Continuum Modelling and Numerical Approaches for Energy Minimisation in Diblock Copolymers

Quentin Parsons

Worcester College

University of Oxford

A thesis submitted for the degree of

Doctor of Philosophy in Computer Science

Trinity Term 2018

Continuum Modelling and Numerical Approaches for Energy Minimisation in Diblock Copolymers

Quentin Parsons

Worcester College, University of Oxford

A thesis submitted for the degree of
Doctor of Philosophy in Computer Science

Trinity Term 2018

Abstract

We use a continuum phase field model to study pattern formation in Diblock Copolymers (DBCs), with an emphasis on terracing in thin films.

Phase separation in DBCs is an important process in nanotechnology that yields an array of highly regular structures on very fine length scales that are of enormous utility. Terraces are ubiquitous in thin film DBC melts. It was long believed that modelling these structures was an intractable problem, but recent attempts to do so using the Self Consistent (Mean) Field Theory (SCFT) were successful.

In this thesis, we use the simpler and more flexible Ohta–Kawasaki (non-local Cahn–Hilliard) Density Functional Theory (DFT) model, derived from the SCFT, with obstacle homogeneous, and long-range energy components. Our main result is that such models can be used to capture terraces in the simplified 2D scenarios we examine, and that these structures form as an inevitable consequence of a simple energy minimisation process.

We consider a 2-phase model for DBC micro-structure evolution, which we analyse rigorously and comprehensively. We study stationary and dynamic (gradient flow) variants of the problem, using the latter as the basis for an efficient but provably convergent numerical method for simulating DBC evolution. Our theoretical analysis and numerical method are based on a common Moreau–Yosida regularisation of the homogeneous energy component. We use the Semi-Smooth Newton (SSN) method to resolve the non-linearities in our numerical method. Comprehensive numerical experiments confirm our theoretical predictions, including a Method of Manufactured Solutions (MMS) test for the order of convergence. We propose a complete specification of the equally spaced global energy minimisers of the symmetric, 2-phase problem in 1D, and offer a practical algorithm for finding them. We explicitly characterise the Order-Disorder Transition (ODT) in parameter space.

We extend our 2-phase model and methods to a 3-phase situation involving a copolymer/homopolymer blend, in which the free surface of the copolymer can adjust to form terraces. We develop energy estimates for energy-minimising 1D morphologies in the sharp interface limit, which we then combine via a double-tangent construction to analyse low energy, 2D structures. We argue that thin films with terraces have a lower free energy than their flat counterparts. Time-dependent numerical simulations in 2D confirm these predictions and provide insight into the evolution of these structures. We replicate and extend recent SCFT results, by performing a numerical experiment in which a terrace forms from a flat initial state.

The model, tools and methods developed in this thesis should serve as a solid foundation for researching more complex, multi-step 3D terraces.

Acknowledgements

There are several people that have helped me on this journey that I would like to thank. Without them, there is no way I would have been able to complete this manuscript.

First, I would like to thank Endre Süli. Endre supervised my Master's thesis and then my initial doctoral work at the Mathematical Institute, before I moved to the Department of Computer Science. Although he didn't directly supervise the research presented in this thesis, he had a major influence on the work, kindly spending many hours teaching me the finer points of how to do the theoretical analysis. He introduced me to pattern formation PDEs, and for that, and his kindness over the last few years, I am very grateful.

Kathryn Gillow was the first 'real' Oxford person I met (she interviewed me for the MMSC MSc) and then the last too, as my internal Oxford examiner! I am extremely grateful that she was prepared to take a chance on me and recommend me for the MSc. I also very much appreciate her feedback on this thesis. I also thank my external examiner, Vanessa Styles, for her piercing questions and meaningful suggestions for improving this piece of work.

I acknowledge too my supervisors David Kay in the Department of Computer Science and Andreas Münch in the Mathematical Institute. I am especially grateful to Andreas for helping me develop the asymptotic results presented here, and for suggesting a number of the 3-phase experiments, as well as for all manner of advice over the last few years. His kind and patient counsel in Munich at the GAMM conference was especially helpful. I wish to thank the EPSRC for funding my work, and the Department of Computer Science for picking me as a DTA award recipient. I am grateful too to Worcester College for kindly funding my attendance at the GAMM and BAMC conferences.

There were several people in the Numerical Analysis Group of the Mathematical Institute who were very good to me. I thank Nick Trefethen for his kindness and personal interest, and also Coralia Cartis for much needed words of encouragement.

A number of people offered me invaluable technical advice in connection with the software. I thank Patrick Farrell for introducing me to FEniCS, and for his

assistance in getting started with the tool. I'm grateful to Chris Richardson, from the BP Institute, Cambridge, who helped me get the graphs I wanted out of FEniCS. I also acknowledge Adrian Jackson at the EPCC for his help in getting my numerical experiments running on Archer.

The University of Oxford is a very grand, very old and complicated institution, with many rules and regulations. I wish to thank Sandy Patel in the Mathematical Institute and Julie Sheppard in the Department of Computer Science for helping me navigate all of these with my sanity (at least nominally) intact.

Miha Troha was an excellent office mate and Nina Otter a great neighbour in Summertown House. Željko Kereta was kind enough not to discard me as a friend through the tough times. I'm grateful for that. I'm also indebted to Marissa Drouillard and her family for their encouragement and support when I started this journey. I'm very thankful to Sally Mullins for her infectious smile, and Helen Taylor for some excellent political conversations as we watched the English-speaking West stumble into self harm.

I wish to thank my sister Julie for her hospitality and kindness, especially over the last year as those final few weeks of writing-up stretched to months and months of back-and-forth to Germany. I am very thankful for her putting me up, lending me her car for the drive to Oxford for the umpteenth time, and for shielding me from the very worst attacks of Oscar the Cat.

Last, I wish to thank Almut for her love, support and patience (especially the part where she would repeatedly and fearlessly (!) walk across the room to calmly offer some advice as I screamed at Matlab – or whatever was refusing to cooperate on my laptop) and for indulging me as I finished this thing off. I am more than lucky to have her in my life. And am well aware of it. Lastly, lastly, I mention Shida (Swahili for 'trouble' – an apt moniker if ever there was one!) our Rhodesian Ridgeback ~~monster~~ puppy, and our (nameless) black cat. They were both blissfully unaware of all of this, but provided the perfect distraction as the research and writing process came to a close. I'd say I'm grateful for their friendship, but if I did that (out loud), they'd both wake up and immediately demand treats and/or belly rubs.

Contents

Acronyms **xxi**

Notation and terminology **xxiii**

I Introduction **1**

1 Introduction **3**

1.1 Core research question and approach 6

1.2 Existing results in the literature 7

1.3 Thesis outline 15

1.4 Highlights and key contributions 18

2 Essential background **19**

2.1 Mathematical essentials 19

2.1.1 Notation, function spaces, norms 19

2.1.2 The Poisson equation with zero Neumann BC 21

2.2 Basic modelling principles 22

2.2.1 Multi-phase materials 22

2.2.2 Energy 23

2.2.3 A stationary energy minimisation problem 24

2.2.4 A dynamic approach: gradient flows 25

2.3 Outlook 26

2.4 Codes and numerical experiments 26

II Two Phase Materials **27**

3 Models of 2-phase materials **29**

3.1 Modelling DBCs 29

3.1.1 2-Phase energy 31

3.1.2 2-Phase incompressibility . . . 32
3.1.3 The Ohta–Kawasaki energy functional . . . 33
3.2 2-Phase dynamics by gradient flow . . . 35
3.2.1 A Lagrange parameter: dynamics in ϕ_A, ϕ_B . . . 35
3.2.2 Dynamics for φ . . . 38
3.2.3 Incompressibility in the energy: a model in φ . . . 39
3.3 Basic properties . . . 40
3.4 Mass control: a local model . . . 41
3.5 Simple, exact solutions . . . 41
3.6 Summary . . . 42

4 Energy minimisation: analysis **47**
4.1 Preliminaries . . . 48
4.1.1 Admissible sets . . . 48
4.1.2 The non-local chemical potential . . . 49
4.1.3 A regularisation of the homogeneous energy density . . . 49
4.2 The stationary problem: a variational inequality . . . 53
4.2.1 A regularised (stationary) problem . . . 54
4.3 A gradient flow, non-local evolutionary problem . . . 56
4.3.1 A regularisation . . . 58
4.3.2 Properties of problems (**P**) and (**Q**) . . . 61
4.3.3 Regularity of solutions . . . 62
4.3.4 Behaviour as $t \to \infty$ . . . 62
4.4 An alternate splitting . . . 62
4.4.1 A local problem: mass *control* . . . 63
4.4.2 Boundedness . . . 65
4.4.3 Stability, continuous dependence on ICs, uniqueness . . . 65
4.4.4 Energy monotonicity . . . 66
4.5 Summary and conclusions . . . 66
4.5.1 Opportunities for further study . . . 67

5 Gradient flow numerical approximations **73**
5.1 A time (only) discretisation . . . 75
5.1.1 Well-posedness of the family of in-time approximations . . . 78
5.1.2 Two local time-discretisations: mass conservation and control . . . 79
5.1.3 Boundedness . . . 82
5.1.4 Stability, continuous dependence on ICs . . . 83
5.1.5 Energy monotonicity . . . 83
5.2 Solving non-linear, non-differentiable problems . . . 84

5.2.1 A fourth degree regularisation . . . 88
5.3 A fully discrete approximation . . . 88
5.3.1 Spatial discretisation, function spaces . . . 88
5.3.2 The discrete Neumann Laplacian . . . 89
5.3.3 Projection operators . . . 90
5.3.4 Formulation of the fully discrete problem . . . 91
5.3.5 ICs . . . 92
5.3.6 Existence of fully discrete solutions . . . 92
5.3.7 Boundedness . . . 92
5.3.8 Stability, continuous dependence on ICs . . . 93
5.3.9 Fully discrete SSN . . . 93
5.3.10 Energy monotonicity . . . 93
5.3.11 Order of convergence . . . 94
5.4 Numerical experiments . . . 95
5.4.1 Mass control . . . 95
5.4.2 MMS testing: order of convergence . . . 98
5.4.3 Regularisation parameter (μ) effects . . . 102
5.5 Summary . . . 105
5.5.1 Opportunities for further study . . . 106

6 Energy minimisation in 1D **113**
6.1 The single monolayer problem . . . 114
6.1.1 A Lagrangian . . . 115
6.1.2 The P2P integro-differential Euler–Lagrange equation . . . 117
6.1.3 A linear, fourth-order ODE . . . 118
6.1.4 An equivalent form of the ID-ELE: an affine function . . . 120
6.1.5 Finding candidate minimisers . . . 121
6.2 Re-scalings: reducing the parameter space . . . 125
6.2.1 Varying models in un-scaled parameter space . . . 126
6.2.2 A rigorous result for disorder; dynamic stability analysis . . . 127
6.2.3 The cool, single monolayer, symmetric morphology . . . 128
6.2.4 The structure of cool, symmetric interface layers . . . 130
6.2.5 Scaling back to the original material parameters . . . 134
6.2.6 A singular problem in scaled parameter space . . . 135
6.2.7 An alternate re-scaling: the sharp interface limit . . . 136
6.3 Multi-monolayer morphologies . . . 138
6.3.1 Energy . . . 139
6.3.2 Stationarity . . . 141

6.4 Summary and conclusions 143

7 Equal-spacing in 1D **149**

7.1 A set of cool, single monolayer, symmetric morphologies 150

7.1.1 Energy-minimising, M1I, cool, single monolayer morphologies 151

7.1.2 Energy symmetry: reflecting morphologies about $x = 0$ 155

7.2 Symmetric, multi-monolayer morphologies 155

7.2.1 Energy minimisation: preliminaries and challenges 155

7.2.2 An equally spaced candidate minimiser 157

7.2.3 Somewhat unequal (Type $\mathrm{A}_{(\nu)}$) morphologies, prescribed ν 160

7.2.4 Very unequal (Type $\mathrm{B}_{(\nu)}$) morphologies, prescribed ν 161

7.2.5 M1I morphologies, variable ν 168

7.2.6 Arbitrary bounded morphologies, variable ν 170

7.3 Summary and conclusions 174

7.3.1 Discussion, limitations 175

8 Implications of equal-spacing in 1D energy minimisers **181**

8.1 Locating ordered and disordered minimisers 182

8.1.1 The disordered candidate minimiser 182

8.1.2 Validating and extending the results with gradient flow experiments 183

8.2 Semi-explicit, P2P minimisers 195

8.2.1 Energy minimisation in un-scaled parameter space 197

8.3 Comparison with Cahn–Hilliard: the effect of $\alpha = 0$ 200

8.4 Implications for modelling phase separation in DBCs 202

8.5 Sharp interface limits 203

8.6 The asymmetric case 206

8.7 Summary and conclusions 208

8.7.1 Discussion, limitations 209

8.7.2 Opportunities for further study 210

III Three Phase Materials **215**

9 3-Phase materials. Terracing **217**

9.1 Modelling 3-phase materials 218

9.1.1 Order parameters, incompressibility, mass 218

9.2 Energy minimisation and gradient flow dynamics 221

9.2.1 Free energy in three phases ϕ_A, ϕ_B, ϕ_V 222

9.2.2 Free energy in two order parameters (φ, ψ) 224

9.2.3 Stationary energy minimisation: variational inequalities 227

9.2.4 Gradient flows . . . 228
9.2.5 Regularisation . . . 229
9.2.6 Symmetric 3-phase materials: general considerations . . . 237
9.3 Symmetric 3-phase materials in 1D . . . 238
9.3.1 The no-V scenario . . . 238
9.3.2 Clean interface scenarios . . . 240
9.3.3 A heuristic *ansatz* for low energy, symmetric morphologies in 1D . . . 241
9.3.4 A convenient re-scaling . . . 243
9.3.5 Sharp interface limit . . . 246
9.3.6 Selecting experimental parameters ($\varepsilon > 0$) . . . 248
9.3.7 Numerical experiments: parameter validation . . . 252
9.4 2D terracing: steps . . . 258
9.4.1 A double tangent construction . . . 258
9.4.2 Gradient flow numerical simulations . . . 262
9.4.3 Open and closed configurations: the effect of χ^{Δ} . . . 263
9.4.4 Triple-phase contact point angles . . . 266
9.4.5 Higher monolayer counts: the closed configuration . . . 268
9.4.6 Spontaneous step formation . . . 268
9.4.7 The effect of inverting χ^{Δ} . . . 275
9.5 Summary and conclusions . . . 277
9.5.1 Opportunities for further study . . . 278

IV Conclusion **287**

10 Conclusions, contributions and further opportunities **289**
10.1 Contributions and results . . . 289
10.1.1 2-Phase results: Chapters 3–8 . . . 289
10.1.2 3-Phase results: Chapter 9 . . . 292
10.1.3 Other contributions . . . 293
10.2 Opportunities for further research . . . 296

References **303**

V Supplementary Material **319**

A Background material **321**
A.1 Further mathematical theory . . . 321
A.1.1 The zero Neumann Poisson equation . . . 324

A.1.2 The $H^{-1}(\Omega)$ inner product . . . 326
A.1.3 Imbeddings . . . 328
A.1.4 Elliptic regularity, BCs . . . 329
A.1.5 Miscellaneous technical results . . . 335
A.1.6 A fully discrete approximation . . . 335
A.2 The n-phase energy minimisation problem . . . 340
A.2.1 A stationary problem . . . 340
A.2.2 A Lagrange function: the $H^{-1}(\Omega)$ gradient flow . . . 341
A.2.3 Applying incompressibility to the energy . . . 343
A.2.4 Regularising a non-smooth homogeneous energy density . . . 343

B Analysis of the 2-phase model **345**
B.1 Proof of Lemma 4.1.2 . . . 345
B.2 Proof of Lemma 4.2.1 . . . 345
B.3 Proof of Lemma 4.2.2 . . . 347
B.4 Proof of Lemma 4.2.4 . . . 348
B.5 Proof of Theorem 4.2.5 . . . 354
B.6 Proof of Lemma 4.2.6 . . . 358
B.7 Proof of Lemma 4.2.7 . . . 359
B.8 Proof of Lemma 4.3.1 . . . 362
B.9 Proof of Lemma 4.3.2 . . . 363
B.10 Proof of Theorem 4.3.3 . . . 370
B.11 Proof of Theorem 4.3.4 . . . 375
B.12 Proof of Theorem 4.3.5 . . . 376
B.13 Proof of Theorem 4.3.6 . . . 378
B.14 Proof of Theorem 4.3.7 . . . 383
B.15 Proof of Lemma 4.3.8 . . . 384
B.16 Proof of Theorem 4.3.9 . . . 387
B.17 Proof of Lemma 4.4.1 . . . 390
B.18 Proof of Corollary 4.4.2 . . . 390
B.19 Boundedness: proof of Lemma 4.4.3 . . . 390
B.20 Stability: proof of Lemma 4.4.4 . . . 395
B.21 Energy decay: proof of Lemma 4.4.5 . . . 396
B.22 Well-posedness: proof of Lemma 5.1.2 . . . 397
B.23 Proof of Lemma 5.1.3 . . . 401
B.24 Proof of Lemma 5.1.4 . . . 401
B.25 Proof of Corollary 5.1.5 . . . 402
B.26 Proof of Lemma 5.1.6 . . . 403

B.27 Boundedness: proof of Lemma 5.1.7 405
B.28 Stability: proof of Lemma 5.1.8 414
B.29 Energy decay: proof of Lemma 5.1.9 418
B.30 Proof of Lemma 5.2.4 421
B.31 Proof of Lemma 5.3.6 425
B.32 Fully discrete boundedness: proof of Lemma 5.3.7 426
B.33 Fully discrete stability: proof of Lemma 5.3.8 430
B.34 Fully discrete energy decay: proof of Lemma 5.3.9 430
B.35 Convergence: proof of Theorem 5.3.10 431

C The 2-phase problem in 1D **451**
C.1 Alternative proof of Lemma 6.1.1 451
C.2 Interfacial structure in Region I 453
C.2.1 The effect of sending $\widehat{L} \downarrow 0$ 455
C.3 Interfacial structure outside of Region I 457
C.4 Interface layer feasibility in $\left(\widehat{\ell}, \widehat{\alpha}\right)$ parameter space 462
C.5 The function $\widetilde{g}$ in the ID-ELE 466

D Models of 3-phase materials **471**
D.1 Dynamics: a Lagrange parameter for incompressibility 471
D.2 A 3-phase model in two order parameters 480
D.2.1 Energy 480
D.2.2 Dynamics 481
D.2.3 Mass conservation: from non-local to local dynamics 481
D.3 Mass control 482
D.3.1 Exact solutions: constant ICs 485
D.4 Numerical simulations of gradient flow dynamics 486
D.4.1 Discrete time mass control 486

List of Figures

1.1 DBCs and micro-structure self-assembly 4
1.2 A terraced thin film droplet 5
1.3 DBC ground state phase diagram 9

3.1 Schematic of a DBC molecule 30
3.2 The effect of increasing the Flory–Huggins parameter 35

4.1 The non-smooth, 2-phase homogeneous energy and its regulariser 52
4.2 Energy evolution for $f \neq 0$ 66
4.3 Summary – Chapter 4 67

5.1 Existence and uniqueness of a family of in-time approximations 80
5.2 Mass control experiment results (2-phase, 1D) 96
5.3 Mass control convergence test 96
5.4 Fully explicit non-local mass control experiment (2-phase, 1D) 97
5.5 MMS convergence testing results in 1D 101
5.6 The IC and the seven end-states 103
5.7 Results of a 2-phase μ-study for four mesh sizes 104
5.8 Summary – Chapter 5 105
5.9 Comparison of second and fourth order regularisation approaches 108
5.10 SSN mesh (in)dependence investigation 109

6.1 A BA monolayer morphology schematic 115
6.2 Three types of 1D, 2-phase candidate energy minimiser 117
6.3 Zero contours of R in (x_L, x_R)–space 124
6.4 Cool parameter space 131
6.5 The effect of varying Θ and ε_φ in scaled parameter space 131
6.6 Four sample interface layers 132
6.7 Properties of interface layers as a function of scaled parameter space 134
6.8 A consistent, singular problem 136
6.9 A 3-monolayer, 2-phase morphology 140

7.1 Summary M1I single monolayer minimum energy source indicator 152
7.2 A sample constrained, continuous optimisation problem in $\widehat{\ell}$ 152
7.3 The M1I, single monolayer minimum energy surface over cool parameter space 153
7.4 Second derivative of the minimum energy surface 154
7.5 An illustrative AB/BA reflection 155
7.6 Two sample profiles: one of Type $\mathrm{A}_{(5)}$, and the other Type $\mathrm{B}_{(5)}$ 158
7.7 Snippet of a raised morphology in $-\Phi'$ 163
7.8 The energy equivalence of elevated single monolayer profiles in $-\Phi'$ 164
7.9 Elevated and non-elevated 2-monolayer minimisers 165
7.10 Elevated and non-elevated 2-monolayer minimisers 165
7.11 A very unequally spaced morphology profile 166
7.12 Contour map of ν_{opt} 168
7.13 Minimum multi-monolayer energy surface 169
7.14 Minimum-energy surfaces for various monolayer counts 171
7.15 Minimiser component layer source indicator 172
7.16 The bounded, single monolayer minimum energy over cool parameter space 173
7.17 Minimiser component layer source indicator 174

8.1 Comparison with the disordered (constant zero) morphology 183
8.2 Revised energy minimising layer count contour plot 184
8.3 Gradient flow experiment Set 1 summary results 187
8.4 Summary results: 2-phase pulse shift experiments 188
8.5 Gradient flow experiment Set 2 summary results (part 1 of 2) 189
8.6 Gradient flow experiment Set 2 summary results (part 2 of 2) 190
8.7 Gradient flow experiment Set 3 summary results 191
8.8 Gradient flow experiment Set 4 summary results 192
8.9 Gradient flow experiment Set 5 summary results 193
8.10 Minimum energy vs layer count ν 197
8.11 Explicit minimisers in scaled parameter space 198
8.12 Energy-minimising layer counts in un-scaled parameter space 199
8.13 Cooling and heating 202
8.14 Zero contours of G and H in (x_L, x_R)–space 207
8.15 Candidate asymmetric minimisers 207
8.16 Comparison of various forms of the 2-phase homogeneous energy density . . 211
8.17 Vastly different timescales for similar gradient flow experiments 213

9.1 A 3-phase morphology in 1D using (φ, ψ) order parameters 219
9.2 The (φ, ψ)–parameter triangle 220
9.3 A polymer (melt) with a void above, in 2D 222

9.4 Two regularised homogeneous energy densities 230
9.5 Partial derivatives of a homogeneous energy density function 230
9.6 MMS results: 3-phase/1D 236
9.7 Schematic of a 3-monolayer DBC 238
9.8 Resolved 1D, 3-phase morphologies 239
9.9 The 3-phase sharp interface limit process 246
9.10 Summary for $\gamma = 32$ 249
9.11 Results of the 3-phase μ-study for three mesh sizes 251
9.12 An experiment illustrating the effect of μ in 3-phase simulations 252
9.13 Drill-down results: the effect of μ in 3-phase simulations 252
9.14 Energy minimising 2-phase parameters in the pure polymer 254
9.15 3-Phase morphologies and energy comparison in 1D: Scenario 1 255
9.16 3-Phase morphologies and energy comparison in 1D: Scenario 2 256
9.17 3-Phase morphologies and energy comparison in 1D: Scenario 3 257
9.18 The jump in the gradient flow end-state energy 258
9.19 A 2D stepped configuration and its flat alternative 259
9.20 The 3-phase, double tangent construction schematic 260
9.21 Plots of φ and corresponding views in (φ, ψ)-space 264
9.22 Energy evolution 265
9.23 The sharp interface double tangent construction 265
9.24 Schematic of a triple point from Young's relation 266
9.25 Two triple points in the open stepped configuration 267
9.26 $L_2^{||}$–$L_4^{||}$ ICs and end-states 269
9.27 Sharp interface double tangent construction for the $L_2^{||}$–$L_4^{||}$ configuration . . 269
9.28 A wedge of well-mixed material 271
9.29 Energy evolution for spontaneous step formation 271
9.30 Spontaneous step formation 272
9.31 Spontaneous step formation: evolution of the polymer–void free surface . . 273
9.32 Spontaneous step formation: evolution in (φ, ψ)-space 274
9.33 The effect of inverting χ^{Δ}: φ snapshots 275
9.34 The effect of inverting χ^{Δ}: ψ snapshots 276
9.35 The effect of inverting χ^{Δ}: views in (φ, ψ) parameter space 276
9.36 A DBC 'staircase' 281

C.1 The function $c_A\left(\widehat{\ell}, \widehat{\alpha}\right)$ over Region I 454
C.2 Small $\widehat{\ell}$ morphological response. 456
C.3 Un-scaled single-layer energy minimisers inside Region I 458
C.4 Finding M1I regions in (scaled) parameter space 465

C.5 View of a typical function $\widetilde{g}$ 467

D.1 Converting from dynamics in $\boldsymbol{\phi}$ to dynamics in (φ, ψ) 474
D.2 Ratio of macro to micro mobilities 477
D.3 Mass evolution for an asymmetric DBC 486
D.4 Predicted discrete time mass evolution for an asymmetric DBC 489

List of Tables

5.1 Mass control test parameters (2-phase, 1D) 95
5.2 2-Phase MMS test parameters 100
5.3 Second degree regularisation MMS test parameters 101
5.4 Fourth degree regularisation MMS test parameters 101
5.5 2-Phase μ-experiment parameter set (1D) 102

8.1 Common 2-phase gradient flow experiment parameters 185
8.2 Gradient flow experiments from ICs with $\nu \neq \nu_{\text{opt}}$ 187

9.1 3-Phase MMS test parameters 236
9.2 3-Phase gradient-flow experiment parameters 253
9.3 Start/finish energy comparison data 264

C.1 Sample intersections of $\cos\left(\sqrt{\widehat{q}_h}\frac{\widehat{\ell}}{2}\right)$ and $\cos\left(\sqrt{\widehat{q}_\ell}\frac{\widehat{\ell}}{2}\right)$ 461
C.2 Sample intersections of $\sin\left(\sqrt{\widehat{q}_h}\frac{\widehat{\ell}}{2}\right)$ and $\sin\left(\sqrt{\widehat{q}_\ell}\frac{\widehat{\ell}}{2}\right)$ 462

Acronyms

1D One dimension.

2D Two dimensions.

3D Three dimensions.

BC Boundary Condition. xxiii, xxiv, 19–22, 25, 36, 38, 39, 55, 56, 62, 71, 73, 90, 113, 116, 117, 119, 122, 125, 137, 141, 142, 146, 149, 155, 156, 162, 163, 170, 174, 176, 177, 179, 196, 200, 224, 240, 241, 245, 278, 283, 291, 324, 325, 330, 331, 333, 336, 340–342, 354, 356, 358, 384, 385, 387, 394, 401, 402, 410, 414, 448, 455, 469, 472, 480–482

BCP Block Copolymer. 3

CDS Cell-Dynamical-System. 11–13, 300

CHC Cahn–Hilliard–Cook. 11, 298

DBC Diblock Copolymer. iii, xxiii, xxv, 3–12, 14–18, 23, 24, 29–31, 33, 42, 43, 74, 113, 139, 145, 181, 202, 208, 212, 217–221, 238, 240, 243, 244, 277, 281, 289, 292, 293, 297, 340, 344, 482–484, 486–489

DDFT Dynamic Density Functional Theory. 7, 8, 14

DFT Density Functional Theory. iii, 6–8, 11, 12, 18, 202, 289

ELE Euler–Lagrange Equation. 200, 201, 241

GMRES Generalized Minimal Residual Method. 280

IC Initial Condition. 25, 35, 38, 39, 41, 45, 56, 58, 60–66, 73, 74, 76, 80, 83, 91, 93, 95, 100, 102, 103, 105, 111, 112, 146, 184–188, 212, 213, 228, 231, 234, 237, 239, 245, 250, 252–258, 263, 264, 267–269, 271–275, 277, 278, 280, 284, 285, 292, 293, 295–297, 363, 365, 374, 375, 378, 380, 382–384, 388, 393, 395, 449, 472, 480, 483, 485

ID-ELE Integro-Differential Euler–Lagrange Equation. xxvi, xxvii, 55, 114, 117, 120, 121, 124, 129, 130, 137, 138, 142, 143, 150–152, 156, 159, 164, 169, 170, 173–177, 185, 195, 201, 206, 209, 212, 290, 291, 466, 468

ISR Intermediate Segregation Regime. 11, 34, 203

M1I Monotone with a Single Inflexion Point. xxvi, 130, 132, 134, 149–153, 156, 162, 165, 168, 170, 172–176, 182, 194, 195, 207–210, 214, 455, 456, 464, 465

MMS Method of Manufactured Solutions. iii, 16–18, 63, 66, 94, 98–101, 105–108, 111, 112, 231, 233, 235, 236, 290

MPI Message Passing Interface. 294, 295

ODE Ordinary Differential Equation. 41, 64, 114, 118, 120, 121, 124, 125, 130, 136, 142, 143, 149–151, 170, 172, 174–176, 291, 363, 453, 483, 485

ODT Order-Disorder Transition. iii, xxvi, 9, 11, 17, 18, 176, 182, 184, 194, 199, 202, 208, 291, 297

P2P Pure-Phase to Pure-Phase. xxiv, xxvi, 114–117, 119, 130, 132, 139, 149, 151, 155–157, 160, 161, 168–170, 172–178, 180–183, 186, 194–196, 200, 201, 203, 208, 212, 219, 220, 459, 463, 466, 468

PDAS Primal-Dual Active Set. 14, 107, 290, 300, 302

PDE Partial Differential Equation. 12, 25, 35, 39, 41, 73, 299, 340, 472, 473, 478, 480, 482

PETSc Portable and Extendable Toolkit for Scientific Computing. 280, 295

PS-PMMA Polystyrene-Polymethylmethacrylate. 5

SCFT Self Consistent (Mean) Field Theory. iii, 6–8, 11–15, 17, 18, 34, 202, 208, 218, 262, 277, 282, 285, 292, 293, 297, 300

SSN Semi-Smooth Newton. iii, 14, 84–86, 88, 106–109, 234, 251, 279, 280, 283, 284, 290, 294, 300

SSR Strong Segregation Regime. 11, 34, 203

WSR Weak Segregation Regime. 34, 203

Notation and terminology

Ω Spatial domain in $\mathbb{R}^d$ occupied by the material. 19

L The length of a single monolayer (containing an interface layer of width ℓ) in the 2-phase case. In 3-phase, the (vertical) extent of the domain Ω. 114, 238, 258

L_x The (horizontal) extent of the 2D rectangular domain, Ω in the 3-phase case. 258

$\mathcal{D}$ The length of the domain in the (general) multi-monolayer energy minimisation problem. 138, 139

$\overline{\varphi}$ The integral average of φ over Ω. 19, 20

$(-\Delta_n)^{-1}$ The zero mass, inverse Laplacian of a function (with zero Neumann Boundary Condition (BC)). 21

$\|\cdot\|_{-1}$ The $H^{-1}(\Omega)$ norm of a zero mass function. 22

$\mathscr{F}$ The set of elements in $\left(H^1(\Omega)\right)'$ mapping constant functions to zero. See (2.8b). 21

C An arbitrary constant, which can change from line to line and term to term. 52

Θ Absolute temperature. 31

N Index of polymerisation; the total number of A and B monomers in a single DBC chain molecule. 30

a Type A monomer density. 30, 221

b Type B monomer density. 30, 221

v Type V monomer (homopolymer, 3$^{\text{rd}}$ phase) density. 221

m The average difference between the A and B monomer densities; $\overline{\varphi} = m$ in two phases and $\overline{\varphi} = m\mathcal{M}$ in three phases. 30, 33, 221

$\mathcal{M}$ Volume fraction or proportion of copolymer material in a 3-phase copolymer/homopolymer blend. 220

ℓ Kuhn statistical length, measuring the average distance between adjacent monomers. Also the width of a Pure-Phase to Pure-Phase (P2P) AB/BA interface layer. 31, 114

ε_φ^2 Square of the interfacial thickness parameter for φ in two and three phases. 33, 225

$\varepsilon_{\varphi\psi}^2$ Square of the interfacial thickness parameter in three phases. 225

ε_ψ^2 Square of the interfacial thickness parameter for ψ in three phases. 225

χ^{AB} AB Flory–Huggins interaction parameter, modelling the excess incompatibility of A and B monomers in two and three phases. 34, 226

χ^{BV} BV Flory–Huggins interaction parameter, modelling the excess incompatibility of B and V monomers in three phases. 226

χ^{AV} AV Flory–Huggins interaction parameter, modelling the excess incompatibility of A and V monomers in three phases. 226

α Non-local energy coefficient in two and three phases. 34, 226

β Non-local energy coefficient in three phases; $\beta = 0$ in the symmetric case. 226

γ Non-local energy coefficient in three phases; $\gamma = 0$ in the symmetric case. Also used for that part of the non-local coefficient (written as $\varepsilon\gamma$) that is held constant in the sharp interface limit ($\varepsilon \downarrow 0$) in the 2- and 3-phase models.. 136, 226, 244

φ *Micro*-phase order parameter as a function of (x, t): the *difference* between the A and B monomer densities in the 2- and 3-phase models.

- φ_j denotes the exact function φ at $t = t_j$;
- φ^j is an approximation of φ_j not based on any particular spatial discretisation; and
- φ_h^j denotes a fully discrete (finite element in space) approximation of φ.

$\varphi = 1 \Rightarrow$ pure A and $\varphi = -1 \Rightarrow$ pure B. See also Section 5.1 and 9.2.5.3. 32, 218

$\widetilde{\varphi}$ φ inside a P2P interface layer. 115

$-\Phi$ Inverse Laplacian of φ with zero Neumann BC, in the 1D problem. $-\Phi'$ is the first derivative of $-\Phi$, and appears in the energy functional. 113

ψ *Macro*-phase order parameter as a function of (x, t): the *sum* of the A and B monomer densities in the 3-phase model.

- ψ_j denotes the exact function ψ at $t = t_j$;

- ψ^j is an approximation of ψ_j not based on any particular spatial discretisation; and
- ψ_h^j denotes a fully discrete (finite element in space) approximation of ψ.

$\psi = 0 \Rightarrow$ pure V and $\varphi = 1 \Rightarrow$ pure copolymer (some combination of A and B material). See also Section 9.2.5.3.

Also the non-local chemical potential in two phases. 49, 218

M_φ The mobility of φ in the 2- and 3-phase gradient flow dynamics. 39, 229

M_ψ The mobility of ψ in the 3-phase gradient flow dynamics. 229

$\mathcal{B}$ The homogeneous (or bulk) energy density component (and its matrix of coefficients), favouring pure phases at low temperatures. Modelled as a double obstacle in this thesis. 24, 31

$\mathcal{B}_\mu$ The regularised homogeneous energy density component as in (3.19), (9.32). 34, 229

μ Moreau–Yosida regularisation parameter for the double obstacle homogeneous energy component in two and three phases. 32, 34, 229

Υ_μ Moreau–Yosida penalty component of the regularised double-obstacle homogeneous energy density in the 2- and 3-phase models. 49, 229

ζ_μ Derivative of Υ_μ in the 2-phase problem i.e. $\zeta_\mu(r) = \Upsilon_\mu'(r)$. Appears in all of the regularised dynamics. 50

$\mathcal{I}$ The interfacial energy density component (and its matrix of coefficients), favouring constant phase field variables. 23, 31

$\mathcal{N}$ The non-local energy density component, favouring constant phase field variables at their averages. Models the covalent bond and periodic structure of phase separated DBCs. 24, 32

$\mathcal{E}$ Ginzburg–Landau approximation to the Gibbs free energy. 23

$\mathcal{E}_\mu$ Regularised free energy obtained by replacing the double obstacle homogeneous density component $\mathcal{B}$, with its regularised counterpart, $\mathcal{B}_\mu$. 32, 33

$\mathcal{E}_\mu^{(m)}$ Regularised free energy of a morphology with integral/mass average m; and the non-local component involves $\varphi - m$ (instead of $\varphi - \overline{\varphi}$). 64

$\mathcal{E}_{\mathbf{min}}^{(1)}$ Minimum energy of a single monolayer morphology. 151

$\mathcal{E}^{(\nu)}$ Minimum energy of a multi-monolayer morphology with ν monolayers (ν given). 195

$\widehat{L}$ Scaled length parameter in the 2-phase problem as in (6.47). Generally used in the context of the single monolayer energy minimisation problem. 126

$\widehat{\mathcal{D}}$ The scaled length of the domain in the (general) multi-monolayer energy minimisation problem; scales from $\mathcal{D}$ in the same way as $\widehat{L}$. 139

$\widehat{\ell}$ The re-scaled width of a P2P AB/BA interface layer. 129

$\widehat{\alpha}$ Scaled non-local energy coefficient parameter in the 2-phase problem as in (6.47). 126

$\widehat{\alpha}_{\max}$ The upper bound of structure in scaled parameter space for the symmetric problem in 1D. If $\widehat{\alpha} > \widehat{\alpha}_{\max}$, the (unique) global energy minimiser is disordered (constant); if $\widehat{\alpha} \leq \widehat{\alpha}_{\max}$, the global minimiser is not unique and one of the minimisers is comprised of equally spaced monolayers. Also defines the ODT in scaled parameter space for the symmetric problem in 1D. See Conjectures 8.1.1 and 8.2.2. 133, 184

warm Warm (scaled) parameter space corresponding to $\widehat{\alpha} > \frac{1}{4}$. The unique (global) energy minimiser is disordered in this part of parameter space. 119, 127

critical Critical (scaled) parameter space corresponding to $\widehat{\alpha} = \frac{1}{4}$. See also (6.25) and Conjecture 8.2.2. 128

cool Cool parameter space, corresponding to $\widehat{\alpha} < \frac{1}{4}$ (cf. (6.58)). Ordered minimisers are possible in this part of parameter space. See Fig's 6.4, 6.5. 128

cold Cold parameter space. A subset of cool parameter space with the property that if Θ is made small enough, all models enter this region and never leave. Bounded in parameter space by the first zero contour of $\cos\left(\sqrt{\widehat{q}_h}\frac{\widehat{\ell}}{2}\right)$ on the left and the first zero contour of $\cos\left(\sqrt{\widehat{q}_\ell}\frac{\widehat{\ell}}{2}\right)$ on the right. See Fig's 6.4, 6.5. 130

$\widetilde{\ell}$ The smallest solution of $\widetilde{g}\left(\widehat{\ell}\right) = \widehat{\ell}$ as in (6.63a). The corresponding monolayer width is denoted $\widetilde{L}$. $\widetilde{\ell}$ and $\widetilde{L}$ are used interchangeably. They both measure the width of the thinnest possible P2P interface/monolayer solving the Integro-Differential Euler–Lagrange Equation (ID-ELE). 466

$\widehat{\ell}_{\min}$ The smallest solution of the ID-ELE with zero right-hand side. 468

$\widehat{\ell}_{\mathbf{opt}}$ Scaled interface layer width in the minimum energy, single monolayer morphology. The corresponding quantity in unscaled length units is denoted ℓ_{opt}. 151, 195

$\widehat{\ell}_{\max}$ Maximum (scaled) width of a P2P interface layer that is Monotone with a Single Inflexion Point (M1I). See Fig. 6.7(a) on p. 134. 132

$\widetilde{L}$ The upper bound on Region I in scaled parameter space (as a function of $\widehat{\alpha}$). See also $\widetilde{\ell}$. 130, 195

$\widehat{L}_{\mathbf{opt}}$ The (scaled) width of each monolayer in the energy-minimising configuration. The corresponding un-scaled quantity is L_{opt}. 169

$\widehat{L}_{\max}$ The (scaled) width of the monolayer which has an energy minimising interface layer of width $\widehat{\ell}_{\max}$ according to the ID-ELE, viz. $\widehat{L}_{\max} = \widetilde{g}\left(\widehat{\ell}_{\max}\right)$. 195

ν The number of monolayers in a lamellar configuration (two and three phases). 114

$\nu_{\min}$ The smallest possible number of monolayers in an energy minimising 1D morphology, viz. $\nu_{\min} \leq \nu_{\mathrm{opt}}$. 196

$\nu_{\mathbf{opt}}$ Number of monolayers in an energy-minimising, 1D configuration. 168, 195

$\nu_{\max}$ The highest possible number of monolayers in an energy minimising 1D morphology, viz. $\nu_{\mathrm{opt}} \leq \nu_{\max}$. 196

q_h Coefficient of high frequency interface layer solution component. 120

$\widehat{q_h}$ Coefficient of scaled high frequency interface layer solution component. 129

q_ℓ Coefficient of low frequency interface layer solution component. 120

$\widehat{q_\ell}$ Coefficient of scaled low frequency interface layer solution component. 129

$\mathcal{K}$ 3-Phase sharp interface limit re-scaling interface polymer–void thickness parameter. 244

χ^{Δ} Re-scaled measure of the asymmetry in the repulsion of the $B \leftrightarrow V$ and $A \leftrightarrow V$ phases in the 3-phase model. 244

ε The scaled interfacial width parameter that goes to zero ($\varepsilon \downarrow 0$) in the sharp interface limit (in two and three phases). Also used to denote $\frac{1}{\sqrt{6}} \times \ell$ (the Kuhn statistical length) in the 3-phase model. 136, 223, 244

$w_{\min}$ Practical minimum width of each monolayer inside the copolymer, in an energy-minimising (esp. sharp interface limit) 3-phase configuration. The smallest solution w of $g(w;\gamma) = w$ in (6.83c). 249

$w_{\mathbf{opt}}$ Width of each monolayer inside the copolymer, in an energy-minimising (esp. sharp interface limit) 3-phase configuration. 246

$w_{\max}$ Practical maximum width of each monolayer inside the copolymer, in an energy-minimising (esp. sharp interface limit) 3-phase configuration. 249

T Total simulation time horizon. 75

τ Size of the time-step in a time-discrete approximation; $t_{j+1} = t_j + \tau$. 75, 233

M The number of time-steps in a discrete-in-time approximation, viz. $T = M\tau$. 75, 233

h A measure of how fine a finite element spatial discretisation is. The longest diameter of any simplex in a triangulation $\mathcal{T}^h$. 110

V^h Conforming finite element (piecewise linear approximation) function space on the triangulation $\mathcal{T}^h$. 88

$(-\Delta_h)^{-1}$ The discrete, zero mass, inverse Laplacian of a function in V^h (cf. $(-\Delta_n)^{-1}$). 89

$\|\cdot\|_{-h}$ The discrete $H^{-1}(\Omega)$ norm of a zero mass function in V^h (cf. $\|\cdot\|_{-1}$). 90

$\mathcal{E}_{\mu,h}^{(m)}$ Regularised free energy of a function in V^h, in which the non-local component is based on the $\|\cdot\|_{-h}$ norm (instead of $\|\cdot\|_{-1}$; cf. $\mathcal{E}_{\mu}^{(m)}$). 91

Part I

Introduction

Chapter 1

Introduction

Contents

1.1 Core research question and approach 6

1.2 Existing results in the literature 7

1.3 Thesis outline 15

1.4 Highlights and key contributions 18

Block Copolymers (BCPs) are important materials with a range of industrial and scientific applications. The molecules making up these materials are organised into sub-chains or linear blocks of like monomers. In the simplest case, the Diblock Copolymer (DBC), each molecule consists of a linear block of type A monomers connected by a covalent bond to a linear block of type B monomers. More generally, repeated blocks, combinations with more than two types of monomer, and topologies other than linear chains, such as triblock and branched copolymers are also possible (see Fig. 1 of Bates and Fredrickson (1999)). We restrict our attention to DBCs.

DBC molecules usually prefer arrangements in which blocks of the same monomer species are close to each other. At the molecular level according to Choksi (2003), '*below a critical temperature, even a weak repulsion between unlike monomers A and B induces a strong repulsion between the sub-chains causing [them] to segregate*'. It is this repulsive action that gives these molecules their remarkable ability to self-assemble into ordered, periodic structures organised into highly regular patterns of like monomers including, lamellae, cylinders, spheres and so-called gyroids, by a process called *phase separation* (see Fig. 1.3 and also Bates and Fredrickson (1999)). The size of the resulting segregated regions is limited by the fact that the blocks are chemically bonded, and by the tendency of the chains to coil up. Phase separation thus occurs on a micro- but not a macro-scale, making them extremely useful as functional nano-materials (Kim et al. (2010); Fasolka and Mayes (2001)). We depict a schematic of a DBC and the way in which these molecules rearrange themselves in

Fig. 1.1. A large collection of such molecules is called a *melt*.

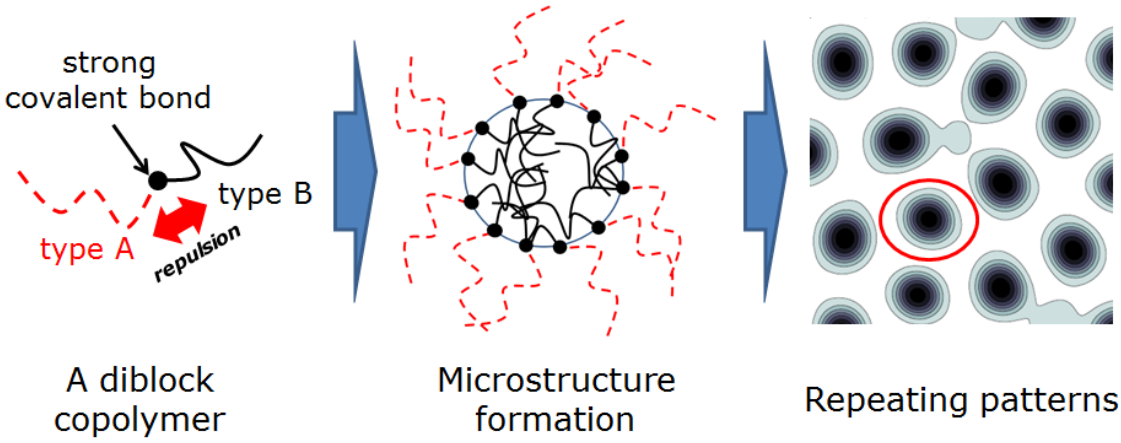

Figure 1.1: DBCs and micro-structure self-assembly

DBC molecules can be precisely synthesized on a large scale to create diverse materials with properties that are determined by the structure of the molecules. Because of this, such materials are often referred to as *designer soft materials* (Bates and Fredrickson (1999)). Applications are, for example, in gel electrophoresis, where the lamellae are chemically tuned to have a preference for certain species in the material to be analysed, the manufacture of high efficiency solar cells and biological applications where the fine length scale of the repeating patterns can be used in blood analysis (Lyakhova et al. (2006); Kim et al. (2010)). In other cases, the bulk properties that arise from the micro-structures are exploited in commodity products such as box tape adhesives or as toughening additives for tarmacs (Bates and Fredrickson (1999)). According to De Gennes (1990), the production of just three such materials (polyethylene, polystyrene and polyvinylchloride) '*exceeds that of metals*'. At least in part because of their enormous commercial value, the literature related to polymers is vast. Doi and Edwards (1988), Hamley (2003) and Fredrickson (2006) provide a general background to these materials and their properties.

Terracing

Interesting structures appear when a DBC is confined to a thin film, because the confinement introduces an additional length scale that is not typically compatible with the natural length scale selected by a layered pattern in free space (Knoll et al. (2002); Feng et al. (2004); Nikoubashman et al. (2013)). In *hard confinement*, a layer of DBC is confined between two non-deformable substrates. If the gap between these substrates is highly incommensurate with the natural lamella period in the bulk, the system may switch to a state where the lamellae are perpendicular to the substrate, or a mixed state with both parallel and perpendicular interfaces (Matsen (1997); Carvalho and Thomas (1994)). In

soft confinement, one of the surfaces is free, and the system can change thickness locally to create steps and, in 3D, terraces (McGraw et al. (2011)). In 3D, micro-structures other than lamellae can appear, such as cylinders of various orientations, or spheres, adding further complexity to the possible interactions between the structure in the polymer bulk and the shape of the free surface (Lyakhova et al. (2006); van Dijk and van den Berg (1995); Yokoyama et al. (2000)).

Croll et al. (2006) includes a top-down atomic force microscopy error signal scan (see Fig. 1(a) of that reference reproduced as our Fig. 1.2) of such a structure from experimental observations. The papers by Carvalho and Thomas (1994) and Gido et al. (1993) suggest the existence of intricate twist geometries in the micro-structure between successive steps, as thin film DBCs form terraces.

That terracing is an interesting and important topic is confirmed by the remark in Lyakhova et al. (2006) that '*[t]heoretical studies of terrace formation in thin films are sparse*' and '*the fundamentals of terrace formation, that is, how a developing and rearranging micro-structure determines (or is determined by) the shape of the free interface, remain to be uncovered*'. More recently, Stasiak et al. (2012) state that *'[t]he presence of step edges separating different film thicknesses is ubiquitous in block copolymer films, and yet they have received relatively little theoretical attention'.*

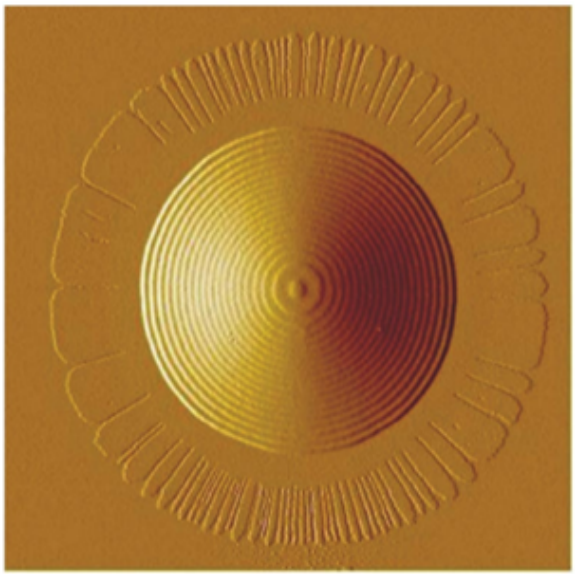

Figure 1.2: A droplet of Polystyrene-Polymethylmethacrylate (PS-PMMA) DBC material with clearly visible, concentric steps, or terraces. Reprinted with permission from Fig. 1(a) of Croll et al. (2006) – Droplet Shape of an Anisotropic Liquid. Phys. Rev. Lett., 97:204502, Nov. 2006 © 2006 by the American Physical Society. See http://dx.doi.org/10.1103/PhysRevLett.97.204502.

Having confirmed that terraces are important and interesting structures that are worthy

of investigation, we pose our basic research question together with our proposed approach to answering it.

1.1 Core research question and approach

As we will discuss in some detail presently, DBCs are frequently modelled using two techniques: i) the Self Consistent (Mean) Field Theory (SCFT), and ii) Density Functional Theorys (DFTs), both of which are based on the notion of free energy minimisation. We do not attempt to comprehensively compare these approaches. At a high level however, it would appear that SCFT-based models are superior to their DFT counterparts in their predictive power, but DFT models tend to yield more flexible numerical methods. Our informal interpretation of the situation is that the SCFT is favoured by physicists, while DFT models appear to be preferred by mathematicians. SCFT-based models have successfully been applied to model terracing in DBCs but, as far as we are aware (as at this writing), this has not been attempted using a DFT approach. In this spirit, we ask:

Is it possible to use a DFT model of phase separation in DBCs to capture and study terrace formation?

Our interest in this question is motivated by various references. In Lyakhova et al. (2006) the authors '*[wonder] if it would be possible to simplify the [SCFT] model further (e.g., by replacing our computational-intensive SCF free energy with more computational-efficient phenomenological descriptions, such as a Landau-Ginzburg Hamiltonian in a cell dynamics method)*'. That this is a difficult problem is confirmed by the same authors: '*modeling [sic] of the terrace formation in block copolymer systems was long believed to be intractable because of the complexety [sic] of the interface phenomena and the many different length and time scales involved*'.

Capturing and theoretically predicting the complex twist and other morphologies discussed in Carvalho and Thomas (1994); Gido et al. (1993); Nishikawa et al. (1993) is a very ambitious, long-term goal. Our more modest plan is to consider simplified versions of these structures. As such, we work in 1D and 2D, but anticipate that our results should serve as a stepping stone to the 3D terracing problem.

Approach

Several building blocks are required to answer our core research question.

1. An energy-minimisation based **phase field model** for DBCs and their evolution, that is strongly motivated by the underlying physics.

2. **Analysis** of the energy minimisation problem to ensure the existence of minimisers,

and understand their structure. Analysis of dynamic variants of the problem to ensure that these are well-posed.

3. Efficient, convergent **numerical methods** for approximating the dynamical methods. Assurances that they lead either to provably global energy minimisers or, at the very least, low energy morphologies that are morphologically similar to energy minimisers.

4. Detailed **experimental results** (physical and from simulations) and further insights into the literature related to models of terrace formation. Such insights should shape our experimental programme, and give us expected results that our model and simulations should be able to replicate.

1.2 Existing results in the literature

We review some of the key results as they pertain to the four building blocks above.

Modelling

In the context of DBC modelling, we distinguish three types of model, the first of which is a stepping-stone to the other two:

i) As 2-phase (A and B) materials, in which the DBC *completely* fills a domain (viz. a container), and we consider only the micro-structure that results from self-assembly.

ii) As 3-phase materials, in which the polymer *partially* fills a container, and a third material (the void, most likely air) interacts with the copolymer. We consider the AB (2-phase) micro-structure inside the copolymer, and the free surface by which the void and polymer interact.

iii) As n-phase materials ($n > 2$). We do not consider such models in this thesis, but draw the reader's attention to some items in the literature that deal with them.

The basic principle in both SCFT and DFT-based models is that DBCs rearrange themselves to minimise a particular free energy. Stationary (time independent) and dynamic variants of the energy minimisation problem exist; the latter attempt to capture the time evolution of DBC phase separation.

Remark. The acronym/term SCFT appears to be well-defined and understood in the literature. The abbreviation DFT, on the other hand, seems less well-defined. We use it to describe models in which phase field variables are used to model a material, in the context of minimising a free energy functional of those variables, as in Choksi and Ren (2003, 2005). This approach is quite distinct from the Dynamic Density Functional Theory (DDFT) (note the similar nomenclature) of Fraaije et al. (1997), which is a time-dependent version of the

SCFT that, according to Section 5.3.6 of Fredrickson (2006), can '*at least qualitatively capture the kinetic pathway of a complex fluid towards its equilibrium state.*'

The SCFT, which considers the average effect of the surrounding monomers for each molecule (see Edwards (1965); de Gennes (1969); Fredrickson (2006)), is an important theoretical tool for predicting structures and patterns in DBCs, '*which is regarded as the state-of-the-art for block copolymer melts*' (Maher et al. (2016)). In Matsen and Schick (1994), the authors developed a spectral method whereby predictions of low energy morphologies could be made as a function of the physical properties of the underlying molecule, as depicted in Fig. 1.3 (see also Matsen (2002)). The match between this figure and that constructed from physical observations (see Fig's 5.15 and 5.17 of Fredrickson (2006)) is striking (the numerical/theoretical and measured phase diagrams can be seen side-by-side in Fig. 2 of Choksi et al. (2009)). Time-dependent variants of the SCFT also exist, such as the DDFT we mentioned earlier (see Fraaije (1993); Fraaije et al. (1997); Maurits and Fraaije (1997); Morita et al. (2001)), and the dynamical mean-field theory/dynamical SCFT variants (see Yeung and Shi (1999); Reister et al. (2001); Hasegawa and Doi (1997); Müller and Schmid (2005)).

We have mentioned the spectral method associated with the SCFT and given some indication of its predictive power. Unfortunately, such numerical methods are computationally expensive (see Choksi et al. (2009); Uneyama and Doi (2004), and Fredrickson et al. (2002) for a review). Tracking terraces on large 3D domains for long times, via dynamical variants of the SCFT, to observe the behaviour of surface structures, is prohibitively expensive. As such, the results in the literature appear to be limited to a small number of carefully chosen domains (see Lyakhova et al. (2006)).

Another key limitation of this approach, is that the associated numerical methods are *ansatz*-based and assume certain structural symmetries, which means that '*[s]uch calculations run the risk of overlooking complex [3D] micro-phases that have not been previously identified*' (Bates and Fredrickson (1999)) in, for instance, laboratory experiments (see the Introduction to Choksi and Ren (2003) for a more detailed discussion).

These limitations have renewed the interest in DFT-based modelling approaches, and their associated numerical methods. DFT-based approaches involving phase field models for micro-structure evolution have been studied for several decades. According to Qin and Bhadeshia (2011), '*[a] phase field method is in principle able to compute the evolution of microstructure without explicit intervention. The domain of interest is the field in which the value of an order parameter at a particular location identifies the nature of the phase, the presence of an interface or other parameters such as chemical composition or strain. The heterogeneous system is incorporated into a grand functional representing its free energy. Assumptions are then made about how the field evolves as the free energy is minimized. Interfaces do not need to be tracked but can be inferred from the field parameters during*

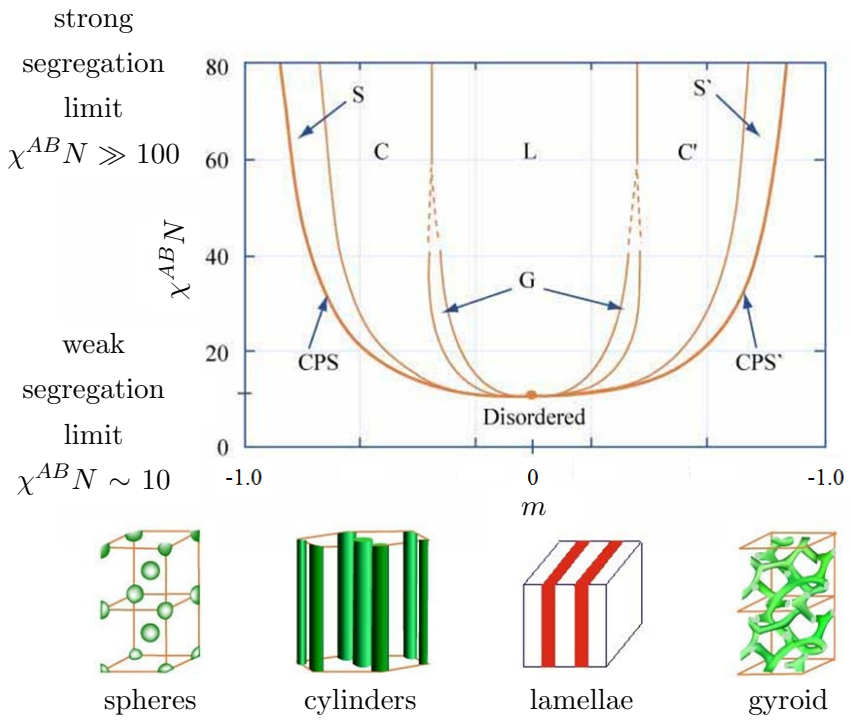

Figure 1.3: DBC '*ground state phase diagram*' (adapted from mitopencourseware (2012)). The Order-Disorder Transition (ODT) separates the disordered region in which energy minimisers have no discernible structure, from those parameters which lead to structured minimisers. On the vertical axis, $\chi^{AB}N$ captures the combination of the length of each molecule and the strength of the repulsion between unlike A and B monomers (see Chapter 3 for details). The horizontal axis measures the relative proportion of A and B monomers in each molecule ($m = 0$ corresponds to equal proportions of A and B monomers).
S = spheres; C = cylinders; L = lamellae; G = gyroids; CPS = close-packed spheres.

the calculation. The number of equations to be solved can therefore be far smaller than the number of particles which form the structure. The phase field method is also eyecatching because it produces remarkable visual outputs, particularly of morphology, capturing features which are often realistic in appearance.' Phase field models are used to describe a diverse set of phenomena (see Chen (2002), Emmerich (2003), Moelans et al. (2008), Steinbach (2009), Qin and Bhadeshia (2010) and the references therein) and are favoured, at least in part, because of their (relative) simplicity and amenability to rigorous analysis.

One of the most popular phase field models is the Cahn–Hilliard model (Cahn and Hilliard (1958); Cahn (1961); Elliott (1989); Bates and Fife (1993); Fife (2000); Novick-Cohen (2008)) which has a free energy functional (of the phase field variable(s)) comprising interfacial and homogeneous components. Minimisation of the interfacial component yields constant (zero gradient) phase field solutions, while minimisation of the homogeneous com-

ponent leads to pure phases (hence the name). The time-dependent Cahn–Hilliard equation is based on the so-called H^{-1}-gradient flow, and is mass-conserving, in that it preserves the overall proportions of the modelled phases. This, combined with the two energy minimisation effects, leads to energy minimisers with very thin interface layers separating (large) regions of pure-phase material.

A number of different forms of the homogeneous energy component of the Cahn–Hilliard model have been studied, including i) the double-well: a quartic polynomial in the phase field variable(s) whose roots correspond to the pure phases of the material being modelled, as in Novick-Cohen and Segel (1984); Choksi et al. (2009), ii) a double-obstacle: similar to the double-well but involving a concave function that is not defined outside some modelling range which is minimised at values of the phase field variable which correspond to pure phases, as in Blowey and Elliott (1991); Choksi and Ren (2003), and iii) logarithmic (see (1.1) in Barrett et al. (1999)). The choice of the form of the homogeneous term has significant implications. Various mobilities have also been studied in the context of the dynamic problem, most notably, the degenerate mobility (see Elliott and Garcke (1996)) which (locally) turns the dynamics off whenever/wherever the system achieves a pure-phase, so as to limit the size of the pure-phase regions.

The Cahn–Hilliard model has been used as a standalone model to study a large number of pattern formation phenomena especially in the area of metallic alloys (Hoyt (1989, 1990)). A variant of Cahn–Hilliard, involving an additional 'fidelity term' was even used in Bosch et al. (2014a) in connection with image in-painting viz. solving a modified Cahn–Hilliard equation inside a damaged/missing part of an image to reconstruct it. The equation has also been coupled to secondary models such as the Navier–Stokes equations for flow as in Boyer and Lapuerta (2006) and Boyer et al. (2010) (which considers a 3-phase situation (oil, water, gas) in which gas bubbles ascend through separated layers of oil and water) to biological applications, such as tumour growth in Garcke et al. (2016).

As popular as the Cahn–Hilliard model is, it is not appropriate as a standalone model for DBCs, as it lacks a mechanism for restricting the size of the segregated A and B regions. The addition of a non-local energy component satisfies this requirement and leads to the so-called Ohta–Kawasaki model (sometimes referred to as *the non-local Cahn–Hilliard model*, as in Choksi et al. (2009)). This third energy component favours morphologies in which the phase field variable(s) are constant at their averages. The competition between the three minimisation effects leads to energy minimising phase field functions that oscillate between pure-phase values (cf. the Introduction to Ren and Wei (2003)). As such, they capture the regular/repeating nature of structures in phase separated DBCs.

The Ohta–Kawasaki free-energy functional, was first derived in Ohta and Kawasaki (1986), using mean field theory with the specific aim of modelling '*microphase separation of diblock copolymers*' (see also Leibler (1980)). More recently, in Choksi and Ren (2003),

the authors '*re-examine the derivation of the Ohta–Kawasaki DFT theory*' to show how it is '*an offspring of the well-established SCMFT*' of DBCs, and can be regarded essentially as a first term linearisation thereof (subject to various approximations and re-scalings).

One of the principle advantages of DFT-type models is that they lead to numerical approaches that do not require any assumptions of solution symmetry. The Cell-Dynamical-System (CDS) approach (Bahiana and Oono (1990); Shinozaki and Oono (1993); Ren and Hamley (2001); Hamley (2000); Guo et al. (2007)) has been applied extensively to Ohta–Kawasaki-like models. It is '*a relatively fast method*' that has been extensively validated against various SCFT variants (Dessí et al. (2013)), and can be adapted to capture a large number of secondary effects. The review by Pinna and Zvelindovsky (2012) shows how electric field, confinement, and shear flow effects can be catered for; more recently in Dessí et al. (2013), confinement of thin film DBCs in patterned substrates for applications in '*circuit design in nanoelectronics*' was studied using the same technique. Other effects such as thermal fluctuations in the medium are modelled via the addition of a stochastic source to the Cahn–Hilliard equation leading to the so-called Cahn–Hilliard–Cook (CHC) equation, or *Model B* (cf. (3.6) in Elliott (1989), Section 2 of Ren and Hamley (2001) and Oono and Puri (1988); Puri and Oono (1988); Pinna and Zvelindovsky (2012)).

On the other hand, the validity of Ohta–Kawasaki models for the study of DBCs has been challenged, particularly in the Intermediate Segregation Regime (ISR) and Strong Segregation Regime (SSR), which is intensively studied in experiments. However, computations based on the DFT have reproduced all of the phases predicted by the SCFT, including gyroids (see Choksi et al. (2009) and esp. Teramoto and Nishiura (2002)). Significant effort has been devoted to trying to replicate the SCFT phase diagram in Fig. 1.3 using minimisers of the Ohta–Kawasaki free-energy functional. Finding and characterising these is difficult (see Ren and Wei (2003); Chen and Oshita (2005); Choksi (2012)), and so numerical methods are frequently used. In Müller and Rey (2018), the authors compare various approaches to modelling DBCs, including the SCFT and Ohta–Kawasaki equation. They conclude with a suggestion that simulations based on the Ohta–Kawasaki equation could be used in conjunction with more detailed SCFT simulations '*to gain a better understanding of the structure formation process*'. In Choksi et al. (2011); Choksi et al. (2009), the authors attempt to characterise the 2D minimisers in terms of the underlying input parameters with a combination of numeric and asymptotic analysis (including a weakly non-linear stability analysis to locate the ODT).

The papers by Ohta and Ito (1995) and Ito (1998) are the first that we are aware of to use DFT-models to study 3-phase DBC copolymer/homopolymer blends, albeit in a fairly general context, on the basis of a re-scaled quartic approximation of the homogeneous term (other references that model similar situations include Uneyama and Doi (2004)). Unfortunately, as noted in Choksi and Ren (2005), '*[n]o details were presented on its derivation,*

and we are unaware of any systematic derivation of such a nonlocal functional for homopolymer/copolymer blend'. The rest of Choksi and Ren (2005) is then devoted to deriving a 3-phase Ohta–Kawasaki type model for copolymer/homopolymer blends from the SCFT (extending the 2-phase developments in Choksi and Ren (2003)). The authors '*consider a mixture of A-B copolymers with homo-polymers of monomer species C, where the species C is thermodynamically incompatible with both the A and B monomer species*'. This latter model is the basis for our 3-phase work. A similar approach for films and droplets with a DBC and a solvent species was pursued in Cohen and Andelman (2014), using the Brazovskii free energy. This form uses a different representation of the long-range interaction, and a different (logarithmic) homogeneous free energy.

Remarks. We have discussed CDS as if it were a *model*, but it may also make sense to regard it as a numerical method. In the literature it is regarded as an 'a priori *discrete space-time model*' that is '*not a PDE solver in any standard sense of numerical analysis*', and is thus quite distinct from '*PDE models*' like Cahn–Hilliard (Shinozaki and Oono (1993)). This same reference goes on to say that '*there is no particular reason to favour the PDE model over the CDS model or vice versa*' since '*the CDS model and the [Cahn–Hilliard] equation give identical asymptotic macroscopic results*'. On the other hand, '*for sufficiently small δt and fine spatial discretization [sic], the CDS models reduce to the simple Euler scheme*'. The authors claim that '*when seen as a discretization [sic] scheme the CDS ... model is a qualitatively accurate discretization [sic] method for the [Cahn–Hilliard] equation*'. This is the sense in which we could also classify it as a numerical method, and the reason we associate it with the Ohta–Kawasaki equation above. See also Teixeira and Mulder (1997) which comments on the relationship between CDS and Cahn–Hilliard PDE methods.

The Allen–Cahn equation has the same energy functional as Cahn–Hilliard, but has dynamics based on an L^2-gradient flow, which is not mass conserving (see Sections 1–3 of Guillén-González and Tierra (2014)). We mention this model mostly for completeness, and because some of the numerical methods that have been used to study it are applicable. It is not suitable as a standalone model for studying DBCs.

Analysis

The mathematical analysis of SCFT and CDS models appears to be quite limited, and since we do not use these methods in our research, we sample some of the (vast) literature devoted to analysing relevant DFT phase field models. Whereas the Cahn–Hilliard equation is of limited use in *modelling* DBCs, the local and non-local Cahn–Hilliard models are *very* similar from the perspective of analysis. The analysis takes several flavours.

The first is applied analysis, which relates to the existence, smoothness and other fundamental properties of minimisers, and the well-posedness, and energy properties of the associated gradient flow systems. Many results exist in this space. Blowey and Elliott (1991)

studied the 2-phase Cahn–Hilliard model with an obstacle homogeneous term; Elliott and Luckhaus (1991) then analysed an n-phase model with constant mobility and logarithmic homogeneous energy. The combination of a degenerate mobility and singular homogeneous energy was studied in Elliott and Garcke (1996); systems of such equations were then studied in Elliott and Garcke (1997); Garcke et al. (2000). A coupled Allen–Cahn/Cahn–Hilliard model with degenerate mobility and logarithmic homogeneous free energy was analysed in Dal Passo et al. (1999).

As we noted above, phase field formulations have several desirable features, but solving them analytically to find energy minimisers is hard. Asymptotic analysis is one way to gain qualitative insights into the structure of energy minimisers. The idea is to simplify the problem by exploiting the small interfacial thickness parameter and eliminate some of the solution complexity by considering the so-called sharp interface limit. We only make limited application of some well-known asymptotic results in this thesis, and so we merely list some of the main results.

The Cahn–Hilliard equation has been studied extensively using asymptotic techniques (Cahn et al. (1996); Garcke et al. (1998, 1999)). Kohn and Otto (2002) considers the coarsening rates for constant and degenerate mobility variants of the Cahn–Hilliard equation, and reveals how both of these can be regarded as limits of a stochastic Ising model. Lee et al. (2015) derives a third order asymptotic solution of the 1D Cahn–Hilliard problem assuming the quartic polynomial homogeneous density and degenerate mobility. Similar results in connection with the 2- and 3-phase Ohta–Kawasaki equations can be found in Choksi (2001); van Gennip and Peletier (2008, 2009); Choksi and Peletier (2010, 2011); Le (2010). The most relevant reference for our purposes was Section 4 of Choksi and Ren (2005) in which 1D (local) minimisers of the 3-phase (copolymer/homopolymer blend model), sharp-interface problem are characterised, and expressions given for the surface tensions of a stationary configuration, in terms of the underlying model parameters.

Work has also been done using the calculus of variations to characterise and count energy minimisers for the Ohta–Kawasaki functional. Well known references in this regard are Ohnishi et al. (1999); Ren and Wei (2003); Chen and Oshita (2005), which relate to the 1D problem.

Numerical methods

We discussed the SCFT and CDS numerical methods in the Modelling section above; we reiterate here that the analysis of these approaches (as numerical methods or otherwise) appears to be lacking. The numerical analysis of methods specifically developed for the Ohta–Kawasaki equation is also quite limited (for instance Benesová et al. (2014) studies a second-order accurate temporal discretisation (the implicit midpoint approximation) with a Fourier–Galerkin spatial approximation). On the other hand, numerical methods and their

analysis for the Cahn–Hilliard model are numerous and can (generally) easily be adapted to the Ohta–Kawasaki case.

In Blowey and Elliott (1992), the authors study a numerical approximation of the dynamics associated with the Cahn–Hilliard model with an obstacle homogeneous term. Other major pieces of numerical analysis are Barrett and Blowey (1996), Barrett and Blowey (1997), Barrett et al. (1999) (which studies a finite element approximation of the problem with degenerate mobility and logarithmic/obstacle homogeneous energies), Barrett and Blowey (1999a,b, 2001) (see the references in the last publication).

Other first order accurate (in time) methods have been proposed and discussed in Du and Nicolaides (1991); Elliott and Stuart (1993); Feng and Prohl (2004); He et al. (2007). Second order (in time) methods were considered in Furihata (2001); Guillén-González and Tierra (2014, 2013); Diegel et al. (2015) and others. In the unpublished (but highly cited) Eyre (1998a) and Eyre (1998b), the author proposes a series of one-step Euler time-splitting methods for the Cahn–Hilliard equation. The latter reference introduces the idea of 'convex splitting' of the homogeneous term; an idea we will examine in depth.

Numerical methods, including approaches to pre-conditioning and performance tuning of solvers of the resulting linear systems for some of the coupled models we mentioned earlier, can be found in references such as Kay et al. (2002); Feng (2006); Kay and Welford (2007); Kay et al. (2008, 2009); Boyer and Minjeaud (2009).

There has also been significant interest in applying methods of optimisation (as in Meyer et al. (2006); Neitzel and Tröltzsch (2009)) to the Cahn–Hilliard and (mass-constrained) Allen–Cahn problems with an obstacle homogeneous energy via the Primal-Dual Active Set (PDAS) method (Hintermüller et al. (2002); Ito and Kunisch (2003); Blank et al. (2011, 2012, 2013)). Our chosen numerical method (which involves a regularisation/penalty method) shares some properties with this iterative method. Solvers based on a Moreau–Yosida regularisation of the obstacle homogeneous term, combined with the Semi-Smooth Newton (SSN) method were studied in Hintermüller et al. (2011); Bosch et al. (2014a,b); we draw heavily on these references.

Existing terracing results

As we note above, the literature pertaining to the modelling and analysis of the '*fundamentals of terrace formation*' is limited (Lyakhova et al. (2006)), but some results do exist. In Belyi and Witten (2004) the authors present a model for the way terraced DBCs spread. In Lyakhova et al. (2006), the authors use the DDFT to examine terrace formation in triblock copolymers. More recently, in Kim and Matsen (2009), the authors use the SCFT to address the question of terrace formation in circular droplets of polymer fluid sitting on a flat substrate, where the terraces express as '*concentric circular disks with a terraced profile*'. They model an interaction between the A and B phases and the substrate and attempt to

understand the contact angle between the droplet and the surface.

Arguably the most interesting pieces of work in this regard are Stasiak et al. (2012); Maher et al. (2016), in which the authors use the SCFT to examine terracing. In the first of these, the authors explicitly omit any device to model the interaction of the copolymer and the substrate but attempt to capture terraces using a model in which a homopolymer takes the place of the void and interacts with the copolymer (which has a free surface which can buckle to form terraces). An energy minimisation approach is used to show that terraced configurations involving ν lamellae on one half of (and oriented parallel to) a substrate, and $\nu + 2$ lamellae on the other (with the same orientation), with a step separating them, have a lower energy than uniform (viz. flat) configurations involving the same amount of copolymer material. We design our numerical experiments to replicate these results. Maher et al. (2016) explores substantially more complex terracing situations (using the SCFT), including so-called '*islands*' and '*holes*'. These are beyond the scope of our research.

1.3 Thesis outline

To answer the question we posed in Section 1.1, and in light of our understanding of the current literature, we structure this thesis into four parts.

In the current part, we motivate the problem of interest, describe the generic model(s) we will use, and summarise the relevant mathematics and notation.

We study 2-phase materials (where the DBC material completely fills the container/-domain) in Part II. Terraces cannot form in these circumstances, but we will see that our 3-phase model (which does allow for terracing) reduces to a 2-phase model under certain conditions. An understanding of 2-phase materials is therefore extremely beneficial.

In the first three chapters, we pose the 2-phase energy minimisation problem and analyse basic properties of its solutions. In Chapter 3, we present our 2-phase Ohta–Kawasaki model for phase separation in DBCs via energy minimisation, which we adopt from Choksi and Ren (2003). We review essential properties of the stationary problem, and also discuss and pose the H^{-1} gradient flow/dynamic approach. Noteworthy properties of the model include i) the non-local component of the energy, and ii) the obstacle homogeneous energy component. We pick the obstacle form over the (ostensibly simpler) quartic polynomial form for two reasons. First, it arises naturally from the SCFT, as discussed in Choksi and Ren (2003), and therefore appears to most closely model the underlying physics. Second, our simulations involving the polynomial homogeneous term yielded solutions in which the phase field variables are bounded well away from their pure phase values (see also Fig. 5.2 of Zhang (2006)). This makes it extremely difficult to analytically determine the shape of the interface layers. In Chapters 6–8, we will find the obstacle form (surprisingly) much easier to work with.

In Chapter 4, we rigorously analyse the 2-phase model from the previous chapter, in the context of a variational inequality (due to the obstacle homogeneous energy component). We consider the existence and regularity of minimisers of the stationary problem, before posing a set of gradient flow dynamics which incorporate a time-like dependency. We establish the well-posedness (existence, stability/uniqueness), regularity, energy decay and mass conservation (and control) properties of these dynamics. A key focus of this chapter is the Moreau–Yosida regularisation of the homogeneous term, and the non-local energy component. Blowey and Elliott (1991) was the most influential piece of literature in this chapter. Those authors omit the non-local component and studied a C^2 regularisation; ours is C^1, and was adapted from Bosch et al. (2014a).

In Chapter 5, we develop and rigorously analyse a numerical method for approximating solutions of the gradient flow problem, based on an Euler-in-time, $\mathbb{P}_1$ finite-element in space approximation. We work with finite elements as they can be used in (virtually) arbitrary physical domains. Indeed, talking in the context of complex 2-phase geometries, Remark 4.3 of Choksi et al. (2009) suggests that '*[i]t would be interesting to investigate this numerically with ... finite element methods on general domains*'. We prove that our method is well-posed, convergent and, crucially, that the free energy we seek to minimise is a monotonically non-increasing function of time. We implement the method in FEniCS (see https://fenicsproject.org/ and Alnæs et al. (2015)), and conduct a series of numerical experiments that prove that our method has the properties predicted by the theory. These culminate in a novel Method of Manufactured Solutions (MMS)-experiment to confirm the order of convergence of the method. We also pay special attention to the time discretisation of the non-local term, by attaching a θ-method to this term.

Most of our theoretical numerical analysis is adapted from Blowey and Elliott (1992). For simplicity, we consider a first order (in time) accurate family of discretisations. The primary innovation in our approach is that we use the same regularisation in the applied analysis in Chapter 4 and the numerical analysis in Chapter 5. This approach puts our applied and numerical analysis on the same footing.

We explore the stationary 1D problem in the next three chapters. We pose and characterise the problem in Chapter 6, and establish all of the infrastructure necessary to solve it, by specialising the results of Chapter 4 to 1D. A key realisation in this chapter is the *substantial* simplification which results from restricting our attention to symmetric DBCs, in which the A and B sub-chains comprising each molecule are of equal length.

We propose a complete and explicit solution of the 1D problem, in the symmetric case, in Chapters 7–8, together with an efficient algorithm for finding global energy-minimisers. We provide numerical evidence that energy minimisers are periodic (or *equally spaced*) and characterise them completely. Even though these are the most speculative chapters in the thesis, our results are entirely consistent with those in Chen and Oshita (2005). We reveal

how our results are consistent with the predictions of sharp interface limit analysis, precisely locate the ODT in parameter space (cf. Fig. 1.3), and link our results back to models for DBC structure formation, as well as the Cahn–Hilliard case (no non-local energy).

In Part III, we consider a 2-phase DBC interacting via a free surface with a third, void phase. We develop our 3-phase model and energy minimisation problem from that presented in Choksi and Ren (2005) (once again, derived from the SCFT), and establish its basic properties. A key aspect of the model is the fact that the free (upper) boundary of the copolymer can change shape as it interacts with a third phase, and is not constrained by the geometry of a container. We adopt the same approach as Stasiak et al. (2012) in modelling this third phase, viz. '*the air* [is replaced by] *a homo-polymer*'. The modelling advantage of this approach is its simplicity. We regard the filler as another phase that exists on the same mathematical footing as the A and B phases of the DBC. On the other hand, this approach has some unintended consequences (since air is not a homopolymer), which we explore, as a result of which, we propose a modification to the 3-phase model.

Our 3-phase modelling approach is a natural extension of our 2-phase approach in that we study an obstacle homogeneous energy component. Likewise, we propose a numerical method for approximating 3-phase gradient flow dynamics based on an analogous regularisation of the obstacle homogeneous energy component. We sketch out the steps that would be required to analyse the 3-phase case (extending ideas from our work in two phases), and offer compelling numerical evidence of the order of convergence of the method, with an MMS-experiment.

We propose and discuss two types of low energy, 1D morphology. First, we develop a heuristic *ansatz* based on the idea that the monolayers in the copolymer bulk are equally-spaced, as in the 2-phase model. Second, we apply the sharp interface limit results in Section 4 of Choksi and Ren (2005). The simplicity of this latter approach allows us to estimate the free energy and surface tensions in (locally) energy-minimising configurations. We conduct a large set of numerical experiments that confirm that our *ansatz* based morphologies are very similar to their sharp interface limit counterparts. Hence we can use sharp interface limit results to guide the selection of parameters for our gradient flow numerical experiments.

We then combine our sharp interface 1D insights in a double tangent construction to develop our main result, which is that **terraces are inevitable, low energy configurations in 2D**. We confirm our predictions with a series of numerical experiments inspired by the SCFT experiments in Stasiak et al. (2012). We replicate key elements of their results, and extend them to a situation in which a terrace forms spontaneously from a flat initial state.

Finally, in Part IV, we conclude and summarise our results and contributions. We close with suggestions for further research.

1.4 Highlights and key contributions

Our main result is that a DFT-based model of DBCs can be used to study and capture terrace formation. To the best of our knowledge, this is the first time such models have been applied to this problem. An examination of our numerical results suggests that our capabilities are comparable to the current state of the art (i.e. the SCFT approach), for the scenarios we considered.

We make a number of contributions in the build-up to our main result. We classify these according to the four building blocks listed in Section 1.1.

1. **Modelling**. We extract our 2- and 3-phase models from the literature, and comprehensively treat the issue of incompressibility. We propose a change to the DFT-model derived in Choksi and Ren (2005) to cater for a copolymer that is interacting with air (that is modelled as a homopolymer).

2. **Analysis**. Our applied and numerical analysis of the 2-phase model is rigorous and exhaustive. As far as we are aware, this end-to-end analysis, combining our choice of Moreau–Yosida regularisation of the homogeneous energy component with a non-local energy component, is new.

   Our proposed, explicit solution of the symmetric 2-phase energy minimisation problem in 1D is new, as is our suggestion for the location of the ODT in parameter space.

   The way we combine our 1D sharp interface limit energy estimates, using a double tangent construction to analyse 3-phase, 2D morphologies, is simple and novel. It allows us to predict the conditions under which terraces (steps) should form, having lower free energy than their flat counterparts.

3. **Numerical methods**. We develop and exhaustively analyse gradient flow numerical methods in two and three phases based on the same regularisation of the obstacle homogeneous term, as we use in the analysis. In the 2-phase case, we prove that our method is convergent; we provided compelling numerical evidence of this in two and three phases. Our approach to MMS-testing appears to be novel in the context of the obstacle Ohta–Kawasaki equation. Finally, we propose an efficient algorithm for finding (global) energy minimisers for the symmetric energy minimisation problem in 1D.

4. **Experiments**. We report on a very large number of numerical experiments in this thesis, the most significant of which confirms our theoretical predictions in respect of terrace formation in 2D. The crown jewel of our experimental work is a numerical experiment in which a terrace spontaneously forms from a flat initial state. As far as we are aware, this has not been achieved before with any modelling or numerical approach.

Chapter 2

Essential background

In this brief chapter, we present some of the key mathematical notation we will use, together with the high-level modelling context for the problem.

Contents

2.1 Mathematical essentials 19
2.2 Basic modelling principles 22
2.3 Outlook 26
2.4 Codes and numerical experiments 26

2.1 Mathematical essentials

This brief section is augmented by Appendix A.1, starting on p. 321.

2.1.1 Notation, function spaces, norms

Ω denotes an open, bounded set in $\mathbb{R}^d, d = 1, 2, 3$ with Lipschitz boundary $\partial\Omega$ that satisfies a cone condition, as in Fig. 6 of Braess (2001).[1] Intervals (in 1D) and rectangles (in 2D) are examples of such domains. The mass of a function on Ω is its integral average over Ω, which we denote

$$\overline{\varphi} := \fint_\Omega \varphi \, \mathrm{d}\Omega := \frac{1}{|\Omega|} \int_\Omega \varphi \, \mathrm{d}\Omega. \tag{2.1}$$

Since Ω will be clear from the context, we generally avoid the explicit '$_{(\Omega)}$' subscript notation of Evans (1998), unless we use a domain other than Ω (for instance, a sub-domain).

For functions having zero Neumann Boundary Condition (BC), we use the shorthand

$$\partial_n \varphi|_{\partial\Omega} = 0. \tag{2.2}$$

We will work in the function spaces

$$H^k_m(\Omega) := \left\{ \varphi \in H^k(\Omega) \,:\, \overline{\varphi} = m \right\} \tag{2.3}$$

where $H^k(\Omega)$ is the Sobolev space of functions $\varphi \in W^{k,2}(\Omega)$ (without a prescribed mass) with the property that $D^\alpha \varphi \in L^2(\Omega)$ for $|\alpha| \leq k$ (see Evans (1998), Section 5.2.2). When $m = 0$, we use the '$_*$' subscript, as in

$$H^1_*(\Omega) := \left\{ \varphi \in H^1(\Omega) \,:\, \overline{\varphi} = 0 \right\} \tag{2.4}$$

to avoid confusion with the space of functions in $H^1(\Omega)$ with zero Dirichlet BC, viz.

$$H^1_0(\Omega) := \left\{ \varphi \in H^1(\Omega) \,:\, \varphi|_{\partial\Omega} = 0 \right\}. \tag{2.5}$$

Remark. $H^k_m(\Omega)$ is not a vector space (let alone a Hilbert space) unless $m = 0$.

Likewise,

$$L^2_*(\Omega) := \left\{ \varphi \in L^2(\Omega) \,:\, \overline{\varphi} = 0 \right\}. \tag{2.6}$$

We use round brackets $(\cdot,\cdot)$ for inner products, double bars, $\|\cdot\|$, for norms and single bars, $|\cdot|$, for semi-norms. We use angled brackets, $\langle\cdot,\cdot\rangle$, to denote duality pairings between elements of a dual space in the first component, and the subscripted space in the second. We will work mostly in $L^2(\Omega)$, $H^1(\Omega)$ and $H^2(\Omega)$:

- In $L^2(\Omega)$, $(\cdot,\cdot)$ (no subscript) denotes the inner product, and $\|\cdot\|$, the norm. In particular, from (2.1),

$$\overline{\varphi} = \frac{1}{|\Omega|}(\varphi, 1). \tag{2.7}$$

  In the dual space $\left(L^2(\Omega)\right)'$, we use $\|\cdot\|_{'}$ and $(\cdot,\cdot)_{'}$ for norms and inner products. Duality pairings between $\left(L^2(\Omega)\right)'$ and $L^2(\Omega)$ are denoted $\langle\cdot,\cdot\rangle$, with no subscript.

- In $H^k(\Omega)$, $(\cdot,\cdot)_k$ denotes the inner product and $\|\cdot\|_k$, the (full) norm; the corresponding semi-norm is denoted $|\cdot|_k$. In the dual space $\left(H^k(\Omega)\right)'$, we use $\|\cdot\|_{k'}$ and $(\cdot,\cdot)_{k'}$ for norms and inner products. Duality pairings between members of $\left(H^k(\Omega)\right)'$ and $H^k(\Omega)$ are denoted $\langle\cdot,\cdot\rangle_k$.

Remark. $|\cdot|$ (no subscript) denotes the absolute value or measure, and not a semi-norm. For $v \in H^1(\Omega)$, $|v|_1 := \|\nabla v\|$.

On the rare occasion that we need to work in $W^{k,p}(\Omega)$ ($p \neq 2$), we use $\|\cdot\|_{k,p}$, $|\cdot|_{k,p}$ and $(\cdot,\cdot)_{k,p}$ ($\|\cdot\|_{k,p,\Omega}$, $|\cdot|_{k,p,\Omega}$ or $(\cdot,\cdot)_{k,p,\Omega}$ if there is ambiguity about Ω) for the norm, semi-norm and inner product (cf. Paragraph 2.3 and 3.1 of Adams and Fournier (2003)). In the dual space $\left(W^{k,p}(\Omega)\right)'$, we use $\|\cdot\|_{(k,p)'}$ and $(\cdot,\cdot)_{(k,p)'}$ for norms and inner products; for duality

pairings, we use $\langle \cdot, \cdot \rangle_{k,p}$. For $L^p(\Omega)$, we explicitly write '0' for k; for instance $\|\cdot\|_{0,3}$ denotes the $L^3(\Omega)$–norm, and $\|\cdot\|_{0,\infty}$ the $L^\infty(\Omega)$–norm. $|\cdot|_{0,p} = \|\nabla \cdot\|_{0,p}$ is the $L^p(\Omega)$–semi-norm. Our notation for Banach-space valued and Hölder continuous functions is standard. We use explicit subscripts,[2] such as $\|\varphi\|_{L^\infty(0,T;H^1(\Omega))}$, $\|\varphi\|_{C([0,T];L^2(\Omega))}$ and $\|\varphi\|_{C^{0,\lambda}(\overline{\Omega})}$. $C_c^\infty(\Omega)$ denotes the set of smooth functions with compact support in Ω.

2.1.2 The Poisson equation with zero Neumann BC

Much of our analysis hinges on properties of the Poisson equation with a zero Neumann BC. The classical problem is to find φ, for given f, such that

$$-\Delta\varphi = f \qquad \text{subject to} \qquad \partial_n \varphi|_{\partial\Omega} = 0. \tag{2.8a}$$

The weak problem is,[3]

($\mathscr{P}^{\mathbf{n}}$): given

$$f \in \mathscr{F} := \left\{ f \in \left(H^1(\Omega)\right)' : \langle f, 1 \rangle = 0 \right\}, \tag{2.8b}$$

find

$$\varphi \in H^1(\Omega) \qquad \text{s.t.} \qquad (\nabla\varphi, \nabla\nu) = \langle f, \nu \rangle \qquad \text{for every} \qquad \nu \in H^1(\Omega). \tag{2.8c}$$

The compatibility condition, $\langle f, 1 \rangle = 0$, ensures that solutions of ($\mathscr{P}^{\mathbf{n}}$) exist (cf. (1.4) in Elman et al. (2008)). We abbreviate this problem as

$$-\Delta_n \varphi = f. \tag{2.8d}$$

We also make the following important definition.

Definition 2.1.1. (The inverse Neumann Laplacian $(-\Delta_n)^{-1}$) *We define the inverse Neumann Laplacian $(-\Delta_n)^{-1}$ such that, given $f \in \mathscr{F}$, $(-\Delta_n)^{-1} f \in H^1_*(\Omega)$ is the unique solution of ($\mathscr{P}^{\mathbf{n}}$), viz.*

$$\left(\nabla (-\Delta_n)^{-1} f, \nabla\nu\right) = \langle f, \nu \rangle \qquad \textit{for every} \qquad \nu \in H^1(\Omega) \tag{2.9a}$$

$$\textit{where} \qquad \left((-\Delta_n)^{-1} f, 1\right) = 0. \tag{2.9b}$$

If $u \in H^1(\Omega)$ and $f \in L^2_*(\Omega)$, then

$$(u, \nu) = \left((-\Delta_n)^{-1} f, \nu\right) \quad \Leftrightarrow \quad (\nabla u, \nabla\nu) = (f, \nu) \quad \textit{for every} \quad \nu \in H^1(\Omega). \tag{2.9c}$$

Remark. Our $(-\Delta_n)^{-1}$ notation implies the zero Neumann BC *and* the well-posedness zero mass condition in (2.9b). It corresponds to the Green's operator '$\mathscr{G}_N$' of Blowey and Elliott (1991).

The '$_n$' subscript in $(-\Delta_n)^{-1}$ represents the zero Neumann BC. This notation is used in the context of solutions of (2.8c), i.e. *weak* solutions of (2.8a). On the other hand, we generally make the necessary assumptions to obtain strong solutions from weak ones via elliptic regularity theory (see Lemma A.1.9.)

An alternative inner product on $L^2_*(\Omega)$

Finally, we define a new inner product on $L^2_*(\Omega)$, the so-called $H^{-1}(\Omega)$ inner product.

Definition 2.1.2. (The $H^{-1}(\Omega)$ inner product on $L^2_*(\Omega)$) *Define the $H^{-1}(\Omega)$ inner product of $\omega, \nu \in L^2_*(\Omega)$ as*

$$(\omega, \nu)_{-1} := \left((-\Delta_n)^{-1/2} \omega, (-\Delta_n)^{-1/2} \nu \right), \tag{2.10}$$

with induced norm $\|\cdot\|_{-1}$ given by,[4]

$$\|\omega\|_{-1} = \left\| (-\Delta_n)^{-1/2} \omega \right\| = \left\| (-\Delta_n)^{1/2} (-\Delta_n)^{-1} \omega \right\| = \left| (-\Delta_n)^{-1} \omega \right|_1 . \tag{2.11}$$

The $H^{-1}(\Omega)$ norm of $\omega \in L^2_*(\Omega)$ is the $H^1(\Omega)$ semi-norm (viz. the $L^2(\Omega)$ norm of the gradient) of its inverse Laplacian (with zero Neumann BC).

The $H^{-1}(\Omega)$ inner product can be written in three equivalent forms:

$$(\omega, \nu)_{-1} := \begin{cases} \left((-\Delta_n)^{-1} \omega, \nu \right) \\ \left((-\Delta_n)^{-1/2} \omega, (-\Delta_n)^{-1/2} \nu \right) \\ \left(\omega, (-\Delta_n)^{-1} \nu \right) \end{cases} \quad \text{for every} \quad \omega, \nu \in L^2_*(\Omega) . \tag{2.12}$$

We discuss this inner product in more detail in Appendix A.1.2. See also Defn A.1.6 on p. 325.

2.2 Basic modelling principles

We now pose the mathematical problem for n-phase materials.

2.2.1 Multi-phase materials

We consider a material described by the n–vector

$$\boldsymbol{\phi}(x) = (\phi_1(x), \ldots, \phi_n(x))^\top ,$$

in some $\Omega \subset \mathbb{R}^d$. Each $\phi_i(x)$ encodes the local concentration or density of the i-th phase of the material, and

$$\phi_i(x) = \begin{cases} 0 & \Rightarrow \text{ no phase } i \text{ material at } x \\ 1 & \Rightarrow \text{ pure-phase } i \text{ material at } x, \end{cases} \tag{2.13}$$

where we insist that

$$0 \le \phi_i(x) \le 1, \qquad 1 \le i \le n, \qquad \text{for a.e. } x \in \Omega. \tag{2.14a}$$

We consider only incompressible materials for which

$$\boldsymbol{\phi}^{\top}(x) \cdot \mathbf{1} = \sum_{i=1}^{n} \phi_i(x) = 1, \qquad \text{for a.e. } x \in \Omega, \tag{2.14b}$$

i.e. the domain is entirely filled with the n-phase material, and *only* the n-phase material. Extending our interpretation in (2.13), $0 < \phi_i(x) < 1$ means that the material at x is only partly phase-i. Finally, we specify the global ratio of the various phases in Ω as

$$\overline{\phi_i} = m_i, \qquad 1 \leq i \leq n, \tag{2.14c}$$

for some mass control vector $\boldsymbol{m} := (m_1, \ldots, m_n)^{\top}$, with the property that

$$\boldsymbol{m}^{\top} \cdot \mathbf{1} = \sum_{i=1}^{n} m_i = 1. \tag{2.14d}$$

This requirement will arise naturally in the modelling of DBCs as a statement about the composition of the molecules under consideration.

2.2.2 Energy

We consider a Ginzburg–Landau approximation to the Gibbs free energy of the form

$$\mathcal{E}(\boldsymbol{\phi}) = \int_{\Omega} \underbrace{\mathcal{I}(\boldsymbol{\phi}, \nabla\boldsymbol{\phi})}_{\underline{\text{i}}\text{nterfacial}} + \underbrace{\mathcal{B}(\boldsymbol{\phi})}_{\underline{\text{b}}\text{ulk}} + \underbrace{\mathcal{N}(\boldsymbol{\phi})}_{\underline{\text{n}}\text{on-local}} \, \mathrm{d}\Omega. \tag{2.15}$$

We refer to the sum of the bulk/homogeneous and interfacial energies as the short-range energy contribution, $\mathcal{E}_S$, and the non-local component as the long-range part, $\mathcal{E}_L$. We solve:

$$\text{find } \boldsymbol{\phi}(x) \text{ s.t. } \mathcal{E}(\boldsymbol{\phi}) \to \min \tag{2.16}$$

subject to:

- Concentration consistency/boundedness, in the sense of (2.14a).
- Local incompressibility as in (2.14b).
- Predefined mass as in (2.14c)–(2.14d).

We briefly describe each component of the energy in (2.15).

Interfacial energy

The interfacial energy captures the energy present in the material interfaces, as (cf. Boyer and Lapuerta (2006))

$$\mathcal{I}(\nabla\boldsymbol{\phi}) = \frac{1}{2} \sum_{i,j=1}^{n} \varepsilon_{ij}^2 \left| \nabla\phi_i \cdot \nabla\phi_j \right| = \frac{1}{2} (\nabla\boldsymbol{\phi})^{\top} \mathcal{I}(\nabla\boldsymbol{\phi}), \tag{2.17a}$$

$$\text{where} \quad \mathcal{I} = (\mathcal{I}_{ij}) \quad \text{with} \quad \mathcal{I}_{ij} = \varepsilon_{ij}^2, \tag{2.17b}$$

is the (symmetric) matrix of interfacial coefficients. We use $\mathcal{I}$ for the density function and its matrix of coefficients.

Homogeneous (bulk) free energy

The homogeneous (sometimes called bulk) free energy density is given by

$$\mathcal{B}(\boldsymbol{\phi}) = \frac{1}{2}\boldsymbol{\phi}^{\top}\mathcal{B}\boldsymbol{\phi} - \langle \text{linear terms} \rangle, \tag{2.18a}$$

$$\text{where we define} \qquad \mathcal{B} := (\mathcal{B}_{ij}) \quad \text{with} \quad \mathcal{B}_{ij} = \alpha_{ij}, \tag{2.18b}$$

as the (symmetric) matrix of interaction coefficients $\alpha_{ij} \geq 0$ and the linear terms are chosen so that $\mathcal{B}(\boldsymbol{\phi}) \geq 0$, and is minimised (zero) for pure phase materials (these terms do not otherwise impact the minimisation). $\mathcal{B}$ denotes the density function and its matrix of coefficients.

We refine (2.18a) to include a mechanism for enforcing (2.14a) via

$$\mathcal{B}_{[0,1]}(\boldsymbol{\phi})(x) = \begin{cases} \mathcal{B}(\boldsymbol{\phi}) & \text{if } 0 \leq \phi_i(x) \leq 1 \\ \infty & \text{otherwise.} \end{cases} \tag{2.18c}$$

Vector functions $\boldsymbol{\phi}$ with finite homogeneous energy are those for which (2.14a) holds a.e. $\mathcal{B}_{[0,1]}$ is not differentiable; this has far-reaching consequences.

Non-local energy

The non-local energy can be written using (2.12) as

$$\int_{\Omega} \mathcal{N}(\boldsymbol{\phi})\,\mathrm{d}\Omega = \frac{1}{2}\sum_{i,j=1}^{n} \gamma_{ij}\left(\phi_i - \overline{\phi_i}, \phi_j - \overline{\phi_j}\right)_{-1} = \frac{1}{2}\sum_{i,j=1}^{n} \gamma_{ij}\left((-\Delta_n)^{-1}\left(\phi_i - \overline{\phi_i}\right), \phi_j - \overline{\phi_j}\right) \tag{2.19a}$$

for a symmetric, constant coefficient non-local interaction matrix

$$\Gamma = (\gamma_{ij}) \qquad \text{in which each} \qquad \gamma_{ij} \geq 0. \tag{2.19b}$$

This somewhat obtuse definition of $\mathcal{N}(\boldsymbol{\phi})$ is justified once we start taking functional derivatives. In DBCs, this component of the energy models the fact that the AB molecules do not break apart, even though the A and B parts repel each other.

2.2.3 A stationary energy minimisation problem

To start, we consider the incompressibility constraint in (2.14b). Imposing this constraint allows us to formulate an n-phase problem in $n-1$ unknowns. Any such $(n-1)$-parameter formulation should be consistent with the underlying n-phase problem. Consider the scalar Lagrange function $\lambda = \lambda(x) : \mathbb{R}^d \to \mathbb{R}$, and the Lagrangian

$$\mathscr{L}(\boldsymbol{\phi}, \lambda) = \underbrace{\mathcal{E}(\boldsymbol{\phi})}_{\text{Energy}} \underbrace{- \int_{\Omega} \lambda\left(\sum_{i=1}^{n} \phi_i - 1\right)\mathrm{d}\Omega}_{\text{Incompressibility}}. \tag{2.20}$$

Necessary first order conditions for minimising $\mathcal{E}$ subject to (2.14b) are that (cf. Theorem 12.1 of Nocedal and Wright (2006))

$$\frac{\delta \mathscr{L}}{\delta \boldsymbol{\phi}} = \mathbf{0} \quad \Rightarrow \quad \frac{\delta \mathcal{E}}{\delta \phi_i} = \lambda, \quad 1 \leq i \leq n, \quad \text{and} \quad \frac{\delta \mathscr{L}}{\delta \lambda} = 0 \quad \Rightarrow \quad \boldsymbol{\phi}^\top \cdot \mathbf{1} = 1, \tag{2.21}$$

where we understand the notation

$$\frac{\delta \mathscr{L}}{\delta \boldsymbol{\phi}} \quad \text{to mean the } n\text{–vector} \quad \left(\frac{\delta \mathscr{L}}{\delta \phi_1} \dots \frac{\delta \mathscr{L}}{\delta \phi_n} \right)^\top.$$

2.2.4 A dynamic approach: gradient flows

We will also consider a dynamic approach for finding low energy morphologies. To do so, we replace the spatial Lagrange function $\lambda(x)$ with $\lambda = \lambda(x,t)$ and the stationary (2.20) with

$$\mathscr{L}(t) = \mathscr{L}(\boldsymbol{\phi}(t), \lambda(t)) = \mathcal{E}(\boldsymbol{\phi}(t)) - \int_\Omega \lambda(t) \left(\sum_{i=1}^n \phi_i(t) - 1 \right) \mathrm{d}\Omega. \tag{2.22}$$

We introduce a mobility matrix $M^{(k)}$ for each ϕ_k and define a system of n PDEs for the dynamics, as

$$\partial_t \phi_k + \nabla \cdot \boldsymbol{j}^{(k)} = 0 \qquad \text{where} \qquad \boldsymbol{j}^{(k)} = -M^{(k)} \nabla \left(\frac{\delta \mathscr{L}}{\delta \phi_k} \right), \tag{2.23a}$$

where $\boldsymbol{j}^{(k)}$ is called the k–th chemical potential flux. We insist that

$$\boldsymbol{j}^{(k)} \cdot \hat{\boldsymbol{n}} \Big|_{\partial\Omega} = 0 \qquad \text{for each} \qquad 1 \leq k \leq n, \tag{2.23b}$$

i.e. we impose zero flux BCs, along with the zero Neumann spatial BC

$$\partial_n \phi_i|_{\partial\Omega} = 0 \qquad \text{for each} \qquad 1 \leq i \leq n \qquad \text{and a.e. } t \in (0,T], \tag{2.23c}$$

and the Initial Condition (IC)

$$\boldsymbol{\phi}(x,0) = \boldsymbol{\phi}(t=0) = \boldsymbol{\phi}_0 = (\phi_{10}, \dots, \phi_{n0})^\top. \tag{2.23d}$$

We also demand that (cf. (2.14c))

$$\overline{\phi_i(\cdot,0)} = \overline{(\boldsymbol{\phi}_0)_i} = \overline{\phi_{i0}} = m_i \qquad \text{for each} \qquad 1 \leq i \leq n, \tag{2.23e}$$

with $\boldsymbol{m} = (m_1, \dots, m_n)^\top$ as in (2.14d), and finally that

$$\sum_{i=1}^n \phi_{i0}(x) = 1 \quad \text{for a.e. } x \in \Omega. \tag{2.23f}$$

This problem is known as the **Cahn–Hilliard equation** when $\alpha = 0$; when $\alpha > 0$, we call it the **Ohta–Kawasaki equation**. Its solutions should have two properties:

i) Mass conservation, in the sense that (cf. (2.14c))

$$\overline{\phi_i(t)} = \overline{\phi_i(0)} = m_i \qquad \text{for every} \qquad 0 < t \leq T \qquad \text{and each} \qquad 1 \leq i \leq n. \tag{2.24}$$

ii) Local incompressibility in the sense that

$$\sum_{i=1}^{n} \phi_i(x,t) = 1 \quad \text{for a.e. } (x,t) \in \Omega \times [0,T]. \tag{2.25}$$

The Lagrange function $\lambda(x,t)$ ensures that this last condition is satisfied.

2.3 Outlook

In Appendix A.2 on p. 340, we discuss some of the principles of solving the n-phase problem (2.16) using the stationary and dynamic approaches outlined above. Having posed the basic context for the energy minimisation problem, we are ready to dive into the details for $n = 2$ (Part II) and $n = 3$ (Part III).

2.4 Codes and numerical experiments

A large set of codes was created in support of the research presented in the rest of this thesis. They have been saved to two `bitbucket` repositories:

1. `MATLAB OKDE` (https://bitbucket.org/quentin_parsons/matlab-okde/src/master/): MATLAB code and data from the sweep and other experiments of Chapters 6–8, as well as the codes used to create most of the pictures in this thesis.

2. `3 Phase FEniCS` (https://bitbucket.org/quentin_parsons/3-phase-fenics/src/master/): `Python` codes in support of 2- and 3-phase gradient flow simulations in FEniCS.

Relevant experimental data (including binary data, summary pictures etc.) generated with the FEniCS code has been archived to `figshare` (see https://figshare.com/), and each set attributed a Digital Object Identifier (DOI). Links to these appear in endnotes to all of the relevant figures in the thesis (a `figshare` account is not required).

Notes

[1] A domain Ω is Lipschitz (cf. Defn 7.10 of Renardy and Rogers (2004)) '*if every point on $\partial\Omega$ has a neighbourhood N such that, after an affine change of coordinates (translation and rotation), $\partial\Omega \cap N$ is described by the equation $x_d = \phi(x_1, \ldots, x_{d-1})$, where ϕ is uniformly Lipschitz continuous. Moreover, $\Omega \cap N$ is on one side of $\partial\Omega \cap N$, e.g., $\omega \cap N = \{x \in N | x_d < \phi(x_1, \ldots, x_{d-1})\}$.*' See also the footnote associated with Theorem 1.9 of Braess (2001).

[2] See for instance Example 11.2 of Renardy and Rogers (2004) and Section 5.1 of Evans (1998).

[3] In what follows, $\mathscr{F}$ comes from Blowey and Elliott (1991)—see their Section 2.1.

[4] See also (2.4) of Blowey and Elliott (1991)

Part II

Two Phase Materials

Chapter 3

Models of 2-phase materials

In this chapter, we present our 2-phase model for DBCs.

Contents

3.1 Modelling DBCs 29
3.2 2-Phase dynamics by gradient flow 35
3.3 Basic properties 40
3.4 Mass control: a local model 41
3.5 Simple, exact solutions 41
3.6 Summary 42

Chapter outline

We start in Section 3.1 with a review of the model of Choksi and Ren (2003), in terms of the framework we developed in Section 2.2. In Section 3.2 we develop a dynamic model for energy minimisation in which a Lagrange parameter enforces incompressibility in the underlying dynamical equations (see also Appendix A.2.2).

In Section 3.3 we develop a one-parameter, time-dependent dynamic model with a non-local component. In Section 3.4, we replace this non-local model with a *local* version that is better suited to numerical work. We conclude in Section 3.5 by examining some simple, exact solutions of this model.

3.1 Modelling DBCs

Fig. 3.1 depicts a schematic of a linear DBC molecule comprised of two sub-chains, consisting of identical monomers (red for type A and black, type B). We study a melt of such molecules inside the domain Ω.

We use N_A to denote the number of type A monomers in each molecule, and likewise for N_B; N, the *index of polymerisation*, measures the total number of monomers per DBC

molecule with $N = N_A + N_B$. As in Choksi and Ren (2003), n denotes the number of AB molecules in Ω, for a total of nN monomers. We designate the average type A (type B) monomer density[1] in Ω by a (or b) where,

$$a = \frac{N_A}{N_A + N_B} \qquad \text{and} \qquad b = \frac{N_B}{N_A + N_B}.$$

We assume incompressibility: $a + b = 1$. The molecular mass m, is defined as the difference between the type A and B densities viz.

$$m := a - b = a - (1 - a) = 2a - 1 = 1 - 2b \quad \Rightarrow \quad a = \frac{m+1}{2}, \quad b = \frac{1-m}{2}. \tag{3.1}$$

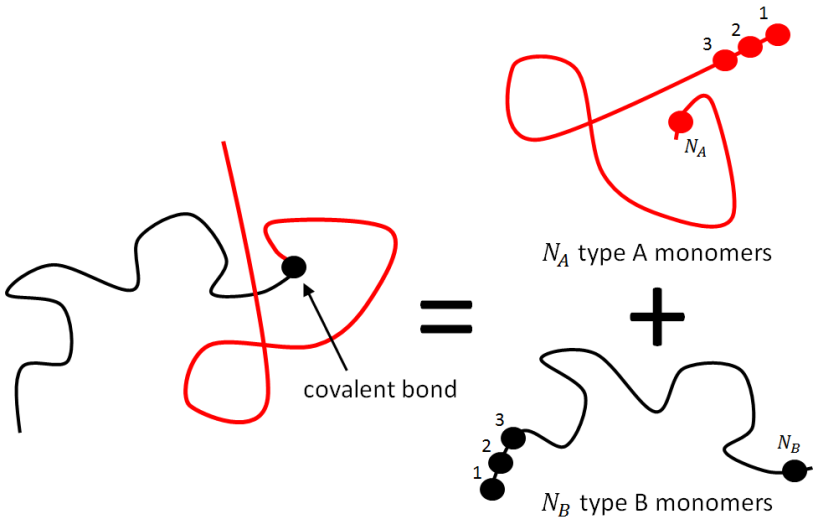

Figure 3.1: Schematic of a DBC molecule comprising $N = N_A + N_B$ individual monomers in two sub-chains, connected by a strong covalent bond.

For our 2-phase DBC model, $\boldsymbol{\phi}(x) = (\phi_A(x), \phi_B(x))$ denotes the local concentrations of the A, B monomers with mass control vector $\boldsymbol{m} = (a, b)$ (cf. (2.14d)). Then (cf. (2.13))

$$\phi_A(x) = \begin{cases} 0 & \Rightarrow \text{ no phase } A \text{ material at } x \\ 1 & \Rightarrow \text{ pure phase } A \text{ material at } x, \end{cases} \tag{3.2}$$

and similarly for $\phi_B(x)$. We insist on **boundedness** in that (cf. (2.14a))

$$0 \le \phi_A(x), \phi_B(x) \le 1, \qquad \text{for a.e. } x \in \Omega, \tag{3.3a}$$

local incompressibility (cf. (2.14b))

$$\phi_A(x) + \phi_B(x) = 1, \qquad \text{for a.e. } x \in \Omega, \tag{3.3b}$$

and that ϕ_A, ϕ_B have the correct **mass** with (cf. (2.14c), (2.14d))

$$\overline{\phi_A} = a \qquad \text{and} \qquad \overline{\phi_B} = b \qquad \text{where} \qquad a + b = 1. \tag{3.3c}$$

a, b and m above are invariant material parameters.

3.1.1 2-Phase energy

DBC molecules tend to self-assemble into structures that minimise the contact between unlike monomers, and in so doing, minimise their free energy (Choksi (2003)). We model this free energy with the Ohta–Kawasaki energy functional of Ohta and Kawasaki (1986). We define (cf. (2.15))

$$\mathcal{E}(\boldsymbol{\phi}) = \int_{\Omega} \mathcal{I}(\nabla\boldsymbol{\phi}) + \mathcal{B}(\boldsymbol{\phi}) + \mathcal{N}(\boldsymbol{\phi}) \ \mathrm{d}\Omega, \tag{3.4}$$

in terms of $\boldsymbol{\phi} = (\phi_A, \phi_B)^\top$, where:

- We define the interfacial energy density (cf. (2.17a), (A.88)),

$$\mathcal{I}(\nabla\boldsymbol{\phi}) = \frac{\varepsilon_A^2}{2}|\nabla\phi_A|^2 + \varepsilon_{AB}^2|\nabla\phi_A \cdot \nabla\phi_B| + \frac{\varepsilon_B^2}{2}|\nabla\phi_B|^2. \tag{3.5a}$$

  From the matrix K in (4.15) of Choksi and Ren (2003), we deduce that our matrix of interfacial coefficients is (cf. (2.17b))

$$\mathcal{I} = \begin{pmatrix} \varepsilon_A^2 & \varepsilon_{AB}^2 \\ \varepsilon_{AB}^2 & \varepsilon_B^2 \end{pmatrix} = \frac{\ell^2}{12}\mathrm{diag}\left(a^{-1}, b^{-1}\right) = \frac{\ell^2}{12}\mathrm{diag}\left(\frac{N}{N_A}, \frac{N}{N_B}\right), \tag{3.5b}$$

  where ℓ is the *Kuhn statistical length* measuring the average distance between two adjacent monomers or '*the average monomer space size*' (Choksi et al. (2009)). Hence

$$\varepsilon_A^2 = \frac{\ell^2 N}{12N_A}, \qquad \varepsilon_{AB}^2 = 0, \qquad \text{and} \qquad \varepsilon_B^2 = \frac{\ell^2 N}{12N_B}. \tag{3.5c}$$

- For the homogeneous energy component, we have the symmetric 2×2 monomer interaction parameter matrix (cf. (2.18b)),

$$\mathcal{B} = \begin{pmatrix} \mathcal{B}^{AA} & \mathcal{B}^{AB} \\ \mathcal{B}^{BA} & \mathcal{B}^{BB} \end{pmatrix}. \tag{3.6a}$$

  The entries of $\mathcal{B}$ are '*all positive*'[2] and the '*interaction is short ranged ... and repulsive by taking* $\mathcal{B}^{km} > 0$'.[3] Using the matrix $\mathcal{B}$, we define the function

$$\mathcal{B}(\boldsymbol{\phi}) = \frac{1}{2\Theta}\left(\sum_{k,m\in\{A,B\}} \mathcal{B}^{km}\phi_k\phi_m - \sum_{k\in\{A,B\}} \mathcal{B}^{kk}\phi_k\right), \tag{3.6b}$$

  where Θ is the absolute temperature. Equation (4.25) of Choksi and Ren (2003) defines the homogeneous energy density as (cf. (2.18c))

$$\mathcal{B}_{[0,1]}(\boldsymbol{\phi}) = \begin{cases} \mathcal{B}(\boldsymbol{\phi}) & \phi_A + \phi_B = 1; \phi_A, \phi_B \geq 0 \\ \infty & \text{otherwise.} \end{cases} \tag{3.6c}$$

The subtracted linear terms ensure that $\mathcal{B}_{[0,1]}(\boldsymbol{\phi}) \geq 0$ for all $\boldsymbol{\phi}$ and $\mathcal{B}_{[0,1]}(\boldsymbol{\phi}) = 0 \Leftrightarrow \boldsymbol{\phi} = (1,0)$ or $(0,1)$ i.e. for pure A/B phases. We regularise this as (cf. (A.100))

$$\mathcal{B}_{\mu}(\boldsymbol{\phi}) = \mathcal{B}(\boldsymbol{\phi}) + \frac{1}{2\mu}\left((\phi_A - 1)_+^2 + (\phi_A)_-^2 + (\phi_B - 1)_+^2 + (\phi_B)_-^2\right), \tag{3.6d}$$

for $0 < \mu \ll 1$, so as to be able to take partial derivatives, and replace $\mathcal{E}$ in (3.4) with the penalised

$$\mathcal{E}_{\mu}(\boldsymbol{\phi}) = \int_{\Omega} \mathcal{I}(\nabla\boldsymbol{\phi}) + \mathcal{B}_{\mu}(\boldsymbol{\phi}) + \mathcal{N}(\boldsymbol{\phi})\ \mathrm{d}\Omega. \tag{3.7}$$

- For the non-local energy, we have (cf. (2.19a), (A.89))

$$\int_{\Omega} \mathcal{N}(\boldsymbol{\phi})\,\mathrm{d}\Omega = \frac{\gamma_A}{2}\left\|\phi_A - \overline{\phi_A}\right\|_{-1}^2 + \gamma_{AB}\left(\phi_A - \overline{\phi_A}, \phi_B - \overline{\phi_B}\right)_{-1} + \frac{\gamma_B}{2}\left\|\phi_B - \overline{\phi_B}\right\|_{-1}^2, \tag{3.8a}$$

where we define

$$\Phi_A := (-\Delta_n)^{-1}\left(\phi_A - \overline{\phi_A}\right) \qquad \text{and} \qquad \Phi_B := (-\Delta_n)^{-1}\left(\phi_B - \overline{\phi_B}\right), \tag{3.8b}$$

and, to ensure well-posedness, demand that

$$\partial_n \Phi_A|_{\partial\Omega} = \partial_n \Phi_B|_{\partial\Omega} = 0 \qquad \text{and} \qquad \overline{\Phi_A} = \overline{\Phi_B} = 0. \tag{3.8c}$$

An examination of the matrix L in (4.15) of Choksi and Ren (2003) reveals that the 2-phase, non-local interaction matrix is (cf. (2.19b))

$$\boldsymbol{\Gamma} = \begin{pmatrix} \gamma_A & \gamma_{AB} \\ \gamma_{AB} & \gamma_B \end{pmatrix} = \frac{9}{\ell^2}\begin{pmatrix} \frac{1}{N_A^2} & \frac{-1}{N_A N_B} \\ \frac{-1}{N_A N_B} & \frac{1}{N_B^2} \end{pmatrix} = \frac{9}{\ell^2 N^2}\begin{pmatrix} a^{-2} & -(ab)^{-1} \\ -(ab)^{-1} & b^{-2} \end{pmatrix}, \tag{3.9}$$

and so

$$\gamma_A = \frac{9}{\ell^2 N_A^2}, \qquad \gamma_{AB} = -\frac{9}{\ell^2 N_A N_B}, \qquad \text{and} \qquad \gamma_B = \frac{9}{\ell^2 N_B^2}. \tag{3.10}$$

3.1.2 2-Phase incompressibility

We now impose incompressibility (3.3b) with

$$\varphi := \phi_A - \phi_B, \tag{3.11a}$$

as the difference between the type A and type B monomer densities, so that

$$\varphi = 1 - 2\phi_B = 2\phi_A - 1, \qquad \phi_A = \frac{1+\varphi}{2} \qquad \text{and} \qquad \phi_B = \frac{1-\varphi}{2}. \tag{3.11b}$$

Using (3.1), (3.3c), we conclude that

$$\overline{\varphi} = m \qquad \text{where} \qquad m = a - b, \tag{3.11c}$$

and so (cf. (3.1), (3.11b))

$$m = 1 - 2b = 2a - 1, \qquad a = \frac{1+m}{2} \qquad \text{and} \qquad b = \frac{1-m}{2}. \tag{3.11d}$$

We will also make use of the order parameter

$$\phi_A = \phi_A(\phi) = \phi \qquad \text{so that} \qquad \phi_B = \phi_B(\phi) = 1 - \phi. \tag{3.12a}$$

Using (3.11b), we conclude that

$$\varphi = \phi_A - \phi_B = \phi - (1-\phi) = 2\phi - 1 \qquad \Rightarrow \qquad \phi = \frac{\varphi + 1}{2}. \tag{3.12b}$$

(3.3a) and (3.11a) imply that

$$|\varphi(x)| \leq 1 \qquad \text{for a.e. } x \in \Omega. \tag{3.13}$$

We identify $\varphi(x) = 1$ with the (local) presence of pure A material, $\varphi(x) = -1$ with pure B material, and $\varphi(x) = 0$ with a mixture (cf. (3.2)). Interfacial regions in which φ transitions from ± 1 to ∓ 1 model the connections between the A and B sub-chains, and m encodes the relative excess proportion of A over B monomers in each molecule: $m = 1$ (or -1) models a pure A (or B) DBC, and $m = 0$ a symmetric DBC with $N_A = N_B$.

3.1.3 The Ohta–Kawasaki energy functional

We now express the (penalised) free energy $\mathcal{E}_\mu$ in (3.7), in terms of φ, as

$$\mathcal{E}_\mu(\varphi) = \int_\Omega \mathcal{I}(\nabla\varphi) + \mathcal{B}_\mu(\varphi) + \mathcal{N}(\varphi) \ \mathrm{d}\Omega, \tag{3.14}$$

which has three components. For the **interfacial** component,[4]

$$\mathcal{I}(\nabla\varphi) = \frac{\varepsilon_\varphi^2}{2} |\nabla\varphi|^2, \tag{3.15}$$

where, using (3.5c), we define

$$\varepsilon_\varphi^2 := \frac{1}{4}\left(\varepsilon_A^2 - 2\varepsilon_{AB}^2 + \varepsilon_B^2\right) = \frac{\ell^2}{48}\left(\frac{N}{N_A} + \frac{N}{N_B}\right) = \frac{\ell^2}{48a(1-a)}. \tag{3.16}$$

$\varepsilon_\varphi = C\ell$ and so ε_φ is related to the interfacial thickness, ℓ.

The **homogeneous** energy density is[5]

$$\mathcal{B}_{[-1,1]}(\varphi) = \begin{cases} \dfrac{\chi^{AB}}{4}\left(1 - \varphi^2\right) & |\varphi| \leq 1 \\ \infty & \text{otherwise,} \end{cases} \tag{3.17}$$

where in turn (cf. (4.22) of Choksi and Ren (2003) and our (3.6a)),

$$\chi^{AB} := \frac{1}{\Theta}\left(\mathcal{B}^{AB} - \frac{1}{2}\left(\mathcal{B}^{AA} + \mathcal{B}^{BB}\right)\right) > 0. \tag{3.18}$$

The quantity χ^{AB} is the *Flory–Huggins interaction parameter* measuring the excess incompatibility of type A and B monomers.[6] A regularised version of $\mathcal{B}_{[-1,1]}$ is

$$\mathcal{B}_\mu(\varphi) = \frac{\chi^{AB}}{4}\left(1-\varphi^2\right) + \frac{1}{2\mu}\left((\varphi-1)_+^2 + (\varphi+1)_-^2\right). \tag{3.19}$$

The effect of changing χ^{AB} can be seen in Fig. 3.2: as χ^{AB} increases, $\mathcal{B}_\mu(0)$ increases, but $\mathcal{B}_\mu(\pm 1)$ remain small (identically zero as $\mu \downarrow 0$). Since $\varphi = 0$ is identified with a well-mixed morphology (in which the A and B monomers are not phase separated) it is clear that increasing χ^{AB} makes phase separation energetically favourable. (3.18) suggests that this is achieved by lowering the temperature, Θ. According to the Introduction of Choksi and Ren (2003), SCFT theory predicts the following temperature response:

i) at high temperatures, '*a disordered regime wherein the melt exhibits no observable phase separation*'. In our model, this state is represented by $\varphi \equiv m$.

ii) the '*Weak Segregation Regime (WSR) where the size of the*' pure-phase, '*A and B-rich domains are of roughly of the same order as the interfacial . . . regions*'.

iii) as the temperature is further reduced, the so-called *ISR* and *SSR* where the pure-phase domains are '*much larger than the interfacial length*'.

We investigate the predictions of our model in this regard in Section 8.4.

Remark. We use the double obstacle version of $\mathcal{B}$ (and its regularisation) in this thesis, but note that the so-called double-well (quartic) polynomial approximation has also been studied extensively. To use this, as in Choksi et al. (2011), we would replace $\mathcal{B}_\mu$ with

$$\mathcal{B}_q(\varphi) = \frac{\chi^{AB}}{4}\left(1-\varphi^2\right)^2. \tag{3.20}$$

For the **non-local** energy component, we write[8]

$$\int_\Omega \mathcal{N}(\varphi)\,\mathrm{d}\Omega = \frac{\alpha}{2}\left\|\varphi - \overline{\varphi}\right\|_{-1}^2, \tag{3.21a}$$

where we have defined

$$\alpha := \frac{1}{4}\left(\gamma_A - 2\gamma_{AB} + \gamma_B\right) = \frac{9N^2}{4N_A^2N_B^2\ell^2} = \frac{9}{4a^2\left(1-a\right)^2\ell^2N^2}. \tag{3.21b}$$

We also insist that (cf. (3.8b), (3.8c))

$$\Phi := (-\Delta_n)^{-1}\left(\varphi - \overline{\varphi}\right), \qquad \partial_n\Phi|_{\partial\Omega} = 0 \qquad \text{and} \qquad \overline{\Phi} = 0, \tag{3.21c}$$

to ensure the well-posedness of this energy component.[9]

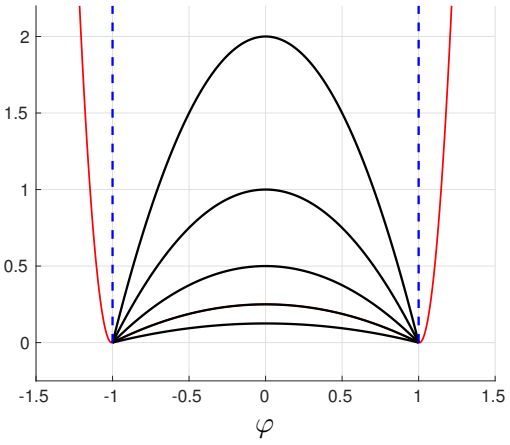

Figure 3.2: The effect of increasing the Flory–Huggins parameter (decreasing Θ in (3.18)): $\mathcal{B}_{[-1,1]}(\varphi)$ in (3.17) is depicted in black on $|\varphi| \leq 1$ for $\chi^{AB} \in \left\{\frac{1}{2}, 1, 2, 4, 8\right\}$. $\mathcal{B}_\mu$ from (3.19) is depicted in **red** for $\mu = 10^{-2}$ (a relatively large value) and $\chi^{AB} = 1$ on $|\varphi| > 1$. The dashed **blue** lines depict the obstacle ('infinite penalty') for $|\varphi| > 1$ as $\mu \downarrow 0$. The higher χ^{AB} is (the lower Θ is), the more energetically favourable phase separation ($\varphi = \pm 1$) is.[7]

3.2 2-Phase dynamics by gradient flow

3.2.1 A Lagrange parameter: dynamics in ϕ_A, ϕ_B

We use a Lagrange function $\lambda = \lambda(x,t)$ for the incompressibility (cf. Section 2.2.4), and assume that ϕ_A, ϕ_B have constant, scalar mobilities M_A, M_B. The 4-part system of PDEs for the 2-phase $H^{-1}(\Omega)$ gradient-flow dynamics is (cf. (A.91))

$$\partial_t \phi_A - M_A \Delta \left(\frac{\delta \mathcal{E}}{\delta \phi_A} - \lambda \right) = 0 \qquad \text{or} \qquad \begin{cases} \partial_t \phi_A - M_A \Delta \mu_A = 0 \\ \text{where} \quad \mu_A = \dfrac{\delta \mathcal{E}}{\delta \phi_A} - \lambda, \end{cases} \tag{3.22a}$$

and

$$\partial_t \phi_B - M_B \Delta \left(\frac{\delta \mathcal{E}}{\delta \phi_B} - \lambda \right) = 0 \qquad \text{or} \qquad \begin{cases} \partial_t \phi_B - M_B \Delta \mu_B = 0 \\ \text{where} \quad \mu_B = \dfrac{\delta \mathcal{E}}{\delta \phi_B} - \lambda, \end{cases} \tag{3.22b}$$

subject to the local incompressibility requirement (cf. (2.25))

$$\phi_A(x,t) + \phi_B(x,t) = 1 \qquad \text{for a.e. } (x,t) \in \Omega \times [0,T], \tag{3.22c}$$

along with the ICs (cf. (2.23d), (2.23e))

$$\boldsymbol{\phi}(x,0) = \boldsymbol{\phi}_0(x) = (\phi_{A0}(x), \phi_{B0}(x))^\top \qquad \text{where} \qquad \overline{\phi_{A0}} = a, \qquad \overline{\phi_{B0}} = b, \tag{3.22d}$$

and the zero Neumann BCs (cf. (2.23c), (A.91c))

$$\partial_n \phi_A|_{\partial\Omega} = \partial_n \phi_B|_{\partial\Omega} = 0, \qquad \text{and} \qquad \partial_n \mu_A|_{\partial\Omega} = \partial_n \mu_B|_{\partial\Omega} = 0. \tag{3.22e}$$

To start, we find λ. If we add (3.22a) and (3.22b) and use (3.3b), we see that

$$\underbrace{\partial_t \left(\phi_A + \phi_B\right)}_{=0} - \Delta \left(M_A \frac{\delta \mathcal{E}}{\delta \phi_A} + M_B \frac{\delta \mathcal{E}}{\delta \phi_B} - \lambda \left(M_A + M_B\right) \right) = 0 \tag{3.23}$$

or, assuming the invertibility of Δ (cf. (A.93a)),

$$\lambda = \frac{1}{M_A + M_B} \left(M_A \frac{\delta \mathcal{E}}{\delta \phi_A} + M_B \frac{\delta \mathcal{E}}{\delta \phi_B} \right). \tag{3.24}$$

Substitution back into (3.22a) and (3.22b) leads to

$$\partial_t \phi_A - \frac{M_A M_B}{M_A + M_B} \Delta \left(\frac{\delta \mathcal{E}}{\delta \phi_A} - \frac{\delta \mathcal{E}}{\delta \phi_B} \right) = 0, \tag{3.25a}$$

and

$$\partial_t \phi_B - \frac{M_A M_B}{M_A + M_B} \Delta \left(\frac{\delta \mathcal{E}}{\delta \phi_B} - \frac{\delta \mathcal{E}}{\delta \phi_A} \right) = 0. \tag{3.25b}$$

From (3.5a), we find that

$$\nabla \cdot \partial_{\nabla \phi_i} \mathcal{I} = \varepsilon_{ij}^2 \Delta \phi_j + \varepsilon_i^2 \Delta \phi_i; \tag{3.26}$$

likewise, using (3.6d) we find that (cf. (A.101))

$$\partial_{\phi_i} \mathcal{B}_\mu \left(\boldsymbol{\phi} \right) = \frac{1}{\Theta} \left(\mathcal{B}^{ij} \phi_j + \mathcal{B}^{ii} \left(\phi_i - 2 \right) \right) + \frac{1}{\mu} \left(\left(\phi_i - 1 \right)_+ + \left(\phi_i \right)_- \right), \tag{3.27}$$

while (3.8a) gives

$$\partial_{\phi_i} \mathcal{N} = \left(-\Delta_n \right)^{-1} \left(\gamma_{ij} \left(\phi_j - \overline{\phi_j} \right) + \gamma_i \left(\phi_i - \overline{\phi_i} \right) \right), \tag{3.28}$$

for $i, j = A, B$, $i \neq j$.[10] Summing, we see that (cf. (A.87)),

$$\begin{aligned} \frac{\delta \mathcal{E}}{\delta \phi_i} = \varepsilon_{ij}^2 \Delta \phi_j + \varepsilon_i^2 \Delta \phi_i + \left(-\Delta_n \right)^{-1} \left(\gamma_{ij} \left(\phi_j - \overline{\phi_j} \right) + \gamma_i \left(\phi_i - \overline{\phi_i} \right) \right) \\ + \frac{1}{\Theta} \left(\mathcal{B}^{ij} \phi_j + \mathcal{B}^{ii} \left(\phi_i - 2 \right) \right) + \frac{1}{\mu} \left(\left(\phi_i - 1 \right)_+ + \left(\phi_i \right)_- \right) \end{aligned} \tag{3.29}$$

for $i, j = A, B$, $i \neq j$.[11] Substituting (3.29) into (3.25) gives

$$\partial_t \phi_A + \frac{M_A M_B}{M_A + M_B} \left(-\Delta \right) \widetilde{\omega_A} = 0 \tag{3.30a}$$

where

$$\widetilde{\omega_A} := \frac{\delta\mathcal{E}}{\delta\phi_A} - \frac{\delta\mathcal{E}}{\delta\phi_B} = \left(\varepsilon_A^2 - \varepsilon_{AB}^2\right)(-\Delta)\,\phi_A + \left(\varepsilon_{AB}^2 - \varepsilon_B^2\right)(-\Delta)\,\phi_B$$
$$+ (-\Delta_n)^{-1}\left((\gamma_A - \gamma_{AB})\left(\phi_A - \overline{\phi_A}\right) + (\gamma_{AB} - \gamma_B)\left(\phi_B - \overline{\phi_B}\right)\right)$$
$$+ \frac{1}{\Theta}\left(\left(\mathcal{B}^{AA} - \mathcal{B}^{AB}\right)\phi_A + \left(\mathcal{B}^{AB} - \mathcal{B}^{BB}\right)\phi_B - 2\left(\mathcal{B}^{AA} - \mathcal{B}^{BB}\right)\right)$$
$$+ \frac{1}{\mu}\left((\phi_A - 1)_+ - (\phi_B - 1)_+ + (\phi_A)_- - (\phi_B)_-\right), \quad (3.30b)$$

and likewise

$$\partial_t\phi_B + \frac{M_A M_B}{M_A + M_B}(-\Delta)\,\widetilde{\omega_B} = 0, \quad (3.30c)$$

$$\text{where} \quad \widetilde{\omega_B} = \frac{\delta\mathcal{E}}{\delta\phi_B} - \frac{\delta\mathcal{E}}{\delta\phi_A} = -\widetilde{\omega_A}. \quad (3.30d)$$

Now define

$$\omega_A := \widetilde{\omega_A} - (-\Delta_n)^{-1}\left((\gamma_A - \gamma_{AB})\left(\phi_A - \overline{\phi_A}\right) + (\gamma_{AB} - \gamma_B)\left(\phi_B - \overline{\phi_B}\right)\right), \quad (3.31a)$$

by subtracting the non-local terms from $\widetilde{\omega_A}$, so that

$$(-\Delta)\,\widetilde{\omega_A} = (-\Delta)\,\omega_A + \left((\gamma_A - \gamma_{AB})\left(\phi_A - \overline{\phi_A}\right) + (\gamma_{AB} - \gamma_B)\left(\phi_B - \overline{\phi_B}\right)\right). \quad (3.31b)$$

Substitution into (3.30) then yields

$$\partial_t\phi_A + \frac{M_A M_B}{M_A + M_B}\left((-\Delta)\,\omega_A + (\gamma_A - \gamma_{AB})\left(\phi_A - \overline{\phi_A}\right) + (\gamma_{AB} - \gamma_B)\left(\phi_B - \overline{\phi_B}\right)\right) = 0 \quad (3.32a)$$

where ω_A is specified by (3.31a) and (3.30b), viz.

$$\omega_A = \frac{\delta\mathcal{E}}{\delta\phi_A} - \frac{\delta\mathcal{E}}{\delta\phi_B} = \left(\varepsilon_A^2 - \varepsilon_{AB}^2\right)(-\Delta)\,\phi_A + \left(\varepsilon_{AB}^2 - \varepsilon_B^2\right)(-\Delta)\,\phi_B$$
$$+ \frac{1}{\Theta}\left(\left(\mathcal{B}^{AA} - \mathcal{B}^{AB}\right)\phi_A + \left(\mathcal{B}^{AB} - \mathcal{B}^{BB}\right)\phi_B - 2\left(\mathcal{B}^{AA} - \mathcal{B}^{BB}\right)\right)$$
$$+ \frac{1}{\mu}\left((\phi_A - 1)_+ - (\phi_B - 1)_+ + (\phi_A)_- - (\phi_B)_-\right), \quad (3.32b)$$

and, similarly

$$\partial_t\phi_B + \frac{M_A M_B}{M_A + M_B}\left((-\Delta)\,\omega_B + (\gamma_{AB} - \gamma_A)\left(\phi_A - \overline{\phi_A}\right) + (\gamma_B - \gamma_{AB})\left(\phi_B - \overline{\phi_B}\right)\right) = 0 \quad (3.32c)$$

$$\text{where} \qquad \omega_B = -\omega_A. \quad (3.32d)$$

As we explore in Appendix A.2.2, this model is mass conserving and exhibits energy decay.

Remark. In going from (3.30) to (3.32), we moved the non-local terms $(-\Delta_n)^{-1}\left(\phi_i - \overline{\phi_i}\right)$ from the second to the first line of each sub-system. These problems are equivalent because the mapping in (3.31) is well-defined (cf. Defn 2.1.1).

3.2.2 Dynamics for φ

We now derive gradient flow dynamics for φ from the ϕ_A, ϕ_B dynamics above. In the next section, we re-write the energy (3.14) using (3.11a), and re-derive the φ dynamics, and then reconcile the two sets. In so doing, we will discover a restriction on M_φ, the mobility of φ.

To start, we *add* (3.32b) and (3.32d) and find that $\omega_A + \omega_B \equiv 0$; similarly, adding (3.32a) and (3.32c) leads to $0 = 0$ (for $\phi_A + \phi_B = 1$) i.e. the systems comprise a redundant pair, as expected. Retaining the first of these and writing it in terms of ϕ from (3.12a) yields

$$\partial_t \phi + \frac{M_A M_B}{M_A + M_B} \left((-\Delta) \widetilde{\omega} + 4\alpha \left(\phi - \overline{\phi} \right) \right) = 0 \tag{3.33a}$$

with α as in (3.21b), and

$$\widetilde{\omega} = 4\varepsilon_\varphi^2 (-\Delta) \phi + \partial_\phi \mathcal{B}_\mu = 4 \left(\varepsilon_\varphi^2 (-\Delta) \phi + \frac{\chi^{AB}}{4} (1 - 2\phi) + \frac{1}{2\mu} \left((\phi - 1)_+ + (\phi)_- \right) \right), \tag{3.33b}$$

with ε_φ given by (3.16) and χ^{AB} by (3.18), we used the Chain Rule to conclude that

$$\partial_\phi \mathcal{B} = \partial_{\phi_A} \mathcal{B} \partial_\phi \phi_A + \partial_{\phi_B} \mathcal{B} \partial_\phi \phi_B = \partial_{\phi_A} \mathcal{B} - \partial_{\phi_B} \mathcal{B}, \tag{3.34}$$

and, finally, substituted (3.12a) into (3.6d) to write

$$\begin{aligned} \mathcal{B}_\mu (\phi) = \frac{1}{\Theta} \left(\phi \left(\mathcal{B}^{AB} - \frac{1}{2} \left(\mathcal{B}^{AA} + \mathcal{B}^{BB} \right) \right) - \phi^2 \left(\mathcal{B}^{AB} - \frac{1}{2} \left(\mathcal{B}^{AA} + \mathcal{B}^{BB} \right) \right) \right) \\ + \frac{1}{\mu} \left((\phi - 1)_+^2 + (\phi)_-^2 \right) = \chi^{AB} \left(\phi - \phi^2 \right) + \frac{1}{\mu} \left((\phi - 1)_+^2 + (\phi)_-^2 \right), \end{aligned}$$

after noting that $(\phi - 1)_+^2 = (1 - \phi)_-^2$ and $(\phi)_-^2 = (-\phi)_+^2$. Using (3.12b) we now transform (3.33) to the pair (cf. (3.19))[12]

$$\partial_t \varphi + \frac{4 M_A M_B}{M_A + M_B} \left((-\Delta) \omega_\varphi + \alpha (\varphi - \overline{\varphi}) \right) = 0 \tag{3.35a}$$

$$\omega_\varphi := \varepsilon_\varphi^2 (-\Delta) \varphi - \frac{\chi^{AB}}{2} \varphi + \frac{1}{\mu} \left((\varphi - 1)_+ + (\varphi + 1)_- \right), \tag{3.35b}$$

where μ in (3.35b) is re-scaled to four times the μ in (3.33), and we have re-used the symbol.[13] To close this system, we transform the ICs in (3.22) to

$$\varphi (x, 0) = \varphi_0 (x) = \phi_{A0} (x) - \phi_{B0} (x) \quad \text{where} \quad \overline{\varphi_0} = \overline{\phi_{A0}} - \overline{\phi_{B0}} = a - b = m, \tag{3.35c}$$

and, likewise, the zero Neumann BCs

$$\partial_n \varphi|_{\partial\Omega} = \partial_n (\phi_A - \phi_B)|_{\partial\Omega} = 0, \qquad \text{and} \qquad \partial_n \omega_\varphi|_{\partial\Omega} = \partial_n (\mu_A - \mu_B)|_{\partial\Omega} = 0. \tag{3.35d}$$

Remark. We take the zero Neumann (natural) BC on φ from the stationary problem

$$\frac{\delta \mathcal{E}}{\delta \varphi} = 0 \tag{3.36}$$

and *impose* the same condition on ω_φ to guarantee mass conservation.

3.2.3 Incompressibility in the energy: a model in φ

We now work directly from the energy (3.14) to re-derive φ-dynamics of the form (cf. (3.22))

$$\partial_t \varphi + M_\varphi \left(-\Delta\right) \omega_\varphi = 0 \qquad \text{where} \qquad \omega_\varphi = \frac{\delta \mathcal{E}}{\delta \varphi}, \tag{3.37}$$

subject to the ICs and zero Neumann BCs in (3.35). Our first observation is that for (3.37) to be consistent with (3.35), we must have[14]

$$M_\varphi = \frac{4 M_A M_B}{M_A + M_B}. \tag{3.38}$$

Working from (A.87), we determine that:

- for the interfacial energy, (3.15) gives

$$-\nabla \cdot \partial_{\nabla \varphi} \mathcal{I} = \varepsilon_\varphi^2 \left(-\Delta\right) \varphi; \tag{3.39a}$$

- for the homogeneous component, (3.19) implies that

$$\partial_\varphi \mathcal{B}_\mu = -\frac{\chi^{AB}}{2} \varphi + \frac{1}{\mu} \left((\varphi - 1)_+ + (\varphi + 1)_- \right); \tag{3.39b}$$

- for the non-local component, (3.21a) leads to

$$\partial_\varphi \mathcal{N} = \alpha \left(-\Delta_n\right)^{-1} \left(\varphi - \overline{\varphi}\right). \tag{3.39c}$$

Combining all of the above leads to the pair

$$\partial_t \varphi + \frac{4 M_A M_B}{M_A + M_B} \left(-\Delta\right) \psi = 0 \tag{3.40a}$$

$$\psi := \varepsilon_\varphi^2 \left(-\Delta\right) \varphi - \frac{\chi^{AB}}{2} \varphi + \frac{1}{\mu} \left((\varphi - 1)_+ + (\varphi + 1)_- \right) + \alpha \left(-\Delta_n\right)^{-1} \left(\varphi - \overline{\varphi}\right). \tag{3.40b}$$

Shifting the non-local terms, as we did in (3.31), leads to (3.35). We can also write this system as the (single) fourth order PDE

$$\partial_t \varphi + M_\varphi \left(-\Delta \left(\varepsilon_\varphi^2 \left(-\Delta\right) \varphi - \frac{\chi^{AB}}{2} \varphi + \frac{1}{\mu} \left((\varphi - 1)_+ + (\varphi + 1)_- \right) \right) + \alpha \left(\varphi - \overline{\varphi}\right) \right) = 0, \tag{3.41a}$$

in which the BC in (3.35d) is replaced with

$$\partial_n \varphi |_{\partial\Omega} = \partial_n \Delta \varphi |_{\partial\Omega} = 0. \tag{3.41b}$$

Remark. We can write these dynamics with a unit mobility by rescaling time $t \to \widehat{t}$ with

$$\widehat{t} = \frac{4 M_A M_B}{M_A + M_B} t. \tag{3.42}$$

Moreover, in the event that $M_A = M_B = \widehat{M}$ as in (A.94),

$$\frac{M_A M_B}{M_A + M_B} = \frac{\widehat{M}^2}{2\widehat{M}} = \frac{\widehat{M}}{2}, \qquad \Rightarrow \qquad M_\varphi = 2\widehat{M}.$$

For all of our further analysis, without any loss of generality, we set $M_\varphi = 1$.

3.3 Basic properties

Mass conservation

To establish mass conservation, we use (3.35a) with a unit mobility to deduce that

$$\frac{\mathrm{d}\overline{\varphi}}{\mathrm{d}t} = \frac{1}{|\Omega|}\int_\Omega \partial_t\varphi \ \mathrm{d}\Omega = \frac{1}{|\Omega|}\int_\Omega (\Delta)\,\omega_\varphi \ \mathrm{d}\Omega - \frac{\alpha}{|\Omega|}\int_\Omega \varphi - \overline{\varphi} \ \mathrm{d}\Omega = 0. \tag{3.43}$$

Hence, $\overline{\varphi}(t)$ is constant in time, and so using (3.35c), we obtain

$$\overline{\varphi}(t) = \overline{\varphi}(0) = \overline{\varphi_0} = m \qquad \text{for a.e. } t \in (0,T]. \tag{3.44}$$

Energy monotonicity (decay)

We now present an informal demonstration of energy monotonicity, which relies on several implicit assumptions about the existence and smoothness of solutions to (3.35); a rigorous treatment appears in Chapter 4. We base our approach on Appendix B of Choksi et al. (2009). To start, we write (3.37) with unit mobility as

$$\partial_t\varphi = -(-\Delta)\frac{\delta\mathcal{E}}{\delta\varphi} \qquad \Rightarrow \qquad \frac{\delta\mathcal{E}}{\delta\varphi} = -(-\Delta_n)^{-1}(\partial_t\varphi), \tag{3.45}$$

making all of the necessary assumptions about solvability. Now we write (cf. (3.14))

$$\mathcal{E}(t) = \mathcal{E}(\varphi(t)) = \int_\Omega E(\varphi(t)) \ \mathrm{d}\Omega, \qquad E(\varphi) = \mathcal{I}(\nabla\varphi) + \mathcal{B}(\varphi) + \mathcal{N}(\varphi). \tag{3.46}$$

(The Latin E for the integrand is deliberate.) Then

$$\begin{aligned}\frac{\mathrm{d}\mathcal{E}}{\mathrm{d}t} &= \frac{\mathrm{d}}{\mathrm{d}t}\int_\Omega E(\varphi(t)) \ \mathrm{d}\Omega = \int_\Omega \partial_t E(\varphi(t)) \ \mathrm{d}\Omega \\ &= \left(\frac{\delta\mathcal{E}}{\delta\varphi}, \partial_t\varphi\right) = -\left((-\Delta_n)^{-1}(\partial_t\varphi), \partial_t\varphi\right) = -\|\partial_t\varphi\|_{-1}^2 \le 0,\end{aligned} \tag{3.47}$$

which means that the energy is a non-increasing function of t.

Two kinds of stationarity

If φ solves the stationary problem (3.36), viz. $\frac{\delta\mathcal{E}}{\delta\varphi} = 0$, then $\Delta\left(\frac{\delta\mathcal{E}}{\delta\varphi}\right) = 0$, so $\partial_t\varphi = 0$ in (3.37) i.e. φ is a stationary solution of the dynamic equation (in the sense of having zero time derivative). On the other hand, if $\partial_t\varphi = 0$ in (3.37), then $\Delta\left(\frac{\delta\mathcal{E}}{\delta\varphi}\right) = 0$, but this does not necessarily imply that $\frac{\delta\mathcal{E}}{\delta\varphi} = 0$ i.e. we cannot, at this level, *guarantee* that the corresponding φ solves the stationary problem. However, we will show rigorously in Section 4.3.4, that we recover stationary minimisers from gradient flows as $t \to \infty$.

3.4 Mass control: a local model

(3.35) is non-local by virtue of the $\overline{\varphi}$ term. In light of mass conservation, however, we can replace $\overline{\varphi}$ in (3.35a) with the *control mass* m, and re-scale time to obtain

$$\partial_t \varphi + (-\Delta)\,\omega_\varphi + \alpha\,(\varphi - m) = 0. \tag{3.48}$$

This PDE is local and thus easier to work with (especially numerically). Note however that (3.35a) and (3.48) are *not* equivalent: (3.35a) is mass conserving, but (3.48) is not. This becomes clear if we drop the requirement in (3.35c) that $\overline{\varphi_0} = m$, and suppose that $\overline{\varphi_0} = \widetilde{m} \neq m$. As in Section (2.3.1) of Parsons (2012), integrating (3.48) in space yields

$$(\partial_t \varphi, 1) + \underbrace{((-\Delta)\,\omega_\varphi, 1)}_{=0} + \alpha\,(\varphi - m, 1) = 0 \quad \Rightarrow \quad \frac{\mathrm{d}}{\mathrm{d}t}\,(\varphi - m, 1) = -\alpha\,(\varphi - m, 1) \tag{3.49}$$

since m is time independent. We recognise this as an ODE in time for $(\varphi - m, 1)$ with IC $(\varphi - m, 1)\,(0) = (\varphi\,(0) - m, 1) = (\varphi_0, 1) - (m, 1) = |\Omega|\,(\widetilde{m} - m)$, and solution

$$(\varphi - m, 1)\,(t) = |\Omega|\,(\widetilde{m} - m)\,\mathrm{e}^{-\alpha t} \qquad \Rightarrow \qquad \overline{\varphi\,(t)} = m + (\widetilde{m} - m)\,\mathrm{e}^{-\alpha t} \to m \tag{3.50}$$

as $t \to \infty$ (for $\alpha > 0$). We term (3.48) mass *controlling* because of this tendency to drive the solution mass average $\overline{\varphi} \to m$ exponentially quickly.[15]

Remark. For $\alpha = 0$, (3.50) becomes $\overline{\varphi\,(t)} = \widetilde{m} = \overline{\varphi_0}$ and mass control reduces to mass conservation. For any IC satisfying $\overline{\varphi_0} = m$, (3.48) yields $\overline{\varphi}\,(t) = m$ for a.e. $t \in (0, T]$.

3.5 Simple, exact solutions

We now explore some simple, exact solutions of (3.48). Consider the mass controlling

$$\partial_t \varphi - \Delta\left(\varepsilon_\varphi^2\,(-\Delta)\,\varphi - \frac{\chi^{AB}}{2}\varphi + \frac{1}{\mu}\left((\varphi - 1)_+ + (\varphi + 1)_-\right)\right) + \alpha\,(\varphi - m) = 0, \tag{3.51}$$

unit mobility version of (3.41), with the constant IC (cf. (3.35c))

$$\varphi_0\,(x) \equiv \widetilde{m}, \qquad -1 \leq \widetilde{m} \leq 1, \qquad \text{viz.} \qquad \overline{\varphi_0} = \widetilde{m}. \tag{3.52}$$

At $t = 0$,

$$\partial_t \varphi \equiv -\alpha\,(\widetilde{m} - m)\,, \tag{3.53}$$

since the Laplacian $-\Delta$ of any constant is zero, and $-1 \leq \widetilde{m} \leq 1$ means that there is no penalty contribution i.e. $\partial_t \varphi$ is constant in space (and zero if $\widetilde{m} = m$). Using $\varphi = \widetilde{m}$ and re-writing (3.53) (cf. (3.49), (3.50)) yields

$$\partial_t\,(\varphi - m) \equiv -\alpha\,(\varphi - m) \quad \Rightarrow \quad \varphi\,(x, t) \equiv m + (\widetilde{m} - m)\,\mathrm{e}^{-\alpha t} \to m \quad \text{as } t \to \infty. \tag{3.54}$$

Hence this (simple) exact solution is constant in space.

3.6 Summary

In this brief chapter, we derived our 2-phase model for DBCs, and explored some of its basic properties. The main idea is that DBCs self-assemble so as to minimise their free energy, which we expressed as a functional of a phase variable which, in turn, captures the structure of the DBC. We thus seek to solve an energy minimisation problem. To facilitate this process, we wrote down a set of mass conserving, energy decaying, local gradient flow dynamics in terms of the aforementioned phase variable. We explore this energy minimisation problem in detail in the forthcoming chapters.

Notes

[1]Equivalently, the length of the type A monomer chain as a proportion of the total length of each DBC macromolecule.

[2]See the sentence just above (4.22) in Choksi and Ren (2003). Our matrix $\mathcal{B}$ is equivalent to the V of that reference.

[3]See the sentence just below (2.1) in Choksi and Ren (2003).

[4]Details are as follows:

$$\begin{aligned}
\mathcal{I}(\boldsymbol{\phi}) &= \frac{\varepsilon_A^2}{2}|\nabla\phi_A|^2 + \varepsilon_{AB}^2|\nabla\phi_A\cdot\nabla\phi_B| + \frac{\varepsilon_B^2}{2}|\nabla\phi_B|^2 \\
&= \frac{\varepsilon_A^2}{2}|\nabla\phi|^2 + \varepsilon_{AB}^2|\nabla\phi\cdot\nabla(1-\phi)| + \frac{\varepsilon_B^2}{2}|\nabla(1-\phi)|^2 \\
&= \frac{\varepsilon_A^2}{2}|\nabla\phi|^2 - \varepsilon_{AB}^2|\nabla\phi|^2 + \frac{\varepsilon_B^2}{2}|\nabla\phi|^2 \\
&= \left(\frac{\varepsilon_A^2}{2} - \varepsilon_{AB}^2 + \frac{\varepsilon_B^2}{2}\right)|\nabla\phi|^2 \\
&= \left(\frac{\varepsilon_A^2}{2} - \varepsilon_{AB}^2 + \frac{\varepsilon_B^2}{2}\right)\left|\nabla\frac{1+\varphi}{2}\right|^2 \\
&= \frac{1}{2}\left(\frac{1}{4}\left(\varepsilon_A^2 - 2\varepsilon_{AB}^2 + \varepsilon_B^2\right)\right)|\nabla\varphi|^2 = \frac{\varepsilon_\varphi^2}{2}|\nabla\varphi|^2 = \mathcal{I}(\nabla\varphi)
\end{aligned}$$

where ε_φ^2 is defined in (3.16).

[5]Details are as follows:

$$\begin{aligned}
\mathcal{B}(\boldsymbol{\phi}) &= \frac{1}{2\Theta}\left(\mathcal{B}^{AA}(\phi_A)^2 + 2\mathcal{B}^{AB}\phi_A\phi_B + \mathcal{B}^{BB}(\phi_B)^2 - \left(\mathcal{B}^{AA}\phi_A + \mathcal{B}^{BB}\phi_B\right)\right) \\
&= \frac{1}{2\Theta}\left(\mathcal{B}^{AA}\left(\frac{1+\varphi}{2}\right)^2 + \mathcal{B}^{AB}\frac{1-\varphi^2}{2} + \mathcal{B}^{BB}\left(\frac{1-\varphi}{2}\right)^2 - \left(\mathcal{B}^{AA}\frac{1+\varphi}{2} + \mathcal{B}^{BB}\frac{1-\varphi}{2}\right)\right) \\
&= \frac{1}{2\Theta}\left(\frac{\mathcal{B}^{AA}}{4} - \frac{\mathcal{B}^{AB}}{2} + \frac{\mathcal{B}^{BB}}{4}\right)\left(\varphi^2 - 1\right) \\
&= \frac{1}{4\Theta}\left(\mathcal{B}^{AB} - \frac{1}{2}\left(\mathcal{B}^{AA} + \mathcal{B}^{BB}\right)\right)\left(1-\varphi^2\right) = \frac{\chi^{AB}}{4}\left(1-\varphi^2\right),
\end{aligned}$$

where χ^{AB} is defined in (3.18).

[6]$\mathcal{B}^{AB}$ measures the interaction and repulsion of dislike A and B monomers, $\mathcal{B}^{AA}$ and $\mathcal{B}^{BB}$ the repulsion of like monomers with themselves. $\chi^{AB} > 0$ means that $\mathcal{B}^{AB} > \frac{1}{2}\left(\mathcal{B}^{AA} + \mathcal{B}^{BB}\right)$, or in words, the (dislike) AB repulsion effect is greater than the average of the (like) AA and BB effects i.e. '*in a block copolymer, dislike monomers repel each other more than like ones do*' – see the comment just after (4.22) in Choksi and Ren (2003).

[7]See the MATLAB working script `plot_regularised_energy_bulk.m` in the `bitbucket` repository.

[8]The detailed working is as follows: using (3.8a),

$$\begin{aligned}
\int_\Omega \mathcal{N}(\boldsymbol{\phi})\,\mathrm{d}\Omega &= \frac{\gamma_A}{2}\left\|\phi_A - \overline{\phi_A}\right\|_{-1}^2 + \gamma_{AB}\left(\phi_A - \overline{\phi_A}, \phi_B - \overline{\phi_B}\right)_{-1} + \frac{\gamma_B}{2}\left\|\phi_B - \overline{\phi_B}\right\|_{-1}^2 \\
&= \frac{\gamma_A}{2}\left\|\frac{1+\varphi}{2} - \overline{\frac{1+\varphi}{2}}\right\|_{-1}^2 + \gamma_{AB}\left(\frac{1+\varphi}{2} - \overline{\frac{1+\varphi}{2}}, \frac{1-\varphi}{2} - \overline{\frac{1-\varphi}{2}}\right)_{-1} \\
&\quad + \frac{\gamma_B}{2}\left\|\frac{1-\varphi}{2} - \overline{\frac{1-\varphi}{2}}\right\|_{-1}^2 \\
&= \frac{1}{4}\Big(\frac{\gamma_A}{2}\left\|1+\varphi - \overline{1+\varphi}\right\|_{-1}^2 + \gamma_{AB}\left(1+\varphi - \overline{1+\varphi}, 1-\varphi - \overline{1-\varphi}\right)_{-1} \\
&\quad + \frac{\gamma_B}{2}\left\|1-\varphi - \overline{1-\varphi}\right\|_{-1}^2\Big) \\
&= \frac{1}{4}\left(\frac{\gamma_A}{2}\left\|\varphi - \overline{\varphi}\right\|_{-1}^2 + \gamma_{AB}\left(\varphi - \overline{\varphi}, -\varphi + \overline{\varphi}\right)_{-1} + \frac{\gamma_B}{2}\left\|-\varphi + \overline{\varphi}\right\|_{-1}^2\right)
\end{aligned}$$

$$= \frac{1}{2}\left(\frac{1}{4}\left(\gamma_A - 2\gamma_{AB} + \gamma_B\right)\right)\left\|\varphi - \overline{\varphi}\right\|_{-1}^2 = \frac{\alpha}{2}\left\|\varphi - \overline{\varphi}\right\|_{-1}^2,$$

where α is defined in (3.21b).

[9]The closest version of the energy in Choksi and Ren (2003) to ours, and the one on which we base the above is their (5.1), in which

$$C_1 = \frac{\ell^2}{24a\left(1-a\right)}, \qquad\qquad C_2 = \frac{9}{2\ell^2 N^2 a^2\left(1-a\right)^2}.$$

To get from (5.1) to (5.2) in Choksi and Ren (2003), the authors re-scale space $x \to \widehat{x}$ i.e. $\Omega \to D$, where each spatial dimension scales as $\widehat{x} = |\Omega|^{-1/3}x$, which means that $|D| = 1$. They then also (presumably) replace their u_A with $\frac{1+\psi}{2}$ (cf. our (3.11b)) but this is not entirely clear given the errors ('$\psi = 1 - 2u_A$' and '$m = 1 - 2a$') on the line immediately after their definition of C_1 and C_2. They also scale the energy by the volume $|\Omega|$ as in their (4.20) in which $I = \beta F/\left(\rho_0|\Omega|\right)$. However, in going from (5.1) to (5.2), it would appear that the authors erroneously *multiplied* (instead of dividing) C_1 and C_2 by 4 to arrive at their ϵ^2 and σ. We contest that their ϵ^2 and σ should therefore be

$$\epsilon^2 = \frac{\ell^2}{48a\left(1-a\right)\chi|\Omega|^{2/3}}, \qquad\qquad \sigma = \frac{9|\Omega|^{2/3}}{4a^2\left(1-a\right)^2\ell^2\chi N^2}.$$

We do not re-scale the volume $\Omega \to D$, and leave χ^{AB} as-is in $\mathcal{B}$ (cf. Fig. 3.2). We do not scale the energy by $|\Omega|$ to work with an energy volume density, and neither do we scale the energy by χ^{AB}. To scale the effects of their transformations out of the above, we therefore use

$$\varepsilon_\varphi^2 = \frac{C_1}{2} = \frac{\ell^2}{48a\left(1-a\right)}, \qquad \text{and} \qquad \alpha = \frac{C_2}{2} = \frac{9}{4a^2\left(1-a\right)^2\ell^2 N^2}.$$

[10]In detail,

$$\nabla\cdot\partial_{\nabla\phi_A}\mathcal{I} = \varepsilon_{AB}^2\Delta\phi_B + \varepsilon_A^2\Delta\phi_A \qquad \text{and} \qquad \nabla\cdot\partial_{\nabla\phi_B}\mathcal{I} = \varepsilon_{AB}^2\Delta\phi_A + \varepsilon_B^2\Delta\phi_B; \tag{3.55}$$

$$\partial_{\phi_A}\mathcal{B}_\mu\left(\boldsymbol{\phi}\right) = \frac{1}{\Theta}\left(\mathcal{B}^{AB}\phi_B + \mathcal{B}^{AA}\phi_A - 2\mathcal{B}^{AA}\right) + \frac{1}{\mu}\left(\left(\phi_A - 1\right)_+ + \left(\phi_A\right)_-\right), \tag{3.56a}$$

and

$$\partial_{\phi_B}\mathcal{B}_\mu\left(\boldsymbol{\phi}\right) = \frac{1}{\Theta}\left(\mathcal{B}^{AB}\phi_A + \mathcal{B}^{BB}\phi_B - 2\mathcal{B}^{BB}\right) + \frac{1}{\mu}\left(\left(\phi_B - 1\right)_+ + \left(\phi_B\right)_-\right). \tag{3.56b}$$

and

$$\partial_{\phi_A}\mathcal{N} = \left(-\Delta_n\right)^{-1}\left(\gamma_{AB}\left(\phi_B - \overline{\phi_B}\right) + \gamma_A\left(\phi_A - \overline{\phi_A}\right)\right) \tag{3.57a}$$

and

$$\partial_{\phi_B}\mathcal{N} = \left(-\Delta_n\right)^{-1}\left(\gamma_{AB}\left(\phi_A - \overline{\phi_A}\right) + \gamma_B\left(\phi_B - \overline{\phi_B}\right)\right). \tag{3.57b}$$

[11]In detail,

$$\frac{\delta\mathcal{E}}{\delta\phi_A} = \varepsilon_A^2\left(-\Delta\right)\phi_A + \varepsilon_{AB}^2\left(-\Delta\right)\phi_B + \left(-\Delta_n\right)^{-1}\left(\gamma_A\left(\phi_A - \overline{\phi_A}\right) + \gamma_{AB}\left(\phi_B - \overline{\phi_B}\right)\right) + \frac{1}{\Theta}\left(\mathcal{B}^{AA}\phi_A + \mathcal{B}^{AB}\phi_B - 2\mathcal{B}^{AA}\right) + \frac{1}{\mu}\left(\left(\phi_A - 1\right)_+ + \left(\phi_A\right)_-\right), \tag{3.58a}$$

and

$$\frac{\delta\mathcal{E}}{\delta\phi_B} = \varepsilon_{AB}^2\left(-\Delta\right)\phi_A + \varepsilon_B^2\left(-\Delta\right)\phi_B + \left(-\Delta_n\right)^{-1}\left(\gamma_{AB}\left(\phi_A - \overline{\phi_A}\right) + \gamma_B\left(\phi_B - \overline{\phi_B}\right)\right) + \frac{1}{\Theta}\left(\mathcal{B}^{AB}\phi_A + \mathcal{B}^{BB}\phi_B - 2\mathcal{B}^{BB}\right) + \frac{1}{\mu}\left(\left(\phi_B - 1\right)_+ + \left(\phi_B\right)_-\right). \tag{3.58b}$$

[12]The detailed working is as follows: substitute $\phi = (\varphi+1)/2$ to arrive at

$$\partial_t\left(\frac{\varphi+1}{2}\right) + \frac{M_A M_B}{M_A+M_B}\left((-\Delta)\,\widetilde{\omega} + 4\alpha\left(\frac{\varphi+1}{2} - \overline{\frac{\varphi+1}{2}}\right)\right) = 0$$

or

$$\partial_t\varphi + \frac{4M_A M_B}{M_A+M_B}\left((-\Delta)\,\frac{\widetilde{\omega}}{2} + \alpha\,(\varphi-\overline{\varphi})\right) = 0$$

and

$$\widetilde{\omega} = 4\left(\varepsilon_\varphi^2\,(-\Delta)\left(\frac{\varphi+1}{2}\right) - \frac{\chi^{AB}}{4}\varphi + \frac{1}{2\mu}\left(\left(\frac{\varphi+1}{2}-1\right)_+ + \left(\frac{\varphi+1}{2}\right)_-\right)\right),$$

or

$$\frac{\widetilde{\omega}}{2} = 2\left(\varepsilon_\varphi^2\,(-\Delta)\left(\frac{\varphi}{2}\right) - \frac{\chi^{AB}}{4}\varphi + \frac{1}{2\mu}\left(\left(\frac{\varphi-1}{2}\right)_+ + \left(\frac{\varphi+1}{2}\right)_-\right)\right),$$

or equivalently

$$\frac{\widetilde{\omega}}{2} = \left(\varepsilon_\varphi^2\,(-\Delta)\,\varphi - \frac{\chi^{AB}}{2}\varphi + \frac{1}{4\mu}\left((\varphi-1)_+ + (\varphi+1)_-\right)\right).$$

Setting $\omega := \frac{\widetilde{\omega}}{2}$ and transforming $\mu \to \frac{\mu}{4}$ (but retaining the same symbol) yields (3.35).

[13]This is risk free as we never actually compute with (3.33), or indeed the ϕ_A, ϕ_B dynamical equations.

[14]Another way to see this is as follows: using (3.12a), we see that

$$\frac{\delta\mathcal{E}}{\delta\phi} = \frac{\delta\mathcal{E}}{\delta\phi_A}\partial_\phi\phi_A + \frac{\delta\mathcal{E}}{\delta\phi_B}\partial_\phi\phi_B = \frac{\delta\mathcal{E}}{\delta\phi_A} - \frac{\delta\mathcal{E}}{\delta\phi_B}. \tag{3.59}$$

Substituting this into (3.25), leads to the (redundant) pair

$$\partial_t\phi - \frac{M_A M_B}{M_A+M_B}\Delta\left(\frac{\delta\mathcal{E}}{\delta\phi}\right) = 0 \qquad \text{and} \qquad -\partial_t\phi + \frac{M_A M_B}{M_A+M_B}\Delta\left(\frac{\delta\mathcal{E}}{\delta\phi}\right) = 0. \tag{3.60}$$

We transform the first of these (either will do) using our preferred 2-phase order parameter φ as in (3.11a) and (3.11b) to arrive at

$$\partial_\varphi\phi\partial_t\varphi - \frac{M_A M_B}{M_A+M_B}\Delta\left(\frac{\delta\mathcal{E}}{\delta\varphi}\partial_\phi\varphi\right) = 0$$

whence

$$\frac{1}{2}\partial_t\varphi - \frac{M_A M_B}{M_A+M_B}\Delta\left(2\frac{\delta\mathcal{E}}{\delta\varphi}\right) = 0 \qquad \Rightarrow \qquad \partial_t\varphi + \frac{4M_A M_B}{M_A+M_B}\,(-\Delta)\left(\frac{\delta\mathcal{E}}{\delta\varphi}\right) = 0. \tag{3.61}$$

It is clear then, that we need dynamics for φ in which

$$\partial_t\varphi - \frac{4M_A M_B}{M_A+M_B}\Delta\left(\frac{\delta\mathcal{E}}{\delta\varphi}\right) = \partial_t\varphi - \nabla\cdot\left(\frac{4M_A M_B}{M_A+M_B}I\nabla\frac{\delta\mathcal{E}}{\delta\varphi}\right) = 0.$$

[15]This is a useful property, because it means that we can compute with random ICs that have nearly, but not exactly the control mass average.

Chapter 4

Energy minimisation: analysis

Problem description

We define the energy functional

$$\mathcal{E}[\varphi] = \frac{\varepsilon_\varphi^2}{2}|\varphi|_1^2 + (\mathcal{B}(\varphi), 1) + \frac{\alpha}{2}\|\varphi - \overline{\varphi}\|_{-1}^2, \tag{4.1a}$$

with homogeneous free energy density

$$\mathcal{B}(\varphi) := \frac{\chi^{AB}}{4}\left(1 - \varphi^2\right). \tag{4.1b}$$

Our problem is to: find $\varphi \in H^1(\Omega)$ such that

$$\mathcal{E}[\varphi] \to \min, \tag{4.1c}$$

with the integral (isoperimetric) constraint that

$$\overline{\varphi} = m, \tag{4.1d}$$

for a given control mass m, with $|m| \leq 1$, and where we insist that

$$|\varphi(x)| \leq 1 \qquad \text{a.e. in } \Omega. \tag{4.1e}$$

Contents

4.1 Preliminaries **48**
4.2 The stationary problem: a variational inequality **53**
4.3 A gradient flow, non-local evolutionary problem **56**
4.4 An alternate splitting **62**
4.5 Summary and conclusions **66**

Chapter outline and solution approach

We consider a 2-phase energy minimisation problem involving the double-obstacle homogeneous free energy, in which we combine (4.1b) and (4.1e) into

$$\mathcal{B}_{[-1,1]}(\varphi) := \begin{cases} \mathcal{B}(\varphi), & |\varphi| \leq 1 \\ \infty, & \text{otherwise.} \end{cases} \tag{3.17}$$

According to Blowey and Elliott (1991), this form of the free energy[1] originates with Oono and Puri (1988) and caters for the boundedness constraint (4.1e) in that the energy becomes unbounded unless (4.1e) holds a.e. A key focus is on approximating $\mathcal{B}_{[-1,1]}$ in (3.17).

- In Section 4.2, we pose the **stationary 2-phase energy minimisation problem** and derive the **variational inequality** that minimisers must satisfy. We establish key existence and smoothness properties of solutions of this inequality.

  This section is similar to Section 3 of Blowey and Elliott (1991), and also draws on elements of Section 2 of Blank et al. (2011).

- We consider a **dynamic version of the problem** in Section 4.3. We introduce a gradient flow, and seek a trajectory along which the energy is guaranteed to decay. Finding low energy morphologies thus involves solving a non-linear, time-dependent variational inequality.

  This section is similar to Section 2 of Blowey and Elliott (1991).

Remark. This chapter draws heavily on Blowey and Elliott (1991). Most of the proofs of our results are adapted from the corresponding portions of that paper. **For brevity and clarity, our proofs appear in Appendix B.** Key differences include the fact that a) we use a C^1 regularisation of $\mathcal{B}_{[-1,1]}$ in (3.17) (theirs is C^2) and, b) we include a non-local component i.e. $\alpha > 0$.

4.1 Preliminaries

4.1.1 Admissible sets

We work with two sets of admissible functions.

Definition 4.1.1. (Admissible sets) *We define the admissible sets*[2]

$$\mathscr{A} := \left\{ \varphi \in H^1(\Omega) \mid |\varphi(x)| \leq 1 \text{ a.e. in } \Omega. \right\}, \tag{4.2a}$$

$$\mathscr{A}_m := \{ \varphi \in \mathscr{A} \mid \overline{\varphi} = m \}. \tag{4.2b}$$

Lemma 4.1.2. (Convexity) *The sets $\mathscr{A}$ and $\mathscr{A}_m$ are convex.*

We prove this result in Appendix B.1 on p. 345.

Remark. For $\mathcal{E} < \infty$, it is necessary that $\varphi \in H^1(\Omega)$. We do not anticipate the non-local operator $(-\Delta_n)^{-1}$ putting additional smoothness restrictions on φ because it is applied to the zero mass function $\varphi - \overline{\varphi}$. Since $H^1(\Omega) \subset \left(H^1(\Omega)\right)'$, we infer the existence of Φ (at least as smooth as φ), with $-\Delta\Phi = \varphi - \overline{\varphi}$. In general, for a given φ, Φ need not be unique, but *the energy in* (4.1a) *is*.[3]

Definition 4.1.3. (Subsets of Ω) *For $\varphi \in \mathscr{A}, \mathscr{A}_m$, define the (potentially disjoint) sets*

$$\Omega_{AB} := \{x \in \Omega \,|\, |\varphi(x)| < 1\}, \tag{4.3a}$$

$$\Omega_{\overline{A}} := \left\{x \in \overline{\Omega} \,|\, \varphi(x) = 1\right\}, \tag{4.3b}$$

$$\Omega_{\underline{B}} := \left\{x \in \overline{\Omega} \,|\, \varphi(x) = -1\right\}. \tag{4.3c}$$

While we have no *a priori* expectation that any of these sets should be non-empty, we must have $\Omega_{\overline{A}} \cup \Omega_{\underline{B}} \cup \Omega_{AB} = \Omega$.

We identify Ω_{AB} with AB and BA interface layers and $\Omega_{\overline{A}}$ ($\Omega_{\underline{B}}$) with the regions/s of pure phase A (B) material (at which $\varphi = \pm 1$). Ω_{AB} is the part of Ω on which the obstacle constraint (4.1e) is *inactive*; the obstacle is *active* on $\Omega_{\overline{A}}$ and $\Omega_{\underline{B}}$. If $m = \pm 1$, then $\Omega_{AB} = \emptyset$ and either $\Omega_{\overline{A}} = \Omega$ or $\Omega_{\underline{B}} = \Omega$.[4]

4.1.2 The non-local chemical potential

Definition 4.1.4. (Chemical potential) *Define the non-local chemical potential,*[5] *as*

$$\psi := \varepsilon_\varphi^2 (-\Delta)\varphi - \frac{\chi^{AB}}{2}\varphi + \alpha(-\Delta_n)^{-1}(\varphi - \overline{\varphi}). \tag{4.4}$$

4.1.3 A regularisation of the homogeneous energy density

In order to work with (3.17), we introduce the Moreau–Yosida[6] regularisation,[7]

$$W^{2,\infty}(\mathbb{R}) \supset C^1(\mathbb{R}) \ni \mathcal{B}_\mu(\varphi) := \mathcal{B}(\varphi) + \Upsilon_\mu(\varphi), \tag{4.5a}$$

for $0 < \mu \ll 1$, where the regularisation is governed by the convex function[8]

$$\Upsilon_\mu(r) := \frac{1}{2\mu}\left[(r-1)_+^2 + (r+1)_-^2\right] = \mathcal{B}_\mu(r) - \frac{\chi^{AB}}{4}\left(1 - r^2\right) \geq 0 \quad \forall \quad r \in \mathbb{R}. \tag{4.5b}$$

The corresponding regularised energy (cf. (4.1a)) is defined as[9]

$$\mathcal{E}_\mu[\varphi] := \frac{\varepsilon_\varphi^2}{2}|\varphi|_1^2 + (\mathcal{B}_\mu(\varphi), 1) + \frac{\alpha}{2}\|\varphi - \overline{\varphi}\|_{-1}^2 = \mathcal{E}[\varphi] + \mathcal{E}_{\text{penalty}}$$
$$\text{where} \qquad \mathcal{E}_{\text{penalty}} := (\Upsilon_\mu(\varphi), 1) \geq 0. \tag{4.6}$$

If $\varphi \in \mathscr{A} \supset \mathscr{A}_m$, then $\mathcal{E}_{\text{penalty}} = 0$, and (4.6) reduces to (4.1a). The value of μ regulates the degree to which violations of the boundedness constraint (4.1e) are penalised. We expect

smaller values of μ to yield functions which more closely adhere to (4.1e). To retrieve and solve our original problem, we will send $\mu \downarrow 0$.

The first derivative of the regularised homogeneous energy density $\mathcal{B}_\mu$ is

$$\mathcal{B}'_\mu(r) = -\frac{\chi^{AB}}{2} r + \Upsilon'_\mu(r) \tag{4.7}$$

where[10]

$$\Upsilon'_\mu(r) = \zeta_\mu(r) = \zeta^+_\mu(r) + \zeta^-_\mu(r); \quad \zeta^+_\mu(r) := \frac{1}{\mu}(r-1)_+; \quad \zeta^-_\mu(r) := \frac{1}{\mu}(r+1)_-. \tag{4.8}$$

$\mathcal{B}'_\mu$ is a Lipschitz continuous, piecewise linear function with

$$\mathcal{B}'_\mu(-1) = \frac{\chi^{AB}}{2} \qquad \text{and} \qquad \mathcal{B}'_\mu(1) = -\frac{\chi^{AB}}{2}, \tag{4.9}$$

and

$$\left|\mathcal{B}'_\mu(r) - \mathcal{B}'_\mu(s)\right| \leq L(\mu)|r-s| \qquad \text{with Lipschitz constant} \qquad L(\mu) = \frac{1}{\mu} < \infty \tag{4.10}$$

for $\mu > 0$. The minima of $\mathcal{B}_\mu$ occur at

$$\mathcal{B}'_\mu(r) = 0 \qquad \Leftrightarrow \qquad r = \frac{\pm 2}{2 - \chi^{AB}\mu}, \tag{4.11}$$

so that as $\mu \downarrow 0$, these tend to $r = \pm 1$ (for any $\chi^{AB} > 0$). Hence,

$$\begin{aligned}\mathcal{B}_\mu(r) &\geq \frac{\chi^{AB}}{4}\left(1 - \left(\frac{2}{2-\chi^{AB}\mu}\right)^2\right) + \frac{1}{2\mu}\left(\frac{2}{2-\chi^{AB}\mu} - 1\right)^2 \\ &= \frac{\left(\chi^{AB}\right)^2\left(\frac{\mu}{4} - \frac{1}{2}\right)}{\left(2-\chi^{AB}\mu\right)^2}\mu \geq -C_0\left(\chi^{AB}\right)\mu\end{aligned} \tag{4.12}$$

for C_0 a positive constant, which is independent of μ, as long as

$$0 < \mu < \min\left\{2, \frac{2}{\chi^{AB}}\right\} =: \mu_{\max}. \tag{4.13}$$

The second derivative of $\mathcal{B}_\mu$ is the piecewise-constant, discontinuous $L^\infty(\mathbb{R})$ function

$$\mathcal{B}''_\mu(r) = -\frac{\chi^{AB}}{2} + \zeta'_\mu(r) \qquad \text{where} \qquad 0 \leq \zeta'_\mu(r) = \frac{1}{\mu}\begin{Bmatrix} 0 & |r| \leq 1 \\ 1 & |r| > 1 \end{Bmatrix} \leq \frac{1}{\mu}. \tag{4.14a}$$

It follows that

$$0 \leq \mu\zeta'_\mu(r) \leq 1 \qquad \text{for every} \qquad r \in \mathbb{R}. \tag{4.14b}$$

Finally,[11]

$$\Upsilon_\mu(r) = \frac{(\mu\zeta_\mu(r))^2}{2\mu} = \frac{\mu}{2}(\zeta_\mu(r))^2, \tag{4.15}$$

and likewise, since Υ_μ is convex,[12]

$$\frac{\Upsilon_\mu(r) - \Upsilon_\mu(s)}{r-s} \geq \Upsilon'_\mu(s) = \zeta_\mu(s) \qquad \Rightarrow \qquad \Upsilon_\mu(r) \geq \Upsilon_\mu(s) + \zeta_\mu(s)(r-s) \tag{4.16}$$

for any $r, s \in \mathbb{R}$.[13] Notice that (4.10) holds for any finite $\chi^{AB} \in \mathbb{R}$. Setting $\chi^{AB} = 0$, we find that $\zeta_\mu(r)$ is also Lipschitz continuous, with the same Lipschitz constant, viz.

$$|\zeta_\mu(r) - \zeta_\mu(s)| \leq \frac{1}{\mu}|r-s|. \tag{4.17}$$

Setting $s = 0$ in (4.10) and then (4.17) yields

$$\left|\mathcal{B}'_\mu(r)\right| \leq \frac{|r|}{\mu} \qquad \text{and} \qquad |\zeta_\mu(r)| \leq \frac{|r|}{\mu}. \tag{4.18}$$

It is also clear that $\zeta_\mu(r)$ is a monotone non-decreasing function, and so

$$(\zeta_\mu(r) - \zeta_\mu(s))(r-s) \geq 0 \qquad \text{for every} \qquad r, s \in \mathbb{R}; \tag{4.19a}$$

since $\zeta_\mu(0) = 0$,

$$r\zeta_\mu(r) \geq 0 \qquad \text{for every} \qquad r \in \mathbb{R}. \tag{4.19b}$$

Finally, we define[14] (cf. (4.8))

$$\zeta(r) := \mu\left(\frac{\chi^{AB}}{2}r + \mathcal{B}'_\mu(r)\right) = \mu\zeta_\mu(r) = (r-1)_+ + (r+1)_-. \tag{4.20a}$$

This μ-independent function is Lipschitz continuous with

$$|\zeta(r) - \zeta(s)| \leq |r-s| \qquad \text{for every} \qquad r, s \in \mathbb{R}. \tag{4.20b}$$

It has a piecewise-constant, discontinuous $L^\infty(\mathbb{R})$ derivative,[15]

$$\zeta'(r) = \begin{Bmatrix} 0 & |r| \leq 1 \\ 1 & |r| > 1 \end{Bmatrix} \qquad \Rightarrow \qquad 0 \leq \zeta'(r) \leq 1 \qquad \text{for every} \qquad r \in \mathbb{R}, \tag{4.21}$$

and is monotone non-decreasing (see Fig. 4.1d and (4.19a)), which means that

$$(\zeta(r) - \zeta(s))(r-s) \geq 0 \qquad \text{for every} \qquad r, s \in \mathbb{R}. \tag{4.22a}$$

Setting $s = 0$, and noting that $\zeta(0) = 0$, gives (cf. (4.19b))

$$r\zeta(r) \geq 0 \qquad \text{for every} \qquad r \in \mathbb{R}. \tag{4.22b}$$

Moreover, according to (4.20a), $\zeta \equiv 0$ on $[-1,1]$, and so for any $r \in \mathbb{R}$,[16]

$$|\zeta(r)| = \left.\begin{cases} -(r+1) & r < -1 \\ 0 & |r| \leq 1 \\ r-1 & r > 1. \end{cases}\right\} \leq r\zeta(r) = \begin{cases} r(r+1) & r < -1 \\ 0 & |r| \leq 1 \\ r(r-1) & r > 1 \end{cases} \quad \Rightarrow \quad |\zeta_\mu(r)| \leq r\zeta_\mu(r). \tag{4.22c}$$

We depict $\mathcal{B}_\mu$ and the various functions related to it, for various μ, in Fig. 4.1 (cf. Fig. 6 of Blowey and Elliott (1991) and Fig. 3.2 on p. 35 of this thesis). Note that[17]

$$\nu \in H^1(\Omega) \qquad \Rightarrow \qquad \zeta_\mu(\nu), \zeta(\nu) \in H^1(\Omega) \qquad \text{for } \mu > 0. \tag{4.23}$$

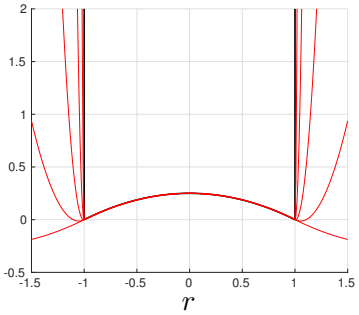

(a) $\mathcal{B}_\mu$ from (4.5a) for various μ in **red**, with the non-smooth $\mathcal{B}_{[-1,1]}$ from (3.17) in **black**

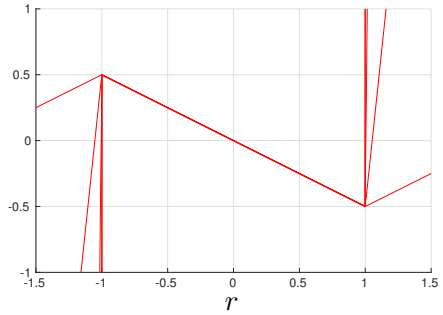

(b) Corresponding first derivatives of $\mathcal{B}_\mu$

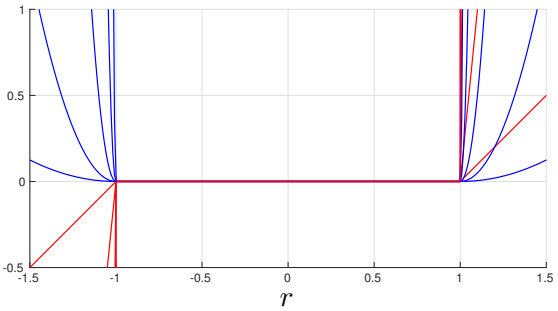

(c) The convex Υ_μ from (4.5b) in **blue** and its monotone, piecewise-linear, first derivative ζ_μ from (4.8) in **red**, for various μ.

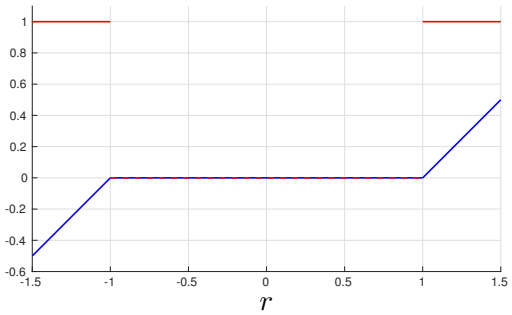

(d) The piecewise-linear, monotone function ζ from (4.20a) in **blue** and its piecewise-constant (discontinuous) first derivative in **red**. Both are μ-independent.

Figure 4.1: The non-smooth $\mathcal{B}_{[-1,1]}$, its Moreau–Yosida regularised version $\mathcal{B}_\mu$, and its first derivative for $\chi^{AB} = 1$ and $\mu \in \{10^0, \ldots, 10^{-4}\}$. The smaller μ is, the more closely $\mathcal{B}_\mu$ resembles $\mathcal{B}_{[-1,1]}$. $\mathcal{B}_{[-1,1]}(r)$ and $\mathcal{B}_\mu(r)$ coincide for $|r| \leq 1$.[18]

Remark. For the rest of this chapter and the next, C **denotes an arbitrary constant, the value of which can change from line to line and term to term.**

4.2 The stationary problem: a variational inequality

We pose (4.1) as the minimisation problem[19]

$$(\mathbf{M}): \qquad \text{given } |m| \leq 1, \text{ find } \varphi \in \mathscr{A}_m \text{ such that} \qquad \mathcal{E}[\varphi] = \min_{\eta \in \mathscr{A}_m} \mathcal{E}[\eta]. \tag{4.24}$$

Lemma 4.2.1. (Existence of a minimiser) *$\mathscr{A}_m$ is non-empty.* (**M**) *has a solution $\varphi \in \mathscr{A}_m$.*

We prove this result in Appendix B.2 on p. 345.

Remark. The minimisers above are not unique.[20]

Going forward, we assume that $|m| < 1$ (*strictly*) since the problem is trivial if $m = \pm 1$. In order to further analyse the problem, we construct the Lagrangian

$$\mathscr{L}(\varphi; \lambda) = \mathcal{E}[\varphi] - \lambda(\overline{\varphi} - m), \tag{4.25}$$

with scalar Lagrange multiplier λ to enforce the mass condition (4.1d).

Lemma 4.2.2. (Variational characterisation of a minimiser) *Suppose that $\varphi \in \mathscr{A}_m$ minimises $\mathscr{L}$, with corresponding $\lambda \in \mathbb{R}$. Then, for every $\psi \in \mathscr{A}$,*

$$\varepsilon_\varphi^2 (\nabla\varphi, \nabla(\psi - \varphi)) - \frac{\chi^{AB}}{2}(\varphi, \psi - \varphi) - \lambda(1, \psi - \varphi) + \alpha\left((-\Delta_n)^{-1}(\varphi - \overline{\varphi}), \psi - \varphi\right) \geq 0. \tag{4.26}$$

We prove this result in Appendix B.3 on p. 347.

We now define two problems which we will analyse in detail.[21]

Definition 4.2.3. (Two problems) *Define the* stationary *problem*

(**S**)*: Find $\{\varphi, \lambda\} \in \mathscr{A}_m \times \mathbb{R}$ such that for every $\psi \in \mathscr{A}$,*

$$\varepsilon_\varphi^2 (\nabla\varphi, \nabla(\psi - \varphi)) - \frac{\chi^{AB}}{2}(\varphi, \psi - \varphi) - \lambda(1, \psi - \varphi) + \alpha\left((-\Delta_n)^{-1}(\varphi - \overline{\varphi}), \psi - \varphi\right) \geq 0, \tag{4.27a}$$

and the critical point *problem,*

(**S**$_C$)*: Find $\varphi \in \mathscr{A}_m$ such that for every $\psi \in \mathscr{A}_m$,*

$$\varepsilon_\varphi^2 (\nabla\varphi, \nabla(\psi - \varphi)) - \frac{\chi^{AB}}{2}(\varphi, \psi - \varphi) + \alpha\left((-\Delta_n)^{-1}(\varphi - \overline{\varphi}), \psi - \varphi\right) \geq 0. \tag{4.27b}$$

Remarks.

i) Problem (**S**) is identical to the variational inequality in (4.26). Solving it yields candidate minimisers, viz. solutions of problem (**M**) in (4.24).

ii) The constant solution $\{\varphi, \lambda\} \equiv \left\{m, -\frac{\chi^{AB}}{2}m\right\}$ solves (**S**), and $\varphi \equiv m$ solves (**S**$_C$).[22]

iii) If we take λ inside the integral in (4.27a), and set $\lambda = \psi$ as in (4.4), then (4.27a) is identically zero. As in Blowey and Elliott (1991), we can regard λ as '*the constant steady state value of the chemical potential*'.

Approach

We have shown that solutions of the stationary problem (**S**) are candidate solutions of the minimisation problem, (**M**). We also introduced problem ($\mathbf{S}_C$). We proceed as follows:

1. We examine problem (**S**) and establish its well-posedness and solution regularity properties via a 2-stage approximation process.

   i) We use the machinery of Section 4.1.3 to regularise (**S**), converting it from an inequality in the set $\mathscr{A}_m$ to an equality over $H^1(\Omega)$; the result is a problem we designate ($\mathbf{S}_\mu$), which involves the regularisation parameter $0 < \mu \ll 1$.

   ii) We approximate ($\mathbf{S}_\mu$) with a finite dimensional Galerkin approximation problem, designated $\left(\mathbf{S}_\mu^{(N)}\right)$. We establish a series of uniform bounds on the solutions of $\left(\mathbf{S}_\mu^{(N)}\right)$, and then invoke compactness results from Lions (1969) to prove various claims about the solutions of ($\mathbf{S}_\mu$). We then send $\mu \downarrow 0$ to recover (**S**).

2. We show that (**S**) and ($\mathbf{S}_C$) are equivalent.

4.2.1 A regularised (stationary) problem

We study the regularised problem:[23]

($\mathbf{S}_\mu$): for given $f \in \mathscr{A}_m$ find $\varphi_\mu \in H^1(\Omega)$ such that

$$\varepsilon_\varphi^2 (\nabla\varphi_\mu, \nabla\eta) + (\varphi_\mu, \eta) + (\zeta_\mu(\varphi_\mu), \eta) + \alpha\left((-\Delta_n)^{-1}(\varphi_\mu - \overline{\varphi_\mu}), \eta\right) = (f, \eta) \tag{4.28}$$

for every $\eta \in H^1(\Omega)$, with ζ_μ as in (4.8).

Remark. We do *not* assert that $\overline{\varphi_\mu} = m$.

Lemma 4.2.4. (Well-posedness, regularity of solutions of ($\mathbf{S}_\mu$)) *Problem* ($\mathbf{S}_\mu$) *has a unique solution* $\varphi_\mu \in H^1(\Omega)$. *If* $\partial\Omega$ *satisfies the requirements of Lemma A.1.9, then*

$$\varphi_\mu \in H^2(\Omega) \qquad \textit{and} \qquad \partial_n\varphi_\mu|_{\partial\Omega} = 0 \qquad \textit{in the sense of trace.} \tag{4.29}$$

[24]The basic idea of the proof is to consider a finite-dimensional, Galerkin approximation of the problem, namely,

$\left(\mathbf{S}_\mu^{(N)}\right)$: for each $N \geq 1$, find $\varphi_\mu^{(N)} \in V^N \in V^N = \operatorname{span}\{e_j\}_{j=1}^N$ such that, for given $f \in \mathscr{A}_m(\Omega)$,

$$\varphi_\mu^{(N)} = \sum_{j=1}^N c_j^N e_j = \boldsymbol{c}\cdot\boldsymbol{e}; \qquad \boldsymbol{c} := \left(c_1^N, c_2^N, \ldots, c_N^N\right)^\top; \qquad \boldsymbol{e} := (e_1, e_2, \ldots, e_N)^\top, \tag{4.30a}$$

where, for every $\eta^{(N)}$,

$$\begin{aligned}\varepsilon_\varphi^2 \left(\nabla\varphi_\mu^{(N)}, \nabla\eta^{(N)}\right) + \left(\varphi_\mu^{(N)}, \eta^{(N)}\right) + \left(P^N\zeta_\mu\left(\varphi_\mu^{(N)}\right), \eta^{(N)}\right) \\ + \alpha\left(P^N(-\Delta_n)^{-1}\left(\varphi_\mu^{(N)} - \overline{\varphi_\mu^{(N)}}\right), \eta^{(N)}\right) = \left(P^N f, \eta^{(N)}\right),\end{aligned} \tag{4.30b}$$

where P^N is from (A.62) and the e_ks are eigenfunctions of $\mathscr{P}$ in Lemma A.1.11. Full details of the proof appear in Appendix B.4 on p. 348.

Theorem 4.2.5. (Existence, regularity of solutions of problem (**S**)) *Problem* (**S**) *in* (4.27a) *has a solution* $\{\varphi, \lambda\} \in \mathscr{A}_m \times \mathbb{R}$. *In particular,*

$$|\varphi| \leq 1 \qquad \text{a.e. in } \Omega, \tag{4.31a}$$

$$\overline{\varphi} = m. \tag{4.31b}$$

If $\partial\Omega$ *is smooth enough to satisfy the requirements of Lemma A.1.9, and* $f \in H^2(\Omega)$, *then*

$$\varphi \in W^{2,p}(\Omega) \quad \text{for every} \quad 1 \leq p < \infty \quad \Rightarrow \quad \varphi \in C^{1,\alpha}\left(\overline{\Omega}\right) \quad \text{for} \quad 0 < \alpha < 1 \tag{4.32}$$

and $d = 1, 2, 3$, *and*

$$\partial_n \varphi|_{\partial\Omega} = 0 \qquad \text{in the sense of trace.} \tag{4.33}$$

This result is a partial counterpart to Lemma 3.2 of Blowey and Elliott (1991); we prove it in Appendix B.5 on p. 354.

We now investigate the structural properties of candidate minimisers in more detail.

Lemma 4.2.6. (Structure of a candidate minimiser) *Suppose that* $\{\varphi, \lambda\} \in \mathscr{A}_m \times \mathbb{R}$ *solves problem* (**S**) *in* (4.27a) *and that* $\partial\Omega$ *satisfies the requirements of Lemma A.1.9. Then* Ω_{AB} *in* (4.3) *is open. Moreover,*

$$-sign(\varphi)\left(\varepsilon_\varphi^2(-\Delta\varphi) - \frac{\chi^{AB}}{2}\varphi - \lambda + \alpha(-\Delta_n)^{-1}(\varphi - m)\right) \geq 0 \quad \text{a.e. in } \Omega, \tag{4.34a}$$

$$\left(\varepsilon_\varphi^2(-\Delta)\varphi - \frac{\chi^{AB}}{2}\varphi - \lambda + \alpha(-\Delta_n)^{-1}(\varphi - m)\right)(|\varphi| - 1) = 0 \qquad \text{a.e. in } \Omega, \tag{4.34b}$$

$$\lambda = -\frac{\chi^{AB}}{2|\Omega_{AB}|}\int_{\Omega_{AB}} \varphi \, \mathrm{d}\Omega + \frac{\alpha}{|\Omega_{AB}|}\int_{\Omega_{AB}} (-\Delta_n)^{-1}(\varphi - \overline{\varphi}) \, \mathrm{d}\Omega. \tag{4.34c}$$

We prove this result in Appendix B.6 on p. 358.

Remarks.

i) (4.34b) says that either $|\varphi| = 1$ (on $\Omega_{\overline{A}} \cup \Omega_{\underline{B}}$) or the 2-phase Integro-Differential Euler–Lagrange Equation (ID-ELE),

$$\varepsilon_\varphi^2(-\Delta)\varphi - \frac{\chi^{AB}}{2}\varphi - \lambda + \alpha(-\Delta_n)^{-1}(\varphi - m) = 0,$$

holds (on Ω_{AB}). We discuss this equation at length, starting in Chapter 6. It governs energy-minimising $A \to B$ and $B \to A$ transitions. Where these transitions impact $\partial\Omega$, a zero Neumann BC holds (cf. (4.33)), whereas a Dirichlet BC ($\varphi(x) = \pm 1$) *and* a tangent condition (zero Neumann BC) hold where they impact $\Omega_{\overline{A}} \cup \Omega_{\underline{B}}$, viz. on the free boundaries $\partial\Omega_{AB} \cap \partial\Omega_{\overline{A}}$ and $\partial\Omega_{AB} \cap \partial\Omega_{\underline{B}}$, because of the global regularity (4.32).

ii) $\overline{(-\Delta_n)^{-1}(\varphi-\overline{\varphi})}=0$, but this does not mean that

$$\int_{\Omega_{AB}}(-\Delta_n)^{-1}(\varphi-\overline{\varphi})\,\mathrm{d}\Omega=0$$

in (4.34c), since we have no information about $(-\Delta_n)^{-1}(\varphi-\overline{\varphi})$ on $\partial\Omega_{AB}$. This is a fundamental difference between this and the Cahn–Hilliard ($\alpha=0$) case.

Corresponding to Proposition 3.3 of Blowey and Elliott (1991), we have the following, which we prove in Appendix B.7 on p. 359.

Lemma 4.2.7. (Equivalence of stationary and critical point problems) *Problems* (**S**) *and* ($\mathbf{S}_C$) *are equivalent.*

Remark. We have *not* asserted (much less proved) that problem (**S**) and ($\mathbf{S}_C$) have unique solutions. As we will see in Chapter 8, minimisers are not generally unique.

We have characterised candidate minimisers in and away from regions of pure phase A/B material, but we have not considered the location of the free boundary. We consider these and other questions in the 1D case, in detail, starting in Chapter 6. For the remainder of this chapter, we consider a dynamic approach to finding low energy morphologies.

4.3 A gradient flow, non-local evolutionary problem

This section corresponds to Section 2 of Blowey and Elliott (1991), and includes elements of the approach followed in Elliott and Garcke (1996).[25] We study the free-boundary, gradient-flow problem (cf. (1.1) in Le (2010)):

Find $\{\varphi(x,t),\psi(x,t)\}$ such that on $\Omega_T:=\Omega\times(0,T)$

$$\partial_t\varphi-\Delta\psi=0, \tag{4.35a}$$

$$(|\varphi|-1)\left(\varepsilon_\varphi^2(-\Delta)\varphi-\frac{\chi^{AB}}{2}\varphi+\alpha(-\Delta_n)^{-1}(\varphi-\overline{\varphi})-\psi\right)=0, \tag{4.35b}$$

$$-\operatorname{sign}(\varphi)\left(\varepsilon_\varphi^2(-\Delta)\varphi-\frac{\chi^{AB}}{2}\varphi+\alpha(-\Delta_n)^{-1}(\varphi-\overline{\varphi})-\psi\right)\geq 0, \tag{4.35c}$$

$$|\varphi|\leq 1, \tag{4.35d}$$

and $|\varphi|=1$, $\nabla\varphi=0$ on the free boundary, subject to the IC

$$\varphi(x,0)=\varphi_0(x), \tag{4.35e}$$

and the zero Neumann BCs

$$\partial_n\varphi|_{\partial\Omega}=\partial_n\psi|_{\partial\Omega}=0. \tag{4.35f}$$

(4.35b)–(4.35d) say that either $\varphi=\pm1$, or,[26]

$$\psi=\varepsilon_\varphi^2(-\Delta)\varphi-\frac{\chi^{AB}}{2}\varphi+\alpha(-\Delta_n)^{-1}(\varphi-\overline{\varphi})\qquad\text{where}\qquad|\varphi|<1. \tag{4.36}$$

Approach

Our three-step approach is as follows:

1. To start, we introduce μ as a parameter governing the regularisation of the double-obstacle (3.17). Using this, we approximate the inequality in (4.35) as an equality.
2. We approximate solutions to the equality problem via an N-dimensional Galerkin approximation. For each N, we establish the well-posedness of the approximation.
3. We retrieve solutions of our original problem by first sending $N \to \infty$, which tells us something about solutions to the equality problem, and then sending $\mu \downarrow 0$, so as to recover solutions of the inequality problem, (4.35).

Mobilities, re-scaling

Notice that (4.35a) excludes a scalar mobility like the M of (1.4b) in Blowey and Elliott (1991). We are able to do this without any loss of generality by re-scaling time to absorb the mobility. On the other hand, we retain χ^{AB}, so as to keep our system as close as possible to the full, physical model.

Two problems

We define the non-local counterparts to problems (**P**) and (**Q**) of Blowey and Elliott (1991):

(**P**): Find $\{\varphi, \psi\}$ with $\varphi \in H^1\left(0,T;\left(H^1(\Omega)\right)'\right) \cap L^\infty\left(0,T;H^1(\Omega)\right)$, $\varphi(\cdot,t) \in \mathscr{A}$ for a.e. $t \in (0,T)$, and $\psi \in L^2\left(0,T;H^1(\Omega)\right)$ such that

$$\langle \partial_t \varphi, \nu_1 \rangle + (\nabla \psi, \nabla \nu_1) = 0 \tag{4.37a}$$

$$\varepsilon_\varphi^2 (\nabla \varphi, \nabla \nu_2 - \nabla \varphi) - \frac{\chi^{AB}}{2} (\varphi, \nu_2 - \varphi) + \alpha \left((-\Delta_n)^{-1} (\varphi - \overline{\varphi}), \nu_2 - \varphi \right) \geq (\psi, \nu_2 - \varphi), \tag{4.37b}$$

for any $\nu_1 \in H^1(\Omega)$, $\nu_2 \in \mathscr{A}$ and a.e. $t \in (0,T)$, and

$$\varphi(0) = \varphi_0 \qquad \text{such that} \qquad \overline{\varphi_0} = m. \tag{4.37c}$$

(**Q**): Find $\varphi \in H^1\left(0,T;\left(H^1(\Omega)\right)'\right) \cap L^\infty\left(0,T;H^1(\Omega)\right)$, $\varphi(t) \in \mathscr{A}_m$ for a.e. $t \in (0,T)$, such that

$$\left((-\Delta_n)^{-1} (\partial_t \varphi), \nu - \varphi \right) + \varepsilon_\varphi^2 (\nabla \varphi, \nabla \nu - \nabla \varphi) - \frac{\chi^{AB}}{2} (\varphi, \nu - \varphi) + \alpha \left((-\Delta_n)^{-1} (\varphi - \overline{\varphi}), \nu - \varphi \right) \geq 0, \tag{4.38}$$

for any $\nu \in \mathscr{A}_m$ and a.e. $t \in (0,T)$, and (4.37c) holds.

Remark. Problems (**S**) and ($\mathbf{S}_C$) in (4.27) are clearly the stationary versions (for which $\partial_t \varphi = 0$) of (**P**) and (**Q**) above. Moreover, there is an *a priori* assumption in posing problem (**Q**), that $\overline{\partial_t \varphi} = 0$.[27]

4.3.1 A regularisation

We now introduce a regularised version of problem ($\mathbf{P}$), which we study in detail.[28]

($\mathbf{P}_\mu$): For given $\mu > 0$, find $\{\varphi_\mu, \psi_\mu\}$ with $\varphi_\mu \in H^1\left(0,T;\left(H^1(\Omega)\right)'\right) \cap L^\infty\left(0,T;H^1(\Omega)\right)$, and $\psi_\mu \in L^2\left(0,T;H^1(\Omega)\right)$ such that

$$\langle \partial_t \varphi_\mu, \nu_1 \rangle + (\nabla \psi_\mu, \nabla \nu_1) = 0, \tag{4.39a}$$

$$\varepsilon_\varphi^2 (\nabla \varphi_\mu, \nabla \nu_2) + \left(\mathcal{B}'_\mu(\varphi_\mu), \nu_2\right) + \alpha\left((-\Delta_n)^{-1}(\varphi_\mu - \overline{\varphi_\mu}), \nu_2\right) = (\psi_\mu, \nu_2) \tag{4.39b}$$

for any $\nu_1, \nu_2 \in H^1(\Omega)$ and a.e. $t \in (0,T)$, along with the IC

$$\varphi_\mu(0) = \varphi_0 \in \mathscr{A}_m. \tag{4.39c}$$

4.3.1.1 A Galerkin approximation to the regularised problem

Our approach matches Section 7.1.2 of Evans (1998) and Sections 3.2 and 4.2.3 of Temam (1997). Let $\mathscr{P}$, $\{e_k\}_{k=1}^\infty$ and V^N be as in Section A.1.3 and Lemma 4.2.4 for the stationary problem. A Galerkin approximation of problem ($\mathbf{P}_\mu$) is (cf. (4.30))

$\left(\mathbf{P}_\mu^{(N)}\right)$: given $0 < \mu < 1$, find $\varphi_\mu^{(N)}(t), \psi_\mu^{(N)}(t) : [0,T] \to V^N$ such that

$$\varphi_\mu^{(N)}(t) = \sum_{j=1}^N c_j^N(t)\, e_j, \qquad \psi_\mu^{(N)}(t) = \sum_{j=1}^N d_j^N(t)\, e_j, \tag{4.40a}$$

$$\left(\partial_t \varphi_\mu^{(N)}, \eta^{(N)}\right) + \left(\nabla \psi_\mu^{(N)}, \nabla \eta^{(N)}\right) = 0 \tag{4.40b}$$

$$\varepsilon_\varphi^2 \left(\nabla \varphi_\mu^{(N)}, \nabla \eta^{(N)}\right) + \left(P^N \mathcal{B}'_\mu\left(\varphi_\mu^{(N)}\right), \eta^{(N)}\right) + \alpha\left(P^N (-\Delta_n)^{-1}\left(\varphi_\mu^{(N)} - \overline{\varphi_\mu^{(N)}}\right), \eta^{(N)}\right) = \left(\psi_\mu^{(N)}, \eta^{(N)}\right), \tag{4.40c}$$

for all $\eta^{(N)} \in V^N$, subject to the IC

$$\varphi_\mu^{(N)}(0) = P^N \varphi_0 \qquad \text{has} \qquad \overline{\varphi_\mu^{(N)}(0)} = m, \tag{4.40d}$$

where in turn φ_0 is as in (4.39c), and the projection P^N is from (A.62). Re-stating (B.11) and (B.14) for every $t \in [0,T]$[29] and considering (4.7),[30] we replace (4.40c) with

$$\varepsilon_\varphi^2 \left(\nabla \varphi_\mu^{(N)}, \nabla \eta^{(N)}\right) - \frac{\chi^{AB}}{2}\left(\varphi_\mu^{(N)}, \eta^{(N)}\right) + \left(\zeta_\mu\left(\varphi_\mu^{(N)}\right), \eta^{(N)}\right) + \alpha\left((-\Delta_n)^{-1}\left(\varphi_\mu^{(N)} - \overline{\varphi_\mu^{(N)}}\right), \eta^{(N)}\right) = \left(\psi_\mu^{(N)}, \eta^{(N)}\right). \tag{4.40e}$$

Remark. The Galerkin approximation is posed for every $t \in [0,T]$: $\varphi_\mu^{(N)}$ and $\psi_\mu^{(N)}$ are in $C\left([0,T]; V^N\right)$, whereas the test functions are from V^N. There are $2N$ coefficient functions (of time) $c_j^N(t), d_j^N(t)$.

Well-posedness of the Galerkin approximation problem

Lemma 4.3.1. (Approximate solutions) *For each integer $N = 1, 2, \ldots$ there exists a unique pair of functions $\left\{\varphi_\mu^{(N)}(t), \psi_\mu^{(N)}(t)\right\}$ satisfying problem $\left(\mathbf{P}_\mu^{(N)}\right)$ in (4.40). Each solution exhibits mass conservation in that*

$$\frac{\mathrm{d}\overline{\varphi_\mu^{(N)}(t)}}{\mathrm{d}t} = 0, \qquad \Rightarrow \qquad \overline{\varphi_\mu^{(N)}(t)} = m, \tag{4.41}$$

for $N = 1, \ldots$ and all $t \in [0, T]$. Moreover, for each N,

$$c_1^N(t) =: c_1(t) = m\,|\Omega|^{1/2} \qquad \text{for every} \qquad t \in [0, T]. \tag{4.42}$$

The proof can be found in Appendix B.8 on p. 362.

Energy estimates

Lemma 4.3.2. (Energy estimates, monotonicity) *For $\varphi_0 \in \mathscr{A}_m$, problem $\left(\mathbf{P}_\mu^{(N)}\right)$ in (4.40) exhibits energy monotonicity in the sense that there exists an N' such that for every $N > N'$,*

$$\mathcal{E}_\mu\left[\varphi_\mu^{(N)}(t)\right] \leq \mathcal{E}_\mu\left[P^N\varphi_0\right] \qquad \text{for any} \qquad 0 \leq t \leq T. \tag{4.43}$$

Likewise for $N > N'$, solutions are bounded uniformly as follows:

$$\left\|\varphi_\mu^{(N)}\right\|_{L^\infty(0,T;H^1(\Omega))} \leq C, \tag{4.44a}$$

$$\left\|\varphi_\mu^{(N)}\right\|_{L^2(0,T;H^1(\Omega))} \leq C, \qquad \left\|\partial_t\varphi_\mu^{(N)}\right\|_{L^2\left(0,T;(H^1(\Omega))'\right)} \leq C, \tag{4.44b}$$

$$\left\|\varphi_\mu^{(N)}\right\|_{H^1\left(0,T;(H^1(\Omega))'\right)} \leq C, \tag{4.44c}$$

$$\left\|\varphi_\mu^{(N)}\right\|_{H^1(\delta,T;H^1(\Omega))} \leq C, \qquad \left\|\varphi_\mu^{(N)}\right\|_{C([\delta,T];H^1(\Omega))} \leq C, \tag{4.44d}$$

$$\text{and} \qquad \left\|\psi_\mu^{(N)}\right\|_{L^2(0,T;H^1(\Omega))} \leq C\left(1 + T^{1/2}\right), \tag{4.44e}$$

for any $\delta > 0$. The constants C are independent of μ and N.

The proof can be found in Appendix B.9 on p. 363.

Remark. We conclude from (4.44c) and (A.37) that each $\varphi_\mu^{(N)} \in C\left([0, T]; \left(H^1(\Omega)\right)'\right)$. However, all this says is that each $\varphi_\mu^{(N)}$ maps continuously from $t \in [0, T]$ to the fairly 'rough' (dual) function space $\left(H^1(\Omega)\right)'$. A more useful consequence of (4.44a)–(4.44c) is (4.45c) in the next theorem.

4.3.1.2 Well-posedness of the regularised problem

Having established the well-posedness of the Galerkin approximation problem, we now hold $\mu > 0$ constant, and send $N \to \infty$ to find a solution to problem $(\mathbf{P}_\mu)$.

Theorem 4.3.3. (Existence of solutions to $(\mathbf{P}_\mu)$) *There exists a weak solution* $\{\varphi_\mu, \omega_\mu\}$ *of problem* $(\mathbf{P}_\mu)$ *in* (4.39)*, with* $\mathcal{B}_\mu$ *as in* (4.5a)*, for which*

$$\|\varphi_\mu\|_{H^1\left(0,T;(H^1(\Omega))'\right)} \leq C, \tag{4.45a}$$

$$\|\varphi_\mu\|_{L^\infty(0,T;H^1(\Omega))} \leq C, \tag{4.45b}$$

$$\|\varphi_\mu\|_{C([0,T];L^2(\Omega))} \leq C, \tag{4.45c}$$

$$\|\varphi_\mu\|_{H^1(\delta,T;H^1(\Omega))} \leq C, \tag{4.45d}$$

$$\text{and} \qquad \|\psi_\mu\|_{L^2(0,T;H^1(\Omega))} \leq C\left(1 + T^{1/2}\right), \tag{4.45e}$$

for any $\delta > 0$*. The constants* C *are independent of* μ*. As a consequence of* (4.45d)*,* $\varphi_\mu \in C\left([\delta, T]; H^1(\Omega)\right)$ *for any* $\delta > 0$*. Moreover,* φ_μ *is mass conserving in that*

$$\overline{\varphi_\mu(t)} = m \qquad \text{for every} \qquad t \in [0, T]. \tag{4.46}$$

The proof of these assertions is very similar to the corresponding parts of Theorems 2.1, 2.2 of Blowey and Elliott (1991), and depends on a standard argument (as in Section 7.4.3 of Robinson (2001)). Details can be found in Appendix B.10 on p. 370.

We now show that solutions to $(\mathbf{P}_\mu)$ are unique.

Theorem 4.3.4. (Uniqueness of solutions) *Suppose that problem* $(\mathbf{P}_\mu)$ *with* $\mathcal{B}_\mu$ *as in* (4.5a) *has two solutions* $U_1 = \{\varphi_1, \psi_1\}$ *and* $U_2 = \{\varphi_2, \psi_2\}$ *with ICs* $(\varphi_1)_0, (\varphi_2)_0 \in \mathscr{A}_m$*. Define their difference as* $U = \{\varphi_\mu, \psi_\mu\} := \{\varphi_1 - \varphi_2, \psi_1 - \psi_2\} = U_1 - U_2$*. If* $(\varphi_1)_0 = (\varphi_2)_0$*, then* $U \equiv \mathbf{0}$*, viz. any solution to problem* $(\mathbf{P}_\mu)$ *is unique.*

The proof is adapted from that of Theorem 2.1 of Blowey and Elliott (1991). Details can be found in Appendix B.11 on p. 375. An alternate version of this result, with some different conclusions is presented in Lemma 4.4.4.

Having established the existence and uniqueness of solutions to $(\mathbf{P}_\mu)$, we now explore their energy properties (cf. Lemma 4.3.1).

Theorem 4.3.5. (Energy monotonicity of $(\mathbf{P}_\mu)$) *The energy defined in* (4.6) *is a Lyapunov functional*[31] *for* $(\mathbf{P}_\mu)$*, in that, for* $\{\varphi_\mu(t), \psi_\mu(t)\}$ *a solution of the problem with IC* (4.39c)*,*

$$\mathcal{E}_\mu[\varphi_\mu(t)] + \int_0^t |\psi_\mu(s)|_1^2 \,\mathrm{d}s \leq \mathcal{E}_\mu[\varphi_0] \qquad \text{for any} \qquad 0 < t \leq T, \tag{4.47a}$$

$$\mathcal{E}_\mu[\varphi_\mu(t)] + \int_{t'}^t |\psi_\mu(s)|_1^2 \,\mathrm{d}s \leq \mathcal{E}_\mu\left[\varphi\left(t'\right)\right] \qquad \text{for any} \qquad 0 < t' \leq t \leq T, \tag{4.47b}$$

i.e. the regularised energy is a non-increasing function of increasing time, and

$$\mathcal{E}_\mu[\varphi_\mu(t)] \leq \mathcal{E}_\mu\left[\varphi_\mu\left(t'\right)\right] \leq \mathcal{E}_\mu[\varphi_0] \qquad \text{for any} \qquad 0 < t' \leq t \leq T. \tag{4.48}$$

Our result is stronger than that in the remark following Theorem 2.1 of Blowey and Elliott (1991); it is the regularised version of the result in their Theorem 2.2.[32] Details of the proof appear in Appendix B.12 on p. 376.

4.3.2 Properties of problems (P) and (Q)

Having established that the regularised problem $(\mathbf{P}_\mu)$ is well-posed, we now study problems $(\mathbf{P})$ and $(\mathbf{Q})$. Recall that we sent $N \to \infty$ for *fixed* $\mu > 0$ in Theorem 4.3.3, but that the bounds in (4.45), (4.58) were uniform in μ. We exploit this property in what follows.

Theorem 4.3.6. (Problems $(\mathbf{P})$ and $(\mathbf{Q})$ have solutions and are equivalent) *Problems* $(\mathbf{P})$ (4.37) *and* $(\mathbf{Q})$ (4.38) *have unique solutions and are equivalent. Moreover,*

$$\overline{\varphi(t)} = m \qquad \text{for every} \qquad t \in [0,T]. \tag{4.49}$$

Suppose that problem $(\mathbf{P})$ *has two solutions* $U_1 = \{\varphi_1, \psi_1\}$ *and* $U_2 = \{\varphi_2, \psi_2\}$ *with ICs* $(\varphi_1)_0, (\varphi_2)_0 \in \mathscr{A}_m$*, and define* $U = U_1 - U_2 = \{\varphi_1 - \varphi_2, \psi_1 - \psi_2\} := \{\varphi, \psi\}$*. Then*[33]

$$\|\varphi(t)\|_{-1}^2 \leq C(t)\,\|\varphi_0\|_{-1}^2 \qquad \text{where} \qquad \varphi_0 := (\varphi_1)_0 - (\varphi_2)_0 \in \mathscr{A}_0. \tag{4.50}$$

An analogous result holds for problem $(\mathbf{Q})$*. Moreover, for* φ *solving problems* $(\mathbf{P})$ *and* $(\mathbf{Q})$*,*

$$\varphi \in H^1\left(\delta, T; H^1(\Omega)\right) \quad \Rightarrow \quad \varphi \in C\left([\delta, T]; H^1(\Omega)\right) \quad \text{for any} \quad \delta > 0. \tag{4.51}$$

Our statement above and proof mimic the first part of Theorem 2.2 of Blowey and Elliott (1991); we send $\mu \downarrow 0$ in problem $(\mathbf{P}_\mu)$, and recover a solution (φ, ψ) of problem $(\mathbf{P})$. The complete proof appears in Appendix B.13 on p. 378.

Remark. Equivalently, $\varphi \in C\left((0,T]; H^1(\Omega)\right)$ in (4.51), above.

Having confirmed the existence, uniqueness and mass conservation of solutions of $(\mathbf{P})$ and $(\mathbf{Q})$, we explore their energy properties.

Theorem 4.3.7. (Energy monotonicity of solutions of $(\mathbf{P})$ and $(\mathbf{Q})$) *The energy defined in* (4.1a) *is a Lyapunov functional for* $(\mathbf{P})$ *and* $(\mathbf{Q})$*, in that, for* $\{\varphi(t), \psi(t)\}$ *a solution of* $(\mathbf{P})$ *and* $\varphi(t)$ *a solution of* $(\mathbf{Q})$*, with IC* (4.37c)*,*[34]

$$\mathcal{E}[\varphi(t)] + \int_0^t |\psi(s)|_1^2 \,\mathrm{d}s \leq \mathcal{E}[\varphi_0] \qquad \text{for any} \qquad 0 < t \leq T, \tag{4.52a}$$

$$\mathcal{E}[\varphi(t)] + \int_{t'}^t |\psi(s)|_1^2 \,\mathrm{d}s \leq \mathcal{E}\left[\varphi\left(t'\right)\right] \qquad \text{for any} \qquad 0 < t' \leq t \leq T. \tag{4.52b}$$

A detailed proof appears in Appendix B.14 on p. 383.

4.3.3 Regularity of solutions

This brief section corresponds to Section 2.2 of Blowey and Elliott (1991).

Lemma 4.3.8. (Higher regularity of solutions of problems $(\mathbf{P}_\mu)$, $(\mathbf{P})$ and $(\mathbf{Q})$) *If $\partial\Omega$ is smooth enough to satisfy the conditions of Lemma A.1.9, then*

$$\varphi, \varphi_\mu \in L^2\left(0,T; H^2(\Omega)\right) \quad \text{and} \quad \partial_n\varphi|_{\partial\Omega} = \partial_n\varphi_\mu|_{\partial\Omega} = 0 \quad \text{for a.e. } t \in (0,T) \tag{4.53}$$

for φ_μ solving problem $(\mathbf{P}_\mu)$ and φ solving $(\mathbf{P})$ and $(\mathbf{Q})$. The normal BCs are in the sense of trace. Moreover, φ_μ and φ are in $C^0\left(\overline{\Omega}\right)$ for a.e. $t \in (0,T)$ and $d = 1, 2, 3$.

If, in addition, the IC is such that $-\Delta\varphi_0 \in H^1(\Omega)$ and $\partial_n\varphi_0|_{\partial\Omega} = 0$, then[35]

$$\varphi, \varphi_\mu \in H^1\left(0,T; H^1(\Omega)\right) \cap L^\infty\left(0,T; H^2(\Omega)\right), \tag{4.54a}$$

$$\psi, \psi_\mu \in L^\infty\left(0,T; H^1(\Omega)\right). \tag{4.54b}$$

We prove these assertions in Appendix B.15 on p. 384.

4.3.4 Behaviour as $t \to \infty$

We now show that we recover minimisers of the stationary problem $(\mathbf{M})$ in (4.24) (viz. solutions of $(\mathbf{S})$ in (4.27a)) as $t \to \infty$.[36] This linchpin result links the stationary and dynamic strands of the work in this chapter.

Lemma 4.3.9. (Asymptotic behaviour as $t \to \infty$) *If $\partial\Omega$ is smooth enough to satisfy the conditions of Lemma A.1.9, then as $t \to \infty$ the solution φ of problems $(\mathbf{P})$ and $(\mathbf{Q})$ satisfies the stationary problems $(\mathbf{S})$ and $(\mathbf{S}_C)$ in (4.27); that is, φ is a candidate solution of the minimisation problem $(\mathbf{M})$ in (4.24).*

The proof of this result appears in Appendix B.16 on p. 387.

Remark. This result, along with those in Theorems 4.3.7 and 4.3.5, explain our interest in gradient flow techniques for energy minimisation. The energy (4.1a) at any time t is always bounded above by that of the IC, and is a non-increasing function of time. We recover (candidate) energy minimisers as $t \to \infty$.

4.4 An alternate splitting

We now propose an alternative to problem $(\mathbf{P}_\mu)$ (4.39) by, in effect, altering the definition of the chemical potential.

$(\mathbf{R}_{\mu,\mathbf{f}})$: given $0 < \mu \ll 1$ and

$$f \in C^1\left([0,T]; L^2_*(\Omega)\right), \tag{4.55}$$

find $\{\varphi_\mu, \omega_\mu\}$ with $\varphi_\mu \in H^1\left(0,T;\left(H^1(\Omega)\right)'\right) \cap L^\infty\left(0,T;H^1(\Omega)\right) \cap H^1\left(\delta,T;H^1(\Omega)\right)$ for any $\delta > 0$, and $\omega_\mu \in L^2\left(0,T;H^1(\Omega)\right)$ such that

$$\langle \partial_t \varphi_\mu, \nu_1 \rangle + (\nabla \omega_\mu, \nabla \nu_1) + \alpha\left(\varphi_\mu - \overline{\varphi_\mu}, \nu_1\right) = (f, \nu_1) \tag{4.56a}$$

$$\varepsilon_\varphi^2 (\nabla \varphi_\mu, \nabla \nu_2) + \left(\mathcal{B}_\mu'(\varphi_\mu), \nu_2\right) = (\omega_\mu, \nu_2), \tag{4.56b}$$

for any $\nu_1, \nu_2 \in H^1(\Omega)$ and a.e. $t \in (0,T)$, and the IC (4.39c) holds.

We have moved the non-local term from (4.39b) in $(\mathbf{P}_\mu)$ to (4.56a) in $(\mathbf{R}_{\mu,\mathbf{f}})$. We have also introduced the function f to support our MMS numerical experiments (in the next chapter). Observe that $\overline{f(t)} = 0$ for every $t \in [0,T]$. We set $f \equiv 0$ to recover $(\mathbf{P}_\mu)$ from $(\mathbf{R}_{\mu,\mathbf{f}})$.

Lemma 4.4.1. (Problems $(\mathbf{P}_\mu)$ and $(\mathbf{R}_{\mu,\mathbf{0}})$ are equivalent) *Problems* $(\mathbf{P}_\mu)$ *and* $(\mathbf{R}_{\mu,\mathbf{0}})$ *are equivalent: if* $\{\varphi_\mu, \psi_\mu\}$ *solves* $(\mathbf{P}_\mu)$*, then* $\{\varphi_\mu, \omega_\mu\}$ *with*

$$(\omega_\mu, \nu) = (\psi_\mu, \nu) - \alpha\left(\left(-\Delta_n\right)^{-1}\left(\varphi_\mu - \overline{\varphi_\mu}\right), \nu\right) \qquad \text{for any} \qquad \nu \in H^1(\Omega), \tag{4.57a}$$

or equivalently (cf. (2.9c)*),*

$$(\nabla \omega_\mu, \nabla \nu) = (\nabla \psi_\mu, \nabla \nu) - \alpha\left(\varphi_\mu - \overline{\varphi_\mu}, \nu\right) \qquad \text{for any} \qquad \nu \in H^1(\Omega), \tag{4.57b}$$

solves $(\mathbf{R}_{\mu,\mathbf{0}})$*, and vice versa.*

The proof of this result appears in Appendix B.17 on p. 390. The equivalence of problems $(\mathbf{R}_{\mu,\mathbf{0}})$ and $(\mathbf{P}_\mu)$ means that solutions of $(\mathbf{R}_{\mu,\mathbf{0}})$ inherit all of the properties of those of $(\mathbf{P}_\mu)$. We summarise these properties in the following Lemma.

Corollary 4.4.2. (Solutions of $(\mathbf{R}_{\mu,\mathbf{f}})$) *There exists a unique solution* $\{\varphi_\mu, \omega_\mu\}$ *of problem* $(\mathbf{R}_{\mu,\mathbf{0}})$ *in* (4.39)*, with* $\mathcal{B}_\mu$ *as in* (4.5a)*, for which*

$$\varphi_\mu \in H^1\left(0,T;\left(H^1(\Omega)\right)'\right) \cap L^\infty\left(0,T;H^1(\Omega)\right) \cap H^1\left(\delta,T;H^1(\Omega)\right)$$

for any $\delta > 0$*, as in* (4.45a)–(4.45d)*, and also (cf.* (4.45e)*)*

$$\|\omega_\mu\|_{L^2(0,T;H^1(\Omega))} \leq C\left(1 + T^{1/2}\right). \tag{4.58}$$

C *is independent of* μ *and* T*. Solutions of* $(\mathbf{R}_{\mu,\mathbf{f}})$ *are mass conserving as in* (4.46)*.* $(\mathbf{R}_{\mu,\mathbf{0}})$ *exhibits energy monotonicity in that* (4.48) *holds for its solutions.*

We prove this result in Appendix B.18 on p. 390.

4.4.1 A local problem: mass *control*

We saw in Corollary 4.4.2 that solutions to $(\mathbf{R}_{\mu,\mathbf{f}})$ in (4.56) having an IC in $\mathscr{A}_m$ (cf. (4.39c)) are mass conserving as in (4.46). We also observe the non-local mass average term $\overline{\varphi_\mu}$ in

$(\mathbf{R}_{\mu,\mathbf{f}})$ which could introduce significant computational difficulty if left in place. We thus replace $\overline{\varphi_\mu}$ with the control mass m in (4.56a) and work with the following (final) version of the problem:

$\left(\mathbf{R}^{(\mathbf{m})}_{\mu,\mathbf{f}}\right)$: given $0 < \mu \ll 1$, $|m| < 1$ and f as in (4.55), find $\{\varphi_\mu, \omega_\mu\}$ as in problem $(\mathbf{R}_{\mu,\mathbf{f}})$ such that

$$\langle \partial_t \varphi_\mu, \nu_1 \rangle + (\nabla \omega_\mu, \nabla \nu_1) + \alpha \left(\varphi_\mu - m, \nu_1\right) = (f, \nu_1) \qquad \text{for every} \qquad \nu_1 \in H^1(\Omega), \tag{4.59}$$

along with (4.56b) for a.e. $t \in (0, T)$, and the IC (4.39c).

If $\varphi_0 \in \mathscr{A}_m$, $\left(\mathbf{R}^{(\mathbf{m})}_{\mu,\mathbf{f}}\right)$ is equivalent to $(\mathbf{R}_{\mu,\mathbf{f}})$, and conserves mass, even if $f \neq 0$. However, if we relax the requirement that $\overline{\varphi_0} = m$, then the two problems are *not* equivalent, and $\left(\mathbf{R}^{(\mathbf{m})}_{\mu,\mathbf{f}}\right)$ *is not mass conserving.* To see this, suppose that $\varphi_0 \equiv m + \delta m$ i.e. $\overline{\varphi_0} = m + \delta m \neq m$. As in Section (2.3.1) of Parsons (2012), setting $\nu_1 = 1$ in (4.59) yields

$$\left(\partial_t \varphi_\mu, 1\right) + \alpha \left(\varphi_\mu - m, 1\right) = 0 \qquad \Rightarrow \qquad \frac{\mathrm{d}}{\mathrm{d}t}\left(\varphi_\mu - m, 1\right) = -\alpha \left(\varphi_\mu - m, 1\right) \tag{4.60}$$

after noting that $\overline{f(t)} = 0$ for every $t \in [0, T]$, which is an ODE for $\left(\varphi_\mu - m, 1\right)(t)$, with IC $\left(\varphi_\mu - m, 1\right)(0) = \left(\varphi_\mu(0) - m, 1\right) = (\varphi_0, 1) - (m, 1) = |\Omega|\, \delta m$, and solution

$$\left(\varphi_\mu - m, 1\right)(t) = |\Omega|\, \delta m \mathrm{e}^{-\alpha t} \qquad \Rightarrow \qquad \overline{\varphi_\mu(t)} = m + \delta m \mathrm{e}^{-\alpha t} \to m \tag{3.50}$$

as $t \to \infty$ (for $\alpha > 0$). We term $\left(\mathbf{R}^{(\mathbf{m})}_{\mu,\mathbf{f}}\right)$ 'mass *controlling*' because of this tendency to drive the mass $\overline{\varphi_\mu} \to m$ exponentially quickly. For problems with $\varphi_0 \in \mathscr{A}_m$, we can replace the energy functional in (4.6), with

$$\mathcal{E}^{(m)}_\mu(t) = \mathcal{E}^{(m)}_\mu\left[\varphi_\mu(t)\right] := \frac{\varepsilon_\varphi^2}{2} \left|\varphi_\mu(t)\right|_1^2 + \left(\mathcal{B}_\mu\left(\varphi_\mu(t)\right), 1\right) + \frac{\alpha}{2} \left\|\varphi_\mu(t) - m\right\|_{-1}^2 \tag{4.61}$$

and be assured of the well-posedness of the non-local energy component for a.e. t.

Remark. Considering ICs in $\mathscr{A}$, but not $\mathscr{A}_m$, has practical value because we anticipate performing simulations of $\left(\mathbf{R}^{(\mathbf{m})}_{\mu,\mathbf{f}}\right)$ in which we cannot guarantee that $\overline{\varphi_0} = m$ exactly.

Outlook

We changed the problem when we introduced the function f and 'localised' it. That said, we will not establish the well-posedness of $\left(\mathbf{R}^{(\mathbf{m})}_{\mu,\mathbf{f}}\right)$ as we did $\left(\mathbf{P}^{(N)}_\mu\right)$ and $(\mathbf{P}_\mu)$, assessing that f is not a core part of the problem. In preparation for our (discrete) numerical analysis, we now (re-)establish boundedness and stability for $\left(\mathbf{R}^{(\mathbf{m})}_{\mu,\mathbf{f}}\right)$, **assuming only that solutions exist if** $f \neq 0$. These results will, in turn, allow us to establish the order of convergence of our numerical method assuming $f \neq 0$, with confidence that the results hold for $f \equiv 0$.

Our analysis of $\left(\mathbf{R}^{(\mathbf{m})}_{\mu,\mathbf{f}}\right)$ in the next two sections uses substantially enhanced versions of the techniques we used in Parsons (2012).[37]

4.4.2 Boundedness

Lemma 4.4.3. (Boundedness of solutions of $\left(\mathbf{R}_{\mu,\mathbf{f}}^{(\mathbf{m})}\right)$) *If* $0 < \mu < \mu_{\max}$ *as in* (4.13), *and* $\mathcal{B}_\mu$ *is as in* (4.5a), *then solutions* φ_μ *of* $\left(\mathbf{R}_{\mu,\mathbf{f}}^{(\mathbf{m})}\right)$ *satisfy*

$$\|\varphi_\mu\|_{L^\infty(0,T;H^1(\Omega))} \leq C \tag{4.62}$$

If, in addition, $\partial\Omega$ *satisfies the smoothness conditions of Lemma A.1.9, and*

$$-\Delta\varphi_0 \in H^1(\Omega) \qquad \text{with} \qquad \partial_n\varphi_0|_{\partial\Omega} = 0, \tag{4.63}$$

then

$$\|\varphi_\mu\|_{H^1(0,T;H^1(\Omega))}, \|\varphi_\mu\|_{L^\infty(0,T;H^2(\Omega))} < C. \tag{4.64}$$

The constants C *are independent of* μ.

The proof of this result appears in Appendix B.19 on p. 390.

Remark. By Sobolev embedding, $\|\varphi_\mu\|_{L^\infty(\Omega)} \lesssim \|\varphi_\mu\|_{H^2(\Omega)}$ for $d = 1, 2, 3$, and so

$$\|\varphi_\mu\|_{L^\infty(0,T;L^\infty(\Omega))} < C \tag{4.65}$$

follows from the second part of (4.64).[38]

4.4.3 Stability, continuous dependence on ICs, uniqueness

Lemma 4.4.4. (Stability, continuous dependence on ICs) *Suppose that* $\left(\mathbf{R}_{\mu,\mathbf{f}}^{(\mathbf{m})}\right)$ *has two solutions* $U_1 = (\varphi_1, \omega_1)$ *and* $U_2 = (\varphi_2, \omega_2)$, *with* $\varphi_1(t), \varphi_2(t) \in H_m^1(\Omega)$ *for a.e.* $t \in (0,T)$, *corresponding to the ICs* $(\varphi_1)_0, (\varphi_2)_0 \in \mathscr{A}_m$. *Define the difference*

$$U = (\varphi_\mu, \omega_\mu) := (\varphi_1 - \varphi_2, \omega_1 - \omega_2) = U_1 - U_2, \qquad \varphi_0 := \varphi_1(0) - \varphi_2(0)$$

in which $\varphi_\mu(t) \in H_*^1(\Omega)$ *for a.e.* $t \in (0,T)$ *and* $\varphi_0 \in \mathscr{A}_0$. $\left(\mathbf{R}_{\mu}^{(\mathbf{m})}\right)$ *is stable and its solutions are continuously dependent on the ICs in that*

$$\|U\|_{L^\infty(0,T;L^2(\Omega))\times L^2(0,T;L^2(\Omega))} \leq C(T,\mu)\|\varphi_0\| \tag{4.66}$$

where $C(T,\mu)$ *depends on* μ, *and*

$$\|U\|^2_{L^\infty(0,T;L^2(\Omega))\times L^2(0,T;L^2(\Omega))} := \|\varphi_\mu\|^2_{L^\infty(0,T;L^2(\Omega))} + \|\omega_\mu\|^2_{L^2(0,T;L^2(\Omega))}. \tag{4.67}$$

Solutions of $\left(\mathbf{R}_{\mu,\mathbf{f}}^{(\mathbf{m})}\right)$ *are unique. In addition,*

$$\|\varphi_\mu\|_{L^\infty\left(0,T;(H^1(\Omega))'\right)} := \operatorname*{ess\,sup}_{t\in(0,T)} \left\{\|\varphi_\mu(t)\|_{-1}\right\} \leq C(T)\|\varphi_0\|_{-1} \tag{4.68}$$

where $C(T)$ *depends on* T, *but is independent of* μ

The proof of this result appears in Appendix B.20 on p. 395.

4.4.4 Energy monotonicity

Finally, we explicitly prove that the energy of solutions of the localised problem $\left(\mathbf{R}^{(\mathbf{m})}_{\mu,\mathbf{0}}\right)$ is monotonically non-increasing in time.

Lemma 4.4.5. (Energy monotonicity of solutions of $\left(\mathbf{R}^{(\mathbf{m})}_{\mu,\mathbf{0}}\right)$) *If $\varphi_0 \in \mathscr{A}_m$, then $\left(\mathbf{R}^{(\mathbf{m})}_{\mu,\mathbf{0}}\right)$ exhibits energy monotonicity in that its solutions satisfy (cf.* (4.48), (4.61)*)*

$$\mathcal{E}^{(m)}_{\mu}\left[\varphi_{\mu}(t)\right] \leq \mathcal{E}^{(m)}_{\mu}\left[\varphi_{\mu}\left(t'\right)\right] \leq \mathcal{E}^{(m)}_{\mu}\left[\varphi_0\right] \qquad \textit{for any} \qquad 0 < t' \leq t \leq T. \tag{4.69}$$

We prove this result in Appendix B.21 on p. 396.

Remark. We set $f \equiv 0$ in considering the energy evolution for $(\mathbf{R}_{\mu,\mathbf{0}})$ and $\left(\mathbf{R}^{(\mathbf{m})}_{\mu,\mathbf{0}}\right)$. In the latter, we also demanded that $\overline{\varphi_0} = m$. For $f \neq 0$, we have no expectation of energy monotonicity, as illustrated in Fig. 4.2.

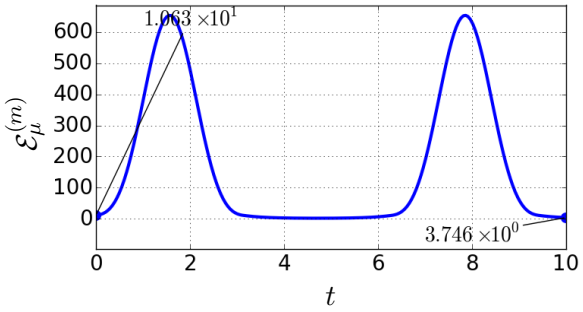

Figure 4.2: An example of the energy evolution for $f \neq 0$; $\mathcal{E}^{(m)}_{\mu}(t)$ is clearly not monotone. (Data taken from the seventh MMS experiment in Set A in Table 5.3 on p. 101.)

4.5 Summary and conclusions

We started this chapter by posing the 2-phase energy minimisation problem. We confirmed that this problem has (potentially non-unique) solutions in the feasible set $\mathscr{A}_m$, and then characterised candidate energy minimisers as solutions of a certain variational inequality. We studied this inequality in detail via a 2-stage approximation process. First, we regularised the obstacle defining $\mathscr{A}_m$ using a C^1-regularisation function to arrive at an equality approximation involving the small parameter, μ. We then studied this equation using an N-dimensional Galerkin approximation. Sending $N \to \infty$, and then $\mu \downarrow 0$, we were able to prove that solutions to the variational inequality exist that are globally C^1.

We then defined a dynamic version of the minimisation problem via a time-dependent gradient flow, which we initially defined as a partial differential inequality. Our approach here was analogous to the time-independent case: we employed a 2-stage approximation to confirm the existence and uniqueness (in the sense of continuous dependence on the ICs)

of solutions to the dynamic inequality. The key advantage of this approach is that it yields solutions for which the energy is non-increasing in time. Finally, we defined and analysed a 'local' version of the gradient flow system, which is a suitable basis for a numerical method.

Most of the results and proofs of this chapter are adapted from the corresponding parts of Blowey and Elliott (1991), and to this extent, we make no claims as to the originality of the ideas in this chapter. We were, however, able to confirm that our C^1 regularisation function could be used in conjunction with a non-local energy component (this was not studied in Blowey and Elliott (1991)).

We studied a number of problems (stationary and dynamic) in this chapter. We summarise their relationships in Fig. 4.3.

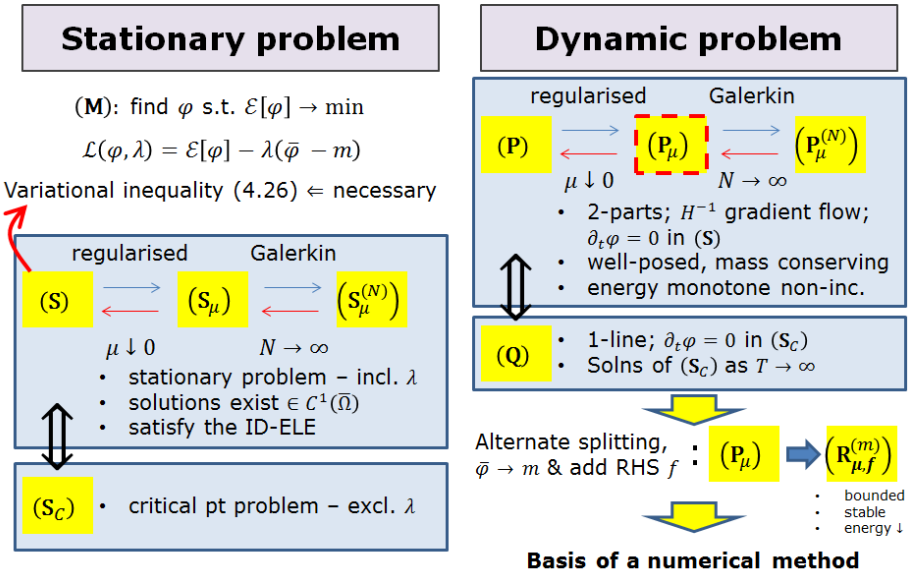

Figure 4.3: Summary of the relationships between the results in Chapter 4

4.5.1 Opportunities for further study

We close by listing possible extensions to the work in this chapter.

i) We did not (re-)establish counterparts for *all* of the results in Blowey and Elliott (1991). For instance, we did not establish a version of the complementarity problem in their Corollary 2.4.

ii) Re-scalings. We deliberately chose not to re-scale the model in this chapter (beyond absorbing the mobility into time). On the one hand, this makes our results cosmetically similar to those in the literature for the Cahn–Hilliard ($\alpha = 0$) model, and this is of particular value in the next chapter where we start assessing the effect of discretising in time and space. On the other hand, without re-scaling, our results above and in the

next chapter could obscure the *actual* dependencies between various parameters, and so our approach could limit our insights. There are several ways to re-scale the model. We explore two of them in Chapters 6–8. It might be useful (albeit tedious) to apply one/both of them to the results of this and the next chapter.

iii) It seems reasonable (and our numerical experiments in Section 5.4.3 suggest) that

$$\|\varphi_\mu\|_{L^\infty(0,T,L^\infty(\Omega))} \leq 1 + C\mu \tag{4.70}$$

with C independent of μ and T, at least in 1D. On the other hand, (B.153) and (B.155) suggest that

$$\|\zeta(\varphi_\mu(t))\|^2 \leq C\mu^2 \qquad \text{and} \qquad |\zeta(\varphi_\mu(t))|_1^2 \leq C\mu \tag{4.71}$$

for a.e. $t \in (0,T)$ (by assumption, $\varphi_\mu(0) = \varphi_0 \in \mathscr{A}$ so $\zeta(\varphi_0) \equiv 0$). Consequently,

$$\|\zeta(\varphi_\mu)\|_1^2 \leq C\mu \qquad \Rightarrow \qquad \operatorname*{ess\,sup}_{t\in(0,T)} \|\zeta(\varphi_\mu(t))\|_1 \leq C\mu^{1/2}.$$

Sobolev embedding (in 1D) implies that $\|\zeta(\varphi_\mu(t))\|_{0,\infty} \lesssim \|\zeta(\varphi_\mu(t))\|_1$, and so

$$\|\zeta(\varphi_\mu)\|_{L^\infty(0,T,L^\infty(\Omega))} \leq C\mu^{1/2}.$$

This and (4.20a) imply that $\|\varphi_\mu\|_{L^\infty(0,T,L^\infty(\Omega))} \leq 1 + C\mu^{1/2}$. It would be useful to reconcile these statements.

Remark. One possibility is that the bound we observed experimentally is due to the solution, and not the regularisation i.e. instead of examining the effect of ζ_μ, we should seek a bound on something like $\|\varphi - \varphi_\mu\|_{L^\infty(0,T;L^\infty(\Omega))}$, as in the next point. Theorem 2.2 (see equation (2.17)) of Barrett and Blowey (2001) is an intriguing result, albeit in the context of a different (logarithmic) homogeneous energy, that may be of use.

iv) In the next chapter, we will approximate φ_μ (numerically) by φ_h, and estimate the resulting numerical error. We may also wish to estimate

$$\begin{aligned} \overbrace{\|\varphi - \varphi_h\|_{X(0,T;Y)}}^{\text{approximation error}} &= \|\varphi - \varphi_\mu + \varphi_\mu - \varphi_h\|_{X(0,T;Y)} \\ &\leq \underbrace{\|\varphi - \varphi_\mu\|_{X(0,T;Y)}}_{\text{regularisation error}} + \underbrace{\|\varphi_\mu - \varphi_h\|_{X(0,T;Y)}}_{\text{numerical error}}. \end{aligned}$$

We saw in this chapter (in Theorem 4.3.6) that $\varphi_\mu \to \varphi$ (in an appropriate sense; cf. (B.149)) as $\mu \downarrow 0$, but we did not attach a rate (in μ) to this convergence. It would be useful to estimate this regularisation error, in order to estimate the total approximation error (in an appropriate norm). Hintermüller and Hinze (2009) could be a helpful reference in any further examination of this issue.

v) We could replace the second degree (4.5b) with the fourth degree

$$\Upsilon_\mu(r) := \frac{1}{4\mu}\left[(r-1)_+^4 + (r+1)_-^4\right] = \mathcal{B}_\mu - \frac{\chi^{AB}}{4}\left(1-r^2\right) \geq 0 \quad \forall \quad r \in \mathbb{R}, \tag{4.72a}$$

for which $\mathcal{B}_\mu(\varphi) \in C^3(\mathbb{R}) \subset W^{4,\infty}(\mathbb{R})$, and (cf. (4.8))

$$\Upsilon'_\mu(r) = \zeta_\mu(r) = \frac{1}{\mu}\left((r-1)_+^3 + (r+1)_-^3\right). \tag{4.72b}$$

In principle, as long as all of the statements in Section 4.1.3 are true of this alternate regularisation, it should be possible to make all of the statements of this chapter using (4.72). We could then use (4.72) as the basis for a different numerical method (to the one we propose in the next chapter). We do some basic numerical experimentation with (4.72) in the next chapter, but make no comparison of this regularisation and the one in (4.5b). An investigation of this topic may be fruitful.

Outlook for the next chapter

In the next chapter, we use the regularisation approach above as the basis for a practical numerical approximation of the dynamic version of the problem, which we then analyse in detail. Our principle interest is in finding low energy morphologies that we hope will be similar to the energy minimisers we characterised in the first part of this chapter.

Notes

[1]See their equation (1.14).

[2]The sets $\mathscr{A}$ and $\mathscr{A}_m$ are the $H^1(\Omega)$ functions satisfying (4.1e), and correspond to K and K_m in Blowey and Elliott (1991). We define the mass, m, in normalised fashion as

$$m := \frac{1}{|\Omega|}(\varphi_0, 1) \in (-1, 1),$$

whereas in Blowey and Elliott (1991), the definition is $m \equiv (\varphi_0, 1) \in (-|\Omega|, |\Omega|)$.

[3]To see this, write (4.1a) as

$$\begin{aligned}\mathcal{E}[\varphi; \Phi + C] &= \int_\Omega \frac{\varepsilon_\varphi^2}{2}|\nabla\varphi|^2 + \frac{\chi^{AB}}{4}\left(1-\varphi^2\right) + \frac{\alpha}{2}(\varphi - \overline{\varphi})(\Phi + C)\ \mathrm{d}\Omega \\ &= \int_\Omega \frac{\varepsilon_\varphi^2}{2}|\nabla\varphi|^2 + \frac{\chi^{AB}}{4}\left(1-\varphi^2\right) + \frac{\alpha}{2}(\varphi - \overline{\varphi})\Phi\ \mathrm{d}\Omega + C\frac{\alpha}{2}\underbrace{\int_\Omega \varphi - \overline{\varphi}\ \mathrm{d}\Omega}_{=0} = \mathcal{E}[\varphi; \Phi].\end{aligned}$$

Consequently, we set $\Phi = (-\Delta_n)^{-1}(\varphi - \overline{\varphi})$ viz. $\overline{\Phi} = 0$ (cf. (2.9) and Lemma A.1.5).

[4]The sets Ω_{AB}, $\Omega_{\overline{A}}$ and $\Omega_{\underline{B}}$ correspond to what Blowey and Elliott (1991) call Ω_0, Ω_+ and Ω_-. We will regard $\Omega_{AB} = \emptyset$ as trivial.

[5]See (1.19) of Blowey and Elliott (1991).

[6]See Hintermüller et al. (2011) and Section 3.2.2 of Grisvard (1985). In this latter reference, an approximation like (4.5) is called the 'Yosida approximation', while that of the derivative in (4.7) is called the 'Moreau approximation'.

[7]See $\psi_\varepsilon \in C^2(\mathbb{R})$ in (2.9) of Blowey and Elliott (1991).

[8]This is our counterpart to $\widehat{\psi}_\varepsilon$ in (2.13), (2.14) of Blowey and Elliott (1991); notice their typo.

[9]See (2.23) of Blowey and Elliott (1991).

[10]See the λ_c in Hintermüller et al. (2011), just after their equation (20).

[11]See (2.15) of Blowey and Elliott (1991).

[12]See (2.16) of Blowey and Elliott (1991).

[13]A simple graphical argument shows that if f is convex, and $b > a$ then

$$\frac{f(b) - f(a)}{b - a} \geq f'(a) \qquad \Rightarrow \qquad f(b) \geq f(a) + f'(a)(b - a).$$

Likewise, for $a > b$,

$$\frac{f(a) - f(b)}{a - b} = \frac{f(b) - f(a)}{b - a} \leq f'(a) \qquad \Rightarrow \qquad f(b) \geq f(a) + f'(a)(b - a).$$

[14]This is our counterpart to β_ε in (2.11) of Blowey and Elliott (1991).

[15]See (2.12) of Blowey and Elliott (1991)

[16]In what follows,

$$r > 1 \quad \Rightarrow \quad r - 1 > 0 \quad \Rightarrow \quad r - 1 < r(r - 1).$$
$$\text{Similarly,} \quad r < -1 \quad \Rightarrow \quad -(r + 1) > 0 \quad \text{and} \quad -r > 1 \quad \Rightarrow \quad -(r + 1) < r(r + 1).$$

Our ζ is identical to the β in (2.43) of Blowey and Elliott (1991).

[17]The proof is as follows: let $\Omega_{|\varphi|>1}$ denote that part of Ω on which $|\varphi(x)| > 1$. Using (4.8),

$$\begin{aligned}\|\zeta_\mu(\varphi)\|^2 = \int_\Omega (\zeta_\mu(\varphi))^2\,\mathrm{d}\Omega &= \frac{1}{\mu^2}\int_{\Omega_{|\varphi|>1}} (|\varphi| - 1)^2\,\mathrm{d}\Omega \\ &\leq \frac{1}{\mu^2}\int_{\Omega_{|\varphi|>1}} \varphi^2\ \mathrm{d}\Omega \leq \frac{1}{\mu^2}\int_\Omega \varphi^2\ \mathrm{d}\Omega = \frac{\|\varphi\|^2}{\mu^2} < \infty\end{aligned}$$

as long as $\mu > 0$. For the semi-norm, $\nabla(\zeta_\mu(\varphi)) = \zeta'_\mu(\varphi)\nabla\varphi$, and so

$$|\zeta_\mu(\varphi)|_1 = \left\|\zeta'_\mu(\varphi)\nabla\varphi\right\| \leq \frac{1}{2}\left(\left\|\zeta'_\mu(\varphi)\right\|^2 + |\varphi|_1^2\right) < \infty \qquad \text{for} \qquad \mu > 0,$$

since, by (4.14a),

$$\left\|\zeta'_\mu(\varphi)\right\|^2 = \int_\Omega \left(\zeta'_\mu(\varphi)\right)^2 \mathrm{d}\Omega \leq \frac{|\Omega|}{\mu^2}.$$

We do not assume that $\varphi \in L^\infty(\Omega)$ above; there is no need to, thanks to (4.8), (4.14a). The proofs for $\zeta(\varphi)$ are similar (except that there is no $1/\mu$ factor or μ restriction). Blowey and Elliott (1991) use this fact immediately below their equation (2.47), but never prove it.

[18]See the MATLAB working script `plot_regularised_energy_bulk.m` in the `bitbucket` repository.

[19]See ($\mathbf{M}_\gamma$), (3.2) of Blowey and Elliott (1991).

[20]See Theorem 3 of Section 8.4 of Evans (1998) for a similar situation which *does* have a unique minimiser.

[21]These correspond to ($\mathbf{S}_\gamma$), ($\mathbf{C}_\gamma$) in (3.1), (3.3) of Blowey and Elliott (1991).

[22]See the first remark in Section 3.1 of Blowey and Elliott (1991).

[23]This problem corresponds to ($\mathbf{S}_{\gamma,\epsilon}$) in Blowey and Elliott (1991).

[24]For further information on trace operators, see Section 5.5 of Evans (1998). The idea is that $\partial\Omega$ has d-dimensional Lebesgue measure zero, which means that we cannot speak of *the* function value there. Trace operators allow us to map from $W^{1,p}(\Omega)$ to $L^p(\Omega)$ and define functions that agree a.e. on the boundary i.e. they define Dirichlet BCs. Functions in $L^p(\Omega)$ only (viz. that cannot sustain at least one derivative) do not have traces (see exercise 14 of Chapter 5 of Evans (1998)). Hence, for a function to have zero Neumann BC, it needs to be able to take two derivatives: a zero Neumann BC on $\varphi \in H^2(\Omega)$, is a zero *Dirichlet* BC on $\varphi' \in H^1(\Omega)$, for which a trace operator exists.

[25]The later reference relates to the Cahn–Hilliard model with a generic homogeneous energy component (quartic polynomial, logarithmic), in which the mobility is multiplied by a function that is zero when $\varphi = \pm 1$.

[26]See (1.19) of Blowey and Elliott (1991).

[27]This is so that $(-\Delta_n)^{-1}(\partial_t\varphi)$ in the first term is well-posed.

[28]See (2.17) of Blowey and Elliott (1991).

[29]In the build-up to these results, we replace each c_i^N with $c_i^N(t)$ for the time-dependent problem.

[30]See (2.21c) of Blowey and Elliott (1991).

[31]The basic idea is that a Lyapunov functional is a function (of $\varphi(t)$) that is non-increasing in time, with the property that if it becomes constant beyond some $t = T'$, then $\varphi(t)$ stops changing. See Defn 10.11 of Robinson (2001).

[32]Evidently, (4.47b) holds for $0 < t' \leq t \leq T$, not $0 < t' < t \leq T$ as in Blowey and Elliott (1991). (4.47a) corresponds to (2.42) in Blowey and Elliott (1991).

[33]See (2.45) of Blowey and Elliott (1991).

[34]What follows corresponds to (2.46) of Blowey and Elliott (1991). In their (2.46b), they assert that the inequality holds '$\forall\, 0 \leq t$'. This inequality should be strict as in our (4.52a) since, as they show in their (2.57), $u \in C\left([\delta, T]; H^1(\Omega)\right)$ for any $\delta > 0$ (strictly).

[35]This next part corresponds to Proposition 2.5 of Blowey and Elliott (1991).

[36]See Section 2.3 of Blowey and Elliott (1991).

[37]This piece of work assumed a quartic homogeneous density function.

[38]Sobolev embedding (cf. Theorem (5.29) of Robinson (2001)) could be invoked for $d = 1$ based on the uniform bound on $\|\varphi_\mu(t)\|_{H^1(\Omega)}$ for a.e. t. In higher dimensions ($d = 2, 3$), $H^2(\Omega)$ membership is required.

Chapter 5

Gradient flow numerical approximations

Earlier, we wrote down the regularised fourth order gradient flow problem with unit mobility (cf. (3.42)), as the pair of second order PDEs,

$$\partial_t \varphi_\mu + (-\Delta)\,\omega_\mu + \alpha\,(\varphi_\mu - m) = 0, \tag{3.48}$$

$$\text{and} \qquad \omega_\mu := \varepsilon_\varphi^2\,(-\Delta)\,\varphi_\mu + \mathcal{B}'_\mu\,(\varphi_\mu)\,, \tag{3.35b}$$

$$\text{with} \qquad \mathcal{B}'_\mu\,(\varphi_\mu) = -\frac{\chi^{AB}}{2}\varphi_\mu + \zeta_\mu\,(\varphi_\mu)\,; \quad \zeta_\mu\,(\varphi_\mu) = \frac{1}{\mu}\,(\varphi_\mu - 1)_+ + \frac{1}{\mu}\,(\varphi_\mu + 1)_-\,, \tag{4.7}$$

subject to the IC

$$\varphi_\mu\,(x,0) = \varphi_0\,(x) \qquad \text{where} \qquad \overline{\varphi_0} = m, \tag{3.35c}$$

and the zero Neumann BCs

$$\partial_n \varphi_\mu|_{\partial\Omega} = 0, \qquad \text{and} \qquad \partial_n \omega_\mu|_{\partial\Omega} = 0. \tag{3.35d}$$

In Chapter 4, we proved that the regularised energy $\mathcal{E}_\mu^{(m)}$ of (4.61) is a non-increasing function of time under these dynamics, and then rigorously analysed the problem,

$\left(\mathbf{R}_{\mu,\mathbf{f}}^{(\mathbf{m})}\right)$: given $0 < \mu \ll 1$ and f as in (4.55), find $\varphi_\mu \in H^1\left(0,T;\left(H^1\,(\Omega)\right)'\right) \cap L^\infty\left(0,T;H^1\,(\Omega)\right)$, and $\omega_\mu \in L^2\left(0,T;H^1\,(\Omega)\right)$ such that

$$\langle \partial_t \varphi_\mu, \nu_1\rangle + (\nabla\omega_\mu, \nabla\nu_1) + \alpha\,(\varphi_\mu - m, \nu_1) = (f, \nu_1)\,, \tag{4.59}$$

$$\text{where} \qquad \varepsilon_\varphi^2\,(\nabla\varphi_\mu, \nabla\nu_2) + \left(\mathcal{B}'_\mu\,(\varphi_\mu)\,, \nu_2\right) = (\omega_\mu, \nu_2)\,, \tag{4.39b}$$

for every $\nu_1, \nu_2 \in H^1\,(\Omega)$ and a.e. $t \in (0,T]$, subject to the IC

$$\varphi_\mu\,(x,0) = \varphi_0\,(x) \in \mathscr{A}_m. \tag{4.39c}$$

We recovered the variational inequality minimising the exact energy $\mathcal{E}$ with double obstacle homogeneous component, as $\mu \downarrow 0$. At this stage, we thus have:

i) A double-obstacle, energy-minimisation problem with corresponding (gradient flow variational inequality) dynamics, based firmly in the physics of DBCs;

ii) Gradient flow equality dynamics involving a regularisation parameter μ; and

iii) A rigorous proof that these problems are well-posed and equivalent in the sense that we recover the variational inequality dynamics (i) as $\mu \downarrow 0$ in (ii).

Contents

5.1 A time (only) discretisation 75
5.2 Solving non-linear, non-differentiable problems 84
5.3 A fully discrete approximation 88
5.4 Numerical experiments 95
5.5 Summary 105

Chapter outline and solution approach

In the current chapter, we pose and analyse a numerical approximation of the regularised gradient flow problem $\left(\mathbf{R}^{(\mathbf{m})}_{\mu,\mathbf{f}}\right)$ for a given $0 < \mu \ll 1$. We regard the solutions of $\left(\mathbf{R}^{(\mathbf{m})}_{\mu,\mathbf{f}}\right)$ as exact, even though they are approximate solutions of the underlying energy-minimisation problem. This approximation forms the basis of a code we then implement to find and visualise approximate minimisers of $\mathcal{E}$. In this respect, our approach differs from that in Blowey and Elliott (1992); those authors analyse a discretisation of the underlying variational inequality (without any regularisation).

- In Section 5.1 we consider a family of time (only) one-step Euler discretisations of the problem. We prove that the approximation is well-posed, bounded, stable (in the sense that solutions depend continuously on the ICs), and exhibits energy monotonicity.
- Section 5.2 then addresses the practical matter of dealing with the non-linearities of the problem via the semi-smooth Newton (SSN) method.
- In Section 5.3, we consider a fully discrete approximation, as we attach a $\mathbb{P}_1$ finite element spatial approximation to each time-step. The conforming nature of the spatial discretisation means that the boundedness, stability and energy decay properties of Section 5.1 hold (almost) immediately. We extend the results in Section 5.1 to the $\mathbb{P}_1$ approximation, and establish its order of convergence.
- Finally, in Section 5.4, we report on a series of numerical experiments that confirm our theoretical predictions. The most important of these is the method of manufactured solutions (MMS) demonstration of the order of convergence of the scheme. We also investigate mass control and the effect of the regularisation parameter, μ.

Remark. We henceforth drop the '$_\mu$' solution subscripts to ease notational burden i.e. φ_μ becomes φ, and ω_μ, ω. μ is a fixed, small parameter that we (generally) do not vary.

For brevity and clarity, the proofs of this chapter are in Appendix B.

5.1 A time (only) discretisation

We discretise in time seeking approximate solutions to $\left(\mathbf{R}^{(\mathbf{m})}_{\mu,\mathbf{f}}\right)$ at $t \in (t_j)_{j=1}^M \subset (0,T]$. Let $\tau = T/M, M \geq 1$, be the (uniform) time-step size and M the number of time-steps over which we simulate, i.e. $t_j := j\tau$. φ_j will denote the exact solution to $\left(\mathbf{R}^{(\mathbf{m})}_{\mu,\mathbf{f}}\right)$ at time t_j, and φ^j the discrete-in-time approximation of φ_j. Later on, φ^j_h will denote the fully discrete (in space and time) approximation of φ_j.

We define a family of time discretisations, inspired by the schemes in Hintermüller et al. (2011), Bosch et al. (2014b) and Benesová et al. (2014).

Definition 5.1.1. (One-step Euler approximations) *Define the notation*

$$\delta^{(\tau)} u^j := \frac{u^j - u^{j-1}}{\tau}. \tag{5.2}$$

Let $0 < \mu \ll 1$, $\varphi^{j-1} \in H^2_m(\Omega)$ *having* $\partial_n \varphi^{j-1}\big|_{\partial\Omega} = 0$ *and (cf.* (4.55)*, but notice the additional spatial smoothness)*

$$f \in C^1\left([0,T]; H^1_*(\Omega)\right), \tag{5.3}$$

and define $\widetilde{f}^j$ *as a linear combination*

$$\widetilde{f}^j := \begin{cases} \sum_i a_i f(t_i) & j \geq 1 \\ f(0) & j = 0 \end{cases} \qquad \text{where} \qquad \{t_i\} \subset (t_{j-1}, t_j]. \tag{5.4}$$

Consider the family of in-time discretisations (cf. (3.41)*)*

($\mathbf{P}_{\tau,\theta}$)*: Find* $\varphi^j \in H^2_m(\Omega)$ *with* $\partial_n \varphi^j\big|_{\partial\Omega} = \partial_n(-\Delta)\varphi^j\big|_{\partial\Omega} = 0$ *for which*

$$\delta^{(\tau)}\varphi^j - \Delta\left(\varepsilon_\varphi^2(-\Delta)\varphi^j - \frac{\chi^{AB}}{2}\varphi^{j-1} + \zeta_\mu\left(\varphi^j\right)\right) + \alpha\left(\varphi^j - \overline{\varphi^j}\right)_{\{\theta\}} = \widetilde{f}^j, \tag{5.5a}$$

for $j = 1, \ldots, M$*, where*

$$\varphi^0 = \varphi_0 \in \mathscr{A} \cap H^2_m(\Omega). \tag{5.5b}$$

The shorthand $\varrho^j_{\{\theta\}} := \theta\varrho^j + (1-\theta)\varrho^{j-1}$ *indicates a (local)* θ*–method. In* (5.5a)*, we require*

$$\frac{1}{2} \leq \theta \leq 1. \tag{5.5c}$$

Define

$$\omega^j := \varepsilon_\varphi^2(-\Delta)\varphi^j - \frac{\chi^{AB}}{2}\varphi^{j-1} + \zeta_\mu\left(\varphi^j\right) \qquad \text{with} \qquad \partial_n \omega^j\big|_{\partial\Omega} = 0, \tag{5.5d}$$

so that (5.5a) *is equivalent to*

$$\delta^{(\tau)}\varphi^j - \Delta\omega^j + \alpha\left(\varphi^j - \overline{\varphi^j}\right)_{\{\theta\}} = \widetilde{f}^j. \tag{5.5e}$$

The weak form of $(\mathbf{P}_{\tau,\theta})$ *is:*

$\left(\mathbf{R}^{(-)}_{\tau,\theta}\right)$*: given* μ, f, φ^{j-1} *as above, find* $\varphi^j \in H^1_m(\Omega)$ *such that*

$$\left(\delta^{(\tau)}\varphi^j, \nu_1\right) + \left(\nabla\omega^j, \nabla\nu_1\right) + \alpha\left(\left(\varphi^j - \overline{\varphi^j}\right)_{\{\theta\}}, \nu_1\right) = \left(\widetilde{f}^j, \nu_1\right), \tag{5.6}$$

for every $\nu_1 \in H^1(\Omega)$*, and (cf.* (4.8)*)*

$$\left(\omega^j, \nu_2\right) = \varepsilon_\varphi^2\left(\nabla\varphi^j, \nabla\nu_2\right) - \frac{\chi^{AB}}{2}\left(\varphi^{j-1}, \nu_2\right) + \left(\zeta_\mu\left(\varphi^j\right), \nu_2\right) \tag{5.20c}$$

for every $\nu_2 \in H^1(\Omega)$ *and each* $j = 1, \ldots, M$*, subject to the IC*

$$\varphi^0 = \varphi_0 \in \mathscr{A}_m. \tag{5.7}$$

Finally, we define

$(\mathbf{Q}_{\tau,\theta})$*: given* μ, f, φ^{j-1} *above, find* $\varphi^j \in H^1_m(\Omega)$ *such that*

$$\begin{aligned}\left((-\Delta_n)^{-1}\delta^{(\tau)}\varphi^j, \nu\right) + \varepsilon_\varphi^2\left(\nabla\varphi^j, \nabla\nu\right) - \frac{\chi^{AB}}{2}\left(\varphi^{j-1}, \nu\right) \\ + \left(\zeta_\mu\left(\varphi^j\right), \nu\right) + \alpha\left((-\Delta_n)^{-1}\left(\varphi^j - \overline{\varphi^j}\right)_{\{\theta\}}, \nu\right) = \left((-\Delta_n)^{-1}\widetilde{f}^j, \nu\right),\end{aligned} \tag{5.8}$$

for every $\nu \in H^1_*(\Omega)$ *and each* $j = 1, \ldots, M$ *subject to the IC* (5.7)*.*

We also define the ***fully implicit versions*** *of these problems, each of which has the same IC as the corresponding non-implicit version. Corresponding to* $(\mathbf{P}_{\tau,\theta})$*, we consider:*

$(\mathbf{P}_\tau)$*: Find* $\varphi^j \in H^2_m(\Omega)$ *with* $\partial_n\varphi^j\big|_{\partial\Omega} = \partial_n(-\Delta)\varphi^j\big|_{\partial\Omega} = 0$ *for which*

$$\delta^{(\tau)}\varphi^j - \Delta\omega^j + \alpha\left(\varphi^j - \overline{\varphi^j}\right) = \widetilde{f}^j. \tag{5.9a}$$

where

$$\omega^j := \varepsilon_\varphi^2(-\Delta)\varphi^j - \frac{\chi^{AB}}{2}\varphi^j + \zeta_\mu\left(\varphi^j\right) \qquad \text{with} \qquad \partial_n\omega^j\big|_{\partial\Omega} = 0. \tag{5.9b}$$

The weak form of $(\mathbf{P}_\tau)$ *is:*

$\left(\mathbf{R}^{(-)}_{\tau}\right)$*: given* μ, f, φ^{j-1} *as above, find* $\varphi^j \in H^1_m(\Omega)$ *such that*

$$\left(\delta^{(\tau)}\varphi^j, \nu_1\right) + \left(\nabla\omega^j, \nabla\nu_1\right) + \alpha\left(\left(\varphi^j - \overline{\varphi^j}\right), \nu_1\right) = \left(\widetilde{f}^j, \nu_1\right), \tag{5.10a}$$

for every $\nu_1 \in H^1(\Omega)$*, and*

$$\left(\omega^j, \nu_2\right) = \varepsilon_\varphi^2\left(\nabla\varphi^j, \nabla\nu_2\right) - \frac{\chi^{AB}}{2}\left(\varphi^j, \nu_2\right) + \left(\zeta_\mu\left(\varphi^j\right), \nu_2\right) \tag{5.10b}$$

for every $\nu_2 \in H^1(\Omega)$ *and each* $j = 1, \dots, M$. *The fully implicit version of* $(\mathbf{Q}_{\tau,\theta})$ *is:*

$(\mathbf{Q}_\tau)$: *given* μ, f, φ^{j-1} *as above, find* $\varphi^j \in H^1_m(\Omega)$ *such that*

$$\left((-\Delta_n)^{-1}\delta^{(\tau)}\varphi^j, \nu\right) + \varepsilon_\varphi^2\left(\nabla\varphi^j, \nabla\nu\right) - \boxed{\frac{\chi^{AB}}{2}\left(\varphi^j, \nu\right)} + \left(\zeta_\mu\left(\varphi^j\right), \nu\right) + \alpha\left((-\Delta_n)^{-1}\left(\varphi^j - \overline{\varphi^j}\right), \nu\right) = \left((-\Delta_n)^{-1}\widetilde{f}^j, \nu\right), \quad (5.11)$$

for every $\nu \in H^1_*(\Omega)$ *and each* $j = 1, \dots, M$.

Remarks.

i) $(\mathbf{Q}_{\tau,\theta})$ corresponds approximately to $\left(\mathbf{Q}_\mathbf{1}^\mathbf{h}\right)$ in Blowey and Elliott (1992); $\left(\mathbf{R}_{\tau,\theta}^{(-)}\right)$ corresponds to their $\left(\mathbf{P}_\mathbf{2}^\mathbf{h}\right)$. Formally, we can derive $(\mathbf{Q}_{\tau,\theta})$ from (5.5a) by applying $(-\Delta_n)^{-1}$ throughout, and taking a weak form.

ii) $\widetilde{f}^j$ is to approximate f in (5.3) in such a way that $\tau\widetilde{f}^j \approx \int_{t_{j-1}}^{t_j} f \, \mathrm{d}t$. In our numerical experiments in Section 5.4.2, $\widetilde{f}^j = \frac{1}{2}\left(f\left(t_{j-1}\right) + f\left(t_j\right)\right)$. Thanks to Lemma A.1.5, we can split f into two parts and infer the existence of $F_1 \in H^1_*(\Omega)$ with (cf. (B.215b))

$$f = f_1 - f_2 \quad \text{where} \quad f_2 = -\Delta F_1; \quad \partial_n F_1|_{\partial\Omega} = 0 \quad \Leftrightarrow \quad H^1_*(\Omega) \ni F_1 = (-\Delta_n)^{-1} f_2. \quad (5.12a)$$

We could then replace (5.6) and (5.20c) with

$$\left(\delta^{(\tau)}\varphi^j, \nu_1\right) + \left(\nabla\omega^j, \nabla\nu_1\right) + \alpha\left(\left(\varphi^j - \overline{\varphi^j}\right)_{\{\theta\}}, \nu_1\right) = \left(\widetilde{f}_1^j, \nu_1\right), \quad (5.12b)$$

$$\left(\omega^j, \nu_2\right) = \varepsilon_\varphi^2\left(\nabla\varphi^j, \nabla\nu_2\right) - \frac{\chi^{AB}}{2}\left(\varphi^{j-1}, \nu_2\right) + \left(\zeta_\mu\left(\varphi^j\right), \nu_2\right) + \left(\widetilde{F}_1^j, \nu_2\right). \quad (5.12c)$$

Our FEniCS code is based on (5.12). There is no need to carry F_1 into the analysis, however, and so we analyse (5.6) and (5.20c).

We demand somewhat higher spatial regularity of f in (5.3) than in (4.55) so as to be able to use certain interpolation results in the numerical analysis.

iii) The regularisation component involving ζ_μ is fully implicit,[1] whereas the linear term involving χ^{AB} in $(\mathbf{Q}_{\tau,\theta})$ is fully explicit. As such, the method resembles the 'convex splitting' scheme of Eyre (1998a), Eyre (1998b) and Wu et al..

iv) In comparing the convex splitting ((5.5)–(5.8)) and fully implicit ((5.9)–(5.11)) formulations, observe that the latter problems have the linear term $-\frac{\chi^{AB}}{2}\varphi$ (marked in red in (5.9)–(5.11)) at the *upper* (implicit) time-level, and $\theta = 1$. This difference has *significant* implications for the analysis of these problems.

v) The rationale for (5.5c) will become clear presently: this restriction says that the nonlocal term has to be (at least partially) implicit. It cannot be explicit.

vi) $(\mathbf{Q}_{\tau,\theta})$ and $(\mathbf{Q}_{\tau})$ have the test space $H^1_*(\Omega)$; not $H^1(\Omega)$. This makes intuitive sense given that we defined $(-\Delta_n)^{-1}$ in Lemma 2.1.1 to denote the zero mass inverse Laplacian i.e. most of the terms on the left of the inner products in (5.8) and (5.11) have zero mass.[2]

We defined two sets of three problems above. We now use $(\mathbf{Q}_{\tau,\theta})$ to show that $(\mathbf{P}_{\tau,\theta})$ is well-posed (under appropriate conditions) and use $\left(\mathbf{R}^{(-)}_{\tau,\theta}\right)$ as the basis of a numerical method for finding approximate solutions of $(\mathbf{P}_{\tau,\theta})$ (and similarly for $(\mathbf{Q}_{\tau})$, $(\mathbf{P}_{\tau})$ and $\left(\mathbf{R}^{(-)}_{\tau}\right)$).

5.1.1 Well-posedness of the family of in-time approximations

We now prove that the time-stepping scheme of Defn 5.1.1 is well-posed. To start, we prove that $(\mathbf{Q}_{\tau,\theta})$ has a unique solution.

Lemma 5.1.2. (Existence, uniqueness of solutions) *Problem* $(\mathbf{Q}_{\tau,\theta})$ *in* (5.8) *has a unique solution* $\varphi^j \in H^1(\Omega)$*, for any* $\tau > 0$ *satisfying*

$$\frac{1}{\tau} + \alpha\theta \geq 0 \qquad \Leftrightarrow \qquad 1 + \tau\alpha\theta \geq 0. \tag{5.13}$$

In particular, if $\theta \geq \frac{1}{2}$ *as in* (5.5c) *or* $\alpha = 0$*, the problem has a unique solution for any* $\tau > 0$*. The fully implicit formulation* $(\mathbf{Q}_{\tau})$ *in* (5.11) *has a unique solution if* $\tau \lesssim \varepsilon^2_{\varphi}$*. Both formulations are mass conserving in that*

$$\overline{\varphi^j} = \overline{\varphi^{j-1}} \qquad \Rightarrow \qquad \overline{\varphi^j} = m \qquad \text{for each} \qquad j = 0, 1, \ldots, M.$$

We prove this result using the Browder–Minty theorem (cf. Theorem 10.49 of Renardy and Rogers (2004) and Section 9.1 of Evans (1998)). We write

$$\mathring{\varphi}^j := \varphi^j - \overline{\varphi^j} \quad \Leftrightarrow \quad \varphi^j = \mathring{\varphi}^j + \overline{\varphi^j} \quad \Rightarrow \quad \overline{\mathring{\varphi}^j} = 0 \quad \text{and} \quad \mathring{\varphi}^j_{\{\theta\}} = \varphi^j_{\{\theta\}} - \overline{\varphi^j_{\{\theta\}}} \tag{5.14}$$

for every j.[3] Hence $\mathring{\varphi}^j \in H^1_*(\Omega)$ for each j. Using this, we formulate the problem

$\left(\mathbf{Q}^{(*)}\right)$: Given $\mathring{\varphi}^{j-1} \in H^1_*(\Omega)$, find $\mathring{\varphi}^j \in H^1_*(\Omega)$ such that

$$B\left(\mathring{\varphi}^j, \nu\right) = g\left(\mathring{\varphi}^{j-1}, \nu\right) \qquad \text{for every} \qquad \nu \in H^1_*(\Omega), \tag{5.15}$$

where, for given $m \in \mathbb{R}$ and $\widetilde{f}^j \in L^2_*(\Omega)$,

$$B(\varphi, \nu) : \left(H^1_*(\Omega)\right)^2 \mapsto \mathbb{R} := \frac{1}{\tau}\left(\left(-\Delta_n\right)^{-1}\varphi, \nu\right) + \varepsilon^2_{\varphi}(\nabla\varphi, \nabla\nu) + \left(\zeta_{\mu}(\varphi + m), \nu\right) + \alpha\theta\left(\left(-\Delta_n\right)^{-1}\varphi, \nu\right), \tag{5.16a}$$

and

$$g(\omega, \nu) : \left(H^1_*(\Omega)\right)^2 \mapsto \mathbb{R} := \left(\left(-\Delta_n\right)^{-1}\widetilde{f}^j, \nu\right) + \frac{1}{\tau}\left(\left(-\Delta_n\right)^{-1}\omega, \nu\right) - \alpha(1-\theta)\left(\left(-\Delta_n\right)^{-1}\omega, \nu\right) + \frac{\chi^{AB}}{2}(\omega + m, \nu). \tag{5.16b}$$

For the fully implicit problem $(\mathbf{Q}_\tau)$, B and g in (5.16) are replaced with

$$B(\varphi,\nu):\left(H^1_*(\Omega)\right)^2\mapsto\mathbb{R}:=\frac{1}{\tau}\left(\left(-\Delta_n\right)^{-1}\varphi,\nu\right)+\varepsilon_\varphi^2\left(\nabla\varphi,\nabla\nu\right)+\left(\zeta_\mu\left(\varphi+m\right),\nu\right)$$
$$-\frac{\chi^{AB}}{2}\left(\varphi+m,\nu\right)+\alpha\left(\left(-\Delta_n\right)^{-1}\varphi,\nu\right), \quad (5.17a)$$

$$\text{and}\qquad g(\omega,\nu):\left(H^1_*(\Omega)\right)^2\mapsto\mathbb{R}:=\left(\left(-\Delta_n\right)^{-1}\widetilde{f}^j,\nu\right)+\frac{1}{\tau}\left(\left(-\Delta_n\right)^{-1}\omega,\nu\right). \quad (5.17b)$$

We present a detailed proof of this result in Appendix B.22 on p. 397. We now establish the conditions under which $(\mathbf{P}_{\tau,\theta})$ has solutions.

Lemma 5.1.3. (Solutions of $(\mathbf{P}_{\tau,\theta})$) *Suppose that $\partial\Omega$ is smooth enough to satisfy the requirements of Lemma A.1.9. If θ satisfies* (5.5c) *or $\alpha=0$, $(\mathbf{P}_{\tau,\theta})$ in* (5.5) *has a solution for any $\tau>0$. In particular, with ω^j as in* (5.5d)*,*

$$\partial_n\varphi^j\big|_{\partial\Omega}=\partial_n\omega^j\big|_{\partial\Omega}=0 \qquad \textit{(in the sense of trace).} \quad (5.18)$$

The solutions of $(\mathbf{P}_{\tau,\theta})$ are mass conserving in that $\overline{\varphi^j}=\overline{\varphi^{j-1}}=m$ for $j=1,\ldots,M$.

We prove this result in Appendix B.23 on p. 401. We now consider $\left(\mathbf{R}^{(-)}_{\tau,\theta}\right)$.

Lemma 5.1.4. (Existence of solutions of $\left(\mathbf{R}^{(-)}_{\tau,\theta}\right)$) ***Existence**: If $\partial\Omega$ is sufficiently smooth, as in Lemma A.1.9, then $\left(\mathbf{R}^{(-)}_{\tau,\theta}\right)$ has a solution $\left(\varphi^j,\omega^j\right)_{j=1}^M$ with each $\varphi^j\in H^1(\Omega)$, for any $\tau>0$ satisfying* (5.13)*. **Mass conservation**: The problem is mass conserving in that $\overline{\varphi^j}=\overline{\varphi^{j-1}}$ for $j=1,\ldots,M$ viz. each $\varphi^j\in H^1_m(\Omega)$.*

The (short) proof of this result appears in Appendix B.24 on p. 401.

Corollary 5.1.5. (Uniqueness of solutions) *The solutions of $(\mathbf{Q}_{\tau,\theta})$, $(\mathbf{P}_{\tau,\theta})$ and $\left(\mathbf{R}^{(-)}_{\tau,\theta}\right)$ are unique under the conditions of Lemma 5.1.2, as long as $\partial\Omega$ is sufficiently smooth.*

The fully implicit scheme problem chain, $(\mathbf{Q}_\tau)$, $(\mathbf{P}_\tau)$ and $\left(\mathbf{R}^{(-)}_{\tau}\right)$, has unique solutions if all of these conditions hold and $\tau\lesssim\varepsilon_\varphi^2$.

We establish this corollary in Appendix B.25 on p. 402. The conclusions of and logic underpinning Lemmas 5.1.2–5.1.4 and Corollary 5.1.5 are summarised in Fig. 5.1.

5.1.2 Two local time-discretisations: mass conservation and control

We have established conditions under which $\left(\mathbf{R}^{(-)}_{\tau,\theta}\right)$ and $\left(\mathbf{R}^{(-)}_{\tau}\right)$ have unique solutions in $H^1(\Omega)$, and that these problems are mass conserving. We therefore replace the non-local $\overline{\varphi^j}$ term in (5.6) with the control mass m, viz.

$$\overline{\varphi^j_{\{\theta\}}}=\theta\overline{\varphi^j}+(1-\theta)\,\overline{\varphi^{j-1}}=\theta m+(1-\theta)\,m=m, \quad (5.19)$$

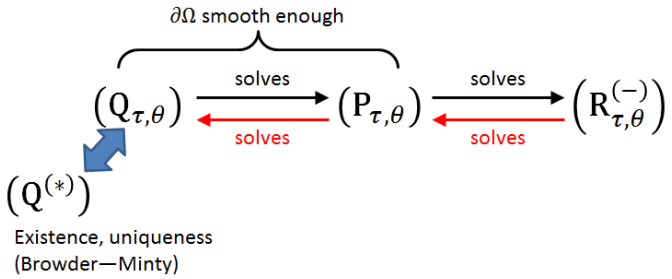

Figure 5.1: Schematic: existence and uniqueness of a family of in-time approximations

to arrive at two time discretisations, which we study in the rest of this chapter:

$\left(\mathbf{R}_{\tau,\theta}^{(m)}\right)$: given $0 < \mu \ll 1$, f as in (5.3) and $\varphi^{j-1} \in H_m^1(\Omega)$, find $\varphi^j \in H_m^1(\Omega)$ such that

$$\left(\delta^{(\tau)}\varphi^j, \nu_1\right) + \left(\nabla\omega^j, \nabla\nu_1\right) + \alpha\left(\varphi_{\{\theta\}}^j - m, \nu_1\right) = \left(\widetilde{f}^j, \nu_1\right), \tag{5.20a}$$

or (cf. (5.6))

$$\begin{aligned}\left(\varphi^j, \nu_1\right) + \tau\left(\nabla\omega^j, \nabla\nu_1\right) + \tau\alpha\theta\left(\varphi^j - m, \nu_1\right) \\ = \tau\left(\widetilde{f}^j, \nu_1\right) + \left(\varphi^{j-1}, \nu_1\right) - \tau\alpha\left(1-\theta\right)\left(\varphi^{j-1} - m, \nu_1\right),\end{aligned} \tag{5.20b}$$

for every $\nu_1 \in H^1(\Omega)$ and $j = 1, \ldots, M$, where (5.5c) holds and (cf. (4.8))

$$\left(\omega^j, \nu_2\right) = \varepsilon_\varphi^2\left(\nabla\varphi^j, \nabla\nu_2\right) - \frac{\chi^{AB}}{2}\left(\varphi^{j-1}, \nu_2\right) + \left(\zeta_\mu\left(\varphi^j\right), \nu_2\right) \tag{5.20c}$$

for every $\nu_2 \in H^1(\Omega)$ and $j = 1, \ldots, M$, subject to the IC (5.7).

We also consider the fully implicit alternative to $\left(\mathbf{R}_{\tau,\theta}^{(m)}\right)$, which is:

$\left(\mathbf{R}_{\tau}^{(m)}\right)$: given $0 < \mu \ll 1$, f as in (5.3) and $\varphi^{j-1} \in H_m^1(\Omega)$, find $\varphi^j \in H_m^1(\Omega)$ with

$$\left(\delta^{(\tau)}\varphi^j, \nu_1\right) + \left(\nabla\omega^j, \nabla\nu_1\right) + \alpha\left(\varphi^j - m, \nu_1\right) = \left(\widetilde{f}^j, \nu_1\right), \tag{5.21a}$$

for every $\nu_1 \in H^1(\Omega)$ and $j = 1, \ldots, M$, and

$$\left(\omega^j, \nu_2\right) = \varepsilon_\varphi^2\left(\nabla\varphi^j, \nabla\nu_2\right) - \frac{\chi^{AB}}{2}\left(\varphi^j, \nu_2\right) + \left(\zeta_\mu\left(\varphi^j\right), \nu_2\right) \tag{5.21b}$$

for every $\nu_2 \in H^1(\Omega)$ and $j = 1, \ldots, M$, subject to the IC (5.7).

Remark. These time discretisations have very similar properties. $\left(\mathbf{R}_{\tau}^{(m)}\right)$ is (generally) easier to work with, and so we usually develop the proofs of various statements for $\left(\mathbf{R}_{\tau}^{(m)}\right)$, and then adapt them for $\left(\mathbf{R}_{\tau,\theta}^{(m)}\right)$.

We now ensure that the two schemes have the same mass control properties as the underlying continuous time model; we drop the requirement that $\overline{\varphi^0} = m$. Setting $\nu_1 = 1$ in (5.20b) and dividing by $|\Omega|$ yields

$$\left(\overline{\varphi^j} - m\right) - \left(\overline{\varphi^{j-1}} - m\right) + \tau\alpha\left(\theta\left(\overline{\varphi^j} - m\right) + (1-\theta)\left(\overline{\varphi^{j-1}} - m\right)\right) = 0,$$

after noting that $\left(\widetilde{f}^j, 1\right) = 0$ for each j, which means that

$$\overline{\varphi^j} = \frac{1 - \tau\alpha(1-\theta)}{1 + \tau\alpha\theta}\overline{\varphi^{j-1}}, \tag{5.22}$$

for $j = 1, \ldots, M$. Hence, for $\left(\mathbf{R}^{(m)}_{\tau,\theta}\right)$,

$$\overline{\varphi^j} = \left(\frac{1 + \tau\alpha\theta - \tau\alpha}{1 + \tau\alpha\theta}\right)^j \overline{\mathring{\varphi}^0} \to 0 \quad \text{as} \quad j \to \infty \qquad \Leftarrow \qquad \left|\frac{1 + \tau\alpha\theta - \tau\alpha}{1 + \tau\alpha\theta}\right| < 1. \tag{5.23}$$

This last condition certainly holds if, for $\tau, \alpha > 0$,[4] (cf. (5.13))

$$1 + \tau\alpha\theta > \frac{\tau\alpha}{2} > 0 \qquad \text{i.e.} \qquad \theta > \frac{1}{2} - \frac{1}{\tau\alpha}. \tag{5.24}$$

The first half of (5.23) is an explicit prediction of the discrete mass at each time-step. For $\left(\mathbf{R}^{(m)}_{\tau}\right)$, we set $\theta = 1$ in (5.23)–(5.24) and obtain

$$\overline{\varphi^j} = \frac{\overline{\mathring{\varphi}^0}}{(1 + \tau\alpha)^j} \to 0 \quad \text{as} \quad j \to \infty \qquad \Leftarrow \qquad \text{any } \tau, \alpha > 0. \tag{5.25}$$

Our first indication of the accuracy of the schemes is the following result.

Lemma 5.1.6. (Mass control) *Let $\mathring{\varphi} := \varphi - m$. The mass-control problem is (cf.* (4.60)*)*

$$\frac{\mathrm{d}\overline{\mathring{\varphi}}}{\mathrm{d}t}(t) = -\alpha\overline{\mathring{\varphi}}(t) =: \varpi\left(t, \overline{\mathring{\varphi}}(t)\right) \qquad \textit{where} \qquad \overline{\mathring{\varphi}}(0) = \delta m, \tag{5.26a}$$

with the exact solution (cf. (3.50)*)*

$$\overline{\mathring{\varphi}}(t) = \delta m \mathrm{e}^{-\alpha t}. \tag{5.26b}$$

Setting $\nu_1 = 1/|\Omega|$ in (5.20a) *leads to the mass control approximation in which $\overline{\mathring{\varphi}}(\tau_j) \approx \overline{\mathring{\varphi}^j}$, $\tau = t_j - t_{j-1}$ viz. $\tau_j = j\tau$, and*

$$\overline{\mathring{\varphi}^j} = \overline{\mathring{\varphi}^{j-1}} + \tau\left((1-\theta)\varpi\left(t_{j-1}, \overline{\mathring{\varphi}^{j-1}}\right) + \theta\varpi\left(t_j, \overline{\mathring{\varphi}^j}\right)\right). \tag{5.27}$$

Define the global mass error as

$$\overline{e}_j = \overline{\mathring{\varphi}}(\tau_j) - \overline{\mathring{\varphi}^j} = \overline{\varphi}(\tau_j) - \overline{\varphi^j}. \tag{5.28}$$

Then:

i) (5.27) *is zero-stable, consistent with* (5.26) *and convergent. In particular,*

$$\theta = \frac{1}{2} \quad \Rightarrow \quad \max\{|\overline{e}_j|\}_{j=1}^M \leq C\tau^2; \quad \theta = 1 \quad \Rightarrow \quad \max\{|\overline{e}_j|\}_{j=1}^M \leq C\tau. \tag{5.29}$$

ii) If $\theta \geq \frac{1}{2}$*, the mass control problem is A-stable and mass controlling (i.e.* (5.23) *holds) for any* τ*.*

The statements above are elementary—see Chapter 12 of Süli and Mayers (2006) and Section 2 of Süli (2010). For completeness, we prove them in Appendix B.26 on p. 403.

Remarks.

i) In the terminology of finite difference methods, setting $\theta = \frac{1}{2}$ in (5.27) yields the trapezium rule method; $\theta = 0$ ($\theta = 1$) corresponds to the explicit (implicit) Euler method for the mass control problem.

ii) Our condition for mass control in (5.23) corresponds to the A-stability of the method. Demanding that $\theta \geq \frac{1}{2}$ ensures that the scheme is (otherwise) unconditionally mass conserving/controlling. We test (5.29) numerically in Section 5.4.1.

5.1.3 Boundedness

Lemma 5.1.7. (Boundedness) *The sequences of approximations* $\left(\varphi^j\right)_{j=0}^M$ *solving* $\left(\mathbf{R}_\tau^{(m)}\right)$*,* $\left(\mathbf{R}_{\tau,\theta}^{(m)}\right)$ *are bounded uniformly in* μ *and* τ *in that*

$$\left\|\left(\varphi^j\right)_{j=0}^M\right\|_{\ell^\infty\left((j\tau)_{j=0}^M;H^1(\Omega)\right)} := \max_{0\leq j\leq M}\left\|\varphi^j\right\|_1 \leq C, \tag{5.30a}$$

independent of μ *and* τ*, if* $\tau \lesssim \varepsilon_\varphi^2$*,* $\theta \geq \frac{1}{2}$ *or* $\alpha = 0$*. In fact,*

$$\max_{0\leq j\leq M}\left\|\varphi^j\right\|_1^2 + \sum_{j=1}^M \tau\left\|\delta^{(\tau)}\varphi^j\right\|_{-1}^2 + \sum_{j=1}^M\left\|\varphi^j - \varphi^{j-1}\right\|_1^2 \leq C, \tag{5.30b}$$

independent of τ *and* μ*. If, in addition,* $\partial\Omega$ *is smooth as in Lemma 5.1.4, and* (4.63) *and* (5.3) *hold, then*

$$\left\|\left(\varphi^j\right)_{j=0}^M\right\|_{\ell^\infty\left((j\tau)_{j=0}^M;H^2(\Omega)\right)} := \max_{0\leq j\leq M}\left\|\varphi^j\right\|_2 \leq C \tag{5.31}$$

independent of μ *and* τ*.*

Solutions of $\left(\mathbf{R}_{\tau,\theta}^{(m)}\right)$ *are bounded as above for any* $\tau > 0$*, if* $\alpha = 0$*.*

The proof is adapted from the proof of Lemma 4.4.3; see Appendix B.27 on p. 405.

Remarks.

i) An examination of the proof of this result reveals that if we allow $\|\varphi_0\|_{0,\infty} > 1$, then the solutions are bounded independent of τ, but may depend on μ.

ii) By Sobolev embedding, we infer from (5.31) that

$$\left\|\left(\varphi^j\right)_{j=0}^M\right\|_{\ell^\infty\left((j\tau)_{j=0}^M;L^\infty(\Omega)\right)} := \max_{0\le j\le M}\left\|\varphi^j\right\|_{0,\infty} \le C, \tag{5.32}$$

independent of μ and τ, if $\tau \lesssim \varepsilon_\varphi^2$, $\theta \ge \frac{1}{2}$ or $\alpha = 0$.

5.1.4 Stability, continuous dependence on ICs

Lemma 5.1.8. (Stability of solutions) *Suppose that* $\left(\mathbf{R}_\tau^{(m)}\right)$ *or* $\left(\mathbf{R}_{\tau,\theta}^{(m)}\right)$ *has two solution sequences,* $\left(\varphi_1^j,\omega_1^j\right)_{j=1}^M$ *and* $\left(\varphi_2^j,\omega_2^j\right)_{j=1}^M$*, corresponding to the ICs* φ_1^0 *and* φ_2^0*, with* $\varphi_1^j,\varphi_2^j \in H_m^1(\Omega)$ *for* $j = 0,1,\ldots,M$*. Define their difference as*

$$U_\tau^j := \left(\varphi^j,\omega^j\right) = \left(\varphi_1^j,\omega_1^j\right) - \left(\varphi_2^j,\omega_2^j\right), \tag{5.33}$$

in which each $\varphi^j \in H_*^1(\Omega)$*. Define also the sequence*

$$\varphi_\tau := \left(\varphi^j\right)_{j=0}^M.$$

Then $\varphi_\tau \in \ell^\infty\left(0,T;\left(H^1(\Omega)\right)'\right)$ *and the sequence is stable, uniformly in* τ *and* μ *in that if* $\tau \lesssim \varepsilon_\varphi^2$*, then*

$$\|\varphi_\tau\|_{\ell^\infty\left(0,T;(H^1(\Omega))'\right)} := \max_{0\le k\le M}\left\|\varphi^k\right\|_{-1} \le C(T)\|\varphi_0\|_{-1}, \qquad \varphi_0 := \varphi_1^0 - \varphi_2^0, \tag{5.34}$$

with $C(T)$ *independent of* τ *and* μ*.*

Remark. Each φ^j in the sequence φ_τ above is in $H_*^1(\Omega)$.

The proof of this result is modelled on that for Lemma 4.4.4. We defer the details to Appendix B.28 on p. 414.

5.1.5 Energy monotonicity

Lemma 5.1.9. (Energy monotonicity) *Suppose that* $\overline{\varphi_0} = m$*,* $\partial\Omega$ *is sufficiently smooth and* $f \equiv 0$*. Then (cf.* (4.69)*)*

$$\mathcal{E}_\mu^{(m)}\left[\varphi^j\right] \le \mathcal{E}_\mu^{(m)}\left[\varphi^{j-1}\right] \le \ldots \le \mathcal{E}_\mu^{(m)}\left[\varphi_0\right] \qquad \text{for each} \qquad j = 1,\ldots,M, \tag{5.35}$$

for solutions of

- $\left(\mathbf{R}_\tau^{(m)}\right)$*, as long as* $\tau \lesssim \varepsilon_\varphi^2$*;*
- $\left(\mathbf{R}_{\tau,\theta}^{(m)}\right)$*, for any* $\tau > 0$*.*

Remark. $\left(\mathbf{R}_\tau^{(m)}\right)$ is termed conditionally gradient stable and $\left(\mathbf{R}_{\tau,\theta}^{(m)}\right)$ unconditionally gradient stable.

The proof is modelled on that of Lemma 4.4.5; see Appendix B.29 on p. 418.

5.2 Solving non-linear, non-differentiable problems

We have confirmed that our time discretisation is well-posed, convergent and gradient stable (under appropriate conditions). In so doing, we have implicitly assumed that we can advance from φ^{j-1} at t_{j-1} to φ^j at t_j, despite the presence of the non-differentiable ζ_μ.

In the current section, we show how the iterative SSN method can solve the problem at each t_j, using the (converged) solution φ^{j-1} (from the previous time-step) as the initial guess. For SSN to converge requires i) a well-posed problem, i.e. that a unique solution φ^j exists for a given φ^{j-1} (which we have), and ii) an initial guess (viz. φ^{j-1}) sufficiently close to φ^j. We define

$$\boldsymbol{x}^{(j)} = \left(\varphi^j, \omega^j\right), \tag{5.36}$$

and write (5.20b)–(5.20c) as (cf. (46), (47) of Hintermüller et al. (2011) and F_ν in (3.1) of Bosch et al. (2014a))

$$\boldsymbol{g}\left(\boldsymbol{x}^{(j)}\right) = \left(g_1\left(\boldsymbol{x}^{(j)}\right), g_2\left(\boldsymbol{x}^{(j)}\right)\right) = \mathbf{0}, \tag{5.37a}$$

where in turn,

$$\begin{aligned}\left(g_1\left(\boldsymbol{x}^{(j)}\right), \boldsymbol{\nu}\right) = \left(\varphi^j, \nu_1\right) + \tau\left(\nabla\omega^j, \nabla\nu_1\right) + \tau\alpha\theta\left(\varphi^j, \nu_1\right) \\ - \left[\left(\tau\widetilde{f}^j + \varphi^{j-1} - \tau\alpha\left(1-\theta\right)\left(\varphi^{j-1} - m\right), \nu_1\right)\right] = 0,\end{aligned} \tag{5.37b}$$

$$\begin{aligned}\left(g_2\left(\boldsymbol{x}^{(j)}\right), \boldsymbol{\nu}\right) = \left(\omega^j, \nu_2\right) - \varepsilon_\varphi^2\left(\nabla\varphi^j, \nabla\nu_2\right) - \left(\zeta_\mu\left(\varphi^j\right), \nu_2\right) \\ - \left[-\frac{\chi^{AB}}{2}\left(\varphi^{j-1}, \nu_2\right)\right] = 0;\end{aligned} \tag{5.37c}$$

for every $\boldsymbol{\nu} = (\nu_1, \nu_2) \in H^1(\Omega)$. Each of these equations has form

$$\left(g_i\left(\boldsymbol{x}^{(j)}\right), \boldsymbol{\nu}\right) = [t_j \text{ terms}] - [t_{j-1} \text{ terms}] = 0.$$

The form for (5.21) is adapted from (5.37) in the obvious way.

The Newton method

The Newton and SSN methods iterate in the same way, and so we develop the basic ideas behind SSN using the more familiar Newton method. Consider the generic

$$\boldsymbol{g}(\boldsymbol{x}) = \mathbf{0} \tag{5.38}$$

for $\boldsymbol{g} : \mathbb{R}^q \to \mathbb{R}^q$, $q \geq 1$. Newton's method involves iterating as follows:

$$\begin{aligned}\boldsymbol{x}^{(n+1)} &= \boldsymbol{x}^{(n)} - \left[\mathcal{F}\left(g\left(\boldsymbol{x}^{(n)}\right)\boldsymbol{\delta}\right)\right]^{-1}\boldsymbol{g}\left(\boldsymbol{x}^{(n)}\right) \\ \text{viz.} \qquad \mathcal{F}\left(g\left(\boldsymbol{x}^{(n)}\right)\boldsymbol{\delta}\right)&\left(\boldsymbol{x}^{(n)} - \boldsymbol{x}^{(n+1)}\right) = \boldsymbol{g}\left(\boldsymbol{x}^{(n)}\right),\end{aligned} \tag{5.39}$$

for $n = 0, 1, \ldots$ i.e. n counts the iteration number, where $\mathcal{F}\left(g\left(\boldsymbol{x}^{(n)}\right)\boldsymbol{\delta}\right)$ is defined as the Fréchet derivative of $\boldsymbol{g}$ evaluated at $\boldsymbol{x}^{(n)}$ in the (unknown) direction $\boldsymbol{\delta}$. In order to arrive at a scheme suitable for a time evolution problem, we introduce a time index j, since we are progressing from t_{j-1} to t_j, and rearrange (5.39) as

$$\mathcal{F}\left(g\left(\boldsymbol{x}^{(j-1,n)}\right)\underbrace{\left(\boldsymbol{x}^{(j-1,n)}-\boldsymbol{x}^{(j-1,n+1)}\right)}_{:=\boldsymbol{\delta}^{(j-1,n)}}\right)=\boldsymbol{g}\left(\boldsymbol{x}^{(j-1,n)}\right), \tag{5.40a}$$

and observe that

$$\boldsymbol{\delta}^{(j-1,n)}=\boldsymbol{x}^{(j-1,n)}-\boldsymbol{x}^{(j-1,n+1)} \qquad \Rightarrow \qquad \boldsymbol{x}^{(j-1,n+1)}=\boldsymbol{x}^{(j-1,n)}-\boldsymbol{\delta}^{(j-1,n)}, \tag{5.40b}$$

i.e. we will solve a linear system for the decrement $\boldsymbol{\delta}^{(j-1,n)}$ on each iteration. We identify

$$\boldsymbol{x}^{(j-1,n)}:=\left(\varphi^{(j-1,n)},\omega^{(j-1,n)}\right) \qquad \text{and} \qquad \boldsymbol{\delta}^{(j-1,n)}:=\left(\delta\varphi^{(j-1,n)},\delta\omega^{(j-1,n)}\right);$$

the solution at each t_j is defined as

$$\boldsymbol{x}^{(j)}:=\boldsymbol{x}^{(j,0)}:=\lim_{n\to\infty}\boldsymbol{x}^{(j-1,n)} \qquad \text{i.e.} \qquad \begin{cases}\varphi^{j}:=\lim_{n\to\infty}\varphi^{(j-1,n)}\\ \omega^{j}:=\lim_{n\to\infty}\omega^{(j-1,n)}\end{cases}$$

where each $\boldsymbol{\delta}^{(j-1,n)}$ solves (5.40a). Multiplying (5.40a) by the (spatial) test function $\boldsymbol{\nu}$ and integrating over Ω leads to the weak form,

$$\mathcal{F}\left(g\left(\boldsymbol{x}^{(j-1,n)}\right)\boldsymbol{\delta}^{(j-1,n)},\boldsymbol{\nu}\right)=\left(\boldsymbol{g}\left(\boldsymbol{x}^{(j-1,n)}\right),\boldsymbol{\nu}\right). \tag{5.40c}$$

SSN

The iteration framework for the SSN method is the same as for the Newton method, except that we relax our requirement of Fréchet differentiability, and instead use the more general Newton derivative. We use $\mathcal{N}\left(\left(g\left(\boldsymbol{x}\right),\boldsymbol{\nu}\right),\boldsymbol{\delta}\right)$ to denote the Newton derivative of the inner product $\left(g\left(\boldsymbol{x}\right),\boldsymbol{\nu}\right)$ in the direction $\boldsymbol{\delta}$, replacing (5.40c) with

$$\mathcal{N}\left(g\left(\boldsymbol{x}^{(j-1,n)}\right)\boldsymbol{\delta}^{(j-1,n)},\boldsymbol{\nu}\right)=\left(\boldsymbol{g}\left(\boldsymbol{x}^{(j-1,n)}\right),\boldsymbol{\nu}\right). \tag{5.41}$$

We take the following definition of the Newton derivative from Defn 3.1 of Bosch et al. (2014a) (cf. Defn 5.1 of Hintermüller et al. (2011)):

Definition 5.2.1. (Newton Derivative) *Let X and Z be Banach spaces, and let $E \subset X$ be an open subset. A mapping $G : E \to Z$ is called Newton-differentiable in $U \subset E$ if there exists a family of mappings $N : U \to Z$ such that*

$$\lim_{h\to 0}\frac{\left\|G\left(x+h\right)-G\left(x\right)-N\left(x+h\right)h\right\|_Z}{\left\|h\right\|_X}=0 \qquad \textit{for every} \qquad x\in U.$$

The operator N is called a Newton derivative of G on U.

We also quote Theorem 5.2 from Hintermüller et al. (2011) (cf. Lemma 3.4 of Bosch et al. (2014a))

Theorem 5.2.2. (Super-linear convergence of the SSN method) *Let $G(x^*) = 0$, and suppose that $G : E \subset X \to Z$ is Newton-differentiable in a neighbourhood U of x^*, with $\left\{ \left\| [N(x)]^{-1} \right\|_{\mathcal{L}(Z,X)} : x \in U \right\}$ bounded. Then the sequence $\left(x^{(n)}\right)_{n\in\mathbb{N}}$ generated by*

$$x^{(n+1)} = x^{(n)} - \left[N\left(x^{(n)}\right) \right]^{-1} G\left(x^{(n)}\right),$$

with N a Newton derivative of G as in Defn 5.2.1, converges super-linearly to x^*, provided $\left\|x^{(0)} - x^*\right\|_X$ is sufficiently small.

Remarks.

i) The proof of this result appears in Theorem 1.1 of Hintermüller et al. (2002).

ii) We have stated the result above with reference to a generic iteration scheme to reduce notational overhead. We will apply it to our scheme in (5.41), identifying the initial guess $x^{(0)}$ with $\boldsymbol{x}^{(j-1)}$ (the known solution at the lower time level), and x^* with $\boldsymbol{x}^{(j)}$ (the solution we seek at the upper time level).

iii) As with all such results, there is no easy way to *a priori* quantify the 'sufficiently small' requirement at the end of the theorem (cf. Newton's method in Theorem 3.5 of Nocedal and Wright (2006)). *Practically*, this means that we iterate until subsequent iterates are close together (viz. $\left\|x^{(n+1)} - x^{(n)}\right\|_X \leq \texttt{TOL}$ for some predefined tolerance), and then assume that we have an approximation of the solution.

iv) The Newton method typically exhibits quadratic convergence, which (generally) implies convergence in fewer iterations than SSN.[5]

Fréchet derivatives are Newton derivatives. For $\left(\mathbf{R}_{\tau,\theta}^{(m)}\right)$, the left side of (5.41) is

$$\mathcal{N}_\theta\left(g\left(\boldsymbol{x}^{(j-1,n)}\right)\boldsymbol{\delta}^{(j-1,n)}, \boldsymbol{\nu}\right) = \begin{pmatrix} \left(\delta\varphi^{(j-1,n)}, \nu_1\right) + \tau\left(\nabla\delta\omega^{(j-1,n)}, \nabla\nu_1\right) + \tau\alpha\theta\left(\delta\varphi^{(j-1,n)}, \nu_1\right) \\ \left(\delta\omega^{(j-1,n)}, \nu_2\right) - \varepsilon_\varphi^2\left(\nabla\delta\varphi^{(j-1,n)}, \nabla\nu_2\right) - \mathscr{N}\left(\zeta_\mu\left(\varphi^j\right)\boldsymbol{\delta}^{(j-1,n)}, \nu_2\right) \end{pmatrix}. \quad (5.42a)$$

For $\left(\mathbf{R}_{\tau}^{(m)}\right)$, we use (notice the additional term in the derivative)

$$\mathcal{N}\left(g\left(\boldsymbol{x}^{(j-1,n)}\right)\boldsymbol{\delta}^{(j-1,n)}, \boldsymbol{\nu}\right) = \mathcal{N}_{(\theta=1)}\left(g\left(\boldsymbol{x}^{(j-1,n)}\right)\boldsymbol{\delta}^{(j-1,n)}, \boldsymbol{\nu}\right) + \begin{pmatrix} 0 \\ \frac{\chi^{AB}}{2}\left(\delta\varphi^{(j-1,n)}, \nu_2\right) \end{pmatrix}. \quad (5.42b)$$

We propose the following Newton derivative for the penalty component (which involves min/max functions and is not Fréchet differentiable),

$$\mathscr{N}\left(\zeta_\mu\left(\varphi^j\right)\boldsymbol{\delta}^{(j-1,n)},\nu_2\right) = \frac{1}{\mu}\left[\left(\mathbf{1}\left\{\varphi^{(j-1,n)}>1\right\}\delta\varphi^{(j-1,n)},\nu_2\right)+\left(\mathbf{1}\left\{\varphi^{(j-1,n)}<-1\right\}\delta\varphi^{(j-1,n)},\nu_2\right)\right], \quad (5.42c)$$

where we define the conditional characteristic or indicator function,

$$\mathbf{1}\{A\} := \begin{cases} 1 & A \text{ is true} \\ 0 & \text{otherwise.} \end{cases} \quad (5.43)$$

We solve for the direction $\boldsymbol{\delta}^{(j-1,n)} = \left(\delta\varphi^{(j-1,n)}, \delta\omega^{(j-1,n)}\right)$ in each iteration. The right-hand side of (5.41) is found by evaluating (5.37) at the prior iterate, viz. $\boldsymbol{x}^{(j-1,n)}$.

The following `UFL` code snippets (from FEniCS) are for $\left(\mathbf{R}_{\tau,\theta}^{(m)}\right)$. The unknowns are `dphi` ($= \delta\varphi^{(j-1,n)}$) and `dw_phi` ($= \delta\omega^{(j-1,n)}$). The two rows of (5.42a) are `L1` and `L2` below.

```
# Micro separation parameter:
#-------------------------------
L1 = (dphi*vh1*dx(mesh)
      + tau*dot(grad(dw_phi), grad(vh1))*dx(mesh)
      + tau*( alpha*theta*dphi )*vh1*dx(mesh) )

# Micro separation 'potential':
#-------------------------------
L2 = (dw_phi*vh2*dx(mesh)
      - e_ph2*dot(grad(dphi), grad(vh2))*dx(mesh)
      - Newton_B_phi(phi,dphi)*vh2*dx(mesh) )

# and sum the parts
newton_derivative = L1 + L2
```

where

```
Newton_B_phi = \
    ( (1/mu)*(conditional(phi>1.0,
                          Constant(1.0), # true
                          Constant(0.0)) # false
                          *dphi)
    + (1/mu)*(conditional(phi<-1.0,
                          Constant(1.0), # true
                          Constant(0.0)) # false
                          *dphi) )
```

We now demonstrate that our selections above lead to a numerical method exhibiting super-linear convergence.

Lemma 5.2.3. (A Newton derivative) (5.42a) *and* (5.42b) *together with* (5.42c) *are Newton derivatives, as in Defn 5.2.1, of* $\boldsymbol{g}$ *in* (5.37a) *for* $\left(\mathbf{R}_{\tau,\theta}^{(m)}\right)$ *and* $\left(\mathbf{R}_{\tau}^{(m)}\right)$.

We do not provide a proof of this statement (the core of which relates to (5.42c)), but refer to Lemma 3.3 of Bosch et al. (2014a) and Lemma 5.3 of Hintermüller et al. (2011). We use this fact to establish the following important result.

Lemma 5.2.4. (Superlinear convergence) *The SSN method encapsulated in* (5.42) *converges superlinearly to* $\boldsymbol{x}^{(j)} = \left(\varphi^j, \omega^j\right)$ *for* $\left(\mathbf{R}_{\tau,\theta}^{(m)}\right)$ *for any* $\tau > 0$ *and* $\left(\mathbf{R}_{\tau}^{(m)}\right)$ *if* $\tau \lesssim \varepsilon_\varphi^2$, *and,*

$$\left\|\boldsymbol{x}^{(j-1)} - \boldsymbol{x}^{(j)}\right\|_{H^1(\Omega)\times H^1(\Omega)} \quad \text{is sufficiently small.} \tag{5.44}$$

We adapt the proof of Lemma 3.4 of Bosch et al. (2014a) to prove this result, in Appendix B.30 on p. 421. See also Proposition 5.5 of Hintermüller et al. (2011).

5.2.1 A fourth degree regularisation

Alternatively, we could use the degree four regularisation in (4.72). The additional regularity of this approach means we replace $\mathscr{N}\left(\zeta_\mu\left(\varphi^j\right)\boldsymbol{\delta}^{(j-1,n)}, \nu_2\right)$ in (5.42c) with the fully implicit

$$\frac{3}{\mu}\Bigg[\left(\mathbf{1}\left\{\varphi^{(j-1,n)} > 1\right\}\left(\varphi^{(j-1,n)} - 1\right)^2 \delta\varphi^{(j-1,n)}, \nu_2\right) + \left(\mathbf{1}\left\{\varphi^{(j-1,n)} < -1\right\}\left(\varphi^{(j-1,n)} + 1\right)^2 \delta\varphi^{(j-1,n)}, \nu_2\right)\Bigg]. \tag{5.45}$$

5.3 A fully discrete approximation

Having established the basic properties of the time discretisation above, we consider a fully discrete (time and space) approximation of the problem.

5.3.1 Spatial discretisation, function spaces

Suppose that Ω is an interval (for $d = 1$), convex polygon (for $d = 2$) or polyhedron ($d = 3$) so that it can be triangulated exactly, and let $\left\{\mathcal{T}^h\right\}_{h>0}$ be a quasi-uniform family of partitions of Ω into disjoint, open simplices K.[6] We define h_K as the diameter (longest side) of simplex K and $h := \max_{K\in\mathcal{T}^h} h_K$. Then $\overline{\Omega} = \cup_{K\in\mathcal{T}^h}\overline{K}$. We associate the following conforming finite element (piecewise linear approximation) function spaces with $\mathcal{T}^h$,

$$V^h := \left\{v_h \in C\left(\overline{\Omega}\right) : v_h|_K \text{ is linear } \forall\, K \in \mathcal{T}^h\right\} \subset H^1\left(\Omega\right); \tag{5.46a}$$

$$V_*^h := \left\{v_h \in V^h : \overline{v_h} = 0\right\}; \tag{5.46b}$$

$$V_m^h := \left\{v_h \in V^h : \overline{v_h} = m \neq 0\right\}. \tag{5.46c}$$

Our spatial discretisation is conforming in that $V^h \subset H^1(\Omega)$. The advantage of this selection, in combination with our results in the Section 5.1, is that we are able to examine the effects of the time discretisation *separately* from those of the spatial discretisation.

The set of nodes in a discretisation is denoted J, with coordinates $J_x := \{x_i\}_{i=1}^{N_h} \subset \overline{\Omega}$. The standard basis ('hat') functions $\phi = \{\phi_i\}$ have the property that $\phi_i(x_j) = \delta_{ij}$, and

$$\dim V^h =: N_h \qquad \text{with} \qquad V^h = \operatorname{span}\{\phi_i\}_{1 \le i \le N_h}. \tag{5.47}$$

N_h counts the dimension of V^h and the number of nodes in $\mathcal{T}^h$. We approximate each φ^j and ω^j in problems $\left(\mathbf{R}_\tau^{(m)}\right)$ and $\left(\mathbf{R}_{\tau,\theta}^{(m)}\right)$ as a finite sum in V^h, viz.

$$\varphi^j \approx \varphi_h^j = \sum_{i=1}^{N_h} \varphi_{h,i}^j \phi_i \qquad \text{and} \qquad \omega^j \approx \omega_h^j = \sum_{i=1}^{N_h} \omega_{h,i}^j \phi_i, \qquad j = 1, \dots M, \tag{5.48}$$

in which we anticipate that $\varphi_{h,i}^j \approx \varphi^j(x_i) \approx \varphi(x_i, t_j)$ (and likewise for ω), in a sense we will make precise shortly.[7]

If $u_h \in V_h$, then ∇u_h is a piecewise constant vector function with d components (assuming $\Omega \subset \mathbb{R}^d$).

Remark. For simplicity, **we ignore any quadrature effects** as a result of working in V^h. We do not define an approximate $L^2(\Omega)$ inner-product like the $(\cdot,\cdot)^h$ of Blowey and Elliott (1992) and Barrett et al. (1999).

5.3.2 The discrete Neumann Laplacian

We consider discrete counterparts to the operators $-\Delta_n$ and $(-\Delta_n)^{-1}$ which we will use extensively.

Definition 5.3.1. (The discrete Neumann Laplacian $-\Delta_h$) *The discrete Neumann Laplacian $-\Delta_h : V^h \to V_*^h$ is defined such that for $u_h \in V^h$,*

$$-\Delta_h u_h = f_h \qquad \Leftrightarrow \qquad (f_h, v_h) = (\nabla u_h, \nabla v_h) \qquad \textit{for any} \qquad v_h \in V^h. \tag{5.49}$$

The '$_h$'-subscript reminds us that $-\Delta_h u_h$ depends on the discretisation being considered. Notice that $\overline{f_h} = 0$ i.e. $f_h \in V_*^h$ above because, if we set $v_h = 1$ in (5.49), then $(f_h, 1) = 0$. Hence, $-\Delta_n$ and $-\Delta_h$ share the same compatibility condition. The mapping $-\Delta_h$ is well-defined in that for any $u_h \in V^h$, $-\Delta_h u_h \in V^h$ exists and is unique.[8]

We also define the inverse of $-\Delta_h$.

Definition 5.3.2. (The *inverse* discrete Neumann Laplacian $(-\Delta_h)^{-1}$) *The inverse discrete Neumann Laplacian $(-\Delta_h)^{-1} : V_*^h \to V_*^h$ is defined such that*

$$V_*^h \ni u_h = (-\Delta_h)^{-1} f_h \quad \Leftrightarrow \quad \left((-\Delta_h)^{-1} f_h, v_h\right) = (u_h, v_h) \quad \Leftrightarrow \quad (f_h, v_h) = (\nabla u_h, \nabla v_h) \tag{5.50}$$

for any $v_h \in V^h$.

In Lemma A.1.5, we specified that $\overline{(-\Delta_n)^{-1}\nu} = 0$ for $\nu \in L^2_*(\Omega)$, to ensure the uniqueness of solutions of the Poisson equation with zero Neumann BC. Likewise, in this context and for the same reason, we demand that $\overline{(-\Delta_h)^{-1}u_h} = 0$ for (any) $u_h \in V^h_*$.[9] For any $f_h \in V^h_*$, there is a unique $u_h \in V^h_*$ for which

$$u_h = (-\Delta_h)^{-1} f_h \qquad \Leftrightarrow \qquad -\Delta_h u_h = f_h$$

i.e. the discrete Poisson equation is well-posed. In correspondence with (2.9a) and (4.15) of Blank et al. (2011), we note that for any $f_h \in V^h_*$,

$$\left(\nabla(-\Delta_h)^{-1} f_h, \nabla u_h\right) = (f_h, u_h) \qquad \text{for every} \qquad u_h \in V^h. \tag{5.51}$$

For $u_h, v_h \in V^h_*$, we use $(-\Delta_h)^{-1}$ to define the inner product (cf. (2.10) and (5.51))

$$(u_h, v_h)_{-h} := \left((-\Delta_h)^{-1} u_h, v_h\right) = \left(u_h, (-\Delta_h)^{-1} v_h\right) = \left(\nabla(-\Delta_h)^{-1} u_h, \nabla(-\Delta_h)^{-1} v_h\right), \tag{5.52}$$

on V^h_*, with induced norm $\|\cdot\|_{-h}$, defined as (cf. (2.11) and (2.6) of Blowey and Elliott (1992))

$$\|u_h\|^2_{-h} := \left((-\Delta_h)^{-1} u_h, u_h\right) = \left(\nabla(-\Delta_h)^{-1} u_h, \nabla(-\Delta_h)^{-1} u_h\right) = \left|(-\Delta_h)^{-1} u_h\right|^2_1. \tag{5.53}$$

We present a more detailed discussion of these and other issues related to the spatial discretisation in Appendix A.1.6, starting on p. 335.

5.3.3 Projection operators

For given $\psi \in H^1(\Omega)$, we consider three projection operators.

Definition 5.3.3. ($H^1_*(\Omega)$ orthogonal projection) *Define* $P^{(\star)}_m : H^1(\Omega) \to V^h$ *as*

$$\left(\nabla P^{(\star)}_m \varphi, \nabla v_h\right) = (\nabla\varphi, \nabla v_h) \quad \forall\, v_h \in V^h \qquad \textit{such that} \qquad \overline{P^{(\star)}_m \varphi} = m. \tag{5.54}$$

Definition 5.3.4. ($L^2(\Omega)$ projection) *Define the projector* $P^{(h)} : L^2(\Omega) \to V^h$ *as*

$$\left(P^{(h)}\varphi, v_h\right) = (\varphi, v_h) \qquad \textit{for every} \qquad v_h \in V^h. \tag{5.55}$$

Definition 5.3.5. (Lagrange interpolation operator) *The piecewise linear Lagrange interpolation operator* $\mathcal{I}^{(h)} : C\left(\overline{\Omega}\right) \to V^h$ *is defined as*

$$\left(\mathcal{I}^{(h)} v\right)(x_i) = v(x_i) \tag{5.56}$$

for each node x_i *in* $\mathcal{T}^h$.

We discuss these (well-known) operators in Appendix A.1.6.3, starting on p. 337.

5.3.4 Formulation of the fully discrete problem

Using the above, we formulate our fully discrete, Euler-in-time, $\mathbb{P}_1$-in-space problem:

$\left(\mathbf{R}^{(m)}_{\tau,\theta,h}\right)$: given $0 < \mu \ll 1$, $f_h^j = P^{(h)}\widetilde{f}^j$, $\varphi_h^{j-1} \in V^h$ for each j, and $\varphi^0 \in H^2_m(\Omega)$ with $\partial_n u|_{\partial\Omega} = 0$ and $-\Delta\varphi^0 \in H^1(\Omega)$,

$$\varphi_h^0 = P_m^{(\star)}\varphi^0 \quad \text{viz.} \quad \left(\nabla\varphi_h^0, \nabla v_h\right) = \left(\nabla\varphi^0, \nabla v_h\right) \quad \forall \quad v_h \in V^h \quad \text{and} \quad \overline{\varphi_h^0} = m, \tag{5.57a}$$

find $\varphi_h^j \in V^h$ such that (cf. (5.20b))

$$\left(\delta^{(\tau)}\varphi_h^j, u_h\right) + \left(\nabla\omega_h^j, \nabla u_h\right) + \alpha\theta\left(\varphi_h^j - m, u_h\right) = \left(f_h^j, u_h\right) - \alpha(1-\theta)\left(\varphi_h^{j-1} - m, u_h\right) \tag{5.57b}$$

for every $u_h \in V^h$, and (cf. (5.20c))

$$\left(\omega_h^j, v_h\right) = \varepsilon_\varphi^2\left(\nabla\varphi_h^j, \nabla v_h\right) + \left(\zeta_\mu\left(\varphi_h^j\right), v_h\right) - \frac{\chi^{AB}}{2}\left(\varphi_h^{j-1}, v_h\right) \tag{5.57c}$$

or, equivalently, if we use (4.7),

$$\left(\omega_h^j, v_h\right) = \varepsilon_\varphi^2\left(\nabla\varphi_h^j, \nabla v_h\right) + \left(\mathcal{B}'_\mu\left(\varphi_h^j\right), v_h\right) + \frac{\chi^{AB}}{2}\left(\varphi_h^j - \varphi_h^{j-1}, v_h\right), \tag{5.57d}$$

for every $v_h \in V^h$, for $j = 1, \ldots, M$ with $T = M\tau$.

The convex splitting scheme above corresponds to $\left(\mathbf{P_2^h}\right)$ of Blowey and Elliott (1992). A fully implicit scheme, corresponding to $\left(\mathbf{P_1^h}\right)$ of Blowey and Elliott (1992) and (5.11), is:

$\left(\mathbf{R}^{(m)}_{\tau,h}\right)$: given $0 < \mu \ll 1$, $f_h^j = P^{(h)}\widetilde{f}^j$ and $\varphi_h^{j-1} \in V^h$ for each j, and the IC (5.57a) as above, find $\varphi_h^j \in V^h$ such that

$$\left(\delta^{(\tau)}\varphi_h^j, u_h\right) + \left(\nabla\omega_h^j, \nabla u_h\right) + \alpha\left(\varphi_h^j - m, u_h\right) = \left(f_h^j, u_h\right) \tag{5.58a}$$

for every $u_h \in V^h$, and

$$\left(\omega_h^j, v_h\right) = \varepsilon_\varphi^2\left(\nabla\varphi_h^j, \nabla v_h\right) + \left(\mathcal{B}'_\mu\left(\varphi_h^j\right), v_h\right), \tag{5.58b}$$

for every $v_h \in V^h$, for $j = 1, \ldots, M$ with $T = M\tau$.

Remarks.

i) We do *not* require $\left\|\varphi^0\right\|_{0,\infty} \leq 1$ in the fully discrete problem. φ^0 denotes the source of φ_h^0 in (5.57a) and Section 5.3.5 below, as distinct from $\varphi_0 \in \mathscr{A}_m$ in (5.7).

ii) Each $\overline{f_h^j} = 0$ by (A.74) and (5.3).

Energy

Finally, we define the (discrete) energy of φ_h^j as (cf. (4.61))

$$\mathcal{E}^{(m)}_{\mu,h}\left[\varphi_h^j\right] := \frac{\varepsilon_\varphi^2}{2}\left|\varphi_h^j\right|_1^2 + \left(\mathcal{B}_\mu\left(\varphi_h^j\right), 1\right) + \frac{\alpha}{2}\left\|\varphi_h^j - m\right\|_{-h}^2. \tag{5.59}$$

This is the energy we measure in numerical experiments.

5.3.5 ICs

For the fully-discrete problem, we relax the requirement that $\left\|\varphi^0\right\|_{0,\infty} \leq 1$, and insist only that $\overline{\varphi^0} = m$. According to Lemma A.1.17, (5.57a) and our assumptions on φ^0 imply that

$$\left\|\varphi_h^0\right\|_1 \leq C\left(\varphi^0, m, c_P, |\Omega|\right), \tag{5.60}$$

independent of h and τ. For $h < 1$,

$$\left\|\varphi_h^0\right\|_{0,\infty} \leq C\left(\varphi^0\right), \tag{5.61}$$

independent of h.

Remark. $\left\|\varphi^0\right\|_{0,\infty} \leq 1$ **does *not* necessarily imply that** $\left\|\varphi_h^0\right\|_{0,\infty} \leq 1$ for φ_h^0 as in (5.57a), although Lemma A.1.17 on 338 shows that this must be true in the limit as $h \downarrow 0$. We explore two other (unsatisfactory) definitions of φ_h^0 in an endnote.[10]

We will also need the fictitious solution, φ^{-1}, which we define as

$$\varphi^{-1} = \varphi^0. \tag{5.62}$$

5.3.6 Existence of fully discrete solutions

Lemma 5.3.6. (Existence, uniqueness of discrete solutions, mass control) $\left(\mathbf{R}_{\tau,\theta,h}^{(m)}\right)$ *has unique solutions* $\left(\varphi_h^j, \omega_h^j\right)_{j=1}^M$ *for any* $\tau > 0$*;* $\left(\mathbf{R}_{\tau,h}^{(m)}\right)$ *has unique solutions as long as* $\tau \lesssim \varepsilon_\varphi^2$*. In both cases, if* $\overline{\varphi_h^0} = m$*, then* $\overline{\varphi_h^j} = m$ *for* $j = 1, \ldots, M$*.*

The proof of this result appears in Appendix B.31 on p. 425.

5.3.7 Boundedness

Lemma 5.3.7. (Boundedness) *The sequences of finite element approximations* $\left(\varphi_h^j\right)_{j=0}^M$ *solving* $\left(\mathbf{R}_{\tau,h}^{(m)}\right)$ *and* $\left(\mathbf{R}_{\tau,\theta,h}^{(m)}\right)$ *are bounded uniformly in* h *and* τ *(but not* μ*), in that*

$$\left\|\left(\varphi_h^j\right)_{j=0}^M\right\|_{\ell^\infty\left((j\tau)_{j=0}^M; H^1(\Omega)\right)} := \max_{0\leq j\leq M}\left\|\varphi_h^j\right\|_1 \leq C, \tag{5.63a}$$

$$\max_{0\leq j\leq M}\left\|\varphi_h^j\right\|_1^2 + \sum_{j=1}^M \tau\left\|\delta^{(\tau)}\varphi_h^j\right\|_{-h}^2 + \sum_{j=1}^M\left\|\varphi_h^j - \varphi_h^{j-1}\right\|_1^2 \leq C, \tag{5.63b}$$

$$\left\|\left(\varphi_h^j\right)_{j=0}^M\right\|_{\ell^\infty\left((j\tau)_{j=0}^M; \ell^\infty(\Omega)\right)} := \max_{0\leq j\leq M}\left\|\varphi_h^j\right\|_{0,\infty} \leq C, \tag{5.63c}$$

independent of h *and* τ*, if* $\tau \lesssim \varepsilon_\varphi^2$*,* $\theta \geq \frac{1}{2}$*, and the triangulation is quasi-uniform.*

If $\alpha = 0$*, then solutions of* $\left(\mathbf{R}_{\tau,\theta,h}^{(m)}\right)$ *are bounded for any* $\tau > 0$*.*[11]

The proof mimics that of Lemma 5.1.7. Details appear in Appendix B.32 on p. 426.

Remark. For φ_h^j as in (5.48) and a $\mathbb{P}_1$ spatial discretisation,

$$\left\|\varphi_h^j\right\|_{0,\infty} = \max_{1\le i\le N_h}\left|\varphi_{h,i}^j\right| = \max_{x_i\in J_x}\left|\varphi_h^j\left(x_i\right)\right|.$$

5.3.8 Stability, continuous dependence on ICs

Lemma 5.3.8. (Stability) *Suppose that* $\left(\mathbf{R}_{\tau,h}^{(m)}\right)$ *or* $\left(\mathbf{R}_{\tau,\theta,h}^{(m)}\right)$ *has two solution sequences,* $\left(\varphi_{h,1}^j,\omega_1^j\right)_{j=1}^M$ *and* $\left(\varphi_{h,2}^j,\omega_2^j\right)_{j=1}^M$*, corresponding to the ICs* $\varphi_{h,1}^0$ *and* $\varphi_{h,2}^0$*. Define their difference at* $t=t_j$ *as*

$$U_h^j := \left(\varphi_h^j,\omega_h^j\right) = \left(\varphi_{h,1}^j,\omega_{h,1}^j\right) - \left(\varphi_{h,2}^j,\omega_{h,2}^j\right), \tag{5.64}$$

and the sequence $\varphi_h := \left(\varphi_h^j\right)_{j=0}^M$*. Then* $\varphi_h\in\ell^\infty\left(0,T;\left(V_*^h\right)'\right)$ *and the sequence is stable, uniformly in* h *and* τ *in that*

$$\left\|\varphi_h\right\|_{\ell^\infty\left(0,T;\left(V_*^h\right)'\right)} := \max_{0\le k\le M}\left\|\varphi_h^k\right\|_{-h} \le C\left(T\right)\left\|\varphi_h^0\right\|_{-h}, \qquad \varphi_h^0 := \varphi_{h,1}^0-\varphi_{h,2}^0, \tag{5.65}$$

where C *is independent of* h *and* τ*, as long as* $\tau\lesssim\varepsilon_\varphi^2$*.*

Remark. Each φ_h^k in the sequence φ_h above is in V_*^h.

This is the fully discrete version of Lemma 5.1.8; Appendix B.33 on p. 430 has a proof.

5.3.9 Fully discrete SSN

For brevity, we do not state or prove a fully discrete version of Theorem 5.2.2, but observe that our conforming spatial discretisation gives such a result (almost) immediately.

5.3.10 Energy monotonicity

Lemma 5.3.9. (Conditional gradient stability) $\left(\mathbf{R}_{\tau,\theta,h}^{(m)}\right)$ *and* $\left(\mathbf{R}_{\tau,h}^{(m)}\right)$ *are conditionally gradient stable if* $f\equiv 0$ *for each* $j=1,\ldots,M$*, in that, as long as* $\tau\lesssim\varepsilon_\varphi^2$*,*

$$\mathcal{E}_{\mu,h}^{(m)}\left[\varphi_h^j\right] \le \mathcal{E}_{\mu,h}^{(m)}\left[\varphi_h^{j-1}\right] \le \ldots \le \mathcal{E}_{\mu,h}^{(m)}\left[\varphi_h^0\right] \qquad \textit{for each} \qquad j=1,\ldots,M. \tag{5.66}$$

The proof mimics that of Lemma 5.1.9; we present details in Appendix B.34 on p. 430.

Remark. This result and its proof also hold for $\mathcal{E}_\mu^{(m)}$ instead of $\mathcal{E}_{\mu,h}^{(m)}$, viz.

$$\mathcal{E}_{\mu}^{(m)}\left[\varphi_h^j\right] \le \mathcal{E}_{\mu}^{(m)}\left[\varphi_h^{j-1}\right] \le \ldots \le \mathcal{E}_{\mu}^{(m)}\left[\varphi_h^0\right] \qquad \text{for each} \qquad j=1,\ldots,M. \tag{5.67}$$

This is an interesting and reassuring result, but is of little practical value because in our code, we can only measure the fully discrete $\mathcal{E}_{\mu,h}^{(m)}$, not $\mathcal{E}_\mu^{(m)}$.

5.3.11 Order of convergence

Theorem 5.3.10. (Order of convergence) *Suppose that $\partial\Omega$ is smooth enough that the exact solutions to $\left(\mathbf{R}^{(\mathbf{m})}_{\mu,\mathbf{f}}\right)$, (φ,ω), are such that*

$$\varphi \in H^1\left(0,T;\left(H^1(\Omega)\right)'\right) \cap L^\infty\left(0,T;H^1(\Omega)\right) \cap L^2\left(0,T;H^2(\Omega)\right). \tag{5.68}$$

Define[12]

$$\varphi_h(t) := \begin{cases} \varphi_h^j & t \in (t_{j-1},t_j]\,; \\ \varphi_h^0 & t = 0, \end{cases} \tag{5.69a}$$

$$\text{and} \qquad e_{\varphi,h}(t) := \varphi(t) - \varphi_h(t)\,; \qquad e^j_{\varphi,h} := e_{\varphi,h}(t_j) = \varphi_j - \varphi_h^j. \tag{5.69b}$$

The finite element approximation $\varphi_h(t)$ converges to $\varphi(t)$ as $h \to 0$ and $\tau \to 0$ in that

$$\|e_{\varphi,h}\|^2_{L^\infty\left(0;T;(H^1(\Omega))'\right)} + \|e_{\varphi,h}\|^2_{L^2(0,T;H^1(\Omega))} \leq C\left(\tau + h^2 + \frac{h^4}{\tau}\right) \tag{5.70}$$

with C independent of h and τ, as long as $\tau \lesssim \varepsilon_\varphi^2$.

This result has no counterpart in our time-discretisation analysis. We present a proof, adapted from that of Theorem 3.5 of Blowey and Elliott (1992), in Appendix B.35 on p. 431.

Remarks.

i) The function φ_h is a piecewise-constant (in time) version of φ_h^j. The error function $e_{\varphi,h}(t)$ measures the difference between the exact solution $\varphi(t)$ and this approximation.

ii) If $\tau = Ch^2$, then an immediate consequence of (5.70) is that

$$\|e_{\varphi,h}\|_{L^2(0,T;H^1(\Omega))} \leq Ch, \tag{5.71}$$

and so it makes sense to try and improve this result to one/both of

$$\|e_{\varphi,h}\|_{\ell^\infty\left((j\tau)_{j=0}^M;H^1(\Omega)\right)} \leq Ch \qquad \text{or} \qquad \|e_{\varphi,h}\|_{\ell^\infty\left((j\tau)_{j=0}^M;L^2(\Omega)\right)} \leq Ch^2; \tag{5.72}$$

the latter being particularly appealing for its experimental tractability. We were able to prove a theorem which said that

$$\|e_{\varphi,h}\|_{\ell^\infty\left((j\tau)_{j=0}^M;L^2(\Omega)\right)} := \max_{0\leq j\leq M}\left\|e^j_{\varphi,h}\right\| \leq C\left(\tau + h^2\right) \tag{5.73}$$

with C independent of h and τ, as long as $\tau \lesssim \mu^2\varepsilon_\varphi^2$.[13] This condition is *prohibitively* restrictive, and makes this result virtually useless. In practice, however, we were able to use *much* larger time-steps ($\lesssim \varepsilon_\varphi^2$) in our Method of Manufactured Solutions (MMS) experiments in Section 5.4.2, which are based on, and confirm (5.73).[14]

5.4 Numerical experiments

We conducted a series of numerical experiments to demonstrate various properties of our numerical methods.

i) In Section 5.4.1 we investigate mass control;

ii) In Section 5.4.2, we demonstrate the convergence of the methods; and

iii) In Section 5.4.3, we examine the impact of the regularisation parameter, μ.

The experiments in Sections 5.4.1, 5.4.2 confirm that we have correctly implemented our code.

5.4.1 Mass control

We performed three investigations using the parameters in Table 5.1.

Type	**Parameter**	**Values**
Model	ε_φ^2	1.0
	χ^{AB}	1.0
	m	0
	Ω	$x \in (0,1)$ (1D)
	ICs	$\varphi_0 \equiv \overline{\varphi_0}$; constant ICs
Control	h	10^{-3}
	Regularisation	$\mu = 10^{-6}$

Table 5.1: Default mass control test parameters (2-phase, 1D)

i) We investigated the mass control expression (5.23) with

$$\theta \in \left\{1, \frac{1}{2}\right\}, \qquad \alpha = 10, \qquad \overline{\varphi_0} \in \{\pm 0.8, \pm 0.5, 0\} \qquad \text{and} \qquad \tau = 10^{-3}. \tag{5.74}$$

Summary results appear in Fig. 5.2. The actual and expected masses were indistinguishable; there was no visible difference between the results for $\theta = 1$ and $\theta = \frac{1}{2}$.

ii) We then tested our code to ensure that (5.29) holds with $h = 0.1$ and

$$\alpha = 10, \quad \overline{\varphi_0} = 0.8, \quad T = 1 \quad \text{and} \quad \tau \in \left\{10^{-1}, 10^{-2}, 5 \times 10^{-3}, 10^{-3}, 5 \times 10^{-4}, 10^{-4}\right\}. \tag{5.75}$$

Summary results of this (successful) experiment appear in Fig. 5.3.

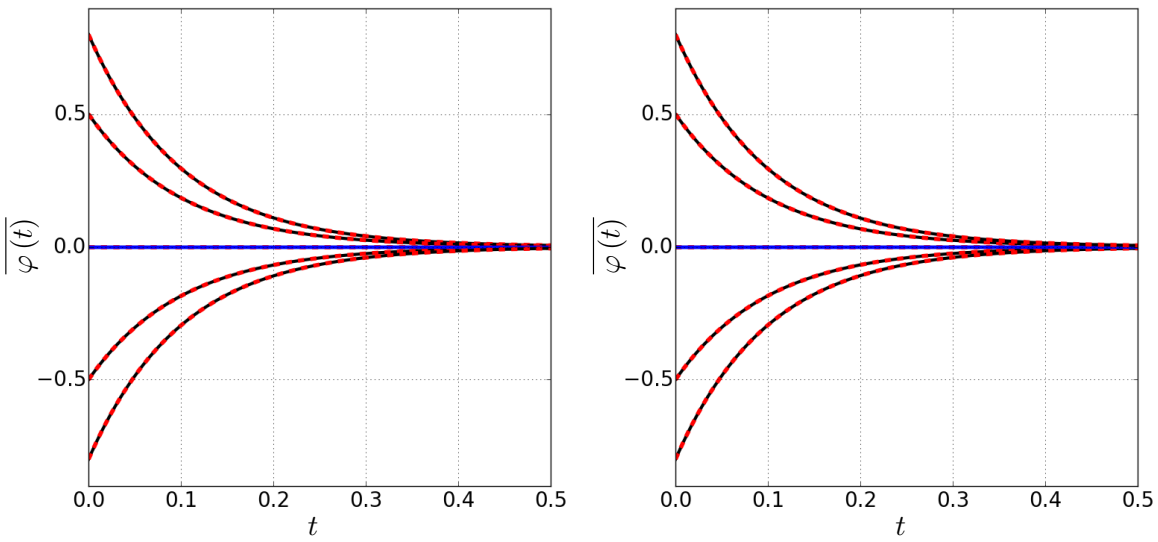

(a) $\theta = 1$: fully-implicit non-local term

(b) $\theta = \frac{1}{2}$: semi-implicit non-local term

Figure 5.2: Mass control experiment results (2-phase, 1D) with parameters as in (5.74) and Table 5.1. The actual, recorded mass evolution trajectory for each experiment is drawn in **black**; the expected trajectories from (5.23) are drawn in dashed **red**. The control mass $m = 0$ is marked in solid **blue**.[15]

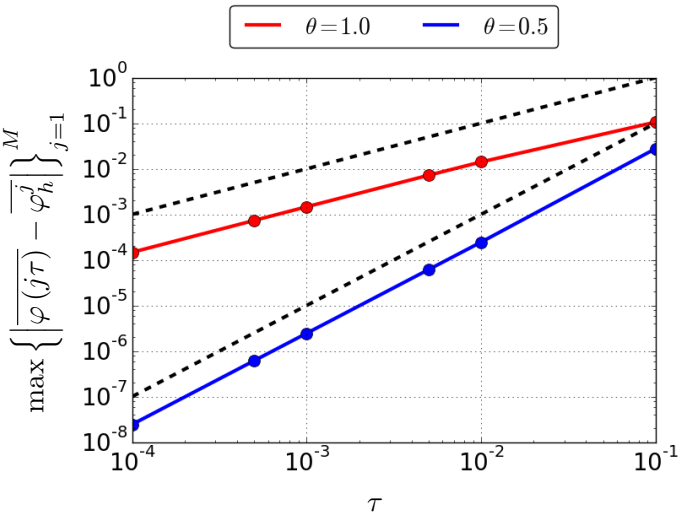

Figure 5.3: Mass control convergence test based on parameters in (5.75). For $\theta = 1$ in **red**, the convergence appears to be linear (the corresponding guideline has unit gradient); for $\theta = \frac{1}{2}$ in **blue**, the convergence appears to be quadratic (the corresponding guideline has gradient two), as predicted by (5.29).[16]

iii) Finally, we explored the effect of deliberately violating the requirement in (5.23) that

$$\left|\frac{1+\tau\alpha\theta-\tau\alpha}{1+\tau\alpha\theta}\right|<1.$$

To achieve this, we selected τ, α and θ such that

$$0\leq\theta<\frac{1}{2}-\frac{1}{\tau\alpha}\qquad\text{viz.}\qquad\tau\alpha>2.$$

In particular, we made the non-local term fully explicit, with

$$\theta=0,\qquad\alpha=210,\qquad\overline{\varphi_0}=10^{-4}\qquad\text{and}\qquad\tau=10^{-2}.$$

Results appear in Fig. 5.4. These results are understandable in light of our analysis in Section 5.1.2. Even though $\tau\ll\varepsilon_\varphi^2$, there is a major instability; this cannot occur if $\theta\geq\frac{1}{2}$. There is no such effect in the mass *conserving* Cahn–Hilliard case.

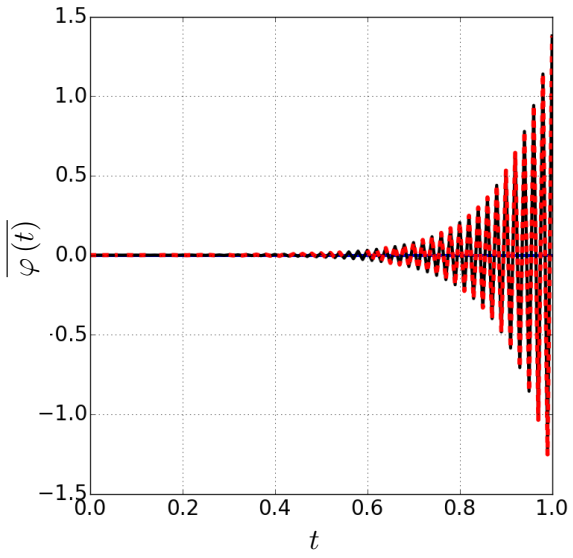

Figure 5.4: Fully explicit ($\theta=0$) non-local mass control experiment (2-phase, 1D). The recorded mass evolution trajectory of the experiment is drawn in **black**; the expected trajectory from (5.23) is drawn in dashed **red**. The control mass $m=0$ is marked in solid **blue**, but is largely hidden beneath the other lines.[17]

Remark. We tested a second degree regularisation, but the mass control results are independent of the homogeneous term (cf. Section 5.2.1).

5.4.2 MMS testing: order of convergence

Consider a numerical method $A\left(\varphi_h^j\right) = 0$ with unknown φ_h^j, for which exact, analytical solutions are not available. The idea behind the MMS technique is to manufacture an exact solution φ_{E} and solve for f in $f\left(\varphi_{\mathrm{E}}\right) = A\left(\varphi_{\mathrm{E}}\right)$. $f\left(\varphi_{\mathrm{E}}\right)$ is then injected into the right-hand side of the numerical method as $A\left(\varphi_h^j\right) = f\left(\varphi_{\mathrm{E}}\right)$ to (hopefully) recover the manufactured solution $\varphi_h^j = \varphi_{\mathrm{E}}$ (up to numerical and other approximation errors).

We explore two ways of doing this, and numerically test our (preferred) second degree regularisation and the fourth degree regularisation of Section 5.2.1.

Type I MMS

First, we put f on the first line of the problem, viz. (cf. (3.35))

$$\begin{gathered}\partial_t\varphi + (-\Delta)\,\omega + \alpha\,(\varphi - m) = \boxed{f\,(\varphi)} \leftarrow \\ \omega := \varepsilon_\varphi^2\,(-\Delta)\,\varphi - \frac{\chi^{AB}}{2}\varphi + \zeta_\mu\,(\varphi)\,.\end{gathered}$$

Given a manufactured φ_{E}, we use the second equation above to find that

$$\omega_{\mathrm{E}}\left(\varphi_{\mathrm{E}}\right) := \varepsilon_\varphi^2\,(-\Delta)\,\varphi_{\mathrm{E}} + \mathcal{B}'_\mu\left(\varphi_{\mathrm{E}}\right) = \underbrace{\varepsilon_\varphi^2\,(-\Delta)\,\varphi_{\mathrm{E}} - \frac{\chi^{AB}}{2}\varphi_{\mathrm{E}}}_{:=\,\omega_{\mathrm{base}}} + \underbrace{\zeta_\mu\left(\varphi_{\mathrm{E}}\right)}_{:=\,\omega_{\mathrm{penalty}}}\,, \tag{5.76}$$

so that (cf. (3.41), (3.51))

$$\begin{aligned}f\left(\varphi_{\mathrm{E}}\right) &= \partial_t\varphi_{\mathrm{E}} - \Delta\omega_{\mathrm{E}}\left(\varphi_{\mathrm{E}}\right) + \alpha\left(\varphi_{\mathrm{E}} - m\right) \\ &= \underbrace{\partial_t\varphi_{\mathrm{E}} + \varepsilon_\varphi^2\Delta^2\varphi_{\mathrm{E}} + \frac{\chi^{AB}}{2}\Delta\varphi_{\mathrm{E}} + \alpha\left(\varphi_{\mathrm{E}} - m\right)}_{:=\,f_{\mathrm{base}}} + \underbrace{(-\Delta)\,\zeta_\mu\left(\varphi_{\mathrm{E}}\right)}_{:=\,f_{\mathrm{penalty}}}.\end{aligned} \tag{5.77}$$

We define $f_{\mathrm{E}}^j := f\left(\varphi_{\mathrm{E}}\left(t_j\right)\right)$, and inject $f\left(\varphi_{\mathrm{E}}\right)$ into the numerical method using

$$\begin{gathered}\left(\frac{\varphi_{\mathrm{N}}^j - \varphi_{\mathrm{N}}^{j-1}}{\tau}, \nu_1\right) + M_\varphi\left(\left(\nabla\omega_{\mathrm{N}}^j, \nabla\nu_1\right) + \alpha\left(\varphi_{\mathrm{N}} - m, \nu_1\right)\right) = \left(\frac{f_{\mathrm{E}}^{j-1} + f_{\mathrm{E}}^j}{2}, \nu_1\right) \\ \varepsilon_\varphi^2\left(\nabla\varphi_{\mathrm{N}}, \nabla\nu_2\right) + \left(\mathcal{B}'_\mu\left(\varphi_{\mathrm{N}}\right), \nu_2\right) = \left(\omega_{\mathrm{N}}^j, \nu_2\right),\end{gathered} \tag{5.78}$$

to recover the numerical solution $\left(\varphi_{\mathrm{N}}^j, \omega_{\mathrm{N}}^j\right)$.

Remarks.

i) In the abstract analysis of the first part of this chapter, type I MMS corresponds to setting $f_2 \equiv 0$ in (5.12), and specifying/injecting a given $f = f_1$.

ii) We experimented with different time integration rules for f; (5.78) demonstrates the trapezium rule.[18] See also the second remark immediately after Defn 5.1.1, on p. 77.

For the second degree regularisation scheme in (4.8), finding f_{penalty} in (5.77) explicitly is not possible, and so we seek $f = f_{\text{base}} + f_{\text{penalty}}$ with

$$\left(f_{\text{penalty}}\left(\varphi_{\text{E}}\right), \nu\right) = \frac{1}{\mu}\left(\mathbf{1}\left\{\left|\varphi_{\text{E}}\right| > 1\right\}\nabla\varphi_{\text{E}}, \nabla\nu\right) \qquad \text{for every} \qquad \nu \in H^1\left(\Omega\right) \tag{5.79a}$$

where, using (4.14a) and (5.43),

$$\nabla\zeta_\mu\left(\varphi_{\text{E}}\right) = \zeta_\mu'\left(\varphi_{\text{E}}\right)\nabla\varphi_{\text{E}} = \frac{1}{\mu}\mathbf{1}\left\{\left|\varphi_{\text{E}}\right| > 1\right\}\nabla\varphi_{\text{E}}. \tag{5.79b}$$

Solving (5.79) numerically introduced an error which was larger than the overall approximation error, and so we could not use type I MMS for the second degree regularisation. However, we could determine an explicit, strong f from (5.77) for the fourth degree regularisation, in which (cf. (5.45)),

$$\begin{aligned}\Delta\zeta_\mu\left(\varphi_{\text{E}}\right) &= \frac{1}{\mu}\Delta\left(\left(\varphi_{\text{E}} - 1\right)_+^3 + \left(\varphi_{\text{E}} + 1\right)_-^3\right) \\ &= \frac{1}{\mu}\left(6\left(\left(\varphi_{\text{E}} - 1\right)_+ + \left(\varphi_{\text{E}} + 1\right)_-\right)\left|\nabla\varphi_{\text{E}}\right|^2 + 3\left(\left(\varphi_{\text{E}} - 1\right)_+^2 + \left(\varphi_{\text{E}} + 1\right)_-^2\right)\Delta\varphi_{\text{E}}\right).\end{aligned} \tag{5.80}$$

Type II MMS

Alternatively, we define F_1 as part of the chemical potential as in (5.12), so that

$$\begin{gathered}\partial_t\varphi + \left(-\Delta\right)\omega + \alpha\left(\varphi - m\right) = 0 \\ \omega := \varepsilon_\varphi^2\left(-\Delta\right)\varphi - \frac{\chi^{AB}}{2}\varphi + \zeta_\mu\left(\varphi\right) + \boxed{F_1\left(\varphi\right)}, \leftarrow\end{gathered}$$

i.e. for given φ_{E},

$$F_1\left(\varphi_{\text{E}}\right) = \omega_{\text{E}} + \varepsilon_\varphi^2\Delta\varphi_{\text{E}} - \mathcal{B}_\mu'\left(\varphi_{\text{E}}\right) = \underbrace{\omega_{\text{E}} + \varepsilon_\varphi^2\Delta\varphi_{\text{E}} + \frac{\chi^{AB}}{2}\varphi_{\text{E}}}_{:= F_{\text{base}}} - \underbrace{\zeta_\mu\left(\varphi_{\text{E}}\right)}_{:= F_{\text{penalty}}}, \tag{5.81a}$$

$$\text{where} \qquad \omega_{\text{E}} = \left(-\Delta_n\right)^{-1}\left(-\frac{\partial_t\varphi_{\text{E}}}{M_\varphi} - \alpha\left(\varphi_{\text{E}} - m\right)\right). \tag{5.81b}$$

We define $F_{\text{E}}^j := F_1\left(\varphi_{\text{E}}\left(t_j\right)\right)$, and replace (5.78) with

$$\begin{aligned}\left(\frac{\varphi_{\text{N}}^j - \varphi_{\text{N}}^{j-1}}{\tau}, \nu_1\right) + M_\varphi\left(\left(\nabla\omega_{\text{N}}^j, \nabla\nu_1\right) + \alpha\left(\varphi_{\text{N}} - m, \nu_1\right)\right) &= 0 \\ \varepsilon_\varphi^2\left(\nabla\varphi_{\text{N}}, \nabla\nu_2\right) + \left(\mathcal{B}_\mu'\left(\varphi_{\text{N}}\right), \nu_2\right) = \left(\omega_{\text{N}}^j, \nu_2\right) + \left(\frac{F_{\text{E}}^{j-1} + F_{\text{E}}^j}{2}, \nu_2\right).\end{aligned} \tag{5.82}$$

This approach could be used for both of our regularisation approaches.

Remark. In the abstract analysis of the first part of this chapter, type II MMS corresponds to setting $f_1 \equiv 0$ in (5.12), and specifying/injecting a given f_2.

Experiment setup: parameters

We tested various combinations of the parameters in Table 5.2.[19] φ_{E} in the table is smooth, and $\partial_n \varphi_{\mathrm{E}}(0,t) = \partial_n \varphi_{\mathrm{E}}(1,t) = 0$ and $\overline{\varphi_{\mathrm{E}}(t)} = m$ for every t. (5.76) reveals that $\partial_n \omega_{\mathrm{E}}(0,t) = \partial_n \omega_{\mathrm{E}}(1,t) = 0$. Moreover, $\|\varphi_{\mathrm{E}}\|_{L^\infty(0,T;L^\infty(\Omega))} > 1$ i.e. we should have $f_{\text{penalty}}(\varphi_{\mathrm{E}}) \neq 0$ for part of each simulation. We set $\tau = Ch^2$ in anticipation of an $\mathcal{O}\left(\tau + h^2\right)$ result.

Remark. Our experimental IC differed from that in (5.57a): instead of using the $P_m^{(\star)}$ projection, we set $\varphi_h^0 = \mathcal{I}^{(h)}\varphi_{\mathrm{E}}(0)$. This had no noticeable effect on the results.[20]

Type	**Parameter**	**Values**						
Model	ε_φ^2	1.0						
	χ^{AB}	1.0						
	α	100						
	Ω	$x \in (0,1)$						
$\varphi_{\mathrm{E}}(x,t)$		$m + \mathrm{e}^{C\sin(t)}\cos(2\pi x)$, $C \in \left\{\frac{1}{2}, 1\right\}$						
Control	T	10.0						
	h (test)	1/10	1/20	1/50	1/100	1/200	1/500	1/1 000
	τ $\left(= 100h^2\right)$	1.0	0.25	0.04	0.01	0.0025	0.0004	10^{-4}
	# time-steps (M)	10	40	250	1 000	4 000	25 000	10^5
	Time-splitting	Non-local: $\theta \in \left\{\frac{1}{2}, 1\right\}$						
		χ^{AB} term: implicit and explicit (convex splitting)						
	Regularisation	$\mu \in \left\{10^{-3}, 10^{-4}, 10^{-6}\right\}$						

Table 5.2: 2-Phase MMS test parameters (1D). For each test there are seven (h, τ) pairs.

Second degree regularisation experiments

We ran four sets (A, B, C, D) of type II MMS experiments to test the second degree regularisation. Details are in Table 5.3; summary results appear in Fig. 5.5(a).

Fourth degree regularisation experiments

We ran four sets (E, F, G, H) of type II MMS experiments to test the fourth degree regularisation. Setup details are in Table 5.4; summary results appear in Fig. 5.5(b).

Set	$\varphi_{\mathrm{E}}(x,t)$	m	χ^{AB} term	Non-local term	μ
A	$\mathrm{e}^{\sin(t)}\cos(2\pi x)$	0	explicit	$\theta = 1$	10^{-3}
B	$\mathrm{e}^{\sin(t)}\cos(2\pi x)$	0	implicit	$\theta = \frac{1}{2}$	10^{-6}
C	$\frac{1}{2} + \mathrm{e}^{\sin(t)}\cos(2\pi x)$	$\frac{1}{2}$	implicit	$\theta = 1$	10^{-3}
D	$\frac{1}{2} + \mathrm{e}^{\sin(t)}\cos(2\pi x)$	$\frac{1}{2}$	explicit	$\theta = \frac{1}{2}$	10^{-6}

Table 5.3: Second degree regularisation MMS test parameters

Set	$\varphi_{\mathrm{E}}(x,t)$	m	χ^{AB} term	Non-local term	μ
E	$\mathrm{e}^{\sin(t)}\cos(2\pi x)$	0	implicit	$\theta = \frac{1}{2}$	10^{-4}
F	$\mathrm{e}^{\sin(t)}\cos(2\pi x)$	0	explicit	$\theta = \frac{1}{2}$	10^{-6}
G	$\frac{1}{2} + \mathrm{e}^{\frac{1}{2}\sin(t)}\cos(2\pi x)$	$\frac{1}{2}$	explicit	$\theta = 1$	10^{-6}
H	$\frac{1}{2} + \mathrm{e}^{\sin(t)}\cos(2\pi x)$	$\frac{1}{2}$	implicit	$\theta = 1$	10^{-4}

Table 5.4: Fourth degree regularisation MMS test parameters

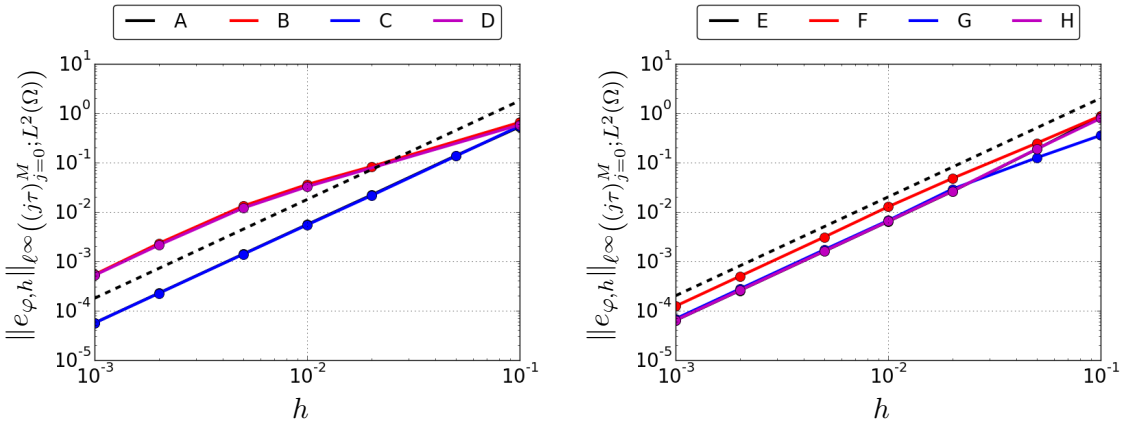

(a) Results of the second degree regularisation MMS experiments in Table 5.3

(b) Results of the fourth degree regularisation MMS experiments in Table 5.4

Figure 5.5: MMS convergence results in 1D for two sets of MMS experiments as specified in the indicated tables, with common configuration in Table 5.2. The dashed, black lines indicate a quadratic relationship for comparison.[21]

Discussion, observations

As expected, our observed error was $\mathcal{O}\left(h^2\right)$, matching the prediction in (5.73). The rate of convergence appears to be unaffected by the way we time-split the homogeneous and non-local terms. The solution mass $\overline{\varphi_{\mathrm{E}}}$ has no material impact on the error, either. We went further than our theoretical result, and provided numerical evidence of the rate of convergence for two different regularisations of the homogeneous term.[22]

For the second degree regularisation (cf. Fig. 5.5(a), the errors for $\mu = 10^{-6}$ (sets B and D; the **red** and **magenta** lines) were significantly larger (by an order of magnitude) than for $\mu = 10^{-3}$ (sets A and C; the **blue** and **black** lines). For the smaller μ-value, finer meshes and smaller time-steps were required to observe the asymptotic order of convergence.

Remark. This suggests that C in (5.73) may depend on μ.

5.4.3 Regularisation parameter (μ) effects

Next, we explored the effect of the regularisation parameter, μ on the second degree regularisation. We ran a series of experiments with the parameters listed in Table 5.5. We started each of the experiments from the same IC, which we depict in Fig. 5.6(a). The IC was constructed using techniques we will discuss in Section 8.2. We believe it is the interpolant of a (non-unique) global energy minimiser of problem (**M**) in (4.24), for these parameters. Summary results appear in Fig. 5.7.[23]

Type	**Parameter**	**Values**
Model	ε_φ^2	10^{-4}
	χ^{AB}	1.0
	α	100
	m	0
	Ω	$x \in (0,1)$
	Substrate phase	B
Control	T	5.0
	h	10^{-3} $\quad 5\times10^{-4}$ $\quad 2\times10^{-4}$ $\quad 10^{-4}$
	τ	10^{-4}
	Time-splitting	$\theta = 1$ (implicit)
		χ^{AB} term: semi-implicit
	Regularisation	$\mu \in \left\{10^{-2}, 10^{-3}, \ldots, 10^{-8}\right\}$

Table 5.5: 2-Phase μ-experiment parameter set (1D)

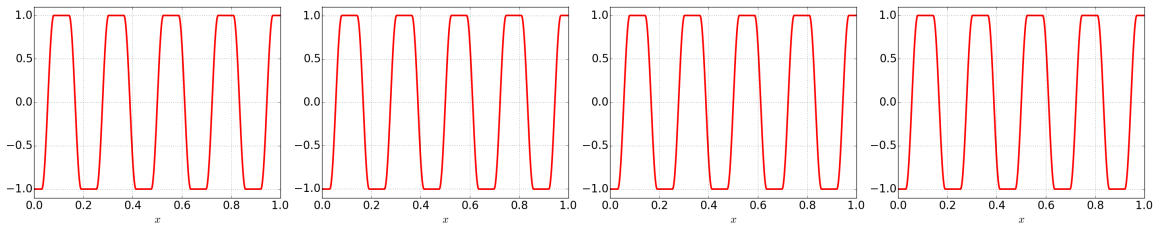

(a) Common IC (b) $\mu = 10^{-2}$ (c) $\mu = 10^{-3}$ (d) $\mu = 10^{-4}$

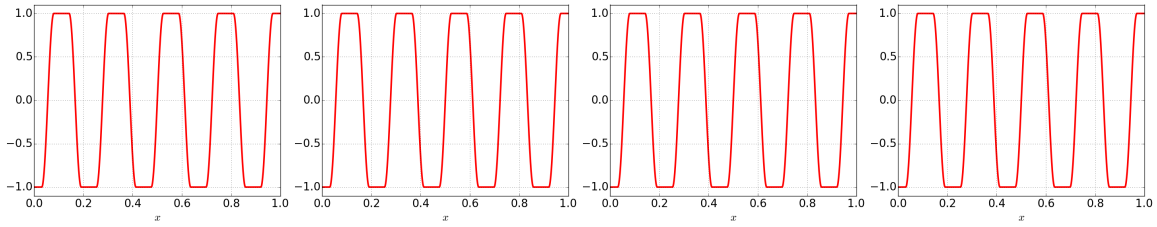

(e) $\mu = 10^{-5}$ (f) $\mu = 10^{-6}$ (g) $\mu = 10^{-7}$ (h) $\mu = 10^{-8}$

Figure 5.6: The IC, with nine equally spaced monolayers, and the seven end-states for the tested μ-values. The end-states all had the same number of monolayers as the IC.[24]

Discussion, observations

For $\mu \in \left\{10^{-2}, 10^{-3}, \ldots, 10^{-8}\right\}$, the results in Fig. 5.7(a) suggest that (cf. (4.70), (4.5b))

$$\Upsilon_{\mu,\infty} := \max\left\{\left(\varphi\left(T\right)-1\right)_{+}, -\left(\varphi\left(T\right)+1\right)_{-}\right\} = \left\|\varphi\left(T\right)\right\|_{0,\infty} - 1 \sim \mathcal{O}\left(\mu\right) \quad \text{as} \quad \mu \downarrow 0. \tag{5.83}$$

The results in Fig. 5.7(b) are consistent with these. If $\Upsilon_{\mu,\infty} \sim \mathcal{O}\left(\mu\right)$, then (cf. (4.6))

$$\mathcal{E}_{\text{penalty}}\left[\varphi\left(T\right)\right] := \frac{1}{2\mu}\int_{\Omega}\left[\left(\varphi\left(T\right)-1\right)_{+}^{2} + \left(\varphi\left(T\right)+1\right)_{-}^{2}\right]\mathrm{d}\Omega \sim \mathcal{O}\left(\mu\right). \tag{5.84}$$

The results in Fig's 5.7(c)–(d) suggest that we should be able to reliably estimate the energy of global minimisers if $\mu < 10^{-6}$. Smaller values of μ yield higher accuracy energy estimates (viz. end-states that are more similar to energy minimisers), but we can practically work with $\mu \sim 10^{-6}$.

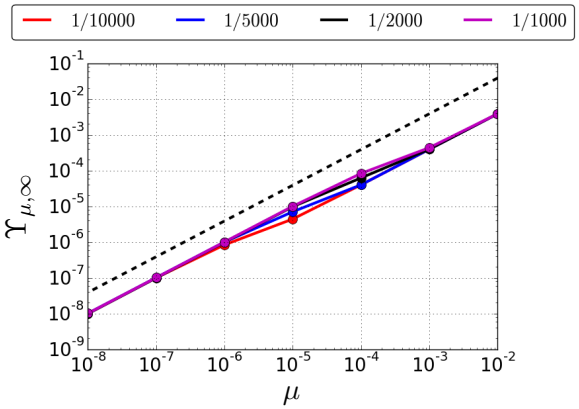

(a) Log-log plot of $\Upsilon_{\mu,\infty}$ in (5.83) against μ for the four indicated h-values.

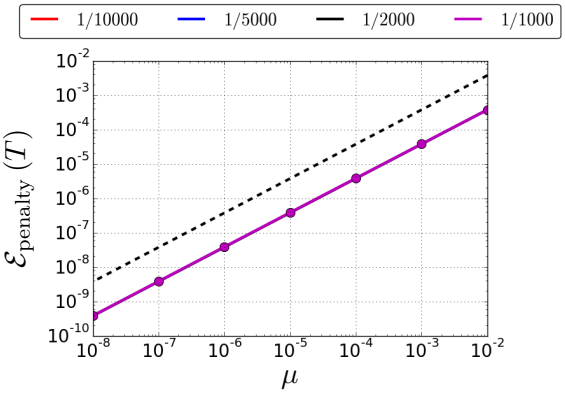

(b) Log-log plot of the end-state penalty energy $\mathcal{E}_{\text{penalty}}$ against μ for four h-values.

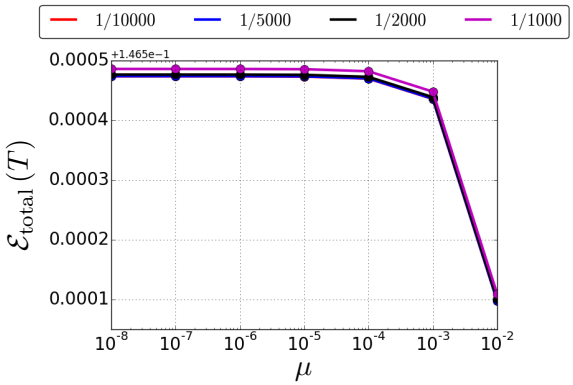

(c) Semi-log (x) plot of the end-state total energy $\mathcal{E}_{\text{total}}$ against μ for four h-values. For $\mu \lesssim 10^{-4}$, the total energy is approximately constant w.r.t. μ. The end-state energy decreases with increasing μ, and can be negative.

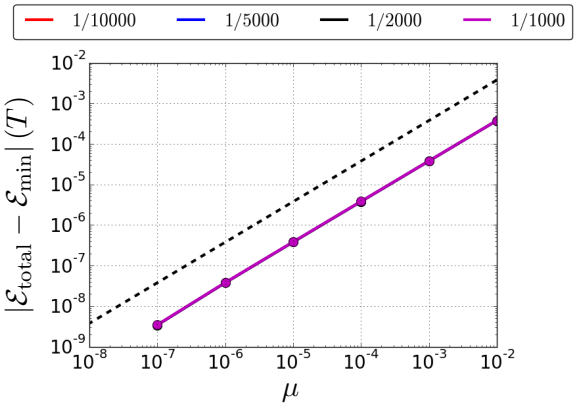

(d) Log-log plot of the magnitude of the difference between each end-state energy and that recorded for the smallest μ in the test set, against μ for four h-values.

Figure 5.7: Results of a 2-phase μ-study for four h-values. In the log-log plots, the reference, dashed black lines indicate a linear relationship. In all instances, the individual lines are close, becoming indistinguishable for very small μ-values. This suggests that these effects are asymptotically mesh independent.[25]

5.5 Summary

In this chapter, we proposed and analysed practical techniques for finding approximate solutions to the variational inequalities of Chapter 4, using gradient flows. The second degree regularisation of the homogeneous term was intrinsic to our numerical methods. We summarise the relationships between the problems we studied in Fig. 5.8.

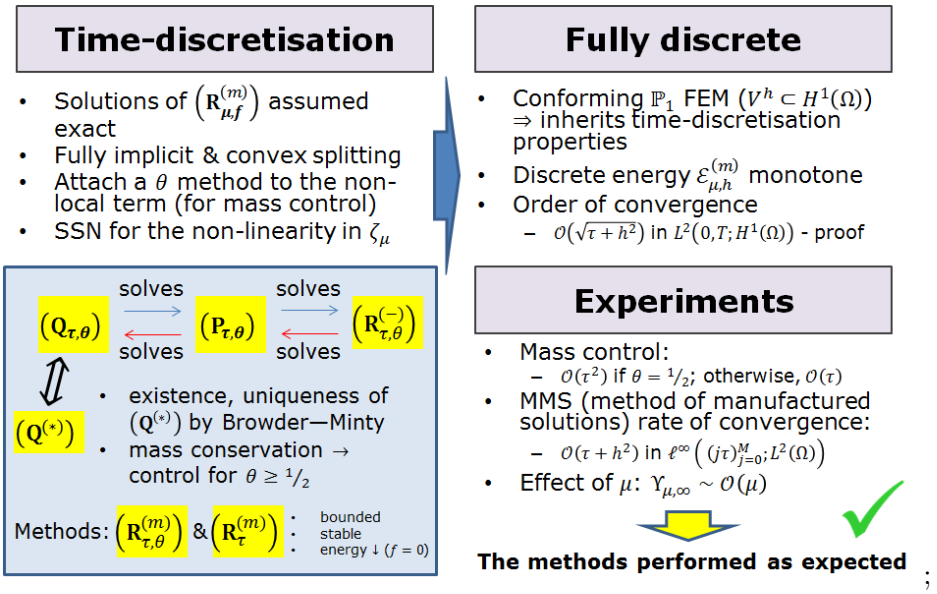

Figure 5.8: Summary of the relationships between the results in Chapter 5

To start, we posed a family of in-time, single-step Euler discretisations (step size τ) of the gradient flow system (with an $H^1(\Omega)$ solution at each time-step), which we then analysed in detail. We proved that our proposed discretisations are well-posed (solutions exist and are unique), bounded, stable (solutions have a continuous dependence on the ICs), mass controlling and energy decaying (or 'gradient stable'). We then addressed the question of resolving the non-linear, non-differentiable part of the calculation at each time-step. We proposed and analysed the semi-smooth Newton (SSN) method, which generalises the Newton method, and proved that this technique would converge to the unique solution that we previously established exists.

We then proposed a (conforming) $\mathbb{P}_1$ finite-element discretisation (mesh-size parameter h) of the spatial part of the problem, and analysed the fully discrete scheme, in detail. Our choice of conforming spatial approximation allowed us to focus on the effects of the *time* discretisation as distinct from the *spatial* discretisation. Crucially, we predicted that the error in our fully discrete approximation φ_h^j of φ_μ should be $\mathcal{O}\left(\tau + h^2\right)$ (as $h, \tau \downarrow 0$).

Finally, we subjected our FEniCS code to a battery of tests, the most important of which was the MMS-test, which confirmed the order of convergence of the method.

5.5.1 Opportunities for further study

We close by listing possible extensions to the work in this chapter.

i) In this chapter, we regarded the solutions of the regularised version of the underlying variational inequality as exact. Another approach would be to **discretise the variational inequality directly**, using techniques such as those in Section 11.4 of Atkinson and Weimin (2009), and Blowey and Elliott (1992). Our approach facilitated the MMS experiments we performed in Section 5.4.2.[26] We adapted the results in Blowey and Elliott (1992) and so, in some sense, our approach encapsulates the variational inequality approach.[27]

   Our regularisation is core to the code we will use for our numerical investigations in subsequent chapters. That is, we have analysed the numerical approximation we will actually use.

ii) In the previous chapter, we established a series of results about the gradient flow problem assuming a Galerkin approximation based on the eigenfunctions of a certain differential operator. Another, more streamlined approach, might be based on the approximation of this chapter (we would send $h \downarrow 0$, then $\tau \downarrow 0$ and finally $\mu \downarrow 0$).[28]

iii) All of our results assumed that $\overline{\varphi_0} = m$. We also analysed mass control under which $\overline{\varphi_j} \to m$ exponentially quickly in the event that $\overline{\varphi_0} \neq m$ (we showed that all of our approximation schemes have the same property). We did not show that the problem is well-posed if $\overline{\varphi_0} \neq m$.[29]

iv) We **ignored quadrature effects** for the sake of simplicity (by deliberately not defining the $(\cdot,\cdot)^h$ inner product). Such effects could impact additional numerical experiments (see below), and for this reason, understanding them could be valuable.

v) There are numerous **additional numerical experiments** that could be conducted. For instance, we did not verify the *unconditional* gradient stability of $\left(\mathbf{R}^{(m)}_{\tau,\theta,h}\right)$, by comparison with the *conditional* gradient stability of the fully implicit $\left(\mathbf{R}^{(m)}_{\tau,h}\right)$. It should also be possible to use our MMS testing framework to verify and demonstrate the super-linear convergence of the SSN scheme at each time-step.

vi) **Convergence/MMS**. We opted to verify (5.73) in our MMS experiments because of its simplicity. For completeness, an experimental verification of (5.70) should also be conducted (although this would be non-trivial). Conversely, a theorem predicting (5.73) *without* the requirement that $\tau \lesssim \mu^2\varepsilon_\varphi^2$ would be useful.[30]

vii) We did not establish **discrete versions of the semi-flow result** of Lemma 4.3.9. Such a result would imply that (numerical) solutions of our discretised gradient flow

problem approximate solutions of a certain stationary energy minimisation problem, as $T \to \infty$.

Remark. Practically, when computing, we assume that we have an approximation of a stationary morphology whenever $\mathrm{d}\mathcal{E}_{\mu,h}^{(m)}/\mathrm{d}t$ is very small.[31]

viii) We deliberately used a simple time-stepping scheme so as to focus on the C^1 regulariser and the non-local term. Consequently, our scheme is only first order accurate in time. Having dealt with the regularisation scheme and the non-local term, it would be beneficial to consider second or higher order accurate time-stepping schemes like the **multi-step approach** discussed in Diegel et al. (2015).

Remark. A word of caution may be in order: in Diegel et al. (2015), the authors study a quartic polynomial homogeneous energy, which can be readily bounded above. For our regularised obstacle homogeneous term, the upper bound involves a $1/\mu$ factor which becomes unbounded as $\mu \downarrow 0$. Bounding ζ_μ from *below* (independent of μ) by monotonicity is possible (we used this fact repeatedly in the proofs in Appendix B), but this could make the analysis somewhat more awkward.

ix) **Comparing second and fourth degree regularisation schemes.** We focused on the second degree regularisation of the homogeneous double obstacle term, and only mentioned the fourth order regularisation scheme in passing. It would be useful to compare these two schemes. One way to do this, is on a like-for-like basis as illustrated in Fig. 5.9, where we compare how the two methods performed for a common MMS experiment. The advantage of this approach is that the two methods are forced to progress from one predefined state to the next, on each time-step (as forced by our forcing function), and so they 'do the same work' on each step.

x) **SSN mesh (in)dependence**: non-linear iteration counts. In Blank et al. (2013), the authors numerically investigate mesh independence of their PDAS method (which is typically analysed as equivalent to a type of SSN scheme). They report that '*the number of PDAS iterations might depend on the mesh size h. Analytical results on this are still lacking.*' In their Table VII, they report a mild increase in the average number of PDAS iterations as h decreases. Inspired by this, we did an initial investigation of the relationship between h and the number of SSN iterations per time-step, using a variant of MMS Test Set D (cf. Table 5.3, Fig. 5.5(a)). Whereas $\tau = Ch^2$ in the MMS experiments, this time we set $\tau = 0.01$ and,

$$h \in \left\{10^{-1}, 10^{-2}, 10^{-3}, 10^{-4}, 10^{-5}\right\} \quad \text{and} \quad \tau = 0.01, \quad T = 5, \quad M = 500. \tag{5.85}$$

The only parameter that varies from one experiment to the next is h. Summary results in Fig. 5.10 suggest that the iteration count *increases* (albeit slowly) with decreasing h. The implications of this are not clear.

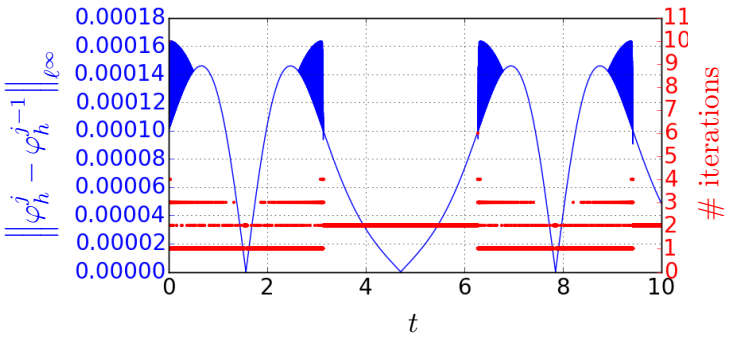

(a) Second degree regularisation: the seventh experiment in Set B. Wall-time: 2h25mins. A large proportion of the time-steps converged in one or two SSN iterations.

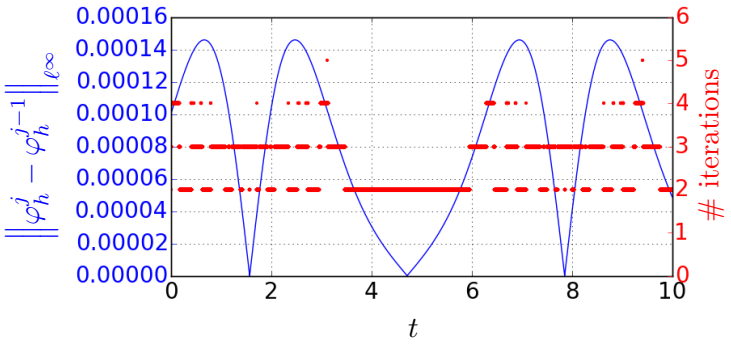

(b) Fourth degree regularisation: the seventh experiment in Set F. Wall-time: 2h45mins. None of the time-steps converged in a single Newton iteration; a significant proportion converged in two or three iterations.

Figure 5.9: Solver performance comparison for the second and fourth degree regularisation approaches in the MMS experiments we reported on in Section 5.4.2. Same spatial ($h = 10^{-3}$) and temporal ($\tau = 10^{-4}$) discretisation; same μ-value (10^{-6}). We plot the maximum change in the numerical solution from one time-step to the next against the left y-axis (in blue). We use this measure of solution change on each time-step as a proxy for the amount of work the solver has to do. The number of iterations inside each time-step is plotted on the right y-axis (in red). Both quantities are plotted against the simulation time, t.

Remark. In the earlier reference Hintermüller et al. (2011), the authors report that (see Section 8) '*[a]s expected, the [Moreau–Yosida] SSN solver features mesh-independent convergence*', although they do not say why this is expected (their list of citations includes Hintermüller and Ulbrich (2004) which is suggestive). In any case, our results in this regard are quite different from theirs, and it may be interesting and useful to understand why.

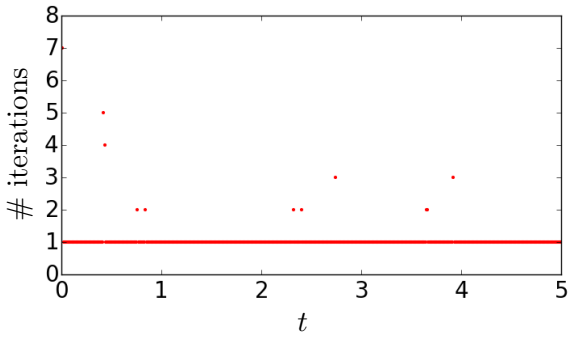

(a) $h = 10^{-1}$; avg. # iterations: 1.05

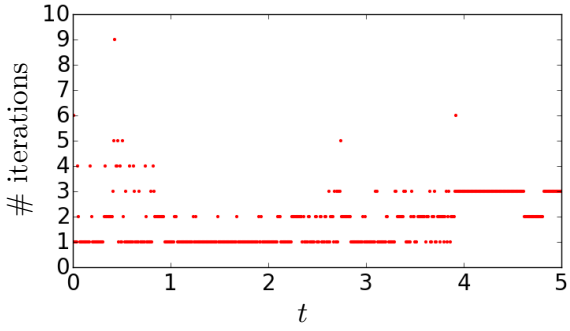

(b) $h = 10^{-2}$; avg. # iterations: 1.82

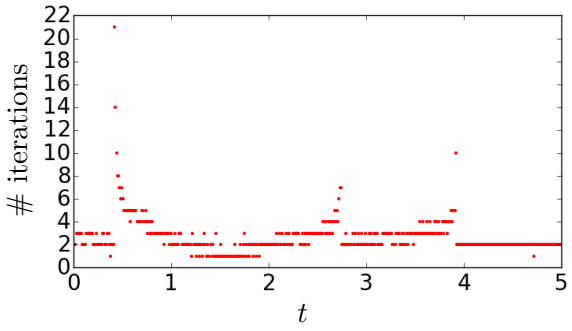

(c) $h = 10^{-3}$; avg. # iterations: 2.65

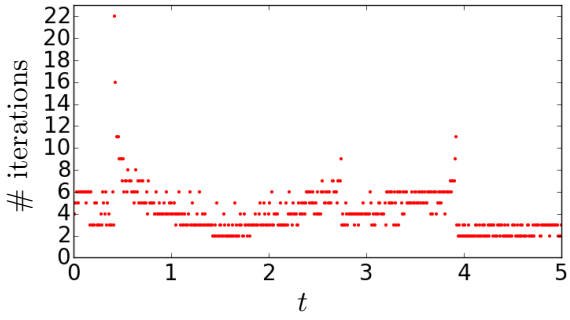

(d) $h = 10^{-4}$; avg. # iterations: 4.19

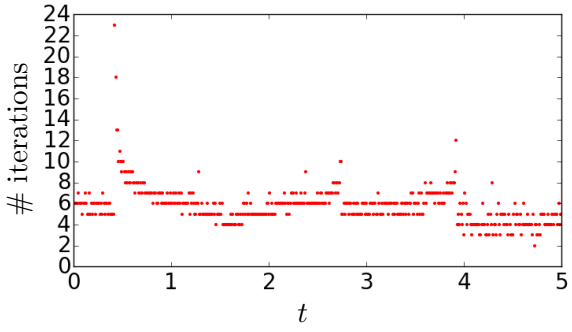

(e) $h = 10^{-5}$; avg. # iterations: 5.82

Figure 5.10: Mesh (in)dependence investigation. It looks like the SSN iteration count scales (roughly) as $-\log(h)$.[32]

Notes

[1]It could be possible to split this term across time, but making it fully *explicit* would likely lead to a disaster on the first time-step, assuming $\varphi_0 \in \mathscr{A}_m$ since the non-penalised portion of the bulk density (i.e. the entire thing) would be unbounded below.

[2]We will see that they all have zero mass.

[3]The last equality comes from

$$\mathring{\varphi}^j_{\{\theta\}} = \theta\mathring{\varphi}^j + (1-\theta)\,\mathring{\varphi}^{j-1} = \theta\left(\varphi^j - \overline{\varphi^j}\right) + (1-\theta)\left(\varphi^{j-1} - \overline{\varphi^{j-1}}\right) = \varphi^j_{\{\theta\}} - \overline{\varphi^j_{\{\theta\}}}.$$

[4]This is because

$$1 + \tau\alpha\theta > \frac{\tau\alpha}{2} > 0 \qquad \Rightarrow \qquad -(1 + \tau\alpha\theta - \tau\alpha) < 1 + \tau\alpha\theta,$$

but also

$$\tau\alpha > 0 \qquad \Rightarrow \qquad 1 + \tau\alpha\theta - \tau\alpha < 1 + \tau\alpha\theta$$

which means that

$$|1 + \tau\alpha\theta - \tau\alpha| < 1 + \tau\alpha\theta < |1 + \tau\alpha\theta| \qquad \text{i.e.} \qquad \left|\frac{1 + \tau\alpha\theta - \tau\alpha}{1 + \tau\alpha\theta}\right| < 1.$$

[5]As in Lecture 25 (see exercise 25.2) of Trefethen and Bau III (1997), let $|e_1|, |e_2|, |e_3|, \ldots$ be a sequence of non-negative (magnitudes of) errors in an iterative process. Suppose there is a constant C and an exponent α such that, for sufficiently large k, $|e_{k+1}| \leq C\,(|e_k|)^\alpha$. If $\alpha = 2$, the process is said to exhibit *quadratic* convergence. Typically, the number of digits of accuracy doubles at each iteration in such schemes, and machine precision can be achieved in $\sim$4 iterations. *Linear* (or geometric) convergence occurs when $\alpha = 1$ and $C < 1$; (approximately) each iteration yields one more digit of accuracy. Superlinear convergence means that

$$\lim_{k\to\infty} \frac{|e_{k+1}|}{|e_k|} = 0.$$

In practice, we expect superlinearly convergent schemes to converge faster than linearly, but not as fast as quadratically.

[6]In 1D, we divide $\Omega = (a, b)$ into segments—by defining the nodes $a = x_1 \leq x_2 \leq \ldots \leq x_{N_h} = b$—with lengths $h_K = x_K - x_{K-1}$, and $h := \max h_K$. In 2D, we discretise Ω using a quasi-uniform triangulation. This is a family of triangulations with the property that the ratio of the shortest side of any triangle therein, $\underline{h}$, to the longest side, h, is bounded below by some positive constant, ρ, for every grid in the sequence i.e. as $h \to 0$ (see Defn 1.30 of Elman et al. (2008)). The remarks in 4.4.17 of Brenner and Scott (2007) give an insight as to how one might think of constructing such a family: '*start with an arbitrary triangulation in [2D] and sub-divide by connecting edge midpoints*'. Our assumption of quasi-uniformity implies shape regularity, which is equivalent to the minimum angle condition in the case of a triangulation. Note that we make slightly stronger assumptions on Ω (i.e. we consider a smaller set of domains) than in Blowey and Elliott (1992), where domains with curved edges are admitted. Our approach is consistent with other works such as Elliott and Garcke (1996) and the more recent Blank et al. (2011).

[7]We thus identify each *function* $\varphi^j_h \in V^h$ with a **vector** $\boldsymbol{\varphi}^j_h \in \mathbb{R}^{N_h}$, with components $\varphi^j_{h,i}$. In particular, when we say $u_h = 1 \in V^h$, we mean the constant unit function $u_h = \sum_{i=1}^{N_h} \phi_i$ which we identify with $\mathbf{1} \in \mathbb{R}^{N_h}$ (an N_h–vector of ones). Likewise, by $u_h = 0 \in V^h$, we mean the constant zero function, which we identify with $\mathbf{0} \in \mathbb{R}^{N_h}$ (an N_h–vector of zeros).

[8]As in Süli (2018), suppose we are given any $u_h \in V^h$ and seek $\omega_h \in V^h_*$ such that

$$(\omega_h, v_h) = (\nabla u_h, \nabla v_h) \quad \forall\, v_h \in V^h.$$

We will show that there exists one such $\omega_h \in V^h$ and label it '$-\Delta_h u_h$'. Define the linear functional $\ell(v_h) := (\nabla u_h, \nabla v_h)$ and observe by the Cauchy–Schwarz inequality that

$$|\ell(v_h)| \leq |u_h|_1 |v_h|_1 \leq |u_h|_1 \|v_h\|_1 \leq C(h) |u_h|_1 |v_h|_1$$

since all norms on the finite-dimensional space V^h are equivalent. It follows that ℓ is a bounded linear functional on V^h; consequently by the Riesz Representation Theorem there exists a unique $\omega_h \in V^h$ such that $\ell(v_h) = (\omega_h, v_h)$ for every $v_h \in V^h$, which we label $-\Delta_h u_h$. For any given $u_h \in V^h$, we have shown that $-\Delta_h u_h \in V^h$ is unique, and therefore exists.

[9]Without this restriction, suppose that $u_h = (-\Delta_h)^{-1} f_h \Rightarrow (f_h, v_h) = (\nabla u_h, \nabla v_h)$ for any $v_h \in V^h$. Trivially, $(f_h, v_h) = (\nabla(u_h + c), \nabla v_h)$ for any $c \in \mathbb{R}$ i.e. we could also assert that $u_h + c = (-\Delta_h)^{-1} f_h$. The restriction that $\overline{u_h} = 0$ removes this ambiguity. In fact, $-\Delta_h$ is a bijection (and $(-\Delta_h)^{-1}$ is defined) on V^h_*, but not all of V^h.

[10]We explore two other options:

1. Set $\varphi^0_h = P^{(h)}\varphi^0$ (the $L^2(\Omega)$ projection of φ^0). Note that $\overline{P^{(h)}\varphi^0} = \overline{\varphi^0} = m$. The issue with this approach is that $\left\|\varphi^0_h\right\|_{0,\infty}$ cannot be bounded, independent of h, which has serious consequences for our boundedness result.

   In Blowey and Elliott (1992), the authors use an $L^2(\Omega)$ projection to ensure that their IC has the correct mass, *but* they also assume (see just below their (3.24)) that '$U^0 = P^h u_0 \in K^h$' i.e. that their IC U^0 is the L^2 projection of u_0 *and* is uniformly bounded $\left\|U^0\right\|_{0,\infty} \leq 1$, independent of h. This cannot be guaranteed.

2. Set $\varphi^0_h = \mathcal{I}^{(h)}\varphi^0$ (the piecewise linear interpolant of φ^0). For such a φ^0_h,

   $$\left\|\varphi^0_h\right\|_{0,\infty} \leq \left\|\varphi^0\right\|_{0,\infty} \qquad \Rightarrow \qquad \left\|\varphi^0_h\right\| \leq |\Omega|^{1/2} \left\|\varphi^0_h\right\|_{0,\infty} \leq |\Omega|^{1/2} \left\|\varphi^0\right\|_{0,\infty}$$

   which is independent of h (and τ). In particular, if $\varphi^0 \in \mathscr{A}$, then $\left\|\varphi^0_h\right\|_{0,\infty} \leq 1$. The problem with this approach is that $\overline{\mathcal{I}^{(h)}\varphi^0} \neq m$ as the interpolant of $\varphi^0 \in \mathscr{A}_m$, which is clearly an issue, because all of our proofs assume that the IC has mass m.

[11]Our (5.63b) corresponds to (3.3) in Blowey and Elliott (1992).

[12]The following definition is lifted from (3.23)–(3.24) of Blowey and Elliott (1992).

[13]The μ^2 part of the coefficient resulted from an interaction between the regularisation term and others; as happened in (B.243). We were unable to resolve this entanglement. For this reason, we omit this result and its proof.

[14]It is clear that (5.73) demands a continuous (in time) solution φ, so that it can be sampled at arbitrary points in time.

[15]See http://dx.doi.org/10.6084/m9.figshare.7029242 for the source data for these experiments; fig. (a) is in `exp_group_run_232,` fig. (b) is in `exp_group_run_233.`

[16]See http://dx.doi.org/10.6084/m9.figshare.7029248 for the source data for these experiments; the red line comes from `exp_group_run_269,` and the blue line from `exp_group_run_270.`

[17]See http://dx.doi.org/10.6084/m9.figshare.7029275 for the source data for this figure.

[18]We also experimented with backward Euler time-integration (in which $\left(f_{\mathrm{E}}^{j-1} + f_{\mathrm{E}}^{j}\right)/2$ is replaced with f_{E}^{j}). There was no significant difference in the results, which is consistent with (B.428).

[19]Our code was written to be dimension independent. The problem with testing in 2D and 3D is that we wish to examine the test results in log-log graphs. MMS tests conducted in higher dimensions can only practically cover very small ranges of $\log(h)$ values.

[20]The effect of this choice was that $\overline{\varphi^0_h} \neq m$ (although it was close). On the other hand, we chose a very large value for α, which meant that $\overline{\varphi^j_h} \to m$ very rapidly.

[21]See http://dx.doi.org/10.6084/m9.figshare.7029287 for the second degree regularisation MMS source data, and http://dx.doi.org/10.6084/m9.figshare.7029296 for the fourth degree regularisation MMS source data.

[22]Although we do not report on them here, the results of our MMS test for a polynomial approximation of the homogeneous term were quite similar, displaying the same order of convergence.

[23]The energy at each end-state in Fig. 5.6 is lower than that of the IC in Fig. 5.6(a), even though the latter is a global energy minimiser. This is because the IC minimises $\mathcal{E}$ in (4.1a), but $\mathcal{E}_{\mu}^{(m)}$ in (4.61) decays under the action of the gradient flow.

[24]See `exp_group_run`201 in http://dx.doi.org/10.6084/m9.figshare.7029329 for the source data for these figures.

[25]See http://dx.doi.org/10.6084/m9.figshare.7029329 for the source data for these figures.

[26]It is not clear how one could manufacture 'exact' solutions in the context of a variational inequality.

[27]Crudely speaking, we could arrive at all of the variational inequality results by simply removing all of our references to the regularisation term.

[28]We chose the approach we did for two reasons: i) we were able to draw on the work of Blowey and Elliott (1991), and ii) this approach more easily deals with curved domains.

[29]Some results, like energy decay, are not expected to hold if $\overline{\varphi_0} \neq m$.

[30]Despite committing considerable resource to this effort, we were unable to construct such a proof.

[31]We approximate this using

$$\frac{\mathrm{d}\mathcal{E}_{\mu,h}^{(m)}}{\mathrm{d}t} \approx \frac{\mathcal{E}_{\mu,h}^{(m)}\left(t_j\right) - \mathcal{E}_{\mu,h}^{(m)}\left(t_{j-1}\right)}{\tau}.$$

[32]See http://dx.doi.org/10.6084/m9.figshare.7029344 for the source data for these figures.

Chapter 6

Energy minimisation in 1D

We study the energy minimisation problem: find $\varphi \in C^1\left(\overline{\Omega}\right)$ (cf. Theorem 4.2.5) such that the Ohta–Kawasaki energy functional

$$\mathcal{E}\left[\varphi\right] = \int_\Omega \left\{ \frac{\varepsilon_\varphi^2}{2}\left(\varphi'\right)^2 + \frac{\chi^{AB}}{4}\left(1-\varphi^2\right) + \frac{\alpha}{2}\left(\varphi - \overline{\varphi}\right)\Phi \right\} \mathrm{d}x \to \min, \tag{6.1a}$$

where $\Omega = (0, \mathcal{D})$, and (cf. (3.21c))

$$-\Phi''\left(x\right) = \varphi\left(x\right) - \overline{\varphi}, \qquad -\Phi'\left(0\right) = -\Phi'\left(\mathcal{D}\right) = 0, \qquad \text{and} \qquad \int_\Omega \Phi \ \mathrm{d}x = 0, \tag{6.1b}$$

and we demand that φ satisfy the global **mass constraint**,

$$\overline{\varphi} = m \qquad \text{viz.} \qquad \frac{1}{\mathcal{D}}\int_\Omega \varphi \ \mathrm{d}x = m. \tag{6.1c}$$

Finally, we impose the **boundedness constraint**

$$\left|\varphi\left(x\right)\right| \leq 1 \qquad \text{for every } x \in \overline{\Omega}. \tag{6.1d}$$

The second part of (6.1b) is two zero Neumann BCs on Φ; the third makes Φ unique. After integrating the non-local term by parts, we replace (6.1a) with

$$\mathcal{E}\left[\varphi\right] = \int_\Omega \frac{\varepsilon_\varphi^2}{2}\left(\varphi'\right)^2 + \frac{\chi^{AB}}{4}\left(1-\varphi^2\right) + \frac{\alpha}{2}\left(-\Phi'\right)^2 \mathrm{d}x \to \min. \tag{6.1e}$$

The boundedness constraint in (6.1d) and our intuition about the effect each of the three energy components has on the minimisation process, suggest that energy minimisers will oscillate back and forth from regions in which $\varphi = \pm 1$. Consistent with the physical model of Chapter 3, we identify regions in which $\varphi = -1$ $(+1)$ with pure phase B (A) DBC material, and transitions between these (the interface layers) as the approximate locations of the covalent bond(s) connecting them (see the lower parts of Fig's 6.1 and 6.9 for a graphical depiction). We will discover that minimisers are completely characterised by the number

(ν), location, thickness (ℓ) and shape of the Pure-Phase to Pure-Phase (P2P) $A \to B$ or $B \to A$ transitions.

Contents

6.1 The single monolayer problem . . . 114
6.2 Re-scalings: reducing the parameter space . . . 125
6.3 Multi-monolayer morphologies . . . 138
6.4 Summary and conclusions . . . 143

Chapter outline

Our approach in this and the next two chapters is elementary and emulates Section 3.2 of Blowey and Elliott (1991), which studies this problem with $\alpha = 0$. In the current, very technical chapter, we tee the problem up, and develop all of the infrastructure we need for the analysis in Chapters 7–8.

- In Section 6.1, we consider **the single monolayer problem**. We study 1D morphologies on a domain of width L, that include a single P2P transition from A to B (or vice versa) of width ℓ (see Fig. 6.1). We pose the energy minimisation problem, and derive an Integro-Differential Euler–Lagrange Equation (ID-ELE), under which the first variation of the energy is stationary. We differentiate this condition to arrive at a linear, fourth-order ODE, which we solve. We then consider the symmetric ($m = 0$) case, in which solutions of the ODE are particularly simple.
- In Section 6.2, we **re-scale** and simplify the parameter space, and then investigate how individual P2P interface layers (solving the ODE) depend on these new parameters.
- Finally, in Section 6.3, we define a framework for solving the **multi-monolayer** problem. We find that the multi-monolayer energy minimisation problem is equivalent to a *system* of single monolayer energy minimisation problems.

6.1 The single monolayer problem

We consider morphologies of the sort depicted in Fig. 6.1 and solve (6.1) on $\Omega = \left(-\frac{L}{2}, \frac{L}{2}\right)$. We assume there is a single P2P interface layer on (x_L, x_R), of width

$$\ell := x_R - x_L > 0. \tag{6.2}$$

A **monolayer** of width L contains one **interface layer** of width $\ell \leq L$.

The energy minimisation problem is to: find $\varphi \in C^1\left(-\frac{L}{2}, \frac{L}{2}\right)$ such that

$$\mathcal{E}[\varphi] = \int_{-L/2}^{L/2} \left\{ \frac{\varepsilon_\varphi^2}{2} \left(\varphi'\right)^2 + \frac{\chi^{AB}}{4} \left(1 - \varphi^2\right) + \frac{\alpha}{2} \left(\varphi - \overline{\varphi}\right) \Phi \right\} \mathrm{d}x \to \min, \tag{6.3}$$

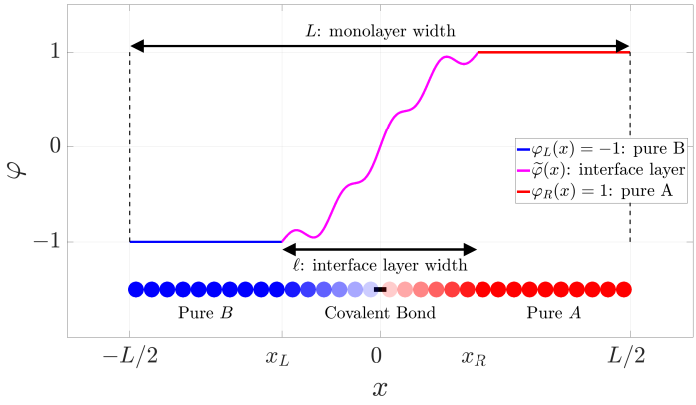

Figure 6.1: A single BA monolayer morphology φ-schematic of length L, and the underlying molecule it represents. It has three parts: a pure B end (in which type B monomers occur with probability one), a P2P interface layer of width $\ell = x_R - x_L$, from pure B to pure A (in which B monomers become less likely and A monomers more so) which we label $\widetilde{\varphi}$, and the pure A end (in which A monomers occur with probability one). The covalent bond connecting the pure B and A sections is in the P2P interface layer. The figure suggests that the structure is odd about $x = 0$; in what follows, we make no such assumption.[1]

where we demand that φ and $-\Phi'$ satisfy shifted versions of (6.1b), (6.1c) and (6.1d). Finally, we impose the BA interface layer *ansatz*,

$$\varphi_{BA}(x_L) = -1, \qquad \varphi_{BA}(x_R) = 1, \tag{6.4a}$$

and insist that (as in Fig. 6.1),

$$\varphi_{BA}(x) = \begin{cases} \varphi_L(x) \equiv -1 & x \in \left[-\frac{L}{2}, x_L\right), \\ \widetilde{\varphi}(x) & x \in [x_L, x_R], \\ \varphi_R(x) \equiv 1 & x \in \left(x_R, \frac{L}{2}\right]. \end{cases} \tag{6.4b}$$

As we will see, AB and BA minimisers are energetically equivalent. We study the BA case, but drop the '$_{BA}$' subscript going forward.[2]

6.1.1 A Lagrangian

We pose the Lagrangian

$$\mathscr{L}[\varphi; \boldsymbol{x}, \lambda] = \int_{x_L}^{x_R} \frac{\varepsilon_\varphi^2}{2}(\varphi')^2 + \frac{\chi^{AB}}{4}(1-\varphi^2)\,\mathrm{d}x + \frac{\alpha}{2}\int_{-L/2}^{L/2}(-\Phi')^2\,\mathrm{d}x - \lambda\left(\int_{-L/2}^{L/2}\varphi\,\mathrm{d}x - mL\right), \tag{6.5}$$

in which λ is a scalar Lagrange parameter for the mass constraint, and $\boldsymbol{x} := (x_L, x_R)^\top$ defines the width and location of the interface layer. We do not (yet) impose the pointwise constraints (6.1d) in (6.5); we will deal with them in Section 7.1.

Necessary conditions for an energy minimising morphology include

$$\nabla_{\boldsymbol{x}} \mathscr{L} = 0, \qquad \frac{\delta \mathscr{L}}{\delta \widetilde{\varphi}} = 0, \qquad \text{and} \qquad \partial_\lambda \mathscr{L} = 0, \tag{6.6}$$

where, in the second condition, we vary the morphology φ in the interface layer ($\varphi =: \widetilde{\varphi}$) and demand that admissible functions $\widetilde{\varphi}$ satisfy the Dirichlet BCs in (6.4a). We now specify Φ' in terms of φ. Using (6.1b), we find that

$$-\Phi'(x) + \Phi'\left(\frac{-L}{2}\right) = -\Phi'(x) = \int_{-L/2}^{x} \varphi(t) - \overline{\varphi} \, \mathrm{d}t, \tag{6.7}$$

and so[3]

$$-\Phi'(x) = \begin{cases} -\left(x + \dfrac{L}{2}\right)(1 + \overline{\varphi}) & x \in \left[-\dfrac{L}{2}, x_L\right) \\ \displaystyle\int_{x_L}^{x} \widetilde{\varphi}(t) - \overline{\varphi} \, \mathrm{d}t - \left(x_L + \frac{L}{2}\right)(1 + \overline{\varphi}) & x \in [x_L, x_R] \\ \left(x - \dfrac{L}{2}\right)(1 - \overline{\varphi}) & x \in \left(x_R, \dfrac{L}{2}\right]. \end{cases} \tag{6.8}$$

We now explore the consequences of the necessary conditions in (6.6) in detail.[4]

Lemma 6.1.1. ($\varphi' = 0$ at each interfacial end-point of a single monolayer minimiser) *For a single monolayer morphology to be an energy minimiser, it is necessary that*

$$\widetilde{\varphi}'(x_L) = 0 \qquad \textit{and} \qquad \widetilde{\varphi}'(x_R) = 0. \tag{6.9}$$

The Euler–Lagrange equation

$$\frac{\delta \mathscr{L}}{\delta \widetilde{\varphi}} = 0 \quad \Leftrightarrow \quad \varepsilon_\varphi^2 \left(-\widetilde{\varphi}''\right) - \frac{\chi^{AB}}{2} \widetilde{\varphi} - \lambda + \alpha \Phi = 0 \quad \textit{for} \quad x \in (x_L, x_R), \tag{6.10}$$

is necessary for a stationary BA interface layer. Finally, (cf. Defn 4.1.3)

$$(1 + m) \left|\Omega_{\underline{B}}\right| - (1 - m) \left|\Omega_{\overline{A}}\right| = \int_{x_L}^{x_R} \widetilde{\varphi} - m \, \mathrm{d}x. \tag{6.11}$$

This result follows immediately from the global regularity we established in Theorem 4.2.5, in 1D. We present an alternate, elementary proof in Appendix C.1 on p. 451.

The choice of pure-phase at the ends of the P2P transition is irrelevant. This is important because minimisers could potentially involve non-pure-phase to pure-phase transitions on $\partial\Omega$, or non-pure to non-pure transitions, with no pure phase material in Ω. We depict all of the possibilities in Fig. 6.2 (cf. Types 1, 2 and 3 in Section 3.2 of Blowey and Elliott (1991)). According to Lemma 6.1.1, a minimiser must have **zero Neumann BCs** and zero derivative at the ends of all non-pure to pure-phase transitions. Likewise, the constant, so-called *disordered* morphology ($\varphi \equiv m$), has zero first derivative on $\partial\Omega$.

We now study P2P minimisers in detail. Non-P2P (disordered) minimisers appear again in Section 8.1.

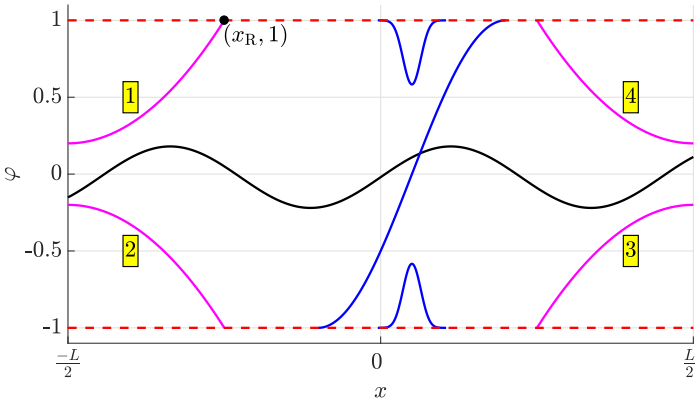

Figure 6.2: A schematic of three types of 1D, 2-phase candidate energy minimiser: the **blue** layers are of type P2P (BA as discussed in Lemma 6.1.1 as well as AA and BB); the **black** transition involves no pure-phase material; the **magenta** snippets are the four possible non-pure to pure transitions from the left/right ends of the domain.

6.1.2 The P2P integro-differential Euler–Lagrange equation

We integrate (6.10) on (x_L, x_R) and use the BCs in (6.9) to conclude that

$$-\varepsilon_\varphi^2 \underbrace{\widetilde{\varphi}'\big|_{x_L}^{x_R}}_{=0} - \frac{\chi^{AB}}{2}\int_{x_L}^{x_R} \widetilde{\varphi}\,\mathrm{d}x - \lambda\,(x_R - x_L) + \alpha\int_{x_L}^{x_R} \Phi\,(t)\,\mathrm{d}t = 0,$$

or, since $\widetilde{\varphi} = -\Phi'' + m$,

$$\lambda = \frac{\chi^{AB}}{2}\left(\frac{\Phi'\,(x_R) - \Phi'\,(x_L)}{x_R - x_L} - m\right) + \frac{\alpha}{x_R - x_L}\int_{x_L}^{x_R} \Phi\,(t)\,\mathrm{d}t. \tag{6.12}$$

Consequently, the Euler–Lagrange equation (6.10) becomes the integro-differential (cf. (4.34b))

$$\varepsilon_\varphi^2\left(-\widetilde{\varphi}''\right) - \frac{\chi^{AB}}{2}\left(\widetilde{\varphi} - m + \frac{\Phi'\,(x_R) - \Phi'\,(x_L)}{x_R - x_L}\right) + \alpha\left(\Phi - \frac{1}{x_R - x_L}\int_{x_L}^{x_R} \Phi\,(t)\,\mathrm{d}t\right) = 0 \tag{6.13a}$$

or, if we use (6.8) and (6.11), we can define the integro-differential operator

$$\mathbb{L}\,[\varphi] := \varepsilon_\varphi^2\left(-\widetilde{\varphi}''\right) - \frac{\chi^{AB}}{2}\left(\widetilde{\varphi} - \frac{mL + x_L + x_R}{x_R - x_L}\right) + \alpha\left(\Phi - \frac{1}{x_R - x_L}\int_{x_L}^{x_R} \Phi\,(t)\,\mathrm{d}t\right) = 0 \tag{6.13b}$$

for $x \in (x_L, x_R)$. We call this equation the ID-ELE, and describe its solutions as stationary.

Remarks.

i) For $\alpha = 0$, (6.13) is a second order *differential* equation (as in Blowey and Elliott (1991)). We consider $\alpha = 0$ in Section 8.3, but otherwise **assume that** $\alpha > \mathbf{0}$.

ii) Integrating (6.13b) over (x_L, x_R), we conclude that the integral of $\widetilde{\varphi}$ over (x_L, x_R) is

$$\int_{x_L}^{x_R} \widetilde{\varphi} \, \mathrm{d}x = \frac{mL + x_L + x_R}{x_R - x_L}.$$

Equivalently, a minimiser must have interfacial mass

$$\overline{\widetilde{\varphi}}_{(x_L, x_R)} = mL + x_L + x_R, \tag{6.14}$$

irrespective of the temperature (in the sense of (6.20)); this restates (6.11).

iii) The term $\Phi - \dfrac{1}{x_R - x_L} \displaystyle\int_{x_L}^{x_R} \Phi(t) \, \mathrm{d}t$ always yields a zero average version of Φ *inside the interface*. If we replace Φ in (6.13a) with $\Phi + C$, the last term on the left becomes

$$\alpha \left(\Phi + C - \frac{1}{x_R - x_L} \int_{x_L}^{x_R} (\Phi + C) \ \mathrm{d}x \right) = \alpha \left(\Phi - \frac{1}{x_R - x_L} \int_{x_L}^{x_R} \Phi(t) \, \mathrm{d}t \right). \tag{6.15}$$

We conclude that when working with (6.13), any first integral Φ of Φ' can be used i.e. the mass of Φ is irrelevant.

Despite the simplification implied by this last remark, we will still need to write down an explicit version of Φ if we are to calculate with (6.13b). Integrating (6.8) up once more (taking due care of signs and continuity), we arrive at

$$\Phi(x) = \begin{cases} \left(\dfrac{x^2}{2} + \dfrac{Lx}{2} + \dfrac{x_L^2}{2} \right) (\overline{\varphi} + 1) + \widetilde{E} & x \in \left[-\dfrac{L}{2}, x_L \right) \\ -\displaystyle\int_{x_L}^{x} \int_{x_L}^{\xi} \widetilde{\varphi} - \overline{\varphi} \ \mathrm{d}t \ \mathrm{d}\xi + \left(x_L + \dfrac{L}{2} \right) (\overline{\varphi} + 1) \, x + \widetilde{E} & x \in [x_L, x_R] \\ \left(\dfrac{x^2}{2} - \dfrac{Lx}{2} - \left(\dfrac{x_R^2}{2} - \dfrac{Lx_R}{2} \right) \right) (\overline{\varphi} - 1) & \\ + \left(x_L + \dfrac{L}{2} \right) (\overline{\varphi} + 1) \, x_R - \displaystyle\int_{x_L}^{x_R} \int_{x_L}^{\xi} \widetilde{\varphi} - \overline{\varphi} \ \mathrm{d}t \ \mathrm{d}\xi + \widetilde{E} & x \in \left(x_R, \dfrac{L}{2} \right]. \end{cases} \tag{6.16}$$

From our remarks above, we conclude that we can set $\widetilde{E} = 0$ when calculating.[5]

6.1.3 A linear, fourth-order ODE

Returning now to (6.13b) with $\alpha > 0$, we differentiate twice in x, and arrive at the linear, fourth-order ODE

$$\varepsilon_\varphi^2 \widetilde{\varphi}^{(\mathrm{iv})} + \frac{\chi^{AB}}{2} \widetilde{\varphi}'' + \alpha (\widetilde{\varphi} - m) = 0 \qquad \text{for} \qquad x \in (x_L, x_R). \tag{6.17a}$$

We impose the BA interface layer *ansatz* (Dirichlet) BCs

$$\widetilde{\varphi}\,(x_L) = -1, \qquad\qquad \widetilde{\varphi}\,(x_R) = 1, \tag{6.17b}$$

along with the minimising (Neumann) condition (6.9) from Lemma 6.1.1,

$$\widetilde{\varphi}'\big|_{x=x_L,x_R} = 0. \tag{6.17c}$$

Setting $\varphi - m = \mathrm{e}^{px}$ and $q = p^2$ (viz. $p = \pm\sqrt{q}$) leads to the auxiliary equation

$$\varepsilon_\varphi^2 q^2 + \frac{\chi^{AB}}{2} q + \alpha = 0 \tag{6.18a}$$

which has roots

$$q_\pm := \frac{-\chi^{AB} \pm \sqrt{\Delta}}{4\varepsilon_\varphi^2} \qquad \text{with discriminant} \qquad \Delta := \left(\chi^{AB}\right)^2 - 16\alpha\varepsilon_\varphi^2. \tag{6.18b}$$

Clearly, the sign of Δ will have a significant impact on the solution(s) of (6.17a).

A restriction: cool P2P morphologies

We recall from (3.18) and Section 4 of Choksi and Ren (2005), that the homogeneous Flory–Huggins parameter χ^{AB} is a fraction involving the absolute temperature Θ, that can be written

$$\chi^{AB} = \frac{\widetilde{\chi^{AB}}}{\Theta} \tag{6.19}$$

for a temperature independent constant, $\widetilde{\chi^{AB}}$. Consequently, we identify small values of χ^{AB} with high temperatures and vice versa, and interpret (6.18b) as follows:

$$\Delta < 0 \quad \Leftrightarrow \quad \varepsilon_\varphi > \frac{\chi^{AB}}{4\sqrt{\alpha}} \quad \Leftrightarrow \quad \Theta > \frac{\widetilde{\chi^{AB}}}{4\sqrt{\alpha}\varepsilon_\varphi} \quad : \quad \text{warm conditions;} \tag{6.20a}$$

$$\Delta = 0 \quad \Leftrightarrow \quad \varepsilon_\varphi = \frac{\chi^{AB}}{4\sqrt{\alpha}} \quad \Leftrightarrow \quad \Theta = \frac{\widetilde{\chi^{AB}}}{4\sqrt{\alpha}\varepsilon_\varphi} \quad : \quad \text{critical conditions;} \tag{6.20b}$$

$$\Delta > 0 \quad \Leftrightarrow \quad \varepsilon_\varphi < \frac{\chi^{AB}}{4\sqrt{\alpha}} \quad \Leftrightarrow \quad \Theta < \frac{\widetilde{\chi^{AB}}}{4\sqrt{\alpha}\varepsilon_\varphi} \quad : \quad \text{cool conditions.} \tag{6.20c}$$

We only consider solutions satisfying (6.20c), since we are primarily interested in P2P morphologies. An equivalent condition is

$$\Delta > 0 \quad \Leftrightarrow \quad \chi^{AB} > 4\sqrt{\alpha}\varepsilon_\varphi \quad (\text{small } \varepsilon_\varphi, \Theta; \text{ large } \chi^{AB} \Rightarrow \text{cool conditions}) \tag{6.21}$$

i.e. χ^{AB} is large. As we saw in Fig. 3.2 on p. 35, this gives ordered structures (with $\varphi = \pm 1$) a relative energy advantage over disordered ones ($\varphi = 0$). This suggests that P2P interface layers are more likely if χ^{AB} is large. We explore this topic rigorously in Section 6.2.2.

Under cool conditions, with $\alpha, \Delta > 0$, the solutions $q_\pm$ of the auxiliary equation (6.18) are distinct and strictly negative.[6] We define

$$q_\ell\left(\alpha, \varepsilon_\varphi, \chi^{AB}\right) = |q_+| = -q_+ = \frac{\chi^{AB} - \sqrt{\left(\chi^{AB}\right)^2 - 16\alpha\varepsilon_\varphi^2}}{4\varepsilon_\varphi^2} > 0 \tag{6.22a}$$

for a $\underline{\boldsymbol{\ell}}$ow frequency/high wavelength contribution, and

$$q_h\left(\alpha, \varepsilon_\varphi, \chi^{AB}\right) = |q_-| = -q_- = \frac{\chi^{AB} + \sqrt{\left(\chi^{AB}\right)^2 - 16\alpha\varepsilon_\varphi^2}}{4\varepsilon_\varphi^2} > q_\ell > 0, \tag{6.22b}$$

for a $\underline{\boldsymbol{h}}$igher frequency contribution.[7] The general solution can be written compactly as

$$\widetilde{\varphi}(x) = m + \widetilde{c}_1 \sin\left(\sqrt{q_\ell}x + \widetilde{c}_2\right) + \widetilde{c}_3 \sin\left(\sqrt{q_h}x + \widetilde{c}_4\right), \tag{6.23}$$

but we will generally favour the longer form

$$\widetilde{\varphi}(x) = m + c_1 \sin\left(\sqrt{q_\ell}x\right) + c_2 \cos\left(\sqrt{q_\ell}x\right) + c_3 \sin\left(\sqrt{q_h}x\right) + c_4 \cos\left(\sqrt{q_h}x\right), \tag{6.24a}$$

with

$$\widetilde{\varphi}'(x) = c_1\sqrt{q_\ell}\cos\left(\sqrt{q_\ell}x\right) - c_2\sqrt{q_\ell}\sin\left(\sqrt{q_\ell}x\right) + c_3\sqrt{q_h}\cos\left(\sqrt{q_h}x\right) - c_4\sqrt{q_h}\sin\left(\sqrt{q_h}x\right). \tag{6.24b}$$

Remark. We do not explore the critical or warm problems at all (see Section 6.2.2) beyond remarking that critical interfaces are governed by the general solution

$$\widetilde{\varphi}(x) = m + \sin\left(\frac{\sqrt{\chi^{AB}}}{2\varepsilon_\varphi}x\right)(c_1 + c_3 x) + \cos\left(\frac{\sqrt{\chi^{AB}}}{2\varepsilon_\varphi}x\right)(c_2 + c_4 x). \tag{6.25}$$

6.1.4 An equivalent form of the ID-ELE: an affine function

We now consider the ID-ELE (6.13), which we write as $\mathbb{L}(x) = 0$. The ODE (6.17a) has form $\mathbb{L}''(x) = 0$ on the interface layer, since it results from differentiating the ID-ELE twice. Consequently, the ID-ELE can be expressed as the affine

$$\mathbb{L}(x) = Gx + H = 0 \qquad \text{for} \qquad x \in (x_L, x_R). \tag{6.26}$$

For the ID-ELE to hold, we therefore demand that $G = 0$ and $H = 0$. Substituting (6.24) back into (6.13b) and simplifying (for $\alpha, \ell > 0$) yields the two conditions

$$G(x_L, x_R, c_1, c_2, c_3, c_4) = 0 \qquad \text{and} \qquad H(x_L, x_R, c_1, c_2, c_3, c_4) = 0, \tag{6.27a}$$

if and only if

$$-\frac{c_1}{\sqrt{q_\ell}}\cos\left(\sqrt{q_\ell}x_L\right) + \frac{c_2}{\sqrt{q_\ell}}\sin\left(\sqrt{q_\ell}x_L\right) - \frac{c_3}{\sqrt{q_h}}\cos\left(\sqrt{q_h}x_L\right) + \frac{c_4}{\sqrt{q_h}}\sin\left(\sqrt{q_h}x_L\right) + \left(x_L + \frac{L}{2}\right)(m+1) = 0, \tag{6.27b}$$

and

$$\frac{\chi^{AB}}{2}\left(x_R + x_L + m\left(L - (x_R - x_L)\right)\right) + \alpha\left(\frac{c_1\left(\cos\left(\sqrt{q_\ell}x_R\right) - \cos\left(\sqrt{q_\ell}x_L\right)\right) + c_2\left(\sin\left(\sqrt{q_\ell}x_L\right) - \sin\left(\sqrt{q_\ell}x_R\right)\right)}{q_\ell^{3/2}} + \frac{c_3\left(\cos\left(\sqrt{q_h}x_R\right) - \cos\left(\sqrt{q_h}x_L\right)\right) + c_4\left(\sin\left(\sqrt{q_h}x_L\right) - \sin\left(\sqrt{q_h}x_R\right)\right)}{q_h^{3/2}}\right) = 0. \quad (6.27c)$$

6.1.5 Finding candidate minimisers

The integro-differential equation (6.13b) contains all of the information required to determine the location *and* thickness of any candidate (stationary) interface layer.[8] We can:

i) Solve the ODE (6.17) to characterise the interface layer in terms of the constants c_1, c_2, c_3 and c_4 (cf. (6.24)), each of which depends on x_L and x_R; and

ii) Substitute these results back into the ID-ELE (6.13b) (expressed as the system (6.27)) to locate the interface layer, finding x_L and x_R (and ℓ).

We begin with step (i), assuming a general solution of the form (6.24). The conditions in (6.17b)–(6.17c) can be expressed in a 4×4 system $A\boldsymbol{c} = \boldsymbol{b}$, where

$$\boldsymbol{c} = (c_1, c_2, c_3, c_4)^\top, \qquad \boldsymbol{b} = (0, 0, -1-m, 1-m)^\top \quad (6.28a)$$

and

$$A = \begin{pmatrix} \sqrt{q_\ell}\cos\left(\sqrt{q_\ell}x_L\right) & -\sqrt{q_\ell}\sin\left(\sqrt{q_\ell}x_L\right) & \sqrt{q_h}\cos\left(\sqrt{q_h}x_L\right) & -\sqrt{q_h}\sin\left(\sqrt{q_h}x_L\right) \\ \sqrt{q_\ell}\cos\left(\sqrt{q_\ell}x_R\right) & -\sqrt{q_\ell}\sin\left(\sqrt{q_\ell}x_R\right) & \sqrt{q_h}\cos\left(\sqrt{q_h}x_R\right) & -\sqrt{q_h}\sin\left(\sqrt{q_h}x_R\right) \\ \sin\left(\sqrt{q_\ell}x_L\right) & \cos\left(\sqrt{q_\ell}x_L\right) & \sin\left(\sqrt{q_h}x_L\right) & \cos\left(\sqrt{q_h}x_L\right) \\ \sin\left(\sqrt{q_\ell}x_R\right) & \cos\left(\sqrt{q_\ell}x_R\right) & \sin\left(\sqrt{q_h}x_R\right) & \cos\left(\sqrt{q_h}x_R\right) \end{pmatrix}. \quad (6.28b)$$

With assistance from MATLAB, we find that the coefficient matrix A has determinant

$$\det(A) = -4c_A(\ell)\, c_B(\ell), \quad (6.29a)$$

where (cf. (6.22)),

$$c_A\left(\alpha, \varepsilon_\varphi, \chi^{AB}, \ell\right) := \sqrt{q_h}\cos\left(\sqrt{q_h}\frac{\ell}{2}\right)\sin\left(\sqrt{q_\ell}\frac{\ell}{2}\right) - \sqrt{q_\ell}\cos\left(\sqrt{q_\ell}\frac{\ell}{2}\right)\sin\left(\sqrt{q_h}\frac{\ell}{2}\right), \quad (6.29b)$$

and

$$c_B\left(\alpha, \varepsilon_\varphi, \chi^{AB}, \ell\right) := \sqrt{q_\ell}\cos\left(\sqrt{q_h}\frac{\ell}{2}\right)\sin\left(\sqrt{q_\ell}\frac{\ell}{2}\right) - \sqrt{q_h}\cos\left(\sqrt{q_\ell}\frac{\ell}{2}\right)\sin\left(\sqrt{q_h}\frac{\ell}{2}\right). \quad (6.29c)$$

There are two cases to consider: $\det(A) = 0$ and $\det(A) \neq 0$.

6.1.5.1 A singular coefficient matrix: $\det(A) = 0$

Notice that $\det(A)$ in (6.29) is independent of m, and all of its components depend on ℓ, the interface layer *width* (not its location). We exploit this insight by 'shifting' the problem to the right so that in (6.28b), $x_L \to 0$ and $x_R \to \ell$. This transformation has no effect on the BCs, but the coefficient vector $\boldsymbol{c}$ 'shifts right' to $\overrightarrow{\boldsymbol{c}}$, the matrix A becomes

$$\overrightarrow{A} = \begin{pmatrix} \sqrt{q_\ell} & 0 & \sqrt{q_h} & 0 \\ \sqrt{q_\ell}\cos\left(\sqrt{q_\ell}\ell\right) & -\sqrt{q_\ell}\sin\left(\sqrt{q_\ell}\ell\right) & \sqrt{q_h}\cos\left(\sqrt{q_h}\ell\right) & -\sqrt{q_h}\sin\left(\sqrt{q_h}\ell\right) \\ 0 & 1 & 0 & 1 \\ \sin\left(\sqrt{q_\ell}\ell\right) & \cos\left(\sqrt{q_\ell}\ell\right) & \sin\left(\sqrt{q_h}\ell\right) & \cos\left(\sqrt{q_h}\ell\right) \end{pmatrix}, \quad (6.30a)$$

and the shifted problem is $\overrightarrow{A}\,\overrightarrow{\boldsymbol{c}} = \boldsymbol{b}$. From the first equation above,

$$\overrightarrow{c_1}\sqrt{q_\ell} + \overrightarrow{c_3}\sqrt{q_h} = 0 \qquad \Rightarrow \qquad \overrightarrow{c_3} = -\sqrt{\frac{q_\ell}{q_h}}\overrightarrow{c_1}; \quad (6.30b)$$

and the third equation yields

$$\overrightarrow{c_2} + \overrightarrow{c_4} = -1 - m \qquad \Rightarrow \qquad \overrightarrow{c_4} = -1 - m - \overrightarrow{c_2}. \quad (6.30c)$$

Consequently, the original 4×4 system collapses to the 2×2 problem $\overrightarrow{\mathcal{A}}\boldsymbol{C} = \overrightarrow{\boldsymbol{b}}$ in which

$$\boldsymbol{C} = \begin{pmatrix} \overrightarrow{c_1} \\ \overrightarrow{c_2} \end{pmatrix}, \qquad \overrightarrow{\boldsymbol{b}} = \begin{pmatrix} \sqrt{q_h}\sin\left(\sqrt{q_h}\ell\right)(1+m) \\ \sqrt{q_h}\left(1 - m + \cos\left(\sqrt{q_h}\ell\right)(1+m)\right) \end{pmatrix}, \quad (6.31a)$$

and

$$\overrightarrow{\mathcal{A}} = \begin{pmatrix} -\sqrt{q_\ell}\left[\cos\left(\sqrt{q_\ell}\ell\right) - \cos\left(\sqrt{q_h}\ell\right)\right] & \sqrt{q_\ell}\sin\left(\sqrt{q_\ell}\ell\right) - \sqrt{q_h}\sin\left(\sqrt{q_h}\ell\right) \\ \sqrt{q_h}\sin\left(\sqrt{q_\ell}\ell\right) - \sqrt{q_\ell}\sin\left(\sqrt{q_h}\ell\right) & \sqrt{q_h}\left[\cos\left(\sqrt{q_\ell}\ell\right) - \cos\left(\sqrt{q_h}\ell\right)\right] \end{pmatrix}. \quad (6.31b)$$

Our first observation is that $\det(A) = \det\left(\overrightarrow{\mathcal{A}}\right)$ and so $\overrightarrow{\mathcal{A}}$ captures the singularities of A. Consider now the singular 2×2 system

$$\begin{pmatrix} a & b \\ c & d \end{pmatrix}\begin{pmatrix} x \\ y \end{pmatrix} = \begin{pmatrix} p \\ q \end{pmatrix} \qquad \text{in which} \qquad ad = bc. \quad (6.32)$$

The row operation $\mathcal{R}_2 \to b\mathcal{R}_2 - d\mathcal{R}_1$ zeros out the second row. Hence, if $\det(A) = 0$, the system admits an infinite set of solutions if/where $\mathscr{C} := bq - dp = 0$ on the right. Solving this for (6.31) exactly is difficult, but a numerical investigation is possible. We need the intersection(s) of

$$\begin{aligned} \mathscr{C}(\ell, \alpha) = &\left(\sqrt{q_\ell}\sin\left(\sqrt{q_\ell}\ell\right) - \sqrt{q_h}\sin\left(\sqrt{q_h}\ell\right)\right)\left(\sqrt{q_h}\left(1 - m + \cos\left(\sqrt{q_h}\ell\right)(1+m)\right)\right) \\ &- \left(\sqrt{q_h}\left[\cos\left(\sqrt{q_\ell}\ell\right) - \cos\left(\sqrt{q_h}\ell\right)\right]\right)\left(\sqrt{q_h}\sin\left(\sqrt{q_h}\ell\right)(1+m)\right) = 0 \end{aligned} \quad (6.33)$$

and $c_A = 0$ or $c_B = 0$ (viz. $\det(A) = 0$ as in (6.29b)–(6.29c)). We defer this investigation, for $m = 0$, to Section 6.2.6.

6.1.5.2 An invertible coefficient matrix: $\det(A) \neq 0$

For the non-singular case $\det(A) \neq 0$, it is convenient to work with our original (unshifted) problem. We find that c_1, c_2, c_3, c_4 are fractions of the form

$$c_i = \frac{c_i^{\text{num}}}{\det(A)}, \qquad i \in \{1,2,3,4\}, \tag{6.34a}$$

with a common denominator $\det(A)$, and numerators

$$\begin{aligned} c_1^{\text{num}} &= (1+m)\sqrt{q_h q_\ell}\sin\left(\sqrt{q_\ell}x_L\right) - (1-m)\sqrt{q_h q_\ell}\sin\left(\sqrt{q_\ell}x_R\right) \\ &\quad + (1-m)\,q_h\cos\left(\sqrt{q_\ell}x_L\right)\sin\left(\sqrt{q_h}\ell\right) + (1+m)\,q_h\cos\left(\sqrt{q_\ell}x_R\right)\sin\left(\sqrt{q_h}\ell\right) \\ &\quad + (1-m)\sqrt{q_h q_\ell}\sin\left(\sqrt{q_\ell}x_L\right)\cos\left(\sqrt{q_h}\ell\right) - (1+m)\sqrt{q_h q_\ell}\sin\left(\sqrt{q_\ell}x_R\right)\cos\left(\sqrt{q_h}\ell\right), \end{aligned} \tag{6.34b}$$

and

$$\begin{aligned} c_2^{\text{num}} &= (1+m)\sqrt{q_h q_\ell}\cos\left(\sqrt{q_\ell}x_L\right) - (1-m)\sqrt{q_h q_\ell}\cos\left(\sqrt{q_\ell}x_R\right) \\ &\quad - (1-m)\,q_h\sin\left(\sqrt{q_\ell}x_L\right)\sin\left(\sqrt{q_h}\ell\right) - (1+m)\,q_h\sin\left(\sqrt{q_\ell}x_R\right)\sin\left(\sqrt{q_h}\ell\right) \\ &\quad + (1-m)\sqrt{q_h q_\ell}\cos\left(\sqrt{q_\ell}x_L\right)\cos\left(\sqrt{q_h}\ell\right) - (1+m)\sqrt{q_h q_\ell}\cos\left(\sqrt{q_\ell}x_R\right)\cos\left(\sqrt{q_h}\ell\right); \end{aligned} \tag{6.34c}$$

we can find c_3 and c_4 from the observation that

$$c_1(q_h, q_\ell) = c_3(q_\ell, q_h) \qquad \text{and} \qquad c_2(q_h, q_\ell) = c_4(q_\ell, q_h). \tag{6.34d}$$

6.1.5.3 Mass in the interface layer

The combination of (6.24a) and (6.34) allows us to completely characterise the interface layer for a given (x_L, x_R).[9] Substituting (6.34) into (6.24a) allows us to write $\widetilde{\varphi} = \widetilde{\varphi}(x_L, x_R)$; a tedious integration gives the mass inside a general interface layer as the fraction

$$\int_{x_L}^{x_R} \widetilde{\varphi}(x_L, x_R)\ \mathrm{d}x = \frac{P(x_L, x_R)}{Q(x_L, x_R)}, \tag{6.35a}$$

where

$$\begin{aligned} P(\ell) = 2m\Big[&\left(q_h^{3/2} + q_\ell^{3/2} - \sqrt{q_h q_\ell}\left(\sqrt{q_h} + \sqrt{q_\ell}\right)\right)\sin\left(\left(\sqrt{q_h} + \sqrt{q_\ell}\right)\ell\right) \\ &+ \left(q_h^{3/2} - q_\ell^{3/2} + \sqrt{q_h q_\ell}\left(\sqrt{q_h} - \sqrt{q_\ell}\right)\right)\sin\left(\left(\sqrt{q_h} - \sqrt{q_\ell}\right)\ell\right) \\ &+ 2\left(q_h - q_\ell\right)\left(\sqrt{q_\ell}\sin\left(\sqrt{q_\ell}\ell\right) - \sqrt{q_h}\sin\left(\sqrt{q_h}\ell\right)\right) - 2q_h q_\ell \ell \\ &- \frac{\ell}{2}\sqrt{q_h q_\ell}\left(\left(\sqrt{q_h} - \sqrt{q_\ell}\right)^2\cos\left(\left(\sqrt{q_h} + \sqrt{q_\ell}\right)\ell\right) - \left(\sqrt{q_h} + \sqrt{q_\ell}\right)^2\cos\left(\left(\sqrt{q_h} - \sqrt{q_\ell}\right)\ell\right)\right)\Big], \end{aligned} \tag{6.35b}$$

and

$$Q(\ell) = 2\sqrt{q_h q_\ell}\det(A); \tag{6.35c}$$

both of which are explicit functions of ℓ, the interface layer width (not its location). Combined with (6.14), we can thus locate minimisers in (x_L, x_R)–space by solving

$$R\left(x_L, x_R\right) := mL + x_L + x_R - \frac{P\left(x_L, x_R\right)}{Q\left(x_L, x_R\right)} = 0. \tag{6.36}$$

We depict the zero contours of R in (6.36) for various m in Fig. 6.3. The mass restriction applies to all solutions of the ODE (6.17), including those solving the ID-ELE (6.13).

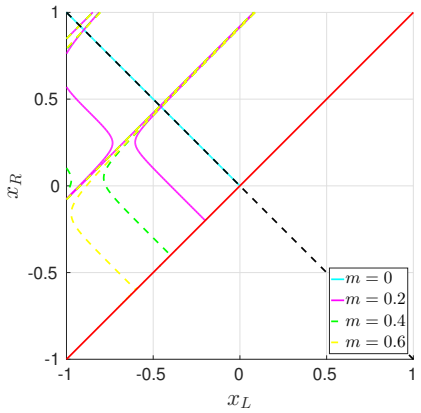

Figure 6.3: Zero contours of R in (6.36) for $\varepsilon_\varphi^2 = 10^{-2}$, $\chi^{AB} = 1$, $\alpha = 0.5$, $L = 2$ and various m. The minimisers for these values of m *must* occur on the corresponding contour line(s). In particular, for $m = 0$, $x_R = -x_L = \frac{\ell}{2}$. The red line is $x_R = x_L$; the dashed black line $x_R = -x_L$. We insist that $x_R > x_L$ (cf. (6.2)).[10]

6.1.5.4 A *substantial* simplification: symmetry

We now focus on the symmetric case, $m = 0$.[11] For $m = 0$, (6.35) says that *any* interface layer solving the ODE (6.17) will have zero (local) mass. Substituting into (6.36), we see that zero mass minimisers *must* have $x_L = -x_R$ with $x_R = \frac{\ell}{2}$ (see also Fig. 6.3). Using (6.34), we conclude that $c_2 = c_4 = 0$, and so for $m = 0$ we have an odd interface layer, which is the sum of two sine functions.[12]

We discover another significant simplification when we substitute these results back into the ID-ELE system (6.27), in that the second condition (6.27c) holds identically, and the ID-ELE reduces to the single condition $G = 0$ as in (6.27b). For $m = 0$, $c_2 = c_4 = 0$ and $x_L = -\frac{\ell}{2}$, satisfying the ID-ELE is therefore equivalent to the requirement that

$$\frac{c_1}{\sqrt{q_\ell}} \cos\left(\sqrt{q_\ell}\frac{\ell}{2}\right) + \frac{c_3}{\sqrt{q_h}} \cos\left(\sqrt{q_h}\frac{\ell}{2}\right) - \frac{L-\ell}{2} = 0. \tag{6.37}$$

6.2 Re-scalings: reducing the parameter space

The problem parameter space has five dimensions. In this section, we reduce this to three, and in the next, we set $m = 0$, to arrive at a 2D parameter space. We refer to each distinct point or physical configuration $\left(\alpha, \varepsilon_\varphi, \chi^{AB}, m, L\right)$ as a *model*, in *un-scaled* parameter space. To start, we introduce the scaling

$$x = s\widehat{x} \qquad \Rightarrow \qquad \frac{\mathrm{d}}{\mathrm{d}x} = \frac{\mathrm{d}}{\mathrm{d}\widehat{x}}\frac{\mathrm{d}\widehat{x}}{\mathrm{d}x} = \frac{1}{s}\frac{\mathrm{d}}{\mathrm{d}\widehat{x}} \qquad \Rightarrow \qquad \frac{\mathrm{d}^n}{\mathrm{d}x^n} = \frac{1}{s^n}\frac{\mathrm{d}}{\mathrm{d}\widehat{x}^n}, \tag{6.38}$$

where we will determine s presently.

Remark. We use hats (as in $x \to \widehat{x}$) to describe a scaled problem. For a function $f(x)$ of an un-scaled spatial variable, when we set $x = s\widehat{x}$ to scale, we will write

$$f(s\widehat{x}) = \widehat{f}(\widehat{x}) \tag{6.39}$$

i.e. a hat is used to denote any function (in $\widehat{x}$) that results from replacing each x with $s\widehat{x}$.

Applying the scaling (6.38) to (6.17a), and writing $\widehat{\widetilde{\varphi}}(\widehat{x}) = \widetilde{\varphi}(sx)$ yields

$$\frac{\varepsilon_\varphi^2}{s^4}\frac{\mathrm{d}^4\widehat{\widetilde{\varphi}}}{\mathrm{d}\widehat{x}^4} + \frac{\chi^{AB}}{2s^2}\frac{\mathrm{d}^2\widehat{\widetilde{\varphi}}}{\mathrm{d}\widehat{x}^2} + \alpha\left(\widehat{\widetilde{\varphi}} - m\right) = 0 \qquad \text{for} \qquad \widehat{x} \in (\widehat{x_L}, \widehat{x_R})\,. \tag{6.40}$$

We now choose $s > 0$ so that

$$\frac{\varepsilon_\varphi^2}{s^4} = \frac{\chi^{AB}}{2s^2} \qquad \text{viz.} \qquad s = \sqrt{\frac{2\varepsilon_\varphi^2}{\chi^{AB}}} \qquad \Rightarrow \qquad \frac{\varepsilon_\varphi^2}{s^4} = \frac{\chi^{AB}}{2s^2} = \frac{\left(\chi^{AB}\right)^2}{4\varepsilon_\varphi^2}, \tag{6.41}$$

viz. (cf. Fig. 6.1)

$$\widehat{x} = \sqrt{\frac{\chi^{AB}}{2\varepsilon_\varphi^2}}x, \quad \Rightarrow \quad \widehat{L} = \sqrt{\frac{\chi^{AB}}{2\varepsilon_\varphi^2}}L, \quad \widehat{x_L} = \sqrt{\frac{\chi^{AB}}{2\varepsilon_\varphi^2}}x_L, \quad \text{and} \quad \widehat{x_R} = \sqrt{\frac{\chi^{AB}}{2\varepsilon_\varphi^2}}x_R. \tag{6.42}$$

We then divide (6.40) by $\left(\chi^{AB}\right)^2/4\varepsilon_\varphi^2$ to arrive at the canonical ODE

$$\frac{\mathrm{d}^4\widehat{\widetilde{\varphi}}}{\mathrm{d}\widehat{x}^4} + \frac{\mathrm{d}^2\widehat{\widetilde{\varphi}}}{\mathrm{d}\widehat{x}^2} + \widehat{\alpha}\left(\widehat{\widetilde{\varphi}} - m\right) = 0 \qquad \text{where} \qquad \widehat{\alpha} := \frac{4\alpha\varepsilon_\varphi^2}{\left(\chi^{AB}\right)^2}, \tag{6.43a}$$

inside the interface layer, for which we specify the BA Dirichlet BCs (cf. (6.17b))

$$\widehat{\widetilde{\varphi}}(\widehat{x_L}) = -1, \qquad \widehat{\widetilde{\varphi}}(\widehat{x_R}) = 1, \tag{6.43b}$$

and the Neumann conditions (cf. (6.17c))

$$\frac{\mathrm{d}\widehat{\widetilde{\varphi}}}{\mathrm{d}\widehat{x}}(\widehat{x_L}) = \frac{\mathrm{d}\widehat{\widetilde{\varphi}}}{\mathrm{d}\widehat{x}}(\widehat{x_R}) = 0. \tag{6.43c}$$

Remark. We can recover (6.43a) from (6.17a) if we set

$$\varepsilon_{\varphi}^2 = 1 \qquad \text{and} \qquad \chi^{AB} = 2 \tag{6.44}$$

in the latter.[13] In particular, if $\widehat{\mathcal{E}}\left[\widehat{\varphi}\right]$ denotes the energy of the scaled morphology $\widehat{\varphi}$,

$$\widehat{\mathcal{E}}\left[\widehat{\varphi}\right] = \int_0^{\widehat{L}} \left\{ \frac{1}{2}\left(\widehat{\varphi}'\right)^2 + \frac{1}{2}\left(1 - \widehat{\varphi}^2\right) + \frac{\widehat{\alpha}}{2}\left(-\widehat{\Phi}'\right)^2 \right\} \mathrm{d}\widehat{x}. \tag{6.45}$$

Likewise, the auxiliary equation we presented in (6.18) is replaced with

$$\widehat{q}^2 + \widehat{q} + \widehat{\alpha} = 0 \tag{6.46a}$$

which has roots

$$\widehat{q}_{\pm}\left(\widehat{\alpha}\right) := \frac{-1 \pm \sqrt{1 - 4\widehat{\alpha}}}{2} \qquad \text{and discriminant} \qquad \widehat{\Delta}\left(\widehat{\alpha}\right) := 1 - 4\widehat{\alpha}. \tag{6.46b}$$

An un-scaled model with five parameters thus maps to our scaled space via

$$\widehat{\alpha} = \frac{4\varepsilon_{\varphi}^2}{\left(\chi^{AB}\right)^2}\alpha \qquad \text{and} \qquad \widehat{L} = \sqrt{\frac{\chi^{AB}}{2\varepsilon_{\varphi}^2}}L. \tag{6.47}$$

The mapping *to* scaled parameters is unique, but the reverse is not i.e. there is a family of models in $\left(\alpha, \varepsilon_{\varphi}, \chi^{AB}, m, L\right)$-parameter space for each point in $\left(\widehat{\alpha}, m, \widehat{L}\right)$–space.

6.2.1 Varying models in un-scaled parameter space

We now consider what happens in $\left(\widehat{L}, \widehat{\alpha}\right)$–space as we vary each of the model parameters $(\alpha, \varepsilon_{\varphi}, L)$ in un-scaled space.

- Varying α:

  Models with the same $\left(\varepsilon_{\varphi}, \chi^{AB}, L, m\right)$, but different α, map to the same $\widehat{L}$ value. If we use (6.47), it is clear that for such models,

  $$\frac{\widehat{\alpha}_2}{\widehat{\alpha}_1} = \frac{\alpha_2}{\alpha_1}, \tag{6.48}$$

  i.e. $\widehat{\alpha}$ scales (vertically) like α (all other parameters held constant).

- Varying L:

  The situation is analogous for models that differ in L only; for these, we observe that

  $$\frac{\widehat{L}_2}{\widehat{L}_1} = \frac{L_2}{L_1}, \tag{6.49}$$

  i.e. $\widehat{L}$ scales (horizontally) like L (all other parameters held constant). This observation will be useful when we analyse multi-monolayer morphologies.

- Varying ε_φ:

  Eliminating ε_φ between $\widehat{\alpha}$ and $\widehat{L}$ (cf. (6.47)) leads to

  $$f_\varepsilon\left(\widehat{L},\widehat{\alpha}\right)=\widehat{\alpha}\widehat{L}^2=\frac{2\alpha L^2}{\chi^{AB}}, \tag{6.50}$$

  which is constant for any given $\left(\alpha,\chi^{AB},L\right)$ as we vary ε_φ. We depict a series of contours of f_ε under cool conditions (each of which corresponds to a family of models), as the dashed red lines in Fig. 6.5. In this plot, decreasing ε_φ corresponds to moving down and to the right along the contours of f_ε. Under cool conditions,

  $$\lim_{\varepsilon_\varphi\to 0}\widehat{\alpha}=0 \qquad \text{and} \qquad \lim_{\varepsilon_\varphi\to 0}\widehat{L}=\infty. \tag{6.51}$$

- Varying χ^{AB} (heating and cooling):

  We recall that temperature Θ, is scaled into χ^{AB} (cf. (6.19)) so that if we hold $(\varepsilon_\varphi,\alpha,L)$ constant as we vary Θ, then this increases (*decreases*) χ^{AB} as we cool (*heat*) a given system. Eliminating χ^{AB} between $\widehat{\alpha}$ and $\widehat{L}$ in (6.47) leads to

  $$f_\Theta\left(\widehat{L},\widehat{\alpha}\right)=\widehat{\alpha}\widehat{L}^4=\frac{\alpha L^4}{\varepsilon_\varphi^2}, \tag{6.52}$$

  which is constant for any given $(\varepsilon_\varphi,\alpha,L)$ as we heat/cool. We depict a series of contours of f_Θ as the solid black lines in Fig. 6.5. Increasing χ^{AB} in this plot (cooling/reducing Θ) corresponds to moving down and to the right along the contours of f_Θ, and vice versa for heating. Under cool conditions,

  $$\lim_{\Theta\to 0}\widehat{\alpha}=0 \qquad \text{and} \qquad \lim_{\Theta\to 0}\widehat{L}=\infty. \tag{6.53}$$

  See also Section 8.4 on p. 202.

6.2.2 A rigorous result for disorder; dynamic stability analysis

We now justify our interest in cool parameters by showing that non-constant minimisers can only occur if $\widehat{\alpha}\leq\frac{1}{4}$. We emulate Theorem 3.1 of Choksi et al. (2009).

Lemma 6.2.1. (A unique, disordered minimiser) *For any $m\in(-1,1)$, the constant state $\widehat{\varphi}\equiv m$ is the unique, global minimiser of* (6.45) *if $\widehat{\alpha}>\frac{1}{4}$ (viz. warm conditions).*

Remark. For simplicity, we have stated and will prove this result in 1D. As in Choksi et al. (2009), it actually holds in any space dimension, and for any $\widehat{L}$.

Proof. Define $W(\varphi)=\frac{1}{2}\left(1-\varphi^2\right)$. Then for $|u|\leq 1$, a Taylor expansion gives

$$W(u)=W(m)+W'(m)(u-m)-\frac{1}{2}(u-m)^2.$$

For the disordered $\varphi \equiv m$, the energy in (6.45) is $\widehat{\mathcal{E}}^{(m)} := \widehat{\mathcal{E}}\left[\varphi \equiv m\right] = W\left(m\right)\left|\widehat{L}\right| \geq 0$. More generally, for any $\varphi \in \mathscr{A}_m$ the energy is (cf. (3.11) of Choksi et al. (2009))

$$\widehat{\mathcal{E}}\left[\varphi\right] = W\left(m\right)\left|\widehat{L}\right| + \frac{1}{2}\int_0^{\widehat{L}} \left(\varphi'\right)^2 \mathrm{d}x + \frac{\widehat{\alpha}}{2}\int_0^{\widehat{L}} \left(-\Phi'\right)^2 \mathrm{d}x + W'\left(m\right) \underbrace{\int_0^{\widehat{L}} \left(\varphi - m\right)\ \mathrm{d}x}_{= 0 \text{ since } \overline{\varphi} = m}$$

$$- \frac{1}{2}\int_0^{\widehat{L}} \left(\varphi - m\right)^2 \mathrm{d}x = \widehat{\mathcal{E}}^{(m)} + \sum_{k\neq 0}\left(\frac{1}{2}\frac{4\pi^2k^2}{\widehat{L}^2} - \frac{1}{2} + \frac{\widehat{\alpha}}{2}\frac{\widehat{L}^2}{4\pi^2k^2}\right)\left|\widehat{u}_k\right|^2 \quad (6.54)$$

where, as in Choksi et al. (2009), for $k \in \mathbb{Z}$, the $\widehat{u}_k$ are the Fourier coefficients for φ on $\left[0, \widehat{L}\right]$ with respect to normalised basis functions, viz.

$$\varphi = \sum_{k\in\mathbb{Z}} \widehat{u}_k \exp\left\{\frac{i2k\pi x}{\widehat{L}}\right\}; \qquad\qquad i = \sqrt{-1}.$$

The sum at the end is positive, viz. $\widehat{\mathcal{E}}\left[\varphi\right] \geq \widehat{\mathcal{E}}^{(m)}$ if (cf. (3.12) of Choksi et al. (2009))

$$\digamma\left(k\right) = \frac{1}{2}\frac{4\pi^2k^2}{\widehat{L}^2} - \frac{1}{2} + \frac{\widehat{\alpha}}{2}\frac{\widehat{L}^2}{4\pi^2k^2} \geq 0 \quad (6.55)$$

for every $k = 1, 2, \ldots$. Minimising $\digamma$ with respect to k^2, we find that

$$\frac{\mathrm{d}\digamma}{\mathrm{d}\left(k^2\right)} = 0 \qquad \Leftarrow \qquad \frac{1}{2}\frac{4\pi^2}{\widehat{L}^2} = \frac{\widehat{\alpha}}{2}\frac{\widehat{L}^2}{4\pi^2k^4} \qquad \Leftrightarrow \qquad k^2 = \sqrt{\widehat{\alpha}}\frac{\widehat{L}^2}{4\pi^2}; \quad (6.56)$$

and so (6.55) holds if $\widehat{\alpha} \geq \frac{1}{4}$. Under such conditions, $\varphi \equiv m$ is the global minimiser; it is unique for $\alpha > \frac{1}{4}$. □

We arrive at the same conclusion via a dynamic stability argument as in Section 4.1 of Choksi et al. (2009): this approach says that $\widehat{\alpha} = \frac{1}{4}$ is a critical value above which the well-mixed state $\varphi \equiv m$ is stable against small perturbations, at all wave numbers. We defer the details to an endnote.[14] It follows from (6.47), that warm conditions, under which the disordered state (viz. $\varphi \equiv m$) is stable, correspond to (cf. (6.20))

$$\widehat{\alpha} > \frac{1}{4} \qquad\qquad \Leftrightarrow \qquad\qquad \varepsilon_\varphi > \frac{\chi^{AB}}{4\sqrt{\alpha}}. \quad (6.57)$$

6.2.3 The cool, single monolayer, symmetric morphology

We now scale the cool, symmetric ($m = 0$) single monolayer solution into scaled $\left(\widehat{L}, \widehat{\alpha}\right)$ parameter space. The cool condition (6.20c) becomes

$$\widehat{\Delta} > 0: \qquad 0 < \widehat{\alpha} < \frac{1}{4} \qquad (\textit{relatively} \text{ small } \widehat{\alpha} \Rightarrow \text{cool conditions})$$

and so we restrict our attention to

$$\left(\widehat{L}, \widehat{\alpha}\right)_{\text{cool}} := \left\{\left(\widehat{L}, \widehat{\alpha}\right) \in (0, \infty) \times \left(0, \frac{1}{4}\right)\right\}. \quad (6.58)$$

Any cool, symmetric ($m = 0$) energy minimising interface layer must have

$$\widehat{x_R} = -\widehat{x_L} = \frac{\widehat{\ell}}{2}, \tag{6.59a}$$

and scaled structural form (cf. (6.24a))

$$\widetilde{\varphi}\left(\widehat{x};\widehat{\ell},\widehat{\alpha}\right) = c_1\left(\widehat{\ell},\widehat{\alpha}\right)\sin\left(\sqrt{\widehat{q_\ell}\,(\widehat{\alpha})}\widehat{x}\right) + c_3\left(\widehat{\ell},\widehat{\alpha}\right)\sin\left(\sqrt{\widehat{q_h}\,(\widehat{\alpha})}\widehat{x}\right), \tag{6.59b}$$

for $\widehat{x} \in \left(\frac{-\widehat{\ell}}{2}, \frac{\widehat{\ell}}{2}\right)$, where

$$c_1\left(\widehat{\ell},\widehat{\alpha}\right) = \frac{\sqrt{\widehat{q_h}}\cos\left(\sqrt{\widehat{q_h}}\frac{\widehat{\ell}}{2}\right)}{c_A\left(\widehat{\ell},\widehat{\alpha}\right)}, \qquad \text{and} \qquad c_3\left(\widehat{\ell},\widehat{\alpha}\right) = \frac{-\sqrt{\widehat{q_\ell}}\cos\left(\sqrt{\widehat{q_\ell}}\frac{\widehat{\ell}}{2}\right)}{c_A\left(\widehat{\ell},\widehat{\alpha}\right)}, \tag{6.59c}$$

and in turn,

$$c_A\left(\widehat{\ell},\widehat{\alpha}\right) = \sqrt{\widehat{q_h}}\cos\left(\sqrt{\widehat{q_h}}\frac{\widehat{\ell}}{2}\right)\sin\left(\sqrt{\widehat{q_\ell}}\frac{\widehat{\ell}}{2}\right) - \sqrt{\widehat{q_\ell}}\cos\left(\sqrt{\widehat{q_\ell}}\frac{\widehat{\ell}}{2}\right)\sin\left(\sqrt{\widehat{q_h}}\frac{\widehat{\ell}}{2}\right), \tag{6.29b}$$

$$c_B\left(\widehat{\ell},\widehat{\alpha}\right) := \sqrt{\widehat{q_\ell}}\cos\left(\sqrt{\widehat{q_h}}\frac{\widehat{\ell}}{2}\right)\sin\left(\sqrt{\widehat{q_\ell}}\frac{\widehat{\ell}}{2}\right) - \sqrt{\widehat{q_h}}\cos\left(\sqrt{\widehat{q_\ell}}\frac{\widehat{\ell}}{2}\right)\sin\left(\sqrt{\widehat{q_h}}\frac{\widehat{\ell}}{2}\right). \tag{6.29c}$$

Finally (cf. (6.22), (6.46b))

$$\widehat{q_\ell}\,(\widehat{\alpha}) = -\widehat{q}_+ = \frac{1-\sqrt{1-4\widehat{\alpha}}}{2} > 0 \quad \text{and} \quad \widehat{q_h}\,(\widehat{\alpha}) = -\widehat{q}_- = \frac{1+\sqrt{1-4\widehat{\alpha}}}{2} > \widehat{q_\ell} > 0. \tag{6.60}$$

Observe that:

- The scaled and un-scaled frequency coefficients are related via

$$\sqrt{\widehat{q_h}} = \sqrt{q_h\frac{2\varepsilon_\varphi^2}{\chi^{AB}}} = s\sqrt{q_h} \qquad \text{and likewise} \qquad \sqrt{\widehat{q_\ell}} = \sqrt{q_\ell\frac{2\varepsilon_\varphi^2}{\chi^{AB}}} = s\sqrt{q_\ell}. \tag{6.61}$$

- $\widehat{q_h}$ *decreases* with increasing $\widehat{\alpha}$, viz. $\widehat{q_h} = \widehat{q_h}\,(\widehat{\alpha}) \in \left(\frac{1}{2}, 1\right)$ for $\widehat{\alpha} \in \left(0, \frac{1}{4}\right)$.
- $\widehat{q_\ell}$ *increases* with increasing $\widehat{\alpha}$, viz. $\widehat{q_\ell} = \widehat{q_\ell}\,(\widehat{\alpha}) \in \left(0, \frac{1}{2}\right)$ for $\widehat{\alpha} \in \left(0, \frac{1}{4}\right)$.
- Moreover,

$$\widehat{q_h}\left(\frac{1}{4}\right) = \widehat{q_\ell}\left(\frac{1}{4}\right) = \frac{1}{2} \qquad \text{and} \qquad \sqrt{\frac{\widehat{q_h}}{\widehat{q_\ell}}} \to \infty \qquad \text{as} \qquad \widehat{\alpha} \downarrow 0. \tag{6.62}$$

Using MATLAB, we verify that the symmetric ID-ELE condition (6.37) rearranges to

$$\widetilde{g}\left(\widehat{\ell},\widehat{\alpha}\right) := \widehat{\ell} + \frac{g_{\text{num}}\left(\widehat{\ell},\widehat{\alpha}\right)}{c_A\left(\widehat{\ell},\widehat{\alpha}\right)} = \widehat{L}; \tag{6.63a}$$

where

$$g_{\text{num}}\left(\widehat{\ell},\widehat{\alpha}\right) = 2\left(\frac{\widehat{q_h}-\widehat{q_\ell}}{\sqrt{\widehat{q_\ell}\widehat{q_h}}}\right)\cos\left(\sqrt{\widehat{q_h}}\frac{\widehat{\ell}}{2}\right)\cos\left(\sqrt{\widehat{q_\ell}}\frac{\widehat{\ell}}{2}\right). \tag{6.63b}$$

Remarks.

i) The left side of (6.63a) involves $\widehat{\ell}$ (for given $\widehat{\alpha}$) and the right depends on $\widehat{L}$ (only). We can therefore fix $\widehat{L}$ and $\widehat{\alpha}$, and solve for $\widehat{\ell}$.

ii) The coefficients c_1 and c_3 in (6.59c) are functions of $\widehat{\ell}$ and $\widehat{\alpha}$ only. **These two parameters completely characterise any candidate P2P interface layer**. Likewise, for a given $\left(\widehat{L},\widehat{\alpha}\right)$-pair, we could solve (6.63) to find $\widehat{\ell}$, and given $\left(\widehat{\ell},\widehat{\alpha}\right)$ and $\widehat{L}$, we could then **calculate the energy** (cf. (6.3)) for a complete single monolayer morphology.

6.2.4 The structure of cool, symmetric interface layers

We have shown that minimisers are constant for $\widehat{\alpha} > \frac{1}{4}$. In this section, we start examining the possibilities for $\widehat{\alpha} \leq \frac{1}{4}$ and $m = 0$. We saw in the last section that individual P2P interface layers are completely characterised by $\widehat{\alpha}$ and their width, $\widehat{\ell}$, **independent of the monolayer or domain width** within which they occur. We now examine the structure of BA interface layers in cool $\left(\widehat{\ell},\widehat{\alpha}\right)$ parameter space. The following non-standard terminology and notation is useful:

Definition 6.2.2. (A type M1I interface) *An M1I P2P interface layer, $\widetilde{\varphi}$, is i) bounded $\|\widetilde{\varphi}\|_{0,\infty,\left(\frac{-\widehat{\ell}}{2},\frac{\widehat{\ell}}{2}\right)} \leq 1$, ii) monotone and, iii) has a single inflexion point. Going forward, we abbreviate $\|\widetilde{\varphi}\|_{0,\infty,\left(\frac{-\widehat{\ell}}{2},\frac{\widehat{\ell}}{2}\right)}$, the maximum magnitude of φ inside its interface layer, by $\|\widetilde{\varphi}\|_{\infty}$. A sample M1I interface layer appears in Fig. 6.6(d).*

Fig's 6.4–6.5 depict two regions of parameter space that we label **Region I** and the **cold region**. The **cold region** is defined by[15]

$$\widehat{\alpha} \leq \frac{1}{4}\left(1-\left(2\left(\frac{\pi}{\widehat{\ell}}\right)^2-1\right)^2\right) \qquad \text{for} \qquad \widehat{\ell} \in (\pi,\infty)\,,$$

and is infinitely wide at its base. Since $\widehat{q}_\ell \downarrow 0$ as $\widehat{\alpha} \downarrow 0$,

$$\widehat{\ell} = \frac{\pi}{\sqrt{\widehat{q}_\ell\left(\widehat{\alpha}\right)}} = \frac{\sqrt{2}\pi}{\sqrt{1-\sqrt{1-4\widehat{\alpha}}}} \to \infty \qquad \text{as} \qquad \widehat{\alpha} \downarrow 0. \tag{6.64}$$

This region is so named because as models cool along the solid black contours of f_Θ in Fig. 6.5, they enter the cold region and never leave.[16] **Region I** is to the left of the cold region, and is defined by

$$\widehat{\alpha} \in \left(0,\frac{1}{4}\right) \quad \text{and} \quad \widehat{\ell}\left(\widehat{\alpha}\right) \in \left(0,\widetilde{L}\left(\widehat{\alpha}\right)\right); \quad \widetilde{L}\left(\widehat{\alpha}\right) := \frac{\sqrt{2}\pi}{\sqrt{1+\sqrt{1-4\widehat{\alpha}}}} = \frac{\pi}{\sqrt{\widehat{q}_h\left(\widehat{\alpha}\right)}}. \tag{6.65}$$

P2P interface layers satisfying the ODE and drawn from $\left(\widehat{\ell},\widehat{\alpha}\right)$ parameters in Region I, cannot satisfy the ID-ELE. Additionally, such structures are always of type M1I.

Remark. We have defined Region I and the cold region above in $\left(\widehat{\ell},\widehat{\alpha}\right)$, but we use the same terminology in $\left(\widehat{L},\widehat{\alpha}\right)$–space.

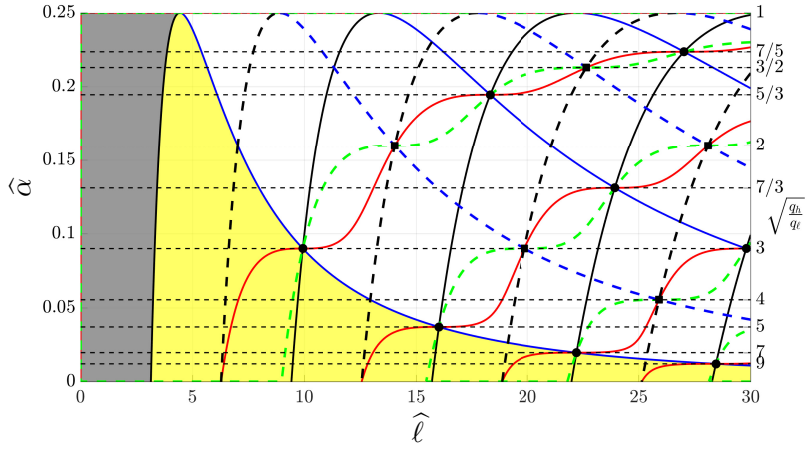

Figure 6.4: The cold region is shaded yellow, and Region I, grey, along with a set of useful contours in cool parameter space. The solid **black** lines are the zero contours of $\cos\left(\sqrt{\widehat{q}_h}\frac{\widehat{\ell}}{2}\right)$, and the solid **blue** lines those of $\cos\left(\sqrt{\widehat{q}_\ell}\frac{\widehat{\ell}}{2}\right)$; the dashed black lines are the zero contours of $\sin\left(\sqrt{\widehat{q}_h}\frac{\widehat{\ell}}{2}\right)$, and the dashed blue lines those of $\sin\left(\sqrt{\widehat{q}_\ell}\frac{\widehat{\ell}}{2}\right)$. Their intersections are marked with solid black dots/filled squares. The dashed **green** lines are the zero contours of $c_A\left(\widehat{\ell};\widehat{\alpha}\right)$; this function is zero along $\widehat{\ell}=0$, $\widehat{\alpha}=\frac{1}{4}$ and along parts of $\widehat{\alpha}=0$. The solid **red** lines trace out the zero contours of $c_B\left(\widehat{\ell};\widehat{\alpha}\right)$; this function is zero along $\widehat{\ell}=0$ and $\widehat{\alpha}=\frac{1}{4}$. We depict $\sqrt{\frac{\widehat{q}_h}{\widehat{q}_\ell}}$ from (6.60) on the right axis. The horizontal, dashed, black lines are for $\sqrt{\frac{\widehat{q}_h}{\widehat{q}_\ell}}\in\left\{1,\frac{7}{5},\frac{3}{2},\frac{5}{3},2,\frac{7}{3},3,4,5,7,9\right\}$.[17]

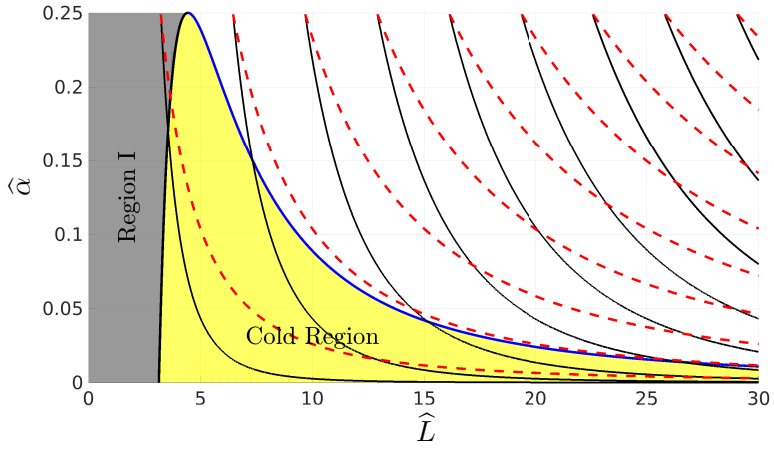

Figure 6.5: The dashed **red** lines are contours of f_ε from (6.50), for decreasing ε_φ (down/right). The solid black lines sweeping from top left to bottom right are contours of f_Θ from (6.52). Each one represents a different model $(\varepsilon_\varphi,\alpha,L)$ as it is heated (up/left) or cooled (down/right). The black lines enter the cold region as Θ is reduced.[18]

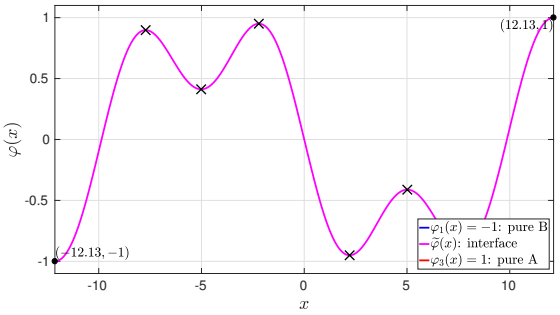

(a) An interface layer that is bounded, but extremely 'wiggly'; it has six turning points. $\left(\widehat{\ell}, \widehat{\alpha}\right) = (24.266, 0.094)$.

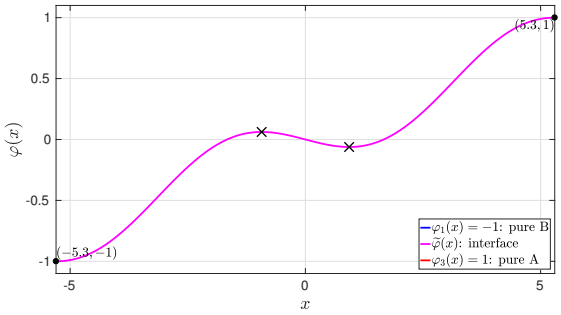

(b) An interface layer that is bounded, but not monotone; it has two turning points and three inflexion points. $\left(\widehat{\ell}, \widehat{\alpha}\right) = (10.6, 0.008)$.

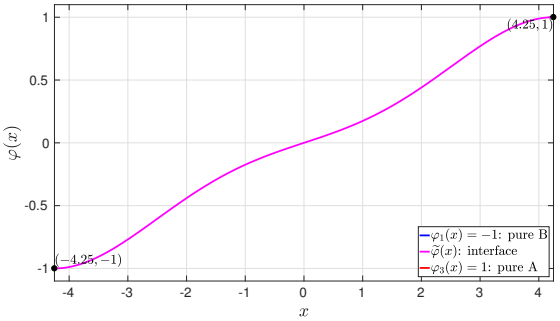

(c) An interface layer that is monotone, but has multiple inflexion points. $\left(\widehat{\ell}, \widehat{\alpha}\right) = (8.5, 0.206)$.

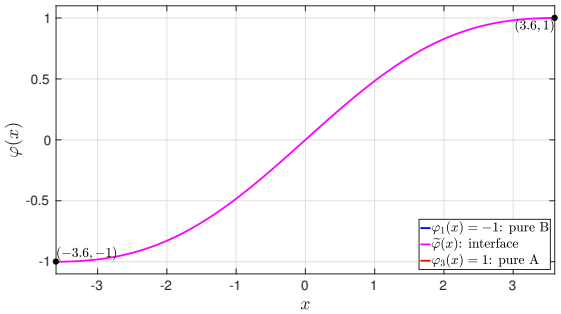

(d) An M1I interface layer; $\left(\widehat{\ell}, \widehat{\alpha}\right) = (7.2, 0.099)$.

Figure 6.6: Four bounded interface layers with $\|\widetilde{\varphi}\|_\infty \leq 1$: (a) and (b) are 'wiggly', (c) is monotone (but not M1I) and, (d) is M1I (as in Defn 6.2.2).[19]

Interfacial structure in Region I

We present a detailed investigation of the interfacial structures occurring in Region I in Appendix C.2, starting on p. 453. Our key observation is that if $\widehat{\ell} \leq \pi/\sqrt{\widehat{q}_h}$, then the interface layer satisfying (6.59) is M1I, viz. *any* P2P morphology in Region I is M1I.

Features in the cold region and beyond

The situation is more complicated outside of Region I. We defer a detailed discussion of some of the possibilities to Appendix C.3 on p. 457, and summarise our findings in Fig. 6.7:

- Fig. 6.7(a) depicts the regions in which M1I (yellow), monotone (blue), and bounded ($\|\widetilde{\varphi}\|_\infty \leq 1$) (grey) interface layers occur. $\widehat{\ell}_{\max}(\widehat{\alpha})$ is defined as the right edge of the left-most (yellow) M1I region.

- Fig. 6.7(b) summarises the properties of interface layers satisfying (6.59). These figures reveal that the zero contours of $\cos\left(\sqrt{\widehat{q}_h}\frac{\widehat{\ell}}{2}\right)$, $\cos\left(\sqrt{\widehat{q}_\ell}\frac{\widehat{\ell}}{2}\right)$, $\sin\left(\sqrt{\widehat{q}_h}\frac{\widehat{\ell}}{2}\right)$ and

$\sin\left(\sqrt{\widehat{q}_\ell}\frac{\widehat{\ell}}{2}\right)$ separate important regions in the parameter space. They are

$$\cos\left(\sqrt{\widehat{q}_h}\frac{\widehat{\ell}}{2}\right)=0 \quad \Rightarrow \quad \begin{cases}\widehat{\ell}=\dfrac{(2r+1)\,\pi}{\sqrt{\widehat{q}_h}}=\dfrac{\sqrt{2}\,(2r+1)\,\pi}{\sqrt{1+\sqrt{1-4\widehat{\alpha}}}}\\ \widehat{\alpha}=\left(\dfrac{(2r+1)\,\pi}{\widehat{\ell}}\right)^2\left(1-\left(\dfrac{(2r+1)\,\pi}{\widehat{\ell}}\right)^2\right)\end{cases} \tag{6.66a}$$

for $\widehat{\ell}\in(2r+1)\,\pi\left(1,\sqrt{2}\right)$ and

$$\cos\left(\sqrt{\widehat{q}_\ell}\frac{\widehat{\ell}}{2}\right)=0 \quad \Rightarrow \quad \begin{cases}\widehat{\ell}=\dfrac{(2s+1)\,\pi}{\sqrt{\widehat{q}_\ell}}=\dfrac{\sqrt{2}\,(2s+1)\,\pi}{\sqrt{1-\sqrt{1-4\widehat{\alpha}}}}\\ \widehat{\alpha}=\left(\dfrac{(2s+1)\,\pi}{\widehat{\ell}}\right)^2\left(1-\left(\dfrac{(2s+1)\,\pi}{\widehat{\ell}}\right)^2\right)\end{cases} \tag{6.66b}$$

for $\widehat{\ell}\in\pi\left(\sqrt{2}\,(2s+1)\,,\infty\right)$ and some $r,s\in\mathbb{N}_0$. For the zeros of the sine functions,

$$\sin\left(\sqrt{\widehat{q}_h}\frac{\widehat{\ell}}{2}\right)=0 \quad \Rightarrow \quad \begin{cases}\widehat{\ell}=\dfrac{2r\pi}{\sqrt{\widehat{q}_h}}=\dfrac{2\sqrt{2}r\pi}{\sqrt{1+\sqrt{1-4\widehat{\alpha}}}}\\ \widehat{\alpha}=\left(\dfrac{2r\pi}{\widehat{\ell}}\right)^2\left(1-\left(\dfrac{2r\pi}{\widehat{\ell}}\right)^2\right)\end{cases} \tag{6.67a}$$

for $\widehat{\ell}\in 2r\pi\left(1,\sqrt{2}\right)$ and

$$\sin\left(\sqrt{\widehat{q}_\ell}\frac{\widehat{\ell}}{2}\right)=0 \quad \Rightarrow \quad \begin{cases}\widehat{\ell}=\dfrac{2s\pi}{\sqrt{\widehat{q}_\ell}}=\dfrac{2\sqrt{2}s\pi}{\sqrt{1-\sqrt{1-4\widehat{\alpha}}}}\\ \widehat{\alpha}=\left(\dfrac{2s\pi}{\widehat{\ell}}\right)^2\left(1-\left(\dfrac{2s\pi}{\widehat{\ell}}\right)^2\right)\end{cases} \tag{6.67b}$$

for $\widehat{\ell}\in\pi\left(2\sqrt{2}s,\infty\right)$ and some $r,s\in\mathbb{N}_0$ ($\widehat{\ell}=0$ is also a solution). The border of the cold region comes from (6.66) with $r=s=0$.

- The solid black line in Fig. 6.4 traces out the first zero contour of $\cos\left(\sqrt{\widehat{q}_h}\frac{\widehat{\ell}}{2}\right)$, viz.

$$\widehat{\ell}=\frac{\pi}{\sqrt{\widehat{q}_h}} \quad \Rightarrow \quad \widehat{\alpha}=\left(\frac{\pi}{\widehat{\ell}}\right)^2\left(1-\left(\frac{\pi}{\widehat{\ell}}\right)^2\right) \quad \text{for} \quad \widehat{\ell}\in\pi\left(1,\sqrt{2}\right), \tag{6.68a}$$

  if we use (6.60). The solid blue line is the first zero contour of $\cos\left(\sqrt{\widehat{q}_\ell}\frac{\widehat{\ell}}{2}\right)$, viz.

$$\widehat{\ell}=\frac{\pi}{\sqrt{\widehat{q}_\ell}} \quad \Rightarrow \quad \widehat{\alpha}=\left(\frac{\pi}{\widehat{\ell}}\right)^2\left(1-\left(\frac{\pi}{\widehat{\ell}}\right)^2\right) \quad \text{for} \quad \widehat{\ell}\in\pi\left(\sqrt{2},\infty\right). \tag{6.68b}$$

  (6.68) is the same as (6.66) with $r=s=0$.

It is also useful at this point to define the important

$$\widehat{\alpha}_{\max}\left(\widehat{\ell}\right):=\max_{\substack{r\in\mathbb{N}_0\\ \widehat{\ell}\geq\pi}}\left\{\left(\frac{r\pi}{\widehat{\ell}}\right)^2\left(1-\left(\frac{r\pi}{\widehat{\ell}}\right)^2\right)\right\} \tag{6.69}$$

as the upper envelope of the regions enclosed by the contours (6.65), (6.66), (6.67). **Region II is the disconnected part of phase space above $\widehat{\alpha}_{\max}$, to the right of Region I.**

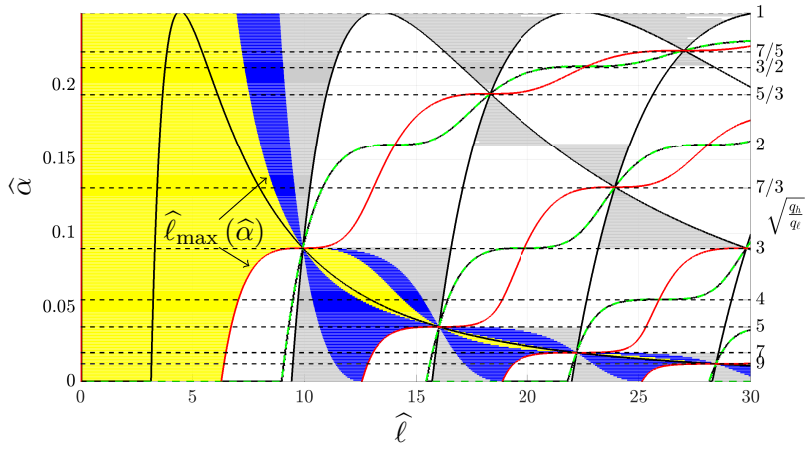

(a) Regions in which $\widehat{\ell}$ corresponds to bounded interface layers with $\|\widetilde{\varphi}\|_\infty \leq 1$ are shaded grey; monotone sub-domains are **blue** and M1I sub-domains of those, yellow. Inside the cold region, the zero contours of $\cos\left(\sqrt{q_h}\frac{\widehat{\ell}}{2}\right)$ (in black) correspond to lower limits of regions where $\|\widetilde{\varphi}\|_\infty \leq 1$; the zero contours of $c_B\left(\widehat{\ell},\widehat{\alpha}\right)$ (in **red**) correspond to upper limits of regions where $\|\widetilde{\varphi}\|_\infty \leq 1$. $\|\widetilde{\varphi}\|_\infty > 1$ on the zero contours of $c_A\left(\widehat{\ell},\widehat{\alpha}\right)$ (black and green). $\widehat{\ell}_{\max}(\widehat{\alpha})$ is the right edge of the left-most (yellow) M1I region.

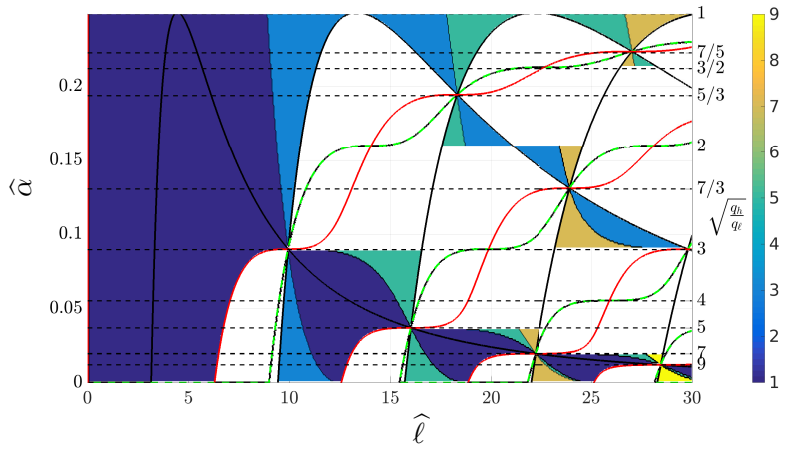

(b) Filled contour plot of the interface layer internal oscillation count. The dark blue regions correspond to monotone interface layers (cf. the blue and yellow areas in (a), above). We observe odd oscillation counts $1, 3, 5, 7, 9$, only (as expected).

Figure 6.7: Properties of interface layers, as a function of scaled parameter space.[20]

6.2.5 Scaling back to the original material parameters

We now place this re-scaling process into the context of solving a problem posed in un-scaled parameters. The end-to-end process is as follows:

Step 1. Scale the given/measured material parameters $\left(\alpha, \varepsilon_\varphi, \chi^{AB}, m, L\right) \to \left(\widehat{\alpha}, m, \widehat{L}\right)$;

Step 2. Find energy minimisers in scaled parameter space; and

Step 3. Scale back to $\left(\alpha, \varepsilon_\varphi, \chi^{AB}, m, L\right)$.

The result of step (2) is a morphology function of the form $\widehat{\widetilde{\varphi}}\left(\widehat{x}\right)$, in scaled variables. To retrieve the solution in un-scaled variables we replace $\widehat{x}$ with $\frac{x}{s}$ (cf. (6.39)) to arrive at

$$\varphi\left(x\right) = \widehat{\widetilde{\varphi}}\left(\frac{x}{s}\right) \tag{6.70}$$

with s as in (6.41). For (scaled) first integrals such as (6.7), we have,

$$-\frac{\mathrm{d}\widehat{\Phi}}{\mathrm{d}\widehat{x}}\left(\widehat{x}\right) = \int_{-\widehat{L}/2}^{\widehat{x}} \widehat{\varphi}\left(\widehat{t}\right) - \overline{\varphi}\ \mathrm{d}\widehat{t} \qquad \text{and} \qquad -\frac{\mathrm{d}\Phi}{\mathrm{d}x}\left(x\right) = \int_{-L/2}^{x} \varphi\left(t\right) - \overline{\varphi}\ \mathrm{d}t \tag{6.71}$$

and so in order to transform from $\widehat{\Phi}' \to \Phi'$, we set $x = s\widehat{x}$ and write

$$-\frac{\mathrm{d}\Phi}{\mathrm{d}x}\left(x\right) = \underbrace{\int_{-L/2}^{s\widehat{x}} \varphi\left(t\right) - \overline{\varphi}\ \mathrm{d}t}_{\text{set } t = s\widehat{t}} = \underbrace{s\int_{-\widehat{L}/2}^{\widehat{x}} \widehat{\varphi}\left(\widehat{t}\right) - \overline{\varphi}\ \mathrm{d}\widehat{t}}_{\widehat{L} = \frac{L}{s} \text{ by (6.42)}} = s\left(-\frac{\mathrm{d}\widehat{\Phi}}{\mathrm{d}\widehat{x}}\left(\widehat{x}\right)\right). \tag{6.72}$$

Alternatively, we could set $n = -1$ in (6.38). Moreover,

$$\begin{aligned}
\mathcal{E}\left[\varphi\right] &= \int_0^L \frac{\varepsilon_\varphi^2}{2}\left(\varphi'\right)^2 + \frac{\chi^{AB}}{4}\left(1-\varphi^2\right) + \frac{\alpha}{2}\left(-\Phi'\right)^2 \mathrm{d}x \\
&= \sqrt{\frac{2\varepsilon_\varphi^2}{\chi^{AB}}}\int_0^{\widehat{L}} \left\{ \frac{\varepsilon_\varphi^2}{2}\frac{\chi^{AB}}{2\varepsilon_\varphi^2}\left(\frac{\mathrm{d}\widehat{\varphi}}{\mathrm{d}\widehat{x}}\right)^2 + \frac{\chi^{AB}}{4}\left(1-\widehat{\varphi}^2\right) + \frac{\widehat{\alpha}\left(\chi^{AB}\right)^2}{8\varepsilon_\varphi^2}\frac{2\varepsilon_\varphi^2}{\chi^{AB}}\left(-\frac{\mathrm{d}\widehat{\Phi}}{\mathrm{d}\widehat{x}}\left(\widehat{x}\right)\right)^2 \right\} \mathrm{d}\widehat{x} \\
&= \frac{\chi^{AB}}{2}\sqrt{\frac{2\varepsilon_\varphi^2}{\chi^{AB}}}\int_0^{\widehat{L}} \left\{ \frac{1}{2}\left(\widehat{\varphi}'\right)^2 + \frac{1}{2}\left(1-\widehat{\varphi}^2\right) + \frac{\widehat{\alpha}}{2}\left(-\widehat{\Phi}'\right)^2 \right\} \mathrm{d}\widehat{x} = \varepsilon_\varphi\sqrt{\frac{\chi^{AB}}{2}}\widehat{\mathcal{E}}\left[\widehat{\varphi}\right],
\end{aligned} \tag{6.73}$$

where $'$ denotes the derivative in $\widehat{x}$ on the last line, after using (6.1e), (6.42), (6.43a), (6.45).

6.2.6 A singular problem in scaled parameter space

With the re-scaling above in hand, we are now ready to explore the singular condition (6.33) in scaled parameter space. With $m = 0$, the consistency condition reduces to

$$\begin{aligned}
\mathscr{C}\left(\widehat{\ell}, \widehat{\alpha}\right) = &\left(\sqrt{\widehat{q}_\ell}\sin\left(\sqrt{\widehat{q}_\ell}\widehat{\ell}\right) - \sqrt{\widehat{q}_h}\sin\left(\sqrt{\widehat{q}_h}\widehat{\ell}\right)\right)\left(\sqrt{\widehat{q}_h}\left(1+\cos\left(\sqrt{\widehat{q}_h}\widehat{\ell}\right)\right)\right) \\
&- \left(\sqrt{\widehat{q}_h}\left[\cos\left(\sqrt{\widehat{q}_\ell}\widehat{\ell}\right) - \cos\left(\sqrt{\widehat{q}_h}\widehat{\ell}\right)\right]\right)\left(\sqrt{\widehat{q}_h}\sin\left(\sqrt{\widehat{q}_h}\ell\right)\right) = 0
\end{aligned} \tag{6.74}$$

and so we plot this zero contour together with $c_A = 0$ and $c_B = 0$ from (6.29b), (6.29c) in Fig. 6.8. We find that the zero contours of $\mathscr{C}$ (solutions of (6.74)) coincide with those of c_B, $\cos\left(\sqrt{\widehat{q}_h}\frac{\widehat{\ell}}{2}\right)$ and $\cos\left(\sqrt{\widehat{q}_\ell}\frac{\widehat{\ell}}{2}\right)$. This means that it should be possible to write

$$\mathscr{C}\left(\widehat{\ell}, \widehat{\alpha}\right) = c_B\left(\widehat{\ell}, \widehat{\alpha}\right)\cos\left(\sqrt{\widehat{q}_h}\frac{\widehat{\ell}}{2}\right)\cos\left(\sqrt{\widehat{q}_\ell}\frac{\widehat{\ell}}{2}\right)\mathscr{G}\left(\widehat{\ell}, \widehat{\alpha}\right) \tag{6.75}$$

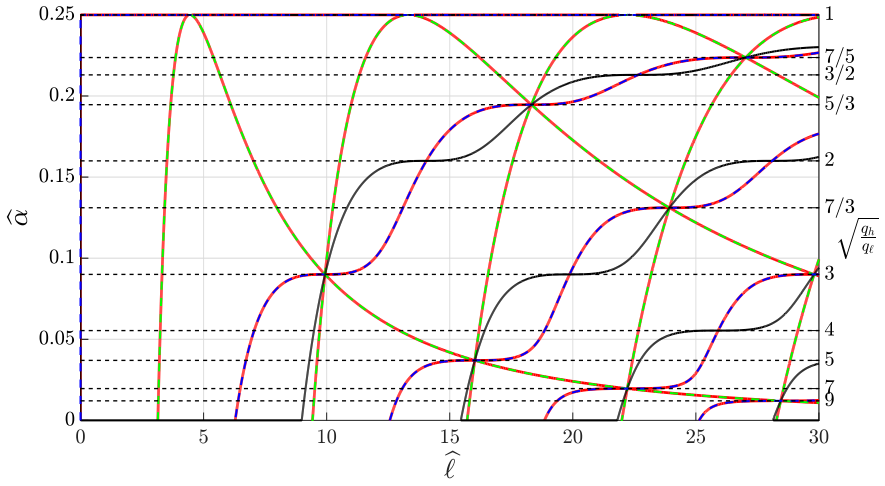

Figure 6.8: Zero contours of the consistency function $\mathscr{C}$ in (6.74) in solid **red**, as well as those of c_A (solid black lines) and c_B (dashed **blue** lines) over scaled $\left(\widehat{\ell}, \widehat{\alpha}\right)$ parameter space. The contours of $\mathscr{C}\left(\widehat{\ell}, \widehat{\alpha}\right) = 0$ coincide with $c_B\left(\widehat{\ell}, \widehat{\alpha}\right) = 0$, suggesting that at such points, the problem (6.28) is singular but consistent, and admits an infinite family of solutions. The dashed green lines are the zero contours of $\cos\left(\sqrt{\widehat{q}_h}\frac{\widehat{\ell}}{2}\right)$ and $\cos\left(\sqrt{\widehat{q}_\ell}\frac{\widehat{\ell}}{2}\right)$.[21]

for some function $\mathscr{G}\left(\widehat{\ell}, \widehat{\alpha}\right)$. We conclude that when $\det(A) = 0$, and (6.28) is singular, it has no solutions where $c_A\left(\widehat{\ell}, \widehat{\alpha}\right) = 0$, and an infinite set where $c_B\left(\widehat{\ell}, \widehat{\alpha}\right) = 0$.

Fig. 6.7(a) and the coefficients in (6.59c) suggest we can ignore parameters corresponding to the solutions of $c_A\left(\widehat{\ell}, \widehat{\alpha}\right) = 0$ as these lead to $\|\widetilde{\varphi}\|_\infty > 1$. It would appear that the interface layer satisfying the ODE (6.17) with parameters specified by $c_A\left(\widehat{\ell}, \widehat{\alpha}\right) = 0$ has $\|\widetilde{\varphi}\|_\infty \to \infty$. On the other hand, parameters corresponding to $c_B\left(\widehat{\ell}, \widehat{\alpha}\right) = 0$ yield an infinite family of single monolayer solutions satisfying (6.17). Fig. 6.7(a) suggests that these either yield interface layers with $\|\widetilde{\varphi}\|_\infty > 1$ or they are on the edge of boundedness.

6.2.7 An alternate re-scaling: the sharp interface limit

The re-scaling above will prove adequate for most of our requirements. A second re-scaling, more suited to sharp interface limit analysis (see Section 8.5), is one in which we define

$$\mathcal{E}_{BA} := \frac{\mathcal{E}[\varphi]}{\chi^{AB}}, \quad \varepsilon^2 := \frac{\varepsilon_\varphi^2}{\chi^{AB}}, \quad \text{and} \quad \varepsilon\gamma := \frac{\alpha}{\chi^{AB}}, \quad \text{viz.} \quad \gamma = \frac{\alpha}{\varepsilon\chi^{AB}} = \frac{\alpha}{\varepsilon_\varphi\sqrt{\chi^{AB}}}. \tag{6.76}$$

For simplicity, we work on a symmetric interval $x \in \left[\frac{-L}{2}, \frac{L}{2}\right]$, and seek a continuous profile φ of the form (6.4b). The energy of a single BA monolayer φ on $\left(-\frac{L}{2}, \frac{L}{2}\right)$ is therefore given

by (cf. (6.1e), (6.73))

$$\mathcal{E}_{BA} = \int_{x_L}^{x_R} \frac{\varepsilon^2}{2} \left(\varphi'\right)^2 + \frac{1}{4}\left(1-\varphi^2\right)\ \mathrm{d}x + \frac{\varepsilon\gamma}{2}\int_{-L/2}^{L/2} \left(-\Phi'\right)^2 \mathrm{d}x. \tag{6.77}$$

The symmetric case

To find a critical point φ of the 2-phase energy functional (6.77) (cf. (5.1) of Choksi and Ren (2003)), under the constraint $\overline{\varphi} = 0$, we re-scale as in (6.76) and use (6.7) with $\overline{\varphi} = m = 0$ to define the Lagrangian (cf. (6.5))

$$\mathscr{L}\left[\varphi; x_L, x_R, \lambda\right] = \int_{x_L}^{x_R} \frac{\varepsilon^2}{2}\left(\widetilde{\varphi}'\right)^2 + \frac{1}{4}\left(1-\widetilde{\varphi}^2\right)\ \mathrm{d}x + \frac{\varepsilon\gamma}{2}\int_{-L/2}^{L/2}\left(\int_{-L/2}^{x}\varphi\left(t\right)\ \mathrm{d}t\right)^2 \mathrm{d}y - \lambda\int_{-L/2}^{L/2}\varphi\ \mathrm{d}x. \tag{6.78}$$

The stationarity condition (6.10) becomes

$$\varepsilon^2\widetilde{\varphi}''\left(x\right) + \frac{1}{2}\widetilde{\varphi}\left(x\right) + \varepsilon\gamma\int_{-L/2}^{x}\left(\int_{-L/2}^{\zeta}\varphi\left(\eta\right)\ \mathrm{d}\eta\right)\mathrm{d}\zeta + \lambda = 0 \quad \text{for} \quad x \in \left(x_L, x_R\right). \tag{6.79a}$$

Integrating over the interface layer as in (6.12) leads to

$$\lambda = \frac{-1}{\ell}\left[\frac{x_R + x_L}{2} + \varepsilon\gamma\int_{x_L}^{x_R}\int_{-L/2}^{x}\left(\int_{-L/2}^{\zeta}\varphi\left(\eta\right)\mathrm{d}\eta\right)\mathrm{d}\zeta\ \mathrm{d}x\right], \tag{6.79b}$$

and we impose the BCs (6.17b)–(6.17c). The ID-ELE (6.13b) becomes

$$\varepsilon^2\widetilde{\varphi}'' + \frac{1}{2}\left(\widetilde{\varphi} - \frac{x_L + x_R}{\ell}\right) - \varepsilon\gamma\left(\Phi - \overline{\Phi}_{(x_L,x_R)}\right) = 0, \tag{6.80}$$

where (cf. (6.1b)),

$$-\Phi\left(x\right) = \int_{-L/2}^{x}\left(\int_{-L/2}^{\zeta}\varphi\left(\eta\right)\ \mathrm{d}\eta\right)\mathrm{d}\zeta;$$

integrating (6.80) over (x_L, x_R) then yields (6.14) with $m = 0$. Differentiating (6.79a) twice leads to the linear (cf. (6.17a))

$$\varepsilon^2\widetilde{\varphi}^{(\mathrm{iv})} + \frac{1}{2}\widetilde{\varphi}'' + \varepsilon\gamma\widetilde{\varphi} = 0, \tag{6.81}$$

which we solve to arrive at the general solution (6.24), in which (cf. (6.22))

$$q_h = \frac{1+\sqrt{1-\rho}}{4\varepsilon^2}, \qquad q_\ell = \frac{1-\sqrt{1-\rho}}{4\varepsilon^2}, \qquad \text{provided} \qquad \rho < 1, \qquad \rho := 16\gamma\varepsilon^3. \tag{6.82}$$

Clearly $\rho = 1$ is equivalent to $\widehat{\alpha} = \frac{1}{4}$, and is the critical value above which minimisers are disordered (as we demonstrated in Section 6.2.2). As we saw in Section 6.1.5.4, symmetry

$(m = 0)$ allows us to conclude that $x_R = -x_L = \frac{\ell}{2}$, and $c_2 = c_4 = 0$, as long as $c_A, c_B \neq 0$ as in (6.29). Under these conditions, the Dirichlet conditions (6.17b) yield

$$c_1 \sin\left(\sqrt{q_\ell}\frac{\ell}{2}\right) + c_3 \sin\left(\sqrt{q_h}\frac{\ell}{2}\right) = 1, \tag{6.83a}$$

and the zero Neumann conditions yield

$$c_1\sqrt{q_\ell}\cos\left(\sqrt{q_\ell}\frac{\ell}{2}\right) + c_3\sqrt{q_h}\cos\left(\sqrt{q_h}\frac{\ell}{2}\right) = 0. \tag{6.83b}$$

The condition (6.63) for the ID-ELE becomes

$$g\left(\ell;\gamma\right) := \frac{2\left(q_h - q_\ell\right)}{c_A\sqrt{q_h q_\ell}}\cos\left(\sqrt{q_h}\frac{\ell}{2}\right)\cos\left(\sqrt{q_\ell}\frac{\ell}{2}\right) + \ell = L. \tag{6.83c}$$

We will use these three conditions (for the three unknowns c_1, c_3 and ℓ) in our sharp interface analysis of the problem.

6.3 Multi-monolayer morphologies

We close this chapter by presenting our notation and terminology for describing multi-monolayer morphologies, and then relate these to single monolayer configurations.

Notation and terminology

We characterise the morphology by the usual parameters $\varepsilon_\varphi^2, \chi^{AB}, \alpha$ as well as:

- A set $\{X_i\}_{i=0,\ldots,\nu}$ with $0 = X_0 < X_1 < \ldots < X_\nu = \mathcal{D}$ and $\varphi\left(X_i\right) = \pm 1$ for each i. These points locate the midpoints of the pure phase regions separating the interface layers, as illustrated in Fig. 6.9. X_i is the right end of the i-th (of ν) monolayer(s). We collect the set of X-values into the $(\nu+1)$–vector $\boldsymbol{X} = \left(X_0, \ldots, X_\nu\right)^\top$, and define the set of monolayer lengths $\{L_i\}_{i=1,\ldots,\nu}$ with

  $$L_i := X_i - X_{i-1}, \tag{6.84a}$$

  and collect these into the ν–vector $\boldsymbol{L} = \left(L_1, \ldots, L_\nu\right)^\top$.

- A set of intervals $\left\{\left(x_L^{(i)}, x_R^{(i)}\right)\right\}_{i=1,\ldots,\nu}$ in which $X_{i-1} \leq x_L^{(i)} < x_R^{(i)} \leq X_i$ for $i = 1, \ldots, \nu$ (cf. Section 3.2 of Blowey and Elliott (1991)) and a corresponding set of interface layer widths $\{\ell_i\}_{i=1,\ldots,\nu}$ with each

  $$\ell_i := x_R^{(i)} - x_L^{(i)}. \tag{6.84b}$$

  These intervals define the locations of the interface layers inside each monolayer. We collect the end-points into the 2ν–vector $\boldsymbol{x} = \left(x_L^{(1)}, x_R^{(2)}, \ldots, x_L^{(\nu)}, x_R^{(\nu)}\right)^\top$ and their lengths into the ν–vector $\boldsymbol{\ell} = \left(\ell_1, \ldots, \ell_\nu\right)^\top$, with

  $$X_i = \frac{x_R^{(i)} + x_L^{(i+1)}}{2} \qquad \text{for} \qquad i = 1, \ldots, \nu - 1. \tag{6.84c}$$

- Interfacial functions $\widetilde{\varphi}^{(i)}$ that define the P2P transitions on the $\left(x_L^{(i)}, x_R^{(i)}\right)$.
- A specification that φ correspond to a pure phase at $x = 0$, viz. $\varphi(0) = \pm 1$.

We use $\mathcal{D}$ (un-scaled) and $\widehat{\mathcal{D}}$ (scaled) to describe the multi-monolayer situation, and L (un-scaled) and $\widehat{L}$ (scaled) for individual monolayers. Finally, we define a *pulse*.

Definition 6.3.1. (A pulse) *We define the j-th pulse as the structure comprised of the j-th and $(j+1)$-st monolayers in a multi-monolayer configuration.*

Remarks.

i) We require $\nu \geq 2$ for this definition to make sense. A ν-layer morphology will consist of $\nu - 1$ pulses as in Fig. 6.9.

ii) Our definition of a monolayer neatly models a row of DBC molecules lying end-to-end as in Fig. 6.9; each φ monolayer corresponds to one DBC molecule.

iii) We allow zero width A/B pure-phase regions, but insist that each $\ell_i > 0$.

6.3.1 Energy

The energy of a multi-monolayer configuration is given by (cf. (6.1e))

$$\begin{aligned}\mathcal{E}[\varphi] &= \int_0^{\mathcal{D}} \left\{ \frac{\varepsilon_\varphi^2}{2} \left(\varphi'\right)^2 + \frac{\chi^{AB}}{4}\left(1-\varphi^2\right) + \frac{\alpha}{2}\left(-\Phi'\right)^2 \right\} \mathrm{d}x \\ &= \underbrace{\sum_{i=1}^{\nu} \int_{x_L^{(i)}}^{x_R^{(i)}} \left\{ \frac{\varepsilon_\varphi^2}{2} \left(\varphi'\right)^2 + \frac{\chi^{AB}}{4}\left(1-\varphi^2\right) + \frac{\alpha}{2}\left(-\Phi'\right)^2 \right\} \mathrm{d}x}_{\text{interfacial energy: } \nu \text{ interface layers}} \\ &\qquad + \underbrace{\frac{\alpha}{2} \sum_{i=1}^{\nu} \left(\int_{X_{i-1}}^{x_L^{(i)}} \left(-\Phi'\right)^2 \mathrm{d}x + \int_{x_R^{(i)}}^{X_i} \left(-\Phi'\right)^2 \mathrm{d}x \right)}_{\text{non-local energy: } \nu \text{ monolayers}} \end{aligned} \tag{6.85}$$

where we specify that

$$-\Phi''(x) = \varphi(x) - \overline{\varphi}, \qquad \Phi'(0) = \Phi'(\mathcal{D}) = 0, \qquad \text{and} \qquad \int_0^{\mathcal{D}} \Phi(t)\,\mathrm{d}t = 0, \tag{6.1b}$$

and require that

$$\overline{\varphi} = m \qquad \Rightarrow \qquad \frac{1}{\mathcal{D}} \int_0^{\mathcal{D}} \varphi \,\mathrm{d}x = m. \tag{6.1c}$$

We also assume the *ansatz* (cf. (6.4))

$$\varphi(0) = -1 \tag{6.86a}$$

i.e. the left side of the domain is pure phase B, which in turn means that

$$\varphi\left(x_L^{(2i-1)}\right) = \varphi\left(x_R^{(2i)}\right) = -1, \quad \varphi\left(x_L^{(2i)}\right) = \varphi\left(x_R^{(2i-1)}\right) = 1 \quad i = 1, \dots \lceil \frac{\nu}{2} \rceil, \tag{6.86b}$$

and in particular that

$$\varphi(x) = \begin{cases} -1 & x \in \left[x_0, x_L^{(1)}\right), \left(x_R^{(2)}, x_L^{(3)}\right), \left(x_R^{(4)}, x_L^{(5)}\right), \dots \\ \widetilde{\varphi}^{(i)} & x \in \left[x_L^{(i)}, x_R^{(i)}\right], i = 1, \dots, \nu \\ 1 & x \in \left(x_R^{(1)}, x_L^{(2)}\right), \left(x_R^{(3)}, x_L^{(4)}\right), \left(x_R^{(5)}, x_L^{(6)}\right), \dots . \end{cases} \tag{6.86c}$$

We depict such a morphology for $\nu = 3$ in Fig. 6.9.

Remark. The energy expression (6.85) says that the interfacial and homogeneous energy are concentrated in the interface layers (only). These energy components are not present in the pure phase A,B regions at all. Non-local energy is distributed throughout Ω.

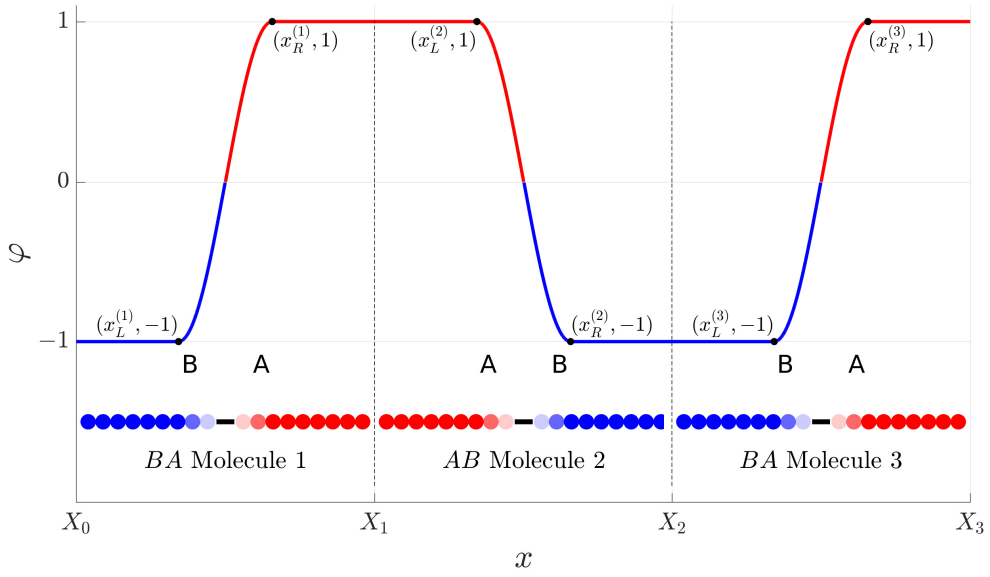

Figure 6.9: A 3-monolayer morphology as in (6.86c). The set $\{X_i\}$ defines the end-points of the monolayers; end-points of the interface layers are indicated as pairs $\left\{x_L^{(i)}, x_R^{(i)}\right\}$. We interpret $\varphi > 0$ as phase A (red), and $\varphi < 0$ as phase B (blue). The three molecules represented by φ are depicted, lying end-to-end, in the lower part of the figure (cf. Fig 6.1). The morphology consists of two pulses: an upright one (the first and second monolayers), and an inverted one (the second and third monolayers).[22]

6.3.2 Stationarity

We now construct the Lagrangian we will use and determine conditions under which a morphology is a stationary point of the energy. We define (cf. (6.5))

$$\mathscr{L}(\varphi, \boldsymbol{x}, \boldsymbol{X}, \lambda) = \sum_{i=1}^{\nu} \int_{x_L^{(i)}}^{x_R^{(i)}} \left\{ \frac{\varepsilon_\varphi^2}{2} \left(\varphi'\right)^2 + \frac{\chi^{AB}}{4} \left(1 - \varphi^2\right) \right\} \mathrm{d}x + \frac{\alpha}{2} \sum_{i=1}^{\nu} \left(\int_{x_{i-1}}^{x_i} \left(-\Phi'\right)^2 \mathrm{d}x \right) - \lambda \left(\int_0^{\mathcal{D}} \varphi \, \mathrm{d}x - m\mathcal{D} \right). \quad (6.87)$$

Necessary conditions for a stationary (energy minimising) morphology include (cf. (6.6))

$$\nabla_{\boldsymbol{x}} \mathscr{L} = 0, \qquad \frac{\delta \mathscr{L}}{\delta \widetilde{\varphi}^{(i)}} = 0, \qquad \text{and} \qquad \partial_\lambda \mathscr{L} = 0, \quad (6.88)$$

where, in the second condition, we vary the φ in each interface layer ($\varphi =: \widetilde{\varphi}^{(i)}$).

Lemma 6.3.2. ($\varphi' = 0$ at each interfacial end-point of a multi-monolayer minimiser) *For a multi-monolayer minimiser, it is necessary that*

$$\left(\widetilde{\varphi}^{(i)}\right)' \left(x_L^{(i)}\right) = \left(\widetilde{\varphi}^{(i)}\right)' \left(x_R^{(i)}\right) = 0 \qquad \textit{for each} \qquad i = 1, \ldots, \nu, \quad (6.89)$$

i.e. on every interface layer in the morphology.

This follows immediately from Theorem 4.2.5 as in the single monolayer case.

A *system* of ID-ELEs

The stationarity condition must hold separately in each interface layer, and so

$$\varepsilon_\varphi^2 \left(- \left(\widetilde{\varphi}^{(i)}\right)'' \right) - \frac{\chi^{AB}}{2} \widetilde{\varphi}^{(i)} - \lambda + \alpha\Phi = 0 \quad (6.90)$$

in each interfacial sub-domain $\left(x_L^{(i)}, x_R^{(i)}\right)$. Integrating this on each $\left(x_L^{(i)}, x_R^{(i)}\right)$ using our new BCs leads to a system of ν integro-differential equations on the interface layers,

$$-\frac{\chi^{AB}}{2} \int_{x_L^{(i)}}^{x_R^{(i)}} \widetilde{\varphi}^{(i)} \, \mathrm{d}x - \lambda \left(x_R^{(i)} - x_L^{(i)} \right) + \alpha \int_{x_L^{(i)}}^{x_R^{(i)}} \Phi(t) \, \mathrm{d}t = 0;$$

whence (cf. (6.12)),

$$\lambda = \frac{\chi^{AB}}{2} \left(\frac{\Phi'\left(x_R^{(i)}\right) - \Phi'\left(x_L^{(i)}\right)}{x_R^{(i)} - x_L^{(i)}} - m \right) + \frac{\alpha}{x_R^{(i)} - x_L^{(i)}} \int_{x_L^{(i)}}^{x_R^{(i)}} \Phi(t) \, \mathrm{d}t. \quad (6.91)$$

Hence, we have a system of ν ID-ELEs, one in each interface, and (6.90) becomes

$$\varepsilon_\varphi^2 \left(\left(-\widetilde{\varphi}^{(i)} \right)'' \right) - \frac{\chi^{AB}}{2} \left(\widetilde{\varphi}^{(i)} - m + \frac{\Phi' \left(x_R^{(i)} \right) - \Phi' \left(x_L^{(i)} \right)}{x_R^{(i)} - x_L^{(i)}} \right) + \alpha \left(\Phi - \frac{1}{x_R^{(i)} - x_L^{(i)}} \int_{x_L^{(i)}}^{x_R^{(i)}} \Phi(t)\, \mathrm{d}t \right) = 0; \ i = 1, \ldots, \nu, \quad (6.92)$$

where we demand that:

- Φ' is to be continuous on the domain;
- the interface layers should alternate BA, AB, ... and so on;
- $x_L^{(1)} < x_R^{(1)} \leq x_L^{(2)} < x_R^{(2)} \leq \ldots \leq x_L^{(\nu)} < x_R^{(\nu)}$ i.e. the interface layers are sequenced appropriately and have non-zero thickness.

As in the single monolayer case, we can write each (6.92) as

$$G^{(i)} x + H^{(i)} = 0 \qquad \text{which is to hold for every} \qquad x \in \left(x_L^{(i)}, x_R^{(i)} \right). \quad (6.26)$$

Remark. Morphologies satisfying the system of ID-ELEs in (6.92) are termed stationary.[23]

A *system* of linear fourth-order ODEs

We obtain a system of ν fourth order ODEs when we differentiate each component of (6.92) twice. For $i = 1, \ldots, \nu$, we have (cf. (6.17a) and (3.16) of Blowey and Elliott (1991))

$$\varepsilon_\varphi^2 \left(\widetilde{\varphi}^{(i)} \right)^{(\mathrm{iv})} + \frac{\chi^{AB}}{2} \left(\widetilde{\varphi}^{(i)} \right)'' + \alpha \left(\left(\widetilde{\varphi}^{(i)} \right) - m \right) = 0, \quad (6.93a)$$

with BCs

$$\widetilde{\varphi}^{(i)} \left(x_L^{(i)} \right) = -1, \quad \widetilde{\varphi}^{(i)} \left(x_R^{(i)} \right) = 1 \quad \text{and} \quad \left(\widetilde{\varphi}^{(i)} \right)' \left(x_L^{(i)} \right) = \left(\widetilde{\varphi}^{(i)} \right)' \left(x_R^{(i)} \right) = 0 \quad (6.93b)$$

for the BA interface layers, and

$$\widetilde{\varphi}^{(i)} \left(x_L^{(i)} \right) = 1, \quad \widetilde{\varphi}^{(i)} \left(x_R^{(i)} \right) = -1 \quad \text{and} \quad \left(\widetilde{\varphi}^{(i)} \right)' \left(x_L^{(i)} \right) = \left(\widetilde{\varphi}^{(i)} \right)' \left(x_R^{(i)} \right) = 0 \quad (6.93c)$$

for the AB transitions.

Remark. The re-scalings of Sections 6.2, 6.2.7 can be applied to multi-monolayer morphologies in the obvious way.

6.4 Summary and conclusions

We started our study of the 1D problem in this chapter. We posed the single-monolayer minimisation problem over the symmetric domain $\left(-\frac{L}{2}, \frac{L}{2}\right)$ and derived a necessary first order minimisation condition, which we found to be an integro-differential equation (the ID-ELE). We found that solutions of the ID-ELE also satisfy a certain linear, fourth order ODE and started bracketing solutions of the latter in terms of the discriminant of the underlying auxiliary equation. We reduced the ID-ELE to an affine function which in turn led to a system of two non-linear equations governing all candidate energy minimisers. This system serves as the link between the large set of solutions of the ODE (which are easy to write down) and those candidates satisfying the ID-ELE (a small subset of the former). After exploring a number of technicalities related to the ODE, we discovered that the single monolayer minimisation problem is substantially simplified under the assumption of symmetry ($m = 0$).

We then studied two re-scalings of the underlying parameter space.

i) The first involves $\widehat{\alpha}$ and a scaled length parameter ($\widehat{L}$ or $\widehat{\ell}$) and will prove useful in Chapter 7, when we attempt to solve the minimisation problem exactly in cool parameter space ($\widehat{\alpha} \leq \frac{1}{4}$). We showed that minimisers are disordered if $\alpha > \frac{1}{4}$ (hence our interest in cool parameters), and then examined the nature of individual symmetric BA interface layers over $\left(\widehat{\ell}, \widehat{\alpha}\right)$-space, for $\widehat{\alpha} \leq \frac{1}{4}$.

ii) The second is well suited to the study of solutions of the sharp interface limit problem, in which we will send $\varepsilon_\varphi \downarrow 0$ in a very specific way, in Section 8.5.

Finally, we extended our notation and terminology to consider the multi-monolayer minimisation problem. We found that the first order minimisation condition for these structures is a *system* of ID-ELEs, each of which is similar to that of the single monolayer problem.

Outlook for the next chapter

We now use the infrastructure above to start developing an exact solution to the stationary symmetric energy minimisation problem in 1D.

Notes

[1]See the MATLAB working script `three_phase_1D_asymp_one_ARB_BApiece.m` in the `bitbucket` repository. Run as `three_phase_1D_asymp_one_ARB_BApiece(0.1,`true).

[2]The AB-interface layer *ansatz* is

$$\varphi_{AB}(x_L) = 1, \qquad \varphi_{AB}(x_R) = -1.$$

[3]Detailed working is as follows:

$$-\Phi'(x) = -(1+\overline{\varphi})\,x + A \qquad \text{for} \qquad x \in \left(-\frac{L}{2}, x_L\right), \tag{6.94a}$$

and

$$-\Phi'(x) = (1-\overline{\varphi})\,x + B \qquad \text{for} \qquad x \in \left(x_R, \frac{L}{2}\right). \tag{6.94b}$$

For $x \in (x_L, x_R)$, we specify that

$$-\Phi'(x) = \int_{x_L}^{x} \widetilde{\varphi} - \overline{\varphi}\,\mathrm{d}t + C \tag{6.95}$$

where A, B, C can be found by consideration of the relevant boundary/mass conditions. In particular, from $\Phi'(-L/2) = 0$, we determine that

$$(1+\overline{\varphi})\frac{L}{2} + A = 0 \qquad \Rightarrow \qquad A = \frac{-L}{2}(1+\overline{\varphi}), \tag{6.96a}$$

and from $\Phi'(L/2) = 0$, we find

$$(1-\overline{\varphi})\frac{L}{2} + B = 0 \qquad \Rightarrow \qquad B = \frac{-L}{2}(1-\overline{\varphi}). \tag{6.96b}$$

Consequently,

$$-\Phi'(x) = \begin{cases} -\left(x + \dfrac{L}{2}\right)(1+\overline{\varphi}) & x \in \left(-\dfrac{L}{2}, x_L\right) \\ \displaystyle\int_{x_L}^{x} \widetilde{\varphi} - \overline{\varphi}\,\mathrm{d}t + C & x \in (x_L, x_R) \\ \left(x - \dfrac{L}{2}\right)(1-\overline{\varphi}) & x \in \left(x_R, \dfrac{L}{2}\right). \end{cases} \tag{6.97}$$

We have two continuity conditions at x_L, x_R available to resolve the remaining constant. We require

$$-\Phi'(x)\big|_{x_L-}^{x_L+} = 0 \qquad \Rightarrow \qquad -\left(x_L + \frac{L}{2}\right)(1+\overline{\varphi}) = C \tag{6.98a}$$

and

$$-\Phi'(x)\big|_{x_R-}^{x_R+} = 0 \qquad \Rightarrow \qquad \left(x_R - \frac{L}{2}\right)(1-\overline{\varphi}) = \int_{x_L}^{x_R} \widetilde{\varphi} - \overline{\varphi}\,\mathrm{d}x + C. \tag{6.98b}$$

Combining these, we arrive at the trivial (so-called because it is equivalent to $\int_{-L/2}^{L/2} \varphi - \overline{\varphi}\,\mathrm{d}x = 0$)

$$(1+\overline{\varphi})\underbrace{\left(x_L + \frac{L}{2}\right)}_{|\Omega_{\underline{B}}|} - (1-\overline{\varphi})\underbrace{\left(\frac{L}{2} - x_R\right)}_{|\Omega_{\overline{A}}|} = \int_{x_L}^{x_R} \widetilde{\varphi} - \overline{\varphi}\,\mathrm{d}x.$$

[4]We use Leibnitz's rule extensively in what follows:

$$\frac{\mathrm{d}}{\mathrm{d}y}\int_{h(y)}^{g(y)} f(x,y)\,\mathrm{d}x = f(g(y),y)\,g'(y) - f(h(y),y)\,h'(y) + \int_{h(y)}^{g(y)} \partial_y f(x,y)\,\mathrm{d}x.$$

[5]Picking $\widetilde{E}$ so that Φ has zero integral on $\left(-\frac{L}{2},\frac{L}{2}\right)$ leads to

$$\widetilde{E}=(m+1)\left(\frac{L^2}{24}-\frac{Lx_R}{4}+\frac{x_R^2}{4}-\frac{x_L^3}{6L}-\frac{x_L^2}{4}+\frac{x_Lx_R^2}{2L}-\frac{x_Lx_R}{2}\right)+(m-1)\left(\frac{L^2}{24}-\frac{Lx_R}{4}+\frac{x_R^2}{2}-\frac{x_R^3}{3L}\right)$$
$$+\frac{1}{L}\int_{x_L}^{x_R}\int_{x_L}^{x}\int_{x_L}^{\xi}\widetilde{\varphi}-m\;\mathrm{d}t\;\mathrm{d}\xi\;\mathrm{d}x+\left(\frac{1}{2}-\frac{x_R}{L}\right)\int_{x_L}^{x_R}\int_{x_L}^{\xi}\widetilde{\varphi}-m\;\mathrm{d}t\;\mathrm{d}\xi. \quad (6.99)$$

[6]The roots $q_\pm$ will be always be real *and negative* for a sufficiently low temperature/small ε_φ; in particular, for a non-negative discriminant,

$$\Delta\geq 0 \qquad \Leftrightarrow \qquad \chi^{AB}\geq 4\sqrt{\alpha}\varepsilon_\varphi \qquad \Leftrightarrow \qquad 0<\Theta\leq\frac{\widetilde{\chi^{AB}}}{4\sqrt{\alpha}\varepsilon_\varphi}; \quad (6.100)$$

this latter inequality defines a temperature range within which $q_\pm\leq 0$ i.e. both roots are non-positive (and finite). There are several points worth making in respect of parameter studies:

a) For given values of α and ε_φ, (6.100) implies there is a lower bound on allowed values of χ^{AB}: equivalently, conditions have to be cold enough or these solutions do not hold;

b) For given values of χ^{AB} and ε_φ, there is an upper bound on α given by

$$\alpha\leq\frac{\left(\chi^{AB}\right)^2}{16\varepsilon_\varphi^2}; \quad (6.101)$$

c) For given values of χ^{AB} and α, ε_φ must be suitably small; in particular, we must have

$$\varepsilon_\varphi\leq\frac{\chi^{AB}}{4\sqrt{\alpha}}. \quad (6.102)$$

[7]The frequency increases with *increasing* α (cf. (6.101)) and *decreasing* Θ. The inequalities in (6.22a)–(6.22b) are strict since $\alpha>0$.

[8]A count of unknowns and free parameters suggests that we appear to be one short i.e. we have no way of relating x_L and x_R. However, (6.13b) provides full information about x_L and x_R.

[9]These are unknown at this stage in our solution process.

[10]See the MATLAB numerical experiment `work_with_general_1D_2phase_energy.m` in the `bitbucket` repository.

[11]From a modelling perspective, $m=0$ corresponds to the pure A and B parts of the DBC molecule having equal length.

[12]Another way of seeing this, which gives some indication as to why this is such a useful result is as follows: consider the general solution in the 'shifted' form (6.23); we will determine the values of c_2 and c_4 for $m=0$. Expanding the '$\sqrt{q_\ell}$' term, we see that

$$\bar{c}_1\sin\left(\sqrt{q_\ell}x+\bar{c}_2\right)=\underbrace{\bar{c}_1\cos\left(\bar{c}_2\right)}_{=c_1}\sin\left(\sqrt{q_\ell}x\right)+\underbrace{\bar{c}_1\sin\left(\bar{c}_2\right)}_{=c_2}\cos\left(\sqrt{q_\ell}x\right) \qquad \Rightarrow \qquad \bar{c}_2=\arctan\left(\frac{c_2}{c_1}\right).$$

(For our purposes, there is little value in working out $\bar{c}_1$.) With $m=0$, (6.34) then gives

$$\frac{c_2}{c_1}=\frac{\left(\begin{array}{r}\sqrt{q_\ell}\left[1+\cos\left(\sqrt{q_h}\left(x_L-x_R\right)\right)\right]\left[\cos\left(\sqrt{q_\ell}x_L\right)-\cos\left(\sqrt{q_\ell}x_R\right)\right]\\+\sqrt{q_h}\sin\left(\sqrt{q_h}\left(x_L-x_R\right)\right)\left[\sin\left(\sqrt{q_\ell}x_L\right)+\sin\left(\sqrt{q_\ell}x_R\right)\right]\end{array}\right)}{\left(\begin{array}{r}\sqrt{q_\ell}\left[1+\cos\left(\sqrt{q_h}\left(x_L-x_R\right)\right)\right]\left[\sin\left(\sqrt{q_\ell}x_L\right)-\sin\left(\sqrt{q_\ell}x_R\right)\right]\\+\sqrt{q_h}\sin\left(\sqrt{q_h}\left(x_R-x_L\right)\right)\left[\cos\left(\sqrt{q_\ell}x_L\right)+\cos\left(\sqrt{q_\ell}x_R\right)\right]\end{array}\right)}$$
$$=\tan\left(\frac{-\sqrt{q_\ell}\left(x_L+x_R\right)}{2}\right),$$

from which it follows that

$$\bar{c}_2=\frac{-\sqrt{q_\ell}\left(x_L+x_R\right)}{2}. \quad (6.103a)$$

Likewise, for the $\sqrt{q_h}$ term in (6.23) we determine that (cf. (6.34d))

$$\frac{c_4}{c_3}\left(q_\ell, q_h\right) = \frac{c_2}{c_1}\left(q_h, q_\ell\right) \qquad \Rightarrow \qquad \overline{c}_4 = \arctan\left(\frac{c_4}{c_3}\right) = \frac{-\sqrt{q_h}\left(x_L + x_R\right)}{2}. \tag{6.103b}$$

Consequently, for the zero mass case, the interface layer can be described by a shifted function of the form

$$\widetilde{\varphi}_{(m=0)}\left(x\right) = \overline{c}_1 \sin\left(\sqrt{q_\ell}\left(x - \frac{x_L + x_R}{2}\right)\right) + \overline{c}_3 \sin\left(\sqrt{q_h}\left(x - \frac{x_L + x_R}{2}\right)\right), \tag{6.104}$$

which is obviously odd about $x = \frac{x_L + x_R}{2}$ and thus integrates to zero over (x_L, x_R). In particular, we conclude that any zero mass interface layer is comprised of two sine components (one of high frequency, the other low) and $c_2 = c_4 = 0$ if we write the solution as in (6.24a). We conclude that the zero mass, single monolayer minimiser *must* be such that $x_L = -x_R$ (where we set $x_R = \frac{\ell}{2}$, cf. (6.2)) i.e. we have morphological (a)symmetry and in fact, according to (6.104), oddness.

[13]This observation will prove useful as we switch back and forth between the original and scaled problems, especially when working with MATLAB (and other) codes that investigate these problems.

[14]Starting from (3.51) and using (6.43a), we arrive at the dynamic equation

$$\partial_t \widehat{\varphi} + \widehat{\varphi}^{(\mathrm{iv})} + \widehat{\varphi}'' - \frac{1}{\mu}\left(\left(\widehat{\varphi} - 1\right)_+ + \left(\widehat{\varphi} + 1\right)_-\right)'' + \widehat{\alpha}\left(\widehat{\varphi} - m\right) = 0, \tag{6.105a}$$

on $\widehat{x} \in \left(0, \widehat{L}\right)$, where we have re-scaled time to absorb a possible non-unit mobility, with BCs (cf. (3.35d))

$$\varphi'\big|_{0,\widehat{L}} = 0, \qquad \text{and} \qquad \varphi^{(\mathrm{iii})}\Big|_{0,\widehat{L}} = 0, \tag{6.105b}$$

and an appropriate IC of form (3.35c). We now perform a stability analysis of (6.105). We start at $t = 0$, and assume that $|\varphi|_{0,\infty}\left(0\right) \leq 1$ i.e. the penalty is zero. This is a valid assumption for all candidates close to the disordered, $\varphi \equiv m$. Then

$$\partial_t \widehat{\varphi} + \widehat{\varphi}^{(\mathrm{iv})} + \widehat{\varphi}'' + \widehat{\alpha}\left(\widehat{\varphi} - m\right) = 0$$

where the initial (conserved) mass is $\overline{\widehat{\varphi}_0} = m$, $|m| < 1$. We rescale the above as in Section 2.1 of Choksi et al. (2009) with $u := \widehat{\varphi} - m$ to arrive at the *linear* equation

$$\partial_t u + u^{(\mathrm{iv})} + u'' + \widehat{\alpha} u = 0,$$

with $u'\big|_{0,\widehat{L}} = u^{(\mathrm{iii})}\Big|_{0,\widehat{L}} = 0$, and $u\left(x, 0\right) = u_0\left(x\right)$, with $\overline{u_0} = 0$. From the *ansatz* $u = \mathrm{e}^{\lambda t + ikx}$, we find that

$$\lambda = -|k|^4 + |k|^2 - \widehat{\alpha}$$

and so $\lambda > 0$ and there are growing modes (instability) if

$$-|k|^4 + |k|^2 - \widehat{\alpha} > 0 \qquad \Leftrightarrow \qquad \left(|k|^2 - \frac{1}{2}\right)^2 < \frac{1}{4} - \widehat{\alpha}.$$

As in Lemma 6.2.1, this result is m–independent, which is fundamentally different to (3.10) and (4.15) of Choksi et al. (2009), both of which relate to a 2-phase model in which the homogeneous energy density is approximated by a quartic polynomial.

[15]The definition that follows is correct, but could be regarded as somewhat obtuse. The cold region is bounded in parameter space by the first zero contour of $\cos\left(\sqrt{\widehat{q}_h}\frac{\widehat{\ell}}{2}\right)$ on the left and the first zero contour of $\cos\left(\sqrt{\widehat{q}_\ell}\frac{\widehat{\ell}}{2}\right)$ on the right.

[16]We prove this as follows: consider the intersection $\left(\underline{\widehat{L}}, \underline{\widehat{\alpha}}\right)$ of $F = \widehat{\alpha}\widehat{L}^4$ as in (6.52), and the first zero contour of $\cos\left(\sqrt{\widehat{q}_\ell}\frac{\widehat{L}}{2}\right)$,

$$\widehat{L} = \frac{\sqrt{2}\pi}{\sqrt{1 - \sqrt{1 - 4\widehat{\alpha}}}} \qquad \Rightarrow \qquad \widehat{\alpha} = \frac{\pi^2}{\widehat{L}^2}\left(1 - \frac{\pi^2}{\widehat{L}^2}\right). \tag{6.106}$$

Notice that $\widehat{\alpha} \in \left(0, \frac{1}{4}\right]$ with $\widehat{\alpha} = \frac{1}{4}$ when $\widehat{L} = \sqrt{2}\pi$, and $\widehat{\alpha} \downarrow -\infty$ as $\widehat{L} \to 0$, but $\widehat{\alpha} \downarrow 0$ as $\widehat{L} \to \infty$. Eliminating $\widehat{\alpha}$ to solve $\widehat{L} > 0$ in terms of F, we find that

$$\frac{\pi^2}{\widehat{L}^2}\left(1 - \frac{\pi^2}{\widehat{L}^2}\right) = \frac{F}{\widehat{L}^4} \qquad \Rightarrow \qquad \underline{\widehat{L}} = \frac{\sqrt{\pi^4 + F}}{\pi} \qquad \text{and so} \qquad \underline{\widehat{\alpha}} = \frac{F\pi^4}{\left(\pi^4 + F\right)^2}.$$

For $F < \pi^4$, we must have $\underline{\widehat{\alpha}} > \frac{1}{4}$ and $\underline{\widehat{L}} < \sqrt{2}\pi$ and so there are no points of intersection inside cool parameter space for such an F. The line of cooling through $\left(\underline{\widehat{L}}, \underline{\widehat{\alpha}}\right) = \left(\sqrt{2}\pi, \frac{1}{4}\right)$ (where the cold region touches $\widehat{\alpha} = \frac{1}{4}$) corresponds to $F = \pi^4$. Consequently, there are two sub-cases to consider:

i) $F < \pi^4$: these contours enter cool parameter space directly into Region I.

ii) $F \geq \pi^4$: the points of intersection are inside cool parameter space.

For $F = \pi^4$, $\left(\underline{\widehat{L}}, \underline{\widehat{\alpha}}\right) = \left(\sqrt{2}\pi, \frac{1}{4}\right)$ and

$$\widehat{\alpha} = \frac{F}{\widehat{L}^4} < \frac{\pi^2}{\widehat{L}^2}\left(1 - \frac{\pi^2}{\widehat{L}^2}\right) \qquad \Leftrightarrow \qquad \widehat{L} > \sqrt{2}\pi.$$

Finally, for $F > \pi^4$, any contour of (6.52) intersects the edge of the cold region at the single point, $\left(\underline{\widehat{L}}, \underline{\widehat{\alpha}}\right)$, at which

$$\left.\frac{\mathrm{d}\widehat{\alpha}}{\mathrm{d}\widehat{L}}\left(\underline{\widehat{L}}, \underline{\widehat{\alpha}}\right)\right|_{\text{contour}} = \frac{-4F}{\underline{\widehat{L}}^5} < \left.\frac{\mathrm{d}\widehat{\alpha}}{\mathrm{d}\widehat{L}}\left(\underline{\widehat{L}}, \underline{\widehat{\alpha}}\right)\right|_{\text{cold region}} = \frac{4\pi^4 - 2\pi^2\underline{\widehat{L}}^2}{\underline{\widehat{L}}^5}$$

i.e. the contours of (6.52) enter the cold region, and never leave.

[17]See the MATLAB code `qp_okfef_1D_2phase_plot_fundamentals.m` in the `bitbucket` repository, which is called inside `scaled_alpha_L_sweep_1D_2phase.m`.

[18]See the MATLAB code `qp_okfef_1D_2phase_plot_cool2cold.m` in the `bitbucket` repository, which is called inside `scaled_alpha_L_sweep_1D_2phase.m`.

[19]See the MATLAB numerical experiment `scaled_alpha_L_sweep_1D_2phase.m` in the `bitbucket` repository.

[20]See the MATLAB code `qp_okfef_1D_2phase_physical_regions_plot.m` in the `bitbucket` repository, which is called inside `scaled_alpha_L_sweep_1D_2phase.m`.

[21]See the MATLAB code `qp_okfef_1D_2phase_singularA_plot.m` in the `bitbucket` repository.

[22]See the MATLAB working script `two_phase_1D_asymp.m` in the `bitbucket` repository. Run this script as `two_phase_1D_asymp(0.1,3, 'B')`.

[23]These are stationary in the sense that if we vary *one* interfacial anchor point (an $x_L^{(i)}$ or $x_R^{(i)}$ value) or *one* interfacial profile (a single function $\widetilde{\varphi}^{(i)}$) *holding all of the other monolayers constant*, then the energy will increase/decrease according to whether the monolayer being varied is a (single monolayer) minimiser or maximiser.

Chapter 7

Equal-spacing in 1D

It is well known that 1D energy minimisers of the Ohta–Kawasaki energy functional with double-well homogeneous energy are equally spaced (Ohnishi et al. (1999); Choksi (2001); Ren and Wei (2003); Chen and Oshita (2005)). Inspired by these results, and armed with the infrastructure we developed in the previous chapter, we now investigate the situation for our obstacle homogeneous energy, using an elementary, constructive approach.

Contents

7.1 A set of cool, single monolayer, symmetric morphologies 150

7.2 Symmetric, multi-monolayer morphologies 155

7.3 Summary and conclusions 174

Chapter outline

In Section 7.1, we characterise the minimum energy of **symmetric, single monolayer morphologies of width** $\widehat{L}$, in which the P2P interface layer solves the ODE

$$\varepsilon_{\varphi}^{2}\widetilde{\varphi}^{(\mathrm{iv})}+\frac{\chi^{AB}}{2}\widetilde{\varphi}''+\alpha\widetilde{\varphi}=0 \qquad \text{on} \qquad x\in(x_L,x_R) \tag{6.17a}$$

subject to the BA interface *ansatz* (Dirichlet) conditions $\widetilde{\varphi}(x_L)=-1$ and $\widetilde{\varphi}(x_R)=1$ from (6.17b), the zero Neumann conditions $\widetilde{\varphi}'|_{x=x_L,x_R}=0$ from (6.17c) and the boundedness constraint $|\varphi(x)|\leq 1$ for every $x\in\overline{\Omega}$ from (6.1d). We will also impose the global first integral, non-local BC $-\Phi'(0)=-\Phi'\left(\widehat{L}\right)=0$ from (6.1b), and insist that the interface layer is of type M1I. Our first result suggests that the **minimum energy** of such morphologies is a **convex function of the monolayer width,** $\widehat{L}$.[1]

In Section 7.2, we study **multi-monolayer morphologies**.

i) In Section 7.2.3, we consider configurations in which each monolayer satisfies all of the conditions above, including the non-local (6.1b) in the sense that $-\Phi'=0$ ***strictly between*** **each monolayer**, as in Fig. 7.6(a). The convexity result of Section 7.1 means

that the energy minimiser in this set is equally spaced i.e. the individual monolayers must be identical, translated/reflected copies of each other.

ii) In Section 7.2.4, we consider ν-layer (ν prescribed) configurations in which the **zeros of $-\Phi'$ are *not* strictly between each monolayer**, as in Fig. 7.6(b).[2] We argue that any such configuration can be rearranged so as to have $-\Phi' = 0$ *strictly between* each monolayer, and lower energy. By the previous section, we further reduce the energy by rearranging the morphology until it is equally spaced.

iii) In Section 7.2.5, **we relax the imposed layer count constraint** ν, and let the system 'choose' the number of layers that minimises the energy, ν_{opt}. The main result in this section is that the energy is minimised when each of the equally spaced interface layers satisfies the ODE, *as well as the ID-ELE* (6.13b).

iv) Section 7.2.6 then generalises further by **relaxing the requirement that each interface layer be monotone**: we insist only that the interface layers be bounded as in (6.1d). For such morphologies, we can reduce the system energy by replacing any monolayer that has a non-monotone, 'wiggly' interface layer, with a set of equally spaced monolayers with type M1I interface layers. In this way, we can replace *any* layered morphology satisfying $\|\varphi\|_{0,\infty} \leq 1$, with one that is a member of the set we considered in Section 7.2.4, having lower energy.

Our investigation suggests that the monolayers in a multi-monolayer energy minimiser are equally spaced, and have (identical) M1I interface layers that solve the ID-ELE. We are unable to provide an analytical expression for ν_{opt} in scaled parameter space, but we do present a numerical result.

7.1 A set of cool, single monolayer, symmetric morphologies

We consider interface layers that satisfy a **boundedness constraint** (cf. Defn 6.2.2)

$$\|\widetilde{\varphi}\|_{\infty} \leq 1, \tag{7.1a}$$

so that $\|\varphi\|_{0,\infty} \leq 1$ on the entire monolayer (cf. (6.1d)), a **monotonicity constraint**,

$$\frac{\mathrm{d}\widetilde{\varphi}}{\mathrm{d}x} \geq 0 \qquad \text{for every} \qquad x \in [x_L, x_R]\,, \tag{7.1b}$$

and the **single inflexion point constraint**,

$$\frac{\mathrm{d}^2\widetilde{\varphi}}{\mathrm{d}x^2} = 0 \qquad \text{has one solution for} \qquad x \in (x_L, x_R)\,. \tag{7.1c}$$

The conditions in (7.1) define our **initial, feasible set**; we depicted samples of these in Fig. 6.6. It is clear that feasible interface layers are in $C^1_{[x_L,x_R]} \cap C^{\infty}_{(x_L,x_R)}$. Hence,

the morphologies satisfying (7.1c) form a subset of those satisfying (7.1b) which, in turn, comprise a subset of those satisfying (7.1a).[3] The M1I interface layers of Defn 6.2.2 satisfy all three of the constraints in (7.1).

7.1.1 Energy-minimising, M1I, cool, single monolayer morphologies

We now solve the single monolayer energy minimisation problem (6.3) for a given $\left(\widehat{L},\widehat{\alpha}\right)_{\text{cool}}$, with the additional restriction that the minimiser should have one M1I P2P interface layer. For a given $\widehat{\alpha},\widehat{L}$, we seek that $\widehat{\ell}\leq\widehat{L}$, in the yellow region of Fig. 6.7(a), which minimises the energy.

Remark. We use $\widehat{\ell}_{\text{opt}}=\widehat{\ell}_{\text{opt}}\left(\widehat{L},\widehat{\alpha}\right)$ to denote the width of an energy-minimising interface layer, for a given set of parameters. The energy of the corresponding M1I, single monolayer morphology is denoted

$$\mathcal{E}^{(1)}_{\text{min}}=\mathcal{E}\left(\widehat{\ell}_{\text{opt}}\left(\widehat{L},\widehat{\alpha}\right),\widehat{L},\widehat{\alpha}\right)=\mathcal{E}^{(1)}_{\text{min}}\left(\widehat{L},\widehat{\alpha}\right). \tag{7.2}$$

The problem thus reduces to a constrained, continuous optimisation problem in one unknown, $\widehat{\ell}$, with candidate $\widehat{\ell}$-values coming from:

Source (1). Solutions of the ID-ELE (6.63): corresponding to smooth local minima of the energy function.

We discuss $\widetilde{g}$ from the ID-ELE (6.63) in detail in Appendix C.5, and find that the ID-ELE has no P2P solutions if $\widehat{L}<\pi/\sqrt{\widehat{q}_h}$ (viz. inside Region I), and solution $\widehat{\ell}=\widehat{L}$ when $\widehat{L}=\pi/\sqrt{\widehat{q}_h}$ (at the right edge of Region I). Inside Region I, $\widehat{\ell}_{\text{opt}}=\widehat{L}$ (cf. Fig. 7.1) i.e. minimum energy interface layers completely fill the domain. They satisfy the ODE, but not the ID-ELE.

Source (2). Edge morphologies: $\widehat{\ell}$-values on the boundaries of the yellow regions in Fig. 6.7(a), as well as the zero width ($\widehat{\ell}=0$) interface layer and $\widehat{\ell}=\widehat{L}$ morphologies.

The principle difficulty in finding Source (2) $\widehat{\ell}$-values is calculating the edges of the regions of interest, especially $\widehat{\ell}_{\text{max}}\left(\widehat{\alpha}\right)$ (as in Fig. 6.7). We investigate these issues in Appendix C.4 on p. 462.

Finding the set of candidate $\widehat{\ell}$-values by hand is impossible, and so we perform a numerical sweep over a grid in $\left(\widehat{L},\widehat{\alpha}\right)_{\text{cool}}$. Our first result is Fig. 7.1 which shows the Source of $\widehat{\ell}_{\text{opt}}$ in $\left(\widehat{L},\widehat{\alpha}\right)_{\text{cool}}$.

We present a sample energy minimisation problem for a particular $\left(\widehat{L},\widehat{\alpha}\right)$-pair in Fig. 7.2.[5]

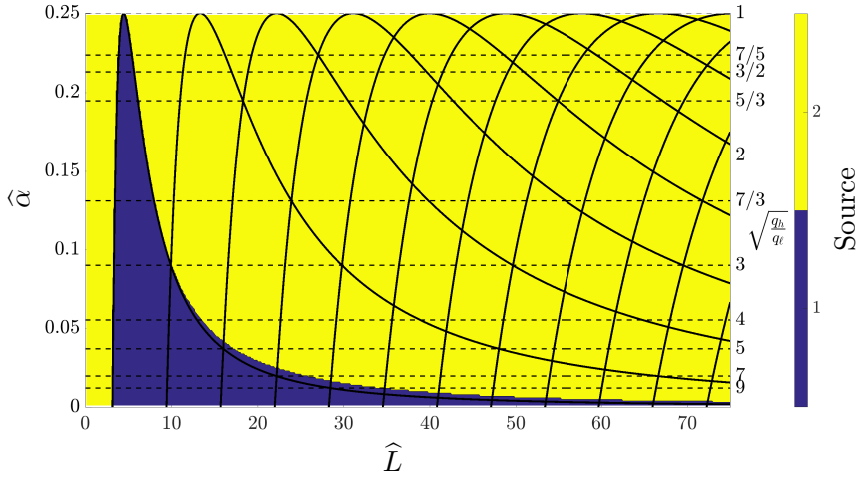

Figure 7.1: Summary M1I single monolayer minimum energy Source plot. The cosine function zero contours (6.66) are black. Region I is in the yellow Source (2) area. Key: Source (1): $\widehat{\ell}_{\text{opt}}$ solves the ID-ELE (6.63); Source (2): an edge morphology.[4]

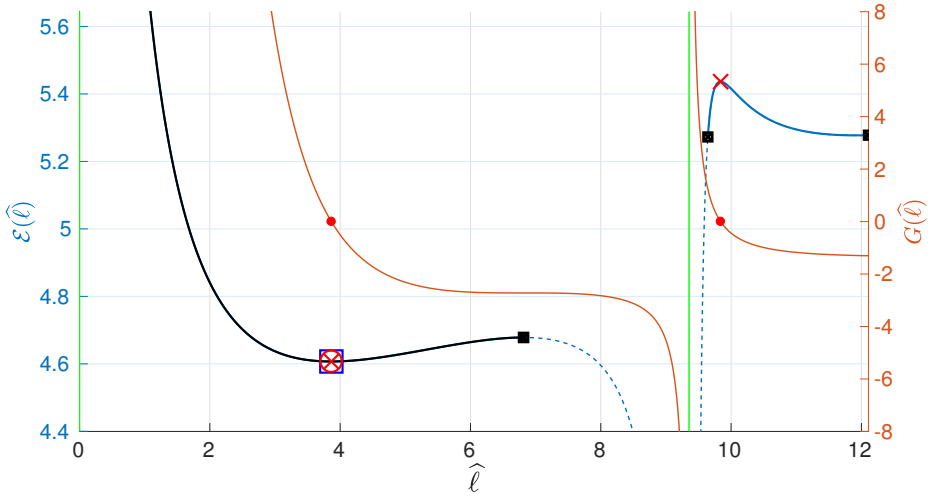

Figure 7.2: Energy minimisation for $\left(\widehat{L},\widehat{\alpha}\right) = (12.108, 0.043)$. Energy is plotted against the left y-axis: the solid **black** segment is M1I, the solid **blue** portion is bounded (but 'wiggly') and the dashed blue parts have $\|\widetilde{\varphi}\|_\infty > 1$. $G\left(\widehat{\ell}\right)$ from (6.37) is against the right y-axis in brown; its zeros and their energies are marked as **red** dots and ×s. Edge morphology energies are marked as thick, crossed black squares. The $\|\widetilde{\varphi}\|_\infty \leq 1$ minimiser is marked with a **blue** square; the M1I minimiser with a **red** circle (they coincide at $\widehat{\ell} = 3.865$).

Summary observations

Conjecture 7.1.1. ($\mathcal{E}^{(1)}_{\min}\left(\widehat{L}\right)$ smooth and convex for $\widehat{L} > 0$) *For given* $0 < \widehat{\alpha} < \frac{1}{4}$, $\widehat{\ell}_{opt} = \widehat{\ell}_{opt}\left(\widehat{L}\right) \leq \widehat{\ell}_{\max}$, *and* $\mathcal{E}^{(1)}_{min}$ *is a smooth, convex function of* $\widehat{L}$. $\mathcal{E}^{(1)}_{min} = \mathcal{E}^{(1)}_{min}\left(\widehat{L}\right)$ *and*

$$\frac{\left(\mathcal{E}^{(1)}_{min}\right)'\left(\widehat{L}_1\right) - \left(\mathcal{E}^{(1)}_{min}\right)'\left(\widehat{L}_2\right)}{\widehat{L}_1 - \widehat{L}_2} > 0 \qquad \textit{for any} \qquad \widehat{L}_1, \widehat{L}_2 > 0, \qquad \widehat{L}_1 \neq \widehat{L}_2;$$

or ${\mathcal{E}^{(1)}_{min}}''\left(\widehat{L}\right) > 0$ *for every* $\widehat{L} > 0$. *Moreover, for any* $\widehat{\alpha} \in \left(0, \frac{1}{4}\right)$,

$$\lim_{\widehat{L}\downarrow 0} \mathcal{E}^{(1)}_{min}\left(\widehat{L}\right) = \lim_{\widehat{L}\to\infty} \mathcal{E}^{(1)}_{min}\left(\widehat{L}\right) = \infty \tag{7.3a}$$

$$\Rightarrow \quad \lim_{\widehat{L}\downarrow 0} {\mathcal{E}^{(1)}_{min}}'\left(\widehat{L}\right) = -\infty \qquad \textit{and} \qquad \lim_{\widehat{L}\to\infty} {\mathcal{E}^{(1)}_{min}}'\left(\widehat{L}\right) = \infty. \tag{7.3b}$$

Remark. This result does not relate to the *global* energy minimiser, but rather the lowest energy, M1I, single monolayer morphology.[6]

Evidence.

i) We depict the numerically constructed $\mathcal{E}^{(1)}_{\min}$ surface over cool parameter space in Fig. 7.3, with the corresponding map of the sign of its second derivative (in $\widehat{L}$) in Fig. 7.4. Second derivatives were approximated by the finite difference

$$\left.\frac{\mathrm{d}^2\mathcal{E}^{(1)}_{\min}}{\mathrm{d}\widehat{L}^2}\right|_{\widehat{L}=i\Delta\widehat{L}} \approx \frac{{\mathcal{E}^{(1)}_{\min}}^{(i+1)} - 2{\mathcal{E}^{(1)}_{\min}}^{(i)} + {\mathcal{E}^{(1)}_{\min}}^{(i-1)}}{\left(\Delta\widehat{L}\right)^2}, \tag{7.4}$$

with $\Delta\widehat{L}$ the (fixed) difference between successive sampled $\widehat{L}$ values.

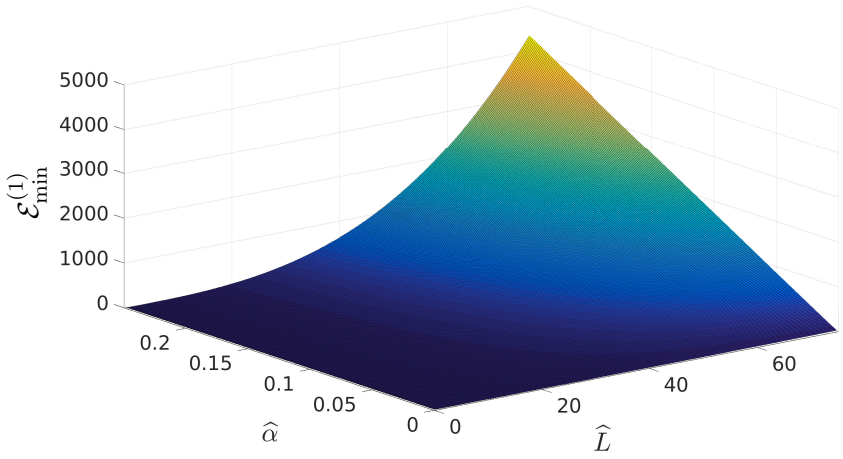

Figure 7.3: The M1I, single monolayer minimum energy surface $\mathcal{E}^{(1)}_{\min}\left(\widehat{L}, \widehat{\alpha}\right)$. Although not visible in the plot, $\mathcal{E}^{(1)}_{\min} \to \infty$ as $\widehat{L} \downarrow 0$ as in (7.3a).[7]

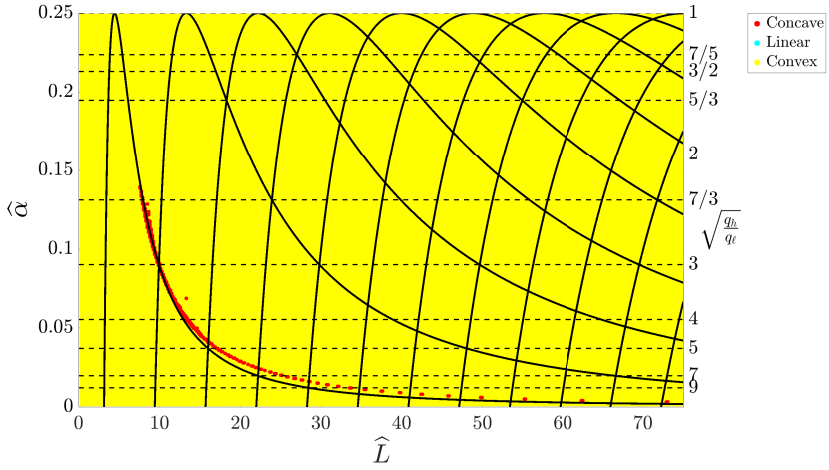

Figure 7.4: Sign of the second derivative of $\mathcal{E}^{(1)}_{\min}$ with respect to $\widehat{L}$ (approximated by (7.4)). $\mathcal{E}^{(1)}_{\min}$ is convex in $\widehat{L}$ in the yellow regions; areas of non-convexity are marked with **red** dots (the smallest value of (7.4) was -0.03). For small $\widehat{\alpha}$ ($\lesssim 0.1$), we observed a (small) non-convexity at every sampled $\widehat{\alpha}$-value. The gaps between the red dots for $\widehat{L} \gtrsim 30$ reflect our vertical ($\widehat{\alpha}$) sampling rate, not sparse non-convexity. A comparison with Fig. 7.1 suggests that the non-convexity has to do with the transition from Source (1) to Source (2) minimisers (see the edge of the dark blue region in that plot). *We believe the red dots are numerical artefacts.* There are no **cyan** dots viz. no regions where the energy is linear.[8]

ii) To demonstrate (7.3), we consider the un-scaled single monolayer minimiser. We set $\chi^{AB} = 1$ and $L = 1$, and vary (un-scaled) ε_φ and α and consider the effect in (scaled) $\left(\widehat{L}, \widehat{\alpha}\right)$-space. According to (6.47),

$$\alpha = \frac{\widehat{L}^2 \widehat{\alpha}}{2} \qquad \text{and} \qquad \varepsilon_\varphi = \frac{1}{\sqrt{2}\widehat{L}}. \tag{7.5}$$

Hence, using (6.73), we find that the *scaled* energy is

$$\widehat{\mathcal{E}}\left[\widehat{\varphi}\right] = \int_{-1/2}^{1/2} \left\{ \frac{1}{2\widehat{L}} \left(\varphi'\right)^2 + \frac{\widehat{L}}{2}\left(1-\varphi^2\right) + \frac{\widehat{L}^3\widehat{\alpha}}{2}\left(-\Phi'\right)^2 \right\} \mathrm{d}x. \tag{7.6}$$

From our sweep results, we conclude that $|\varphi'|$ is bounded and finite for $\widehat{\alpha} \in \left(0, \frac{1}{4}\right)$, independent of $\widehat{L} \leq \frac{\pi}{\sqrt{\widehat{q}_h}}$, and so $\widehat{\mathcal{E}}\left[\widehat{\varphi}\right] \to \infty$ as $\widehat{L} \downarrow 0$ (see Appendix C.2.1). Likewise, $\widehat{\ell}_{\text{opt}}$ is bounded for each $\widehat{\alpha}$ and so $|\Phi'| > 0$ on a region which grows with increasing $\widehat{L}$, viz. for $\widehat{\alpha} > 0$, $\widehat{\mathcal{E}}\left[\widehat{\varphi}\right] \to \infty$ as $\widehat{L} \to \infty$.

□

Remark. Sending $\widehat{L} \downarrow 0$ is *not* the same as taking a sharp interface limit. According to (7.5), as $\widehat{L} \downarrow 0$, the (un-scaled) $\varepsilon_\varphi \to \infty$, and so the interfacial energy becomes unbounded, even though the morphology itself is perfectly reasonable (see Appendix C.2.1). Likewise, sending $\widehat{L} \to \infty$ sends (un-scaled) $\alpha \to \infty$, which makes the non-local energy infinite.

7.1.2 Energy symmetry: reflecting morphologies about $x = 0$

We have worked thus far assuming a BA *ansatz* morphology. Given any BA monolayer φ_{BA}, we can create a corresponding AB morphology by reflecting φ_{BA} about $x = 0$, and defining $\varphi_{AB}(x) = \varphi_{BA}(-x)$, as in Fig. 7.5.

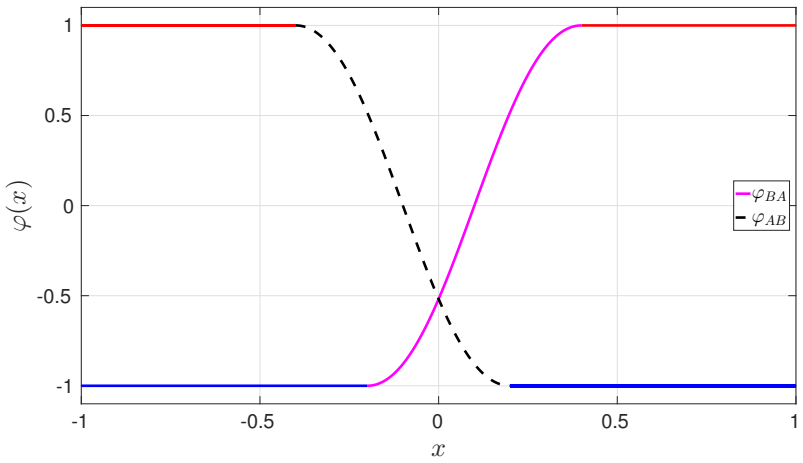

Figure 7.5: A reflection: a BA monolayer, φ_{BA}, is depicted with a **magenta** interface layer alongside its reflected AB–counterpart, φ_{AB}; its interface layer is the dashed black line. The two morphologies have the same energy and mass.[9]

All of the results we derived above hold: reflected morphologies have the same mass, $m_{BA} = m_{AB}$ (we only change the *ansatz* at the ends of the interface), $x_L \to -x_R$ and $x_R \to -x_L$ and energy is the same, viz. $\mathcal{E}(\varphi_{BA}) = \mathcal{E}(\varphi_{AB})$. This AB/BA energy symmetry will be crucial when we work with multi-monolayer morphologies, and follows because of the symmetry of the non-local energy about $-\Phi' = 0$ and our choice of non-local BC.

7.2 Symmetric, multi-monolayer morphologies

We now consider 1D, 2-phase P2P morphologies comprising several ($\nu > 1$) monolayers on $x \in (0, \mathcal{D})$. We wish to apply the single monolayer results of the previous section. There are substantial difficulties in doing so, however, as we need to consider the number, thickness and location of each of the component monolayers, as well as the thickness of each of their interface layers. To manage this complexity, we initially impose a layer count ν.

7.2.1 Energy minimisation: preliminaries and challenges

To start, we restrict attention to cool, symmetric ($m = 0$) configurations of the type we studied for the single monolayer problem. We proceed as we did in Section 6.1.5 to arrive

at a general solution involving the coefficients $c_1^{(i)}$, $c_2^{(i)}$, $c_3^{(i)}$ and $c_4^{(i)}$ as in (6.34), solving a system of the form (6.28) (one for each monolayer). Notice that we would replace x_L, x_R and ℓ with the appropriate $x_L^{(i)}$, $x_R^{(i)}$ and $\ell^{(i)}$ (still unknowns at this stage) if we were to write down these coefficients. As in the single monolayer problem, we can also specify the mass in each of the interface layers according to a local version of (6.35) which would depend on the width of the particular interface layer, $\ell^{(i)}$. We have established most of the following:

Lemma 7.2.1. (Multi-layer, symmetric interface layers) *For $m = 0$, any candidate morphology has zero mass in all of its interface layers. In particular,*

$$m = 0 \qquad \Rightarrow \qquad \Phi'\left(x_L^{(i)}\right) = \Phi'\left(x_R^{(i)}\right) \qquad \text{for each} \qquad i = 1, \ldots, \nu. \tag{7.7}$$

Proof. For the first part, substitute $m = 0$ into the i-th instance of (6.35a) to conclude that

$$\int_{x_L^{(i)}}^{x_R^{(i)}} \widetilde{\varphi}^{(i)}\left(x_L^{(i)}, x_R^{(i)}\right) \, \mathrm{d}x = 0. \tag{7.8}$$

For the second part, we integrate $-\Phi''(x) = \varphi - \overline{\varphi}$ (setting $\overline{\varphi} = m = 0$ for a zero mass minimiser) once on $\left(x_L^{(i)}, x_R^{(i)}\right)$ to conclude that

$$\Phi'\left(x_L^{(i)}\right) - \Phi'\left(x_R^{(i)}\right) = 0. \tag{7.9}$$

□

The principle complexity in going from single to multi-monolayer energy minimisation is that the extra freedom in placing the interface layers in the latter case means that the zero BCs we had on the first integral $-\Phi'$, in (6.1b) no longer necessarily hold separately on each component monolayer (they must hold at the ends of the domain). Instead, we have the more general condition in (7.7). We illustrate this difficulty in Fig. 7.6: Fig. 7.6(a) is a morphology with zeros in $-\Phi'$ at the end of each monolayer (to which our single monolayer results might apply), whereas Fig. 7.6(b) shows a configuration in which $\overline{\varphi} = 0$ globally, each interface layer has zero mass (cf. (7.7)), but the monolayers all have different (local) masses (cf. (6.1b)).

Consequently, we distinguish two types of multi-monolayer morphology.

Definition 7.2.2. (Two types of multi-monolayer morphology) *For given $\left(\varepsilon_\varphi, \chi^{AB}, \alpha, \mathcal{D}\right)$, a BC $\varphi(0)$ and a prescribed number of M1I monolayers $\nu \geq 1$, we define two types of multi-monolayer morphology:*

Type $A_{(\nu)}$: P2P, ν monolayer morphologies in which each of the interface layers is M1I and satisfies a differential equation (6.93a) *(but* not *necessarily the ID-ELE system* (6.92)*), and $-\Phi'$ has $\nu + 1$ zeros strictly between the monolayers (two of which*

are at the ends of the domain) at points where $\varphi = \pm 1$ (i.e. not in any of the interface layers). We term such zeros 'pure-phase', and refer to any other zero of $-\Phi'$ as 'non-pure-phase'.

An example of such a morphology is depicted in Fig. 7.6(a).

Type $B_{(\nu)}$: P2P, ν monolayer morphologies of Type $A_{(\nu)}$, as well as those with monolayers in which $-\Phi'$ either has no zeros or has non-pure-phase zeros (i.e. $-\Phi' = 0$ inside the interface layer). We draw an example of a morphology of this type in Fig. 7.6(b).

We will refer to the sets of all such morphologies as Morphology Sets $A_{(\nu)}$ and $B_{(\nu)}$.

Remark. Type A configurations can be thought of as *moderately, but not very unequally spaced*. Type B monolayers with 'missing' zeros of $-\Phi'$ or $-\Phi' = 0$ inside their interface layers, occur when ν is relatively small and/or $\mathcal{D}$ is large. The interface layers are *very* unequally spaced, being separated by one or more very long or very short sections of pure phase material (cf. the long pure B section to the right of monolayer $\boxed{5}$, and the short pure B section between monolayers $\boxed{3}$ and $\boxed{4}$ in Fig. 7.6(b)).

Clearly, the pattern of zeros of $-\Phi'$ is important. We designate the zeros of $-\Phi'$ by (cf. (6.84a)),

$$\{\underline{X}_i\}_{i=0,\ldots,\nu} \qquad \text{with} \qquad \underline{L}_i := \left|\underline{X}_i - \underline{X}_{i-1}\right|; \tag{7.10}$$

i.e. we assign each monolayer an alternate length measure, as the distance between the two zeros of $-\Phi'$ associated with it. **We identify $\widehat{L}$ in the single monolayer problem with $\underline{\widehat{L}}$ in the multi-monolayer case.** Clearly $X_0 = \underline{X}_0$ and $X_\nu = \underline{X}_\nu$ i.e. the microstructure and its first integral always match at the ends, but it is *not* necessarily true that $\underline{X}_0 \leq \underline{X}_1 \leq \ldots \leq \underline{X}_\nu$. There is clearly a complication in dealing with morphologies like those in Fig. 7.6(b) in which the $-\Phi'$ profile admits one or more of the following pathologies:

i) A length $\underline{\widehat{L}}_i$ which is too small to accommodate the interface layer ($\widehat{\ell}_i > \underline{\widehat{L}}_i$ such as $\boxed{2}$ in Fig. 7.6(b)); and/or

ii) Monolayers with missing zeros of $-\Phi'$, such as monolayers $\boxed{3}$ and $\boxed{4}$ in Fig. 7.6(b).

We will apply the same approach to both of these situations.

7.2.2 An equally spaced candidate minimiser

In this section, we define equally spaced morphologies and discover some of their properties.

Definition 7.2.3. (An equally spaced morphology) *An equally spaced morphology has:*

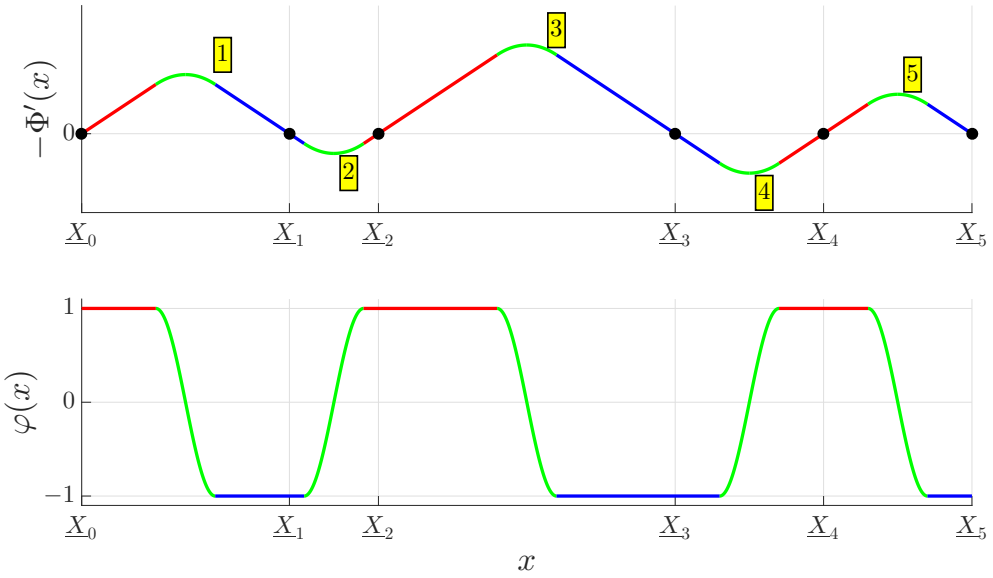

(a) Schematic of a Type $A_{(5)}$ profile ($-\Phi'$ above; φ below) with $\nu + 1 = 6$ pure-phase zeros strictly between the monolayers, which are labelled $\boxed{1}$ through $\boxed{5}$ in yellow. $-\Phi' = 0$ on the marked set $\{\underline{X}_0, \ldots, \underline{X}_5\}$ (as in the main text). The pure-phase sections are all approximately the same length.

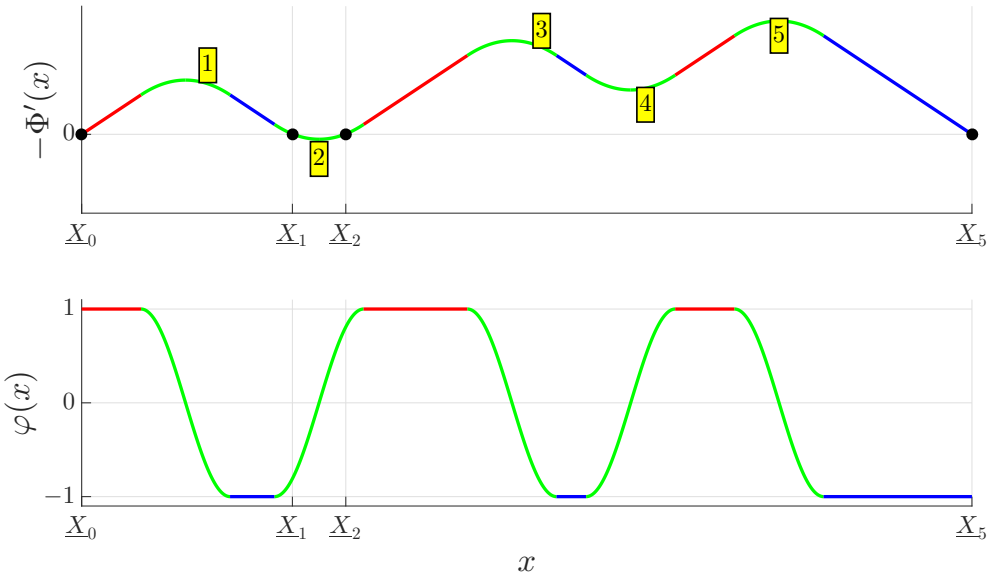

(b) Schematic of a Type $B_{(5)}$ profile ($-\Phi'$ above; φ below). Monolayer $\boxed{2}$ has $-\Phi'(\underline{X}_1) = -\Phi'(\underline{X}_2) = 0$ and these zeros are inside the (green) interface layer. $-\Phi'$ is not zero anywhere inside monolayers $\boxed{3}$ and $\boxed{4}$ (cf. $\underline{X}_2$, $\underline{X}_3$ and $\underline{X}_4$ in (a) above). The rightmost section of pure B is relatively long, whereas the pure B section between monolayers $\boxed{3}$ and $\boxed{4}$ is very short.

Figure 7.6: Profiles illustrating Defn 7.2.2: one of Type $A_{(5)}$, and the other Type $B_{(5)}$. Both have pure phase A at $x = 0$ and B at $x = \mathcal{D} = X_5$. The spacing in the φ profile in (b) is visibly more unequal than that in (a).[10]

- *The monolayers are all of the same width:* $\widehat{L}_i = X_i - X_{i-1} = \frac{\widehat{\mathcal{D}}}{\nu} =: \widehat{L}$.
- *The BA–monolayers are all translated copies of a prototypical monolayer,* $\varphi_{BA}^{(P)}$*, which is the (unique) minimiser of the BA single monolayer problem on* $\left(\frac{-\widehat{L}}{2}, \frac{\widehat{L}}{2}\right)$*, and likewise for the AB–monolayers.* $\varphi_{AB}^{(P)}$*, the prototype AB interface layer, is a reflection of* $\varphi_{BA}^{(P)}$ *about* $\widehat{x} = 0$.[11]
- *Sections of pure material have the same length in all of the monolayers viz.* $\left|\Omega_A^{(i)}\right| = \left|\Omega_A^{(j)}\right|$ *for* $i, j = 1, \ldots, \nu$*, and likewise for* B*. For* $m = 0$*, the pure* A *sections have the same length as the pure* B *sections.*
- *The non-local function* Φ *and its derivative* Φ' *are also translated piecewise from their prototypes on* $\left(\frac{-\widehat{L}}{2}, \frac{\widehat{L}}{2}\right)$.[12] $\Phi'(X_i) = 0$ *for each* i *i.e. at the ends of each of the monolayers.* Φ' *and* Φ *are* $2\widehat{L}$ *periodic.*

Remarks. If we specify φ at one end of the domain (say $\varphi(0) = \pm 1$) then, for a given layer count ν, we may speak of *the* (unique) equally spaced morphology.[13]

Lemma 7.2.4. (A candidate minimising structure) *The equally spaced morphology of Defn 7.2.3 has the following properties:*

- $X_i = \underline{X}_i$ *for each* $0 \leq i \leq \nu$ *and* $\widehat{L}_i = \widehat{\underline{L}}_i =: \widehat{L} = \frac{\widehat{\mathcal{D}}}{\nu}$ *for* $1 \leq i \leq \nu$*, since the zeros of* $-\Phi'$ *occur precisely at the ends of the monolayers.*
- *The energy of the total configuration is*

$$\mathcal{E}_{total} = \nu \mathcal{E}_{min}^{(1)}\left(\widehat{L}, \widehat{\alpha}\right) \tag{7.11}$$

where $\mathcal{E}_{min}^{(1)}\left(\widehat{L}, \widehat{\alpha}\right)$ *is the energy of the minimising single monolayer morphology as in* (7.2)*;*

- *Each monolayer has the global mass, viz.*

$$\frac{1}{\widehat{L}_i}\int_{X_{i-1}}^{X_i} \varphi \, \mathrm{d}\widehat{x} = m \, (= \overline{\varphi}) \qquad \text{for each} \qquad i = 1, \ldots, \nu. \tag{7.12}$$

- *If* ν *is high enough that each monolayer is in Region I (cf.* (6.65)*), i.e.*

$$\widehat{L} = \frac{\widehat{\mathcal{D}}}{\nu} < \widetilde{L} = \frac{\pi}{\sqrt{\widehat{q}_h}}, \tag{7.13}$$

then the morphology cannot satisfy the system of ID-ELEs in (6.92)*.*

- *The morphology is a (local) minimum of the energy under pulse variations if* $\widehat{L} > \widetilde{L}$.

Proof.

i) (7.11) is trivial, albeit important.

ii) For (7.12), $-\Phi''(x) = \varphi - \overline{\varphi} = \varphi - m$ (cf. (6.1b)) in Ω if $\overline{\varphi} = m$. Integrating over any (X_i, X_{i+1}) yields

$$\int_{X_i}^{X_{i+1}} \left(-\Phi''\right) \mathrm{d}x = -\left(\Phi'(X_{i+1}) - \Phi'(X_i)\right) = 0 = \int_{X_i}^{X_{i+1}} \varphi - m \, \mathrm{d}x. \tag{7.14}$$

since $\Phi'(X_i) = 0$ for each i i.e. at the ends of each of the monolayers.

iii) The second-last statement follows from our work on the single monolayer problem.

iv) We omit the details of the proof of the last statement. The idea is that the total energy of an equally spaced configuration increases if any pair of consecutive monolayers is shifted left/right. Such variations are mass-conserving.

□

We now review the key properties of the morphology sets we defined earlier.

Lemma 7.2.5. (Properties of Morphology Sets $\mathrm{A}_{(\nu)}$, $\mathrm{B}_{(\nu)}$)

i) Morphology Set $A_{(\nu)}$ includes one equally spaced morphology.

ii) Configurations in Morphology Set $A_{(\nu)}$ are those for which the zeros of $-\Phi'$ are all pure-phase; φ and its first integral $-\Phi'$ coincide in that

$$\sum_{i=1}^{\nu} L_i = \sum_{i=1}^{\nu} \underline{L}_i = \mathcal{D}. \tag{7.15}$$

iii) Morphology Set $A_{(\nu)} \subset$ Set $B_{(\nu)}$, which includes one equally spaced morphology.

We now show that the equally spaced morphology is the energy minimiser in the set of all P2P morphologies. Our first result concerns Type $\mathrm{A}_{(\nu)}$ morphologies.

7.2.3 Somewhat unequal (Type $\mathrm{A}_{(\nu)}$) morphologies, prescribed ν

Conjecture 7.2.6. (The Type $\mathrm{A}_{(\nu)}$ energy minimiser is equally spaced) *The (unique) equally spaced member of Morphology Set $A_{(\nu)}$ has the lowest energy in the set.*

Evidence. Consider any Type $\mathrm{A}_{(\nu)}$ morphology as in Fig. 7.6(a). If the morphology is equally spaced, we are done. If not, this morphology must be comprised of a set of monolayers of different widths (width referring to the distance between successive zeros of $-\Phi'$). We write the energy (6.85) of such a configuration using the set $\{\underline{X}_i\}_{i=0,\ldots,\nu}$ from (7.10) as

$$\mathcal{E}[\varphi] = \sum_{i=1}^{\nu} \left(\int_{\underline{X}_{i-1}}^{\underline{X}_i} \frac{\varepsilon_\varphi^2}{2} \left(\varphi'\right)^2 + \frac{\chi^{AB}}{4} \left(1 - \varphi^2\right) + \frac{\alpha}{2} \left(-\Phi'\right)^2 \mathrm{d}x \right), \tag{7.16}$$

where on each sub-domain $\left[\underline{X}_{i-1}, \underline{X}_i\right]$, we have the same setup as we had for our single monolayer minimisation problem. Consequently, minimising the energy in each of these sub-domains (separately) reduces the total energy. Our first step is to replace each of the interface layers with its (M1I) minimiser; for each of these, $\widehat{\ell}_{\text{opt}} \leq \widehat{\underline{L}}_i$ and so each such minimiser fits without affecting the pattern of zeros in $-\Phi'$. The total energy becomes

$$\mathcal{E}_{\text{total}} = \sum_{i=1}^{\nu} \mathcal{E}_{\min}^{(1)}\left(\widehat{\underline{L}}_i\right)$$

where $\mathcal{E}_{\min}^{(1)}\left(\widehat{\underline{L}}_i\right)$ is the (minimum) energy of the i-th monolayer, and is a function of $\widehat{\underline{L}}_i$ *only* (for a given $\widehat{\alpha}$), and the entire configuration has width $|\Omega| = \widehat{\mathcal{D}} = \sum_{i=1}^{\nu} \widehat{\underline{L}}_i = \sum_{i=1}^{\nu} \widehat{L}_i$ (because of the pattern of the zeros of $-\Phi'$). But then from (7.15),

$$\frac{1}{\nu}\sum_{i=1}^{\nu} \mathcal{E}_{\min}^{(1)}\left(\widehat{\underline{L}}_i\right) \geq \mathcal{E}_{\min}^{(1)}\left(\frac{\widehat{\mathcal{D}}}{\nu}\right) \quad \Leftrightarrow \quad \frac{1}{\nu}\sum_{i=1}^{\nu} \mathcal{E}_{\min}^{(1)}\left(\widehat{\underline{L}}_i\right) \geq \mathcal{E}_{\min}^{(1)}\left(\frac{1}{\nu}\sum_{i=1}^{\nu} \widehat{\underline{L}}_i\right) = \mathcal{E}_{\min}^{(1)}\left(\frac{1}{\nu}\sum_{i=1}^{\nu} \widehat{L}_i\right) \tag{7.17}$$

by the (strict) convexity of $\mathcal{E}_{\min}$ (as a function of $\widehat{\underline{L}} > 0$), which we proposed in Conjecture 7.1.1. Hence, the energy of any member of Morphology Set $\text{A}_{(\nu)}$ is bounded below by that of the equally spaced member of the set.[14] □

Remark. Our single monolayer energy convexity result was for BA monolayers, but we have just applied it to alternating BA, AB monolayers. This is possible because of the symmetry of the non-local energy about $-\Phi' = 0$. Setting $-\Phi' = a \neq 0$ at both ends of the domain would not change the mass, but it would mean that equally spaced AB and BA monolayers have different non-local energies (since the non-local energy is a multiple of $\|-\Phi'\|^2$).

We now consider a more general class of P2P configurations.

7.2.4 Very unequal (Type $\text{B}_{(\nu)}$) morphologies, prescribed ν

We now show that any Type B_ν morphology can be rearranged into one of Type A_ν, with the same monolayer count, but lower energy. To do so, we require a better understanding of the possible Type B_ν configurations and the corresponding patterns of zeros of $-\Phi'$.

Understanding and exploiting the zeros of $-\Phi'$

Lemma 7.2.7. (Pure-phase zeros of $-\Phi'$) *If ν is even and $-\Phi'(0) = -\Phi'(\mathcal{D}) = 0$, then $-\Phi'$ has an odd number of pure-phase zeros (at least one) inside $(0, \mathcal{D})$ viz. $-\Phi'(x_i) = 0$ and $\varphi(x_i) = \pm 1$ for some $\{x_i\}_{i=1}^{2k+1} \subset (0, \mathcal{D})$ with $\mathbb{N} \ni k \geq 0$. But if ν is odd, then $-\Phi'$ has an even number of pure-phase zeros (possibly none). An odd number of monolayers exists between successive pure-phase zeros of $-\Phi'$.*

This follows easily from symmetry, (7.7) and the continuity of $-\Phi'$.

In what follows, we will make extensive use of the idea of splitting the problem into smaller pieces at the zeros of $-\Phi'$.

Definition 7.2.8. (Splitting the problem) *By splitting the problem, we mean considering the sub-problem on (x_1, x_2), where x_1 and x_2 are successive, pure-phase zeros of $-\Phi'$ (it may also have non-pure-phase zeros in (x_1, x_2)) and $\varphi(x_2) = -\varphi(x_1)$.*

The sub-problem above has i) an odd number of monolayers in (x_1, x_2) by Lemma 7.2.7; ii) the global mass, $\overline{\varphi}_{(x_1,x_2)} = \overline{\varphi}$; and iii) the same non-local BCs (at x_1, x_2) as on $\partial\Omega$. Anything reducing the energy of the sub-problem will reduce the energy of the whole configuration, without affecting any other part.[15]

Re-arranging very unequally spaced morphologies

In all of our work thus far, we have used the energy symmetry of AB and BA monolayers, which follows from the non-local BC $-\Phi' = 0$. In the current section, this assumption is not valid. Consider the morphology snippet in Fig. 7.7(a) comprising layers $\boxed{j}$ and $\boxed{j+1}$, with $-\Phi' = a > 0$ at the ends. We wish to replace this 'elevated' (in $-\Phi'$) arrangement with the equally spaced, 2-monolayer minimiser in Fig. 7.7(b), with $-\Phi' = 0$ at the ends.

To work with elevated, two-layer morphologies, we need to solve a new minimisation problem. To ease the notation, we drop hats in this section, and let $\mathcal{E}^{(a)}_{AB}(L)$ denote the minimum M1I single monolayer energy for an AB monolayer of width L, with $-\Phi' = a$ at the ends, and similarly for $\mathcal{E}^{(a)}_{BA}(L)$ (so that $\mathcal{E}^{(0)}_{AB}(L) \equiv \mathcal{E}^{(1)}_{\min}(L)$). With reference to Fig. 7.7(a), our problem is to

$$(\mathbf{P}_a): \quad \text{find } \underline{\overline{L}}_1, \underline{\overline{L}}_2 \quad \text{s.t.} \quad \mathcal{E}^{(a)}_{BA}\left(\underline{\overline{L}}_1\right) + \mathcal{E}^{(a)}_{AB}\left(\underline{\overline{L}}_2\right) \to \min \quad \text{where} \quad \underline{\overline{L}}_1 + \underline{\overline{L}}_2 = L'. \tag{7.18}$$

The notation $\underline{\overline{L}}_i$ suggests that these lengths are elevated (i.e. not at $-\Phi' = 0$), and relate to distances between points that will become zeros of $-\Phi'$.

The asymmetry in the non-local energy for $a \neq 0$ suggests that we should *not* expect $\underline{\overline{L}}_1 = \underline{\overline{L}}_2$ in the solution of (7.18). We recover the multi-monolayer problem we studied earlier if we set $a = 0$, and under such circumstances, symmetry in the non-local energy, combined with convexity of the single monolayer minimum energy from Conjecture 7.1.1 imply that $\underline{\overline{L}}_1^{(a=0)} = \underline{\overline{L}}_2^{(a=0)}$. The problem in (7.18) can thus be regarded as a generalisation of our earlier problem, which we could label $(\mathbf{P}_0)$. As in Conjecture 7.1.1, we offer numerical evidence of the following conjecture.[17]

Conjecture 7.2.9. (Elevated, two-layer energy minimisers) *The solutions $\underline{\overline{L}}_1, \underline{\overline{L}}_2$ to (7.18) with $a \neq 0$ are such that*

$$\mathcal{E}^{(a)}_{BA}\left(\underline{\overline{L}}_1\right) + \mathcal{E}^{(a)}_{AB}\left(\underline{\overline{L}}_2\right) > 2\mathcal{E}^{(0)}_{BA}\left(\frac{L'}{2}\right); \tag{7.19}$$

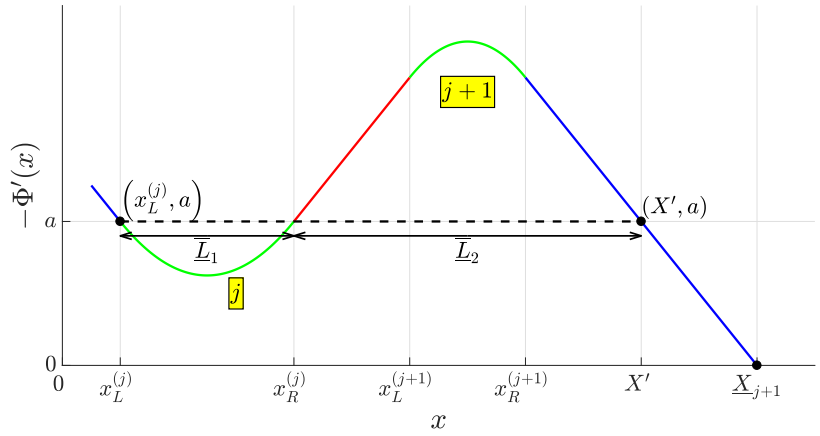

(a) $-\Phi'_{\text{start}}$ is an elevated morphology (in $-\Phi'$) comprising monolayers j and $j+1$ between $x_L^{(j)}$ and X' ($X' - x_L^{(j)} =: L'$), with $-\Phi' = a \neq 0$ at the ends. Pure phase B (A) sections are **blue** (**red**); interface layers are **green**.

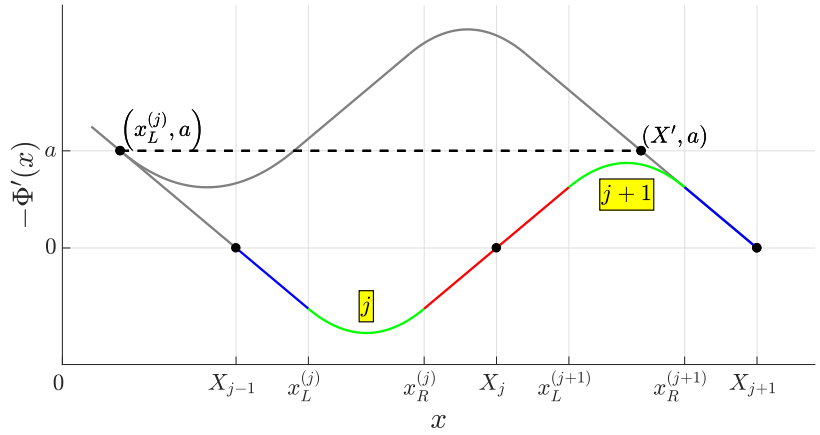

(b) $-\Phi'_{\text{start}}$ (from (a)) in grey alongside $-\Phi'_{\text{end}}$ in colour; an equally spaced 2-monolayer minimiser with $-\Phi' = 0$ at the ends. It has the same width, mass and monolayer count (two) as $-\Phi'_{\text{start}}$, but lower energy.

Figure 7.7: The starting morphology snippet $-\Phi'_{\text{start}}$ with non-zero BCs, and its replacement, $-\Phi'_{\text{end}}$ with zero BCs, and lower energy.[16]

i.e. the minimum energy of the elevated two-layer snippet is always greater than that of the corresponding equally spaced minimiser with $-\Phi' = 0$ at the ends.

In a $BAAB$ morphology with $a > 0$ (equivalently $ABBA$ with $a < 0$), $\underline{L}_1 > \underline{L}_2$ i.e. the left monolayer is wider than the right one. More generally, the monolayer with $-\Phi'$ closer to the $-\Phi' = 0$ axis (depicted in the left part of Fig. 7.8) is the wider of the two.

Remarks. If we adapt the energy expression (6.1e), and assume the structural *ansatz* (6.4), then the energy of an elevated single BA monolayer, φ on $\left(-\frac{\widehat{L}}{2}, \frac{\widehat{L}}{2}\right)$, is

$$\mathcal{E}_{BA}^{(a)}[\varphi] = \int_{-\widehat{L}/2}^{\widehat{L}/2} \frac{\varepsilon_\varphi^2}{2} (\varphi')^2 + \frac{\chi^{AB}}{4} (1 - \varphi^2) + \frac{\alpha}{2} (-\Phi' + a)^2 \, \mathrm{d}x. \tag{7.20a}$$

By symmetry of the local (interfacial and bulk) energies, and Fig. 7.8, we see that

$$\mathcal{E}_{BA}^{(a)}\left[\varphi\right] = \mathcal{E}_{AB}^{(-a)}\left[r\left(\varphi\right)\right], \tag{7.20b}$$

where $r\left(\varphi\right)$ is the AB reflection of φ about its midpoint, viz.

$$\mathcal{E}_{AB}^{(a)}\left[\varphi\right] = \int_{-\widehat{L}/2}^{\widehat{L}/2} \frac{\varepsilon_\varphi^2}{2}\left(\varphi'\right)^2 + \frac{\chi^{AB}}{4}\left(1-\varphi^2\right) + \frac{\alpha}{2}\left(\Phi'-a\right)^2 \mathrm{d}x, \tag{7.20c}$$

where, on the right of (7.20c), we assume a BA *ansatz*.[18] To solve the problem for a $BAAB$ pair, we can minimise the energy for a pair of values $\pm a$ assuming each monolayer is BA. Note too that $ABBA$ and $BAAB$ snippets are energetically equivalent i.e. we can solve the problem using our BA *ansatz*.[19] However, the ID-ELE condition (6.37) is not applicable, and so for simplicity in our numerical investigation, we found the turning points of the energy and picked the one with the lowest energy.

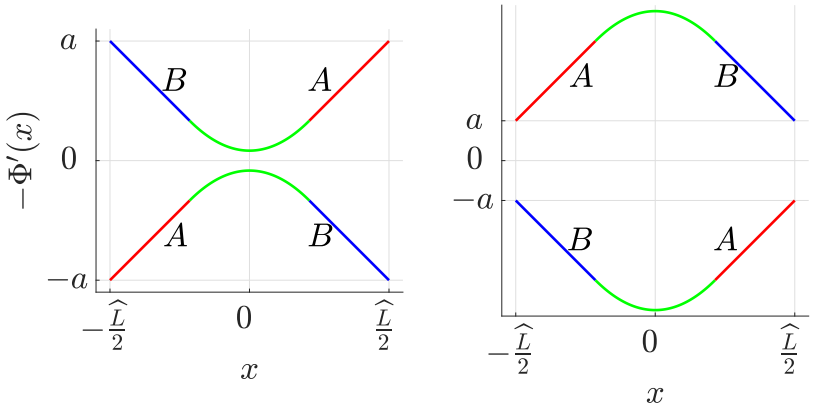

Figure 7.8: The energy equivalence of elevated single monolayer profiles in $-\Phi'$: on the left, a BA (upper) and AB (lower) pair, with the same non-local ($\frac{\widehat{\alpha}}{2}\left\|-\Phi'\right\|^2$) and total energies, and similarly on the right. To investigate the energy of a $BA-AB$ pair (top left and right) we combine the top left ($-\Phi' = +a$ at the ends) and bottom right ($-\Phi' = -a$ at the ends) BA monolayers; we do not need to work with AB monolayers.[20]

Evidence. It is more difficult to visualise these results than those of Conjecture 7.1.1. We depict summary energy data for $\widehat{\alpha} = 0.005, 0.2$ and $a \in \{0, \pm 1, \ldots \pm 10\}$ in Fig. 7.9. Fig. 7.10 shows the ratio $\underline{L}_1/\underline{L}_2$ as a function of $\widehat{L}$ for the two $\widehat{\alpha}$-values.[21]

□

We now generalise the above to account for arbitrary, elevated 2-monolayer snippets.

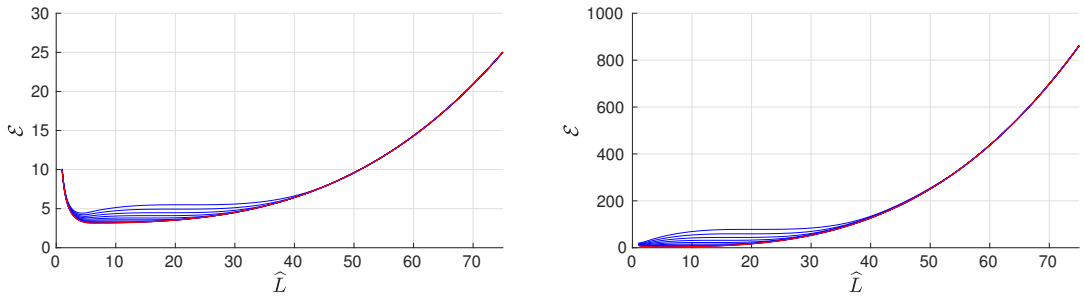

(a) $\widehat{\alpha} = 0.005$ (b) $\widehat{\alpha} = 0.2$

Figure 7.9: Elevated and non-elevated 2-monolayer solutions of (7.18) for $\widehat{\alpha} = 0.005, 0.2$ and $a \in \{0, \pm 1, \ldots \pm 10\}$. In each case, the red line is the minimum 2-monolayer energy for $a = 0$, the blue lines correspond to various $\pm a \neq 0$ (i.e. elevated 2-monolayer minimisers). As $|a|$ increases, the difference between the elevated and $a = 0$ energies increases.[22]

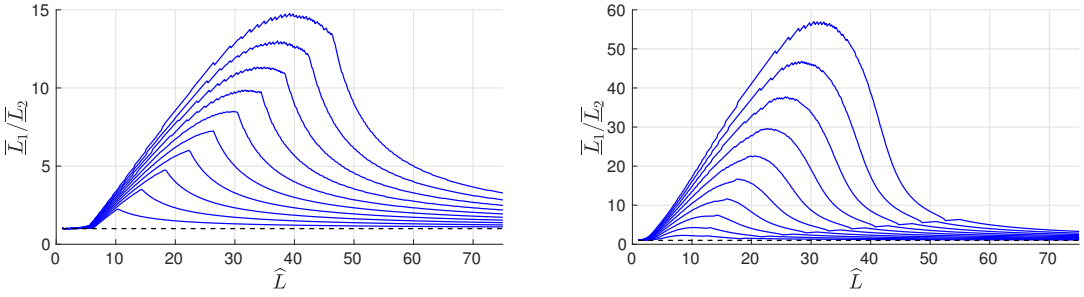

(a) $\widehat{\alpha} = 0.005$ (b) $\widehat{\alpha} = 0.2$

Figure 7.10: The fraction $\overline{L}_1/\overline{L}_2$ in the solution of (7.18) for the $\widehat{\alpha}$ and a-values in Fig. 7.9. The dashed black line marks off the unit ratio. Notice that $\overline{L}_1 > \overline{L}_2$.[23]

Conjecture 7.2.10. (Elevated 2-monolayer morphologies have higher energy) *The energy of* any *elevated 2-monolayer, M1I morphology with* $-\Phi' = a \neq 0$ *at the ends, is bounded below by that of the corresponding 2-monolayer, M1I energy minimiser with* $-\Phi' = 0$ *at the ends.*

Evidence. Consider the raised 2-monolayer morphology snippet $-\Phi'_{\text{start}}$ in Fig. 7.7(a). Re-arrange pulse j (comprising layers $\boxed{j}$ and $\boxed{j+1}$, cf. Defn 6.3.1), and move it down to $-\Phi' = 0$ as follows:

i) Replace $-\Phi'_{\text{start}}$ at $-\Phi' \neq 0$ with its elevated, 2-monolayer energy minimiser, $-\Phi'_{\text{temp}}$.

ii) Replace $-\Phi'_{\text{temp}}$ with the 2-monolayer minimiser with $-\Phi'(X_{j-1}) = -\Phi'(X_{j+1}) = 0$.[24]

The first step bounds the energy since we replace $-\Phi'_{\text{start}}$ with its (local) energy minimiser;

the second further reduces the energy by Conjecture 7.2.9. □

By conservation of energy, we may replace the process above with one in which we slide the pulse until we obtain the additional zeros we need in $-\Phi'$, and then replace the 2-monolayer snippet with its (global) energy minimiser.

To use this result in a ν-layer morphology ($\nu \geq 3$), consider the Type $\mathrm{B}_{(5)}$ profile depicted in Fig. 7.11. It has no pure-phase interior zeros and, for example, monolayer $\boxed{4}$ has no $-\Phi'$ zeros (of any kind). Layers $\boxed{4}$ and $\boxed{5}$ form a snippet of the sort depicted in Fig. 7.7(a). We can reduce the energy of the entire structure if we replace this elevated snippet with the grey, 2-monolayer minimiser as depicted. We use processes of this kind as we prove our main result.

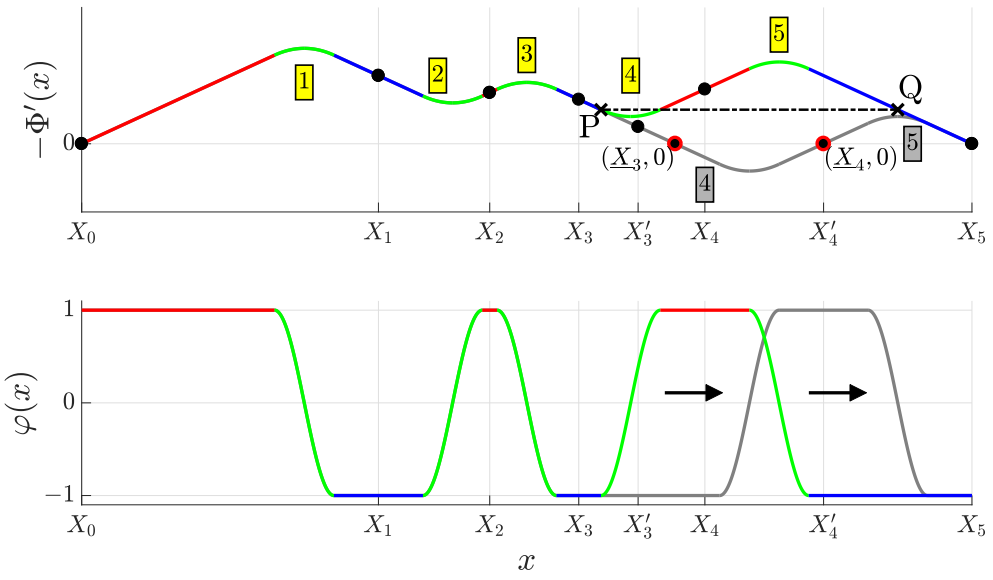

Figure 7.11: The full-colour profile ($-\Phi'$ above; φ below) is very unequally spaced (with long pure phase sections at the ends) and comprises an odd number of monolayers with no pure-phase interior zeros i.e. $\Phi' = 0$ at $x = 0, \mathcal{D}$ only. Monolayer end-points are marked by black dots at $X_0, \ldots, X_5$. In the evidence for Conjecture 7.2.10, monolayers $\boxed{4}$ and $\boxed{5}$ along PQ are shifted right and then replaced with the equally spaced, 2-monolayer energy-minimiser (depicted in grey) with $-\Phi = 0$ at the ends. As a result, $-\Phi'$ obtains two more pure-phase zeros ($\underline{X}_3$ and $\underline{X}_4$), and the energy of the entire configuration is reduced. Monolayer end-points X_3 and X_4, are shifted to X'_3 and $X'_4 (= \underline{X}_4)$; monolayers $\boxed{1}$–$\boxed{3}$ are unaffected.[25] [26]

Conjecture 7.2.11. (The equally spaced morphology is the energy minimiser in Morphology Set $\mathrm{B}_{(\nu)}$) *The (unique) equally spaced Type $A_{(\nu)}$ member of Morphology Set $B_{(\nu)}$ (cf. Conjecture 7.2.6) minimises the energy in that set.*

Evidence. Consider any Type $B_{(\nu)}$ morphology. We split and reassemble the problem, proceeding by induction on ν:

- $\nu = 1$: this is the single monolayer case; the morphology is trivially equally spaced.
- $\nu = 2$: $-\Phi'$ has three $(\nu+1)$ pure-phase zeros by Lemma 7.2.7. We apply Conjecture 7.2.6.[27]
- $\nu > 2$ and even: $-\Phi'$ has at least one pure-phase interior zero by Lemma 7.2.7. Split the problem into (at least) two parts on the pure-phase zeros of $-\Phi'$, as in Defn 7.2.8. Each sub-domain will comprise an odd number of monolayers (less than ν) by Lemma 7.2.7, and so the component morphologies may be separately redefined (by the induction hypothesis) in such a way as to bound the energy from below, by Conjecture 7.2.10. Recombine to arrive at a problem on $\left(0, \widehat{\mathcal{D}}\right)$ in which $-\Phi'$ has $\nu+1$ pure-phase zeros and lower total energy, and apply Conjecture 7.2.6.
- $\nu > 2$ and odd: there are two sub-cases:

  i) $-\Phi'$ has pure-phase interior zeros: split the problem into sub-domains each containing less than ν monolayers (some combination of even and odd), rearrange each sub-problem by the induction hypothesis, and then recombine to arrive at a problem on $\left(0, \widehat{\mathcal{D}}\right)$ in which $-\Phi'$ has $\nu+1$ pure-phase zeros and lower total energy. Apply Conjecture 7.2.6.

  ii) $-\Phi'$ has no pure-phase interior zeros: perform the variation described in Conjecture 7.2.10 to bound the energy from below, and split the domain into two parts, with $\nu-2$ monolayers on one part and two on the other. Invoke the induction hypothesis on the part with $\nu-2$ monolayers (an odd number) to bound the energy from below. Recombine to get a problem on $\left(0, \widehat{\mathcal{D}}\right)$ in which $-\Phi'$ has $\nu+1$ pure-phase zeros. Apply Conjecture 7.2.6.

In each case, we bound the total energy from below by re-arranging the morphology so that $-\Phi'$ has $\nu+1$ pure-phase zeros, and then apply Conjecture 7.2.6. □

Remarks.

i) The result above can be regarded as a generalisation of Conjecture 7.2.9. It shows that the energy of an elevated ν-layer morphology can be bounded below by that of the corresponding equally spaced, ν-layer minimiser with $-\Phi' = 0$ at the ends.

ii) We never explicitly write down the energy of a morphology with missing or non-pure-phase zeros of $-\Phi'$.

7.2.5 M1I morphologies, variable ν

For any *given* $1 \leq \nu < \infty$, we minimise the energy in a P2P configuration by making it equally spaced. We now find the energy-minimising monolayer count, ν_{opt}.

A numerical investigation

For given $\widehat{\alpha}$, the minimum energy of an equally spaced, ν-layer configuration of width $\widehat{\mathcal{D}}$, is

$$\nu \times \mathcal{E}^{(1)}_{\text{min}}\left(\widehat{L}_\nu\right) \qquad \text{where} \qquad \widehat{L}_\nu = \frac{\widehat{\mathcal{D}}}{\nu}.$$

Consequently, given $\left(\widehat{\mathcal{D}}, \widehat{\alpha}\right)$, we can exploit our single monolayer results and find ν_{opt} by solving

$$\nu_{\text{opt}}\left(\widehat{\mathcal{D}}, \widehat{\alpha}\right) = \arg\min_{\nu\in\mathbb{N}}\left\{\nu\mathcal{E}^{(1)}_{\text{min}}\left(\frac{\widehat{\mathcal{D}}}{\nu}, \widehat{\alpha}\right)\right\} = \arg\min_{\nu\in\mathbb{N}}\left\{\nu\mathcal{E}^{(1)}_{\text{min}}\left(\widehat{L}_\nu, \widehat{\alpha}\right)\right\}. \tag{7.21}$$

Numerically, we evaluate

$$\mathcal{E}_\nu\left(\widehat{\mathcal{D}}, \widehat{\alpha}\right) := \nu\mathcal{E}\left(\widehat{L}_\nu, \widehat{\alpha}\right) \qquad \text{for} \qquad \nu \in \{1, 2, \ldots, \nu_{\text{max}}\}, \tag{7.22}$$

up to some maximum ν_{max},[28] at each sampled $\left(\widehat{\mathcal{D}}, \widehat{\alpha}\right)$, and pick the minimum. Summary results are presented in Fig. 7.12, which reveals that increasing $\widehat{\alpha}$ and/or $\widehat{\mathcal{D}}$ (moving up and to the right) increases ν_{opt}.[29] It is also clear that ν_{opt} is not generally unique; the energies for a given ν and $\nu+1$ are identical along the contour lines separating distinct ν_{opt} values.

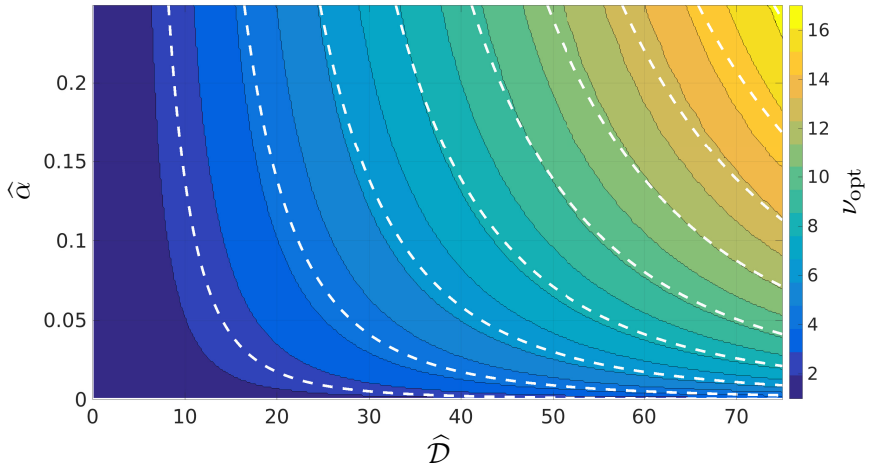

Figure 7.12: Contour map of ν_{opt} taken from the M1I, single monolayer minimum energy. The dashed white lines are discussed in Section 8.5.[30]

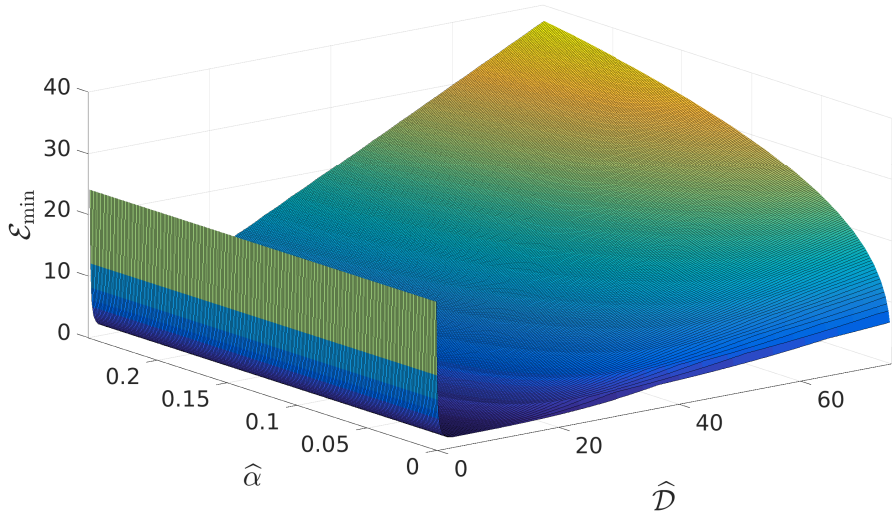

Figure 7.13: The multi-monolayer, minimum-energy surface corresponding to Fig. 7.12, with corrugations within each band of ν. These can be explained by reference to Fig. 7.14 which depicts the minimum-energy surface for a pre-defined set of monolayer count values ($\nu = 1, 2, \ldots, 7$). The current graph could be constructed by gluing together patches of graphs like those in Fig. 7.14 where they present a minimum energy.[31]

The nature of the interface layers in a multi-monolayer energy minimiser

We now investigate the individual interface layers in the structures of Fig. 7.12.

Fig. 7.13 depicts the minimum, multi-monolayer energy over $\left(\widehat{\mathcal{D}}, \widehat{\alpha}\right)_{\text{cool}}$, assuming that the number of equally spaced monolayers is the energy-minimising ν_{opt} depicted in Fig. 7.12. The energies are *substantially* lower than the single monolayer values depicted in Fig. 7.3, and there are corrugations in the energy surface, corresponding to distinct ν_{opt} values. We examine these corrugations in Fig. 7.14. We define (cf. (7.21))

$$\widehat{L}_{\text{opt}} := \frac{\widehat{\mathcal{D}}}{\nu_{\text{opt}}} \tag{7.23}$$

as the width of each monolayer in the energy-minimising configuration. Using our single monolayer problem data, we numerically interpolate the corresponding, energy-minimising interfacial thickness, $\widehat{\ell}_{\text{opt}}\left(\widehat{L}_{\text{opt}}, \widehat{\alpha}\right)$ over $\left(\widehat{\mathcal{D}}, \widehat{\alpha}\right)_{\text{cool}}$. The pair $\left(\widehat{L}_{\text{opt}}, \widehat{\ell}_{\text{opt}}\right)$ comprises the solution of the multi-monolayer problem.

To create Fig. 7.15, we analyse the Source (in the sense of Section 7.1.1) of the interfacial thickness $\widehat{\ell}_{\text{opt}}$, found above. Everywhere other than Regions I and II, the energy minimisers have identical P2P interface layers which solve the ID-ELE.[32] To give context to this figure, we recall Fig. 7.1, which shows where the Source (1) and (2) minimisers originate in $\left(\widehat{L}, \widehat{\alpha}\right)$-space. Source (1) minimisers come from a region dominated by the cold region. Fur-

ther analysis suggests that the minimising $\widehat{\ell}$-values in this region are the smallest/thinnest solutions of the ID-ELE (i.e. on the first branch of $\widetilde{g}$ as in Appendix C.5).

7.2.6 Arbitrary bounded morphologies, variable ν

We now investigate (and eliminate) the possibility of a minimiser containing one or more 'wiggly' (but bounded) interface layers of the sort depicted in Fig's 6.6(a)–(c). We offer a conjecture with supporting numerical evidence, assuming $-\Phi' = 0$ at the ends.

Conjecture 7.2.12. (Arbitrary bounded layers) *Consider an arbitrary bounded, single monolayer morphology of width $\widehat{\mathcal{D}}$, satisfying the ODE* (6.43) *and the integral BCs* (6.1b)*. Its energy is bounded below by that of a morphology with $\nu_{opt}\left(\widehat{\mathcal{D}}, \widehat{\alpha}\right)$ (cf.* (7.21)*) M1I P2P layers.*

Evidence. We re-run the numerical sweep simulation, but this time admit any and all bounded candidates, and construct a second minimum energy surface (trivially bounded *above* by the one we found when we insisted that the interface layers be M1I) over cool parameter space. The result is Fig. 7.16(a). We then argue as we did in (7.22), finding the minimum total energy as ν times the energy on a domain of width $\widehat{\mathcal{D}}/\nu$, to construct the contour plot in Fig. 7.16(b). This graph is identical to Fig. 7.12, except for the curved dark blue lines at the top of the $\nu = 3, 5, \ldots$ regions; we address these in the next section. The implication is that we can replace an arbitrary bounded monolayer of width $\widehat{\mathcal{D}}$ with $\nu_{\text{opt}}\left(\widehat{\mathcal{D}}, \widehat{\alpha}\right) \geq 1$ (cf. (7.21) and Fig. 7.16(a)) equally spaced (bounded) monolayers, and reduce the energy.

In Fig. 7.17, we demonstrate that each of the replacement interface layers in the process above is M1I. For this graph, we calculated $\widehat{L}_{\text{opt}}$ as in (7.23) as $\widehat{\mathcal{D}}$ divided by ν using Fig. 7.16(a). To calculate $\widehat{\ell}_{\text{opt}}\left(\widehat{L}_{\text{opt}}\right)$, we interpolated the source of each of the single monolayer minimisers of width $\widehat{L}_{\text{opt}}$, and compared results with the corresponding M1I data in Fig. 7.15. It is clear that each replacement multi-monolayer structure consists of M1I P2P monolayers.

□

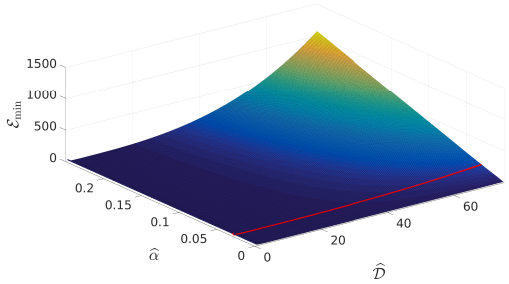

(a) 2-layer, minimum-energy surface

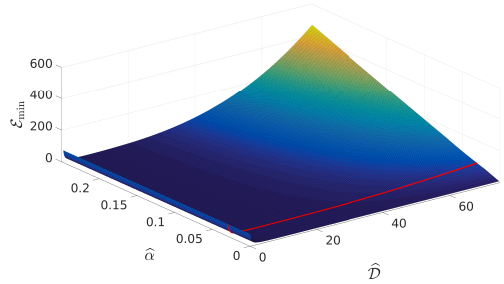

(b) 3-layer, minimum-energy surface

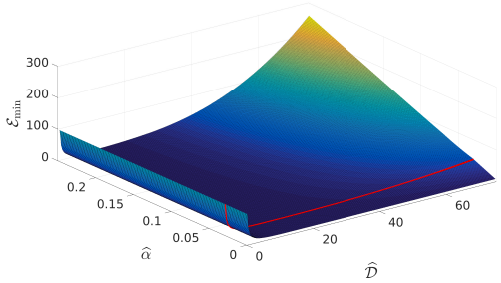

(c) 4-layer, minimum-energy surface

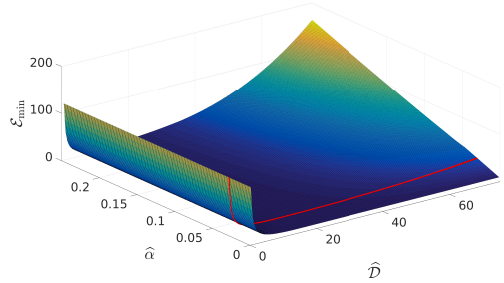

(d) 5-layer, minimum-energy surface

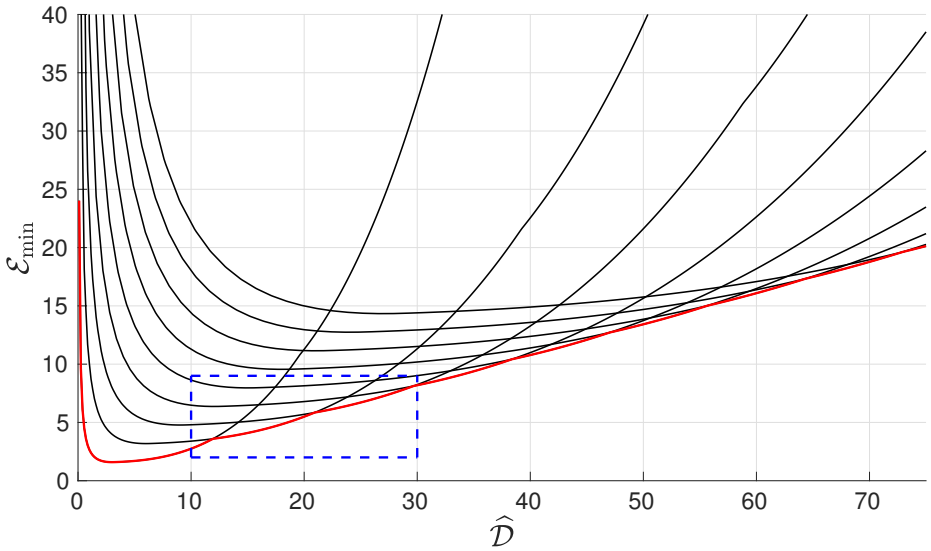

(e) Composite minimum energy surface section at $\widehat{\alpha} = 0.03$. The black lines trace out the minimum energies for $\nu = 1, \ldots, 9$ (extracted from the red section indicated in (a)–(d) above); the red line picks off the minimum energy in this set, creating the corrugated effect. Ridges occur where ν_{opt} is not unique. We explore the dashed blue box in more detail in Fig. 8.3.

Figure 7.14: Minimum-energy surfaces for $\nu = 2, \ldots, 5$, along with the summary, compound minimiser through $\widehat{\alpha} = 0.03$.[33]

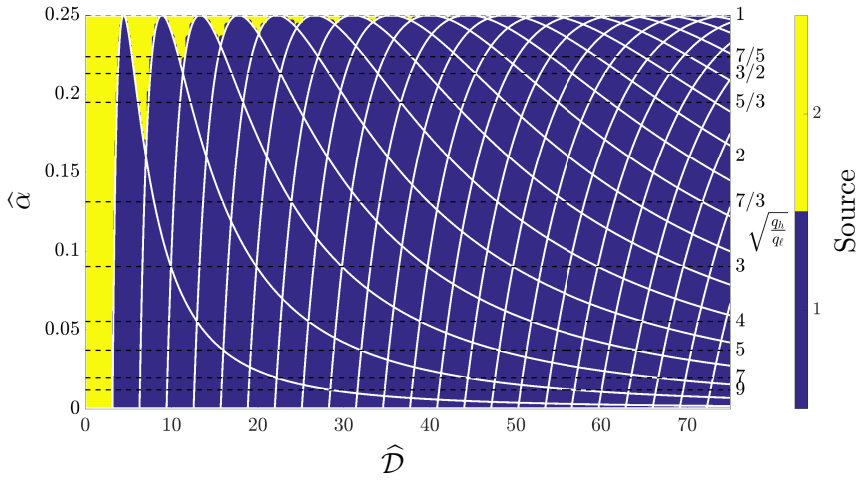

Figure 7.15: Energy minimising, equally spaced multi-monolayer component interface layer source indicator plot, with the sine and cosine function zero contours (in white).[34]

An end-to-end minimisation process

Given *any* reference bounded configuration comprised of a set of ν_{ref} P2P monolayers on $\left(0, \widehat{\mathcal{D}}\right)$ that i) have interface layers solving the ODE (6.43), ii) are connected by pure phase regions in which $\varphi = \pm 1$ and, iii) have $-\Phi' = 0$ at the ends as in (6.1b), we argue as follows:

Step 1. Replace each interface layer by its bounded, single-transition energy minimiser (ignoring M1I requirements entirely).

Step 2. Replace any remaining bounded, 'wiggly' monolayers with a set of equally spaced, M1I monolayers as in Fig. 7.16(b), but note that the replacement structure should transition from AB (or BA) and not AA/BB.

- Suppose we wish to replace a 'wiggly' monolayer on (x_1, x_2) with $x_2 - x_1 = \widehat{L}_w$, with a set of $\nu_{\text{opt}}\left(\widehat{L}_w, \widehat{\alpha}\right)$ M1I P2P monolayers. If ν_{opt} is odd, we simply insert the replacement configuration. If ν_{opt} is even, we insert the replacement monolayers, and reflect the remainder of the original morphology (on $x \geq x_2$), about $\varphi = 0$. Doing so has no effect on the monolayer count, energy or mass of φ on $\left(x_2, \widehat{\mathcal{D}}\right)$, but will swap the pure phase at $x = \widehat{\mathcal{D}}$.

The result is a Type B_ν configuration with $\nu \geq \nu_{\text{ref}}$ and lower energy.

Step 3. As in Conjecture 7.2.11, rearrange this Type B_ν morphology into an equally spaced Type A_ν arrangement.

Step 4. Replace the result with the equally spaced Type $\text{A}_{\nu_{\text{opt}}}$ morphology of Fig. 7.12.

□

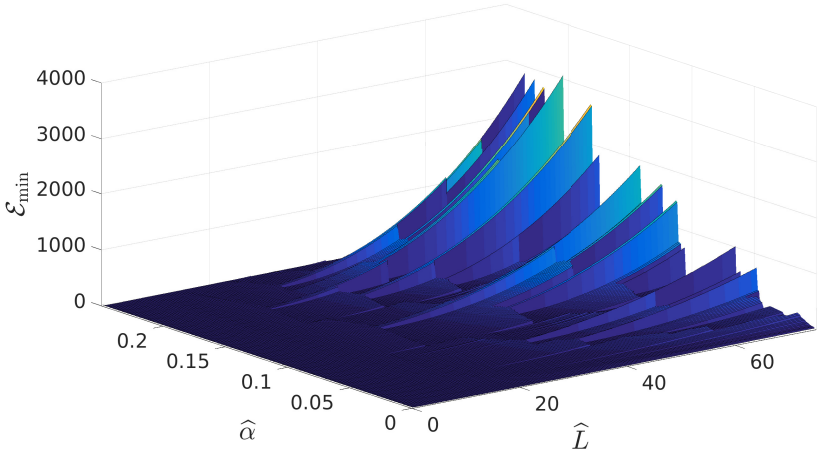

(a) Bounded single monolayer minimum energy surface (corresponding to that depicted in Fig. 7.3). This surface is obviously not convex in $\widehat{L}$.

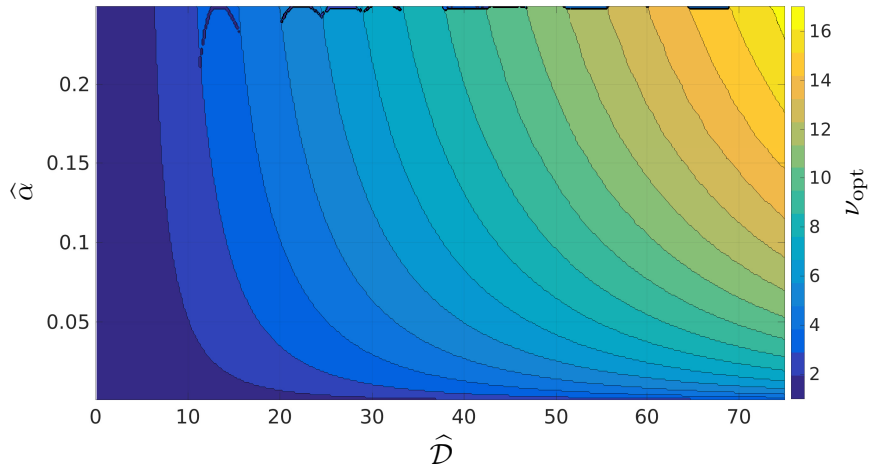

(b) Corresponding contour map of ν_{opt}, the energy minimising equally spaced monolayer count based on the energy in (a) above. This plot is (mostly) identical to that in Fig. 7.12.

Figure 7.16: The bounded, single monolayer minimum energy over cool parameter space.[35]

We conclude that **the energy of *any* P2P morphology is bounded below by that of a stationary set of M1I, equally spaced monolayers with interface layers solving the ID-ELE system** (6.92)**.**

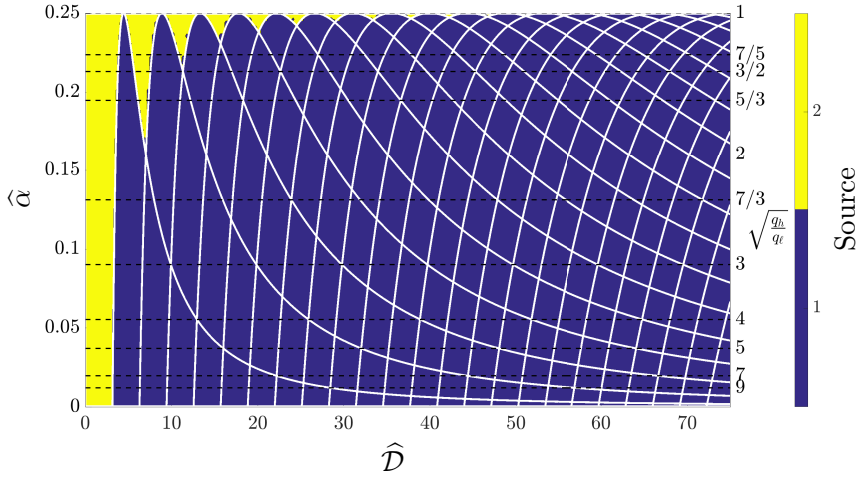

Figure 7.17: Component interface layer source indicator plot, for the equally spaced, multi-monolayer minimiser with $\|\widetilde{\varphi}\|_{0,\infty} \leq 1$. This figure is identical to Fig. 7.15, but is based on different data.[36]

7.3 Summary and conclusions

In this chapter, we offered evidence to suggest that layered, 1D symmetric minimisers are equally spaced. Given any bounded P2P morphology, in which the individual interface layers satisfy the ODE, we were able to re-arrange the configuration (by moving and/or replacing interface layers) to arrive at an equally spaced arrangement of M1I solutions of the ID-ELE (6.13), with lower energy. We considered larger and larger sets of P2P morphologies.

- To start, we considered M1I, single monolayer morphologies on symmetric domains, in which the interface layer satisfies the ODE, and the morphology has zero non-local BCs $-\Phi'\left(\pm\frac{\widehat{L}}{2}\right) = 0$. Our numerical evidence suggests that the minimum energy of such configurations is a convex function of the monolayer width, $\widehat{L}$.

- We then considered Type $\mathrm{A}_{(\nu)}$ configurations (ν prescribed) in which each interface layer is M1I and has zero non-local BCs. Our single monolayer set result means that we minimise the energy in this set by making each monolayer an identical copy/reflection/translation of the corresponding single monolayer minimiser.

- We then analysed Type $\mathrm{B}_{(\nu)}$ morphologies. Given any such morphology, we are able to re-arrange the interface layers to create a member of Set $\mathrm{A}_{(\nu)}$, with lower energy. We could thus rearrange *any* M1I P2P morphology, into an equally spaced arrangement with the same monolayer count (no matter how high), and lower energy.

  We constructed the energy-minimising monolayer count ν_{opt}, numerically, as a (non-

unique) function of scaled $\left(\widehat{L},\widehat{\alpha}\right)$-parameter space, and discovered that in energy-minimising configurations, interface layers satisfy the ODE *and* the ID-ELE.

- Finally, we dropped the requirement that each interface layer be M1I, insisting only that they be bounded. We found that we could replace any 'wiggly' interface layer, with a set of equally spaced, M1I interface layers with lower total energy.

  We concluded that *any* bounded P2P morphology can be rearranged into a set of stationary, equally spaced, M1I layers, with lower energy.

7.3.1 Discussion, limitations

The main result of this chapter is our claim that any layered P2P minimiser of the 2-phase 1D problem *must* be equally spaced. We do not (yet) assert that these equally spaced morphologies are global energy minimisers, as we cannot categorically exclude the possibility that some other class of morphology exists with lower energy.

Our demonstration was suggestive, but not rigorous. The biggest weakness was the numerical demonstration of energy convexity in Conjecture 7.1.1. Fig. 7.4 gives some indication of the problem with this demonstration, and calls into question whether this result is valid. A number of factors suggest that the red dots of Fig. 7.4, where non-convexity was observed, could be numerical artefacts:

- Not every sampled value of $\widehat{\alpha}$ yielded a region of non-convexity (although most did), even when we resorted to using CHEBFUN (the most accurate tool of its kind that we are aware of – see http://www.chebfun.org/) to construct the minimum energy surface.

- Energy is clearly convex for large $\widehat{\alpha}$ (> 0.14) and $\widehat{L}$, but this is easy to explain since the energy includes an $\widehat{\alpha}\widehat{L}^3$ term for the non-local portion. For small $\widehat{\alpha}$ and/or $\widehat{L}$ there is a transition region as the non-local energy starts to dominate, and it is hard to decide (numerically at least) whether the total energy is convex in this region.

- The pattern of red dots in Fig. 7.4 is somewhat noisy, but appears to be centred on the point $\left(\widehat{\mathcal{D}},\widehat{\alpha}\right) = (10, 0.9)$. Candidate morphologies involve rational trigonometric functions (cf. (6.59b)), with repeating poles. Some of these were hard to classify as essential or removable. Despite the author's best efforts, $\left(\widehat{\mathcal{D}},\widehat{\alpha}\right) = (10, 0.9)$ proved impossible to classify (by hand). The impact of these poles (which trace out lines in parameter space) on the energy and our numerical method, is difficult to assess.

- The most difficult numerical task was finding the edge of the M1I region in parameter space (i.e. $\widehat{\ell}_{\max}(\widehat{\alpha})$ on the right edge of the leftmost yellow region in Fig. 6.7(a)). This

is because i) the underlying $\widehat{\ell}$-intervals are open, and ii) the ends of the intervals are exceptionally difficult to work with.

For $\widehat{\alpha} > 0.09$, we were unable to identify $\widehat{\ell}_{\max}$ analytically. That said, the energy non-convexity for large $\widehat{\alpha}$ values was not too severe. The situation is far more opaque for $\widehat{\alpha} < 0.09$. In this range, interface layers are M1I for every $\widehat{\ell}$ less than the first zero of c_B. Precisely on this zero, the problem admits an infinite set of solutions (cf. Fig. 6.8), but it is not at all clear what this means for the structure of the corresponding interface layer. Could it be, for instance, that whereas (6.28) admits an infinite set of solutions, they all describe the same (bounded) morphology (noting that $\|\widetilde{\varphi}\|_\infty > 1$ whenever $\widehat{\ell}$ exceeds this first zero)? If so, is the corresponding morphology M1I, or does it have a second inflexion point (cf. Fig. C.4)? We were unable to answer these questions definitively, and so, in our numerical sweep, we simply restricted the set of candidate $\widehat{\ell}$-values to within 10^{-11} of this first zero of c_B.

Fig. 7.1 suggests that the red dots in Fig. 7.4 correspond to the transition from Source (1) to (2) single monolayer minimisers (i.e. for $\widehat{\alpha} < 0.09$, $\widehat{\ell}_{\text{opt}}$ tends precisely to the first zero of c_B). But whereas $\widehat{\ell}_{\text{opt}}$ can assume values that are close, but not equal, to this value, the energy surface has to transition across this pole. This uncertainty in $\widehat{\ell}_{\text{opt}}$ makes it hard to decide numerically whether the energy in this region is convex.

Another weakness of our argument was Conjecture 7.2.9. We plugged solutions of the ODE into the modified energy (7.20) and found the turning points of the latter. A better, more complicated, approach would have been to generalise Section 6.1 (and all subsequent results) to cater for non-zero, non-local BCs, $-\Phi' = a \neq 0$.

Outlook for the next chapter

In the next chapter, we explore the consequences of our equal-spacing proposal. We seek to understand where (in parameter space) equally spaced P2P structures are global energy minimisers, and look for the ODT separating these structured morphologies from disordered (constant) minimisers of the energy. We also present a series of gradient flow experiments (using the method we developed and analysed in Chapter 5) that offer further corroboration of our main claim in this chapter. We will present evidence that the energy is minimised when *either* all of the equally spaced P2P interface layers satisfy the ID-ELE (6.13b) *or* the morphology is disordered, which is consistent with our theoretical prediction in Lemma 4.2.6. We will also propose a complete solution of the global energy minimisation problem as a function of parameter space.

Notes

[1]The choice of the BA *ansatz* turns out to be irrelevant; reflected AB interface layers have identical properties.

[2]We do insist that (6.1b) holds globally, viz. at the ends of Ω.

[3]This observation will prove useful when we try to bound these sets numerically.

[4]See the MATLAB numerical experiment `scaled_alpha_L_sweep_1D_2phase.m` in the `bitbucket` repository, and especially `qp_okfef_1D_2phase_ellEmin_source_plot.`

[5]Our numerical study suggests the presence of turning points in the function $\mathcal{E}\left(\widehat{\ell}\right)$ (zeros of the derivative $\frac{\mathrm{d}\mathcal{E}}{\mathrm{d}\widehat{\ell}}$) that do not correspond to any of the energy minimising candidates we have considered. Intuition would suggest that the variational process we followed to get to the ID-ELE should have the same effect as taking the $\widehat{\ell}$ derivative of the (minimum) energy $\mathcal{E}$. However, this is not the case, as the following argument, due to Münch (2017), shows: For a given $\left(\widehat{L},\widehat{\alpha}\right)$, $\mathcal{E}=\mathcal{E}\left(\widehat{\ell}\right)$ is constructed by substituting $\varphi=\varphi\left(x,\widehat{\ell}\right)$, which depends on x and has $\widehat{\ell}$ as a parameter, into the energy. $\partial_{\widehat{\ell}}\varphi$ will denote the $\widehat{\ell}$-derivative of φ, and $\mathcal{E}'$ the $\widehat{\ell}$ derivative of $\mathcal{E}$. Differentiating underneath the integral and doing integration by parts yields

$$\mathcal{E}'=\int_{-\widehat{\ell}/2}^{\widehat{\ell}/2}\mathbb{L}\left[\varphi\right]\partial_{\widehat{\ell}}\varphi\,\mathrm{d}x$$

where the boundary terms that emerge during integration by parts vanish, and $\mathbb{L}$ is the integro-differential operator of (6.13b). If $\mathbb{L}\left[\varphi\right]=0$ (i.e. $F=G=0$), then obviously $\mathcal{E}'=0$ and we also have a turning point for $\mathcal{E}\left(\widehat{\ell}\right)$. However, in general, $G\neq 0$ so $\mathbb{L}\left[\varphi\right]$ is a non-trivial, linear function in x. Nevertheless, $\mathcal{E}'$ can be zero if

$$\int_{-\widehat{\ell}/2}^{\widehat{\ell}/2}x\,\partial_{\widehat{\ell}}\varphi\,\mathrm{d}x=0$$

(notice the factor x). This can easily happen, for instance when $\partial_{\widehat{\ell}}\varphi$ is an even function of x. In those cases, we have turning points in $\mathcal{E}\left(\widehat{\ell}\right)$ i.e. where $\mathcal{E}'=0$, but for which $\mathbb{L}[\varphi]\neq 0$. The corresponding $\varphi\left(x;\widehat{\ell}\right)$ is then not an optimal solution for $\mathcal{E}$, because the ID-ELE is not satisfied.

[6]For instance, in Region I, there is strong evidence to suggest that we have imposed the 'wrong' BCs i.e. global minimisers do not entail P2P monolayers. In Region I, we could, for instance, consider (6.17a) with

$$\left.\frac{\mathrm{d}\varphi}{\mathrm{d}\widehat{x}}\right|_{\widehat{x}=\pm\frac{\widehat{L}}{2}}=\left.\frac{\mathrm{d}^3\varphi}{\mathrm{d}\widehat{x}^3}\right|_{\widehat{x}=\pm\frac{\widehat{L}}{2}}=0. \tag{7.24}$$

[7]See the MATLAB numerical experiment `scaled_alpha_L_sweep_1D_2phase.m` in the `bitbucket` repository.

[8]See the MATLAB numerical experiment `scaled_alpha_L_sweep_1D_2phase.m` and especially the function call to `qp_okfef_convex_energy_regions_plot` in the `bitbucket` repository.

[9]See the MATLAB numerical experiment `work_with_general_1D_2phase_energy.m` in the `bitbucket` repository.

[10]See the MATLAB working script `plot_type_A_B_nu_layer_schematics.m` in the `bitbucket` repository.

[11]We have (cf. (6.4b))

$$\varphi_{BA}^{(P)}\left(\widehat{x}\right)=\begin{cases}-1 & \widehat{x}\in\left[\dfrac{-\widehat{L}}{2},x_L\right)\\ \widetilde{\varphi}_{BA}^{(P)}\left(\widehat{x}\right) & \widehat{x}\in[\widehat{x_L},\widehat{x_R}]\\ +1 & \widehat{x}\in\left(\widehat{x_R},\dfrac{\widehat{L}}{2}\right],\end{cases}\qquad\text{and}\qquad\varphi_{AB}^{(P)}\left(\widehat{x}\right)=\varphi_{BA}^{(P)}\left(-\widehat{x}\right).$$

For the translation of the i-th monolayer,

$$\varphi_{BA}^{(i)}\left(\widehat{x}\right)=\varphi_{BA}^{(P)}\left(\widehat{x}-\left(X_{i-1}+\frac{\widehat{L}}{2}\right)\right)\qquad\text{and}\qquad\varphi_{AB}^{(j)}\left(\widehat{x}\right)=\varphi_{AB}^{(P)}\left(\widehat{x}-\left(X_{j-1}+\frac{\widehat{L}}{2}\right)\right)=\varphi_{BA}^{(P)}\left(\left(X_{j-1}+\frac{\widehat{L}}{2}\right)-\widehat{x}\right),$$

i.e. we shift the relevant prototype so that it occupies $[X_{i-1},X_i]$ or $[X_{j-1},X_j]$, depending on the choice of $\varphi\left(0\right)$.

[12]We have that (cf. (6.8), (6.16))

$$\Phi_{BA}'\left(\widehat{x}\right)=\begin{cases}\left(\widehat{x}-X_{i-1}\right)\left(1+m\right) & \widehat{x}\in\left[X_{i-1},\widehat{x_L}^{(i)}\right)\\ -\displaystyle\int_{\widehat{x_L}^{(i)}}^{\widehat{x}}\widetilde{\varphi}^{(i)}-m\ \mathrm{d}t+\left(\widehat{x_L}^{(i)}-X_{i-1}\right)\left(1+m\right) & \widehat{x}\in\left[\widehat{x_L}^{(i)},\widehat{x_R}^{(i)}\right]\\ -\left(\widehat{x}-X_i\right)\left(1-m\right) & \widehat{x}\in\left(\widehat{x_R}^{(i)},X_i\right].\end{cases}\tag{7.25}$$

Similarly,

$$\begin{cases}\left(\dfrac{\widehat{x}^2}{2}-X_{i-1}x+\dfrac{\left(\widehat{x_L}^{(i)}\right)^2}{2}\right)\left(1+m\right) & \widehat{x}\in\left[X_{i-1},\widehat{x_L}^{(i)}\right)\\ -\displaystyle\int_{\widehat{x_L}^{(i)}}^{x}\int_{\widehat{x_L}^{(i)}}^{\xi}\widetilde{\varphi}^{(i)}-m\ \mathrm{d}t\ \mathrm{d}\xi+\left(\widehat{x_L}^{(i)}-X_{i-1}\right)\left(1+m\right)\widehat{x} & \widehat{x}\in\left[\widehat{x_L}^{(i)},\widehat{x_R}^{(i)}\right]\\ -\left(\dfrac{\widehat{x}^2}{2}-X_i\widehat{x}-\left(\dfrac{\left(\widehat{x_R}^{(i)}\right)^2}{2}-X_i\widehat{x_R}^{(i)}\right)\right)\left(1-m\right)\\ -\displaystyle\int_{\widehat{x_L}^{(i)}}^{\widehat{x_R}^{(i)}}\int_{\widehat{x_L}^{(i)}}^{\xi}\widetilde{\varphi}^{(i)}-m\ \mathrm{d}t\ \mathrm{d}\xi+\left(\widehat{x_L}^{(i)}-X_{i-1}\right)\left(1+m\right)\widehat{x_R}^{(i)} & \widehat{x}\in\left(\widehat{x_R}^{(i)},X_i\right].\end{cases}\tag{7.26}$$

Note that we set $E=0$ above (cf. (6.16)).

[13]ν is prescribed but not restricted at this stage. For very high values of ν, we might expect the equally spaced morphology to have an energy that is higher than that of another configuration with fewer (or no) P2P layers. We explore topics of this nature in Section 7.2.5.

[14]We demonstrate that convexity of the minimum single monolayer energy over $\widehat{L}$ (cf. Conjecture 7.1.1) implies an equally spaced minimiser: consider the constrained minimisation problem

$$\left(\mathbf{P}_\nu\right):\qquad\text{find}\qquad\left\{\underline{\widehat{L}}_i\right\}_{i=1}^{\nu}\qquad\text{s.t.}\qquad\sum_{i=1}^{\nu}\mathcal{E}_{\min}^{(1)}\left(\underline{\widehat{L}}_i\right)\to\min\qquad\text{where}\qquad\sum_{i=1}^{\nu}\underline{\widehat{L}}_i=\widehat{\mathcal{D}}.\tag{7.27}$$

To solve this problem, we pose the Lagrangian

$$\mathscr{L}\left[\left\{\underline{\widehat{L}}_i\right\}_{i=1}^{\nu},\lambda\right]=\sum_{i=1}^{\nu}\mathcal{E}_{\min}^{(1)}\left(\underline{\widehat{L}}_i\right)-\lambda\left(\sum_{i=1}^{\nu}\underline{\widehat{L}}_i-\widehat{\mathcal{D}}\right).\tag{7.28}$$

The first order, necessary KKT conditions for minimisation are

$$\nabla_{\underline{\widehat{L}}}\mathscr{L}=\mathbf{0}\qquad\text{and}\qquad\partial_\lambda\mathscr{L}=0;\tag{7.29}$$

expanding these for clarity, we obtain the system of $\nu+1$ equations (using $'=\mathrm{d}/\mathrm{d}\underline{L}$),

$$\begin{aligned}\partial_{\underline{\widehat{L}}_1}\mathscr{L}=0\qquad&\Rightarrow\qquad\mathcal{E}_{\min}^{(1)\,\prime}\left(\underline{\widehat{L}}_1\right)=\lambda;\\ &\cdots\\ \partial_{\underline{\widehat{L}}_\nu}\mathscr{L}=0\qquad&\Rightarrow\qquad\mathcal{E}_{\min}^{(1)\,\prime}\left(\underline{\widehat{L}}_\nu\right)=\lambda;\end{aligned}$$

and;

$$\partial_\lambda \mathscr{L} = 0 \qquad \Rightarrow \qquad \sum_{i=1}^{\nu} \widehat{\underline{L}}_i = \widehat{\mathcal{D}}. \tag{7.30}$$

The Lagrange multiplier λ is the gradient of the tangent to $\mathcal{E}^{(1)}_{\min}$ at each $\widehat{\underline{L}}_i$. For suitably smooth, (strictly) convex $\mathcal{E}^{(1)}_{\min}$ as in Conjecture 7.1.1, its first derivative $\mathcal{E}^{(1)\,\prime}_{\min} : \mathbb{R}^+ \to \mathbb{R}$ is a strictly increasing, invertible function. Consequently, for any given $\lambda \in \mathbb{R}$, $\mathcal{E}^{(1)\,\prime}_{\min}\left(\widehat{\underline{L}}\right) = \lambda$ has a unique solution, $\widehat{L}$. Combining this observation with the last condition in (7.30), we conclude that a necessary condition for a minimising set $\left\{\widehat{\underline{L}}_i\right\}_{i=1}^{\nu}$ is that each

$$\widehat{\underline{L}}_i = \frac{\widehat{\mathcal{D}}}{\nu}.$$

[15]Note: we never split a problem at a non-pure-phase zero of $-\Phi'$, as doing so would create sub-problems with BCs to which our single monolayer results do not apply.

[16]In the `bitbucket` repository, see the MATLAB working scripts `scaled_alpha_L_sweep_1D_2phase.m` and `draw_sealevel_morph_snippet.m`.

[17]One way to solve (7.18), would be to pose the Lagrangian

$$\mathscr{L}\left[\overline{\underline{L}}_1, \overline{\underline{L}}_2, \lambda\right] = \mathcal{E}^{(a)}_{BA}\left(\overline{\underline{L}}_1\right) + \mathcal{E}^{(a)}_{AB}\left(\overline{\underline{L}}_2\right) - \lambda\left(\overline{\underline{L}}_1 + \overline{\underline{L}}_2 - L'\right) \tag{7.31}$$

and solve it in the form of the double tangent problem (using $' = \mathrm{d}/\mathrm{d}\overline{\underline{L}}$),

$$\partial_{\overline{\underline{L}}_1} \mathscr{L} = 0 \qquad \Rightarrow \qquad \left(\mathcal{E}^{(a)}_{BA}\right)'\left(\overline{\underline{L}}_1\right) = \lambda; \tag{7.32a}$$

$$\partial_{\overline{\underline{L}}_2} \mathscr{L} = 0 \qquad \Rightarrow \qquad \left(\mathcal{E}^{(a)}_{AB}\right)'\left(\overline{\underline{L}}_2\right) = \lambda, \tag{7.32b}$$

and;

$$\partial_\lambda \mathscr{L} = 0 \qquad \Rightarrow \qquad \overline{\underline{L}}_1 + \overline{\underline{L}}_2 = L'. \tag{7.32c}$$

Our numerical approach was simpler and more direct.

[18]If $\varphi_{(a)}$ denotes the single monolayer morphology minimising $\mathcal{E}^{(a)}_{AB}[\varphi]$, then it is *not* true that

$$\mathcal{E}^{(a)}_{AB,\min}\left(\widehat{L}\right) = \int_{-\widehat{L}/2}^{\widehat{L}/2} \frac{\varepsilon_\varphi^2}{2}\left(\varphi'_{(0)}\right)^2 + \frac{\chi^{AB}}{4}\left(1 - \varphi^2_{(0)}\right) + \frac{\alpha}{2}\left(-\Phi' + a\right)^2 \mathrm{d}x$$

i.e. the elevated and 'non-elevated' minimisers are *not* the same.

[19]We can also reuse much of the code we developed for Conjecture 7.1.1.

[20]See the MATLAB working script `plot_one_AB_morph_elevated.m` in the `bitbucket` repository.

[21]These results suggest that (cf. (7.19))

$$\mathcal{E}^{(a)}_{BA}\left(\overline{\underline{L}}_1\right) + \mathcal{E}^{(a)}_{AB}\left(L' - \overline{\underline{L}}_1\right) \to 2\mathcal{E}^{(0)}_{BA}\left(\frac{L'}{2}\right), \qquad \overline{\underline{L}}_1, \overline{\underline{L}}_2 \to \frac{L'}{2} \qquad \text{as} \qquad L' \to \infty, \tag{7.33}$$

i.e. the minimum energy of the elevated 2-monolayer snippet tends to that with $a = 0$ as the width of the configuration becomes unbounded, which seems intuitively correct.

[22]See the MATLAB code `qp_okfef_1D_2phase_draw_elevated_energies.m` in the `bitbucket` repository.

[23]See the MATLAB code `qp_okfef_1D_2phase_draw_elevated_energies.m` in the `bitbucket` repository.

[24]This part of the process can be regarded as a mass-preserving, *non* shape-preserving pulse variation.

[25]We could equivalently slide $\boxed{1}$ and $\boxed{2}$ to the left by an analogous process (leaving monolayers $\boxed{3}$ through $\boxed{5}$ unaffected).

[26]See the MATLAB working script `plot_type_A_B_nu_layer_schematics.m` in the `bitbucket` repository.

[27]It is not possible to construct a (pathological) 2-layer morphology in which one of the $\underline{L}_i$'s has $\underline{L}_i < \widetilde{L}$ and one of the zeros is non-pure-phase, since doing so would result in an interface layer in which $-\Phi' = 0$, on one end of the domain (viz. inside the interface layer) – which is impossible.

[28]The fact that $\mathcal{E}_{\min}^{(1)} \to \infty$ as $\widehat{L} \to 0$ (cf. Conjecture 7.1.1) means that $\nu_{\max}$ is generally quite modest. For our numerical investigations, we set $\nu_{\max} = 50$.

[29]In addition, as ε_φ is reduced along the dashed, white lines, the minimum energy monolayer count increases: the lines of decreasing ε_φ are 'shallower' than the contour lines separating the regions of distinct monolayer count.

[30]See the MATLAB numerical experiment `scaled_alpha_L_sweep_1D_2phase.m` in the `bitbucket` repository, and especially `qp_okfef_1D_2phase_plot_min_energy_nu_map`.

[31]See the MATLAB numerical experiment `scaled_alpha_L_sweep_1D_2phase.m` in the `bitbucket` repository.

[32]We anticipate that energy minimisers are not P2P in Region I – see the next chapter.

[33]See the MATLAB numerical experiment `scaled_alpha_L_sweep_1D_2phase.m` in the `bitbucket` repository, and especially `qp_okfef_1D_2phase_min_nu_layer_energy`.

[34]See the MATLAB numerical experiment `scaled_alpha_L_sweep_1D_2phase.m` in the `bitbucket` repository.

[35]See the MATLAB numerical experiment `scaled_alpha_L_sweep_1D_2phase.m` in the `bitbucket` repository, and especially `qp_okfef_1D_2phase_plot_min_energy_nu_map`.

[36]See the MATLAB numerical experiment `scaled_alpha_L_sweep_1D_2phase.m` in the `bitbucket` repository, and especially `qp_okfef_1D_2phase_analyse_Emin_source_layers`.

Chapter 8

Implications of equal-spacing in 1D energy minimisers

In this chapter, we put the theoretical predictions of the previous chapter into context.

Contents

8.1 Locating ordered and disordered minimisers 182
8.2 Semi-explicit, P2P minimisers 195
8.3 Comparison with Cahn–Hilliard: the effect of $\alpha = 0$ 200
8.4 Implications for modelling phase separation in DBCs 202
8.5 Sharp interface limits 203
8.6 The asymmetric case 206
8.7 Summary and conclusions 208

Chapter outline

- In Section 8.1, we attempt to verify our prediction of the equal-spacing of P2P minimisers using numerical (gradient flow) experiments. We then explore and locate disordered/constant (non P2P) minimisers in parameter space.
- In Section 8.2, we propose and implement a practical, efficient algorithm for finding explicit global energy minimisers.
- In Section 8.3, we focus on the effect of the non-local energy coefficient α, summarising and comparing our results ($\alpha > 0$) with those noted in the literature for $\alpha = 0$.
- In Section 8.4, we explore the implications of our results in the context of modelling symmetric DBCs.

- In Section 8.5, we confirm that our results match established, sharp interface, asymptotic predictions from the literature.
- Finally, in Section 8.6, we introduce the asymmetric problem ($m \neq 0$).

8.1 Locating ordered and disordered minimisers

We have provided evidence suggesting that energy minimising, P2P morphologies must have equally spaced, identical, M1I interface layers. In the literature, such configurations are referred to as ordered, as distinct from disordered (i.e. constant, $\varphi \equiv m$) morphologies. While analysing the single monolayer problem, we suggested that global minimisers drawn from the parameters in Region I were unlikely to be P2P. In this section, we use gradient flow and other techniques to i) search for the ODT (cf. Choksi et al. (2009), Choksi et al. (2011)) separating ordered and disordered minimisers in scaled parameter space, and ii) confirm that the layer counts of Fig. 7.12 minimise the energy. In so doing, we will confirm our suspicion about the structure of minimisers in Region I.

8.1.1 The disordered candidate minimiser

Our first attempt at finding and understanding the ODT is to explore the disordered solution $\varphi \equiv m$ to (6.43a). Regions of parameter space in which the disordered morphology has lower energy than any P2P morphology cannot admit a P2P global minimiser.[1] The energy of a constant morphology is simple as it has no interfacial or non-local energy. Extracting the homogeneous energy component from (6.1e) yields

$$\mathcal{E}\left[\varphi \equiv m\right] = \int_0^{\mathcal{D}} \frac{\chi^{AB}}{4}\left(1-m^2\right) \mathrm{d}x = \frac{\chi^{AB}}{4}\left(1-m^2\right)\mathcal{D}, \tag{8.1a}$$

so that in the symmetric ($m = 0$) case,

$$\mathcal{E}\left[\varphi \equiv 0\right] = \frac{\chi^{AB}\mathcal{D}}{4}. \tag{8.1b}$$

Scaling into $\left(\widehat{\mathcal{D}}, \widehat{\alpha}\right)$ via (6.43b), we conclude that

$$\mathcal{E}\left[\varphi \equiv 0\right] = \frac{\widehat{\mathcal{D}}}{2}, \tag{8.1c}$$

which is a linear function of $\widehat{\mathcal{D}}$. In particular, $\lim_{\widehat{\mathcal{D}}\downarrow 0} \mathcal{E}\left[\varphi \equiv 0\right] = 0$, which is quite different from what we observed for P2P morphologies in Fig. 7.13.

Doing a numerical comparison of the energy surface in Fig. 7.13 with that implied by (8.1c) leads to Fig. 8.1. In comparing these plots with Fig. 7.15, we see that the Source (2) (edge morphology minimiser) regions in Fig. 7.15 have been replaced by the Source (0) disordered morphology. Fig. 8.2 depicts the impact of the disordered morphology on ν_{opt};

$\nu_{\text{opt}} = 0$ indicates that the disordered morphology has a lower energy than any layered morphology.

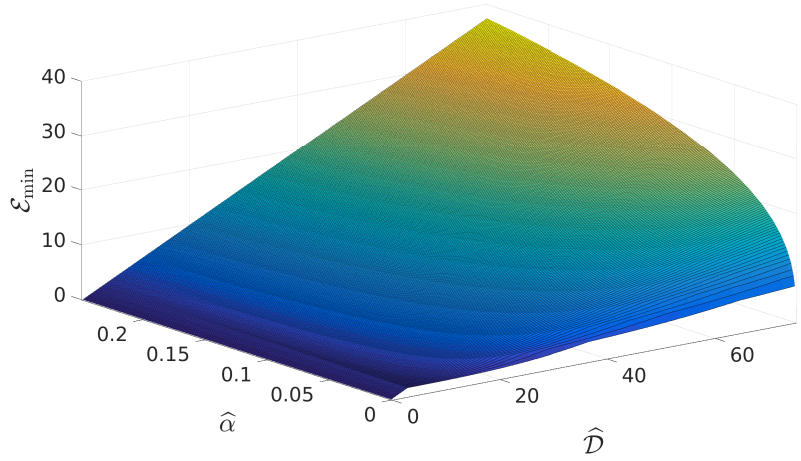

(a) Refined minimum energy surface. The shape of this surface near $\widehat{\mathcal{D}} = 0$ is different to what we observed in Fig. 7.13. This graph suggests that the disordered morphology is an energy minimiser along $\widehat{\alpha} = \frac{1}{4}$.

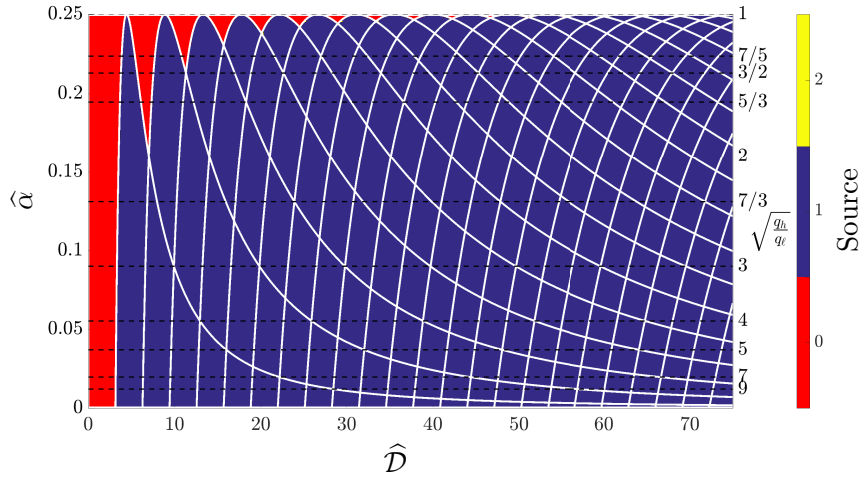

(b) Corresponding minimiser source indicator contour plot. The new Source, '0', shaded in **red** indicates that the disordered morphology $\varphi \equiv 0$ has lower energy than *any* P2P morphology. The Source (0) morphology has displaced the Source (2) energy minimising region from Fig. 7.15 in its entirety.

Figure 8.1: Comparison with the disordered (zero) morphology.[2]

8.1.2 Validating and extending the results with gradient flow experiments

In this section we test our predictions in Fig. 8.2 using the gradient flow techniques we defined and discussed in Chapter 4. Sending $t \to T$, T large enough for the solution to become (nearly) stationary, allows us to explore low energy configurations **without any of the *ansatz* constraints of our previous work**.

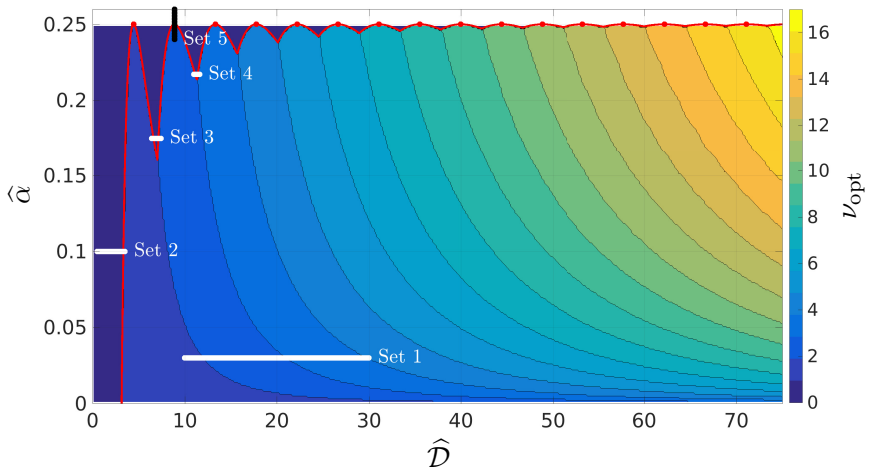

Figure 8.2: Revised ν_{opt} contour plot (cf. Fig. 7.12). We identify $\nu = 0$ (shaded dark **blue**) with the disordered (zero) morphology energy minimiser; this is the same as the **red** region in Fig. 8.1(b). The **red** line is the ODT ($\widehat{\alpha} = \widehat{\alpha}_{\max}\left(\widehat{\mathcal{D}}\right)$ as in (6.69)) from Conjecture 8.1.1 on p. 194. The white/black patches mark the five $\left(\widehat{\mathcal{D}}, \widehat{\alpha}\right)$ test sets of Section 8.1.2.[3]

The following experiments are similar to the 1D experiment in Section 8.1 of Hintermüller et al. (2011). Those authors tested their numerical method against exact solutions of the Cahn–Hilliard equation from Blowey and Elliott (1991). We test our method using the minimisers we proposed in the previous chapter.

Experiment design

We worked with five sets of $\left(\widehat{\mathcal{D}}, \widehat{\alpha}\right)$ pairs, marked as the white and black patches in Fig. 8.2. For each pair, we ran a gradient flow experiment with time-step τ, spatial discretisation h, and the *un-scaled* parameters in Table 8.1 to stationarity.[4] Using these and (6.47) yields

$$\alpha = \frac{\widehat{\alpha}\widehat{\mathcal{D}}^2}{2} \qquad \text{and} \qquad \varepsilon_\varphi^2 = \frac{1}{2\widehat{\mathcal{D}}^2}. \tag{8.2}$$

The parameters in Table 8.1 together with (8.1b) imply that the energy of the disordered solution $\varphi \equiv 0$ is $\mathcal{E}_{\text{total}} = \frac{1}{4}$ for all of our experiments. We were thus able to to compare our end-state energies with a known, low energy. Details are as follows:

Set 1. This set of experiments was intended to confirm the predictions of Fig. 7.14(e). We set $\widehat{\alpha} = 0.03$ and worked with three subsets of 150 equally spaced $\widehat{\mathcal{D}}$-values in $10 \leq \widehat{\mathcal{D}} \leq 30$, and $h = 10^{-3}$. ICs were selected as follows:

a) The 150 $\widehat{\mathcal{D}}$-values using interpolants of the theoretical $\nu = \nu_{\text{opt}} = 1, 2, 3$ or 4-layer energy minimisers, as in Fig. 7.14(e). We set $\tau = 0.001$ and $T = 5$.

Parameter	Value	Comments
μ	10^{-8}	Based on our experiments and observations in Section 5.4.3.
$\mathcal{D}$	1	A unit (un-scaled) interval.
χ^{AB}	1	

Table 8.1: Common 2-phase gradient flow experiment parameters

Results are summarised in Fig. 8.3: all of the experiments ended at the theoretical ν_{opt}. The observed/end-state and predicted/minimum energies were very similar.

b) Morphologies with $\nu \neq \nu_{\text{opt}}$, using selected $\widehat{\mathcal{D}}$ values in the set of 150.

We selected two $\widehat{\mathcal{D}}$ values that were close to the 2-to-3 monolayer transition depicted in Fig. 8.3: $\widehat{\mathcal{D}} \in \{20.738, 21.141\}$. For $\widehat{\mathcal{D}} = 20.738$, $\nu_{\text{opt}}^{(\text{predicted})} = 2$, so we used an IC with three monolayers (one too many). For $\widehat{\mathcal{D}} = 22.483$, $\nu_{\text{opt}}^{(\text{predicted})} = 3$; we used an IC with two monolayers (one too few).

We then considered $\widehat{\mathcal{D}} = 15.101$, a value far from the 2-to-3 monolayer transition value $\nu_{\text{opt}}^{(\text{predicted})} = 2$. We conducted experiments with $\nu = 1, 3, 4, 5$; the $1, 3, 4$-monolayer ICs were stationary in the sense of satisfying the ID-ELE system (6.92); for $\nu = 5$, the interface layers came from Region I, and so the IC was not stationary. In all cases, we set $\tau = 0.005$ and $T = 400$.

Results are presented in Table 8.2.[5] The experiments with $\widehat{\mathcal{D}} = 20.738, 22.483$ (close to the 2-to-3 monolayer transition) failed in the sense that the stationary solutions remained at non-optimal monolayer counts. However, both end-state energies were higher than the theoretically predicted minima, and so they were successful insofar as they did not yield alternative morphologies with lower energies. The experiments with $\widehat{\mathcal{D}} = 15.101$ yielded similar results. Only with $\nu_{\text{IC}} = 5$ did the morphology evolve to $\nu_{\text{end}} = 3$, which was still not the theoretical minimiser, but was closer.

c) Ten mass-conserving pulse variations of an equally spaced, theoretical minimiser. We used $\widehat{\mathcal{D}} = 25.034$ which has $\nu_{\text{opt}}^{(\text{predicted})} = 3$, and shifted pulse 2 (cf. Defn 6.3.1) to the right by $0.01 \times \{1, 2, \ldots, 10\}$ (equivalent to $0.2503\,\{1, 2, \ldots, 10\}$ in scaled units). In all cases, we set $\tau = 0.005$ and $T = 400$.

Results are summarised in Fig. 8.4. In all cases, the unequally spaced ICs evolved to equally spaced end-states that matched the theoretical minimiser exactly. All end-state energies were the same to (at least) ten significant digits: $\widehat{\mathcal{E}}_{\text{end}} = 0.134$. Monolayer counts were unchanged by the dynamics.[6]

Set 2. $\widehat{\alpha} = 0.1$ and we chose two sets of 20 $\widehat{\mathcal{D}}$ values, equally spaced in part 1: $0.5 \leq \widehat{\mathcal{D}} \leq 2.9$ and part 2: $3.0 \leq \widehat{\mathcal{D}} \leq 3.5$ (40 experiments in total). We set $h = 10^{-3}$, $\tau = 0.005$ and $T = 400$. For each $\left(\widehat{\mathcal{D}}, \widehat{\alpha}\right)$ pair, the minimum energy, 1-monolayer P2P configuration was used as the IC.[7]

We know that minimisers in Region I cannot be P2P, and so we were interested in understanding the transition from disorder to order as we crossed from Region I into the cold region.

Summary results appear in Fig's 8.5–8.6: all experiments in Region I converged to the disordered solution having $\mathcal{E}_{\text{total}} = \frac{1}{4}$; those in the cold region converged to a 1-monolayer morphology with $\mathcal{E}_{\text{total}} < \frac{1}{4}$.

Set 3. $\widehat{\alpha} = 0.175$ and we chose a set of 20 equally spaced $\widehat{\mathcal{D}}$ values in $6.4 \leq \widehat{\mathcal{D}} \leq 7.4$, with $h = 10^{-3}$, $\tau = 0.005$ and $T = 400$.[8]

As in the previous set, we did not expect P2P minimisers for $\widehat{\alpha} > \widehat{\alpha}_{\max}$ (cf. (6.69), (8.4)). Fig. 8.2 predicts a 1-monolayer P2P minimiser near $\widehat{\mathcal{D}} = 6.4$ and a 2-monolayer minimiser near $\widehat{\mathcal{D}} = 7.4$. We wished to understand the transition from one to two monolayers. As such, the minimum energy, 1-monolayer P2P configuration was used as the IC for $\widehat{\mathcal{D}} < 6.6$ (the first four experiments), 1- and 2-monolayer P2P configurations were used in the transition area (the next eleven experiments), and 2-monolayer configurations for the rest.

Summary results appear in Fig. 8.7. For those parameters with two ICs (Fig's 8.7(e)–(o)), we present the end-state with the lower energy (the choice was arbitrary since in every case, both experiments converged to the disordered morphology). All of the experiments with $\widehat{\alpha} > \widehat{\alpha}_{\max}$ converged to the disordered solution having $\mathcal{E}_{\text{total}} = \frac{1}{4}$; those with $\widehat{\alpha} < \widehat{\alpha}_{\max}$ converged to a 1- or 2-monolayer morphology with $\mathcal{E}_{\text{total}} < \frac{1}{4}$.

Set 4. $\widehat{\alpha} = 0.217$ and we chose 20 equally spaced $\widehat{\mathcal{D}}$ values in $11 \leq \widehat{\mathcal{D}} \leq 11.6$. This set was similar to the previous one (same space-time discretisation), but that we anticipated a transition from two to three monolayers. Our approach to using multiple ICs between regions of predicted P2P structure was analogous to the previous set (the middle nine experiments were started separately from minimum energy, 2- and 3-monolayer P2P morphologies).

Summary results appear in Fig. 8.8; those with two ICs are in Fig's 8.8(f)–(n) (we depict the end-state with the lower energy; arbitrary once again). The results were analogous to those in Set 3.

Set 5. In this set (the vertical set of black dots in Fig. 8.2), we explored the effects of transitioning $\widehat{\alpha}$ through $\frac{1}{4}$ for $\widehat{\mathcal{D}} = \sqrt{8}\pi$. ICs were created as follows: for $\widehat{\alpha} < \frac{1}{4}$, we used our theoretical 2-monolayer minimiser. For $\widehat{\alpha} \geq \frac{1}{4}$, for which the cool,

sine/cosine *ansatz* (6.24) is not appropriate, we used the 2-monolayer minimiser corresponding to $\widehat{\alpha} = 0.2499$, and set $h = 10^{-3}$, $\tau = 0.005$ and $T = 400$.

Summary results are in Fig. 8.9: experiments with $\widehat{\alpha} \leq \frac{1}{4}$ converged to a 2-monolayer morphology with $\mathcal{E}_{\text{total}} < \frac{1}{4}$; those with $\widehat{\alpha} > \frac{1}{4}$ converged to $\varphi \equiv 0$ with $\mathcal{E}_{\text{total}} = \frac{1}{4}$.

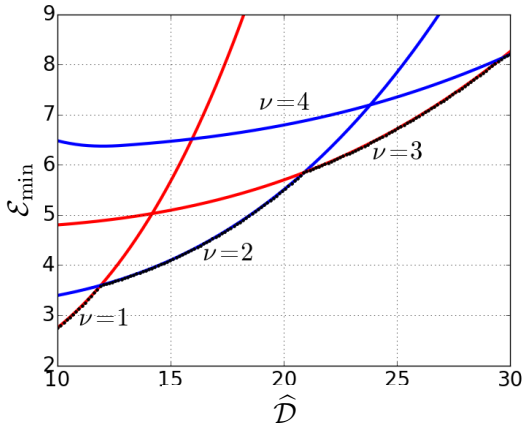

Figure 8.3: Theoretical minimum energy vs observed end-state energies (cf. the dashed blue box in Fig. 7.14(e)). The theoretical minima are **red** and **blue** according to whether an odd/even number of monolayers ($1, 2, 3$ or 4) was proposed. The 150 experimental end-state energies are plotted as **black** dots.[9]

$\widehat{\mathcal{D}}$	ν_{opt}	$\widehat{\mathcal{E}}_{\text{min}}$	ν_{IC}	ν_{end}	$\widehat{\mathcal{E}}_{\text{end}}$	**Comments**
20.738	2	5.785	3	3	5.820	The monolayer count remained too high.
21.141	3	5.891	2	2	5.946	The monolayer count remained too low.
15.101	2	4.120	1	1	5.760	
			3	3	5.102	
			4	4	6.472	
			5	3	5.102	$\widehat{\mathcal{E}}_{\text{end}}$ for this and the 4^{th} row matched to (at least) 13 significant digits.

Table 8.2: Gradient flow experiments from ICs with $\nu \neq \nu_{\text{opt}}$. We used $\widehat{\alpha} = 0.03$ and the parameters in Table 8.1. Energies were scaled as in Fig. 8.3 using (6.73).[10]

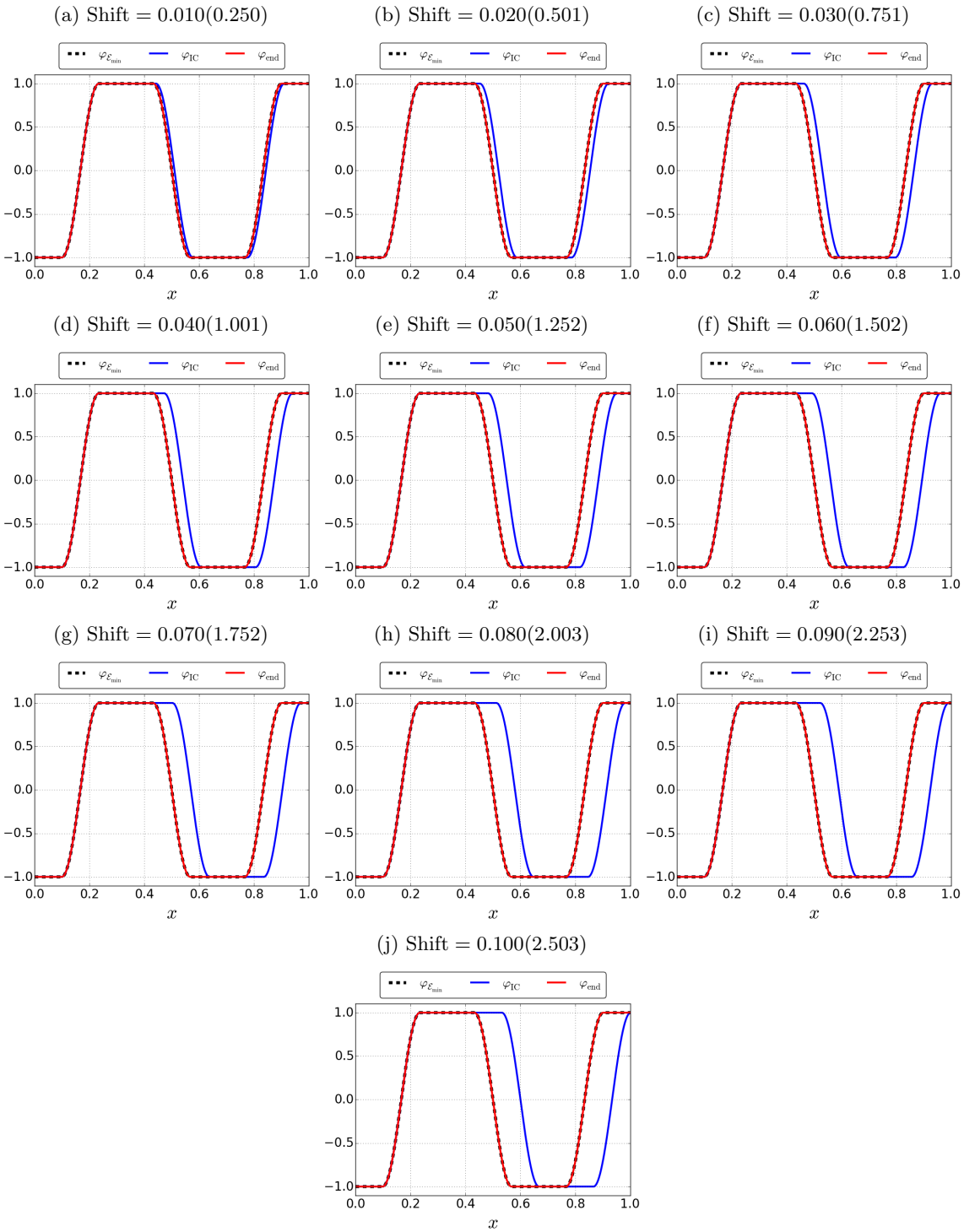

Figure 8.4: Summary results: comparisons of pulse-shifted ICs (solid **blue**), end-states (solid **red**), and theoretical energy minimisers (dashed **black**) for $\left(\widehat{D}, \widehat{\alpha}\right) = (25.034, 0.030)$. Un-scaled (scaled) pulse shift distances were as indicated.[11]

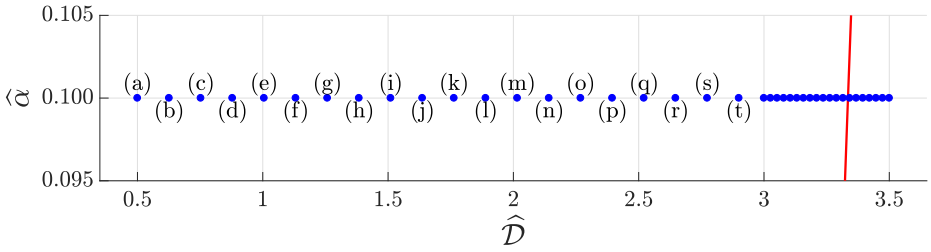

Set 2 (part 1) parameters. The **red** line is the right edge of Region I (cf. (6.65)).

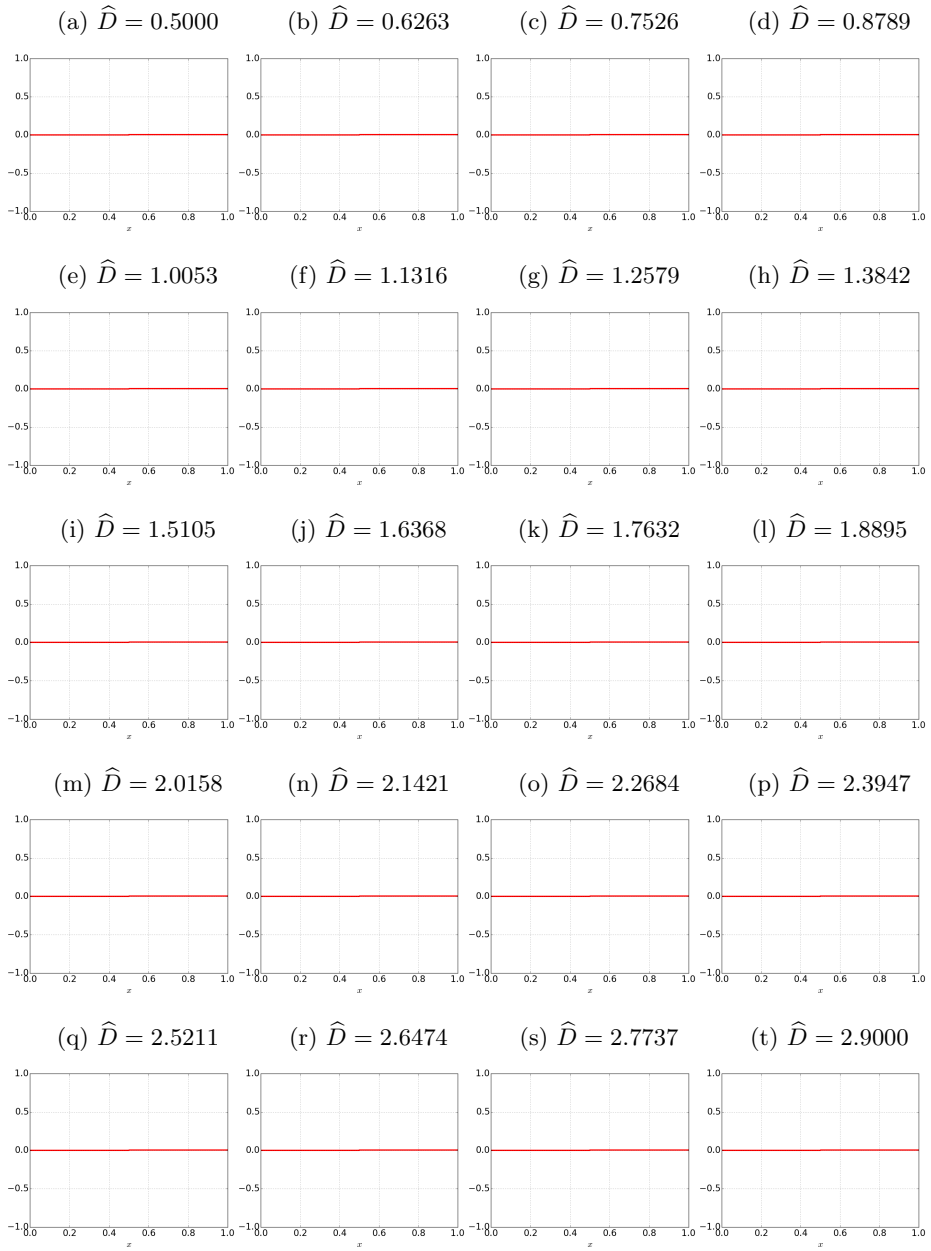

Figure 8.5: Set 2 parameters and summary results (part 1 of 2): end-state morphologies for $\widehat{\alpha} = 0.1000$ and $\widehat{D} \in (0.5, 2.9)$, as indicated.[12]

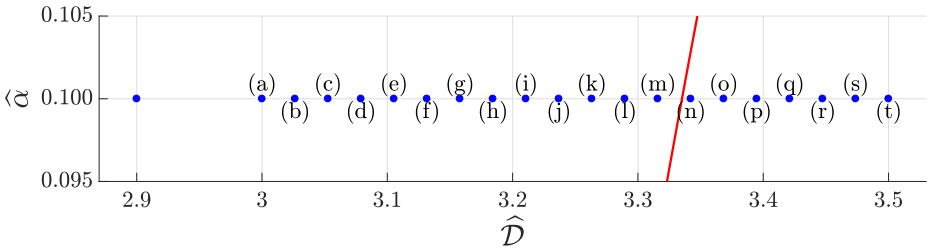

Set 2 (part 2) parameters. The **red** line is the right edge of Region I (cf. (6.65)).

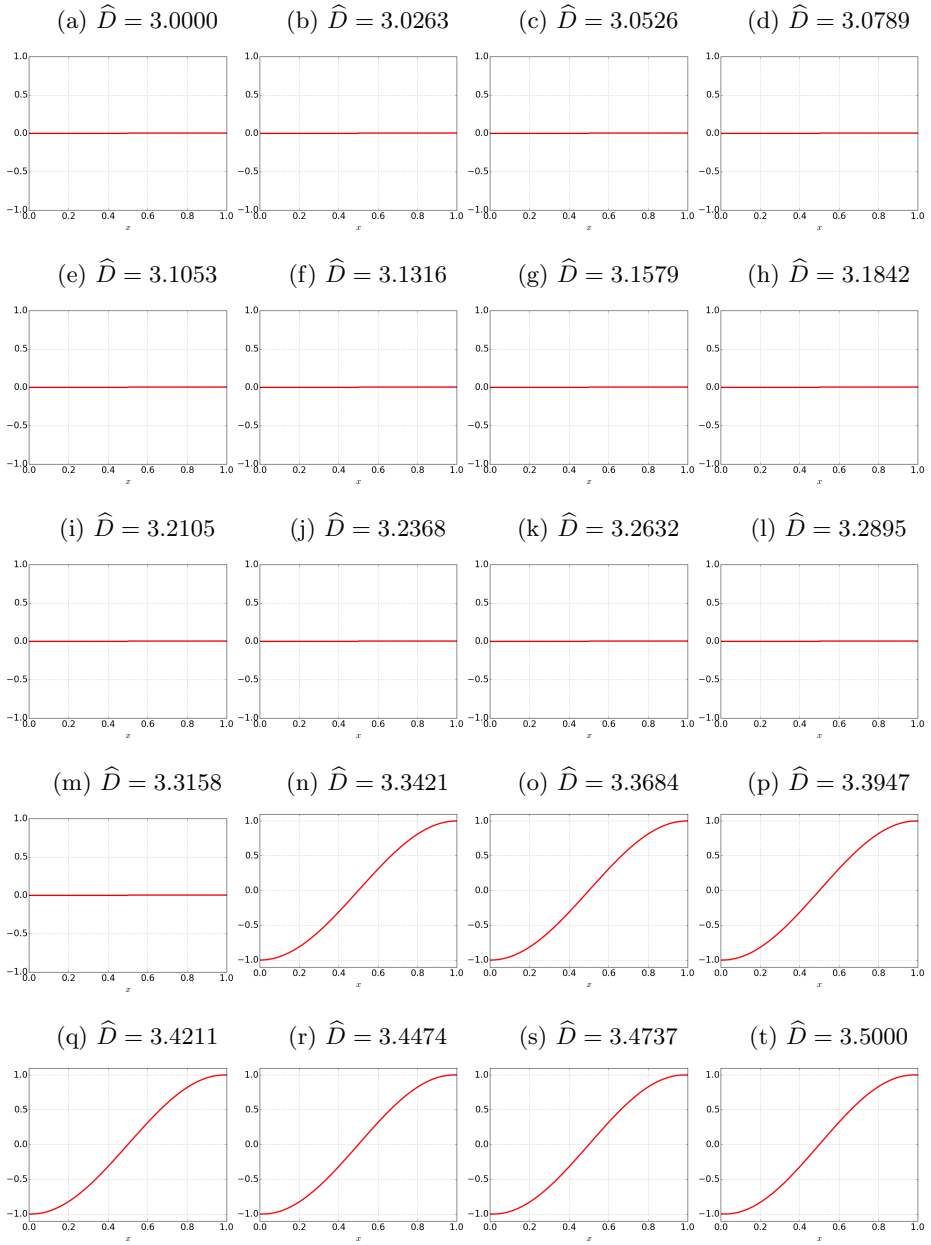

Figure 8.6: Set 2 summary results (part 2 of 2): end-state morphologies for $\widehat{\alpha} = 0.1000$ and varying $\widehat{D} \in (3.0, 3.5)$ as indicated.[13]

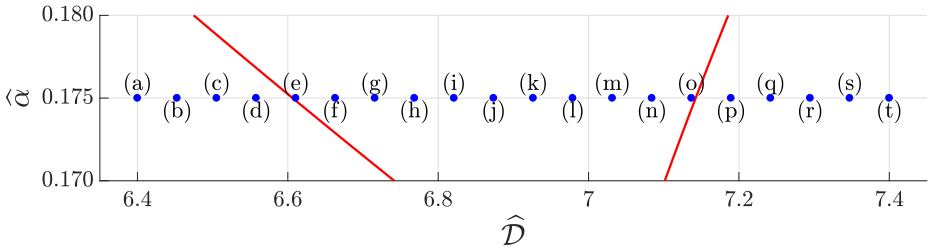

Set 3 parameters. The **red** line is $\widehat{\alpha} = \widehat{\alpha}_{\max}\left(\widehat{\mathcal{D}}\right)$ (cf. (8.4)).

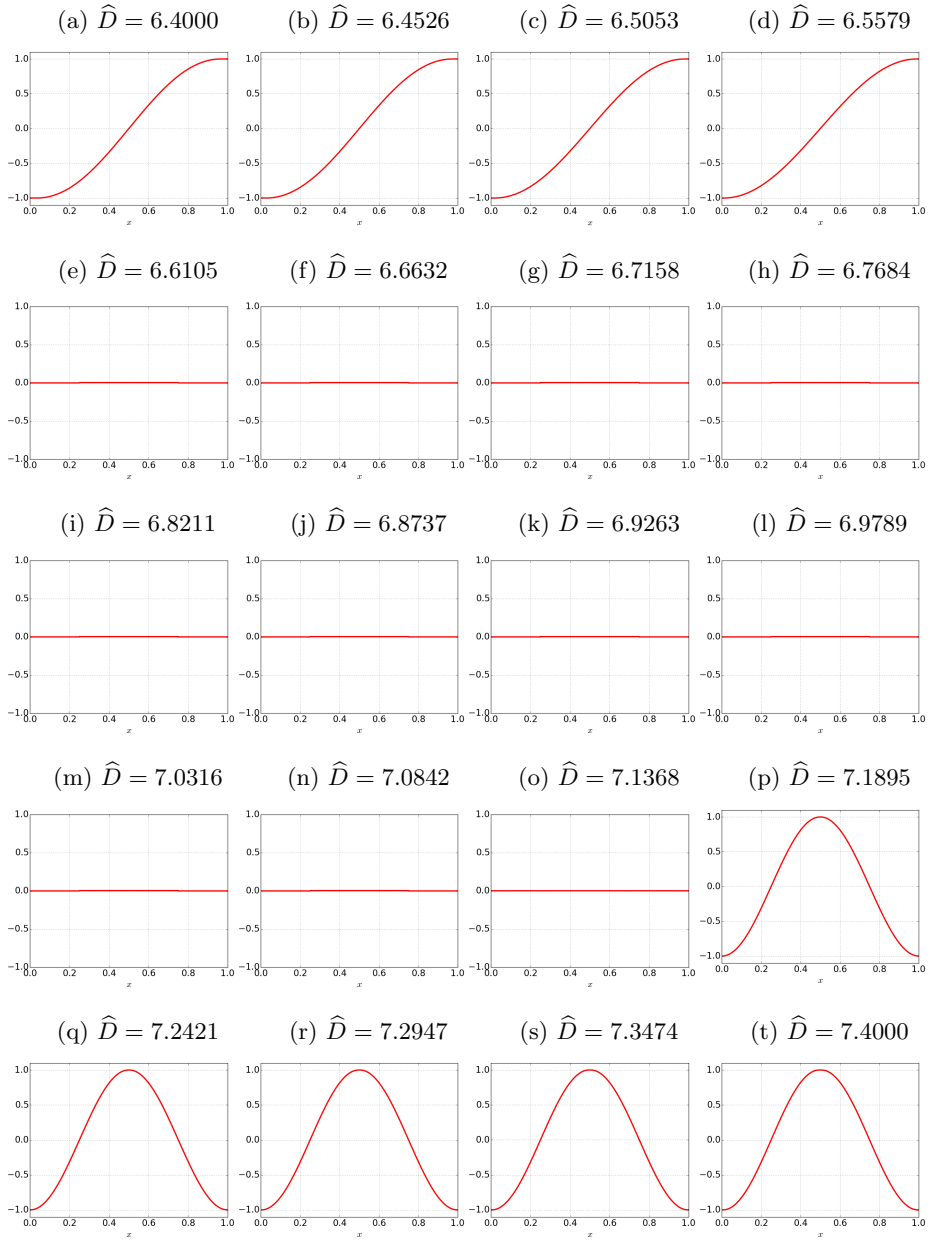

Figure 8.7: Set 3 parameters and summary results: end-state morphologies for $\widehat{\alpha} = 0.175$ and varying $\widehat{D}$ as indicated.[14]

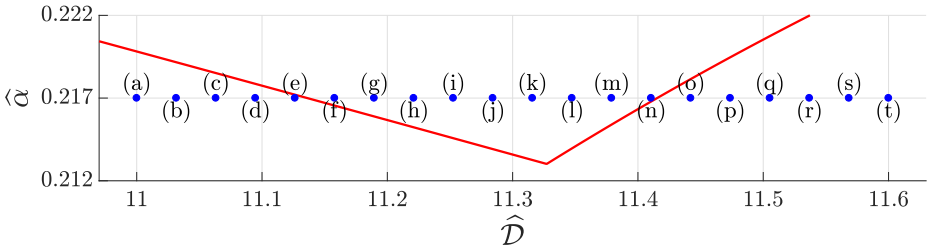

Set 4 parameters: the **red** line is $\widehat{\alpha} = \widehat{\alpha}_{\max}\left(\widehat{\mathcal{D}}\right)$ (cf. (8.4)).

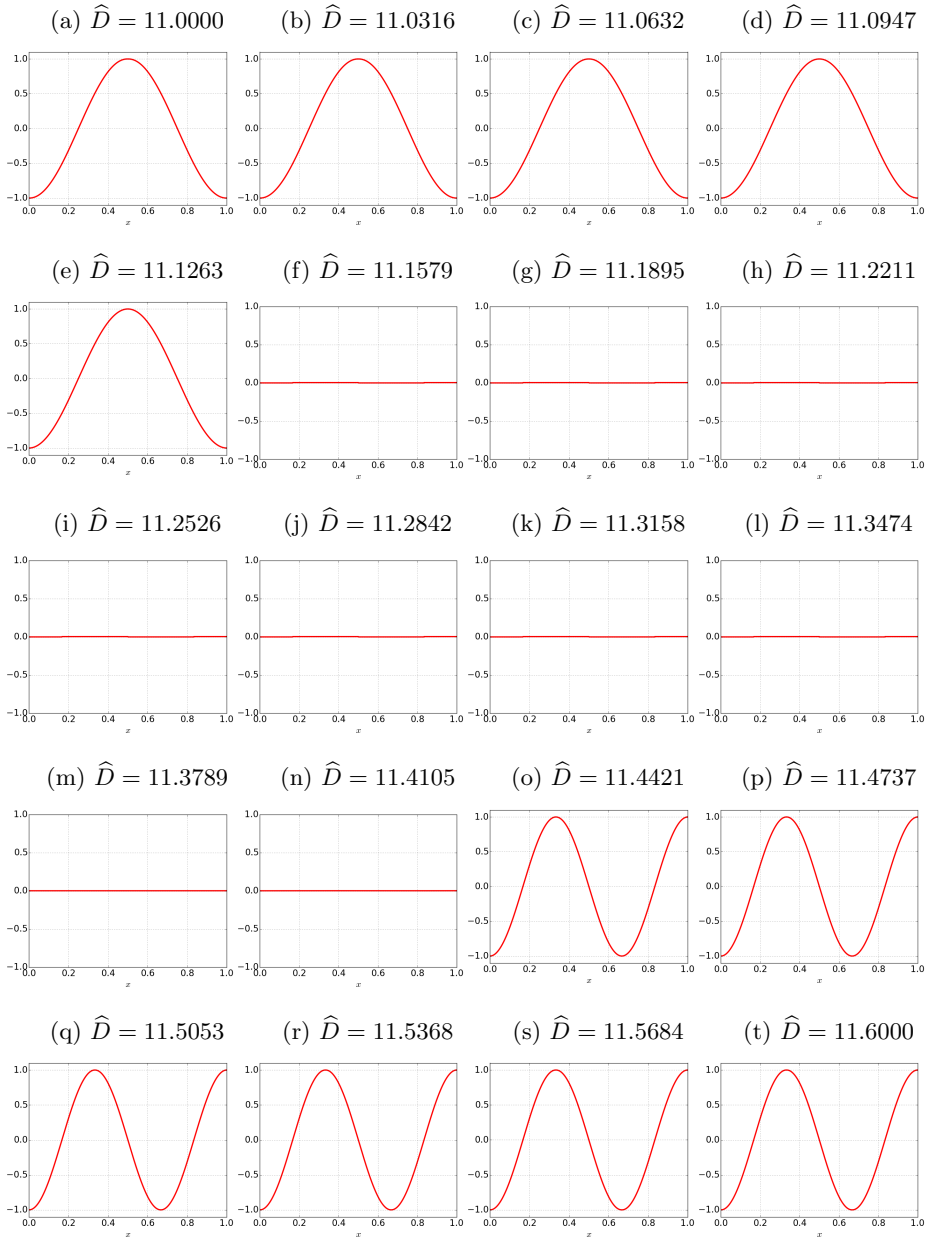

Figure 8.8: Set 4 parameters and summary results: end-state morphologies for $\widehat{\alpha} = 0.217$ and various $\widehat{D}$-values, as indicated.[15]

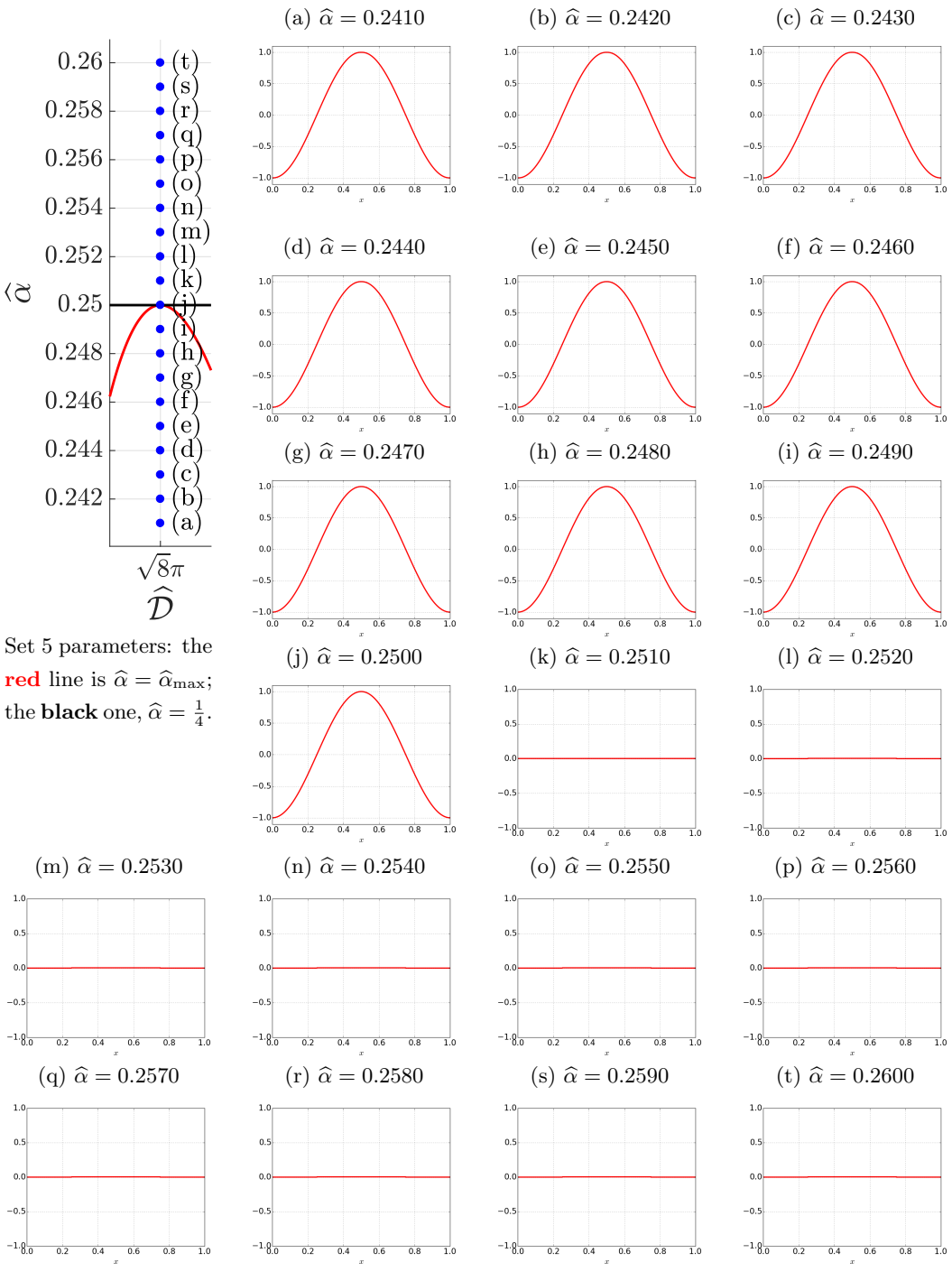

Set 5 parameters: the **red** line is $\widehat{\alpha} = \widehat{\alpha}_{\max}$; the **black** one, $\widehat{\alpha} = \frac{1}{4}$.

Figure 8.9: Set 5 parameters and summary results: end-state morphologies for $\widehat{D} = \sqrt{8}\pi$ and various $\widehat{\alpha}$-values, as indicated.[16]

Discussion and preliminary conclusions

The results above suggest that the global energy minimisers in Regions I and II and for $\widehat{\alpha} \geq \frac{1}{4}$ (the dark blue and white regions of Fig. 8.2) are disordered, whereas the rest of parameter space admits equally spaced, M1I, P2P minimisers with monolayer counts as predicted in the figure. The energies of stationary morphologies appear to be quantised according to the number of P2P layers: our gradient flow experiments were only able to converge at discrete energy levels like those depicted in Fig. 8.3.[17] [18]

Furthermore, the transition from disordered to ordered minimisers is sudden as we exit Regions I and II. In particular:

- The (unique) global energy minimiser inside Region I and where $\widehat{\alpha} > \widehat{\alpha}_{\max}$ is the disordered morphology $\varphi \equiv 0$.
- On the boundaries of Regions I ($\widehat{\mathcal{D}} = \pi/\sqrt{\widehat{q}_h}$, cf. (6.65)) and II ($\widehat{\alpha} = \widehat{\alpha}_{\max} < \frac{1}{4}$, cf. (8.4)), minimisers are not unique. The disordered morphology has the same energy as the P2P morphology predicted by Fig. 8.2.
- For $\left(\widehat{\mathcal{D}}, \widehat{\alpha}\right) = \left(\nu\sqrt{2}\pi, \frac{1}{4}\right)$, $\nu \in \mathbb{N}$ (the red dots along $\widehat{\alpha} = \frac{1}{4}$ in Fig. 8.2), the global minimiser is not unique: the disordered and ν-monolayer morphologies satisfying the *ansatz* (6.25) have equal energies. Setting $c_1 = 1$ and $c_2 = c_3 = c_4 = 0$ in (6.25) gives

$$\widehat{\varphi}\left(\widehat{x}\right) = \sin\left(\frac{\widehat{x}}{\sqrt{2}}\right), \quad -\widehat{\Phi}'\left(\widehat{x}\right) = -\sqrt{2}\cos\left(\frac{\widehat{x}}{\sqrt{2}}\right) \quad \text{on} \quad \widehat{x} \in \left(-\frac{\pi}{\sqrt{2}}, \frac{\pi}{\sqrt{2}}\right). \tag{8.3a}$$

  Using (6.73) with $\widehat{\alpha} = \frac{1}{4}$ and $\widehat{L} = \sqrt{2}\pi$ we find that

$$\widehat{\mathcal{E}}\left[\widehat{\varphi}\right] = \int_{-\pi/\sqrt{2}}^{\pi/\sqrt{2}} \frac{1}{2}\left(\widehat{\varphi}'\right)^2 + \frac{1}{2}\left(1 - \widehat{\varphi}^2\right) + \frac{1}{8}\left(-\widehat{\Phi}'\right)^2 \mathrm{d}\widehat{x}$$
$$= \int_{-\pi/\sqrt{2}}^{\pi/\sqrt{2}} \cos^2\left(\frac{\widehat{x}}{\sqrt{2}}\right) \mathrm{d}\widehat{x} = \frac{\pi}{\sqrt{2}}, \tag{8.3b}$$

  i.e. $\widehat{\mathcal{E}}\left[\widehat{\varphi}\right] = \frac{\widehat{L}}{2}$ which matches what we found for the disordered morphology in (8.1c). Each additional monolayer ($\nu \to \nu + 1$) adds half of the sine wave in (8.3a) to the morphology and $\pi/\sqrt{2}$ to the energy; the result is a P2P morphology with the same energy as $\varphi \equiv 0$. For other values of $\widehat{\mathcal{D}}$ ($\widehat{\alpha} = \frac{1}{4}$), the disordered morphology is the unique, global energy minimiser.

This is all evidence in support of the following conjecture:

Conjecture 8.1.1. (ODT) *The ODT in scaled parameter space is the line* $\widehat{\alpha} = \widehat{\alpha}_{\max}\left(\widehat{\mathcal{D}}\right)$ *from* (6.69).

8.2 Semi-explicit, P2P minimisers

With the confidence gained from the previous section, we now assume that our conclusions in respect of P2P minimisers hold generally, and propose a (semi) explicit, terminating algorithm for finding a (non-unique) P2P energy minimiser for a given $\left(\widehat{\mathcal{D}},\widehat{\alpha}\right)$ in cool parameter space. The main idea is to find that combination of $\left(\nu,\widehat{L},\widehat{\ell}\right)$ that minimises the energy over the set of all equally spaced morphologies associated with a given $\left(\widehat{\mathcal{D}},\widehat{\alpha}\right)$, where in turn we assume *a priori* that $\widehat{\ell}$ is the smallest solution of the associated ID-ELE. It turns out that there are properties of the energy that allow us to bracket ν and search a (relatively) small set of integer values, using a variant of a binary search algorithm. The result is an extremely fast, albeit non-explicit way of finding P2P minimisers.

Conjecture 8.2.1. (Semi-explicit, ordered, cool, global energy minimisers) *If*

$$\widehat{\mathcal{D}} \geq \widetilde{L} = \frac{\pi}{\sqrt{\widehat{q}_h}} \qquad \textit{and} \qquad 0 < \widehat{\alpha} \leq \widehat{\alpha}_{\max}\left(\widehat{\ell}\right) \tag{8.4}$$

as in (6.69)*, then the global energy minimiser is equally spaced and comprised of ν_{opt} identical (translated, reflected) monolayers of width $\widehat{L}_{opt}$, each of which contains a P2P interface layer of width $\widehat{\ell}_{opt}$. In turn, ν_{opt} solves (cf.* (7.21)*)*

$$\nu_{opt} = \arg\min_{\nu\in\mathbb{N}} \mathcal{E}^{(\nu)} \qquad \textit{where} \qquad \mathcal{E}^{(\nu)} := \left\{ \nu\widetilde{\mathcal{E}}\left(\frac{\widehat{\mathcal{D}}}{\nu}, \widehat{\ell}_{opt}\left(\frac{\widehat{\mathcal{D}}}{\nu}\right)\right)\right\} \tag{8.5}$$

where, $\widetilde{\mathcal{E}}\left(\widehat{L},\widehat{\ell}\right)$ is the energy of the monolayer of total width $\widehat{L}$ with single prototypical P2P interface layer $\widetilde{\varphi}^{(\nu)}$ of width $\widehat{\ell}$ (as in Defn 7.2.3). For a candidate monolayer width $\widehat{L} = \frac{\widehat{\mathcal{D}}}{\nu}$, $\widehat{\ell}_{opt}$ should be the smallest, non-zero solution of (6.63)*, viz.*

$$\widehat{\ell}_{opt}\left(\widehat{L}\right) = \min\left\{ \widehat{\ell} > 0 : \widehat{\ell} + \frac{g_{num}\left(\widehat{\ell},\widehat{\alpha}\right)}{c_A\left(\widehat{\ell},\widehat{\alpha}\right)} = \widehat{L} \right\}. \tag{8.6}$$

Two further requirements allow us to bound ν_{opt} from below and above:

i) Individual monolayers cannot be in Region I (because the ID-ELE has no solutions there), and so (cf. (6.65)*)*

$$\frac{\pi}{\sqrt{\widehat{q}_h}} = \widetilde{L} \leq \widehat{L}_{opt}. \tag{8.7a}$$

ii) The interface layers must be M1I with $0 < \widehat{\ell} \leq \widehat{\ell}_{\max}(\widehat{\alpha})$ (i.e. from the left-most yellow patch of Fig. 6.7(a)), and fit in the sense that $\widehat{\ell} \leq \widehat{L}$. In light of (8.6)*, and the fact that $\widetilde{g}$ is an increasing function of $\widehat{\ell}$ (cf.* (6.63a)*)*

$$\widehat{L}_{opt} \leq \widetilde{g}\left(\widehat{\ell}_{\max}\right) =: \widehat{L}_{\max}. \tag{8.7b}$$

Any value of $\widehat{L}_{opt}$ greater than $\widehat{L}_{\max}$ would admit a non M1I solution to (8.6)*.*

Combining these, we find that

$$\widetilde{L} < \widehat{L}_{opt} \leq \widehat{L}_{\max} \qquad \textit{whence} \qquad \lceil \frac{\widehat{\mathcal{D}}}{\widetilde{L}_{\max}} \rceil =: \nu_{\min} \leq \nu_{opt} \leq \nu_{\max} := \lfloor \frac{\widehat{\mathcal{D}}}{\widetilde{L}} \rfloor. \tag{8.7c}$$

ν_{opt} is not generally unique. Only one of the following is true:

a. $\nu_{opt} = 1$ *and* $\mathcal{E}^{(2)} > \mathcal{E}^{(1)}$*;*

b. $\nu_{opt} > 1$ *and either* $\mathcal{E}^{(\nu_{opt}-1)} > \mathcal{E}^{(\nu_{opt})} < \mathcal{E}^{(\nu_{opt}+1)}$ *or* $\nu_{opt} - 1 < \nu_{\min}$ *and* $\mathcal{E}^{(\nu_{opt})} < \mathcal{E}^{(\nu_{opt}+1)}$*;*

c. $\mathcal{E}^{(\nu_{opt})} = \mathcal{E}^{(\nu_{opt}+1)} < \mathcal{E}^{(\nu_{opt}+2)}$*;*

The implication is that there is no need to solve the energy minimisation problem for every $\nu \in \{\nu_{\min}, \ldots, \nu_{\max}\}$. Instead, we can search the set by a modified binary search. We illustrate these effects in Fig. 8.10 with data gathered from our sweep.

The conjecture above forms the basis for a practical way to find $\left(\widehat{L}_{\text{opt}}, \nu_{\text{opt}}, \widehat{\ell}_{\text{opt}}\right)$ for a given $\left(\widehat{\mathcal{D}}, \widehat{\alpha}\right)$ inside the region of P2P minimisers, as follows:

1. Calculate $\widehat{\ell}_{\max}(\widehat{\alpha})$, fix $\widetilde{g}\left(\widehat{\ell}; \widehat{\alpha}\right)$, and calculate $\widehat{L}_{\max}$ and $\nu_{\min}$ as in (8.7b), (8.7c).
2. Calculate $\pi/\sqrt{\widehat{q_h}(\widehat{\alpha})}$, and use it to find $\nu_{\max}$ as in (8.7c).
3. Perform a modified binary search of $\{\nu_{\min}, \ldots, \nu_{\max}\}$. For each ν, determine $\widehat{L} = \frac{\widehat{\mathcal{D}}}{\nu}$ and solve (8.6) to find the corresponding candidate $\widehat{\ell}$. Evaluate the energy of the configuration $\mathcal{E}^{(\nu)}$ using (8.5). ν_{opt} is that value of ν with the smallest $\mathcal{E}^{(\nu)}$.

We compared the results of the technique with those depicted in Fig. 8.2 and found agreement (up to computational rounding/interpolation errors). We then used the process to predict minimisers on a *substantially* bigger block of scaled space, as in Fig. 8.11.[19] [20]

An examination of Fig. 8.2 suggests the following:

Conjecture 8.2.2. (Number of global minimisers) *The symmetric ($m = 0$), 1D energy minimisation problem* (6.1) *has a unique, disordered minimiser ($\varphi \equiv 0$) for $\widehat{\alpha} > \widehat{\alpha}_{\max}$ and up to five global minimisers for $\widehat{\alpha} \leq \widehat{\alpha}_{\max}$. For $\widehat{\alpha} = \widehat{\alpha}_{\max}$, the problem has:*

- *five minimisers where successive 'caps' of the ODT, corresponding to successive r-values in $\widehat{\alpha}_{\max}$ intersect (cf.* (6.69)*): the disordered morphology, two with $\nu = r$ equally spaced monolayers (corresponding to the two possible BCs, $\varphi(0) = \pm 1$; vertical reflections of each other) and, similarly, two with $\nu = r+1$ equally spaced monolayers.*
- *three minimisers elsewhere: the disordered morphology and two with $\nu = r$ equally spaced monolayers.*

For $\widehat{\alpha} < \widehat{\alpha}_{\max}$, the problem has four equally spaced minimisers if $\left(\widehat{\mathcal{D}}, \widehat{\alpha}\right)$ is on a contour line separating two ν_{opt}-values in Fig. 8.2 or 8.11(a). Otherwise, it has two equally spaced minimisers (that are vertical reflections of each other). □

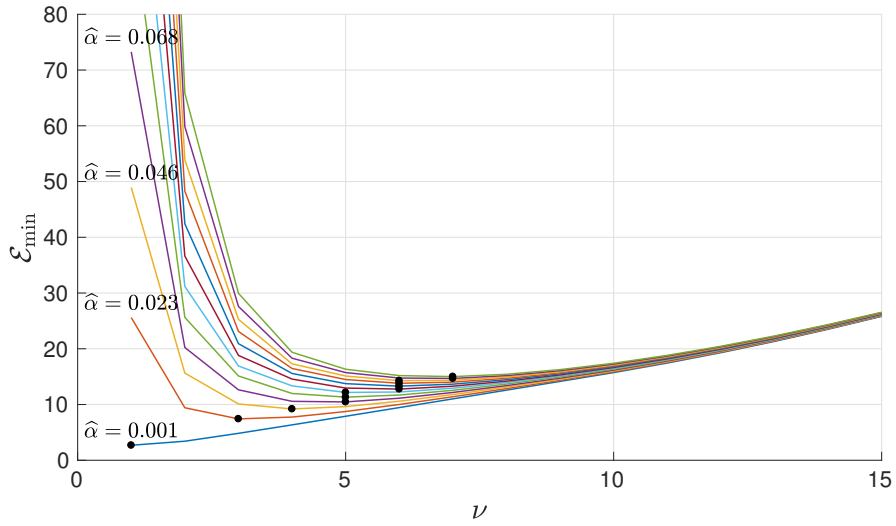

Figure 8.10: Plot of the minimum energy vs layer count ν for twelve equally spaced $\widehat{\alpha}$-values between 0.001 and 0.249. Energy increases with increasing $\widehat{\alpha}$, and is minimised at a particular ν_{opt} for each $\widehat{\alpha}$ (the black dot), increasing to the left and right of this value.[21]

8.2.1 Energy minimisation in un-scaled parameter space

We now summarise the properties of global minimisers in *un-scaled* parameter space, with

$$\mathcal{D} = 1, \quad \chi^{AB} = 1, \quad \alpha \in [0, 400]\,, \quad \text{and} \quad \varepsilon_\varphi \in \left[10^{-3}, 0.5\right] \Leftrightarrow \varepsilon_\varphi^2 \in \left[10^{-6}, 0.25\right]. \tag{8.8a}$$

For these choices of $\mathcal{D}, \chi^{AB}$, the transformations in (6.47) reduce to

$$\widehat{\alpha} = 4\alpha\varepsilon_\varphi^2 \quad \text{and} \quad \widehat{\mathcal{D}} = \frac{1}{\sqrt{2}\varepsilon_\varphi} \quad \Leftrightarrow \quad \alpha = \frac{\widehat{\alpha}\widehat{\mathcal{D}}^2}{2} \quad \text{and} \quad \varepsilon_\varphi = \frac{1}{\sqrt{2}\widehat{\mathcal{D}}}. \tag{8.8b}$$

The boundary of cool parameter space ($\widehat{\alpha} = \frac{1}{4}$), maps to

$$\alpha = \frac{1}{16\varepsilon_\varphi^2}. \tag{8.8c}$$

We map regions of $(\varepsilon_\varphi, \alpha)$–space from/to regions of $\left(\widehat{\mathcal{D}}, \widehat{\alpha}\right)$–space in Fig. 8.12. We map ν_{opt} in scaled parameter space in Fig. 8.12(a) (which is the same as Fig. 7.12, but with equivalent blocks of un-scaled parameter space indicated) to un-scaled space in Fig. 8.12(b). Lines of constant α in Fig. 8.12(a) are found by eliminating ε_φ in (8.8b) to arrive at

$$\widehat{\alpha}\widehat{\mathcal{D}}^2 = 2\alpha. \tag{8.8d}$$

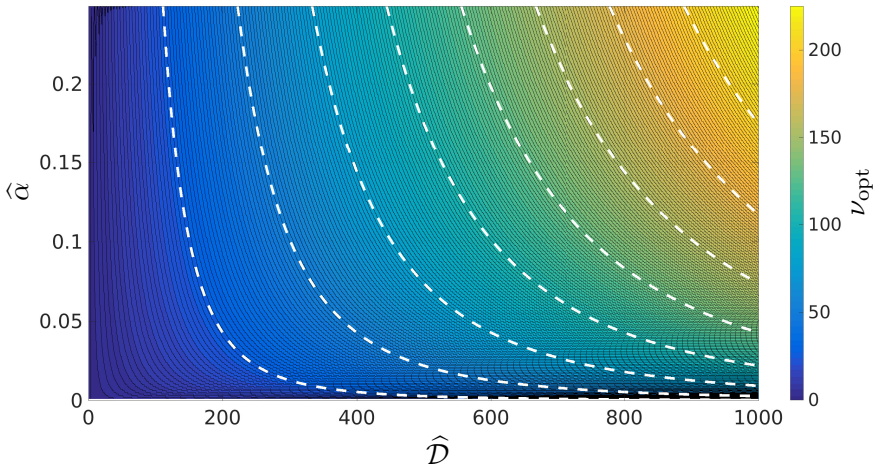

(a) ν_{opt} over scaled parameter space (ordered minimisers) for $0 < \widehat{\mathcal{D}} \leq 1000$. On these length scales, we achieve structures with ~ 200 layers. The dashed white lines are discussed in Section 8.5.

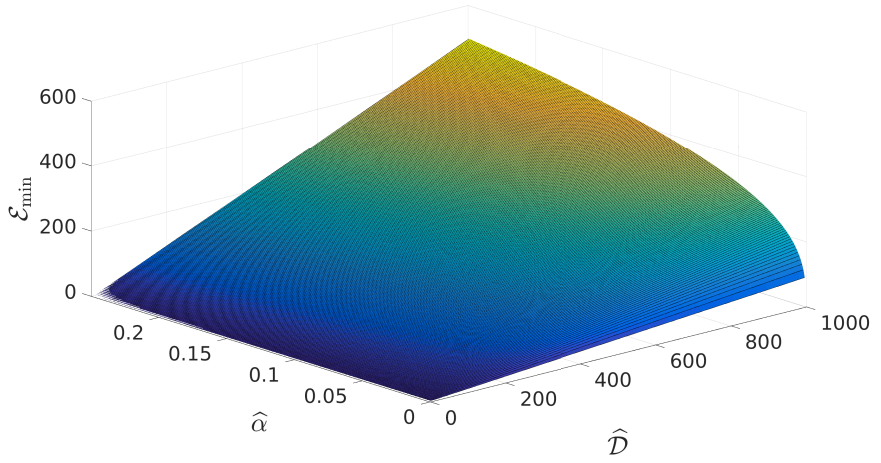

(b) $\mathcal{E}_{\text{min}}$ surface over scaled parameter space (ordered minimisers) for $0 < \widehat{\mathcal{D}} \leq 1000$.

Figure 8.11: P2P minimisers over cool parameter space (with $0 < \widehat{\mathcal{D}} \leq 1000$) constructed using Conjecture 8.2.1. These results greatly extend those depicted in Fig. 8.1 (but match those up to numerical and rounding errors on $0 < \widehat{\mathcal{D}} \leq 75$).[22]

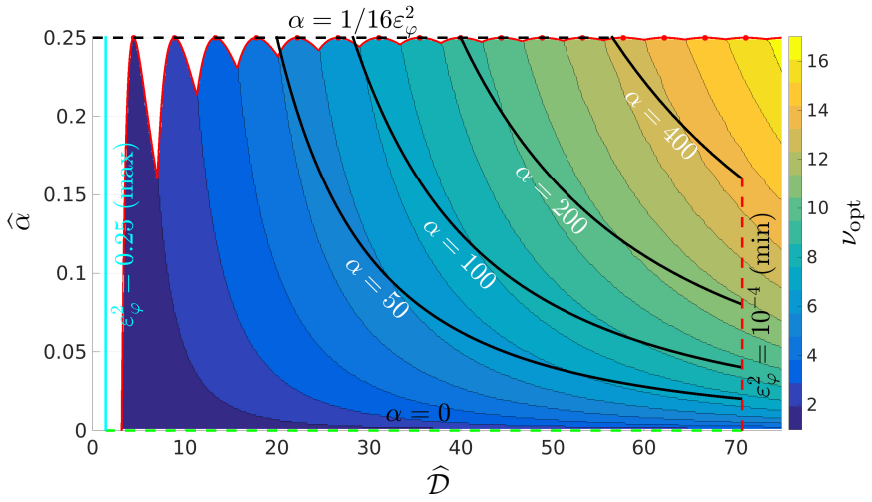

(a) Blocks of un-scaled parameter space over a contour plot of ν_{opt}, for $\mathcal{D} = 1$, $\chi^{AB} = 1$, $0.01 \leq \varepsilon_\varphi \leq 0.5$ and $0 \leq \alpha \leq 400$, in scaled $\left(\widehat{\mathcal{D}}, \widehat{\alpha}\right)$–space. For $\mathcal{D} = 1$ and $\chi^{AB} = 1$, (8.8b) specifies that $\varepsilon_\varphi^2 = 10^{-4}$ occurs on the dashed **red** line at $\widehat{\mathcal{D}} = 70.7$; $\varepsilon_\varphi^2 = 0.25$ is on the **cyan** line inside Region I at $\widehat{\mathcal{D}} = 1.4$ (where the global minimisers are disordered).

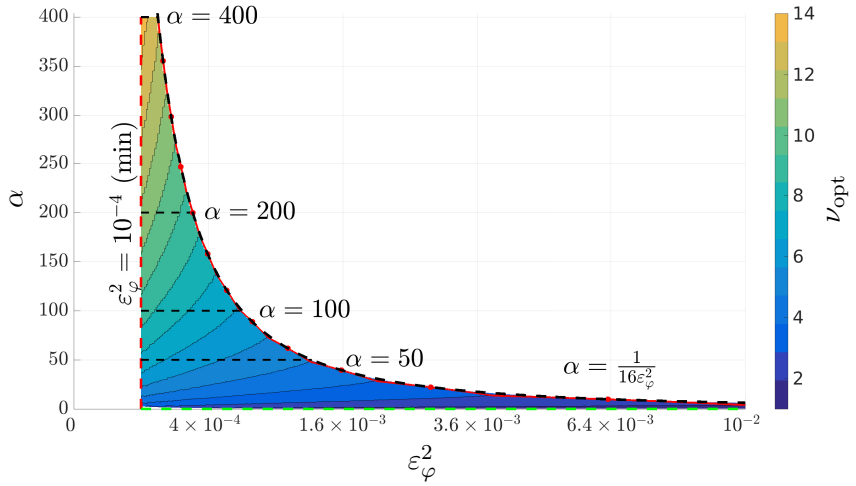

(b) ν_{opt} in un-scaled $\left(\varepsilon_\varphi^2, \alpha\right)$–parameter space for varying ε_φ and α (for $\varepsilon_\varphi^2 \leq 0.01$). The dimpling effect of the **red** ODT is barely visible.

Figure 8.12: Energy-minimising (equally spaced) layer counts for $\mathcal{D} = 1$, $\chi^{AB} = 1$ and varying ε_φ and α. The thick, black dashed line represents $\widehat{\alpha} = \frac{1}{4}$ (equivalent to $\alpha = 1/16\varepsilon_\varphi^2$). The ODT is solid **red** and its intersections with $\widehat{\alpha} = \frac{1}{4}$ are marked with **red** dots. We include lines corresponding to $\alpha \in \{50, 100, 200, 400\}$ in scaled and un-scaled space.[23] [24]

8.3 Comparison with Cahn–Hilliard: the effect of $\alpha = 0$

We now compare our results with those for the Cahn–Hilliard $\alpha = 0$ ($\widehat{\alpha} = 0$) case. For reference we consider Section 3.2 of Blowey and Elliott (1991), especially their Theorem 3.6 which states that Cahn–Hilliard energy minimisers are those with the thinnest interface layers.

There are two differences for $\alpha = 0$: i) the Cahn–Hilliard Euler–Lagrange Equation (ELE) is a second order differential equation, not an integro-differential equation, and ii) there is no non-local energy. There is no energy in the pure phase regions and the location of the interface layers is limited only by mass constraints (their spacing may vary without changing the energy). That said, visually taking $\widehat{\alpha} \downarrow 0$ in Fig. 8.2 suggests that the global energy minimiser for $\widehat{\alpha} = 0$ is disordered for $\widehat{\mathcal{D}} \leq \pi$, and a single P2P layer in the middle of the domain (which is trivially equally spaced) to ensure $\overline{\varphi} = 0$, for $\widehat{\mathcal{D}} \geq \pi$.

The Euler-Lagrange equation, energy, stationarity

For $\alpha = 0$, the ELE is the *differential* equation

$$\varepsilon_\varphi^2 \widetilde{\varphi}'' + \frac{\chi^{AB}}{2}\left(\widetilde{\varphi} - \frac{x_L + x_R}{x_R - x_L}\right) = 0 \tag{8.9}$$

for $x \in (x_L, x_R)$. Setting

$$\widetilde{\varphi} - \frac{x_L + x_R}{x_R - x_L} = \mathrm{e}^{px}$$

leads to the auxiliary equation

$$\varepsilon_\varphi^2 p^2 + \frac{\chi^{AB}}{2} = 0 \qquad \Rightarrow \qquad p = \pm i\sqrt{q}; \qquad q := \frac{\chi^{AB}}{2\varepsilon_\varphi^2} > 0, \tag{8.10}$$

for $\chi^{AB} > 0, \varepsilon_\varphi \in \mathbb{R}$ i.e. the roots of the auxiliary equation are in a (strictly) complex conjugate pair. We are thus led to the general solution

$$\widetilde{\varphi}(x) = \frac{x_L + x_R}{x_R - x_L} + c_1 \sin(\sqrt{q}x) + c_2 \cos(\sqrt{q}x) \tag{8.11}$$

for the interface layer. Arguing in much the same way we did for the $\alpha > 0$ case, assuming the same BA *ansatz* and BCs, we find that stationary P2P interface layers must have zero mass (cf. Case A and (3.19) of Blowey and Elliott (1991)), which leads us to conclude (for a symmetric domain) that $x_R = -x_L = \frac{\ell}{2}$, so that (8.11) reduces to

$$\widetilde{\varphi}(x) = \sin\left(\sqrt{\frac{\chi^{AB}}{2\varepsilon_\varphi^2}}x\right) \qquad \text{for} \qquad x \in \left(-\frac{\pi\varepsilon_\varphi}{\sqrt{2\chi^{AB}}}, \frac{\pi\varepsilon_\varphi}{\sqrt{2\chi^{AB}}}\right). \tag{8.12}$$

There is one interfacial width, $\ell = \sqrt{2}\pi\varepsilon_\varphi/\sqrt{\chi^{AB}}$, which is quite unlike the $\alpha > 0$ case.

Scaling, single monolayer morphology characteristics

We now scale the problem from $(0, \mathcal{D}) \to \left(0, \widehat{\mathcal{D}}\right)$ (there is no $\widehat{\alpha}$ this time) as we did in Section 6.2. Setting $x = s\widehat{x}$ with

$$s = \sqrt{\frac{2\varepsilon_\varphi^2}{\chi^{AB}}} \tag{6.41}$$

leads from (8.12) to the (scaled), prototypical stationary single monolayer

$$\widetilde{\widehat{\varphi}}\left(\widehat{x}\right) = \sin\left(\widehat{x}\right) \qquad \text{for} \qquad \widehat{x} \in \left(-\frac{\pi}{2}, \frac{\pi}{2}\right), \tag{8.13}$$

viz. $\widehat{\ell} = \pi$ (half the period of the sine function). The ELE becomes (cf. (6.43a))

$$\widetilde{\widehat{\varphi}}'' + \widetilde{\widehat{\varphi}} = 0. \tag{8.14}$$

If we define Region I as $0 < \widehat{x} \leq \pi$, we see that our ELE has no solutions there (the $\alpha > 0$ ID-ELE had no solutions in Region I either) because stationary interface layers cannot fit inside monolayers of width $\widehat{L} < \pi$.

Energy minimisation

The scaled and un-scaled energies of a single monolayer morphology are related via (cf. (6.73))

$$\mathcal{E}\left[\varphi\right] = \varepsilon_\varphi \sqrt{\frac{\chi^{AB}}{2}} \widehat{\mathcal{E}}\left[\widehat{\varphi}\right]; \quad \widehat{\mathcal{E}}\left[\widehat{\varphi}\right] = \int_0^{\widehat{\mathcal{D}}} \left\{ \frac{1}{2}\left(\widehat{\varphi}'\right)^2 + \frac{1}{2}\left(1 - \widehat{\varphi}^2\right) \right\} \mathrm{d}\widehat{x} = \int_{-\pi/2}^{\pi/2} \cos^2\left(\widehat{x}\right) \, \mathrm{d}\widehat{x} = \frac{\pi}{2} \tag{8.15}$$

which matches Case A in Theorem 3.6 of Blowey and Elliott (1991). The disordered morphology has energy (cf. (8.1))

$$\widehat{\mathcal{E}}\left[\widehat{\varphi} \equiv 0\right] = \frac{\widehat{\mathcal{D}}}{2} \qquad \Rightarrow \qquad \mathcal{E}\left[\varphi \equiv 0\right] = \frac{\chi^{AB}\mathcal{D}}{4} \tag{8.16}$$

which suggests a disordered minimiser for $\widehat{\mathcal{D}} < \pi$, a non-unique minimiser (disordered, single monolayer) at $\widehat{\mathcal{D}} = \pi$ and a single monolayer, P2P minimiser for $\widehat{\mathcal{D}} > \pi$.

It is possible to impose a layer count ν, as we did in the $\widehat{\alpha} > 0$ case, and still have a stationary configuration in the sense that each individual interface layer satisfies the ELE (8.14). The locations of the interface layers are restricted to the extent that we require $\overline{\varphi} = 0$ (there is no non-local energy or $-\Phi'$ function impacting where they must go), but ν itself is restricted in that a scaled domain of width $\widehat{\mathcal{D}}$ only has space for $\lfloor \frac{\widehat{\mathcal{D}}}{\pi} \rfloor$ stationary interface layers (cf. M from Case A in Theorem 3.5 of Blowey and Elliott (1991)). Each additional interface layer contributes a scaled energy of $\frac{\pi}{2}$.

8.4 Implications for modelling phase separation in DBCs

We mentioned in Section 3.1.3 that SCFT theory makes specific predictions about the effects of reducing the temperature on structure formation in DBCs. In this section we explore what our DFT model says in this regard.

We superimpose a set of contours of f_Θ from (6.52) (on p. 127) under cool conditions[25] onto the phase diagram for ν_{opt}, as the dashed white lines in Fig. 8.13 (cf. Fig. 8.2). As the system is cooled (χ^{AB} increased), Fig. 8.13 suggests that the layer count ν_{opt} decreases.[26] This effect is easily explained by what we observed in Fig. 3.2 (p. 35): if the homogeneous density term dominates, and favours phase separation ($\varphi = \pm 1$), we expect a morphology comprised mostly of pure phase sections with minimal interfacial material.[27]

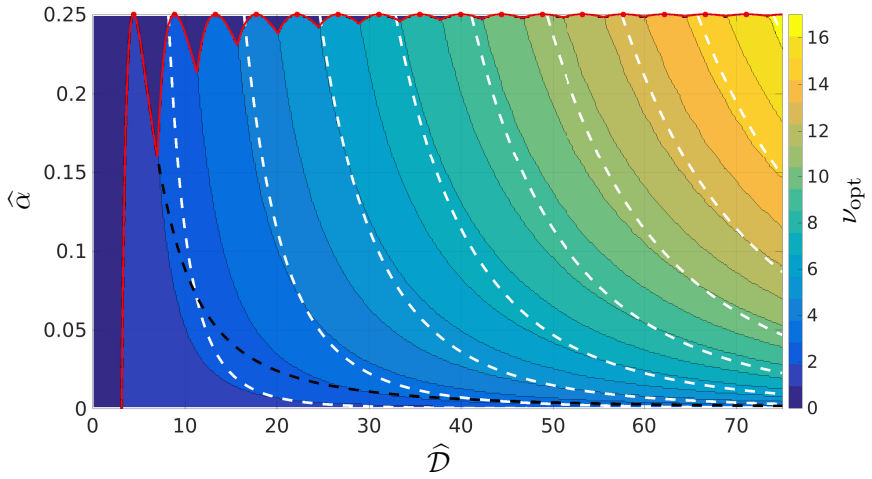

Figure 8.13: Cooling and heating of DBCs. The family of dashed white lines sweeping from top left to bottom right are contours of the function f_Θ we defined in (6.52). Each one represents a different (un-scaled) model $(\varepsilon_\varphi, \alpha, \mathcal{D})$ as it is heated (up and to the left) or cooled (down and to the right). The dashed **black** line is the edge of the cold region; the solid **red** line marks the ODT.[28]

The cold region revisited: segregation regimes

We saw in Section 6.2.4 that any line of cooling (the dashed white lines in Fig. 8.13) will enter the cold region (bounded by the dashed black line) and never leave. In light of this and our other observations, it seems reasonable to propose the following identifications (see the discussion on p. 34 immediately following (3.18)):

- Regions I and II and $\widehat{\alpha} > \frac{1}{4}$ might correspond to the disordered region of DBCs. Persistent structures do not form in these areas of parameter space.

- The SSR could be that region of parameter space in which $\nu_{\text{opt}} = 1$. We showed above that any contour of (6.52) will eventually enter the cold region, but Fig. 8.13 suggests they also, eventually, enter the region in which $\nu_{\text{opt}} = 1$ (viz. the SSR). **Our model predicts that any sufficiently cold model will have a unique, global energy minimiser comprised of a single P2P layer**.

- We might propose that the ISR is that part of the cold region excluding the SSR. Fig. 8.13 suggests that all layer counts in excess of one are possible minimisers in this regime.

- The WSR is the remainder of cool parameter space.

Remark. The second bullet point above suggests that individual molecules can become arbitrarily long if they are cooled to sufficiently low temperatures. This is clearly nonsensical from the perspective of the physics and suggests that the model may only be valid in the ISR and WSR (defined as suggested above).

8.5 Sharp interface limits

We now compare our results with sharp interface limit results. The basic idea is to define a process whereby the interface layers in an energy minimising multi-monolayer morphology are sharpened i.e. their number and locations remain fixed, but each interface layer width $\ell \to 0$. We use the re-scaling of Section 6.2.7.

Energy minimisers are equally spaced (periodic) in the sharp interface limit as $\varepsilon \downarrow 0$ to (at least) first order, according to Choksi (2001), Ohnishi et al. (1999) and the references therein, which is consistent with our claims above for $\varepsilon > 0$.

An informal argument

We consider a ν-layer morphology of width $\mathcal{D}$. To identify the scaling for the optimal number of monolayers, ν_{opt}, and their width

$$L_{\text{opt}} := \frac{\mathcal{D}}{\nu_{\text{opt}}}, \tag{8.17}$$

we need to balance the energy contribution from the interface layers, which *grows* with ν, against that from the long-range interactions, which *decays* with ν. If we assume that a single interface layer can be approximated as (cf. (6.4b))

$$\widetilde{\varphi}(x) \sim \frac{x}{\varepsilon} \qquad \text{having width} \qquad \ell \sim \mathcal{O}(\varepsilon), \tag{8.18}$$

we can estimate the energy of each of the interfacial, homogeneous and long-range contributions to the energy in (6.77):

- Interfacial: since the width of the interface layer scales like ε and the gradient of $\widetilde{\varphi}$ like $1/\varepsilon$, the gradient energy term is $\mathcal{O}(1)$ inside the interface layer (zero elsewhere).
- Homogeneous: the homogeneous energy is $\mathcal{O}(\varepsilon)$ inside each interface layer.

Hence, the total local (interfacial + homogeneous) energy of ν identical, equally spaced interface layers is $\sim \nu\varepsilon$.

- Long-range: for a single monolayer of width $L = \mathcal{D}/\nu$, the energy integrand scales like $\varepsilon\gamma L^2$ (cf. (6.8) and the last term in (6.77)) and is non-zero over the entire width of the monolayer, L. Hence the total long-range energy of ν monolayers is $\sim \nu\varepsilon\gamma L^3$.

We can thus approximate the total energy of such a ν-layer morphology, to first order, as

$$\mathcal{E} \sim \Big(\underbrace{c_1\nu}_{\text{local}} + \underbrace{c_2\nu\gamma L^3}_{\text{non-local}} \Big)\varepsilon = \left(\frac{c_1}{L} + c_2\gamma L^2\right)\varepsilon, \tag{8.19}$$

since $L = \mathcal{D}/\nu$, and $\mathcal{D}$ is a fixed constant that we have absorbed into the second c_1, c_2. For a first order minimiser, we require

$$\left.\frac{\mathrm{d}\mathcal{E}}{\mathrm{d}L}\right|_{L=L_{\text{opt}}} = \frac{-c_1}{L_{\text{opt}}^2} + c_2\gamma L_{\text{opt}} = 0 \qquad \text{viz.} \qquad L_{\text{opt}} \sim \gamma^{-1/3},$$

and so the optimal width depends on γ, *only*. To keep the width and number of monolayers constant for an optimal configuration, we therefore consider the sharp interface limit in which γ and $\mathcal{D}$ are constant as $\varepsilon \downarrow 0$.

Remark. Our γ above corresponds to the $\frac{\sigma}{\varepsilon}$ of Section 2.1 of Choksi et al. (2009). They refer to $\gamma^{-1/3}$ = their $\left(\frac{\varepsilon}{\sigma}\right)^{1/3}$ as the '*intrinsic length for the phase patterns*'.

A formal argument

We now expand our conclusions above using formal asymptotic expansions. The optimal monolayer width $L = L_{\text{opt}}$ is defined as that L for which the energy density $\mathcal{E}_{BA}/L$ in (6.77) is minimal. To find this value in the sharp interface limit, we first determine an asymptotic approximation for the solution of (6.83), as $\varepsilon \downarrow 0$, with γ and $\mathcal{D}$ fixed. We obtain the expansion for ℓ from (6.83c), and

$$q_h = \frac{1}{2\varepsilon^2} - 2\gamma\varepsilon + \mathcal{O}\left(\varepsilon^4\right), \qquad\qquad q_\ell = 2\gamma\varepsilon + \mathcal{O}\left(\varepsilon^4\right) \tag{8.20}$$

(from (6.82)), and then use this to expand the solutions for c_1 and c_3 of (6.83a) and (6.83b). We find (using MAPLE) that

$$\ell \sim \sqrt{2}\pi\varepsilon + 4\gamma L\varepsilon^3, \qquad c_1 \sim \frac{\sqrt{2}}{2}\gamma^{1/2}L\varepsilon^{1/2}, \qquad \text{and} \qquad c_3 \sim 1. \tag{8.21}$$

Using these, we approximate the interface layer in (6.4b) (cf. (8.18)) as

$$\widetilde{\varphi}\,(x) = \frac{x}{\sqrt{2}\pi\varepsilon} + \mathcal{O}\,(\varepsilon)\,; \tag{8.22}$$

substituting this into the energy (6.77) gives, to first order,

$$\mathcal{E}_{BA} \sim \left(\frac{\gamma L^3}{24} + \frac{\pi}{2\sqrt{2}}\right)\varepsilon. \tag{8.23}$$

The energy density $\mathcal{E}_{BA}/L$ is thus minimized (to first order) when

$$\frac{\mathrm{d}}{\mathrm{d}L}\left(\frac{\mathcal{E}_{BA}}{L}\right) \sim \frac{\mathrm{d}}{\mathrm{d}L}\left(\frac{\gamma L^2}{24} + \frac{\pi}{2\sqrt{2}L}\right)\varepsilon = \left(\frac{\gamma L}{12} - \frac{\pi}{2\sqrt{2}L^2}\right)\varepsilon = 0$$

viz. (cf. (8.19))

$$L_{\mathrm{opt}} \sim \frac{\left(3\sqrt{2}\pi\right)^{1/3}}{\gamma^{1/3}}. \tag{8.24}$$

The view in scaled $\left(\widehat{\mathcal{D}}, \widehat{\alpha}\right)$–space

We now take $\varepsilon_\varphi \downarrow 0$ with γ fixed, and map the resulting trajectories in scaled $\left(\widehat{\mathcal{D}}, \widehat{\alpha}\right)$–parameter space. For convenience, we set $\mathcal{D} = 1$ and $\chi^{AB} = 1$ in *un-scaled* parameter space,[29] and define (cf. (6.76))

$$\gamma := \frac{\alpha}{\varepsilon_\varphi} \qquad \text{so that} \qquad \alpha = \varepsilon_\varphi \gamma. \tag{8.25}$$

Substituting this into our scaling equations in (6.47) leads to

$$\widehat{\alpha} = 4\varepsilon_\varphi^3\gamma \quad \text{and} \quad \widehat{\mathcal{D}} = \frac{1}{\sqrt{2}\varepsilon_\varphi} \quad \Rightarrow \quad \widehat{\alpha}\widehat{\mathcal{D}}^3 = \sqrt{2}\gamma \quad \text{viz.} \quad \widehat{\mathcal{D}} = \left(\frac{\sqrt{2}\gamma}{\widehat{\alpha}}\right)^{1/3}, \tag{8.26}$$

upon eliminating ε_φ. Sending $\varepsilon_\varphi \downarrow 0$ on the left of (8.26) has the effect of sending $\widehat{\alpha} \to 0$ and $\widehat{\mathcal{D}} \to \infty$. Superimposing the resulting trajectories over our contour map of ν_{opt} leads to the dashed white lines in Fig's 7.12 and 8.11(a). As $\varepsilon_\varphi \downarrow 0$, we move down and to the right along these lines, each of which maps the effect for a different γ in an (un-scaled) model with $\chi^{AB} = 1$ and $\mathcal{D} = 1$. We expect ν_{opt} to be constant along these trajectories. As expected, the dashed white lines in Fig. 8.11(a) are approximately parallel to the contour lines separating distinct ν_{opt} values. A visual inspection suggests that the gradients of the dashed white sharp interface lines and ν_{opt} contour lines become more similar as ε_φ becomes smaller (down and to the right). This is what we would expect for a first order approximation. Different values of γ can thus be identified (approximately) with distinct ν_{opt} values.

Further opportunities

An examination of Fig. 8.2 indicates that the contour lines separating regions of distinct ν_{opt} in $\left(\widehat{\mathcal{D}}, \widehat{\alpha}\right)$–space, originate from the intersections of successive caps of

$$\widehat{\alpha}\left(\widehat{\ell}\right) = \left(\frac{r\pi}{\widehat{\ell}}\right)^2 \left(1 - \left(\frac{r\pi}{\widehat{\ell}}\right)^2\right), \qquad r \in \mathbb{N}_0, \tag{8.27}$$

corresponding to successive values of r (cf. $\widehat{\alpha}_{\max}$ in (6.69)). These intersections could be found exactly and substituted into a more accurate approximation for the γ–trajectories above. The result would be a family of explicit contours separating parameter space into regions of distinct ν_{opt}. Ideally we would want an exact expression for the ν_{opt} contours, but a good approximation would also be useful. We also reiterate the intriguing relationship between r in (8.27) and ν_{opt} that we summarised in Conjecture 8.2.2. We were unable to explain this, but our results suggest that these two quantities are related.

8.6 The asymmetric case

We close this chapter with a brief survey of the asymmetric problem, $m \neq 0$. In Section 6.1.5.4, the assumption of symmetry yielded several simplifications:

i) each interface layer had zero mass (cf. (6.35)) with $-\Phi'(x_L) = -\Phi'(x_R)$, and could be written as a two-term sum like (6.59b), instead of the five-term (6.24a); and,

ii) the ID-ELE as expressed by the system (6.27) collapsed to the single condition (6.37).

Finding candidate stationary interface layers

Neither of these simplifications applies if $m \neq 0$. However, the process defined in Section 6.1.5 for finding candidate, stationary, single monolayers should still work:

1. Solve the linear system (6.34) to express the coefficients $c_1, \ldots, c_4$ in terms of x_L, x_R;

2. Substitute the results back into the system (6.27) to obtain a 2×2 system of non-linear equations in x_L, x_R, of the form $G = 0$ and $H = 0$, and solve.

We illustrate the process in unscaled parameter space, using the same parameters as in Fig. 6.3, viz. $\varepsilon_\varphi^2 = 10^{-2}$, $\chi^{AB} = 1$, $\alpha = 0.5$, $L = 2$ and $m = \frac{1}{4}$. We plot the zero contours of G and H in (x_L, x_R)–space in Fig. 8.14. As in the symmetric case, the process can generate a number of candidates, corresponding to the intersections of the zero contours above. The two candidates in our example are depicted in Fig. 8.15.[30]

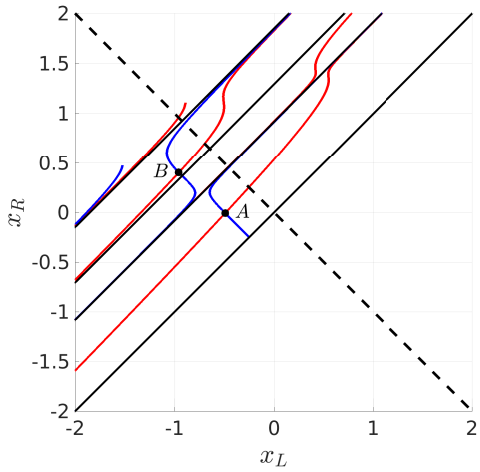

Figure 8.14: Zero contours of G (in **red**) and H (**blue**) as in (6.27) in (x_L, x_R)–space for $x_L < x_R \leq x_L + L$ (viz. $0 < \ell \leq L$, cf. (6.2)) with $\varepsilon_\varphi^2 = 10^{-2}$, $\chi^{AB} = 1$, $\alpha = 0.5$, $L = 2$ and $m = \frac{1}{4}$. The dashed black line is $x_R = -x_L$. The solid black lines of unit gradient are the oblique asymptotes $x_R = x_L + \widetilde{\ell}$ for $\widetilde{\ell}$ a zero of c_A and/or c_B. At these values of ℓ, the candidate c_i coefficients blow up. The process has yielded two candidate minimisers at the points marked A and B.[31]

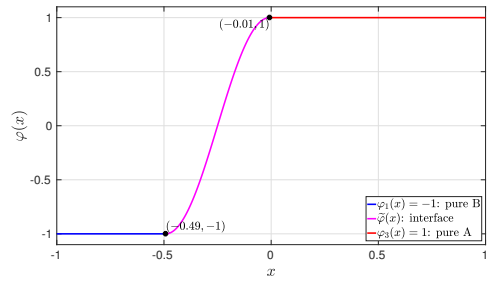

(a) A in Fig. 8.14: $x_L = -0.492$, $x_R = -0.007$, $\ell = 0.485$

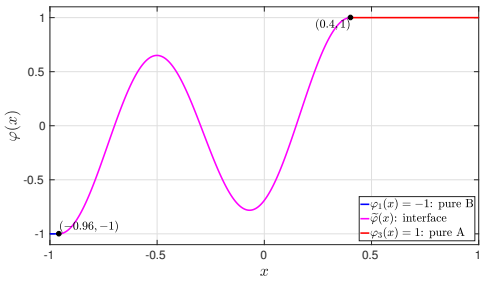

(b) B in Fig. 8.14: $x_L = -0.958$, $x_R = 0.402$, $\ell = 1.360$

Figure 8.15: Two candidate asymmetric minimisers $\widetilde{\varphi}$: both appear to have $\|\widetilde{\varphi}\|_{0,\infty} \leq 1$. Whereas A appears to be of type M1I, B is clearly not.[32]

Towards a demonstration of equal-spacing

There is every reason to expect that our equal-spacing result carries over to the asymmetric case. Some of the anticipated difficulties include:

i) The non-linear 2D system (6.27) admits multiple solutions in (x_L, x_R), in much the same way the 1D (6.37) did in ℓ, for $m = 0$. Whereas it was relatively easy to construct a code to find all of the $m = 0$ solutions (by bracketing solutions between the poles of $\widetilde{g}$), the corresponding $m \neq 0$ process in 2D is likely to be more technically demanding.

ii) The 'cutting and pasting' rearrangements we performed for $m = 0$ should also be possible for $m \neq 0$, taking note, however, that $-\Phi'(x_L) \neq -\Phi'(x_R)$. For instance, with $m = 0$ in Section 7.2.4 (Fig. 7.11), we were able to shift interface layers around at will. Care would need to be exercised to make sure that similar moves are possible if $m \neq 0$.

iii) Using our approach, we would have to perform a numerical convexity demonstration for each m of interest, which is a major weakness. A superior approach would be to establish exactly the convexity of the minimum energy over the space of M1I interface layer functions, for any m (if this statement is indeed true).

iv) In Section 7.2.6, we replaced individual 'wiggly' interface layers with ν_{opt} M1I replacements, and noted that we could reflect the remainder of the morphology if ν_{opt} is even. It is not clear how to do this for $m \neq 0$.

On the other hand, the contours that gave rise to Fig. 6.7 (which in turn governed the regions of physicality, monotonicity etc.) were mass independent, and stemmed from the zero contours of c_A and c_B in the determinant of A in (6.29). We would therefore expect these contours to be of use for $m \neq 0$, too. In the best case, we might hope for the same regions of physicality etc., in the same way that Lemma 6.2.1 was mass independent.

It seems reasonable to hope that the equal-spacing demonstration we devised for the symmetric case might also apply, at least in principle, for $m \neq 0$.

8.7 Summary and conclusions

The most important results of this chapter are:

i) Fig. 8.2: a phase diagram depicting the energy minimising P2P monolayer count ν_{opt} over scaled parameter space, together with a proposal for the location of the ODT (cf. Conjecture 8.1.1) separating ordered and disordered minimisers. The phase diagram resulted from the equal-spacing result of Chapter 7 (cf. Fig. 7.12); here we used gradient flow numerical experiments to further validate it. We also explored the structure transitions across the ODT.

ii) Conjecture 8.2.1: an algorithm for finding P2P minimisers (semi)-explicitly.

iii) We reconciled our results with those of the Cahn–Hilliard case ($\alpha = 0$), and compared our results with those from sharp interface limit analysis. We made proposals relating the SCFT DBC segregation regimes to specific regions of our scaled parameter space. We briefly considered the asymmetric problem.

8.7.1 Discussion, limitations

We have made some bold claims in this and the previous chapter in connection with the global energy minimisers of the symmetric problem in 1D. Our results are certainly suggestive, but by no means rigorous.

A pessimistic perspective

As we noted at the end of the previous chapter, our demonstration of equal-spacing was not rigorous, and there were non-trivial weaknesses in our approach. The most serious outcome would be that the single monolayer minimum energy is not convex (viz. the red dots in Fig. 7.4 are not numerical artefacts) and/or we may be working in the wrong set of interface layer functions (viz. the set of M1I functions). A rigorous proof of our claim of single monolayer minimum energy convexity, a modification to the M1I function set, or a counter example would be required to settle the issue.

An optimistic perspective

On the other hand, there are reasons to be optimistic that our proposed result is valid.

- Most of our pessimism above stems from uncertainty about the validity of our suggestion that the single monolayer minimum energy is a convex function (in Conjecture 7.1.1). Energy convexity is sufficient for our equal-spacing result (at least part of it), but it is not clear that it is necessary. Intuition suggests that some notion of 'sufficient convexity' (viz. that any non-convexity is sufficiently far away from the single monolayer minimum energy) may suffice.

  The most serious consequence of non-convexity would be that it necessarily implies the existence of an unequally spaced energy minimiser. But if this was true, it should be possible to find such a structure for any $\nu_{\text{opt}} > 1$. In this regard, the pulse shift numerical experiments we reported on in Fig. 8.4 are reassuring because we offered the gradient flow process the chance to fall into a (local) energy valley while unequally spaced – and this never happened. These experiments do not constitute a proof (and further tests could be conceived to further investigate this idea), but they are at least consistent with our claim.

- Our proposed global minimisers satisfy the ID-ELE, and also have the smoothness demanded by the theoretical analysis we presented in Chapter 4.

- All of the gradient flow numerical experiments we reported on in the current chapter are consistent with an equal-spacing result. We conducted a number of informal gradient flow experiments which we do not report on here involving much higher

monolayer counts. Every single one converged to something indistinguishable from the equally spaced configuration, with ν_{opt} as predicted in the current chapter.

- Another source of optimism is that our approach (albeit elementary) very closely follows the basic idea developed in Chen and Oshita (2005) (our energy functional is almost a special case of theirs, with their $\gamma = 0$.) They study a homogeneous term that is smoother than ours, but the overall gist of their argument is that energy minimisers have the property that the zeros of $-\Phi'$ (their v_x) '*are equally spaced*' (see their Theorem 2). Ren and Wei (2003) study an energy functional that is very similar to ours. It has a double well instead of double obstacle homogeneous term, but exactly the same non-local term. Key results in this paper are that, in 1D, '*[f]or small ε every global minimum ... is necessarily periodic*', and '*for small ε [the functional] has either two or four global minima*' – this is exactly what we suggested in Conjecture 8.2.2.

  Our proposal is thus consistent with well-established results in the literature, although we believe we have been more explicit in characterising global minimisers and locating them in parameter space.

8.7.2 Opportunities for further study

We close by listing possible extensions to the work in this chapter.

i) A rigorous proof of our equal-spacing result would be extremely desirable. Rigorous results have been found for quite smooth homogeneous energy densities ($C^3(\mathbb{R})$ in Chen and Oshita (2005) and others); these are not directly applicable to our case. However it might be possible to construct a sufficiently smooth regularisation function[33] for our obstacle homogeneous term, apply known equal-spacing results to that, and then take the regularisation parameter $\mu \downarrow 0$ to establish the result for the obstacle term. A more challenging task would be to rigorously establish the fact that interface layers of energy minimisers are always in the set of M1I functions.

ii) The most obvious, and difficult direct extension to the current chapter would involve analysing the **asymmetric** case. We provided some ideas in Section 8.6, which may prove useful in this regard.

iii) We presented $\nu_{\text{opt}}\left(\widehat{\mathcal{D}}, \widehat{\alpha}\right)$ numerically in Fig. 8.2, and offered further experimental evidence in support of its correctness, but we didn't analyse its properties.

  There are other ways to think about our results which may prove fruitful. For instance, we defined and analysed the variable ν_{opt}, the number of monolayers with minimum energy at each point $\left(\widehat{\mathcal{D}}, \widehat{\alpha}\right)$ of parameter space. Another alternative, which might give a useful insight, is the quantity $\widehat{\mathcal{D}}/\nu_{\text{opt}}$ which is the spatial monolayer density.

A related and basic question of interest is how ν_{opt} grows with $\widehat{\mathcal{D}}$ (for given $\widehat{\alpha}$). Our results indicate that energy minimisers on wider domains (bigger $\widehat{\mathcal{D}}$) have more monolayers, as expected, but is $\nu_{\text{opt}} \sim C\widehat{\mathcal{D}}$ (i.e. linear/affine) for fixed $\widehat{\alpha}$? Intuition suggests that it should be (which would correspond to a constant average spatial monolayer density). If so, how does the gradient C vary with $\widehat{\alpha}$? Likewise, we saw in Fig. 8.2 that ν_{opt} increases with $\widehat{\alpha}$ (for fixed $\widehat{\mathcal{D}}$), but we have not analysed this relationship.

iv) **Energy minimisers of the 2-phase double-well (quartic polynomial) approximation in 1D**. In Chapters 6–8 we suggested that 1D minimisers are equally spaced. A key factor in being able to construct Fig. 8.2 was the fact that we could isolate and estimate the energy of a single monolayer. This approach is clearly not (directly) applicable if we use the quartic polynomial $\mathcal{B}_q$ of (3.20) for the homogeneous energy density. However, it should be possible to perform a sweep of $\left(\widehat{\mathcal{D}}, \widehat{\alpha}\right)$-parameter space (using gradient flow methods as we did in Section 8.1.2) and to compare the ν_{opt} resulting from $\mathcal{B}_q$ with what we presented in Fig. 8.2. We might expect the these two functions to yield somewhat similar ν_{opt} functions by virtue of Fig. 8.16. Analysing the effect of $\mathcal{B}$ (the obstacle density) has proved much more tractable than $\mathcal{B}_q$. It might therefore be possible to get an insight into the morphological implications of $\mathcal{B}_q$ by reference to our $\mathcal{B}$ results (although the 1D problem for the double-well problem has been studied in detail – see Ohnishi et al. (1999); Ren and Wei (2003); Chen and Oshita (2005)).

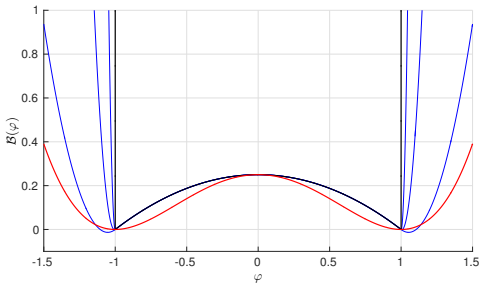

(a) The quadratic double obstacle $\mathcal{B}$ (**black**), its regularised version for various μ (in **blue**, and the quartic approximation $\mathcal{B}_q$ (in **red**). The black and **blue** functions agree exactly for $|\varphi| \leq 1$; $\mathcal{B}_q$ is similar.

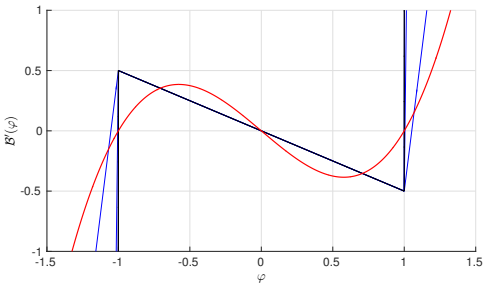

(b) Derivatives of the functions in (a).

Figure 8.16: Comparison of $\mathcal{B}$, $\mathcal{B}_\mu$ and $\mathcal{B}_q$ for $\chi^{AB} = 1$. We might expect $\mathcal{B}_\mu$ and $\mathcal{B}_q$ to lead to similar functions $\nu_{\text{opt}}\left(\widehat{\mathcal{D}}, \widehat{\alpha}\right)$.[34]

Outlook

This concludes our study of 2-phase materials. We now consider 3-phase materials, in which micro-structures inside a polymer are like the 2-phase structures above, and the polymer melt itself has a free surface in contact with a third, void phase.

Notes

[1]This does not necessarily imply that the disordered morphology is the minimiser; merely that the minimiser cannot be P2P.

[2]See the MATLAB numerical experiment `scaled_alpha_L_sweep_1D_2phase.m` in the `bitbucket` repository, and especially `qp_okfef_1D_2phase_compare_zero_const_energy`.

[3]See the MATLAB numerical experiment `scaled_alpha_L_sweep_1D_2phase.m` in the `bitbucket` repository, and especially `qp_okfef_1D_2phase_compare_zero_const_energy`.

[4]The method was fully implicit in all terms, except for the linear/homogeneous term, which was semi-implicit.

[5]We also repeated them with $\mu = 10^{-3}$: the results were structurally very similar, albeit with different energies.

[6]The movement of the pulses in these experiments resembles the process we defined in the evidence for Conjecture 7.2.11.

[7]To be consistent with the Set 3 and 4 experimental design, we might also have considered the disordered IC, but this was unnecessary based on the results observed.

[8]With one exception: the experiment with the 1-monolayer IC leading to Fig. 8.7(e) had to be run for an additional $T \sim 600$ to converge (for a total simulation horizon of $T \sim 1\,000$) The data for this experiment can be found in `exp_run_3215` in http://dx.doi.org/10.6084/m9.figshare.7029002; data for the simulation horizon extension is in http://dx.doi.org/10.6084/m9.figshare.7029035.

[9]See http://dx.doi.org/10.6084/m9.figshare.7028270 for the source data for these 150 experiments.

[10]See `exp_run_1758, exp_run_1764, exp_run_1760, exp_run_1761, exp_run_1762,` and `exp_run_1763` in http://dx.doi.org/10.6084/m9.figshare.7028270 for the source data for this table.

[11]See http://dx.doi.org/10.6084/m9.figshare.7028969 for the source data for these figures.

[12]See `exp_run_3170` to `exp_run_3189` in http://dx.doi.org/10.6084/m9.figshare.7028984 for the source data for these figures.

[13]See `exp_run_3190` to `exp_run_3209` in http://dx.doi.org/10.6084/m9.figshare.7028984 for the source data for these figures.

[14]See http://dx.doi.org/10.6084/m9.figshare.7029002 for the source data for these figures.

[15]See http://dx.doi.org/10.6084/m9.figshare.7029008 for the source data for these figures.

[16]See http://dx.doi.org/10.6084/m9.figshare.7029029 for the source data for these figures.

[17]It is intriguing to think about whether this result captures anything physical about the way DBC molecules form patterns.

[18]We are also able to make some general observations about gradient flow numerical methods:

i) The methods appear to be quite poor at finding the global minimisers for this problem, in the sense that we would have had to let them run longer (bigger T) and/or used smaller time-steps for them to converge to these structures. When offered our theoretical minimisers as ICs, the method was unable to find lower energy morphologies (in the given T), but, likewise, when offered low energy, but non-optimal ICs, it was unable to find the global minimiser (at all). Care should therefore be exercised in examining the results of experiments with, for instance, random ICs. It would be interesting to create ICs satisfying the ID-ELE system (6.92) but with *non-uniform* interface layer thicknesses. Pulse variations of these would also be interesting.

ii) We observed *much* slower convergence in Regions I and II (where the methods were reliable (in the sense that they *always* 'found' the disordered minimiser) than in areas where P2P minimisers were predicted (ones vs up to hundreds of simulated time units). This is one of the primary difficulties in using gradient flow experiments to search for global energy minimisers. We illustrate the issue in Fig. 8.17; see `exp_run_3262` and `exp_run_3263` in http://dx.doi.org/10.6084/m9.figshare.7029008 for

the source data for these experiments.

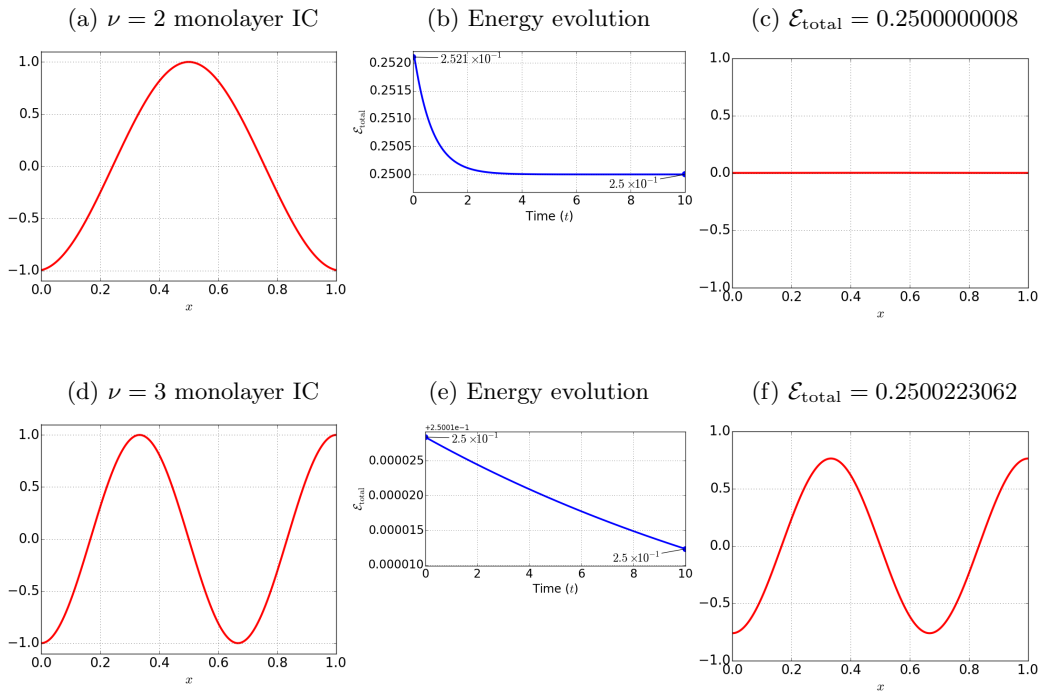

Figure 8.17: Results over the first ten time units for the same experiment with two different ICs illustrate the risk of vastly different timescales ($\widehat{D} = 11.4105$ in Set 4).

Both experiments ran with the same dynamic parameters, differing only in their ICs. Whereas the first experiment converged to the constant minimiser in $T \sim 15$, the second one had to run for a total of $T \sim 350$ (i.e. 20× as long) before it finally converged (also to the constant morphology). We saw in Chapter 4 that the gradient flow problem and our numerical approximation thereof are well-posed and gradient stable under appropriate conditions. These results imply that gradient flow methods can be used to find low energy morphologies, but there are no guarantees about how practical such methods are, and it is quite possible to run experiments with the same dynamic parameters (but different ICs) that require *vastly* different convergence horizons. In the experiments above, these extremes were most pronounced close to the transition from ordered to disordered minimisers. Presumably, this is because on these transitions, the energy differences between these morphologies are very small creating small temporal energy gradients for the gradient flow experiments to exploit.

A comparison of Fig's 8.17(c) and (f) reveals two morphologies that have very similar energies, but quite different structures. A more extreme example of this can be seen in the Set 5 result for $\widehat{\alpha} = \frac{1}{4}$ depicted in Fig. 8.8(j): this 2-monolayer morphology has an energy of *exactly* $\frac{1}{4}$ i.e. precisely the same (to machine precision) as the disordered solution. This is a consequence of the non-uniqueness of minimisers of the problem.

iii) It is worth reiterating that our analysis in Chapter 5 predicts that gradient flow methods with small enough time-steps and large enough T will *eventually* converge to the global energy minimisers.

[19] We implemented this algorithm in MATLAB and `Python;` the relevant codes can be found in the appropriate `bitbucket` repositories. The MATLAB code is `qp_okfef_1D_2phase_energy_MIN.m` in `1D_2phase_sweep/.`

For `Python,` see `utils_from_MATLAB_codes.py` and especially `minimise_alphaset` and `minimise_Dset.`

[20]A re-examination of Fig. 6.7(a) (on p. 134) reveals a significant change at $\widehat{\alpha} = 0.09$: for $\widehat{\alpha} < 0.09$, we observe physical and indeed M1I morphologies for $0 < \widehat{\ell} < \widehat{\ell}_B$, where $\widehat{\ell}_B$ is the smallest non-zero solution of $c_B\left(\widehat{\ell}, \widehat{\alpha}\right) = 0$ (corresponding to the leftmost **red** contour in that Figure). We anticipate that $\widehat{\ell}_{\max}$ can be made arbitrarily close to $\widehat{\ell}_B$. As $\widehat{\alpha} \uparrow 0.09$, we find that $\widehat{\ell}_B \to \widehat{\ell}_A$, where $\widehat{\ell}_A$ is the smallest non-zero solution of $c_A\left(\widehat{\ell}, \widehat{\alpha}\right) = 0$, which is the first pole of $\widetilde{g}$. But that means that $\widehat{\ell}_{\max} \to \widehat{\ell}_A$ at $\widehat{\alpha} = 0.09$, which effectively means that when $\widehat{\alpha} = 0.09$, $\widehat{L}_{\max} \to \infty$ and the range of feasible layer counts becomes infinite (we have to consider every $\nu \in \mathbb{N}$). For $\alpha > 0.09$, we observe the right edge of the space of M1I interface layers (viz. $\widehat{\ell}_{\max}$) moving far away from the first pole of $\widetilde{g}$ (above $\widehat{\alpha} = 0.09$, the left-most green and black contour separates quickly from the right edge of the yellow region of M1I interface layers), suggesting difficulties in the numerical method proposed above near $\widehat{\alpha} = 0.09$.

[21]See the MATLAB numerical experiment `scaled_alpha_L_sweep_1D_2phase.m` in the `bitbucket` repository, and especially `qp_okfef_1D_2phase_plot_energy_vs_nu.`

[22]See the MATLAB numerical experiment `scaled_alpha_L_sweep_1D_2phase.m` in the `bitbucket` repository, and especially `qp_okfef_1D_2phase_scaled_alpha_L_MIN_sweep.`

[23]The (degenerate) case $\alpha = 0$, could be depicted in (a) as an '$\llcorner$'-shaped line along the axes $\widehat{\mathcal{D}} = 0$ and $\widehat{\alpha} = 0$. We draw the relevant portion of this line as the dashed green line along $\widehat{\alpha} = 0$. From (a), it is clear that we would need to increase $\widehat{\mathcal{D}}_{\max}$ to investigate even smaller values of ε_φ. For instance, to investigate energy minimisation down to $\varepsilon_\varphi^2 = 10^{-6}$ (viz. $(\varepsilon_\varphi)_{\min} = 10^{-3}$) with all other parameters held constant, we would need to set,

$$\widehat{\mathcal{D}}_{\max}\left((\varepsilon_\varphi)_{\min} = 10^{-3}\right) = \left.\frac{1}{\sqrt{2}\varepsilon_\varphi}\right|_{\varepsilon_\varphi = 10^{-3}} \approx 710.$$

according to the second part of (8.8b). The graphs of these results were unintelligible.

[24]See the MATLAB working script `plot_Phi_prime_profiles.m` in the `bitbucket` repository.

[25]Each one corresponds to a family of models.

[26]Because the lines of cooling are steeper than the contour lines separating distinct ν_{opt} values.

[27]In the extreme case, we would expect only a single interface layer to ensure the correct total mass (a constant solution is not valid because of the mass constraint).

[28]See the MATLAB numerical experiment `scaled_alpha_L_sweep_1D_2phase.m` in the `bitbucket` repository, and especially `qp_okfef_1D_2phase_compare_zero_const_energy.`

[29]Alternatively we could start from the scaled model of Section 6.2.7.

[30]We have not used the mass condition R from (6.36) in the example. This is because a numerical investigation suggested that $R = 0$ is equivalent to (6.27c) i.e. this is not an additional piece of information. This may ultimately explain the source of the simplification of (6.27) for $m = 0$; we replaced $H = 0$ with $R = 0$.

[31]See the MATLAB numerical experiment `mass_Asymmetric_candidates.m` in the `bitbucket` repository.

[32]See the MATLAB numerical experiment `mass_Asymmetric_candidates.m` in the `bitbucket` repository.

[33]This would have to be smoother than the one we used in Chapter 4.

[34]See the MATLAB code `two_phase_double_obstacle_densities.m` in the `bitbucket` repository.

Part III

Three Phase Materials

Chapter 9

3-Phase materials. Terracing

We are finally in a position to study terracing in DBCs.

Contents

9.1 Modelling 3-phase materials 218
9.2 Energy minimisation and gradient flow dynamics 221
9.3 Symmetric 3-phase materials in 1D 238
9.4 2D terracing: steps 258
9.5 Summary and conclusions 277

Chapter outline

We now study 3-phase materials. We model the situation in which a 2-phase DBC interacts with a third, void phase, which we think of as representing air, a solvent or some other non-interacting fluid. Our approach to modelling and numerical simulations is similar to what we did for 2-phase materials, and extends those ideas. For brevity and so that we can get to our main results in Section 9.4 quickly, the first three sections of this chapter are brief, with much of the detail deferred to Appendix D.

- In Section 9.1, we present our model of 3-phase materials.
- In Section 9.2, we describe the stationary (energy minimisation) and dynamic (gradient flow) problems we wish to solve, and discuss their basic properties. We develop a numerical method to approximate the gradient flow mentioned above.
- Section 9.3 discusses symmetric 3-phase morphologies in 1D.
- In Section 9.4 we consider a class of low energy, symmetric DBC morphologies in 2D that have terraces (steps).

This chapter is based on Parsons et al. (2017), and greatly expands on that manuscript.

9.1 Modelling 3-phase materials

We consider a model for 3-phase materials, with two polymer phases A and B for the monomers comprising a DBC, and a third phase which models the void above a polymer melt. The polymer and void occupy the domain Ω. The main idea, based on Ohta and Ito (1995), Ito (1998) and Choksi and Ren (2005), is that we treat the void as a homopolymer with a very large index of polymerisation and an extremely unfavourable interaction with the two DBC phases. The same approach was used more recently in Stasiak et al. (2012) and Maher et al. (2016) in the context of an SCFT model. We take our free energy from Choksi and Ren (2005) (see their (3.22)–(3.26)) which, in turn, is derived from the SCFT in that reference. According to Maher et al. (2016), ' *SCFT ... is ... the state-of-the-art for block copolymer melts*', which is why we adopt a model derived from it.

9.1.1 Order parameters, incompressibility, mass

We use three order parameters $\phi_A = \phi_A(x)$, $\phi_B = \phi_B(x)$ and $\phi_V = \phi_V(x)$ as the (local) volume fractions (concentrations) of the A, B and V monomer species, in which

$$\boldsymbol{\phi} := (\phi_A, \phi_B, \phi_V) \qquad \text{where each} \qquad \phi_A, \phi_B, \phi_V \in [0,1]\,. \tag{9.1}$$

For matrix indexing, we identify A with the first row/column, B with the second, and V with the third. We impose the incompressibility condition

$$\phi_A + \phi_B + \phi_V = 1. \tag{9.2}$$

Following the example of Ohta and Ito (1995), Ito (1998) and Appendix A of Choksi and Ren (2005) we also define our preferred order parameters:

i) a *micro*-phase separation order parameter $\varphi = \varphi(x)$, with

$$\varphi = \phi_A - \phi_B \tag{9.3a}$$

as the local excess concentration of the A polymer over the B species, where

$$\varphi \in [-1,1] \quad \text{and we identify} \quad \begin{cases} \varphi = 1 \text{ with pure phase } A; \\ \varphi = 0 \text{ with mixed phase } A \text{ and } B; \text{ and} \\ \varphi = -1 \text{ with pure phase } B. \end{cases} \tag{9.3b}$$

Transitions in φ from $\pm 1 \leftrightarrow \mp 1$ correspond to AB interface layers in a way that is consistent with our definitions in two phases (cf. (3.11)).

ii) a *macro*-phase parameter parameter $\psi = \psi(x)$, with

$$\psi = \phi_A + \phi_B. \tag{9.3c}$$

From (9.2) we find that $\psi = 1 - \phi_V$ and so

$$\psi \in [0,1] \qquad \text{and we identify} \qquad \begin{cases} \psi = 0 \text{ with pure void; and} \\ \psi = 1 \text{ with pure melt;} \end{cases} \tag{9.3d}$$

that is, we treat ψ as a device for modelling the separation of the void and the polymer melt. Since $|\nabla\psi| = |\nabla\phi_V|$, transitions in ψ from $0 \leftrightarrow 1$ correspond to polymer–void interface layers.

We depict a sample 3-phase morphology in 1D using (φ, ψ) order parameters in Fig. 9.1.

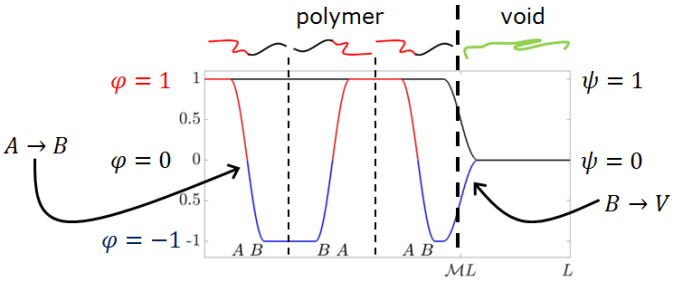

Figure 9.1: A 3-phase morphology in 1D on $[0, L]$, using (φ, ψ) order parameters. φ models the micro-phase separation viz. the AB DBC and ψ, the polymer. An $ABBAABV$ morphology is depicted, with three DBC molecules end-to-end inside a polymer melt (in which $\psi \equiv 1$), which is to the left of a void (in which $\varphi = \psi \equiv 0$). The void is modelled as a homopolymer. Transitions in φ from $\pm 1 \leftrightarrow \mp 1$, inside the melt, correspond to AB interface layers. The polymer–void transition is captured by the transition in ψ from $1 \to 0$ and that in φ from $-1 \to 0$, centred on $\mathcal{M}L$.

The combination of (9.2), (9.3a) and (9.3c) leads to

$$\phi_A = \frac{1}{2}(\psi + \varphi) \qquad \text{and} \qquad \phi_B = \frac{1}{2}(\psi - \varphi) \qquad \text{and} \qquad \phi_V = 1 - \psi. \tag{9.4}$$

The constraint (9.1) is then equivalent to

$$\psi \leq 1 \qquad \text{and} \qquad \psi \geq |\varphi| \qquad \text{a.e. in } \Omega, \tag{9.5}$$

i.e. we require $(\varphi(x), \psi(x)) \in \Omega_\nabla$ for a.e. $x \in \Omega$. We depict Ω_∇ in Fig. 9.2.

P2P transitions (interface layers)

According to (9.3), (9.4),

$$\phi_A = 0 \quad \Leftrightarrow \quad \psi + \varphi = 0; \quad \phi_B = 0 \quad \Leftrightarrow \quad \psi - \varphi = 0; \quad \text{and} \quad \phi_V = 0 \quad \Leftrightarrow \quad \psi = 1, \tag{9.6}$$

each of which corresponds to one of the edges of Ω_∇. We thus identify the edges of Ω_∇ with the three possible *clean* P2P transitions (AB, AV, BV). Conversely, a morphology

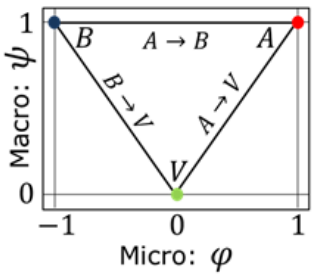

Figure 9.2: The (φ, ψ)–parameter triangle, Ω_∇. Clean P2P transitions run along its edges, as indicated. The pure void at $(\varphi, \psi) = (0, 0)$ is light **green**; pure phase A at $(\varphi, \psi) = (1, 1)$ is **red**, pure B at $(\varphi, \psi) = (-1, 1)$ is **blue**.

with points in (φ, ψ)-space *not* on the edges of Ω_∇, must include phase transitions that are not clean. For instance, the morphology in Fig's 9.21(b), (e) includes a BV transition with some phase A material in it, whereas that in Fig's 9.21(c), (f) has only clean AB and AV transitions.

Remark. We will use the term *internal interface layer* for an AB or BA P2P interface layer (in φ) inside the polymer (where $\psi \equiv 1$). For the transition from the polymer to the void (which involves ψ and φ), we use the term *polymer–void transition.*

Component average masses

As in Choksi and Ren (2005), we assume that the material is comprised of n DBC molecules with polymerisation index N (i.e. each one consists of N monomers of type A or B) and ν type V homopolymer molecules having polymerisation index N_V. Each DBC molecule comprises a linear chain of N_A type A monomers, covalently bonded to a chain of N_B type A monomers i.e. $N_A + N_B = N$ (cf. Fig. 3.1). We assume that:

- all of the monomers have the same average volume so that their molar and volume fractions are equivalent; and
- the domain Ω is completely filled with the material. This leads to the incompressibility condition (9.2).

We define $\mathcal{M}$ as the volume fraction of polymer material inside Ω. In terms of monomers,

$$\mathcal{M} = \frac{\text{total \# of } A, B \text{ monomers}}{\text{total \# of all monomers}} = \frac{nN}{nN + \nu N_V}. \tag{9.7}$$

Consequently, using $\boldsymbol{\phi}$, we define

$$\begin{aligned} a := \overline{\phi_A} &= \frac{N_A}{N}\mathcal{M} = \frac{N_A}{N}\left(\frac{nN}{nN+\nu N_V}\right) = \frac{nN_A}{nN+\nu N_V}; \\ b := \overline{\phi_B} &= \frac{N_B}{N}\mathcal{M} = \frac{N_B}{N}\left(\frac{nN}{nN+\nu N_V}\right) = \frac{nN_B}{nN+\nu N_V}; \\ \text{and} \qquad v := \overline{\phi_V} &= 1-\mathcal{M} = 1-\frac{nN}{nN+\nu N_V} = \frac{\nu N_V}{nN+\nu N_V}, \end{aligned} \tag{9.8a}$$

which is equivalent to (3.26) of Choksi and Ren (2005). That is, a, b and v are the volume (equivalently, the average mass) fractions of the A, B and V phases, viz. $a+b+v=1$. We can thus relate the integral averages of φ and ψ to monomer counts via

$$\overline{\varphi} = a-b = \frac{N_A-N_B}{N}\mathcal{M} \qquad \text{and} \qquad \overline{\psi} = a+b = \frac{N_A+N_B}{N}\mathcal{M} = \mathcal{M} = 1-v. \tag{9.8b}$$

Inside the polymer, we wish to define something akin to the mass we defined for 2-phase materials (cf. (3.1)). We define the *molecular ratio*

$$m := \frac{a-b}{\mathcal{M}} = \frac{a-b}{a+b} = \frac{N_A-N_B}{N} = \frac{\overline{\varphi}}{\overline{\psi}} \quad \text{whence} \quad \overline{\varphi} = m\mathcal{M} = \frac{N_A-N_B}{N}\mathcal{M} = a-b, \tag{9.9}$$

which is consistent with the 2-phase mass of (3.1). We also find that

$$a+b=\mathcal{M}, \qquad a-b=m\mathcal{M} \qquad \Rightarrow \qquad a=\frac{\mathcal{M}\,(1+m)}{2}, \qquad b=\frac{\mathcal{M}\,(1-m)}{2}. \tag{9.10}$$

If we regard 2-phase materials as 3-phase materials with $\mathcal{M}=1$ (i.e. no void), then $m\mathcal{M}=m$ and the two definitions coincide. Crucially, m encodes a a property of the DBC molecule that is independent of $\mathcal{M}$, as follows:

$$m = \frac{\overline{\varphi}}{\overline{\psi}} \in [-1,1] \qquad \text{and} \qquad \begin{cases} m=-1 & \Rightarrow \text{a pure type-}B\text{ DBC;} \\ m=0 & \Rightarrow \text{an equally mixed } A/B\text{ DBC;} \\ m=1 & \Rightarrow \text{a pure type-}A\text{ DBC.} \end{cases} \tag{9.11}$$

We use the term *symmetric* to describe molecules with $m=0$. We can thus gain an understanding of the underlying DBC molecules by measuring $\overline{\varphi}$ and $\overline{\psi}$, and calculating m. We summarise the situation in Fig. 9.3.

9.2 Energy minimisation and gradient flow dynamics

As in two phases, we are ultimately looking to solve an energy minimisation problem. It is possible to work either in the underlying order parameters $\boldsymbol{\phi}$, or in terms of (φ,ψ)-parameters, and there is a process for ensuring consistency between these two formulations. We defer the details of this to Appendix D, and merely state all of the results we need here.

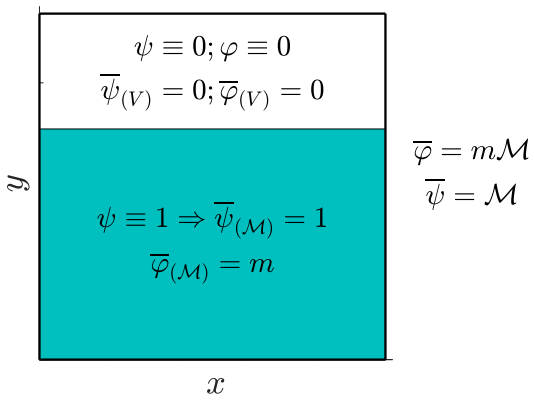

Figure 9.3: A polymer (melt) with a void above, in 2D. The polymer (shaded blue/green) is labelled $\mathcal{M}$ (in which $\psi \equiv 1$ and $\overline{\varphi}_{(\mathcal{M})} = m$), and the (white) void, V (in which $\varphi = \psi \equiv 0$). The molecular ratio is $\frac{\overline{\varphi}}{\overline{\psi}} = m$.[1]

9.2.1 Free energy in three phases ϕ_A, ϕ_B, ϕ_V

We use the free energy in (3.22)–(3.26) of Choksi and Ren (2005), which we write in our notation (cf. Appendix A.2 and (2.15)) as

$$\mathcal{E}(\boldsymbol{\phi}) = \underbrace{\int_\Omega \underbrace{\underbrace{\mathcal{I}(\nabla\boldsymbol{\phi})}_{\text{interfacial}} + \underbrace{\mathcal{N}(\boldsymbol{\phi})}_{\text{non-local}}}_{\text{entropy}} \,\mathrm{d}\Omega}_{} + \underbrace{\int_\Omega \underbrace{\mathcal{B}(\boldsymbol{\phi})}_{\text{bulk}} \,\mathrm{d}\Omega}_{\text{enthalpy}} = \int_\Omega \underbrace{\mathcal{I}(\nabla\boldsymbol{\phi}) + \mathcal{B}(\boldsymbol{\phi})}_{\text{short-range}} + \underbrace{\mathcal{N}(\boldsymbol{\phi})}_{\text{long-range}} \,\mathrm{d}\Omega. \tag{9.12}$$

The minimisation problem we wish to solve is to

$$\text{find } \boldsymbol{\phi} \text{ s.t. } \mathcal{E}(\boldsymbol{\phi}) \to \min \tag{9.13a}$$

subject to the constraints

$$\sum_{i\in\{A,B,V\}} \phi_i(x) = 1 \quad \text{a.e.} \quad \text{and} \quad \|\phi_i\|_{0,\infty} \le 1 \quad \text{for } i \in \{A,B,V\}, \tag{9.13b}$$

and (cf. (9.8a))

$$\overline{\phi_A} = a, \quad \overline{\phi_B} = b \quad \text{and} \quad \overline{\phi_V} = v \quad \text{where} \quad a+b+v = 1. \tag{9.13c}$$

We now describe each component of the energy.

Interfacial energy

The interfacial energy density (cf. (3.5a)) is

$$\mathcal{I}(\nabla\boldsymbol{\phi}) = \frac{1}{2} \sum_{i,j\in\{A,B,V\}} \varepsilon_{ij}^2 \,|\nabla\phi_i \cdot \nabla\phi_j|. \tag{9.14a}$$

Using the matrix K of Choksi and Ren (2005) (see their (3.23)–(3.27)), we specify that the (symmetric) matrix $\mathcal{I} = \mathcal{I}^\top = \left(\varepsilon_{ij}^2\right)_{i,j\in\{A,B,V\}}$ is (cf. (2.17b) and (3.5b))

$$\mathcal{I} = \frac{\varepsilon^2}{2}\mathrm{diag}\left(\frac{nN+\nu N_V}{nN_A}, \frac{nN+\nu N_V}{nN_B}, \frac{nN+\nu N_V}{\nu N_V}\right) = \frac{\varepsilon^2}{2}\mathrm{diag}\left(\frac{1}{a}, \frac{1}{b}, \frac{1}{1-(a+b)}\right), \tag{9.14b}$$

where[2] $\varepsilon^2 = \ell^2/6$ viz. $\varepsilon = \ell/\sqrt{6}$, and ℓ is the Kuhn statistical length we defined on p. 31. All off-diagonal entries of $\mathcal{I}$ are zero, and

$$\varepsilon_A^2 = \frac{\varepsilon^2}{2a}, \qquad \varepsilon_B^2 = \frac{\varepsilon^2}{2b} \qquad \text{and} \qquad \varepsilon_V^2 = \frac{\varepsilon^2}{2v}. \tag{9.15}$$

Homogeneous energy

As in Choksi and Ren (2003, 2005), we use a symmetric 3×3 monomer interaction parameter matrix $\mathcal{B} = \left(\mathcal{B}^{km}\right)$ (their V, our $\mathcal{B}$) to denote the interaction between the three underlying phases ϕ_A, ϕ_B, ϕ_V. The entries $\mathcal{B}^{km}$ are all positive, the '*interaction is short ranged, and* $\mathcal{B}^{km}$ *is large compared to* $\mathcal{B}^{kk}$ *and* $\mathcal{B}^{mm}$ *for all* $k, m \in \{A, B, C\}, k \neq m$' i.e. the off-diagonal terms are relatively large. We use the same label for the matrix $\mathcal{B}$, and the density function[3]

$$\mathcal{B}(\boldsymbol{\phi}) = \begin{cases} \dfrac{1}{2\Theta}\left(\displaystyle\sum_{k,m\in\{A,B,V\}} \mathcal{B}^{km}\phi_k\phi_m - \sum_{k\in\{A,B,V\}} \mathcal{B}^{kk}\phi_k\right) & \sum\phi_k = 1; \phi_k \geq 0 \\ \infty & \text{otherwise,} \end{cases} \tag{9.16}$$

where Θ denotes the absolute temperature.[4] The linear terms are added for convenience, and imply that $\mathcal{B}(\boldsymbol{\phi}) \geq 0$ for all $\boldsymbol{\phi}$ and is zero for pure phases, viz.

$$\mathcal{B}(\boldsymbol{\phi}) = 0 \qquad \Leftrightarrow \qquad \boldsymbol{\phi} \in \{(1,0,0), (0,1,0), (0,0,1)\}. \tag{9.17}$$

Non-local energy

For the non-local component, we have (cf. (2.19a) and (3.8a))

$$\int_\Omega \mathcal{N}(\boldsymbol{\phi})\,\mathrm{d}\Omega = \frac{1}{2}\sum_{i,j\in\{A,B,V\}} \gamma_{ij}\left(\phi_i - \overline{\phi_i}, \phi_j - \overline{\phi_j}\right)_{-1}, \tag{9.18a}$$

where we define the matrix $\boldsymbol{\Gamma} = \boldsymbol{\Gamma}^\top = \left(\gamma_{ij}^2\right)_{i,j\in\{A,B,V\}}$ of non-local coefficients (cf. (2.19b) and (3.9))

$$\boldsymbol{\Gamma} = \frac{3\varepsilon\gamma_c\mathcal{M}}{2}\begin{pmatrix} \left(\frac{nN+\nu N_V}{nN_A}\right)^2 & -\frac{(nN+\nu N_V)^2}{nN_AN_B} & 0 \\ -\frac{(nN+\nu N_V)^2}{nN_AN_B} & \left(\frac{nN+\nu N_V}{nN_B}\right)^2 & 0 \\ 0 & 0 & 0 \end{pmatrix} = \frac{3\varepsilon\gamma_c\mathcal{M}}{2}\begin{pmatrix} \frac{1}{a^2} & -\frac{1}{ab} & 0 \\ -\frac{1}{ab} & \frac{1}{b^2} & 0 \\ 0 & 0 & 0 \end{pmatrix}, \tag{9.18b}$$

from the matrix J of (3.25) of Choksi and Ren (2005), where, as in (3.23) of that reference,[5]

$$\varepsilon\gamma_c := \frac{6}{\ell^2 N^2} \qquad \text{viz.} \qquad \gamma_c = \frac{6\sqrt{6}}{N^2\ell^3}. \tag{9.18c}$$

The zeros in the bottom row and rightmost column reflect the fact that there are no non-local interactions (i.e. covalent bonds) between the void and the A/B monomers. For completeness, we also define (cf. (3.8b))

$$\Phi_A := (-\Delta_n)^{-1}\left(\phi_A - \overline{\phi_A}\right), \quad \Phi_B := (-\Delta_n)^{-1}\left(\phi_B - \overline{\phi_B}\right), \quad \Phi_V := (-\Delta_n)^{-1}\left(\phi_V - \overline{\phi_V}\right), \tag{9.18d}$$

and, to ensure that the non-local energy is well-defined, demand that[6] (cf. (3.8c))

$$\partial_n\Phi_A|_{\partial\Omega} = \partial_n\Phi_B|_{\partial\Omega} = \partial_n\Phi_V|_{\partial\Omega} = 0 \qquad \text{and} \qquad \overline{\Phi_A} = \overline{\Phi_B} = \overline{\Phi_V} = 0. \tag{9.18e}$$

9.2.2 Free energy in two order parameters (φ, ψ)

Re-stating the energy in terms of φ, ψ from (9.3) yields

$$\begin{aligned}\mathcal{E}(\varphi,\psi) = \int_\Omega \frac{\varepsilon_\psi^2}{2}|\nabla\psi|^2 + \varepsilon_{\varphi\psi}^2|\nabla\psi\cdot\nabla\varphi| + \frac{\varepsilon_\varphi^2}{2}|\nabla\varphi|^2 + \mathcal{B}(\varphi,\psi)\,\mathrm{d}\Omega \\ + \frac{\alpha}{2}\|\varphi-\overline{\varphi}\|_{-1}^2 + \beta\left(\varphi-\overline{\varphi},\psi-\overline{\psi}\right)_{-1} + \frac{\gamma}{2}\left\|\psi-\overline{\psi}\right\|_{-1}^2.\end{aligned} \tag{9.19}$$

The minimisation problem thus transforms to

$$\begin{aligned}\text{find } (\varphi,\psi) \text{ s.t.} \quad \mathcal{E}[\varphi,\psi] = \int_\Omega \Bigg(\underbrace{\frac{\varepsilon_\psi^2}{2}|\nabla\psi|^2 + \varepsilon_{\varphi\psi}^2|\nabla\psi\cdot\nabla\varphi| + \frac{\varepsilon_\varphi^2}{2}|\nabla\varphi|^2}_{\mathcal{I}(\varphi,\psi)} + \mathcal{B}(\varphi,\psi) \\ \underbrace{+\frac{\alpha}{2}\Phi(\varphi-\overline{\varphi}) + \beta\Psi(\varphi-\overline{\varphi}) + \frac{\gamma}{2}\Psi\left(\psi-\overline{\psi}\right)}_{\mathcal{N}(\varphi,\psi)} \Bigg)\,\mathrm{d}\Omega \to \min,\end{aligned} \tag{9.20a}$$

where (cf. (9.18d))

$$\Phi := (-\Delta)^{-1}(\varphi-\overline{\varphi}) \qquad \text{and} \qquad \Psi := (-\Delta)^{-1}\left(\psi-\overline{\psi}\right), \tag{9.20b}$$

with the zero Neumann BCs

$$\partial_n\varphi|_{\partial\Omega} = 0 \qquad \text{and} \qquad \partial_n\psi|_{\partial\Omega} = 0, \tag{9.20c}$$

and where we demand that (cf. (3.21c), (9.18e))

$$\partial_n\Phi|_{\partial\Omega} = \partial_n\Psi|_{\partial\Omega} = 0 \qquad \text{and} \qquad \overline{\Phi} = \overline{\Psi} = 0, \tag{9.20d}$$

to ensure the well-posedness of the (non-local) Poisson equations in (9.20b). We also insist that (9.5) holds (i.e. that $(\varphi(x), \psi(x)) \in \Omega_\nabla$ a.e.), along with the integral constraints

$$\overline{\varphi} = m\mathcal{M} \qquad \text{and} \qquad \overline{\psi} = \mathcal{M}, \tag{9.20e}$$

for given molecular ratio $|m| < 1$ and polymer volume fraction $0 < \mathcal{M} < 1$.

We now relate the parameters in (9.20a) to those in Section 9.2.1. The details and derivation of these connections, are discussed in Appendix D.

Interfacial parameters

We have that

$$\varepsilon_\varphi^2 := \frac{1}{4}\left(\varepsilon_A^2 - 2\varepsilon_{AB}^2 + \varepsilon_B^2\right) = \frac{\varepsilon^2}{8}\left(\frac{a+b}{ab}\right) = \frac{\varepsilon^2}{2\mathcal{M}(1-m^2)}, \tag{9.21a}$$

$$\varepsilon_{\varphi\psi}^2 := \frac{1}{4}\left(\varepsilon_A^2 - \varepsilon_B^2 + 2\varepsilon_{BV}^2 - 2\varepsilon_{AV}^2\right) = \frac{\varepsilon^2}{8}\left(\frac{a-b}{ab}\right) = m\varepsilon_\varphi^2, \tag{9.21b}$$

and

$$\begin{aligned}\varepsilon_\psi^2 &:= \frac{1}{4}\left(\varepsilon_A^2 + \varepsilon_B^2 + 2\varepsilon_{AB}^2 - 4\varepsilon_{AV}^2 - 4\varepsilon_{BV}^2 + 4\varepsilon_V^2\right) \\ &= \frac{\varepsilon^2}{4}\left(\frac{1+\mathcal{M}\left(1-2m^2\right)}{\mathcal{M}(1-\mathcal{M})(1-m^2)}\right) = \varepsilon_\varphi^2 + \frac{\varepsilon^2}{2(1-\mathcal{M})},\end{aligned} \tag{9.21c}$$

after noting (9.15) and using (9.10) to conclude that

$$a = \frac{\mathcal{M}(1+m)}{2}, \qquad b = \frac{\mathcal{M}(1-m)}{2} \qquad \Rightarrow \qquad ab = \frac{\mathcal{M}^2\left(1-m^2\right)}{4}.$$

Remarks.

i) According to (9.21c), $\varepsilon_\psi^2 \geq \varepsilon_\varphi^2$, irrespective of the parameter values, with equality only if $\varepsilon_V^2 = 0$. This is impossible for $\varepsilon > 0$, according to (9.15).

ii) $\varepsilon_{\varphi\psi}^2$ could be negative (since we allow $m < 0$). This anomaly stems from the way we defined $\mathcal{I}$ in (9.14) as a matrix of squares, $\left(\varepsilon_{ij}^2\right)$. We never work with $\varepsilon_{\varphi\psi}$, and so we leave this as-is.[7] For $\varepsilon > 0$, $\varepsilon_{\varphi\psi}^2 = 0 \Leftrightarrow m = 0$.

iii) Each of $\varepsilon_\varphi^2, \varepsilon_{\varphi\psi}^2, \varepsilon_\varphi^2$ is a multiple of ε^2 (which is a multiple of ℓ^2).

iv) $\mathcal{M}$ has a strong effect on ε_φ^2 and ε_ψ^2.

Homogeneous energy density parameters

In order to work in (φ,ψ)-parameters, we define the Flory–Huggins parameters,[8]

$$\chi^{AB} := \frac{1}{\Theta}\left(\mathcal{B}^{AB} - \frac{1}{2}\left(\mathcal{B}^{AA}+\mathcal{B}^{BB}\right)\right) > 0, \tag{9.22a}$$

$$\chi^{AV} := \frac{1}{\Theta}\left(\mathcal{B}^{AV} - \frac{1}{2}\left(\mathcal{B}^{AA}+\mathcal{B}^{VV}\right)\right) > 0, \tag{9.22b}$$

$$\text{and} \qquad \chi^{BV} := \frac{1}{\Theta}\left(\mathcal{B}^{BV} - \frac{1}{2}\left(\mathcal{B}^{BB}+\mathcal{B}^{VV}\right)\right) > 0. \tag{9.22c}$$

In each case, the repulsion between each pair of unlike material phases exceeds the average repulsion of the corresponding pairs of like phases, since the diagonal entries of the matrix $\mathcal{B}$ in (9.16) are relatively small. Using (9.22) and (9.2), we define

$$\begin{aligned}\mathcal{B}(\varphi,\psi) &= \frac{1}{2}\left(\frac{\chi^{AB}}{2}\left(\psi^2-\varphi^2\right)+\chi^{AV}(\psi+\varphi)(1-\psi)+\chi^{BV}(\psi-\varphi)(1-\psi)\right)\\ &= \frac{1}{2}\Bigg(\left(\frac{\chi^{AB}}{2}-\chi^{AV}-\chi^{BV}\right)\psi^2-\frac{\chi^{AB}}{2}\varphi^2-\left(\chi^{AV}-\chi^{BV}\right)\varphi\psi\\ &\qquad +\left(\chi^{AV}+\chi^{BV}\right)\psi+\left(\chi^{AV}-\chi^{BV}\right)\varphi\Bigg),\end{aligned} \tag{9.23a}$$

and then transform (9.16) to (cf. (3.17) and Fig. 9.2)

$$\mathcal{B}_\nabla(\varphi(x),\psi(x)) = \begin{cases}\mathcal{B}(\varphi(x),\psi(x)) & (\varphi(x),\psi(x))\in\Omega_\nabla\\ \infty & \text{otherwise.}\end{cases} \tag{9.23b}$$

As in two phases, with $\mathcal{B}$ defined in this way, configurations with finite energy are those for which $(\varphi,\psi)\notin\Omega_\nabla$ only on a set of measure zero i.e. such morphologies satisfy (9.5). Additionally, as in (9.17), for pure phases,

$$\mathcal{B}_\nabla(0,0) = \mathcal{B}_\nabla(\pm1,1) = 0.$$

Non-local parameters

We have that

$$\alpha := \frac{1}{4}\left(\gamma_A - 2\gamma_{AB} + \gamma_B\right) = \frac{3\varepsilon\gamma_c\mathcal{M}}{8}\left(\frac{a+b}{ab}\right)^2 = \frac{6\varepsilon\gamma_c}{\mathcal{M}\left(1-m^2\right)^2} > 0, \tag{9.24a}$$

$$\beta := \frac{1}{4}\left(\gamma_A - \gamma_B + 2\gamma_{BV} - 2\gamma_{AV}\right) = \frac{3\varepsilon\gamma_c\mathcal{M}}{8}\left(\frac{b^2-a^2}{(ab)^2}\right) = -m\alpha, \tag{9.24b}$$

and

$$\begin{aligned}\gamma &:= \frac{1}{4}\left(\gamma_A+\gamma_B+2\gamma_{AB}-4\gamma_{AV}-4\gamma_{BV}+4\gamma_V\right)\\ &= \frac{3\varepsilon\gamma_c\mathcal{M}}{8}\left(\frac{b-a}{ab}\right)^2 = (-m)^2\alpha = -m\beta,\end{aligned} \tag{9.24c}$$

after using (9.10) and (9.18b).

Remarks.

i) As with the interfacial parameters in (9.21), $\mathcal{M}$ is present in all of the non-local coefficients. Each one is a multiple of $1/\ell^2$.

ii) For $\varepsilon > 0$, $\alpha > 0$ and so $\beta = 0 \Leftrightarrow \gamma = 0 \Leftrightarrow m = 0$.

iii) $\mathcal{N}(\varphi, \psi)$ in (9.20a), is identical to $F_L\{\eta, \phi\}$ in (7) of Ito (1998).

9.2.3 Stationary energy minimisation: variational inequalities

Corresponding to Defn 4.1.1, we have

Definition 9.2.1. (Admissible sets: 3-phase energy minimisation) *Define*

$$\boldsymbol{m} := \mathcal{M}(m, 1)^{\top}, \tag{9.25}$$

and the 3-phase admissible sets

$$\mathscr{A} := \left\{(\varphi, \psi) \in \left(H^1(\Omega)\right)^2 \mid (\varphi(x), \psi(x)) \in \Omega_{\nabla} \text{ a.e. in } \Omega.\right\}, \tag{9.26a}$$

$$\mathscr{A}_{\boldsymbol{m}} := \left\{(\varphi, \psi) \in \mathscr{A} \,|\, \overline{\varphi} = m\mathcal{M},\, \overline{\psi} = \mathcal{M}\right\}. \tag{9.26b}$$

Using these admissible sets, we have the following short-hand for the minimisation problem (cf. the 2-phase problem in (4.24))

$$(\mathbf{M}): \qquad \text{Find } (\varphi, \psi) \in \mathscr{A}_{\boldsymbol{m}} \text{ such that} \qquad \mathcal{E}[\varphi, \psi] = \min_{(\eta,\nu)\in\mathscr{A}_{\boldsymbol{m}}} \mathcal{E}[\eta, \nu] \tag{9.27}$$

with $\mathcal{E}$ as in (9.20a). Corresponding to the 2-phase critical point problem $(\mathbf{S}_C)$ in (4.27b), we have the 3-phase system of inequalities,

$(\mathbf{S}_C)$: Find $(\varphi, \psi) \in \mathscr{A}_{\boldsymbol{m}}$ such that

$$\begin{aligned}\varepsilon_{\varphi}^2(\nabla\varphi, \nabla\nu - \nabla\varphi) + \varepsilon_{\varphi\psi}^2(\nabla\psi, \nabla\nu - \nabla\varphi) + \frac{1}{2}\left(-\chi^{AB}\varphi + \left(\chi^{BV} - \chi^{AV}\right)\psi, \nu - \varphi\right) \\ + \left(\alpha(-\Delta_n)^{-1}(\varphi - \overline{\varphi}) + \beta(-\Delta_n)^{-1}\left(\psi - \overline{\psi}\right), \nu - \varphi\right) \geq 0,\end{aligned} \tag{9.28a}$$

and

$$\begin{aligned}\varepsilon_{\varphi\psi}^2(\nabla\varphi, \nabla\upsilon - \nabla\psi) + \varepsilon_{\psi}^2(\nabla\psi, \nabla\upsilon - \nabla\psi) \\ + \frac{1}{2}\left(\left(\chi^{BV} - \chi^{AV}\right)\varphi + \left(\chi^{AB} - 2\left(\chi^{AV} + \chi^{BV}\right)\right)\psi, \upsilon - \psi\right) \\ + \left(\beta(-\Delta_n)^{-1}(\varphi - \overline{\varphi}) + \gamma(-\Delta_n)^{-1}\left(\psi - \overline{\psi}\right), \upsilon - \psi\right) \geq 0,\end{aligned} \tag{9.28b}$$

for every $(\nu, \upsilon) \in \mathscr{A}_{\boldsymbol{m}}$.

For brevity, we do not prove that the solutions of (9.28) are candidate 3-phase minimisers, viz. solutions of (9.27), but it seems reasonable that this should be the case in light of our work on the 2-phase problem.

9.2.4 Gradient flows

As in two phases, solving the stationary problem above is difficult, and so we resort to gradient flow methods. Corresponding to the 2-phase problem (**P**) in (4.37), we have the 3-phase version of the problem,

(**P**): Find $(\varphi, \psi) \in \mathscr{A}_{\boldsymbol{m}}$ for a.e. $t \in (0,T)$ such that

$$\langle \partial_t \varphi, \nu_1 \rangle + M_\varphi \left[\left(\nabla \omega^{(\varphi)}, \nabla \nu_1 \right) + \left(\alpha \left(\varphi - \overline{\varphi} \right) + \beta \left(\psi - \overline{\psi} \right), \nu_1 \right) \right] = 0, \tag{9.29a}$$

for which

$$\varepsilon_\varphi^2 \left(\nabla \varphi, \nabla \nu - \nabla \varphi \right) + \varepsilon_{\varphi\psi}^2 \left(\nabla \psi, \nabla \nu - \nabla \varphi \right) + \frac{1}{2} \left(-\chi^{AB} \varphi + \left(\chi^{BV} - \chi^{AV} \right) \psi, \nu - \varphi \right) \geq \left(\omega^{(\varphi)}, \nu - \varphi \right), \tag{9.29b}$$

and

$$\langle \partial_t \psi, \nu_3 \rangle + M_\psi \left[\left(\nabla \omega^{(\psi)}, \nabla \nu_3 \right) + \left(\beta \left(\varphi - \overline{\varphi} \right) + \gamma \left(\psi - \overline{\psi} \right), \nu_3 \right) \right] = 0, \tag{9.29c}$$

with

$$\varepsilon_{\varphi\psi}^2 \left(\nabla \varphi, \nabla \upsilon - \nabla \psi \right) + \varepsilon_\psi^2 \left(\nabla \psi, \nabla \upsilon - \nabla \psi \right) + \frac{1}{2} \left(\left(\chi^{BV} - \chi^{AV} \right) \varphi, \upsilon - \psi \right) + \frac{1}{2} \left(\left(\chi^{AB} - 2 \left(\chi^{AV} + \chi^{BV} \right) \right) \psi, \upsilon - \psi \right) \geq \left(\omega^{(\psi)}, \upsilon - \psi \right) \tag{9.29d}$$

for any $\nu_1, \nu_3 \in H^1(\Omega)$ and $(\nu, \upsilon) \in \mathscr{A}$ and a.e. $t \in (0,T)$, and we have the ICs

$$\varphi(0) = \varphi_0, \qquad \overline{\varphi_0} = m\mathcal{M} \qquad \text{and} \qquad \psi(0) = \psi_0, \qquad \overline{\psi_0} = \mathcal{M}. \tag{9.29e}$$

Corresponding to the 2-phase problem (**Q**) in (4.38), we have

(**Q**): Find $(\varphi(t), \psi(t)) \in \mathscr{A}_{\boldsymbol{m}}$ for a.e. $t \in (0,T)$, such that

$$\frac{1}{M_\varphi} \left((-\Delta_n)^{-1} (\partial_t \varphi), \nu - \varphi \right) + \varepsilon_\varphi^2 \left(\nabla \varphi, \nabla \nu - \nabla \varphi \right) + \varepsilon_{\varphi\psi}^2 \left(\nabla \psi, \nabla \nu - \nabla \varphi \right) + \frac{1}{2} \left(-\chi^{AB} \varphi + \left(\chi^{BV} - \chi^{AV} \right) \psi, \nu - \varphi \right) + \left(\alpha (-\Delta_n)^{-1} \left(\varphi - \overline{\varphi} \right) + \beta (-\Delta_n)^{-1} \left(\psi - \overline{\psi} \right), \nu - \varphi \right) \geq 0, \tag{9.30a}$$

and

$$\frac{1}{M_\psi} \left((-\Delta_n)^{-1} (\partial_t \psi), \upsilon - \psi \right) + \varepsilon_{\varphi\psi}^2 \left(\nabla \varphi, \nabla \upsilon - \nabla \psi \right) + \varepsilon_\psi^2 \left(\nabla \psi, \nabla \upsilon - \nabla \psi \right) + \frac{1}{2} \left(\left(\chi^{BV} - \chi^{AV} \right) \varphi + \left(\chi^{AB} - 2 \left(\chi^{AV} + \chi^{BV} \right) \right) \psi, \upsilon - \psi \right) + \left(\beta (-\Delta_n)^{-1} \left(\varphi - \overline{\varphi} \right) + \gamma (-\Delta_n)^{-1} \left(\psi - \overline{\psi} \right), \upsilon - \psi \right) \geq 0, \tag{9.30b}$$

for any $(\nu, \upsilon) \in \mathscr{A}_{\boldsymbol{m}}$ and a.e. $t \in (0,T)$, and (9.29e) holds.

Remark. While it seems reasonable to pose these problems with $\varphi, \psi \in H^1\left(0,T; \left(H^1(\Omega)\right)'\right) \cap L^\infty\left(0,T; H^1(\Omega)\right)$ and the two potentials $\omega^{(\varphi)}, \omega^{(\psi)} \in L^2\left(0,T; H^1(\Omega)\right)$, as in the 2-phase case, we do not (at this stage) prove that solutions exist in these spaces.

Mobilities

We have introduced the two mobilities M_φ and M_ψ above. Notice that, unlike the 2-phase case, we *cannot* re-scale time to absorb these parameters (unless they are equal). These mobilities should be consistent with the underlying 3-phase dynamics stated in terms of ϕ_A, ϕ_B, ϕ_V, and their mobilities M_A, M_B, M_V. We explore this question in detail in Appendix D.1 and conclude that for $M_A = M_B = M_V$, we need to set (cf. (D.27))

$$M_\psi = \frac{2}{3} \qquad \text{and} \qquad M_\varphi = 2. \tag{9.31}$$

9.2.5 Regularisation

As in two phases, we cannot differentiate $\mathcal{B}_\nabla$ in (9.23b). For a computational model, we again introduce a regularisation parameter $0 < \mu \ll 1$, and replace the obstacle form of $\mathcal{B}_\nabla$ in (9.23b) with (cf. (4.5b))

$$\begin{aligned} \mathcal{B}_\mu(\varphi,\psi) &:= \mathcal{B}(\varphi,\psi) + \Upsilon_\mu(\varphi,\psi), \\ \text{with} \quad \Upsilon_\mu(\varphi,\psi) &:= \frac{1}{2\mu}\left[(\psi-1)_+^2 + (\varphi-\psi)_+^2 + (\varphi+\psi)_-^2\right], \end{aligned} \tag{9.32}$$

where $(\cdot)_+$ indicates the positive, and $(\cdot)_-$ the negative part of the expressions in the bracket. $\mathcal{B}_\mu$ is thus defined for all values of φ and ψ. We will use $\mathcal{E}_\mu$ to denote the regularised energy obtained whenever we replace $\mathcal{B}$ with $\mathcal{B}_\mu$; $\mathcal{E}_\mu$ includes a penalty component defined as (cf. (4.6))

$$\mathcal{E}_{\text{penalty}} := (\Upsilon_\mu(\varphi,\psi), 1) > 0. \tag{9.33}$$

We expect that $\mathcal{E}_{\text{penalty}} \downarrow 0$ as $\mu \downarrow 0$ (cf. Fig. 9.11(b)). We depict two sample $\mathcal{B}_\mu$ surfaces in Fig. 9.4.

The partial derivatives of $\mathcal{B}_\mu$ in (9.32) are

$$\partial_\varphi \mathcal{B}_\mu(\varphi,\psi) = \frac{1}{2}\left(-\chi^{AB}\varphi + \left(\chi^{BV} - \chi^{AV}\right)\psi + \chi^{AV} - \chi^{BV}\right) + \zeta_\mu^{(\varphi)}(\varphi,\psi), \tag{9.34a}$$

where (cf. (4.8))

$$\zeta^{(\varphi)}(\varphi,\psi) := (\varphi-\psi)_+ + (\varphi+\psi)_- \qquad \text{and} \qquad \zeta_\mu^{(\varphi)}(\varphi,\psi) := \frac{1}{\mu}\zeta^{(\varphi)}(\varphi,\psi), \tag{9.34b}$$

and

$$\begin{aligned} \partial_\psi \mathcal{B}_\mu(\varphi,\psi) = \frac{1}{2}\left(\left(\chi^{BV} - \chi^{AV}\right)\varphi + \left(\chi^{AB} - 2\left(\chi^{AV} + \chi^{BV}\right)\right)\psi + \chi^{AV} + \chi^{BV}\right) \\ + \zeta_\mu^{(\psi)}(\varphi,\psi), \end{aligned} \tag{9.34c}$$

where (cf. (4.8))

$$\zeta^{(\psi)}(\varphi,\psi) := (\psi-1)_+ - (\varphi-\psi)_+ + (\varphi+\psi)_- \quad \text{and} \quad \zeta_\mu^{(\psi)}(\varphi,\psi) := \frac{1}{\mu}\zeta^{(\psi)}(\varphi,\psi). \tag{9.34d}$$

We drop the constants in these derivatives as they have no impact on the gradient flow dynamics. Each derivative is (piecewise) *linear* in (φ,ψ) as can be seen in Fig. 9.5.

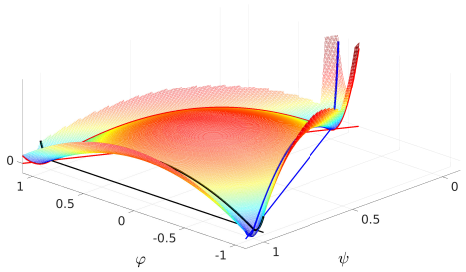

(a) The χ-symmetric case: $\chi^{AB} = \chi^{AV} = \chi^{BV}$

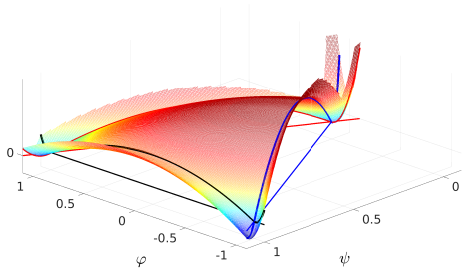

(b) The χ-asymmetric case: $\chi^{BV} > \chi^{AV}$

Figure 9.4: Two regularised homogeneous densities $\mathcal{B}_\mu$ with $\mu = 10^{-3}$, over Ω_∇: in (a), the three Flory–Huggins parameters are equal (to 30). In (b), $\chi^{BV} - \chi^{AV} = 30 > 0$ denoting the fact that BV interactions are more unfavourable (have higher energy) than AV interactions: the surface is visibly higher along the **blue** BV interface line $\varphi + \psi = 0$. The penalty for (φ, ψ) outside of Ω_∇ is clearly visible.[9]

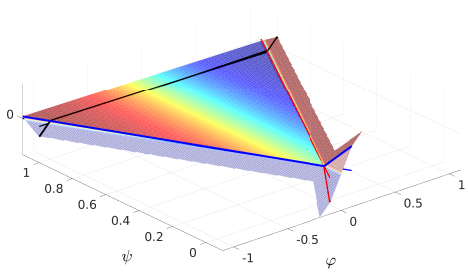

(a) φ partial derivative

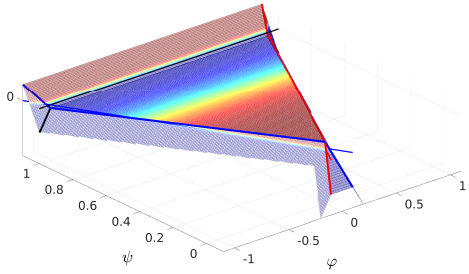

(b) ψ partial derivative

Figure 9.5: φ and ψ partial derivatives of the χ-symmetric surface of Fig. 9.4(a). Both are piecewise linear.[10]

9.2.5.1 Gradient flow dynamics

The dynamics of the regularised system have the form

$$\partial_t \psi_\mu - \Delta\left(M_\psi \frac{\delta \mathcal{E}_\mu}{\delta \psi_\mu}\right) = 0 \qquad \text{and} \qquad \partial_t \varphi_\mu - \Delta\left(M_\varphi \frac{\delta \mathcal{E}_\mu}{\delta \varphi_\mu}\right) = 0, \tag{9.35}$$

or, after splitting the system into four second order problems,

$$\partial_t \varphi_\mu - M_\varphi\left(\Delta \omega_\mu^{(\varphi)} - \left(\alpha\left(\varphi_\mu - \overline{\varphi_\mu}\right) + \beta\left(\psi_\mu - \overline{\psi_\mu}\right)\right)\right) = f_1, \tag{9.36a}$$

$$\omega_\mu^{(\varphi)} = \varepsilon_\varphi^2\left(-\Delta\right)\varphi_\mu + \varepsilon_{\varphi\psi}^2\left(-\Delta\right)\psi_\mu + \partial_{\varphi_\mu}\mathcal{B}_\mu\left(\varphi_\mu, \psi_\mu\right) + F_1; \tag{9.36b}$$

$$\partial_t \psi_\mu - M_\psi\left(\Delta \omega_\mu^{(\psi)} - \left(\beta\left(\varphi_\mu - \overline{\varphi_\mu}\right) + \gamma\left(\psi_\mu - \overline{\psi_\mu}\right)\right)\right) = f_2, \tag{9.36c}$$

$$\omega_\mu^{(\psi)} = \varepsilon_{\varphi\psi}^2\left(-\Delta\right)\varphi_\mu + \varepsilon_\psi^2\left(-\Delta\right)\psi_\mu + \partial_{\psi_\mu}\mathcal{B}_\mu\left(\varphi_\mu, \psi_\mu\right) + F_2. \tag{9.36d}$$

The functions f_1, f_2, F_1, F_2 have been inserted for MMS-testing (cf. Section 5.4.2), and are zero in the underlying model. We impose the zero Neumann boundary conditions (cf. (3.35d))

$$\partial_n \varphi_\mu|_{\partial\Omega} = 0, \qquad \partial_n \omega_\mu^{(\varphi)}\Big|_{\partial\Omega} = 0 \qquad \text{and} \qquad \partial_n \psi_\mu|_{\partial\Omega} = 0, \qquad \partial_n \omega_\mu^{(\psi)}\Big|_{\partial\Omega} = 0, \tag{9.36e}$$

along with the ICs in which $(\varphi_0, \psi_0) \in \mathscr{A}_{\boldsymbol{m}}$ and (cf. (3.35c), (9.8))

$$\psi_\mu(0) = \psi_0, \quad \overline{\psi_0} = a + b = \mathcal{M}, \quad \text{and} \quad \varphi_\mu(0) = \varphi_0, \quad \overline{\varphi_0} = a - b = m\mathcal{M}. \tag{9.36f}$$

Extending the weak form of the 2-phase problem $(\mathbf{P}_\mu)$ in (4.39) to three phases, yields $\left(\mathbf{P}_\mu^{(\mathbf{m})}\right)$: given $0 < \mu \ll 1$, find $\left\{\varphi_\mu, \omega_\mu^{(\varphi)}, \psi_\mu, \omega_\mu^{(\psi)}\right\}$ with $\varphi_\mu, \psi_\mu \in H^1\left(0,T;\left(H^1(\Omega)\right)'\right) \cap L^\infty\left(0,T;H^1(\Omega)\right)$, and $\omega_\mu^{(\varphi)}, \omega_\mu^{(\psi)} \in L^2\left(0,T;H^1(\Omega)\right)$, such that

$$\langle \partial_t \varphi_\mu, \nu_1\rangle + M_\varphi\left[\left(\nabla\omega_\mu^{(\varphi)}, \nabla\nu_1\right) + \left(\alpha\left(\varphi_\mu - \overline{\varphi_\mu}\right) + \beta\left(\psi_\mu - \overline{\psi_\mu}\right), \nu_1\right)\right] = (f_1, \nu_1) \tag{9.37a}$$

where

$$\begin{aligned}\left(\omega_\mu^{(\varphi)}, \nu_2\right) &= \varepsilon_\varphi^2\left(\nabla\varphi_\mu, \nabla\nu_2\right) + \varepsilon_{\varphi\psi}^2\left(\nabla\psi_\mu, \nabla\nu_2\right) \\ &\quad + \frac{1}{2}\left(-\chi^{AB}\varphi_\mu + \left(\chi^{BV} - \chi^{AV}\right)\psi_\mu, \nu_2\right) + \left(\zeta_\mu^{(\varphi)}\left(\varphi_\mu, \psi_\mu\right), \nu_2\right) + \left(F_1, \nu_2\right),\end{aligned} \tag{9.37b}$$

and

$$\langle \partial_t \psi_\mu, \nu_3\rangle + M_\psi\left[\left(\nabla\omega_\mu^{(\psi)}, \nabla\nu_3\right) + \left(\beta\left(\varphi_\mu - \overline{\varphi_\mu}\right) + \gamma\left(\psi_\mu - \overline{\psi_\mu}\right), \nu_3\right)\right] = \left(f_2, \nu_3\right), \tag{9.37c}$$

where, in turn,

$$\begin{aligned}\left(\omega_\mu^{(\psi)}, \nu_4\right) &= \varepsilon_{\varphi\psi}^2\left(\nabla\varphi_\mu, \nabla\nu_4\right) + \varepsilon_\psi^2\left(\nabla\psi_\mu, \nabla\nu_4\right) + \frac{1}{2}\left(\chi^{BV} - \chi^{AV}\right)\left(\varphi_\mu, \nu_4\right) \\ &\quad + \frac{1}{2}\left(\chi^{AB} - 2\left(\chi^{AV} + \chi^{BV}\right)\right)\left(\psi_\mu, \nu_4\right) + \left(\zeta_\mu^{(\psi)}\left(\varphi_\mu, \psi_\mu\right), \nu_4\right) + \left(F_2, \nu_4\right),\end{aligned} \tag{9.37d}$$

for every $\nu_1, \nu_2, \nu_3, \nu_4 \in H^1(\Omega)$ and a.e. $t \in (0,T)$, subject to the ICs (9.36f).

9.2.5.2 Key properties of the regularised dynamics

Recovering the underlying variational inequalities as $\mu \downarrow 0$

We do not perform a full analysis of the 3-phase problem at this stage, but outline the process for recovering the system (9.29) from (9.37) as $\mu \downarrow 0$.

i) First we would need to establish the convergence results of the form (cf. (B.149))

$$\varphi_\mu \rightharpoonup \varphi, \quad \psi_\mu \rightharpoonup \psi \quad \text{in} \quad H^1\left(0,T;\left(H^1(\Omega)\right)'\right) \cap L^2\left(0,T;H^1(\Omega)\right), \tag{9.38a}$$

$$\varphi_\mu \to \varphi, \quad \psi_\mu \to \psi \quad \text{in} \quad L^2(\Omega_T), \tag{9.38b}$$

$$\omega_\mu^{(\varphi)} \rightharpoonup \omega_\varphi, \quad \omega_\mu^{(\psi)} \rightharpoonup \omega_\psi \quad \text{in} \quad L^2\left(0,T;H^1(\Omega)\right) \tag{9.38c}$$

as $\mu \downarrow 0$.

ii) We would then apply these to each of the equations in (9.37).

Working term-by-term in (9.37a) and (9.37c) (by taking appropriate sub-sequences), we could recover (9.29a) and (9.29c). For the remaining two equations, we pick any $(\nu, \upsilon) \in \mathscr{A}$, for which

$$\zeta^{(\varphi)}(\nu, \upsilon) = \zeta^{(\psi)}(\nu, \upsilon) = 0 \quad \text{a.e.} \tag{9.39}$$

Setting $\nu_2 = \nu - \varphi_\mu$ in (9.37b), it should be possible to show that (cf. (B.150))

$$\begin{aligned}\varepsilon_\varphi^2(\nabla\varphi_\mu, \nabla\nu - \nabla\varphi_\mu) + \varepsilon_{\varphi\psi}^2(\nabla\psi_\mu, \nabla\nu - \nabla\varphi_\mu) + \frac{1}{2}\left(-\chi^{AB}\varphi_\mu + \left(\chi^{BV} - \chi^{AV}\right)\psi_\mu, \nu - \varphi_\mu\right) \\ - \left(\omega_\mu^{(\varphi)}, \nu - \varphi_\mu\right) = \frac{1}{\mu}\left(\zeta^{(\varphi)}(\nu, \upsilon) - \zeta^{(\varphi)}(\varphi_\mu, \psi_\mu), \nu - \varphi_\mu\right) \geq 0, \end{aligned} \tag{9.40}$$

since $\zeta^{(\varphi)}$ is monotone non-decreasing in its first coordinate. Likewise, setting $\nu_4 = \upsilon - \psi_\mu$ in (9.37d) should yield

$$\begin{aligned}\varepsilon_{\varphi\psi}^2(\nabla\varphi_\mu, \nabla\upsilon - \nabla\psi_\mu) + \varepsilon_\psi^2(\nabla\psi_\mu, \nabla\upsilon - \nabla\psi_\mu) + \frac{1}{2}\left(\left(\chi^{BV} - \chi^{AV}\right)\varphi_\mu, \upsilon - \psi_\mu\right) \\ + \frac{1}{2}\left(\left(\chi^{AB} - 2\left(\chi^{AV} + \chi^{BV}\right)\right)\psi_\mu, \upsilon - \psi_\mu\right) - \left(\omega_\mu^{(\psi)}, \upsilon - \psi_\mu\right) \\ = \frac{1}{\mu}\left(\zeta^{(\psi)}(\nu, \upsilon) - \zeta^{(\psi)}(\varphi_\mu, \psi_\mu), \upsilon - \psi_\mu\right) \geq 0 \end{aligned} \tag{9.41}$$

since $\zeta^{(\psi)}$ is monotone non-decreasing in its second coordinate.

iii) Finally, we would need to show that the (φ, ψ) in (9.38) are in $\mathscr{A}$ i.e. as in (B.158), that $\zeta^{(\varphi)}(\varphi, \psi) = \zeta^{(\psi)}(\varphi, \psi) = 0$.

Having sketched out the major elements of the constrained 3-phase minimisation problem, we focus now on practical methods for finding low energy morphologies (φ_μ, ψ_μ) that are at least approximately in $\mathscr{A}_{\boldsymbol{m}}$. **From this point forward, we work exclusively with regularised order parameters φ_μ, ψ_μ and their potentials $\omega_\mu^{(\varphi)}$, $\omega_\mu^{(\psi)}$. To simplify the notation, we henceforth omit all solution '$_\mu$' subscripts.**

Mass conservation and control: a local problem

We investigate 3-phase mass conservation and control in detail in Appendix D.3. We replace the non-local elements (9.37a) and (9.37c) of (9.37) (after dropping all μ-subscripts) with

$$\langle \partial_t\varphi, \nu_1\rangle + M_\varphi\left[\left(\nabla\omega^{(\varphi)}, \nabla\nu_1\right) + \left(\alpha(\varphi - m\mathcal{M}) + \beta(\psi - \mathcal{M}), \nu_1\right)\right] = 0 \tag{9.42a}$$

and

$$\langle \partial_t\psi, \nu_3\rangle + M_\psi\left[\left(\nabla\omega^{(\psi)}, \nabla\nu_3\right) + \left(\beta(\varphi - m\mathcal{M}) + \gamma(\psi - \mathcal{M}), \nu_3\right)\right] = 0. \tag{9.42b}$$

We think of $\boldsymbol{m}$ in (9.25) as a 3-phase mass control vector; we have replaced the non-local $\overline{\varphi}$ and $\overline{\psi}$ terms with the components of $\boldsymbol{m}$.

Energy monotonicity (decay)

We make no attempt to generalise the rigorous demonstration of energy monotonicity in two phases (as in Corollary 4.4.2) to the 3-phase case. Rather, we informally demonstrate that the (regularised) energy, $\mathcal{E}_\mu = \mathcal{E}_\mu(t)$, is a non-increasing function of time, under the action of the dynamics above. We use our scalar mobilities to re-arrange (9.35) to

$$\frac{\delta \mathcal{E}_\mu}{\delta \psi} = \frac{-1}{M_\psi}\left(-\Delta_n\right)^{-1}\left(\partial_t \psi\right) \qquad \text{and} \qquad \frac{\delta \mathcal{E}_\mu}{\delta \varphi} = \frac{-1}{M_\varphi}\left(-\Delta_n\right)^{-1}\left(\partial_t \varphi\right).$$

Then

$$\frac{\mathrm{d}\mathcal{E}_\mu}{\mathrm{d}t} = \int_\Omega \frac{\delta \mathcal{E}_\mu}{\delta \varphi}\partial_t \varphi + \frac{\delta \mathcal{E}_\mu}{\delta \psi}\partial_t \psi \,\mathrm{d}\Omega = -\left(\frac{\|\partial_t \psi\|_{-1}^2}{M_\psi} + \frac{\|\partial_t \varphi\|_{-1}^2}{M_\varphi}\right) \leq 0. \tag{9.43}$$

It is this property that makes gradient flows so useful.

Remark. A complete analysis of (9.29) should reveal that $\mathrm{d}\mathcal{E}/\mathrm{d}t \leq 0$ too (i.e. that the exact energy is monotonically non-increasing in time as in Lemma 4.3.2). We omit this.

9.2.5.3 Numerical methods for regularised gradient flow dynamics

We use a backward Euler time discretisation and discretise the spatial part of the problem using $\mathbb{P}_1$ finite elements, as we did in the 2-phase problem.

A one-step Euler time discretisation

We solve on the time interval $t \in (0, T]$, with $\tau = T/M, M \geq 1$, the (uniform) time-step size and M the number of time-steps i.e. $t_j := j\tau$. φ_j and ψ_j denote the exact solutions to the 3-phase problem at time t_j, φ^j and ψ^j the discrete-in-time approximations of φ_j and ψ_j. Later on, φ_h^j and ψ_h^j will denote the fully discrete (in space and time) approximations of our order parameters. In what follows, we suppress the MMS functions f_1, f_2, F_1, F_2.

Definition 9.2.2. (A fully implicit one-step Euler time discretisation) *Consider the fully implicit one-step Euler time discretisation, of problem* $\left(\mathbf{P}_\mu^{(\mathbf{m})}\right)$ *in* (9.37)*:*

$\left(\mathbf{P}_{\mu,\tau}^{(\mathbf{m})}\right)$*: for* $j = 1, \ldots, M$*, given (fixed)* $0 < \mu \ll 1$ *and* $\varphi^{j-1}, \psi^{j-1} \in H^1(\Omega)$*, find* $\varphi^j, \psi^j \in H^1(\Omega)$ *such that*

$$\left(\varphi^j, \nu_1\right) + \tau M_\varphi\left[\left(\nabla \omega_\varphi^j, \nabla \nu_1\right) + \left(\alpha\left(\varphi^j - m\mathcal{M}\right) + \beta\left(\psi^j - \mathcal{M}\right), \nu_1\right)\right] = \left(\varphi^{j-1}, \nu_1\right) \tag{9.44a}$$

$$\begin{aligned}\left(\omega_\varphi^j, \nu_2\right) = \varepsilon_\varphi^2\left(\nabla \varphi^j, \nabla \nu_2\right) + \varepsilon_{\varphi\psi}^2\left(\nabla \psi^j, \nabla \nu_2\right) \\ + \frac{1}{2}\left(-\chi^{AB}\varphi^j + \left(\chi^{BV} - \chi^{AV}\right)\psi^j, \nu_2\right) + \left(\zeta_\mu^{(\varphi)}\left(\varphi^j, \psi^j\right), \nu_2\right)\end{aligned} \tag{9.44b}$$

and

$$\left(\psi^j, \nu_3\right) + \tau M_\psi\left[\left(\nabla \omega_\psi^j, \nabla \nu_3\right) + \left(\beta\left(\varphi^j - m\mathcal{M}\right) + \gamma\left(\psi^j - \mathcal{M}\right), \nu_3\right)\right] = \left(\psi^{j-1}, \nu_3\right) \tag{9.44c}$$

$$\left(\omega_\psi^j, \nu_4\right) = \varepsilon_{\varphi\psi}^2 \left(\nabla\varphi^j, \nabla\nu_4\right) + \varepsilon_\psi^2 \left(\nabla\psi^j, \nabla\nu_4\right) + \frac{1}{2}\left(\chi^{BV} - \chi^{AV}\right)\left(\varphi^j, \nu_4\right)$$
$$+ \frac{1}{2}\left(\chi^{AB} - 2\left(\chi^{AV} + \chi^{BV}\right)\right)\left(\psi^j, \nu_4\right) + \left(\zeta_\mu^{(\psi)}\left(\varphi^j, \psi^j\right), \nu_4\right) \quad (9.44d)$$

for every $(\nu_1, \nu_2, \nu_3, \nu_4) \in \left(H^1(\Omega)\right)^4$*, subject to the ICs*

$$\varphi^0 = \varphi_0, \qquad \overline{\varphi^0} = m\mathcal{M} \qquad \textit{and} \qquad \psi^0 = \psi_0, \qquad \overline{\psi^0} = \mathcal{M}. \quad (9.44e)$$

SSN

As in two phases, we cannot use the Newton method to resolve the non-linearities in $\zeta_\mu^{(\varphi)}\left(\varphi^j, \psi^j\right)$ and $\zeta_\mu^{(\psi)}\left(\varphi^j, \psi^j\right)$, because the min and max functions are not Fréchet differentiable. Instead we use the SSN method of Section 5.2. The iteration framework is the same for three as for two phases. In three phases, we have the 4×4 system (cf. (5.42a)

$$\mathcal{N}\left(g\left(\boldsymbol{x}^{(j-1,n)}\right)\boldsymbol{\delta}^{(j-1,n)}, \boldsymbol{\nu}\right) =$$
$$\begin{pmatrix}
\left(\delta\varphi^{(j-1,n)}, \nu_1\right) + \tau M_\varphi\left(\nabla\delta\omega_\varphi^{(j-1,n)}, \nabla\nu_1\right) + \tau M_\varphi\left(\alpha\delta\varphi^{(j-1,n)} + \beta\delta\psi^{(j-1,n)}, \nu_1\right) \\
\left(\delta\omega_\varphi^{(j-1,n)}, \nu_2\right) - \varepsilon_\varphi^2\left(\nabla\delta\varphi^{(j-1,n)}, \nabla\nu_2\right) - \varepsilon_{\varphi\psi}^2\left(\nabla\delta\psi^{(j-1,n)}, \nabla\nu_2\right) + \frac{\chi^{AB}}{2}\left(\delta\varphi^{(j-1,n)}, \nu_2\right) \\
\quad + \frac{\chi^{AV} - \chi^{BV}}{2}\left(\delta\psi^{(j-1,n)}, \nu_2\right) - \mathcal{N}\left(\zeta_\mu^{(\varphi)}\left(\varphi^j, \psi^j\right)\boldsymbol{\delta}^{(j-1,n)}, \nu_2\right) \\
\left(\delta\psi^{(j-1,n)}, \nu_3\right) + \tau M_\psi\left(\nabla\delta\omega_\psi^{(j-1,n)}, \nabla\nu_3\right) + \tau M_\psi\left(\beta\delta\varphi^{(j-1,n)} + \gamma\delta\psi^{(j-1,n)}, \nu_3\right) \\
\left(\delta\omega_\psi^{(j-1,n)}, \nu_4\right) - \varepsilon_{\varphi\psi}^2\left(\nabla\delta\varphi^{(j-1,n)}, \nabla\nu_4\right) - \varepsilon_\psi^2\left(\nabla\delta\psi^{(j-1,n)}, \nabla\nu_4\right) \\
\quad + \frac{\chi^{AV} - \chi^{BV}}{2}\left(\delta\varphi^{(j-1,n)}, \nu_4\right) - \frac{\chi^{AB} - 2\left(\chi^{AV} + \chi^{BV}\right)}{2}\left(\delta\psi^{(j-1,n)}, \nu_4\right) \\
\quad - \mathcal{N}\left(\zeta_\mu^{(\psi)}\left(\varphi^j, \psi^j\right)\boldsymbol{\delta}^{(j-1,n)}, \nu_4\right)
\end{pmatrix}, \quad (9.45)$$

with Newton derivatives (cf. (5.42c))

$$\mathcal{N}\left(\zeta_\mu^{(\varphi)}\left(\varphi^j, \psi^j\right)\boldsymbol{\delta}^{(j-1,n)}, \nu_2\right)$$
$$= \frac{1}{\mu}\Bigg[\left(\mathbf{1}\left\{\varphi^{(j-1,n)} - \psi^{(j-1,n)} > 0\right\}\left(\delta\varphi^{(j-1,n)} - \delta\psi^{(j-1,n)}\right), \nu_2\right)$$
$$+ \left(\mathbf{1}\left\{\varphi^{(j-1,n)} + \psi^{(j-1,n)} < 0\right\}\left(\delta\varphi^{(j-1,n)} + \delta\psi^{(j-1,n)}\right), \nu_2\right)\Bigg], \quad (9.46a)$$

and

$$\mathcal{N}\left(\zeta_\mu^{(\psi)}\left(\varphi^j, \psi^j\right)\boldsymbol{\delta}^{(j-1,n)}, \nu_4\right) = \frac{1}{\mu}\Bigg[\left(\mathbf{1}\left\{\psi^{(j-1,n)} > 1\right\}\delta\psi^{(j-1,n)}, \nu_4\right)$$
$$- \left(\mathbf{1}\left\{\varphi^{(j-1,n)} - \psi^{(j-1,n)} > 0\right\}\left(\delta\varphi^{(j-1,n)} - \delta\psi^{(j-1,n)}\right), \nu_4\right)$$
$$+ \left(\mathbf{1}\left\{\varphi^{(j-1,n)} + \psi^{(j-1,n)} < 0\right\}\left(\delta\varphi^{(j-1,n)} + \delta\psi^{(j-1,n)}\right), \nu_4\right)\Bigg]. \quad (9.46b)$$

Remarks.

i) Our bespoke FEniCS code supports substantially more general time-stepping than the fully-implicit method in (9.44). All of the numerical experiments in this chapter used fully-implicit time-stepping.

ii) Much of the analysis that follows relates to symmetric ($m = 0$) materials, for which we define a re-scaling in Section 9.3.4. Our FEniCS code was based on the more general model above, in support of exploring more complicated scenarios as/when appropriate.

iii) We assume (but do not prove) that our numerical scheme inherits the key properties we discussed in Section 9.2.5.2 i.e. it is mass controlling and exhibits energy monotonicity.

Order of convergence demonstration: 3-phase MMS

We conducted an MMS convergence experiment, similar to that in Section 5.4.2. We manufactured two exact solutions φ_{E} and ψ_{E} as in Table 9.1, and used them to derive and inject four functions f_1, f_2, F_1 and F_2 into (9.36) (cf. (5.82)) using (9.34b), (9.34d) as

$$\omega_{\mathrm{E}}^{(\varphi)} = \varepsilon_{\varphi}^2 (-\Delta)\, \varphi_{\mathrm{E}} + \varepsilon_{\varphi\psi}^2 (-\Delta)\, \psi_{\mathrm{E}} + \partial_{\varphi_{\mathrm{E}}} \mathcal{B}(\varphi_{\mathrm{E}}, \psi_{\mathrm{E}}), \tag{9.47a}$$

$$f_1 = \partial_t \varphi_{\mathrm{E}} - M_{\varphi} \left(\Delta \omega_{\mathrm{E}}^{(\varphi)} - (\alpha(\varphi_{\mathrm{E}} - m\mathcal{M}) + \beta(\psi_{\mathrm{E}} - \mathcal{M})) \right), \tag{9.47b}$$

$$F_1 = -\zeta_{\mu}^{(\varphi)}(\varphi_{\mathrm{E}}, \psi_{\mathrm{E}}); \tag{9.47c}$$

$$\omega_{\mathrm{E}}^{(\psi)} = \varepsilon_{\varphi\psi}^2 (-\Delta)\, \varphi_{\mathrm{E}} + \varepsilon_{\psi}^2 (-\Delta)\, \psi_{\mathrm{E}} + \partial_{\psi_{\mathrm{E}}} \mathcal{B}(\varphi_{\mathrm{E}}, \psi_{\mathrm{E}}), \tag{9.47d}$$

$$f_2 = \partial_t \psi_{\mathrm{E}} - M_{\psi} \left(\Delta \omega_{\mathrm{E}}^{(\psi)} - (\beta(\varphi_{\mathrm{E}} - m\mathcal{M}) + \gamma(\psi_{\mathrm{E}} - \mathcal{M})) \right), \tag{9.47e}$$

$$F_2 = -\zeta_{\mu}^{(\psi)}(\varphi_{\mathrm{E}}, \psi_{\mathrm{E}}). \tag{9.47f}$$

We ran seven experiments using the parameters in Table 9.1 and plotted the errors in Fig. 9.6 (cf. Fig. 5.5). Based on these results, it seems reasonable to assume/hope that our method converges in the sense that (cf. (5.72)),

$$\|e_{\varphi,h}\|_{\ell^\infty\left((j\tau)_{j=0}^{M}; L^2(\Omega)\right)} + \|e_{\psi,h}\|_{\ell^\infty\left((j\tau)_{j=0}^{M}; L^2(\Omega)\right)} \leq C\left(\tau + h^2\right).$$

We make no attempt to prove this analytically.

Remarks. Compared to the 2-phase MMS demonstration, we were forced to use much smaller τ-values ($10h^2$ instead of $100h^2$) in our 3-phase experiments. As a result, we selected $T = 1$ (instead of 10). Despite this limitation, we had $(\varphi_{\mathrm{E}}, \psi_{\mathrm{E}})$ outside of Ω_{∇} for part of the simulation spacetime domain i.e. we made sure to test the penalty components.

We only MMS-tested with $\beta = \gamma = 0$, partly because of our interest in symmetric models (see the next section).[12]

Type	Parameter	Values						
Model	$\left(\varepsilon_{\varphi}^2, \varepsilon_{\varphi\psi}^2, \varepsilon_{\psi}^2\right)$	$(1.0, 0, 1.0)$						
	$\left(\chi^{AB}, \chi^{AV}, \chi^{BV}\right)$	$(1.0, 1.5, 10.0)$						
	(α, β, γ)	$(20, 0, 0)$						
	(M_{φ}, M_{ψ})	$\left(2, \frac{2}{3}\right)$						
	$(m, \mathcal{M})$	$\left(\frac{1}{3}, \frac{1}{2}\right)$						
	Ω	$x \in (0, 1)$						
	$\varphi_{\mathrm{E}}(x,t) = m\mathcal{M} + \mathrm{e}^{\sin(t)}\cos(2\pi x)$; $\psi_{\mathrm{E}}(x,t) = \mathcal{M} + \cos(t)\cos(4\pi x)$							
Control	T	1.0						
	h (test)	$1/10$	$1/20$	$1/50$	$1/100$	$1/200$	$1/500$	$1/1\,000$
	τ $\left(= 10h^2\right)$	0.1	0.025	0.04	10^{-3}	2.5×10^{-4}	4×10^{-5}	10^{-5}
	Time-splitting	Fully implicit						
	Regularisation	2^{nd} degree; $\mu = 10^{-4}$						

Table 9.1: 3-Phase MMS test parameters (1D) (cf. Table 5.2).

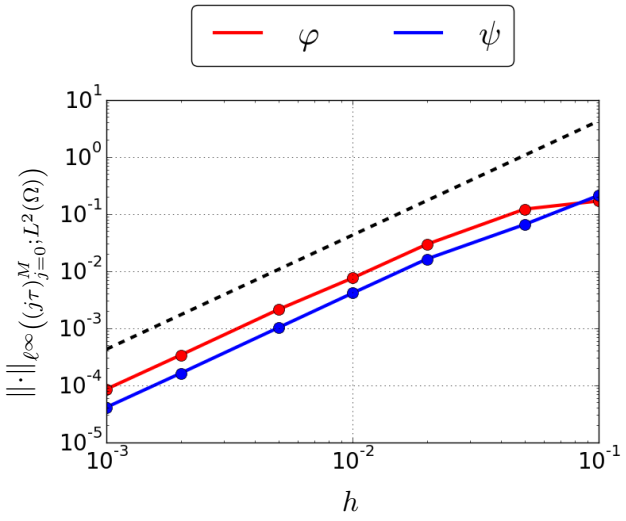

Figure 9.6: MMS results: 3-phase/1D in a log-log plot. The **red** line indicates $\|e_{\varphi,h}\|_{\ell^\infty\left((j\tau)_{j=0}^{M};L^2(\Omega)\right)}$; the **blue** line $\|e_{\psi,h}\|_{\ell^\infty\left((j\tau)_{j=0}^{M};L^2(\Omega)\right)}$. The dashed, black line indicates a quadratic relationship (gradient two) for comparison.[11]

9.2.6 Symmetric 3-phase materials: general considerations

As in two phases, the assumption of symmetry ($m = 0$) leads to a substantial simplification. For $m = 0$, (9.21) yields

$$\varepsilon_\varphi^2 = \frac{\varepsilon^2}{2\mathcal{M}}, \qquad \varepsilon_{\varphi\psi}^2 = 0, \qquad \text{and} \qquad \varepsilon_\psi^2 = \frac{\varepsilon^2}{2\mathcal{M}\left(1-\mathcal{M}\right)}. \tag{9.48a}$$

Under such conditions,

$$\frac{\varepsilon_\psi^2}{\varepsilon_\varphi^2} = \frac{1}{1-\mathcal{M}} \geq 1 \qquad \Rightarrow \qquad \varepsilon_\psi^2 \geq \varepsilon_\varphi^2, \tag{9.48b}$$

with equality only if $\mathcal{M} = 0$ (which is clearly nonsensical). Since $m = 0 \Rightarrow a = b = \frac{\mathcal{M}}{2}$, the non-zero part of $\mathbf{\Gamma}$ in (9.18) is

$$\gamma_{ij} = (-1)^{i+j}\,\widehat{\gamma} \qquad \text{where} \qquad \widehat{\gamma} = \frac{6\varepsilon\gamma_c}{\mathcal{M}} \tag{9.49a}$$

and so α, β and γ in (9.24) simplify to

$$\alpha = \frac{6\varepsilon\gamma_c}{\mathcal{M}}, \qquad \beta = 0 \qquad \text{and} \qquad \gamma = 0. \tag{9.49b}$$

As such there is no non-local energy in ψ, and the regularised energy becomes

$$\begin{aligned}\mathcal{E}_\mu(\varphi,\psi) &= \int_\Omega \frac{\varepsilon_\psi^2}{2}\left|\nabla\psi\right|^2 + \frac{\varepsilon_\varphi^2}{2}\left|\nabla\varphi\right|^2 + \mathcal{B}_\mu(\varphi,\psi)\ \mathrm{d}\Omega + \frac{\alpha}{2}\left\|\varphi\right\|_{-1}^2 \\ &= \int_\Omega \frac{\varepsilon^2}{4\mathcal{M}}\left(\frac{1}{1-\mathcal{M}}\left|\nabla\psi\right|^2 + \left|\nabla\varphi\right|^2\right) + \mathcal{B}_\mu(\varphi,\psi)\ \mathrm{d}\Omega + \frac{3\varepsilon\gamma_c}{\mathcal{M}}\left\|\varphi\right\|_{-1}^2.\end{aligned} \tag{9.50}$$

The gradient flow problem $\left(\mathbf{P}_\mu^{(\mathbf{m})}\right)$ in (9.37) simplifies to:

$\left(\mathbf{P}_\mu^{(\mathrm{sym})}\right)$: For given $\mu > 0$, find $\left\{\varphi, \omega^{(\varphi)}, \psi, \omega^{(\psi)}\right\}$ with $\varphi, \psi \in H^1\left(0,T;\left(H^1(\Omega)\right)'\right) \cap L^\infty\left(0,T;H^1(\Omega)\right)$, and $\omega^{(\varphi)}, \omega^{(\psi)} \in L^2\left(0,T;H^1(\Omega)\right)$, such that

$$\left\langle \partial_t\varphi, \nu_1\right\rangle + M_\varphi\left[\left(\nabla\omega^{(\varphi)}, \nabla\nu_1\right) + \alpha\left(\varphi,\nu_1\right)\right] = 0 \tag{9.51a}$$

$$\left(\omega^{(\varphi)}, \nu_2\right) = \varepsilon_\varphi^2\left(\nabla\varphi, \nabla\nu_2\right) + \frac{1}{2}\left(-\chi^{AB}\varphi + \left(\chi^{BV} - \chi^{AV}\right)\psi, \nu_2\right) + \left(\zeta_\mu^{(\varphi)}(\varphi,\psi), \nu_2\right), \tag{9.51b}$$

$$\left\langle \partial_t\psi, \nu_3\right\rangle + M_\psi\left(\nabla\omega^{(\psi)}, \nabla\nu_3\right) = 0, \tag{9.51c}$$

$$\begin{aligned}\left(\omega^{(\psi)}, \nu_4\right) &= \varepsilon_\psi^2\left(\nabla\psi, \nabla\nu_4\right) \\ &\quad + \frac{1}{2}\left(\left(\chi^{BV} - \chi^{AV}\right)\varphi + \left(\chi^{AB} - 2\left(\chi^{AV} + \chi^{BV}\right)\right)\psi, \nu_4\right) + \left(\zeta_\mu^{(\psi)}(\varphi,\psi), \nu_4\right),\end{aligned} \tag{9.51d}$$

for every $\nu_1, \nu_2, \nu_3, \nu_4 \in H^1(\Omega)$ and a.e. $t \in (0,T)$, subject to the ICs

$$\varphi(0) = \varphi_0, \qquad \overline{\varphi_0} = 0 \qquad \text{and} \qquad \psi(0) = \psi_0, \qquad \overline{\psi_0} = \mathcal{M}. \tag{9.51e}$$

9.3 Symmetric 3-phase materials in 1D

We continue our focus on symmetric materials for the rest of this chapter, starting with an in-depth look at 1D morphologies.

Motivation: an interesting DBC configuration

We are interested in DBC configurations in which the molecules have arranged themselves perpendicular to a substrate ($y = 0$) so as to form A and B-rich sub-domains lying parallel to the substrate, below a region of void extending from the top of the polymer to $y = L$, as in Fig. 9.7 (see also Fig. 1 of Stasiak et al. (2012) on which our drawing is based).

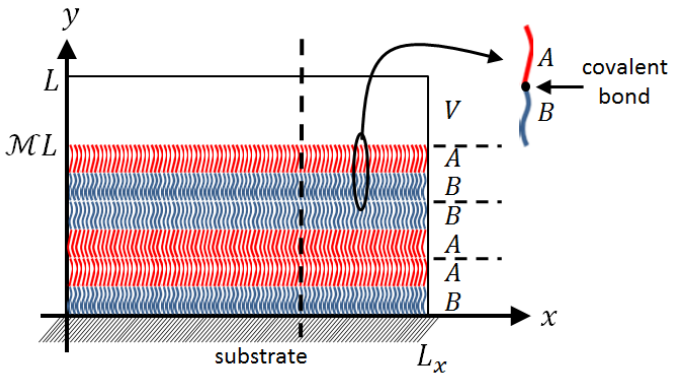

Figure 9.7: Schematic of a $\nu = 3$ monolayer $BAABBA$ DBC, stacked on the substrate from $y = 0$ to $y = \mathcal{M}L$, below a void in $\mathcal{M}L < y \leq L$. The DBC molecules, of length $\mathcal{M}L/\nu$, are stacked vertically end-on-end perpendicular to the substrate (at $y = 0$) so as to form A and B-rich microdomains that run parallel to the substrate. We take a section along the vertical dashed black line, and study the resulting 1D morphology.

We consider 1D vertical sections through such morphologies of the sort shown in Fig. 9.8 (see also Fig. 9.1). We use y as our 1D spatial coordinate; the substrate is at $y = 0$. In Fig. 9.8, we observe $\nu = 3$ monolayers inside the pure polymer ($\psi \equiv 1$). ν odd (even) implies different (the same) polymer phases at $y = 0$ (the substrate) and $\mathcal{M}L$ (the polymer–void transition). Consistent with the sharp interface limit morphology, **we assume that $\varphi = \pm\psi$ inside the polymer–void transition** centred at $\mathcal{M}L$. We will return to this point later.

We therefore investigate the following special cases:

i) The no-V ($\psi = 1$) scenario; and

ii) The no-A ($\varphi = -\psi$) and no-B ($\varphi = \psi$) clean interface scenarios.

9.3.1 The no-V scenario

There are two global cases, and one local case to consider:

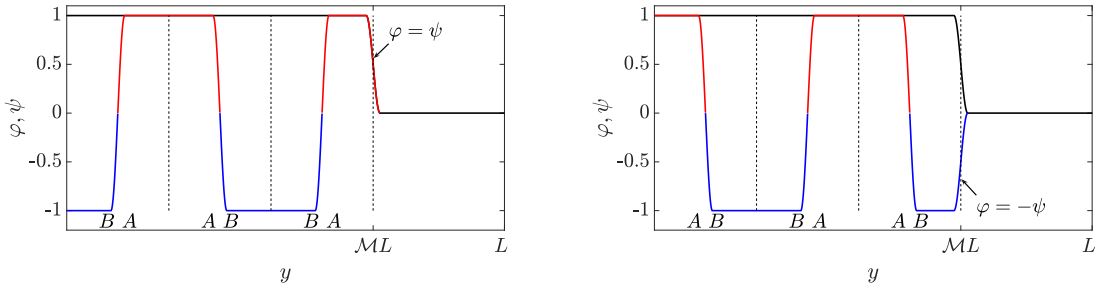

(a) $\nu = 3$: $BAABBAV$ (b) $\nu = 3$: $ABBAABV$

Figure 9.8: Resolved 1D, 3-phase morphologies: $\psi(y)$ is drawn in black, $\varphi(y)$ in red ($\varphi(y) > 0$) and blue ($\varphi(y) < 0$). Inside the polymer ($y < \mathcal{M}L$), $\psi \equiv 1$, and there are three monolayers. Their ends are indicated in the figure by vertical dashed black lines. There is a single polymer–void transition centred at $y = \mathcal{M}L$, inside which we assume that $\varphi = \pm\psi$. The void, $\psi \equiv 0$, occupies $y > \mathcal{M}L$.[13]

$\psi = 1$ globally (*a priori*)

Suppose that there is no void whatsoever in Ω. According to (9.8b), this is equivalent to

$$\overline{\psi} = a + b = \mathcal{M} = 1, \qquad \psi \equiv 1 \qquad \text{and} \qquad \psi - \overline{\psi} \equiv 0.$$

Since ψ is constant, its spatial derivatives are zero, and the energy (9.19) becomes

$$\begin{aligned}\mathcal{E}(\varphi, \psi \equiv 1) &= \int_\Omega \frac{\varepsilon_\varphi^2}{2} |\nabla\varphi|^2 + \mathcal{B}(\varphi, \psi = 1)\,\mathrm{d}\Omega + \frac{\alpha}{2}\|\varphi - \overline{\varphi}\|_{-1}^2 \\ &= \int_\Omega \frac{\varepsilon_\varphi^2}{2} |\nabla\varphi|^2 + \mathcal{B}(\varphi)\,\mathrm{d}\Omega + \frac{\alpha}{2}\|\varphi - \overline{\varphi}\|_{-1}^2 \end{aligned} \tag{9.52}$$

with $\mathcal{B}(\varphi)$ as in (3.17), after using (9.23). But this is identical to the 2-phase energy we studied in Chapter 3, and so if we construct gradient flow dynamics for φ with $\psi \equiv 1$, we arrive at 2-phase dynamics; it is as if there is no third phase at all.

$\psi_0 \equiv 1$ (an IC)

An alternate perspective is that the IC $\psi_0 \equiv 1$ and $\|\varphi_0\|_{0,\infty} \leq 1$. For a mass conserving system, $\overline{\psi} = \mathcal{M} = 1$, which means that $\psi \equiv \mathcal{M}$. All of the spatial derivatives of ψ (a constant) vanish, and so we have the (instantaneous) dynamics

$$\partial_t\varphi + M_\varphi\left(\varepsilon_\varphi^2\varphi^{(\mathrm{iv})} + \frac{\chi^{AB}}{2}\varphi'' + \alpha\varphi\right) = 0 \qquad \text{and} \qquad \partial_t\psi = M_\psi\frac{\chi^{BV} - \chi^{AV}}{2}\varphi'' \tag{9.53}$$

after noting that we can write

$$\partial_\varphi\mathcal{B}_\mu(\varphi, \psi = 1) = \frac{-\chi^{AB}}{2}\varphi \qquad \text{and} \qquad \partial_\psi\mathcal{B}_\mu(\varphi, \psi = 1) = \frac{\chi^{BV} - \chi^{AV}}{2}\varphi, \tag{9.54}$$

after dropping constants once again.

Suppose now that $\partial_t\psi < 0$ at some point in Ω. By mass conservation, there must be some other point at which $\partial_t\psi > 0$ (for otherwise we would have $\overline{\psi} \neq \mathcal{M}$). But this violates the obstacle condition that $\psi \leq 1$. Hence $\partial_t\psi \equiv 0$, and the second equation in (9.53) yields $\varphi'' = 0$ which, together with the mass and BCs (9.36e) implies that we must have $\varphi \equiv 0$. Substituting this into the first equation in (9.53), we find that $\partial_t\varphi = 0$, i.e. these dynamics break down.

$\psi_0 = 1$ on a small patch

Finally, we suppose that $\psi_0 = 0$ on a small patch of the domain (for instance inside the pure polymer) and that $\|\varphi_0\|_{0,\infty} \leq 1$. The 3-phase dynamics at any point inside such a patch are the same as in (9.53), after noting that the spatial derivatives of ψ are zero (locally), except that this time, there is no guarantee that $\partial_t\psi = 0$ (unless $\chi^{BV} = \chi^{AV}$). The key observation is that the first equation in (9.53) is the same as the 2-phase (3.41). We conclude that φ (i.e. the DBC micro-structure) evolves in the polymer as if it is comprised of two phases only.

9.3.2 Clean interface scenarios

Our first observation is that it is not possible to have $\varphi \equiv \pm\psi$ (a.e. in Ω) if $m = \overline{\varphi} = 0$, for this would imply that $\mathcal{M} = \overline{\psi} = 0$ too, which is degenerate. Consequently, we consider only the case where the conditions are imposed on a small (local) patch, as may be the case in a polymer–void transition of the type depicted in Fig. 9.8.

$\psi = \varphi$ on a small patch: a clean AV interface

This is the same condition governing what we previously termed a clean AV interface (in which $\phi_B = 0$). Using (D.39) and (9.48), and assuming that $0 \leq \psi \leq 1$ (i.e. we can discard the penalty) we find that

$$\partial_t\varphi + M_\varphi\left(\varepsilon_\varphi^2\varphi^{(\mathrm{iv})} + \frac{\chi^{AB} + \chi^{AV} - \chi^{BV}}{2}\varphi'' + \alpha\varphi\right) = 0 \tag{9.55a}$$

and

$$\partial_t\psi + M_\psi\left(\varepsilon_\psi^2\psi^{(\mathrm{iv})} + \frac{-\chi^{AB} + 3\chi^{AV} + \chi^{BV}}{2}\psi''\right) = 0, \tag{9.55b}$$

after noting, from (9.34), that

$$\partial_\varphi\mathcal{B}_\mu(\varphi,\varphi) = \frac{-\chi^{AB} - \chi^{AV} + \chi^{BV}}{2}\varphi \quad \text{and} \quad \partial_\psi\mathcal{B}_\mu(\psi,\psi) = \frac{\chi^{AB} - 3\chi^{AV} - \chi^{BV}}{2}\psi, \tag{9.55c}$$

after dropping constants once again.

$\psi = -\varphi$ on a small patch: a clean BV interface

The clean BV interface is similar. We replace (9.55) with

$$\partial_t \varphi + M_\varphi \left(\varepsilon_\varphi^2 \varphi^{(\mathrm{iv})} + \frac{\chi^{AB} - \chi^{AV} + \chi^{BV}}{2} \varphi'' + \alpha \varphi \right) = 0 \tag{9.56a}$$

and

$$\partial_t \psi + M_\psi \left(\varepsilon_\psi^2 \psi^{(\mathrm{iv})} + \frac{-\chi^{AB} + \chi^{AV} + 3\chi^{BV}}{2} \psi'' \right) = 0, \tag{9.56b}$$

where

$$\partial_\varphi \mathcal{B}_\mu (\varphi, -\varphi) = \frac{-\chi^{AB} + \chi^{AV} - \chi^{BV}}{2} \varphi \quad \text{and} \quad \partial_\psi \mathcal{B}_\mu (-\psi, \psi) = \frac{\chi^{AB} - \chi^{AV} - 3\chi^{BV}}{2} \psi. \tag{9.56c}$$

Remarks.

i) In both cases, φ evolves like a 2-phase material having non-zero, non-local interaction, while ψ evolves like a 2-phase Cahn–Hilliard material (with zero non-local term).

ii) The two models are symmetric in the sense that we can recover one from the other by switching $\chi^{AV} \leftrightarrow \chi^{BV}$.

9.3.3 A heuristic *ansatz* for low energy, symmetric morphologies in 1D

Motivated by our observations above, we pose a heuristic *ansatz* for low energy morphologies in 1D. For ψ, we suppose that (cf. (6.4b))

$$\psi(y) = \begin{cases} 1 & 0 \le y < \mathcal{M}L - \dfrac{\ell_{\mathrm{mAc}}}{2} \\ \widetilde{\psi}(y) & \mathcal{M}L - \dfrac{\ell_{\mathrm{mAc}}}{2} \le y \le \mathcal{M}L + \dfrac{\ell_{\mathrm{mAc}}}{2} \\ 0 & \mathcal{M}L + \dfrac{\ell_{\mathrm{mAc}}}{2} < y \le L \end{cases} \tag{9.57}$$

where the interface layer function $\widetilde{\psi}$ satisfies a 2-phase Cahn–Hilliard ELE, that depends on the nature of the polymer–void transition as follows (cf. (8.9)),

$$A \to V: \quad \varepsilon_\psi^2 \widetilde{\psi}^{(\mathrm{iv})} + \frac{\chi_{A\to V}}{2} \widetilde{\psi}'' = 0, \qquad \chi_{A\to V} := -\chi^{AB} + 3\chi^{AV} + \chi^{BV} > 0 \tag{9.58a}$$

$$B \to V: \quad \varepsilon_\psi^2 \widetilde{\psi}^{(\mathrm{iv})} + \frac{\chi_{B\to V}}{2} \widetilde{\psi}'' = 0, \qquad \chi_{B\to V} := -\chi^{AB} + \chi^{AV} + 3\chi^{BV} > 0, \tag{9.58b}$$

subject to the BCs

$$\widetilde{\psi}\left(\mathcal{M}L - \frac{\ell_{\mathrm{mAc}}}{2}\right) = 1, \quad \widetilde{\psi}\left(\mathcal{M}L + \frac{\ell_{\mathrm{mAc}}}{2}\right) = 0 \quad \text{and} \quad \widetilde{\psi}'\left(\mathcal{M}L \pm \frac{\ell_{\mathrm{mAc}}}{2}\right) = 0. \tag{9.59}$$

This problem is similar to what we discussed in Section 8.3. ψ thus has a single transition of width $\ell_{\rm mAc}$, that is symmetric about $\mathcal{M}L$ (so that $\overline{\psi} = \mathcal{M}$), with

$$\widetilde{\psi}\left(y\right) = \frac{1}{2}\left(1 - \sin\left(\frac{\pi\left(y - \mathcal{M}L\right)}{\ell_{\rm mAc}}\right)\right); \qquad \mathcal{M}L - \frac{\ell_{\rm mAc}}{2} \leq y \leq \mathcal{M}L + \frac{\ell_{\rm mAc}}{2} \tag{9.60a}$$

as in (9.57). We suppose that an $A \to V$ polymer–void transition has

$$\text{width:} \qquad \ell_{\rm mAc} =: \ell_{\rm mAc}^{A\to V} = \frac{\pi\varepsilon_\psi}{\sqrt{\chi_{A\to V}/2}} \qquad \text{and} \qquad \widetilde{\varphi}\left(y\right) = \widetilde{\psi}\left(y\right). \tag{9.60b}$$

Similarly, a $B \to V$ transition has

$$\text{width:} \qquad \ell_{\rm mAc} =: \ell_{\rm mAc}^{B\to V} = \frac{\pi\varepsilon_\psi}{\sqrt{\chi_{B\to V}/2}} \qquad \text{and} \qquad \widetilde{\varphi}\left(y\right) = -\widetilde{\psi}\left(y\right). \tag{9.60c}$$

Notice that,

$$\frac{\ell_{\rm mAc}^{A\to V}}{\ell_{\rm mAc}^{B\to V}} = \sqrt{\frac{\chi_{B\to V}}{\chi_{A\to V}}} = \sqrt{\frac{-\chi^{AB} + \chi^{AV} + 3\chi^{BV}}{-\chi^{AB} + 3\chi^{AV} + \chi^{BV}}},$$

and so:

- If $\chi^{BV} = \chi^{AV}$, the two possible interface layer widths are equal; but
- For a χ-asymmetric homogeneous density in which $\chi^{BV} > \chi^{AV}$,

  $$-\chi^{AB} + \chi^{AV} + 3\chi^{BV} > -\chi^{AB} + 3\chi^{AV} + \chi^{BV} \qquad \text{i.e.} \qquad \ell_{\rm mAc}^{A\to V} > \ell_{\rm mAc}^{B\to V}$$

  (and vice versa if $\chi^{AV} > \chi^{BV}$). Hence, if $A \to V$ transitions are energetically favoured by the homogeneous density (i.e. have lower energy), they will be *thicker* than their $B \to V$ counterparts (and vice versa).

We assume that φ minimises the 2-phase energy on $0 \leq y \leq \mathcal{M}L$. As in Chapter 8, we assume that φ has $\nu_{\rm opt}$ equally spaced monolayers between $y = 0$ and $y = \mathcal{M}L$, each of width $\mathcal{M}L/\nu_{\rm opt}$. We insert an additional polymer–void transition on $\mathcal{M}L - \ell_{\rm mAc}/2 \leq y \leq \mathcal{M}L + \ell_{\rm mAc}/2$, with $\widetilde{\varphi} = \pm\widetilde{\psi}$ as in (9.60). It is clear that this construction yields $\overline{\varphi} = 0$, as required. We now define the BA monolayer function

$$u\left(y, y_k, \mathcal{D}\right) := \begin{cases} -1, & y < y_k - \dfrac{\ell_{\rm mic}}{2} \\ \widetilde{\varphi}_{BA}\left(y - y_k, \mathcal{D}\right), & |y - y_k| \leq \dfrac{\ell_{\rm mic}}{2} \\ 1, & y > y_k + \dfrac{\ell_{\rm mic}}{2} \end{cases}; \qquad \ell_{\rm mic} = \ell_{\rm opt}\left(\mathcal{D}\right), \tag{9.61a}$$

where $\widetilde{\varphi}_{BA}\left(y, \mathcal{D}\right)$ is the minimum energy, BA interface layer of width $\ell_{\rm opt}\left(\mathcal{D}\right)$ inside a 2-phase monolayer of width $\mathcal{D}$, constructed using the techniques of Section 8.2. Using this and (9.60) for a ν-layer morphology with phase B at the substrate, we propose the *ansatz*,

$$\varphi^B\left(y\right) = \left(\sum_{k=1}^{\nu}\left(-1\right)^{k+1} u\left(y, \frac{\mathcal{M}L\left(k - \frac{1}{2}\right)}{\nu}, \frac{\mathcal{M}L}{\nu}\right)\right) + \left\{\begin{array}{ll} \text{odd } \nu: & \psi\left(y\right) - 1 \\ \text{even } \nu: & -\psi\left(y\right) \end{array}\right\}. \tag{9.61b}$$

with $\psi(y)$ as in (9.57), (9.60). For a configuration with phase A at the substrate, we propose

$$\varphi^A(y) = \left(\sum_{k=1}^{\nu} (-1)^k \, u\left(y, \frac{\mathcal{M}L\left(k-\frac{1}{2}\right)}{\nu}, \frac{\mathcal{M}L}{\nu}\right)\right) + \left\{\begin{array}{ll} \text{odd } \nu: & 1-\psi(y) \\ \text{even } \nu: & \psi(y) \end{array}\right\}. \tag{9.61c}$$

$\mathcal{M}$, L and the other material parameters above are prescribed; we will select $\nu = \nu_{\text{opt}}$ according to the 2-phase equal-spacing results of Chapter 8.[14]

To summarise: the first $\nu - 1$ monolayers (counting from the substrate) have width $\frac{\mathcal{M}L}{\nu}$; each one has two regions of pure A/B material of (equal) width $\frac{1}{2}\left(\frac{\mathcal{M}L}{\nu} - \ell_{\text{mic}}\right)$, on either side of an internal interface layer, of width ℓ_{mic}. The last monolayer before the void has total length $\frac{\mathcal{M}L}{\nu} - \frac{\ell_{\text{mAc}}}{2}$ and, depending on the nature of the polymer–void transition, is comprised of a section of pure B (or A) material of width $\frac{1}{2}\left(\frac{\mathcal{M}L}{\nu} - \ell_{\text{mic}}\right)$, an internal interface layer of width ℓ_{mic}, and the last section of pure A (or B) material before the polymer–void transition, of width $\frac{1}{2}\left(\frac{\mathcal{M}L}{\nu} - (\ell_{\text{mic}} + \ell_{\text{mAc}})\right)$. The region of pure polymer $\psi \equiv 1$, has measure $\mathcal{M}L - \frac{\ell_{\text{mAc}}}{2}$, the polymer–void transition has width ℓ_{mAc}, and the pure void region $\psi \equiv 0$, has measure $L - \left(\mathcal{M}L + \frac{\ell_{\text{mAc}}}{2}\right)$. For simplicity, we demand that the last section of pure polymer material before the void have positive width, viz.

$$\frac{\mathcal{M}L}{\nu} > \ell_{\text{mic}} + \ell_{\text{mAc}}.$$

This restricts the *ansatz* to catering for low monolayer counts ν and/or small ε_φ and ε_ψ, since the internal interface layers will be of width $\mathcal{O}(\varepsilon_\varphi)$, and the polymer–void transition of width $\mathcal{O}(\varepsilon_\psi)$.

Remark. While it seems reasonable that the morphologies above should have low energy, there is nothing to suggest that they are local, let alone global minimisers. The biggest difference between two and three phases is the polymer–void interface layer, which means we cannot construct a convexity argument based on a single interface as we did in two phases. As such, our assumption of equal-spacing above is supported by intuition, only. Our insistence that $\varphi = \pm\psi$ for the polymer–void transition is convenient, and also matches the structure of provably local minimisers in the sharp interface limit (see Theorem 4.4 of Choksi and Ren (2005)). However, for non-zero $\varepsilon_\varphi, \varepsilon_\psi$, this assumption is clearly an approximation, as is evident from a comparison of (9.55a), (9.55b) and (9.58a): the latter condition makes $\partial_t \psi = 0$ in (9.55b) (making ψ stationary), but this clearly does not guarantee that $\partial_t \varphi \equiv 0$ on the interface layer in (9.55a).

9.3.4 A convenient re-scaling

In the previous section, we proposed low energy morphologies involving a set of internal interface layers of width $\mathcal{O}(\varepsilon_\varphi)$, and a polymer–void transition of width $\mathcal{O}(\varepsilon_\psi)$. As we noted in the remarks following (9.21), ε_φ and ε_ψ both depend on $\mathcal{M}$ in the DBC model of Choksi and Ren (2005); for $m = 0$, they are related as in (9.48).

We could thus envisage a situation in which a fixed amount of polymer material is placed inside a box in which the lid is lifted, so that L increases and $\mathcal{M}$ decreases. Our DBC model predicts that the interface widths, ε_φ and ε_ψ, would then change; ε_φ (viz. the width of the internal DBC interface layers) would increase with increasing L. This strange consequence is a side-effect of our treatment of the void as a homopolymer that interacts with the DBC via the interfacial parameters.

A refinement to our DBC model

To avoid this situation, and as we did in Parsons et al. (2017), we remove the dependence of ε_φ and ε_ψ on $\mathcal{M}$. We re-write the interfacial energy component as (cf. (9.14a), (9.14b))

$$\mathcal{I}\left(\nabla\boldsymbol{\phi}\right) = \frac{\widehat{\varepsilon}^2}{2}\sum_{i\in\{A,B,V\}}\widehat{K}_i\left|\nabla\phi_i\right|^2 \quad \text{viz.} \quad \varepsilon_A^2 = \widehat{K}_1\widehat{\varepsilon}^2, \quad \varepsilon_B^2 = \widehat{K}_2\widehat{\varepsilon}^2, \quad \text{and} \quad \varepsilon_V^2 = \widehat{K}_3\widehat{\varepsilon}^2, \tag{9.62}$$

with $\widehat{\varepsilon} \ll 1$, and $\widehat{K}_1 = \widehat{K}_2$ for a symmetric DBC, and the non-local energy as (cf. (9.18a)),

$$\mathcal{N}\left(\boldsymbol{\phi}\right) = \frac{1}{2}\sum_{i,j\in\{A,B\}}\widehat{\varepsilon}\widehat{\gamma}_{ij}\left(\left(-\Delta_n\right)^{-1}\left(\phi_i - \overline{\phi_i}\right)\right)\left(\phi_j - \overline{\phi_j}\right), \tag{9.63}$$

where (cf. (3.25) of Choksi and Ren (2005), (9.18b) and (9.49a)),

$$\widehat{\gamma}_{ij} = (-1)^{i+j}\widehat{\gamma}, \qquad \text{viz.} \qquad \begin{pmatrix} \gamma_A & \gamma_{AB} \\ \gamma_{BA} & \gamma_B \end{pmatrix} = \widehat{\varepsilon}\widehat{\gamma}\begin{pmatrix} 1 & -1 \\ -1 & 1 \end{pmatrix}, \tag{9.64}$$

with $\widehat{\gamma}$ a constant parameter, independent of $\mathcal{M}$. Using (9.21) and (9.24), we conclude that

$$\varepsilon_\varphi^2 = \frac{\widehat{K}_1\widehat{\varepsilon}^2}{2}, \quad \varepsilon_\psi^2 = \frac{\widehat{\varepsilon}^2}{2}\left(\widehat{K}_1 + 2\widehat{K}_3\right), \quad \frac{\varepsilon_\varphi^2}{\varepsilon_\psi^2} = \frac{1}{1 + 2\widehat{K}_3/\widehat{K}_1} \leq 1 \quad \text{and} \quad \alpha = \widehat{\varepsilon}\widehat{\gamma}, \tag{9.65}$$

in which ε_φ and ε_ψ no longer depend on $\mathcal{M}$. The energy (9.50) becomes

$$\mathcal{E}\left(\varphi,\psi\right) = \int_\Omega \frac{1}{2}\frac{\widehat{K}_1\widehat{\varepsilon}^2}{2}\left(\left(1 + \frac{2\widehat{K}_3}{\widehat{K}_1}\right)\left|\nabla\psi\right|^2 + \left|\nabla\varphi\right|^2\right) + \mathcal{B}\left(\varphi,\psi\right)\,\mathrm{d}\Omega + \frac{\widehat{\varepsilon}\widehat{\gamma}}{2}\left\|\varphi\right\|_{-1}^2.$$

It is convenient to divide this by $\widehat{\chi^{AB}}$, and define

$$\varepsilon^2 := \frac{\widehat{K}_1\widehat{\varepsilon}^2}{2\widehat{\chi^{AB}}}, \qquad \mathcal{K} := 1 + \frac{2\widehat{K}_3}{\widehat{K}_1} = 1 + \frac{2\widehat{K}_3}{\widehat{K}_2} \geq 1, \qquad \varepsilon\gamma := \frac{\widehat{\varepsilon}\widehat{\gamma}}{\widehat{\chi^{AB}}},$$

$$\chi^{AV} := \frac{\widehat{\chi^{AV}}}{\widehat{\chi^{AB}}}, \qquad \text{and} \qquad \chi^{\Delta} := \frac{\widehat{\chi^{BV}} - \widehat{\chi^{AV}}}{\widehat{\chi^{AB}}}. \tag{9.66}$$

The regularised energy thus transforms to

$$\mathcal{E}_\mu(\varphi,\psi)=\int_\Omega \frac{\varepsilon^2}{2}\left(\mathcal{K}\left|\nabla\psi\right|^2+\left|\nabla\varphi\right|^2\right)+\mathcal{B}_\mu(\varphi,\psi)\,\mathrm{d}\Omega+\frac{\varepsilon\gamma}{2}\left\|\varphi\right\|_{-1}^2, \tag{9.67a}$$

in which (cf. (9.23), (9.32))

$$\mathcal{B}_\mu(\varphi,\psi)=\frac{1}{2}\left[\left(\frac{1}{2}-2\chi^{AV}-\chi^{\Delta}\right)\psi^2-\frac{1}{2}\varphi^2+\chi^{\Delta}\varphi(\psi-1)+\left(2\chi^{AV}+\chi^{\Delta}\right)\psi\right]+\Upsilon_\mu(\varphi,\psi) \tag{9.67b}$$

for $0<\mu\ll 1$. This is the 3-phase version of the 2-phase re-scaling of Section 6.2.7.

Remark. γ in (9.66) is not the same as the non-local coefficient in (9.48). Since the latter is zero if $m=0$, we reuse the symbol as above in our further work on the symmetric problem. To map back into the parameters of Section 9.2, we use the specified χ^{AV}, and

$$\varepsilon_\varphi=\varepsilon,\qquad \varepsilon_\psi=\sqrt{\mathcal{K}}\varepsilon,\qquad \chi^{AB}=1,\qquad \chi^{BV}=\chi^{AV}+\chi^{\Delta},\qquad \alpha=\varepsilon\gamma. \tag{9.68}$$

Re-scaled dynamics

With the re-scaling above and $m=0$, the dynamics in (9.35), (9.36) simplify to

$$\partial_t\psi=M_\psi\Delta\omega_\psi \qquad \text{where} \qquad \omega_\psi=\mathcal{K}\varepsilon^2(-\Delta)\psi+\partial_\psi\mathcal{B}(\varphi,\psi); \tag{9.69a}$$

$$\partial_t\varphi=M_\varphi\Delta\omega_\varphi-M_\varphi\varepsilon\gamma\varphi \qquad \text{where} \qquad \omega_\varphi=\varepsilon^2(-\Delta)\varphi+\partial_\varphi\mathcal{B}(\varphi,\psi), \tag{9.69b}$$

for $t\in(0,T]$ with $M_\varphi=2$ and $M_\psi=\frac{2}{3}$ as in (9.31), after noting that the first variations of $\mathcal{E}_\mu$ in (9.67a) are

$$\frac{\delta\mathcal{E}_\mu}{\delta\psi}=\mathcal{K}\varepsilon^2(-\Delta)\psi+\partial_\psi\mathcal{B}_\mu(\varphi,\psi), \tag{9.69c}$$

$$\frac{\delta\mathcal{E}_\mu}{\delta\varphi}=\varepsilon^2(-\Delta)\varphi+\partial_\varphi\mathcal{B}_\mu(\varphi,\psi)+\varepsilon\gamma(-\Delta_n)^{-1}(\varphi-\overline{\varphi}), \tag{9.69d}$$

and setting the non-local $\overline{\varphi}=0$ in (9.69d) due to (9.70) below. The zero Neumann BCs in (9.36e) are unchanged. The ICs in (9.36f) simplify to those in (9.51e).

Mass control/conservation

Arguing as in Appendix D.3, we integrate (9.69) over Ω and divide by $|\Omega|$ to obtain

$$\partial_t\overline{\psi}=0 \qquad \text{and} \qquad \partial_t\overline{\varphi}=-M_\varphi\varepsilon\gamma\overline{\varphi}, \tag{9.70a}$$

after recalling the zero Neumann BCs on ω_ψ and ω_φ. It follows that

$$\overline{\psi}(t)=\overline{\psi_0}\quad\text{for a.e. } t \qquad \text{and} \qquad \overline{\varphi}(t)=c_1\exp(-M_\varphi\varepsilon\gamma t). \tag{9.70b}$$

If $\overline{\varphi}(0)=\overline{\varphi_0}=\widetilde{m}\neq 0$, the second of these yields (cf. (D.52))

$$\overline{\varphi}(t)=\widetilde{m}\mathrm{e}^{-M_\varphi\varepsilon\gamma t}\to 0 \qquad \text{as} \qquad t\to\infty, \tag{9.70c}$$

as long as $M_\varphi\varepsilon\gamma>0$. These dynamics thus *conserve* $\overline{\psi}(t)$, but *control* $\overline{\varphi}(t)$, in the sense that $\overline{\varphi}(t)\to 0$ exponentially fast if $\overline{\varphi_0}\neq 0$ and $\gamma>0$.

Energy monotonicity (decay)

Energy monotonicity follows (informally) by the argument at the end of Section 9.2.5.2.

9.3.5 Sharp interface limit

We now use this refined model to investigate symmetric 1D morphologies in which the monolayer width is close to optimal, in the limit as $\varepsilon \downarrow 0$. We consider 1D morphologies of the type discussed in Section 9.3 (Fig. 9.8) above, which correspond to those in Section 4 of Choksi and Ren (2005).

We saw in Section 9.3.1 that the energy in the pure polymer (where $\psi \equiv 1$) is the same as that of a 2-phase material. Consequently, arguing informally as we did in Section 8.5 to balance local and non-local components of the energy (in φ), we conclude that each of the ν_{opt} copolymer monolayers has width (to first order)

$$w_{\text{opt}} := \frac{\mathcal{M}L}{\nu_{\text{opt}}} \qquad \text{where} \qquad w_{\text{opt}} \sim \gamma^{-1/3}, \tag{8.24}$$

which depends on γ, *only*. To keep the width and number of monolayers in the polymer (viz. on $[0, \mathcal{M}L]$) constant and optimal, we therefore consider the sharp interface limit in which γ is held fixed as $\varepsilon \downarrow 0$, as illustrated in Fig. 9.9.

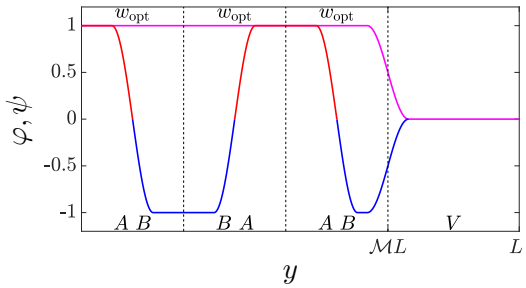

(a) A configuration with $\nu_{\text{opt}} = 3$ and w_{opt} as drawn. The interface layers all have non-zero thickness for $\varepsilon > 0$. $\psi(y)$ is drawn in **magenta**, A (B) φ-sections are coloured **red** (**blue**).

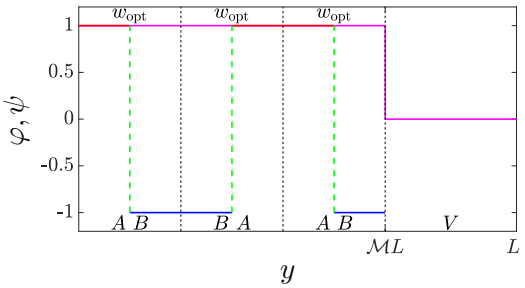

(b) The sharp interface limit of (a) with $\varepsilon \downarrow 0$ and (φ, ψ) as in (9.72). The pure-phase A/B sections have lengths $w_{\text{opt}}/2, w_{\text{opt}}, w_{\text{opt}}, w_{\text{opt}}/2$ inside the polymer; the internal interfaces are dashed, **green** lines.

Figure 9.9: The sharp interface limit process in which we hold $\mathcal{K}$ and γ constant, and send $\varepsilon \downarrow 0$. The number and width of the monolayers in the polymer stays constant, but all of the interface layers tend to zero width.[15]

Remark. w_{opt} in three phases corresponds to L_{opt} in two phases (cf. (8.17)).

According to Choksi and Ren (2005) (see $Q(u)$ in (4.34) of this reference, and also Baldo (1990)), in the sharp interface limit $\varepsilon \downarrow 0$ with $\gamma, \mathcal{K}$ fixed, the rescaled 1D free energy

$\mathcal{I}_\varepsilon = \mathcal{E}/\varepsilon$ (with $\psi = 1$) tends to the functional

$$\mathcal{I}_0 = \sigma_{AB}\nu + \sigma_{AV}\nu_{AV} + \sigma_{BV}\nu_{BV} + \frac{\gamma}{2}\int_0^{\mathcal{M}L}\left(\int_0^y \varphi(z)\,\mathrm{d}z\right)^2 \mathrm{d}y, \tag{9.71}$$

defined on the admissible set

$$\left\{\boldsymbol{u} = (\varphi,\psi) : [0,L] \to \{(\pm 1,1),(0,0)\};\, \varphi,\psi \in \mathcal{BV}([0,L]),\ \overline{\varphi} = 0,\, \overline{\psi} = \mathcal{M}\right\}, \tag{9.72}$$

and the minimisers of $\mathcal{I}_\varepsilon$ tend to the minimisers of $\mathcal{I}_0$. Here, $\mathcal{BV}([0,L])$ denotes the set of functions with bounded variation, and ν, ν_{AV}, ν_{BV} the number of AB, AV, and BV interface layers. The set in (9.72) is comprised of functions (φ,ψ) that take only a finite set of values on $[0,L]$ (each ψ is 0 (pure void) or 1 (pure polymer); each φ is one of 0 (pure void) or ± 1 (pure A or B)) and jump between these at finitely many points. If $\psi = 1$, then $\varphi = \pm 1$, but if $\psi = 0$, then $\varphi = 0$, only. We can thus identify each $\boldsymbol{u}$ with a sequence of characters describing a 1D morphology (as in Section 4 Choksi and Ren (2005)).

The surface tension of each of these interface layers is given by

$$\sigma_{AB} = \inf_\eta \left\{\varrho[\eta];\, \eta \in C^1,\, \eta(0) = (-1,1),\, \eta(1) = (1,1)\right\} = \frac{\pi}{2\sqrt{2}}, \tag{9.73a}$$

$$\sigma_{AV} = \inf_\eta \left\{\varrho[\eta];\, \eta \in C^1,\, \eta(0) = (1,1),\, \eta(1) = (0,0)\right\} = \frac{\pi\sqrt{(1+\mathcal{K})\,\chi^{AV}}}{4\sqrt{2}}, \tag{9.73b}$$

$$\sigma_{BV} = \inf_\eta \left\{\varrho[\eta];\, \eta \in C^1,\, \eta(0) = (-1,1),\, \eta(1) = (0,0)\right\} = \frac{\pi\sqrt{(1+\mathcal{K})\,(\chi^{AV}+\chi^{\Delta})}}{4\sqrt{2}}, \tag{9.73c}$$

where we have used the abbreviation (cf. (4.35) of Choksi and Ren (2005))

$$\varrho[\eta] := \sqrt{2}\int_0^1 \sqrt{\mathcal{B}(\eta(t))\left((\eta_1')^2 + \mathcal{K}(\eta_2')^2\right)}\,\mathrm{d}t. \tag{9.73d}$$

In Choksi and Ren (2005), the authors show that the microdomains of solutions with an alternating $\ldots AB\ldots$ pattern, which are local minimisers of $\mathcal{I}_0$, all have width $w = \frac{\mathcal{M}L}{\nu}$, except for those adjacent to the substrate and the polymer–void transition, which are half as wide (cf. Fig. 9.9(b)). Consequently, the contribution from the last term in (9.71) to $\mathcal{I}_0$ is ν times the contribution from a single monolayer which extends symmetrically to both sides of an internal interface layer. The first layer starts at $y = 0$, ends at $y = \frac{\mathcal{M}L}{\nu}$, and has an AB interface layer centred at $y = \frac{\mathcal{M}L}{2\nu}$ (consistent with the *ansatz* in Section 9.3.3). Hence, the contribution of the last integral in (9.71) to $\mathcal{I}_0$ is

$$\nu\left(\frac{\gamma}{2}\int_0^w \left(\int_0^x \varphi(\xi)\,\mathrm{d}\xi\right)^2 \mathrm{d}x\right) = \nu\frac{\gamma}{2}\int_0^w \left(\left|x - \frac{w}{2}\right| - \frac{w}{2}\right)^2 \mathrm{d}x = \nu\frac{\gamma w^3}{24}.$$

Evaluating $\mathcal{I}_0$ for such a 1D pattern gives the three-part energy estimate

$$I_0(\nu, \mathcal{M}) := \underbrace{\frac{\pi}{2\sqrt{2}}\nu}_{AB \text{ interfacial}} + \overbrace{\frac{\gamma}{24}\frac{\mathcal{M}^3 L^3}{\nu^2}}^{\text{non-local}} + \underbrace{\frac{\pi}{4\sqrt{2}}\sqrt{1+\mathcal{K}}\left[\sqrt{\chi^{AV}}\nu_{AV} + \sqrt{(\chi^{AV}+\chi^{\Delta})}\nu_{BV}\right]}_{\text{polymer–void transition}}, \tag{9.74}$$

where we have emphasised the dependence of I_0 on ν and $\mathcal{M}$. We assume there is one polymer–void transition ($A \to V$ or $B \to V$), so either $\nu_{AV} = 1$ and $\nu_{BV} = 0$, or vice versa. To determine the monolayer width w_{opt} which minimises I_0, we replace ν in (9.74) with $\frac{\mathcal{M}L}{w}$ to obtain

$$I_0(w) = \frac{\pi \mathcal{M} L}{2\sqrt{2}w} + \frac{\gamma \mathcal{M} L w^2}{24} + \frac{\pi}{4\sqrt{2}}\sqrt{1+\mathcal{K}}\left[\sqrt{\chi^{AV}}\nu_{AV} + \sqrt{(\chi^{AV}+\chi^{\Delta})}\nu_{BV}\right],$$

so that

$$\frac{\mathrm{d}I_0}{\mathrm{d}w} = \mathcal{M}L\left(-\frac{\pi}{2\sqrt{2}w^2} + \frac{\gamma w}{12}\right).$$

Setting this derivative equal to zero, to minimise I_0 with respect to w, yields

$$w_{\text{opt}} = \frac{\left(3\sqrt{2}\pi\right)^{1/3}}{\gamma^{1/3}}, \tag{9.75}$$

which is independent of $\mathcal{M}$ and L and matches our 2-phase estimate in (8.24). On the other hand, $\frac{\mathcal{M}L}{w_{\text{opt}}}$ is not generally an integer, and so the *actual* value of ν_{opt}, is whichever of $\{\lfloor \mathcal{M}L/w_{\text{opt}} \rfloor, \lceil \mathcal{M}L/w_{\text{opt}} \rceil\}$ yields the smaller I_0 (both, if the value is the same) i.e. ν_{opt} is not generally unique.

9.3.6 Selecting experimental parameters ($\varepsilon > 0$)

We will use the estimates from the previous section (for morphologies like the one in Fig. 9.9(b)), to guide a series of numerical experiments involving morphologies like the one in Fig. 9.9(a). In this section, we select parameters to ensure that our experimental morphologies are close to their sharp interface limit counterparts and, in particular, that they have the same numbers of monolayers.

When setting up our numerical experiments, we will choose $w_{\text{opt}} = 0.75$ along with a specific geometric scenario of interest (number of monolayers ν, domain size L and volume fraction $\mathcal{M}$), and aim to ensure that the optimal monolayer spacing fits with these constraints. In view of (9.75), this amounts to setting $\gamma = 32$; there is usually more flexibility in the choice of ε. Small ε makes the interface layers thinner and improves the accuracy of the sharp interface estimates, but increases the computational cost by requiring finer spatial grids.

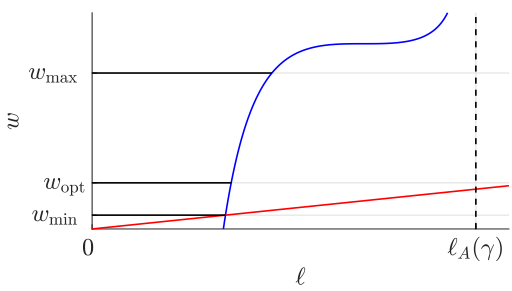

(a) The function $g(\ell)$ in (6.83c) is **blue** for the parameters in (9.79). The **red** line is $w = \ell$. $w_{\min} = 0.224$ as in (9.76), $w_{\text{opt}} = 0.747$ as in (8.24), and $w_{\max} = 2.525$ as in (9.77). The smallest non-zero pole of g occurs at $\ell = \ell_A = 0.644$.

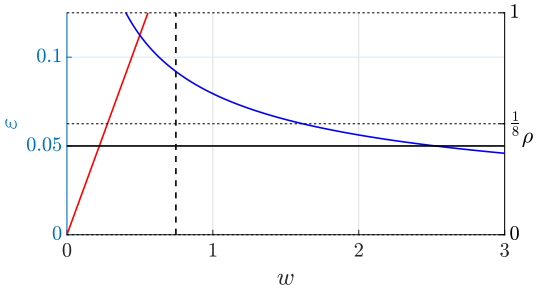

(b) $w_{\min}$, w_{opt} and $w_{\max}$ for $0 < \varepsilon < 0.125$ viz. the right y-axis, $0 < \rho < 1$ as in (6.82). the **red** line is $w_{\min}(\varepsilon)$ as in (9.76); the **blue** line is $w_{\max}(\varepsilon)$ as in (9.77). The vertical dashed line is $w_{\text{opt}} = 0.747$ as in (9.75) (independent of ε).

Figure 9.10: Summary for $\gamma = 32$.[16]

To gain the qualitative insight we need for the 3-phase situation, and in light of our observations in Section 9.3.1, we consider a single 2-phase BA interface layer of width ℓ inside a monolayer of width w, modelled in the absence of the void, and study this using the tools we developed in Section 6.2.7. We recall the solutions $\ell > 0$ of

$$g(\ell;\gamma) := \frac{2(q_h - q_\ell)}{c_A\sqrt{q_h q_\ell}} \cos\left(\sqrt{q_h}\frac{\ell}{2}\right) \cos\left(\sqrt{q_\ell}\frac{\ell}{2}\right) + \ell = w. \tag{6.83c}$$

We fix γ and vary ε, but refer to $\rho = 16\gamma\varepsilon^3$ from (6.82) where this is useful. We first consider $\varepsilon \downarrow 0$ which, for fixed γ, is equivalent to $\rho \ll 1$. We work with the parameters (9.79), for which $\rho = 0.064$, which led to the function g shown in Fig. 9.10(a). For $\ell > 0$, $g(\ell;\gamma)$ has poles where $c_A(\ell,\gamma) = 0$ (see (6.29b)). Between these poles, g increases monotonically, and thus (6.83c) has one solution ℓ between each pair of consecutive poles, for a given $w > 0$. We focus on solutions corresponding to the thinnest interface layers, for which $0 < \ell < \ell_A(\gamma)$, where $\ell_A(\gamma)$ is the first non-zero pole of g (for a given γ).

Since the *ansatz* (6.4b) implicitly assumes that $w \geq \ell$, we are only interested in solutions of (6.83c) where $g > \ell$. This holds if and only if $w > w_{\min}$ (or equivalently, $\ell > w_{\min}$), where $w_{\min}$ is the smallest solution w of $g(w;\gamma) = w$ in (6.83c). To first order,

$$w_{\min} := \frac{\pi}{\sqrt{q_h}} \sim \sqrt{2}\pi\varepsilon \tag{9.76}$$

by (8.20). On the other hand, we recall from Fig. 6.7(a) that it is easy to end up with $\|\widetilde{\varphi}\|_{0,\infty} > 1$ if ℓ is too large. To avoid such profiles in the current situation, we found that it was sufficient to have $\ell < \frac{1}{2}\ell_A(\gamma)$, but this effectively imposes the upper bound $w < w_{\max} := g\left(\frac{\ell_A}{2}\right)$. In the sharp interface limit,[17] the implication is that

$$w_{\max} \sim \frac{0.202}{\gamma\varepsilon^2}. \tag{9.77}$$

This value satisfies $w_{\min} < w_{\text{opt}} < w_{\max}$ (cf. Fig. 9.10(b)) as $\varepsilon \downarrow 0$.

Remark. $w < w_{\min}$ (left of the red line in Fig. 9.10(b)) corresponds to Region I in (6.65).

We observed earlier that $\rho = 1$ is the threshold above which 2-phase candidate minimisers are disordered.[18] Hence we insist that

$$\rho = 16\varepsilon\gamma^3 < 1 \qquad \Leftrightarrow \qquad \varepsilon < \frac{1}{2\,(2\gamma)^{1/3}} \qquad \text{i.e. for } \gamma = 32, \qquad \varepsilon < \frac{1}{8}. \tag{9.78}$$

To accommodate thin monolayers, ε needs to be even smaller than this. Our (simple) approach is to halve the bound in (9.78), and require that $\varepsilon < \frac{1}{16} = 0.0625$; we select $\varepsilon = 0.05$. This has a manageable impact on grid resolution and guarantees that $\rho < \frac{1}{8} \ll 1$, so that the estimates in (8.21)–(8.23) are valid. In all of our experiments, we set

$$\gamma = 32, \qquad \varepsilon = 0.05 \qquad \text{and} \qquad \mathcal{K} = 1. \tag{9.79}$$

For χ^{AV} close to 1, $\mathcal{K} = 1$ results in similar thicknesses for the internal and polymer–void interface layers.

Choosing a regularisation parameter, μ

We conducted a series of 1D gradient flow experiments on $\Omega = (0, 4.5)$ to understand the effect of μ. We used as an IC the interpolant of

$$\varphi\,(y) = 0.5 + \sum_{i=1}^{4} (-1)^i H_\delta\left(y, \frac{3(i-0.5)}{4}, 0.07\right) - 0.5 H_\delta\,(y, 3, 0.04) \tag{9.80a}$$

$$\psi\,(y) = 0.5\,(1 - H_\delta\,(y, 3, 0.04))\,, \tag{9.80b}$$

where

$$H_\delta\,(y, Y, \delta) = \begin{cases} -1 & \dfrac{y-Y}{\delta} < \dfrac{-\pi}{2} \\ \sin\left(\dfrac{y-Y}{\delta}\right) & \left|\dfrac{y-Y}{\delta}\right| \le \dfrac{\pi}{2} \\ +1 & \dfrac{y-Y}{\delta} > \dfrac{\pi}{2}, \end{cases}$$

comprising four zero-mass, internal interface layers, equally spaced between $y = 0$ and $y = 3$ (the midpoint of the polymer–void transition). We used (9.79), along with

$$\chi^{AV} = 1.5, \qquad \chi^{\Delta} = 18.5, \qquad \mathcal{M} = \frac{2}{3}, \tag{9.81}$$

and experimented with $\mu \in 10^{-2}, 10^{-3}, \ldots, 10^{-8}$ and a number of different mesh sizes. Each monolayer thus had width $w = 0.75$. We present summary results in Fig. 9.11, and drill-down into the results for $\mu = 10^{-3}, 10^{-8}$ in Fig's 9.12 and 9.13.

Discussion, observations

For $\mu \in \{10^{-3}, 10^{-4}, \ldots, 10^{-8}\}$, the results in Fig. 9.11(a) suggest that (cf. (5.83))

$$\Upsilon_{\mu,\infty} := \max\left\{(\psi-1)_+, (\varphi-\psi)_+, -(\varphi+\psi)_-\right\}(T) \sim \mathcal{O}(\mu) \qquad \text{as} \qquad \mu \downarrow 0. \tag{9.82}$$

As expected, the smaller μ was, the more closely we came to achieving $(\varphi, \psi) \in \Omega_\nabla$. Fig's 9.12 and 9.13(a) indicate that, for $\mu = 10^{-3}$, φ and ψ were visibly and substantially outside of Ω_∇, whereas for $\mu = 10^{-8}$ this discrepancy was *much* smaller ($\sim 2 \times 10^{-7}$). Besides altering the plateau values between the interface layers, Fig. 9.12 also suggests that the regularisation shifts the layers horizontally by a similar amount.

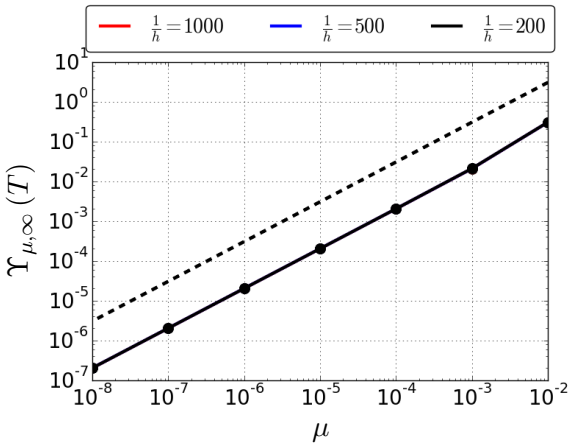

(a) Log-log plot of the end-state $\Upsilon_{\mu,\infty}$ in (9.82) against μ for the three indicated mesh sizes.

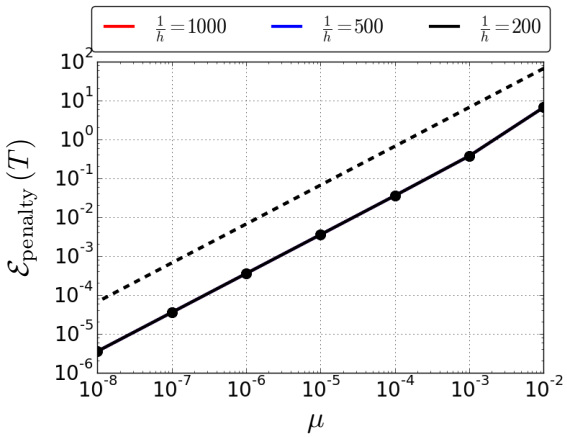

(b) Log-log plot of the end-state $\mathcal{E}_{\text{penalty}}$ in (9.33) against μ for the three indicated mesh sizes.

Figure 9.11: Results of the 3-phase μ-study for three mesh sizes. In the log-log plots, the straight dashed, black lines have unit gradient (suggesting an $\mathcal{O}(\mu)$ relationship). The mesh-specific lines are indistinguishable, suggesting these relationships are mesh-independent.[19]

Fig. 9.11(b) suggests that the energy of the stationary state (with $(\varphi, \psi) \in \Omega_\nabla$ a.e.) converges linearly in μ. At $\mu = 10^{-8}$, we get $\mathcal{E}_\mu = 0.37745$, and only the last digit changes if μ is increased by a factor of 10; hence we take $\mathcal{E} = 0.3775$ as the converged value. In contrast, $\mathcal{E}_\mu = 0.016$ and 0.342 if $\mu = 10^{-3}$ and $\mu = 10^{-4}$. This is consistent with a linear convergence in μ, but also suggests that for $\mathcal{E}_\mu$ to be within 10% of $\mathcal{E}$, we must have $\mu \leq 10^{-4}$. The sharp interface energy estimate from (9.74), with $\nu = 4$, $\nu_{AV} = 1$, $\nu_{BV} = 0$, $L = 4.5$, is $I_0 = 0.383$, which is close to $\mathcal{E}$. That said, Fig. 9.12 suggests that the profile shape is qualitatively morphologically correct, even with the relatively large $\mu = 10^{-3}$. On the other hand, informal experimentation in 2D suggested that average SSN iteration counts grow as $-\log \mu$. To balance the desire for accuracy against our (modest) computational budget, **we selected $\mu = 10^{-6}$ as the default for our 2D experiments**.

Remark. These basic experiments suggest that the effect of μ is mesh independent.[22]

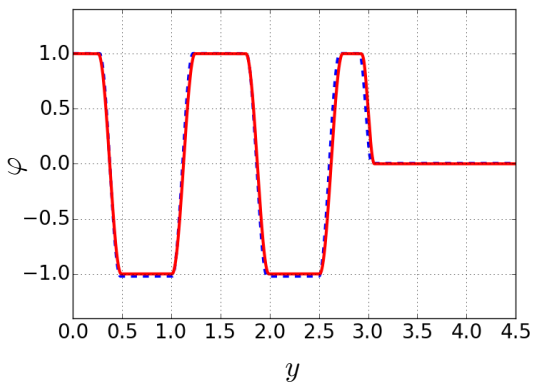

(a) Superimposed φ profiles for $\mu = 10^{-3}, 10^{-8}$

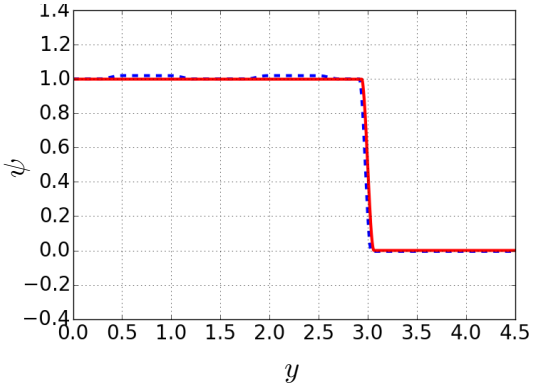

(b) Superimposed ψ profiles for $\mu = 10^{-3}, 10^{-8}$

Figure 9.12: 1D end-state solutions from the time-dependent model (9.69) with IC (9.80), the parameters (9.79), (9.81) with $\mu = 10^{-3}$ (dashed **blue**) and $\mu = 10^{-8}$ (**red**).[20]

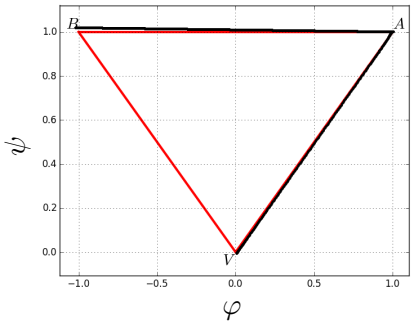

(a) $\mu = 10^{-3}$

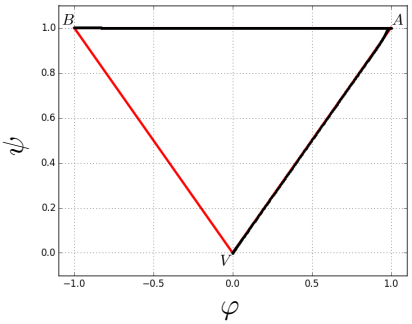

(b) $\mu = 10^{-8}$

Figure 9.13: 1D end-state solutions in (φ, ψ)-space corresponding to the morphologies in Fig. 9.12, with the indicated μ values.[21]

9.3.7 Numerical experiments: parameter validation

At this stage, we can construct low energy 1D morphologies in two ways: i) with the *ansatz* of Section 9.3.3, and ii) the sharp interface limit approach of Section 9.3.5. We now compare the energies of these two types of morphology. We investigated three scenarios involving six specific cases of interest:

Scenario 1:

$$L = 3; \quad (\mathcal{M}, \nu) \in \left\{ \left(\frac{1}{4}, 1\right), \left(\frac{3}{4}, 3\right) \right\}; \quad \chi^{AV} = 1.5; \quad \chi^{\Delta} = 1.5; \quad \varphi(0) = -1. \tag{9.83}$$

Scenario 2: As in (9.83) but with $\chi^{\Delta} = 18.5$.

Scenario 3:

$$L = 4.5; \quad (\mathcal{M}, \nu) \in \left\{ \left(\frac{1}{3}, 2\right), \left(\frac{2}{3}, 4\right) \right\}; \quad \chi^{AV} = 1.5; \quad \chi^{\Delta} = 18.5; \quad \varphi(0) = 1. \tag{9.84}$$

The parameters in (9.79) were used in all cases. $\mathcal{E}_{1D}^{\varepsilon\downarrow 0} = I_0\varepsilon$ with I_0 as in (9.74) denotes the sharp interface limit energy. $\mathcal{E}_{1D}^{\varepsilon>0}$ denotes the energy of the *ansatz* morphologies. It is theoretically possible to create an analytical expression for the energy of an *ansatz* morphology as a function ν, $\mathcal{M}$ and L.[23] The expressions are too complicated to offer any real insight, and so we used CHEBFUN to numerically construct (and plot) these morphologies, and calculate their energies to high precision. In order to use the 2-phase results from Chapter 8 in building the *ansatz* morphologies, we scaled the parameters above to (cf. (9.68), (6.47))

$$\widehat{\alpha} = 4\varepsilon^3\gamma = \frac{2}{125} = 0.016 \quad \text{with} \quad \widehat{q_h} = 0.9837 \quad \text{and} \quad \widehat{q_\ell} = 0.0163; \quad \widehat{\mathcal{D}} = \frac{\mathcal{M}L}{\sqrt{2}\varepsilon}. \tag{9.85}$$

The end-state energy of the experiments was denoted $\mathcal{E}_h(T)$.

We ran three sets of gradient flow experiments with interpolants of our *ansatz* morphologies as ICs (cf. Section 8.1.2 and Fig. 8.3). For the discretisation, we set

$$\tau = 10^{-3}, \qquad T = 5 \quad \text{(i.e. } M = 5\,000\text{)} \qquad \text{and} \qquad h = 10^{-3}. \tag{9.86}$$

$\mathcal{M}$ was varied according to Table (9.2).

Scenario	$\mathcal{M}_{\min}$	$\mathcal{M}_{\max}$	# experiments	Remark
1	$\frac{1}{8}$	$\frac{7}{8}$	200	$\frac{1}{4}, \frac{3}{4} \in [\mathcal{M}_{\min}, \mathcal{M}_{\max}]$
2	$\frac{1}{8}$	$\frac{7}{8}$	200	$\frac{1}{4}, \frac{3}{4} \in [\mathcal{M}_{\min}, \mathcal{M}_{\max}]$
3	$\frac{1}{6}$	$\frac{5}{6}$	200	$\frac{1}{3}, \frac{2}{3} \in [\mathcal{M}_{\min}, \mathcal{M}_{\max}]$

Table 9.2: 3-Phase gradient-flow experiment parameters (1D). Each test set (one per scenario) included 200 $\mathcal{M}$-values, equally spaced between $\mathcal{M}_{\min}$ and $\mathcal{M}_{\max}$.

Discussion, observations

Summary results are presented in Fig's 9.15– 9.17. Summary energy data is plotted in Fig's 9.15(a), 9.16(a) and 9.17(a). Sample sharp interface morphologies are depicted (as in Fig. 9.9(b)) alongside the corresponding *ansatz* morphologies (the dashed black lines) in Fig's 9.15(b)–(c) and 9.17(b)–(c). We also provide the 2-phase $\left(\widehat{\mathcal{D}}, \widehat{\alpha}\right)$ parameters we used to find $\widehat{\ell}$. The *ansatz* and gradient flow end-state morphologies for the six cases of interest are depicted in Fig's 9.15(d)–(e), 9.16(b)–(c) and 9.17(d)–(e).

The most striking feature in the energy plots in Fig's 9.15(a), 9.16(a) and 9.17(a) is how similar the gradient flow experiment end-state energies (the black dots) are to the minimum sharp interface energy estimates (the solid red and blue lines). The match is generally quite good and excellent for small χ^Δ, but comparatively poor when χ^Δ is high (viz. $B \to V$ polymer–void transitions are energetically expensive) *and* the polymer–void transition is

$A \to V$, as evidenced by the gaps between the solid and dashed red lines in Fig's 9.16(a), 9.17(a).[24]

In Fig's 9.15(d)–(e), 9.16(b)–(c) and 9.17(d)–(e), we observed that the sample *ansatz* morphologies (the ICs) were structurally quite similar to the gradient flow end-states they generated. Their energies were also close. Initial and end-states differed consistently and noticeably in the polymer–void transition region. This suggests that our *ansatz* assumption that $\varphi = \pm\psi$ in these areas is poor. Crucially, for our chosen parameters, all three types of morphology have the same energy-minimising monolayer count in each of the six specific cases of interest. Fig. 9.14 shows how our parameters are safely in the middle of the $\nu_{\text{opt}} = 1, \ldots, 4$ regions of 2-phase parameter space. This suggests that the parameter selections we made in Section 9.3.6 are fit for purpose, and that we can use our sharp interface estimates to guide our gradient flow experiments. It also seems reasonable to use our 1D *ansatz* morphologies as IC building blocks in our 2D gradient flow experiments.[25] We provide details starting in Section 9.4.2.

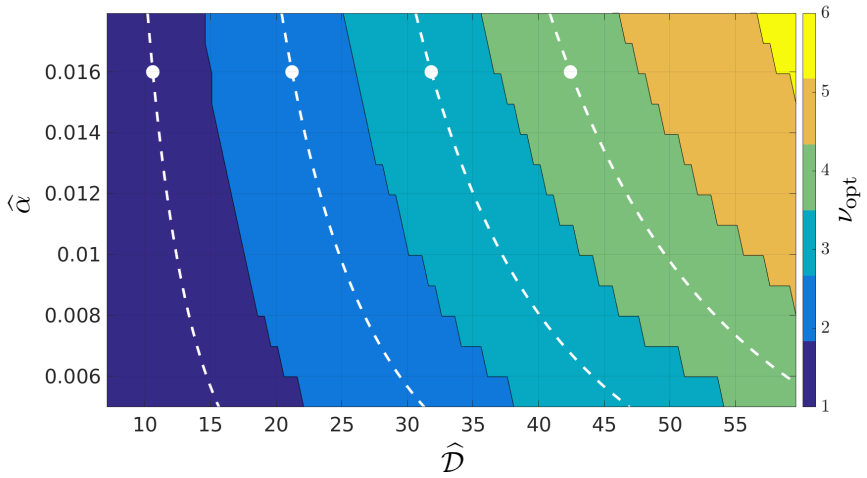

Figure 9.14: A magnified section of Fig. 8.11(a). The white dots indicate $\widehat{\alpha} = 0.016$ and $\widehat{\mathcal{D}} \in \{10.607, 21.213, 31.820, 42.426\}$, as in Fig's 9.15(b), 9.17(b), 9.15(c) and 9.17(c). We take a 2-phase sharp interface limit ($\varepsilon \downarrow 0$, γ constant) along the white dashed lines, as in Section 8.5.[26] This suggests that these monolayer counts should persist as $\varepsilon \downarrow 0$.

Another interesting feature is the discontinuous jumps observed in the gradient flow end-state energies. Their location suggests that this has something to do with the number of monolayers increasing (by one) as $\mathcal{M}$ increases. We do not explore this phenomenon in any detail beyond drilling into our detailed results in Fig. 9.18. The assumption that $\varphi = \pm\psi$ in the polymer–void transition appears to break down in Fig. 9.18(b).

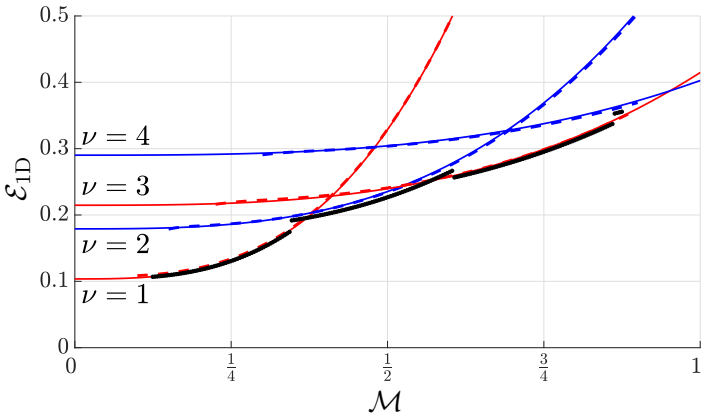

(a) Comparison of *ansatz* (dashed lines) and sharp interface limit (solid lines) energies. **Red** implies an $A \to V$ transition, and **blue**, $B \to V$. The agreement between the *ansatz* and sharp interface energies is excellent. End-state gradient-flow energies (cf. the first row of Table 9.2) are marked as **black** dots. These are very close to the sharp interface limit values.

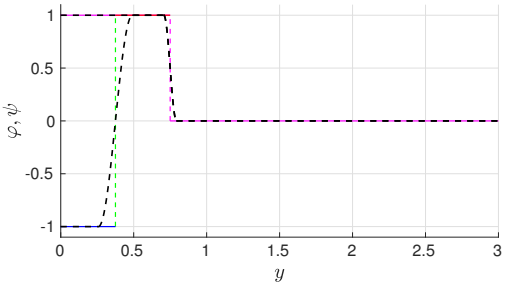

(b) $\mathcal{M} = \frac{1}{4}$, $\nu = 1$. $\mathcal{E}_{1D}^{\varepsilon>0} = 0.1341$, $\mathcal{E}_{1D}^{\varepsilon\downarrow 0} = 0.1318$. $\left(\widehat{\mathcal{D}}, \widehat{\alpha}\right) = (10.607, 0.016)$.

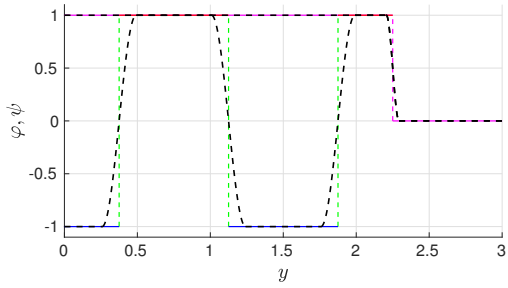

(c) $\mathcal{M} = \frac{3}{4}$, $\nu = 3$. $\mathcal{E}_{1D}^{\varepsilon>0} = 0.2987$, $\mathcal{E}_{1D}^{\varepsilon\downarrow 0} = 0.2991$. $\left(\widehat{\mathcal{D}}, \widehat{\alpha}\right) = (31.820, 0.016)$.

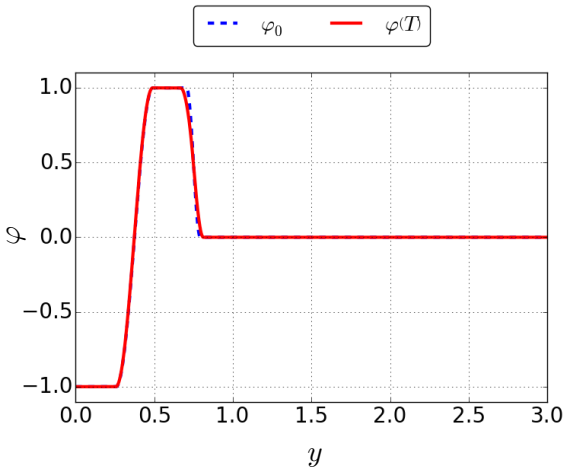

(d) $\nu = 1$ ($M = \frac{1}{4}$)φ *ansatz* IC and gradient-flow end-state morphologies. $\mathcal{E}_{1D}^{\varepsilon>0} = 0.1341$ (the IC), $\mathcal{E}_h(T) = 0.1302$ (end-state).

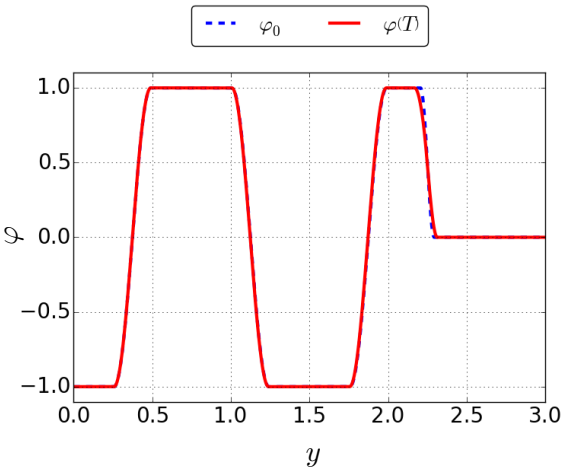

(e) $\nu = 3$ ($M = \frac{3}{4}$)φ *ansatz* IC and gradient-flow end-state morphologies. $\mathcal{E}_{1D}^{\varepsilon>0} = 0.2987$ (the IC), $\mathcal{E}_h(T) = 0.2949$ (end-state).

Figure 9.15: Scenario 1 comparison. For the internal interface layers, $\ell_{\text{mic}} = 0.234$; in the 2-phase process, $\widehat{\ell} = 3.304$, $c_1 = 0.484$ and $c_3 = 0.901$ in (6.59b). $\ell_{\text{mAc}} = 0.087$.[27]

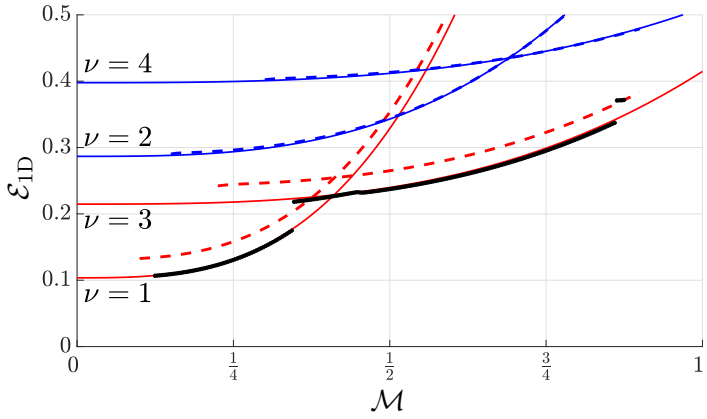

(a) Comparison of *ansatz* (dashed lines) and sharp interface limit (solid lines) energies, as in Fig. 9.15. The agreement between the *ansatz* and sharp interface energies is good for $\nu = 1, 3$, and excellent for $\nu = 2, 4$. End-state gradient-flow energies (cf. the second row of Table 9.2) are marked as **black** dots. These are very close to the sharp interface limit values.

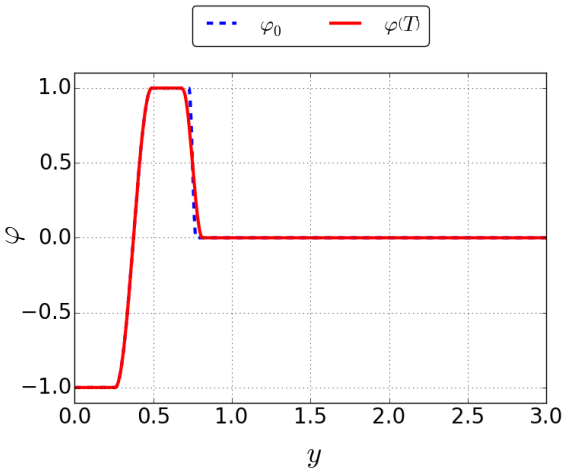

(b) $\nu = 1$ ($M = \frac{1}{4}$) φ *ansatz* IC and gradient-flow end-state morphologies. $\mathcal{E}_{1D}^{\varepsilon>0} = 0.1582$ (the IC), $\mathcal{E}_h(T) = 0.1302$ (end-state) and $\mathcal{E}_{1D}^{\varepsilon\downarrow 0} = 0.1318$ (sharp interface).

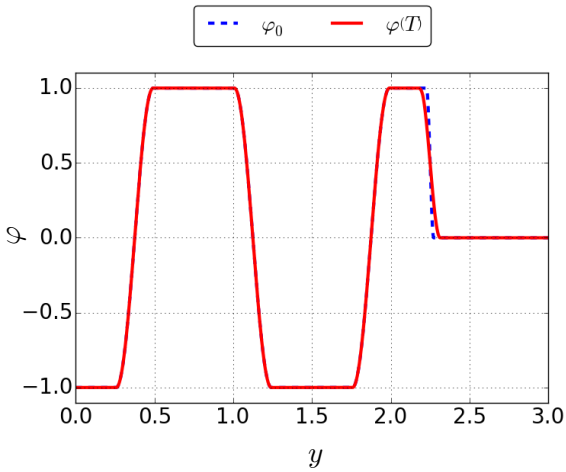

(c) $\nu = 3$ ($M = \frac{3}{4}$) φ *ansatz* IC and gradient-flow end-state morphologies. $\mathcal{E}_{1D}^{\varepsilon>0} = 0.3229$ (the IC), $\mathcal{E}_h(T) = 0.2948$ (end-state) and $\mathcal{E}_{1D}^{\varepsilon\downarrow 0} = 0.2991$ (sharp interface).

Figure 9.16: Scenario 2 comparison. The morphologies for $\mathcal{M} = \frac{1}{4}$, $\nu = 1$ and $\mathcal{M} = \frac{3}{4}$, $\nu = 3$ are visually indistinguishable from those in Fig. 9.15 (as expected, the internal interface layers are identical). $\ell_{\mathrm{mAc}} = 0.046$. The *ansatz* IC and gradient-flow end-state morphologies look very similar; their energies are somewhat different.[28]

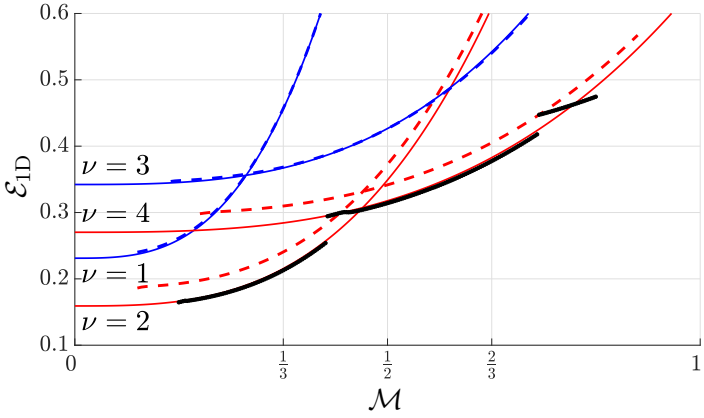

(a) Comparison of *ansatz* (dashed lines) and sharp interface limit (solid lines) energies. The agreement between the *ansatz* and sharp interface energies is good for $\nu = 2, 4$, and excellent for $\nu = 1, 3$. End-state gradient-flow energies (cf. the third row of Table 9.2) are marked as **black** dots. These are very close to the sharp interface limit values.

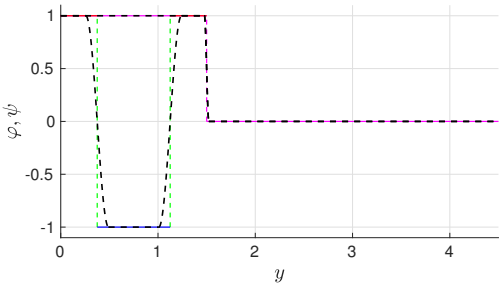

(b) $\mathcal{M} = \frac{1}{3}$, $\nu = 2$. $\mathcal{E}_{1D}^{\varepsilon>0} = 0.2406$, $\mathcal{E}_{1D}^{\varepsilon\downarrow 0} = 0.2154$. $\left(\widehat{\mathcal{D}}, \widehat{\alpha}\right) = (21.213, 0.016)$.

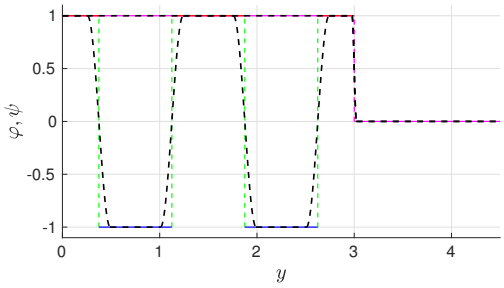

(c) $\mathcal{M} = \frac{2}{3}$, $\nu = 4$. $\mathcal{E}_{1D}^{\varepsilon>0} = 0.4052$, $\mathcal{E}_{1D}^{\varepsilon\downarrow 0} = 0.3827$. $\left(\widehat{\mathcal{D}}, \widehat{\alpha}\right) = (42.426, 0.016)$.

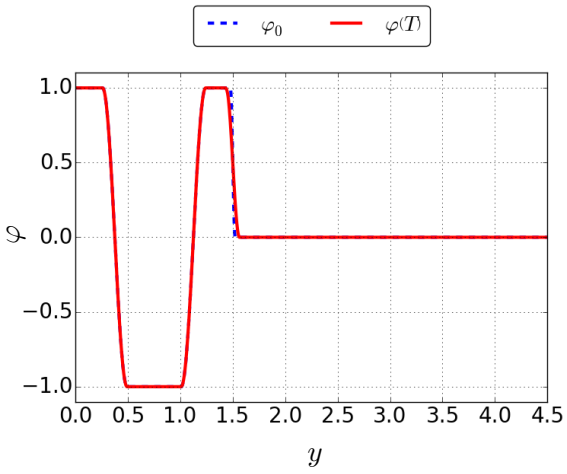

(d) $\nu = 2$ ($M = \frac{1}{3}$) φ *ansatz* IC and gradient-flow end-state morphologies. $\mathcal{E}_{1D}^{\varepsilon>0} = 0.2406$ (the IC), $\mathcal{E}_h(T) = 0.2125$ (end-state).

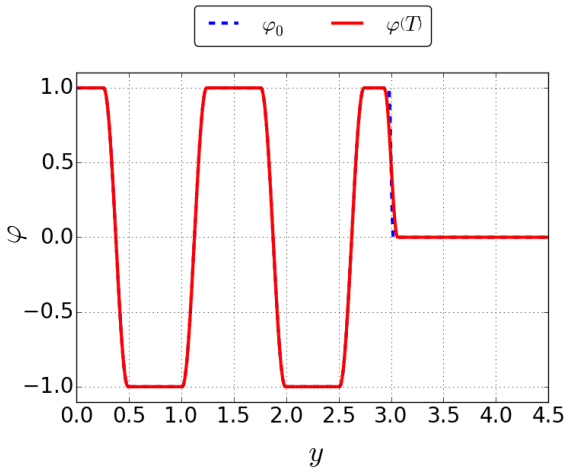

(e) $\nu = 4$ ($M = \frac{2}{3}$) φ *ansatz* IC and gradient-flow end-state morphologies. $\mathcal{E}_{1D}^{\varepsilon>0} = 0.4052$ (the IC), $\mathcal{E}_h(T) = 0.3771$ (end-state).

Figure 9.17: Scenario 3 comparison. ℓ_{mic} and ℓ_{mAc} are as in Scenario 2.[29]

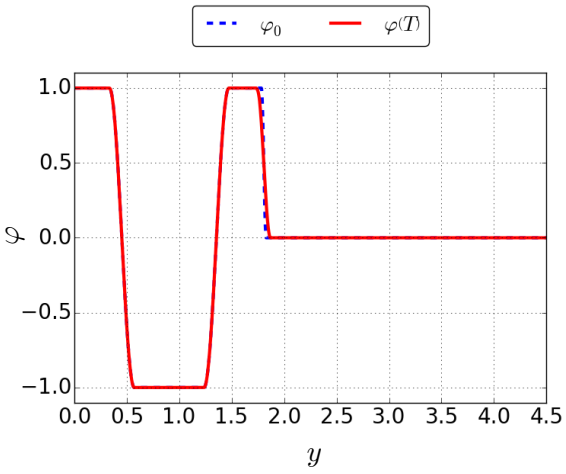

(a) $M = 0.4012$; $\mathcal{E}(T) = 0.2536$. The IC and end-state are structurally quite similar.

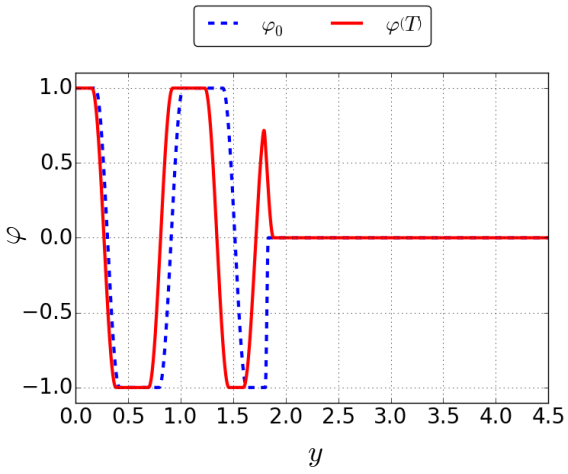

(b) $M = 0.4045$; $\mathcal{E}(T) = 0.2940$. The IC has three monolayers, but the end-state has started to develop an additional monolayer.

Figure 9.18: The jump in the gradient flow end-state energy in Fig. 9.17(a) near $\mathcal{M} = 0.4$. Sharp interface estimates suggest that the additional monolayer should not develop until $\mathcal{M} \approx 0.46$, but for $\varepsilon > 0$, this happens at a lower $\mathcal{M}$.[30]

9.4 2D terracing: steps

We now consider a simplified 2D problem, in which terraces express as steps.[31] We will show that, under appropriate conditions, stepped configurations like the one in Fig. 9.19(a) (Stasiak et al. (2012) refer to this as an $L_1^{||}$–$L_3^{||}$ configuration – see their Fig. 1), have lower energy than their flat alternatives, as in Fig. 9.19(b) (a so-called $L_2^{||}$ configuration).

Our approach in comparing these alternatives is two-fold:

i) In Section 9.4.1 we consider a stationary minimisation approximation that leads to a double tangent construction. We apply our 1D sharp interface limit estimates to the left/right plateaux, and find (simplified) conditions under which the energy of a stepped configuration is lower than a flat one.

ii) Starting in Section 9.4.2, we execute a set of dynamic gradient flow numerical experiments to explore low energy, stepped morphologies. These methods allow us to study far more complicated situations than we can using stationary arguments.

9.4.1 A double tangent construction

We consider a 2D domain $[0, L_x] \times [0, L]$, where $0 < x < L_x$ is the coordinate along the substrate, and $0 < y < L$ is normal to it. We suppose that the domain is occupied by a

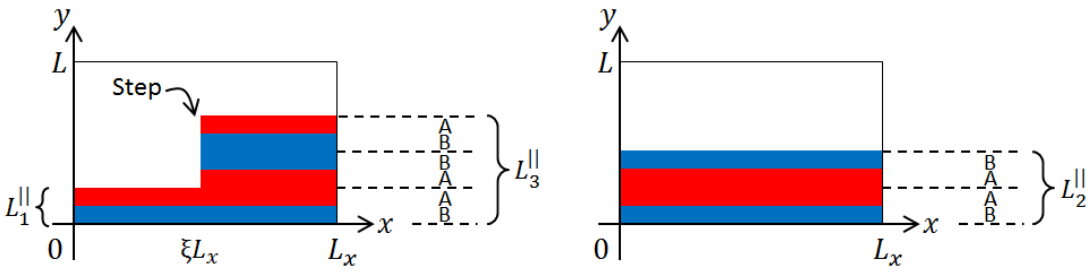

(a) An $L_1^{||}$–$L_3^{||}$ configuration. The step at $x = \xi L_x$, $0 < \xi < 1$, forms the edge of a bilayer on top of an $L_1^{||}$ monolayer.

(b) The corresponding flat $L_2^{||}$ configuration, $BAABV$.

Figure 9.19: A 2D $L_1^{||}$–$L_3^{||}$ stepped configuration in (a) and its flat $L_2^{||}$ alternative in (b). Distinct monolayers are indicated on the right of each figure with horizontal, dashed lines. The A-microdomains are red; the B-microdomains blue. We identify the plane $y = 0$ with a substrate. The microdomains closest to the substrate and void are half as wide as the others. Both configurations have the same copolymer volume fraction, $\mathcal{M}$.

(pure) copolymer of area $V_p = \mathcal{M}L \times L_x$ and a void with area $(1 - \mathcal{M})\, L \times L_x$, as in Fig. 9.19. We assume that the vertical sections of these configurations have been constructed as sharp interface limits, i.e. taking a vertical section through either figure in Fig. 9.19 will yield a 1D morphology like the one in Fig. 9.9(b).

The flat film in Fig. 9.19(b) thus occupies the area $0 < y < \mathcal{M}L$, and comprises ν_{opt} layers of thickness w_{opt} parallel to the substrate, with ν_{opt} as specified immediately after (9.75). If, however, w_{opt} is not commensurate with an integer number of monolayers, the copolymer film could attain a non-uniform profile as an alternative to being flat (with monolayers of sub-optimal width $w \neq w_{\text{opt}}$). The film surface could adjust to accommodate different numbers of layers on different parts of the substrate, all of optimal width w_{opt}. The simplest possibility is a single step change in the film thickness at $x = \xi L_x$, $0 < \xi < 1$, at which the number of monolayers changes from ν_ℓ on the left (each of width w_ℓ) to ν_r on the right (each of width w_r), as in Fig. 9.19(a). It is useful to define

$$\mathcal{M}_\ell := \nu_\ell w_\ell \qquad \text{and} \qquad \mathcal{M}_r := \nu_r w_r \tag{9.87}$$

as the mass fractions on the left and right of the step. If we ignore the energy due to the step edge, the total energy in the configuration is

$$\mathcal{E}_{\text{2D}}\left(\mathcal{M}_\ell, \mathcal{M}_r, \xi\right) = \underbrace{\xi L_x I_0\left(\mathcal{M}_\ell\right)}_{\text{left plateau}} + \underbrace{\left(1-\xi\right) L_x I_0\left(\mathcal{M}_r\right)}_{\text{right plateau}}, \tag{9.88a}$$

with I_0 as in (9.74), but where we have suppressed the ν dependence since we will assume that ν_ℓ, ν_r are given *a priori*. We assume that the entirety of the top of the film surface

(on both sides of the step) is made up of the same A or B species i.e. one of ν_{AV} or ν_{BV} is non-zero for both contributions to $\mathcal{E}_{2\mathrm{D}}$. For a given $\mathcal{M}$, we require

$$\xi\mathcal{M}_\ell + (1-\xi)\,\mathcal{M}_r = \mathcal{M}L. \tag{9.88b}$$

We wish to minimise the energy $\mathcal{E}_{2\mathrm{D}}$ in (9.88a), subject to the mass constraint (9.88b), for given ν_ℓ, ν_r. To solve this problem, we define the Lagrangian

$$\mathscr{L}\left(\mathcal{M}_\ell, \mathcal{M}_r, \xi, \eta\right) = \xi L_x I_0\left(\mathcal{M}_\ell\right) + (1-\xi)\, L_x I_0\left(\mathcal{M}_r\right) - \eta\left(\xi\mathcal{M}_\ell + (1-\xi)\,\mathcal{M}_r - \mathcal{M}L\right), \tag{9.89}$$

with Lagrange parameter η. Necessary first order minimisation conditions are (assuming $'$ denotes $\mathrm{d}/\mathrm{d}\mathcal{M}$)

$$\partial_{\mathcal{M}_\ell}\mathscr{L} = 0 \qquad \Rightarrow \qquad I_0'\left(\mathcal{M}_\ell\right) = \frac{\eta}{L_x}; \tag{9.90a}$$

$$\partial_{\mathcal{M}_r}\mathscr{L} = 0 \qquad \Rightarrow \qquad I_0'\left(\mathcal{M}_r\right) = \frac{\eta}{L_x}; \tag{9.90b}$$

$$\partial_{\xi}\mathscr{L} = 0 \qquad \Rightarrow \qquad \frac{I_0\left(\mathcal{M}_\ell\right) - I_0\left(\mathcal{M}_r\right)}{\mathcal{M}_\ell - \mathcal{M}_r} = \frac{\eta}{L_x}; \tag{9.90c}$$

$$\text{and} \quad \partial_{\eta}\mathscr{L} = 0 \qquad \Rightarrow \qquad \xi\mathcal{M}_\ell + (1-\xi)\,\mathcal{M}_r = \mathcal{M}L. \tag{9.90d}$$

The first three of these lead to the double tangent construction depicted in Fig. 9.20, which we can use to solve for $\mathcal{M}_\ell$, $\mathcal{M}_r$ and η. We find ξ by rearranging (9.90d) to

$$\xi = \frac{\mathcal{M}_r - \mathcal{M}L}{\mathcal{M}_r - \mathcal{M}_\ell}. \tag{9.91}$$

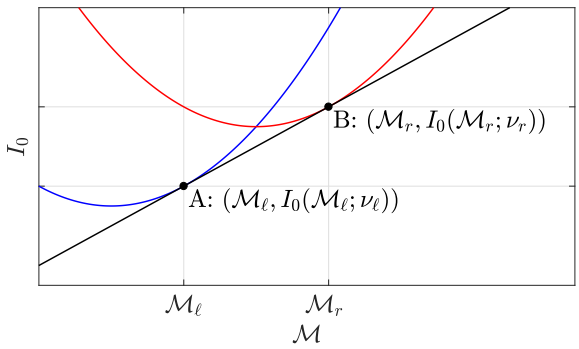

Figure 9.20: The double tangent construction schematic: the blue line is $I_0\left(\mathcal{M};\nu_\ell\right)$ (for a given $\nu = \nu_\ell$) and the red one, $I_0\left(\mathcal{M};\nu_r\right)$ (for a given $\nu = \nu_r$). The black line through A and B of gradient $\left(I_0\left(\mathcal{M}_\ell;\nu_\ell\right) - I_0\left(\mathcal{M}_r;\nu_r\right)\right)/\left(\mathcal{M}_\ell - \mathcal{M}_r\right)$ (cf. (9.90c)) is tangent to $I_0\left(\mathcal{M}_\ell;\nu_\ell\right)$ at A as in (9.90a)), and likewise to $I_0\left(\mathcal{M}_r;\nu_r\right)$ at B, as in (9.90b).

We recall from (9.75) that I_0 is minimised when $w = w_{\mathrm{opt}}$, and that w_{opt} is *independent of* $\mathcal{M}$. Consequently, $\mathcal{E}_{2\mathrm{D}}$ is minimised when $w_\ell = w_r = w_{\mathrm{opt}}$, i.e. all of the monolayers on

the left/right have the same width as for the 1D minimum. Under these conditions, (9.91) yields (using (9.87))

$$\xi = \frac{\nu_r w_{\rm opt} - \mathcal{M}L}{\nu_r w_{\rm opt} - \nu_\ell w_{\rm opt}} = \frac{\nu_r - \mathcal{M}L/w_{\rm opt}}{\nu_r - \nu_\ell}. \tag{9.92}$$

A special case: the $L^{||}_\nu$–$L^{||}_{\nu+2}$ configuration

We focus on the case where $\nu_\ell = \nu$, $\nu_r = \nu + 2$, $\mathcal{M}L = (\nu + 1)\, w_{\rm opt}$. Then $\xi = \frac{1}{2}$ and if the polymer–void transition is $A \to V$ (i.e. $\nu_{AV} = 1$, $\nu_{BV} = 0$), then the lateral energy density (in x) of the $L^{||}_\nu$–$L^{||}_{\nu+2}$ configuration is, according to (9.88a),

$$\frac{\mathcal{E}_{\rm 2D}}{L_x} = \frac{1}{2}\Big[I_0\left(\nu, \nu w_{\rm opt}\right) + I_0\left(\nu + 2, (\nu + 2)\, w_{\rm opt}\right)\Big] = \frac{3\pi}{4\sqrt{2}}\,(\nu + 1) + \frac{\pi}{4\sqrt{2}}\sqrt{(1 + \mathcal{K})\,\chi^{AV}}, \tag{9.93}$$

where we used (9.75). $\mathcal{E}_{\rm 2D}$ is independent of γ. An alternate flat $L^{||}_{\nu+1}$ configuration with $\nu + 1$ microdomains of optimal width $w_{\rm opt}$ is also possible, with a $B \to V$ polymer–void transition, and lateral energy density

$$I_0\left(\nu + 1, \mathcal{M}\right) = \frac{3\pi}{4\sqrt{2}}\,(\nu + 1) + \frac{\pi}{4\sqrt{2}}\sqrt{(1 + \mathcal{K})\,(\chi^{AV} + \chi^{\Delta})}, \tag{9.94}$$

using (9.75) once again. In this simple, sharp interface approximation, it is clear that if $\chi^\Delta > 0$, then the configuration with the step has lower energy than the flat, $(\nu + 1)$-layer alternative. Since this approximation neglects the energy due to the step edge, we expect that χ^Δ should be above some threshold for the stepped configuration to be energetically advantageous (for a fixed L_x). On the other hand, the third term in I_0 in (9.74), which measures the energy in the polymer–void transition, does not depend on ν (or w), and thus has no impact on $w_{\rm opt}$ in (9.75). This simplification thus entirely discounts the effect of the polymer–void transition on the monolayer count. Specifically, for very high χ^Δ, we might expect a nett energetic advantage from a higher/lower monolayer count (i.e. monolayers of width other than $w_{\rm opt}$) if this puts the lower energy polymer species at the polymer–void transition. We illustrate this effect in Fig. 9.23. In the example above, we thus anticipate at least three possibilities: i) a flat film with $\nu+1$ monolayers of width $w_{\rm opt}$, but a very high energy polymer–void transition, ii) a flat film with ν or $\nu + 2$ monolayers and a low energy polymer–void transition, but monolayer width not close to $w_{\rm opt}$, and iii) a configuration with ν and $\nu + 2$ monolayers to the left/right of a step, with the lower energy polymer–void transition covering at least the majority of the film, and all of the monolayers having width at or near $w_{\rm opt}$.

The relative advantage of this last configuration grows with increasing L_x. We illustrate this as follows: for the flat alternative and the $L^{||}_{\nu_\ell}$–$L^{||}_{\nu_r}$ stepped configuration, we have

$$\mathcal{E}_{\rm flat}\left(\mathcal{M}; \nu\right) = I_0\left(\mathcal{M}; \nu\right) L_x \varepsilon, \tag{9.95a}$$

$$\mathcal{E}_{\text{step}}\left(\nu_\ell, \nu_r\right) = \frac{\mathcal{E}_{\text{flat}}\left(\mathcal{M}_\ell; \nu_\ell\right) + \mathcal{E}_{\text{flat}}\left(\mathcal{M}_r; \nu_r\right)}{2} = \frac{I_0\left(\mathcal{M}_\ell; \nu_\ell\right) + I_0\left(\mathcal{M}_r; \nu_r\right)}{2} L_x \varepsilon, \qquad (9.95b)$$

where we suppress the $\mathcal{M}_\ell, \mathcal{M}_r$ dependency on the left; $\xi = \frac{1}{2}$, so $\frac{1}{2}\left(\mathcal{M}_\ell + \mathcal{M}_r\right) = \mathcal{M} = \frac{1}{2}$. If we use (9.93) and (9.94) in (9.95), we find that, to first order,

$$\mathcal{E}_{\text{flat}} - \mathcal{E}_{\text{step}} = \frac{\pi\sqrt{1+\mathcal{K}}}{4\sqrt{2}} \left(\sqrt{\chi^{AV} + \chi^{\Delta}} - \sqrt{\chi^{AV}}\right) L_x \varepsilon. \qquad (9.96)$$

Hence stepped configurations should be energetically favoured for sufficiently large L_x.

9.4.2 Gradient flow numerical simulations

We report on a set of 2D gradient flow numerical experiments that we conducted to test our predictions above.

Experimental setup

We used the fully implicit time-stepping numerical scheme and FEniCS code of Section 9.2.5.3, and mapped the parameters of Section 9.3.6 to those in the numerical method using (9.68). We used a fixed spatial grid and and manual, adaptive time-stepping.[32] We extended T in each simulation until the energy decay was essentially zero, and the profiles could be considered stationary (see Fig. 9.22).[33]

We worked with two rectangular geometries $(0, L_x) \times (0, L)$, similar to those used in the first numerical SCFT experiments in Stasiak et al. (2012):

i) the $L_1^{\parallel}$–$L_3^{\parallel}$ configuration, with $L_x = 16$ and $L = 3$.

ii) the $L_2^{\parallel}$–$L_4^{\parallel}$ configuration, with $L_x = 8$ and $L = 4.5$.

Unless otherwise stated, we set the polymer volume fraction to $\mathcal{M} = 0.5$. In both geometries, these combinations fixed the optimal (vertical) width of the monolayers in equilibrium at $w_{\text{opt}} = 0.75$, and we chose the remaining parameters as in (9.79).

Interpreting results

We explain the shaded φ contour map in Fig. 9.21(a). Light green represents $\varphi = 0$, dark **red** $\varphi = 1$ (phase A), and dark **blue** $\varphi = -1$ (phase B), with other colours indicating the interface layers between them. ψ has a simple topology so we do not introduce a separate colour scheme. Instead, we include the dashed white line marking the contour line $\psi = \frac{1}{2}$, to indicate the middle of the polymer–void transition. The light green area above the dashed white line represents the region with the (nearly) pure V (void) species, $\psi, \varphi \approx 0$, while the region below is occupied by the polymer, $\psi \approx 1$.

Where appropriate, we compared our 2D end-state energies with the corresponding minimum flat film energy, defined as the product of L_x and the minimum energy of a

vertical 1D section configuration (obtained by simulation) with $\mathcal{M} = \frac{1}{2}$. We then compared these with the sharp interface estimates (with $\xi = \frac{1}{2}$) in (9.95).

9.4.3 Open and closed configurations: the effect of χ^{Δ}

Small χ^{Δ}. For our first pair of 2D experiments, we used the IC in Fig. 9.21(a), in which the domain was split into left and right halves. On the left, $0 < x < \frac{1}{2}L_x$, we used a configuration with a B-micro-domain at the substrate ($y = 0$) of width $w_{\text{opt}}/2$, below an A-micro-domain of the same width (i.e. a one monolayer configuration) as in Fig. 9.15(b). For $\frac{1}{2}L_x < x < L_x$, we had four microdomains $BAABBA$ (three monolayers), of width $w_{\text{opt}}/2$, w_{opt}, w_{opt} and $w_{\text{opt}}/2$, as in Fig. 9.15(c). Because of our spatial discretisation, $\overline{\varphi_0}$ was not exactly zero (this was true for all of our 2D experiments), but thanks to the mass control property in (9.70c), this was not a serious issue. Finally, we set

$$\chi^{AV} = 1.5 \qquad \text{and} \qquad \chi^{\Delta} = 1.5. \tag{9.97}$$

Since w_{opt} is the optimal monolayer width in the sharp interface limit, we expected the IC to be close to the end-state in equilibrium. The expression (9.92) predicts that for $\nu_\ell = 1$, $\nu_r = 3$, and $\mathcal{M}L = (\nu_\ell + \nu_r)\, w_{\text{opt}}/2$, the step should remain very close to $x = \xi L_x = L_x/2$. When we ran the simulation, there was initially a fairly rapid evolution as the side of the step relaxed and the polymer–void transition adjusted. At $T = 202$, the solution shown in Fig. 9.21(b) was essentially stationary, as confirmed in Fig. 9.22(a). The step was still centred around $x = L_x/2$. The topology at the surface was largely unchanged, with the A phase occupying most of the interface layer with the void, except for a small portion in the step transition near $x = 8$. We also observed two triple points near $(x, y) = (7.7, 1.2)$ and $(8.5, 1.8)$, where all three pure phases were close to each other (see Section 9.4.4). The flat configuration with the lowest energy was the 2-monolayer $BAABV$ with $\mathcal{E}_\mu = 3.619$ (which exceeds that noted below Fig. 9.21(b) and in Table 9.3). The sharp interface energy estimates (9.95) (cf. Fig. 9.23) were

$$\mathcal{E}_{\text{flat}}\left(\frac{1}{2}; 1\right) = 5.258, \quad \mathcal{E}_{\text{flat}}\left(\frac{1}{2}; 2\right) = 3.765, \quad \mathcal{E}_{\text{flat}}\left(\frac{1}{2}; 3\right) = 3.835, \quad \mathcal{E}_{\text{step}}\,(1, 3) = 3.447,$$

with $\mathcal{E}_{\text{step}}$ the smallest, in good agreement with our dynamic numerical results.

Large χ^{Δ}. If the surface tension of one of the interface layers, say BV, exceeds the sum of the other two, $\sigma_{BV} > \sigma_{AB} + \sigma_{AV}$, then it is energetically favourable to remove the triple-phase contact points by eliminating the interface layer between B and V completely. This is the situation in the rightmost column of Fig. 9.21, in which we increased χ^{Δ}, setting

$$\chi^{AV} = 1.5, \qquad \chi^{\Delta} = 18.5. \tag{9.98}$$

The other parameters and the IC were unchanged. According to (9.73), the surface tensions are $\sigma_{AB} = 1.11$, $\sigma_{AV} = 0.96$, and $\sigma_{BV} = 3.51$. In Fig. 9.21(c), recorded at $T = 102$, the

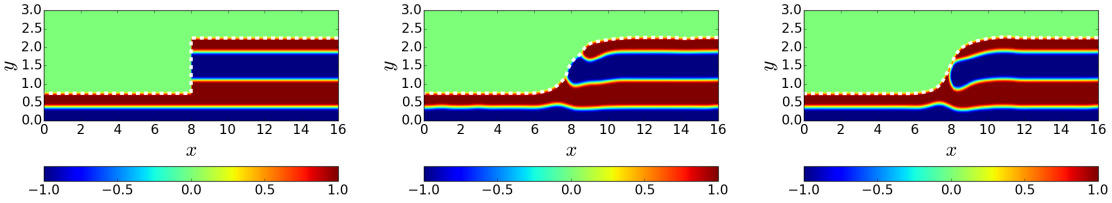

(a) Shared IC: $t = 0$

(b) The open configuration: $\chi^{\Delta} = 1.5$; (9.97). $\mathcal{E}_{\mu} = 3.441$

(c) The closed configuration: $\chi^{\Delta} = 18.5$; (9.98). $\mathcal{E}_{\mu} = 3.461$

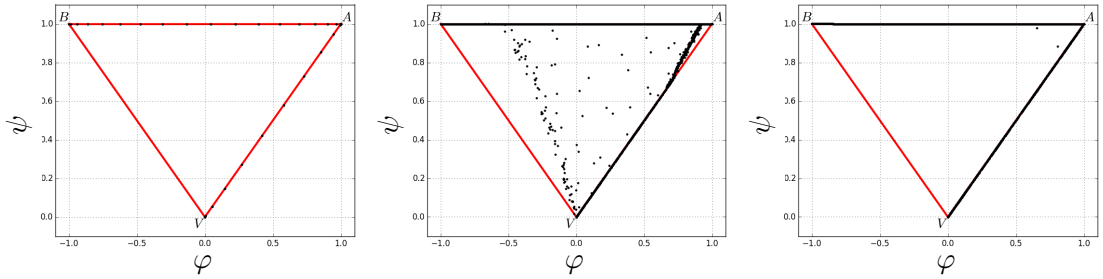

(d) The IC in (φ, ψ)-space

(e) The end-state open configuration in (φ, ψ)-space

(f) The end-state closed configuration in (φ, ψ)-space

Figure 9.21: Plots of φ and corresponding views in (φ, ψ)-space (cf. Fig. 9.2), for the first and second 2D simulations. The colour map in the top row, and the dashed white lines are explained in the text. The parameters in (9.79) were used in both experiments. Fig's (b) and (c) are $L_1^{||}$–$L_3^{||}$ configurations in Stasiak et al. (2012): (b) corresponds to the open (O) morphology of Fig. 2 of Stasiak et al. (2012), and (c) to their closed (C_0) morphology.[34]

	Open		**Closed**	
Energy bucket	$t = 0.0$	$T = 202$	$t = 0.0$	$T = 102$
Bulk (ex. penalty)	1.313	1.359	1.366	1.376
Penalty	0	$< 10^{-4}$	0	0.003
Total homogeneous	1.313	1.359	1.366	1.379
Long-range	0.849	0.844	0.849	0.842
φ-interfacial	1.141	1.019	1.141	1.046
ψ-interfacial	0.264	0.219	0.264	0.194
$\mathcal{E}_{\text{total}}$	3.568	3.441	3.621	3.461

Table 9.3: Start/finish energy comparison data for the open and closed morphology experiments, summarised by energy bucket. For $\mu = 10^{-6}$, the penalty energy is very small.[36]

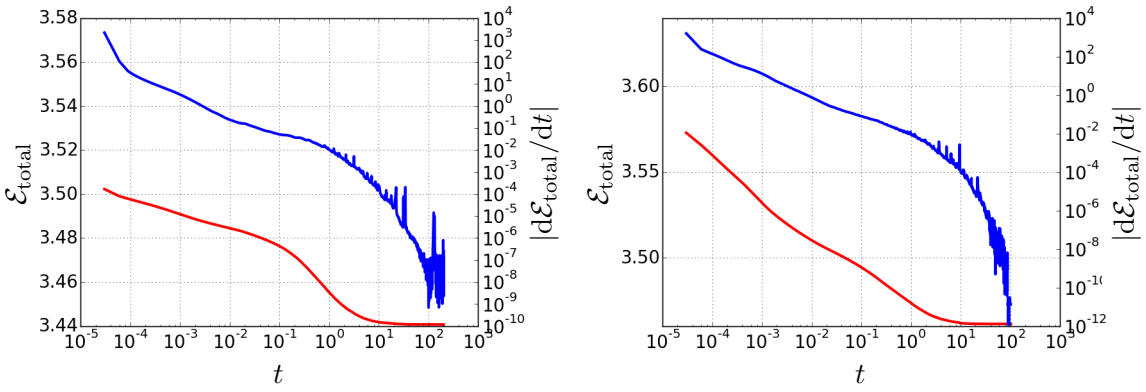

(a) Open configuration energy evolution

(b) Closed configuration energy evolution

Figure 9.22: Log-log plots of energy evolution against t. On the left y-axis, we show total energy in **red**; on the right, $\left|\frac{\mathrm{d}\mathcal{E}}{\mathrm{d}t}\right|$ in **blue** (see Table 9.3 for complete start/finish energy information). In each case, there is a steep drop in the energy, early in the simulation (it is not possible to plot data against $t = 0$ on a log scale). We ran the simulations until the energy essentially stopped changing and $\left|\frac{\mathrm{d}\mathcal{E}}{\mathrm{d}t}\right|$ was very close to zero.[35]

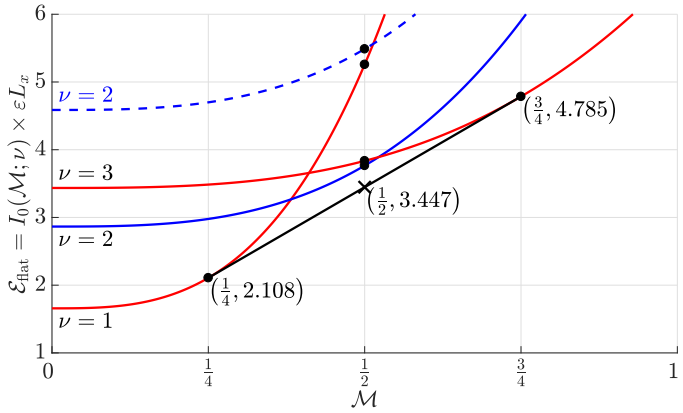

Figure 9.23: Sharp interface double tangent construction for (flat) $\nu = 1, 2, 3$ with phase B at the substrate, and the parameters in (9.79). Configurations with an odd number of monolayers ($A \to V$ polymer–void transition) are **red**; even number monolayer configurations ($B \to V$ polymer–void transition) are **blue**. $\mathcal{M}_\ell = \frac{1}{4}$, $\mathcal{M} = \frac{1}{2}$ and $\mathcal{M}_r = \frac{3}{4}$ in (9.88), (9.90). The solid lines relate to the small χ^Δ parameters (in (9.97)): $\mathcal{E}_{\text{flat}}\left(\frac{1}{2}; 1\right) = 5.258$, $\mathcal{E}_{\text{flat}}\left(\frac{1}{2}; 2\right) = 3.765$, $\mathcal{E}_{\text{flat}}\left(\frac{1}{2}; 3\right) = 3.835$ and $\mathcal{E}_{\text{step}}(1, 3) = 3.447$. The results for large χ^Δ (viz. (9.98)) are the same, except for $\nu = 2$, which is drawn as the dashed **blue** line. The 2-monolayer, large χ^Δ morphology has a *much* higher energy, $\mathcal{E}_{\text{flat}}\left(\frac{1}{2}; 2\right) = 5.487$, than the corresponding small χ^Δ morphology. See also Fig's 9.15(a), 9.16.[37]

triple points have moved towards each other leading to the closed configuration, in which B and V do not share an interface layer. This is also clearly visible in Fig. 9.21(f) (cf. the open configuration of Fig's 9.21(b), (e)). The energy evolution of this experiment is depicted in Fig. 9.22(b).

For this much higher value of χ^{Δ}, the simulated flat configuration with the lowest energy was the 3-monolayer $BAABBAV$ (notice the AV interface layer) with $\mathcal{E}_{\mu} = 3.792$ (exceeding that noted below Fig. 9.21(c) and in Table 9.3). The sharp interface energy estimates (9.95) (cf. Fig. 9.23) were the same as those above, except for $\mathcal{E}_{\text{flat}}(2) = 5.487$ (because of the BV interface layer). The value of w_{opt} in (9.75) corresponded to the flat 2-monolayer configuration which had much higher energy; see the discussion immediately preceding section 9.3.6.

9.4.4 Triple-phase contact point angles

We consider the triple points in the open configuration of Fig. 9.21(b) near $(x, y) = (7.7, 1.2)$ and $(8.5, 1.8)$, at which all three pure phases are close to each other. Young's relation (as in Fig. 3 of Boyer and Lapuerta (2006) and Chapter 11 (p. 283) of Lee (2012)) relates the angles between tangent lines at a triple point, $\boldsymbol{\theta} = \{\theta_A, \theta_B, \theta_V\}$, to the surface tensions exerted by the interface layers, $\boldsymbol{\sigma} = \{\sigma_{AB}, \sigma_{AV}, \sigma_{BV}\}$, via

$$\frac{\sin\theta_A}{\sigma_{BV}} = \frac{\sin\theta_B}{\sigma_{AV}} = \frac{\sin\theta_V}{\sigma_{AB}} \qquad \text{and} \qquad \theta_A + \theta_B + \theta_V = 2\pi, \qquad \theta_A, \theta_B, \theta_V > 0. \tag{9.99}$$

We depicted this relationship in the schematic of Fig. 9.24.

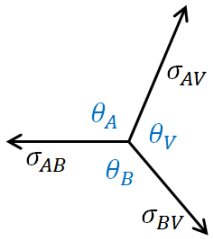

Figure 9.24: Schematic of a triple point from Young's relation. The arrows represent the surface tensions exerted by the interface layers as vectors tangent to the contour lines of each phase, originating at the triple point. The contact angles are blue.

Substituting the parameters (9.79) and (9.97) into the sharp interface limit approximation (9.73), we find that the surface tensions are $\sigma_{AB} = 1.11$, $\sigma_{AV} = 0.96$, and $\sigma_{BV} = 1.36$. Substituting these into (9.99) we calculate that $\theta_A = 0.2728 = 98.2°$, $\theta_B = 0.3769 = 135.7°$ and $\theta_V = 0.3503 = 126.1°$.[38]

In Fig. 9.25, we manually superimposed the angles solving (9.99) as in Fig. 9.24, over the magnified triple points extracted from Fig. 9.21b. We attempted to visually identify

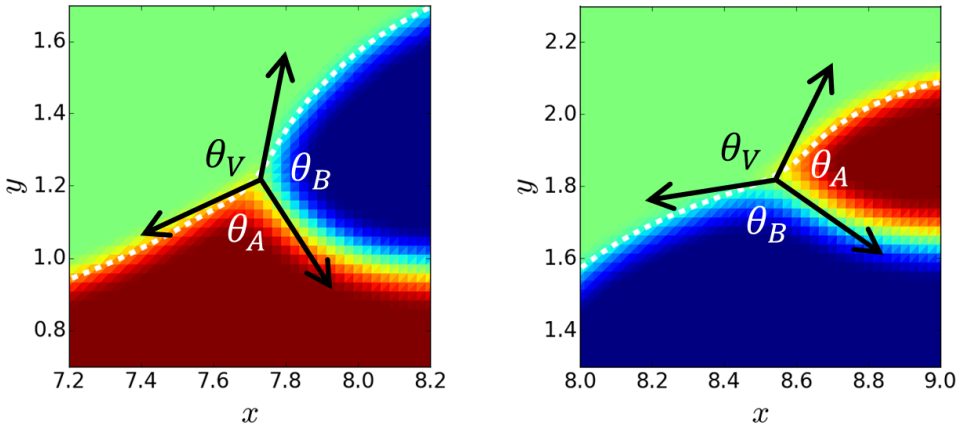

(a) The triple point near $(x, y) = (7.7, 1.2)$ (b) The triple point near $(x, y) = (8.5, 1.8)$

Figure 9.25: Zoomed view of the triple points in the open end-state of Fig. 9.21, with contact angles solving (9.99) overlaid manually. We superimpose the contour line $\psi = \frac{1}{2}$ (dashed, white) as a visual cue to the approximate location of the triple points.

the point closest to the centre of the transitional region between the three pure phases, and then align the surface tension vectors[39] manually to the edges of the red ($\phi_A \approx 1$), blue ($\phi_B \approx 1$) and light green ($\phi_V \approx 1$) regions in the underlying filled contour plot. We wished to understand how closely the angles in $\boldsymbol{\theta}$ matched those on the edges of these coloured regions, where they meet (i.e. at the triple point).

Discussion, observations

- Manually locating the triple points was difficult because the interfacial regions were relatively thick at the depicted magnification. It was difficult to visually superimpose contour lines separating the coloured regions, and impossible to identify tangents at their contact points.[40]

- It looks like the two sets of contact angles in Fig. 9.25 are different, which suggests that the morphology is not at equilibrium. We cannot dismiss this possibility entirely, but note that this is unlikely in view of the energy evolution plot in Fig. 9.22(a). This impression is also at least, in part, likely due to the very different sizes/shapes of the dark red regions.

In light of the above, it is very difficult to assess how closely our results matched the sharp interface limit predictions. To improve the situation we could project the morphology in Fig. 9.21(b) onto a finer mesh/grid and use it as the IC in a new gradient flow experiment. Ideally, we could also use a smaller value of ε (keeping γ and $\mathcal{K}$ fixed) and experiment with a model that is closer to the sharp interface limit. It might also be possible to numerically

extract the $\psi = \frac{1}{2}$ and $\varphi = 0$ contours from the finite element solution,[41] and then estimate their intersection and tangent vectors. This would allow us to estimate $\boldsymbol{\theta}$ *from the data*, instead of superimposing the theoretical sharp interface limit values as we did above.

9.4.5 Higher monolayer counts: the closed configuration

In our second pair of 2D experiments, summarised in Fig. 9.26, we used the same parameters (9.79) and (9.98) as in Fig. 9.21(a) and (c), but used ICs having two and four monolayers to the left and right of the step, and an A-micro-domain at the substrate (cf. Fig's 9.17(b), (c)). In the first experiment, the top B-micro-domain to the right of the step (the second blue layer in Fig. 9.26(a)) was a semi-layer; in the second (Fig. 9.26(c)), the second A-micro-domain was a truncated layer. As in Stasiak et al. (2012), we call these the C_0 and C_1 topologies. To keep the polymer volume fraction constant at $\mathcal{M} = \frac{1}{2}$ (for the same optimal layer width as our previous experiments), the vertical extent of the domain was increased to $L = 4.5$. The lateral extent was decreased to limit computational cost. These very different topologies were preserved as the systems evolved, giving the results in Fig's 9.26(b) (recorded at $T = 133$) and (d) (recorded at $T = 193$). At the time for which the results are shown, the energy decay had essentially stopped, suggesting that both configurations were very close to stable steady states, that is, local energetic minima. The total energies of these states are very similar to those noted in Stasiak et al. (2012). However, while those authors recorded a lower energy for the C_1 than for the C_0 topology, our energy values were too close for a reliable comparison, given our spatial grid resolution ($\sim$40 nodes per unit length in each direction).

The corresponding flat configuration with the lowest energy, for both of these scenarios, was the four-layer $ABBAABBAV$ configuration with $\mathcal{E}_\mu = 2.509$, which exceeds both of the values noted in Fig's 9.26(b), (d). The sharp interface estimates (9.95) (cf. Fig. 9.27) were

$$\mathcal{E}_{\text{flat}}\left(\frac{1}{2}; 2\right) = 2.792, \quad \mathcal{E}_{\text{flat}}\left(\frac{1}{2}; 3\right) = 3.413, \quad \mathcal{E}_{\text{flat}}\left(\frac{1}{2}; 4\right) = 2.542, \quad \mathcal{E}_{\text{step}}\left(2, 4\right) = 2.393,$$

with $\mathcal{E}_{\text{step}}$ the smallest. Once again, our sharp interface and gradient flow numerical results were in good, qualitative agreement.

9.4.6 Spontaneous step formation

We conducted a gradient flow experiment with the random wedge of polymer material depicted in Fig. 9.28 as the IC,[44] and the same material and dynamic parameters as in Section 9.4.5. We wished to investigate i) whether a step would form spontaneously from a flat IC and, if so, examine the kinematics of the process; ii) whether we would recover the optimal monolayer width, w_{opt}; and iii) which of the C_0 and C_1 configurations in Fig's 9.26(b)–(d) (if either) would emerge as the preferred (lower energy) morphology.

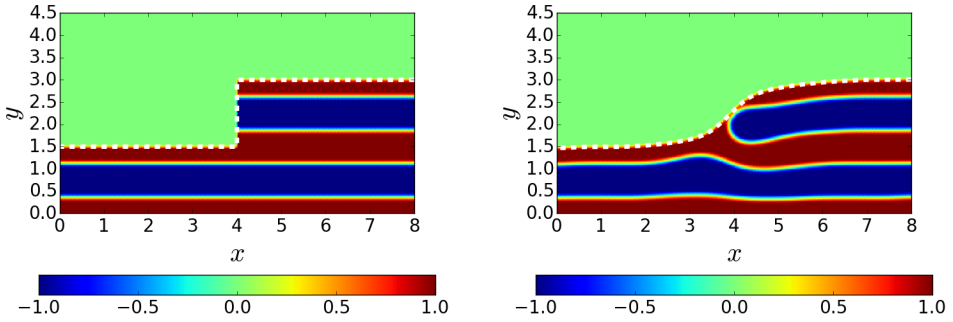

(a) $t = 0$

(b) The C_0 closed configuration. $\chi^{\Delta} = 18.5$ as in (9.98). $\mathcal{E}_{\mu} = 2.408$

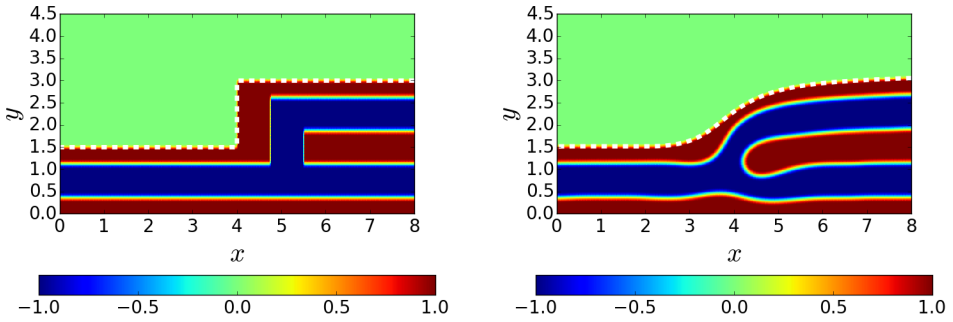

(c) $t = 0$

(d) The C_1 closed configuration. $\chi^{\Delta} = 18.5$ as in (9.98). $\mathcal{E}_{\mu} = 2.411$

Figure 9.26: ICs and end-states. These are $L_2^{||}$–$L_4^{||}$ configurations in Stasiak et al. (2012): (b) corresponds to the closed C_0 morphology of Fig. 4 of Stasiak et al. (2012), and (d) to their C_1 morphology.[42]

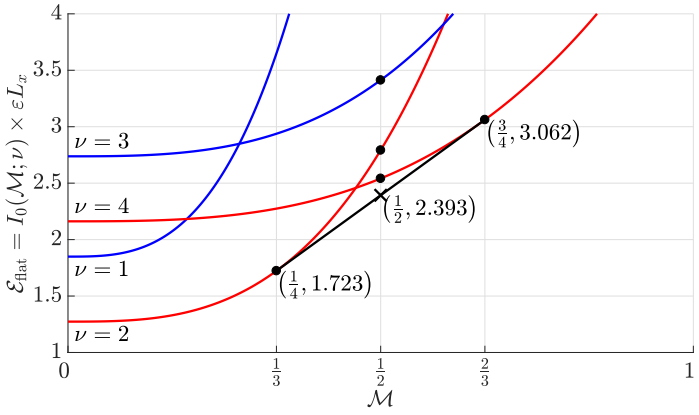

Figure 9.27: Sharp interface double tangent construction for the parameters in (9.79), (9.98), with substrate phase A, and a higher layer count. $\mathcal{E}_{\text{flat}}\left(\frac{1}{2}; 2\right) = 2.792$, $\mathcal{E}_{\text{flat}}\left(\frac{1}{2}; 3\right) = 3.413$, $\mathcal{E}_{\text{flat}}\left(\frac{1}{2}; 4\right) = 2.542$ and $\mathcal{E}_{\text{step}}\left(2, 4\right) = 2.393$. $\mathcal{M}_{\ell} = \frac{1}{3}$, $\mathcal{M} = \frac{1}{2}$ and $\mathcal{M}_r = \frac{2}{3}$. See also Fig. 9.17(a).[43]

Discussion, observations

We depict snapshots of our results in Fig's 9.30– 9.32. The energy evolution is in Fig. 9.29. In Fig's 9.30– 9.32, we observe:

- As expected, φ initially evolved extremely rapidly, forming a set of fine, concentric wedges, that were parallel to the substrate ($y = 0$) and the polymer–void transition, and perpendicular to the right edge of Ω (at $x = 8$). These fine structures coarsened and appeared to diffuse through the right edge of Ω.

- Most of the change in φ occurred before $t \approx 10$, after which the evolution slowed.

- By $T \approx 396$, the energy was no longer monotonically decreasing,[45] and $\mathrm{d}\mathcal{E}_\mu/\mathrm{d}t \approx 10^{-12}$ as in Fig. 9.29, and so we concluded the experiment. The end-state morphology in Fig. 9.30(o) was visually indistinguishable from the C_1 closed configuration of Fig. 9.26(d). The end-state AB monolayers had width very close to $w_{\mathrm{opt}} = 0.75$.

- Fig. 9.31 suggests a different temporal evolution profile for ψ compared to φ. Whereas φ changed very quickly initially, ψ and the polymer–void free surface (i.e. the shape of the pure polymer region) changed substantially between $t \approx 10$ and $T = 396$.

- Fig. 9.32 reveals that by $t \approx 10$, the morphology was comprised entirely of pure phase A, B and V areas, and clean AB and BV interface layers.

Remarks.

i) The shading in Fig. 9.30(a) is different to that of the other figures; dark blue corresponds to $\varphi \approx -0.5$, and light blue (not the usual light green) to $\varphi \approx 0$.

ii) The light green area inside the wedge of polymer in Fig. 9.30(b) consisted of mixed A and B material in which $\varphi \approx 0$. There was no void inside the polymer (i.e. $\psi \approx 1$ in this area as in Fig. 9.31(b)). The dashed white contour line $\psi = \frac{1}{2}$ is at the top of the wedge of polymer material.

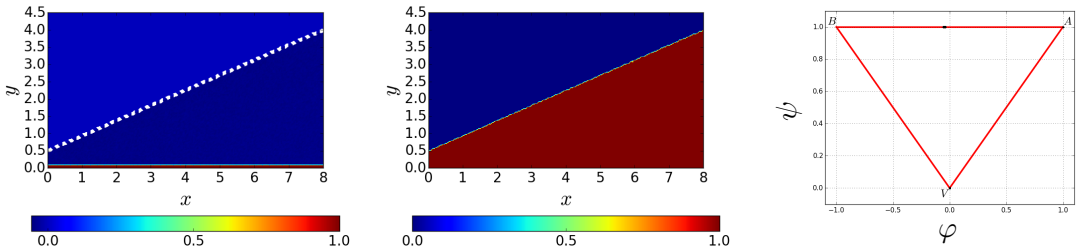

(a) Filled φ-contour plot (b) Filled ψ-contour plot (c) The view in (φ, ψ)

Figure 9.28: A wedge of well-mixed material. In (a), a thin layer (height 0.1) of pure phase A material ($\varphi = 1$) lies on the substrate ($y = 0$); the remainder of the polymer is randomly perturbed inside the polymer,[46] so that $\overline{\varphi} \approx 0$ (we achieved $\overline{\varphi} = -0.00282$).[47] The polymer–void transition (the thick dashed white line) is a random perturbation of the straight line from $y = 0.5$ on the left ($x = 0$) to $y = 4$ on the right ($x = 8$) for $\mathcal{M} = 0.500$.[48] Below this line we set $\psi = 1$, and above $\psi = 0$ i.e. there was no smooth polymer–void transition. The random polymer–void transition is visible in (b). In (c), the IC is represented by three dots: the pure void is at $(0, 0)$ and the thin layer of A material is at $(1, 1)$; the random values inside the wedge are the smeared black patch near $(0, 1)$.[49]

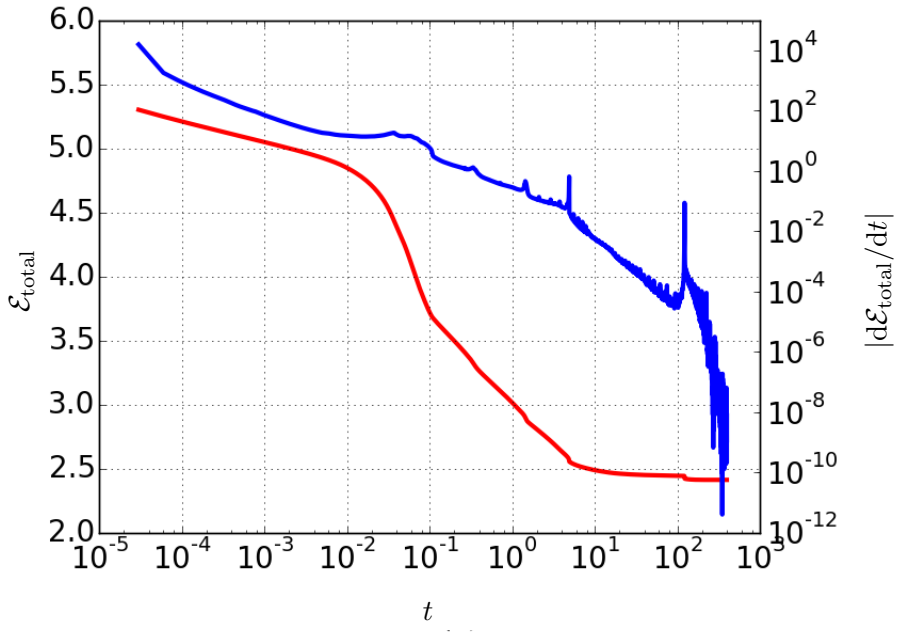

Figure 9.29: Energy evolution for spontaneous step formation. The starting energy was $\mathcal{E}_\mu(t = 0) = 5.772$; the final energy was $\mathcal{E}_\mu(T = 396.6) = 2.411$.[50]

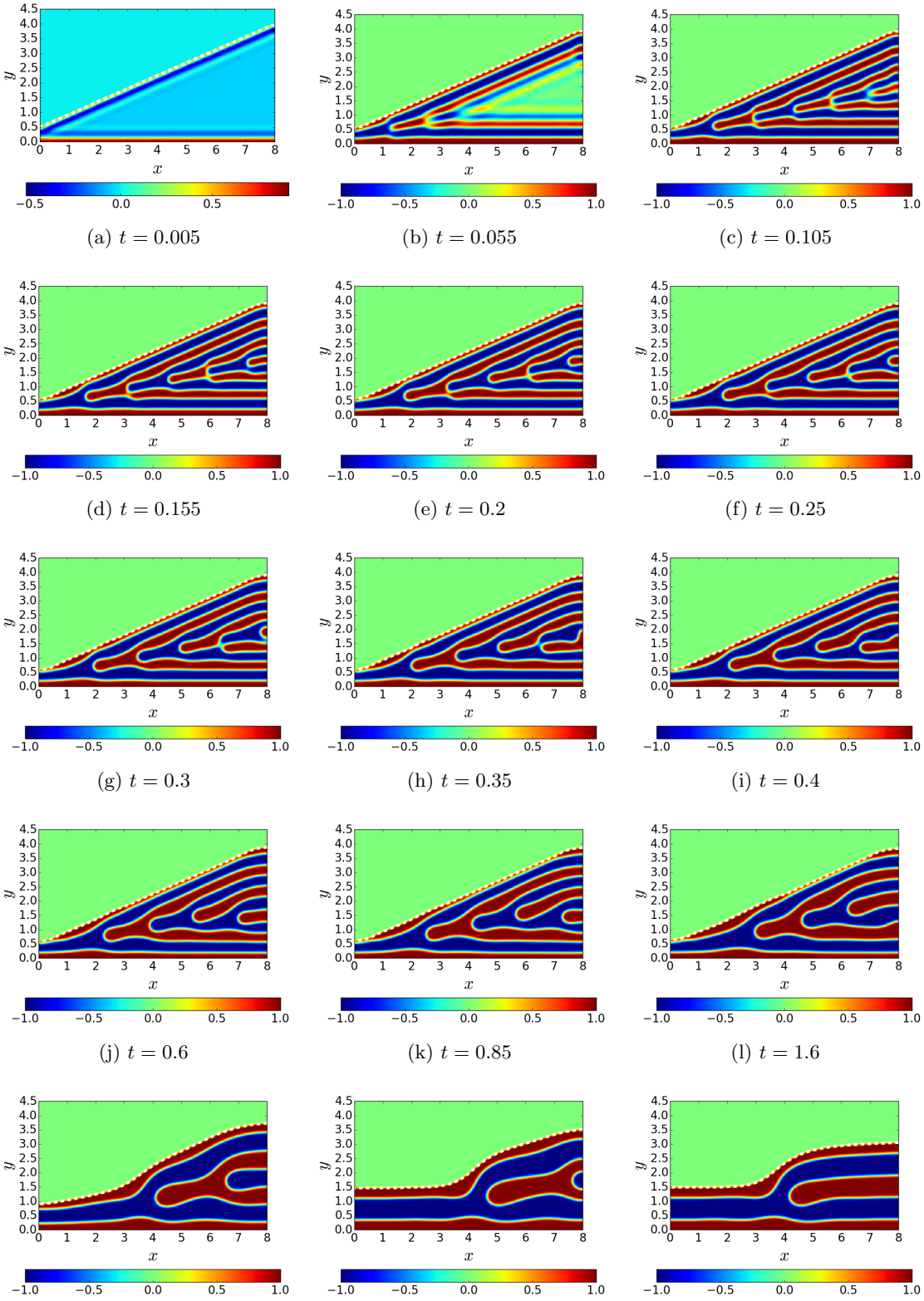

(a) $t = 0.005$ (b) $t = 0.055$ (c) $t = 0.105$

(d) $t = 0.155$ (e) $t = 0.2$ (f) $t = 0.25$

(g) $t = 0.3$ (h) $t = 0.35$ (i) $t = 0.4$

(j) $t = 0.6$ (k) $t = 0.85$ (l) $t = 1.6$

(m) $t = 8.6$ (n) $t = 116.6$ (o) $T = 396.6$; $\mathcal{E}_\mu = 2.411$

Figure 9.30: Spontaneous step formation from the flat wedge IC in Fig. 9.28.[51]

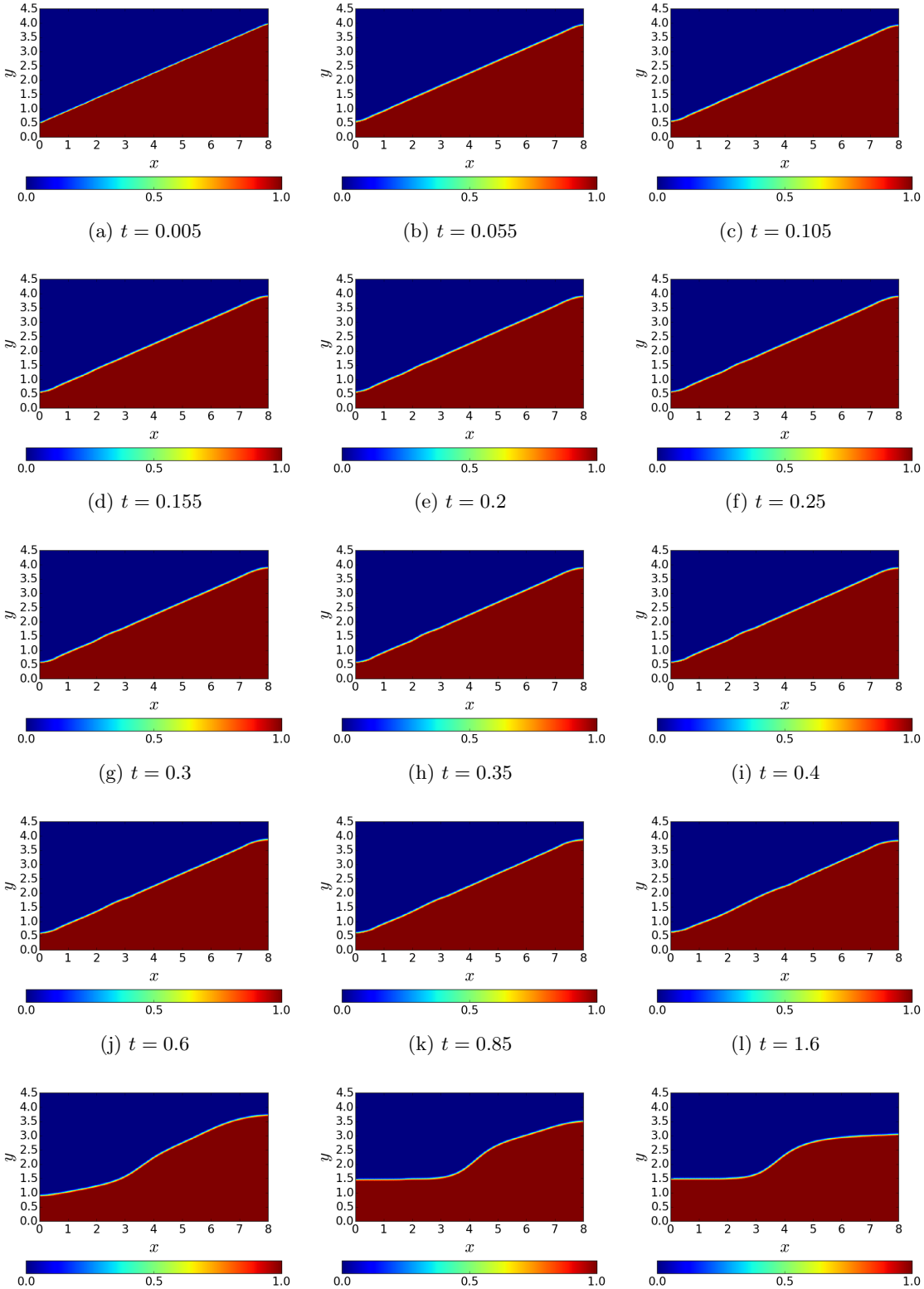

(a) $t = 0.005$ (b) $t = 0.055$ (c) $t = 0.105$

(d) $t = 0.155$ (e) $t = 0.2$ (f) $t = 0.25$

(g) $t = 0.3$ (h) $t = 0.35$ (i) $t = 0.4$

(j) $t = 0.6$ (k) $t = 0.85$ (l) $t = 1.6$

(m) $t = 8.6$ (n) $t = 116.6$ (o) $T = 396.6$

Figure 9.31: Spontaneous step formation from the flat wedge IC in Fig. 9.28; evolution of the polymer–void free surface as modelled by ψ.[52]

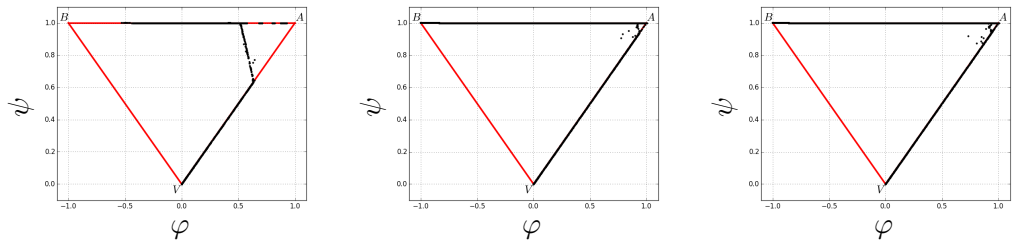

(a) $t = 0.005$ (b) $t = 0.055$ (c) $t = 0.105$

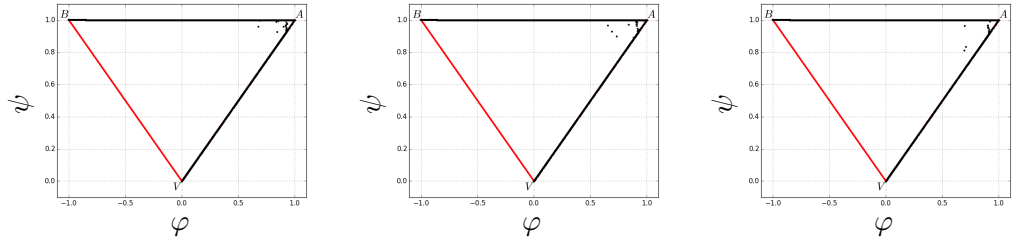

(d) $t = 0.155$ (e) $t = 0.2$ (f) $t = 0.25$

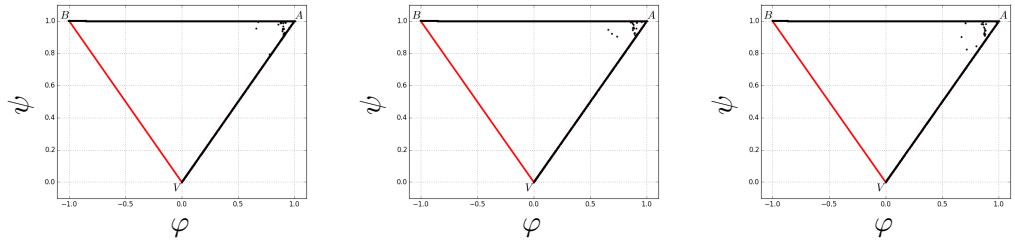

(g) $t = 0.3$ (h) $t = 0.35$ (i) $t = 0.4$

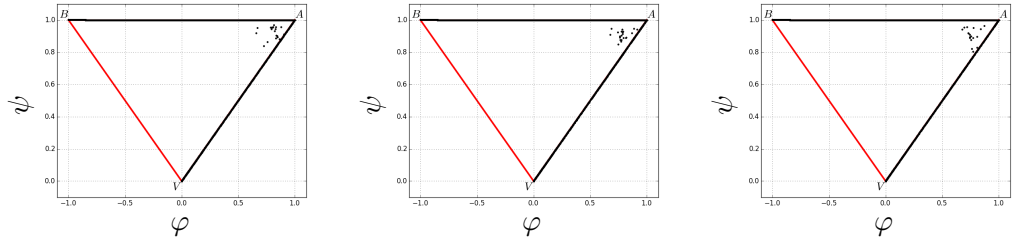

(j) $t = 0.6$ (k) $t = 0.85$ (l) $t = 1.6$

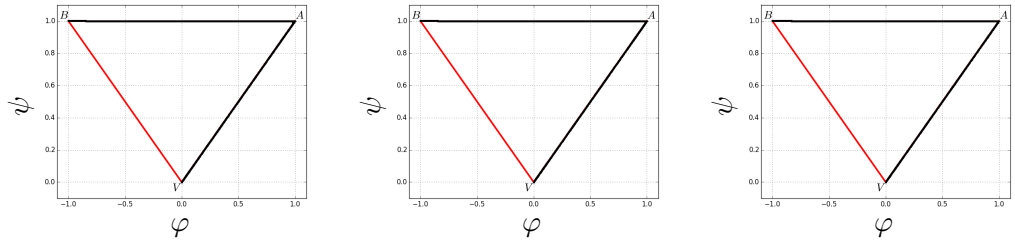

(m) $t = 8.6$ (n) $t = 116.6$ (o) $T = 396.6$

Figure 9.32: Spontaneous step formation from the flat wedge IC in Fig. 9.28 in (φ, ψ)-space.[53]

9.4.7 The effect of inverting χ^{Δ}

Our final, somewhat unusual, 2D experiment on $(0, 16) \times (0, 3)$ is summarised in Fig. 9.33. We started with the configuration depicted in Fig. 9.21(a) and the parameters in (9.79), but inverted the preferences between the void and the polymer species by setting

$$\chi^{AV} = 10, \qquad \chi^{\Delta} = -8.5. \tag{9.100}$$

The $B \to V$ polymer–void transition was thus preferred to the $A \to V$ transition. As a result, the blue semi-layer spread over the AV interface layer to the left and right. At the same time, the top red semi-layer retracted as the A-species diffused across the blue B-micro-domain into the other A-micro-domain, until all that remained was a small semi-circle at $x = L_x$. At this stage, the evolution had effectively stopped, suggesting that a solution close to a (stable) stationary state had been reached. The persistence of the semi-circle was counter-intuitive. For this much longer running simulation ($T \approx 1530$), we used $\mu = 10^{-3}$.

Remark. In Section 8 of Hintermüller et al. (2011), the authors describe their experimental approach to selecting c (our $\frac{1}{\mu}$). We could apply their technique here by taking the end-state in Fig. 9.33(d) as the IC for an experiment with $\mu = 10^{-4}$, use that end-state as an IC with $\mu = 10^{-5}$ and so on, until $\mu_{\min}$ is reached. As noted previously, we expect the configurations depicted in Fig's 9.33, 9.34 and 9.35 to be qualitatively correct.

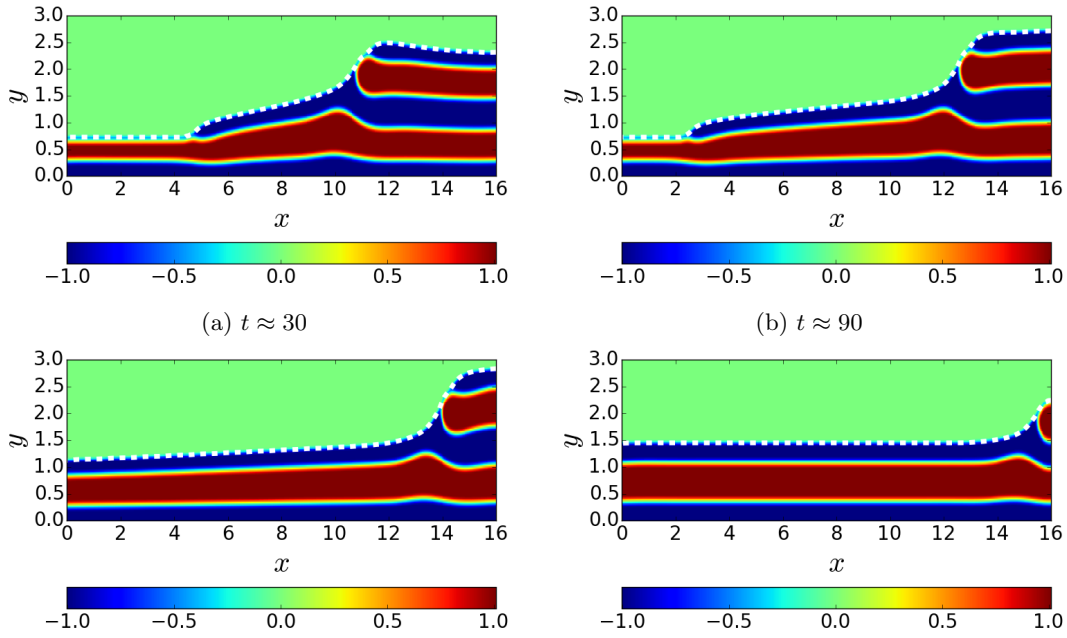

(a) $t \approx 30$ (b) $t \approx 90$

(c) $t \approx 280$ (d) $T \approx 1530$

Figure 9.33: Results at the times indicated for parameters (9.79) and (9.100), for which a $B \to V$ polymer–void transition is energetically preferred to an $A \to V$ transition.[54]

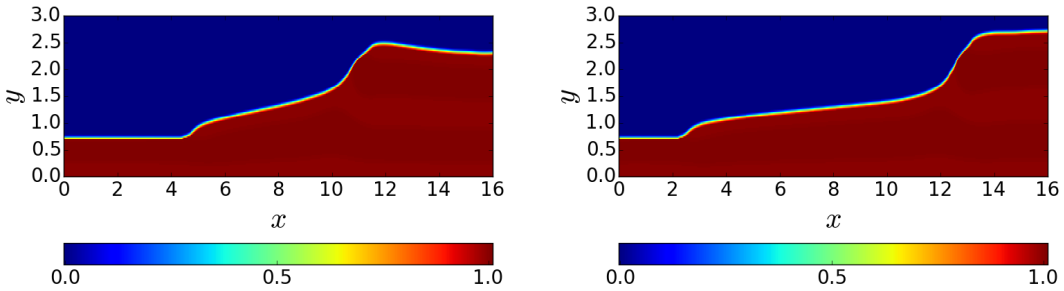

(a) $t \approx 30$ (b) $t \approx 90$

(c) $t \approx 280$ (d) $T \approx 1530$

Figure 9.34: The effect of inverting χ^{Δ}: ψ snapshots at the indicated times.[55]

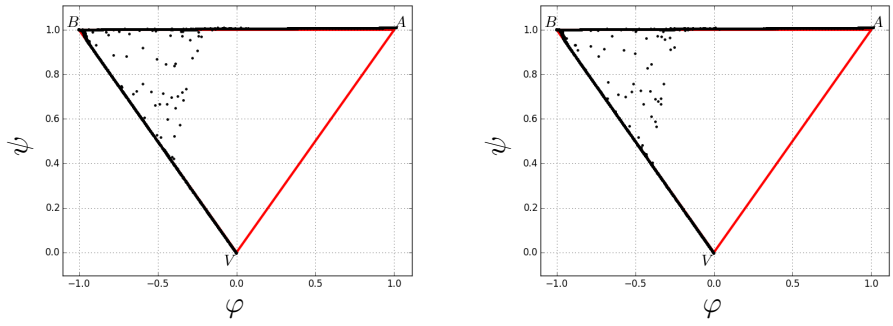

(a) $t \approx 30$ (b) $t \approx 90$

(c) $t \approx 280$ (d) $T \approx 1530$

Figure 9.35: The effect of inverting χ^{Δ}: views in (φ, ψ) parameter space.[56]

9.5 Summary and conclusions

We started this chapter by developing a model for 3-phase materials, involving two DBC polymer phases A and B, and a third void phase V, which we modelled as a homopolymer. Our 3-phase model is a natural extension of the 2-phase model we presented in Chapter 3, and was derived in Choksi and Ren (2005) from the SCFT. One of the consequences of this choice is that the homogeneous energy density involves an obstacle. As in the 2-phase case, this led us to working with variational inequalities, which we regularised to arrive at a practical, computational model for simulating the time evolution of 3-phase materials.

We were particularly interested in symmetric materials. After a brief introduction to these in Section 9.2.6, we studied the 1D case in some detail in Section 9.3. We considered a number of special cases and proposed a heuristic *ansatz* for low energy morphologies. The primary basis for the *ansatz* was the observation that, inside the pure polymer region, models of 3-phase materials reduce to the 2-phase case. We thus used our 2-phase energy minimisation results to propose 1D structures that were useful for our 2D numerical computations.

After proposing a re-scaling of the problem, we studied the sharp interface limit in 1D. Using this simplified version of the problem, we made predictions about the structure (number, location and thickness of monolayers) of (local) 1D energy minimisers. We used our 1D sharp interface limit results to predict conditions under which 2D stepped configurations would have lower energy than their flat counterparts. These predictions, in turn, served as the basis for a series of 2D gradient flow numerical experiments.

Our first four 2D experiments emulated those in Stasiak et al. (2012); we chose ICs that were structurally similar to the stable (local) energy minimisers we expected, and executed a set of gradient flow simulations.[57] In each case, the observed end-states closely matched our predictions.

We then executed two very long-running simulations in which we attempted to capture more physically realistic DBC evolution. In the first, we observed a step forming spontaneously from a wedge IC. The profile and monolayer widths associated with this step matched our predictions, and were also consistent with results reported using the SCFT, in Stasiak et al. (2012). In the second, we studied a situation in which the top layer in the initial step configuration was the less preferred layer, and observed the step retract as the preferred species wet the free surface. This eventually led to a nearly flat film that was only perturbed near the boundary of the domain. Such a configuration may be amenable to experimental investigation using the technique in Maher et al. (2016), whereby the film is covered by an additional top layer of a specifically chosen homopolymer.

We were thus able to identify conditions under which stepped 3-phase configurations have lower energy than their flat counterparts.

9.5.1 Opportunities for further study

We close by listing possible extensions to the work in this chapter.

i) **Equal-spacing in three phases**. It would appear that 3-phase energy-minimisers are not (exactly) equally spaced, but an indication as to how unequal the spacing is could be of interest. In Section 9.3.2 we suggested that our 3-phase model reduces to a 2-phase model when $\psi \equiv 1$. However, we were unable to (directly) apply the 2-phase reasoning from Chapter 7 because of the BC on φ at the polymer–void transition ($\varphi = 0$ instead of ± 1). As such there was no way to work with the 3-phase equivalent of a single monolayer morphology inside the polymer, and no way to arrive at an energy convexity result. Moreover, equal-spacing in the 2-phase case implied that the monolayers all had the same thickness (and identical interface layers). As such, we are interested in the location *and* thickness of each monolayer in an energy-minimising morphology.

   Another complexity stems from the fact that there are two 3-phase interfacial thickness parameters: ε_φ and ε_ψ. In the sharp interface limit analysis of Choksi and Ren (2005) and our Section 9.3.5, both of these were sent to zero, but studying a problem involving two such *non-zero* (different) parameters is much more difficult. One approach may be to consider a sharp interface limit in which $\varepsilon_\psi > 0$ is held constant, and $\varepsilon_\varphi \downarrow 0$.

   We could also conduct a numerical investigation involving a set of 3-phase experiments similar to the 2-phase experiments of Section 8.1.2 (see Fig. 8.3). We could systematically construct ICs using the *ansatz* of Section 9.3.3 for various ε_φ, ε_ψ values, and then run a series of gradient flow experiments to stationarity. We would then examine the locations and thickness of the monolayers in the end-states to get some sense as to how their spacing depends on ε_φ and ε_ψ. The results in Fig. 9.18 suggest that this could be complicated.

ii) A systematic exploration of the effects of **the Flory–Huggins parameters**, χ^{AB}, χ^{AV} and χ^{BV}, would be useful. We set $\chi^{AB} < \chi^{AV}, \chi^{BV}$ (cf. Section 9.3.7 and (9.68)), and found that the internal interface layers always ran parallel to the polymer–void transition (and the substrate). This was consistent with observations from Ohta and Ito (1995) and Ito (1998) (albeit with a different approximation of the homogeneous density $\mathcal{B}$). Those papers offered numerical evidence suggesting the existence of parameter ranges in which the internal interface layers run *perpendicular* to the polymer–void transition (see Fig. 2 in Ohta and Ito (1995)). We attempted to reproduce these results, but were unable to do so. In any case, the effects of these Flory–Huggins parameters should be better understood.

iii) **Asymmetry**. As in two phases, most of our work on the 3-phase problem assumed symmetry because, according to Choksi and Ren (2005), setting $m = 0$ dramatically

simplifies the model. In particular, the non-local terms involving β and γ fall away (cf. Section 9.2.6), which suggests that energy minimisers should involve a single body of polymer material (as in the Cahn–Hilliard case). But this also suggests that we would only ever see lamellar micro-structure (not spheres, cylinders etc.). It would be interesting to explore these other non-local terms, and potentially combine $m \neq 0$ with $\beta = \gamma = 0$.[58]

iv) **Convex splitting**. We showed that there is an advantage to placing the linear term at the lower time level in the 2-phase problem (unconditional existence and uniqueness of solutions, as well as energy monotonicity). It is not clear how to achieve the 3-phase version of this, but clearly any scheme with the same advantages as 2-phase convex splitting would be valuable.

v) A **polynomial approximation of the homogeneous density function $\mathcal{B}$**, leading to a 3-phase double-well approximation to our double-obstacle would facilitate a numerical method based on the Newton method instead of SSN (which converges more slowly). We tried to create such a polynomial approximation, without success. The papers Ohta and Ito (1995) and Ito (1998) made use of a polynomial version of $\mathcal{B}$, but included no information as to its source. In our opinion, the results of our numerical experiments that used their function f_{int} were quite poor (the structures were not well defined and the phase separation was quite weak) compared to the far clearer results obtained using $\mathcal{B}_\mu$.

Remark. At first blush, our choice of obstacle homogeneous energy component appears more complicated than the polynomial alternative. However, in the detail, we found that its (quadratic) simplicity away from the obstacle facilitated a very detailed analysis of energy minimising interface layers. Our numerical methods were also quite fast. Care should thus be taken to ensure that any such polynomial homogeneous term really does simplify the problem and/or facilitate an easier analysis. A naïve selection may actually prove less useful than our (ostensibly more complicated) obstacle term.

Another option might be to consider higher (fourth) order versions of Υ_μ in (4.5b) and (9.32), such as

$$\text{2-phase:} \qquad \Upsilon_\mu(\varphi) := \frac{1}{4\mu}\left[(\varphi-1)_+^4 + (\varphi+1)_-^4\right] \tag{9.101a}$$

$$\text{3-phase:} \qquad \Upsilon_\mu(\varphi,\psi) := \frac{1}{4\mu}\left[(\psi-1)_+^4 + (\varphi-\psi)_+^4 + (\varphi+\psi)_-^4\right]. \tag{9.101b}$$

These regularisers can sustain more derivatives, and would thus support a numerical method based on the Newton method. *It is not clear what effect such choices would have on the work we did in Chapters 4– 5.*

vi) We did not perform a **rigorous analysis of the 3-phase problem** corresponding to the 2-phase work we did in Chapters 4–5, but rather sketched a small part of this in Section 9.2.5.2. As such, we have not *proved* that our 3-phase regularisation has the required convergence properties (to the underlying obstacle problem as $\mu \downarrow 0$) or that our 3-phase numerical method converges (as $h, t \downarrow 0$), although these do seem like reasonable conclusions. Applying the ideas of Chapters 4–5 to the 3-phase problem should be relatively straightforward, although this is likely to be a large piece of work.

vii) **Pre-conditioners and performance tuning**. We used an additive Schwarz pre-conditioner in the Portable and Extendable Toolkit for Scientific Computing (PETSc) (see Balay et al. (2018)) with the Generalized Minimal Residual Method (GMRES) as the underlying iterative solver, as this offered the best performance of the standard options we tested. This simple approach seemed appropriate, given our limited computational resources. Far more sophisticated methods are possible, and significant improvements would be required before we can consider tackling large (3D) simulations on shared supercomputing resources.

As at this writing, an MSc student at the University of Oxford is exploring this topic in detail, extending the ideas of Farrell and Pearson (2017) to 3-phase problems. A multigrid approach to the Cahn–Hilliard problem was studied in Baňas and Nürnberg (2009), and may also be of use.

viii) Automatic **time and space h-adaptivity**.

- We built limited time adaptivity and recovery capabilities into our FEniCS code. There is no guarantee that the SSN method will converge for a given time-step, τ. We therefore built a capability whereby our non-linear solver attempts a certain number of SSN iterations[59] and re-starts the calculation using a smaller value of τ, should the method not converge. On the other hand, it seems reasonable to assume that very small time-steps are required for stability, energy monotonicity etc. We wished to take larger and larger time-steps, whenever possible, so as to be able to calculate over long simulation horizons.

  We were only able to run individual numerical experiments for up to $\sim$12 hours at a time, because of our limited hardware. We therefore stitched together sequences of constant τ experiments, using the end-state of one experiment as the IC for the next one, and manually increasing τ as we progressed from one experiment to the next. For much longer running experiments on a shared supercomputer (running for up to several weeks at a time), this is not practical, and a fully automatic time adaptivity capability (that can increase and decrease τ in response to the progress of the method) would be required to make efficient use of the hardware.

- Likewise, for simplicity, we used fixed spatial grids in all of our numerical experiments. Combined with our limited computational power, this choice restricted the size of the experiments we could conduct, and also the ε we used (cf. (9.79)). In the short term, a simple mesh refinement/coarsening strategy based on $|\varphi|_1$ might prove useful. This would add grid points to the (micro and macro) interface layers and remove them from areas of (nearly) pure phase material, especially the large voids that were present in our 3-phase experiments. We could thus select a smaller ε, for little to no additional computational cost (see Hintermüller et al. (2011) for ideas around mesh refinement/coarsening for the Cahn–Hilliard problem in the context of a very similar numerical approximation).

With these enhancements, the more complex structures of Stasiak et al. (2012) and the '*islands*' and '*holes*' of Maher et al. (2016), as well as larger, multi-step structures should be accessible (cf. Fig. 9.36). With access to a supercomputer like ARCHER (see http://www.archer.ac.uk/), it would likely also be possible to simulate entire terraced structures such as the radially symmetric droplet of Fig. 1.2.[60]

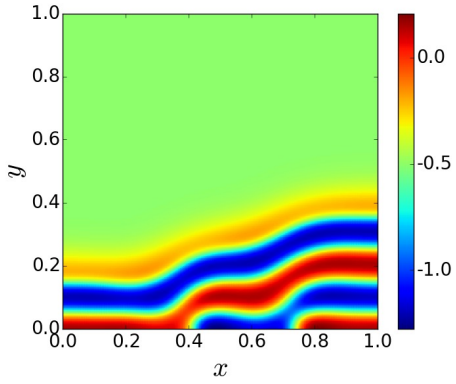

Figure 9.36: A DBC 'staircase' obtained as the end-state of an experiment based on the model of Ohta and Ito (1995), conducted on the UK national supercomputer, ARCHER. The morphology has two steps that formed spontaneously from a random initial wedge of polymer material.

ix) Other **geometries**: one of the strengths of our model and the spatial finite element method, is that it can be applied to virtually arbitrary spatial domains, as suggested in Remark 4.3 of Choksi et al. (2009). Indeed, as noted in Kim and Matsen (2009), '*researchers are turning their attention to block copolymers in confined geometries which exhibit much richer phase behaviours*'. We have used simple 2D rectangles for simplicity, but it should be relatively straightforward to simulate on other domains with our FENICS code.

x) **Molecular parameters**. We attempted to scale the physical parameters, describing

the molecules used in Stasiak et al. (2012), through the model of Choksi and Ren (2005), and then our own re-scaling in Section 9.3.4. As we noted in the endnote marked on p. 34, we strongly suspect there is a scaling error in Choksi and Ren (2005), which we were unable to resolve. It is therefore not clear what physical situation we simulated in this chapter. On the other hand, in Maher et al. (2016), the authors admit that '*[t]he one shortcoming of the SCFT is that we cannot solve the field equations for realistic values of*' χ^{AV} *and* χ^{BV} (see the end of their 'Materials and Methods' section),[61] which suggests that this issue should not be taken as a reason to discard our results.

In any case, if our methods are to be of practical use to materials scientists, there must be some way for them to provide a set of material parameters (obtained by measurement or otherwise), that we can then convert to parameters suitable for analysis and simulation using our model.

Notes

[1]See the MATLAB working script `draw_3phase_polymer_box_schematic.m` in the `bitbucket` repository.

[2]We do not scale x by the L of Choksi and Ren (2005).

[3]This corresponds to W in Choksi and Ren (2003, 2005).

[4]The β in Choksi and Ren (2005) is equivalent to our $1/\Theta$.

[5]We do not scale x by L.

[6]The following BCs are, strictly speaking, redundant as they are implied by the $(-\Delta_n)^{-1}$ operators in (9.18d).

[7]A better approach might be to replace $\left(\varepsilon_{ij}^2\right)$ with (ε_{ij}), but that would make all of our equations inconsistent with the literature.

[8]See the material between equations (4.35) and (4.36) of Choksi and Ren (2005).

[9]See the MATLAB code `check_bulk_densities.m` in the `bitbucket` repository.

[10]See the MATLAB code `check_bulk_densities.m` in the `bitbucket` repository.

[11]See http://dx.doi.org/10.6084/m9.figshare.7028216 for the source data for this experiment.

[12]We conducted very few experiments with $\beta, \gamma \neq 0$, and observed the following:

i) There were *significant* instabilities when the (non-zero) β and γ non-local terms were run on a fully explicit basis (cf. Section 5.4.1);

ii) When these terms were fully implicit, there were extremely severe time-stepping restrictions (the SSN method failed to converge even when τ was very small).

[13]See the working scripts `OKDE_asymptotic_solns.m` and `three_phase_1D_asymp.m` in the `bitbucket` MATLAB repository.

[14]We have written these definitions as if the substrate phase (A, B) and ν (even/odd) are given, so that the nature of the polymer–void transition follows. We could just as easily specify the phase at the polymer together with ν, and infer the phase at the substrate.

[15]See the MATLAB working script `OKDE_asymptotic_solns.m` in the `bitbucket` repository.

[16]See the MATLAB working script `draw_g_for_paper1.m` in the `bitbucket` repository.

[17]As in Münch (2017), the process is as follows: solve for the smallest zero of c_A in (6.29b), for fixed γ and $\varepsilon > 0$. The result is a transcendental equation from which we extract the smallest positive zero – this is ℓ_A; numerically we find that $\ell_A = 2.709\varepsilon$. Substitute half of this into the expression for g; the leading order term is given in (9.77).

[18]See the sentence immediately following (6.82).

[19]See http://dx.doi.org/10.6084/m9.figshare.7028300, and esp. `exp_group_run_196` for the source data for these figures.

[20]See http://dx.doi.org/10.6084/m9.figshare.7025621 for the source data for these figures.

[21]See http://dx.doi.org/10.6084/m9.figshare.7025621 and especially `exp_run_3469` and `exp_run_3474,` for the source data for these figures.

[22]This implies that we *should* be able to choose a mesh according to ε (i.e. sufficient to resolve the interface layers), without worrying about the effect of μ. Our study is by no means conclusive on this issue.

[23]This could be done by hand, or with a symbolic algebra tool.

[24]The match for $B \to V$ polymer–void transitions (viz. the blue lines in the energy comparison figures) is excellent in all cases.

[25]In fact, we were able to use less precise versions of these structures as in (9.80). The most important consideration was the monolayer count.

[26]Each dashed white line is the contour of $f_\gamma := \widehat{\alpha}\widehat{\mathcal{D}}^3$, as in (8.26), through the marked $\left(\widehat{\mathcal{D}}, \widehat{\alpha}\right)$ point.

[27]See the MATLAB code `1D_3phase_sweep/qp_okfef_1D_3phase_low_e_morphs.m` in the `bitbucket` repository, and also http://dx.doi.org/10.6084/m9.figshare.7028288 for the simulation data, and `exp_run_4707`

for fig. (d) and `exp_run_4708` for fig. (e). The source simulation data for the 200 black dots in fig. (a) can be found at http://dx.doi.org/10.6084/m9.figshare.7025723.

[28]See the MATLAB code `1D_3phase_sweep/qp_okfef_1D_3phase_low_e_morphs.m` in the `bitbucket` repository, and also http://dx.doi.org/10.6084/m9.figshare.7028291 for the simulation data, and `exp_run_4709` for fig. (b) and `exp_run_4710` for fig. (c). The source simulation data for the 200 black dots in fig. (a) can be found at http://dx.doi.org/10.6084/m9.figshare.7025828.

[29]See the MATLAB code `1D_3phase_sweep/qp_okfef_1D_3phase_low_e_morphs.m` in the `bitbucket` repository, and also http://dx.doi.org/10.6084/m9.figshare.7028297 for the simulation data, and `exp_run_4711` for fig. (d) and `exp_run_4712` for fig. (e). The source simulation data for the 200 black dots in fig. (a) can be found at http://dx.doi.org/10.6084/m9.figshare.7026035.

[30]See `exp_run_4578` and `exp_run_4579` in http://dx.doi.org/10.6084/m9.figshare.7026035 for the source data for these figures.

[31]Terracing has no 1D expression. We regard terraces as 3D objects, and refer to their 2D counterparts, in this chapter, as steps.

[32]The main reason for this was that the simulations were extremely long-running: in the order of several days. We therefore managed each simulation as a series of consecutive, chained experiments with increasing (fixed) time-step size, τ. In this way, we were able to simply increase the time-step without the risk and complexity of developing a fully automatic adaptive time-stepping capability.

[33]We anticipate that energy should be a monotonically non-increasing function of time, for sufficiently small τ. We therefore increased T until either the energy stopped decaying, and started to fluctuate about a certain value, or the non-linear SSN iteration count dropped to zero. In each case, we made sure that the quantity

$$\max\left\{\left\|\varphi_h^n - \varphi_h^{n-1}\right\|, \left\|\psi_h^n - \psi_h^{n-1}\right\|\right\},$$

measuring the change in the morphology from one time-step to the next, was small ($\sim 10^{-7}$), before declaring an experiment complete.

[34]See http://dx.doi.org/10.6084/m9.figshare.7028327 for the source data for these experiments. The IC in fig's (a), (d) is from `exp_run_3547,` fig's (b), (e) are from `exp_run_3568,` and fig's (c), (f) are from `exp_run_3566.`

[35]See http://dx.doi.org/10.6084/m9.figshare.7028327 for the source data for these experiments.

[36]See http://dx.doi.org/10.6084/m9.figshare.7028327 for the source data for these experiments.

[37]See the MATLAB working script `draw_sharp_interface_double_tgt.m` in the `bitbucket` repository.

[38]We solved this problem using the MATLAB function `fsolve` from an initial guess of $\boldsymbol{\theta} = \left\{\frac{\pi}{2}, \frac{\pi}{2}, \frac{\pi}{2}\right\}$.

[39]Note that the arrows we used are all the same length and are not scaled according to the magnitude of each surface tension.

[40]In preparing Fig. 9.25, we experimented with the $\varphi = 0$ contour (separating the blue and red regions), but found that it was only marginally helpful.

[41]Other contours may be more useful, but these seem reasonable.

[42]See http://dx.doi.org/10.6084/m9.figshare.7028345 for the source data for these figures. Fig. (a) is from `exp_run_3514,` (b) is from `exp_run_3540,` (c) is from `exp_run_3515,` and (d) is from `exp_run_3543.`

[43]See the MATLAB working script `draw_sharp_interface_double_tgt.m` in the `bitbucket` repository.

[44]The graphics package `matplotlib` (see https://matplotlib.org/) scaled the colours in Fig. 9.28(a) according to the represented values of φ. Hence, $\varphi = 0$ is blue (above the dashed white line) instead of the usual pale green in this plot.

[45]At this point, the time-step had increased to $\tau = 0.02$.

[46]We set $\varphi = \widetilde{m} + \varepsilon$ with $\varepsilon \sim U([-0.01, 0.01))$ and

$$\widetilde{m} = -0.0465 = \frac{0 - 1 \times 0.1 \times 8}{(0.5 + 4) \times 8/2 - 0.1 \times 8}.$$

[47]Note that the horizontal light green line (corresponding to $\varphi \approx 0$) in the figure just above the pure phase A layer, is a graphical artefact due to the transition from $\varphi = 1$ to the average. We did not insert a second line of constant φ.

[48]We set $y = mx + 0.5 + \varepsilon$ with $\varepsilon \sim U([-0.01, 0.01))$ and $m = 0.4375$ such that $\overline{\psi} = \frac{1}{2}$ in the absence of the perturbation. Note that $y(0) = 0.5 + \varepsilon$ and $y(8) = 4 + \varepsilon$.

[49]See http://dx.doi.org/10.6084/m9.figshare.7026119 for the source data, esp. `exp_run_3569.`

[50]See http://dx.doi.org/10.6084/m9.figshare.7026119 for the source data, esp. `exp_run_3595.`

[51]See http://dx.doi.org/10.6084/m9.figshare.7026119 for the source data.

[52]See http://dx.doi.org/10.6084/m9.figshare.7026119 for the source data.

[53]See http://dx.doi.org/10.6084/m9.figshare.7026119 for the source data.

[54]See http://dx.doi.org/10.6084/m9.figshare.7026146 for the source data.

[55]See http://dx.doi.org/10.6084/m9.figshare.7026146 for the source data.

[56]See http://dx.doi.org/10.6084/m9.figshare.7026146 for the source data.

[57]The language in Maher et al. (2016) suggests that their SCFT numerical method uses an initial guess that approximately corresponds to our IC, and is chosen to be morphologically similar to the (stepped) end-state they are interested in.

[58]It is not clear what this last suggestion corresponds to in the underlying physical model.

[59]We generally set this number to ten.

[60]An assumption of radial symmetry would reduce this 3D structure to a 2D one.

[61]The authors use the symbols χ_{Ah} and χ_{Bh} for our χ^{AV} and χ^{BV}.

Part IV

Conclusion

Chapter 10

Conclusions, contributions and further opportunities

In this short, final chapter we summarise our key results and contributions, and explore opportunities for further research.

Contents

10.1 Contributions and results 289
10.2 Opportunities for further research 296

10.1 Contributions and results

This thesis has been written for the next student wishing to work on this problem. As noted in Appendix B of Choksi et al. (2009), much of the material on which study of these problems is based is '*folklore*' that is '*surprisingly written down in very few places*'. Significant effort has therefore been expended to present a coherent and complete account connecting the mathematics of DFTs and the physical models of DBCs. We focused on 2-phase (DBC-only) models, and then considered 3-phase (2-phase DBC + void/homopolymer) models.

In terms of core research outcomes and with reference to the question we posed in the Introduction, we conclude that,

yes, it is possible to use a phase field model to capture and study terrace formation in DBCs.

10.1.1 2-Phase results: Chapters 3–8

In Chapter 3, we presented our non-local, 2-phase model for phase separation in DBCs. In this chapter we synthesized and applied the model of Choksi and Ren (2003), presenting

it in a simple and easy-to-understand way. A key outcome of this chapter was the energy functional (3.4) and the corresponding minimisation formulation of the problem.

Chapters 4–5 were the most technical and rigorous of the thesis.

In Chapter 4, we studied the theoretical properties of the 2-phase energy minimisation problem, and established counterparts of many of the results in Blowey and Elliott (1991). There were two innovations in this chapter: first, we used a C^1 Moreau–Yosida regularisation of the homogeneous energy density term (instead of the C^2 regularisation of Blowey and Elliott (1991). Second, we included the non-local term in our analysis.

In Chapter 5 we devised and analysed a family of numerical methods based on the regularisation of the previous chapter. We considered a family of time-splitting schemes, established their theoretical convergence and other properties, and then confirmed these experimentally with a code written in FEniCS. Our method is based on the same Moreau–Yosida regularisation scheme as that used in Bosch et al. (2014b,a); Hintermüller et al. (2011), combined with the SSN method to deal with non-linearities inside each time-step. We additionally considered a *family* of time-stepping approximations of the non-local term. Our method can be regarded as equivalent to the PDAS method explored in Blank et al. (2011) (in the sense that the well-posedness of PDAS methods is established by showing that they are equivalent to SSN). However, the implementation and core algorithm are different.

Our inclusion of a forcing function in this context appears to be somewhat unusual (we could find no other relevant literature that employed this device). The advantage of this technique is that it obviates the need for exact/analytical solutions, but meant that we could still perform a compelling set of MMS numerical experiments to demonstrate the order of convergence of our method. We regard our results in Fig. 5.5 as easier to understand and more compelling than, say, Table 1 of Hintermüller et al. (2011) or Table 1 of Blowey and Elliott (1992).[1]

Our analysis in Chapters 4–5 is comprehensive in that we relate our numerical approximation all the way back to the underlying (continuous) energy minimisation problem. Our regularisation of the homogeneous energy term is fundamental, and puts our applied and numerical analysis on the same footing. By contrast, works like Hintermüller et al. (2011) (which uses a very similar numerical procedure to ours) include only part of this analysis chain, to show how their regularised approximation solves a specific time-discrete Cahn–Hilliard variational inequality (see their equations (15)–(17)). Our approach was more general and fundamental; we added a non-local term to the problem, and completely (re-)analysed it.

We studied the 2-phase problem on 1D domains in Chapters 6–8, with particular emphasis on the symmetric case. In Chapter 6, we reformulated the 1D energy stationarity condition as an ID-ELE which governs the interface layer inside each monolayer in a candi-

date energy minimiser. It also encodes non-local information about the minimiser (viz. BCs at the ends of the domain). Our key insight was that we could analyse the problem by differentiating the ID-ELE, and working with a linear, fourth order ODE which admits a far larger set of solutions. We thus explored the structure of candidate interface layers (viz. solutions of the ODE), independent of the energy minimisation process.

In Chapter 7, we presented an argument which considered morphologies constructed using interface layers taken from larger and larger sets of solutions of this ODE, and offered evidence suggesting that layered energy minimisers are equally spaced, in that all of the monolayers are copies/translations/reflections of each other. We suggested that:

i) For a prescribed, finite monolayer count, the 2-phase energy is minimised if the monolayers are equally spaced *and* each interface layer solves the ODE and is monotone with a single inflexion point.

ii) The global energy minimiser is either disordered or comprises ν_{opt} equally spaced monolayers, each of which contains an interface layer that satisfies the ODE *and* the ID-ELE.

In Chapter 8, we put these ideas into context. We produced a phase diagram of the energy-minimising monolayer count ν_{opt} as a function of scaled parameter space, that includes an analytical specification of the ODT in parameter space. **Given any set of symmetric model parameters, we believe we can completely describe the (non-unique) global energy minimiser in 1D**.

Our results go further than Section 3.2 of Blowey and Elliott (1991), because the non-local term in our model opens the door to minimisers with a far richer structure than in the Cahn–Hilliard case. In Section 8.3, we showed how the **Cahn–Hilliard results are a special case of ours**. Our ODT result is much more precise than that proposed for a similar model in Choksi et al. (2009). In Fig. 8 of that paper, the authors depict three lines; two dashed lines obtained by stability analysis for upper and lower bounds on the location of the ODT, and a solid line that was '*numerically computed*' by performing a large number of simulations in phase space, reflecting the '*best fit separating these regions*'. **We proposed an ODT in closed form**.

We devised and implemented an **efficient numerical algorithm** for finding and characterising the global energy minimisers above. We used this tool in conjunction with our gradient flow numerical method (implemented in FEniCS) to conduct a novel set of numerical experiments in support of our claim that such configurations are indeed minimisers. These experiments are very much in keeping with the spirit of other published works such as Choksi et al. (2009), Choksi et al. (2011) and Choksi (2012).

We demonstrated that our proposals for energy minimisers are **consistent with** other, established results in the **calculus of variations** (in respect of the equal spacing of 1D minimisers) and **sharp interface limit analysis** (in respect of the width of the monolayers).

We also linked the temperature response of our models back to well known **segregation regimes of physical models** of DBC phase separation.

As we noted in the Introduction, a significant body of literature exists studying (local) energy minimisers in the sharp interface limit (Alberti et al. (2007); Nunzio Spadaro (2009); Choksi (2012) and others). As we noted at the outset of Chapter 7, the 1D minimisation problem has been studied very extensively. In Alberti et al. (2007), the authors state that '*[i]n [1D], it can be proven that minimizers of [the sharp interface limit problem] or its diffuse interface representation (the Ohta–Kawasaki functional) are periodic*'. Our results are drawn from an elementary, constructive process, but they are consistent with this statement. We were unable to *prove* that symmetric, 2-phase minimisers are equally spaced using our technique. We were however able to use it to exploit the form of our homogeneous energy approximation (viz. the quadratic nature of the term away from the obstacle), and attempt a systematic and complete analysis of the (global) energy minimisers in a highly simplified situation (symmetric, 1D). We went further than claiming that such minimisers are layered and periodic, and proposed an *explicit and complete* characterisation (number, location and detailed shape of the component structures) of the minimisers *for any set of parameters* i.e. *away* from the sharp interface limit. To the best of our knowledge, this process and the explicit predictions we made with it do not appear in any published work.

10.1.2 3-Phase results: Chapter 9

As in the 2-phase case, we started this chapter by presenting a summary of a physical model of 3-phase materials, and elucidating the appropriate free energy functional and the minimisation problem of interest. Our model was drawn from Choksi and Ren (2005) because of its strong connection to the SCFT (which is regarded as the state of the art model of DBCs). We then presented our framework for gradient flows and a gradient flow numerical method which was a generalisation of our 2-phase method.

We were primarily interested in symmetric 3-phase materials and, as in our study of the 2-phase problem, we studied the 1D problem in detail. We posed an ***ansatz* for low energy symmetric morphologies in 1D** that made use of our 2-phase equal-spacing result. We asserted that this is a reasonable approach because of the way our 3-phase model reduces to the 2-phase case inside the pure copolymer. We then used and **extended the 3-phase sharp interface limit results** of Choksi and Ren (2005) to predict the energy minimising monolayer width (and count) in the class of 1D morphologies of interest. A comparison between the sharp interface limit results and the heuristic *ansatz* approach above enabled us to make meaningful parameter selections, and construct useful ICs for our subsequent gradient flow numerical experiments.

We then **applied our 3-phase model to step formation (terracing) in 2D thin films**. We modelled these as thin layers of polymer material resting atop a substrate with

a free surface to the void. The **free surface could evolve** (and form a step) so as to minimise the energy functional. The films were thin in that they could accommodate a small number monolayers oriented parallel to the substrate. Our application of a phase field model to the terracing problem is, to the best of our knowledge, entirely novel. We restricted our attention to single-step configurations, taking inspiration from the results of the SCFT experiments and physical observations reported in Stasiak et al. (2012).

Our work made an additional contribution compared to Stasiak et al. (2012) in two respects:

i) Our simplified model facilitated a sharp interface analysis which led to the **novel double tangent construction** of Section 9.4.1, which is a simple but powerful tool for analysing, predicting and explaining terracing.

   Remark. Stasiak et al. (2012) also reference a double-tangent construction (see their Fig. 10 and the paragraph immediately preceding their 'Theory' section). However, very little detail is given as to how it was constructed or what it was used for.

ii) The SCFT numerical simulations in Stasiak et al. (2012) were not dynamic, in that the authors did not report on the kinetic pathway of the fluids to their equilibrium state (cf. Section 5.3.6 of Fredrickson (2006)). In some respects the experiments in this reference are similar to those we reported on in Sections 9.4.3, 9.4.5, where we constructed ICs that we believed to be morphologically similar to an end-state of interest (the initial guesses are not described in Stasiak et al. (2012)).

   We performed **two large numerical experiments to showcase our capabilities in simulating the physical evolution of DBCs**. First, the spontaneous terrace formation experiment in Section 9.4.6 is the first we are aware of that captures the formation of a step from a random, flat IC. Second, our numerical experiment in Section 9.4.7 corresponds to what we believe to be a physical situation. We were able to make a prediction about the time evolution of a complex situation which could, in principle, be verified experimentally.

We do not expect the results of our numerical experiments to accurately reflect every detail of the underlying time evolution. Realistically, we hope to have captured some of its essential features. It seems reasonable, however, to hope that the models and techniques upon which our experiments are based, are a meaningful first step towards models and simulations that do. At the very least, it appears that our capabilities are comparable to the current state of the art (i.e. the SCFT approach) for the scenarios we considered.

10.1.3 Other contributions

We draw the reader's attention to the extensive appendices at the end of this manuscript.

- Appendix A includes two useful sections: Appendix A.1 describes the **mathematical tools** we used in Chapters 4 and 5. Much of the material underlying papers such as Blowey and Elliott (1991) is hard to find written down anywhere. Appendix A.2 provides further insight into the overall **modelling context** of solving the n-dimensional energy minimisation problem posed in Section 2.2.

- Appendix B includes **full and detailed proofs of the results** in Chapters 4 and 5.

- Appendix C provides further details of the 1D/2-phase numerical experiments and further analysis we conducted for Chapters 6–8.

- Appendix D provides substantial **detail in connection with 3-phase modelling** in support of Chapter 9. Two minor, but interesting results are developed:

  i) we reconcile the two ways of writing down dynamics for the problem (viz. in ϕ_A, ϕ_B, ϕ_V and φ, ψ order parameters) and find **restrictions on the mobilities** M_φ **and** M_ψ in terms of M_A, M_B, M_V. We assert that M_φ and M_ψ cannot be equal, which suggests there is a problem with the assumption in Ito (1998) that their $L_1 = L_2 = 1$ (see the comment immediately following their equation (8)).

  ii) we explore **mass conservation and control in 3-phase systems**. It is well known for 2-phase Ohta–Kawasaki systems (i.e. with non-zero non-local component), that if $\overline{\varphi_0} \neq m$ then $\varphi(t) \to m$ exponentially quickly (cf. (3.50)). However, we are not aware of any analysis for the 3-phase situation, in which $\left(\overline{\varphi_0}, \overline{\psi_0}\right) \neq \boldsymbol{m}$. We find that mass control in three phases is different to that in two, and that generally, instead of $\left(\overline{\varphi}, \overline{\psi}\right) \to \boldsymbol{m}$, the *ratio* of $\overline{\varphi}(t)$ to $\overline{\psi}(t)$ is controlled.

Finally, we list the **software codes and tools** we developed in support of this thesis.

- A very substantial MATLAB code was written in support of the 2-phase energy minimisation process. Apart from the code required to perform the parameter space sweep in Chapters 6–7, we also implemented the semi-explicit 2-phase optimisation process defined in Section 8.2. Substantial use was made of the CHEBFUN tool in this code.

- We developed a Message Passing Interface (MPI), FENICS code (using the `Python` front-end) for our 2- and 3-phase gradient flow experiments (cf. Chapter 5 and Section 9.2.5.3), that supports almost arbitrary time-splitting capabilities (from fully implicit to fully explicit in every component term via the use of a number of θ time-splitting parameters).

  Because our 3-phase numerical experiments were so long running, a significant amount of effort was dedicated to building a code that was robust and, in particular, could cope with non-convergence of the SSN method (the method frequently failed to converge).

- We wrapped our FEniCS code inside an experiment management suite, built on a bespoke `mySQL` database, that supported the following functionality:

  i) The ability to define and save spatial and time discretisations, together with scenarios describing various combinations of the problem parameters of interest. These could be combined into experiments which could be executed (automatically and repeatedly) on different platforms (the author's laptop and Archer, the UK national supercomputing facility – see http://www.archer.ac.uk/), with different configurations for the PETSc backend. We were also able to plug-and-play different homogeneous energy density components in two and three phases, from the regularised $\mathcal{B}_\mu$, used in this thesis, to the double-well polynomial versions studied elsewhere.

  ii) We developed a number of IC creation capabilities, supporting random ICs, as well as the sorts of structures depicted in Fig's 9.21(a), 9.28. To support these requirements, much of the Matlab 2-phase optimisation code we wrote for Section 8.2 was redeveloped in `Python`, so that we could use interpolants of these structures as ICs in gradient flow experiments (cf. Section 8.1.2).

  iii) We developed an experiment 'chaining' capability which allowed us to stitch together sequences of individual experiments into very long simulations, in which the end-state of one experiment was the IC for the next one. Each individual experiment used a fixed time-step τ, but the chain capability allowed us to (manually) increase the time-step as we progressed the very long time-horizon simulations (cf. Section 9.4.7).

  iv) We developed a bespoke task-farm capability, which allowed us to design and create large groups of individual gradient flow experiments (tens to hundreds in a set, such as in Section 8.1.2), that were then executed by a set of independent MPI processes (we generally used between four and six). The root process managed the process of handing out individual experiments to the 'farm hands' (the individual MPI processes) until all of the experiments in a set were completed. We could thus devise and manage very large, complex groups of experiments, like the set of 600+ experiments we report on in Section 9.3.7.

  v) Extensive, automated analysis and reporting capabilities. We developed a reporting tool that created solution snapshot pictures, analysis of various metrics of interest (energy and mass evolution, performance of the solver, execution time/SSN iteration counts etc.), and then combined these into a standard `.pdf` report. Our reporting capabilities worked across chains and groups.

These codes (see Section 2.4) will be made public in due course. Hopefully they will be of use to other researchers.

10.2 Opportunities for further research

We note several opportunities for further research. These would likely entail significant extensions to the work presented in this manuscript.

i) The **non-local Hele–Shaw/Mullins–Sekerka** problem. In Pego (1989), the author showed that taking the sharp interface limit ($\varepsilon \downarrow 0$) of the Cahn–Hilliard gradient flow equation (with double-well [quartic polynomial] homogeneous energy density) leads to the Hele–Shaw/Mullins–Sekerka problem (cf. p. 265 of Chen (1996)). Alikakos et al. (1994) then established the same result rigorously. Le (2010) then established the convergence of the (non-local) Ohta–Kawasaki gradient flow equation, to motion by the non-local Mullins–Sekerka law, using the Gamma-convergence technique developed in Sandier and Serfaty (2004). The Mullins–Sekerka free boundary problem, as $\varepsilon \downarrow 0$, was given in (1.3) of Le (2010) as

$$
\begin{aligned}
u^0 &= \pm 1 && \text{in } \Omega_t^{\pm},\ t \in [0,T] \\
v &= \Delta^{-1}\left(u^0 - \overline{u^0}\right) && \text{in } \Omega \times [0,T] \\
\Delta w &= 0 && \text{in } \Omega \backslash \Gamma(t),\ t \in [0,T] \\
\partial_n w &= 0 && \text{on } \partial\Omega \times [0,T] \\
w &= \sigma\kappa - \lambda v && \text{on } \Gamma(t), [0,T] \\
\partial_t \Gamma &= \frac{1}{2}\left[\partial_n w\right]_{\Gamma(t)} && \text{on } \Gamma(t), [0,T] \\
\Gamma(0) &= \Gamma_0. &&
\end{aligned}
$$

In this problem u^0 and v are the sharp interface limits of our φ and $\Delta^{-1}(\varphi - \overline{\varphi})$. Γ is the interface separating Ω^+ (its exterior) from Ω^- (its interior) in Ω, on which $u^0 = \pm 1$ (with IC Γ_0). κ is the mean curvature of Γ and $\partial_t \Gamma$ is the normal velocity of Γ (taken to be positive if Γ encloses an expanding domain) and $\hat{\boldsymbol{n}}$ is the unit outward normal to Γ. $\left[\partial_n w\right]_{\Gamma(t)} = \partial_n w^+ - \partial_n w^-$ is the jump in the restriction of w to Ω^+ and Ω^-, across Γ. The non-local coefficient above is λ, and is equivalent to our α; setting $\lambda = 0$ recovers the Cahn–Hilliard equation and the Mullins–Sekerka law (see (1.8) in Cahn et al. (1996)).

There are several interesting questions to consider: does the regularised version of the model that we have used, lead to the non-local Mullins–Sekerka/Hele–Shaw problem in the sharp interface limit (as $\varepsilon \downarrow 0$) in two phases? Does the obstacle problem (with $\mu \downarrow 0$) also tend to this problem? Can corresponding results be developed in three phases? If so, what can we learn from studying/simulating the dynamics of these sharp interface problems?

The 2-phase version of this piece of work, using matched asymptotics, was initially

slated for inclusion in this thesis, but was deferred to control scope.

ii) **Explicit characterisation of energy minimisers**. In Choksi et al. (2011) the authors attempt to find the ODT for a 2-phase model in 2D, using a spectral numerical method. We considered a different form of the homogeneous energy density, and the simplified situation of symmetry in 1D, but the basic intention was the same, and we were able to make more precise claims than those authors. Obvious extensions to our work include the asymmetric case in 1D, as well as the 2D and 3D problems. The main aim would be to predict, explain and reproduce the phase diagram in Fig. 1.3.

We should hope to go further than this. If we can extend our 1D ideas and results above, we should be able to a) exactly and explicitly locate the 2-phase ODT in parameter space for any spatial dimension, b) classify the morphologies associated with sub-regions in the ordered part of parameter space, and define the functions separating them, and c) generalise our ν_{opt} variable in Fig. 8.2 to quantify the structures in parameter space. For instance, in 3D we might measure the number of close-packed spheres (cf. Fig. 1.3) in an energy minimiser, at each point in the relevant region of parameter space, and so on, for each distinct type of component structure.

We could then extend these ideas to 3-phase models, although this would be a very large piece of work. Ultimately, we would wish to exploit the fundamentally *ansatz*-free nature of the method to investigate DBC structures and morphologies that have *not* been observed experimentally.

These are extremely ambitious objectives. A major source of our confidence that they may be achievable stems from the (surprising) simplifications resulting from our chosen form of the homogeneous energy density. Indeed, in Alberti et al. (2007) the authors observe that '*it is ... natural to conjecture that in higher dimensions, minimizers are at least nearly periodic. Surprisingly, proving such a simple statement is a formidable task*'. More recently, in Choksi (2012), the authors note that '*[w]hether or not a global minimizer is exactly periodic remains open and, perhaps, debatable*'.

iii) **Surface interaction terms**. Our 3-phase model includes a device (we called it χ^{Δ}) for capturing the asymmetry in the degree to which the two polymer phases A, B repel the void. However, we did not model the preferential interaction between the polymer phases and the substrate. Instead, we inserted layers of pure phase material into our numerical experiment ICs.

Remark. The SCFT model used in Stasiak et al. (2012) also explicitly excludes any way of capturing the polymer–substrate interaction. The authors remark that '*[t]he substrate is assumed to have a strong affinity for one of the components, but there is no need for a parameter specifying the strength of this preference. The affinity is accounted*

for by simply limiting our attention to morphologies that only have one component in contact with the substrate, which is achieved by having one of the continuous monolayers next to the substrate'.

We briefly attempted work in this direction. One of the difficulties we encountered (as with all such non-trivial model enhancements), was how to parameterise the additional terms, without obscuring the remainder of our model. The third term in equation (3) of Dessí et al. (2013) (see also their equation (6)) illustrates the basic idea in the context of chemical patterns on substrates. Fraaije et al. (1997) also includes ideas related to these surface terms, which could be used as the basis for an enhancement of our model.

iv) **Time evolution**. We used (mass conserving) H^{-1} gradient flows in formulating our gradient flow dynamics. As such we introduced a (formal) gradient flow variable t and mobilities that make it reasonable to think of t as time. We made simplifying assumptions on the mobilities, assuming them to be constant scalars. As such, it is not clear how well the evolution we presented, for instance in Fig. 9.30, captures the underlying physics.

We could consider other forms of mobility matrix, as a first step towards making our results more physically realistic. For example, solution dependent, degenerate mobilities have been widely studied (see for instance Elliott and Garcke (1996), Barrett and Blowey (2001) and Lee et al. (2015)), albeit in the context of Cahn–Hilliard-type models.

Remark. Such degenerate mobilities generally turn the dynamics off (set a mobility function to zero) wherever a pure phase $\varphi = \pm 1$ is achieved. In contrast to Cahn–Hilliard models, non-local models based on the double-well homogeneous energy density $\mathcal{B}_q$ of (3.20) lead to morphologies in which $\|\varphi\|_{0,\infty} < 1$, and so degenerate mobilities would have little to no effect. On the other hand, the double-obstacle homogeneous energy density leads to morphologies with $\|\varphi\|_{0,\infty} = 1$, and so combining degenerate mobilities with this homogeneous density would have a substantial effect.

Likewise, it is not clear that the H^{-1} gradient flow correctly captures the underlying physical evolution, although this is the choice made in, for instance, Ohta and Ito (1995) and Ito (1998) and in the CHC theory.

Remark. One simple option would be to replace the H^{-1} gradient flow with a mass-constrained L^2 gradient flow. The result would be a mass-constrained Allen–Cahn type model. This may seem like a simplification, but apart from questions about physical relevance, this approach is unlikely to offer much of an improvement to the underlying numerical method because:

1. The H^{-1} gradient flow exactly cancels out the non-local energy terms making them

linear. On the other hand, when we operator split the H^{-1} gradient flow PDE, we introduce chemical potentials which make the problem large. With an L^2 gradient flow, we would need to solve for non-local variables instead of these chemical potentials, and so the result would be a problem of the same size.

2. The mass constraints would likely express as one or two lines in the underlying linear algebra systems. These would potentially destroy any matrix symmetry and could make the resulting numerics extremely expensive.

With suitable enhancements to the model, improvements in our numerical methods and access to a large supercomputing facility, genuine 3D structures like 'Scherk's double periodic surface' which connects successive steps, as noted in Gido et al. (1993) and Carvalho and Thomas (1994), may become accessible. *These are extremely complex structures that are (likely) well beyond our current capabilities.*

v) **Coupling of our phase separation models to additional models**: temperature, Flory–Huggins and the Navier–Stokes equations:

In Parsons (2013), we proposed a model coupling the 2-phase Ohta–Kawasaki and Navier–Stokes equations, using the natural extension of the coupling discussed in Feng (2006) and some technical results from Feng and Prohl (2004). We extended this model using the relationship between the Flory–Huggins parameter and temperature noted in Section 6.1 (equation (58)) of Matsen (2002), and then included the heat equation (including diffusion and transport effects due to the underlying continuum) to try and replicate the results in Hashimoto et al. (1999), Mita et al. (2007) and Campbell et al. (2013).

We created a bespoke 2D implementation of the model in MATLAB based on proposals for implementing the fully non-linear Navier–Stokes equations from Kay and Welford (2007) and Kay et al. (2008). Results from our numerical experiments were encouraging and suggested that the model is, at least conceptually, correct. We observed the microstructures being carried by the moving fluid. The structures 'dissolved' in warmer regions, and then (re-)formed in cooler regions.

Our treatment of temperature was, we believe, new: all of the literature we are aware of treats temperature as a constant. We regarded it as a scalar that could evolve in space and time according to the heat equation. That this might be reasonable is hinted at in Section 2 of Pinna and Zvelindovsky (2012).

The difficulty with these enhancements, and the reason we avoided pursuing them in depth, is two-fold:

1. There are deep questions around the thermodynamic consistency of these models. Our assumption that temperature evolves according to the heat equation made good

intuitive sense, but was not based on fundamental physical modelling.

2. Each additional model introduces its own physical parameters. Finding physically correct values for these and/or non-dimensionalising them could be extremely challenging. A telling remark in this regard is found in Stasiak et al. (2012). In the context of their model for terrace formation (very similar to ours) they say that '*four parameters is a lot*'. It would seem we are justified in being hesitant to work with models involving several more parameters than that.

Such models are interesting mathematical objects, but it is essential that they be confirmed as physically meaningful and consistent. This could be achieved, for instance, by showing that they correspond to the thermodynamic limits of models with a solid basis in physics.

vi) We note two additional modelling opportunities that we have not investigated in any depth, but that could significantly enhance the predictive power of the model:

   i) **Visco-elasticity**: for instance by coupling in the Oldroyd-B model; and

   ii) A **temperature/viscosity dependency** to capture the way in which such materials become brittle as they cool.

vii) **PDAS**. In Blank et al. (2011, 2013), the authors implemented PDAS for the Cahn–Hilliard and mass-constrained Allen–Cahn models. This method is similar to ours in that it depends on an SSN method for its convergence, but differs in that the solutions it generates do not exceed unit norm (our method yields solutions with $\|\varphi_\mu\|_{0,\infty} \leq 1+C\mu$). In principle, the method could be extended to cater for non-local models in a higher number of phases. The main theoretical advantage of the method is that it iterates over portions of the problem (on the active and inactive sets), which means that it works on a series of sub-problems that are smaller than the overall problem (most of the computational effort is focused on interfacial regions), and should be *significantly* faster (or at least more efficient).[2]

We implemented PDAS for our non-local, 2-phase model in FEniCS. *For technical reasons, we were unable to exploit its potential for a speed-up relative to our Moreau–Yosida regularised SSN method.*

viii) **Comparison of numerical methods**. Our numerical method (Euler-in-time, FEM-in-space) could be compared to the CDS method discussed in references such as Ren and Hamley (2001), Pinna and Zvelindovsky (2012) and Dessí et al. (2013), PDAS (as above), as well as the SCFT-method used in Stasiak et al. (2012), Maher et al. (2016) (see the section 'Theory' under 'Materials and Methods'). For instance, in Dessí et al. (2013), the authors state that '*SCFT remains one of the best available tools to study*

complex [block copolymer] systems, however it is computationally expensive even with modern computational power.'

It would be useful to understand which method(s) offer the most performance efficient support for high fidelity simulations involving long simulation time-horizons and large physical domains, bearing in mind that advances in multi-processor computer technology may make methods that were historically prohibitively expensive, more attractive. An analysis and comparison of the various modelling and computational options would also need to take various trade-offs (modelling requirements [such as domain geometry], speed, accuracy, user objectives [e.g. research mathematician vs practising material scientist] etc.) into account.

Notes

[1]It is not clear how to adapt this approach for the PDAS method.

[2]By 'efficient', we mean the following: we attempted (unsuccessfully, see the next sentence) to implement PDAS in combination with a mesh refinement/coarsening strategy involving refinement inside interfacial regions and coarsening in pure phase areas. Such a strategy would not necessarily reduce the problem size (as measured by the number of degrees of freedom) compared to a non-refined approach, but would focus computational resource on resolving the interfacial structures to extremely high accuracy.

References

R. A. Adams and J. J. F. Fournier. *Sobolev Spaces*. Pure and Applied Mathematics. Elsevier Science, second edition, 2003.

G. Alberti, R. Choksi, and F. Otto. *Uniform Energy Distribution for Minimizers of an Isoperimetric Problem Containing Long-range Interactions*. SFB 611, 2007.

N. D. Alikakos, P. W. Bates, and X. Chen. Convergence of the Cahn–Hilliard equation to the Hele–Shaw model. *Archive for rational mechanics and analysis*, 128(2):165–205, 1994.

M. S. Alnæs, J. Blechta, J. Hake, A. Johansson, B. Kehlet, A. Logg, C. Richardson, J. Ring, M. E. Rognes, and G. N. Wells. The FEniCS Project Version 1.5. *Archive of Numerical Software*, 3(100), 2015. doi: 10.11588/ans.2015.100.20553.

K. Atkinson and H. Weimin. *Theoretical Numerical Analysis, A Functional Analysis Framework*. Texts in Applied Mathematics. Springer, third edition, 2009.

M. Bahiana and Y. Oono. Cell dynamical system approach to block copolymers. *Physical Review A*, 41(12):6763, 1990.

S. Balay, S. Abhyankar, M. F. Adams, J. Brown, P. Brune, K. Buschelman, L. Dalcin, V. Eijkhout, W. D. Gropp, D. Kaushik, M. G. Knepley, D. A. May, L. C. McInnes, R. T. Mills, T. Munson, K. Rupp, P. Sanan, B. F. Smith, S. Zampini, and H. Zhang. PETSc Web page. `http://www.mcs.anl.gov/petsc`, 2018. URL `http://www.mcs.anl.gov/petsc`.

S. Baldo. Minimal interface criterion for phase transitions in mixtures of Cahn–Hilliard fluids. In *Annales de l'Institut Henri Poincare (C) Non Linear Analysis*, volume 7, pages 67–90. Elsevier, 1990.

J. Ball. *Dynamical Systems and Energy Minimization*. 2014. Tutorial notes supplied for this Part B course at the University of Oxford.

L. Baňas and R. Nürnberg. A multigrid method for the Cahn–Hilliard equation with obstacle potential. *Applied Mathematics and Computation*, 213(2):290–303, 2009.

J. W. Barrett and J. F. Blowey. An error bound for the finite element approximation of a model for phase separation of a multi-component alloy. *IMA Journal of Numerical Analysis*, 16(2):257–287, 1996. doi: 10.1093/imanum/16.2.257.

J. W. Barrett and J. F. Blowey. Finite element approximation of a model for phase separation of a multi-component alloy with non-smooth free energy. *Numerische Mathematik*, 77(1):1–34, 1997.

J. W. Barrett and J. F. Blowey. An improved error bound for a finite element approximation of a model for phase separation of a multi-component alloy. *IMA Journal of Numerical Analysis*, 19(1):147–168, 1999a.

J. W. Barrett and J. F. Blowey. An optimal error bound for a finite element approximation of a model for phase separation of a multi-component alloy with non-smooth free energy. *ESAIM: Mathematical Modelling and Numerical Analysis*, 33(5):971–987, 1999b.

J. W. Barrett and J. F. Blowey. An improved error bound for a finite element approximation of a model for phase separation of a multi-component alloy with a concentration dependent mobility matrix. *Numerische Mathematik*, 88:255–297, 2001. ISSN 0029-599X.

J. W. Barrett, J. F. Blowey, and H. Garcke. Finite Element Approximation of the Cahn–Hilliard Equation with Degenerate Mobility. *SIAM Journal on Numerical Analysis*, 37 (1):286–318, 1999.

R.G. Bartle and D.R. Sherbert. *Introduction to Real Analysis*. Wiley, 2011. ISBN 9780471433316.

F. S. Bates and G. H. Fredrickson. Block Copolymers – Designer Soft Materials. *Phys. Today*, 52(2), 1999.

P. W. Bates and P. C. Fife. The dynamics of nucleation for the Cahn–Hilliard equation. *SIAM Journal on Applied Mathematics*, 53(4):990–1008, 1993.

V. A. Belyi and T. A. Witten. Spreading of block copolymer films and domain alignment at moving terrace steps. *The Journal of chemical physics*, 120(11):5476–5485, 2004.

B. Benesová, C. Melcher, and E. Süli. An Implicit Midpoint Spectral Approximation of Nonlocal Cahn–Hilliard Equations. *SIAM Journal on Numerical Analysis*, 52(3):1466–1496, 2014.

L. Blank, M. Butz, and H. Garcke. Solving the Cahn-Hilliard variational inequality with a semi-smooth Newton method. *ESAIM: COCV*, 17(4):931–954, 2011.

L. Blank, M. Butz, H. Garcke, L. Sarbu, and V. Styles. *Allen-Cahn and Cahn-Hilliard Variational Inequalities Solved with Optimization Techniques*, pages 21–35. Springer Basel, Basel, 2012.

L. Blank, H. Garcke, L. Sarbu, and V. Styles. Primal-dual active set methods for AllenCahn variational inequalities with nonlocal constraints. *Numerical Methods for Partial Differential Equations*, 29(3):999–1030, 2013.

J. F. Blowey and C. M. Elliott. The Cahn-Hilliard gradient theory for phase separation with non-smooth free energy Part I: Mathematical analysis. *European Journal of Applied Mathematics*, 2(03):233–280, 1991. doi: 10.1017/S095679250000053X.

J. F. Blowey and C. M Elliott. The Cahn–Hilliard gradient theory for phase separation with non-smooth free energy Part II: Numerical analysis. *European Journal of Applied Mathematics*, 3(2):147–179, 1992.

J. Bosch, D. Kay, M. Stoll, and A. J. Wathen. Fast Solvers for Cahn–Hilliard Inpainting. *SIAM Journal on Imaging Sciences*, 7(1):67–97, 2014a.

J. Bosch, M. Stoll, and P. Benner. Fast solution of Cahn–Hilliard variational inequalities using implicit time discretization and finite elements. *Journal of Computational Physics*, 262:38–57, 2014b.

F. Boyer and C Lapuerta. Study of a three component Cahn–Hilliard flow model. *ESAIM: Mathematical Modelling and Numerical Analysis*, 40(04):653–687, 2006.

F. Boyer and S. Minjeaud. Fully discrete approximation of a three component cahn–hilliard model. In *Proceedings of ALGORITMY*, pages 143–152, 2009.

F. Boyer, C. Lapuerta, S. Minjeaud, B. Piar, and M. Quintard. Cahn–Hilliard/Navier–Stokes model for the simulation of three-phase flows. *Transport in porous media*, 82(3): 463–483, 2010.

D. Braess. *Finite Elements: Theory, Fast Solvers, and Applications in Solid Mechanics*. Cambridge University Press, second edition, 2001.

S. C. Brenner and R. Scott. *The Mathematical Theory of Finite Element Methods*. Texts in Applied Mathematics. Springer, 2007.

J. W. Cahn. On spinodal decomposition. *Acta Metallurgica*, 9(9):795 – 801, 1961. doi: https://doi.org/10.1016/0001-6160(61)90182-1.

J. W. Cahn and J. E. Hilliard. Free Energy of a Nonuniform System. i. Interfacial Free Energy. *The Journal of chemical physics*, 28(2):258–267, 1958.

J. W. Cahn, C. M. Elliott, and A. Novick-Cohen. The Cahn–Hilliard equation with a concentration dependent mobility: motion by minus the Laplacian of the mean curvature. *European Journal of Applied Mathematics*, 7(03):287–301, 1996.

I. P. Campbell, C. He, and M. P. Stoykovich. Topologically Distinct Lamellar Block Copolymer Morphologies Formed by Solvent and Thermal Annealing. *ACS Macro Letters*, 2(10): 918–923, 2013.

B. L. Carvalho and E. L. Thomas. Morphology of Steps in Terraced Block Copolymer Films. *Physical review letters*, 73(24):3321, 1994.

L. Chen. Phase-Field Models for Microstructure Evolution. *Annual Review of Materials Research*, 32(1):113–140, 2002. doi: 10.1146/annurev.matsci.32.112001.132041.

X. Chen. Global asymptotic limit of solutions of the cahn-hilliard equation. *J. Differential Geom.*, 44(2):262–311, 1996.

X. Chen and Y. Oshita. Periodicity and Uniqueness of Global Minimizers of an Energy Functional Containing a Long-Range Interaction. *SIAM Journal on Mathematical Analysis*, 37(4):1299–1332, 2005. doi: 10.1137/S0036141004441155.

R. Choksi. Scaling Laws in Microphase Separation of Diblock Copolymers. *Journal of Nonlinear Science*, 11(3):223–236, Jun 2001. ISSN 1432-1467.

R. Choksi. Mathematical Aspects of Microphase Separation of Diblock Copolymers. In *Surikaisekikenkyusko Kokyuroku*, volume 1330 of *Conference Proceedings*, pages 10–17. RIMS, 2003.

R. Choksi. On global minimizers for a variational problem with long-range interactions. *Quarterly of Applied Mathematics*, 70(3):517–537, 2012.

R. Choksi and M. A Peletier. Small volume fraction limit of the diblock copolymer problem: I. sharp-interface functional. *SIAM Journal on Mathematical Analysis*, 42(3):1334–1370, 2010.

R. Choksi and M. A Peletier. Small volume-fraction limit of the diblock copolymer problem: Ii. diffuse-interface functional. *SIAM Journal on Mathematical Analysis*, 43(2):739–763, 2011.

R. Choksi and X. Ren. On the Derivation of a Density Functional Theory for Microphase Separation of Diblock Copolymers. *J. Statist. Phys.*, 113:151–176, 2003.

R. Choksi and X. Ren. Diblock Copolymer/Homopolymer Blends: Derivation of a Density Functional Theory. *Physica D: Nonlinear Phenomena*, 203(1):100–119, 2005.

R. Choksi, M. A. Peletier, and J. F. Williams. On the Phase Diagram for Microphase Separation of Diblock Copolymers: An Approach via a Nonlocal Cahn–Hilliard Functional. *SIAM Journal on Applied Mathematics*, 69(6):1712–1738, 2009.

R. Choksi, M. Maras, and J. F. Williams. 2D Phase Diagram for Minimizers of a Cahn–Hilliard Functional with Long-Range Interactions. *ArXiv e-prints*, March 2011.

P. G. Ciarlet. *The finite element method for elliptic problems*. North–Holland Publishing Company, 1978.

S. Cohen and D. Andelman. Interfacial Phenomena of Solvent–Diluted Block Copolymers. *Macromolecules*, 47(1):460–469, 2014.

A. B. Croll, M. V. Massa, M. W. Matsen, and K. Dalnoki-Veress. Droplet Shape of an Anisotropic Liquid. *Phys. Rev. Lett.*, 97:204502, Nov 2006. doi: 10.1103/PhysRevLett.97.204502. URL `https://link.aps.org/doi/10.1103/PhysRevLett.97.204502`.

B. Dacorogna. *Direct methods in the calculus of variations*, volume 78. Springer Science & Business Media, second edition, 2007.

R. Dal Passo, L. Giacomelli, and A. Novick-Cohen. Existence for an Allen–Cahn/Cahn–Hilliard system with degenerate mobility. *Interfaces and free boundaries*, 1(2):199–226, 1999.

P. G. de Gennes. Some conformation problems for long macromolecules. *Reports on Progress in Physics*, 32(1):187, 1969.

P. G. De Gennes. *Introduction to Polymer Dynamics*. CUP Archive, 1990.

R. Dessí, M. Pinna, and A. V. Zvelindovsky. Cell Dynamics Simulations of Cylinder-Forming Diblock Copolymers in Thin films on Topographical and Chemically Patterned Substrates. *Macromolecules*, 46(5):1923–1931, 2013.

A. E. Diegel, C. Wang, and S. M. Wise. Stability and Convergence of a Second Order Mixed Finite Element Method for the Cahn–Hilliard Equation. *IMA Journal of Numerical Analysis*, 36(4):1867–1897, 2015.

M. Doi and S. F. Edwards. *The Theory of Polymer Dynamics*, volume 73. Oxford University Press, 1988.

Q. Du and R. A Nicolaides. Numerical analysis of a continuum model of phase transition. *SIAM journal on numerical analysis*, 28(5):1310–1322, 1991.

S. F. Edwards. The statistical mechanics of polymers with excluded volume. *Proceedings of the Physical Society*, 85(4):613, 1965.

C. M. Elliott. The Cahn–Hilliard Model for the Kinetics of Phase Separation. 88:35–73, 1989.

C. M. Elliott and H. Garcke. On the Cahn–Hilliard equation with degenerate mobility. *Siam journal on mathematical analysis*, 27(2):404–423, 1996.

C. M. Elliott and H. Garcke. Diffusional phase transitions in multicomponent systems with a concentration dependent mobility matrix. *Physica D: Nonlinear Phenomena*, 109(3-4): 242–256, 1997.

C. M. Elliott and S. Luckhaus. A generalised diffusion equation for phase separation of a multi-component mixture with interfacial free energy'. 1991.

C. M. Elliott and A. M. Stuart. The Global Dynamics of Discrete Semilinear Parabolic Equations. *SIAM Journal on Numerical Analysis*, 30(6):pp. 1622–1663, 1993.

H. Elman, D Silvester, and A. Wathen. *Finite Elements and Fast Iterative Solvers*. Oxford University Press, reprinted edition, 2008.

H. Emmerich. *The diffuse interface approach in materials science: thermodynamic concepts and applications of phase-field models*, volume 73. Springer Science & Business Media, 2003.

L.C. Evans. *Partial Differential Equations*. Graduate Studies in Mathematics. American Mathematical Society, 1998. ISBN 9780821807729.

D. J. Eyre. An Unconditionally Stable One-Step Scheme for Gradient Systems. *Unpublished article*, 1998a.

D. J. Eyre. Unconditionally gradient stable time marching the Cahn–Hilliard equation. In *MRS Proceedings*, volume 529, page 39. Cambridge Univ Press, 1998b.

P. E. Farrell and J. W. Pearson. A preconditioner for the Ohta–Kawasaki equation. *SIAM Journal on Matrix Analysis and Applications*, 38(1):217–225, 2017.

M. J. Fasolka and A. M. Mayes. Block copolymer thin films: physics and applications. *Annual Review of Materials Research*, 31(1):323–355, 2001.

J. Feng, H. Liu, and J. M. Hu, Y. Prausnitz. Micro-phase separation of diblock-copolymer melts confined in a slit from simulation calculations-effect of coarse-graining scale. *Chemical Engineering Science*, 59(8):1701–1710, 2004. doi: https://doi.org/10.1016/j.ces.2004.01.026. URL `http://www.sciencedirect.com/science/article/pii/S0009250904000855`. Complex Systems and Multi-scale Methodology.

X. Feng. Fully discrete finite element approximations of the Navier–Stokes–Cahn–Hilliard diffuse interface model for two-phase fluid flows. *SIAM journal on numerical analysis*, 44 (3):1049–1072, 2006.

X. Feng and A. Prohl. Error analysis of a mixed finite element method for the Cahn–Hilliard equation. *Numerische Mathematik*, 99(1):47–84, 2004.

P. C. Fife. Models for phase separation and their mathematics. *Electronic Journal of Differential Equations*, 2000(48):1–26, 2000.

J. G. E. M. Fraaije. Dynamic density functional theory for microphase separation kinetics of block copolymer melts. *The Journal of chemical physics*, 99(11):9202–9212, 1993.

J. G. E. M. Fraaije, B. A. C. Van Vlimmeren, N. M. Maurits, M. Postma, O. A. Evers, C. Hoffmann, P. Altevogt, and G. Goldbeck-Wood. The dynamic mean-field density functional method and its application to the mesoscopic dynamics of quenched block copolymer melts. *The Journal of chemical physics*, 106(10):4260–4269, 1997.

G. H. Fredrickson. *The Equilibrium Theory of Inhomogeneous Polymers*, volume 134. Oxford University Press, 2006.

G. H. Fredrickson, V. Ganesan, and F. Drolet. Field-theoretic computer simulation methods for polymers and complex fluids. *Macromolecules*, 35(1):16–39, 2002.

D. Furihata. A stable and conservative finite difference scheme for the cahn-hilliard equation. *Numerische Mathematik*, 87(4):675–699, 2001.

H. Garcke, B. Nestler, and B. Stoth. On anisotropic order parameter models for multi-phase systems and their sharp interface limits. *Physica D: Nonlinear Phenomena*, 115 (1):87–108, 1998.

H. Garcke, B. Stoth, and B. Nestler. Anisotropy in multi-phase systems: a phase field approach. *Interfaces and Free Boundaries*, 1(2):175–198, 1999.

H. Garcke, A. Novick-Cohen, et al. A singular limit for a system of degenerate cahn–hilliard equations. *Advances in Differential Equations*, 5(4-6):401–434, 2000.

H. Garcke, K. F. Lam, E. Sitka, and V. Styles. A Cahn–Hilliard–Darcy model for tumour growth with chemotaxis and active transport. *Mathematical Models and Methods in Applied Sciences*, 26(06):1095–1148, 2016.

I. M. Gelfand and S. V. Fomin. *Calculus of Variations*. Dover Books on Mathematics. Dover Publications, 2012.

S. P. Gido, J. Gunther, E. L. Thomas, and D. Hoffman. Lamellar Diblock Copolymer Grain Boundary Morphology. 1. Twist Boundary Characterization. *Macromolecules*, 26 (17):4506–4520, 1993.

D. Gilbarg and N.S. Trudinger. *Elliptic Partial Differential Equations of Second Order*. Classics in Mathematics. Springer, 2001.

J. L. Goldberg and A. J. Schwartz. *Systems of Ordinary Differential Equations: An Introduction*. Harper & Row Publishers, 1972.

P. Grisvard. *Elliptic problems in nonsmooth domains*. Monographs and studies in mathematics. Pitman Advanced Pub. Program, 1985.

F. Guillén-González and G. Tierra. On linear schemes for a Cahn–Hilliard diffuse interface model. *Journal of Computational Physics*, 234:140–171, 2013. doi: https://doi.org/10.1016/j.jcp.2012.09.020.

F. Guillén-González and G. Tierra. Second order schemes and time-step adaptivity for Allen–Cahn and Cahn–Hilliard models. *Computers & Mathematics with Applications*, 68 (8):821–846, 2014.

X. Guo, M. Pinna, and A. V. Zvelindovsky. Parallel algorithm for cell dynamics simulation of block copolymers. *Macromolecular Theory and Simulations*, 16(9):779–784, 2007.

I. W. Hamley. Cell dynamics simulations of block copolymers. *Macromolecular theory and simulations*, 9(7):363–380, 2000.

I. W. Hamley. *The Physics of Block Copolymers*. Oxford, reprinted edition, 2003.

R. Hasegawa and M. Doi. Adsorption dynamics. Extension of self-consistent field theory to dynamical problems. *Macromolecules*, 30(10):3086–3089, 1997.

T. Hashimoto, J. Bodycomb, Y. Funaki, and K. Kimishima. The effect of temperature gradient on the microdomain orientation of diblock copolymers undergoing an order-disorder transition. *Macromolecules*, 32(3):952–954, 1999.

Y. He, Y. Liu, and T. Tang. On large time-stepping methods for the Cahn–Hilliard equation. *Applied Numerical Mathematics*, 57(5):616 – 628, 2007. ISSN 0168-9274. doi: https://doi.org/10.1016/j.apnum.2006.07.026. Special Issue for the International Conference on Scientific Computing.

M. Hintermüller and M. Hinze. Moreau–Yosida Regularization in State Constrained Elliptic Control Problems: Error Estimates and Parameter Adjustment. *SIAM Journal on Numerical Analysis*, 47(3):1666–1683, 2009. doi: 10.1137/080718735.

M. Hintermüller and M. Ulbrich. A mesh-independence result for semi-smooth Newton methods. *Mathematical Programming*, 101(1):151–184, Aug 2004. doi: 10.1007/s10107-004-0540-9.

M. Hintermüller, K. Ito, and K. Kunisch. The Primal-Dual Active Set Strategy as a Semismooth Newton Method. *SIAM Journal on Optimization*, 13(3):865–888, 2002.

M. Hintermüller, M. Hinze, and M. H. Tber. An adaptive finite-element Moreau–Yosida-based solver for a non-smooth Cahn–Hilliard problem. *Optimization Methods and Software*, 26(4-5):777–811, 2011.

J. J. Hoyt. Spinodal decomposition in ternary alloys. *Acta Metallurgica*, 37(9):2489 – 2497, 1989. doi: https://doi.org/10.1016/0001-6160(89)90047-3.

J. J. Hoyt. Linear spinodal decomposition in a regular ternary alloy. *Acta Metallurgica et Materialia*, 38(2):227 – 231, 1990. doi: https://doi.org/10.1016/0956-7151(90)90052-I.

W. Hurewicz. *Lectures on ordinary differential equations*. Courier Corporation, 1990.

A. Ito. Domain patterns in copolymer-homopolymer mixtures. *Physical Review E*, 58(5): 6158, 1998.

K. Ito and K. Kunisch. Semismooth Newton methods for variational inequalities of the first kind. *ESAIM: Mathematical Modelling and Numerical Analysis - Modélisation Mathmatique et Analyse Numérique*, 37(1):41–62, 2003.

D. W. Jordan and P. Smith. *Nonlinear Ordinary Differential Equations: An Introduction for Scientists and Engineers*. Oxford Texts in Applied and Engineering Mathematics Series. New York, 2007.

D. Kay and R. Welford. Efficient numerical solution of Cahn–Hilliard–Navier–Stokes fluids in 2D. *SIAM Journal on Scientific Computing*, 29(6):2241–2257, 2007.

D. Kay, D. Loghin, and A. Wathen. A Preconditioner for the Steady-State Navier–Stokes Equations. *SIAM Journal on Scientific Computing*, 24(1):237–256, 2002.

D. Kay, V. Styles, and R. Welford. Finite element approximation of a Cahn–Hilliard–Navier–Stokes system. *Interfaces and free Boundaries*, 10(1):15–43, 2008.

D. Kay, V. Styles, and E. Süli. Discontinuous Galerkin finite element approximation of the cahn–hilliard equation with convection. *SIAM Journal on Numerical Analysis*, 47(4): 2660–2685, 2009.

J. K. Kim, S. Y. Yang, Y. Lee, and Y. Kim. Functional nanomaterials based on block copolymer self-assembly. *Progress in Polymer Science*, 35(11):1325–1349, 2010.

J. U. Kim and M. W. Matsen. Droplets of structured fluid on a flat substrate. *Soft Matter*, 5(15):2889–2895, 2009.

A. Knoll, A. Horvat, K. S. Lyakhova, G. Krausch, G. J. A. Sevink, A. V. Zvelindovsky, and R. Magerle. Phase behavior in thin films of cylinder-forming block copolymers. *Phys. Rev. Lett.*, 89:035501, Jun 2002. doi: 10.1103/PhysRevLett.89.035501.

R. V. Kohn and F. Otto. Upper Bounds on Coarsening Rates. *Communications in Mathematical Physics*, 229(3):375–395, 2002.

E. Kreyszig. *Introductory functional analysis with applications*. Wiley. com, 1978.

N. Q Le. On the convergence of the Ohta–Kawasaki equation to motion by nonlocal Mullins–Sekerka law. *SIAM Journal on Mathematical Analysis*, 42(4):1602–1638, 2010.

A. A. Lee, A. Münch, and E. Süli. Sharp interface limits of the Cahn–Hilliard equation with degenerate mobility. *IFAC-PapersOnLine*, 48(1):401–402, 2015.

H.G. Lee. *Materials Thermodynamics: With Emphasis on Chemical Approach (With CD-ROM)*. 2012. ISBN 9789813108257.

L. Leibler. Theory of Microphase Separation in Block Copolymers. *Macromolecules*, 13(6): 1602–1617, 1980.

J. L. Lions. Quelques méthodes de résolution des problemes aux limites non linéaires. 1969.

K. S. Lyakhova, A. Horvat, A. V. Zvelindovsky, and G. J. A. Sevink. Dynamics of Terrace Formation in a Nanostructured Thin Block Copolymer Film. *Langmuir*, 22(13):5848–5855, 2006.

M. J. Maher, J. L. Self, P. Stasiak, G. Blachut, C. J. Ellison, M. W. Matsen, C. M. Bates, and C. G. Willson. Structure, Stability, and Reorganization of 0.5 L_0 Topography in Block Copolymer Thin Films. *ACS nano*, 10(11):10152–10160, 2016.

M. W. Matsen. Thin films of block copolymer. *The Journal of Chemical Physics*, 106(18): 7781, 1997.

M. W. Matsen. The standard Gaussian model for block copolymer melts. *Journal of Physics: Condensed Matter*, 14(2):R21, 2002.

M. W. Matsen and M. Schick. Stable and unstable phases of a diblock copolymer melt. *Phys. Rev. Lett.*, 72:2660–2663, Apr 1994.

N. M. Maurits and J. G. E. M. Fraaije. Mesoscopic dynamics of copolymer melts: from density dynamics to external potential dynamics using nonlocal kinetic coupling. *The Journal of chemical physics*, 107(15):5879–5889, 1997.

J. D. McGraw, I. D. W. Rowe, M. W. Matsen, and K. Dalnoki-Veress. Dynamics of interacting edge defects in copolymer lamellae. *The European Physical Journal E*, 34(12):1–7, 2011.

C. Meyer, A. Rösch, and F. Tröltzsch. Optimal Control of PDEs with Regularized Pointwise State Constraints. *Computational Optimization and Applications*, 33(2):209–228, 2006.

K. Mita, H. Tanaka, K. Saijo, M. Takenaka, and T. Hashimoto. Cylindrical domains of block copolymers developed via ordering under moving temperature gradient. *Macromolecules*, 40(16):5923–5933, 2007.

mitopencourseware. Diblock Copolymer Morphology Diagram. 2012. URL `http://www.flickr.com/photos/mitopencourseware/3323137283/in/set-72157614617563539`. This work is licensed under the Creative Commons Attribution-NonCommercial-ShareAlike 3.0 Unported License. To view a copy of this license, visit http://creativecommons.org/licenses/by-nc-sa/3.0/ or send a letter to Creative Commons, 444 Castro Street, Suite 900, Mountain View, California, 94041, USA.

N. Moelans, B. Blanpain, and P. Wollants. An introduction to phase-field modeling of microstructure evolution. *Calphad*, 32(2):268 – 294, 2008. ISSN 0364-5916. doi: https://doi.org/10.1016/j.calphad.2007.11.003.

H. Morita, T. Kawakatsu, and M. Doi. Dynamic density functional study on the structure of thin polymer blend films with a free surface. *Macromolecules*, 34(25):8777–8783, 2001.

M. Müller and J. C. O. Rey. Continuum models for directed self-assembly. *Molecular Systems Design & Engineering*, 3(2):295–313, 2018.

M. Müller and F. Schmid. Incorporating fluctuations and dynamics in self-consistent field theories for polymer blends. In *Advanced Computer Simulation Approaches for Soft Matter Sciences II*, pages 1–58. Springer, 2005.

Andreas Münch. Private communication. 2017.

I. Neitzel and F. Tröltzsch. On regularization methods for the numerical solution of parabolic control problems with pointwise state constraints. *ESAIM: COCV*, 15(2):426–453, 2009.

A. Nikoubashman, R. A. Register, and A. Z. Panagiotopoulos. Self-Assembly of Cylinder-Forming Diblock Copolymer Thin Films. *Macromolecules*, 46(16):6651–6658, 2013. doi: 10.1021/ma400867s.

Y. Nishikawa, H. Kawada, H. Hasegawa, and T. Hashimoto. Grain boundary morphology of lamellar microdomains. *Acta polymerica*, 44(4):192–200, 1993.

J. Nocedal and S. Wright. *Numerical Optimization*. Springer Series in Operations Research and Financial Engineering. Springer, second edition, 2006.

A. Novick-Cohen. The cahn–hilliard equation. *Handbook of differential equations: evolutionary equations*, 4:201–228, 2008.

A. Novick-Cohen and L. A. Segel. Nonlinear aspects of the cahn-hilliard equation. *Physica D: Nonlinear Phenomena*, 10(3):277–298, 1984. doi: https://doi.org/10.1016/0167-2789(84)90180-5.

E. Nunzio Spadaro. Uniform energy and density distribution: diblock copolymers functional. *Interfaces and Free Boundaries*, 11(3):447–474, 2009.

I. Ohnishi, Y. Nishiura, M. Imai, and Y. Matsushita. Analytical solutions describing the phase separation driven by a free energy functional containing a long-range interaction term. *Chaos: An Interdisciplinary Journal of Nonlinear Science*, 9(2):329–341, 1999.

T. Ohta and A. Ito. Dynamics of phase separation in copolymer-homopolymer mixtures. *Physical Review E*, 52(5):5250, 1995.

T. Ohta and K. Kawasaki. Equilibrium morphology of block copolymer melts. *Macromolecules*, 19(10):2621–2632, 1986.

Y. Oono and S. Puri. Study of phase-separation dynamics by use of cell dynamical systems. i. Modeling. *Physical Review A*, 38(1):434, 1988.

Q. K. Parsons. *Numerical Approximation of the Ohta–Kawasaki Functional*. 2012. URL `http://people.maths.ox.ac.uk/parsons/Dissertation.pdf`. MSc thesis.

Q. K. Parsons. *Finite element approximation of an Ohta-Kawasaki/Navier-Stokes system*. 2013. A paper submitted for the course 'Mixed Finite Element Methods and Iterative Methods' at Oxford University, Trinity Term 2013.

Q. K. Parsons, D. Kay, and A. Münch. Step evolution in two-dimensional diblock copolymer films. *ArXiv e-prints*, December 2017.

R. L. Pego. Front migration in the nonlinear Cahn–Hilliard equation. In *Proceedings of the Royal Society of London A: Mathematical, Physical and Engineering Sciences*, volume 422, pages 261–278. The Royal Society, 1989.

M. Pinna and A.V. Zvelindovsky. Large scale simulation of block copolymers with cell dynamics. *The European Physical Journal B*, 85(6):1–18, 2012.

S. Puri and Y. Oono. Study of phase-separation dynamics by use of cell dynamical systems. ii. Two-dimensional demonstrations. *Physical Review A*, 38(3):1542, 1988.

R. S. Qin and H. K. Bhadeshia. Phase field method. *Materials science and technology*, 26 (7):803–811, 2010.

R. S. Qin and H. K. D. H. Bhadeshia. Applications of phase field modeling. *Current Opinion in Solid State and Materials Science*, 15(3):81 – 82, 2011. ISSN 1359-0286. doi: https://doi.org/10.1016/j.cossms.2011.04.004. Applications of Phase Field Modeling in Materials Science and Engineering.

E. Reister, M. Müller, and K. Binder. Spinodal decomposition in a binary polymer mixture: dynamic self-consistent-field theory and monte carlo simulations. *Physical Review E*, 64 (4):041804, 2001.

S. R. Ren and I. W. Hamley. Cell dynamics simulations of microphase separation in block copolymers. *Macromolecules*, 34(1):116–126, 2001.

X. Ren and J. Wei. On energy minimizers of the diblock copolymer problem. *Interfaces and Free Boundaries*, 5(2):193–238, 2003.

M. Renardy and R. C. Rogers. *An Introduction to Partial Differential Equations*. Texts in Applied Mathematics. Springer, 2004.

J. C. Robinson. *Infinite-Dimensional Dynamical Systems: An Introduction to Dissipative Parabolic PDEs and the Theory of Global Attractors*. Cambridge Texts in Applied Mathematics. Cambridge University Press, 2001.

H. Sagan. *Introduction to the Calculus of Variations*. Dover Books on Mathematics. New York: Dover, 1969.

E. Sandier and S. Serfaty. Gamma-convergence of gradient flows with applications to Ginzburg-Landau. *Communications on Pure and Applied mathematics*, 57(12):1627–1672, 2004.

G. Seregin. *Methods of Functional Analysis for PDEs*. 2013. Tutorial notes supplied for this Part C course at the University of Oxford.

A. Shinozaki and Y. Oono. Spinodal decomposition in 3-space. *Phys. Rev. E*, 48:2622–2654, Oct 1993. doi: 10.1103/PhysRevE.48.2622.

J. Simon. Compact sets in the space $L^p(0,T;B)$. *Annali di Matematica Pura ed Applicata*, 146(1):65–96, Dec 1986.

P. Stasiak, J.D. McGraw, K. Dalnoki-Veress, and M.W. Matsen. Step Edges in Thin Films of Lamellar-Forming Diblock Copolymer. *Macromolecules*, 45(23):9531–9538, 2012.

I. Steinbach. Phase-field models in materials science. *Modelling and Simulation in Materials Science and Engineering*, 17(7):073001, 2009.

E. Süli. *Numerical Solution of Ordinary Differential Equations*. 2010. Tutorial notes supplied for this course as part of the Mathematical Modelling and Scientific Computing MSc at the University of Oxford.

E. Süli. Private communication. 2018.

E. Süli and D. Mayers. *An Introduction to Numerical Analysis*. Cambridge University Press, first edition, 2006.

W. A. Sutherland. *Introduction to Metric & Topological Spaces*. Oxford University Press, second edition, 2009.

P. I. C. Teixeira and B. M. Mulder. scomment on "study of phase-separation dynamics by use of cell dynamical systems. i. modeling". *Physical Review E*, 55(3):3789, 1997.

R. Temam. *Infinite Dimensonal Dynamical Systems in Mechanics and Physics*. Applied Mathematical Sciences. Springer, 1997.

T. Teramoto and Y. Nishiura. Double Gyroid Morphology in a Gradient System with Nonlocal Effects. *Journal of the Physical Society of Japan*, 71(7):1611–1614, 2002.

L. N. Trefethen and D. Bau III. *Numerical linear algebra*, volume 50. Siam, 1997.

T. Uneyama and M. Doi. Density Functional Theory for Block Copolymer Melts and Blends. *Macromolecules*, 38(1):196–205, 2004.

M. A. van Dijk and R. van den Berg. Ordering Phenomena in Thin Block Copolymer Films Studied Using Atomic Force Microscopy. *Macromolecules*, 28(20):6773–6778, 1995.

Y. van Gennip and M. A. Peletier. Copolymer-homopolymer blends: global energy minimisation and global energy bounds. *Calculus of Variations and Partial Differential Equations*, 33(1):75–111, 2008.

Y. van Gennip and M. A. Peletier. Stability of monolayers and bilayers in a copolymer-homopolymer blend model. *Interfaces and Free Boundaries*, 11(3):331–373, 2009.

X. Wu, G. J. Zwieten, and K. G. Zee. Stabilized second-order convex splitting schemes for Cahn–Hilliard models with application to diffuseinterface tumor-growth models. *International Journal for Numerical Methods in Biomedical Engineering*, 30(2):180–203.

C. Yeung and A. Shi. Formation of interfaces in incompatible polymer blends: a dynamical mean field study. *Macromolecules*, 32(11):3637–3642, 1999.

H. Yokoyama, T. E. Mates, and E. J. Kramer. Structure of Asymmetric Diblock Copolymers in Thin Films. *Macromolecules*, 33(5):1888–1898, 2000.

K. Yosida. *Functional Analysis*. Springer-Verlag, 1980.

E. Zeidler. *Nonlinear functional analysis and its applications*, volume 2. Springer, 1990.

J. Zhang, G. Jin, and Y. Ma. Phase separations in a copolymer–copolymer mixture. *Journal of Physics: Condensed Matter*, 18(3):837, 2005.

P. Zhang. *Periodic Phase Separation: A Numerical Study via a Modified Cahn–Hilliard Equation*. 2006. MSc Thesis, Simon Fraser University.

Part V

Supplementary Material

Appendix A

Background material

A.1 Further mathematical theory

We state some well known results to introduce constants and further notation. To start, we introduce the Poincaré constant, c_P.

Theorem A.1.1. (Poincaré's inequality) *Let $\Omega \subset \mathbb{R}^d$ be a bounded, Lipschitz domain and $v \in H^1(\Omega)$. There exists a constant $c_P = c_P(d, \Omega) > 0$ with*

$$\|v - \overline{v}\| \leq c_P |v|_1 , \tag{A.1}$$

and,[1]

$$\|v\| \leq c_P \left\{ |\Omega| \, |\overline{v}| + |v|_1 \right\} = c_P \left\{ |(v,1)| + |v|_1 \right\} \qquad \text{for every} \qquad v \in H^1(\Omega) . \tag{A.2}$$

More generally, for every $v \in W^{1,p}(\Omega)$,

$$\|v - \overline{v}\|_{0,p} \leq \|v - \overline{v}\|_{1,p} \leq c_P |v|_{1,p} . \tag{A.3}$$

(A.1) is from Lemma 8.3 of Seregin (2013), and is called the Poincaré-Sobolev inequality in that reference. See also Theorem 1 from Section 5.8 of Evans (1998) and Section 4.4 of Dacorogna (2007). According to (7.45) in Gilbarg and Trudinger (2001), (A.1) holds for any convex domain Ω. A proof of (A.1) appears as Ex. 5.9 of Robinson (2001) for bounded C^1 domains; solutions are available at `https://homepages.warwick.ac.uk/~masdh/Public/solutions.pdf`. (A.3) is from Lemma 4.3.14 of Brenner and Scott (2007).

We refer to all such results simply as Poincaré's inequality.

Proof. We derive (A.2) from (A.1): noting that $\|\overline{v}\| = \left(\int_\Omega \overline{v}^2 \, \mathrm{d}\Omega \right)^{1/2} = |\Omega|^{1/2} |\overline{v}|$,

$$\|v\| = \|v - \overline{v} + \overline{v}\| \leq \|v - \overline{v}\| + \|\overline{v}\| \qquad \Rightarrow \qquad \|v\| - |\Omega|^{1/2} |\overline{v}| \leq \|v - \overline{v}\|$$

by Minkowski's inequality (Lemma 1.10 of Robinson (2001)). Using (A.1) then leads to

$$\|v\| - |\Omega|^{1/2} |\overline{v}| \leq c_P |v|_1 \qquad \Rightarrow \qquad \|v\| \leq |\Omega|^{1/2} |\overline{v}| + c_P |v|_1 ,$$

which is (A.2) with c_P suitably redefined. □

Using this we have the following:

Lemma A.1.2. (The Hilbert space $H^1_*(\Omega)$) *$H^1_*(\Omega)$ is a Hilbert space with inner product*

$$(\omega, v)_* := (\nabla\omega, \nabla v), \tag{A.4}$$

and $H^1_*(\Omega)$–norm

$$\|\omega\|_* := |\omega|_1. \tag{A.5}$$

This norm is equivalent to the $H^1(\Omega)$–norm in that

$$\|\omega\|_* \leq \|\omega\|_1 \leq \left(c_P^2 + 1\right)^{1/2} \|\omega\|_* \tag{A.6}$$

for every $\omega \in H^1_*(\Omega)$.

Proof.

i) In this function space, (A.5) defines a norm because

$$\|\omega\|_* = 0 \qquad \Rightarrow \qquad |\omega|_1 = 0 \qquad \Rightarrow \qquad \omega(x) = c \in \mathbb{R} \qquad \text{for a.e.} \qquad x \in \Omega$$

i.e. ω is a.e. constant. But since $\overline{\omega} = 0$, we must have $\omega = 0$ a.e.

ii) The left inequality in (A.6) follows because the $H^1(\Omega)$ semi-norm is trivially bounded above by the full norm. For the inequality on the right,

$$\|\omega\|_1^2 = \|\omega\|^2 + |\omega|_1^2 \leq \left(c_P^2 + 1\right) \|\omega\|_*^2$$

by Poincaré's inequality.

□

Next, we consider the bounded linear functionals on $H^1(\Omega)$ and $H^1_*(\Omega)$. According to the Riesz Representation theorem, $\left(H^1(\Omega)\right)'$ and $H^1(\Omega)$ are isometrically isomorphic and there exists a Riesz mapping

$$R_1 : \left(H^1(\Omega)\right)' \to H^1(\Omega) \qquad \text{in which} \qquad \left(H^1(\Omega)\right)' \ni \ell_\omega \mapsto \omega \in H^1(\Omega)$$

in which case we write $R_1(\ell_\omega) = \omega$.

Remark. The Riesz Representation theorem appears in many places, including as Theorem 6.52 of Renardy and Rogers (2004), Theorem 4.9 of Robinson (2001), 3.8-1 of Kreyszig (1978), and Theorem 2 of Appendix D of Evans (1998).

In this case, $\ell_\omega \in \left(H^1(\Omega)\right)'$ is uniquely represented in $H^1(\Omega)$ by ω, in that the pairing between $\ell_\omega \in \left(H^1(\Omega)\right)'$ and any $v \in H^1(\Omega)$ can be written,

$$\ell_\omega(\nu) := \langle \ell_\omega, \nu \rangle_1 = (\nu, \omega)_1 = (\nu, \omega) + (\nabla\nu, \nabla\omega). \tag{A.7}$$

$\left(H^1(\Omega)\right)'$ is a Hilbert space with inner product

$$(\ell_\varphi, \ell_\omega)_{1'} := (\varphi, \omega)_1 \qquad \text{for} \qquad \varphi = R_1(\ell_\varphi), \omega = R_1(\ell_\omega) \in H^1(\Omega). \tag{A.8}$$

The norm of $\ell_\omega \in \left(H^1(\Omega)\right)'$ is

$$\|\ell_\omega\|_{1'} = \sup_{\nu \in H^1(\Omega)\setminus\{0\}} \frac{|\ell_\omega(\nu)|}{\|\nu\|_1} = \sup_{\nu \in H^1(\Omega)\setminus\{0\}} \frac{\left|(\nu, \omega)_1\right|}{\|\nu\|_1} = \sup_{\|\nu\|_1 = 1} \left|(\nu, \omega)_1\right|. \tag{A.9}$$

The isometry in the Riesz mapping means that

$$\|\ell_\varphi\|_{1'} = \|\varphi\|_1. \tag{A.10}$$

Remark. The easiest way to see this is to set $\varphi = \omega$ in (A.8).

The definition above is standard. We also use the following bespoke dual space.

Definition A.1.3. (The dual space $\left(H_*^1(\Omega)\right)'$) *We use $\left(H_*^1(\Omega)\right)'$ to denote the dual of the Hilbert space $H_*^1(\Omega)$. As above, $\left(H_*^1(\Omega)\right)'$ and $H_*^1(\Omega)$ are isometrically isomorphic, and we write $R_\Delta(\ell_\omega) = \omega$ for the Riesz mapping,*

$$R_\Delta : \left(H_*^1(\Omega)\right)' \to H_*^1(\Omega) \qquad \text{in which} \qquad \left(H_*^1(\Omega)\right)' \ni \ell_\omega \mapsto \omega \in H_*^1(\Omega).$$

The pairing between $\ell_\omega \in \left(H_*^1(\Omega)\right)'$ and any $v \in H_*^1(\Omega)$ can be written,

$$\ell_\omega(\nu) := \langle \ell_\omega, \nu \rangle_* = (\nu, \omega)_* = (\nabla\nu, \nabla\omega). \tag{A.11}$$

Moreover, $\left(H_*^1(\Omega)\right)'$ is a Hilbert space with inner product

$$(\ell_\varphi, \ell_\omega)_{*'} := (\varphi, \omega)_* \qquad \text{for} \qquad \varphi = R_\Delta(\ell_\varphi), \omega = R_\Delta(\ell_\omega) \in H_*^1(\Omega). \tag{A.12}$$

By the isometry in the Riesz mapping,

$$\|\ell_\varphi\|_{*'} = \|\varphi\|_*. \tag{A.13}$$

We now explore the relationship between $\left(H_*^1(\Omega)\right)'$ and $\left(H^1(\Omega)\right)'$.

Lemma A.1.4. (Equivalent duals of $H^1(\Omega)$) *The duals $\left(H_*^1(\Omega)\right)'$ and $\left(H^1(\Omega)\right)'$ are equivalent in that any $\ell \in \left(H_*^1(\Omega)\right)'$ can be extended all over $H^1(\Omega)$ to yield a member of $\left(H^1(\Omega)\right)'$, and vice versa. Moreover,*

$$\|\ell\|_{1'} = \|\ell\|_{*'} \qquad \text{for any} \qquad \ell \in \left(H^1(\Omega)\right)', \left(H_*^1(\Omega)\right)'. \tag{A.14}$$

Proof.

i) Suppose that $\ell \in \left(H^1(\Omega)\right)'$, with $\omega_1 = R_1(\ell) \in H^1(\Omega)$. Then for any $\nu \in H^1(\Omega)$,

$$\ell(\nu) = (\nu, \omega_1)_1 = (\nu, \omega_1) + (\nabla\nu, \nabla\omega_1).$$

In particular, for any $\varphi \in H_*^1(\Omega) \subset H^1(\Omega)$,

$$|\ell(\varphi)| = \left|(\varphi, \omega_1)_1\right| \le \|\omega_1\|_1 \|\varphi\|_1 \le \|\omega_1\|_1 \left(c_P^2 + 1\right)^{1/2} \|\varphi\|_*$$

by the Cauchy–Schwarz inequality in $H^1(\Omega)$ and (A.6), which means that $\ell \in \left(H_*^1(\Omega)\right)'$ too. But Lemma A.1.3 then implies the existence of a (unique) $\omega_2 = R_\Delta(\ell) \in H_*^1(\Omega)$ such that, for any $\varphi \in H_*^1(\Omega)$,

$$\ell(\varphi) = (\nu, \omega_2)_* = (\nabla\varphi, \nabla\omega_2),$$

viz. given any $\omega_1 \in H^1(\Omega)$, there is a unique $\omega_2 = R_\Delta(\ell) \in H_*^1(\Omega)$ such that

$$(\nu, \omega_1)_1 = (\nu, \omega_1) + (\nabla\nu, \nabla\omega_1) = (\nabla\nu, \nabla\omega_2) \qquad \text{for any} \qquad \nu \in H_*^1(\Omega). \tag{A.15}$$

Setting $\nu = \omega_2$ in (A.15), we find that (cf. (A.5))

$$\|\omega_2\|_*^2 = |\omega_2|_1^2 = (\omega_2, \omega_1)_1 \le \|\omega_2\|_1 \|\omega_1\|_1 \le \|\omega_1\|_1 \left(c_P^2 + 1\right)^{1/2} \|\omega_2\|_*$$

by the Cauchy–Schwarz inequality and (A.6) again. Hence, by the isometry in the two Riesz mappings above,

$$\|\ell\|_{*'} = \|\omega_2\|_* \le \left(c_P^2 + 1\right)^{1/2} \|\omega_1\|_1 = \left(c_P^2 + 1\right)^{1/2} \|\ell\|_{1'}. \tag{A.16}$$

ii) Conversely, suppose that $\ell \in \left(H^1_*(\Omega)\right)'$, with $\omega_1 = R_\Delta(\ell) \in H^1_*(\Omega)$. Then,

$$\ell(\nu) = (\nu, \omega_1)_* = (\nabla\nu, \nabla\omega_1) \qquad \text{for any} \qquad \nu \in H^1_*(\Omega).$$

However, for any $\varphi \in H^1(\Omega)$ we can define $\varphi_* := \varphi - \overline{\varphi} \in H^1_*(\Omega)$, and so

$$\ell(\varphi_*) = (\nabla\varphi_*, \nabla\omega_1) = (\nabla(\varphi_* + \overline{\varphi}), \nabla\omega_1) = (\nabla\varphi, \nabla\omega_1) = \ell(\varphi)$$

provides a sensible definition of $\ell(\varphi)$ for any $\varphi \in H^1(\Omega)$. Moreover,

$$|\ell(\varphi)| = |(\nabla\varphi, \nabla\omega_1)| \leq |\omega_1|_1 |\varphi|_1 \leq \|\omega_1\|_* \|\varphi\|_1$$

by the Cauchy–Schwarz inequality, which means that $\ell \in \left(H^1(\Omega)\right)'$ too. As in part (i) above, we infer the existence of a (unique) $\omega_2 = R_1(\ell) \in H^1(\Omega)$ such that (cf. (A.15))

$$(\nu, \omega_1)_* = (\nabla\nu, \nabla\omega_1) = (\nu, \omega_2) + (\nabla\nu, \nabla\omega_2) \qquad \text{for any} \qquad \nu \in H^1(\Omega). \tag{A.17}$$

Setting $\nu = \omega_2$ in (A.17) yields

$$\|\omega_2\|_1^2 = (\nabla\omega_2, \nabla\omega_1) \leq |\omega_2|_1 |\omega_1|_1 \leq \|\omega_2\|_1 \|\omega_1\|_*$$

or (cf. (A.16))

$$\|\ell\|_{1'} = \|\omega_2\|_1 \leq \|\omega_1\|_* = \|\ell\|_{*'}. \tag{A.18}$$

See also the first part of the proof of Theorem 7.2 of Robinson (2001). □

A.1.1 The zero Neumann Poisson equation

We use the $L^2(\Omega)$ duality pairing on the right-hand side of (2.8c). However, if $f \in L^2(\Omega)$, then $H^1(\Omega) \ni \nu \mapsto \langle f, \nu\rangle$ defines a bounded linear functional on $H^1(\Omega)$.

Lemma A.1.5. (The Poisson equation with zero Neumann BC) *Problem* ($\mathscr{P}^{\mathbf{n}}$) *in* (2.8c) *has a solution* $\varphi \in H^1(\Omega)$ *for a given* $f \in \left(H^1(\Omega)\right)'$*, if and only if,*

$$f \in \mathscr{F} \qquad \textit{viz.} \qquad f \in L^2_*(\Omega). \tag{A.19}$$

The solution is unique if $\overline{\varphi} = 0$ *viz.* $\varphi \in H^1_*(\Omega)$*.*

Remark. We write $L^2_*(\Omega) \subset \left(H^1_*(\Omega)\right)' \subset \left(H^1(\Omega)\right)'$.

Proof. The first part of Lemma A.1.5 is Ex. 6.5 of Robinson (2001). Solutions were available from `https://homepages.warwick.ac.uk/~masdh/Public/solutions.pdf` at the time of writing. We present a proof here for completeness.

i) Suppose that (2.8a) has a solution φ. Setting $\nu \equiv 1 \in H^1(\Omega)$ in (2.8c) yields

$$0 = \langle f, 1\rangle.$$

ii) Suppose that $\overline{f} = 0$, and that

$$(\nabla\varphi, \nabla\nu) = (f, \nu) \tag{A.20}$$

for every $\nu \in H^1(\Omega)$. Since $H^1_*(\Omega) \subset H^1(\Omega)$, (A.20) trivially holds for every $\nu \in H^1_*(\Omega)$ too. Conversely, suppose that (A.20) holds for every $\nu \in H^1_*(\Omega)$. Clearly $H^1(\Omega) = H^1_*(\Omega) \oplus k$, $k \in \mathbb{R}$, and so we have

$$(\nabla\varphi, \nabla(\nu + k)) = (f, \nu + k) = (f, \nu) + k(f, 1) = (f, \nu)$$

for any $\nu \in H^1_*(\Omega)$ and $k \in \mathbb{R}$, since $(f, 1) = 0$. But that is the same as saying that (A.20) holds for every $\nu \in H^1(\Omega)$. Our original weak problem is thus equivalent to (A.20) for every $\nu \in H^1_*(\Omega)$.

iii) We analyse (A.20) over the set of test functions from $H^1_*(\Omega)$. For $f \in L^2_*(\Omega)$ and $\langle f, \nu\rangle = (f, \nu)$ for every $\nu \in H^1_*(\Omega)$, we can identify f with an element of $\left(H^1_*(\Omega)\right)'$ since

$$|(f,\nu)| \leq \|f\| \, \|\nu\| \leq c_P \, \|f\| \, |\nu|_1 = c_P \, \|f\| \, \|\nu\|_*$$

by the Cauchy–Schwarz and Poincaré inequalities, and the properties of $H^1_*(\Omega)$ we established in Lemma A.1.2. The Riesz Representation theorem thus implies the existence of a unique $\omega \in H^1_*(\Omega)$ such that

$$\langle f, \nu\rangle = (\nabla\omega, \nabla\nu) \qquad \text{for every} \qquad \nu \in H^1_*(\Omega).$$

Clearly this $\omega \in H^1(\Omega)$ which implies the existence of a solution $\varphi = \omega$ to $(\mathscr{P}^{\mathbf{n}})$ in (2.8c).

iv) Observe that if φ solves $(\mathscr{P}^{\mathbf{n}})$ in (2.8c), so does $\varphi + k$ for any $k \in \mathbb{R}$ i.e. the solution to $(\mathscr{P}^{\mathbf{n}})$ above is not unique. However, if we insist that the solution be in $H^1_*(\Omega)$, then we have a unique solution (cf. problem $(\mathscr{P}^{\mathbf{n}}_*)$ in (A.22)).

Using (2.8a), we see that

$$\overline{f} = \frac{1}{|\Omega|}\int_\Omega f \, \mathrm{d}\Omega = \frac{1}{|\Omega|}\int_\Omega (-\Delta)\,\varphi \, \mathrm{d}\Omega = -\frac{1}{|\Omega|}\underbrace{\int_{\partial\Omega} \partial_n\varphi \, \mathrm{d}s}_{=0} = 0, \tag{A.21}$$

by the Divergence Theorem and the zero Neumann BC. □

The result above implies that following problem is well-posed:
$(\mathscr{P}^{\mathbf{n}}_*)$: given any $f \in \mathscr{F}$ as in (2.8b), find

$$\varphi \in H^1_*(\Omega) \qquad \text{s.t.} \qquad (\nabla\varphi, \nabla\nu) = \langle f, \nu\rangle \qquad \text{for every} \qquad \nu \in H^1_*(\Omega). \tag{A.22}$$

We could also apply $-\Delta$ to non-zero mass elements of $H^1(\Omega)$, but we restrict attention to zero mass elements so as to make sense of the inverse operator $(-\Delta_n)^{-1}$, which carries a BC and well-posedness condition with it.

Remark. $(-\Delta_n)^{-1}$ in Defn 2.1.1 is none other than the Riesz map R_Δ from Defn A.1.3, restricted to $L^2_*(\Omega)$. Notice that whereas $(-\Delta_n)^{-1}$ is defined on all of $L^2_*(\Omega)$ (because problem $(\mathscr{P}^{\mathbf{n}}_*)$ in (A.22) is well-posed), it is not surjective onto $H^1_*(\Omega)$. In particular, it is *not* true that given *any* $\varphi \in H^1_*(\Omega)$, there exists an $f \in L^2_*(\Omega)$ with $(\nabla\varphi, \nabla\nu) = (f, \nu)$ for every $\nu \in H^1_*(\Omega)$. This is because there are functionals in $\left(H^1_*(\Omega)\right)'$ that cannot be represented using the $L^2_*(\Omega)$ duality pairing. We expect this since the Riesz Representation theorem says that functionals on $H^1_*(\Omega)$ can always be represented by elements of $H^1_*(\Omega)$, but $H^1_*(\Omega)$ is a proper subset of $L^2_*(\Omega)$. In fact, $H^1_*(\Omega) \subset L^2_*(\Omega) = \left(L^2_*(\Omega)\right)' \subset \left(H^1_*(\Omega)\right)'$.

In correspondence with the idea that the Laplacian is the trace of the Hessian matrix, $\Delta = \nabla\cdot\nabla$, we define two fractional powers of $-\Delta_n$ as follows:

Definition A.1.6. (Half powers of the Neumann Laplacian: $(-\Delta_n)^{\pm 1/2}$) *Define the operators* $(-\Delta_n)^{\pm 1/2}$ *such that*

$$\left((-\Delta_n)^{1/2}\, u, (-\Delta_n)^{1/2}\, v\right) := (\nabla u, \nabla v) \qquad \textit{for any} \qquad u, v \in H^1(\Omega), \tag{A.23a}$$

and

$$\left((-\Delta_n)^{-1/2}\, \omega, (-\Delta_n)^{-1/2}\, \nu\right) := \left((-\Delta_n)^{-1}\, \omega, \nu\right) \qquad \textit{for every} \qquad \omega, \nu \in L^2_*(\Omega). \tag{A.23b}$$

For $\alpha, \beta = \pm\frac{1}{2}$,

$$(-\Delta_n)^{\alpha}\,(-\Delta_n)^{\beta} = (-\Delta_n)^{\alpha+\beta} \tag{A.23c}$$

with $(-\Delta_n)^0$ *equivalent to the identity operator.*

Remarks.

- We can think of $(-\Delta_n)^{1/2}$ as a (weak) first derivative, and $(-\Delta_n)^{-1/2}$ as a first integral. A rigorous description of the fractional powers of $-\Delta_n$ involves its spectral properties, as in Section 3.10 of Robinson (2001). The informal treatment above suffices for our purposes.

- Whereas $\nabla\varphi$ is a *vector* function in $\mathbb{R}^d$, $(-\Delta_n)^{1/2}\varphi$ is a *scalar* i.e. $\nabla\varphi \neq (-\Delta_n)^{1/2}\varphi$. However, (A.23a) implies that we can use ∇ or $(-\Delta_n)^{1/2}$ in integrals.

- We could rewrite the $H^1_*(\Omega)$ inner product in (A.4) as

$$(\omega, v)_* = (\nabla\omega, \nabla v) = \left((-\Delta_n)^{1/2}\omega, (-\Delta_n)^{1/2} v\right), \tag{A.24a}$$

  with induced norm (cf. (A.5))

$$\|\omega\|_* = |\omega|_1 = \left\|(-\Delta_n)^{1/2}\omega\right\|. \tag{A.24b}$$

- We could also re-write Poincaré's inequality in (A.1) as

$$\|v - \overline{v}\| \leq c_P \left\|(-\Delta_n)^{1/2} v\right\| \qquad \text{for any} \qquad v \in H^1(\Omega). \tag{A.25}$$

A.1.2 The $H^{-1}(\Omega)$ inner product

We discuss the $H^{-1}(\Omega)$ inner product of Defn 2.1.2 in further detail. $(\cdot,\cdot)_{-1}$ is an inner product because it is symmetric and linear, and

$$\|\omega\|^2_{-1} = 0 \qquad \Leftrightarrow \qquad (-\Delta_n)^{-1/2}\omega = 0 \qquad \Leftrightarrow \qquad \omega = 0$$

since $\overline{\omega} = 0$.

As in Appendix B of Choksi et al. (2009), and using our notation above, we relate this inner product to $\left(H^1_*(\Omega)\right)'$ as follows: suppose that for given $f, g \in L^2_*(\Omega)$,

$$-\Delta_n\omega = f \qquad \text{and} \qquad -\Delta_n\varphi = g, \qquad \text{viz.} \qquad \omega = (-\Delta_n)^{-1} f \qquad \text{and} \qquad \varphi = (-\Delta_n)^{-1} g.$$

Then, ω and φ are well-defined functions in $H^1_*(\Omega)$, and

$$\begin{aligned}(f,g)_{-1} = \left((-\Delta_n)^{-1/2} f, (-\Delta_n)^{-1/2} g\right) &= \left((-\Delta_n)^{-1/2}(-\Delta_n)\omega, (-\Delta_n)^{-1/2}(-\Delta_n)\varphi\right) \\ &= \left((-\Delta_n)^{1/2}\omega, (-\Delta_n)^{1/2}\varphi\right) = (\omega,\varphi)_* = (\ell_\omega, \ell_\varphi)_{*'}\end{aligned} \tag{A.26}$$

by (2.10) and (A.23c), where the two functionals $\ell_\omega = R_\Delta(\omega)$ and $\ell_\varphi = R_\Delta(\varphi)$ are in $\left(H^1_*(\Omega)\right)'$. For $f \in \mathscr{F}$ (cf. (2.8b)), (1.35) in Barrett and Blowey (1999a) states that

$$C\|f\|_{1'} \leq \|f\|_{-1} \leq C\|f\|_{1'}, \tag{A.27}$$

i.e. the standard dual norm on $\left(H^1(\Omega)\right)'$ is equivalent to $\|\cdot\|_{-1}$. For further intuition about this, setting $g = f$ in (A.26), and using Lemma A.1.4 yields

$$\|f\|_{-1} = \|f\|_{*'} = \|f\|_{1'},$$

where the second and third norms are understood to refer to the functionals in $\left(H^1_*(\Omega)\right)'$ uniquely associated to f by the Riesz map R_Δ of Lemma A.1.3. This equivalence of the $H^{-1}(\Omega)$ and dual norms will prove useful. We summarise some properties of this inner product and its norm.

Lemma A.1.7. (Properties of the $H^{-1}(\Omega)$ inner product and norm)

i) If $u \in L^2_*(\Omega)$, then (cf. (2.6) of Blowey and Elliott (1991))

$$\|u\|_{-1} \leq c_P \|u\| . \tag{A.28a}$$

If in addition, $u \in H^1_*(\Omega)$, then $\|u\| \leq c_P \|u\|_*$ and

$$\|u\|_{-1} \leq c_P^2 \|u\|_* \, (= c_P^2 \, |u|_1). \tag{A.28b}$$

ii) If $u \in H^1_*(\Omega)$, we have the Sobolev interpolation inequality,

$$\|u\|^2 \leq \|u\|_{-1} \|u\|_* \, (= \|u\|_{-1} \, |u|_1). \tag{A.29}$$

Proof.

i) For $u \in L^2_*(\Omega)$,

$$\|u\|_{-1} = \left\|(-\Delta_n)^{-1/2} u\right\| \leq c_P \left\|(-\Delta_n)^{1/2} \left((-\Delta_n)^{-1/2} u\right)\right\| = c_P \|u\| .$$

by Poincaré's inequality, since $(-\Delta_n)^{-1/2} u \in H^1_*(\Omega)$. If $u \in H^1_*(\Omega)$, then Poincaré's inequality gives

$$\|u\| \leq c_P \left\|(-\Delta_n)^{1/2} u\right\| .$$

ii) If $u \in H^1_*(\Omega)$, then

$$\|u\|^2 = \left((-\Delta_n)^{1/2} (-\Delta_n)^{-1/2} u, u\right) = \left((-\Delta_n)^{-1/2} u, (-\Delta_n)^{1/2} u\right) \leq \underbrace{\left\|(-\Delta_n)^{-1/2} u\right\|}_{= \|u\|_{-1}} \underbrace{\left\|(-\Delta_n)^{1/2} u\right\|}_{= \|u\|_*}$$

by the Cauchy–Schwarz inequality, and noting that $(-\Delta_n)^{1/2}$ is symmetric in the $L^2(\Omega)$ inner product.

□

As a consequence of (A.25), (2.11) and (A.28),

$$\left\|(-\Delta_n)^{-1} \nu\right\| \leq c_P \left\|(-\Delta_n)^{1/2} (-\Delta_n)^{-1} \nu\right\| = c_P \|\nu\|_{-1} \leq c_P^2 \|\nu\| , \tag{A.30a}$$

for any $\nu \in L^2_*(\Omega)$. Likewise, if $\nu \in H^1_*(\Omega) \subset L^2_*(\Omega)$, then

$$\left\|(-\Delta_n)^{-1} \nu\right\| \leq c_P^2 \|\nu\| \leq c_P^3 \, |\nu|_1 , \tag{A.30b}$$

since $\overline{(-\Delta_n)^{-1} \nu} = 0$. For $p > 2$, we define the $-p$–norm (cf. (2.11))

$$\|\omega\|_{0,-p} := \left\|(-\Delta_n)^{-1/2} \omega\right\|_{0,p} \qquad \text{for} \qquad \omega \in L^p_*(\Omega) \subset L^2_*(\Omega) . \tag{A.31}$$

There is no inner product this time because $L^p(\Omega)$ is only a Hilbert space for $p = 2$. Moreover, since $L^q(\Omega) \hookrightarrow L^p(\Omega)$ for $1 \leq p \leq q \leq \infty$ (see the next section for an explanation of this notation) for $|\Omega| < \infty$ (cf. Theorem 2.14 of Adams and Fournier (2003)), $\|\omega\|_{-1} < \infty$ does not guarantee that $\|\omega\|_{0,-p} < \infty$. However, it is true that $\|\omega\|_{0,-p} = 0 \Leftrightarrow \omega = 0$ a.e.. We can also use the Poincaré inequality (A.3) to find that (cf. (A.30)), for $p > 2$ and any $\nu \in L^p_*(\Omega)$,

$$\left\|(-\Delta_n)^{-1} \nu\right\|_{0,p} \leq c_P \left\|(-\Delta_n)^{-1/2} \nu\right\|_{0,p} = c_P \|\nu\|_{0,-p} \leq c_P^2 \|\nu\|_{0,p} . \tag{A.32a}$$

Likewise, if $\nu \in W^{1,p}_*(\Omega) \subset L^p_*(\Omega)$, then

$$\left\|(-\Delta_n)^{-1} \nu\right\|_{0,p} \leq c_P^2 \|\nu\|_{0,p} \leq c_P^3 \, |\nu|_{0,p} . \tag{A.32b}$$

A.1.3 Imbeddings

The Banach space X is *continuously* imbedded in Y (written $X \hookrightarrow Y$) if $X \subset Y$ and there is a constant C, independent of u, with (cf. Defn (7.15) of Renardy and Rogers (2004))

$$\|u\|_Y \leq C \|u\|_X \qquad \text{for every} \qquad u \in X. \tag{A.33}$$

X is *compactly* imbedded in Y (written $X \overset{c}{\hookrightarrow} Y$) if $X \hookrightarrow Y$ and every bounded sequence in X has a subsequence that converges (strongly) in Y. See Defn (7.25) of Renardy and Rogers (2004) or the first definition of Section 5.7 of Evans (1998); see also Paragraph 1.25 of Adams and Fournier (2003). We list the imbeddings we will use in the following lemma.

Lemma A.1.8. (Imbeddings) *Suppose that Ω is bounded and is either a 1D interval, or has a Lipschitz boundary satisfying a cone condition.*

i) Sobolev imbeddings*: see Case A in Part I and II of the theorem in Paragraph 4.12 of Adams and Fournier (2003):*

1. *For $d = 1$: $H^1(\Omega) \hookrightarrow L^\infty(\Omega)$, $H^1(\Omega) \hookrightarrow C^{0,\lambda}(\overline{\Omega})$ and $H^2(\Omega) \hookrightarrow C^{1,\lambda}(\overline{\Omega})$ with $0 < \lambda \leq \frac{1}{2}$.*
   Remark. Theorem 2 of Section 5.6 of Evans (1998) gives the result for $d = 1$ and $\partial\Omega$ of class C^1.
2. *For $d = 2, 3$: $H^2(\Omega) \hookrightarrow L^\infty(\Omega)$, $H^2(\Omega) \hookrightarrow C^{0,\lambda}(\overline{\Omega})$ and $W^{2,p}(\Omega) \hookrightarrow C^{1,\lambda}(\overline{\Omega})$ if $p \geq d + 1$ for appropriate $0 < \lambda < \lambda'$. As $p \to \infty$, $\lambda' \to 1$.*

We thus identify any function in $W^{m,p}(\Omega)$ with its continuous version in $C^0(\overline{\Omega})$, or more specifically, the equivalence class associated with each such function includes one that is continuous. In any spatial dimension, $C^{1,\lambda}(\overline{\Omega}) \hookrightarrow C^1(\overline{\Omega}) \hookrightarrow C^0(\overline{\Omega}) \hookrightarrow L^\infty(\Omega)$ for any $\lambda \geq 0$. Moreover,

$$H^2(\Omega) \hookrightarrow L^p(\Omega) \qquad \textit{for every} \qquad 1 \leq p \leq \infty \qquad \textit{and} \qquad d = 1, 2, 3. \tag{A.34}$$

Remark. The cone condition is defined in Paragraph 4.6 of Adams and Fournier (2003); according to Paragraph 4.11, the Lipschitz condition implies the cone condition. Theorem 1.9 of Braess (2001) and especially Fig. 6 illustrate the practical implications of the cone condition.

Remark. In Paragraph 4.12 of Adams and Fournier (2003),

- $H^1(\Omega) = W^{1,2}(\Omega) = W^{j+m,p}(\Omega) \hookrightarrow C^{j,\lambda}(\overline{\Omega})$. For 1D, $n = 1$ and we set $j = 0$, $m = 1$, $p = 2$ whence $mp = 2 > n = 1 > 0$, and we have $0 < \lambda \leq \frac{1}{2}$.
- $H^2(\Omega) = W^{2,2}(\Omega) = W^{j+m,p}(\Omega) \hookrightarrow C^{j,\lambda}(\overline{\Omega})$. In 1D, $n = 1$ and we set $j = 1$, $m = 1$, $p = 2$ whence $mp = 2 > n = 1 > 0$, and we have $0 < \lambda \leq \frac{1}{2}$. In 2D and 3D, $n = 2$ or 3, we set $j = 0$, $m = 2$, $p = 2$ so $mp = 4 > 2, 3 = n > 0$. For $n = 2$, $0 < \lambda \leq m - \frac{n}{p} = 1$ and for $n = 3$, $0 < \lambda \leq m - \frac{n}{p} = \frac{1}{2}$.
- 2D: $W^{2,p}(\Omega) \hookrightarrow C^{1,\lambda}(\overline{\Omega})$ if $p \geq 3$, in which case $0 < \lambda \leq \lambda'$, $\lambda' = 1 - \frac{2}{p} \geq \frac{1}{3}$. We set $j = 1$ and $m = 1$ so $j + m = 2$. In 2D, $n = 2$ and $mp > 2 = n$ if $p \geq 3$. As $p \to \infty$, $\lambda' \to 1$ and $0 < \lambda \leq 1$.
- 3D: $W^{2,p}(\Omega) \hookrightarrow C^{1,\lambda}(\overline{\Omega})$ if $p \geq 4$, in which case $0 < \lambda \leq \lambda'$, $\lambda' = 1 - \frac{3}{p} \geq \frac{1}{4}$. We set $j = 1$ and $m = 1$ so $j + m = 2$. In 3D, $n = 3$ and $mp > 3 = n$ if $p \geq 4$. As in 2D, as $p \to \infty$, $\lambda' \to 1$ and $0 < \lambda \leq 1$.

Remark. For (A.34), use Case A in Part I of the theorem in Paragraph 4.12 of Adams and Fournier (2003) as follows: $H^2(\Omega) = W^{2,2}(\Omega)$ so $m = p = 2$, but notice also Remark 3 in Paragraph 4.13 for Ω of finite volume.

ii) Compact imbeddings*: the Rellich Selection or Rellich-Kondrachov Theorem says that*

$$H^2(\Omega) \overset{c}{\hookrightarrow} H^1(\Omega) \overset{c}{\hookrightarrow} L^2(\Omega) = \left(L^2(\Omega)\right)' \hookrightarrow \left(H^1(\Omega)\right)'. \tag{A.35}$$

Remark. Notice that the '=' in the above is by identification. See also Section 5.8 of Robinson (2001), and the Rellich-Kondrachov Theorem in Paragraph 6.3 of Adams and Fournier (2003) and Theorem 1 of Section 5.7 of Evans (1998).

For any bounded sequence $\left(\eta^{(N)}\right)$ *in* $H^1(\Omega)$ *there exists an* $\eta \in L^2(\Omega)$ *and a subsequence* $\left(\eta^{(N_j)}\right)$ *of* $\left(\eta^{(N)}\right)$ *that converges strongly in* $L^2(\Omega)$ *to* η*, viz.*

$$\left\|\eta^{(N_j)} - \eta\right\| \to 0, \qquad \left\|\eta^{(N_j)}\right\| \to \|\eta\|, \qquad \text{as } N_j \to \infty. \tag{A.36}$$

iii) Suppose X *is any real Banach space and* $u \in H^1(0,T;X)$*. Then*

$$H^1(0,T;X) \hookrightarrow C([0,T];X) \qquad \text{and} \qquad \|u\|_{C([0,T];X)} \leq C(T)\|u\|_{H^1(0,T;X)}, \tag{A.37a}$$

and also

$$u(t) = u(s) + \int_s^t u'(\tau)\,\mathrm{d}\tau \qquad \text{for every} \qquad 0 \leq s \leq t \leq T. \tag{A.37b}$$

See Theorem 2 of Section 5.9 of Evans (1998) or Proposition 7.1 of Robinson (2001).

iv) The Aubin–Lions–Simon Lemma *(cf. Simon (1986)). In the context of* (A.35)*,*

$$W := \left\{\varphi \in L^2\left(0,T;H^1(\Omega)\right); \partial_t\varphi \in L^2\left(0,T;\left(H^1(\Omega)\right)'\right)\right\} \overset{c}{\hookrightarrow} L^2\left(0,T;L^2(\Omega)\right). \tag{A.38}$$

Remark. As in Blowey and Elliott (1991), we use $L^2(\Omega_T)$ to denote this last function space. Any sequence (φ_i) in W, has a (strongly) convergent subsequence in $L^2(\Omega_T)$.

v) Dense imbedding: $C_c^\infty\left(\overline{\Omega}\right)$ *dense in* $L^2(\Omega)$ *(cf. Corollary 1.14 of Robinson (2001)) and, likewise,* $H^1(\Omega)$ *is dense in* $L^2(\Omega)$*, since* $C_c^\infty\left(\overline{\Omega}\right) \subset H^1(\Omega) \subset L^2(\Omega)$*. Hence, for any* $u \in L^2(\Omega)$ *there is a sequence* $\left(u^{(n)}\right) \subset H^1(\Omega)$ *such that* $u^{(n)} \to u$ *in* $L^2(\Omega)$*, or* $\lim_{n\to\infty}\left\|u^{(n)} - u\right\| \to 0$*. If* $Lu - f \in L^2(\Omega)$ *and* $(Lu - f, v) = 0$ *for every* $v \in H^1(\Omega)$*, then* $(Lu - f, v) = 0$ *for every* $v \in L^2(\Omega)$ *too.*

Proof. Given any $v \in L^2(\Omega)$, let $\left(v^{(n)}\right) \in H^1(\Omega)$ be a sequence converging to v in $L^2(\Omega)$. Then $\left(Lu - f, v^{(n)}\right) = 0$ for every $v^{(n)}$ and so

$$(Lu - f, v) = \left(Lu - f, v - v^{(n)}\right) \leq \underbrace{\|Lu - f\|}_{<\infty}\left\|v - v^{(n)}\right\| \to 0 \qquad \text{as } n \to \infty, \tag{A.39}$$

by the Cauchy–Schwarz inequality. Hence $(Lu - f, v) = 0$ for any $v \in L^2(\Omega)$. We use density arguments of this sort repeatedly. □

A.1.4 Elliptic regularity, BCs

We now quote a well-known result from elliptic regularity theory, which gives conditions under which weak solutions of the Poisson equation in $H^1(\Omega)$ have higher regularity viz. are in $H^2(\Omega)$.

Lemma A.1.9. (Elliptic regularity) *Suppose that $\varphi \in H^1(\Omega)$ is the (unique) solution of*

$$(\nabla u, \nabla v) + (\lambda u, v) = (f, v) \qquad \text{for every} \qquad v \in H^1(\Omega), \tag{A.40}$$

for given $f \in L^2(\Omega)$ and any $\lambda \geq 0$. If Ω is a 1D interval, or $\partial\Omega$ is of class C^2 or Ω is a convex polygonal ($d = 2$) or polyhedral domain ($d = 3$), then $\varphi \in H^2(\Omega)$ and,

$$\|\varphi\|_2 \leq C \|f\|. \tag{A.41}$$

In particular, $\|-\Delta\varphi\|$ is equivalent to the $H^2(\Omega)$ norm in that

$$\|-\Delta\varphi\| \leq \|\varphi\|_2 \leq C \|-\Delta\varphi\|, \tag{A.42}$$

for $C = C(d, \Omega)$, and

$$|\varphi|_2 \leq C \|(-\Delta)\varphi\|. \tag{A.43}$$

Moreover, if $\lambda = 0$ and $f \in L^p(\Omega)$, then

$$\|\varphi\|_{2,p} \leq C \|-\Delta\varphi\|_{0,p}. \tag{A.44}$$

Remark. We recover (2.8c) by setting $\lambda = 0$ in (A.40); in this case, $\varphi \in H^2_*(\Omega)$.

Elliptic regularity is a vast subject; finding an exact statement of the result above was not possible, and so we inferred it from Süli (2018) and Chapter 4 of Grisvard (1985) (esp. (4,1,2) which is established in Section 4.3.1 for $p = 2$ and Section 4.3.2 for $p \neq 2$). See also Theorem 6.16 of Robinson (2001), Theorem 4 of Section 6.3 of Evans (1998) and Chapter 8 of Gilbarg and Trudinger (2001). See also Section 2.2 of Blowey and Elliott (1991).

Lemma A.1.10. (Zero Neumann BCs) *For any $u \in H^2(\Omega)$,*

$$(\nabla u, \nabla v) = (-\Delta u, v) \qquad \text{for every } v \in H^1(\Omega) \qquad \Leftrightarrow \qquad \partial_n u|_{\partial\Omega} = 0. \tag{A.45}$$

Suppose that $u \in H^1(\Omega)$ is the (unique) solution of (A.40) *and that Ω satisfies the conditions of Lemma A.1.9. Then*

$$\partial_n u|_{\partial\Omega} = 0 \qquad \text{in the sense of trace.} \tag{A.46}$$

Moreover, $u \in H^2(\Omega)$ is a strong solution of the problem in that

$$(-\Delta u + \lambda u, v) = (f, v) \qquad \text{for every} \qquad v \in L^2(\Omega) \tag{A.47}$$

and in fact

$$-\Delta u + \lambda u = f \qquad \text{a.e. in } \Omega. \tag{A.48}$$

Proof.

i) For $u \in H^2(\Omega)$ and any $v \in H^1(\Omega)$, Green's formula (cf. (1.2.5) of Ciarlet (1978) and Lemma 6.4 of Seregin (2013)) says that

$$(-\Delta u, v) = (\nabla u, \nabla v) + \int_{\partial\Omega} v\, \partial_n u \, \mathrm{d}S, \tag{A.49}$$

where the normal derivative ∂_n is understood in the sense of trace i.e.

$$\partial_n u = \nabla u \cdot \hat{\boldsymbol{n}} = \sum_{i=1}^{d} \mathrm{tr}\,(\partial_i u)\, n_i.$$

Hence, if $(-\Delta u, v) = (\nabla u, \nabla v)$ for every $v \in H^1(\Omega)$, then $\int_{\partial\Omega} v \partial_n u \, \mathrm{d}S = 0$ and so $\partial_n u|_{\partial\Omega} = 0$. Conversely, if $\partial_n u|_{\partial\Omega} = 0$, then $(-\Delta u, v) = (\nabla u, \nabla v)$ for every $v \in H^1(\Omega)$.

ii) Suppose that u is the solution of (A.40) and that Ω satisfies the conditions of Lemma A.1.9. According to that result, $u \in H^2(\Omega)$, and if we substitute (A.40) into (A.49) and rearrange, we find that

$$(-\Delta u + \lambda u - f, v) = \int_{\partial\Omega} v\, \partial_n u \, \mathrm{d}S \qquad \text{for every} \qquad v \in H^1(\Omega). \tag{A.50}$$

This statement is true for any $v \in C_c^\infty(\Omega)$ and so

$$(-\Delta u + \lambda u - f, v) = 0 \quad \text{for every} \quad v \in C_c^\infty(\Omega) \quad \Rightarrow \quad -\Delta u + \lambda u - f = 0 \quad \text{a.e. in } \Omega.$$

If we substitute this back into the left side of (A.50), we see that

$$\int_{\partial\Omega} v\, \partial_n u \, \mathrm{d}S = 0 \quad \text{for every} \quad v \in H^1(\Omega) \quad \Rightarrow \quad \partial_n u = 0 \quad \text{a.e. in } \partial\Omega.$$

iii) From the BC above, it is clear that u is a strong solution of (A.40), and that

$$(-\Delta u + \lambda u, v) = (f, v) \qquad \text{for every} \qquad v \in H^1(\Omega).$$

However, since $H^1(\Omega)$ is dense in $L^2(\Omega)$, we can pick any $v \in L^2(\Omega)$ if we argue as in (A.39). The result is (A.47).

□

We now consider the differential operator $-\Delta + I$, whose eigenfunctions form an orthogonal basis of $H^1(\Omega)$ and an orthonormal basis of $L^2(\Omega)$ (cf. (2.19) of Blowey and Elliott (1991)).

Lemma A.1.11. (Properties of $\mathscr{P} := (-\Delta + I)$) *The operator*

$$\mathscr{P} : H^1(\Omega) \to L^2(\Omega) \qquad \text{such that} \qquad (\mathscr{P}\varphi, \nu) = (\varphi, \nu)_1 \qquad \forall \qquad \nu \in H^1(\Omega), \tag{A.51}$$

is invertible and surjective i.e. $\mathcal{R}(\mathscr{P}) = L^2(\Omega)$. *Its inverse,*

$$\mathscr{P}^{-1} : L^2(\Omega) \to H^1(\Omega) \overset{c}{\hookrightarrow} L^2(\Omega), \tag{A.52}$$

is compact, linear and symmetric.

Remark. From the definition in Appendix D.5 of Evans (1998): An operator $K : X \to Y$ is compact if every bounded sequence $(u_k)_{k=1}^\infty \subset X$ has a sub-sequence $\left(u_{k_j}\right)_{j=1}^\infty$ for which $\left(Ku_{k_j}\right)_{j=1}^\infty$ converges in Y.

$\mathscr{P}$ *and* $\mathscr{P}^{-1}$ *have the same eigenfunctions* $\{e_k\}_{k=1}^\infty$ *for which* $\mathscr{P}e_k = \lambda_k e_k$ *and* $\mathscr{P}^{-1}e_k = (1/\lambda_k)\, e_k$, *where*

$$\mathscr{P}e_k = \lambda_k e_k \qquad \Leftrightarrow \qquad (\nabla e_k, \nabla \nu) + (e_k, \nu) = (\lambda_k e_k, \nu) \qquad \textit{for every} \qquad \nu \in H^1(\Omega). \tag{A.53}$$

The $\{e_k\}_{k=1}^\infty$ *form an orthonormal basis of* $L^2(\Omega)$ *and an orthogonal basis of* $H^1(\Omega)$. *The first eigenfunction is the constant function*

$$e_1 = \frac{1}{|\Omega|^{1/2}} \qquad \textit{corresponding to the eigenvalue} \qquad \lambda_1 = 1 > 0. \tag{A.54}$$

Every e_k, *other than the first one, has zero mass viz.*

$$\overline{e_k} = \begin{cases} \dfrac{1}{|\Omega|^{1/2}} & k = 1 \\ 0 & k > 1. \end{cases} \tag{A.55}$$

The eigenvalues $\{\lambda_k\}_{k=1}^{\infty}$ *of* $\mathscr{P}$ *are such that*

$$0 < 1 = \lambda_1 < \lambda_2 \leq \lambda_3 \leq \dots \qquad \text{and} \qquad \lambda_k \to \infty \qquad \text{as } k \to \infty. \tag{A.56a}$$

Likewise, for $\mathscr{P}^{-1}$*, the eigenvalues* $\{1/\lambda_k\}_{k=1}^{\infty} = \left\{\widetilde{\lambda_k}\right\}_{k=1}^{\infty}$ *are such that*

$$1 = \lambda_1 = \widetilde{\lambda_1} > \widetilde{\lambda_2} \geq \widetilde{\lambda_3} \geq \dots \qquad \text{and} \qquad \widetilde{\lambda_k} \to 0 \qquad \text{as } k \to \infty. \tag{A.56b}$$

The principle eigenvalue of both operators, $\lambda_1 = 1$*, is simple.*

Under the conditions of Lemma A.1.9, each $e_k \in H^2(\Omega)$*, and*

$$(-\Delta e_k, \nu) = (\nabla e_k, \nabla \nu) \qquad \text{for every} \qquad \nu \in H^1(\Omega) \qquad \text{viz.} \qquad \partial_n e_k|_{\partial\Omega} = 0 \tag{A.57}$$

(in the sense of trace). Moreover, by (A.42)*,* (A.43)*, with* $C = C(d, \Omega)$*, each*

$$|e_k|_2 \leq \|e_k\|_2 \leq C \|(-\Delta) e_k\|. \tag{A.58}$$

Proof.

i) $\mathscr{P}$ is invertible: clearly if $\varphi = 0$, $\mathscr{P}\varphi = 0$. For the converse, suppose that $\mathscr{P}\varphi = 0$ i.e. $(\varphi, \nu)_1 = 0$ for every $\nu \in H^1(\Omega)$. In particular, $(\varphi, \varphi)_1 = \|\varphi\|_1^2 = 0$ i.e. $\varphi = 0$. Hence, $\mathscr{P}$ is invertible and injective, and zero is not one of its eigenvalues.

ii) The range of $\mathscr{P}$ is all of $L^2(\Omega)$: given any $\omega \in L^2(\Omega)$, $H^1(\Omega) \ni \nu \mapsto (\omega, \nu)$ defines a bounded linear functional in $\left(H^1(\Omega)\right)'$. By the Riesz Representation theorem, this functional has a (unique) representative $\varphi \in H^1(\Omega)$, such that $(\omega, \nu) = (\varphi, \nu)_1$ for every $\nu \in H^1(\Omega)$. But then $\omega = \mathscr{P}\varphi$.

iii) The linearity of $\mathscr{P}^{-1}$ follows from that of $\mathscr{P}$; compactness follows from the compact embedding of $H^1(\Omega)$ into $L^2(\Omega)$ by (A.35).

iv) $\mathscr{P}$ is symmetric: for any $v, w \in H^1(\Omega)$,

$$(\mathscr{P}v, w) = (v, w)_1 = (w, v)_1 = (\mathscr{P}w, v) = (v, \mathscr{P}w).$$

Now define $\widetilde{v} := \mathscr{P}v$ so that $v = \mathscr{P}^{-1}\widetilde{v}$ and $\widetilde{w} := \mathscr{P}w$ i.e. $w = \mathscr{P}^{-1}\widetilde{w}$. By the symmetry of $\mathscr{P}$,

$$(\mathscr{P}v, w) = (v, \mathscr{P}w) \qquad \Rightarrow \qquad \left(\widetilde{v}, \mathscr{P}^{-1}\widetilde{w}\right) = \left(\mathscr{P}^{-1}\widetilde{v}, \widetilde{w}\right)$$

i.e. $\mathscr{P}^{-1}$ is symmetric, too.

v) $L^2(\Omega)$ is a separable Hilbert space and so, by the Hilbert-Schmidt theorem, (cf. Theorem 7 of Appendix E of Evans (1998) or Theorem 3.18 of Robinson (2001)) there exists a countable orthonormal basis of $L^2(\Omega)$, consisting of eigenfunctions of $\mathscr{P}^{-1}$. We denote this set $\{e_k\}_{k=1}^{\infty}$.

vi) $\mathscr{P}$ and $\mathscr{P}^{-1}$ have the same eigenfunctions: suppose that $\mathscr{P}^{-1}e_k = \widetilde{\lambda_k}e_k$ i.e.

$$\left(\mathscr{P}^{-1}e_k, \nu\right) = \left(\widetilde{\lambda_k}e_k, \nu\right) \qquad \text{for every} \qquad \nu \in H^1(\Omega), \tag{A.59}$$

which immediately yields (A.53). By linearity and invertibility,

$$e_k = \mathscr{P}\left(\widetilde{\lambda_k}e_k\right) \qquad \Rightarrow \qquad \mathscr{P}e_k = \frac{1}{\widetilde{\lambda_k}}e_k$$

and conversely. We denote the eigenvalues of $\mathscr{P}$ by $\{\lambda_k\}_{k=1}^{\infty}$ and those of $\mathscr{P}^{-1}$ by $\left\{\widetilde{\lambda}_k\right\}_{k=1}^{\infty}$. By the above, $\widetilde{\lambda}_k = 1/\lambda_k$ for each k. The constant function $1/|\Omega|^{1/2}$ is an eigenfunction of $\mathscr{P}$ corresponding to the eigenvalue $\lambda_1 = \widetilde{\lambda}_1 = 1$ because (cf. (A.59))

$$\left(\mathscr{P}\left(\frac{1}{|\Omega|^{1/2}}\right), \nu\right) = \underbrace{\left(\nabla\left(\frac{1}{|\Omega|^{1/2}}\right), \nabla\nu\right)}_{:=0} + \left(\frac{1}{|\Omega|^{1/2}}, \nu\right) = \left(\lambda \frac{1}{|\Omega|^{1/2}}, \nu\right)$$

for every $\nu \in H^1(\Omega)$, if $\lambda = 1$. Hence, we *define* the first eigenfunction in $\{e_k\}_{k=1}^{\infty}$ as in (A.54). Clearly, $\|e_1\| = 1$.

vii) For $\lambda_k \neq 1$, each eigenfunction e_k satisfies (A.53). In particular, for $\nu = 1$, we find that

$$(e_k, 1) = (\lambda_k e_k, 1) \qquad \Rightarrow \qquad (1 - \lambda_k)(e_k, 1) = 0,$$

and so for $\lambda_k \neq 1$, $(e_k, 1) = 0$ viz. $\overline{e_k} = 0$. For $\lambda_k = 1$, (A.53) reduces to the requirement that $(\nabla e_1, \nabla\nu) = 0$ for every $\nu \in H^1(\Omega)$, which is not well-posed. However, there is a unique eigenfunction e_1 having $\|e_1\| = 1$, corresponding to the eigenvalue $\lambda_1 = 1$, and we arrive at (A.55).

viii) $\mathscr{P}$, $-\Delta$ and $(-\Delta_n)^{-1}$ share eigenfunctions. If $\mathscr{P}e_k = (-\Delta + I)e_k = \lambda_k e_k$, then for $k = 1$, we *define*

$$-\Delta e_1 = 0 \times e_1 \qquad \text{but} \qquad (-\Delta_n)^{-1} 0 = 0, \tag{A.60a}$$

since $\lambda_k = 1$, and for $k \geq 2$,

$$-\Delta e_k = (\lambda_k - 1) e_k \qquad \Rightarrow \qquad (-\Delta_n)^{-1} e_k = \frac{1}{\lambda_k - 1} e_k. \tag{A.60b}$$

If λ_k is an eigenvalue of $\mathscr{P}$ for eigenfunction e_k, $-\Delta$ has eigenvalue $\lambda_k - 1$ (for the same eigenfunction).

ix) Theorem 2 of Section 6.5 of Evans (1998) gives (A.56a) for $-\Delta$ with Dirichlet BCs; similar reasoning can be applied to the zero Neumann BC case. See also Section 8.12 of Gilbarg and Trudinger (2001). (A.56b) follows by (A.60). Theorem 8.3-1 of Kreyszig (1978) says that the set $\left\{\widetilde{\lambda_k}\right\}_{k=1}^{\infty}$ is countable, and that the only possible accumulation point is $\lambda = 0$. Theorem 8.38 of Gilbarg and Trudinger (2001) shows that the minimum eigenvalue of $\mathscr{P}$ (i.e. $\lambda_1 = 1$) is simple.

x) Finally, any basis of $L^2(\Omega)$ also spans $H^1(\Omega)$, since $H^1(\Omega) \subset L^2(\Omega)$. But since each e_k is an eigenfunction of $\mathscr{P}^{-1}$, each $e_k \in H^1(\Omega)$ too, since it is a weak solution of the Poisson equation. The eigenfunctions $\{e_k\}_{k=1}^{\infty}$ are orthonormal in $L^2(\Omega)$, which means that $(e_j, e_k) = \delta_{jk}$. However, as in (A.59) and Section 7.3 of Robinson (2001), $(e_j, e_k)_1 = (\mathscr{P}e_j, e_k) = \lambda_j (e_j, e_k) = \lambda_j \delta_{jk}$, which means that the $\{e_k\}_{k=1}^{\infty}$ form an orthogonal basis of $H^1(\Omega)$.

xi) Suppose that the conditions of Lemma A.1.9 hold. Then (A.57) follows by Lemma A.1.10 if we set $\lambda = 1$ in (A.40).

□

For any $\varphi \in H^1(\Omega)$, we have the eigenfunction expansion

$$\varphi = \sum_{j=1}^{\infty} (\varphi, e_j)\, e_j. \tag{A.61}$$

Let V^N denote the N-dimensional span $\{e_j\}_{j=1}^N \subset H^1(\Omega)$, and V_*^N the zero mass subspace of V^N. $P^N : H^1(\Omega) \to V^N$ is the L^2-projection of a function onto V^N in which (cf. (2.22) of Blowey and Elliott (1991)),

$$P^N\varphi = \sum_{j=1}^{N} (\varphi, e_j)\, e_j \qquad \text{with} \qquad \left(P^N\varphi - \varphi, e_k\right) = 0, \qquad k = 1, \ldots, N. \tag{A.62}$$

According to Lemma 7.5 of Robinson (2001), for any $\varphi \in H^1(\Omega)$,

$$\left\|P^N\varphi\right\| \le \|\varphi\| \qquad \text{and} \qquad P^N\varphi \to \varphi \qquad \text{in } L^2(\Omega) \qquad \text{viz.} \qquad \lim_{N\to\infty} \left\|P^N\varphi - \varphi\right\| \to 0, \tag{A.63a}$$

i.e. $\lim_{N\to\infty} \left\|P^N\varphi\right\| = \|\varphi\|$, and likewise,

$$\left\|P^N\varphi\right\|_1 \le \|\varphi\|_1 \qquad \text{and} \qquad P^N\varphi \to \varphi \qquad \text{in } H^1(\Omega) \qquad \text{viz.} \qquad \lim_{N\to\infty} \left\|P^N\varphi - \varphi\right\|_1 \to 0. \tag{A.63b}$$

Remark. For a general proof of the second part of the previous result, we show that $\|x_N - y\| \to 0$ as $N \to \infty$ implies that $\|x_N\| \to \|y\|$. Clearly,

$$\|x_N\| = \|x_N - y + y\| \le \|x_N - y\| + \|y\|,$$

whence

$$\|x_N\| - \|y\| \le \|x_N - y\| \to 0 \quad \text{as } N \to \infty.$$

But similarly,

$$\|y\| = \|y - x_N + x_N\| \le \|x_N - y\| + \|x_N\|,$$

which means that

$$|\|y\| - \|x_N\|| \le \|x_N - y\| \to 0 \quad \text{as } N \to \infty.$$

Hence $\|x_N\| \to \|y\|$ as $N \to \infty$. This result holds for any norm.

Finally, for any $\varphi \in H^1(\Omega)$ and $N \ge 1$ (cf. just after (2.25) in Blowey and Elliott (1991)),

$$\left\|P^N\varphi\right\| \le \|\varphi\| \qquad \text{and} \qquad \left|P^N\varphi\right|_1 \le |\varphi|_1. \tag{A.64}$$

Remark. The first part above is taken directly from Lemma 7.5 of Robinson (2001). For the second part, define the projection orthogonal to P^N as $Q^N = I - P^N$ (cf. Section 7.3 of Robinson (2001)), where

$$Q^N\varphi = \sum_{j=N+1}^{\infty} (\varphi, e_j)\, e_j. \tag{A.65}$$

Clearly, $P^N\varphi \perp Q^N\varphi$ in that $\left(P^N\varphi, Q^N\varphi\right) = 0$. But for any $\varphi \in H^1(\Omega)$, we also have that $\left(P^N\varphi, Q^N\varphi\right)_1 = 0$ since $\{e_k\}_{k=1}^{\infty}$ is orthogonal in $H^1(\Omega)$. We conclude that

$$\left(\nabla Q^N\varphi, \nabla P^N\varphi\right) = 0 \qquad \text{for any} \qquad \varphi \in H^1(\Omega).$$

Hence,

$$\begin{aligned} |\varphi|_1^2 &= \left(\nabla\left(\varphi - P^N\varphi + P^N\varphi\right), \nabla\left(\varphi - P^N\varphi + P^N\varphi\right)\right) \\ &= \left|Q^N\varphi\right|_1^2 + 2\underbrace{\left(\nabla Q^N\varphi, \nabla P^N\varphi\right)}_{=0} + \left|P^N\varphi\right|_1^2 = \left|Q^N\varphi\right|_1^2 + \left|P^N\varphi\right|_1^2, \end{aligned}$$

Remark. When we approximate functions $\varphi \in H^1(\Omega)$ using $\{e_k\}_{k=1}^{\infty}$, the first term encodes the mass, $\overline{\varphi}$.

A.1.5 Miscellaneous technical results

We close this section with statements of some of the technical results we will use repeatedly. We start with a special case of Lemma 1.8 of Robinson (2001) with $p = q = 2$.

Lemma A.1.12. (Young's Inequality) *If $a, b \geq 0$ and $\gamma > 0$, then*

$$ab \leq \frac{\gamma}{2}a^2 + \frac{1}{2\gamma}b^2. \tag{A.66}$$

We now quote two useful forms of Gronwall's Lemma. The first is taken from Section 5.2 of Atkinson and Weimin (2009).

Lemma A.1.13. (Gronwall's Lemma – continuous) *Suppose $f \in C[a, b]$ satisfies*

$$f(t) \leq g(t) + \int_a^t h(s) f(s) \, \mathrm{d}s \qquad\qquad t \in [a, b]$$

where g is continuous, $h \in L^1(a, b)$ and $h(t) \geq 0$ a.e.. Then

$$f(t) \leq g(t) + \int_a^t g(s) h(s) \exp\left\{\int_s^t h(\tau) \, \mathrm{d}\tau\right\} \mathrm{d}s \qquad \text{for every} \qquad t \in [a, b].$$

In addition, if g is non-decreasing, then

$$f(t) \leq g(t) \exp\left\{\int_a^t h(s) \, \mathrm{d}s\right\} \qquad \text{for every} \qquad t \in [a, b].$$

In the case where $h(s) = c > 0$, these inequalities reduce to

$$f(t) \leq g(t) + c\int_a^t g(s) \exp\{c(t - s)\} \, \mathrm{d}s \qquad \text{for every} \qquad t \in [a, b],$$

and

$$f(t) \leq g(t) \exp\{c(t - a)\} \qquad \text{for every} \qquad t \in [a, b].$$

We take the discrete counterpart to this from a result in Section 3.4.2 of Süli (2010).

Lemma A.1.14. (Gronwall's Lemma – discrete) *If the non-negative sequence $(|e_k|)$ has*

$$|e_n| \leq P + \Delta t Q \sum_{k=0}^{n-1} |e_k|, \qquad\qquad n \geq 0,$$

for $P, Q > 0$, then

$$|e_n| \leq P\mathrm{e}^{(Qn\Delta t)}, \qquad\qquad n \geq 0.$$

A.1.6 A fully discrete approximation

A.1.6.1 Norms

We introduce two norms on V_*^h. The first is the counterpart to Lemma A.1.2.

Lemma A.1.15. (V_*^h and its dual $\left(V_*^h\right)'$) *V_*^h is a Hilbert space with inner product as in* (A.4) *and the same norm as that specified in* (A.5) *i.e.*

$$\|\omega_h\|_{V_*^h} := |\omega_h|_1 = \|\omega_h\|_* . \tag{A.67}$$

We denote the dual of V_*^h by $\left(V_*^h\right)'$, with norm (cf. (A.9)*)*

$$\|\ell_{\omega_h}\|_{(V_*^h)'} = \sup_{\nu_h \in V_*^h \setminus \{0\}} \frac{|\ell_{\omega_h}(\nu_h)|}{\|\nu_h\|_{V_*^h}} = \sup_{\nu \in V_*^h \setminus \{0\}} \frac{\left|(\nu_h, \omega_h)_{V_*^h}\right|}{\|\nu_h\|_{V_*^h}} = \sup_{\|\nu_h\|_{V_*^h} = 1} \left|(\nu_h, \omega_h)_{V_*^h}\right|. \tag{A.68}$$

The result is immediate since V_*^h is a finite dimensional subspace of $H_*^1(\Omega)$.

The second is the discrete counterpart to the $H^{-1}(\Omega)$ inner product of Defn 2.1.2 in (5.52), with the induced norm (5.53). That this is a norm follows immediately from Lemma A.1.15. Note that

$$(u_h, v_h)_{-h} \leq \left|(-\Delta_h)^{-1} u_h\right|_1 \left|(-\Delta)^{-1} v_h\right|_1 = \|u_h\|_{-h} \|v_h\|_{-h}, \tag{A.69}$$

which is essentially the Cauchy–Schwarz inequality in the $(\cdot,\cdot)_{-h}$ inner product. We also have the discrete counterpart to Lemma A.1.7

Lemma A.1.16. (Properties of $(\cdot,\cdot)_{-h}$) *If $u_h \in V_*^h$, then (cf.* (A.28)*)*

$$\|u_h\|_{-h} \leq c_P \|u_h\| \leq c_P^2 |u_h|_1. \tag{A.70}$$

Likewise, (cf. (A.29)*)*

$$\|u_h\|^2 \leq \|u_h\|_{-h} |u_h|_1. \tag{A.71}$$

Proof. To establish (A.70), we use (5.53) to argue that

$$\begin{aligned}\|u_h\|_{-h}^2 = \left((-\Delta_h)^{-1} u_h, u_h\right) &\leq \left\|(-\Delta_h)^{-1} u_h\right\| \|u_h\| \\ &\leq c_P \left|(-\Delta_h)^{-1} u_h\right|_1 \|u_h\| = c_P \|u_h\|_{-h} \|u_h\| \quad \Rightarrow \quad \|u_h\|_{-h} \leq c_P \|u_h\|,\end{aligned}$$

by the Cauchy–Schwarz and Poincaré inequalities (the latter holds since $V^h \subset H^1(\Omega)$). For (A.71), we use (5.51), the Cauchy–Schwarz inequality and (5.53) to write

$$\|u_h\|^2 = (u_h, u_h) = \left(\nabla (-\Delta_h)^{-1} u_h, \nabla u_h\right) \leq \left|(-\Delta_h)^{-1} u_h\right|_1 |u_h|_1 = \|u_h\|_{-h} |u_h|_1.$$

□

Finally, we note that (cf. (A.27))

$$C \|u_h\|_{(V_*^h)'} \leq \|u_h\|_{-h} \leq C \|u_h\|_{(V_*^h)'}. \tag{A.72}$$

The intuition for (A.72) is as follows: suppose that $f_h, g_h \in V_*^h$ and

$$-\Delta_h v_h = f_h \qquad \text{and} \qquad -\Delta_h u_h = g_h, \qquad \text{viz.} \qquad v_h = (-\Delta_h)^{-1} f_h \qquad \text{and} \qquad u_h = (-\Delta_h)^{-1} g_h.$$

Then, v_h and u_h are well-defined functions in V_*^h, and using (5.52),

$$(f_h, g_h)_{-h} = \left(\nabla (-\Delta_h)^{-1} f_h, \nabla (-\Delta_h)^{-1} g_h\right) = (\nabla v_h, \nabla u_h) = (\ell_{v_h}, \ell_{u_h})_{*'}.$$

A.1.6.2 Elliptic regularity, BCs

In Lemma A.1.5 (p. 324), we saw that $(-\Delta\varphi, \nu) = (\nabla\varphi, \nabla\nu)$ for every $\nu \in H^1(\Omega)$ if and only if $\partial_n \varphi|_{\partial\Omega} = 0$ i.e. in this case, $-\Delta$ (weakly) enforces a zero Neumann BC on φ. On the other hand, $-\Delta_h$ is defined all over V^h and is onto V_*^h i.e. $-\Delta_h$ does not enforce a BC.

In previous sections, we saw that if $f \in L_*^2(\Omega)$, then $(-\Delta_n)^{-1} f$ is smoother than f, being a member of $H^1(\Omega)$. We could infer higher regularity (membership of $H^2(\Omega)$) if we made appropriate assumptions on $\partial\Omega$. There is no corresponding increase in smoothness when we apply $(-\Delta_h)^{-1}$ to members of V_*^h. Given any $u_h, v_h \in V^h$, (cf. (A.45))

$$(\nabla u_h, \nabla v_h) = (-\Delta_h u_h, v_h).$$

Non-constant elements of V^h are not in $H^2(\Omega)$. We replace results about $H^2(\Omega)$ (which bounds $L^\infty(\Omega)$ in $d = 1, 2, 3$) with results in $\ell^\infty(\Omega)$ (the discrete counterpart in V^h to $L^\infty(\Omega)$). On other other hand, our assumption that Ω is a convex polygon to which we apply a quasi-uniform triangulation (see Section 5.3.1), implies that for any $u_h \in V^h$,

$$\|u_h - \overline{u_h}\|_{0,\infty} \leq C \|u_h\|^{1-\Theta} \|-\Delta_h u_h\|^{\Theta} \leq C < \infty, \tag{A.73}$$

independent of h, where $\Theta = \frac{1}{2}$ if $d = 2$, and $\Theta = \frac{3}{4}$ if $d = 3$ (see Barrett and Blowey (1999a) and Barrett and Blowey (2001)). This is the discrete counterpart to (A.42).

A.1.6.3 Properties of the projection operators of Section 5.3.3

We observe that:

i) $P^{(h)}$ preserves mass in that, for any $\varphi \in L^2(\Omega)$,

$$\overline{P^{(h)}\varphi} = \overline{\varphi}. \tag{A.74}$$

$P^{(h)}$ is well-defined and linear: for any $\varphi \in L^2(\Omega)$,

$$\left\|\varphi - P^{(h)}\varphi\right\| \leq \|\varphi - v_h\| \qquad \text{for every} \qquad v_h \in V^h, \tag{A.75a}$$

and the orthogonality relation

$$\left(\varphi - P^{(h)}\varphi, v_h\right) = 0 \qquad \text{for every} \qquad v_h \in V^h \tag{A.75b}$$

holds. Moreover,

$$\left\|P^{(h)}\varphi\right\| \leq \|\varphi\|. \tag{A.75c}$$

We prove the last statement as follows: by definition

$$\left(P^{(h)}\varphi, v_h\right) = (\varphi, v_h) \qquad \text{for every} \qquad v_h \in V^h.$$

Setting $v_h = P^{(h)}\varphi$ and using the Cauchy–Schwarz inequality yields

$$\left\|P^{(h)}\varphi\right\|^2 \leq \|\varphi\| \left\|P^{(h)}\varphi\right\| \qquad \Rightarrow \qquad \left\|P^{(h)}\varphi\right\| \leq \|\varphi\|.$$

ii) $P_m^{(\star)}$ is not well-defined without the mass condition in (5.54). With it, $P_m^{(\star)}$ is well-defined and linear: for $\varphi_1, \varphi_2 \in H^1(\Omega)$

$$P_m^{(\star)}(\alpha\varphi_1 + \beta\varphi_2) = \alpha P_m^{(\star)}\varphi_1 + \beta P_m^{(\star)}\varphi_2, \tag{A.76a}$$

for any $\alpha, \beta \in \mathbb{R}$. Furthermore, for $\varphi \in H^1(\Omega)$,

$$\left|\varphi - P_m^{(\star)}\varphi\right|_1 \leq |\varphi - v_h|_1 \qquad \text{for every} \qquad v_h \in V^h. \tag{A.76b}$$

Finally, for $\varphi \in H^1(\Omega)$, we have the orthogonality relation

$$\left(\nabla\left(\varphi - P_m^{(\star)}\varphi\right), \nabla v_h\right) = 0 \qquad \text{for every} \qquad v_h \in V^h. \tag{A.76c}$$

The following results are useful.

Lemma A.1.17. (Properties of the $P_m^{(\star)}$ and $P^{(h)}$ projections.) *Suppose that $u \in H_m^2(\Omega)$ with $\partial_n u|_{\partial\Omega} = 0$, and that $u_h = P_m^{(\star)} u \in V^h$. Then $-\Delta_h u_h = P^{(h)}(-\Delta u)$, and*

$$\|-\Delta_h u_h\| \leq \|-\Delta u\|. \tag{A.77}$$

In addition,

$$\|u_h\|_1 = \left(\|u_h\|^2 + |u_h|_1^2\right)^{1/2} \leq C(u, m, c_P, |\Omega|), \tag{A.78}$$

i.e. $|u_h|_1$, $\|u_h\|$ and $\|u_h\|_1$ are bounded independent of h and τ. Moreover,

$$\|u_h\|_{0,\infty} \leq \|u_h - u\|_{0,\infty} + \|u\|_{0,\infty} \leq Ch^{2-(d/2)} \|u\|_2 + \|u\|_{0,\infty} \leq C\|u\|_2 = C(u), \tag{A.79}$$

for $d = 1, 2, 3$. If $h < 1$ (for instance, as $h \downarrow 0$) then $h^{2-(d/2)} < 1$, and the bound in (A.79) is h–independent.

Suppose that $f_h \in V_*^h$. Let $u_h = (-\Delta_h)^{-1} f_h$ and $u = (-\Delta_n)^{-1} f_h \in H^1(\Omega)$. Then

$$\|f_h\|_{-h} \leq \|f_h\|_{-1}, \tag{A.80}$$

and $u_h = P_m^{(\star)} u$ (with $m = 0$).

Proof.

i) If $u \in H_m^2$, then $u \in L^\infty(\Omega), C^0\left(\overline{\Omega}\right)$ for $d = 1, 2, 3$ (by Sobolev embedding).

ii) If $u_h = P_m^{(\star)} u \in V^h$, then

$$(\nabla u_h, \nabla v_h) = (\nabla u, \nabla v_h) \qquad \text{for every} \qquad v_h \in V^h. \tag{A.81}$$

Moreover, by definition,

$$(-\Delta_h u_h, v_h) = (\nabla u_h, \nabla v_h) \qquad \text{for every} \qquad v_h \in V^h.$$

Suppose that $u \in H^2(\Omega)$ and $\partial_n u|_{\partial\Omega} = 0$, so that

$$(-\Delta u, v) = (\nabla u, \nabla v) \qquad \text{for every} \qquad v \in H^1(\Omega).$$

Since, $V^h \subset H^1(\Omega)$, it is also true that

$$(-\Delta u, v_h) = (\nabla u, \nabla v_h) \qquad \text{for every} \qquad v_h \in V^h.$$

Hence

$$(-\Delta_h u_h, v_h) = (\nabla u_h, \nabla v_h) = (\nabla u, \nabla v_h) = (-\Delta u, v_h)$$

for every $v_h \in V^h$, which means that $-\Delta_h u_h = P^{(h)}(-\Delta u)$. Setting $v_h = -\Delta_h u_h$ in the above, we find that

$$\|-\Delta_h u_h\|^2 \leq \|-\Delta u\| \, \|-\Delta_h u_h\| \qquad \Rightarrow \qquad \|-\Delta_h u_h\| \leq \|-\Delta u\|$$

by the Cauchy–Schwarz inequality, which is (A.77).

iii) We see that

$$\|u_h\| = \|u_h - m + m\| \leq \|u_h - \overline{u_h}\| + \|m\| \leq c_P \left|u_h\right|_1 + |m| \left|\Omega\right|^{1/2}, \tag{A.82}$$

by Poincaré's inequality. Setting $v_h = u_h$ in (A.81) reveals that

$$\left|u_h\right|_1^2 = (\nabla u, \nabla u_h) \leq \left|u\right|_1 \left|u_h\right|_1 \qquad \Rightarrow \qquad \left|u_h\right|_1 \leq \left|u\right|_1 = C\left(u\right) \tag{A.83}$$

by the Cauchy–Schwarz inequality. From (A.82), we thus conclude that

$$\|u_h\| \leq C\left(u, m, c_P, |\Omega|\right) \tag{A.84}$$

independent of h and τ. (A.78) follows immediately.

iv) We use the following in establishing (A.79):

$$\begin{aligned}
\left\|u_h - u\right\|_{0,\infty} &\leq \left\|u_h - \mathcal{I}^{(h)} u\right\|_{0,\infty} + \left\|\mathcal{I}^{(h)} u - u\right\|_{0,\infty} \\
&\leq C h^{-d/2} \left\|u_h - \mathcal{I}^{(h)} u\right\|_{L^2(\Omega)} + \left\|\mathcal{I}^{(h)} u - u\right\|_{0,\infty} \\
&\leq C h^{-d/2} \left\|u_h - u\right\|_{L^2(\Omega)} + C h^{-d/2} \left\|u - \mathcal{I}^{(h)} u\right\|_{L^2(\Omega)} \\
&\quad + \left\|\mathcal{I}^{(h)} u - u\right\|_{0,\infty} \\
&\leq C h^{-d/2} h^2 \left|u\right|_2 + C h^{-d/2} h^2 \left|u\right|_2 + C h^{2-d/2} \left\|u\right\|_2 \\
&\leq C h^{2-d/2} \left\|u\right\|_2,
\end{aligned}$$

where we used the inverse inequality (Theorem 3.2.6 and inequality 3.2.34 of Ciarlet (1978)), and the quasi-uniformity of our discretisation of Ω in the second line above.

v) For the last part of the Lemma,

$$\begin{aligned}
u_h = \left(-\Delta_h\right)^{-1} f_h \qquad &\Rightarrow \qquad (\nabla u_h, \nabla v_h) = (f_h, v_h) \qquad \text{for every } v_h \in V^h; \\
u = \left(-\Delta_n\right)^{-1} f_h \qquad &\Rightarrow \qquad (\nabla u, \nabla v) = (f_h, v) \qquad \text{for every } v \in H^1\left(\Omega\right).
\end{aligned}$$

Since $V^h \subset H^1\left(\Omega\right)$, $(\nabla u, \nabla v_h) = (f_h, v_h)$ for every $v_h \in V^h$, too, and so

$$(\nabla u_h, \nabla v_h) = (\nabla u, \nabla v_h) \qquad \text{for every} \qquad v_h \in V^h. \tag{A.85}$$

Setting $v_h = u_h$ in this last expression leads to

$$(\nabla u_h, \nabla u_h) = (\nabla u, \nabla u_h) \qquad \Rightarrow \qquad \left|u_h\right|_1 \leq \left|u\right|_1 \qquad \Rightarrow \qquad \left\|f_h\right\|_{-h} \leq \left\|f_h\right\|_{-1},$$

which is (A.80). A comparison of (5.54) and (A.85) above reveals that $u_h = P_m^{(\star)} u$ (with $m = 0$), since $\overline{u} = \overline{u_h} = 0$.

□

A.2 The n-phase energy minimisation problem

A.2.1 A stationary problem

As in Section 7 of Gelfand and Fomin (2012), we define the variational derivative of

$$F[\varphi] = \int_\Omega E(x, \varphi(x), \nabla\varphi(x)) \,\mathrm{d}\Omega \qquad \text{as} \qquad \frac{\delta F}{\delta \varphi} = -\nabla \cdot \partial_{\nabla\varphi} E + \partial_\varphi E. \tag{A.86a}$$

The variational derivative may be defined as that function for which (cf. (A.49))

$$(\partial_{\nabla\varphi} E, \nabla\nu) + (\partial_\varphi E, \nu) = \Bigg(\underbrace{-\nabla \cdot \partial_{\nabla\varphi} E + \partial_\varphi E}_{:= \frac{\delta F}{\delta \varphi}}, \nu \Bigg) + \int_{\partial\Omega} \nu \, \partial_n \varphi \,\mathrm{d}S \qquad \forall \qquad \nu \in C^\infty\left(\overline{\Omega}\right). \tag{A.86b}$$

The Euler–Lagrange equation and its BC, which together comprise the stationarity condition, result from demanding that the above be zero for every test function ν, viz.

$$\frac{\delta F}{\delta \varphi} = 0 \qquad \text{with natural BC} \qquad \partial_n \varphi|_{\partial\Omega} = 0. \tag{A.86c}$$

Combining (2.15) and (A.86a), it is clear that

$$\frac{\delta \mathcal{E}}{\delta \phi_i} = -\nabla \cdot \partial_{\nabla\phi_i} \mathcal{I} + \partial_{\phi_i} (\mathcal{B} + \mathcal{N}). \tag{A.87}$$

For the interfacial energy, (2.17a) implies that

$$-\nabla \cdot \partial_{\nabla\phi_i} \mathcal{I} = \sum_{j=1}^{n} \varepsilon_{ij}^2 (-\Delta) \phi_j \tag{A.88}$$

We assume that each $\partial_{\phi_i} \mathcal{B}$ is well-defined. This is clearly a problem in light of (2.18c), which we will resolve in due course. For the non-local energy, (2.19a) implies that

$$\partial_{\phi_i} \mathcal{N} = \sum_{k=1}^{n} \gamma_{ik} (-\Delta_n)^{-1} \left(\phi_k - \overline{\phi_k}\right). \tag{A.89}$$

Various approaches

We consider two approaches to solving (2.16): i) directly, and ii) using gradient flows.

In gradient flow methods, we define a dynamic process under which the energy (2.15) is a monotonically non-increasing function of t. Such techniques enjoy several advantages:

i) They can be formulated as (systems of) PDEs, for which sophisticated analytical and numerical approximation techniques are available.

ii) As $t \to \infty$, the solution of a gradient flow PDE tends to a candidate energy minimiser. We will prove this for our 2-phase model in Chapter 4. Practically, this means that if we can build convergent codes that approximate gradient flows and run them over sufficiently long time horizons, we *should* retrieve functions that have energies that are similar to energy minimisers.

iii) It is relatively straightforward to introduce mobilities into a gradient flow PDE and recover a model which approximates the time-dynamics of DBC phase separation. As such, we can think of our gradient flow variable, t, as time.

On the other hand:

i) It is very hard to distinguish a low energy configuration from an energy minimiser. Metastability is a phenomenon whereby these methods become 'stuck' (viz. the solution evolution becomes *extremely* slow as the energy gradient becomes flat) at a configuration which is morphologically quite distinct from any minimiser. This issue is discussed at length in Section 4 of Choksi et al. (2011).[2]

ii) When applied to our specific problem, the methods suffer from severe time-stepping restrictions, which makes the associated codes very long running.

Gradient flows: two equivalent formulations

We will consider two equivalent options in constructing time-dependent dynamics:

i) Write down the dynamics for n phases and *then* reformulate the problem in $n-1$ unknowns. This technique is the basis of the work in Boyer and Lapuerta (2006) and Boyer et al. (2010).

ii) Apply incompressibility (2.14b) to the energy, and derive the dynamics in $n-1$ parameters directly.

A.2.2 A Lagrange function: the $H^{-1}(\Omega)$ gradient flow

If we consider only constant, diagonal mobility matrices $M^{(k)} = M_k I_d$,[3] in which I_d is the $d \times d$ identity matrix, then (2.23a) becomes

$$\partial_t \phi_k = \nabla \cdot \left(M_k \nabla \frac{\delta \mathscr{L}}{\delta \boldsymbol{\phi}_k} \right) = M_k \Delta \frac{\delta \mathscr{L}}{\delta \boldsymbol{\phi}_k}. \tag{A.90}$$

We now define the vector of chemical potentials $\boldsymbol{\mu} = (\mu_1, \ldots, \mu_n)$, split each dynamic equation into (cf. (2.22))

$$\partial_t \phi_i = M_i(\Delta)\, \mu_i \tag{A.91a}$$

$$\text{where} \quad \mu_i = \frac{\delta \mathscr{L}}{\delta \phi_i} = \frac{\delta \mathcal{E}}{\delta \phi_i} - \lambda, \tag{A.91b}$$

subject to (2.25), and equip $\boldsymbol{\mu}$ with the zero Neumann BC of (2.23b), viz.

$$\partial_n \mu_i|_{\partial\Omega} = 0 \qquad \text{for each} \qquad 1 \leq i \leq n. \tag{A.91c}$$

To find λ, we sum the n equations (A.91a), and substitute (A.91b) to find that

$$\sum_{i=1}^{n} \partial_t \phi_i = \partial_t \left(\sum_{i=1}^{n} \phi_i \right) = \Delta \left(\sum_{i=1}^{n} M_i \left(\frac{\delta \mathcal{E}}{\delta \phi_i} - \lambda \right) \right) = \Delta \underbrace{\left(\sum_{i=1}^{n} M_i \frac{\delta \mathcal{E}}{\delta \phi_i} - \lambda \sum_{i=1}^{n} M_i \right)}_{:= f(\mathcal{E}, \boldsymbol{\phi}, \lambda)}, \tag{A.92}$$

To ensure that (2.25) holds, we choose λ to make the left-hand side of (A.92) above equal to zero, since

$$\partial_t \left(\sum_{i=1}^{n} \phi_i \right) = 0 \qquad \Rightarrow \qquad \sum_{i=1}^{n} \phi_i(x,t) = \sum_{i=1}^{n} \phi_{i_0}(x) = 1$$

for a.e. $x \in \Omega$, as long as (2.23f) holds. Hence, λ is to (uniquely) solve

$$(-\Delta) f(\mathcal{E}, \boldsymbol{\phi}, \lambda) = 0 \qquad \Leftrightarrow \qquad f(\mathcal{E}, \boldsymbol{\phi}, \lambda) = (-\Delta_n)^{-1} 0 \qquad \text{with} \qquad \overline{f(\mathcal{E}, \boldsymbol{\phi}, \lambda)} = 0.$$

Selecting

$$\lambda(x,t) = \frac{1}{\sum_{i=1}^{n} M_i} \sum_{i=1}^{n} M_i \frac{\delta \mathcal{E}}{\delta \phi_i}(x,t), \tag{A.93a}$$

makes $f(\mathcal{E}, \boldsymbol{\phi}, \lambda) \equiv 0$ with zero Neumann BC and the correct mass average for unique solvability. Then, according to (A.91b),

$$\mu_i = \frac{\delta \mathcal{E}}{\delta \phi_i} - \frac{1}{\sum_{j=1}^{n} M_j} \left(\sum_{j=1}^{n} M_j \frac{\delta \mathcal{E}}{\delta \phi_j} \right) = \frac{1}{\sum_{j=1}^{n} M_j} \left(\left(\sum_{\substack{j=1 \\ j \neq i}}^{n} M_j \right) \frac{\delta \mathcal{E}}{\delta \phi_i} - \sum_{\substack{j=1 \\ j \neq i}}^{n} M_j \frac{\delta \mathcal{E}}{\delta \phi_j} \right). \tag{A.93b}$$

If each of the underlying mobilities is the same, $M_i = \widehat{M}$ for each i, then

$$\lambda = \frac{1}{n} \left(\sum_{i=1}^{n} \frac{\delta \mathcal{E}}{\delta \phi_i} \right) \qquad \Rightarrow \qquad \mu_i = \frac{1}{n} \left((n-1) \frac{\delta \mathcal{E}}{\delta \phi_i} - \sum_{\substack{j=1 \\ j \neq i}}^{n} \frac{\delta \mathcal{E}}{\delta \phi_j} \right). \tag{A.94}$$

These dynamics are **mass conserving** for each i because, if we use (A.91a) and (A.19),

$$\frac{\mathrm{d}\overline{\phi_i}}{\mathrm{d}t} = \frac{1}{|\Omega|} \int_\Omega \partial_t \phi_i \, \mathrm{d}\Omega = \frac{M_i}{|\Omega|} \underbrace{\int_\Omega (\Delta) \, \mu_i \, \mathrm{d}\Omega}_{=0} = 0 \qquad \Rightarrow \qquad \overline{\phi_i(t)} = \overline{\phi_i(0)} = m_i.$$

Remark. We have used the natural BC associated with the stationary problem (2.21) for each ϕ_i, and *imposed* the zero Neumann BC on each μ_i. This has two consequences. The first is mass conservation. Second, if $\boldsymbol{\phi}$ solves the stationary problem, then $(-\Delta) \frac{\delta \mathscr{L}}{\delta \phi_i} = 0$ for each i and consequently, $\boldsymbol{\phi}_t = \mathbf{0}$. In Section 4.3.4 we establish a partial converse to this, by showing (for $n = 2$) that we recover a candidate stationary minimiser $\boldsymbol{\phi}$ as $t \to \infty$, for which $\boldsymbol{\phi}_t = \mathbf{0}$.

The Cahn–Hilliard and Ohta–Kawasaki equations exhibit **energy monotonicity** as we informally demonstrate, adapting the argument in Appendix B of Choksi et al. (2009). We write

$$\mathscr{L}(t) := \mathscr{L}(\boldsymbol{\phi}(t)) = \int_\Omega L(\boldsymbol{\phi}(t)) \, \mathrm{d}\Omega \tag{A.95a}$$

$$\Rightarrow \qquad \frac{\mathrm{d}\mathscr{L}}{\mathrm{d}t} = \frac{\mathrm{d}}{\mathrm{d}t} \int_\Omega L(\boldsymbol{\phi}(t)) \, \mathrm{d}\Omega = \int_\Omega \partial_t L(\boldsymbol{\phi}(t)) \, \mathrm{d}\Omega = \sum_{i=1}^{n} \left(\frac{\delta \mathscr{L}}{\delta \phi_i}, \partial_t \phi_i \right). \tag{A.95b}$$

With (A.90), written as

$$\frac{\delta \mathscr{L}}{\delta \boldsymbol{\phi}_k} = \frac{-1}{M_k} (-\Delta_n)^{-1} \partial_t \phi_k, \tag{A.96}$$

we use (A.95b) to determine that

$$\frac{\mathrm{d}\mathscr{L}}{\mathrm{d}t} = -\sum_{i=1}^{n} \frac{1}{M_i} \left((-\Delta_n)^{-1} \partial_t \phi_i, \partial_t \phi_i \right) = -\sum_{i=1}^{n} \frac{1}{M_i} \| \partial_t \phi_i \|_{-1}^2 \leq 0. \tag{A.97}$$

Hence the dynamics are mass conserving and energy is a monotonically non-increasing function of t.

Remark. We derive the **Allen–Cahn** equation if we replace (2.23a) with

$$\partial_t \phi_k = -\frac{\delta \mathscr{L}}{\delta \phi_k}. \tag{A.98}$$

These dynamics exhibit energy monotonicity by a similar argument to that above, but the model is not mass conserving (see Zhang (2006)). As such, is it not suitable for our purposes.[4]

A.2.3 Applying incompressibility to the energy

Alternatively, we can use incompressibility to reduce the number of phases in the energy. Any of the phases could be eliminated, and consequently, it is hard to be specific about this approach. The basic idea is that we replace $\mathcal{E}(\boldsymbol{\phi}) : \mathbb{R}^n \to \mathbb{R}^+$ with $\mathcal{E}(\boldsymbol{\varphi}) : \mathbb{R}^{n-1} \to \mathbb{R}^+$ with $\boldsymbol{\varphi} : \mathbb{R}^d \to \mathbb{R}^{n-1}$ an incompressible version of $\boldsymbol{\phi} : \mathbb{R}^d \to \mathbb{R}^n$. We then define a set of $n-1$ dynamic equations, with mobilities $M_r^{(k)}$, of the form (cf. (2.23a))

$$\partial_t \varphi_k + \nabla \cdot \boldsymbol{j}^{(k)} = 0 \qquad \text{where} \qquad \boldsymbol{j}^{(k)} = -M_r^{(k)} \nabla \left(\frac{\delta \mathcal{E}(\boldsymbol{\varphi})}{\delta \varphi_k} \right). \tag{A.99}$$

The principle complication is in reconciling the mobilities $M_r^{(k)}$ with those of the underlying n-phase problem. Our assumption is that the n mobilities $M^{(k)}$ in (2.23) are fundamental (measured in some way from physical experiments) and that the $M_r^{(k)}$s depend on these.

A.2.4 Regularising a non-smooth homogeneous energy density

Taking a partial derivative of $\mathcal{B}_{[0,1]}$ in (2.18c) is problematic because it is not differentiable. There are several other ways to deal with this:

i) Regularise $\mathcal{B}_{[0,1]}$ to make it differentiable. Inspired by Blowey and Elliott (1991),[5] we replace $\mathcal{B}_{[0,1]}$ with

$$\mathcal{B}_\mu(\boldsymbol{\phi}) = \mathcal{B}(\boldsymbol{\phi}) + \underbrace{\frac{1}{2\mu} \sum_{i=1}^{n} \left((\phi_i - 1)_+^2 + (\phi_i)_-^2 \right)}_{\text{penalty energy density}}. \tag{A.100}$$

This density penalises any ϕ_i not satisfying (2.14a) with higher energy, thus favouring morphologies that (approximately) satisfy this constraint. Intuition would suggest that we recover (2.18c) from (A.100) as $\mu \downarrow 0$, with deviations from (2.14a) penalised increasingly harshly as μ gets smaller. $\mathcal{B}_\mu$ is differentiable, with

$$\partial_{\phi_i} \mathcal{B}_\mu(\boldsymbol{\phi}) = \partial_{\phi_i} \mathcal{B}(\boldsymbol{\phi}) + \frac{1}{\mu} \left((\phi_i - 1)_+ + (\phi_i)_- \right), \tag{A.101}$$

which we can use in (A.87). We use $\mathcal{E}_\mu$ to denote the corresponding (regularised) energy.

ii) Use variational inequalities, in which the minimisation conditions are stated as inequalities over admissible sets of functions that satisfy (2.14a).

iii) Approximate $\mathcal{B}_{[0,1]}$ with a smooth, double-well function (such as the quartic polynomial $\left(1 - \varphi^2\right)^2$) with zeros at $0, 1$. We do not study this approach in any detail in this thesis.

We regularise $\mathcal{B}_{[0,1]}$ and in Chapter 4, rigorously demonstrate the equivalence of this and the variational inequality approach as $\mu \downarrow 0$, for the 2-phase problem.

Notes

[1]See (2.3) of Blowey and Elliott (1991).

[2]Interestingly, the same sort of thing is observed when DBCs are observed to phase separate physically. It is almost as if the shallow energy gradient in the gradient flows, and the resulting slow evolution reflects something fundamental about the underlying physics.

[3]We use lower case ms for masses and upper case Ms for mobilities.

[4]We comment on the source of the $H^{-1}(\Omega)$ nomenclature. Following the ideas in Appendix B of Choksi et al. (2009), we can think of defining the dynamics in weak form as the problem

$$\text{Find:} \qquad \partial_t\varphi \in L^2_*(\Omega) \qquad \text{s.t.} \qquad (\partial_t\varphi,\omega)_H = -\left(\frac{\delta E}{\delta\varphi},\omega\right) \qquad \text{for every} \qquad \omega \in L^2_*(\Omega), \tag{A.102}$$

and $t \in (0,T]$, where the choice of inner product on the left-hand side is still open. Taking an $L^2(\Omega)$ inner product on the left leads to the problem

$$\text{Find:} \qquad \partial_t\varphi \in L^2_*(\Omega) \qquad \text{s.t.} \qquad (\partial_t\varphi,\omega) = -\left(\frac{\delta E}{\delta\varphi},\omega\right) \qquad \text{for every} \qquad \omega \in L^2_*(\Omega), \tag{A.103}$$

which corresponds to the Allen–Cahn equation, thanks to Lemma 3.8-2 of Kreyszig (1978). Alternatively, using the $H^{-1}_*(\Omega)$ inner product on the left-hand side of (A.102), leads to

$$\begin{aligned}
\text{Find:} \qquad \partial_t\varphi \in L^2_*(\Omega) \qquad \text{s.t.} \qquad & (\partial_t\varphi,\omega)_{-1} = -\left(\frac{\delta E}{\delta\varphi},\omega\right) \qquad \text{for every} \qquad \omega \in L^2_*(\Omega) \\
\Rightarrow \qquad & \left((-\Delta_n)^{-1}\partial_t\varphi,\omega\right) = \left(-\frac{\delta E}{\delta\varphi},\omega\right) \qquad \text{for every} \qquad \omega \in L^2_*(\Omega) \\
\Rightarrow \qquad & (-\Delta_n)^{-1}\partial_t\varphi = -\frac{\delta E}{\delta\varphi},
\end{aligned} \tag{A.104}$$

thanks to Lemma 3.8-2 of Kreyszig (1978). Alternatively, $\partial_t\varphi = \Delta\dfrac{\delta E}{\delta\varphi}$.

[5]Those authors studied a C^2-regularisation of the 2-phase double obstacle density.

Appendix B

Analysis of the 2-phase model

B.1 Proof of Lemma 4.1.2

Proof. Suppose $u, v \in \mathscr{A}$ and $0 \leq \theta \leq 1$. Clearly any linear combination of $H^1(\Omega)$ functions is in $H^1(\Omega)$. In addition, for any $x \in \Omega$ for which $|u(x)|, |v(x)| \leq 1$, we must have, for $0 \leq \theta \leq 1$,

$$|(\theta u + (1-\theta) v)(x)| \leq \theta |u(x)| + (1-\theta) |v(x)| \leq 1.$$

Likewise, if $u, v \in \mathscr{A}_m$ and $0 \leq \theta \leq 1$, then

$$\overline{(\theta u + (1-\theta) v)} = \theta \overline{u} + (1-\theta) \overline{v} = m.$$

□

B.2 Proof of Lemma 4.2.1

Proof. $\mathscr{A}_m$ is non-empty since $\varphi(x) \equiv m$ ($|m| \leq 1$) satisfies all of the requirements of a candidate minimiser. For $|m| = 1$, $\mathscr{A}_m = \{\varphi(x) \equiv m\}$, and the problem is trivial.

Suppose that $|m| < 1$. We base this next part of the proof on Lemma 2.1 in Blank et al. (2011) and Chapter 8 of Evans (1998) (esp. Theorem 2 of Section 8.2.2).[1]

i) For $\varphi \in \mathscr{A}_m$, $|\varphi| \leq 1$ a.e. and so $(\mathcal{B}(\varphi), 1) \geq 0$, which means that $\mathcal{E}[\varphi]$ in (4.1a) is non-negative i.e. bounded below. Hence, the set of real numbers $\{\mathcal{E}[\varphi]\}_{\varphi \in \mathscr{A}_m}$ has an infimum, $\mathcal{E}_{\min} := \inf_{\varphi \in \mathscr{A}_m} \mathcal{E}[\varphi] \geq 0$. This fact alone is *not* sufficient to guarantee the existence of a minimiser,[2] by which we mean a $\varphi^* \in \mathscr{A}_m$ with $\mathcal{E}[\varphi^*] = \mathcal{E}_{\min}$.

ii) However, we can infer the existence of a minimising sequence $(\varphi_k)_{k \in \mathbb{N}}$, for which

$$\lim_{k \to \infty} \mathcal{E}[\varphi_k] = \mathcal{E}_{\min} \geq 0. \tag{B.1}$$

In the trivial case $m = \pm 1$, we can set $(\varphi_k)_{k \in \mathbb{N}} = (m, m, \ldots)$ viz. the (repeating) set of constant functions. Also, $\mathcal{E}[\varphi \equiv m] < \infty$ and so $\mathcal{E}_{\min}$ is finite. In addition, $\mathcal{E}$ is coercive (cf. (5) in Section 8.2.1 of Evans (1998)), since for $\delta = \varepsilon_\varphi^2 / 4 > 0$,

$$\mathcal{E}[\varphi] \geq \delta |\varphi|_1^2 \qquad \text{i.e.} \qquad \mathcal{E}[\varphi] \to \infty \qquad \text{as} \qquad |\varphi|_1 \to \infty. \tag{B.2}$$

iii) (B.1) and (B.2) imply that the sequence $\left(\mathcal{E}\left[\varphi_k\right]\right)_{k\in\mathbb{N}}$ is bounded above,[3] independent of k, say $\mathcal{E}\left[\varphi_k\right] < C$. Since each of the terms of $\mathcal{E}$ in (4.1a) is non-negative for $\left(\varphi_k\right)_{k\in\mathbb{N}} \subset \mathscr{A}_m$, so is each component of the energy. In particular, the sequence $\left(\frac{\varepsilon_\varphi^2}{2}\left|\varphi_k\right|_1^2\right)_{k\in\mathbb{N}}$ is uniformly bounded. But also

$$\left\|\varphi_k\right\| = \left\|\varphi_k - m + m\right\| \leq \left\|\varphi_k - m\right\| + |m|\,|\Omega|^{1/2} \leq c_P\left|\varphi_k\right|_1 + |m|\,|\Omega|^{1/2} \leq C$$

independent of k, by Poincaré's inequality, since each $\varphi_k \in \mathscr{A}_m$. Hence, $\left(\varphi_k\right)_{k\in\mathbb{N}}$ is uniformly bounded in $H^1\left(\Omega\right)$ and therefore has a weakly convergent sub-sequence. This means there is a $\varphi^* \in \mathscr{A}_m$ and a sub-sequence $\left(\varphi_{k_j}\right)_{k_j\in\mathbb{N}}$ of $\left(\varphi_k\right)_{k\in\mathbb{N}}$ such that (after relabelling indices)

$$\varphi_k \rightharpoonup \varphi^* \qquad \text{in} \qquad H^1\left(\Omega\right).$$

Weakly convergent sequences are bounded (Proposition 4.13 of Robinson (2001)). By the Rellich-Kondrachov Theorem (cf. (A.36)), there exists a (further) sub-sequence (also relabelled) $\left(\varphi_k\right)_{k\in\mathbb{N}}$, and $\varphi^* \in L^2\left(\Omega\right)$ (since limits are unique) with

$$\varphi_k \to \varphi^* \qquad \text{(strongly) in} \qquad L^2\left(\Omega\right) \qquad \text{as } k\to\infty. \tag{B.3}$$

This implies the existence of yet another (relabelled) sub-sequence $\left(\varphi_k\right)_{k\in\mathbb{N}}$ with

$$\varphi_k \to \varphi^* \qquad \text{a.e. in } \Omega. \tag{B.4}$$

iv) We show that $\varphi^* \in \mathscr{A}_m$. For this, we need two facts. First, as in Theorem 1 of Section 8.4.1 of Evans (1998), since each $\overline{\varphi_k} = m$,

$$\left|\left(\varphi^* - m, 1\right)\right| = \left|\left(\varphi^* - m, 1\right) - \left(\varphi_k - m, 1\right)\right| = \left|\left(\varphi^* - \varphi_k, 1\right)\right| \leq \left\|\varphi^* - \varphi_k\right\|\,|\Omega|^{1/2} \to 0$$

as $k\to\infty$, by (B.3). Hence, $\left|\left(\varphi^* - m, 1\right)\right| = 0$ since this is k-independent, viz. $\overline{\varphi^*} = m$. Second, arguing as in Theorem 3 of Section 8.4.2 of Evans (1998), $\left|\varphi_k\right| \leq 1$ a.e. for each k. This means that $\left|\varphi\right| \leq 1$ a.e. too, thanks to (B.4). Thus, $\varphi^* \in \mathscr{A}_m$.

v) It remains to show that $\mathcal{E}\left[\varphi^*\right] = \mathcal{E}_{\min}$ i.e. φ^* is a minimiser of $\mathcal{E}$. To prove this, we show that the energy density is convex in $\nabla\varphi$. The interfacial energy density is $\mathcal{I}\left(\nabla\varphi\right)$ with $\mathcal{I} : \mathbb{R}^d \to \mathbb{R}$ defined by $\mathcal{I}\left(x\right) = \frac{\varepsilon_\varphi^2}{2}\left|x\right|^2$. $\mathcal{I}$ is convex because[4]

$$\left|y\right|^2 \geq \left|x\right|^2 + 2x\cdot\left(y-x\right) \qquad \Rightarrow \qquad \mathcal{I}\left(y\right) \geq \mathcal{I}\left(x\right) + \nabla\mathcal{I}\left(x\right)\cdot\left(y-x\right) \qquad \text{for any} \qquad x, y \in \mathbb{R}^d.$$

For the homogeneous energy term, we use (B.3) to see that (cf. (4.1a), (4.1b)),

$$\left(\mathcal{B}\left(\varphi_k\right), 1\right) = \frac{\chi^{AB}}{4}\left(\left|\Omega\right| - \left\|\varphi_k\right\|^2\right) \to \frac{\chi^{AB}}{4}\left(\left|\Omega\right| - \left\|\varphi^*\right\|^2\right) = \left(\mathcal{B}\left(\varphi^*\right), 1\right) \qquad \text{as} \qquad k\to\infty.$$

For the non-local term,

$$\varphi_k - m \rightharpoonup \varphi^* - m \qquad \text{in} \qquad H^1\left(\Omega\right) \qquad \text{as} \qquad k\to\infty.$$

Since $\left(-\Delta_n\right)^{-1} : H^1_*\left(\Omega\right) \to L^2_*\left(\Omega\right)$ is compact (cf. Theorem 4.15 of Robinson (2001)),

$$\left(-\Delta_n\right)^{-1}\left(\varphi_k - m\right) \to \left(-\Delta_n\right)^{-1}\left(\varphi^* - m\right) \qquad \text{(strongly) in} \qquad L^2\left(\Omega\right) \qquad \text{as} \qquad k\to\infty,$$

and hence weakly too, which means that

$$\left((-\Delta_n)^{-1}(\varphi_k - m), \eta\right) \to \left((-\Delta_n)^{-1}(\varphi^* - m), \eta\right) \qquad \text{(in } \mathbb{R}\text{) as} \qquad k \to \infty,$$

for every $\eta \in L^2(\Omega)$. Setting $\eta = \varphi_k - m$ and using weak convergence on the right,

$$\left((-\Delta_n)^{-1}(\varphi^* - m), \varphi_k - m\right) \to \left((-\Delta_n)^{-1}(\varphi^* - m), \varphi^* - m\right) = \|\varphi^* - m\|_{-1}^2$$

and so in fact, $\|\varphi_k - m\|_{-1}^2 \to \|\varphi^* - m\|_{-1}^2$ as $k \to \infty$. It follows that $\mathcal{E}[\cdot]$ is weakly lower semicontinuous on $H^1(\Omega)$,[5] i.e.

$$\mathcal{E}[\varphi^*] \leq \liminf_{k\to\infty} \mathcal{E}[\varphi_k] \qquad \text{whenever} \qquad \varphi_k \rightharpoonup \varphi^* \qquad \text{in} \qquad H^1(\Omega). \tag{B.5}$$

Hence, $\mathcal{E}[\varphi^*] \leq \mathcal{E}_{\min}$, but also by the definition of the infimum $\mathcal{E}_{\min}$, $\mathcal{E}[\varphi^*] \geq \mathcal{E}_{\min}$. We conclude that $\mathcal{E}[\varphi^*] = \mathcal{E}_{\min}$.

□

B.3 Proof of Lemma 4.2.2

Proof. Our proof mimics Theorem 4 of Section 8.4 of Evans (1998).

i) Fix any $\psi \in \mathscr{A}$, $\lambda \in \mathbb{R}$. Since $\mathscr{A}$ is convex (cf. Lemma 4.1.2), $\varphi + \theta(\psi - \varphi) \in \mathscr{A}$ for each $0 \leq \theta \leq 1$. Hence, if

$$i(\theta) := \mathscr{L}(\varphi + \theta(\psi - \varphi); \lambda), \tag{B.6}$$

then $i(0) \leq i(\theta)$ for all $0 \leq \theta \leq 1$, and so

$$i'(0) \geq 0. \tag{B.7}$$

ii) If $0 < \theta \leq 1$,[6] then

$$\begin{aligned}
\frac{i(\theta) - i(0)}{\theta} &= \frac{\mathscr{L}(\varphi + \theta(\psi - \varphi); \lambda) - \mathscr{L}(\varphi; \lambda)}{\theta} \\
&= \int_\Omega \varepsilon_\varphi^2 \left((\nabla\varphi \cdot \nabla(\psi - \varphi)) + \frac{\theta |\nabla(\psi - \varphi)|^2}{2} \right) - \frac{\chi^{AB}}{2} \left(\varphi(\psi - \varphi) + \frac{\theta(\psi - \varphi)^2}{2} \right) - \lambda(\psi - \varphi) \\
&\qquad + \alpha \Bigg[\left((\psi - \varphi) - \overline{(\psi - \varphi)} \right) \left((-\Delta_n)^{-1}(\varphi - \overline{\varphi}) \right) \\
&\qquad\qquad + \frac{\theta \left((\psi - \varphi) - \overline{(\psi - \varphi)} \right) \left((-\Delta_n)^{-1} \left((\psi - \varphi) - \overline{(\psi - \varphi)} \right) \right)}{2} \Bigg] \, \mathrm{d}\Omega
\end{aligned}$$

and so, taking $\theta \downarrow 0$, we use (2.9b) to arrive at (4.26).

□

B.4 Proof of Lemma 4.2.4

Proof.

i) Using (B.11), (B.12) and (B.14) (see the next paragraph), we replace (4.30b) with

$$\varepsilon_\varphi^2 \left(\nabla\varphi_\mu^{(N)}, \nabla\eta^{(N)}\right) + \left(\varphi_\mu^{(N)}, \eta^{(N)}\right) + \left(\zeta_\mu\left(\varphi_\mu^{(N)}\right), \eta^{(N)}\right) + \alpha\left((-\Delta_n)^{-1}\left(\varphi_\mu^{(N)} - \overline{\varphi_\mu^{(N)}}\right), \eta^{(N)}\right) = \left(f, \eta^{(N)}\right). \quad \text{(B.8)}$$

Note that $\varphi_\mu^{(N)} \in V^N \subset H^1(\Omega) \Rightarrow \zeta_\mu\left(\varphi_\mu^{(N)}\right) \in H^1(\Omega)$ but generally, $\zeta_\mu\left(\varphi_\mu^{(N)}\right) \notin V^N$.

ii) In (A.54) we saw that $e_1 = 1/|\Omega|^{1/2}$ with eigenvalue $\lambda_1 = 1$. Hence, (4.30a) becomes

$$\varphi_\mu^{(N)} = \frac{c_1^N}{|\Omega|^{1/2}} + \sum_{j=2}^N c_j^N e_j. \quad \text{(B.9a)}$$

It follows from (A.55) that

$$\overline{\varphi_\mu^{(N)}} = \frac{c_1^N}{|\Omega|^{1/2}} \qquad \Rightarrow \qquad c_1^N = \overline{\varphi_\mu^{(N)}}\,|\Omega|^{1/2} \quad \text{(B.9b)}$$

which is consistent with the remark on p. 334 (just above Section A.1.5), and so

$$\varphi_\mu^{(N)} = \overline{\varphi_\mu^{(N)}} + \sum_{j=2}^N c_j^N e_j. \quad \text{(B.9c)}$$

Consequently,

$$\varphi^{(1)} - \overline{\varphi^{(1)}} = 0 \qquad \text{and} \qquad \varphi_\mu^{(N)} - \overline{\varphi_\mu^{(N)}} = \sum_{j=2}^N c_j^N e_j \qquad \text{for } N \geq 2.$$

As in Lemma A.1.11 and (A.60), since $\mathscr{P}$ and $(-\Delta_n)^{-1}$ share eigenfunctions,

$$(-\Delta_n)^{-1}\left(\varphi^{(1)} - \overline{\varphi^{(1)}}\right) = 0 \in V^1 \quad \text{(B.10a)}$$

$$(-\Delta_n)^{-1}\left(\varphi_\mu^{(N)} - \overline{\varphi_\mu^{(N)}}\right) = \sum_{j=2}^N \frac{c_j^N}{\lambda_j - 1} e_j \in V^N \qquad \text{for } N \geq 2, \quad \text{(B.10b)}$$

which in turn means that

$$P^N (-\Delta_n)^{-1}\left(\varphi_\mu^{(N)} - \overline{\varphi_\mu^{(N)}}\right) = (-\Delta_n)^{-1}\left(\varphi_\mu^{(N)} - \overline{\varphi_\mu^{(N)}}\right). \quad \text{(B.11)}$$

Similarly, for $f \in H^1(\Omega)$, we have the eigenfunction expansion

$$f = \sum_{j=1}^\infty (f, e_j)\, e_j \qquad \Rightarrow \qquad P^N f = \sum_{j=1}^N (f, e_j)\, e_j$$

and so, since the e_js are orthogonal, for any N

$$\left(P^N f, \eta^{(N)}\right) = \left(f, \eta^{(N)}\right) \qquad \text{for every} \qquad \eta^{(N)} \in V^N. \quad \text{(B.12)}$$

Finally, $\zeta_\mu\left(\varphi_\mu^{(N)}\right) \in H^1(\Omega)$ by (4.23), and so there exist $\left\{\zeta_\mu^{N,j}\right\}$ with

$$\zeta_\mu\left(\varphi_\mu^{(N)}\right) = \sum_{j=1}^\infty \zeta_\mu^{N,j} e_j. \quad \text{(B.13)}$$

But since the e_js are orthogonal, for any N

$$\left(P^N \zeta_\mu\left(\varphi_\mu^{(N)}\right), \eta^{(N)}\right) = \left(\zeta_\mu\left(\varphi_\mu^{(N)}\right), \eta^{(N)}\right) \qquad \text{for every} \qquad \eta^{(N)} \in V^N. \quad \text{(B.14)}$$

iii) We show that problem $\left(\mathbf{S}_\mu^{(N)}\right)$ is well-posed for each N. Making the necessary substitutions into the terms in (B.8), we determine that

$$\begin{gathered}\left(\nabla\varphi_\mu^{(N)},\nabla e_k\right)=\sum_{j=1}^{N}c_j^N\left(\nabla e_j,\nabla e_k\right)=\begin{cases}0 & k=1\\ c_k^N\left(\lambda_k-1\right) & k>1,\end{cases}\\ \left(\varphi_\mu^{(N)},e_k\right)=c_k^N\\ \left(\zeta_\mu\left(\varphi_\mu^{(N)}\right),e_k\right)=:\zeta_\mu^{N,k}\\ \left((-\Delta_n)^{-1}\left(\varphi_\mu^{(N)}-\overline{\varphi_\mu^{(N)}}\right),e_k\right)=\begin{cases}0 & k=1 \text{ or } N=1\\ \dfrac{c_k^N}{\lambda_k-1} & \text{otherwise.}\end{cases}\end{gathered}\tag{B.15}$$

We substitute these back into (B.8) for each $N=1,\ldots$. For $N=1$, $k=1$,

$$c_1^N+\zeta_\mu^{1,1}=(f,e_1)=m|\Omega|^{1/2}\tag{B.16}$$

after recalling the definition of e_1 in (A.54) and noting that $\overline{f}=m$. Hence we pick $c_1^N=m|\Omega|^{1/2}$, $\varphi_\mu^{(1)}=m$ and $\zeta_\mu^{1,1}=0$ (for $|m|<1$). For $N>1$, $k=1,\ldots,N$, we substitute into (B.8) for each e_k to arrive at the $N\times N$ system

$$A\boldsymbol{c}=\boldsymbol{f}-\boldsymbol{g}\left(\boldsymbol{c}\right),\tag{B.17a}$$

$$\boldsymbol{g}\left(\boldsymbol{c}\right):=\left(\zeta_\mu^{N,1},\zeta_\mu^{N,2},\ldots,\zeta_\mu^{N,N}\right)^\top,\qquad \boldsymbol{f}:=\left(m|\Omega|^{1/2},(f,e_2),\ldots,(f,e_N)\right)^\top,\tag{B.17b}$$

with the diagonal matrix

$$A=\operatorname{diag}\left(1,A_{22},\ldots,A_{NN}\right);\qquad A_{jj}=\varepsilon_\varphi^2\left(\lambda_j-1\right)+1+\frac{\alpha}{\lambda_j-1}\qquad\text{for}\qquad j\geq 2.\tag{B.17c}$$

All of the (diagonal) entries of A are non-zero; in fact each $A_{ii}\geq 1$, and the inequality is strict for $i\geq 2$ since each such $\lambda_i>1$ by (A.56a). Hence, A is invertible and (B.17) has a unique solution for any $\left\{\zeta_\mu^{N,1},\ldots,\zeta_\mu^{N,N}\right\}$. However, while (B.17) is linear, the underlying problem is non-linear since each $\zeta_\mu^{N,k}$ depends on the c_i coefficients. For instance c_1^N (and consequently $\overline{\varphi_\mu^{(N)}}$) changes as N increases, which is why we wrote $\boldsymbol{g}\left(\boldsymbol{c}\right)$ above. We replace the formulation in (B.17a) with the fixed point problem

$$\boldsymbol{c}=A^{-1}\left(\boldsymbol{f}-\boldsymbol{g}\left(\boldsymbol{c}\right)\right)=:T\boldsymbol{c}.\tag{B.18}$$

iv) We now establish the conditions necessary to be able to use Schaefer's Fixed Point Theorem to infer the existence of a (fixed point) solution to (B.18).

If $\varphi_\mu^{(N)}=\boldsymbol{c}\cdot\boldsymbol{e}$, then for each j, $\zeta_\mu^{N,j}=\left(\zeta_\mu\left(\boldsymbol{c}\cdot\boldsymbol{e}\right),e_j\right)$, and

$$\boldsymbol{g}\left(\boldsymbol{c}\right)=\left(\left(\zeta_\mu\left(\boldsymbol{c}\cdot\boldsymbol{e}\right),e_1\right),\ldots,\left(\zeta_\mu\left(\boldsymbol{c}\cdot\boldsymbol{e}\right),e_N\right)\right)^\top$$

and the explicit dependence on $\boldsymbol{c}$ is exposed. Now let $\|\cdot\|$ denote the Euclidean norm in $\mathbb{R}^n$. If $\varphi_1=\boldsymbol{c}_1\cdot\boldsymbol{e}$ and $\varphi_2=\boldsymbol{c}_2\cdot\boldsymbol{e}$, then

$$\begin{aligned}\|T\boldsymbol{c}_1-T\boldsymbol{c}_2\|^2&=\left(\zeta_\mu\left(\boldsymbol{c}_1\cdot\boldsymbol{e}\right)-\zeta_\mu\left(\boldsymbol{c}_2\cdot\boldsymbol{e}\right),e_1\right)^2+\sum_{i=2}^{N}\frac{\left(\zeta_\mu\left(\boldsymbol{c}_1\cdot\boldsymbol{e}\right)-\zeta_\mu\left(\boldsymbol{c}_2\cdot\boldsymbol{e}\right),e_i\right)^2}{A_{ii}^2}\\&\leq\sum_{i=1}^{N}\left(\zeta_\mu\left(\varphi_1\right)-\zeta_\mu\left(\varphi_2\right),e_i\right)^2\leq\frac{1}{\mu^2}\sum_{i=1}^{N}\left(\varphi_1-\varphi_2,e_i\right)^2=\frac{1}{\mu^2}\left\|\boldsymbol{c}_1-\boldsymbol{c}_2\right\|^2\end{aligned}$$

since $A_{ii} > 1$ for $i \geq 2$, and after using (4.17). Hence,

$$\|T\boldsymbol{c}_1 - T\boldsymbol{c}_2\| \leq \frac{1}{\mu} \|\boldsymbol{c}_1 - \boldsymbol{c}_2\|, \tag{B.19}$$

which means that T is **continuous**. $T : \mathbb{R}^N \to \mathbb{R}^N$ is thus also **compact**.[7]

Consider the set

$$C := \left\{ \boldsymbol{c} \in \mathbb{R}^N | \boldsymbol{c} = \mu^p T\boldsymbol{c} \right\} \qquad \text{where} \qquad 0 < \mu < 1 \qquad \text{and} \qquad p \geq 1. \tag{B.20}$$

We show that C is bounded. Taking 2-norms, we see that

$$\|\boldsymbol{c}\| \leq \mu^p \left\|A^{-1}\right\| (\|\boldsymbol{f}\| + \|\boldsymbol{g}(\boldsymbol{c})\|) \leq \mu^p \left\|A^{-1}\right\| \left(\|\boldsymbol{f}\| + \frac{1}{\mu} \|\boldsymbol{c}\| \right)$$

which means that

$$\|\boldsymbol{c}\| \left(1 - \mu^{p-1} \left\|A^{-1}\right\|\right) \leq \mu^p \left\|A^{-1}\right\| \|\boldsymbol{f}\|.$$

By (B.17c), it is clear that $\left\|A^{-1}\right\| \geq 1$, but for given μ, we can always pick $p > 1$ so that $\mu^{p-1} \left\|A^{-1}\right\| < 1$. Then

$$\|\boldsymbol{c}\| \leq \frac{\mu^p \left\|A^{-1}\right\| \|\boldsymbol{f}\|}{1 - \mu^{p-1} \|A^{-1}\|}, \tag{B.21}$$

and so the set C is bounded. By Schaefer's Fixed Point Theorem (cf. Theorem 4 in Section 9.2 of Evans (1998) with $0 < \lambda = \mu^p < 1$), (B.18) thus has a fixed point, and $\left(\mathbf{S}_\mu^{(N)}\right)$ has a solution $\varphi_\mu^{(N)}$, for each N.

Remarks.

i) Our proof above has established *existence* only, not uniqueness.

ii) Given this result, we can set $\eta^{(N)} = 1, N > 1$ in (B.8) to obtain

$$\left(\varphi_\mu^{(N)}, 1\right) + \left(\zeta_\mu\left(\varphi_\mu^{(N)}\right), 1\right) = (f, 1) = m|\Omega| \qquad \Rightarrow \qquad \overline{\varphi_\mu^{(N)}} \neq m \qquad \text{if } N > 1. \tag{B.22}$$

We will see that $\zeta_\mu\left(\varphi_\mu^{(N)}\right) \to 0$ a.e. as $N \to \infty$ and $\mu \downarrow 0$, viz. $\overline{\varphi} = m$.

v) We now seek a bound on $\left\|\varphi_\mu^{(N)}\right\|_1$, independent of N and μ. Setting $\eta^{(N)} = \varphi_\mu^{(N)}$ in (B.8) yields

$$\varepsilon_\varphi^2 \left|\varphi_\mu^{(N)}\right|_1^2 + \left\|\varphi_\mu^{(N)}\right\|^2 + \underbrace{\left(\zeta_\mu\left(\varphi_\mu^{(N)}\right), \varphi_\mu^{(N)}\right)}_{\geq 0 \text{ by (4.19b)}} + \alpha \left\|\varphi_\mu^{(N)} - \overline{\varphi_\mu^{(N)}}\right\|_{-1}^2 = \left(f, \varphi_\mu^{(N)}\right)$$

after recalling (2.11) and noting that $\left((-\Delta_n)^{-1}\left(\varphi_\mu^{(N)} - \overline{\varphi_\mu^{(N)}}\right), \overline{\varphi_\mu^{(N)}}\right) = 0$. Hence,

$$\varepsilon_\varphi^2 \left|\varphi_\mu^{(N)}\right|_1^2 + \left\|\varphi_\mu^{(N)}\right\|^2 \leq \|f\| \left\|\varphi_\mu^{(N)}\right\| \leq \frac{1}{2}\|f\|^2 + \frac{1}{2}\left\|\varphi_\mu^{(N)}\right\|^2$$

by the Cauchy–Schwarz and Young's inequalities, and so

$$\varepsilon_\varphi^2 \left|\varphi_\mu^{(N)}\right|_1^2 + \frac{1}{2}\left\|\varphi_\mu^{(N)}\right\|^2 \leq \frac{1}{2}\|f\|^2 = C$$

independent of N and μ. Consequently,

$$\left|\varphi_\mu^{(N)}\right|_1^2 + \leq \frac{C}{\varepsilon_\varphi^2} \qquad \text{and} \qquad \left\|\varphi_\mu^{(N)}\right\|^2 \leq 2C \qquad \Rightarrow \qquad \left\|\varphi_\mu^{(N)}\right\|_1 \leq \sqrt{\frac{C}{\varepsilon_\varphi^2} + 2C} = C \tag{B.23}$$

independent of N and μ. For fixed μ, the sequence $\left(\varphi_\mu^{(N)}\right)$ (increasing N) is thus bounded uniformly in the Hilbert space $H^1(\Omega)$. We thus infer the existence of a sub-sequence of Galerkin approximations, (also labelled) $\left(\varphi_\mu^{(N)}\right)$, and $\varphi_\mu \in H^1(\Omega)$ with[8]

$$\varphi_\mu^{(N)} \rightharpoonup \varphi_\mu \qquad \text{in} \qquad H^1(\Omega). \tag{B.24}$$

Weakly convergent sequences are bounded (Proposition 4.13 of Robinson (2001)), and so $\left(\varphi_\mu^{(N)}\right)$ is bounded in $H^1(\Omega)$. Consequently, by the Rellich-Kondrachov Theorem (cf. (A.36)), there exists a (further) sub-sequence $\left(\varphi_\mu^{(N)}\right)$ with $\varphi_\mu \in L^2(\Omega)$ (recalling that limits are unique) with

$$\varphi_\mu^{(N)} \to \varphi_\mu \qquad \text{(strongly) in} \qquad L^2(\Omega) \qquad \text{as } N \to \infty. \tag{B.25}$$

vi) We show that φ_μ above solves $(\mathbf{S}_\mu)$ in (4.28). As in (A.63) we know that, for any $\eta \in H^1(\Omega)$ there is a sequence of functions (cf. (4.30a))

$$\eta^{(N)} = \sum_{j=1}^{N} (\eta, e_j)\, e_j = P^N \sum_{j=1}^{\infty} (\eta, e_j)\, e_j \in V^N \tag{B.26}$$

with the property that (cf. (A.63))

$$\eta^{(N)} \to \eta \qquad \text{in } H^1(\Omega), \text{ viz.} \qquad \left\|\eta^{(N)} - \eta\right\|_1 \to 0 \qquad \text{as } N \to \infty. \tag{B.27}$$

We fix an integer N and choose functions $\eta^{(N)}$ as in (B.26) as the test functions in (B.8), and choose $n \geq N$ in $\varphi_\mu^{(N)}$, so that

$$\varepsilon_\varphi^2 \left(\nabla\varphi_\mu^{(N)}, \nabla\eta^{(N)}\right) + \left(\varphi_\mu^{(N)}, \eta^{(N)}\right) + \left(\zeta_\mu\left(\varphi_\mu^{(N)}\right), \eta^{(N)}\right) + \alpha\left((-\Delta_n)^{-1}\left(\varphi_\mu^{(N)} - \overline{\varphi_\mu^{(N)}}\right), \eta^{(N)}\right) = \left(f, \eta^{(N)}\right). \tag{B.28}$$

We then take limits in a 2-stage process: a) use (B.24) to take weak limits in the sub-sequences of $\left(\varphi^{(n)}\right)$, sending $n \to \infty$, and b) use a density argument in the set of test functions, sending $N \to \infty$ to recover the (arbitrary) test function $\eta \in H^1(\Omega)$. We proceed term-by-term.

1) In the first term,

$$\left(\nabla\varphi_\mu^{(N)}, \nabla\eta^{(N)}\right) \xrightarrow[n\to\infty]{} \left(\nabla\varphi_\mu, \nabla\eta^{(N)}\right) \xrightarrow[N\to\infty]{} (\nabla\varphi_\mu, \nabla\eta).$$

2) Similarly, in the second term

$$\left(\varphi_\mu^{(N)}, \eta^{(N)}\right) \xrightarrow[n\to\infty]{} \left(\varphi_\mu, \eta^{(N)}\right) \xrightarrow[N\to\infty]{} (\varphi_\mu, \eta),$$

and likewise for the $\left(f, \eta^{(N)}\right)$ term on the right (using only the density argument).

3) For the (non-linear) penalty term,

$$\left|\left(\zeta_\mu\left(\varphi_\mu^{(N)}\right), \eta^{(N)}\right) - \left(\zeta_\mu(\varphi_\mu), \eta\right)\right| \leq \frac{1}{\mu}\left\|\varphi_\mu^{(N)} - \varphi_\mu\right\| \left\|\eta^{(N)}\right\| + \|\zeta_\mu(\varphi_\mu)\| \left\|\eta^{(N)} - \eta\right\| \to 0$$

as $n, N \to \infty$, by the Cauchy–Schwarz and Minkowski inequalities, after recalling (4.17) and noting that $\left\|\varphi_\mu^{(N)} - \varphi_\mu\right\| \to 0$ by (B.25), $\left\|\eta^{(N)}\right\| \to \|\eta\| < \infty$, $\|\zeta_\mu(\varphi_\mu)\| < \infty$ and $\left\|\eta^{(N)} - \eta\right\| \to 0$.

4) Finally, for the non-local term, if we set $\eta = 1$ in the first part of (B.461b), then

$$\left(\varphi_\mu^{(N)}, 1\right) \to (\varphi_\mu, 1) \qquad \text{viz.} \qquad \overline{\varphi_\mu^{(N)}} \to \overline{\varphi_\mu},$$

and so (cf. (B.24))

$$\varphi_\mu^{(N)} - \overline{\varphi_\mu^{(N)}} \rightharpoonup \varphi_\mu - \overline{\varphi_\mu} \qquad \text{in} \qquad H^1(\Omega).$$

Since $(-\Delta_n)^{-1} : H^1_*(\Omega) \to H^1_*(\Omega)$ is compact, we obtain the strong convergence (cf. Theorem 4.15 of Robinson (2001))

$$(-\Delta_n)^{-1}\left(\varphi_\mu^{(N)} - \overline{\varphi_\mu^{(N)}}\right) \to (-\Delta_n)^{-1}(\varphi_\mu - \overline{\varphi_\mu}) \qquad \text{in} \qquad H^1(\Omega),$$

which implies the weak convergence (cf. Lemma 4.12 of Robinson (2001))

$$(-\Delta_n)^{-1}\left(\varphi_\mu^{(N)} - \overline{\varphi_\mu^{(N)}}\right) \rightharpoonup (-\Delta_n)^{-1}(\varphi_\mu - \overline{\varphi_\mu}) \qquad \text{in} \qquad H^1(\Omega).$$

This means that

$$\left((-\Delta_n)^{-1}\left(\varphi_\mu^{(N)} - \overline{\varphi_\mu^{(N)}}\right), \eta\right) \to \left((-\Delta_n)^{-1}(\varphi_\mu - \overline{\varphi_\mu}), \eta\right) \qquad (\text{in } \mathbb{R}) \text{ as} \qquad n \to \infty,$$

for every $\eta \in H^1(\Omega)$. The usual density argument implies that

$$\left((-\Delta_n)^{-1}\left(\varphi_\mu^{(N)} - \overline{\varphi_\mu^{(N)}}\right), \eta^{(N)}\right) \to \left((-\Delta_n)^{-1}(\varphi_\mu - \overline{\varphi_\mu}), \eta\right) \tag{B.29}$$

as $n, N \to \infty$.

Combining all of the above, we determine that

$$\varepsilon_\varphi^2(\nabla\varphi_\mu, \nabla\eta) + (\varphi_\mu, \eta) + (\zeta_\mu(\varphi_\mu), \eta) + \alpha\left((-\Delta_n)^{-1}(\varphi_\mu - \overline{\varphi_\mu}), \eta\right) = (f, \eta)$$

for any $\eta \in H^1(\Omega)$, viz. φ_μ solves $(\mathbf{S}_\mu)$ in (4.28).

vii) Having confirmed the *existence* of solutions $\varphi_\mu \in H^1(\Omega)$ of $(\mathbf{S}_\mu)$, we now establish their *uniqueness*. To this end, suppose that $\varphi_1, \varphi_2 \in H^1(\Omega)$ both solve $(\mathbf{S}_\mu)$, and define $\varphi_\mu := \varphi_1 - \varphi_2 \in H^1(\Omega)$. Substituting each of these into (4.28) and subtracting, we conclude that φ_μ must solve

$$\varepsilon_\varphi^2(\nabla\varphi_\mu, \nabla\eta) + (\varphi_\mu, \eta) + (\zeta_\mu(\varphi_1) - \zeta_\mu(\varphi_2), \eta) + \alpha\left((-\Delta_n)^{-1}(\varphi_\mu - \overline{\varphi_\mu}), \eta\right) = 0$$

for every $\eta \in H^1(\Omega)$. Setting $\eta = \varphi_1 - \varphi_2 = \varphi_\mu$ then leads to

$$\varepsilon_\varphi^2 |\varphi_\mu|_1^2 + \|\varphi_\mu\|^2 + \underbrace{(\zeta_\mu(\varphi_1) - \zeta_\mu(\varphi_2), \varphi_1 - \varphi_2)}_{\geq 0 \text{ by (4.19a)}} + \alpha \|\varphi_\mu - \overline{\varphi_\mu}\|_{-1}^2 = 0,$$

whence $\varphi_\mu \equiv 0$ i.e. the solution to $(\mathbf{S}_\mu)$ is unique.

viii) We set $\eta^{(N)} = P^N \zeta_\mu\left(\varphi_\mu^{(N)}\right)$ in (B.8), and obtain

$$\begin{aligned}\varepsilon_\varphi^2\left(\nabla\varphi_\mu^{(N)}, \nabla\zeta_\mu\left(\varphi_\mu^{(N)}\right)\right) + \left(\varphi_\mu^{(N)}, P^N\zeta_\mu\left(\varphi_\mu^{(N)}\right)\right) + \left\|P^N\zeta_\mu\left(\varphi_\mu^{(N)}\right)\right\|^2 \\ + \alpha\left((-\Delta_n)^{-1}\left(\varphi_\mu^{(N)} - \overline{\varphi_\mu^{(N)}}\right), P^N\zeta_\mu\left(\varphi_\mu^{(N)}\right)\right) = \left(f, P^N\zeta_\mu\left(\varphi_\mu^{(N)}\right)\right),\end{aligned} \tag{B.30}$$

after noting that $\nabla P^N \zeta_\mu\left(\varphi_\mu^{(N)}\right) = P^N \nabla \zeta_\mu\left(\varphi_\mu^{(N)}\right)$ so that

$$\left(\nabla\varphi_\mu^{(N)}, \nabla P^N \zeta_\mu\left(\varphi_\mu^{(N)}\right)\right) = \left(\nabla\varphi_\mu^{(N)}, \nabla\zeta_\mu\left(\varphi_\mu^{(N)}\right)\right).$$

In the first term of (B.30),

$$\varepsilon_\varphi^2\left(\nabla\varphi_\mu^{(N)}, \nabla\zeta_\mu\left(\varphi_\mu^{(N)}\right)\right) = \left(\left(\zeta_\mu'\left(\varphi_\mu^{(N)}\right)\right), \nabla\varphi_\mu^{(N)} \cdot \nabla\varphi_\mu^{(N)}\right) \geq 0 \tag{B.31}$$

after recalling (4.14b). Hence,

$$\begin{aligned}\left\|P^N\zeta_\mu\left(\varphi_\mu^{(N)}\right)\right\|^2 &\leq \left(f - \varphi_\mu^{(N)} - \alpha\left(-\Delta_n\right)^{-1}\left(\varphi_\mu^{(N)} - \overline{\varphi_\mu^{(N)}}\right), P^N\zeta_\mu\left(\varphi_\mu^{(N)}\right)\right)\\ &\leq \left(\|f\| + \left\|\varphi_\mu^{(N)}\right\| + \alpha\left\|\left(-\Delta_n\right)^{-1}\left(\varphi_\mu^{(N)} - \overline{\varphi_\mu^{(N)}}\right)\right\|\right)\left\|P^N\zeta_\mu\left(\varphi_\mu^{(N)}\right)\right\|\end{aligned}$$

by the Cauchy–Schwarz and Minkowski inequalities, and so

$$\left\|P^N\zeta_\mu\left(\varphi_\mu^{(N)}\right)\right\| \leq \|f\| + \left\|\varphi_\mu^{(N)}\right\| + \alpha\left\|\left(-\Delta_n\right)^{-1}\left(\varphi_\mu^{(N)} - \overline{\varphi_\mu^{(N)}}\right)\right\| \leq \|f\| + \left\|\varphi_\mu^{(N)}\right\| + \alpha c_P^3\left|\varphi_\mu^{(N)}\right|_1 \tag{B.32}$$

after using (A.30b).

ix) Suppose now that $\partial\Omega$ is smooth enough to satisfy the requirements of Lemma A.1.9. The eigenfunctions e_k are all in $H^2(\Omega)$ and $(\nabla e_k, \nabla v) = (-\Delta e_k, v)$ for each e_k and any $v \in H^1(\Omega)$ (as in (A.45)) which means that $\partial_n e_k|_{\partial\Omega} = 0$ and so $\partial_n\varphi_\mu^{(N)}\Big|_{\partial\Omega} = 0$ for every N, viz. $-\Delta\varphi_\mu^{(N)} = -\Delta\varphi_\mu^{(N)}$ and

$$\left(\nabla\varphi_\mu^{(N)}, \nabla\nu\right) = \left(-\Delta\varphi_\mu^{(N)}, \nu\right) \qquad \text{for every} \qquad \nu \in H^1(\Omega). \tag{B.33}$$

Using this in the first term of (B.8), we find that

$$\begin{aligned}\varepsilon_\varphi^2\left(-\Delta\varphi_\mu^{(N)}, \eta^{(N)}\right) + \left(\varphi_\mu^{(N)}, \eta^{(N)}\right) + \left(\zeta_\mu\left(\varphi_\mu^{(N)}\right), \eta^{(N)}\right)&\\ + \alpha\left(\left(-\Delta_n\right)^{-1}\left(\varphi_\mu^{(N)} - \overline{\varphi_\mu^{(N)}}\right), \eta^{(N)}\right) &= \left(f, \eta^{(N)}\right)\end{aligned} \tag{B.34}$$

for every $\eta^{(N)} \in H^1(\Omega)$. Since $H^1(\Omega)$ is dense in $L^2(\Omega)$, this also holds for every $\eta^{(N)} \in L^2(\Omega)$ (cf. our remarks about density arguments on p. 329). Hence we may set $\eta^{(N)} = -\Delta\varphi_\mu^{(N)} \in V^N$ in (B.34), and use (B.33) in the second term, to get

$$\begin{aligned}\varepsilon_\varphi^2\left\|-\Delta\varphi_\mu^{(N)}\right\|^2 + \underbrace{\frac{\chi^{AB}}{2}\left|\varphi_\mu^{(N)}\right|_1^2}_{\geq 0} + \left(P^N\zeta_\mu\left(\varphi_\mu^{(N)}\right), -\Delta\varphi_\mu^{(N)}\right)&\\ + \alpha\left(\left(-\Delta_n\right)^{-1}\left(\varphi_\mu^{(N)} - \overline{\varphi_\mu^{(N)}}\right), -\Delta\varphi_\mu^{(N)}\right) &= \left(f, -\Delta\varphi_\mu^{(N)}\right).\end{aligned}$$

If we rearrange, make repeated use of the Cauchy–Schwarz inequality and (A.30b), and then divide through by $\left\|-\Delta\varphi_\mu^{(N)}\right\|$, we can use (B.32) to see that[9]

$$\varepsilon_\varphi^2\left\|-\Delta\varphi_\mu^{(N)}\right\| \leq \left\|P^N\zeta_\mu\left(\varphi_\mu^{(N)}\right)\right\| + \alpha c_P^3\left|\varphi_\mu^{(N)}\right|_1 + \|f\| \leq 2\|f\| + \left\|\varphi_\mu^{(N)}\right\| + 2\alpha c_P^3\left|\varphi_\mu^{(N)}\right|_1 \leq C, \tag{B.35}$$

independent of N and μ by the bound in (B.23) and the fact that f is arbitrary. Now since we assumed additional smoothness on $\partial\Omega$, (A.42) holds for each $\varphi_\mu^{(N)}$ as a linear combination of $H^2(\Omega)$ eigenfunctions. It follows that

$$\left\|\varphi_\mu^{(N)}\right\|_2 \leq C\left\|-\Delta\varphi_\mu^{(N)}\right\| \leq C \tag{B.36}$$

independent of N and μ, and so the sequence of Galerkin approximations $\left(\varphi_\mu^{(N)}\right)$ is bounded uniformly in $H^2(\Omega)$. Hence there exists a sub-sequence of the $H^1(\Omega)$ sub-sequence $\left(\varphi_\mu^{(N)}\right)$ in (B.24), and a $\varphi_\mu \in H^2(\Omega)$ (limits are unique) for which

$$\varphi_\mu^{(N)} \rightharpoonup \varphi_\mu \qquad \text{in} \qquad H^2(\Omega). \tag{B.37}$$

x) We establish the BC on φ_μ. Starting from (B.33), we see that

$$\left(\nabla\varphi_\mu^{(N)}, \nabla\nu\right) \to (\nabla\varphi_\mu, \nabla\nu) \qquad \text{and} \qquad \left(-\Delta\varphi_\mu^{(N)}, \nu\right) \to (-\Delta\varphi_\mu, \nu) \tag{B.38}$$

for every $\nu \in H^1(\Omega)$ by the weak convergences (B.24), (B.37), and the fact that $H^2(\Omega) \subset H^1(\Omega) \subset L^2(\Omega) = \left(L^2(\Omega)\right)' \subset \left(H^1(\Omega)\right)' \subset \left(H^2(\Omega)\right)'$. Therefore,

$$(\nabla\varphi_\mu, \nabla\nu) = (-\Delta\varphi_\mu, \nu) \qquad \text{for every} \qquad \nu \in H^1(\Omega) \qquad \Rightarrow \qquad \partial_n\varphi_\mu|_{\partial\Omega} = 0, \tag{B.39}$$

(in the sense of trace). For sufficiently smooth Ω, we may thus replace (4.28) with

$$\varepsilon_\varphi^2 (-\Delta\varphi_\mu, \eta) + (\varphi_\mu, \eta) + (\zeta_\mu(\varphi_\mu), \eta) + \alpha\left((-\Delta_n)^{-1}(\varphi_\mu - \overline{\varphi_\mu}), \eta\right) = (f, \eta) \tag{B.40}$$

for every $\eta \in H^1(\Omega)$, and since $H^1(\Omega)$ is dense in $L^2(\Omega)$, the usual density argument (see p. 329) implies that (B.40) holds for every $\eta \in L^2(\Omega)$.

□

B.5 Proof of Theorem 4.2.5

Proof. We mimic parts of the proof of Lemma 3.2 of Blowey and Elliott (1991).

i) Consider the sequence (φ_μ) of solutions of $(\mathbf{S}_\mu)$ as $\mu \downarrow 0$. In the previous Lemma we established the bound (B.23) independent of μ, which means that (φ_μ) is uniformly bounded (independent of μ) in $H^1(\Omega)$. We thus infer the existence of $\varphi \in H^1(\Omega)$ and a sub-sequence (also labelled) (φ_μ) for which (cf. (B.24))

$$\varphi_\mu \rightharpoonup \varphi \qquad \text{in} \qquad H^1(\Omega) \qquad \text{as } \mu \downarrow 0. \tag{B.41}$$

As in (B.25), we take a further sub-sequence in which

$$\varphi_\mu \to \varphi \qquad \text{(strongly) in} \qquad L^2(\Omega) \qquad \text{as } \mu \downarrow 0. \tag{B.42}$$

We pass to the limit in each term on the left of (4.28); in the first and second,

$$(\nabla\varphi_\mu, \nabla\eta) \xrightarrow[\mu\downarrow 0]{} (\nabla\varphi, \nabla\eta) \qquad \text{and} \qquad (\varphi_\mu, \eta) \xrightarrow[\mu\downarrow 0]{} (\varphi, \eta)$$

for every $\eta \in H^1(\Omega)$. For the non-local term, we argue as we did in the lead-up to (B.29) to conclude that

$$\left((-\Delta_n)^{-1}(\varphi_\mu - \overline{\varphi_\mu}), \eta\right) \to \left((-\Delta_n)^{-1}(\varphi - \overline{\varphi}), \eta\right) \tag{B.43}$$

for every $\eta \in H^1(\Omega)$ as $\mu \downarrow 0$. Finally, for the penalty term, we modify the argument in (2.48)–(2.52) of Blowey and Elliott (1991). Setting $\eta = \mu\zeta_\mu(\varphi_\mu) = \zeta(\varphi_\mu) \in H^1(\Omega)$ (cf. (4.20a)) in (4.28) yields

$$\begin{aligned}\varepsilon_\varphi^2 (\nabla\varphi_\mu, \nabla\zeta(\varphi_\mu)) + \mu\|\zeta_\mu(\varphi_\mu)\|^2 &= \left(f - \varphi_\mu - \alpha(-\Delta_n)^{-1}(\varphi_\mu - \overline{\varphi_\mu}), \mu\zeta_\mu(\varphi_\mu)\right) \\ &\le \left(\|f\| + \|\varphi_\mu\| + \alpha\left\|(-\Delta_n)^{-1}(\varphi_\mu - \overline{\varphi_\mu})\right\|\right)\|\mu\zeta_\mu(\varphi_\mu)\|\end{aligned} \tag{B.44}$$

by the Cauchy–Schwarz inequality. Consider the first term on the left: by (4.14b), $0 \leq \mu\zeta_\mu' \leq 1$, and so[10]

$$(\nabla\varphi_\mu, \nabla\zeta(\varphi_\mu)) = \int_\Omega \mu\zeta_\mu'(\varphi_\mu)\nabla\varphi_\mu \cdot \nabla\varphi_\mu \,\mathrm{d}\Omega \geq \int_\Omega \left(\mu\zeta_\mu'(\varphi_\mu)\right)^2 \nabla\varphi_\mu \cdot \nabla\varphi_\mu \,\mathrm{d}\Omega$$
$$= |\mu\zeta_\mu(\varphi_\mu)|_1^2 = |\zeta(\varphi_\mu)|_1^2 \geq 0. \quad \text{(B.45)}$$

We therefore discard this term. We find that $\left\|(-\Delta_n)^{-1}(\varphi_\mu - \overline{\varphi_\mu})\right\| \leq c_P^3 |\varphi_\mu|_1$ using (A.30b), and so

$$\mu\|\zeta_\mu(\varphi_\mu)\|^2 \leq \underbrace{\left(\|f\| + \|\varphi_\mu\| + \alpha c_P^3 |\varphi_\mu|_1\right)}_{\leq C} \|\mu\zeta_\mu(\varphi_\mu)\| \leq C\mu + \frac{\mu}{2}\|\zeta_\mu(\varphi_\mu)\|^2$$

in which C is μ-independent by the bound in (B.23), and where we used Young's inequality. In particular,[11]

$$\|\zeta_\mu(\varphi_\mu)\|^2 \leq C \qquad \Rightarrow \qquad \|\zeta(\varphi_\mu)\| \leq C\mu \quad \text{(B.46)}$$

by (4.20a). As a result, using the strong convergence in (B.42),

$$\lim_{\mu\downarrow 0}\|\zeta(\varphi_\mu)\| = \|\zeta(\varphi)\| = 0 \qquad \Rightarrow \qquad \zeta(\varphi) = 0 \quad \text{a.e.} \quad \text{(B.47)}$$

The implication is that $|\varphi| \leq 1$ a.e. i.e. $\varphi \in \mathscr{A}$, which establishes (4.31a). From this and (4.28) we conclude that

$$\varepsilon_\varphi^2(\nabla\varphi, \nabla\eta) + (\varphi, \eta) + \alpha\left((-\Delta_n)^{-1}(\varphi - \overline{\varphi}), \eta\right) = (f, \eta)$$

for every $\eta \in H^1(\Omega)$. Setting $\eta = 1$, and recalling that $\overline{(-\Delta_n)^{-1}(\varphi - \overline{\varphi})} = 0$, gives

$$(\varphi, 1) = (f, 1) \qquad \Rightarrow \qquad \overline{\varphi} = m$$

since $f \in \mathscr{A}_m$. Hence, $\varphi \in \mathscr{A}_m$, which confirms (4.31b).

ii) We now return to (4.28) and set $\eta = \psi - \varphi_\mu$ for arbitrary $\psi \in \mathscr{A}$ (so that $\zeta_\mu(\psi) = 0$). Upon rearranging terms, we discover that

$$\varepsilon_\varphi^2(\nabla\varphi_\mu, \nabla\psi - \varphi_\mu) + (\varphi_\mu, \psi - \varphi_\mu) + \alpha\left((-\Delta_n)^{-1}(\varphi_\mu - \overline{\varphi_\mu}), \psi - \varphi_\mu\right)$$
$$= (f, \psi - \varphi_\mu) + (\zeta_\mu(\varphi_\mu) - \zeta_\mu(\psi), \varphi_\mu - \psi) \geq (f, \psi - \varphi_\mu),$$

for any $\psi \in \mathscr{A}$, since $(\zeta_\mu(\varphi_\mu) - \zeta_\mu(\psi), \varphi_\mu - \psi) \geq 0$ by (4.19a). Using our weak convergence results for $\varphi_\mu \rightharpoonup \varphi$ in this inequality, we conclude that $\varphi \in \mathscr{A}_m$ satisfies[12]

$$\varepsilon_\varphi^2(\nabla\varphi, \nabla\psi - \nabla\varphi) + (\varphi, \psi - \varphi) + \alpha\left((-\Delta_n)^{-1}(\varphi - \overline{\varphi}), \psi - \varphi\right) \geq (f, \psi - \varphi), \quad \text{(B.48)}$$

for every $\psi \in \mathscr{A}$ and given $f \in \mathscr{A}_m$. We therefore set

$$f = \left(1 + \frac{\chi^{AB}}{2}\right)\varphi + \lambda \in \mathscr{A}_m(\Omega), \quad \text{(B.49)}$$

and substitute this into (B.48) to find that $\varphi \in \mathscr{A}_m$ satisfies

$$\varepsilon_\varphi^2(\nabla\varphi, \nabla\psi - \nabla\varphi) - \frac{\chi^{AB}}{2}(\varphi, \psi - \varphi) - \lambda(1, \psi - \varphi) + \alpha\left((-\Delta_n)^{-1}(\varphi - \overline{\varphi}), \psi - \varphi\right) \geq 0,$$

for every $\psi \in \mathscr{A}$. This means that $\{\varphi, \lambda\} \in \mathscr{A}_m \times \mathbb{R}$ solves (**S**) in (4.27a).

Remark. Since $f \in \mathscr{A}_m$, integrating (B.49) yields

$$\overline{f} = \left(1 + \frac{\chi^{AB}}{2}\right)\overline{\varphi} + \lambda\,|\Omega| \qquad \Rightarrow \qquad \lambda = -\frac{\chi^{AB}}{2\,|\Omega|}m. \tag{B.50}$$

iii) Suppose now that $\partial\Omega$ is smooth enough to satisfy the requirements of Lemma A.1.9 and that $f \in H^2(\Omega)$. This means we can work with (B.40) or (4.28).

From the μ-independent $H^2(\Omega)$ bound in (B.36), we infer the existence of $\varphi \in H^2(\Omega)$ and a subsequence of (φ_μ) in (B.41) with (cf. (B.37))

$$\varphi_\mu \rightharpoonup \varphi \qquad \text{in} \qquad H^2(\Omega) \qquad \text{as } \mu \downarrow 0 \tag{B.51}$$

after recalling that limits are unique. The BC (4.29) on $\varphi \in H^2(\Omega)$ follows by the reasoning we used in (B.38)–(B.39). Hence,

$$(\nabla\varphi, \nabla\nu) = (-\Delta\varphi, \nu) \qquad \text{for every} \qquad \nu \in H^1(\Omega). \tag{B.52}$$

iv) We establish the regularity of candidate minimisers. As in Lemma 3.2 of Blowey and Elliott (1991), we set $\eta^{(N)} = (\zeta_\mu(\varphi_\mu))^{p-1} \in H^1(\Omega)$ for $p \geq 2$ and even in (4.28), and obtain

$$\begin{aligned}\varepsilon_\varphi^2\left(\nabla\varphi_\mu, \nabla\left(\zeta_\mu(\varphi_\mu)\right)^{p-1}\right) + \frac{\chi^{AB}}{2}\left(\varphi_\mu, (\zeta_\mu(\varphi_\mu))^{p-1}\right) + \|\zeta_\mu(\varphi_\mu)\|_{0,p}^p \\ + \alpha\left((-\Delta_n)^{-1}(\varphi_\mu - \overline{\varphi_\mu}), (\zeta_\mu(\varphi_\mu))^{p-1}\right) = \left(f, (\zeta_\mu(\varphi_\mu))^{p-1}\right),\end{aligned} \tag{B.53}$$

after noting that $\left(\zeta_\mu(\varphi_\mu), (\zeta_\mu(\varphi_\mu))^{p-1}\right) = \|\zeta_\mu(\varphi_\mu)\|_{0,p}^p$. In the first term (cf. (B.31)),

$$\left(\nabla\varphi_\mu, \nabla\left(\zeta_\mu(\varphi_\mu)\right)^{p-1}\right) = (p-1)\int_\Omega (\zeta_\mu(\varphi_\mu))^{p-2}\left(\zeta_\mu'(\varphi_\mu)\right)\nabla\varphi_\mu \cdot \nabla\varphi_\mu \,\mathrm{d}\Omega \geq 0$$

by (4.14b) and the fact that $p \geq 2$, even $\Rightarrow p-2$ even and $(\zeta_\mu(\varphi_\mu))^{p-2} \geq 0$. Hence, we discard the first term on the left of (B.53), rearrange to discover that

$$\begin{aligned}\|\zeta_\mu(\varphi_\mu)\|_{0,p}^p &\leq \left(f - \frac{\chi^{AB}}{2}\varphi_\mu - \alpha(-\Delta_n)^{-1}(\varphi_\mu - \overline{\varphi_\mu}), (\zeta_\mu(\varphi_\mu))^{p-1}\right) \\ &\leq \left\|f - \frac{\chi^{AB}}{2}\varphi_\mu - \alpha(-\Delta_n)^{-1}(\varphi_\mu - \overline{\varphi_\mu})\right\|_{0,p} \left\|(\zeta_\mu(\varphi_\mu))^{p-1}\right\|_{0,q} \\ &\leq \left(\|f\|_{0,p} + \frac{\chi^{AB}}{2}\|\varphi_\mu\|_{0,p} + \alpha\left\|(-\Delta_n)^{-1}(\varphi_\mu - \overline{\varphi_\mu})\right\|_{0,p}\right)\|\zeta_\mu(\varphi_\mu)\|_{0,p}^{p-1},\end{aligned} \tag{B.54}$$

after using Hölders inequality (Lemma 1.9 of Robinson (2001)) with (p,q) a conjugate pair, and then Minkowski's inequality and the fact that, for (p,q) a conjugate pair,[13]

$$\left\|g^{p-1}\right\|_{0,q} = \left(\int_\Omega g^{(p-1)q}\,\mathrm{d}\Omega\right)^{1/q} = \left(\int_\Omega g^p\,\mathrm{d}\Omega\right)^{(p-1)/p} = \|g\|_{0,p}^{p-1}.$$

For the non-local term, (A.32a) and the Minkowski inequality imply that

$$\left\|(-\Delta_n)^{-1}(\varphi_\mu - \overline{\varphi_\mu})\right\|_{0,p} \leq c_P^2\,\|\varphi_\mu - \overline{\varphi_\mu}\|_{0,p} \leq c_P^2\left(\|\varphi_\mu\|_{0,p} + \overline{\varphi_\mu}\,|\Omega|^{1/p}\right).$$

For the stationary problem, we do not know $\overline{\varphi_\mu}$ precisely, but we do know that

$$\int_\Omega \varphi_\mu\,\mathrm{d}\Omega \leq \left|\int_\Omega \varphi_\mu\,\mathrm{d}\Omega\right| \leq \int_\Omega |\varphi_\mu|\,\mathrm{d}\Omega = \|\varphi_\mu\|_{0,1} \leq C\,\|\varphi_\mu\|_{0,p}$$

for any $p > 0$. Hence,

$$\left\|(-\Delta_n)^{-1}(\varphi_\mu - \overline{\varphi_\mu})\right\|_{0,p} \leq C \|\varphi_\mu\|_{0,p} \tag{B.55}$$

with C μ-independent. If we divide (B.54) through by $\|\zeta_\mu(\varphi_\mu)\|_{0,p}^{p-1}$ and use (B.55),

$$\|\zeta_\mu(\varphi_\mu)\|_{0,p} \leq \|f\|_{0,p} + C \|\varphi_\mu\|_{0,p} \tag{B.56}$$

with both constants C independent of μ. By assumption, $f \in H^2(\Omega) \hookrightarrow L^p(\Omega)$ for every $1 \leq p \leq \infty$ and $d \leq 3$ by Sobolev imbedding (A.34), and so $f \in L^p(\Omega)$ with $\|f\|_{0,p} \leq C$ independent of μ. Likewise, by (B.37) $\varphi_\mu \in H^2(\Omega) \hookrightarrow L^p(\Omega)$ and so $\|\varphi_\mu\|_{0,p} \leq C \|\varphi_\mu\|_2 \leq C$, independent of μ. It follows that

$$\|\zeta_\mu(\varphi_\mu)\|_{0,p} \leq C \qquad \text{for every} \qquad 1 \leq p \leq \infty \qquad \text{and} \qquad d = 1, 2, 3$$

independent of μ.

v) We now substitute $\eta = (-\Delta\varphi_\mu)^{p-1} \in L^2(\Omega)$ for $p \geq 2$ and even into (B.40) and conclude that (cf. (B.35))

$$\varepsilon_\varphi^2 \left(-\Delta\varphi_\mu, (-\Delta\varphi_\mu)^{p-1}\right) + \left(\varphi_\mu, (-\Delta\varphi_\mu)^{p-1}\right) + \left(\zeta_\mu(\varphi_\mu), (-\Delta\varphi_\mu)^{p-1}\right) + \alpha \left((-\Delta_n)^{-1}(\varphi_\mu - \overline{\varphi_\mu}), (-\Delta\varphi_\mu)^{p-1}\right) = \left(f, (-\Delta\varphi_\mu)^{p-1}\right).$$

Now $\left(-\Delta\varphi_\mu, (-\Delta\varphi_\mu)^{p-1}\right) = \|-\Delta\varphi_\mu\|_{0,p}^p$ and so, as in (B.54) and using (B.55),

$$\begin{aligned} \varepsilon_\varphi^2 \|-\Delta\varphi_\mu\|_{0,p}^p &= \left(f - \varphi_\mu - \zeta_\mu(\varphi_\mu) - \alpha(-\Delta_n)^{-1}(\varphi_\mu - \overline{\varphi_\mu}), (-\Delta\varphi_\mu)^{p-1}\right) \\ &\leq \left(\|f\|_{0,p} + C\|\varphi_\mu\|_{0,p} + \|\zeta_\mu(\varphi_\mu)\|_{0,p}\right) \|-\Delta\varphi_\mu\|_{0,p}^{p-1}. \end{aligned}$$

As a result of (B.56) and the fact that $\|f\|_{0,p}$ and $\|\varphi_\mu\|_{0,p}$ are bounded independent of μ,

$$\|-\Delta\varphi_\mu\|_{0,p} \leq C \qquad \text{for any even } p \geq 2 \tag{B.57}$$

independent of μ. We showed at the end of the proof of Lemma 4.2.4, that φ_μ is the unique solution of

$$\varepsilon_\varphi^2 (-\Delta)\varphi_\mu = -\varphi_\mu - \zeta_\mu(\varphi_\mu) - \alpha(-\Delta_n)^{-1}(\varphi_\mu - \overline{\varphi_\mu}) + f \in L^p(\Omega),$$

by a rearrangement of (B.40) and our notes above. The implication is that

$$\|\varphi_\mu\|_{2,p} \leq C \qquad \text{for any even } p \geq 2 \tag{B.58}$$

independent of μ, by elliptic regularity (cf. (A.44)). Hence the sequence (φ_μ) is bounded uniformly in every such $W^{2,p}(\Omega)$, each of which is a reflexive Banach space.[14] By reflexive weak compactness (cf. Corollary 4.19 of Robinson (2001)), we infer the existence of $\varphi \in W^{2,p}(\Omega)$ such that (φ_μ) has a set of sub-sequences (also labelled) (φ_μ) with

$$\varphi_\mu \rightharpoonup \varphi \qquad \text{in each} \qquad W^{2,p}(\Omega) \qquad 2 \leq p < \infty \text{ and even} \qquad \text{as } \mu \downarrow 0. \tag{B.59}$$

Hence $\varphi \in W^{2,p}(\Omega)$ for every finite, even p. For $|\Omega| < \infty$, $L^q(\Omega) \hookrightarrow L^p(\Omega)$ for $1 \leq p \leq q < \infty$ (cf. Theorem 2.14 of Adams and Fournier (2003)) and so $\varphi \in W^{2,p}(\Omega)$ for every finite, *odd* p too, which establishes the first part of (4.32).

vi) The second part of (4.32), viz. $C^{1,\alpha}\left(\overline{\Omega}\right)$ continuity, follows from the above by Sobolev imbedding, as noted in Lemma A.1.8.

□

B.6 Proof of Lemma 4.2.6

Proof. Our proof draws heavily on Section 8.4.2 of Evans (1998).

i) That Ω_{AB} is open follows from the continuity of φ.

ii) We now vary the variational inequality (which holds a.e. in Ω) by a non-negative (non-positive) smooth variation with compact support in the pure phase B (A) regions.

Consider the non-negative variation $\eta \in C_c^\infty(\underline{B})$ i.e. having $\eta(x) > 0$ for $x \in \underline{B}$ only. Notice that, necessarily, $\overline{\eta}_{(\underline{B})}, \overline{\eta} > 0$ for all such functions. If $0 < \theta \leq 1$, then $\psi := \varphi + \theta\eta \in \mathscr{A}$ for sufficiently small θ. Substituting into the variational inequality (4.26), we conclude that

$$\theta \int_\Omega \varepsilon_\varphi^2 (\nabla\varphi \cdot \nabla\eta) - \frac{\chi^{AB}}{2}\varphi\eta - \lambda\eta + \alpha(\eta - \overline{\eta})\left((-\Delta_n)^{-1}(\varphi - \overline{\varphi})\right) \mathrm{d}\Omega \geq 0$$

for any sufficiently small θ, and from this we deduce that

$$\int_\Omega \varepsilon_\varphi^2 (\nabla\varphi \cdot \nabla\eta) - \frac{\chi^{AB}}{2}\varphi\eta - \lambda\eta + \alpha\eta\left((-\Delta_n)^{-1}(\varphi - \overline{\varphi})\right) \mathrm{d}\Omega \geq \alpha\overline{\eta}\int_\Omega \left((-\Delta_n)^{-1}(\varphi - \overline{\varphi})\right) \mathrm{d}\Omega = 0$$

for any non-negative $\eta \in C_c^\infty(\underline{B})$ as above, where we have used (2.9b). The regularity we established in Lemma 4.2.5 means that we can integrate by parts in the first term above to obtain

$$\varepsilon_\varphi^2 \int_\Omega (\nabla\varphi \cdot \nabla\eta) \ \mathrm{d}\Omega = \varepsilon_\varphi^2 \left(\oint_{\partial\Omega} \eta \ (\partial_n \varphi) \, \mathrm{d}S + \int_\Omega \eta(-\Delta)\varphi \ \mathrm{d}\Omega \right) = \varepsilon_\varphi^2 \int_{\Omega_{\underline{B}}} \eta(-\Delta)\varphi \ \mathrm{d}\Omega \tag{B.60}$$

for every $\eta \in C_c^\infty(\underline{B})$ by virtue of the BC on φ and the compact support and smoothness of each η in $\Omega_{\underline{B}}$. By the same properties of each η, we conclude that

$$\int_{\Omega_{\underline{B}}} \eta \left(\varepsilon_\varphi^2(-\Delta\varphi) - \frac{\chi^{AB}}{2}\varphi - \lambda + \alpha(-\Delta_n)^{-1}(\varphi - \overline{\varphi}) \right) \mathrm{d}\Omega \geq 0 \tag{B.61}$$

for all non-negative functions $\eta \in C_c^\infty(\underline{B})$ as above; viz.

$$\varepsilon_\varphi^2(-\Delta\varphi) - \frac{\chi^{AB}}{2}\varphi - \lambda + \alpha(-\Delta_n)^{-1}(\varphi - \overline{\varphi}) \geq 0 \quad \text{a.e. in } \underline{B}. \tag{B.62a}$$

Repeating the argument above for the *non-positive* variations $\eta \in C_c^\infty(\overline{A})$, leads to

$$\varepsilon_\varphi^2(-\Delta\varphi) - \frac{\chi^{AB}}{2}\varphi - \lambda + \alpha(-\Delta_n)^{-1}(\varphi - \overline{\varphi}) \leq 0 \quad \text{a.e. in } \overline{A}. \tag{B.62b}$$

iii) Now, fix any test function $\eta \in C_c^\infty(\Omega_{AB})$ (a smooth function with compact support in Ω_{AB} that can be positive or negative), define $\psi := \varphi + \theta\eta$ (i.e. the minimiser φ with a smooth variation in Ω_{AB}). For $|\theta|$ small enough,

$$|\psi| = |\varphi + \theta\eta| \leq 1,$$

whence $\psi \in \mathscr{A}$ (the variation is smooth and is sufficiently small that ψ is admissible). Substituting this ψ into the variational inequality (4.26) leads to

$$\theta \int_\Omega \varepsilon_\varphi^2 (\nabla\varphi \cdot \nabla\eta) - \frac{\chi^{AB}}{2}\varphi\eta - \lambda\eta + \alpha\eta\left((-\Delta_n)^{-1}(\varphi - \overline{\varphi})\right) \mathrm{d}\Omega \geq \theta\alpha\overline{\eta}\int_\Omega \left((-\Delta_n)^{-1}(\varphi - \overline{\varphi})\right) \mathrm{d}\Omega = 0,$$

where we used (2.9b) once again. Notice that θ can be positive or negative and arbitrarily small in magnitude and thus we conclude that, for all such variations $\eta \in C_c^\infty(\Omega_{AB})$,

$$\int_\Omega \varepsilon_\varphi^2 (\nabla\varphi \cdot \nabla\eta) - \frac{\chi^{AB}}{2}\varphi\eta - \lambda\eta + \alpha\eta\left((-\Delta_n)^{-1}(\varphi - \overline{\varphi})\right) \mathrm{d}\Omega = 0.$$

At this stage, we integrate by parts in the first term above again to obtain

$$\varepsilon_\varphi^2 \int_\Omega (\nabla\varphi \cdot \nabla\eta)\ \mathrm{d}\Omega = \varepsilon_\varphi^2 \int_\Omega \eta\,(-\Delta)\,\varphi\ \mathrm{d}\Omega = \varepsilon_\varphi^2 \int_{\Omega_{AB}} \eta\,(-\Delta)\,\varphi\ \mathrm{d}\Omega$$

for every $\eta \in C_c^\infty(\Omega_{AB})$ because $\partial_n\varphi$ is zero on $\partial\Omega$ and each η has compact support in Ω_{AB}. Hence,[15]

$$\varepsilon_\varphi^2\,(-\Delta)\,\varphi - \frac{\chi^{AB}}{2}\varphi + \alpha\,(-\Delta_n)^{-1}\,(\varphi - \overline{\varphi}) = \lambda \qquad \text{a.e. in } \Omega_{AB}. \tag{B.63}$$

Combining (B.62) and (B.63), we conclude that, a.e. in Ω,

$$|\varphi| \le 1, \qquad -\mathrm{sign}\,(\varphi)\left(\varepsilon_\varphi^2\,(-\Delta\varphi) - \frac{\chi^{AB}}{2}\varphi - \lambda + \alpha\,(-\Delta_n)^{-1}\,(\varphi - \overline{\varphi})\right) \ge 0$$

which is (4.34a).[16]

iv) (4.34b) follows from (B.63) and our definition of the sets in (4.3).

v) For the Lagrange parameter, observe that for a minimiser, φ,

$$0 = \oint_{\partial\Omega} \partial_n\varphi\ \mathrm{d}S = \int_\Omega -\Delta\varphi\ \mathrm{d}\Omega = \int_{\Omega_{AB}\cup\Omega_{\overline{A}}\cup\Omega_{\underline{B}}} -\Delta\varphi\ \mathrm{d}\Omega = \int_{\Omega_{AB}} -\Delta\varphi\ \mathrm{d}\Omega,$$

since $\varphi(x) = \pm 1$ on $\Omega_{\overline{A}} \cup \Omega_{\underline{B}}$ means that $-\Delta\varphi = 0$ (φ is constant) in these regions. Consequently, if we integrate (B.63) over Ω_{AB}, we obtain (4.34c).[17]

□

B.7 Proof of Lemma 4.2.7

Proof. We adapt the proof of Proposition 3.3 of Blowey and Elliott (1991).

i) If $\{\varphi, \lambda\}$ solves (**S**), then φ solves ($\mathbf{S}_C$).[18] To see this, suppose (**S**) holds for $\{\varphi, \lambda\} \in \mathscr{A}_m \times \mathbb{R}$, and select any $\psi \in \mathscr{A}_m \subset \mathscr{A}$. For any such function,

$$\lambda\,(1, \psi - \varphi) = \lambda\,|\Omega|\,(m - m) = 0,$$

since $\overline{\psi} = \overline{\varphi} = m$, and (4.27a) reduces to (4.27b); that is ($\mathbf{S}_C$) holds for φ.

ii) Conversely, suppose $\varphi \in \mathscr{A}_m$ satisfies ($\mathbf{S}_C$) in (4.27b), that is, for every $\psi \in \mathscr{A}_m$,

$$\varepsilon_\varphi^2\,(\nabla\varphi, \nabla\,(\psi - \varphi)) + \frac{\chi^{AB}}{2}\,(\varphi, \psi - \varphi) + \alpha\left((-\Delta_n)^{-1}\,(\varphi - \overline{\varphi})\,, \psi - \varphi\right) \ge \chi^{AB}\,(\varphi, \psi - \varphi)\,. \tag{B.64}$$

iii) Consider the problem:[19]

$\left(\widehat{\mathbf{S}}_\delta\right)$: given $\delta \in \left[\frac{-3}{2}\chi^{AB}, \frac{3}{2}\chi^{AB}\right]$ and φ (the red is deliberate) satisfying (B.64), find $\varphi_\delta \in \mathscr{A}$ with

$$\widetilde{\varepsilon_\varphi}^2\,(\nabla\varphi_\delta, \nabla\,(\eta - \varphi_\delta)) + (\varphi_\delta, \eta - \varphi_\delta) + \widetilde{\alpha}\left((-\Delta_n)^{-1}\,(\varphi_\delta - \overline{\varphi_\delta})\,, \eta - \varphi_\delta\right)$$
$$\ge (2\varphi, \eta - \varphi_\delta) + \frac{2\delta}{\chi^{AB}}\,(1, \eta - \varphi_\delta)\,, \tag{B.65a}$$

for every $\eta \in \mathscr{A}$, where we have defined

$$\widetilde{\varepsilon_\varphi}^2 := \frac{2\varepsilon_\varphi^2}{\chi^{AB}} > 0 \qquad \text{and} \qquad \widetilde{\alpha} := \frac{2\alpha}{\chi^{AB}} > 0. \tag{B.65b}$$

This problem has a unique solution by Lemma 4.2.4 (see Appendix B.4). $\left(\widehat{\mathbf{S}}_\delta\right)$ is essentially identical to problem ($\mathbf{S}_\mu$) in (4.28), with f in that result replaced here by $2\varphi + \frac{2\delta}{\chi^{AB}}$.

iv) Define the solution mass function

$$\mathbb{M} : \left[\frac{-3}{2}\chi^{AB}, \frac{3}{2}\chi^{AB}\right] \mapsto \mathbb{R} \qquad \text{by} \qquad \mathbb{M}(\delta) = \overline{\varphi_\delta} \tag{B.66}$$

for φ_δ solving $\left(\widehat{\mathbf{S}}_\delta\right)$.

Claim: $\mathbb{M}$ in (B.66) is monotone and continuous.

Proof. Let $\delta_1, \delta_2 \in \left[\frac{-3}{2}\chi^{AB}, \frac{3}{2}\chi^{AB}\right]$ correspond to $\varphi_1, \varphi_2 \in \mathscr{A}$ solving (B.65). Setting $\delta = \delta_1$, $\eta = \varphi_2$ in (B.65) leads to

$$\widetilde{\varepsilon_\varphi}^2 \left(\nabla\varphi_1, \nabla\left(\varphi_2 - \varphi_1\right)\right) + \left(\varphi_1, \varphi_2 - \varphi_1\right) + \widetilde{\alpha}\left(\left(-\Delta_n\right)^{-1}\left(\varphi_1 - \overline{\varphi_1}\right), \varphi_2 - \varphi_1\right) \\ \geq \left(2\varphi, \varphi_2 - \varphi_1\right) + \frac{2\delta_1}{\chi^{AB}}\left(1, \varphi_2 - \varphi_1\right).$$

Similarly, if $\delta = \delta_2$ and $\eta = \varphi_1$, then

$$\widetilde{\varepsilon_\varphi}^2 \left(\nabla\varphi_2, \nabla\left(\varphi_1 - \varphi_2\right)\right) + \left(\varphi_2, \varphi_1 - \varphi_2\right) + \widetilde{\alpha}\left(\left(-\Delta_n\right)^{-1}\left(\varphi_2 - \overline{\varphi_2}\right), \varphi_1 - \varphi_2\right) \\ \geq \left(2\varphi, \varphi_1 - \varphi_2\right) + \frac{2\delta_2}{\chi^{AB}}\left(1, \varphi_1 - \varphi_2\right).$$

Adding these gives[20]

$$\left\|\varphi_1 - \varphi_2\right\|^2 \leq \frac{2\left|\Omega\right|}{\chi^{AB}}\left(\mathbb{M}(\delta_1) - \mathbb{M}(\delta_2)\right)\left(\delta_1 - \delta_2\right), \tag{B.67}$$

since $\left|\Omega\right|\mathbb{M}(\delta_1) = (\varphi_1, 1)$, $\left|\Omega\right|\mathbb{M}(\delta_2) = (\varphi_2, 1)$, after repeatedly using

$$\overline{\left(-\Delta_n\right)^{-1}\left(\varphi_1 - \overline{\varphi_1}\right)} = \overline{\left(-\Delta_n\right)^{-1}\left(\varphi_2 - \overline{\varphi_2}\right)} = 0,$$

and then discarding

$$\widetilde{\varepsilon_\varphi}^2 \left|\varphi_1 - \varphi_2\right|_1^2 + \widetilde{\alpha}\left\|\varphi_1 - \varphi_2 - \overline{\varphi_1 - \varphi_2}\right\|_{-1}^2 \geq 0,$$

on the left. By the definition of $\mathbb{M}$ in (B.66) and the Cauchy–Schwarz inequality,

$$\left(\mathbb{M}(\delta_1) - \mathbb{M}(\delta_2)\right)^2 = \frac{1}{\left|\Omega\right|^2}\left(\varphi_1 - \varphi_2, 1\right)^2 \leq \frac{1}{\left|\Omega\right|}\left\|\varphi_1 - \varphi_2\right\|^2,$$

and so in combination with (B.67), we determine that

$$0 \leq \left|\Omega\right|\left(\mathbb{M}(\delta_1) - \mathbb{M}(\delta_2)\right)^2 \leq \left\|\varphi_1 - \varphi_2\right\|^2 \leq \frac{2\left|\Omega\right|}{\chi^{AB}}\left(\mathbb{M}(\delta_1) - \mathbb{M}(\delta_2)\right)\left(\delta_1 - \delta_2\right).$$

Consequently

$$\left|\mathbb{M}(\delta_1) - \mathbb{M}(\delta_2)\right| \leq \frac{2}{\chi^{AB}}\left|\delta_1 - \delta_2\right|, \tag{B.68a}$$

which shows that $\mathbb{M}$ is **continuous**, since $\left|\delta_1 - \delta_2\right| \to 0$ implies $\left|\mathbb{M}(\delta_1) - \mathbb{M}(\delta_2)\right| \to 0$. Moreover,

$$\left(\mathbb{M}(\delta_1) - \mathbb{M}(\delta_2)\right)\left(\delta_1 - \delta_2\right) \geq 0, \tag{B.68b}$$

for any δ_1, δ_2, which implies that $\mathbb{M}$ is **monotone** (non-decreasing).

□

v) If we put $\delta = \frac{3}{2}\chi^{AB}$ and $\varphi_\delta \equiv 1$ in (B.65) and rearrange, we find that

$$(1 - 3 - 2\varphi, \eta - 1) \geq 0 \qquad \Leftrightarrow \qquad (1 + \varphi, \eta - 1) \leq 0, \tag{B.69}$$

for any $\varphi \in \mathscr{A}$, after noting that $(-\Delta_n)^{-1} 0 = 0$. But, if $|\varphi| \leq 1$ and $|\eta| \leq 1$, then

$$\underbrace{(1 + \varphi)}_{\geq 0} \underbrace{(\eta - 1)}_{\leq 0} \leq 0,$$

which means that (B.69) is an identity. We conclude that $\varphi_\delta \equiv 1$ is the solution of $\left(\widehat{\mathbf{S}}_\delta\right)$ in (B.65) if $\delta = \frac{3}{2}\chi^{AB}$. According to (B.66),

$$\mathbb{M}\left(\frac{3}{2}\chi^{AB}\right) = \overline{1} = 1. \tag{B.70a}$$

Likewise, setting $\delta = -\frac{3}{2}\chi^{AB}$ and $\varphi_\delta \equiv -1$ in (B.65) yields

$$(-1 + 3 - 2\varphi, \eta + 1) \geq 0 \qquad \Leftrightarrow \qquad \big(\underbrace{1 - \varphi}_{\geq 0}, \underbrace{\eta + 1}_{\geq 0}\big) \geq 0,$$

the second part of which is also identically true if $|\varphi| \leq 1$ and $|\eta| \leq 1$. Hence, $\varphi_\delta \equiv -1$ solves $\left(\widehat{\mathbf{S}}_\delta\right)$ in (B.65) if $\delta = -\frac{3}{2}\chi^{AB}$, and so

$$\mathbb{M}\left(-\frac{3}{2}\chi^{AB}\right) = \overline{-1} = -1. \tag{B.70b}$$

vi) Since $\mathbb{M}$ in (B.66) is monotone and continuous, the intermediate value theorem implies that there is one $\lambda \in \left[\frac{-3}{2}\chi^{AB}, \frac{3}{2}\chi^{AB}\right]$ for which $\mathbb{M}(\lambda) = m \in [-1, 1]$. The corresponding solution of $\left(\widehat{\mathbf{S}}_\delta\right)$ in (B.65) (which we know exists and is unique) is designated φ_λ. Clearly, $\mathbb{M}(\lambda) = \overline{\varphi_\lambda} = m$. Setting $\delta = \lambda$, $\varphi_\delta = \varphi_\lambda$ and $\eta = \varphi$ in (B.65) thus yields

$$\begin{aligned}\varepsilon_\varphi^2 (\nabla\varphi_\lambda, \nabla(\varphi - \varphi_\lambda)) + \frac{\chi^{AB}}{2}(\varphi_\lambda, \varphi - \varphi_\lambda) + \alpha\left((-\Delta_n)^{-1}(\varphi_\lambda - \overline{\varphi_\lambda}), \varphi - \varphi_\lambda\right) \\ \geq \chi^{AB}(\varphi, \varphi - \varphi_\lambda) + \lambda(1, \varphi - \varphi_\lambda),\end{aligned} \tag{B.71}$$

after multiplying through by $\chi^{AB}/2$. Likewise, setting $\psi = \varphi_\lambda \in \mathscr{A}_m$ in (B.64) gives

$$\varepsilon_\varphi^2 (\nabla\varphi, \nabla(\varphi_\lambda - \varphi)) + \frac{\chi^{AB}}{2}(\varphi, \varphi_\lambda - \varphi) + \alpha\left((-\Delta_n)^{-1}(\varphi - \overline{\varphi}), \varphi_\lambda - \varphi\right) \geq \chi^{AB}(\varphi, \varphi_\lambda - \varphi). \tag{B.72}$$

Adding these last two inequalities leads to

$$\varepsilon_\varphi^2 |\varphi - \varphi_\lambda|_1^2 + \frac{\chi^{AB}}{2}\|\varphi_\lambda - \varphi\|^2 \leq \lambda(1, \varphi_\lambda - \varphi) = 0, \tag{B.73}$$

since $\overline{\varphi} = m = \overline{\varphi_\lambda}$, and after discarding

$$\alpha\|\varphi_\lambda - \varphi - \overline{\varphi_\lambda - \varphi}\|_{-1}^2 \geq 0,$$

on the left. It follows that $\varphi_\lambda = \varphi$. But then $\varphi_\delta = \varphi$ solving $(\mathbf{S}_C)$ also solves $\left(\widehat{\mathbf{S}}_\delta\right)$ in (B.65) if $\delta = \lambda$, viz.

$$\varepsilon_\varphi^2 (\nabla\varphi, \nabla(\eta - \varphi)) - \frac{\chi^{AB}}{2}(\varphi, \eta - \varphi) + \alpha\left((-\Delta_n)^{-1}(\varphi - \overline{\varphi}), \eta - \varphi\right) - \lambda(1, \eta - \varphi) \geq 0,$$

for every $\eta \in \mathscr{A}_m \subset \mathscr{A}$, after multiplying through by $\chi^{AB}/2$, and rearranging terms. But this is problem $(\mathbf{S})$ in (4.27a).

□

B.8 Proof of Lemma 4.3.1

Proof.

i) First note that if we rearrange (A.53) for e_k an eigenfunction of $\mathscr{P}$, then

$$(\nabla e_k, \nabla \nu) = (\lambda_k - 1)(e_k, \nu) \qquad \text{for every} \qquad \nu \in H^1(\Omega). \tag{B.74}$$

Substituting (4.40a) into each term in (4.40b)–(4.40e), and noting (4.7), (A.55), (B.74) and (B.11), for a given N, yields (cf. (B.15))

$$\begin{gathered}
\left(\partial_t \varphi_\mu^{(N)}, e_k\right) = \left(\sum_{j=1}^N c_k'(t) e_j, e_k\right) = \sum_{k=1}^N c_k'(t)(e_k, e_j) = c_k'(t), \\
\left(\nabla \psi_\mu^{(N)}, \nabla e_k\right) = \sum_{j=1}^N d_j^N(t)(\nabla e_j, \nabla e_k) = \begin{cases} 0 & k = 1 \\ d_k^N(t)(\lambda_k - 1) & k > 1, \end{cases} \\
\left(\nabla \varphi_\mu^{(N)}, \nabla e_k\right) = \sum_{j=1}^N c_j^N(t)(\nabla e_j, \nabla e_k) = \begin{cases} 0 & k = 1 \\ c_k^N(t)(\lambda_k - 1) & k > 1, \end{cases} \\
\left(\psi_\mu^{(N)}, e_k\right) = \sum_{j=1}^N d_j^N(t)(e_j, e_k) = d_k^N(t), \\
\left(\varphi_\mu^{(N)}, e_k\right) = c_k^N, \qquad \left(\zeta_\mu\left(\varphi_\mu^{(N)}\right), e_k\right) =: \zeta_\mu^{N,k}(t), \\
\left(\mathcal{B}_\mu'\left(\varphi_\mu^{(N)}\right), e_k\right) =: \mathscr{B}_\mu^{N,k}(t) = -\frac{\chi^{AB}}{2} c_k^N(t) + \zeta_\mu^{N,k}(t), \\
\left((-\Delta_n)^{-1}\left(\varphi_\mu^{(N)} - \overline{\varphi_\mu^{(N)}}\right), e_k\right) = \begin{cases} 0 & k = 1 \text{ or } N = 1 \\ \dfrac{c_k^N(t)}{\lambda_k - 1} & \text{otherwise,} \end{cases}
\end{gathered} \tag{B.75}$$

where the $\mathscr{B}_\mu^{N,k}(t)$'s and $\zeta_\mu^{N,k}(t)$'s are continuous functions of t.

Remark. Recall from Lemma A.1.11 that the eigenvalues $\lambda_k \to \infty$ as $k \to \infty$, and $\lambda_1 = 1$ has multiplicity one. The implication is that (B.10b) and the last fraction above are finite.

Hence if we substitute (B.75) into (4.40b)–(4.40e), we arrive at a system of $2N$ differential equations. From the requirement in (4.40d) that $\overline{\varphi_\mu^{(N)}(0)} = m$,

$$c_1^N(0) = m|\Omega|^{1/2} \qquad \Rightarrow \qquad \varphi_\mu^{(N)}(0) = m + \sum_{j=2}^N (\varphi_0, e_j) e_j. \tag{B.76}$$

Thus, for $k = 1$ (any N), $\left(c_1^N(t)\right)' = 0$ subject to $c_1^N(0) = m|\Omega|^{1/2}$. Hence, we define

$$c_1(t) = m|\Omega|^{1/2} \tag{B.77a}$$

independent of N, and the N-dependent

$$d_1^N(t) = \mathscr{B}_\mu^{N,1}(t) = -\frac{\chi^{AB}}{2} m|\Omega|^{1/2} + \zeta_\mu^{N,1}(t). \tag{B.77b}$$

For $|m| < 1$, $\zeta_\mu^{1,1}(t) \equiv 0$ (the $N = 1$ Galerkin approximation is not penalised). For $N > 1$, $2 \le k \le N$,

$$\frac{\mathrm{d}c_k^N(t)}{\mathrm{d}t} + d_k^N(t)(\lambda_k - 1) = 0 \tag{B.78a}$$

$$d_k^N(t) = \left(\varepsilon_\varphi^2(\lambda_k - 1) - \frac{\chi^{AB}}{2} + \frac{\alpha}{\lambda_k - 1}\right) c_k^N(t) + \zeta_\mu^{N,k}(t). \tag{B.78b}$$

Substituting (B.78b) into (B.78a) yields (cf. (B.17))

$$\frac{\mathrm{d}c_k^N(t)}{\mathrm{d}t} + \left(\varepsilon_\varphi^2(\lambda_k - 1)^2 - \frac{\chi^{AB}}{2}(\lambda_k - 1) + \alpha\right) c_k^N(t) = (1 - \lambda_k)\,\zeta_\mu^{N,k}(t) \tag{B.79a}$$

for $k = 1, 2, \ldots, N$, subject to the IC (cf. (B.76))

$$c_k^N(0) = (\varphi_0, e_k)\,. \tag{B.79b}$$

$\zeta_\mu^{N,k}(t)$ depends on the specific eigenfunctions e_k, as well as the coefficients c_k^N. As such, (B.79a) is non-linear, but the system can be written as

$$\dot{\boldsymbol{c}} = \boldsymbol{f}(\boldsymbol{c}, t)\,.$$

This system has a unique solution by well known results for ODEs (cf. Theorem 7.6.1 and 7.6.2 in Goldberg and Schwartz (1972) (proofs in Hurewicz (1990)). Equation (A1) and Theorem A1 of Appendix A of Jordan and Smith (2007) are also useful, but make demands on $\boldsymbol{f}$ that the system above does not satisfy; see also Chapter 2 of Robinson (2001)).

Consequently, the functions $\left\{\varphi_\mu^{(N)}(t), \psi_\mu^{(N)}(t)\right\}$ in (4.40a) exist, are unique and satisfy (4.40b) and (4.40e) subject to (4.40d), for every $t \in [0, T]$ and $N \geq 1$.

ii) Mass conservation is a necessary condition. We substitute $e_1 := 1/|\Omega|^{1/2}$ into (4.40b) and multiply by $|\Omega|^{1/2}$ to obtain

$$\left(\partial_t \varphi_\mu^{(N)}, 1\right) = 0 \qquad \text{viz.} \qquad \frac{\mathrm{d}}{\mathrm{d}t}\left(\varphi_\mu^{(N)}, 1\right) = 0 \tag{B.80}$$

for every $N = 1, 2, \ldots$.[21] This is equivalent to the left part of (4.41); the right part follows from the IC (4.40d). (4.42) follows from substituting (4.41) into (B.9b).

Remark. The dynamic approximations $\varphi_\mu^{(N)}(t)$ have the correct mass because of the IC and the operator splitting (i.e. the potential $\psi_\mu^{(N)}(t)$, cf. (B.77b)). This is quite different to the stationary problem of Lemma 4.2.4.

□

B.9 Proof of Lemma 4.3.2

Proof.

i) By construction, $\partial_t \varphi_\mu^{(N)} \in V^N$ for each t. Hence, setting $\eta^{(N)} = \partial_t \varphi_\mu^{(N)}$ in (4.40e) yields

$$\begin{aligned}\varepsilon_\varphi^2\left(\nabla\varphi_\mu^{(N)}, \nabla\partial_t\varphi_\mu^{(N)}\right) + \left(\mathcal{B}_\mu'\left(\varphi_\mu^{(N)}\right), \partial_t\varphi_\mu^{(N)}\right) \\ + \alpha\left((-\Delta_n)^{-1}\left(\varphi_\mu^{(N)} - \overline{\varphi_\mu^{(N)}}\right), \partial_t\varphi_\mu^{(N)}\right) = \left(\psi_\mu^{(N)}, \partial_t\varphi_\mu^{(N)}\right).\end{aligned} \tag{B.81}$$

Setting $\eta^{(N)} = \psi_\mu^{(N)} \in V^N$ in (4.40b) leads to

$$\left(\partial_t\varphi_\mu^{(N)}, \psi_\mu^{(N)}\right) = -\left|\psi_\mu^{(N)}\right|_1^2. \tag{B.82}$$

Consider the energy functional

$$\mathcal{E}_\mu\left[\varphi_\mu^{(N)}\right] = \frac{\varepsilon_\varphi^2}{2}\left|\varphi_\mu^{(N)}\right|_1^2 + \left(\mathcal{B}_\mu\left(\varphi_\mu^{(N)}\right), 1\right) + \frac{\alpha}{2}\left\|\varphi_\mu^{(N)} - \overline{\varphi_\mu^{(N)}}\right\|_{-1}^2. \tag{4.6}$$

Differentiating this with respect to t and using (B.81)–(B.82) gives

$$\frac{\mathrm{d}\mathcal{E}_\mu\left[\varphi_\mu^{(N)}\right]}{\mathrm{d}t} = \varepsilon_\varphi^2\left(\nabla\varphi_\mu^{(N)}, \nabla\partial_t\varphi_\mu^{(N)}\right) + \left(\mathcal{B}'_\mu\left(\varphi_\mu^{(N)}\right), \partial_t\varphi_\mu^{(N)}\right) + \alpha\left((-\Delta_n)^{-1}\left(\varphi_\mu^{(N)} - \overline{\varphi_\mu^{(N)}}\right), \partial_t\varphi_\mu^{(N)}\right) = \left(\psi_\mu^{(N)}, \partial_t\varphi_\mu^{(N)}\right) = -\left|\psi_\mu^{(N)}\right|_1^2, \quad \text{(B.83)}$$

after interchanging the $\mathrm{d}/\mathrm{d}t$ and inverse Laplacian operators. Hence

$$\frac{\mathrm{d}\mathcal{E}_\mu\left[\varphi_\mu^{(N)}\right]}{\mathrm{d}t} + \left|\psi_\mu^{(N)}\right|_1^2 = 0,$$

and so if we integrate over $(0,t)$, we obtain

$$\mathcal{E}_\mu\left[\varphi_\mu^{(N)}(t)\right] + \int_0^t \left|\psi_\mu^{(N)}(s)\right|_1^2 \mathrm{d}s = \mathcal{E}_\mu\left[\varphi_\mu^{(N)}(0)\right] = \mathcal{E}_\mu\left[P^N\varphi_0\right] \quad \text{(B.84)}$$

by (4.40d). It remains to bound $\mathcal{E}_\mu\left[P^N\varphi_0\right]$ independent of μ, T and N.

ii) Substituting $r = \varphi_0$ and $s = P^N\varphi_0$ into (4.16) using (4.5b) yields

$$\Upsilon_\mu\left(P^N\varphi_0\right) = \mathcal{B}_\mu\left(P^N\varphi_0\right) - \frac{\chi^{AB}}{4}\left(1 - \left(P^N\varphi_0\right)^2\right) \le \Upsilon_\mu(\varphi_0) + \zeta_\mu\left(P^N\varphi_0\right)\left(P^N\varphi_0 - \varphi_0\right)$$

viz.

$$\left(\mathcal{B}_\mu\left(P^N\varphi_0\right), 1\right) \le \frac{\chi^{AB}}{4}\left(1 - \left(P^N\varphi_0\right)^2, 1\right) + \left(\Upsilon_\mu(\varphi_0), 1\right) + \left(\zeta_\mu\left(P^N\varphi_0\right), P^N\varphi_0 - \varphi_0\right).$$

Now since $\varphi_0 \in \mathscr{A}_m$, $|\varphi_0| \le 1$ a.e., $\Upsilon_\mu(\varphi_0(x)) = 0$ a.e. and so $\left(\Upsilon_\mu(\varphi_0), 1\right) = 0$, i.e.

$$\left(\mathcal{B}_\mu\left(P^N\varphi_0\right), 1\right) \le \frac{\chi^{AB}}{4}\left(1 - \left(P^N\varphi_0\right)^2, 1\right) + \left(\zeta_\mu\left(P^N\varphi_0\right), P^N\varphi_0 - \varphi_0\right). \quad \text{(B.85)}$$

iii) From (4.6) and (B.85), we conclude that

$$\mathcal{E}_\mu\left[P^N\varphi_0\right] \le \frac{\varepsilon_\varphi^2}{2}\left|P^N\varphi_0\right|_1^2 + \frac{\chi^{AB}}{4}\left(1 - \left(P^N\varphi_0\right)^2, 1\right) + \left(\zeta_\mu\left(P^N\varphi_0\right), P^N\varphi_0 - \varphi_0\right) + \frac{\alpha}{2}\left\|P^N\varphi_0 - \overline{\varphi_\mu^{(N)}}\right\|_{-1}^2. \quad \text{(B.86)}$$

We consider each term on the right of (B.86) in turn:

- For the first term, we recall (A.64) to conclude that

$$\frac{\varepsilon_\varphi^2}{2}\left|P^N\varphi_0\right|_1^2 \le \frac{\varepsilon_\varphi^2}{2}|\varphi_0|_1^2. \quad \text{(B.87a)}$$

- In the second term,

$$\left(1 - \left(P^N\varphi_0\right)^2, 1\right) = |\Omega| - \left\|P^N\varphi_0\right\|^2 \to |\Omega| - \|\varphi_0\|^2 = \left(1 - (\varphi_0)^2, 1\right)$$

as $N \to \infty$ by (A.63), and so

$$\lim_{N\to\infty}\frac{\chi^{AB}}{4}\left(1 - \left(P^N\varphi_0\right)^2, 1\right) = \frac{\chi^{AB}}{4}\left(1 - (\varphi_0)^2, 1\right) = \left(\mathcal{B}(\varphi_0), 1\right). \quad \text{(B.87b)}$$

- In the third term,

$$\lim_{N\to\infty}\left(\zeta_\mu\left(P^N\varphi_0\right),P^N\varphi_0-\varphi_0\right)\le\lim_{N\to\infty}\left\|\zeta_\mu\left(P^N\varphi_0\right)\right\|\left\|P^N\varphi_0-\varphi_0\right\|$$

by the Cauchy–Schwarz inequality. From the Lipschitz continuity of ζ_μ (cf. (4.17)),

$$\left|\left(\zeta_\mu\left(P^N\varphi_0\right)-\zeta_\mu\left(\varphi_0\right)\right)(x)\right|\le\frac{1}{\mu}\left|\left(P^N\varphi_0-\varphi_0\right)(x)\right|\qquad\text{a.e.}$$

which means that

$$\left\|\zeta_\mu\left(P^N\varphi_0\right)-\zeta_\mu\left(\varphi_0\right)\right\|\le\frac{1}{\mu}\left\|P^N\varphi_0-\varphi_0\right\|\to 0\quad\text{as } N\to\infty$$

for any $\mu>0$. But that means that $\left\|\zeta_\mu\left(P^N\varphi_0\right)\right\|\to\left\|\zeta_\mu\left(\varphi_0\right)\right\|=0$ as $N\to\infty$, since $\varphi_0\in\mathscr{A}_m$. Consequently,

$$\lim_{N\to\infty}\left(\zeta_\mu\left(P^N\varphi_0\right),P^N\varphi_0-\varphi_0\right)\le 0. \tag{B.87c}$$

- For the last term, we use (A.28a) and (A.63) to conclude that[22]

$$0\le\left\|P^N\varphi_0-\varphi_0\right\|_{-1}\le c_P\left\|P^N\varphi_0-\varphi_0\right\|\to 0\quad\text{as } N\to\infty.$$

Hence, $\left\|\left(P^N\varphi_0-\overline{\varphi_0}\right)-\left(\varphi_0-\overline{\varphi_0}\right)\right\|_{-1}^2\to 0$ as $N\to\infty$, and so

$$\frac{\alpha}{2}\left\|P^N\varphi_0-\overline{\varphi_0}\right\|_{-1}^2\to\frac{\alpha}{2}\left\|\varphi_0-\overline{\varphi_0}\right\|_{-1}^2\quad\text{as } N\to\infty. \tag{B.87d}$$

Hence, sending $N\to\infty$ in (B.86) using (B.87) and (4.1a) and noting that $\varphi_0\in\mathscr{A}_m$ (i.e. the IC has no penalty energy) yields[23]

$$\limsup_{N\to\infty}\mathcal{E}_\mu\left[P^N\varphi_0\right]\le\mathcal{E}_\mu\left[\varphi_0\right]=\mathcal{E}\left[\varphi_0\right]=C \tag{B.88a}$$

where C is a finite constant independent of T, μ and N because $\varphi_0\in H^1(\Omega)$. Hence, there exists an N' such that for every $N>N'$,

$$\mathcal{E}_\mu\left[P^N\varphi_0\right]\le C<\infty. \tag{B.88b}$$

(4.43) follows immediately after considering (B.84).

Remark. We will use the constant C above as a uniform bound (in N) for various sequences of norms of $\varphi_\mu^{(N)}$ and $\psi_\mu^{(N)}$; these bounds are uniform in N for $N>N'$.

iv) For $\mu<\mu_{\max}$ as in (4.13), (4.12) gives $\left(\mathcal{B}_\mu\left(\varphi_\mu^{(N)}\right),1\right)\ge -C_0\left|\Omega\right|\mu$. Hence, using (4.6) and (B.84), we conclude that[24]

$$\frac{\varepsilon_\varphi^2}{2}\left|\varphi_\mu^{(N)}\right|_1^2+\left(\mathcal{B}_\mu\left(\varphi_\mu^{(N)}\right),1\right)+\underbrace{\frac{\alpha}{2}\left\|\varphi_\mu^{(N)}-\overline{\varphi_\mu^{(N)}}\right\|_{-1}^2}_{\ge 0}+\int_0^t\left|\psi_\mu^{(N)}(s)\right|_1^2\mathrm{d}s\le C$$

which means that, according to (B.88),

$$\frac{\varepsilon_\varphi^2}{2}\left|\varphi_\mu^{(N)}\right|_1^2+\int_0^t\left|\psi_\mu^{(N)}(s)\right|_1^2\mathrm{d}s\le C+C_0\left|\Omega\right|\mu<C+C_0\left|\Omega\right|\mu_{\max}=:C, \tag{B.89}$$

with C independent of T, μ and N. Hence,

$$\left|\varphi_\mu^{(N)}(t)\right|_1^2\le C\quad\text{for a.e. } t\in[0,T]. \tag{B.90}$$

v) From (A.2) we deduce that

$$\left\|\varphi_\mu^{(N)}\right\| \le c_P \left\{\left|\left(\varphi_\mu^{(N)}, 1\right)\right| + \left|\varphi_\mu^{(N)}\right|_1\right\} \le c_P \left\{\left\|\varphi_\mu^{(N)}\right\| |\Omega|^{1/2} + \left|\varphi_\mu^{(N)}\right|_1\right\}$$

by the Cauchy–Schwarz inequality, and so

$$\left\|\varphi_\mu^{(N)}(t)\right\|^2 \underbrace{\left(\frac{1 - c_P |\Omega|^{1/2}}{c_P}\right)^2}_{:= C_2^2} \le \left|\varphi_\mu^{(N)}(t)\right|_1^2 \quad \text{for a.e. } t \in [0,T]. \tag{B.91}$$

Adding C_2^2 times (B.90) to (B.91) gives, upon rearrangement,

$$C_2^2 \left\|\varphi_\mu^{(N)}(t)\right\|_1^2 - C_2^2 C_1 \le \left|\varphi_\mu^{(N)}(t)\right|_1^2 \qquad \Rightarrow \qquad \left\|\varphi_\mu^{(N)}(t)\right\|_1^2 \le \frac{C_1 + C_2^2 C_1}{C_2^2} =: C,$$

for a.e. $t \in [0,T]$, if we use (B.90) once again. Since C is independent of t,

$$\operatorname*{ess\,sup}_{0 \le t \le T} \left\|\varphi_\mu^{(N)}(t)\right\|_1^2 \le C, \tag{B.92}$$

which is equivalent to (4.44a). Note that $L^\infty(\Omega) \subset L^2(\Omega)$ (cf. (1.16) in Robinson (2001)). Hence

$$\varphi \in L^\infty\left(0,T; H^1(\Omega)\right) \qquad \Rightarrow \qquad \varphi \in L^2\left(0,T; H^1(\Omega)\right). \tag{B.93a}$$

Likewise, $H^1(\Omega) \subset \left(H^1(\Omega)\right)'$, and so

$$\varphi \in L^2\left(0,T; H^1(\Omega)\right) \qquad \Rightarrow \qquad \varphi \in L^2\left(0,T; \left(H^1(\Omega)\right)'\right). \tag{B.93b}$$

Hence, we deduce from (4.44a) that $\left\|\varphi_\mu^{(N)}\right\|_{L^2\left(0,T;H^1(\Omega)\right)} \le C$ independent of μ and N, but not T. This is equivalent to the first part of (4.44b).[25]

vi) Arguing as in (2.28) of Blowey and Elliott (1991), we see that

$$\begin{aligned}
\left\|\partial_t \varphi_\mu^{(N)}\right\|_{-1}^2 &= \left(\partial_t \varphi_\mu^{(N)}, (-\Delta_n)^{-1}\left(\partial_t \varphi_\mu^{(N)}\right)\right) \\
&= \left(\partial_t \varphi_\mu^{(N)}, P^N (-\Delta_n)^{-1}\left(\partial_t \varphi_\mu^{(N)}\right)\right)
\end{aligned}$$

(by (A.62) since $\partial_t \varphi_\mu^{(N)} \in V^N$)

$$= -\left(\nabla \psi_\mu^{(N)}, \nabla\left(P^N (-\Delta_n)^{-1}\left(\partial_t \varphi_\mu^{(N)}\right)\right)\right)$$

((4.40b) with $\nu = P^N (-\Delta_n)^{-1}\left(\partial_t \varphi_\mu^{(N)}\right)$)

$$= -\left(\nabla \psi_\mu^{(N)}, P^N \nabla\left((-\Delta_n)^{-1}\left(\partial_t \varphi_\mu^{(N)}\right)\right)\right)$$

(interchange projection and gradient operations)

$$= -\left(\nabla \psi_\mu^{(N)}, \nabla\left((-\Delta_n)^{-1}\left(\partial_t \varphi_\mu^{(N)}\right)\right)\right)$$

(by (A.62) once again)

$$= -\left(\psi_\mu^{(N)}, \partial_t \varphi_\mu^{(N)}\right)$$

(by (2.9))

$$= \left|\psi_\mu^{(N)}\right|_1^2$$

using (4.40b) with $\nu = \psi_\mu^{(N)} \in V^N$ again. Hence,

$$\left\|\partial_t \varphi_\mu^{(N)}\right\|_{-1}^2 = \left|\psi_\mu^{(N)}\right|_1^2. \tag{B.94}$$

Integrating in time, using (B.84), (B.88) and (A.27), leads to

$$\left\|\partial_t \varphi_\mu^{(N)}\right\|^2_{L^2\left(0,T;\left(H^1(\Omega)\right)'\right)} = \int_0^T \left\|\partial_t \varphi_\mu^{(N)}\right\|_{-1}^2 \,\mathrm{d}t = \int_0^T \left|\psi_\mu^{(N)}(s)\right|_1^2 \,\mathrm{d}s \le \mathcal{E}_\mu\left[P^N \varphi_0\right] = C, \tag{B.95}$$

independent of T, μ and N.

vii) Combining (4.44a) with (B.93) and using (B.95), we conclude that

$$\left\|\varphi_\mu^{(N)}\right\|_{L^2\left(0,T;\left(H^1(\Omega)\right)'\right)} \le C \qquad \text{and} \qquad \left\|\partial_t \varphi_\mu^{(N)}\right\|_{L^2\left(0,T;\left(H^1(\Omega)\right)'\right)} \le C. \tag{B.96}$$

The first C is independent of μ and N, but not T; the second is independent of μ, N and T and is equivalent to the second part of (4.44b). Hence,

$$\left\|\varphi_\mu^{(N)}\right\|_{H^1\left(0,T;\left(H^1(\Omega)\right)'\right)} \le C$$

independent of μ and N, which is (4.44c).

viii) To establish (4.44d), we differentiate (4.40e) in t to find that

$$\begin{aligned}\varepsilon_\varphi^2 \left(\nabla \partial_t \varphi_\mu^{(N)}, \nabla \eta^{(N)}\right) - \frac{\chi^{AB}}{2}\left(\partial_t \varphi_\mu^{(N)}, \eta^{(N)}\right) + \left(\zeta_\mu'\left(\varphi_\mu^{(N)}\right)\partial_t \varphi_\mu^{(N)}, \eta^{(N)}\right) \\ + \alpha\left((-\Delta_n)^{-1}\left(\partial_t \varphi_\mu^{(N)}\right), \eta^{(N)}\right) = \left(\partial_t \psi_\mu^{(N)}, \eta^{(N)}\right),\end{aligned}$$

for every $\eta^{(N)} \in V^N$. Setting $\eta^{(N)} = \partial_t \varphi_\mu^{(N)} \in V^N$ in this result yields

$$\varepsilon_\varphi^2 \left|\partial_t \varphi_\mu^{(N)}\right|_1^2 + \underbrace{\left(\zeta_\mu'\left(\varphi_\mu^{(N)}\right), \left(\partial_t \varphi_\mu^{(N)}\right)^2\right)}_{\ge 0 \text{ by (4.14b)}} + \underbrace{\alpha\left\|\partial_t \varphi_\mu^{(N)}\right\|_{-1}^2}_{\ge 0} = \frac{\chi^{AB}}{2}\left\|\partial_t \varphi_\mu^{(N)}\right\|^2 + \left(\partial_t \psi_\mu^{(N)}, \partial_t \varphi_\mu^{(N)}\right).$$

Hence,

$$\varepsilon_\varphi^2 \left|\partial_t \varphi_\mu^{(N)}\right|_1^2 \le \left(\partial_t \psi_\mu^{(N)}, \partial_t \varphi_\mu^{(N)}\right) + \frac{\chi^{AB}}{2}\left\|\partial_t \varphi_\mu^{(N)}\right\|^2. \tag{B.97}$$

Setting $\eta^{(N)} = \partial_t \psi_\mu^{(N)}$ in (4.40b) yields

$$\left(\partial_t \psi_\mu^{(N)}, \partial_t \varphi_\mu^{(N)}\right) = -\left(\nabla \psi_\mu^{(N)}, \nabla \partial_t \psi_\mu^{(N)}\right) = -\frac{1}{2}\frac{\mathrm{d}}{\mathrm{d}t}\left|\psi_\mu^{(N)}\right|_1^2;$$

if we substitute this into (B.97), we see that

$$\begin{aligned}\varepsilon_\varphi^2 \left|\partial_t \varphi_\mu^{(N)}\right|_1^2 + \frac{1}{2}\frac{\mathrm{d}}{\mathrm{d}t}\left|\psi_\mu^{(N)}\right|_1^2 &\le \frac{\chi^{AB}}{2}\left\|\partial_t \varphi_\mu^{(N)}\right\|^2 \\ &\le \frac{\chi^{AB}}{2}\left|\partial_t \varphi_\mu^{(N)}\right|_1 \left\|\partial_t \varphi_\mu^{(N)}\right\|_{-1} \le \frac{\varepsilon_\varphi^2}{2}\left|\partial_t \varphi_\mu^{(N)}\right|_1^2 + \frac{\left(\chi^{AB}\right)^2}{8\varepsilon_\varphi^2}\left\|\partial_t \varphi_\mu^{(N)}\right\|_{-1}^2,\end{aligned} \tag{B.98}$$

after using (A.29) and then Young's inequality. Rearranging yields

$$\varepsilon_\varphi^2 \left|\partial_t \varphi_\mu^{(N)}\right|_1^2 + \frac{\mathrm{d}}{\mathrm{d}t}\left|\psi_\mu^{(N)}\right|_1^2 \leq \frac{\left(\chi^{AB}\right)^2}{4\varepsilon_\varphi^2}\left\|\partial_t \varphi_\mu^{(N)}\right\|_{-1}^2 = \frac{\left(\chi^{AB}\right)^2}{4\varepsilon_\varphi^2}\left|\psi_\mu^{(N)}\right|_1^2, \tag{B.99}$$

after recalling (B.94).[26] By elementary calculus,

$$\frac{\mathrm{d}}{\mathrm{d}t}\left[t\left|\psi_\mu^{(N)}\right|_1^2\right] = t\frac{\mathrm{d}}{\mathrm{d}t}\left|\psi_\mu^{(N)}\right|_1^2 + \left|\psi_\mu^{(N)}\right|_1^2 \qquad \Rightarrow \qquad t\frac{\mathrm{d}}{\mathrm{d}t}\left|\psi_\mu^{(N)}\right|_1^2 = \frac{\mathrm{d}}{\mathrm{d}t}\left[t\left|\psi_\mu^{(N)}\right|_1^2\right] - \left|\psi_\mu^{(N)}\right|_1^2.$$

If we multiply (B.99) by t and use this last identity, we discover that

$$\frac{\mathrm{d}}{\mathrm{d}t}\left[t\left|\psi_\mu^{(N)}\right|_1^2\right] + t\varepsilon_\varphi^2\left|\partial_t\varphi_\mu^{(N)}\right|_1^2 \leq \left(1 + t\frac{\left(\chi^{AB}\right)^2}{4\varepsilon_\varphi^2}\right)\left|\psi_\mu^{(N)}\right|_1^2. \tag{B.100}$$

If we integrate this over $(0, t')$, we are led to[27]

$$\begin{aligned} t'\left|\psi_\mu^{(N)}\left(t'\right)\right|_1^2 + \varepsilon_\varphi^2\int_0^{t'} t\left|\partial_t\varphi_\mu^{(N)}\right|_1^2 \mathrm{d}t &\leq \int_0^{t'}\left(1 + t\frac{\left(\chi^{AB}\right)^2}{4\varepsilon_\varphi^2}\right)\left|\psi_\mu^{(N)}\right|_1^2 \mathrm{d}t \\ &\leq \left(1 + t'\frac{\left(\chi^{AB}\right)^2}{4\varepsilon_\varphi^2}\right)\int_0^{t'}\left|\psi_\mu^{(N)}\right|_1^2 \mathrm{d}t \leq \left(1 + t'\right)C \end{aligned} \tag{B.101}$$

using (B.89), where $C = C\left(\varphi_0\right)$ is independent of N and μ. Hence, for $0 < \delta = t' \leq T$,

$$0 \leq \int_0^\delta \frac{t}{1+T}\left|\partial_t\varphi_\mu^{(N)}\right|_1^2 \mathrm{d}t \leq C \qquad \text{and} \qquad 0 \leq \int_0^T \frac{t}{1+T}\left|\partial_t\varphi_\mu^{(N)}\right|_1^2 \mathrm{d}t \leq C.$$

Subtracting the first integral above from the second yields

$$\left|\int_\delta^T \frac{t}{1+T}\left|\partial_t\varphi_\mu^{(N)}\right|_1^2 \mathrm{d}t\right| \leq C$$

or since $\delta \leq t$ in the integrand and all terms are positive,

$$\frac{\delta}{1+T}\int_\delta^T \left|\partial_t\varphi_\mu^{(N)}\right|_1^2 \mathrm{d}t \leq C \qquad \Rightarrow \qquad \int_\delta^T \left|\partial_t\varphi_\mu^{(N)}\right|_1^2 \mathrm{d}t \leq \frac{C\left(1+T\right)}{\delta} < \infty \tag{B.102}$$

as long as $\delta > 0$. Since $\overline{\partial_t\varphi_\mu^{(N)}} = 0$, Poincaré's inequality (A.1) implies that

$$\frac{1}{c_P^2}\left\|\partial_t\varphi_\mu^{(N)}\right\|^2 \leq \left|\partial_t\varphi_\mu^{(N)}\right|_1^2 \qquad \Rightarrow \qquad \int_\delta^T \left\|\partial_t\varphi_\mu^{(N)}\right\|_1^2 \mathrm{d}t < \infty \tag{B.103}$$

for any $\delta > 0$.[28] The first part of (4.44b) implies that $\left\|\varphi_\mu^{(N)}\right\|_{L^2\left(\varepsilon,T;H^1(\Omega)\right)} \leq C$ independent of μ and N, for any $\varepsilon \geq 0$. Combining these leads to the first part of (4.44d). The second part of (4.44d) follows from the first by (A.37).[29]

ix) We now develop counterparts of (2.33)–(2.37) of Blowey and Elliott (1991). From (4.39c), (4.40d) and (4.41), we know that

$$\left(\varphi_\mu^{(N)}\left(t\right), 1\right) = \left(\varphi_0, 1\right) = \left(P^N\varphi_0, 1\right) = m\left|\Omega\right|. \tag{B.104a}$$

We estimate $\left|\left(\psi_\mu^{(N)}, 1\right)\right|$: substituting $\eta^{(N)} = 1$ into (4.40e) yields

$$\left(\psi_\mu^{(N)}, 1\right) = -\frac{\chi^{AB}}{2}\left(\varphi_\mu^{(N)}, 1\right) + \left(\zeta_\mu\left(\varphi_\mu^{(N)}\right), 1\right) + \alpha\underbrace{\left(\left(-\Delta_n\right)^{-1}\left(\varphi_\mu^{(N)} - \overline{\varphi_\mu^{(N)}}\right), 1\right)}_{=\,0 \text{ by (2.9b)}}. \tag{B.104b}$$

Using (4.22c) and (B.104a), we conclude that[30]

$$\left|\left(\psi_\mu^{(N)},1\right)\right| - \frac{\chi^{AB}}{2}\,|m|\,|\Omega| \le \left(\zeta_\mu\left(\varphi_\mu^{(N)}\right),\varphi_\mu^{(N)}\right). \tag{B.105}$$

Now we set $\eta^{(N)} = \varphi_\mu^{(N)}$ in (4.40e) and rearrange to obtain

$$\left(\zeta_\mu\left(\varphi_\mu^{(N)}\right),\varphi_\mu^{(N)}\right) \le \frac{\chi^{AB}}{2}\left\|\varphi_\mu^{(N)}\right\|^2 + \left(\psi_\mu^{(N)},\varphi_\mu^{(N)}\right), \tag{B.106}$$

since $\varepsilon_\varphi^2\left|\varphi_\mu^{(N)}\right|_1^2 \ge 0$, and for any $u \in L^2(\Omega)$ (including $\varphi_\mu^{(N)}$),

$$\left(\left(-\Delta_n\right)^{-1}(u-\overline{u}),u\right) = \left(\left(-\Delta_n\right)^{-1}(u-\overline{u}),u-\overline{u}\right) = \|u-\overline{u}\|_{-1}^2 \ge 0. \tag{B.107}$$

Combining (B.105) and (B.106), we discover that

$$\left|\left(\psi_\mu^{(N)},1\right)\right| \le \frac{\chi^{AB}}{2}\left\|\varphi_\mu^{(N)}\right\|^2 + \frac{\chi^{AB}}{2}\,|m|\,|\Omega| + \left(\psi_\mu^{(N)},\varphi_\mu^{(N)}\right). \tag{B.108}$$

x) Finally, we establish (4.44e). For any $u, v \in L^2(\Omega)$,[31]

$$(u,v) = (u,v-\overline{v}) + \overline{u}\,(v,1). \tag{B.109}$$

Setting $u = \psi_\mu^{(N)}$ and $v = \varphi_\mu^{(N)}$ in (B.109) leads to[32]

$$\begin{aligned}\left(\psi_\mu^{(N)},\varphi_\mu^{(N)}\right) &= \left(\psi_\mu^{(N)},\varphi_\mu^{(N)}-\overline{\varphi_\mu^{(N)}}\right) + \overline{\psi_\mu^{(N)}}\left(\varphi_\mu^{(N)},1\right)\\ &= \left(\nabla\psi_\mu^{(N)},\nabla\left(-\Delta_n\right)^{-1}\left(\varphi_\mu^{(N)}-\overline{\varphi_\mu^{(N)}}\right)\right) + \frac{1}{|\Omega|}\left(\psi_\mu^{(N)},1\right)m\,|\Omega|\end{aligned}$$

(using (2.1), (2.9) and (B.104a))

$$\le \left|\psi_\mu^{(N)}\right|_1\left\|\varphi_\mu^{(N)}-\overline{\varphi_\mu^{(N)}}\right\|_{-1} + |m|\left|\left(\psi_\mu^{(N)},1\right)\right|, \tag{B.110}$$

by the Cauchy–Schwarz inequality, (4.41) and (2.11). Combining (B.108) and (B.110), gives[33]

$$\left|\left(\psi_\mu^{(N)},1\right)\right| \le \frac{\frac{\chi^{AB}}{2}\left\|\varphi_\mu^{(N)}\right\|^2 + \frac{\chi^{AB}}{2}\,|m|\,|\Omega|}{1-|m|} + \frac{\left\|\varphi_\mu^{(N)}-\overline{\varphi_\mu^{(N)}}\right\|_{-1}}{1-|m|}\left|\psi_\mu^{(N)}\right|_1, \tag{B.111}$$

after noting that $|m| < 1$. The first fraction on the right side of (B.111) is bounded above by a constant, independent of t, μ and N by (4.44a). Likewise, by (A.28a),

$$\left\|\varphi_\mu^{(N)}-\overline{\varphi_\mu^{(N)}}\right\|_{-1} \le c_P\left\|\varphi_\mu^{(N)}-\overline{\varphi_\mu^{(N)}}\right\| \le \left\|\varphi_\mu^{(N)}\right\| + \left|\overline{\varphi_\mu^{(N)}}\right|\,|\Omega|^{1/2},$$

and so the coefficient of $\left|\psi_\mu^{(N)}\right|_1$ in the second term on the right of (B.111) is also bounded above, independent of t, μ and N. Hence we can write (B.111) as

$$\left|\left(\psi_\mu^{(N)},1\right)\right| \le C + C\left|\psi_\mu^{(N)}\right|_1, \tag{B.112a}$$

for positive constants C, independent of t, μ and N. A comparison with Poincaré's inequality (A.2) reveals that[34]

$$\left\|\psi_\mu^{(N)}\right\| \le c_P\left\{\left|\left(\psi_\mu^{(N)},1\right)\right| + \left|\psi_\mu^{(N)}\right|_1\right\} \le C + C\left|\psi_\mu^{(N)}\right|_1. \tag{B.112b}$$

Integrating in time using (B.112b) yields

$$\begin{aligned}\left\|\psi_\mu^{(N)}\right\|^2_{L^2\left(0,T;H^1(\Omega)\right)} &= \int_0^T \left\|\psi_\mu^{(N)}(s)\right\|^2 + \left|\psi_\mu^{(N)}(s)\right|_1^2 \mathrm{d}s \\ &\leq \int_0^T C\ \mathrm{d}s + \int_0^T C\left|\psi_\mu^{(N)}(s)\right|_1 \mathrm{d}s + \int_0^T C\left|\psi_\mu^{(N)}(s)\right|_1^2 \mathrm{d}s. \end{aligned} \tag{B.112c}$$

Now

$$\int_0^T C\left|\psi_\mu^{(N)}(s)\right|_1 \mathrm{d}s \leq CT^{1/2}\left(\int_0^T C\left|\psi_\mu^{(N)}(s)\right|_1^2 \mathrm{d}s\right)^{1/2} \leq CT^{1/2}$$

by (8) of Theorem 2.14 of Adams and Fournier (2003) and (B.84), (B.88b). Using the latter two results once more and creating a perfect square on the right-hand side, we can write

$$\left\|\psi_\mu^{(N)}\right\|^2_{L^2\left(0,T;H^1(\Omega)\right)} \leq C\left(1+T^{1/2}\right)^2$$

for C independent of N, T and μ, i.e.

$$\int_0^T \left\|\psi_\mu^{(N)}(s)\right\|_1^2 \mathrm{d}s \leq C\left(1+T^{1/2}\right), \tag{B.112d}$$

which is (4.44e).

□

B.10 Proof of Theorem 4.3.3

Proof. Our approach is to show that as we send $N \to \infty$, we can extract a convergent sub-sequence of $\left(\varphi_\mu^{(N)}, \psi_\mu^{(N)}\right)$ with limit (φ_μ, ψ_μ), which solves problem $(\mathbf{R}_{\mu,\mathbf{f}})$.

i) According to (4.44b), for each N,

$$\varphi_\mu^{(N)} \in L^2\left(0,T;H^1(\Omega)\right) \qquad \text{and} \qquad \partial_t\varphi_\mu^{(N)} \in L^2\left(0,T;\left(H^1(\Omega)\right)'\right),$$

the first part of which implies that

$$\nabla\varphi_\mu^{(N)} \in L^2\left(0,T;L^2(\Omega)\right).$$

Consequently, the sequence $\left(\varphi_\mu^{(N)}\right)$ is bounded in $L^2\left(0,T;H^1(\Omega)\right)$, a Hilbert space, and so has a sub-sequence (also called) $\left(\varphi_\mu^{(N)}\right)$ which converges weakly.[35] Hence (cf. (B.461)),

$$\varphi_\mu^{(N)} \rightharpoonup \varphi_\mu \qquad \text{in} \qquad L^2\left(0,T;H^1(\Omega)\right). \tag{B.113a}$$

In particular,

$$\int_0^T \left(\eta, \varphi_\mu^{(N)}\right)\ \mathrm{d}t \to \int_0^T (\eta,\varphi_\mu)\ \mathrm{d}t \qquad (\text{in } \mathbb{R}) \text{ as} \qquad N\to\infty \tag{B.113b}$$

for every $\eta \in L^2\left(0,T;\left(H^1(\Omega)\right)'\right) \supset L^2\left(0,T;H^1(\Omega)\right)$, and

$$\int_0^T \left(\nabla\eta, \nabla\varphi_\mu^{(N)}\right)\ \mathrm{d}t \to \int_0^T (\nabla\eta,\nabla\varphi_\mu)\ \mathrm{d}t \qquad (\text{in } \mathbb{R}) \text{ as} \qquad N\to\infty \tag{B.113c}$$

for every $\nabla\eta \in L^2\left(0,T;\left(L^2(\Omega)\right)^d\right) \supset L^2\left(0,T;\left(H^1(\Omega)\right)^d\right)$.[36]

ii) We now use the uniform bound on $\partial_t \varphi_\mu^{(N)}$ in $L^2\left(0,T;\left(H^1(\Omega)\right)'\right)$ to extract a further sub-sequence (also called) $\left(\varphi_\mu^{(N)}\right)$ which converges weak-$\star$, viz.

$$\partial_t \varphi_\mu^{(N)} \overset{\star}{\rightharpoonup} \dot{\varphi} \qquad \text{in} \qquad L^2\left(0,T;\left(H^1(\Omega)\right)'\right),$$

for some $\dot{\varphi}$.[37] This means that (cf. (B.462))

$$\int_0^T \left(\partial_t \varphi_\mu^{(N)}, \psi\right)_1 \, \mathrm{d}t \to \int_0^T \left(\dot{\varphi}, \psi\right)_1 \, \mathrm{d}t$$

(in $\mathbb{R}$) as $N \to \infty$, for every $\psi \in L^2\left(0,T;H^1(\Omega)\right)$. Arguing as above, we find that

$$\int_0^T \left(\partial_t \varphi_\mu^{(N)}, \psi\right) \mathrm{d}t \to \int_0^T \left(\dot{\varphi}, \psi\right) \mathrm{d}t \tag{B.114}$$

(in $\mathbb{R}$) as $N \to \infty$, for every $\psi \in L^2\left(0,T;H^1(\Omega)\right)$, and in fact,[38]

$$\dot{\varphi} = \frac{\mathrm{d}\varphi_\mu}{\mathrm{d}t} \in L^2\left(0,T;\left(H^1(\Omega)\right)'\right). \tag{B.115}$$

Arguing as we did to obtain (B.96), we conclude that

$$\varphi_\mu \in L^2\left(0,T;H^1(\Omega)\right) \cap H^1\left(0,T;\left(H^1(\Omega)\right)'\right) \tag{B.116}$$

uniformly in μ. Since weakly convergent sequences are bounded (cf. Proposition 4.17 of Robinson (2001)), (4.45a) holds.

iii) If we apply Lemma 11.4 of Renardy and Rogers (2004), or Theorem 3 of Section 5.9 of Evans (1998), which says that

$$u \in L^2\left(0,T;H^1(\Omega)\right) \cap H^1\left(0,T;\left(H^1(\Omega)\right)'\right) \qquad \Rightarrow \qquad u \in C\left([0,T];L^2(\Omega)\right), \tag{B.117}$$

(equivalently, $L^2\left(0,T;H^1(\Omega)\right) \cap H^1\left(0,T;\left(H^1(\Omega)\right)'\right) \hookrightarrow C\left([0,T];L^2(\Omega)\right)$) to (B.116), we discover that each

$$\varphi_\mu^{(N)} \in C\left([0,T];L^2(\Omega)\right) \qquad \text{and} \qquad \varphi_\mu \in C\left([0,T];L^2(\Omega)\right), \tag{B.118}$$

which leads to (4.45c).

Remark. We do not (yet) assert that $\varphi_\mu^{(N)}(t) \to \varphi_\mu(t)$ a.e. in Ω, for every $t \in [0,T]$ (since the imbedding in (B.117) is only continuous and not compact).

iv) The results above also allow us to establish a strong convergence result. Since weakly convergent sequences are bounded, each $\varphi_\mu^{(N)} \in W$ of (A.38) by (B.113a) and (B.115). Accordingly, there is a sequence $\varphi_\mu \in L^2(\Omega_T)$ with

$$\varphi_\mu^{(N)} \to \varphi_\mu \qquad \text{in} \qquad L^2(\Omega_T). \tag{B.119}$$

Consequently, there is a further sub-sequence, (also called) $\left(\varphi_\mu^{(N)}\right)$ which converges pointwise to φ_μ a.e. in Ω, for a.e. $t \in (0,T)$ (cf. Corollary 1.12 of Robinson (2001)), i.e.

$$\left\|\varphi_\mu^{(N)}(t) - \varphi_\mu(t)\right\| \to 0 \qquad \text{for a.e. } t \in (0,T) \qquad \Rightarrow \qquad \lim_{N\to\infty} \varphi_\mu^{(N)}(t) = \varphi_\mu(t) \qquad \text{a.e.} \tag{B.120}$$

for a.e. t, as $N \to \infty$.

v) The uniform bound in (4.44a) of $\varphi_\mu^{(N)}$ in $L^\infty\left(0,T;H^1(\Omega)\right)$ allows us to extract a further sub-sequence, (also called) $\left(\varphi_\mu^{(N)}\right)$ which converges weak-$\star$, viz. $\varphi_\mu \in L^\infty\left(0,T;H^1(\Omega)\right)$ exists with

$$\varphi_\mu^{(N)} \overset{\star}{\rightharpoonup} \varphi_\mu \qquad \text{in} \qquad L^\infty\left(0,T;H^1(\Omega)\right). \tag{B.121}$$

Since weak-$\star$ convergent sequences are bounded (cf. Proposition 4.17 of Robinson (2001)), we infer (4.45b).[39]

vi) We use the N-independent bound in (4.44d) to take yet another sub-sequence, (also called) $\left(\varphi_\mu^{(N)}\right)$ which converges weakly in $H^1\left(\delta,T;H^1(\Omega)\right)$ to φ_μ, viz.

$$\varphi_\mu^{(N)} \rightharpoonup \varphi_\mu \qquad \text{in} \qquad H^1\left(\delta,T;H^1(\Omega)\right) \qquad \text{for any} \qquad \delta>0. \tag{B.122}$$

By imbedding, $\varphi_\mu \in C\left([\delta,T];H^1(\Omega)\right)$. Together, these results imply (4.45d).

vii) According to (4.44e), each $\left\|\psi_\mu^{(N)}\right\|_{L^2\left(0,T;H^1(\Omega)\right)} \leq C$ independent of μ and N. As such, the sequence $\left(\psi_\mu^{(N)}\right)$ is bounded in the Hilbert space $L^2\left(0,T;H^1(\Omega)\right)$ uniformly in N. We therefore infer the existence of $\psi_\mu \in L^2\left(0,T;H^1(\Omega)\right)$ and a sub-sequence of $\left(\psi_\mu^{(N)}\right)$ (similarly labelled) such that

$$\psi_\mu^{(N)} \rightharpoonup \psi_\mu \qquad \text{in} \qquad L^2\left(0,T;H^1(\Omega)\right), \tag{B.123}$$

which leads to (4.45e). In particular,

$$\int_0^T \left(\eta,\psi_\mu^{(N)}\right)\,\mathrm{d}t \to \int_0^T (\eta,\psi_\mu)\,\mathrm{d}t, \tag{B.124a}$$

and also

$$\int_0^T \left(\nabla\eta,\nabla\psi_\mu^{(N)}\right)\,\mathrm{d}t \to \int_0^T (\nabla\eta,\nabla\psi_\mu)\,\mathrm{d}t \tag{B.124b}$$

(in $\mathbb{R}$) as $N\to\infty$, for every $\eta \in L^2\left(0,T;H^1(\Omega)\right)$.

viii) We now show that (φ_μ,ψ_μ) above solves problem $(\mathbf{R}_{\mu,\mathbf{f}})$.

1. As in Theorem 3 of Section 7.1 of Evans (1998), we fix $N\in\mathbb{N}$, and choose functions $\eta^{(N)} \in C^1\left([0,T],H^1(\Omega)\right)$ having the form (cf. (4.40a))

$$\eta^{(N)}(t) = \sum_{j=1}^N \eta_j(t)\,e_j \tag{B.125}$$

where the $\eta_j(t)$ are given, smooth functions. We choose $n\geq N$ in the approximations $\varphi_\mu^{(N)}$ and $\psi_\mu^{(N)}$ in (4.40a), multiply (4.40b)–(4.40e) by $\eta_j(t)$, sum $j=1,\ldots,N$, and integrate with respect to t. We find that

$$\int_0^T \left(\partial_t\varphi_\mu^{(N)},\eta^{(N)}\right) + \left(\nabla\psi_\mu^{(N)},\nabla\eta^{(N)}\right)\mathrm{d}t = 0, \tag{B.126a}$$

and

$$\int_0^T \varepsilon_\varphi^2\left(\nabla\varphi_\mu^{(N)},\nabla\eta^{(N)}\right) + \left(\mathcal{B}'_\mu\left(\varphi_\mu^{(N)}\right),\eta^{(N)}\right) + \alpha\left((-\Delta_n)^{-1}\left(\varphi_\mu^{(N)}-\overline{\varphi_\mu^{(N)}}\right),\eta^{(N)}\right)\mathrm{d}t = \int_0^T \left(\psi_\mu^{(N)},\eta^{(N)}\right)\mathrm{d}t. \tag{B.126b}$$

We now take weak limits in the sub-sequences of $\left(\varphi_\mu^{(N)}\right)$ and $\left(\psi_\mu^{(N)}\right)$ as described above (i.e. send $n \to \infty$), and then use a density argument in the set of test functions (cf. (A.63) and Theorem 1.13 of Robinson (2001)) to assert that, given any $\eta \in L^2\left(0,T;H^1(\Omega)\right)$, there is a sequence $\eta^{(N)} \in C^1\left([0,T],H^1(\Omega)\right)$ with

$$\eta^{(N)} \to \eta \qquad \text{viz.} \qquad \left\|\eta^{(N)}-\eta\right\|_{L^2\left(0,T;H^1(\Omega)\right)} \to 0 \qquad \text{and} \qquad \left\|\eta^{(N)}(t)-\eta(t)\right\| \to 0 \tag{B.127}$$

(i.e. $\left\|\eta^{(N)}(t)\right\| \to \|\eta(t)\|$) for a.e. $t \in (0,T)$, as $N \to \infty$.

2. In the first term of (B.126a), we use (B.114) to see that, for each N,

$$\int_0^T \left(\partial_t \varphi_\mu^{(N)}, \eta^{(N)}\right) \mathrm{d}t \to \int_0^T \left(\partial_t \varphi_\mu, \eta^{(N)}\right) \mathrm{d}t \qquad \text{as} \qquad n \to \infty. \tag{B.128}$$

Using the sequence in (B.127),

$$\int_0^T \left(\partial_t \varphi_\mu, \eta^{(N)}\right) \mathrm{d}t \to \int_0^T \left(\partial_t \varphi_\mu, \eta\right) \mathrm{d}t \qquad \text{in } \mathbb{R} \qquad \text{as} \qquad N \to \infty. \tag{B.129}$$

We argue similarly for the second term of (B.126a) using (B.124b), and for the first and last terms of (B.126b) using (B.113c) and (B.124a).

3. We establish the convergence of the non-linear term in (B.126b). First, since $\varphi_\mu(t) \in L^2(\Omega)$ for every $t \in [0,T]$ by (4.45c) (cf. (B.118)),

$$\left\|\mathcal{B}'_\mu(\varphi_\mu)\right\| \leq \frac{\chi^{AB}}{2}\|\varphi_\mu\| + \frac{1}{\mu}\left\|(\varphi_\mu-1)_+ + (\varphi_\mu+1)_-\right\| \leq \left(\frac{\chi^{AB}}{2}+\frac{1}{\mu}\right)\|\varphi_\mu\| < \infty$$

upon using (4.8) with $\mu < 1$. We use this, together with (B.127), (B.120), (4.7) and (4.17) for $\mu > 0$, to conclude that

$$\begin{aligned}
&\left|\int_0^T \left(\mathcal{B}'_\mu\left(\varphi_\mu^{(N)}\right), \eta^{(N)}\right) - \left(\mathcal{B}'_\mu(\varphi_\mu), \eta\right) \mathrm{d}t\right| \\
&\quad \leq \int_0^T \left|\left(\mathcal{B}'_\mu\left(\varphi_\mu^{(N)}\right) - \mathcal{B}'_\mu(\varphi_\mu), \eta^{(N)}\right) - \left(\mathcal{B}'_\mu(\varphi_\mu), \eta-\eta^{(N)}\right)\right| \mathrm{d}t \\
&\quad \leq \int_0^T \left(\frac{\chi^{AB}}{2}+\frac{1}{\mu}\right)\left\|\varphi_\mu^{(N)}-\varphi_\mu\right\|\left\|\eta^{(N)}\right\| \mathrm{d}t + \int_0^T \left\|\mathcal{B}'_\mu(\varphi_\mu)\right\|\left\|\eta-\eta^{(N)}\right\| \mathrm{d}t \to 0
\end{aligned} \tag{B.130}$$

as $n, N \to \infty$.

4. Finally, we consider the third (non-local) term of (B.126b). The weak convergence in (B.113b) implies that, for any $\eta \in L^2\left(0,T;L^2(\Omega)\right)$,

$$\int_0^T \left(\varphi_\mu^{(N)}, \eta\right)\ \mathrm{d}t \to \int_0^T (\varphi_\mu, \eta)\ \mathrm{d}t \qquad \text{(in } \mathbb{R}\text{) as } n \to \infty.$$

In particular, we may choose $\eta = \phi(t)\,1(x)$ and any $\phi \in C_c^\infty(0,T)$ to see that

$$\int_0^T \overline{\varphi_\mu^{(N)}(t)}\phi(t)\ \mathrm{d}t \to \int_0^T \overline{\varphi_\mu(t)}\phi(t)\ \mathrm{d}t \qquad \text{(in } \mathbb{R}\text{) as } n \to \infty.$$

Taking the limit on the left, noting the uniqueness of limits of sequences of real numbers and recalling (4.41), we discover that

$$\begin{aligned}
&\int_0^T \left(\overline{\varphi_\mu(t)} - m\right)\phi(t)\ \mathrm{d}t = 0 \qquad \text{for any} \qquad \phi \in C_c^\infty(0,T) \\
&\qquad \Rightarrow \qquad \overline{\varphi_\mu(t)} = m \qquad \text{for a.e.} \qquad t \in (0,T).
\end{aligned} \tag{B.131}$$

Consequently, $\overline{\varphi_\mu^{(N)} - \varphi_\mu} = 0$ for any $n \geq 1$, and so for any $\eta \in L^2\left(0,T;H^1(\Omega)\right)$ and a sequence $\eta^{(N)} \to \eta$ as in (B.127) (cf. (B.130)),

$$\begin{aligned}
&\left|\int_0^T \left((-\Delta_n)^{-1}\left(\varphi_\mu^{(N)} - \overline{\varphi_\mu^{(N)}}\right), \eta^{(N)}\right) - \left((-\Delta_n)^{-1}\left(\varphi_\mu - \overline{\varphi_\mu}\right), \eta\right) \mathrm{d}t\right| \\
&\quad \leq \int_0^T \left\|(-\Delta_n)^{-1}\left(\varphi_\mu^{(N)} - \varphi_\mu\right)\right\| \left\|\eta^{(N)}\right\| \mathrm{d}t + \left|\int_0^T \left\|(-\Delta_n)^{-1}\left(\varphi_\mu - \overline{\varphi_\mu}\right)\right\| \left\|\eta^{(N)} - \eta\right\| \mathrm{d}t\right| \\
&\quad \leq c_P^2 \left(\int_0^T \left\|\varphi_\mu^{(N)} - \varphi_\mu\right\| \left\|\eta^{(N)}\right\| + \|\varphi_\mu\| \left\|\eta^{(N)} - \eta\right\| \mathrm{d}t\right) \\
&\quad \leq c_P^2 \left(\left\|\varphi_\mu^{(N)} - \varphi_\mu\right\|_{L^2(\Omega_T)} \left\|\eta^{(N)}\right\|_{L^2(\Omega_T)} + \|\varphi_\mu\|_{L^2(\Omega_T)} \left\|\eta^{(N)} - \eta\right\|_{L^2(\Omega_T)}\right) \to 0
\end{aligned} \tag{B.132}$$

as $n, N \to \infty$, by the Cauchy–Schwarz inequality and (B.127) and where, according to (A.30a) and (B.119), $\left\|(-\Delta_n)^{-1}\left(\varphi_\mu^{(N)} - \varphi_\mu\right)\right\| \to 0$ for a.e. $t \in (0,T)$. We also used (B.113a) to conclude that $\left\|(-\Delta_n)^{-1}\left(\varphi_\mu - \overline{\varphi_\mu}\right)\right\| \leq c_P \|\varphi_\mu\|_{-1} \leq c_P^2 \|\varphi_\mu\|$ and $\|\varphi_\mu\|_{L^2(\Omega_T)} < \infty$.

5. Combining all of the above, we find that

$$\int_0^T \langle \partial_t \varphi_\mu, \nu_1 \rangle + (\nabla \psi_\mu, \nabla \nu_1) \, \mathrm{d}t = 0 \tag{B.133a}$$

$$\int_0^T \varepsilon_\varphi^2 (\nabla \varphi_\mu, \nabla \nu_2) + \left(\mathcal{B}_\mu'(\varphi_\mu), \nu_2\right) + \alpha \left((-\Delta_n)^{-1}\left(\varphi_\mu - \overline{\varphi_\mu}\right), \nu_1\right) \mathrm{d}t = \int_0^T (\psi_\mu, \nu_2) \, \mathrm{d}t \tag{B.133b}$$

for any $\nu_1, \nu_2 \in L^2\left(0,T;H^1(\Omega)\right)$.[40] In particular (cf. Lemma 7.4 of Robinson (2001)),

$$\langle \partial_t \varphi_\mu, \nu_1 \rangle + (\nabla \psi_\mu, \nabla \nu_1) = 0 \tag{B.134a}$$

$$\varepsilon_\varphi^2 (\nabla \varphi_\mu, \nabla \nu_2) + \left(\mathcal{B}_\mu'(\varphi_\mu), \nu_2\right) + \alpha \left((-\Delta_n)^{-1}\left(\varphi_\mu - \overline{\varphi_\mu}\right), \nu_1\right) = (\psi_\mu, \nu_2) \tag{B.134b}$$

for any $\nu_1, \nu_2 \in H^1(\Omega)$ and a.e. $t \in (0,T)$ i.e. (φ_μ, ψ_μ) solves (4.39a)–(4.39b).

ix) We deal with the IC. We know that $\varphi_\mu(0) \in L^2(\Omega)$ as a result of (B.118). We wish to show that $\varphi_\mu(0) = \varphi_0$ as in (4.39c). As in Section 7.4.4 of Robinson (2001), or part 3 of Theorem 3 of Section 7.1 of Evans (1998), we set $\nu_1 = \phi \in C^1\left([0,T]; L^2(\Omega)\right)$ with $\phi(T) = 0$ in (B.134a) and integrate in time from 0 to T. An integration by parts (in time) in the first term then reveals that

$$\int_0^T -\langle \varphi_\mu, \phi' \rangle + (\nabla \psi_\mu, \nabla \phi) \ \mathrm{d}t = (\varphi_\mu(0), \phi(0)) \tag{B.135a}$$

for any ϕ as specified. Likewise, from (B.126a), we find that

$$\int_0^T -\left\langle \varphi_\mu^{(N)}, \phi' \right\rangle + \left(\nabla \psi_\mu^{(N)}, \nabla \phi\right) \mathrm{d}t = \left(\varphi_\mu^{(N)}(0), \phi(0)\right),$$

for each $n \geq N$ and any ϕ as above. From the results above, we can take weak limits in each term above to find that

$$\int_0^T -\langle \varphi_\mu, \phi' \rangle + (\nabla \psi_\mu, \nabla \phi) \, \mathrm{d}t = (\varphi_0, \phi(0)). \tag{B.135b}$$

The last term on the right side follows from the fact that $\varphi_\mu^{(N)}(0) = P^n \varphi_0 \to \varphi_0$ in $L^2(\Omega)$ by (4.40d) and (A.63a), viz.

$$\left|\left(\varphi_\mu^{(N)}(0) - \varphi_0, \phi(0)\right)\right| \leq \left\|\varphi_\mu^{(N)}(0) - \varphi_0\right\| \|\phi(0)\| \to 0.$$

Comparing (B.135a) and (B.135b), we conclude that $(\varphi_\mu(0), \phi(0)) = (\varphi_0, \phi(0))$ for arbitrary $\phi(0)$ i.e. $\varphi_\mu(0) = \varphi_0$. It follows that $\overline{\varphi_\mu(0)} = \overline{\varphi_0} = m$.

x) We can improve on the result in (B.131). We set $\nu_1 \equiv 1$ in (B.134a) to discover that $\langle \partial_t \varphi_\mu, 1 \rangle = 0$ for a.e. $t \in [0,T]$. We then integrate in time from 0 to any t' such that $0 < t' \leq T$, and then integrate by parts (in time) to find that

$$\int_0^T - \langle \varphi_\mu, 1' \rangle \, \mathrm{d}t = 0 = (\varphi_0, 1) - \left(\varphi_\mu\left(t'\right), 1\right) \qquad \Rightarrow \qquad \overline{\varphi_\mu\left(t'\right)} = \overline{\varphi_0} = m,$$

which is (4.46). Note that we needed (4.45c) to make sense of this last equality.

□

B.11 Proof of Theorem 4.3.4

Proof. i) First, observe that $\overline{\varphi_\mu} = \overline{\varphi_1 - \varphi_2} = 0$ by (4.46). U_1 satisfies

$$\langle \partial_t \varphi_1, \nu_1 \rangle + (\nabla \psi_1, \nabla \nu_1) = 0$$
$$(\psi_1, \nu_2) = \varepsilon_\varphi^2 (\nabla \varphi_1, \nabla \nu_2) + \left(\mathcal{B}_\mu'(\varphi_1), \nu_2\right) + \alpha \left((-\Delta_n)^{-1}(\varphi_1 - \overline{\varphi_1}), \nu_1\right)$$

for every $\nu_1, \nu_2 \in H^1(\Omega)$ and a.e. $t \in (0,T)$, and similarly for U_2. Subtracting these leads to the following problem for $U = \{\varphi_\mu, \psi_\mu\}$ as in the statement of the theorem:
$\left(\mathbf{P}_\mu^{(\mathrm{diff})}\right)$: find $\varphi_\mu(t), \psi_\mu(t)$ as in $(\mathbf{P}_\mu)$ such that

$$\langle \partial_t \varphi_\mu, \nu_1 \rangle + (\nabla \psi_\mu, \nabla \nu_1) = 0 \tag{B.136a}$$
$$(\psi_\mu, \nu_2) = \varepsilon_\varphi^2 (\nabla \varphi_\mu, \nabla \nu_2) + (\zeta_\mu(\varphi_1) - \zeta_\mu(\varphi_2), \nu_2) - \frac{\chi^{AB}}{2}(\varphi_\mu, \nu_2) + \alpha \left((-\Delta_n)^{-1} \varphi_\mu, \nu_2\right) \tag{B.136b}$$

for every $\nu_1, \nu_2 \in H^1(\Omega)$ and a.e. $t \in (0,T)$, where

$$\varphi_\mu(0) = (\varphi_1)_0 - (\varphi_2)_0 \tag{B.136c}$$

with $(\varphi_1)_0$ and $(\varphi_2)_0$ two ICs as in (4.39c).

ii) Putting $\nu_2 = \varphi_\mu = \varphi_1 - \varphi_2$ in (B.136b) yields[41]

$$\varepsilon_\varphi^2 |\varphi_\mu|_1^2 - \frac{\chi^{AB}}{2} \|\varphi_\mu\|^2 + \alpha \|\varphi_\mu\|_{-1}^2 = (\psi_\mu, \varphi_\mu) - \underbrace{(\zeta_\mu(\varphi_1) - \zeta_\mu(\varphi_2), \varphi_1 - \varphi_2)}_{\geq 0 \text{ by (4.19)}} \leq (\psi_\mu, \varphi_\mu).$$

After discarding $\alpha \|\varphi_\mu\|_{-1}^2 \geq 0$ on the left, we find that

$$\varepsilon_\varphi^2 |\varphi_\mu|_1^2 - \frac{\chi^{AB}}{2} \|\varphi_\mu\|^2 \leq (\psi_\mu, \varphi_\mu). \tag{B.137}$$

iii) We now set $\nu_1 = (-\Delta_n)^{-1} \varphi_\mu$ (well-defined since $\varphi_\mu \in L_*^2(\Omega)$) in (B.136a) to obtain

$$\frac{1}{2} \frac{\mathrm{d}}{\mathrm{d}t} \|\varphi_\mu\|_{-1}^2 + (\psi_\mu, \varphi_\mu) = 0 \tag{B.138}$$

since $\left(\nabla \psi_\mu, \nabla (-\Delta_n)^{-1} \varphi_\mu\right) = (\psi_\mu, \varphi_\mu)$ by (2.9a), and also

$$\begin{aligned} \frac{\mathrm{d}}{\mathrm{d}t} \|\varphi_\mu\|_{-1}^2 &= \left(\varphi_\mu', (-\Delta_n)^{-1} \varphi_\mu\right) + \left(\varphi_\mu, (-\Delta_n)^{-1} \varphi_\mu'\right) \\ &= \left(\varphi_\mu', (-\Delta_n)^{-1} \varphi_\mu\right) + \left((-\Delta_n)^{-1} \varphi_\mu, \varphi_\mu'\right) = 2 \left\langle \partial_t \varphi_\mu, (-\Delta_n)^{-1} \varphi_\mu \right\rangle, \end{aligned} \tag{B.139}$$

due to (2.12).[42] Substituting (B.138) into (B.137) leads to[43]

$$\frac{1}{2}\frac{\mathrm{d}}{\mathrm{d}t}\left\|\varphi_\mu\right\|_{-1}^2+\varepsilon_\varphi^2\left|\varphi_\mu\right|_1^2\leq\frac{\chi^{AB}}{2}\left\|\varphi_\mu\right\|^2=\frac{\chi^{AB}}{2}\left(\nabla\varphi_\mu,\nabla\left(-\Delta_n\right)^{-1}\varphi_\mu\right)$$
$$\leq\frac{\chi^{AB}}{2}\left|\varphi_\mu\right|_1\left\|\varphi_\mu\right\|_{-1}\leq\frac{\varepsilon_\varphi^2}{2}\left|\varphi_\mu\right|_1^2+\frac{1}{2}\frac{\left(\chi^{AB}\right)^2}{4\varepsilon_\varphi^2}\left\|\varphi_\mu\right\|_{-1}^2, \quad \text{(B.140)}$$

after using the Cauchy–Schwarz and Young's inequalities. Hence,

$$\frac{\mathrm{d}}{\mathrm{d}t}\left\|\varphi_\mu\right\|_{-1}^2+\varepsilon_\varphi^2\left|\varphi_\mu\right|_1^2\leq\frac{\left(\chi^{AB}\right)^2}{4\varepsilon_\varphi^2}\left\|\varphi_\mu\right\|_{-1}^2. \quad \text{(B.141)}$$

Integrating this in time from 0 to t yields

$$\left\|\varphi_\mu\left(t\right)\right\|_{-1}^2+\varepsilon_\varphi^2\int_0^t\left|\varphi_\mu\left(s\right)\right|_1^2\mathrm{d}s\leq\left\|\varphi_0\right\|_{-1}^2+\frac{\left(\chi^{AB}\right)^2}{4\varepsilon_\varphi^2}\int_0^t\left\|\varphi_\mu\left(s\right)\right\|_{-1}^2\mathrm{d}s$$

where $\varphi_0=\varphi_\mu\left(0\right)=\left(\varphi_1\right)_0-\left(\varphi_2\right)_0$. Gronwall's Lemma then implies that

$$\left\|\varphi_\mu\left(t\right)\right\|_{-1}^2+\varepsilon_\varphi^2\int_0^t\left|\varphi_\mu\left(s\right)\right|_1^2\mathrm{d}s\leq\left\|\varphi_0\right\|_{-1}^2\exp\left\{\frac{\left(\chi^{AB}\right)^2}{4\varepsilon_\varphi^2}T\right\}=C\left(T\right)\left\|\varphi_0\right\|_{-1}^2, \quad \text{(B.142)}$$

where $C\left(T\right)$ is independent of μ. If we now set $\left(\varphi_1\right)_0=\left(\varphi_2\right)_0\in\mathscr{A}_m$, so that $\varphi_0\equiv0$ viz. $\left\|\varphi_0\right\|_{-1}^2=0$, then $\left\|\varphi_\mu\left(t\right)\right\|_{-1}^2=0$, whence $\varphi_\mu\left(t\right)\equiv0$, by mass conservation, $\overline{\varphi_\mu\left(t\right)}=0$ i.e. $\varphi_\mu\left(t\right)\in L_*^2\left(\Omega\right)$, for a.e. $t\in\left(0,T\right)$. We conclude that φ_μ solving problem $\left(\mathbf{P}_\mu\right)$ is unique.

iv) We now establish the uniqueness of ψ_μ solving problem $\left(\mathbf{P}_\mu\right)$. If $\varphi_1=\varphi_2$ (viz. $\varphi_\mu\equiv0$) and we set $\psi_\mu=1$ in (B.136b), we find that $\overline{\psi_\mu\left(t\right)}=0$ for a.e. $t\in\left(0,T\right)$, and so the mass of ψ_μ is also conserved i.e. $\psi_\mu\in L_*^2\left(\Omega\right)$. Likewise, if we set $\nu_1=\psi_\mu$ in (B.136a) with $\varphi_\mu\equiv0$, we find that $\left|\psi_\mu\left(t\right)\right|_1^2=0$ for a.e. $t\in\left(0,T\right)$. But since $\psi_\mu\in L_*^2\left(\Omega\right)$, $\psi_\mu\equiv0$. Hence, ψ_μ solving problem $\left(\mathbf{P}_\mu\right)$ is unique.

□

B.12 Proof of Theorem 4.3.5

Proof.

i) We base our argument on the remark above Theorem 2.2 of Blowey and Elliott (1991). Using the energy in (4.6) and setting $r=\varphi_\mu^{(N)}\left(t\right)$ and $s=\varphi_\mu\left(t\right)$ in (4.16), we find that

$$\mathcal{E}_\mu\left[\varphi_\mu^{(N)}\left(t\right)\right]=\mathcal{E}\left[\varphi_\mu^{(N)}\left(t\right)\right]+\left(\Upsilon_\mu\left(\varphi_\mu^{(N)}\left(t\right)\right),1\right)$$
$$\geq\mathcal{E}\left[\varphi_\mu^{(N)}\left(t\right)\right]+\left(\Upsilon_\mu\left(\varphi_\mu\left(t\right)\right),1\right)+\left(\zeta_\mu\left(\varphi_\mu\left(t\right)\right),\varphi_\mu^{(N)}\left(t\right)-\varphi_\mu\left(t\right)\right). \quad \text{(B.143)}$$

We analyse (B.143) in much the same way we did (B.86). We consider the first and third terms on the right as $N\to\infty$ (ignoring the second as it is N-independent).

- For the first term, (4.1) reveals that

$$\liminf_{N\to\infty}\mathcal{E}\left[\varphi_\mu^{(N)}\right]=\liminf_{N\to\infty}\left\{\frac{\varepsilon_\varphi^2}{2}\left|\varphi_\mu^{(N)}\right|_1^2+\left(\mathcal{B}\left(\varphi_\mu^{(N)}\right),1\right)+\frac{\alpha}{2}\left\|\varphi_\mu^{(N)}-\overline{\varphi_\mu^{(N)}}\right\|_{-1}^2\right\}.$$

According to (B.122), $\varphi_\mu^{(N)}\left(t\right)\rightharpoonup\varphi_\mu\left(t\right)$ in $H^1\left(\Omega\right)$ for every $t>0$, and so, arguing as we did in Theorem 4.3.3, we conclude that (cf. (B.113), (B.463)) $\nabla\psi_\mu^{(N)}\rightharpoonup\nabla\psi_\mu$ in $L^2\left(\Omega\right)$ for every $t>0$. Consequently,

$$\left|\varphi_\mu\left(t\right)\right|_1\leq\liminf_{N\to\infty}\left|\varphi_\mu^{(N)}\left(t\right)\right|_1\qquad\text{for every}\qquad0<t\leq T,$$

using well-known properties of weakly convergent sequences (cf. Lemma 4.14 of Robinson (2001)). Hence,

$$|\varphi_\mu(t)|_1^2 \leq \liminf_{N\to\infty} \left|\varphi_\mu^{(N)}(t)\right|_1^2 \qquad \text{for every} \qquad 0 < t \leq T.$$

Also,

$$\liminf_{N\to\infty} \left(\mathcal{B}\left(\varphi_\mu^{(N)}(t)\right), 1\right) = \lim_{N\to\infty} \frac{\chi^{AB}}{4} \left(|\Omega| - \left\|\varphi_\mu^{(N)}(t)\right\|^2\right) = \left(\mathcal{B}\left(\varphi_\mu(t)\right), 1\right)$$

for a.e. $t \in (0,T)$, because $\varphi_\mu^{(N)}(t) \to \varphi_\mu(t)$ (strongly) in $L^2(\Omega)$. Finally, arguing as in (A.30a) and using (4.41), (4.46),

$$\left\|\left(\varphi_\mu^{(N)} - \overline{\varphi_\mu^{(N)}}\right)(t) - \left(\varphi_\mu - \overline{\varphi_\mu}\right)(t)\right\|_{-1} = \left\|\varphi_\mu^{(N)}(t) - \varphi_\mu(t)\right\|_{-1} \leq c_P^2 \left\|\varphi_\mu^{(N)}(t) - \varphi_\mu(t)\right\| \to 0,$$

for a.e. $t \in (0,T)$, again because $\varphi_\mu^{(N)}(t) \to \varphi_\mu(t)$ (strongly) in $L^2(\Omega)$. Hence,

$$\liminf_{N\to\infty} \left\|\varphi_\mu^{(N)} - \overline{\varphi_\mu^{(N)}}\right\|_{-1}^2 = \lim_{N\to\infty} \left\|\varphi_\mu^{(N)} - \overline{\varphi_\mu^{(N)}}\right\|_{-1}^2 = \left\|\varphi_\mu - \overline{\varphi_\mu}\right\|_{-1}^2.$$

Combining the results above, it follows that

$$\mathcal{E}[\varphi_\mu] \leq \liminf_{N\to\infty} \mathcal{E}\left[\varphi_\mu^{(N)}\right] \qquad \text{for every} \qquad 0 < t \leq T. \tag{B.144a}$$

- For the second term,

$$\left(\zeta_\mu\left(\varphi_\mu(t)\right), \varphi_\mu^{(N)}(t) - \varphi_\mu(t)\right) \leq \left\|\zeta_\mu\left(\varphi_\mu(t)\right)\right\| \left\|\varphi_\mu^{(N)}(t) - \varphi_\mu(t)\right\| \to 0 \tag{B.144b}$$

as $N \to \infty$ for a.e. $t \in (0,T)$ by the Cauchy–Schwarz inequality, and using the strong convergence of $\varphi_\mu^{(N)}(t) \to \varphi_\mu(t)$ in $L^2(\Omega)$.

Hence,

$$\mathcal{E}_\mu[\varphi_\mu(t)] = \mathcal{E}[\varphi_\mu(t)] + \left(\Upsilon_\mu\left(\varphi_\mu(t)\right), 1\right) \leq \liminf_{N\to\infty} \mathcal{E}_\mu\left[\varphi_\mu^{(N)}(t)\right] \tag{B.145a}$$

for any $t > 0$ (strictly).[44] The weak convergence of $\psi_\mu^{(N)} \rightharpoonup \psi_\mu$ in $L^2\left(0,T;H^1(\Omega)\right)$ in (B.123) means that $\nabla\psi_\mu^{(N)} \rightharpoonup \nabla\psi_\mu$ in $L^2\left(0,T;L^2(\Omega)\right)$. It follows that,

$$\int_0^t |\psi_\mu(s)|_1^2 \, \mathrm{d}s \leq \liminf_{N\to\infty} \int_0^t \left|\psi_\mu^{(N)}(s)\right|_1^2 \, \mathrm{d}s \qquad \text{for every} \qquad 0 < t \leq T. \tag{B.145b}$$

Combining (B.145a)–(B.145b) and consulting (B.84) and (B.88) yields

$$\begin{aligned}\mathcal{E}_\mu[\varphi_\mu(t)] + \int_0^t |\psi_\mu(s)|_1^2 \, \mathrm{d}s &\leq \liminf_{N\to\infty} \left\{\mathcal{E}_\mu\left[\varphi_\mu^{(N)}(t)\right] + \int_0^t \left|\psi_\mu^{(N)}(s)\right|_1^2 \mathrm{d}s\right\} \\ &\leq \liminf_{N\to\infty} \mathcal{E}_\mu\left[P^N\varphi_0\right] \leq \limsup_{N\to\infty} \mathcal{E}_\mu\left[P^N\varphi_0\right] \leq \mathcal{E}_\mu[\varphi_0], \end{aligned} \tag{B.146}$$

for N sufficiently large. This implies (4.47a).

ii) For the second part, we use the 'stop-start' argument at the end of Theorem 2.2 of Blowey and Elliott (1991). Because of (4.45d) and (4.46), $\varphi_\mu(t') \in H_m^1(\Omega)$ for any $t' > 0$ (strictly). Consequently, the energy $\mathcal{E}_\mu[\varphi_\mu(t')] < \infty$. We therefore re-start problem $(\mathbf{P}_\mu)$ at $t = t'$, and consider the time-shifted problem $\left(\widetilde{\mathbf{P}}_\mu\right)$ with $t \in (0, T - t')$, with solution $\left\{\widetilde{\varphi}_\mu, \widetilde{\psi}_\mu\right\}$, where $\left(\widetilde{\varphi}_\mu(t), \widetilde{\psi}_\mu(t)\right) = \left(\varphi_\mu(t+t'), \psi_\mu(t+t')\right)$

(by the uniqueness of solutions of both of these problems), and $\left(\widetilde{\mathbf{P}}_\mu\right)$ has IC $\widetilde{\varphi}_0 = \varphi_\mu(t') \in H^1(\Omega)$. Stating (4.47a) for problem $\left(\widetilde{\mathbf{P}}_\mu\right)$, yields

$$\mathcal{E}_\mu\left[\widetilde{\varphi}_\mu(t)\right] + \int_0^t \left|\widetilde{\psi}_\mu(s)\right|_1^2 \mathrm{d}s \leq \mathcal{E}_\mu\left[\widetilde{\varphi}_0\right] \qquad \text{for any} \qquad 0 \leq t \leq T - t', \tag{B.147}$$

or, after setting $\tau = t + t'$, so that $t = \tau - t'$,

$$\mathcal{E}_\mu\left[\varphi_\mu(\tau)\right] + \int_{t'}^\tau |\psi_\mu(s)|_1^2 \mathrm{d}s \leq \mathcal{E}_\mu\left[\varphi_0\right] \qquad \text{for any} \qquad 0 < t' \leq \tau \leq T. \tag{B.148}$$

Relabelling τ as t yields (4.47b).

Remark. In the first inequality in (B.147) above, '$0 \leq t$' is not strict, whereas the corresponding part of (4.47a) is. This is because we know that φ_μ solving $(\mathbf{P}_\mu)$ maps continuously into $H^1(\Omega)$ for all $t \geq t' > 0$ (strictly) by (4.45d). But that means that $\widetilde{\varphi}_\mu$ solving $\left(\widetilde{\mathbf{P}}_\mu\right)$ maps continuously into $H^1(\Omega)$ for every t in that problem's time horizon, by the uniqueness of solutions of $(\mathbf{P}_\mu)$.

iii) (4.48) is a pedantic restatement of (4.47).

□

B.13 Proof of Theorem 4.3.6

Proof.

i) Since $\varphi_\mu \in L^\infty\left(0,T;H^1(\Omega)\right) \cap H^1\left(0,T;\left(H^1(\Omega)\right)'\right)$ and $\psi_\mu \in L^2\left(0,T;H^1(\Omega)\right)$ by (4.45), are bounded independent of μ, we may take sub-sequences of (φ_μ) and (ψ_μ) (in which we vary μ) and infer the existence of $\varphi \in H^1\left(0,T;\left(H^1(\Omega)\right)'\right) \cap L^\infty\left(0,T;H^1(\Omega)\right)$ and $\psi \in L^2\left(0,T;H^1(\Omega)\right)$ such that[45]

$$\varphi_\mu \rightharpoonup \varphi \quad \text{in} \quad H^1\left(0,T;\left(H^1(\Omega)\right)'\right) \cap L^2\left(0,T;H^1(\Omega)\right), \tag{B.149a}$$

$$\varphi_\mu \overset{\star}{\rightharpoonup} \varphi \quad \text{in} \quad L^\infty\left(0,T;H^1(\Omega)\right), \tag{B.149b}$$

$$\varphi_\mu \to \varphi \quad \text{in} \quad L^2\left(\Omega_T\right), \tag{B.149c}$$

$$\psi_\mu \rightharpoonup \psi \quad \text{in} \quad L^2\left(0,T;H^1(\Omega)\right), \tag{B.149d}$$

as $\mu \downarrow 0$, in much the same way we did in the proof of Theorem 4.3.3.

ii) We pass $\mu \downarrow 0$ (taking appropriate sub-sequences) in (4.39a) to obtain (4.37a).[46]

iii) We now consider (4.39b). We use (4.7) and integrate in time to see that

$$\int_0^T \varepsilon_\varphi^2\left(\nabla\varphi_\mu, \nabla\nu_2\right) - \frac{\chi^{AB}}{2}\left(\varphi_\mu, \nu_2\right) + \alpha\left(\left(-\Delta_n\right)^{-1}\left(\varphi_\mu - \overline{\varphi_\mu}\right), \nu_2\right) - \left(\psi_\mu, \nu_2\right) \mathrm{d}t = \int_0^T -\left(\zeta_\mu\left(\varphi_\mu\right), \nu_2\right) \mathrm{d}t$$

for every $\nu_2 \in L^2\left(0,T;H^1(\Omega)\right)$. In particular, if $\nu_2 = \nu - \varphi_\mu$, with $\nu \in L^2\left(0,T;\mathscr{A}\right)$ so that $\zeta_\mu(\nu) = 0$ a.e. in Ω, then

$$\begin{aligned}\int_0^T \varepsilon_\varphi^2\left(\nabla\varphi_\mu, \nabla\nu - \nabla\varphi_\mu\right) - \left(\psi_\mu + \frac{\chi^{AB}}{2}\varphi_\mu - \alpha\left(-\Delta_n\right)^{-1}\left(\varphi_\mu - \overline{\varphi_\mu}\right), \nu - \varphi_\mu\right) \mathrm{d}t \\ = \int_0^T \left(\zeta_\mu(\nu) - \zeta_\mu\left(\varphi_\mu\right), \nu - \varphi_\mu\right) \mathrm{d}t = \frac{1}{\mu}\int_0^T \left(\zeta(\nu) - \zeta\left(\varphi_\mu\right), \nu - \varphi_\mu\right) \mathrm{d}t \geq 0\end{aligned} \tag{B.150}$$

by (4.20b). It remains to show that $\varphi(t) \in \mathscr{A}$ (cf. (B.149)) for a.e. $t \in (0,T)$, and that we can use (B.149) to recover (4.37b) from (B.150).

iv) We set $\nu_2 = \mu\zeta_\mu(\varphi_\mu) = \zeta(\varphi_\mu) \in H^1(\Omega)$ using (4.23), (4.20) in (4.39b), and use (4.7) to conclude that

$$\varepsilon_\varphi^2 (\nabla\varphi_\mu, \nabla\zeta(\varphi_\mu)) + \mu \|\zeta_\mu(\varphi_\mu)\|^2 \leq \mu \left(\frac{\chi^{AB}}{2} \|\varphi_\mu\| + \|\psi_\mu\| \right) \|\zeta_\mu(\varphi_\mu)\| + \alpha \left\| (-\Delta_n)^{-1} (\varphi_\mu - \overline{\varphi_\mu}) \right\| \|\mu\zeta_\mu(\varphi_\mu)\|, \quad \text{(B.151)}$$

after using the Cauchy–Schwarz inequality. Now $\left\|(-\Delta_n)^{-1}(\varphi_\mu - \overline{\varphi_\mu})\right\| \leq c_P^3 |\varphi_\mu|_1$ from (A.30b), and so by Young's inequality,

$$\varepsilon_\varphi^2 (\nabla\varphi_\mu, \nabla\zeta(\varphi_\mu)) + \mu \|\zeta_\mu(\varphi_\mu)\|^2 \leq \frac{3\mu}{4} \|\zeta_\mu(\varphi_\mu)\|^2 + \mu \left(\frac{\left(\chi^{AB}\right)^2}{2} \|\varphi_\mu\|^2 + \frac{\alpha^2 c_P^6}{2} |\varphi_\mu|_1^2 + 2\|\psi_\mu\|^2 \right)$$

i.e.

$$\varepsilon_\varphi^2 (\nabla\varphi_\mu, \nabla\zeta(\varphi_\mu)) + \frac{\mu}{4} \|\zeta_\mu(\varphi_\mu)\|^2 \leq \mu \left(C \|\varphi_\mu\|_1^2 + 2\|\psi_\mu\|^2 \right), \quad \text{(B.152)}$$

with C independent of μ.[47]

v) The left-most term of (B.152) is identical to the corresponding term in (B.44). Using (B.45) we therefore discard it and rearrange, to see that (cf. (B.46))

$$\|\zeta_\mu(\varphi_\mu)\|^2 \leq 4\left(C\|\varphi_\mu\|_1^2 + 2\|\psi_\mu\|^2\right) \leq C \quad \Rightarrow \quad \|\zeta(\varphi_\mu)\|^2 \leq C\mu^2, \quad \text{(B.153)}$$

with C independent of μ, by (4.45b) and (4.58). Hence,

$$\|\zeta(\varphi_\mu)\|_{L^2(\Omega_T)} = \left(\int_0^T \|\zeta(\varphi_\mu)\|^2 \, \mathrm{d}t \right)^{1/2} \leq C\mu \quad \Rightarrow \quad \lim_{\mu \downarrow 0} \|\zeta(\varphi_\mu)\|_{L^2(\Omega_T)} = 0 \quad \text{(B.154)}$$

since C is independent of μ.[48] Using (B.45) and (B.152), we discover that

$$|\zeta(\varphi_\mu)|_1^2 \leq (\nabla\varphi_\mu, \nabla\zeta(\varphi_\mu)) \leq C\mu \quad \text{(B.155)}$$

which means that (note the non-standard norm in what follows)

$$|\zeta(\varphi_\mu)|_{L^2\left(0,T;H^1(\Omega)\right)} := \left(\int_0^T |\zeta(\varphi_\mu)|_1^2 \, \mathrm{d}t \right)^{1/2} \leq C\mu^{1/2} \quad \text{(B.156)}$$

with C independent of μ. Combining (B.154) and (B.156) for $\mu < 1$ leads to[49]

$$\|\zeta(\varphi_\mu)\|_{L^2\left(0,T;H^1(\Omega)\right)} \leq C\mu^{1/2} \quad \Rightarrow \quad \lim_{\mu \downarrow 0} \|\zeta(\varphi_\mu)\|_{L^2\left(0,T;H^1(\Omega)\right)} = 0 \quad \text{(B.157)}$$

since C is independent of μ.

vi) For any $\eta \in L^2\left(0,T;H^1(\Omega)\right)$ (cf. (B.130) on p. 373), it follows that

$$\begin{aligned} \int_0^T |(\zeta(\varphi), \eta)| \, \mathrm{d}t &\leq \int_0^T \left(\|\zeta(\varphi) - \zeta(\varphi_\mu)\| + \|\zeta(\varphi_\mu)\| \right) \|\eta\| \, \mathrm{d}t \\ &\leq \int_0^T \left(\|\varphi - \varphi_\mu\| + C\mu \right) \|\eta\| \, \mathrm{d}t \\ &\leq C \left(\|\varphi - \varphi_\mu\|_{L^2(\Omega_T)} + \mu \right) \|\eta\|_{L^2(\Omega_T)} \to 0 \quad \text{as } \mu \downarrow 0, \end{aligned} \quad \text{(B.158)}$$

by the Cauchy–Schwarz inequality in $L^2(\Omega_T)$, and after noting (4.20a), (4.20b), (B.149c) and (B.153). Hence, $\zeta(\varphi) = 0$, viz. $|\varphi| \leq 1$ a.e. in Ω for a.e. $t \in (0,T)$, that is, $\varphi(t) \in \mathscr{A}$ for a.e. $t \in (0,T)$.

vii) We consider the non-local term in (B.150). In preparation for this, we consider $\overline{\varphi}$ and the convergence properties of $\overline{\varphi_\mu}$ as $\mu \downarrow 0$. Observe that $\left(\overline{\varphi_\mu(t)}\right)$ is the constant sequence $m, m, \ldots$ as $\mu \downarrow 0$, for a.e. $t \in (0,T)$. As in (B.131), we conclude that

$$\overline{\varphi(t)} = m \qquad \text{for a.e.} \qquad t \in [0,T), \tag{4.49}$$

(with $\overline{\varphi(0)} = m$ by (4.37c)). Hence, $\overline{\varphi_\mu - \varphi} = 0$ for any $\mu \geq 0$, and so for any $\nu \in L^2\left(0,T;H^1(\Omega)\right)$,

$$\begin{aligned}\left|\int_0^T \left((-\Delta_n)^{-1}(\varphi_\mu - \overline{\varphi_\mu}) - (-\Delta_n)^{-1}(\varphi - \overline{\varphi}), \nu\right) \mathrm{d}t\right| \\ = \left|\int_0^T \left((-\Delta_n)^{-1}(\varphi_\mu - \varphi), \nu\right) \mathrm{d}t\right| \leq \int_0^T \left\|(-\Delta_n)^{-1}(\varphi_\mu - \varphi)\right\| \|\nu\| \,\mathrm{d}t \\ \leq c_P^2 \int_0^T \|\varphi_\mu - \varphi\| \|\nu\| \,\mathrm{d}t \leq c_P^2 \|\varphi_\mu - \varphi\|_{L^2(\Omega_T)} \|\nu\|_{L^2(\Omega_T)} \to 0\end{aligned} \tag{B.159}$$

by (B.149c), the Cauchy–Schwarz inequality and (A.30a). Hence,

$$\int_0^T \left((-\Delta_n)^{-1}(\varphi_\mu - \overline{\varphi_\mu}), \nu\right) \mathrm{d}t \to \int_0^T \left((-\Delta_n)^{-1}(\varphi - \overline{\varphi}), \nu\right) \mathrm{d}t, \tag{B.160}$$

as $\mu \downarrow 0$, for any $\nu \in L^2\left(0,T;H^1(\Omega)\right)$.

viii) We use this result and the other convergence properties from (B.149) to pass to the limit $\mu \downarrow 0$ term-by-term in (B.150). We rearrange to conclude that

$$\varepsilon_\varphi^2 (\nabla\varphi, \nabla\nu - \nabla\varphi) - \frac{\chi^{AB}}{2}(\varphi, \nu - \varphi) + \alpha\left((-\Delta_n)^{-1}(\varphi - \overline{\varphi}), \nu - \varphi\right) \geq (\psi, \nu - \varphi)$$

for any $\nu \in \mathscr{A}$ and a.e. $t \in (0,T)$. The implication is that $\{\varphi, \psi\}$ solves (4.37b). Hence, problem (**P**) in (4.37) has a solution.

Remark. No special treatment is required for the IC, because according to (4.39c), we have *defined* each $\varphi_\mu(0) = \varphi(0) \in \mathscr{A}$.

ix) We show that problem (**Q**) in (4.38) has a solution. Suppose that $\{\varphi, \psi\}$ solves (**P**). Then from (4.37a),[50]

$$\partial_t\varphi - \Delta\left(\psi - \overline{\psi}\right) = 0 \qquad \text{viz.} \qquad \psi = -(-\Delta_n)^{-1}\partial_t\varphi + \overline{\psi}, \tag{B.161}$$

in correspondence with (2.53) of Blowey and Elliott (1991). If we substitute this into the right-side of (4.37b), we find that

$$\begin{aligned}\left((-\Delta_n)^{-1}(\partial_t\varphi) - \overline{\psi}, \nu_2 - \varphi\right) + \varepsilon_\varphi^2(\nabla\varphi, \nabla\nu_2 - \nabla\varphi) - \frac{\chi^{AB}}{2}(\varphi, \nu_2 - \varphi) \\ + \alpha\left((-\Delta_n)^{-1}(\varphi - \overline{\varphi}), \nu_2 - \varphi\right) \geq 0\end{aligned} \tag{B.162}$$

for any $\nu_2 \in \mathscr{A}$. We now choose $\nu_2 \in \mathscr{A}_m \subset \mathscr{A}$ above and recall from (4.49) that $\overline{\varphi} = m$. For such ν_2, $\overline{\nu_2 - \varphi} = 0$, and so $\left(\overline{\psi}, \nu_2 - \varphi\right) = \overline{\psi}(1, \nu_2 - \varphi) = 0$ in the first term on the left. In this case, (B.162) reduces to (4.38), and for $\{\varphi, \psi\}$ a solution to (**P**), φ solves (**Q**).[51] Hence (**Q**) has a solution because (**P**) does.

x) We establish the uniqueness of solutions of (**P**). Our approach matches that of the relevant part of Theorem 2.2 of Blowey and Elliott (1991), with modifications for the non-local component. Define

$$\varphi(0) = (\varphi_1)_0 - (\varphi_2)_0 =: \varphi_0 \qquad \text{with} \qquad \overline{\varphi_0} = 0 \tag{B.163}$$

with U, U_1 and U_2 as in the statement of the theorem. U_1 satisfies (4.37a)–(4.37b),

$$\langle \partial_t \varphi_1, \nu_1 \rangle + (\nabla \psi_1, \nabla \nu_1) = 0 \tag{B.164a}$$

$$\varepsilon_\varphi^2 (\nabla \varphi_1, \nabla \nu_2 - \nabla \varphi_1) - \frac{\chi^{AB}}{2} (\varphi_1, \nu_2 - \varphi_1) + \alpha \left((-\Delta_n)^{-1} (\varphi_1 - \overline{\varphi_1}), \nu_2 - \varphi_1 \right) \geq (\psi_1, \nu_2 - \varphi_1) \tag{B.164b}$$

for any $\nu_1 \in H^1(\Omega)$, $\nu_2 \in \mathscr{A}$ and a.e. $t \in (0,T)$, and similarly for U_2, i.e.

$$\langle \partial_t \varphi_2, \nu_1 \rangle + (\nabla \psi_2, \nabla \nu_1) = 0 \tag{B.164c}$$

$$\varepsilon_\varphi^2 (\nabla \varphi_2, \nabla \nu_2 - \nabla \varphi_2) - \frac{\chi^{AB}}{2} (\varphi_2, \nu_2 - \varphi_2) + \alpha \left((-\Delta_n)^{-1} (\varphi_2 - \overline{\varphi_2}), \nu_2 - \varphi_2 \right) \geq (\psi_2, \nu_2 - \varphi_2). \tag{B.164d}$$

Subtracting (B.164c) from (B.164a) leads to

$$\langle \partial_t \varphi, \nu \rangle + (\nabla \psi, \nabla \nu) = 0 \qquad \text{for any} \qquad \nu \in H^1(\Omega) \qquad \text{and a.e. } t \in (0,T). \tag{B.165}$$

xi) We now set $\nu_2 = \varphi_2$ in (B.164b) and $\nu_2 = \varphi_1$ in (B.164d), to find that

$$-\varepsilon_\varphi^2 (\nabla \varphi_1, \nabla \varphi) + \frac{\chi^{AB}}{2} (\varphi_1, \varphi) - \alpha \left((-\Delta_n)^{-1} (\varphi_1 - \overline{\varphi_1}), \varphi \right) \geq -(\psi_1, \varphi)$$
$$\varepsilon_\varphi^2 (\nabla \varphi_2, \nabla \varphi) - \frac{\chi^{AB}}{2} (\varphi_2, \varphi) + \alpha \left((-\Delta_n)^{-1} (\varphi_2 - \overline{\varphi_2}), \varphi \right) \geq (\psi_2, \varphi).$$

If we add these, rearrange and recall that $\overline{\varphi} = \overline{\varphi_1 - \varphi_2} = 0$, viz. $\varphi \in L^2_*(\Omega)$, by (4.49), then

$$-(\psi, \varphi) + \varepsilon_\varphi^2 |\varphi|_1^2 \leq \frac{\chi^{AB}}{2} \|\varphi\|^2 \tag{B.166a}$$

after discarding $\alpha \left((-\Delta_n)^{-1} \varphi, \varphi \right) = \alpha \|\varphi\|_{-1}^2 \geq 0$. Setting $\nu = (-\Delta_n)^{-1} \varphi$ in (B.165) gives

$$\left\langle \partial_t \varphi, (-\Delta_n)^{-1} \varphi \right\rangle + \left(\nabla \psi, \nabla (-\Delta_n)^{-1} \varphi \right) = 0 \qquad \Rightarrow \qquad -(\psi, \varphi) = \left\langle \partial_t \varphi, (-\Delta_n)^{-1} \varphi \right\rangle \tag{B.166b}$$

by (2.9a).[52] Combining the two results in (B.166) yields

$$\left\langle \partial_t \varphi, (-\Delta_n)^{-1} \varphi \right\rangle + \varepsilon_\varphi^2 |\varphi|_1^2 \leq \frac{\chi^{AB}}{2} \|\varphi\|^2 \qquad \Rightarrow \qquad \frac{1}{2} \frac{\mathrm{d}}{\mathrm{d}t} \|\varphi\|_{-1}^2 + \varepsilon_\varphi^2 |\varphi|_1^2 \leq \frac{\chi^{AB}}{2} \|\varphi\|^2 \tag{B.167}$$

if we use (B.139), which is identical to (B.140) in Theorem 4.3.4, with φ_μ replaced by φ. By the same argument, we are led to (4.50) (cf. (B.142)) whence $\varphi(t) \equiv 0$ for a.e. $t \in (0,T)$ i.e. the order parameter component φ of the solution (φ, ψ) of $(\mathbf{P})$ is unique.

xii) We establish uniqueness of the chemical potential component ψ of the solution (φ, ψ) of $(\mathbf{P})$. Using the previous result, if we set $\nu = \psi$ in (B.165), then

$$|\psi|_1^2 = -\langle \partial_t \varphi, \psi \rangle = 0. \tag{B.168}$$

Unlike the situation in Theorem 4.3.4 however, we cannot infer here that $\overline{\psi} = 0$, and so all this shows that ψ is only unique up to a constant. We improve on this as follows: define the open set (cf. (4.3)[53])

$$\Omega_{AB}(t) := \{ x \in \Omega \,|\, |\varphi(x)| < 1 \} \qquad \text{for a.e.} \qquad t \in (0,T) \tag{B.169}$$

and observe that $|\Omega_{AB}(t)| > 0$ since $\varphi \in \mathscr{A}_m$ viz. $|\overline{\varphi}| < 1$. Now set $\nu_2 = \varphi_1 \pm \theta\eta$ in (4.37b), with $\eta \in C_c^\infty(\Omega_{AB}(t))$ and θ small enough that $\nu_2 \in \mathscr{A}$ (cf. Lemma 4.2.6), so that for $\{\varphi_1, \psi_1\}$ a solution of (**P**),

$$\varepsilon_\varphi^2(\nabla\varphi_1, \pm\theta\nabla\eta) + \alpha\left((-\Delta_n)^{-1}(\varphi_1 - \overline{\varphi_1}), \pm\theta\eta\right) \geq \left(\frac{\chi^{AB}}{2}\varphi_1 + \psi_1, \pm\theta\eta\right)$$

$$\text{viz.} \quad \varepsilon_\varphi^2(\nabla\varphi_1, \nabla\eta) + \alpha\left((-\Delta_n)^{-1}(\varphi_1 - \overline{\varphi_1}), \eta\right) = \left(\frac{\chi^{AB}}{2}\varphi_1 + \psi_1, \eta\right)$$

for any $\eta \in C_c^\infty(\Omega_{AB}(t))$ and a.e. $t \in (0,T)$. Likewise, for the solution $\{\varphi_2, \psi_2\}$,

$$\varepsilon_\varphi^2(\nabla\varphi_2, \nabla\eta) + \alpha\left((-\Delta_n)^{-1}(\varphi_2 - \overline{\varphi_2}), \eta\right) = \left(\frac{\chi^{AB}}{2}\varphi_2 + \psi_2, \eta\right),$$

and so if we subtract the second of these from the first, and set $\psi_1 - \psi_2 = c \in \mathbb{R}$,

$$\varepsilon_\varphi^2(\nabla\varphi, \nabla\eta) + \alpha\left((-\Delta_n)^{-1}\varphi, \eta\right) = \left(\frac{\chi^{AB}}{2}\varphi + c, \eta\right) \qquad \Rightarrow \qquad (c, \eta) = 0$$

for any $\eta \in C_c^\infty(\Omega_{AB}(t))$ and a.e. $t \in (0,T)$, since $\varphi = \varphi_1 - \varphi_2 \equiv 0$. Hence, $c = 0$, $\psi_1 = \psi_2$ and the chemical potential portion of the solution of (**P**) is unique.

xiii) We prove that solutions of problem (**Q**) are unique. Suppose that (**Q**) has two solutions $\varphi_1, \varphi_2 \in \mathscr{A}_m$ with ICs $(\varphi_1)_0, (\varphi_2)_0 \in \mathscr{A}_m$, and define $\varphi = \varphi_1 - \varphi_2 \in \mathscr{A}_0$. Then

$$\begin{aligned}
&\left((-\Delta_n)^{-1}(\partial_t\varphi_1), \nu - \varphi_1\right) + \varepsilon_\varphi^2(\nabla\varphi_1, \nabla\nu - \nabla\varphi_1) - \frac{\chi^{AB}}{2}(\varphi_1, \nu - \varphi_1) \\
&\qquad + \alpha\left((-\Delta_n)^{-1}(\varphi_1 - \overline{\varphi_1}), \nu - \varphi_1\right) \geq 0, \\
\text{and} \quad &\left((-\Delta_n)^{-1}(\partial_t\varphi_2), \nu - \varphi_2\right) + \varepsilon_\varphi^2(\nabla\varphi_2, \nabla\nu - \nabla\varphi_2) - \frac{\chi^{AB}}{2}(\varphi_2, \nu - \varphi_2) \\
&\qquad + \alpha\left((-\Delta_n)^{-1}(\varphi_2 - \overline{\varphi_2}), \nu - \varphi_2\right) \geq 0,
\end{aligned}$$

for any $\nu \in \mathscr{A}_m$. If we set $\nu = \varphi_2 \in \mathscr{A}_m$ in the first of these and $\nu = \varphi_1 \in \mathscr{A}_m$ in the second, and add the resulting inequalities, we find that

$$\left((-\Delta_n)^{-1}(\partial_t\varphi), \varphi\right) + \varepsilon_\varphi^2|\varphi|_1^2 - \frac{\chi^{AB}}{2}\|\varphi\|^2 + \alpha\|\varphi\|_{-1}^2 \leq 0. \tag{B.170}$$

We discard $\alpha\|\varphi\|_{-1}^2 \geq 0$ on the left, and then use (2.12) (noting that $\partial_t\varphi, \varphi \in L_*^2(\Omega)$) and (B.139), to rearrange this into a form that is identical to (B.167). (4.50) follows (for problem (**Q**)), and implies that solutions of problem (**Q**) are unique.

xiv) We establish (4.51). As in Theorem 4.3.3 (cf. (B.122)),

$$\varphi_\mu \rightharpoonup \varphi \qquad \text{in} \qquad H^1\left(\delta, T; H^1(\Omega)\right) \qquad \text{for any} \qquad \delta > 0; \tag{B.171}$$

and by imbedding, $\varphi \in C\left([\delta, T]; H^1(\Omega)\right)$. Together, these results give (4.51) for solutions of (**P**) and (**Q**).

xv) Finally, we establish (4.49). Setting $\nu = 1$ in (4.37a), we find that

$$\langle\partial_t\varphi, 1\rangle = \left(\varphi', 1\right) = 0 \qquad \text{for a.e. } t \in (0,T).$$

Since $\varphi_1, \varphi_2 \in H^1\left(0, T; \left(H^1(\Omega)\right)'\right)$ by (B.149a), $\varphi = \varphi_1 - \varphi_2 \in H^1\left(0, T; \left(H^1(\Omega)\right)'\right)$ too, and so (cf. (A.37))

$$\varphi(t) = \varphi(s) + \int_s^t \varphi'(\tau)\,\mathrm{d}\tau \qquad \text{for every} \qquad 0 \leq s \leq t \leq T.$$

Integrating in space, we discover that

$$(\varphi(t),1) = (\varphi(s),1) + \underbrace{\int_s^t \left(\varphi'(\tau),1\right) \mathrm{d}\tau}_{=0} \qquad \text{for every} \qquad 0 \le s \le t \le T,$$

and so, if we set $s = 0$ in the above, (B.163) implies that

$$(\varphi(t),1) = (\varphi_0,1) = 0 \qquad \text{for every} \qquad 0 \le t \le T, \tag{B.172}$$

viz. $\overline{\varphi(t)} = m$ for every $0 \le t \le T$, which is the full statement of (4.49).

□

Remark. We did not explicitly prove that solutions of (**Q**) are also solutions of (**P**). On the other hand the uniqueness that is implied by (B.167), and the fact that solutions of (**P**) solve (**Q**), implies that these problems are equivalent, in that they share φ, given a common IC, φ_0.

B.14 Proof of Theorem 4.3.7

Proof.

i) Since $\varphi_0 \in \mathscr{A}_m$,

$$\mathcal{E}_\mu[\varphi_\mu(t)] + \int_0^t |\psi_\mu(s)|_1^2 \,\mathrm{d}s \le \mathcal{E}_\mu[\varphi_0] = \mathcal{E}[\varphi_0] \qquad \text{for any} \qquad 0 < t \le T. \tag{4.47a}$$

Using (4.6) and the argument at the end of Theorem 2.2 of Blowey and Elliott (1991),

$$\liminf_{\mu\downarrow 0} \mathcal{E}_\mu[\varphi_\mu(t)] = \liminf_{\mu\downarrow 0} \mathcal{E}[\varphi_\mu(t)] + \liminf_{\mu\downarrow 0} \left(\Upsilon_\mu(\varphi_\mu(t)),1\right).$$

As in Theorem 4.3.5, we use the fact that $\varphi_\mu(t) \rightharpoonup \varphi(t)$ in $H^1(\Omega)$ for every $t > 0$ and $\varphi_\mu(t) \to \varphi(t)$ (strongly) in $L^2(\Omega)$ for a.e. $t \in (0,T)$ to conclude that

$$\mathcal{E}[\varphi(t)] \le \liminf_{\mu\downarrow 0} \mathcal{E}[\varphi_\mu(t)] \qquad \text{for any} \qquad 0 < t \le T.$$

In addition, using (4.20a), (4.15) and (B.153), we learn that

$$\liminf_{\mu\downarrow 0} \left(\Upsilon_\mu(\varphi_\mu(t)),1\right) = \liminf_{\mu\downarrow 0} \frac{1}{2\mu} \|\zeta(\varphi_\mu(t))\|^2 = \lim_{\mu\downarrow 0} \frac{1}{2\mu} C\mu^2 = 0.$$

Hence, in fact

$$\mathcal{E}[\varphi(t)] \le \liminf_{\mu\downarrow 0} \mathcal{E}_\mu[\varphi_\mu(t)] \qquad \text{for any} \qquad 0 < t \le T. \tag{B.173a}$$

Since $\psi_\mu \rightharpoonup \psi$ in $L^2\left(0,T;H^1(\Omega)\right)$ in (B.149d), $\nabla\psi_\mu \rightharpoonup \nabla\psi$ in $L^2\left(0,T;L^2(\Omega)\right)$, and so

$$\int_0^t |\psi(s)|_1^2 \,\mathrm{d}s \le \liminf_{N\to\infty} \int_0^t |\psi_\mu(s)|_1^2 \,\mathrm{d}s, \tag{B.173b}$$

for every $t > 0$ (cf. (B.145b)). Combining (B.173a)–(B.173b) yields (cf. (B.146))

$$\mathcal{E}[\varphi(t)] + \int_0^t |\psi(s)|_1^2 \,\mathrm{d}s \le \liminf_{\mu\downarrow 0} \left\{ \mathcal{E}_\mu[\varphi_\mu(t)] + \int_0^t |\psi_\mu(s)|_1^2 \,\mathrm{d}s \right\}$$

for $t > 0$ or, if we recall (4.47a) and (4.51),

$$\mathcal{E}[\varphi(t)] + \int_0^t |\psi(s)|_1^2 \,\mathrm{d}s \le \mathcal{E}[\varphi_0] \qquad \text{for any} \qquad 0 < t \le T,$$

which is (4.52a).

ii) To establish (4.52b), we argue as we did in the second part of our Theorem 4.3.5.[54] The basic idea is that for any $t' > 0$, (4.51) and (4.49) imply that $\varphi(t') \in H_m^1(\Omega)$, which implies that the energy $\mathcal{E}[\varphi(t')] < \infty$. We may therefore re-start the problem at $t = t'$ setting $\varphi(t') \in H_m^1(\Omega)$ as the IC for a new problem (**P**). A result analogous to (4.52a) follows from the first part above, which leads to (4.52b).

□

B.15 Proof of Lemma 4.3.8

Proof.

i) In the Galerkin approximation (4.40), each $-\Delta e_k \in V^N$, since $\mathscr{P} e_k = \lambda_k e_k$ and so $-\Delta e_k = (\lambda_k - 1) e_k$ for $1 \leq k \leq N$. By the smoothness of $\partial\Omega$ and (A.57), any $\varphi_\mu^{(N)} \in V^N$ $(N < \infty)$ satisfies

$$\left(-\Delta\varphi_\mu^{(N)}, \eta^{(N)}\right) = \left(\nabla\varphi_\mu^{(N)}, \nabla\eta^{(N)}\right) \qquad \text{for every} \qquad \eta^{(N)} \in V^N \qquad \text{and} \qquad \partial_n \varphi_\mu^{(N)}\Big|_{\partial\Omega} = 0.$$

Hence, we may re-write (4.40e), for every $\eta^{(N)} \in V^N$, as

$$\varepsilon_\varphi^2 \left(-\Delta\varphi_\mu^{(N)}, \eta^{(N)}\right) - \frac{\chi^{AB}}{2}\left(\varphi_\mu^{(N)}, \eta^{(N)}\right) + \left(\zeta_\mu\left(\varphi_\mu^{(N)}\right), \eta^{(N)}\right) + \alpha\left((-\Delta_n)^{-1}\left(\varphi_\mu^{(N)} - \overline{\varphi_\mu^{(N)}}\right), \eta^{(N)}\right) = \left(\psi_\mu^{(N)}, \eta^{(N)}\right). \quad \text{(B.174)}$$

ii) Using (2.9) and the zero Neumann BC on each $\varphi_\mu^{(N)}$, we find that

$$\begin{aligned} 0 \leq \left\|\varphi_\mu^{(N)} - \overline{\varphi_\mu^{(N)}}\right\|^2 &= \left(\varphi_\mu^{(N)} - \overline{\varphi_\mu^{(N)}}, \varphi_\mu^{(N)}\right) \\ &= \left(\nabla(-\Delta_n)^{-1}\left(\varphi_\mu^{(N)} - \overline{\varphi_\mu^{(N)}}\right), \nabla\varphi_\mu^{(N)}\right) = \left((-\Delta_n)^{-1}\left(\varphi_\mu^{(N)} - \overline{\varphi_\mu^{(N)}}\right), -\Delta\varphi_\mu^{(N)}\right). \end{aligned} \quad \text{(B.175a)}$$

From (4.14b) we determine that

$$\left(\zeta_\mu\left(\varphi_\mu^{(N)}\right), -\Delta\varphi_\mu^{(N)}\right) = \left(\nabla\zeta_\mu\left(\varphi_\mu^{(N)}\right), \nabla\varphi_\mu^{(N)}\right) = \left(\zeta_\mu'\left(\varphi_\mu^{(N)}\right), \left(\nabla\varphi_\mu^{(N)}\right)^2\right) \geq 0. \quad \text{(B.175b)}$$

If we set $\eta^{(N)} = -\Delta\varphi_\mu^{(N)} \in V^N$ in (B.174), and use (B.175), we see that[55]

$$\varepsilon_\varphi^2 \left\|-\Delta\varphi_\mu^{(N)}\right\|^2 - \frac{\chi^{AB}}{2}\left|\varphi_\mu^{(N)}\right|_1^2 \leq \left(\nabla\psi_\mu^{(N)}, \nabla\varphi_\mu^{(N)}\right). \quad \text{(B.176a)}$$

Setting $\eta^{(N)} = \varphi_\mu^{(N)}$ in (4.40b) yields[56]

$$\left(\nabla\psi_\mu^{(N)}, \nabla\varphi_\mu^{(N)}\right) = -\left(\partial_t\varphi_\mu^{(N)}, \varphi_\mu^{(N)}\right) = -\frac{1}{2}\frac{\mathrm{d}}{\mathrm{d}t}\left\|\varphi_\mu^{(N)}\right\|^2, \quad \text{(B.176b)}$$

so if we combine (B.176a)–(B.176b) and rearrange, we conclude that

$$\frac{1}{2}\frac{\mathrm{d}}{\mathrm{d}t}\left\|\varphi_\mu^{(N)}\right\|^2 + \varepsilon_\varphi^2\left\|-\Delta\varphi_\mu^{(N)}\right\|^2 \leq \frac{\chi^{AB}}{2}\left|\varphi_\mu^{(N)}\right|_1^2. \quad \text{(B.177)}$$

Integrating in time over $(0, t)$ for $t \in (0, T]$ leads to[57]

$$\begin{aligned} \left\|\varphi_\mu^{(N)}(t)\right\|^2 + 2\varepsilon_\varphi^2\int_0^t \left\|-\Delta\varphi_\mu^{(N)}(s)\right\|^2 \mathrm{d}s &\leq \left\|P^N\varphi_0\right\|^2 + \int_0^t \chi^{AB}\left|\varphi_\mu^{(N)}(s)\right|_1^2 \mathrm{d}s \\ &\leq \|\varphi_0\|^2 + \chi^{AB}\int_0^T \left|\varphi_\mu^{(N)}(s)\right|_1^2 \mathrm{d}s \leq C, \end{aligned} \quad \text{(B.178)}$$

for sufficiently large N, with C independent of N, T and μ, by (4.44b) and (A.64). From (A.42) we determine that

$$\int_0^t \left\|\varphi_\mu^{(N)}(s)\right\|_2^2 \mathrm{d}s \leq \int_0^t \left\|-\Delta\varphi_\mu^{(N)}(s)\right\|^2 \mathrm{d}s \leq C \tag{B.179}$$

i.e. $\varphi_\mu^{(N)}$ is bounded in $L^2\left(0,T;H^2(\Omega)\right)$, independent of N and μ (but not T).

iii) Given the uniform bound above in the Hilbert space $L^2\left(0,T;H^2(\Omega)\right)$, we infer the existence of φ_μ and $\varphi \in L^2\left(0,T;H^2(\Omega)\right)$ and (re-labelled) sub-sequences of $\left(\varphi_\mu^{(N)}\right)$ (fixed μ, varying N) and (φ_μ) (varying μ), such that

$$\varphi_\mu^{(N)} \rightharpoonup \varphi_\mu \qquad \text{in} \qquad L^2\left(0,T;H^2(\Omega)\right) \tag{B.180a}$$

$$\varphi_\mu \rightharpoonup \varphi \qquad \text{in} \qquad L^2\left(0,T;H^2(\Omega)\right), \tag{B.180b}$$

which yields the first part of (4.53). The zero Neumann BCs on φ_μ and φ follow as in (B.38)–(B.39). From the former BC, we determine that

$$(-\Delta\varphi_\mu,\nu) = (\nabla\varphi_\mu,\nabla\nu) \qquad \text{for every} \qquad \nu \in H^1(\Omega). \tag{B.181}$$

iv) In (B.180a), we send $N\to\infty$ (for fixed $\mu>0$); the sequence $\left(\varphi_\mu^{(N)}\right)$ is a sub-sequence of the sequence we constructed in Theorem 4.3.3. By uniqueness of limits, the φ_μ in (B.180a) is the same as that in (4.45), and therefore solves problem $(\mathbf{P}_\mu)$ by the reasoning in that theorem. For sufficiently smooth Ω, we may thus use (B.181) in (4.39b) to conclude that

$$\left(\varepsilon_\varphi^2(-\Delta)\varphi_\mu + \mathcal{B}_\mu'(\varphi_\mu) + \alpha(-\Delta_n)^{-1}(\varphi_\mu - \overline{\varphi_\mu}) - \psi_\mu, \nu_2\right) = 0 \tag{B.182}$$

for any $\nu_2 \in H^1(\Omega)$, and in fact any $\nu_2 \in L^2(\Omega)$ by density, and a.e. $t\in(0,T)$. Hence, a.e. in Ω_T

$$\psi_\mu = \varepsilon_\varphi^2(-\Delta)\varphi_\mu + \mathcal{B}_\mu'(\varphi_\mu) + \alpha(-\Delta_n)^{-1}(\varphi_\mu - \overline{\varphi_\mu}). \tag{B.183}$$

Likewise, in (B.180b), we send $\mu\downarrow 0$, or equivalently consider a sub-sequence of the sequence we constructed in Theorem 4.3.6. As in that result, the φ in (B.180b) solves problems $(\mathbf{P})$ and $(\mathbf{Q})$.

v) By earlier results, $\varphi_\mu(t), \varphi(t) \in H^1(\Omega)$ for any $t>0$, and so in 1D, $\varphi_\mu(t)$ and $\varphi(t)$ are in $C^0\left(\overline{\Omega}\right)$ for a.e. $t\in(0,T)$ by Sobolev imbedding as in Lemma A.1.8. For 2D and 3D, we know from the first part of this proof that $\varphi_\mu(t), \varphi(t) \in H^2(\Omega)$ for a.e. $t\in(0,T)$; Sobolev embedding gives $C^0\left(\overline{\Omega}\right)$ continuity again.

vi) Suppose that $-\Delta\varphi_0 \in H^1(\Omega)$ and $\partial_n\varphi_0|_{\partial\Omega} = 0$. With $t=0$ in (B.182), we *define*

$$H^1(\Omega) \ni \psi_\mu(0) =: \psi_0 = \varepsilon_\varphi^2(-\Delta)\varphi_0 - \frac{\chi^{AB}}{2}\varphi_0 + \alpha(-\Delta_n)^{-1}(\varphi_0 - \overline{\varphi_0}), \tag{B.184}$$

after noting that $\varphi_0 \in \mathscr{A}$. Differentiating (4.39b) with respect to t yields

$$\varepsilon_\varphi^2(\nabla\partial_t\varphi_\mu,\nabla\nu_2) - \frac{\chi^{AB}}{2}(\partial_t\varphi_\mu,\nu_2) + \left(\zeta_\mu'(\varphi_\mu)\partial_t\varphi_\mu,\nu_2\right) + \alpha\left((-\Delta_n)^{-1}(\partial_t\varphi_\mu),\nu_2\right) = (\partial_t\psi_\mu,\nu_2). \tag{B.185}$$

Setting $\nu_2 = \partial_t\varphi_\mu$ in this leads to

$$\varepsilon_\varphi^2|\partial_t\varphi_\mu|_1^2 + \underbrace{\left(\zeta_\mu'(\varphi_\mu),(\partial_t\varphi_\mu)^2\right)}_{\geq 0 \text{ by (4.14a)}} - \frac{\chi^{AB}}{2}\|\partial_t\varphi_\mu\|^2 + \underbrace{\alpha\|\partial_t\varphi_\mu\|_{-1}^2}_{\geq 0} = (\partial_t\psi_\mu,\partial_t\varphi_\mu);$$

i.e.

$$\varepsilon_\varphi^2 \left|\partial_t \varphi_\mu\right|_1^2 - \frac{\chi^{AB}}{2} \left\|\partial_t \varphi_\mu\right\|^2 \leq \left(\partial_t \psi_\mu, \partial_t \varphi_\mu\right). \tag{B.186a}$$

We now set $\nu_1 = \partial_t \psi_\mu$ in (4.39a) and find that

$$\left(\partial_t \varphi_\mu, \partial_t \psi_\mu\right) + \left(\nabla \psi_\mu, \nabla \partial_t \psi_\mu\right) = 0. \tag{B.186b}$$

Combining (B.186a)–(B.186b) gives (cf. (B.98))

$$\begin{aligned}\varepsilon_\varphi^2 \left|\partial_t \varphi_\mu\right|_1^2 + \left(\nabla \psi_\mu, \nabla \partial_t \psi_\mu\right) \leq \frac{\chi^{AB}}{2} \left\|\partial_t \varphi_\mu\right\|^2 &\leq \frac{\chi^{AB}}{2} \left\|\partial_t \varphi_\mu\right\|_{-1} \left|\partial_t \varphi_\mu\right|_1 \\ &\leq \frac{\varepsilon_\varphi^2}{2} \left|\partial_t \varphi_\mu\right|_1^2 + \frac{\left(\chi^{AB}\right)^2}{8\varepsilon_\varphi^2} \left\|\partial_t \varphi_\mu\right\|_{-1}^2, \end{aligned} \tag{B.187}$$

after using (A.29) and Young's inequality. Rearranging, we find that (cf. (B.99))

$$\varepsilon_\varphi^2 \left|\partial_t \varphi_\mu\right|_1^2 + \frac{\mathrm{d}}{\mathrm{d}t} \left|\psi_\mu\right|_1^2 \leq \frac{\left(\chi^{AB}\right)^2}{4\varepsilon_\varphi^2} \left\|\partial_t \varphi_\mu\right\|_{-1}^2. \tag{B.188}$$

vii) We now integrate (B.188) over $(0,t)$ to obtain[58]

$$\left|\psi_\mu(t)\right|_1^2 + \varepsilon_\varphi^2 \int_0^t \left|\partial_s \varphi_\mu\right|_1^2 \mathrm{d}s \leq \left|\psi_\mu(0)\right|_1^2 + \frac{\left(\chi^{AB}\right)^2}{4\varepsilon_\varphi^2} \int_0^T \left\|\partial_s \varphi_\mu\right\|_{-1}^2 \mathrm{d}s \tag{B.189}$$

for every $t \in [0,T]$. We bound $\left|\psi_\mu(0)\right|_1$. From (B.184), (2.11) and (A.28b),

$$\begin{aligned}\left|\psi_0\right|_1 \leq \varepsilon_\varphi^2 \left|-\Delta \varphi_0\right|_1 + \frac{\chi^{AB}}{2} \left|\varphi_0\right|_1 + \alpha \left|(-\Delta_n)^{-1} \left(\varphi_0 - \overline{\varphi_0}\right)\right|_1 \\ \leq \varepsilon_\varphi^2 \left|-\Delta \varphi_0\right|_1 + \left(\frac{\chi^{AB}}{2} + \alpha c_P^2\right) \left|\varphi_0\right|_1 = C\left(\varphi_0\right) < \infty \end{aligned} \tag{B.190}$$

because we assumed $-\Delta \varphi_0 \in H^1(\Omega)$. $C(\varphi_0)$ in (B.190) is independent of μ and T. Hence, from (B.189) and (4.45a),

$$\left|\psi_\mu(t)\right|_1^2 + \varepsilon_\varphi^2 \int_0^t \left|\partial_s \varphi_\mu\right|_1^2 \mathrm{d}s \leq C \qquad \text{for a.e. } t \in (0,T) \tag{B.191}$$

in which C is independent of μ.

viii) Clearly,

$$\overline{\partial_t \varphi_\mu} = 0 \qquad \Rightarrow \qquad \left\|\partial_t \varphi_\mu\right\| \leq c_P \left|\partial_t \varphi_\mu\right|_1$$

by Poincaré's inequality, and so we conclude that $\partial_t \varphi_\mu \in L^2\left(0,T; H^1(\Omega)\right)$. Combining this with the first part of (B.116) which says that $\varphi_\mu \in L^2\left(0,T; H^1(\Omega)\right)$, we see that $\varphi_\mu \in H^1\left(0,T; H^1(\Omega)\right)$. This is the first part of the result for φ_μ in (4.54a).

ix) We now argue as we did in establishing (B.112b) (with (φ_μ, ψ_μ) in place of $\left(\varphi_\mu^{(N)}, \psi_\mu^{(N)}\right)$) and find that

$$\left\|\psi_\mu(t)\right\| \leq C + C \left|\psi_\mu(t)\right|_1 \qquad \text{for a.e. } t \in (0,T), \tag{B.192}$$

in which the constants are μ-independent. Noting (B.191), we conclude that $\psi_\mu \in L^\infty\left(0,T; H^1(\Omega)\right)$, which is the result for ψ_μ in (4.54b).

x) We now set $\nu_2 = -\Delta\varphi_\mu \in L^2(\Omega)$ in (B.182) and use the zero Neumann BC on φ_μ to see that (cf. (B.175), (B.176a))

$$\varepsilon_\varphi^2 \|-\Delta\varphi_\mu\|^2 - \frac{\chi^{AB}}{2} |\varphi_\mu|_1^2 \leq (\nabla\psi_\mu, \nabla\varphi_\mu) \leq |\psi_\mu|_1 |\varphi_\mu|_1 \leq \frac{1}{2} |\psi_\mu|_1^2 + \frac{1}{2} |\varphi_\mu|_1^2 \tag{B.193}$$

by the Cauchy–Schwarz and Young's inequalities. Rearranging yields

$$\varepsilon_\varphi^2 \|-\Delta\varphi_\mu(t)\|^2 \leq \frac{1}{2} |\psi_\mu|_1^2 + \left(\frac{\chi^{AB}}{2} + \frac{1}{2}\right) |\varphi_\mu|_1^2 \leq C \qquad \text{for a.e. } t \in (0,T)$$

since $\psi_\mu \in L^\infty\left(0,T; H^1(\Omega)\right)$ (as above) and recalling (4.45b), and where C is independent of μ. Since t on the left is arbitrary, we find that

$$\operatorname*{ess\,sup}_{t\in(0,T)} \|-\Delta\varphi_\mu(t)\| \leq C,$$

independent of μ. Our smoothness assumptions on $\partial\Omega$ and (A.43) mean that

$$\operatorname*{ess\,sup}_{t\in(0,T)} \|\varphi_\mu(t)\|_2 \leq C,$$

independent of μ; this is the second part of the result for φ_μ in (4.54a).

xi) Having established (4.54) for the regularised (φ_μ, ψ_μ) solving $(\mathbf{P}_\mu)$, we now establish the results for (φ, ψ) solving $(\mathbf{P})$ and $(\mathbf{Q})$. The bounds above on φ_μ, ψ_μ that led to (4.54) are all independent of μ. Consequently, there exist sub-sequences (φ_μ) and (ψ_μ) of the sequences in (B.149), with

$$\varphi \in H^1\left(0,T; H^1(\Omega)\right) \cap L^\infty\left(0,T; H^2(\Omega)\right) \qquad \text{and} \qquad \psi \in L^\infty\left(0,T; H^1(\Omega)\right),$$

for which

$$\varphi_\mu \rightharpoonup \varphi \quad \text{in} \quad H^1\left(0,T; H^1(\Omega)\right), \tag{B.194a}$$

$$\varphi_\mu \overset{\star}{\rightharpoonup} \varphi \quad \text{in} \quad L^\infty\left(0,T; H^2(\Omega)\right), \tag{B.194b}$$

$$\text{and} \qquad \psi_\mu \overset{\star}{\rightharpoonup} \psi \quad \text{in} \quad L^\infty\left(0,T; H^1(\Omega)\right), \tag{B.194c}$$

as $\mu \downarrow 0$. As in Theorem 4.3.6, the (φ, ψ) in (B.194) solve problems $(\mathbf{P})$ and $(\mathbf{Q})$.

□

B.16 Proof of Theorem 4.3.9

The following proof is adapted from the material in the last part of the proof of Proposition 2.3, and Section 2.3 of Blowey and Elliott (1991). The material in Section 1 of Temam (1997) and Ball (2014) is also useful.

Proof. First we establish a result corresponding to (2.60b) of Blowey and Elliott (1991) for our problem. From (B.193), we deduce that

$$\varepsilon_\varphi^2 \|-\Delta\varphi\|^2 \leq \frac{\chi^{AB}}{2} |\varphi|_1^2 + |\psi|_1 |\varphi|_1 \tag{B.195}$$

after taking $\mu \downarrow 0$. Likewise, from (B.101) and (B.466), we determine that

$$\|\psi\|_1^2 \leq C(\varphi_0)\left(1 + \frac{1}{t}\right) \qquad \Rightarrow \qquad \sqrt{\frac{t}{1+t}} \|\psi\|_1 \leq C(\varphi_0)$$

for a.e. t. (B.224b) and (B.195) imply that

$$\|\Delta\varphi\|^2 \leq C(\varphi_0)\left(1+\frac{1}{t}\right) \qquad \Rightarrow \qquad \sqrt{\frac{t}{1+t}}\,\|\varphi\|_2 \leq C(\varphi_0),$$

after using (A.42). Since

$$\frac{1}{\sqrt{2}}\min\left\{\sqrt{t},1\right\} \leq \sqrt{\frac{t}{1+t}},$$

for any $t \geq 0$, we deduce that, for a.e. $t \in (0,T)$,

$$\min\left\{\sqrt{t},1\right\}\|\psi\|_1 \leq C(\varphi_0) \qquad \text{and} \qquad \min\left\{\sqrt{t},1\right\}\|\varphi\|_2 \leq C(\varphi_0). \tag{B.196}$$

The second result above implies that

$$\begin{cases} t \leq 1 & \|\varphi\|_2 \leq \dfrac{C(\varphi_0)}{\sqrt{t}} \\ t > 1 & \|\varphi\|_2 \leq C(\varphi_0) \end{cases} \qquad \Rightarrow \qquad \|\varphi(t)\|_2 \leq C(\varphi_0,t_0) \qquad \text{for} \qquad t > t_0 > 0. \tag{B.197}$$

Having done all of the work above, the rest of the proof is identical to that presented in Blowey and Elliott (1991), since at this level, our peculiar regularisation and non-local terms do not appear. For completeness and convenience, we present the rest of the proof here, as in that paper.

i) For $t \geq 0$, let $S(t)$ be the solution operator for problem (**Q**) in (4.38) with IC φ_0, so that

$$\varphi(t) = S(t)\,\varphi_0 \tag{B.198}$$

that is, S maps the state of the system at time t to the IC. Observe that

$$\varphi(0) = S(0)\,\varphi_0 \tag{B.199}$$

$$\varphi(t) = S(t)\,\varphi(0) \tag{B.200}$$

$$\varphi(t+s) = S(t)\,S(s). \tag{B.201}$$

Moreover, if we define X as the metric space[59] comprising the functions in $\mathscr{A}_m$ together with the metric

$$d(\varphi,\psi) = \|\varphi-\psi\|_{-1} \qquad \varphi,\psi \in \mathscr{A}_m, \tag{B.202}$$

then $\{S(t)\}_{t\geq 0}$ is a semi-group of operators, or semiflow, mapping X into itself. From (4.50), we determine that

$$\|S(t)\,\varphi - S(t)\,\psi\|_{-1} \leq C(t)\,\|\varphi-\psi\|_{-1} \qquad \text{for any} \qquad \varphi,\psi \in X; \tag{B.203}$$

that is, $S(t): X \to X$ is continuous for every $t \geq 0$ (cf. (1.4) in Temam (1997)).

ii) We define the ω-limit set of $\varphi_0 \in X$, as

$$\omega(\varphi_0) = \{\chi \in X : S(t_n)\,\varphi_0 \to \chi \,\text{for some sequence } t_n \to \infty\} = \bigcap_{t\geq 0}\overline{\bigcup_{\tau\geq t} S(\tau)\,\varphi_0}. \tag{B.204}$$

We deduce from (B.197) that $\bigcup_{\tau\geq t} S(\tau)\,\varphi_0$ is relatively compact in X for every $\tau \geq 0$,[60] because $H^2(\Omega) \overset{c}{\hookrightarrow} H^1(\Omega)$ by (A.35). According to Lemma 1.1 of Temam (1997), $\omega(\varphi_0)$ is therefore non-empty, compact and invariant, meaning that $S(t)\,\omega(\varphi_0) \subset \omega(\varphi_0)$ for every $t \geq 0$.

iii) The energy $\mathcal{E}$ in (4.1a) is continuous on $H^1(\Omega)$. For $\varphi, h \in H^1(\Omega)$,

$$\mathcal{E}[\varphi+h] = \frac{\varepsilon_\varphi^2}{2}|\varphi+h|_1^2 + \frac{\chi^{AB}}{4}\left(1-(\varphi+h)^2,1\right) + \frac{\alpha}{2}\left\|\varphi+h-\overline{\varphi+h}\right\|_{-1}^2 = \mathcal{E}[\varphi]$$
$$+\varepsilon_\varphi^2(\nabla\varphi,\nabla h) + \frac{\varepsilon_\varphi^2}{2}|h|_1^2 - \frac{\chi^{AB}}{2}(\varphi,h) - \frac{\chi^{AB}}{4}\|h\|^2 + \alpha\left(\varphi-\overline{\varphi},h-\overline{h}\right)_{-1} + \frac{\alpha}{2}\left\|h-\overline{h}\right\|_{-1}^2,$$

and so

$$\mathcal{E}[\varphi] - H\left(\varphi,\|h\|_1\right) \leq \mathcal{E}[\varphi+h] \leq \mathcal{E}[\varphi] + H\left(\varphi,\|h\|_1\right), \tag{B.205a}$$

where, for fixed $\varphi \in H^1(\Omega)$, and using the Cauchy-Schwarz inequality and (A.28b),

$$H\left(\varphi,\|h\|_1\right) := \varepsilon_\varphi^2\|\varphi\|_1\|h\|_1 + \frac{\varepsilon_\varphi^2}{2}\|h\|_1^2 + \frac{\chi^{AB}}{2}\|\varphi\|_1\|h\|_1$$
$$+\frac{\chi^{AB}}{4}\|h\|_1^2 + \alpha c_P^4\|\varphi\|_1\|h\|_1 + \frac{\alpha}{2}c_P^4\|h\|_1^2 \to 0 \quad \text{as} \quad \|h\|_1 \to 0. \tag{B.205b}$$

Hence,

$$\lim_{\|h\|_1\to 0}\mathcal{E}[\varphi+h] = \mathcal{E}[\varphi].$$

Setting $\varphi = v$ and $\varphi + h = u$, viz. $h = u - v$, we re-write this in the more familiar

$$\lim_{\|u\|_1\to\|v\|_1}\mathcal{E}[u] = \mathcal{E}[v], \tag{B.206}$$

that is, $\mathcal{E}$ in (4.1a) is continuous on $H^1(\Omega)$.

iv) From (4.52b), we find that

$$\mathcal{E}[S(t)\varphi_0] \leq \mathcal{E}\left[S\left(t'\right)\varphi_0\right] \qquad \text{for any} \qquad 0 < t' \leq t \qquad \text{and any} \qquad \varphi_0 \in \mathscr{A}_m. \tag{B.207}$$

By (4.51), $S(t)\varphi_0 \in C\left((0,T];H^1(\Omega)\right)$ and since $\mathcal{E}$ is bounded below on X, (B.207) implies that

$$\mathcal{E}^\infty := \lim_{t\to\infty}\mathcal{E}[S(t)\varphi_0] \tag{B.208}$$

is well-defined. Moreover, by (B.197) and our remarks above, we can infer the existence of a sub-sequence $(S(t_n)\varphi_0)$ and $\varphi \in \omega(\varphi_0)$ such that

$$\varphi = \lim_{t_n\to\infty} S(t_n)\varphi_0 \in H^1(\Omega). \tag{B.209}$$

Remark. The key here is that we have a bound in $H^2(\Omega)$ and, consequently, a strongly convergent sub-sequence in $H^1(\Omega)$.

But since $\mathcal{E}$ is continuous on $H^1(\Omega)$, in fact, for $\varphi \in \omega(\varphi_0)$,

$$\mathcal{E}[\varphi] = \lim_{t_n\to\infty}\mathcal{E}[S(t_n)\varphi_0] = \mathcal{E}^\infty, \tag{B.210}$$

from (B.208). Hence, $\mathcal{E}[\cdot]$ is constant on $\omega(\varphi_0)$ (since $\mathcal{E}^\infty$ is well-defined), but since the energy is a monotonically non-increasing function of time (cf. (B.207)), the solution has stopped changing. That is

$$\frac{\mathrm{d}}{\mathrm{d}t}(S(t)\varphi) \equiv 0 \qquad \text{for} \qquad \varphi \in \omega(\varphi_0), \tag{B.211}$$

and φ is a fixed point of S. But in terms of problem (**Q**) in (4.38), that means that $\partial_t\varphi = 0$, viz.

$$\varepsilon_\varphi^2(\nabla\varphi,\nabla\nu-\nabla\varphi) - \frac{\chi^{AB}}{2}(\varphi,\nu-\varphi) + \alpha\left(\left(-\Delta_n\right)^{-1}(\varphi-\overline{\varphi}),\nu-\varphi\right) \geq 0, \tag{B.212}$$

for every $\nu \in \mathscr{A}_m$. But this says that φ solves problem (**S**) in (4.27a) (and also problem ($\mathbf{S}_C$) in (4.27b) by Lemma 4.2.7).[61]

□

B.17 Proof of Lemma 4.4.1

Proof.

i) The association between ψ_μ and ω_μ in (4.57) is well-defined due to Lemma A.1.5.

ii) Given a solution $\{\varphi_\mu, \psi_\mu\}$ to $(\mathbf{P}_\mu)$, define the pair $\{\varphi_\mu, \omega_\mu\}$ with ω_μ as in (4.57). Substituting (4.57a) into (4.56b) and (4.57b) into (4.56a) then retrieves $(\mathbf{R}_{\mu,\mathbf{0}})$ with solution $\{\varphi_\mu, \omega_\mu\}$. Add a right-hand (f, ν_1) to (4.56a), for a given f, to arrive at $(\mathbf{R}_{\mu,\mathbf{f}})$.

iii) For the converse, we proceed as above, but for given $\{\varphi_\mu, \omega_\mu\}$ a solution to $(\mathbf{R}_{\mu,\mathbf{f}})$, define the pair $\{\varphi_\mu, \psi_\mu\}$ with ψ_μ as in (4.57), and set $f \equiv 0$.

□

B.18 Proof of Corollary 4.4.2

Proof. We established the equivalence of problems $(\mathbf{P}_\mu)$ and $(\mathbf{R}_{\mu,\mathbf{0}})$ in Lemma 4.4.1. As such, the estimates for φ_μ solving $(\mathbf{P}_\mu)$ (viz. (4.45a)–(4.45d)) apply to φ_μ solving $(\mathbf{R}_{\mu,\mathbf{0}})$. All that remains is to establish (4.58). To do so, we set $\nu = \omega_\mu$ in (4.57a), and find that

$$\|\omega_\mu\|^2 = (\psi_\mu, \omega_\mu) - \alpha\left((-\Delta_n)^{-1}(\varphi_\mu - \overline{\varphi_\mu}), \omega_\mu\right) \leq \|\psi_\mu\|\,\|\omega_\mu\| + \alpha\left\|(-\Delta_n)^{-1}(\varphi_\mu - \overline{\varphi_\mu})\right\|\|\omega_\mu\|$$

by the Cauchy–Schwarz inequality. Using (A.30a), and arguing as we did for (B.112b), we find that

$$\|\omega_\mu\| \leq \alpha c_P^2\,\|\varphi_\mu - \overline{\varphi_\mu}\| + \|\psi_\mu\| \leq \|\psi_\mu\| + C \leq C + C\,|\psi_\mu|_1 \tag{B.213a}$$

for constants C independent of T, μ and N. Setting $\nu = \omega_\mu$ in (4.57b) then leads to

$$|\omega_\mu|_1^2 = (\nabla\psi_\mu, \nabla\omega_\mu) - \alpha\,(\varphi_\mu - \overline{\varphi_\mu}, \omega_\mu - \overline{\omega_\mu}) \leq |\psi_\mu|_1\,|\omega_\mu|_1 + \alpha c_P^2\,|\varphi_\mu|_1\,|\omega_\mu|_1$$

by the Cauchy–Schwarz and Poincaré inequalities, since $\overline{\omega_\mu}\,(\varphi_\mu - \overline{\varphi_\mu}, 1) = 0$. Hence,

$$|\omega_\mu|_1 \leq |\psi_\mu|_1 + \alpha c_P^2\,|\varphi_\mu|_1 \leq C + |\psi_\mu|_1\,, \tag{B.213b}$$

for C independent of T, μ and N by (4.44a). Combining (B.213a)–(B.213b), and integrating in time gives (cf. (B.112d))

$$\int_0^T \|\omega_\mu(s)\|_1^2\,\mathrm{d}s = C\left(1 + T^{1/2}\right)$$

for C independent of T, μ and N, which is (4.58).

□

B.19 Boundedness: proof of Lemma 4.4.3

Proof.

i) We assume that a solution $(\varphi_\mu, \omega_\mu)$ exists for $\left(\mathbf{R}_{\mu,\mathbf{f}}^{(\mathbf{m})}\right)$. If $\overline{\varphi_0} = m$, then $\overline{\varphi_\mu} = m$ for a.e. t as we noted earlier. Setting $\nu_1 = 1$ in (4.59) therefore yields

$$(\partial_t\varphi_\mu, 1) = 0 \qquad \Rightarrow \qquad \overline{\partial_t\varphi_\mu} = 0. \tag{B.214}$$

ii) Since $\varphi_\mu - m, f \in L^2_*(\Omega)$ for a.e. t, we use (2.9) to re-write (4.59) as

$$(\partial_t \varphi_\mu, \nu_1) + (\nabla\psi, \nabla\nu_1) = 0 \tag{B.215a}$$

for every $\nu_1 \in H^1(\Omega)$, where

$$\psi := \omega_\mu + \alpha(-\Delta_n)^{-1}(\varphi_\mu - m) + F, \qquad F := (-\Delta_n)^{-1}(-f) \in C^1\left([0,T]; H^1_*(\Omega)\right), \tag{B.215b}$$

thanks to (A.22). Using (B.215b), we re-write (4.56b) as

$$\varepsilon_\varphi^2(\nabla\varphi_\mu, \nabla\nu_2) + \left(\mathcal{B}'_\mu(\varphi_\mu), \nu_2\right) + \alpha\left((-\Delta_n)^{-1}(\varphi_\mu - m), \nu_2\right) + (F, \nu_2) = (\psi, \nu_2), \tag{B.215c}$$

for every $\nu_2 \in H^1(\Omega)$.

Remark. We have effectively transformed $\left(\mathbf{R}^{(\mathbf{m})}_{\mu,\mathbf{f}}\right)$ 'back' to $\left(\mathbf{P}^{(\mathbf{m})}_{\mu,\mathbf{f}}\right)$. As such, the proofs that follow mimic those above for $(\mathbf{P}_\mu)$ which, in turn, draw heavily on the material in Blowey and Elliott (1991).

iii) Setting $\nu_1 = \psi$, then $\nu_1 = (-\Delta_n)^{-1}(\varphi_\mu - m)$ and finally $\nu_1 = F$ in (B.215a) gives

$$\begin{aligned} (\partial_t\varphi_\mu, \psi) &= -|\psi|_1^2 \\ \left(\partial_t\varphi_\mu, (-\Delta_n)^{-1}(\varphi_\mu - m)\right) &= -(\psi, \varphi_\mu - m) \\ (\partial_t\varphi_\mu, F) &= -(\nabla\psi, \nabla F), \end{aligned} \tag{B.216}$$

where we used (2.9) to get the second result. Setting $\nu_2 = \partial_t\varphi_\mu$ in (B.215c) yields

$$\frac{\varepsilon_\varphi^2}{2}\frac{\mathrm{d}}{\mathrm{d}t}|\varphi_\mu|_1^2 + \frac{\mathrm{d}}{\mathrm{d}t}\left(\mathcal{B}_\mu(\varphi_\mu), 1\right) + \alpha\left((-\Delta_n)^{-1}(\varphi_\mu - m), \partial_t\varphi_\mu\right) + (F, \partial_t\varphi_\mu) = (\psi, \partial_t\varphi_\mu), \tag{B.217}$$

after noting that

$$\frac{\mathrm{d}}{\mathrm{d}t}\left(\mathcal{B}_\mu(\varphi_\mu), 1\right) = \left(\mathcal{B}'_\mu(\varphi_\mu), \partial_t\varphi_\mu\right) \qquad \text{and} \qquad \frac{1}{2}\frac{\mathrm{d}}{\mathrm{d}t}|\varphi_\mu|_1^2 = (\nabla\varphi_\mu, \nabla\partial_t\varphi_\mu).$$

Combining (B.216) and (B.217) leads to

$$\frac{\varepsilon_\varphi^2}{2}\frac{\mathrm{d}}{\mathrm{d}t}|\varphi_\mu|_1^2 + \frac{\mathrm{d}}{\mathrm{d}t}\left(\mathcal{B}_\mu(\varphi_\mu), 1\right) + |\psi|_1^2 = (\nabla\psi, \nabla F) + \alpha(\varphi_\mu - m, \psi). \tag{B.218}$$

iv) In the last term in (B.218),

$$\begin{aligned} (\varphi_\mu - m, \psi) = (\varphi_\mu - m, \psi) - \underbrace{\overline{\psi}}_{\in\mathbb{R}}\underbrace{(\varphi_\mu - m, 1)}_{=0} &= \left(\varphi_\mu - \overline{\varphi_\mu}, \psi - \overline{\psi}\right) \\ &\leq \|\varphi_\mu - \overline{\varphi_\mu}\|\left\|\psi - \overline{\psi}\right\| \leq c_P^2|\varphi_\mu|_1|\psi|_1 \end{aligned} \tag{B.219}$$

by the Cauchy–Schwarz and Poincaré inequalities, and so, by Young's inequality,

$$\alpha(\varphi_\mu - m, \psi) \leq \alpha c_P^2|\varphi_\mu|_1|\psi|_1 \leq \frac{1}{2}\alpha^2 c_P^4|\varphi_\mu|_1^2 + \frac{1}{2}|\psi|_1^2. \tag{B.220}$$

Similarly, using (2.11),

$$(\nabla\psi, \nabla F) \leq |\psi|_1|F|_1 \leq |F|_1^2 + \frac{1}{4}|\psi|_1^2 = \|f\|_{-1}^2 + \frac{1}{4}|\psi|_1^2. \tag{B.221}$$

Using (B.220) and (B.221) in (B.218) leads to

$$\varepsilon_\varphi^2\frac{\mathrm{d}}{\mathrm{d}t}|\varphi_\mu|_1^2 + 2\frac{\mathrm{d}}{\mathrm{d}t}\left(\mathcal{B}_\mu(\varphi_\mu), 1\right) + \frac{1}{2}|\psi|_1^2 \leq \alpha^2 c_P^4|\varphi_\mu|_1^2 + 2\|f\|_{-1}^2. \tag{B.222}$$

Integrating this in time over $[0,t]$ yields

$$\varepsilon_\varphi^2 \left|\varphi_\mu(t)\right|_1^2 + 2\left(\mathcal{B}_\mu\left(\varphi_\mu(t)\right),1\right) + \frac{1}{2}\int_0^t \left|\psi(s)\right|_1^2 \mathrm{d}s \le \varepsilon_\varphi^2 \left|\varphi_0\right|_1^2 + 2\left(\mathcal{B}_\mu\left(\varphi_0\right),1\right) + 2\int_0^t \left\|f(s)\right\|_{-1}^2 \mathrm{d}s + \frac{\alpha^2 c_P^4}{\varepsilon_\varphi^2}\int_0^t \varepsilon_\varphi^2 \left|\varphi_\mu(s)\right|_1^2 \mathrm{d}s.$$

If $\mu < \mu_{\max}$, (4.12) says there is a $C_0 = C_0\left(\chi^{AB}\right) > 0$, independent of μ, for which

$$\mathcal{B}_\mu(r) \ge -C_0\mu \qquad \Rightarrow \qquad -\mathcal{B}_\mu(r) \le C_0\mu \le C_0\mu_{\max} \qquad \text{for any} \qquad r \in \mathbb{R}. \tag{B.223a}$$

Moreover, since $\varphi_0 \in \mathscr{A}$ by (4.39c),

$$\left(\mathcal{B}_\mu\left(\varphi_0\right),1\right) = \left(\mathcal{B}\left(\varphi_0\right),1\right) = \frac{\chi^{AB}}{4}\left(1-\varphi_0^2,1\right) = \frac{\chi^{AB}}{4}\left(|\Omega| - \|\varphi_0\|^2\right), \tag{B.223b}$$

and so

$$\varepsilon_\varphi^2 \left|\varphi_\mu(t)\right|_1^2 + \frac{1}{2}\int_0^t \left|\psi(s)\right|_1^2 \mathrm{d}s \le C + \frac{\alpha^2 c_P^4}{\varepsilon_\varphi^2}\int_0^t \varepsilon_\varphi^2 \left|\varphi_\mu(s)\right|_1^2 \mathrm{d}s,$$

where

$$C := \varepsilon_\varphi^2 \left|\varphi_0\right|_1^2 + 2C_0\mu_{\max}|\Omega| + \frac{\chi^{AB}}{2}\left(|\Omega| + \|\varphi_0\|^2\right) + 2\int_0^t \left\|f(s)\right\|_{-1}^2 \mathrm{d}s > 0 \tag{B.224a}$$

is independent of μ. Gronwall's Lemma implies that (cf. (B.89)[62])

$$\varepsilon_\varphi^2 \left|\varphi_\mu(t)\right|_1^2 + \frac{1}{2}\int_0^t \left|\psi(s)\right|_1^2 \mathrm{d}s \le C\exp\left(\frac{\alpha^2 c_P^4}{\varepsilon_\varphi^2}T\right) < \infty \tag{B.224b}$$

for a.e. $t \in (0,T)$. Hence, (cf. (B.90))

$$\left|\varphi_\mu(t)\right|_1^2 \le C \qquad \text{for a.e. } t \in [0,T], \tag{B.225}$$

independent of μ. Arguing as in the build-up to (B.92), we use Poincaré's inequality to conclude that

$$\operatorname*{ess\,sup}_{t\in[0,T]} \left\|\varphi_\mu(t)\right\|_1 \le C \tag{B.226}$$

independent of μ, which is (4.62).

v) Setting $\nu_1 = \left(-\Delta_n\right)^{-1}\partial_t\varphi_\mu$ (noting (B.214)) and then $\nu_1 = \psi$ in (B.215a) yields (cf. (B.94))

$$\left\|\partial_t\varphi_\mu\right\|_{-1}^2 + \left(\psi, \partial_t\varphi_\mu\right) = 0 \qquad \text{and} \qquad \left(\partial_t\varphi_\mu, \psi\right) = -\left|\psi\right|_1^2 \qquad \Rightarrow \qquad \left\|\partial_t\varphi_\mu\right\|_{-1}^2 = \left|\psi\right|_1^2, \tag{B.227}$$

where we used (2.9). Substituting this into (B.224b) immediately gives (cf. (A.27))

$$\int_0^t \left\|\partial_s\varphi_\mu\right\|_{-1}^2 \mathrm{d}s \le C. \tag{B.228}$$

vi) Suppose $\partial\Omega$ satisfies the conditions of Lemma A.1.9, $-\Delta\varphi_0 \in H^1(\Omega)$, $\partial_n\varphi_0|_{\partial\Omega} = 0$ and (4.55) holds. Our assumptions about $\partial\Omega$ mean that (cf. Lemma A.1.10)

$$\varphi_\mu \in H^2(\Omega), \qquad \left(-\Delta\varphi_\mu, \nu\right) = \left(\nabla\varphi_\mu, \nabla\nu\right) \qquad \forall\ \nu \in H^1(\Omega), \qquad \text{and} \qquad \partial_n\varphi_\mu|_{\partial\Omega} = 0 \tag{B.229}$$

(in the sense of trace) for a.e. t. Hence, we can re-write (B.215c) as

$$\varepsilon_\varphi^2 \left(-\Delta\varphi_\mu, \nu_2\right) + \left(\mathcal{B}_\mu'\left(\varphi_\mu\right), \nu_2\right) + \left(\alpha\left(-\Delta_n\right)^{-1}\left(\varphi_\mu - m\right), \nu_2\right) + \left(F, \nu_2\right) = \left(\psi, \nu_2\right), \tag{B.230a}$$

for every $\nu_2 \in L^2(\Omega)$, viz. a.e. in Ω_T,

$$\psi = \omega_\mu + \alpha\left(-\Delta_n\right)^{-1}\left(\varphi_\mu - m\right) + F; \qquad \omega_\mu = \varepsilon_\varphi^2 - \Delta\varphi_\mu + \mathcal{B}_\mu'\left(\varphi_\mu\right). \tag{B.230b}$$

For $t = 0$, our assumptions on the IC and (4.7) give, with $F_0 := F(0)$,

$$H^1(\Omega) \ni \psi(0) =: \psi_0 = \omega_0 + \alpha\left(-\Delta_n\right)^{-1}\left(\varphi_0 - m\right) + F_0 \tag{B.231a}$$

$$\text{where} \qquad H^1(\Omega) \ni \omega_\mu(0) =: \omega_0 = \varepsilon_\varphi^2 - \Delta\varphi_0 - \frac{\chi^{AB}}{2}\varphi_0. \tag{B.231b}$$

vii) We set $\nu_1 = \mathrm{d}\psi/\mathrm{d}t$ in (B.215a) and arrive at

$$\left(\partial_t\varphi_\mu, \partial_t\psi\right) + \frac{1}{2}\frac{\mathrm{d}}{\mathrm{d}t}\left|\psi\right|_1^2 = 0 \qquad \text{since} \qquad \left(\nabla\psi, \nabla\partial_t\psi\right) = \frac{1}{2}\frac{\mathrm{d}}{\mathrm{d}t}\left|\psi\right|_1^2. \tag{B.232}$$

If we differentiate (B.215c) with respect to t, we obtain (cf. (B.185))

$$\begin{aligned}\left(\partial_t\psi, \nu_2\right) = \varepsilon_\varphi^2\left(\nabla\partial_t\varphi_\mu, \nabla\nu_2\right) - \frac{\chi^{AB}}{2}\left(\partial_t\varphi_\mu, \nu_2\right) + \left(\zeta_\mu'\left(\varphi_\mu\right)\partial_t\varphi_\mu, \nu_2\right) \\ + \alpha\left(\left(-\Delta_n\right)^{-1}\left(\partial_t\varphi_\mu\right), \nu_2\right) + \left(\partial_t F, \nu_2\right).\end{aligned}$$

Setting $\nu_2 = \partial_t\varphi_\mu$ in this latter equation yields

$$\varepsilon_\varphi^2\left|\partial_t\varphi_\mu\right|_1^2 - \frac{\chi^{AB}}{2}\left\|\partial_t\varphi_\mu\right\|^2 + \underbrace{\left(\zeta_\mu'\left(\varphi_\mu\right), \left(\partial_t\varphi_\mu\right)^2\right)}_{\geq 0} + \underbrace{\alpha\left\|\partial_t\varphi_\mu\right\|_{-1}^2}_{\geq 0} + \left(\partial_t F, \partial_t\varphi_\mu\right) = \left(\partial_t\psi, \partial_t\varphi_\mu\right). \tag{B.233}$$

Combining this with (B.232) yields (cf. (B.187))

$$\begin{aligned}\varepsilon_\varphi^2\left|\partial_t\varphi_\mu\right|_1^2 + \frac{1}{2}\frac{\mathrm{d}}{\mathrm{d}t}\left|\psi\right|_1^2 &\leq \left(\frac{\chi^{AB}}{2} + \frac{1}{2}\right)\left\|\partial_t\varphi_\mu\right\|^2 + \frac{1}{2}\left\|\partial_t F\right\|^2 \\ &\leq \left(\frac{\chi^{AB}}{2} + \frac{1}{2}\right)^2 \frac{1}{2\varepsilon_\varphi^2}\left\|\partial_t\varphi_\mu\right\|_{-1}^2 + \frac{\varepsilon_\varphi^2}{2}\left|\partial_t\varphi_\mu\right|_1 + \frac{1}{2}\left\|\partial_t F\right\|^2\end{aligned}$$

or

$$\varepsilon_\varphi^2\left|\partial_t\varphi_\mu\right|_1^2 + \frac{\mathrm{d}}{\mathrm{d}t}\left|\psi\right|_1^2 \leq \left(\frac{\chi^{AB}}{2} + \frac{1}{2}\right)^2 \frac{1}{\varepsilon_\varphi^2}\left\|\partial_t\varphi_\mu\right\|_{-1}^2 + \left\|\partial_t F\right\|^2 \tag{B.234}$$

after using the Cauchy–Schwarz and Young's inequalities, together with (A.29). Integrating this in time over $(0, t)$ for any $t \leq T$ leads to

$$\left|\psi(t)\right|_1^2 + \varepsilon_\varphi^2\int_0^t \left|\partial_s\varphi_\mu\right|_1^2 \mathrm{d}s \leq \left|\psi(0)\right|_1^2 + C\left(\chi^{AB}, \varepsilon_\varphi\right)\int_0^T \left\|\partial_s\varphi_\mu\right\|_{-1}^2 \mathrm{d}s + \int_0^T \left\|\partial_t F\right\|^2 \mathrm{d}t. \tag{B.235}$$

- We bound $\left|\psi(0)\right|_1 := \left|\psi_0\right|_1$ on the right, independent of μ (and T) using (B.231) and (2.11);

$$\begin{aligned}\left|\psi_0\right|_1 &\leq \varepsilon_\varphi^2\left|-\Delta\varphi_0\right|_1 + \frac{\chi^{AB}}{2}\left|\varphi_0\right|_1 + \alpha\left|\left(-\Delta_n\right)^{-1}\left(\varphi_0 - m\right)\right|_1 + \left|F_0\right|_1 \\ &\leq \varepsilon_\varphi^2\left|-\Delta\varphi_0\right|_1 + \left(\frac{\chi^{AB}}{2} + \alpha c_P^2\right)\left|\varphi_0\right|_1 + \left\|f_0\right\|_{-1} = C\left(\varphi_0, f\right) < \infty.\end{aligned} \tag{B.236}$$

- (B.228) gives us a bound for the second integral, independent of μ.

- The integral involving $\partial_t F$ is bounded, independent of μ, because of (B.215b).

Hence, (cf. (B.191))

$$|\psi(t)|_1^2 + \varepsilon_\varphi^2 \int_0^t |\partial_s \varphi_\mu|_1^2 \, \mathrm{d}s \leq C \qquad \text{for a.e. } t \in (0,T) \tag{B.237}$$

in which C is independent of μ.

viii) As in the proof of Lemma 4.3.8, by (B.214) and Poincaré's inequality,

$$\overline{\partial_t \varphi_\mu} = 0 \qquad \Rightarrow \qquad \|\partial_t \varphi_\mu\| \leq c_P \, |\partial_t \varphi_\mu|_1 .$$

We conclude from (B.237) that $\partial_t \varphi_\mu \in L^2\left(0,T; H^1(\Omega)\right)$. But from (4.62),

$$\varphi_\mu \in L^\infty\left(0,T; H^1(\Omega)\right) \qquad \Rightarrow \qquad \varphi_\mu \in L^2\left(0,T; H^1(\Omega)\right)$$

and so $\varphi_\mu \in H^1\left(0,T; H^1(\Omega)\right)$, which is (4.64) (cf. (4.54a)).

ix) Another immediate takeaway from (B.237), is that the semi-norm

$$\operatorname*{ess\,sup}_{t\in(0,T)} |\psi(t)|_1 \leq C, \tag{B.238}$$

independent of μ.[63]

x) We now set $\nu_2 = -\Delta\varphi_\mu \in L^2(\Omega)$ in (B.230a) and use the zero Neumann BC on φ_μ in (B.229) to conclude that (cf. (B.175), (B.176a))

$$\begin{aligned}\varepsilon_\varphi^2 \|-\Delta\varphi_\mu\|^2 - \frac{\chi^{AB}}{2} |\varphi_\mu|_1^2 &\leq (\nabla\psi, \nabla\varphi_\mu) - (\nabla F, \nabla\varphi_\mu) \\ &\leq |\psi|_1 |\varphi_\mu|_1 + |F|_1 |\varphi_\mu|_1 \leq \frac{1}{2}|\psi|_1^2 + |\varphi_\mu|_1^2 + \frac{1}{2}\|f\|_{-1}^2\end{aligned}$$

by (2.11) and the Cauchy–Schwarz and Young's inequalities. Rearranging yields

$$\varepsilon_\varphi^2 \|-\Delta\varphi_\mu(t)\|^2 \leq \frac{1}{2}|\psi|_1^2 + \left(\frac{\chi^{AB}}{2} + 1\right)|\varphi_\mu|_1^2 + \frac{1}{2}\|f\|_{-1}^2 \leq C \qquad \text{for a.e. } t \in (0,T) \tag{B.239}$$

where C is independent of μ, because of (4.62) and (B.238). Since t on the left is arbitrary,

$$\operatorname*{ess\,sup}_{t\in(0,T)} \|-\Delta\varphi_\mu(t)\| \leq C$$

independent of μ. Our smoothness assumptions on $\partial\Omega$ and (A.43) mean that

$$\operatorname*{ess\,sup}_{t\in(0,T)} \|\varphi_\mu(t)\|_2 \leq C$$

independent of μ; this is the second part of the result for φ_μ in (4.64).

□

B.20 Stability: proof of Lemma 4.4.4

Proof. i) Since U_1 and U_2 both satisfy $\left(\mathbf{R}^{(\mathbf{m})}_{\mu,\mathbf{f}}\right)$, we may substitute them into (4.59) and (4.56b). Subtracting the results leads to (cf. (B.136)):

$\left(\mathbf{R}^{(\text{diff})}_{\mu}\right)$: find $\varphi_\mu(t), \omega_\mu(t)$ such that

$$\langle \partial_t \varphi_\mu, \nu_1 \rangle + (\nabla \omega_\mu, \nabla \nu_1) + \alpha (\varphi_\mu, \nu_1) = 0 \tag{B.240a}$$

$$(\omega_\mu, \nu_2) = \varepsilon_\varphi^2 (\nabla \varphi_\mu, \nabla \nu_2) + (\zeta_\mu(\varphi_1) - \zeta_\mu(\varphi_2), \nu_2) - \frac{\chi^{AB}}{2} (\varphi_\mu, \nu_2) \tag{B.240b}$$

for every $\nu_1, \nu_2 \in H^1(\Omega)$ and a.e. $t \in (0,T)$, where

$$\varphi_\mu(0) = (\varphi_1)_0 - (\varphi_2)_0 =: \varphi_0 \tag{B.240c}$$

with $(\varphi_1)_0$ and $(\varphi_2)_0$ two ICs as in (4.39c).

Remark. (B.240) features neither m nor f.

ii) As in Section 2.3.4 of Parsons (2012), we set $\nu_1 = \varphi_\mu$ in (B.240a) to obtain

$$\frac{1}{2}\frac{\mathrm{d}}{\mathrm{d}t} \|\varphi_\mu\|^2 + (\nabla \omega_\mu, \nabla \varphi_\mu) + \alpha \|\varphi_\mu\|^2 = 0, \tag{B.241}$$

using the fact that[64]

$$\langle \partial_t \varphi_\mu, \varphi_\mu \rangle = \frac{1}{2} \int_\Omega \frac{\mathrm{d}}{\mathrm{d}t} \left(\varphi_\mu^2\right) \mathrm{d}\Omega = \frac{1}{2}\frac{\mathrm{d}}{\mathrm{d}t} \|\varphi_\mu\|^2 .$$

Putting $\nu_2 = \omega_\mu$ in (B.240b) then yields

$$\|\omega_\mu\|^2 = \varepsilon_\varphi^2 (\nabla \varphi_\mu, \nabla \omega_\mu) + (\zeta_\mu(\varphi_1) - \zeta_\mu(\varphi_2), \omega_\mu) - \frac{\chi^{AB}}{2} (\varphi_\mu, \omega_\mu), \tag{B.242}$$

so if we subtract ε_φ^2 times (B.241) from (B.242) and rearrange, we find that[65]

$$\begin{aligned} \frac{\varepsilon_\varphi^2}{2}\frac{\mathrm{d}}{\mathrm{d}t} \|\varphi_\mu\|^2 + \|\omega_\mu\|^2 + \varepsilon_\varphi^2 \alpha \|\varphi_\mu\|^2 &= (\zeta_\mu(\varphi_1) - \zeta_\mu(\varphi_2), \omega_\mu) - \frac{\chi^{AB}}{2} (\varphi_\mu, \omega_\mu) \\ &\leq \left(\frac{1}{\mu} + \frac{\chi^{AB}}{2}\right) \|\varphi_\mu\| \|\omega_\mu\| \leq \frac{1}{2}\left(\frac{1}{\mu} + \frac{\chi^{AB}}{2}\right)^2 \|\varphi_\mu\|^2 + \frac{1}{2}\|\omega_\mu\|^2, \end{aligned} \tag{B.243}$$

after using the Lipschitz continuity of ζ_μ from (4.17), and the Cauchy–Schwarz and Young's inequalities. Rearranging, we are led to (cf. (B.141)[66])

$$\varepsilon_\varphi^2 \frac{\mathrm{d}}{\mathrm{d}t} \|\varphi_\mu\|^2 + \|\omega_\mu\|^2 \leq 2C_1\left(\mu, \chi^{AB}\right) \|\varphi_\mu\|^2, \tag{B.244}$$

after discarding the non-negative $\varepsilon_\varphi^2 \alpha \|\varphi_\mu\|^2$ on the left. Note that $C_1\left(\mu, \chi^{AB}\right) > 0$. Integrating this in time yields

$$\varepsilon_\varphi^2 \|\varphi_\mu(t)\|^2 + \int_0^t \|\omega_\mu(s)\|^2 \mathrm{d}s \leq \varepsilon_\varphi^2 \|\varphi_0\|^2 + \frac{2C_1}{\varepsilon_\varphi^2} \int_0^t \varepsilon_\varphi^2 \|\varphi_\mu(s)\|^2 \mathrm{d}s,$$

where $\varphi_0(x) = \varphi_\mu(x,0) = (\varphi_1)_0 - (\varphi_2)_0$. Gronwall's Lemma then implies that

$$\varepsilon_\varphi^2 \|\varphi_\mu(t)\|^2 + \int_0^t \|\omega_\mu(s)\|^2 \mathrm{d}s \leq \varepsilon_\varphi^2 \|\varphi_0\|^2 \exp\left\{\frac{2C_1 T}{\varepsilon_\varphi^2}\right\} = C \|\varphi_0\|^2,$$

where C is a function of μ and T. Consequently, since $\varphi_0 \in L^2(\Omega)$,

$$\operatorname*{ess\,sup}_{t\in[0,T]} \|\varphi_\mu(t)\| \lesssim \|\varphi_0\| < \infty \qquad \text{i.e.} \qquad \varphi_\mu \in L^\infty\left(0,T; L^2(\Omega)\right).$$

Similarly,

$$\left(\int_0^t \|\omega_\mu(s)\|^2 \,\mathrm{d}s\right)^{1/2} \lesssim \|\varphi_0\| < \infty \qquad \text{for a.e.} \qquad t \in [0,T],$$

and so setting $t = T$ on the left implies that $\omega_\mu \in L^2\left(0,T;L^2(\Omega)\right)$. Using (4.67), we obtain (4.66).

The uniqueness of φ_μ and ω_μ follows from stability in the usual way.

iii) (4.66) certainly holds for $\mu > 0$, but is unsatisfactory because C_1 in (B.244) depends on μ, and becomes unbounded up as $\mu \downarrow 0$ (cf. (B.141)). To deal with this problem, we present the following alternate argument: setting $\nu_2 = \varphi_\mu = \varphi_1 - \varphi_2$ in (B.240b), we find that

$$\varepsilon_\varphi^2 |\varphi_\mu|_1^2 + \underbrace{\left(\zeta_\mu(\varphi_1) - \zeta_\mu(\varphi_2), \varphi_1 - \varphi_2\right)}_{>0 \text{ by (4.19a)}} - \frac{\chi^{AB}}{2}\|\varphi_\mu\|^2 = (\omega_\mu, \varphi_\mu)$$

or[67]

$$\varepsilon_\varphi^2 |\varphi_\mu|_1^2 - \frac{\chi^{AB}}{2}\|\varphi_\mu\|^2 \leq (\omega_\mu, \varphi_\mu). \tag{B.245}$$

Setting $\nu_1 = (-\Delta_n)^{-1}\varphi_\mu$ (noting that $\overline{\varphi_\mu} = 0$) in (B.240a) leads to

$$\frac{1}{2}\frac{\mathrm{d}}{\mathrm{d}t}\|\varphi_\mu\|_{-1}^2 + (\omega_\mu, \varphi_\mu) + \underbrace{\alpha\|\varphi_\mu\|_{-1}^2}_{\geq 0} = 0 \qquad \Rightarrow \qquad \frac{1}{2}\frac{\mathrm{d}}{\mathrm{d}t}\|\varphi_\mu\|_{-1}^2 + (\omega_\mu, \varphi_\mu) \leq 0 \tag{B.246}$$

after using (B.139) and noting that $\left(\nabla\omega_\mu, \nabla(-\Delta_n)^{-1}\varphi_\mu\right) = (\omega_\mu, \varphi_\mu)$ by (2.9a). Combining (B.245) and (B.246), we find that

$$\frac{1}{2}\frac{\mathrm{d}}{\mathrm{d}t}\|\varphi_\mu\|_{-1}^2 + \varepsilon_\varphi^2 |\varphi_\mu|_1^2 \leq \frac{\chi^{AB}}{2}\|\varphi_\mu\|^2, \tag{B.247}$$

which is identical to (B.140) in Theorem 4.3.4, and also matches the second equation from the bottom of p. 244 of Blowey and Elliott (1991), for the Cahn–Hilliard problem. We therefore establish (4.68) (cf. (B.142)) and the uniqueness of φ_μ as in Theorem 4.3.4.

To establish uniqueness of the potential component of the solution of $\left(\mathbf{R}_{\mu,\mathbf{f}}^{(\mathbf{m})}\right)$, we set $\varphi_0 \equiv 0 \Rightarrow \varphi_\mu(t) \equiv 0$ for a.e. t and $\nu_2 = 1$ in (B.240b) to see that

$$(\omega_\mu, 1) = 0 \qquad \Rightarrow \qquad \omega_\mu(t) \in L_*^2(\Omega) \qquad \text{for a.e. } t \in (0,T).$$

Likewise, setting $\nu_1 = \omega_\mu$ in (B.240a), and using the above yields

$$|\omega_\mu(t)|_1^2 = 0 \qquad \Rightarrow \qquad \omega_\mu(t) \equiv 0 \qquad \text{for a.e. } t \in (0,T).$$

The non-local part of the problem (involving α) falls away in (B.240a) because $\varphi_\mu \equiv 0$.

□

B.21 Energy decay: proof of Lemma 4.4.5

Proof. The assumption that $\varphi_0 \in \mathscr{A}_m$ means that $\overline{\varphi_\mu(t)} = m$ for a.e. $t \in (0,T)$. At this stage, we can argue in two ways.

i) In the first, we set $\nu_1 = \psi$ in (B.215a), and find that (cf. (B.82))

$$(\partial_t \varphi_\mu, \psi) = -|\psi|_1^2 . \tag{B.248a}$$

We now make the smoothness assumptions on $\partial\Omega$ in Lemma A.1.9. According to (4.64), this means that $\varphi_\mu \in H^1\left(0,T;H^1(\Omega)\right)$, and so $\nabla\partial_t\varphi_\mu \in L^2(\Omega)$ for a.e. t. Setting $\nu_2 = \partial_t\varphi_\mu$ and $f \equiv 0$ in (B.215c) thus yields (cf. (B.81))

$$(\psi, \partial_t\varphi_\mu) = \varepsilon_\varphi^2 (\nabla\varphi_\mu, \nabla\partial_t\varphi_\mu) + \left(\mathcal{B}'_\mu(\varphi_\mu), \partial_t\varphi_\mu\right) + \alpha\left((-\Delta_n)^{-1}(\varphi_\mu - m), \partial_t\varphi_\mu\right). \tag{B.248b}$$

Combining (B.248a) and (B.248b) leads to

$$\varepsilon_\varphi^2 (\nabla\varphi_\mu, \nabla\partial_t\varphi_\mu) + \left(\mathcal{B}'_\mu(\varphi_\mu), \partial_t\varphi_\mu\right) + \alpha\left((-\Delta_n)^{-1}(\varphi_\mu - m), \partial_t\varphi_\mu\right) + |\psi|_1^2 = 0.$$

Integrating this in time from t' to t gives

$$\int_{t'}^t \varepsilon_\varphi^2 (\nabla\varphi_\mu, \nabla\partial_t\varphi_\mu) + \left(\mathcal{B}'_\mu(\varphi_\mu), \partial_t\varphi_\mu\right) + \alpha\left((-\Delta_n)^{-1}(\varphi_\mu - m), \partial_t\varphi_\mu\right) \mathrm{d}s + \int_{t'}^t |\psi(s)|_1^2 \,\mathrm{d}s = 0. \tag{B.249}$$

If we consider $\mathcal{E}_\mu^{(m)}$ in (4.61), we can re-write this as

$$\int_{t'}^t \partial_s \mathcal{E}_\mu^{(m)} [\varphi_\mu(s)] \,\mathrm{d}s + \int_{t'}^t |\psi(s)|_1^2 \,\mathrm{d}s = 0.$$

Hence, for any $0 < t' \leq t \leq T$,

$$\mathcal{E}_\mu^{(m)} [\varphi_\mu(t)] + \int_{t'}^t |\psi(s)|_1^2 \,\mathrm{d}s = \mathcal{E}_\mu^{(m)} \left[\varphi_\mu\left(t'\right)\right], \tag{B.250}$$

and since $\int_{t'}^t |\psi(s)|_1^2 \,\mathrm{d}s \geq 0$, $\mathcal{E}_\mu^{(m)} [\varphi_\mu(t)] \leq \mathcal{E}_\mu^{(m)} [\varphi_\mu(t')]$.

ii) In the second, (B.215a)–(B.215c) is identical to (4.39a)–(4.39b) i.e. we have recovered problem $(\mathbf{P}_\mu)$. The argument in Theorem 4.3.5 can be applied.

□

B.22 Well-posedness: proof of Lemma 5.1.2

Proof. We use the Browder–Minty theorem (cf. Theorem 10.49 of Renardy and Rogers (2004) and Section 9.1 of Evans (1998)).

In what follows, the semi-norm $|\cdot|_1$ in $H^1(\Omega)$ is a norm in $H_*^1(\Omega)$, which we denote $\|\cdot\|_*$.

i) We must have $\overline{\varphi^j} = \overline{\varphi^{j-1}} =: m$ to satisfy the compatibility condition in the left-most term of (5.8). Mass conservation is thus a necessary condition for solutions to exist.

ii) We prove that,[68] for each *fixed* $\varphi \in H_*^1(\Omega)$ and any $\nu \in H_*^1(\Omega)$, the mapping

$$\nu \mapsto B(\varphi, \nu) \in \mathbb{R}$$

with B as in (5.16a), is a bounded linear functional.

The linearity of the mapping (in ν) is clear. For boundedness, if $\varphi \in H^1_*(\Omega)$,

$$\begin{aligned}
|B(\varphi,\nu)| &= \frac{1}{\tau}\left(\left(-\Delta_n\right)^{-1/2}\varphi, \left(-\Delta_n\right)^{-1/2}\nu\right) + \varepsilon_\varphi^2\left(\nabla\varphi,\nabla\nu\right) + \left(\zeta_\mu\left(\varphi+m\right),\nu\right) \\
&\quad + \alpha\theta\left(\left(-\Delta_n\right)^{-1/2}\varphi, \left(-\Delta_n\right)^{-1/2}\nu\right) \\
&\leq \frac{1}{\tau}\left\|\varphi\right\|_{-1}\left\|\nu\right\|_{-1} + \varepsilon_\varphi^2\left|\varphi\right|_1\left|\nu\right|_1 + \frac{1}{\mu}\left\|\varphi+m\right\|\left\|\nu\right\| + \alpha\theta\left\|\varphi\right\|_{-1}\left\|\nu\right\|_{-1} \\
&\leq \underbrace{\left(c_P^2\left(\frac{c_P^2}{\tau}+\frac{1}{\mu}+\alpha\theta c_P^2\right)+\varepsilon_\varphi^2\right)}_{C\left(c_P,\mu,\tau,\alpha,\theta,\varepsilon_\varphi^2\right)}\left\|\varphi\right\|_*\left\|\nu\right\|_* = C\left\|\nu\right\|_*
\end{aligned} \tag{B.251}$$

for $0 < C < \infty$, where we used (2.12) and (A.28b), the Cauchy–Schwarz, Poincaré and Young inequalities and (4.18).[69] From this we infer the existence of a mapping

$$\varphi \mapsto T(\varphi) \in \left(H^1_*(\Omega)\right)' \quad \text{with} \quad \left\langle T(\varphi),\nu\right\rangle_{H^1_*(\Omega)} = B(\varphi,\nu) \quad \text{for all} \quad \varphi,\nu \in H^1_*(\Omega). \tag{B.252}$$

iii) By analogous reasoning and bilinear g as in (5.16b), we conclude that the mapping

$$\nu \mapsto g(\omega,\nu) \in \mathbb{R}$$

is also a bounded linear functional. Hence, we reuse the symbol g in the mapping

$$\omega \mapsto g(\omega) \in \left(H^1_*(\Omega)\right)' \quad \text{with} \quad \left\langle g(\omega),\nu\right\rangle_{H^1_*(\Omega)} = g(\omega,\nu) \quad \text{for all} \quad \omega,\nu \in H^1_*(\Omega). \tag{B.253}$$

iv) T is **bounded**.

$$\begin{aligned}
\left\|T(\varphi)\right\|_{\left(H^1_*(\Omega)\right)'} &:= \sup_{\left\|\nu\right\|_*=1}\left|\left\langle T(\varphi),\nu\right\rangle_{H^1_*(\Omega)}\right| = \sup_{\left\|\nu\right\|_*=1}\left|B(\varphi,\nu)\right| \\
&\leq \sup_{\left\|\nu\right\|_*=1} C\left\|\nu\right\|_* = C\left(c_P,\mu,\tau,\alpha,\theta,\varepsilon_\varphi^2,\left\|\varphi\right\|_*\right) < \infty,
\end{aligned} \tag{B.254}$$

using (B.251) i.e. T maps bounded sets in $H^1_*(\Omega)$ to bounded sets in $\left(H^1_*(\Omega)\right)'$ and is thus bounded. Consequently, we define $T : H^1_*(\Omega) \mapsto \left(H^1_*(\Omega)\right)'$ by writing (B.252) in full using (5.16a), for $\varphi,\nu \in H^1_*(\Omega)$, as

$$\left\langle T(\varphi),\nu\right\rangle_{H^1_*(\Omega)} = \frac{1}{\tau}\left(\left(-\Delta_n\right)^{-1}\varphi,\nu\right) + \varepsilon_\varphi^2\left(\nabla\varphi,\nabla\nu\right) + \left(\zeta_\mu\left(\varphi+m\right),\nu\right) + \alpha\theta\left(\left(-\Delta_n\right)^{-1}\varphi,\nu\right). \tag{B.255}$$

v) The mapping T in (B.255) is **(Lipschitz) continuous**. Let $\varphi,\psi \in H^1_*(\Omega)$. Then

$$\begin{aligned}
&\left\langle T(\varphi)-T(\psi),\nu\right\rangle_{H^1_*(\Omega)} \\
&= \frac{1}{\tau}\left(\left(-\Delta_n\right)^{-1/2}\left(\varphi-\psi\right), \left(-\Delta_n\right)^{-1/2}\nu\right) + \varepsilon_\varphi^2\left(\nabla\left(\varphi-\psi\right),\nabla\nu\right) \\
&\quad + \left(\zeta_\mu\left(\varphi+m\right)-\zeta_\mu\left(\psi+m\right),\nu\right) + \alpha\theta\left(\left(-\Delta_n\right)^{-1/2}\left(\varphi-\psi\right), \left(-\Delta_n\right)^{-1/2}\nu\right) \\
&\leq \frac{1}{\tau}\left\|\varphi-\psi\right\|_{-1}\left\|\nu\right\|_{-1} + \varepsilon_\varphi^2\left\|\varphi-\psi\right\|_*\left\|\nu\right\|_* + \frac{1}{\mu}\left\|\varphi-\psi\right\|\left\|\nu\right\| + \alpha\theta\left\|\varphi-\psi\right\|_{-1}\left\|\nu\right\|_{-1} \\
&\leq \underbrace{\left(c_P^2\left(\frac{c_P^2}{\tau}+\frac{1}{\mu}+\alpha\theta c_P^2\right)+\varepsilon_\varphi^2\right)}_{C\left(c_P,\mu,\tau,\alpha,\theta,\varepsilon_\varphi^2\right)}\left\|\varphi-\psi\right\|_*\left\|\nu\right\|_* \leq C\left\|\varphi-\psi\right\|_*\left\|\nu\right\|_*,
\end{aligned} \tag{B.256}$$

where we have used (2.12) and (A.28b) again, along with (4.17), and the Cauchy–Schwarz, Poincaré and Young inequalities. Since $\varphi, \psi \in H^1_*(\Omega)$, $\varphi - \psi \in L^2_*(\Omega)$, which means that $(-\Delta_n)^{-1}(\varphi - \psi)$ is well-defined. Hence,

$$\begin{aligned}\|T(\varphi) - T(\psi)\|_{\left(H^1_*(\Omega)\right)'} &:= \sup_{\|\nu\|_*=1} \left|\langle T(\varphi) - T(\psi), \nu\rangle_{H^1_*(\Omega)}\right| \\ &\leq \sup_{\|\nu\|_*=1} C\|\varphi - \psi\|_* \|\nu\|_* = C\left(c_P, \mu, \tau, \alpha, \theta, \varepsilon_\varphi^2\right)\|\varphi - \psi\|_* \to 0 \quad \text{(B.257)}\end{aligned}$$

as $\|\varphi - \psi\|_* \to 0$.

vi) The mapping T in (B.255) is **strictly monotone**. Let $\varphi, \psi \in H^1_*(\Omega)$. Then

$$\begin{aligned}\langle T(\varphi) - T(\psi), \varphi - \psi\rangle_{H^1_*(\Omega)} &= \left(\frac{1}{\tau} + \alpha\theta\right)\|\varphi - \psi\|^2_{-1} \\ &\quad + \varepsilon_\varphi^2\|\varphi - \psi\|_*^2 + \underbrace{\langle \zeta_\mu(\varphi + m) - \zeta_\mu(\psi + m), \varphi + m - (\psi + m)\rangle}_{\geq 0 \text{ by (4.19)}}; \quad \text{(B.258)}\end{aligned}$$

from which we obtain

$$\langle T(\varphi) - T(\psi), \varphi - \psi\rangle_{H^1_*(\Omega)} \geq \varepsilon_\varphi^2\|\varphi - \psi\|_*^2 \geq 0, \quad \text{(B.259)}$$

if (5.13) holds. The inequality in (B.259) is strict whenever $\varphi \neq \psi$ which means that T is (conditionally) strictly monotone.

vii) The mapping T in (B.255) is **coercive**. We have established more than (conditional) strict monotonicity. In fact we have *strong* monotonicity (as in Definition 25.2 of Zeidler (1990)),[70] from which we obtain coercivity immediately: setting $\psi = 0$ in (B.259) gives

$$\langle T(\varphi), \varphi\rangle_{H^1_*(\Omega)} \geq \frac{\varepsilon_\varphi^2}{2}\|\varphi\|_*^2,$$

since $T(0)$ is the zero functional. Hence,

$$\frac{\langle T(\varphi), \varphi\rangle_{H^1_*(\Omega)}}{\|\varphi\|_*} \geq \frac{\varepsilon_\varphi^2}{2}\|\varphi\|_* \to \infty \qquad \text{as} \qquad \|\varphi\|_* \to \infty.$$

We conclude by the Browder–Minty theorem that problem $\left(\mathbf{Q}^{(*)}\right)$ in (5.15) has a solution in $H^1_*(\Omega)$ for $j = 1, \ldots, M$, and τ satisfying (5.13).

viii) Solutions are **unique**. Suppose, that the problem has two solutions φ_1 and φ_2, so that

$$\langle T(\varphi_1), \nu\rangle_{H^1_*(\Omega)} = \langle g(\psi), \nu\rangle_{H^1_*(\Omega)} \qquad \text{and} \qquad \langle T(\varphi_2), \nu\rangle_{H^1_*(\Omega)} = \langle g(\psi), \nu\rangle_{H^1_*(\Omega)}$$

for every $\nu \in H^1_*(\Omega)$ and some given $\psi \in H^1_*(\Omega)$. Subtracting these yields

$$\langle T(\varphi_1) - T(\varphi_2), \nu\rangle_{H^1_*(\Omega)} = 0$$

for every $\nu \in H^1_*(\Omega)$. Setting $\nu = \varphi_1 - \varphi_2 \in H^1_*(\Omega)$, leads to

$$\langle T(\varphi_1) - T(\varphi_2), \varphi_1 - \varphi_2\rangle_{H^1_*(\Omega)} = 0.$$

From the strict monotonicity above, $\varphi_1 = \varphi_2$ for any τ satisfying (5.13).

ix) Problems $\left(\mathbf{Q}^{(*)}\right)$ and $(\mathbf{Q}_{\tau,\theta})$ are equivalent in that, for a given $\varphi^{j-1} \in H^1_m(\Omega)$, if $\varphi^j \in H^1_m(\Omega)$ solves $(\mathbf{Q}_{\tau,\theta})$, then $\mathring{\varphi}^j := \varphi^j - m \in H^1_*(\Omega)$ solves $\left(\mathbf{Q}^{(*)}\right)$ (for $\mathring{\varphi}^{j-1} = \varphi^{j-1} - m$), and vice versa.

Given $\varphi^{j-1}, \varphi^j \in H^1_m(\Omega)$ solving $(\mathbf{Q}_{\tau,\theta})$, we define $\mathring{\varphi}^k := \varphi^k - m \in H^1_*(\Omega)$ (so that $\varphi^k = \mathring{\varphi}^k + m$) for $k = j-1, j$. Substituting into (5.8) yields

$$\begin{aligned}\left(\left(-\Delta_n\right)^{-1}\delta^{(\tau)}\mathring{\varphi}^j, \nu\right) + \varepsilon_\varphi^2\left(\nabla\mathring{\varphi}^j, \nabla\nu\right) - \frac{\chi^{AB}}{2}\left(\mathring{\varphi}^{j-1} + m, \nu\right) + \left(\zeta_\mu\left(\mathring{\varphi}^j + m\right), \nu\right) \\ + \alpha\theta\left(\left(-\Delta_n\right)^{-1}\mathring{\varphi}^j, \nu\right) + \alpha(1-\theta)\left(\left(-\Delta_n\right)^{-1}\mathring{\varphi}^{j-1}, \nu\right) = \left(\left(-\Delta_n\right)^{-1}\widetilde{f}^j, \nu\right), \quad \text{(B.260)}\end{aligned}$$

for every $\nu \in H^1(\Omega)$. But since $H^1_*(\Omega) \subset H^1(\Omega)$, this holds for every $\nu \in H^1_*(\Omega)$, too. Hence, $\mathring{\varphi}^j$ solves $\left(\mathbf{Q}^{(*)}\right)$.

Conversely, suppose we are given $\mathring{\varphi}^{j-1} \in H^1_*(\Omega)$. We showed above that there is a unique $\mathring{\varphi}^j \in H^1_*(\Omega)$ solving $\left(\mathbf{Q}^{(*)}\right)$. If we define $\varphi^k = \mathring{\varphi}^k + m \in H^1_m(\Omega)$ for $k = j, j+1$ then we can use (5.15) to conclude that

$$\begin{aligned}\left(\left(-\Delta_n\right)^{-1}\delta^{(\tau)}\left(\mathring{\varphi}^j + m\right), \nu\right) + \varepsilon_\varphi^2\left(\nabla\left(\mathring{\varphi}^j + m\right), \nabla\nu\right) - \frac{\chi^{AB}}{2}\left(\mathring{\varphi}^{j-1} + m, \nu\right) \\ + \frac{\chi^{AB}m}{2}\underbrace{(1, \nu)}_{=0} + \left(\zeta_\mu\left(\mathring{\varphi}^j + m\right), \nu\right) + \alpha\left(\left(-\Delta_n\right)^{-1}\left(\mathring{\varphi}^j + m - \overline{\mathring{\varphi}^j + m}\right)_{\{\theta\}}, \nu\right) \\ = \left(\left(-\Delta_n\right)^{-1}\widetilde{f}^j, \nu\right) \qquad \text{for every } \nu \in H^1_*(\Omega). \quad \text{(B.261)}\end{aligned}$$

That is, φ^j solves $(\mathbf{Q}_{\tau,\theta})$.

x) We showed above that solutions of $\left(\mathbf{Q}^{(*)}\right)$ are unique. The equivalence of $\left(\mathbf{Q}^{(*)}\right)$ and $(\mathbf{Q}_{\tau,\theta})$ means that solutions of $(\mathbf{Q}_{\tau,\theta})$ are also unique.

From the properties of $\left(\mathbf{Q}^{(*)}\right)$, we deduce that $(\mathbf{Q}_{\tau,\theta})$ has a unique solution in $H^1_m(\Omega)$ for $j = 1, \ldots, M$, and τ satisfying (5.13).

A proof of the existence and uniqueness of solutions of $(\mathbf{Q}_\tau)$ is similar to that above; the difference occurs in the establishment of monotonicity. Since $-\frac{\chi^{AB}}{2}\varphi$ is monotone *decreasing*, (B.258) is replaced with

$$\langle T(\varphi) - T(\psi), \varphi - \psi\rangle_{H^1_*(\Omega)} \geq \left(\frac{1}{\tau} + \alpha\theta\right)\|\varphi - \psi\|^2_{-1} \underbrace{-\frac{\chi^{AB}}{2}\|\varphi - \psi\|^2}_{\leq 0} + \varepsilon_\varphi^2\|\varphi - \psi\|^2_* \quad \text{(B.262)}$$

after using (4.19) again. The interpolation inequality (A.29), and Young's inequality give

$$\begin{aligned}\frac{\chi^{AB}}{2}\|\varphi - \psi\|^2 \leq \frac{\chi^{AB}}{2}\|\varphi - \psi\|_{-1}\|\varphi - \psi\|_* \leq \frac{\left(\chi^{AB}\right)^2}{8\varepsilon_\varphi^2}\|\varphi - \psi\|^2_{-1} + \frac{\varepsilon_\varphi^2}{2}\|\varphi - \psi\|^2_* \\ \Rightarrow \qquad -\frac{\chi^{AB}}{2}\|\varphi - \psi\|^2 \geq -\frac{\left(\chi^{AB}\right)^2}{8\varepsilon_\varphi^2}\|\varphi - \psi\|^2_{-1} - \frac{\varepsilon_\varphi^2}{2}\|\varphi - \psi\|^2_*.\end{aligned}$$

Substitution into (B.262) then yields that

$$\langle T(\varphi) - T(\psi), \varphi - \psi\rangle_{H^1_*(\Omega)} \geq \left(\frac{1}{\tau} - \frac{\left(\chi^{AB}\right)^2}{8\varepsilon_\varphi^2}\right)\|\varphi - \psi\|^2_{-1} + \frac{\varepsilon_\varphi^2}{2}\|\varphi - \psi\|^2_* \quad \text{(B.263)}$$

for $\theta \geq \frac{1}{2} > 0$. In turn, this final expression is guaranteed to be positive if

$$\tau \leq \frac{4\varepsilon_\varphi^2}{\left(\chi^{AB}\right)^2} \qquad \Rightarrow \qquad \frac{1}{\tau} - \frac{\left(\chi^{AB}\right)^2}{8\varepsilon_\varphi^2} \geq \frac{1}{2\tau} > 0; \quad \text{(B.264)}$$

i.e. $\tau \lesssim \varepsilon_\varphi^2$.

□

B.23 Proof of Lemma 5.1.3

Proof.

i) From Lemma 5.1.2 and an application of Lemma A.1.10 to the second term in (5.8), we infer the existence of $\varphi^j \in H^2_m(\Omega)$ with $\partial_n \varphi^j\big|_{\partial\Omega} = 0$ (in the sense of trace) satisfying

$$\left((-\Delta_n)^{-1}\delta^{(\tau)}\varphi^j, \nu\right) + \varepsilon_\varphi^2\left(-\Delta\varphi^j, \nu\right) - \frac{\chi^{AB}}{2}\left(\varphi^{j-1}, \nu\right) + \left(\zeta_\mu\left(\varphi^j\right), \nu\right) + \alpha\left((-\Delta_n)^{-1}\left(\varphi^j - \overline{\varphi^j}\right)_{\{\theta\}}, \nu\right) = \left((-\Delta_n)^{-1}\widetilde{f}^j, \nu\right),$$

for every $\nu \in L^2_*(\Omega)$ and each $j = 1, \ldots, M$,[71] and so (cf. (A.48)), a.e. in Ω

$$(-\Delta_n)^{-1}\left(\delta^{(\tau)}\varphi^j + \alpha\left(\varphi^j - \overline{\varphi^j}\right)_{\{\theta\}} - \widetilde{f}^j\right) = -\left(\varepsilon_\varphi^2(-\Delta)\varphi^j - \frac{\chi^{AB}}{2}\varphi^{j-1} + \zeta_\mu\left(\varphi^j\right)\right). \tag{B.265}$$

ii) According to the remarks immediately following Lemma 2.1.1, (B.265) is shorthand for,

$$\left(\delta^{(\tau)}\varphi^j + \alpha\left(\varphi^j - \overline{\varphi^j}\right)_{\{\theta\}} - \widetilde{f}^j, \nu\right) = -\left(\nabla\left(\varepsilon_\varphi^2(-\Delta)\varphi^j - \frac{\chi^{AB}}{2}\varphi^{j-1} + \zeta_\mu\left(\varphi^j\right)\right), \nabla\nu\right) = -\left(\nabla\omega^j, \nabla\nu\right) \tag{B.266}$$

for every $\nu \in H^1(\Omega)$ (notice the test space), after using (5.5d). However, by the assumptions we made above in respect of the smoothness of $\partial\Omega$, elliptic regularity theory immediately allows us to conclude that $\omega^j \in H^2(\Omega)$, $\partial_n\omega^j\big|_{\partial\Omega} = 0$ (in the sense of trace), and that $\left(\varphi^j, \omega^j\right)$ satisfies

$$\delta^{(\tau)}\varphi^j + \alpha\left(\varphi^j - \overline{\varphi^j}\right)_{\{\theta\}} - \widetilde{f}^j = \Delta\left(\varepsilon_\varphi^2(-\Delta)\varphi^j - \frac{\chi^{AB}}{2}\varphi^{j-1} + \zeta_\mu\left(\varphi^j\right)\right) = \Delta\omega^j \tag{B.267}$$

a.e. in Ω. This is a rearrangement of (5.5a) i.e. $\left(\varphi^j, \omega^j\right)$ solves $(\mathbf{P}_{\tau,\theta})$ for $j = 1, \ldots, M$.

iii) For mass conservation, we integrate (5.5a) over Ω and use Green's formula (cf. (1.2.5) of Ciarlet (1978) and Lemma 6.4 of Seregin (2013)) and the BCs above to conclude that,[72]

$$\overline{\varphi^j} = \overline{\varphi^{j-1}} = \ldots = \overline{\varphi_0} = m; \qquad j = 1, \ldots, M. \tag{B.268}$$

Remark. We may also infer the zero Neumann boundary condition on $-\Delta\varphi^j$ from that on φ^j, φ^{j-1} and ω^j.

□

B.24 Proof of Lemma 5.1.4

Proof.

i) The **existence of solutions** is trivial: we simply convert $(\mathbf{P}_{\tau,\theta})$ to weak form using the solution $\left(\varphi^j, \omega^j\right)$ we constructed in the previous lemma, together with the BCs those solution components were shown to have.

Remark. We reduced the regularity requirements on φ^j and ω^j in going from $(\mathbf{P}_{\tau,\theta})$ to $\left(\mathbf{R}^{(-)}_{\tau,\theta}\right)$. The implication is that we may use a conforming (in $H^1(\Omega)$) finite element approximation for the spatial part of the problem. We do this in Section 5.3.

ii) **Mass conservation**. If we set $\nu_1 = 1$ in (5.6) and rearrange,

$$\left(\varphi^j - \varphi^{j-1}, 1\right) + \tau\alpha\theta \underbrace{\left(\varphi^j - \overline{\varphi^j}, 1\right)}_{=0} = \tau \underbrace{\left(\widetilde{f}^j, 1\right)}_{=0 \text{ by (5.3)}} - \tau\alpha\left(1-\theta\right) \underbrace{\left(\varphi^{j-1} - \overline{\varphi^{j-1}}, 1\right)}_{=0} \tag{B.269}$$

which is equivalent to (B.268). Hence, $\left(\varphi^j - \varphi^{j-1}, 1\right) = 0$, viz. $\overline{\varphi^j} = \overline{\varphi^{j-1}}$ for *any* solution of $\left(\mathbf{R}_{\tau,\theta}^{(-)}\right)$, including those in the previous lemma.

□

B.25 Proof of Corollary 5.1.5

Proof.

i) In Lemma 5.1.3, we showed how, if $\partial\Omega$ is smooth enough, solutions of $(\mathbf{P}_{\tau,\theta})$ can be constructed from solutions of $(\mathbf{Q}_{\tau,\theta})$. In Lemma 5.1.2, we showed that $(\mathbf{Q}_{\tau,\theta})$ has a unique solution. In Lemma 5.1.4, we showed that solutions of $(\mathbf{P}_{\tau,\theta})$ are also solutions of $\left(\mathbf{R}_{\tau,\theta}^{(-)}\right)$.

ii) We now argue in reverse. If $\left(\varphi^j, \omega^j\right) \in \left(H^1\left(\Omega\right)\right)^2$ satisfies

$$\left(\delta^{(\tau)}\varphi^j, \nu_1\right) + \left(\nabla\omega^j, \nabla\nu_1\right) + \alpha\left(\left(\varphi^j - \overline{\varphi^j}\right)_{\{\theta\}}, \nu_1\right) = \left(\widetilde{f}^j, \nu_1\right),$$

for every $\nu_1 \in H^1\left(\Omega\right)$, and

$$\left(\omega^j, \nu_2\right) = \varepsilon_\varphi^2\left(\nabla\varphi^j, \nabla\nu_2\right) - \frac{\chi^{AB}}{2}\left(\varphi^{j-1}, \nu_2\right) + \left(\zeta_\mu\left(\varphi^j\right), \nu_2\right)$$

for every $\nu_2 \in H^1\left(\Omega\right)$, and $\partial\Omega$ is sufficiently smooth, then $\left(\varphi^j, \omega^j\right) \in \left(H^2\left(\Omega\right)\right)^2$, $\partial_n\varphi^j\big|_{\partial\Omega} = \partial_n\omega^j\big|_{\partial\Omega} = 0$ (in the sense of trace), and

$$\delta^{(\tau)}\varphi^j - \Delta\omega^j + \alpha\left(\varphi^j - \overline{\varphi^j}\right)_{\{\theta\}} = \widetilde{f}^j, \qquad \omega^j = \varepsilon_\varphi^2\left(-\Delta\right)\varphi^j - \frac{\chi^{AB}}{2}\varphi^{j-1} + \zeta_\mu\left(\varphi^j\right)$$

a.e. in Ω. But this is the same as saying that $\left(\varphi^j, \omega^j\right)$ solves $(\mathbf{P}_{\tau,\theta})$ (cf. (5.5d)–(5.5e)).

iii) Finally, we show that solutions of $(\mathbf{P}_{\tau,\theta})$ solve $(\mathbf{Q}_{\tau,\theta})$. Suppose that $\left(\varphi^j, \omega^j\right)$ satisfies

$$\delta^{(\tau)}\varphi^j - \Delta\left(\varepsilon_\varphi^2 - \Delta\varphi^j - \frac{\chi^{AB}}{2}\varphi^{j-1} + \zeta_\mu\left(\varphi^j\right)\right) + \alpha\left(\varphi^j - \overline{\varphi^j}\right)_{\{\theta\}} = \widetilde{f}^j, \tag{5.5a}$$

for $j = 1, \ldots, M$, and that $\partial_n\varphi^j\big|_{\partial\Omega} = \partial_n\left(-\Delta\right)\varphi^j\big|_{\partial\Omega} = 0$. It follows easily that

$$\partial_n\left(\varepsilon_\varphi^2 - \Delta\varphi^j - \frac{\chi^{AB}}{2}\varphi^{j-1} + \zeta_\mu\left(\varphi^j\right)\right)\Big|_{\partial\Omega} = 0$$

and that each term in (5.5a) is in $L_*^2\left(\Omega\right)$. Consequently, we may apply $\left(-\Delta_n\right)^{-1}$ to (5.5a), and find that

$$\left(-\Delta_n\right)^{-1}\delta^{(\tau)}\varphi^j + \varepsilon_\varphi^2 - \Delta\varphi^j - \frac{\chi^{AB}}{2}\varphi^{j-1} + \zeta_\mu\left(\varphi^j\right) + \alpha\left(-\Delta_n\right)^{-1}\left(\varphi^j - \overline{\varphi^j}\right)_{\{\theta\}} = \left(-\Delta_n\right)^{-1}\widetilde{f}^j.$$

Multiplying by any $\nu \in H_*^1\left(\Omega\right)$ and integrating over Ω leads to (5.8), after using the zero Neumann BC on each φ^j to note that $\left(-\Delta\varphi^j, \nu\right) = \left(\nabla\varphi^j, \nabla\nu\right)$. That is, we have found a solution of $(\mathbf{Q}_{\tau,\theta})$. The conditions for existence and uniqueness of solutions of $(\mathbf{Q}_{\tau,\theta})$ apply to $(\mathbf{P}_{\tau,\theta})$ and $\left(\mathbf{R}_{\tau,\theta}^{(-)}\right)$, too.

iv) The same argument works for the implicit scheme problem chain; the requirement that $\tau \lesssim \varepsilon_\varphi^2$ for uniqueness traces back to Lemma 5.1.2, and (B.264).

□

B.26 Proof of Lemma 5.1.6

We use ideas and the notation from Chapter 12 of Süli and Mayers (2006).

Proof.

i) We rewrite

$$\overline{\mathring{\varphi}^j} = \overline{\mathring{\varphi}^{j-1}} + \tau \underbrace{\left((1-\theta)\,\varpi\left(t_{j-1}, \overline{\mathring{\varphi}^{j-1}}\right) + \theta\varpi\left(t_j, \overline{\mathring{\varphi}^j}\right)\right)}_{:=\,\Phi\left(t_{j-1}, \overline{\mathring{\varphi}^{j-1}}; \tau\right)} = \overline{\mathring{\varphi}^{j-1}} + \tau\Phi\left(t_{j-1}, \overline{\mathring{\varphi}^{j-1}}; \tau\right), \tag{5.27}$$

where in turn

$$\Phi\left(t_{j-1}, \overline{\mathring{\varphi}^{j-1}}; \tau\right) = (1-\theta)\,\varpi\left(t_{j-1}, \overline{\mathring{\varphi}^{j-1}}\right) + \theta\varpi\left(t_j, \overline{\mathring{\varphi}^{j-1}} + \tau\Phi\left(t_{j-1}, \overline{\mathring{\varphi}^{j-1}}; \tau\right)\right). \tag{B.270}$$

Rearranging (5.27) leads to (5.22) and (5.23).

ii) We defined the global error in the approximation at $t_j = j\tau$ in (5.28). We define the truncation error

$$\begin{aligned} T_j &= \frac{\overline{\mathring{\varphi}}(t_j) - \overline{\mathring{\varphi}}(t_{j-1})}{\tau} - \Phi\left(t_{j-1}, \overline{\mathring{\varphi}}(t_{j-1}); \tau\right) \\ &= \frac{\overline{\mathring{\varphi}}(t_j) - \overline{\mathring{\varphi}}(t_{j-1})}{\tau} - \left((1-\theta)\,\varpi\left(t_{j-1}, \overline{\mathring{\varphi}}(t_{j-1})\right) + \theta\varpi\left(t_j, \overline{\mathring{\varphi}}(t_j)\right)\right) \\ &= \frac{\overline{\mathring{\varphi}}(t_j) - \overline{\mathring{\varphi}}(t_{j-1})}{\tau} - \left((1-\theta)\,\overline{\mathring{\varphi}}'(t_{j-1}) + \theta\overline{\mathring{\varphi}}'(t_j)\right), \end{aligned} \tag{B.271}$$

where we have used the definition of ϖ. Taylor's Theorem (Theorem 6.4.1 of Bartle and Sherbert (2011) or Theorem A.4 in Appendix A of Süli and Mayers (2006)) for the exact solution $\overline{\mathring{\varphi}}(t_j)$ about t_{j-1} says that

$$\overline{\mathring{\varphi}}(t_j) = \overline{\mathring{\varphi}}(t_{j-1}) + \tau\overline{\mathring{\varphi}}'(t_{j-1}) + \frac{\tau^2}{2}\overline{\mathring{\varphi}}''(t_{j-1}) + \frac{\tau^3}{6}\overline{\mathring{\varphi}}'''(t_{j-1}) + \mathcal{O}\left(\tau^4\right) \tag{B.272a}$$

and likewise

$$\overline{\mathring{\varphi}}'(t_j) = \overline{\mathring{\varphi}}'(t_{j-1}) + \tau\overline{\mathring{\varphi}}''(t_{j-1}) + \frac{\tau^2}{2}\overline{\mathring{\varphi}}'''(t_{j-1}) + \mathcal{O}\left(\tau^3\right). \tag{B.272b}$$

Substituting these into (B.271) we find that the $\overline{\mathring{\varphi}}'(t_{j-1})$ terms all cancel out, and we are left with

$$T_j = \left(\frac{1}{2} - \theta\right)\tau\overline{\mathring{\varphi}}''(t_{j-1}) + \frac{1}{2}\left(\frac{1}{3} - \theta\right)\tau^2\overline{\mathring{\varphi}}'''(t_{j-1}) + \mathcal{O}\left(\tau^3\right).$$

For $\overline{\mathring{\varphi}}$ sufficiently smooth, this implies that

$$|T_j| \leq C \begin{cases} \tau^2 & \theta = \frac{1}{2} \\ \tau & \text{otherwise} \end{cases} \tag{B.273}$$

with C independent of τ. The mass control approximation problem is second order accurate if $\theta = \frac{1}{2}$; otherwise, it is first order accurate.

iii) We wish to apply Theorem 12.2 of Süli and Mayers (2006) to bound the global error in terms of the truncation error T_j, above. To do so, we argue as in Section 12.4 of that reference, to estimate L_Φ, the Lipschitz constant of Φ in its second argument. We find that

$$\begin{aligned} |\Phi(t_{j-1}, u; \tau) - \Phi(t_{j-1}, v; \tau)| = \big|\,&(1-\theta)\,\varpi(t_{j-1}, u) + \theta\varpi(t_j, u + \tau\Phi(t_{j-1}, u; \tau)) \\ &- (1-\theta)\,\varpi(t_{j-1}, v) - \theta\varpi(t_j, v + \tau\Phi(t_{j-1}, v; \tau))\,\big| \end{aligned}$$

and so, after recalling that $\frac{1}{2} \leq \theta \leq 1$,

$$\begin{aligned}
|\Phi(t_{j-1}, u; \tau) - \Phi(t_{j-1}, v; \tau)| &\leq (1-\theta) |\varpi(t_{j-1}, u) - \varpi(t_{j-1}, v)| \\
&\quad + \theta |\varpi(t_j, u + \tau\Phi(t_{j-1}, u; \tau)) - \varpi(t_j, v + \tau\Phi(t_{j-1}, v; \tau))| \\
&\leq (1-\theta) L_\varpi |u - v| + \theta L_\varpi |u - v + \tau(\Phi(t_{j-1}, u; \tau) - \Phi(t_{j-1}, v; \tau))| \\
&\leq L_\varpi |u - v| + \theta L_\varpi \tau |\Phi(t_{j-1}, u; \tau) - \Phi(t_{j-1}, v; \tau)|
\end{aligned}$$

where L_ϖ is the Lipschitz constant of ϖ in its second argument. In our case, $L_\varpi = \alpha \geq 0$, and so

$$\frac{|\Phi(t_{j-1}, u; \tau) - \Phi(t_{j-1}, v; \tau)|}{|u - v|} \leq \frac{\alpha}{1 - \theta\tau\alpha} \qquad \text{viz.} \qquad L_\Phi \leq \frac{\alpha}{1 - \theta\tau\alpha} \qquad \Leftarrow \qquad \tau \leq \frac{1}{\theta\alpha}.$$

Hence for τ sufficiently small,

$$\max_{0 \leq j \leq M} |\overline{e}_j| \leq C \begin{cases} \tau^2 & \theta = \frac{1}{2} \\ \tau & \text{otherwise} \end{cases} \tag{B.274}$$

with C independent of τ. (5.29) follows immediately.

iv) We write the mass control approximation problem (5.27) as the linear 1-step method

$$\begin{gathered}
-\overline{\mathring{\varphi}^{j-1}} + \overline{\mathring{\varphi}^{j}} = \tau \left((1-\theta) \varpi \left(t_{j-1}, \overline{\mathring{\varphi}^{j-1}} \right) + \theta \varpi \left(t_j, \overline{\mathring{\varphi}^{j}} \right) \right); \\
\alpha_0 = -1, \quad \alpha_1 = 1, \quad \beta_0 = 1 - \theta, \quad \beta_1 = \theta.
\end{gathered}$$

The first and second characteristic polynomials are

$$1^{\text{st}} : \rho(z) = z - 1; \qquad\qquad 2^{\text{nd}} : \sigma(z) = \theta z + 1 - \theta. \tag{B.275}$$

- The only root of the first characteristic polynomial is $z = 1$ which lies on the unit circle, but is simple. The mass control approximation problem thus satisfies the Root Condition, and is therefore **zero-stable** (for any θ).
- Moreover, the method is **consistent** (for any θ), because if we write (B.270) as

$$\Phi(x, y; \tau) = (1-\theta) \varpi(x, y) + \theta \varpi(x + \tau, y + \tau\Phi(x, y; \tau)),$$

with $x = t_{j-1}$ and $y = \overline{\mathring{\varphi}^{j-1}}$, then (cf. (26) in Section 2.3 of Süli (2010))

$$\Phi(x, y; 0) = (1-\theta) \varpi(x, y) + \theta \varpi(x, y) = \varpi(x, y).$$

We wrote down the truncation error in (B.273). Having established consistency and zero-stability, we know that the global error $\overline{e}_j$ has the same asymptotic behaviour with respect to τ, by Dahlquist's Equivalence Theorem (Theorem 12.5 of Süli and Mayers (2006)). This reaffirms (B.274).

v) The stability polynomial of the method is

$$\pi(z; \lambda\tau) = \rho(z) - \lambda\tau\sigma(z) = z - 1 - \lambda\tau(\theta z + 1 - \theta), \tag{B.276}$$

with root

$$z_r(\lambda\tau) = \frac{1 + \lambda\tau(1-\theta)}{1 - \lambda\tau\theta}. \tag{B.277}$$

For the **region of absolute stability**, we find those $\lambda\tau$ for which (cf. (5.23) with $\alpha = -\lambda$)

$$|z_r(\lambda\tau)| < 1 \qquad \text{viz.} \qquad \left|\frac{1+\lambda\tau(1-\theta)}{1-\lambda\tau\theta}\right| < 1. \tag{B.278}$$

As in (5.24), the method is **A-stable** for any θ, λ, τ combination for which (cf. (5.24))

$$\theta > \frac{1}{2} + \frac{1}{\tau\lambda}. \tag{B.279}$$

In particular, if $\theta \geq \frac{1}{2}$, then $|z_r(\lambda\tau)| < 1$ for any $\lambda\tau$ for which $\tau > 0$ and $\mathrm{Re}(\lambda) < 0$.

□

B.27 Boundedness: proof of Lemma 5.1.7

Proof. To start, we present a proof for the implicit problem, $\left(\mathbf{R}_\tau^{(m)}\right)$. Our proof mimics that of Lemma 4.4.3.

i) We saw, in the material preceding Lemma 5.1.6, that if $\overline{\varphi_0} = m$, then $\overline{\varphi^j} = m$ for each $j = 1, \ldots, M$. Hence $\overline{\varphi^j - m} = 0$ for each j, and we may define (cf. (B.215b))

$$\psi^j := \omega^j + \alpha(-\Delta_n)^{-1}\left(\varphi^j - m\right) + \widetilde{F}^j, \qquad \widetilde{F}^j := (-\Delta_n)^{-1}\left(-\widetilde{f}^j\right) \in H^1_*(\Omega), \tag{B.280a}$$

and re-write (5.21a) as (cf. (B.215a))

$$\left(\delta^{(\tau)}\varphi^j, \nu_1\right) + \left(\nabla\psi^j, \nabla\nu_1\right) = 0 \tag{B.280b}$$

for every $\nu_1 \in H^1(\Omega)$. Likewise, we re-write (5.21b) as (cf. (B.215c))

$$\left(\psi^j, \nu_2\right) = \varepsilon_\varphi^2\left(\nabla\varphi^j, \nabla\nu_2\right) - \frac{\chi^{AB}}{2}\left(\varphi^j, \nu_2\right) + \left(\zeta_\mu\left(\varphi^j\right), \nu_2\right) + \alpha\left((-\Delta_n)^{-1}\left(\varphi^j - m\right), \nu_2\right) + \left(\widetilde{F}^j, \nu_2\right) \tag{B.280c}$$

for every $\nu_2 \in H^1(\Omega)$.

ii) Setting $\nu_1 = \psi^j$, then $\nu_1 = (-\Delta_n)^{-1}\left(\varphi^j - m\right)$ and finally $\nu_1 = \widetilde{F}^j$ in (B.280b) gives

$$\begin{aligned} \left(\delta^{(\tau)}\varphi^j, \psi^j\right) &= -\left|\psi^j\right|_1^2 \\ \left(\delta^{(\tau)}\varphi^j, (-\Delta_n)^{-1}\left(\varphi^j - m\right)\right) &= -\left(\psi^j, \varphi^j - m\right) \\ \left(\delta^{(\tau)}\varphi^j, \widetilde{F}^j\right) &= -\left(\nabla\psi^j, \nabla\widetilde{F}^j\right), \end{aligned} \tag{B.281}$$

where we used (2.9) to get the second result. Setting $\nu_2 = \delta^{(\tau)}\varphi^j$ in (B.280c), and writing

$$\varphi^j = \frac{\varphi^j - \varphi^{j-1}}{2} + \frac{\varphi^j + \varphi^{j-1}}{2} \tag{B.282}$$

in the first inner product on the right yields

$$\frac{\varepsilon_\varphi^2}{2\tau}\left(\left|\varphi^j\right|_1^2 - \left|\varphi^{j-1}\right|_1^2\right) + \frac{\varepsilon_\varphi^2}{2\tau}\left|\varphi^j - \varphi^{j-1}\right|_1^2 + \frac{1}{\tau}\left(\mathcal{B}'_\mu\left(\varphi^j\right), \varphi^j - \varphi^{j-1}\right) + \alpha\left((-\Delta_n)^{-1}\left(\varphi^j - m\right), \delta^{(\tau)}\varphi^j\right) + \left(\widetilde{F}^j, \delta^{(\tau)}\varphi^j\right) = \left(\psi^j, \delta^{(\tau)}\varphi^j\right). \tag{B.283}$$

Substituting (B.281) into (B.283) leads to (cf. (B.218))

$$\frac{\varepsilon_\varphi^2}{2\tau}\left(\left|\varphi^j\right|_1^2 - \left|\varphi^{j-1}\right|_1^2\right) + \frac{\varepsilon_\varphi^2}{2\tau}\left|\varphi^j - \varphi^{j-1}\right|_1^2 + \frac{1}{\tau}\left(\mathcal{B}'_\mu\left(\varphi^j\right), \varphi^j - \varphi^{j-1}\right) + \left|\psi^j\right|_1^2 = \left(\nabla\psi^j, \nabla\widetilde{F}^j\right) + \alpha\left(\varphi^j - m, \psi^j\right). \tag{B.284}$$

iii) Consider the third term on the left of (B.284). From (4.7) and (4.14a), we recall that $\mathcal{B}'_\mu(r)$ is continuous i.e. $\mathcal{B}_\mu$ is $C^1(\mathbb{R})$ having a continuous first derivative, and piecewise constant (discontinuous) second derivative. By Taylor's Theorem,

$$\mathcal{B}'_\mu(a)(a-b) = \mathcal{B}_\mu(a) - \mathcal{B}_\mu(b) + \frac{1}{2}\mathcal{B}''_\mu(\eta)(b-a)^2 \qquad \text{for some} \qquad \eta \in [a,b]. \tag{B.285}$$

According to (4.14a) $\mathcal{B}''_\mu(r) \geq -\frac{\chi^{AB}}{2}$ (with $\mathcal{B}''_\mu(r) = -\frac{\chi^{AB}}{2} < 0$ for $|r| \leq 1$), and so

$$\mathcal{B}_\mu(a) - \mathcal{B}_\mu(b) - \frac{\chi^{AB}}{4}(b-a)^2 \leq \mathcal{B}'_\mu(a)(a-b) \qquad \text{for any} \qquad a,b \in \mathbb{R}. \tag{B.286}$$

Consequently, if we set $a = \varphi^j$ and $b = \varphi^{j-1}$ in (B.286), we see that

$$\left(\mathcal{B}_\mu\left(\varphi^j\right),1\right) - \left(\mathcal{B}_\mu\left(\varphi^{j-1}\right),1\right) - \frac{\chi^{AB}}{4}\left\|\varphi^j - \varphi^{j-1}\right\|^2 \leq \left(\mathcal{B}'_\mu\left(\varphi^j\right), \varphi^j - \varphi^{j-1}\right). \tag{B.287}$$

Substituting this into (B.284) leads to

$$\begin{aligned}\frac{\varepsilon_\varphi^2}{2\tau}\left(\left|\varphi^j\right|_1^2 - \left|\varphi^{j-1}\right|_1^2\right) + \frac{\varepsilon_\varphi^2}{2\tau}\left|\varphi^j - \varphi^{j-1}\right|_1^2 + \frac{1}{\tau}\left(\left(\mathcal{B}_\mu\left(\varphi^j\right),1\right) - \left(\mathcal{B}_\mu\left(\varphi^{j-1}\right),1\right)\right) \\ + \left|\psi^j\right|_1^2 \leq \left(\nabla\psi^j, \nabla\widetilde{F}^j\right) + \alpha\left(\varphi^j - m, \psi^j\right) + \frac{\chi^{AB}}{4\tau}\left\|\varphi^j - \varphi^{j-1}\right\|^2.\end{aligned} \tag{B.288}$$

iv) Now consider the first two terms on the right of (B.288). In the first, as in (B.221),

$$\left(\nabla\psi^j, \nabla\widetilde{F}^j\right) \leq 2\left\|\widetilde{f}^j\right\|_{-1}^2 + \frac{1}{8}\left|\psi^j\right|_1^2; \tag{B.289a}$$

for the second, as in (B.220),

$$\alpha\left(\varphi^j - m, \psi^j\right) \leq \frac{\alpha^2 c_P^4}{2}\left|\varphi^j\right|_1^2 + \frac{1}{2}\left|\psi^j\right|_1^2. \tag{B.289b}$$

Combining these with (B.288) yields

$$\begin{aligned}\frac{\varepsilon_\varphi^2}{2\tau}\left(\left|\varphi^j\right|_1^2 - \left|\varphi^{j-1}\right|_1^2\right) + \frac{\varepsilon_\varphi^2}{2\tau}\left|\varphi^j - \varphi^{j-1}\right|_1^2 + \frac{1}{\tau}\left(\left(\mathcal{B}_\mu\left(\varphi^j\right),1\right) - \left(\mathcal{B}_\mu\left(\varphi^{j-1}\right),1\right)\right) \\ + \frac{3}{8}\left|\psi^j\right|_1^2 \leq 2\left\|\widetilde{f}^j\right\|_{-1}^2 + \frac{\alpha^2 c_P^4}{2}\left|\varphi^j\right|_1^2 + \frac{\chi^{AB}}{4\tau}\left\|\varphi^j - \varphi^{j-1}\right\|^2.\end{aligned} \tag{B.290}$$

v) To deal with the $\left\|\varphi^j - \varphi^{j-1}\right\|^2$ term on the right of (B.290), we set $\nu_1 = \frac{1}{4}\chi^{AB}\left(\varphi^j - \varphi^{j-1}\right)$ in (B.280b), and find that

$$\begin{aligned}\frac{\chi^{AB}}{4\tau}\left\|\varphi^j - \varphi^{j-1}\right\|^2 = -\frac{\chi^{AB}}{4}\left(\nabla\psi^j, \nabla\varphi^j - \varphi^{j-1}\right) \leq \frac{\chi^{AB}}{4}\left|\psi^j\right|_1\left|\varphi^j - \varphi^{j-1}\right|_1 \\ \leq \frac{1}{8}\left|\psi^j\right|_1^2 + \frac{\left(\chi^{AB}\right)^2}{8}\left|\varphi^j - \varphi^{j-1}\right|_1^2,\end{aligned} \tag{B.291}$$

by the Cauchy–Schwarz and Young's inequalities. Using this in (B.290) leads to

$$\begin{aligned}\frac{\varepsilon_\varphi^2}{2\tau}\left(\left|\varphi^j\right|_1^2 - \left|\varphi^{j-1}\right|_1^2\right) + \left(\frac{\varepsilon_\varphi^2}{2\tau} - \frac{\left(\chi^{AB}\right)^2}{8}\right)\left|\varphi^j - \varphi^{j-1}\right|_1^2 \\ + \frac{1}{\tau}\left(\left(\mathcal{B}_\mu\left(\varphi^j\right),1\right) - \left(\mathcal{B}_\mu\left(\varphi^{j-1}\right),1\right)\right) + \frac{1}{4}\left|\psi^j\right|_1^2 \leq 2\left\|\widetilde{f}^j\right\|_{-1}^2 + \frac{\alpha^2 c_P^4}{2}\left|\varphi^j\right|_1^2.\end{aligned}$$

If we now assume that

$$\tau < \tau_1 := \frac{4\varepsilon_\varphi^2}{\left(\chi^{AB}\right)^2} \qquad \Rightarrow \qquad \frac{\varepsilon_\varphi^2}{2\tau} - \frac{\left(\chi^{AB}\right)^2}{8} > 0, \tag{B.292}$$

then the second term above is non-negative and may be discarded, yielding (cf. (B.222))

$$\varepsilon_\varphi^2 \left(\left|\varphi^j\right|_1^2 - \left|\varphi^{j-1}\right|_1^2 \right) + 2\left(\left(\mathcal{B}_\mu\left(\varphi^j\right), 1\right) - \left(\mathcal{B}_\mu\left(\varphi^{j-1}\right), 1\right) \right) + \frac{\tau}{2}\left|\psi^j\right|_1^2 \leq 4\tau \left\|\widetilde{f}^j\right\|_{-1}^2 + \alpha^2 c_P^4 \tau \left|\varphi^j\right|_1^2. \tag{B.293}$$

Summing this through $j = 1, \ldots, k$, $(k \leq M)$, using the telescoping sums gives

$$\left(\varepsilon_\varphi^2 - \alpha^2 c_P^4 \tau\right)\left|\varphi^k\right|_1^2 + \frac{1}{2}\sum_{j=1}^{k} \tau \left|\psi^j\right|_1^2 \leq \varepsilon_\varphi^2 \left|\varphi_0\right|_1^2 + 2C_0\mu_{\max}\left|\Omega\right| + \frac{\chi^{AB}}{2}\left(\left|\Omega\right| + \left\|\varphi_0\right\|^2\right) + 4\sum_{j=1}^{k}\tau\left\|\widetilde{f}^j\right\|_{-1}^2 + \frac{2\alpha^2 c_P^4}{\varepsilon_\varphi^2}\sum_{j=1}^{k-1}\tau\frac{\varepsilon_\varphi^2}{2}\left|\varphi^j\right|_1^2, \tag{B.294}$$

after moving the last term in the sum on the right over to the left and using (B.223). If we now assume that (cf. (B.292))

$$\tau < \min\left\{\tau_1, \tau_2\right\} \qquad \text{where} \qquad \tau_2 := \frac{\varepsilon_\varphi^2}{2\alpha^2 c_P^4} \qquad \Rightarrow \qquad \frac{\varepsilon_\varphi^2}{2} < \varepsilon_\varphi^2 - \alpha^2 c_P^4 \tau, \tag{B.295}$$

then,

$$\frac{\varepsilon_\varphi^2}{2}\left|\varphi^k\right|_1^2 + \frac{1}{2}\sum_{j=1}^{k} \tau \left|\psi^j\right|_1^2 \leq \varepsilon_\varphi^2 \left|\varphi_0\right|_1^2 + 2C_0\mu_{\max}\left|\Omega\right| + \frac{\chi^{AB}}{2}\left(\left|\Omega\right| + \left\|\varphi_0\right\|^2\right) + 4\sum_{j=1}^{k}\tau\left\|\widetilde{f}^j\right\|_{-1}^2 + \frac{2\alpha^2 c_P^4}{\varepsilon_\varphi^2}\sum_{j=1}^{k-1}\tau\frac{\varepsilon_\varphi^2}{2}\left|\varphi^j\right|_1^2. \tag{B.296}$$

The discrete Gronwall inequality (Lemma A.1.14) implies that (cf. (B.224))

$$\frac{\varepsilon_\varphi^2}{2}\left|\varphi^k\right|_1^2 + \frac{1}{2}\sum_{j=1}^{k} \tau \left|\psi^j\right|_1^2 \leq C_1 \exp\left\{\frac{2\alpha^2 c_P^4}{\varepsilon_\varphi^2} k\tau\right\} \leq C_1 \exp\left\{\frac{2\alpha^2 c_P^4}{\varepsilon_\varphi^2} T\right\} \tag{B.297a}$$

since $k\tau \leq T$ for $k = 1, \ldots, M$, where

$$C_1 := \varepsilon_\varphi^2 \left|\varphi_0\right|_1^2 + 2C_0\mu_{\max}\left|\Omega\right| + \frac{\chi^{AB}}{2}\left(\left|\Omega\right| + \left\|\varphi_0\right\|^2\right) + 4\sum_{j=1}^{k}\tau\left\|\widetilde{f}^j\right\|_{-1}^2 < \infty \tag{B.297b}$$

is independent of k, τ and μ.

vi) We conclude from (B.297) that (cf. (B.225)) each $\left|\varphi^j\right|_1 \leq C$ for $j = 1, \ldots, M$, independent of τ and μ. Moreover, by Poincaré's inequality

$$\left\|\varphi^j\right\| = \left\|\varphi^j - m + m\right\| \leq \left\|\varphi^j - m\right\| + \left|m\right|\left|\Omega\right|^{1/2} \leq c_P\left|\varphi^j\right|_1 + \left|m\right|\left|\Omega\right|^{1/2} = C$$

for each j, independent of τ and μ. Combining these, we discover that,

$$\left\|\varphi^j\right\|_1 \leq C \qquad \text{independent of } j,\ \tau \text{ and } \mu \qquad \Rightarrow \qquad \max_{0\leq j\leq M}\left\|\varphi^j\right\|_1 \leq C,$$

independent of τ and μ, which is (5.30a).

vii) Another consequence of (B.297) is the fact that, independent of k, τ and μ,

$$\sum_{j=1}^{k} \tau \left|\psi^j\right|_1^2 \leq C \qquad \Rightarrow \qquad \sum_{j=1}^{M} \tau \left|\psi^j\right|_1^2 \leq C \tag{B.298}$$

independent of τ and μ. Setting $\nu_1 = (-\Delta_n)^{-1}\left(\delta^{(\tau)}\varphi^j\right)$ and then $\nu_1 = \psi^j$ in (B.280b) yields (cf. (B.227))

$$\left\|\delta^{(\tau)}\varphi^j\right\|_{-1}^2 = -\left(\psi^j, \delta^{(\tau)}\varphi^j\right); \qquad \left(\delta^{(\tau)}\varphi^j, \psi^j\right) = -\left|\psi^j\right|_1^2 \qquad \Rightarrow \qquad \left\|\delta^{(\tau)}\varphi^j\right\|_{-1}^2 = \left|\psi^j\right|_1^2$$

for each $j = 1, \ldots, M$. Using this in (B.298), we find that (cf. (B.228))

$$\sum_{j=1}^{M} \tau \left\|\delta^{(\tau)}\varphi^j\right\|_{-1}^2 \leq C \tag{B.299}$$

independent of τ and μ.

viii) We will show that

$$\sum_{j=1}^{M} \left\|\varphi^j - \varphi^{j-1}\right\|_1^2 \leq C$$

for the third term on the left of (5.30b), in the last part of the proof of energy decay. See the build-up to (B.353) in the proof of Lemma 5.1.9, starting on p. 419.

ix) Our assumptions about the smoothness of $\partial\Omega$ imply that we can re-write (B.280c) as

$$\left(\psi^j, \nu_2\right) = \varepsilon_\varphi^2\left(-\Delta\varphi^j, \nu_2\right) - \frac{\chi^{AB}}{2}\left(\varphi^j, \nu_2\right) + \left(\zeta_\mu\left(\varphi^j\right), \nu_2\right) + \alpha\left((-\Delta_n)^{-1}\left(\varphi^j - m\right), \nu_2\right) + \left(\widetilde{F}^j, \nu_2\right) \tag{B.300a}$$

for every $\nu_2 \in L^2(\Omega)$ i.e.

$$\psi^j = \varepsilon_\varphi^2(-\Delta)\varphi^j - \frac{\chi^{AB}}{2}\varphi^j + \zeta_\mu\left(\varphi^j\right) + \alpha(-\Delta_n)^{-1}\left(\varphi^j - m\right) + \widetilde{F}^j \tag{B.300b}$$

a.e. with $\varphi^j \in H^2(\Omega)$ and $\partial_n\varphi^j\big|_{\partial\Omega} = 0$, for each $j = 1, \ldots, M$. Suppose, in addition, that (4.63) and (4.55) hold. Then we can *define*

$$H^1(\Omega) \ni \psi_0 = \varepsilon_\varphi^2(-\Delta)\varphi_0 - \frac{\chi^{AB}}{2}\varphi_0 + \alpha(-\Delta_n)^{-1}(\varphi_0 - m) + \widetilde{F}_0, \tag{B.300c}$$

after recalling that $\varphi_0 \in \mathscr{A}$ viz. $\zeta_\mu(\varphi_0) \equiv 0$. Moreover, as in (B.280a) $\widetilde{F}_0 \in H_*^1(\Omega)$.

x) We now write (B.280c) at t_j and t_{j-1}, subtract the second from the first and divide through by τ (in effect, discretely differentiating in time), and obtain

$$\left(\delta^{(\tau)}\psi^j, \nu_2\right) = \varepsilon_\varphi^2\left(\nabla\delta^{(\tau)}\varphi^j, \nabla\nu_2\right) - \frac{\chi^{AB}}{2}\left(\delta^{(\tau)}\varphi^j, \nu_2\right) + \frac{1}{\tau}\left(\zeta_\mu\left(\varphi^j\right) - \zeta_\mu\left(\varphi^{j-1}\right), \nu_2\right) + \alpha\left((-\Delta_n)^{-1}\left(\delta^{(\tau)}\varphi^j\right), \nu_2\right) + \left(\delta^{(\tau)}\widetilde{F}^j, \nu_2\right). \tag{B.301}$$

Setting $\nu_2 = \delta^{(\tau)}\varphi^j$ in the above, leads to (cf. (B.233))

$$\left(\delta^{(\tau)}\psi^j, \delta^{(\tau)}\varphi^j\right) = \varepsilon_\varphi^2\left|\delta^{(\tau)}\varphi^j\right|_1^2 - \frac{\chi^{AB}}{2}\left\|\delta^{(\tau)}\varphi^j\right\|^2 + \underbrace{\frac{1}{\tau^2}\left(\zeta_\mu\left(\varphi^j\right) - \zeta_\mu\left(\varphi^{j-1}\right), \varphi^j - \varphi^{j-1}\right)}_{\geq 0 \text{ by (4.19a)}} + \underbrace{\alpha\left\|\delta^{(\tau)}\varphi^j\right\|_{-1}^2}_{\geq 0} + \left(\delta^{(\tau)}\widetilde{F}^j, \delta^{(\tau)}\varphi^j\right),$$

or

$$\varepsilon_\varphi^2 \left|\delta^{(\tau)}\varphi^j\right|_1^2 - \frac{\chi^{AB}}{2}\left\|\delta^{(\tau)}\varphi^j\right\|^2 + \left(\delta^{(\tau)}\widetilde{F}^j, \delta^{(\tau)}\varphi^j\right) \leq \left(\delta^{(\tau)}\psi^j, \delta^{(\tau)}\varphi^j\right). \tag{B.302}$$

Setting $\nu_1 = \delta^{(\tau)}\psi^j$ and (cf. (B.282))

$$\psi^j = \frac{\psi^j - \psi^{j-1}}{2} + \frac{\psi^j + \psi^{j-1}}{2} \tag{B.303}$$

in (B.280b), we find that

$$\left(\delta^{(\tau)}\varphi^j, \delta^{(\tau)}\psi^j\right) = -\frac{1}{2\tau}\left(\left|\psi^j - \psi^{j-1}\right|_1^2 + \left|\psi^j\right|_1^2 - \left|\psi^{j-1}\right|_1^2\right), \tag{B.304}$$

and so from (B.302), we determine that (cf. (B.234))

$$\begin{aligned}\frac{1}{2\tau}\left(\left|\psi^j\right|_1^2 - \left|\psi^{j-1}\right|_1^2\right) + \varepsilon_\varphi^2\left|\delta^{(\tau)}\varphi^j\right|_1^2 &\leq \frac{\chi^{AB}}{2}\left\|\delta^{(\tau)}\varphi^j\right\|^2 - \left(\delta^{(\tau)}\widetilde{F}^j, \delta^{(\tau)}\varphi^j\right) \\ &\leq \frac{\varepsilon_\varphi^2}{2}\left|\delta^{(\tau)}\varphi^j\right|_1^2 + \left(\frac{\chi^{AB}}{2} + \frac{1}{2}\right)^2 \frac{1}{2\varepsilon_\varphi^2}\left\|\delta^{(\tau)}\varphi^j\right\|_{-1}^2 + \frac{1}{2}\left\|\delta^{(\tau)}\widetilde{F}^j\right\|^2\end{aligned} \tag{B.305}$$

by the Cauchy–Schwarz inequality and (A.29), and after discarding

$$\frac{1}{2\tau}\left|\psi^j - \psi^{j-1}\right|_1^2 \geq 0$$

on the left. Hence,

$$\left|\psi^j\right|_1^2 - \left|\psi^{j-1}\right|_1^2 + \varepsilon_\varphi^2\tau\left|\delta^{(\tau)}\varphi^j\right|_1^2 \leq \left(\frac{\chi^{AB}}{2} + \frac{1}{2}\right)^2 \frac{\tau}{\varepsilon_\varphi^2}\left\|\delta^{(\tau)}\varphi^j\right\|_{-1}^2 + \tau\left\|\delta^{(\tau)}\widetilde{F}^j\right\|^2.$$

Summing this through $j = 1, \ldots, k$ ($k \leq M$) gives (cf. (B.235))

$$\left|\psi^k\right|_1^2 + \varepsilon_\varphi^2\sum_{j=1}^k \tau\left|\delta^{(\tau)}\varphi^j\right|_1^2 \leq |\psi_0|_1^2 + C\left(\chi^{AB}, \varepsilon_\varphi\right)\sum_{j=1}^M \tau\left\|\delta^{(\tau)}\varphi^j\right\|_{-1}^2 + \sum_{j=1}^M \tau\left\|\delta^{(\tau)}\widetilde{F}^j\right\|^2. \tag{B.306}$$

We now bound each of the three terms on the right, independent of k, τ and μ.

- For the first, we use (B.300c) and argue as in (B.236).
- For the second, we appeal to (B.299).
- For the third, we wish to say something like

$$\widetilde{F}^j - \widetilde{F}^{j-1} = \int_{t_{j-1}}^{t_j} \partial_t \widetilde{F}\ \mathrm{d}t,$$

but note that $\widetilde{F}$ is only defined at discrete points in time according to (5.4) and (B.280a), that is

$$\widetilde{F}^j := -\left(-\Delta_n\right)^{-1}\begin{cases}\sum_i a_i f\left(t_i\right) & j \geq 1 \\ f\left(0\right) & j = 0\end{cases} = \begin{cases}\sum_i a_i F\left(t_i\right) & j \geq 1 \\ F\left(0\right) & j = 0\end{cases}$$

with F as in (B.215b). We can, however, define a continuously differentiable (in time) version of $\widetilde{F}$ for $t \in (t_{j-1}, t_j]$, as

$$C^1\left([0,T]; H_*^1\left(\Omega\right)\right) \ni \widetilde{F}_\tau\left(t\right) := \sum_i a_i F\underbrace{\left(t_i - \left(t_j - t\right)\right)}_{:=\,\widetilde{t}_i} \quad \text{with} \quad a_i = 0 \quad \text{if} \quad \widetilde{t}_i < 0 \quad (\text{for } j = 1). \tag{B.307}$$

For this function $\widetilde{F}^j - \widetilde{F}^{j-1} = \int_{t_{j-1}}^{t_j} \partial_t \widetilde{F}_\tau\,(t)\ \mathrm{d}t$, and so

$$\left\|\delta^{(\tau)}\widetilde{F}^j\right\|^2 = \left\|\frac{1}{\tau}\int_{t_{j-1}}^{t_j} 1\cdot\partial_t\widetilde{F}_\tau\ \mathrm{d}t\right\|^2 \le \left\|\frac{1}{\tau}\left(\int_{t_{j-1}}^{t_j} 1^2\ \mathrm{d}t\right)^{1/2}\left(\int_{t_{j-1}}^{t_j}\left|\partial_t\widetilde{F}_\tau\right|^2\mathrm{d}t\right)^{1/2}\right\|^2$$
$$= \frac{1}{\tau}\left\|\left(\int_{t_{j-1}}^{t_j}\left|\partial_t\widetilde{F}_\tau\right|^2\mathrm{d}t\right)^{1/2}\right\|^2 = \frac{1}{\tau}\int_{t_{j-1}}^{t_j}\left\|\partial_t\widetilde{F}_\tau\right\|^2\mathrm{d}t, \quad \text{(B.308)}$$

where we used the Cauchy–Schwarz inequality and then interchanged the sequence of the spatial and temporal integration. Consequently,

$$\sum_{j=1}^{M}\tau\left\|\delta^{(\tau)}\widetilde{F}^j\right\|^2 \le \sum_{j=1}^{M}\int_{t_{j-1}}^{t_j}\left\|\partial_t\widetilde{F}_\tau\right\|^2\mathrm{d}t = \int_0^T\left\|\partial_t\widetilde{F}_\tau\right\|^2\mathrm{d}t = C\left(\widetilde{f},T\right) < \infty, \quad \text{(B.309)}$$

independent of τ and μ.

Hence (cf. (B.237)), for $k = 1,\ldots,M$,

$$\left|\psi^k\right|_1^2 + \varepsilon_\varphi^2\sum_{j=1}^{k}\tau\left|\delta^{(\tau)}\varphi^j\right|_1^2 \le C \qquad \text{independent of } k,\ \tau \text{ and } \mu. \quad \text{(B.310)}$$

We conclude that (cf. (B.238))

$$\max_{0\le j\le M}\left|\psi^j\right|_1 < C \quad \text{(B.311)}$$

independent of τ and μ.

xi) Finally, we set $\nu_2 = -\Delta\varphi^j \in L^2(\Omega)$ for each $j = 1,\ldots,M$ in (B.300a) and use the zero Neumann BC on each φ^j to certify that, as in (B.239),[73]

$$\varepsilon_\varphi^2\left\|-\Delta\varphi^j\right\|^2 \le \frac{1}{2}\left|\psi^j\right|_1^2 + \left(\frac{\chi^{AB}}{2}+1\right)\left|\varphi^j\right|_1^2 + \frac{1}{2}\left\|\widetilde{f}^j\right\|_{-1}^2 \le C < \infty, \quad \text{(B.312)}$$

independent of j, τ and μ, by (5.30a) and (B.311). In combination with our assumptions on φ_0, the implication is that

$$\max_{0\le j\le M}\left\|-\Delta\varphi^j\right\| \le C$$

independent of τ and μ. Our smoothness assumptions on $\partial\Omega$ and (A.43) imply that

$$\max_{0\le j\le M}\left\|\varphi^j\right\|_2 \le C$$

independent of τ and μ for each $j = 0,\ldots,M$, which is (5.31).

We now adapt the proof above for $\left(\mathbf{R}_{\tau,\theta}^{(m)}\right)$.

i) We replace (B.280c) with (cf. (5.57d))

$$\left(\psi^j,\nu_2\right)=\varepsilon_\varphi^2\left(\nabla\varphi^j,\nabla\nu_2\right)+\left(\mathcal{B}'_\mu\left(\varphi^j\right),\nu_2\right)$$
$$+\alpha\left(\left(-\Delta_n\right)^{-1}\left(\varphi^j-m\right)_{\{\theta\}},\nu_2\right)+\left(\widetilde{F}^j,\nu_2\right)+\frac{\chi^{AB}}{2}\left(\varphi^j-\varphi^{j-1},\nu_2\right) \quad \text{(B.313)}$$

for every $\nu_2\in H^1(\Omega)$. Setting $\nu_2=\delta^{(\tau)}\varphi^j$ and using (B.282) yields (cf. (B.283))

$$\left(\psi^j,\delta^{(\tau)}\varphi^j\right)=\frac{\varepsilon_\varphi^2}{2\tau}\left(\left|\varphi^j\right|_1^2-\left|\varphi^{j-1}\right|_1^2\right)+\frac{\varepsilon_\varphi^2}{2\tau}\left|\varphi^j-\varphi^{j-1}\right|_1^2+\left(\mathcal{B}'_\mu\left(\varphi^j\right),\delta^{(\tau)}\varphi^j\right)$$
$$+\alpha\left(\left(-\Delta_n\right)^{-1}\left(\varphi^j-m\right)_{\{\theta\}},\delta^{(\tau)}\varphi^j\right)+\left(\widetilde{F}^j,\delta^{(\tau)}\varphi^j\right)+\frac{\chi^{AB}}{2\tau}\left\|\varphi^j-\varphi^{j-1}\right\|^2. \quad \text{(B.314)}$$

We now set $\nu_1=\left(-\Delta_n\right)^{-1}\left(\varphi^j-m\right)_{\{\theta\}}$ in (B.280b) to obtain (cf. (B.281))

$$\left(\delta^{(\tau)}\varphi^j,\left(-\Delta_n\right)^{-1}\left(\varphi^j-m\right)_{\{\theta\}}\right)=-\left(\psi^j,\left(\varphi^j-m\right)_{\{\theta\}}\right); \quad \text{(B.315)}$$

combining this with the other parts of (B.281) in (B.314) yields (cf. (B.284))

$$\frac{\varepsilon_\varphi^2}{2\tau}\left(\left|\varphi^j\right|_1^2-\left|\varphi^{j-1}\right|_1^2\right)+\frac{\varepsilon_\varphi^2}{2\tau}\left|\varphi^j-\varphi^{j-1}\right|_1^2+\frac{1}{\tau}\left(\mathcal{B}'_\mu\left(\varphi^j\right),\varphi^j-\varphi^{j-1}\right)+\left|\psi^j\right|_1^2$$
$$+\frac{\chi^{AB}}{2\tau}\left\|\varphi^j-\varphi^{j-1}\right\|^2=\left(\nabla\psi^j,\nabla\widetilde{F}^j\right)+\alpha\left(\left(\varphi^j-m\right)_{\{\theta\}},\psi^j\right). \quad \text{(B.316)}$$

ii) If we substitute (B.287) into (B.316), we find that (cf. (B.288))

$$\frac{\varepsilon_\varphi^2}{2\tau}\left(\left|\varphi^j\right|_1^2-\left|\varphi^{j-1}\right|_1^2\right)+\frac{\varepsilon_\varphi^2}{2\tau}\left|\varphi^j-\varphi^{j-1}\right|_1^2+\frac{1}{\tau}\left(\left(\mathcal{B}_\mu\left(\varphi^j\right),1\right)-\left(\mathcal{B}_\mu\left(\varphi^{j-1}\right),1\right)\right)$$
$$+\left|\psi^j\right|_1^2+\frac{\chi^{AB}}{4\tau}\left\|\varphi^j-\varphi^{j-1}\right\|^2\leq\left(\nabla\psi^j,\nabla\widetilde{F}^j\right)+\alpha\left(\left(\varphi^j-m\right)_{\{\theta\}},\psi^j\right). \quad \text{(B.317)}$$

Remark. In (B.317) above, we have $\frac{\chi^{AB}}{4\tau}\left\|\varphi^j-\varphi^{j-1}\right\|^2\geq 0$ on the left, compared to the $\frac{\chi^{AB}}{4\tau}\left\|\varphi^j-\varphi^{j-1}\right\|^2$ on the right of (B.288). This simplifies the proof.

iii) We examine the last term on the right of (B.317), and discover that (cf. (B.289b))

$$\alpha\left(\left(\varphi^j-m\right)_{\{\theta\}},\psi^j\right)=\alpha\theta\left(\varphi^j-m,\psi^j-\overline{\psi^j}\right)+\alpha\left(1-\theta\right)\left(\varphi^{j-1}-m,\psi^j-\overline{\psi^j}\right)$$
$$\leq\theta^2\alpha^2c_P^4\left|\varphi^j\right|_1^2+\left(1-\theta\right)^2\alpha^2c_P^4\left|\varphi^{j-1}\right|_1^2+\frac{1}{2}\left|\psi^j\right|_1^2. \quad \text{(B.318)}$$

Combining this with (B.289a) in (B.317) yields (cf. (B.290), (B.293))

$$\frac{\varepsilon_\varphi^2}{2\tau}\left(\left|\varphi^j\right|_1^2-\left|\varphi^{j-1}\right|_1^2\right)+\frac{1}{\tau}\left(\left(\mathcal{B}_\mu\left(\varphi^j\right),1\right)-\left(\mathcal{B}_\mu\left(\varphi^{j-1}\right),1\right)\right)+\frac{3}{8}\left|\psi^j\right|_1^2$$
$$\leq 2\left\|\widetilde{f}^j\right\|_{-1}^2+\theta^2\alpha^2c_P^4\left|\varphi^j\right|_1^2+\left(1-\theta\right)^2\alpha^2c_P^4\left|\varphi^{j-1}\right|_1^2, \quad \text{(B.319)}$$

after discarding

$$\frac{\varepsilon_\varphi^2}{2\tau}\left|\varphi^j-\varphi^{j-1}\right|_1^2+\frac{\chi^{AB}}{4\tau}\left\|\varphi^j-\varphi^{j-1}\right\|^2\geq 0$$

on the left. Summing (B.319) through $j = 1, \dots, k$, $(k \leq M)$, gives (cf. (B.294))

$$\left(\varepsilon_\varphi^2 - 2\theta^2\alpha^2 c_P^4 \tau\right) \left|\varphi^k\right|_1^2 + \frac{3}{4}\sum_{j=1}^{k} \tau \left|\psi^j\right|_1^2 \leq C_1 \left|\varphi_0\right|_1^2 + 2C_0\mu_{\max}\left|\Omega\right| + \frac{\chi^{AB}}{2}\left(|\Omega| + \|\varphi_0\|^2\right) + 4\sum_{j=1}^{k}\tau \left\|\widetilde{f}^j\right\|_{-1}^2 + C_2 \sum_{j=1}^{k-1} \tau \frac{\varepsilon_\varphi^2}{2}\left|\varphi^j\right|_1^2 \quad \text{(B.320a)}$$

where we have defined

$$C_1 := \varepsilon_\varphi^2 + 2\left(1-\theta\right)^2 \alpha^2 c_P^4 T \qquad \text{and} \qquad C_2 := \frac{4\alpha^2 c_P^4 \left(\theta^2 + (1-\theta)^2\right)}{\varepsilon_\varphi^2}, \quad \text{(B.320b)}$$

both independent of τ and μ. If (cf. (B.295))

$$\tau < \tau_1 := \frac{\varepsilon_\varphi^2}{4\theta^2\alpha^2 c_P^4} \qquad \Rightarrow \qquad \frac{\varepsilon_\varphi^2}{2} < \varepsilon_\varphi^2 - 2\theta^2\alpha^2 c_P^4 \tau, \quad \text{(B.321)}$$

then (B.320) resembles (B.296), and the argument from the fully implicit case (cf. (B.297)) can be applied. We quickly arrive at (5.30a), (B.298) and (B.299).

Remark. As $\alpha \downarrow 0$ (i.e. for the Cahn–Hilliard case), $\tau_1 \to \infty$ in (B.321) and (5.30a) holds for any $\tau > 0$. There is no corresponding result for the fully implicit scheme.

We could also argue that $\tau_1 \to \infty$ as $\theta \downarrow 0$, but as we have noted elsewhere, a fully explicit non-local term can cause catastrophic instability, and we explicitly consider only $\theta \geq \frac{1}{2}$.

iv) We write (B.313) at t_j and t_{j-1}, subtract the second from the first and divide through by τ to obtain (cf. (B.301))

$$\left(\delta^{(\tau)}\psi^j, \nu_2\right) = \varepsilon_\varphi^2 \left(\nabla\delta^{(\tau)}\varphi^j, \nabla\nu_2\right) - \frac{\chi^{AB}}{2}\left(\delta^{(\tau)}\varphi^{j-1}, \nu_2\right) + \frac{1}{\tau}\left(\zeta_\mu\left(\varphi^j\right) - \zeta_\mu\left(\varphi^{j-1}\right), \nu_2\right) + \alpha\left(\left(-\Delta_n\right)^{-1}\left(\delta^{(\tau)}\varphi^j\right)_{\{\theta\}}, \nu_2\right) + \left(\delta^{(\tau)}\widetilde{F}^j, \nu_2\right). \quad \text{(B.322)}$$

We notice the φ^{j-2} terms, which did not appear in the corresponding point in the fully implicit argument. Setting $\nu_2 = \delta^{(\tau)}\varphi^j$ in the above, leads to

$$\left(\delta^{(\tau)}\psi^j, \delta^{(\tau)}\varphi^j\right) \geq \varepsilon_\varphi^2 \left|\delta^{(\tau)}\varphi^j\right|_1^2 - \frac{\chi^{AB}}{2}\left(\delta^{(\tau)}\varphi^{j-1}, \delta^{(\tau)}\varphi^j\right) + \alpha\left(\left(-\Delta_n\right)^{-1}\left(\delta^{(\tau)}\varphi^j\right)_{\{\theta\}}, \delta^{(\tau)}\varphi^j\right) + \left(\delta^{(\tau)}\widetilde{F}^j, \delta^{(\tau)}\varphi^j\right), \quad \text{(B.323)}$$

after recalling that

$$\frac{1}{\tau}\left(\zeta_\mu\left(\varphi^j\right) - \zeta_\mu\left(\varphi^{j-1}\right), \delta^{(\tau)}\varphi^j\right) \geq 0.$$

Using the linearity of $\left(-\Delta_n\right)^{-1}$ in the third term on the right leads to

$$\alpha\left(\left(-\Delta_n\right)^{-1}\left(\delta^{(\tau)}\varphi^j\right)_{\{\theta\}}, \delta^{(\tau)}\varphi^j\right) = \underbrace{\alpha\theta\left\|\delta^{(\tau)}\varphi^j\right\|_{-1}^2}_{\geq 0} + \alpha\left(1-\theta\right)\left(\left(-\Delta_n\right)^{-1}\left(\delta^{(\tau)}\varphi^{j-1}\right), \delta^{(\tau)}\varphi^j\right).$$

We substitute this and (B.304) into (B.323) and rearrange to discover that (cf. (B.305))

$$\frac{1}{2\tau}\left(\left|\psi^j\right|_1^2 - \left|\psi^{j-1}\right|_1^2\right) + \varepsilon_\varphi^2\left|\delta^{(\tau)}\varphi^j\right|_1^2 \leq \frac{\chi^{AB}}{2}\left(\delta^{(\tau)}\varphi^{j-1}, \delta^{(\tau)}\varphi^j\right) - \left(\delta^{(\tau)}\widetilde{F}^j, \delta^{(\tau)}\varphi^j\right) - \alpha\left(1-\theta\right)\left(\left(-\Delta_n\right)^{-1}\left(\delta^{(\tau)}\varphi^{j-1}\right), \delta^{(\tau)}\varphi^j\right) \leq \left(\frac{\chi^{AB}}{2}\right)^2 \frac{c_P^4}{\varepsilon_\varphi^2}\left|\delta^{(\tau)}\varphi^{j-1}\right|_1^2 + \frac{c_P^2}{\varepsilon_\varphi^2}\left\|\delta^{(\tau)}\widetilde{F}^j\right\|^2 + \alpha^2\left(1-\theta\right)^2\frac{c_P^4}{\varepsilon_\varphi^2}\left\|\delta^{(\tau)}\varphi^{j-1}\right\|_{-1}^2 + \frac{3\varepsilon_\varphi^2}{4}\left|\delta^{(\tau)}\varphi^j\right|_1^2$$

after using the Cauchy–Schwarz, Young and Poincaré inequalities and (2.11), or

$$\left|\psi^j\right|_1^2+\frac{\varepsilon_\varphi^2}{2}\tau\left|\delta^{(\tau)}\varphi^j\right|_1^2\leq\left|\psi^{j-1}\right|_1^2+\frac{\left(\chi^{AB}\right)^2}{2}\frac{c_P^4}{\varepsilon_\varphi^2}\tau\left|\delta^{(\tau)}\varphi^{j-1}\right|_1^2 \\ +\frac{2c_P^2}{\varepsilon_\varphi^2}\tau\left\|\delta^{(\tau)}\widetilde{F}^j\right\|^2+\frac{2\alpha^2\left(1-\theta\right)^2c_P^4}{\varepsilon_\varphi^2}\tau\left\|\delta^{(\tau)}\varphi^{j-1}\right\|_{-1}^2, \quad \text{(B.324)}$$

for each $j=1,\ldots,M$. Consider the last two terms on the right of (B.324).

- For any $j=1,\ldots,M$,

$$\tau\left\|\delta^{(\tau)}\widetilde{F}^j\right\|^2\leq\sum_{j=1}^M\tau\left\|\delta^{(\tau)}\widetilde{F}^j\right\|^2\leq C \quad \text{(B.325a)}$$

  independent of τ and μ by (B.309).

- Similarly,

$$\tau\left\|\delta^{(\tau)}\varphi^{j-1}\right\|_{-1}^2\leq\sum_{j=1}^M\tau\left\|\delta^{(\tau)}\varphi^{j-1}\right\|_{-1}^2\leq\tau\left\|\delta^{(\tau)}\varphi^0\right\|_{-1}^2+\sum_{j=1}^M\tau\left\|\delta^{(\tau)}\varphi^j\right\|_{-1}^2 \quad \text{(B.325b)}$$

  for each $j=1,\ldots,M$. Given that φ^{-1} is fictitious, $\overline{\varphi_0}=m$ and we require $\overline{\varphi_0-\varphi^{-1}}=0$, we define $\varphi^{-1}=\varphi_0$ as in (5.62), so that $\left\|\delta^{(\tau)}\varphi^0\right\|_{-1}^2=0$. Combining this with (B.299) in (B.325b), we conclude that

$$\tau\left\|\delta^{(\tau)}\varphi^{j-1}\right\|_{-1}^2\leq C, \quad \text{(B.325c)}$$

  for each $j=1,\ldots,M$, independent of τ and μ.

Using (B.325), we write (B.324) as

$$\left|\psi^j\right|_1^2+\frac{\varepsilon_\varphi^2}{2}\tau\left|\delta^{(\tau)}\varphi^j\right|_1^2\leq\left|\psi^{j-1}\right|_1^2+C\tau\left|\delta^{(\tau)}\varphi^{j-1}\right|_1^2+C \quad \text{(B.326)}$$

for each $j=1,\ldots,M$, where each C is a positive constant, independent of τ and μ.

v) We now argue by induction. Writing (B.326) for $j=1$, using $\varphi^{-1}\equiv\varphi_0$, leads to

$$\left|\psi^1\right|_1^2+\frac{\varepsilon_\varphi^2}{2}\tau\left|\delta^{(\tau)}\varphi^1\right|_1^2\leq\left|\psi^0\right|_1^2+C. \quad \text{(B.327)}$$

We bound $\left|\psi^0\right|_1$: as in (B.300), we write

$$\left(\psi^j,\nu_2\right)=\varepsilon_\varphi^2\left(-\Delta\varphi^j,\nu_2\right)-\frac{\chi^{AB}}{2}\left(\varphi^{j-1},\nu_2\right)+\left(\zeta_\mu\left(\varphi^j\right),\nu_2\right) \\ +\alpha\left(\left(-\Delta_n\right)^{-1}\left(\varphi^j-m\right)_{\{\theta\}},\nu_2\right)+\left(\widetilde{F}^j,\nu_2\right) \quad \text{(B.328a)}$$

for every $\nu_2\in L^2\left(\Omega\right)$, and

$$\psi^j=\varepsilon_\varphi^2\left(-\Delta\right)\varphi^j-\frac{\chi^{AB}}{2}\varphi^{j-1}+\zeta_\mu\left(\varphi^j\right)+\alpha\left(-\Delta_n\right)^{-1}\left(\varphi^j-m\right)_{\{\theta\}}+\widetilde{F}^j \quad \text{(B.328b)}$$

a.e. for each $j=1,\ldots,M$. Likewise, if (4.63) and (4.55) hold, we can write

$$H^1\left(\Omega\right)\ni\psi_0=\varepsilon_\varphi^2\left(-\Delta\right)\varphi_0-\frac{\chi^{AB}}{2}\varphi^{-1}+\alpha\left(-\Delta_n\right)^{-1}\left(\varphi_0-m\right)_{\{\theta\}}+\widetilde{F}_0 \\ =\varepsilon_\varphi^2\left(-\Delta\right)\varphi_0-\frac{\chi^{AB}}{2}\varphi_0+\alpha\left(-\Delta_n\right)^{-1}\left(\varphi_0-m\right)+\widetilde{F}_0,$$

since $\varphi_0 \in \mathscr{A}$, and we assumed that $\varphi^{-1} \equiv \varphi^0 = \varphi_0$. The same argument as we used in the fully implicit case (cf. (B.300c), (B.236)) can be used here to bound $\left|\psi^0\right|_1$, independent of τ and μ.

Hence, $\left|\psi^1\right|_1^2$ and $\tau \left|\delta^{(\tau)}\varphi^1\right|_1^2$ are separately bounded, independent of τ and μ. For arbitrary $j > 1$, each term on the left of (B.326), viz. each $\left|\psi^j\right|_1^2$ and $\tau \left|\delta^{(\tau)}\varphi^j\right|_1^2$ for $j = 0, \ldots, M$ is bounded, independent of μ and τ, by induction. Thus, in the current scheme, we also have that

$$\max_{0 \le j \le M} \left|\psi^j\right|_1 < C. \tag{B.311}$$

vi) We set $\nu_2 = -\Delta\varphi^j \in L^2(\Omega)$ in (B.328a), and using the zero Neumann BC on φ^j, rearrange to get (cf. (B.312))

$$\left(\nabla\psi^j, \nabla\varphi^j\right) \ge \varepsilon_\varphi^2 \left\|-\Delta\varphi^j\right\|^2 - \frac{\chi^{AB}}{2}\left(\nabla\varphi^{j-1}, \nabla\varphi^j\right) + \alpha(1-\theta)\left(\nabla\left(-\Delta_n\right)^{-1}\left(\varphi^{j-1} - m\right), \nabla\varphi^j\right) + \left(\nabla\widetilde{F}^j, \nabla\varphi^j\right)$$

after noting that

$$\alpha\theta\left(\left(-\Delta_n\right)^{-1}\left(\varphi^j - m\right), -\Delta\varphi^j\right) + \left(\zeta_\mu'\left(\varphi^j\right), \left(\nabla\varphi^j\right)^2\right) \ge 0.$$

Hence, using the Cauchy–Schwarz and Young inequalities and (A.28b), we see that

$$\varepsilon_\varphi^2 \left\|-\Delta\varphi^j\right\|^2 \le \frac{1}{2}\left|\psi^j\right|_1^2 + \left(\frac{1}{2}\left(\frac{\chi^{AB}}{2}\right)^2 + \frac{\alpha^2(1-\theta)^2 c_P^4}{2}\right)\left|\varphi^{j-1}\right|_1^2 + 2\left|\varphi^j\right|_1^2 + \frac{1}{2}\left\|\widetilde{f}^j\right\|_{-1}^2 \le C < \infty \tag{B.329}$$

independent of μ and τ by virtue of (B.311) and (5.30a). Arguing as we did after (B.312), we are led to (5.31) once again.

vii) We will show that

$$\sum_{j=1}^{M} \left\|\varphi^j - \varphi^{j-1}\right\|_1^2 \le C$$

for the third term on the left of (5.30b), in the last part of the proof of energy decay. See the build-up to (B.360) in the proof of Lemma 5.1.9, starting on p. 421.

□

B.28 Stability: proof of Lemma 5.1.8

Proof. We establish the stability of solutions of $\left(\mathbf{R}_\tau^{(m)}\right)$.

i) Substituting $\left(\varphi_1^j, \omega_1^j\right)_{j=1}^M$ and $\left(\varphi_2^j, \omega_2^j\right)_{j=1}^M$ into the problem we find that (cf. (B.240))

$$\left(\delta^{(\tau)}\varphi^j, \nu_1\right) + \left(\nabla\omega^j, \nabla\nu_1\right) + \alpha\left(\varphi^j, \nu_1\right) = 0, \tag{B.330a}$$

for every $\nu_1 \in H^1(\Omega)$ and each $j = 1, \ldots, M$ and likewise

$$\left(\omega^j, \nu_2\right) = \varepsilon_\varphi^2\left(\nabla\varphi^j, \nabla\nu_2\right) - \frac{\chi^{AB}}{2}\left(\varphi^j, \nu_2\right) + \left(\zeta_\mu\left(\varphi_1^j\right) - \zeta_\mu\left(\varphi_2^j\right), \nu_2\right) \tag{B.330b}$$

for every $\nu_2 \in H^1(\Omega)$.

Remark. This difference problem features neither $\overline{\varphi^j}$ (i.e. m) nor f.

Setting $\nu_2 = \varphi^j = \varphi_1^j - \varphi_2^j$ in (B.330b) yields

$$\left(\omega^j, \varphi^j\right) = \varepsilon_\varphi^2 \left|\varphi^j\right|_1^2 - \frac{\chi^{AB}}{2} \left\|\varphi^j\right\|^2 + \underbrace{\left(\zeta_\mu\left(\varphi_1^j\right) - \zeta_\mu\left(\varphi_2^j\right), \varphi_1^j - \varphi_2^j\right)}_{>0 \text{ by (4.19a)}}$$

viz. (cf. (B.137))[74]

$$\varepsilon_\varphi^2 \left|\varphi^j\right|_1^2 - \frac{\chi^{AB}}{2} \left\|\varphi^j\right\|^2 \leq \left(\omega^j, \varphi^j\right). \tag{B.331}$$

Setting (cf. (B.282))

$$\nu_1 = (-\Delta_n)^{-1} \varphi^j = (-\Delta_n)^{-1} \left(\frac{\varphi^j - \varphi^{j-1}}{2} + \frac{\varphi^j + \varphi^{j-1}}{2}\right) \tag{B.332}$$

in (B.330a) (recalling mass conservation for the compatibility condition) gives (cf. (B.138))

$$\frac{1}{2\tau}\left(\left\|\varphi^j\right\|_{-1}^2 - \left\|\varphi^{j-1}\right\|_{-1}^2\right) + \left(\omega^j, \varphi^j\right) \leq 0, \tag{B.333}$$

since $\left(\nabla\omega^j, \nabla\left(-\Delta_n\right)^{-1}\varphi^j\right) = \left(\omega^j, \varphi^j\right)$ by (2.9a), and after discarding the non-negative

$$\frac{1}{2\tau}\left\|\varphi^j - \varphi^{j-1}\right\|_{-1}^2 + \alpha\left\|\varphi^j\right\|_{-1}^2 \geq 0$$

on the left. Combining (B.333) with (B.331), we find that (cf. (B.140))

$$\begin{aligned}\frac{1}{2\tau}\left(\left\|\varphi^j\right\|_{-1}^2 - \left\|\varphi^{j-1}\right\|_{-1}^2\right) + \varepsilon_\varphi^2\left|\varphi^j\right|_1^2 \leq \frac{\chi^{AB}}{2}\left\|\varphi^j\right\|^2 &= \frac{\chi^{AB}}{2}\left(\nabla\varphi^j, \nabla\left(-\Delta_n\right)^{-1}\varphi^j\right) \\ &\leq \frac{\chi^{AB}}{2}\left|\varphi^j\right|_1\left\|\varphi^j\right\|_{-1} \leq \frac{\varepsilon_\varphi^2}{2}\left|\varphi^j\right|_1^2 + \frac{1}{2}\frac{\left(\chi^{AB}\right)^2}{4\varepsilon_\varphi^2}\left\|\varphi^j\right\|_{-1}^2,\end{aligned}$$

by the Cauchy–Schwarz and Young inequalities (Lemma A.1.12). If we multiply by 2τ, we obtain

$$\left\|\varphi^j\right\|_{-1}^2 - \left\|\varphi^{j-1}\right\|_{-1}^2 + \varepsilon_\varphi^2\tau\left|\varphi^j\right|_1^2 \leq \frac{\left(\chi^{AB}\right)^2}{4\varepsilon_\varphi^2}\tau\left\|\varphi^j\right\|_{-1}^2. \tag{B.334}$$

Summing (B.334) through $j = 1, \ldots, k$, $(k \leq M)$, using the telescoping sum gives

$$\left(\varepsilon_\varphi^2 - \frac{\left(\chi^{AB}\right)^2}{4}\tau\right)\left\|\varphi^k\right\|_{-1}^2 + \varepsilon_\varphi^4 \sum_{j=1}^{k} \tau\left|\varphi^j\right|_1^2 \leq C_1\left\|\varphi_0\right\|_{-1}^2 + C_2\sum_{j=1}^{k-1}\tau\left\|\varphi^j\right\|_{-1}^2$$

where we have moved the last term in the sum on the right over to the left, multiplied through by ε_φ^2 and defined

$$C_1\left(\varepsilon_\varphi^2\right) := \varepsilon_\varphi^2 \qquad \text{and} \qquad C_2\left(\chi^{AB}\right) := \frac{\left(\chi^{AB}\right)^2}{4},$$

both of which are independent of τ, k and μ. If we now assume that

$$\tau \leq \frac{2\varepsilon_\varphi^2}{\left(\chi^{AB}\right)^2} \qquad \Rightarrow \qquad \frac{\varepsilon_\varphi^2}{2} \leq \varepsilon_\varphi^2 - \frac{\left(\chi^{AB}\right)^2}{4}\tau, \tag{B.335a}$$

(independent of μ) then,

$$\frac{\varepsilon_\varphi^2}{2}\left\|\varphi^k\right\|_{-1}^2+\varepsilon_\varphi^4\sum_{j=1}^{k}\tau\left|\varphi^j\right|_1^2\leq C_1\left\|\varphi_0\right\|_{-1}^2+\frac{2C_2}{\varepsilon_\varphi^2}\sum_{j=1}^{k-1}\frac{\varepsilon_\varphi^2}{2}\tau\left\|\varphi^j\right\|_{-1}^2. \tag{B.335b}$$

The discrete Gronwall inequality (Lemma A.1.14) implies that

$$\frac{\varepsilon_\varphi^2}{2}\left\|\varphi^k\right\|_{-1}^2+\varepsilon_\varphi^4\sum_{j=1}^{k}\tau\left|\varphi^j\right|_1^2\leq C_1\left\|\varphi_0\right\|_{-1}^2\exp\left\{\frac{2C_2}{\varepsilon_\varphi^2}k\tau\right\}\leq C_1\left\|\varphi_0\right\|_{-1}^2\exp\left\{\frac{2C_2}{\varepsilon_\varphi^2}T\right\}$$

since $k\tau\leq T$ for $k=1,\ldots,M$. Hence (cf. (B.142))

$$\frac{\varepsilon_\varphi^2}{2}\left\|\varphi^k\right\|_{-1}^2+\varepsilon_\varphi^4\sum_{j=1}^{k}\tau\left|\varphi^j\right|_1^2\leq C\left\|\varphi_0\right\|_{-1}^2\qquad\text{where}\qquad C=C\left(\varepsilon_\varphi^2,\chi^{AB},T\right),$$

where C is independent of k, τ and μ. (5.34) follows.

ii) If we set $\varphi_1^0=\varphi_2^0$, so that $\varphi_0\equiv 0$ viz. $\left\|\varphi_0\right\|_{-1}^2=0$, then each $\left\|\varphi^k\right\|_{-1}^2=0$ and so $\varphi^k\equiv 0$, too.[75] We conclude that $\left(\varphi^j\right)_{j=1}^M$ solving $\left(\mathbf{R}_\tau^{(m)}\right)$ is unique.

To establish the uniqueness of the potential solution sequence $\left(\omega^j\right)_{j=1}^M$, we first set $\varphi_0\equiv 0\Rightarrow\varphi^j\equiv 0$ for each j and $\nu_2=1$ in (B.330b) to see that

$$\left(\omega^j,1\right)=0\qquad\Rightarrow\qquad\omega^j\in L_*^2\left(\Omega\right)$$

for each j. Likewise, setting $\nu_1=\omega^j$ in (B.330a), and using the above yields

$$\left|\omega^j\right|_1^2=0\qquad\Rightarrow\qquad\omega^j\equiv 0.$$

Remark. We have re-established uniqueness from stability above for completeness. See Fig. 5.1 on p. 80 and the result immediately preceding it.

We now adapt the proof above for problem $\left(\mathbf{R}_{\tau,\theta}^{(m)}\right)$.

i) For the difference problem, we use (5.6) and (5.20c) to conclude that

$$\left(\delta^{(\tau)}\varphi^j,\nu_1\right)+\left(\nabla\omega^j,\nabla\nu_1\right)+\alpha\theta\left(\varphi^j,\nu_1\right)=-\alpha\left(1-\theta\right)\left(\varphi^{j-1},\nu_1\right), \tag{B.336a}$$

for every $\nu_1\in H^1\left(\Omega\right)$ and each $j=1,\ldots,M$, and

$$\left(\omega^j,\nu_2\right)=\varepsilon_\varphi^2\left(\nabla\varphi^j,\nabla\nu_2\right)-\frac{\chi^{AB}}{2}\left(\varphi^{j-1},\nu_2\right)+\left(\zeta_\mu\left(\varphi_1^j\right)-\zeta_\mu\left(\varphi_2^j\right),\nu_2\right) \tag{B.336b}$$

for every $\nu_2\in H^1\left(\Omega\right)$. Setting $\nu_2=\varphi^j=\varphi_1^j-\varphi_2^j$ in (B.336b) yields

$$\varepsilon_\varphi^2\left|\varphi^j\right|_1^2-\frac{\chi^{AB}}{2}\left(\varphi^{j-1},\varphi^j\right)\leq\left(\omega^j,\varphi^j\right). \tag{B.337}$$

Using (B.332) in (B.336a) leads to (cf. (B.333))

$$\frac{1}{2\tau}\left(\left\|\varphi^j\right\|_{-1}^2-\left\|\varphi^{j-1}\right\|_{-1}^2\right)+\left(\omega^j,\varphi^j\right)\leq-\alpha\left(1-\theta\right)\left(\varphi^{j-1},\left(-\Delta_n\right)^{-1}\varphi^j\right), \tag{B.338}$$

after discarding

$$\frac{1}{2\tau}\left\|\varphi^j-\varphi^{j-1}\right\|_{-1}^2+\alpha\theta\left\|\varphi^j\right\|_{-1}^2\geq 0$$

on the left. Then, since $\left(\varphi^{j-1},(-\Delta_n)^{-1}\varphi^j\right)=\left(\nabla(-\Delta_n)^{-1}\varphi^{j-1},\nabla(-\Delta_n)^{-1}\varphi^j\right)$ by (2.9a), and likewise $\left(\varphi^{j-1},\varphi^j\right)=\left(\nabla(-\Delta_n)^{-1}\varphi^{j-1},\nabla\varphi^j\right)$, (B.337) and (B.338) give

$$\begin{aligned}
&\frac{1}{2\tau}\left(\left\|\varphi^j\right\|_{-1}^2-\left\|\varphi^{j-1}\right\|_{-1}^2\right)+\varepsilon_\varphi^2\left|\varphi^j\right|_1^2\\
&\quad\leq-\alpha(1-\theta)\left(\nabla(-\Delta_n)^{-1}\varphi^{j-1},\nabla(-\Delta_n)^{-1}\varphi^j\right)+\frac{\chi^{AB}}{2}\left(\nabla(-\Delta_n)^{-1}\varphi^{j-1},\nabla\varphi^j\right)\\
&\quad\leq\alpha(1-\theta)\left\|\varphi^{j-1}\right\|_{-1}\left\|\varphi^j\right\|_{-1}+\frac{\chi^{AB}}{2}\left\|\varphi^{j-1}\right\|_{-1}\left|\varphi^j\right|_1\\
&\quad\leq\frac{\alpha^2(1-\theta)^2}{2}\left\|\varphi^{j-1}\right\|_{-1}^2+\frac{1}{2}\left\|\varphi^j\right\|_{-1}^2+\frac{\varepsilon_\varphi^2}{2}\left|\varphi^j\right|_1^2+\frac{1}{2}\frac{\left(\chi^{AB}\right)^2}{4\varepsilon_\varphi^2}\left\|\varphi^j\right\|_{-1}^2,
\end{aligned}$$

by the Cauchy–Schwarz and Young inequalities (Lemma A.1.12). If we multiply this by 2τ and rearrange, we find that (cf. (B.334))

$$\left\|\varphi^j\right\|_{-1}^2-\left\|\varphi^{j-1}\right\|_{-1}^2+\varepsilon_\varphi^2\tau\left|\varphi^j\right|_1^2\leq\alpha^2(1-\theta)^2\tau\left\|\varphi^{j-1}\right\|_{-1}^2+\left(1+\frac{\left(\chi^{AB}\right)^2}{4\varepsilon_\varphi^2}\right)\tau\left\|\varphi^j\right\|_{-1}^2. \tag{B.339}$$

If we sum (B.339) through $j=1,\ldots,k$, $(k\leq M)$, multiply by ε_φ^2 and rearrange,

$$\begin{aligned}
\varepsilon_\varphi^2\left\|\varphi^k\right\|_{-1}^2+\varepsilon_\varphi^4\sum_{j=1}^k\tau\left|\varphi^j\right|_1^2\leq{}&\varepsilon_\varphi^2\left\|\varphi^0\right\|_{-1}^2+\varepsilon_\varphi^2\alpha^2(1-\theta)^2\tau\left\|\varphi^0\right\|_{-1}^2\\
&+\varepsilon_\varphi^2\alpha^2(1-\theta)^2\sum_{j=1}^{k-1}\tau\left\|\varphi^j\right\|_{-1}^2+\left(1+\frac{\left(\chi^{AB}\right)^2}{4}\right)\sum_{j=1}^k\tau\left\|\varphi^j\right\|_{-1}^2,
\end{aligned}$$

or, since $\tau\leq T$,

$$\left(\varepsilon_\varphi^2-\left(1+\frac{\left(\chi^{AB}\right)^2}{4}\right)\tau\right)\left\|\varphi^k\right\|_{-1}^2+\varepsilon_\varphi^4\sum_{j=1}^k\tau\left|\varphi^j\right|_1^2\leq C_1\left\|\varphi^0\right\|_{-1}^2+C_2\sum_{j=1}^{k-1}\tau\left\|\varphi^j\right\|_{-1}^2, \tag{B.340}$$

where we have moved the last term in the rightmost series over to the left and defined

$$\begin{aligned}
C_1\left(\alpha,\varepsilon_\varphi^2,\theta,T\right)&:=\varepsilon_\varphi^2\left(1+\alpha^2(1-\theta)^2T\right);\\
C_2\left(\alpha,\varepsilon_\varphi^2,\chi^{AB},\theta\right)&:=\left(\varepsilon_\varphi^2\alpha^2(1-\theta)^2+\left(1+\frac{\left(\chi^{AB}\right)^2}{4}\right)\right),
\end{aligned}$$

both of which are independent of τ, k and μ. Assuming that (cf. (B.335a))

$$\tau\leq\frac{2\varepsilon_\varphi^2}{4+\left(\chi^{AB}\right)^2}\qquad\Rightarrow\qquad\frac{\varepsilon_\varphi^2}{2}\leq\varepsilon_\varphi^2-\left(1+\frac{\left(\chi^{AB}\right)^2}{4}\right)\tau, \tag{B.341}$$

(independent of μ) allows us to write (B.340) in a form that is structurally identical to (B.335b). We can argue exactly as we did in the fully implicit case to establish the stability and uniqueness of solutions of $\left(\mathbf{R}_{\tau,\theta}^{(m)}\right)$.

□

B.29 Energy decay: proof of Lemma 5.1.9

Proof. As noted previously, if $\overline{\varphi_0} = m$, then $\overline{\varphi^j} = m$ for $j = 1, \dots, M$. With this fact in hand, we develop the proof for the fully implicit $\left(\mathbf{R}_\tau^{(m)}\right)$.

i) From (B.280b) with $f \equiv 0$,

$$\left(\delta^{(\tau)}\varphi^j, \nu_1\right) + \left(\nabla\psi^j, \nabla\nu_1\right) = 0 \qquad \Rightarrow \qquad \left(\left(-\Delta_n\right)^{-1}\delta^{(\tau)}\varphi^j, \nu_1\right) + \left(\psi^j, \nu_1\right) = 0 \tag{B.342}$$

for every $\nu_1 \in H^1_*(\Omega)$ by (2.9c). Using this in (B.280c) then yields

$$\left(\left(-\Delta_n\right)^{-1}\delta^{(\tau)}\varphi^j, \nu_2\right) + \varepsilon_\varphi^2\left(\nabla\varphi^j, \nabla\nu_2\right) + \left(\mathcal{B}'_\mu\left(\varphi^j\right), \nu_2\right) + \alpha\left(\left(-\Delta_n\right)^{-1}\left(\varphi^j - m\right), \nu_2\right) = 0 \tag{B.343}$$

for every $\nu_2 \in H^1(\Omega)$ and each j. Setting $\nu_2 = \varphi^j - \varphi^{j-1} \in H^1_*(\Omega)$ in (B.343) leads to

$$\begin{aligned}\frac{1}{\tau}\left\|\varphi^j - \varphi^{j-1}\right\|_{-1}^2 &+ \varepsilon_\varphi^2\left(\nabla\varphi^j, \nabla\left(\varphi^j - \varphi^{j-1}\right)\right) \\ &+ \left(\mathcal{B}'_\mu\left(\varphi^j\right), \varphi^j - \varphi^{j-1}\right) + \alpha\left(\left(-\Delta_n\right)^{-1}\left(\varphi^j - m\right), \varphi^j - \varphi^{j-1}\right) = 0.\end{aligned} \tag{B.344}$$

We consider the second, third and fourth terms on the left of (B.344).

- For the second,

$$\begin{aligned}\varepsilon_\varphi^2\left(\nabla\varphi^j, \nabla\left(\varphi^j - \varphi^{j-1}\right)\right) &= \frac{\varepsilon_\varphi^2}{2}\left(\nabla\left(\varphi^j - \varphi^{j-1} + \varphi^j + \varphi^{j-1}\right), \nabla\left(\varphi^j - \varphi^{j-1}\right)\right) \\ &= \frac{\varepsilon_\varphi^2}{2}\left|\varphi^j - \varphi^{j-1}\right|_1^2 + \frac{\varepsilon_\varphi^2}{2}\left(\left|\varphi^j\right|_1^2 - \left|\varphi^{j-1}\right|_1^2\right).\end{aligned} \tag{B.345a}$$

- For the third, we use (B.287) to conclude that

$$\left(\mathcal{B}_\mu\left(\varphi^j\right), 1\right) - \left(\mathcal{B}_\mu\left(\varphi^{j-1}\right), 1\right) - \frac{\chi^{AB}}{4}\left\|\varphi^j - \varphi^{j-1}\right\|^2 \leq \left(\mathcal{B}'_\mu\left(\varphi^j\right), \varphi^j - \varphi^{j-1}\right). \tag{B.345b}$$

- For the fourth term,

$$\begin{aligned}&\alpha\left(\left(-\Delta_n\right)^{-1}\left(\varphi^j - m\right), \varphi^j - \varphi^{j-1}\right) \\ &\quad= \alpha\left(\left(-\Delta_n\right)^{-1}\left(\frac{\varphi^j - \varphi^{j-1} + \varphi^j + \varphi^{j-1}}{2} - m\right), \varphi^j - \varphi^{j-1}\right) \\ &\quad= \alpha\left(\left(-\Delta_n\right)^{-1}\left(\frac{\varphi^j - \varphi^{j-1}}{2}\right), \varphi^j - \varphi^{j-1}\right) \\ &\qquad+\alpha\left(\left(-\Delta_n\right)^{-1}\left(\frac{\varphi^j - m + \varphi^{j-1} - m}{2}\right), \varphi^j - m - \left(\varphi^{j-1} - m\right)\right) \\ &\quad= \frac{\alpha}{2}\left\|\varphi^j - \varphi^{j-1}\right\|_{-1}^2 + \frac{\alpha}{2}\left(\left\|\varphi^j - m\right\|_{-1}^2 - \left\|\varphi^{j-1} - m\right\|_{-1}^2\right).\end{aligned} \tag{B.345c}$$

ii) Using the energy functional in (4.61), we find that

$$\begin{aligned}\mathcal{E}_\mu^{(m)}\left[\varphi^j\right] - \mathcal{E}_\mu^{(m)}\left[\varphi^{j-1}\right] &= \frac{\varepsilon_\varphi^2}{2}\left(\left|\varphi^j\right|_1^2 - \left|\varphi^{j-1}\right|_1^2\right) \\ &+ \left(\mathcal{B}_\mu\left(\varphi^j\right) - \mathcal{B}_\mu\left(\varphi^{j-1}\right), 1\right) + \frac{\alpha}{2}\left(\left\|\varphi^j - m\right\|_{-1}^2 - \left\|\varphi^{j-1} - m\right\|_{-1}^2\right).\end{aligned} \tag{B.346}$$

iii) Using (B.345) and (B.346) in (B.344), we are led to[76]

$$\mathcal{E}_{\mu}^{(m)}\left[\varphi^{j}\right]-\mathcal{E}_{\mu}^{(m)}\left[\varphi^{j-1}\right]+\left(\frac{1}{\tau}+\frac{\alpha}{2}\right)\left\|\varphi^{j}-\varphi^{j-1}\right\|_{-1}^{2}+\frac{\varepsilon_{\varphi}^{2}}{2}\left|\varphi^{j}-\varphi^{j-1}\right|_{1}^{2}-\frac{\chi^{AB}}{4}\left\|\varphi^{j}-\varphi^{j-1}\right\|^{2}\leq 0. \tag{B.347}$$

Noting that $\overline{\varphi^{j}-\varphi^{j-1}}=0$, and using (A.29) and Young's inequality,[77] yields

$$\frac{\chi^{AB}}{4}\left\|\varphi^{j}-\varphi^{j-1}\right\|^{2}\leq\frac{1}{\tau}\left\|\varphi^{j}-\varphi^{j-1}\right\|_{-1}^{2}+\left(\frac{\chi^{AB}}{4}\right)^{2}\frac{\tau}{4}\left|\varphi^{j}-\varphi^{j-1}\right|_{1}^{2}$$

or

$$-\frac{1}{\tau}\left\|\varphi^{j}-\varphi^{j-1}\right\|_{-1}^{2}-\left(\frac{\chi^{AB}}{4}\right)^{2}\frac{\tau}{4}\left|\varphi^{j}-\varphi^{j-1}\right|_{1}^{2}\leq-\frac{\chi^{AB}}{4}\left\|\varphi^{j}-\varphi^{j-1}\right\|^{2}. \tag{B.348}$$

Substituting this into (B.347) gives[78]

$$\mathcal{E}_{\mu}^{(m)}\left[\varphi^{j}\right]-\mathcal{E}_{\mu}^{(m)}\left[\varphi^{j-1}\right]+\frac{\alpha}{2}\left\|\varphi^{j}-\varphi^{j-1}\right\|_{-1}^{2}+\left(\frac{\varepsilon_{\varphi}^{2}}{2}-\left(\frac{\chi^{AB}}{4}\right)^{2}\frac{\tau}{4}\right)\left|\varphi^{j}-\varphi^{j-1}\right|_{1}^{2}\leq 0. \tag{B.349}$$

iv) If we now assume that

$$\tau\leq\frac{32\varepsilon_{\varphi}^{2}}{\left(\chi^{AB}\right)^{2}}\qquad\Rightarrow\qquad\frac{\varepsilon_{\varphi}^{2}}{2}-\left(\frac{\chi^{AB}}{4}\right)^{2}\frac{\tau}{4}=:C_{\varepsilon}\geq 0, \tag{B.350}$$

then (B.349) leads to (5.35) by a simple induction argument.

v) Under the assumption in (B.350), we sum (B.349) from $j=1,\ldots,k\leq M$, to find that

$$\mathcal{E}_{\mu}^{(m)}\left[\varphi^{k}\right]+\frac{\alpha}{2}\sum_{j=1}^{k}\left\|\varphi^{j}-\varphi^{j-1}\right\|_{-1}^{2}+C_{\varepsilon}\sum_{j=1}^{k}\left|\varphi^{j}-\varphi^{j-1}\right|_{1}^{2}\leq\mathcal{E}_{\mu}^{(m)}\left[\varphi^{0}\right]=C\left(\varphi^{0}\right), \tag{B.351}$$

independent of τ. We have two cases to consider:

1. $\mathcal{E}_{\mu}^{(m)}\left[\varphi^{k}\right]\geq 0$: in this case, we can discard $\mathcal{E}_{\mu}^{(m)}\left[\varphi^{k}\right]$ on the left above and conclude that

$$\sum_{j=1}^{k}\left|\varphi^{j}-\varphi^{j-1}\right|_{1}^{2}\leq C<\infty \tag{B.352}$$

independent of τ and μ, and since each $\overline{\varphi^{j}}=\overline{\varphi^{j-1}}=m$, we may use Poincaré's inequality to conclude that each

$$\left\|\varphi^{j}-\varphi^{j-1}\right\|\leq c_{P}\left|\varphi^{j}-\varphi^{j-1}\right|_{1}\quad\Rightarrow\quad\sum_{j=1}^{k}\left\|\varphi^{j}-\varphi^{j-1}\right\|_{1}^{2}\leq C<\infty,\quad k=1,\ldots,M, \tag{B.353}$$

independent of τ and μ.

2. $\mathcal{E}_{\mu}^{(m)}\left[\varphi^{k}\right]<0$: it is possible for the total, regularised energy to be negative. This happens because regularised solution morphologies can have $\left\|\varphi^{j}\right\|_{0,\infty}>1$, and negative homogeneous energy. In such cases, $\mathcal{E}_{\text{penalty}}$ (see (4.6)) is positive, but there is nothing guaranteeing that $\mathcal{E}_{\mu}^{(m)}\left[\varphi^{k}\right]\geq 0$. In this case, we expand $\mathcal{E}_{\mu}^{(m)}\left[\varphi^{k}\right]<0$ in (B.351) using (4.61) and find that

$$\underbrace{\frac{\varepsilon_{\varphi}^{2}}{2}\left|\varphi^{k}\right|_{1}^{2}+\frac{\alpha}{2}\left\|\varphi^{k}-m\right\|_{-1}^{2}}_{\geq 0}+\left(\mathcal{B}_{\mu}\left(\varphi^{k}\right),1\right)+C_{\varepsilon}\sum_{j=1}^{k}\left|\varphi^{j}-\varphi^{j-1}\right|_{1}^{2}\leq\mathcal{E}_{\mu}^{(m)}\left[\varphi^{0}\right],$$

viz.

$$C_\varepsilon \sum_{j=1}^{k} \left|\varphi^j - \varphi^{j-1}\right|_1^2 \leq \mathcal{E}_\mu^{(m)}\left[\varphi^0\right] - \left(\mathcal{B}_\mu\left(\varphi^k\right), 1\right) \leq C\left(\varphi^0\right) + C_0\mu_{\max}|\Omega| = C < \infty \tag{B.354}$$

independent of τ and μ, after using (B.223), as we did in deriving (B.294). We quickly arrive back at (B.353).

The proof for $\left(\mathbf{R}_{\tau,\theta}^{(m)}\right)$ is an adaptation of that above.

i) Instead of (B.343), we use (B.313) with $f \equiv 0$ to obtain

$$\begin{aligned}\left(\left(-\Delta_n\right)^{-1}\delta^{(\tau)}\varphi^j, \nu_2\right) + \varepsilon_\varphi^2\left(\nabla\varphi^j, \nabla\nu_2\right) + \left(\mathcal{B}_\mu'\left(\varphi^j\right), \nu_2\right) \\ + \alpha\left(\left(-\Delta_n\right)^{-1}\left(\varphi^j - m\right)_{\{\theta\}}, \nu_2\right) + \frac{\chi^{AB}}{2}\left(\varphi^j - \varphi^{j-1}, \nu_2\right) = 0\end{aligned} \tag{B.355}$$

for every $\nu_2 \in H^1(\Omega)$. Setting $\nu_2 = \varphi^j - \varphi^{j-1}$ gives (cf. (B.344))

$$\begin{aligned}\frac{1}{\tau}\left\|\varphi^j - \varphi^{j-1}\right\|_{-1}^2 + \varepsilon_\varphi^2\left(\nabla\varphi^j, \nabla\left(\varphi^j - \varphi^{j-1}\right)\right) + \left(\mathcal{B}_\mu'\left(\varphi^j\right), \varphi^j - \varphi^{j-1}\right) \\ + \alpha\left(\left(-\Delta_n\right)^{-1}\left(\varphi^j - m\right)_{\{\theta\}}, \varphi^j - \varphi^{j-1}\right) + \frac{\chi^{AB}}{2}\left\|\varphi^j - \varphi^{j-1}\right\|^2 = 0.\end{aligned} \tag{B.356}$$

ii) We consider the second last term on the left. As in (B.345c)

$$\begin{aligned}&\alpha\left(\left(-\Delta_n\right)^{-1}\left(\varphi^{j-1} - m\right), \varphi^j - \varphi^{j-1}\right) \\ &\quad = \alpha\left(\left(-\Delta_n\right)^{-1}\left(\frac{-\left(\varphi^j - \varphi^{j-1}\right) + \varphi^j + \varphi^{j-1}}{2} - m\right), \varphi^j - \varphi^{j-1}\right) \\ &\quad = -\frac{\alpha}{2}\left\|\varphi^j - \varphi^{j-1}\right\|_{-1}^2 + \frac{\alpha}{2}\left(\left\|\varphi^j - m\right\|_{-1}^2 - \left\|\varphi^{j-1} - m\right\|_{-1}^2\right).\end{aligned}$$

Consequently,

$$\begin{aligned}&\alpha\left(\left(-\Delta_n\right)^{-1}\left(\varphi^j - m\right)_{\{\theta\}}, \varphi^j - \varphi^{j-1}\right) \\ &\quad = \theta\left(\frac{\alpha}{2}\left\|\varphi^j - \varphi^{j-1}\right\|_{-1}^2 + \frac{\alpha}{2}\left(\left\|\varphi^j - m\right\|_{-1}^2 - \left\|\varphi^{j-1} - m\right\|_{-1}^2\right)\right) \\ &\qquad + (1-\theta)\left(-\frac{\alpha}{2}\left\|\varphi^j - \varphi^{j-1}\right\|_{-1}^2 + \frac{\alpha}{2}\left(\left\|\varphi^j - m\right\|_{-1}^2 - \left\|\varphi^{j-1} - m\right\|_{-1}^2\right)\right) \\ &\quad = \frac{\alpha}{2}(2\theta - 1)\left\|\varphi^j - \varphi^{j-1}\right\|_{-1}^2 + \frac{\alpha}{2}\left(\left\|\varphi^j - m\right\|_{-1}^2 - \left\|\varphi^{j-1} - m\right\|_{-1}^2\right).\end{aligned} \tag{B.357}$$

iii) If we substitute (B.346), (B.357) and the remaining parts of (B.345) into (B.356), we find that (cf. (B.347))

$$\begin{aligned}&\frac{1}{\tau}\left\|\varphi^j - \varphi^{j-1}\right\|_{-1}^2 + \frac{\varepsilon_\varphi^2}{2}\left|\varphi^j - \varphi^{j-1}\right|_1^2 + \frac{\varepsilon_\varphi^2}{2}\left(\left|\varphi^j\right|_1^2 - \left|\varphi^{j-1}\right|_1^2\right) \\ &\quad + \left(\mathcal{B}_\mu\left(\varphi^j\right) - \mathcal{B}_\mu\left(\varphi^{j-1}\right), 1\right) - \frac{\chi^{AB}}{4}\left\|\varphi^j - \varphi^{j-1}\right\|^2 + \frac{\alpha}{2}(2\theta - 1)\left\|\varphi^j - \varphi^{j-1}\right\|_{-1}^2 \\ &\qquad + \frac{\alpha}{2}\left(\left\|\varphi^j - m\right\|_{-1}^2 - \left\|\varphi^{j-1} - m\right\|_{-1}^2\right) + \frac{\chi^{AB}}{2}\left\|\varphi^j - \varphi^{j-1}\right\|^2 \leq 0,\end{aligned}$$

or

$$\mathcal{E}_{\mu}^{(m)}\left[\varphi^{j}\right]-\mathcal{E}_{\mu}^{(m)}\left[\varphi^{j-1}\right]+\left(\frac{1}{\tau}+\frac{\alpha}{2}\left(2\theta-1\right)\right)\left\|\varphi^{j}-\varphi^{j-1}\right\|_{-1}^{2} + \frac{\varepsilon_{\varphi}^{2}}{2}\left|\varphi^{j}-\varphi^{j-1}\right|_{1}^{2}+\frac{\chi^{AB}}{4}\left\|\varphi^{j}-\varphi^{j-1}\right\|^{2}\leq 0. \quad \text{(B.358)}$$

If $\theta \geq \frac{1}{2}$, then $2\theta - 1 \geq 0$ and so the last three terms on the left are non-negative. We conclude that, for any $\tau > 0$,

$$\mathcal{E}_{\mu}^{(m)}\left[\varphi^{j}\right]-\mathcal{E}_{\mu}^{(m)}\left[\varphi^{j-1}\right]\leq 0 \qquad \Rightarrow \qquad \mathcal{E}_{\mu}^{(m)}\left[\varphi^{j}\right]\leq\mathcal{E}_{\mu}^{(m)}\left[\varphi^{j-1}\right],$$

which is (5.35).

iv) As in the fully implicit case, we sum (B.358) from $j = 1, \ldots, k \leq M$ to find that

$$\mathcal{E}_{\mu}^{(m)}\left[\varphi^{k}\right] + \frac{\varepsilon_{\varphi}^{2}}{2}\left|\varphi^{j}-\varphi^{j-1}\right|_{1}^{2} + \frac{\chi^{AB}}{4}\left\|\varphi^{j}-\varphi^{j-1}\right\|^{2} \leq \mathcal{E}_{\mu}^{(m)}\left[\varphi^{0}\right] = C < \infty \quad \text{(B.359)}$$

independent of τ and μ. We conclude that (cf. (B.353))

$$\sum_{j=1}^{k}\left\|\varphi^{j}-\varphi^{j-1}\right\|_{1}^{2}\leq C<\infty, \qquad k=1,\ldots,M, \quad \text{(B.360)}$$

independent of τ and μ.

Remark. $\left(\mathbf{R}_{\tau,\theta}^{(m)}\right)$ is unconditionally gradient stable because the linear term appears on the lower time level, as a result of which we have the additional $\frac{\chi^{AB}}{2}\left\|\varphi^{j}-\varphi^{j-1}\right\|^{2}$ term on the left of (B.356) (compared to (B.347)). Another consequence of this is that we did not need to use Poincaré's inequality to arrive at (B.360).

□

B.30 Proof of Lemma 5.2.4

Proof. To start, we present a proof for $\left(\mathbf{R}_{\tau,\theta}^{(m)}\right)$ as it is simpler than the fully implicit case. We adapt the proof of Lemma 3.4 of Bosch et al. (2014a).

i) We show that $\mathcal{N}_{\theta}$ in (5.42a)–(5.42c) is invertible for every $\left(\varphi^{j-1},\omega^{j-1}\right)\in\left(H^{1}\left(\Omega\right)\right)^{2}$, by proving that

$$\mathcal{N}_{\theta}\left(g\left(\boldsymbol{x}^{(j-1,n)}\right)\boldsymbol{\delta}^{(j-1,n)},\boldsymbol{\nu}\right)=\mathbf{0} \qquad \Leftrightarrow \qquad \boldsymbol{\delta}^{(j-1,n)}=\mathbf{0}.$$

To reduce notational clutter, we set $(\delta\varphi,\delta\omega):=\left(\delta\varphi^{(j-1,n)},\delta\omega^{(j-1,n)}\right)$ and $(\varphi,\omega):=\left(\varphi^{j-1},\omega^{j-1}\right)$, and suppose that

$$\left(1+\tau\alpha\theta\right)\left(\delta\varphi,\nu_{1}\right)+\tau\left(\nabla\delta\omega,\nabla\nu_{1}\right)=0 \quad \text{(B.361a)}$$

$$\left(\delta\omega,\nu_{2}\right)-\varepsilon_{\varphi}^{2}\left(\nabla\delta\varphi,\nabla\nu_{2}\right)-\frac{1}{\mu}\left(\chi_{[-1,1]}\left(\varphi\right)\delta\varphi,\nu_{2}\right)=0, \quad \text{(B.361b)}$$

for every $\nu_1, \nu_2 \in H^1(\Omega)$, where we have adopted the shorthand (cf. (5.43))

$$\chi_{[-1,1]}\left(u\right)=\mathbf{1}\left\{u>1\right\}+\mathbf{1}\left\{u<-1\right\}. \quad \text{(B.362)}$$

We show that this necessarily implies that $(\delta\varphi,\delta\omega)=\mathbf{0}$.

We set $\nu_1 = \delta\omega$ in (B.361a), $\nu_2 = -(1+\tau\alpha\theta)\,\delta\varphi$ in (B.361b), add the results and divide by $1+\tau\alpha\theta > 0$ to obtain

$$\frac{\tau}{1+\tau\alpha\theta}\,|\delta\omega|_1^2 + \varepsilon_\varphi^2\,|\delta\varphi|_1^2 \leq 0, \tag{B.363}$$

after using the fact that

$$\frac{1}{\mu}\left(\chi_{[-1,1]}(\varphi)\,\delta\varphi, \delta\varphi\right) \geq 0. \tag{B.364}$$

Since every term on the left above is non-negative,

$$|\delta\omega|_1 = |\delta\varphi|_1 = 0 \qquad \Rightarrow \qquad \nabla\delta\omega = \nabla\delta\varphi = 0, \tag{B.365}$$

and so $\delta\omega$ and $\delta\varphi$ must both be constant. Using these facts in (B.361a) reveals that

$$(\delta\varphi, \nu_1) = 0 \qquad \text{for every} \qquad \nu_1 \in H^1(\Omega) \qquad \Rightarrow \qquad \delta\varphi = 0. \tag{B.366a}$$

Using this fact together with (B.365) in (B.361b) implies that

$$(\delta\omega, \nu_2) = 0 \qquad \text{for every} \qquad \nu_2 \in H^1(\Omega) \qquad \Rightarrow \qquad \delta\omega = 0. \tag{B.366b}$$

Remark. We made no additional assumptions on τ in the proof above.

This first part of the proof implies that we get a well-defined iterate from *any* initial guess (in $\left(H^1(\Omega)\right)^2$). The next part guarantees that the method iterates towards the solution we are actually looking for.

ii) In the first part of the proof we showed that

$$\mathcal{N}_\theta : \left(H^1(\Omega)\right)^2 \mapsto \left(\left(H^1(\Omega)\right)'\right)^2; \qquad \mathcal{N}_\theta(\varphi,\omega)(\delta\varphi,\delta\omega) = (y_1, y_2) =: \boldsymbol{y},$$

has a kernel that includes only $\mathbf{0}$ for any $(\varphi,\omega) \in \left(H^1(\Omega)\right)^2$. Hence, for any given $(y_1, y_1) \in \left(\left(H^1(\Omega)\right)'\right)^2$, there is a unique pair $(\delta\varphi, \delta\omega) \in \left(H^1(\Omega)\right)^2$ with the property that[79]

$$(1+\tau\alpha\theta)(\delta\varphi, \nu_1) + \tau(\nabla\delta\omega, \nabla\nu_1) = \langle y_1, \nu_1\rangle_1 \tag{B.367a}$$

$$(\delta\omega, \nu_2) - \varepsilon_\varphi^2(\nabla\delta\varphi, \nabla\nu_2) - \frac{1}{\mu}\left(\chi_{[-1,1]}(\varphi)\,\delta\varphi, \nu_2\right) = \langle y_2, \nu_2\rangle_1, \tag{B.367b}$$

for every $\nu_1, \nu_2 \in H^1(\Omega)$, that is

$$(\delta\varphi, \delta\omega) = \mathcal{N}_\theta^{-1}(\varphi,\omega)(\boldsymbol{y}).$$

For given $\boldsymbol{y} \in \left(\left(H^1(\Omega)\right)'\right)^2$, we now show that $\|(\delta\varphi,\delta\omega)\|_{H^1(\Omega)\times H^1(\Omega)} \leq C < \infty$. We set $\nu_1 = \delta\omega$ in (B.367a), $\nu_2 = -(1+\tau\alpha\theta)\,\delta\varphi$ in (B.367b), add the results and divide through by $1+\tau\alpha\theta \geq 1$ to obtain

$$\frac{\tau}{1+\tau\alpha\theta}\,|\delta\omega|_1^2 + \varepsilon_\varphi^2\,|\delta\varphi|_1^2 \leq \frac{1}{1+\tau\alpha\theta}\,\langle y_1, \delta\omega\rangle_1 - \langle y_2, \delta\varphi\rangle_1 \leq \langle y_1, \delta\omega\rangle_1 - \langle y_2, \delta\varphi\rangle_1 \tag{B.368}$$

after using (B.364) again.[80] Recalling the definition of $\langle\cdot,\cdot\rangle_1$ in (A.7), we find that[81]

$$\begin{aligned}\frac{\tau}{1+\tau\alpha\theta}\,|\delta\omega|_1^2 + \varepsilon_\varphi^2\,|\delta\varphi|_1^2 &\leq \left|\langle y_1, \delta\omega\rangle_1\right| + \left|\langle y_2, \delta\varphi\rangle_1\right| \\ &\leq \|y_1\|_{1'}\,\|\delta\omega\|_1 + \|y_2\|_{1'}\,\|\delta\varphi\|_1 \\ &\leq \frac{1}{4\beta_1}\,\|\delta\omega\|_1^2 + \frac{1}{4\beta_2}\,\|\delta\varphi\|_1^2 + C\left(\|y_1\|_{1'}^2 + \|y_2\|_{1'}^2\right)\end{aligned} \tag{B.369}$$

by the Cauchy–Schwarz and Young inequalities, where $0 < \beta_1, \beta_2 < \infty$ can be arbitrarily large, and C in the last line is $\max\{\beta_1, \beta_2\} < \infty$, say. Now by Poincaré's inequality (A.2), and since $\left(a^2+b^2\right)^{1/2} \leq a+b$ (for $a, b \geq 0$),

$$\|\delta\varphi\|_1 = \left(\|\delta\varphi\|^2 + |\delta\varphi|_1^2\right)^{1/2} \leq \|\delta\varphi\| + |\delta\varphi|_1 \leq c_P \left|(\delta\varphi, 1)\right| + (1+c_P)\left|\delta\varphi\right|_1,$$

and since $(a+b)^2 \leq 2a^2 + 2b^2$,

$$\|\delta\varphi\|_1^2 \leq 2c_P^2 \left|(\delta\varphi, 1)\right|^2 + 2\left(1+c_P\right)^2 |\delta\varphi|_1^2, \tag{B.370}$$

and similarly for $\|\delta\omega\|_1$. Setting $\nu_1 = 1$ in (B.367a) and $\nu_2 = 1$ in (B.367b) yields[82]

$$(\delta\varphi, 1) = \frac{1}{1+\tau\alpha\theta}\left\langle y_1, 1\right\rangle_1; \qquad (\delta\omega, 1) = \left\langle y_2, 1\right\rangle_1 + \frac{1}{\mu}\left(\chi_{[-1,1]}(\varphi)\,\delta\varphi, 1\right),$$

and so

$$\left|(\delta\varphi, 1)\right| \leq \frac{|\Omega|}{1+\tau\alpha\theta}\left\|y_1\right\|_{1'}; \tag{B.371a}$$

$$\left|(\delta\omega, 1)\right| \leq |\Omega|\left\|y_2\right\|_{1'} + \frac{1}{\mu}\left|(\delta\varphi, 1)\right| \leq C\left(\left\|y_1\right\|_{1'} + \left\|y_2\right\|_{1'}\right), \tag{B.371b}$$

in which C is independent of (φ, ω), and in particular

$$\left|(\delta\varphi, 1)\right|^2 + \left|(\delta\omega, 1)\right|^2 \leq C\left(\left\|y_1\right\|_{1'}^2 + \left\|y_2\right\|_{1'}^2\right). \tag{B.372}$$

Substituting (B.371) via (B.370) and a similar expression for $\|\delta\omega\|_1^2$ into the right side of (B.369) leads to

$$\underbrace{\left(\frac{\tau}{1+\tau\alpha\theta} - \frac{C}{\beta_1}\right)}_{:=C_1}|\delta\omega|_1^2 + \underbrace{\left(\varepsilon_\varphi^2 - \frac{C}{\beta_2}\right)}_{:=C_2}|\delta\varphi|_1^2 \leq C\left(\left\|y_1\right\|_{1'}^2 + \left\|y_2\right\|_{1'}^2\right), \tag{B.373}$$

in which none of the constants depends on (φ, ω). Crucially, we can always pick β_1 and β_2 so that $C_1, C_2 > 0$, and then divide through by the smaller of these to get

$$|\delta\omega|_1^2 + |\delta\varphi|_1^2 \leq \left\{\begin{array}{ll} \dfrac{C_1}{C_2}|\delta\omega|_1^2 + |\delta\varphi|_1^2, & C_2 \leq C_1 \\ |\delta\omega|_1^2 + \dfrac{C_2}{C_1}|\delta\varphi|_1^2, & C_1 < C_2 \end{array}\right\} \leq C\left(\left\|y_1\right\|_{1'}^2 + \left\|y_2\right\|_{1'}^2\right), \tag{B.374}$$

in which C on the right is independent of (φ, ω), but may depend on μ. Using (B.370) again along with (B.374) and (B.372), we conclude that

$$\begin{aligned}\|(\delta\varphi, \delta\omega)\|_{H^1(\Omega)\times H^1(\Omega)}^2 := \|\delta\varphi\|_1^2 + \|\delta\omega\|_1^2 &\leq 2c_P^2\left(\left|(\delta\varphi, 1)\right|^2 + \left|(\delta\omega, 1)\right|^2\right) \\ &\quad + 2\left(1+c_P\right)^2\left(|\delta\varphi|_1^2 + |\delta\omega|_1^2\right) \leq C\left(\left\|y_1\right\|_{1'}^2 + \left\|y_2\right\|_{1'}^2\right). \end{aligned} \tag{B.375}$$

We now adapt the proof above for the implicit problem, $\left(\mathbf{R}_\tau^{(m)}\right)$.

i) We show that $\mathcal{N}$ in (5.42b)–(5.42c) is invertible for every $\left(\varphi^{j-1}, \omega^{j-1}\right) \in \left(H^1(\Omega)\right)^2$. We replace (B.361) with

$$(1+\tau\alpha)(\delta\varphi, \nu_1) + \tau(\nabla\delta\omega, \nabla\nu_1) = 0 \tag{B.376a}$$

$$(\delta\omega, \nu_2) - \varepsilon_\varphi^2(\nabla\delta\varphi, \nabla\nu_2) + \frac{\chi^{AB}}{2}(\delta\varphi, \nu_2) - \frac{1}{\mu}\left(\chi_{[-1,1]}(\varphi)\,\delta\varphi, \nu_2\right) = 0, \tag{B.376b}$$

for every $\nu_1, \nu_2 \in H^1(\Omega)$. We set $\nu_1 = \delta\omega$ in (B.376a) and $\nu_2 = -(1+\tau\alpha)\,\delta\varphi$ in (B.376b), add the results and divide by $1 + \tau\alpha\theta > 0$ to obtain (cf. (B.363)[83])

$$\frac{\tau}{1+\tau\alpha}\,|\delta\omega|_1^2 + \varepsilon_\varphi^2\,|\delta\varphi|_1^2 \leq \frac{\chi^{AB}}{2}\,\|\delta\varphi\|^2\,. \tag{B.377}$$

For the $\|\delta\varphi\|^2$ term on the right, we set $\nu_1 = \frac{\chi^{AB}}{2}\delta\varphi$ in (B.376a).

- Suppose $\alpha > 0$. Then,

$$\begin{aligned}\frac{\chi^{AB}}{2}\,\|\delta\varphi\|^2 = \frac{-\tau\chi^{AB}}{2\,(1+\tau\alpha)}\,(\nabla\delta\omega, \nabla\delta\varphi) &\leq \frac{\tau\chi^{AB}}{2\,(1+\tau\alpha)}\,|\delta\omega|_1\,|\delta\varphi|_1 \\ &\leq \frac{\tau}{(1+\tau\alpha)^2}\,|\delta\omega|_1^2 + \tau\left(\frac{\chi^{AB}}{2}\right)^2\frac{1}{4}\,|\delta\varphi|_1^2 \end{aligned} \tag{B.378}$$

  by the Cauchy–Schwarz and Young inequalities. Substituting this back into (B.377) gives

$$\underbrace{\frac{\tau^2\alpha}{(1+\tau\alpha)^2}}_{>0}\,|\delta\omega|_1^2 + \left(\varepsilon_\varphi^2 - \frac{\left(\chi^{AB}\right)^2}{16}\tau\right)|\delta\varphi|_1^2 \leq 0 \tag{B.379}$$

  after some rearrangement. If we now assume that

$$\tau \leq \frac{16\varepsilon_\varphi^2}{\left(\chi^{AB}\right)^2} \qquad \Rightarrow \qquad \varepsilon_\varphi^2 - \frac{\left(\chi^{AB}\right)^2}{16}\tau > 0, \tag{B.380}$$

  then both coefficients in (B.379) are non-negative as in (B.363), and we conclude that (B.365) holds here too, viz. $\delta\omega$ and $\delta\varphi$ are both constant. Using these facts in (B.376a), we get to (B.366a) once again viz. $\delta\varphi = 0$. Using this new information in (B.376b) leads to (B.366b) again viz. $\delta\omega = 0$, too.

- Suppose $\alpha = 0$. In this case, (B.377) is actually

$$\tau\,|\delta\omega|_1^2 + \varepsilon_\varphi^2\,|\delta\varphi|_1^2 \leq \frac{\chi^{AB}}{2}\,\|\delta\varphi\|^2\,, \tag{B.381}$$

  and so instead of (B.378), we use

$$\frac{\chi^{AB}}{2}\,\|\delta\varphi\|^2 = \frac{-\tau\chi^{AB}}{2}\,(\nabla\delta\omega, \nabla\delta\varphi) \leq \frac{\tau}{2}\,|\delta\omega|_1^2 + \frac{\tau}{2}\left(\frac{\chi^{AB}}{2}\right)^2|\delta\varphi|_1^2\,. \tag{B.382}$$

  Substituting this back into (B.381) leads to

$$\frac{\tau}{2}\,|\delta\omega|_1^2 + \left(\varepsilon_\varphi^2 - \frac{\left(\chi^{AB}\right)^2}{8}\tau\right)|\delta\varphi|_1^2 \leq 0, \tag{B.383}$$

  which has non-negative coefficients on the left (as in (B.379)) if (cf. (B.380))

$$\tau \leq \frac{8\varepsilon_\varphi^2}{\left(\chi^{AB}\right)^2} \qquad \Rightarrow \qquad \varepsilon_\varphi^2 - \frac{\left(\chi^{AB}\right)^2}{8}\tau > 0. \tag{B.384}$$

  The rest of the argument is the same as for $\alpha > 0$.

Remark. The location of the linear term at the upper time level in $\left(\mathbf{R}_\tau^{(m)}\right)$ resulted in an additional term in the derivative (compared to $\left(\mathbf{R}_{\tau,\theta}^{(m)}\right)$). This, in turn, led to *significant* additional complexity and a restriction on τ in the proof above.

ii) We prove that $\left\| \left[\mathcal{N}\left(\varphi^j, \omega^j\right) \right]^{-1} \right\|_{\mathcal{L}\left(\left(\left(H^1(\Omega)\right)'\right)^2, \left(H^1(\Omega)\right)^2\right)}$ is bounded. (B.367) is replaced with

$$(1+\tau\alpha\theta)\left(\delta\varphi, \nu_1\right) + \tau\left(\nabla\delta\omega, \nabla\nu_1\right) = \left\langle y_1, \nu_1\right\rangle_1 \tag{B.385a}$$

$$\left(\delta\omega, \nu_2\right) - \varepsilon_\varphi^2\left(\nabla\delta\varphi, \nabla\nu_2\right) + \frac{\chi^{AB}}{2}\left(\delta\varphi, \nu_2\right) - \frac{1}{\mu}\left(\chi_{[-1,1]}\left(\varphi\right)\delta\varphi, \nu_2\right) = \left\langle y_2, \nu_2\right\rangle_1, \tag{B.385b}$$

for every $\nu_1, \nu_2 \in H^1(\Omega)$, leading to (cf. (B.369))

$$\frac{\tau}{1+\tau\alpha\theta}\left|\delta\omega\right|_1^2 + \varepsilon_\varphi^2\left|\delta\varphi\right|_1^2 \leq \frac{1}{4\beta_1}\left\|\delta\omega\right\|_1^2 + \frac{1}{4\beta_2}\left\|\delta\varphi\right\|_1^2 + \frac{\chi^{AB}}{2}\left\|\delta\varphi\right\|^2 + C\left(\left\|y_1\right\|_{1'}^2 + \left\|y_2\right\|_{1'}^2\right), \tag{B.386}$$

which once again features the troublesome $\left\|\delta\varphi\right\|^2$ term on the right. To deal with it, we argue as in the first part above: we set $\nu_1 = \frac{1}{2}\chi^{AB}\delta\varphi$ in (B.385a) and rearrange, to find that if $\alpha > 0$, then

$$\frac{\chi^{AB}}{2}\left(1+\tau\alpha\theta\right)\left\|\delta\varphi\right\|^2 + \frac{\chi^{AB}}{2}\tau\left(\nabla\delta\omega, \nabla\delta\varphi\right) = \frac{\chi^{AB}}{2}\left\langle y_1, \delta\varphi\right\rangle_1$$

and so (cf. (B.378))

$$\frac{\chi^{AB}}{2}\left\|\delta\varphi\right\|^2 \leq \frac{\tau}{\left(1+\tau\alpha\right)^2}\left|\delta\omega\right|_1^2 + \tau\left(\frac{\chi^{AB}}{2}\right)^2\frac{1}{4}\left|\delta\varphi\right|_1^2 + \beta_2\left(\frac{\chi^{AB}}{2\left(1+\tau\alpha\theta\right)}\right)^2\left\|y_1\right\|_{1'}^2 + \frac{1}{4\beta_2}\left\|\delta\varphi\right\|_1^2$$

after a judicious application of Young's inequality. Substituting this latter expression into the right side of (B.386) leads to (cf. (B.369))

$$C_1\left|\delta\omega\right|_1^2 + C_2\left|\delta\varphi\right|_1^2 \leq \frac{1}{4\beta_1}\left\|\delta\omega\right\|_1^2 + \frac{1}{2\beta_2}\left\|\delta\varphi\right\|_1^2 + C\left(\left\|y_1\right\|_{1'}^2 + \left\|y_2\right\|_{1'}^2\right) \tag{B.387}$$

in which $C_1, C_2 > 0$ if τ satisfies (B.380). Moreover, all of the constants are independent of (φ, ω).

For $\alpha = 0$, a similar argument, with a time-step restriction like (B.384) leads to an inequality with the same structure as (B.387).

Corresponding to (B.371), we use (B.385) to find that

$$\left(\delta\varphi, 1\right) = \frac{1}{1+\tau\alpha\theta}\left\langle y_1, 1\right\rangle_1; \qquad \left(\delta\omega, 1\right) = \left\langle y_2, 1\right\rangle_1 - \frac{\chi^{AB}}{2}\left(\delta\varphi, 1\right) + \frac{1}{\mu}\left(\chi_{[-1,1]}\left(\varphi\right)\delta\varphi, 1\right),$$

and so

$$\left|\left(\delta\varphi, 1\right)\right| \leq \frac{\left|\Omega\right|}{1+\tau\alpha\theta}\left\|y_1\right\|_{1'}; \tag{B.388a}$$

$$\left|\left(\delta\omega, 1\right)\right| \leq \left|\Omega\right|\left\|y_2\right\|_{1'} + \left(\frac{1}{\mu} + \frac{\chi^{AB}}{2}\right)\left|\left(\delta\varphi, 1\right)\right| \leq C\left(\left\|y_1\right\|_{1'} + \left\|y_2\right\|_{1'}\right). \tag{B.388b}$$

We can thus argue as we did after (B.371) for $\left(\mathbf{R}_{\tau,\theta}^{(m)}\right)$.

□

B.31 Proof of Lemma 5.3.6

Proof.

i) Existence and uniqueness: the proof is essentially identical to what we did in Section 5.1.1, since $V^h \subset H^1(\Omega)$.

Remark. We omit the details, but note that we would need to formulate fully discrete, *non-local* versions of $(\mathbf{Q}_{\tau,\theta})$, $(\mathbf{P}_{\tau,\theta})$ and $\left(\mathbf{R}_{\tau,\theta}^{(-)}\right)$ of Section 5.1.1. We derive $\left(\mathbf{R}_{\tau,\theta,h}^{(m)}\right)$ and $\left(\mathbf{R}_{\tau,h}^{(m)}\right)$ above after replacing each $\overline{\varphi_h^j}$ with m, as we did in the time discretisation.

ii) Mass control: setting $u_h = 1$ in (5.57b), we find, after rearranging, that

$$\left(\varphi_h^j, 1\right) + \tau\alpha\left(\varphi_h^j - m, 1\right)_{\{\theta\}} = \left(\varphi_h^{j-1}, 1\right),$$

after noting that $\overline{f_h^j} = 0$ for each j, and so, as in (5.23),

$$\overline{\mathring{\varphi}_h^j} = \left(\frac{1 + \tau\alpha\theta - \tau\alpha}{1 + \tau\alpha\theta}\right)^j \overline{\mathring{\varphi}_h^0}. \tag{B.389}$$

If $\overline{\varphi_h^0} = m$ as in (5.57a), viz. $\overline{\mathring{\varphi}_h^0} = 0$, then $\overline{\mathring{\varphi}_h^j} = 0$ for every j, that is, $\varphi_h^j \in V_m^h$.

iii) If $\theta = 1$ (fully implicit), we are led to the fully discrete version of (5.25)

□

B.32 Fully discrete boundedness: proof of Lemma 5.3.7

Proof. As usual, the basic idea is that we replace each reference to $H^1(\Omega)$ in the proof in Appendix B.27 with a reference to $V^h \subset H^1(\Omega)$. Each occurrence of $-\Delta_n$ (and its inverse) is replaced with $-\Delta_h$, and every norm $\|\cdot\|_{-1}$ with $\|\cdot\|_{-h}$. We discuss some of the specifics in relation to $\left(\mathbf{R}_{\tau,h}^{(m)}\right)$.

i) The fully discrete version of (B.280) (which forms the basis of most of our analysis) is

$$\psi_h^j := \omega_h^j + \alpha\left(-\Delta_h\right)^{-1}\left(\varphi_h^j - m\right) + F_h^j, \qquad F_h^j := \left(-\Delta_h\right)^{-1}\left(-f_h^j\right), \tag{B.390a}$$

so that (cf. (5.57))

$$\left(\delta^{(\tau)}\varphi_h^j, u_h\right) + \left(\nabla\psi_h^j, \nabla u_h\right) = 0 \tag{B.390b}$$

for every $u_h \in V^h$, and

$$\left(\psi_h^j, v_h\right) = \varepsilon_\varphi^2\left(\nabla\varphi_h^j, \nabla v_h\right) - \frac{\chi^{AB}}{2}\left(\varphi_h^j, v_h\right) + \left(\zeta_\mu\left(\varphi_h^j\right), v_h\right) + \alpha\left(\left(-\Delta_h\right)^{-1}\left(\varphi_h^j - m\right), v_h\right) + \left(F_h^j, v_h\right) \tag{B.390c}$$

for every $v_h \in V^h$.

ii) We replace (B.293) with

$$\varepsilon_\varphi^2\left(\left|\varphi_h^j\right|_1^2 - \left|\varphi_h^{j-1}\right|_1^2\right) + 2\left(\left(\mathcal{B}_\mu\left(\varphi^j\right), 1\right) - \left(\mathcal{B}_\mu\left(\varphi_h^{j-1}\right), 1\right)\right) + \frac{\tau}{2}\left|\psi_h^j\right|_1^2 \leq 4\tau\left\|f_h^j\right\|_{-h}^2 + \alpha^2 c_P^4 \tau\left|\varphi_h^j\right|_1^2; \tag{B.391}$$

summing this through $j = 1, \ldots, k$ yields (cf. (B.294))

$$\left(\varepsilon_\varphi^2 - \alpha^2 c_P^4 \tau\right)\left|\varphi_h^k\right|_1^2 + \frac{1}{2}\sum_{j=1}^k \tau\left|\psi_h^j\right|_1^2 \leq \varepsilon_\varphi^2\left|\varphi_h^0\right|_1^2 + \frac{1}{\mu}\left(\left(\varphi_h^0 - 1\right)_+^2 + \left(\varphi_h^0 + 1\right)_-^2, 1\right) + \frac{\chi^{AB}}{2}\left(|\Omega| + \left\|\varphi_h^0\right\|^2\right) + 2C_0\mu_{\max}|\Omega| + 4\sum_{j=1}^k \tau\left\|f_h^j\right\|_{-h}^2 + \frac{2\alpha^2 c_P^4}{\varepsilon_\varphi^2}\sum_{j=1}^{k-1}\tau\frac{\varepsilon_\varphi^2}{2}\left|\varphi_h^j\right|_1^2. \tag{B.392}$$

We consider each term on the right of (B.392).

- $\left|\varphi_h^0\right|_1 \leq C\left(\varphi^0\right)$ independent of h by (5.60).
- For the second term, we *cannot* appeal to (B.223b), because it is not necessarily true that $\left\|\varphi_h^0\right\|_{0,\infty} \leq 1$, as we noted in Section 5.3.5. On the other hand,

$$\left(\left(\varphi_h^0-1\right)_+^2+\left(\varphi_h^0+1\right)_-^2,1\right) \leq \int_\Omega \left(\left\|\varphi_h^0\right\|_{0,\infty}-1\right)_+^2 \mathrm{d}\Omega = |\Omega|\left(\left\|\varphi_h^0\right\|_{0,\infty}-1\right)_+^2$$

and this term vanishes if $\left\|\varphi_h^0\right\|_{0,\infty} \leq 1$. If $\left\|\varphi_h^0\right\|_{0,\infty} > 1$, then according to (5.61),

$$\begin{aligned}\frac{1}{\mu}\left(\left(\varphi_h^0-1\right)_+^2+\left(\varphi_h^0+1\right)_-^2,1\right) &\leq \frac{|\Omega|}{\mu}\left(\left\|\varphi_h^0\right\|_{0,\infty}-1\right)^2 \\ &= \frac{|\Omega|}{\mu}\left(\left\|\varphi_h^0\right\|_{0,\infty}^2+2\left\|\varphi_h^0\right\|_{0,\infty}+1\right) \leq \frac{C\left(\Omega,\varphi^0\right)}{\mu}\end{aligned}$$

in which C is independent of h (for $h<1$, say), but depends on μ.

Remark. (5.61) says that if $\left\|\varphi^0\right\|_{0,\infty}=1$, then $\left\|\varphi_h^0\right\|_{0,\infty} \downarrow 1$ as $h \downarrow 0$ for any $\mu>0$.

- (5.60) gives us a bound on $\left\|\varphi_h^0\right\|^2$, independent of h and τ.
- For the second last sum on the right, we use (A.70), (A.63a) and the definition of f_h^j in Section 5.3.4, to write

$$\begin{aligned}\sum_{j=1}^k \tau\left\|f_h^j\right\|_{-h}^2 \leq c_P^2\sum_{j=1}^k \tau\left\|f_h^j\right\|^2 &= c_P^2\sum_{j=1}^k \tau\left\|P^{(h)}\widetilde{f}^j\right\|^2 \\ &\leq c_P^2\sum_{j=1}^k \tau\left\|\widetilde{f}^j\right\|^2 \leq c_P^2\left\{\max_{0\leq j\leq M}\left\|\widetilde{f}^j\right\|^2\right\}\underbrace{\sum_{j=1}^M \tau}_{=T} = C<\infty,\end{aligned}$$

independent of h and τ by (5.3) and (5.4).

Hence we can replace the C_1 in the fully discrete version of (B.297b) with something independent of h and τ, but not μ.

iii) The next substantial difference occurs when we try to establish a fully discrete version of (B.300). Certainly (cf. (B.300a)),

$$\begin{aligned}\left(\psi_h^j,u_h\right) = \varepsilon_\varphi^2\left(-\Delta_h\varphi_h^j,u_h\right)-\frac{\chi^{AB}}{2}\left(\varphi_h^j,u_h\right)+\left(\zeta_\mu\left(\varphi_h^j\right),u_h\right) \\ +\alpha\left((-\Delta_h)^{-1}\left(\varphi_h^j-m\right),u_h\right)+\left(F_h^j,u_h\right) \quad \text{(B.393)}\end{aligned}$$

for every $u_h \in V^h$, but since $\zeta_\mu\left(\varphi_h^j\right) \notin V^h$ for $\varphi_h^j \in V^h$, there is no directly comparable, discrete version of (B.300b). Likewise, because of (5.61), $\zeta_\mu\left(\varphi_h^0\right) \neq 0$ and $\zeta_\mu\left(\varphi_h^0\right) \notin V^h$. Hence, we write (B.393) for $j=0$ as (cf. (B.300c))

$$V^h \ni \psi_h^0 = \varepsilon_\varphi^2\left(-\Delta_h\right)\varphi_h^0-\frac{\chi^{AB}}{2}\varphi_h^0+P^{(h)}\underbrace{\zeta_\mu\left(\varphi_h^0\right)}_{\neq 0}+\alpha\left(-\Delta_h\right)^{-1}\left(\varphi_h^0-m\right)+F_h^0. \quad \text{(B.394)}$$

We notice the impact of this when we write down the fully discrete version of (B.306),

$$\left|\psi_h^k\right|_1^2+\varepsilon_\varphi^2\sum_{j=1}^k \tau\left|\delta^{(\tau)}\varphi_h^j\right|_1^2 \leq \left|\psi_h^0\right|_1^2+C\left(\chi^{AB},\varepsilon_\varphi\right)\sum_{j=1}^M \tau\left\|\delta^{(\tau)}\varphi_h^j\right\|_{-h}^2+\sum_{j=1}^M \tau\left\|\delta^{(\tau)}F_h^j\right\|^2, \quad \text{(B.395)}$$

and seek to bound the terms on the right, independent of h and τ.

iv) For $\left|\psi_h^0\right|_1^2$ on the right of (B.395), we use (B.394) to write

$$\nabla\psi_h^0 = \varepsilon_\varphi^2 \nabla\left(-\Delta_h\varphi_h^0\right) - \frac{\chi^{AB}}{2}\nabla\varphi_h^0 + \nabla\left(P^{(h)}\zeta_\mu\left(\varphi_h^0\right)\right) + \alpha\nabla\left(-\Delta_h\right)^{-1}\left(\varphi_h^0 - m\right) + \nabla F_h^0,$$

and so (cf. (B.236)) if we take an $L^2(\Omega)$ norm above, we need to bound each term on the right of

$$\left|\psi_h^0\right|_1 \leq \varepsilon_\varphi^2\left|-\Delta_h\varphi_h^0\right|_1 + \frac{\chi^{AB}}{2}\left|\varphi_h^0\right|_1 + \left|P^{(h)}\zeta_\mu\left(\varphi_h^0\right)\right|_1 + \alpha\left\|\varphi_h^0 - m\right\|_{-h} + \left\|f_h^0\right\|_{-h}, \tag{B.396}$$

independent of h. We have used (5.53) to re-write the last two terms above. We consider each term in turn:

- Since $\varphi_h^0 = P_m^{(\star)}\varphi^0$, Lemma A.1.17 implies that $-\Delta_h\varphi_h^0 = P^{(h)}\left(-\Delta\varphi^0\right)$ and so
$$\left|-\Delta_h\varphi_h^0\right|_1 = \left|P^{(h)}\left(-\Delta\varphi^0\right)\right|_1 \leq \left|-\Delta\varphi^0\right|_1 = C\left(\varphi^0\right),$$
which is independent of h, by the assumptions we made on φ^0 in Section 5.3.4.
- For the second term, $\left|\varphi_h^0\right|_1 \leq C\left(\varphi^0\right)$ independent of h by (5.60).
- For the third term, (A.63b) and (4.14a) give
$$\left|P^{(h)}\zeta_\mu\left(\varphi_h^0\right)\right|_1 \leq \left|\zeta_\mu\left(\varphi_h^0\right)\right|_1 = \left\|\nabla\zeta_\mu\left(\varphi_h^0\right)\right\| = \left\|\zeta_\mu'\left(\varphi_h^0\right)\nabla\varphi_h^0\right\| \leq \frac{1}{\mu}\left|\varphi_h^0\right|_1 = C,$$
which is bounded, independent of h and τ (but not μ), by (5.60).
- Using (A.70) in the fourth term,
$$\alpha\left\|\varphi_h^0 - m\right\|_{-h} \leq \alpha c_P\left\|\varphi_h^0 - m\right\| \leq \alpha c_P\left(\left\|\varphi_h^0\right\| + |m|\,|\Omega|^{1/2}\right) = C < \infty,$$
independent of h and τ by (5.60).
- Finally, using (A.70), (A.63a) and the definition of f_h^0 in Section 5.3.4,
$$\left\|f_h^0\right\|_{-h} \leq c_P\left\|f_h^0\right\| = c_P\left\|P^{(h)}\widetilde{f}^0\right\| \leq c_P\left\|\widetilde{f}^0\right\| = C < \infty,$$
independent of h and τ by (5.3).

Hence, we can bound $\left|\psi_h^0\right|_1^2$, independent of h.

v) We can show that

$$\sum_{j=1}^M \tau\left\|\delta^{(\tau)}\varphi_h^j\right\|_{-h}^2 \leq C, \tag{B.397}$$

independent of h and τ, on the right of (B.395), if we argue as we did to establish (B.299), replacing the reference to $\left(-\Delta_n\right)^{-1}$ with $\left(-\Delta_h\right)^{-1}$.

vi) Finally, we bound $\sum_{j=1}^M \tau\left\|\delta^{(\tau)}F_h^j\right\|^2$ on the right of (B.395). Using the Poincaré and Cauchy–Schwarz inequalities, the linearity of $\left(-\Delta_h\right)^{-1}$, (A.70) and (A.75c), we determine that

$$\begin{aligned}\sum_{j=1}^M \tau\left\|\delta^{(\tau)}F_h^j\right\|^2 &\leq c_P\sum_{j=1}^M \tau\left\|\delta^{(\tau)}f_h^j\right\|_{-h}^2 \leq c_P^3\sum_{j=1}^M \tau\left\|\delta^{(\tau)}f_h^j\right\|^2 \\ &= c_P^3\sum_{j=1}^M\left\|\int_{t_{j-1}}^{t_j}\partial_t f_h\,\mathrm{d}t\right\|^2 \leq c_P^3\sum_{j=1}^M\left\|\tau^{1/2}\left(\int_{t_{j-1}}^{t_j}\left(\partial_t f_h\right)^2\mathrm{d}t\right)^{1/2}\right\|^2 \\ = c_P^3\sum_{j=1}^M \tau\int_{t_{j-1}}^{t_j}\left\|\partial_t f_h\right\|^2\mathrm{d}t &\leq c_P^3\sum_{j=1}^M \tau\int_{t_{j-1}}^{t_j}\left\|\partial_t\widetilde{f}\right\|^2\mathrm{d}t \leq c_P^3T^2\max_{0\leq t\leq T}\left\|\partial_t\widetilde{f}\,(t)\right\|^2 = C,\end{aligned} \tag{B.398}$$

which is bounded, independent of h and τ by the regularity of f (and $\widetilde{f}$ below) in (4.55). We also made (5.4) continuous (in time) by specifying that, for $t \in (t_{j-1}, t_j]$, (cf. (B.307))

$$\widetilde{f}(t) := \sum_i a_i f\big(\underbrace{t_i - (t_j - t)}_{:=\widetilde{t}_i}\big) \quad \text{with} \quad a_i = 0 \quad \text{if} \quad \widetilde{t}_i < 0 \text{ (for } j = 1),$$
$$\text{and} \quad f_h(t) := P^{(h)}\widetilde{f}(t); \qquad \partial_t f_h(t) = P^{(h)} \sum_i a_i f'\left(\widetilde{t}_i\right).$$

Remark. The last part of (B.398) shows that

$$\partial_t f_h \in \ell^2\left((j\tau)_{j=0}^M; L^2(\Omega)\right).$$

vii) It follows from (B.395) and the results above that (cf. (B.311))

$$\max_{0\le k\le M} \left|\psi_h^k\right|_1 \le C \tag{B.399}$$

independent of h and τ (but not necessarily μ). Using this, we bound the sequence $\left(\left\|\psi_h^k\right\|\right)$. According to Poincaré's inequality (A.2),

$$\left\|\psi_h^k\right\| \le c_P\left\{\left|\left(\psi_h^k, 1\right)\right| + \left|\psi_h^k\right|_1\right\}, \tag{B.400}$$

i.e. we need to estimate $\left|\left(\psi_h^k, 1\right)\right|$. Setting $u_h = 1$ in (B.393) gives

$$\left|\left(\psi_h^j, 1\right)\right| \le \frac{\chi^{AB}}{2}\left|\left(\varphi_h^j, 1\right)\right| + \left|\left(\zeta_\mu\left(\varphi_h^j\right), 1\right)\right| \le \frac{\chi^{AB}}{2}|m||\Omega| + \frac{C}{\mu}\left\|\varphi_h^j\right\| < C$$

independent of j, h and τ by (5.63a). Taking this, (B.400) and (B.399) yields

$$\max_{0\le k\le M}\left\|\psi_h^k\right\|_1 \le C \tag{B.401}$$

independent of h and τ (but not necessarily μ).

viii) We set $u_h = -\Delta_h\varphi_h^j$ for each $j = 1, \dots, M$ in (B.393) and find that (cf. (B.312))

$$\varepsilon_\varphi^2\left\|-\Delta_h\varphi_h^j\right\|^2 \le \frac{1}{2}\left|\psi_h^j\right|_1^2 + \left(\frac{\chi^{AB}}{2} + 1\right)\left|\varphi_h^j\right|_1^2 + \frac{1}{2}\left\|f_h^j\right\|_{-h}^2, \tag{B.402}$$

after noting that (cf. (B.175)[84])

$$\left(\zeta_\mu\left(\varphi_h^j\right), -\Delta_h\varphi_h^j\right) = \left(\nabla\zeta_\mu\left(\varphi_h^j\right), \nabla\varphi_h^j\right) = \left(\zeta_\mu'\left(\varphi_h^j\right), \left(\nabla\varphi_h^j\right)^2\right) \ge 0,$$

and

$$0 \le \left\|\varphi_h^j - \overline{\varphi_h^j}\right\|^2 = \left(\nabla\left(-\Delta_h\right)^{-1}\left(\varphi_h^j - \overline{\varphi_h^j}\right), \nabla\varphi_h^j\right) = \left(\left(-\Delta_h\right)^{-1}\left(\varphi_h^j - \overline{\varphi_h^j}\right), -\Delta_h\varphi_h^j\right).$$

Each term on the right of (B.402) is bounded, independent of h and τ. Consequently,

$$\max_{0\le j\le M}\left\|-\Delta_h\varphi_h^j\right\| \le C < \infty, \tag{B.403}$$

independent of h, τ. Using (A.73), we conclude that each

$$\left\|\varphi_h^j - m\right\|_{0,\infty} = \left\|\varphi_h^j - \overline{\varphi_h^j}\right\|_{0,\infty} \le C < \infty,$$

and so

$$\left\|\varphi_h^j\right\|_{0,\infty} = \left\|\varphi_h^j - m + m\right\|_{0,\infty} \le \left\|\varphi_h^j - m\right\|_{0,\infty} + |m||\Omega| \le C < \infty,$$

for $j = 1, \dots, M$ independent of h, τ, and similarly from (5.61) for $j = 0$. Hence

$$\left\|\varphi_h^j\right\|_{0,\infty} \le C < \infty \qquad \text{for} \qquad j = 0, 1, \dots, M,$$

independent of h and τ, which is (5.63c), if $\tau \lesssim \varepsilon_\varphi^2$.

The ideas are the same for $\left(\mathbf{R}^{(m)}_{\tau,\theta,h}\right)$. The main difference is that we replace (B.390c) with (cf. (B.313))

$$\left(\psi^j_h, v_h\right) = \varepsilon^2_\varphi \left(\nabla\varphi^j_h, \nabla v_h\right) - \frac{\chi^{AB}}{2}\left(\varphi^j_h, v_h\right) + \left(\zeta_\mu\left(\varphi^j_h\right), v_h\right) + \alpha\left(\left(-\Delta_h\right)^{-1}\left(\varphi^j_h - m\right)_{\{\theta\}}, v_h\right) + \left(F^j_h, v_h\right) + \frac{\chi^{AB}}{2}\left(\varphi^j_h - \varphi^{j-1}_h, v_h\right) \quad \text{(B.404)}$$

for every $v_h \in V^h$.

Finally, in both schemes, we can prove that

$$\sum_{j=1}^{M}\left\|\varphi^j_h - \varphi^{j-1}_h\right\|^2_1 < C, \quad \text{(B.406)}$$

at the end of the fully discrete version of the energy decay proof, in Appendix B.34 on p. 430 (the details are obvious and we omit them).

□

B.33 Fully discrete stability: proof of Lemma 5.3.8

Proof. The proof is structurally identical to that for Lemma 5.1.8 above. We replace each reference to $H^1(\Omega)$ with $V^h \subset H^1(\Omega)$. Each occurrence of $-\Delta_n$ (and its inverse) is replaced with $-\Delta_h$, and every norm $\|\cdot\|_{-1}$ with $\|\cdot\|_{-h}$.

□

B.34 Fully discrete energy decay: proof of Lemma 5.3.9

Proof.

i) The proof is structurally identical to that of Lemma 5.1.9 above. We replace each reference to $H^1(\Omega)$ with $V^h \subset H^1(\Omega)$. Each occurrence of $-\Delta_n$ (and its inverse) is replaced with $-\Delta_h$, and every norm $\|\cdot\|_{-1}$ with $\|\cdot\|_{-h}$. The main idea is to consider the energy functional in (5.59), from which we determine that

$$\mathcal{E}^{(m)}_{\mu,h}\left[\varphi^j_h\right] - \mathcal{E}^{(m)}_{\mu,h}\left[\varphi^{j-1}_h\right] = \frac{\varepsilon^2_\varphi}{2}\left(\left|\varphi^j_h\right|^2_1 - \left|\varphi^{j-1}_h\right|^2_1\right) + \left(\mathcal{B}_\mu\left(\varphi^j_h\right) - \mathcal{B}_\mu\left(\varphi^{j-1}_h\right), 1\right) + \frac{\alpha}{2}\left(\left\|\varphi^j_h - m\right\|^2_{-h} - \left\|\varphi^{j-1}_h - m\right\|^2_{-h}\right). \quad \text{(B.405)}$$

ii) The fully discrete version of (B.353) and (B.360) is

$$\sum_{j=1}^{k}\left\|\varphi^j_h - \varphi^{j-1}_h\right\|^2_1 \leq C, \quad \text{(B.406)}$$

in which the bound is independent of h and τ, but not μ. To make this statement, we need to bound $\mathcal{E}^{(m)}_{\mu,h}\left[\varphi^0_h\right]$, independent of h and τ. Using (5.59), (B.223b), (5.60) and (A.70), we find that

$$\mathcal{E}^{(m)}_{\mu,h}\left[\varphi^0_h\right] := \frac{\varepsilon^2_\varphi}{2}\left|\varphi^0_h\right|^2_1 + \left(\mathcal{B}_\mu\left(\varphi^0_h\right), 1\right) + \frac{\alpha}{2}\left\|\varphi^0_h - m\right\|^2_{-h} \leq \frac{\varepsilon^2_\varphi}{2}\left\|\varphi^0_h\right\|^2_1 + \frac{\chi^{AB}}{4}\left(|\Omega| + \left\|\varphi^0_h\right\|^2_1\right) + \frac{\alpha c^4_P}{2}\left\|\varphi^0_h\right\|^2_1 \leq C\left(\varphi^0\right)$$

which is clearly independent of h and τ, but not μ. As an immediate consequence of (B.406),

$$\sum_{j=1}^{k} \tau \left\| \varphi_h^j - \varphi_h^{j-1} \right\|_1^2 \leq \tau C \leq CT = C, \tag{B.407}$$

since $0 < \tau \leq T$, in which C depends on T.

□

B.35 Convergence: proof of Theorem 5.3.10

Our proof is adapted from that of Theorem 3.5 of Blowey and Elliott (1992). The following elements of approximation theory are useful:

- We cite equation (4.4.28) of Brenner and Scott (2007) with $p = 2$ and $m = 1, 2$ (cf. (3.17) of Blowey and Elliott (1992) and Theorem 3.1.5 of Ciarlet (1978)), which says that if $\nu \in H^2(\Omega)$, then

$$\left\| \nu - \mathcal{I}^{(h)} \nu \right\|_s \leq C h^{2-s} |\nu|_2 ; \qquad \left\| \nu - \mathcal{I}^{(h)} \nu \right\|_s \leq C h^{1-s} |\nu|_1 ; \qquad \text{for} \qquad s = 0, 1. \tag{B.408}$$

- As in (3.21) of Blowey and Elliott (1992), for every $u_h \in V_*^h$,

$$\left\| \left((-\Delta_n)^{-1} - (-\Delta_h)^{-1} \right) u_h \right\| \leq C h^2 \|u_h\|_1 . \tag{B.409}$$

Proof. From our earlier remarks, we assume that

$$\overline{\varphi(t)} = m \qquad \text{for every } t \in [0, T] \qquad \text{and} \qquad \overline{\varphi_h^j} = m \qquad \text{for each } j = 0, \ldots, M. \tag{B.410}$$

To start, we consider the fully implicit formulation, $\left(\mathbf{R}_{\tau,h}^{(m)} \right)$.

i) If (φ_j, ω_j) solves $\left(\mathbf{R}_{\mu,\mathbf{f}}^{(\mathbf{m})} \right)$ exactly at t_j, then

$$\begin{aligned} (\partial_t \varphi_j, u) + (\nabla \omega_j, \nabla u) + \alpha (\varphi_j - m, u) &= (f_j, u) \\ (\omega_j, v) = \varepsilon_\varphi^2 (\nabla \varphi_j, \nabla v) + \left(\mathcal{B}_\mu'(\varphi_j), v \right) & \end{aligned}$$

for every $u, v \in H^1(\Omega)$ and $j = 1, \ldots, M$. Equivalently, we can write (cf. (B.215b), (B.280), (B.390))

$$(\partial_t \varphi_j, u) + (\nabla \psi_j, \nabla u) = 0 \tag{B.411a}$$

$$(\psi_j, v) = \varepsilon_\varphi^2 (\nabla \varphi_j, \nabla v) - \frac{\chi^{AB}}{2} (\varphi_j, v) + (\zeta_\mu(\varphi_j), v) + \alpha \left((-\Delta_n)^{-1} (\varphi_j - m), v \right) + (F_j, v) \tag{B.411b}$$

for every $u, v \in H^1(\Omega)$ and $j = 1, \ldots, M$. Alternatively, since $\overline{\partial_t \varphi_j} = 0$, we know that (cf. (B.343)[85])

$$\begin{aligned} \left((-\Delta_n)^{-1} \partial_t \varphi_j, u \right) + \varepsilon_\varphi^2 (\nabla \varphi_j, \nabla u) - \frac{\chi^{AB}}{2} (\varphi_j, u) & \\ + (\zeta_\mu(\varphi_j), u) + \alpha \left((-\Delta_n)^{-1} (\varphi_j - m), u \right) + (F_j, u) = 0 & \end{aligned} \tag{B.411c}$$

for every $u \in H^1(\Omega)$ and $j = 1, \ldots, M$. Since $V^h \subset H^1(\Omega)$, the equations above are valid if we replace the test functions $u, v \in H^1(\Omega)$ with $u_h, v_h \in V^h$.

ii) We set $u = \varphi_j - \varphi_h^j \in H^1(\Omega)$ in (B.411c) and obtain

$$\left((-\Delta_n)^{-1}\partial_t\varphi_j, \varphi_j - \varphi_h^j\right) + \varepsilon_\varphi^2\left(\nabla\varphi_j, \nabla\left(\varphi_j - \varphi_h^j\right)\right) - \frac{\chi^{AB}}{2}\left(\varphi_j, \varphi_j - \varphi_h^j\right) + \left(\zeta_\mu(\varphi_j), \varphi_j - \varphi_h^j\right) + \alpha\left((-\Delta_n)^{-1}(\varphi_j - m), \varphi_j - \varphi_h^j\right) + \left(F_j, \varphi_j - \varphi_h^j\right) = 0.$$

Integrating this in time over (t_{j-1}, t_j) gives

$$\begin{aligned}\int_{t_{j-1}}^{t_j}\left((-\Delta_n)^{-1}\varphi_t, \varphi - \varphi_h^j\right)\mathrm{d}t + \int_{t_{j-1}}^{t_j}\varepsilon_\varphi^2\left(\nabla\varphi, \nabla\left(\varphi - \varphi_h^j\right)\right)\mathrm{d}t \\ - \int_{t_{j-1}}^{t_j}\frac{\chi^{AB}}{2}\left(\varphi, \varphi - \varphi_h^j\right)\mathrm{d}t + \int_{t_{j-1}}^{t_j}\left(\zeta_\mu(\varphi), \varphi - \varphi_h^j\right)\mathrm{d}t \\ + \int_{t_{j-1}}^{t_j}\alpha\left((-\Delta_n)^{-1}(\varphi - m), \varphi - \varphi_h^j\right)\mathrm{d}t + \int_{t_{j-1}}^{t_j}\left(F, \varphi - \varphi_h^j\right)\mathrm{d}t = 0, \quad \text{(B.412)}\end{aligned}$$

where φ_h^j is constant (in time) over each such time sub-interval, but $\varphi(t)$ (the exact solution) and $F(t)$ may vary.

iii) We follow the example of Blowey and Elliott (1992) in their (3.15) and define the average time integral

$$\widehat{\varphi}^j := \frac{1}{\tau}\int_{t_{j-1}}^{t_j}\varphi(t)\,\mathrm{d}t \qquad \text{with} \qquad \widehat{\varphi}^0 := \varphi^0, \qquad \text{(B.413)}$$

which is a function of space. The second part of (B.413) is equivalent to the decision we made in (5.62). Setting $v_h = \varphi_h^j - \mathcal{I}^{(h)}\widehat{\varphi}^j \in V^h$ in (B.390c) then leads to

$$\begin{aligned}\varepsilon_\varphi^2\left(\nabla\varphi_h^j, \nabla\left(\varphi_h^j - \mathcal{I}^{(h)}\widehat{\varphi}^j\right)\right) - \frac{\chi^{AB}}{2}\left(\varphi_h^j, \varphi_h^j - \mathcal{I}^{(h)}\widehat{\varphi}^j\right) + \left(\zeta_\mu\left(\varphi_h^j\right), \varphi_h^j - \mathcal{I}^{(h)}\widehat{\varphi}^j\right) \\ + \alpha\left((-\Delta_h)^{-1}\left(\varphi_h^j - m\right), \varphi_h^j - \mathcal{I}^{(h)}\widehat{\varphi}^j\right) + \left(F_h^j, \varphi_h^j - \mathcal{I}^{(h)}\widehat{\varphi}^j\right) = \left(\psi_h^j, \varphi_h^j - \mathcal{I}^{(h)}\widehat{\varphi}^j\right).\end{aligned}$$

Multiplying this by τ (equivalent to discrete integration in time) yields

$$\begin{aligned}\varepsilon_\varphi^2\tau\left(\nabla\varphi_h^j, \nabla\left(\varphi_h^j - \mathcal{I}^{(h)}\widehat{\varphi}^j\right)\right) - \frac{\chi^{AB}}{2}\tau\left(\varphi_h^j, \varphi_h^j - \mathcal{I}^{(h)}\widehat{\varphi}^j\right) \\ + \tau\left(\zeta_\mu\left(\varphi_h^j\right), \varphi_h^j - \mathcal{I}^{(h)}\widehat{\varphi}^j\right) + \alpha\tau\left((-\Delta_h)^{-1}\left(\varphi_h^j - m\right), \varphi_h^j - \mathcal{I}^{(h)}\widehat{\varphi}^j\right) \\ + \tau\left(F_h^j, \varphi_h^j - \mathcal{I}^{(h)}\widehat{\varphi}^j\right) = \tau\left(\psi_h^j, \varphi_h^j - \mathcal{I}^{(h)}\widehat{\varphi}^j\right). \quad \text{(B.414)}\end{aligned}$$

Finally, setting $u_h = (-\Delta_h)^{-1}\left(\varphi_h^j - P^{(h)}\widehat{\varphi}^j\right)$ in (B.390b) gives

$$\left(\nabla\psi_h^j, \nabla(-\Delta_h)^{-1}\left(\varphi_h^j - P^{(h)}\widehat{\varphi}^j\right)\right) = -\left(\delta^{(\tau)}\varphi_h^j, (-\Delta_h)^{-1}\left(\varphi_h^j - P^{(h)}\widehat{\varphi}^j\right)\right). \qquad \text{(B.415)}$$

iv) Consider the term on the right of (B.414).[86] Using (B.415), (5.52) and properties of $P^{(h)}$, we find that

$$\begin{aligned}\left(\psi_h^j, \varphi_h^j - \mathcal{I}^{(h)}\widehat{\varphi}^j\right) &= \left(\psi_h^j, \varphi_h^j - P^{(h)}\widehat{\varphi}^j\right) + \left(\psi_h^j, P^{(h)}\widehat{\varphi}^j - \mathcal{I}^{(h)}\widehat{\varphi}^j\right) \\ &= \left(\nabla\psi_h^j, \nabla(-\Delta_h)^{-1}\left(\varphi_h^j - P^{(h)}\widehat{\varphi}^j\right)\right) + \left(\psi_h^j, \widehat{\varphi}^j\right) - \left(\psi_h^j, \mathcal{I}^{(h)}\widehat{\varphi}^j\right) \\ &= -\left(\delta^{(\tau)}\varphi_h^j, (-\Delta_h)^{-1}\left(\varphi_h^j - P^{(h)}\widehat{\varphi}^j\right)\right) + \left(\psi_h^j, \widehat{\varphi}^j - \mathcal{I}^{(h)}\widehat{\varphi}^j\right) \\ &= \left((-\Delta_h)^{-1}\delta^{(\tau)}\varphi_h^j, \widehat{\varphi}^j - \varphi_h^j\right) + \left(\psi_h^j, \widehat{\varphi}^j - \mathcal{I}^{(h)}\widehat{\varphi}^j\right). \qquad \text{(B.416)}\end{aligned}$$

Adding (B.412) and (B.414) using (B.416) leads to

$$\begin{aligned}A_j \leq \varepsilon_\varphi^2 \tau \left(\nabla \varphi_h^j, \nabla\left(\mathcal{I}^{(h)}\widehat{\varphi}^j - \widehat{\varphi}^j\right)\right) - \frac{\chi^{AB}}{2}\tau\left(\left(\varphi_h^j, \mathcal{I}^{(h)}\widehat{\varphi}^j - \widehat{\varphi}^j\right)\right) \\ + \tau\left(\psi_h^j, \widehat{\varphi}^j - \mathcal{I}^{(h)}\widehat{\varphi}^j\right) + \tau\left(\left(\left(-\Delta_h\right)^{-1} - \left(-\Delta_n\right)^{-1}\right)\delta^{(\tau)}\varphi_h^j, \widehat{\varphi}^j - \varphi_h^j\right) \\ + \tau\left(\zeta_\mu\left(\varphi_h^j\right), \mathcal{I}^{(h)}\widehat{\varphi}^j - \widehat{\varphi}^j\right) + \tau\left(F_h^j, \mathcal{I}^{(h)}\widehat{\varphi}^j - \widehat{\varphi}^j\right) \\ + \alpha\tau\left(\left(\left(-\Delta_h\right)^{-1} - \left(-\Delta_n\right)^{-1}\right)\left(\varphi_h^j - m\right), \widehat{\varphi}^j - \varphi_h^j\right) \\ + \alpha\tau\left(\left(-\Delta_h\right)^{-1}\left(\varphi_h^j - m\right), \mathcal{I}^{(h)}\widehat{\varphi}^j - \widehat{\varphi}^j\right), \end{aligned} \tag{B.417}$$

after significant rearrangement, and where we have:

- discarded
$$\int_{t_{j-1}}^{t_j} \underbrace{\left(\zeta_\mu\left(\varphi\right) - \zeta_\mu\left(\varphi_h^j\right), \varphi - \varphi_h^j\right)}_{\geq 0 \text{ by (4.19a)}} \mathrm{d}t + \alpha\int_{t_{j-1}}^{t_j} \left\|\varphi - \varphi_h^j\right\|_{-1}^2 \mathrm{d}t \geq 0$$
on the left.

- defined (as in Blowey and Elliott (1992))
$$\begin{aligned}A_j \coloneqq \overbrace{\int_{t_{j-1}}^{t_j}\left(\varphi_t - \delta^{(\tau)}\varphi_h^j, \left(-\Delta_n\right)^{-1}\left(\varphi - \varphi_h^j\right)\right)\mathrm{d}t}^{\left(A_j^{(1)}\right)} + \overbrace{\int_{t_{j-1}}^{t_j}\left(F - F_h^j, \varphi - \varphi_h^j\right)\mathrm{d}t}^{\left(A_j^{(4)}\right)} \\ + \underbrace{\varepsilon_\varphi^2\int_{t_{j-1}}^{t_j}\left(\nabla\left(\varphi - \varphi_h^j\right), \nabla\left(\varphi - \varphi_h^j\right)\right)\mathrm{d}t}_{\left(A_j^{(2)}\right)} - \underbrace{\frac{\chi^{AB}}{2}\int_{t_{j-1}}^{t_j}\left(\varphi - \varphi_h^j, \varphi - \varphi_h^j\right)\mathrm{d}t}_{\left(A_j^{(3)}\right)}. \end{aligned} \tag{B.418}$$

- used (B.413) to interchange a number of the temporal and spatial integrations on the right, viz.
$$\begin{aligned}\int_{t_{j-1}}^{t_j}\left(\delta^{(\tau)}\varphi_h^j, \left(-\Delta_n\right)^{-1}\left(\varphi - \varphi_h^j\right)\right)\mathrm{d}t &= \tau\left(\delta^{(\tau)}\varphi_h^j, \left(-\Delta_n\right)^{-1}\left(\widehat{\varphi}^j - \varphi_h^j\right)\right); \\ \int_{t_{j-1}}^{t_j}\varepsilon_\varphi^2\left(\nabla\varphi_h^j, \nabla\left(\varphi - \varphi_h^j\right)\right)\mathrm{d}t &= \varepsilon_\varphi^2\tau\left(\nabla\varphi_h^j, \nabla\left(\widehat{\varphi}^j - \varphi_h^j\right)\right); \\ \int_{t_{j-1}}^{t_j}\frac{\chi^{AB}}{2}\left(\varphi_h^j, \varphi - \varphi_h^j\right)\mathrm{d}t &= \frac{\chi^{AB}}{2}\tau\left(\varphi_h^j, \widehat{\varphi}^j - \varphi_h^j\right); \\ \int_{t_{j-1}}^{t_j}\left(\zeta_\mu\left(\varphi_h^j\right), \varphi - \varphi_h^j\right)\mathrm{d}t &= \tau\left(\zeta_\mu\left(\varphi_h^j\right), \widehat{\varphi}^j - \varphi_h^j\right); \\ \int_{t_{j-1}}^{t_j}\alpha\left(\left(-\Delta_n\right)^{-1}\left(\varphi_h^j - m\right), \varphi - \varphi_h^j\right)\mathrm{d}t &= \alpha\tau\left(\left(-\Delta_n\right)^{-1}\left(\varphi_h^j - m\right), \widehat{\varphi}^j - \varphi_h^j\right); \\ \int_{t_{j-1}}^{t_j}\left(F_h^j, \varphi - \varphi_h^j\right)\mathrm{d}t &= \tau\left(F_h^j, \widehat{\varphi}^j - \varphi_h^j\right), \end{aligned}$$
since each φ_h^j is constant (in time) over (t_{j-1}, t_j).

- used (cf. (B.416))
$$\begin{aligned}&\left(\left(-\Delta_h\right)^{-1}\left(\varphi_h^j - m\right), \varphi_h^j - \mathcal{I}^{(h)}\widehat{\varphi}^j\right) \\ &\qquad = \left(\left(-\Delta_h\right)^{-1}\left(\varphi_h^j - m\right), \varphi_h^j - \widehat{\varphi}^j\right) + \left(\left(-\Delta_h\right)^{-1}\left(\varphi_h^j - m\right), \widehat{\varphi}^j - \mathcal{I}^{(h)}\widehat{\varphi}^j\right)\end{aligned}$$
on the right. Observe that $\overline{\widehat{\varphi}^j - \mathcal{I}^{(h)}\widehat{\varphi}^j} \neq 0$ in the last term above.

v) We analyse the terms comprising A_j in (B.418).[87] The first part is

$$\begin{aligned}\left(A_j^{(1)}\right) = &\overbrace{\int_{t_{j-1}}^{t_j} \left(\varphi_t, (-\Delta_n)^{-1}(\varphi - m)\right) \mathrm{d}t}^{\left(A_j^{(1,1)}\right)} + \overbrace{\int_{t_{j-1}}^{t_j} \left(\delta^{(\tau)}\varphi_h^j, (-\Delta_n)^{-1}\left(\varphi_h^j - m\right)\right) \mathrm{d}t}^{\left(A_j^{(1,2)}\right)} \\ &\underbrace{-\left[\left(\varphi_j - \varphi_{j-1}, (-\Delta_n)^{-1}\left(\varphi_h^j - m\right)\right) + \int_{t_{j-1}}^{t_j} \left(\delta^{(\tau)}\varphi_h^j, (-\Delta_n)^{-1}(\varphi - m)\right) \mathrm{d}t\right]}_{\left(A_j^{(1,3)}\right)}, \end{aligned} \tag{B.419}$$

where we have used (B.410) repeatedly. In turn,[88]

$$\left(A_j^{(1,1)}\right) = \frac{1}{2}\int_{t_{j-1}}^{t_j} \partial_t \left\|\varphi - m\right\|_{-1}^2 \mathrm{d}t = \frac{1}{2}\left(\left\|\varphi_j - m\right\|_{-1}^2 - \left\|\varphi_{j-1} - m\right\|_{-1}^2\right); \tag{B.420a}$$

$$\begin{aligned}\left(A_j^{(1,2)}\right) &= \left(\varphi_h^j - \varphi_h^{j-1}, (-\Delta_n)^{-1}\left(\frac{\varphi_h^j - \varphi_h^{j-1}}{2} + \frac{\varphi_h^j + \varphi_h^{j-1}}{2} - m\right)\right) \\ &= \frac{1}{2}\left(\left\|\varphi_h^j - \varphi_h^{j-1}\right\|_{-1}^2 + \left\|\varphi_h^j - m\right\|_{-1}^2 - \left\|\varphi_h^{j-1} - m\right\|_{-1}^2\right); \end{aligned} \tag{B.420b}$$

$$\begin{aligned}\left(A_j^{(1,3)}\right) = &-\left(\varphi_j, (-\Delta_n)^{-1}\left(\varphi_h^j - m\right)\right) + \left(\varphi_h^{j-1}, (-\Delta_n)^{-1}(\varphi_{j-1} - m)\right) \\ &- \left(\varphi_h^j - \varphi_h^{j-1}, (-\Delta_n)^{-1}\left(\widehat{\varphi}^j - \varphi_{j-1}\right)\right). \end{aligned} \tag{B.420c}$$

Consequently,[89]

$$\begin{aligned}\left(A_j^{(1)}\right) &= \frac{1}{2}\left(\left\|\varphi_j - m\right\|_{-1}^2 - 2\left(\varphi_j, (-\Delta_n)^{-1}\left(\varphi_h^j - m\right)\right) + \left\|\varphi_h^j - m\right\|_{-1}^2\right) \\ &\quad -\frac{1}{2}\left(\left\|\varphi_{j-1} - m\right\|_{-1}^2 - 2\left(\varphi_h^{j-1}, (-\Delta_n)^{-1}(\varphi_{j-1} - m)\right) + \left\|\varphi_h^{j-1} - m\right\|_{-1}^2\right) \\ &\quad +\frac{1}{2}\left\|\varphi_h^j - \varphi_h^{j-1}\right\|_{-1}^2 - \left(\varphi_h^j - \varphi_h^{j-1}, (-\Delta_n)^{-1}\left(\widehat{\varphi}^j - \varphi_{j-1}\right)\right) \\ &= \frac{1}{2}\left\|\varphi_j - \varphi_h^j\right\|_{-1}^2 - \frac{1}{2}\left\|\varphi_{j-1} - \varphi_h^{j-1}\right\|_{-1}^2 + \frac{1}{2}\left\|\varphi_h^j - \varphi_h^{j-1}\right\|_{-1}^2 \\ &\quad - \left(\varphi_h^j - \varphi_h^{j-1}, (-\Delta_n)^{-1}\left(\widehat{\varphi}^j - \varphi_{j-1}\right)\right) \\ &= \frac{1}{2}\left\|e_{\varphi,h}^j\right\|_{-1}^2 - \frac{1}{2}\left\|e_{\varphi,h}^{j-1}\right\|_{-1}^2 + \frac{1}{2}\left\|\varphi_h^j - \varphi_h^{j-1}\right\|_{-1}^2 - \left(\varphi_h^j - \varphi_h^{j-1}, (-\Delta_n)^{-1}\left(\widehat{\varphi}^j - \varphi_{j-1}\right)\right), \end{aligned} \tag{B.421a}$$

after recalling (5.69). Likewise, the second part of A_j is

$$\left(A_j^{(2)}\right) = \varepsilon_\varphi^2 \int_{t_{j-1}}^{t_j} \left|e_{\varphi,h}(t)\right|_1^2 \mathrm{d}t, \tag{B.421b}$$

and the third part is

$$\left(A_j^{(3)}\right) = -\frac{\chi^{AB}}{2}\int_{t_{j-1}}^{t_j} \left\|e_{\varphi,h}(t)\right\|^2 \mathrm{d}t. \tag{B.421c}$$

We leave the fourth part of A_j as-is for now. Combining the results above gives[90]

$$\begin{aligned}A_j = &\frac{1}{2}\left\|e_{\varphi,h}^j\right\|_{-1}^2 - \frac{1}{2}\left\|e_{\varphi,h}^{j-1}\right\|_{-1}^2 + \varepsilon_\varphi^2 \int_{t_{j-1}}^{t_j} \left|e_{\varphi,h}(t)\right|_1^2 \mathrm{d}t - \frac{\chi^{AB}}{2}\int_{t_{j-1}}^{t_j} \left\|e_{\varphi,h}(t)\right\|^2 \mathrm{d}t \\ &+ \frac{1}{2}\left\|\varphi_h^j - \varphi_h^{j-1}\right\|_{-1}^2 - \left(\varphi_h^j - \varphi_h^{j-1}, (-\Delta_n)^{-1}\left(\widehat{\varphi}^j - \varphi_{j-1}\right)\right) + \int_{t_{j-1}}^{t_j} \left(F(t) - F_h^j, e_{\varphi,h}(t)\right) \mathrm{d}t. \end{aligned} \tag{B.422}$$

Summing this from $j = 1, \ldots, k$, $(1 \leq k \leq M)$ yields

$$\sum_{j=1}^{k} A_j = \overbrace{\frac{1}{2}\left\|e_{\varphi,h}^{k}\right\|_{-1}^{2} + \varepsilon_{\varphi}^{2}\int_{0}^{t_k}\left|e_{\varphi,h}\left(t\right)\right|_{1}^{2}\mathrm{d}t - \frac{\chi^{AB}}{2}\int_{0}^{t_k}\left\|e_{\varphi,h}\left(t\right)\right\|^{2}\mathrm{d}t}^{\text{(I)}} \overbrace{-\frac{1}{2}\left\|e_{\varphi,h}^{0}\right\|_{-1}^{2}}^{\text{(II)}}$$
$$\underbrace{+\frac{1}{2}\sum_{j=1}^{k}\left\|\varphi_{h}^{j}-\varphi_{h}^{j-1}\right\|_{-1}^{2} - \sum_{j=1}^{k}\left(\varphi_{h}^{j}-\varphi_{h}^{j-1}, (-\Delta_n)^{-1}\left(\widehat{\varphi}^{j}-\varphi_{j-1}\right)\right)}_{\text{(III)}}$$
$$\underbrace{+\sum_{j=1}^{k}\int_{t_{j-1}}^{t_j}\left(F\left(t\right)-F_{h}^{j}, e_{\varphi,h}\left(t\right)\right)\mathrm{d}t}_{\text{(4)}}, \quad \text{(B.423)}$$

where we have labelled the components to match (3.27) of Blowey and Elliott (1992).

vi) We sum (B.417) from $j = 1, \ldots, k$, $(1 \leq k \leq M)$, and find that[91]

$$\sum_{j=1}^{k} A_j \leq \underbrace{\varepsilon_{\varphi}^{2}\sum_{j=1}^{k}\tau\left(\nabla\varphi_{h}^{j}, \nabla\left(\mathcal{I}^{(h)}\widehat{\varphi}^{j}-\widehat{\varphi}^{j}\right)\right)}_{\text{(IV)}} \underbrace{-\frac{\chi^{AB}}{2}\sum_{j=1}^{k}\tau\left(\varphi_{h}^{j}, \mathcal{I}^{(h)}\widehat{\varphi}^{j}-\widehat{\varphi}^{j}\right)}_{\text{(V)}}$$
$$\underbrace{+\sum_{j=1}^{k}\tau\left(\psi_{h}^{j}, \widehat{\varphi}^{j}-\mathcal{I}^{(h)}\widehat{\varphi}^{j}\right)}_{\text{(VI)}} \underbrace{+\sum_{j=1}^{k}\tau\left(\left((-\Delta_h)^{-1}-(-\Delta_n)^{-1}\right)\delta^{(\tau)}\varphi_{h}^{j}, \widehat{\varphi}^{j}-\varphi_{h}^{j}\right)}_{\text{(VII)}}$$
$$\underbrace{+\sum_{j=1}^{k}\tau\left(\zeta_{\mu}\left(\varphi_{h}^{j}\right), \mathcal{I}^{(h)}\widehat{\varphi}^{j}-\widehat{\varphi}^{j}\right)}_{\text{(8)}} \underbrace{+\sum_{j=1}^{k}\tau\left(F_{h}^{j}, \mathcal{I}^{(h)}\widehat{\varphi}^{j}-\widehat{\varphi}^{j}\right)}_{\text{(9)}}$$
$$\underbrace{+\alpha\sum_{j=1}^{k}\tau\left(\left((-\Delta_h)^{-1}-(-\Delta_n)^{-1}\right)\left(\varphi_{h}^{j}-m\right), \widehat{\varphi}^{j}-\varphi_{h}^{j}\right)}_{\text{(10)}}$$
$$\underbrace{+\alpha\sum_{j=1}^{k}\tau\left((-\Delta_h)^{-1}\left(\varphi_{h}^{j}-m\right), \mathcal{I}^{(h)}\widehat{\varphi}^{j}-\widehat{\varphi}^{j}\right)}_{\text{(11)}}. \quad \text{(B.424)}$$

vii) We estimate the numbered terms above.

(II): using (5.57a), (A.28b) and (A.76b),[92]

$$\left|\text{(II)}\right| = \frac{1}{2}\left\|\varphi^{0}-\varphi_{h}^{0}\right\|_{-1}^{2} = \frac{1}{2}\left\|\varphi^{0}-P_{m}^{(\star)}\varphi^{0}\right\|_{-1}^{2}$$
$$\leq \frac{c_P^4}{2}\left|\varphi^{0}-P_{m}^{(\star)}\varphi^{0}\right|_{1}^{2} \leq \frac{c_P^4}{2}\left|\varphi^{0}-\mathcal{I}^{(h)}\varphi^{0}\right|_{1}^{2} \leq Ch^{2}\left|\varphi^{0}\right|_{2}^{2} = Ch^{2}, \quad \text{(B.425)}$$

after applying (B.408), and recalling that we chose $\varphi^0 \in H_m^2\left(\Omega\right)$.

(III): for brevity, we quote (3.34) of Blowey and Elliott (1992), which says that

$$\left|\text{(III)}\right| \geq -C\tau, \quad \text{(B.426)}$$

where use is made of the fact that $\varphi \in H^1\left(0, T; \left(H^1\left(\Omega\right)\right)'\right)$.

(4): for the forcing function term, we use the Cauchy–Schwarz,[93] Poincaré and Young inequalities to argue that

$$\begin{aligned}
|(4)| &= \left| \sum_{j=1}^{k} \int_{t_{j-1}}^{t_j} \left(F(t) - F_h^j, e_{\varphi,h}(t) \right) \mathrm{d}t \right| \\
&\leq \sum_{j=1}^{k} \int_{t_{j-1}}^{t_j} \left\| F(t) - F_h^j \right\| \left\| e_{\varphi,h}(t) \right\| \mathrm{d}t \\
&\leq \sum_{j=1}^{k} \left(\int_{t_{j-1}}^{t_j} c_P^2 \left| F(t) - F_h^j \right|_1^2 \mathrm{d}t \right)^{1/2} \left(\int_{t_{j-1}}^{t_j} c_P^2 \left| e_{\varphi,h}(t) \right|_1^2 \mathrm{d}t \right)^{1/2} \\
&\leq C \left(\sum_{j=1}^{k} \int_{t_{j-1}}^{t_j} \left| F(t) - F_h^j \right|_1^2 \mathrm{d}t \right)^{1/2} \left(\int_0^{t_k} \left| e_{\varphi,h}(t) \right|_1^2 \mathrm{d}t \right)^{1/2} \\
&\leq \frac{C}{\nu} \sum_{j=1}^{M} \int_{t_{j-1}}^{t_j} \left| F(t) - F_h^j \right|_1^2 \mathrm{d}t + \frac{\varepsilon_\varphi^2 \nu}{4} \int_0^{t_k} \left| e_{\varphi,h}(t) \right|_1^2 \mathrm{d}t
\end{aligned} \tag{B.427}$$

for any $\nu > 0$. In principle, since f is known *a priori*, and we *choose* its approximation (viz. $\widetilde{f}^j$ as in (5.4)) at each time-step, we can make the first term on the right above as small as we wish. To be specific, let as assume that we use fully implicit Euler time integration, viz.

$$\widetilde{f}^j := f(t_j) =: f_j. \tag{B.428}$$

Using (5.12) and (A.28a), we determine that for $t_{j-1} < t \leq t_j$,

$$\begin{aligned}
\left| F(t) - F_h^j \right|_1 &= \left| (-\Delta_n)^{-1} \left(f(t) - P^{(h)} f_j \right) \right|_1 \\
&\leq \left\| f(t) - f_j \right\|_{-1} + \left\| f_j - P^{(h)} f_j \right\|_{-1} \\
&\leq c_P \left\| f(t) - f_j \right\| + c_P \left\| f_j - P^{(h)} f_j \right\| \\
&\leq C \left\| f(t) - f_j \right\|_{0,\infty} + c_P \left\| f_j - \mathcal{I}^{(h)} f_j \right\| \\
&\leq C |\Omega| \left(\left| f'(t_j) \right| \right) \tau + \mathcal{O}\left(\tau^2\right) + Ch \left| f_j \right|_1,
\end{aligned}$$

after using (A.75a) and (B.408) with $s = 0$ and $m = 1$, and noting the regularity we assumed (on f) in (5.3). The constant $C\left(\left|f'(t_j)\right|\right)$ above depends on $f'(t_j)$ and results from taking a Taylor series (in time) of f about t_j. Since $f \in C^1\left([0,T]; H_*^1(\Omega)\right)$,

$$\begin{aligned}
\frac{C}{\nu} \sum_{j=1}^{M} \int_{t_{j-1}}^{t_j} \left| F(t) - F_h^j \right|_1^2 \mathrm{d}t &\leq \frac{C}{\nu} \sum_{j=1}^{M} \int_{t_{j-1}}^{t_j} \left(C\left(\left| f'(t_j) \right| \right) \tau + Ch \left| f_j \right|_1 \right)^2 \mathrm{d}t \\
&\leq \frac{C}{\nu} \left(C\tau \max_{0 \leq t \leq T} \left| f'(t) \right| + Ch \max_{0 \leq t \leq T} \left| f(t) \right|_1 \right)^2 \sum_{j=1}^{M} \tau \leq C\left(\tau^2 + h^2\right).
\end{aligned} \tag{B.429}$$

Remark. The approximation error in (B.429) is a worst case. In practice, we use a more accurate approximation of f, such as the trapezium rule to get a temporal error order τ^p with $p > 2$, and a smoother f to get a spatial error order h^p with $p > 2$ (cf. (B.408)), in (B.428).

(IV): according to (3.37) of Blowey and Elliott (1992),

$$|(\mathrm{IV})| \leq \frac{Ch^2}{\nu} + \frac{\varepsilon_\varphi^2 \nu}{4} \int_0^{t_k} \left| e_{\varphi,h}(t) \right|_1^2 \mathrm{d}t, \tag{B.430}$$

for any $\nu > 0$, where use is made of the fact that $\varphi \in L^2\left(0, T; H^2(\Omega)\right)$.

(V): using $\varphi \in L^2\left(0,T;H^2\left(\Omega\right)\right)$, (3.38) of Blowey and Elliott (1992) says that

$$|(\mathrm{V})| \leq Ch^2. \tag{B.431}$$

(VI): using $\varphi \in L^2\left(0,T;H^2\left(\Omega\right)\right)$, (3.39) of Blowey and Elliott (1992) says that

$$|(\mathrm{VI})| \leq Ch^2, \tag{B.432}$$

where use is made of (B.401).

(VII): according to (3.40) of Blowey and Elliott (1992),

$$|(\mathrm{VII})| \leq \frac{Ch^4}{\varepsilon_\varphi^2 \nu \tau} + \frac{\varepsilon_\varphi^2 \nu}{4} \int_0^{t_k} \left|e_{\varphi,h}\left(t\right)\right|_1^2 \mathrm{d}t, \tag{B.433}$$

for any $\nu > 0$, after using (B.406).

(8): the term arising due to the regularisation is bounded as a result of (4.18), (B.408) (with $s = 0$) and the Cauchy–Schwarz inequality as

$$\begin{aligned}
\sum_{j=1}^{k} \tau \left(\zeta_\mu\left(\varphi_h^j\right), \mathcal{I}^{(h)}\widehat{\varphi}^j - \widehat{\varphi}^j\right) &= \sum_{j=1}^{k} \int_{t_{j-1}}^{t_j} \int_\Omega \zeta_\mu\left(\varphi_h^j\right)\left(\mathcal{I}^{(h)}\varphi\left(t\right) - \varphi\left(t\right)\right) \mathrm{d}\Omega \, \mathrm{d}t \\
&= \sum_{j=1}^{k} \int_{t_{j-1}}^{t_j} \left(\zeta_\mu\left(\varphi_h^j\right), \mathcal{I}^{(h)}\varphi\left(t\right) - \varphi\left(t\right)\right) \mathrm{d}t \\
&\leq \frac{1}{\mu} \sum_{j=1}^{k} \int_{t_{j-1}}^{t_j} \left\|\varphi_h^j\right\| \left\|\mathcal{I}^{(h)}\varphi\left(t\right) - \varphi\left(t\right)\right\| \mathrm{d}t \\
&\leq Ch^2 \sum_{j=1}^{k} \left\|\varphi_h^j\right\| \int_{t_{j-1}}^{t_j} \left|\varphi\left(t\right)\right|_2 \mathrm{d}t \\
&\leq Ch^2 \sum_{j=1}^{k} \left\|\varphi_h^j\right\| \left\{\tau^{1/2} \left(\int_{t_{j-1}}^{t_j} \left|\varphi\left(t\right)\right|_2^2 \, \mathrm{d}t\right)^{1/2}\right\} \\
&\leq Ch^2 \left(\sum_{j=1}^{k} \tau \left\|\varphi_h^j\right\|^2\right)^{1/2} \left(\int_0^{t_k} \left|\varphi\left(t\right)\right|_2^2 \, \mathrm{d}t\right)^{1/2} \\
&\leq Ch^2 \left\|\varphi\right\|_{L^2\left(0,T;H^2\left(\Omega\right)\right)} = Ch^2,
\end{aligned} \tag{B.434}$$

where we have used the fact that $\varphi \in L^2\left(0,T;H^2\left(\Omega\right)\right)$, and the bound in (5.63a).

Remark. The constant C above has absorbed a factor of $1/\mu$.[94]

(9): we bound the error due to the forcing function in a similar way, with F_h^j taking the place of $\zeta_\mu\left(\varphi_h^j\right)$ (without the $1/\mu$ factor). We have

$$\sum_{j=1}^{k} \tau \left(F_h^j, \mathcal{I}^{(h)}\widehat{\varphi}^j - \widehat{\varphi}^j\right) \leq Ch^2 \left(\sum_{j=1}^{k} \tau \left\|F_h^j\right\|^2\right)^{1/2} \left(\int_0^{t_k} \left|\varphi\left(t\right)\right|_2^2 \, \mathrm{d}t\right)^{1/2} = Ch^2, \tag{B.435}$$

since each

$$\begin{aligned}
\left\|F_h^j\right\|^2 = \left\|\left(-\Delta_h\right)^{-1} f_h^j\right\|^2 \leq c_P^2 \left|\left(-\Delta_h\right)^{-1} f_h^j\right|_1^2 = c_P^2 \left\|f_h^j\right\|_{-h}^2 \leq c_P^4 \left\|f_h^j\right\|^2 \\
= c_P^4 \left\|P^{(h)}\widetilde{f}^j\right\|^2 \leq c_P^4 \left\|\widetilde{f}^j\right\|^2 \leq c_P^4 \max_{0\leq t\leq T} \left\|\widetilde{f}\left(t\right)\right\|^2 \leq C < \infty,
\end{aligned}$$

by (5.3).

(10): the first non-local term has a similar structure to term (VII), which was analysed in (3.40) of Blowey and Elliott (1992) (see our (B.433)). Arguing similarly,

$$\begin{aligned}
&\left|\alpha\sum_{j=1}^{k}\tau\left(\left((-\Delta_h)^{-1}-(-\Delta_n)^{-1}\right)\left(\varphi_h^j-m\right),\widehat{\varphi}^j-\varphi_h^j\right)\right| \\
&\quad=\alpha\left|\sum_{j=1}^{k}\int_{t_{j-1}}^{t_j}\left(\left((-\Delta_h)^{-1}-(-\Delta_n)^{-1}\right)\left(\varphi_h^j-m\right),e_{\varphi,h}\left(t\right)\right)\mathrm{d}t\right| \\
&\quad\leq\alpha\sum_{j=1}^{k}\left\|\left((-\Delta_h)^{-1}-(-\Delta_n)^{-1}\right)\left(\varphi_h^j-m\right)\right\|\int_{t_{j-1}}^{t_j}\left\|e_{\varphi,h}\left(t\right)\right\|\mathrm{d}t \\
&\quad\leq\alpha\sum_{j=1}^{k}Ch^2\left\|\varphi_h^j-m\right\|_1\left\{\tau^{1/2}\left(\int_{t_{j-1}}^{t_j}c_P^2\left|e_{\varphi,h}\left(t\right)\right|_1^2\mathrm{d}t\right)^{1/2}\right\} \\
&\quad\leq Ch^2\left(\sum_{j=1}^{k}\tau\left\|\varphi_h^j-m\right\|_1^2\right)^{1/2}\left(\int_0^{t_k}\left|e_{\varphi,h}\left(t\right)\right|_1^2\mathrm{d}t\right)^{1/2} \\
&\quad\leq\frac{Ch^4}{\varepsilon_\varphi^2\nu}+\frac{\varepsilon_\varphi^2\nu}{4}\int_0^{t_k}\left|e_{\varphi,h}\left(t\right)\right|_1^2\mathrm{d}t,
\end{aligned}\tag{B.436}$$

for any $\nu>0$, where we have used (B.409), (5.63a) and the Poincaré (noting that $\overline{e_{\varphi,h}\left(t\right)}=0$ for every $t\in[0,T]$), Cauchy–Schwarz and Young inequalities.

(11): the second non-local term resembles terms (8) (and (9)), with $(-\Delta_h)^{-1}\left(\varphi_h^j-m\right)$ taking the place of $\zeta_\mu\left(\varphi_h^j\right)$ (without the $1/\mu$ factor). We have

$$\begin{aligned}
&\alpha\sum_{j=1}^{k}\tau\left((-\Delta_h)^{-1}\left(\varphi_h^j-m\right),\mathcal{I}^{(h)}\widehat{\varphi}^j-\widehat{\varphi}^j\right) \\
&\qquad\leq Ch^2\left(\sum_{j=1}^{k}\tau\left\|\varphi_h^j-m\right\|^2\right)^{1/2}\left(\int_0^{t_k}\left|\varphi\left(t\right)\right|_2^2\ \mathrm{d}t\right)^{1/2}=Ch^2,
\end{aligned}\tag{B.437}$$

after using (2.11), (A.28a) and (5.63a), together with $\varphi\in L^2\left(0,T;H^2\left(\Omega\right)\right)$, as well as Poincaré's inequality to conclude that

$$\left\|(-\Delta_h)^{-1}\left(\varphi_h^j-m\right)\right\|\leq c_P\left\|\varphi_h^j-m\right\|_{-1}\leq c_P^2\left\|\varphi_h^j-m\right\|.$$

viii) Using (B.423), (B.424) and the estimates above for the numbered terms, we find that

$$\frac{1}{2}\left\|e_{\varphi,h}^k\right\|_{-1}^2+\varepsilon_\varphi^2\int_0^{t_k}\left|e_{\varphi,h}\left(t\right)\right|_1^2\mathrm{d}t\leq\sigma\left(h,\tau\right)+\frac{\chi^{AB}}{2}\int_0^{t_k}\left\|e_{\varphi,h}\left(t\right)\right\|^2\mathrm{d}t+\varepsilon_\varphi^2\nu\int_0^{t_k}\left|e_{\varphi,h}\left(t\right)\right|_1^2\mathrm{d}t,\tag{B.438a}$$

for any $\nu>0$, where we have defined

$$\sigma\left(h,\tau\right):=C\left(\tau+h^2+\frac{h^4}{\tau}\right).\tag{B.438b}$$

The previous inequality is essentially identical to (3.41) of Blowey and Elliott (1992). As such, the rest of the argument is identical to the last part of the proof of their Theorem 3.5. For completeness, we provide the necessary details with some minor modifications below.

ix) Using the fact that $\overline{e_{\varphi,h}\left(t\right)}=0$ for every $t\in[0,T]$, we can use (A.29) and Young's inequality to conclude that

$$\left\|e_{\varphi,h}\right\|^2\leq\left\|e_{\varphi,h}\right\|_{-1}\left|e_{\varphi,h}\right|_1\leq\delta\varepsilon_\varphi^2\left|e_{\varphi,h}\right|_1^2+\frac{1}{4\delta\varepsilon_\varphi^2}\left\|e_{\varphi,h}\right\|_{-1}^2$$

for any $\delta > 0$. Plugging this into the right side of (B.438a) leads to[95]

$$\frac{1}{2}\left\|e_{\varphi,h}^{k}\right\|_{-1}^{2}+\varepsilon_{\varphi}^{2}\left(1-\frac{\delta\chi^{AB}}{2}-\nu\right)\int_{0}^{t_{k}}\left|e_{\varphi,h}\left(t\right)\right|_{1}^{2}\mathrm{d}t\leq\frac{\chi^{AB}}{8\delta\varepsilon_{\varphi}^{2}}\sum_{j=1}^{k}\int_{t_{j-1}}^{t_{j}}\left\|e_{\varphi,h}\left(t\right)\right\|_{-1}^{2}\mathrm{d}t+\sigma\left(h,\tau\right),\tag{B.439}$$

for any $\nu, \delta > 0$. By (3.43) of Blowey and Elliott (1992), if $t_{j-1} < t \leq t_j$, then

$$\left\|e_{\varphi,h}^{j}-e_{\varphi,h}\left(t\right)\right\|_{-1}^{2}=\left\|\varphi_{j}-\varphi\left(t\right)\right\|_{-1}^{2}\leq\tau\left\|\partial_{t}\varphi\right\|_{L^{2}\left(t_{j-1},t_{j};\left(H^{1}(\Omega)\right)'\right)}^{2}.\tag{B.440}$$

For any $\zeta > 0$, Young's inequality implies that

$$(a+b)^{2}=a^{2}+2ab+b^{2}\leq a^{2}+2\left(\frac{1}{2\zeta}a^{2}+\frac{\zeta}{2}b^{2}\right)+b^{2}=\left(1+\frac{1}{\zeta}\right)a^{2}+\left(1+\zeta\right)b^{2}.\tag{B.441}$$

If we set

$$\nu<1\qquad\Rightarrow\qquad\delta=\frac{2\left(1-\nu\right)}{\chi^{AB}}>0\qquad\Rightarrow\qquad1-\frac{\delta\chi^{AB}}{2}-\nu=0,$$

in (B.439) and then use (B.441) with

$$a=e_{\varphi,h}\left(t\right)-e_{\varphi,h}^{j}\qquad\text{and}\qquad b=e_{\varphi,h}^{j},$$

as in (B.440), then (B.439) yields[96]

$$\left(\frac{1}{2}-C\left(1+\zeta\right)\tau\right)\left\|e_{\varphi,h}^{k}\right\|_{-1}^{2}\leq\underbrace{C\left(1+\zeta^{-1}\right)\left\|\partial_{t}\varphi\right\|_{L^{2}\left(0,T;\left(H^{1}(\Omega)\right)'\right)}^{2}\tau^{2}}_{=\mathcal{O}\left(\tau^{2}\right)}+C\left(1+\zeta\right)\tau\sum_{j=1}^{k-1}\left\|e_{\varphi,h}^{j}\right\|_{-1}^{2}+\sigma\left(h,\tau\right);$$

that is

$$C_{\zeta,\nu}\left\|e_{\varphi,h}^{k}\right\|_{-1}^{2}\leq\sigma\left(h,\tau\right)+C\left(1+\zeta\right)\sum_{j=1}^{k-1}\tau\left\|e_{\varphi,h}^{j}\right\|_{-1}^{2},\tag{B.442a}$$

for any $\zeta > 0$ and $0 < \nu < 1$, where we have moved the last term in the sum on the right over to the left and absorbed the $\mathcal{O}\left(\tau^{2}\right)$ term on the right into $\sigma\left(h,\tau\right)$ (using $\varphi\in H^{1}\left(0,T;\left(H^{1}\left(\Omega\right)\right)'\right)$), and defined

$$C_{\zeta,\nu}:=\frac{1}{2}-C\left(1+\zeta\right)\tau\qquad\text{and}\qquad C:=\frac{\left(\chi^{AB}\right)^{2}}{16\varepsilon_{\varphi}^{2}\left(1-\nu\right)}.\tag{B.442b}$$

If we assume that

$$\tau<\frac{8\varepsilon_{\varphi}^{2}\left(1-\nu\right)}{\left(1+\zeta\right)\left(\chi^{AB}\right)^{2}}\qquad\Rightarrow\qquad C_{\zeta,\nu}>0,\tag{B.443}$$

for ζ, ν very small, then (B.442a) can be written as[97]

$$\left\|e_{\varphi,h}^{k}\right\|_{-1}^{2}\leq\sigma\left(h,\tau\right)+C\sum_{j=1}^{k-1}\tau\left\|e_{\varphi,h}^{j}\right\|_{-1}^{2}\tag{B.444}$$

for a redefined constant $C > 0$. The discrete Gronwall inequality implies that

$$\left\|e_{\varphi,h}^{k}\right\|_{-1}^{2}\leq\sigma\left(h,\tau\right)\exp\left\{Ck\tau\right\},\qquad\qquad k=1,\ldots,M,$$

or, since $k\tau \leq T$ for $k = 1, \ldots, M$,[98]

$$\left\| e^k_{\varphi,h} \right\|^2_{-1} \leq \sigma(h,\tau) \exp\{CT\} = \sigma(h,\tau), \qquad k = 1, \ldots, M, \tag{B.445}$$

in which the bound on the right is independent of k, that is

$$\|e_{\varphi,h}\|^2_{\ell^\infty\left((j\tau)_{j=0}^M;\left(H^1(\Omega)\right)'\right)} \leq \sigma(h,\tau). \tag{B.446}$$

x) Using (B.441) with $\zeta = 1$ and (B.440), we determine that if $t_{j-1} < t \leq t_j$, then[99]

$$\|e_{\varphi,h}(t)\|^2_{-1} \leq 2\left\| e^j_{\varphi,h} \right\|^2_{-1} + 2\left\| e_{\varphi,h}(t) - e^j_{\varphi,h} \right\|^2_{-1} \leq \sigma(h,\tau) + \underbrace{2\|\partial_t \varphi\|^2_{L^2\left(0,T;\left(H^1(\Omega)\right)'\right)}}_{\mathcal{O}(\tau)} \tau \leq \sigma(h,\tau), \tag{B.447}$$

after using (B.446) and the fact that $\varphi \in H^1\left(0,T;\left(H^1(\Omega)\right)'\right)$. The bound on the right of (B.447) is independent of t, and so (B.446) can be improved to

$$\|e_{\varphi,h}\|^2_{L^\infty\left(0;T;\left(H^1(\Omega)\right)'\right)} \leq \sigma(h,\tau). \tag{B.448}$$

xi) We now set $\nu = \frac{1}{4}$, $\delta = \left(2\chi^{AB}\right)^{-1}$ and $k = M$ in (B.439) and use (B.448) to discover that

$$\int_0^T |e_{\varphi,h}(t)|^2_1 \, \mathrm{d}t \leq \frac{\left(\chi^{AB}\right)^2}{2\varepsilon^4_\varphi} \sum_{j=1}^M \int_{t_{j-1}}^{t_j} \|e_{\varphi,h}(t)\|^2_{-1} \, \mathrm{d}t + \sigma(h,\tau) \leq \sigma(h,\tau).$$

This last result and Poincaré's inequality imply that

$$\|e_{\varphi,h}\|^2_{L^2\left(0;T;H^1(\Omega)\right)} \leq \sigma(h,\tau), \tag{B.449}$$

since $\overline{e_{\varphi,h}(t)} = 0$. The combination of (B.448) and (B.449) is (5.70).

We adapt the proof above for $\left(\mathbf{R}^{(m)}_{\tau,\theta,h}\right)$.

i) We replace (B.414) with

$$\begin{aligned}
&\varepsilon^2_\varphi \tau\left(\nabla\varphi^j_h, \nabla\left(\varphi^j_h - \mathcal{I}^{(h)}\widehat{\varphi}^j\right)\right) - \frac{\chi^{AB}}{2}\tau\left(\varphi^j_h, \varphi^j_h - \mathcal{I}^{(h)}\widehat{\varphi}^j\right) \\
&\qquad + \tau\left(\zeta_\mu\left(\varphi^j_h\right), \varphi^j_h - \mathcal{I}^{(h)}\widehat{\varphi}^j\right) + \alpha\tau\left((-\Delta_h)^{-1}\left(\varphi^j_h - m\right), \varphi^j_h - \mathcal{I}^{(h)}\widehat{\varphi}^j\right) \\
&\qquad\qquad + \tau\left(F^j_h, \varphi^j_h - \mathcal{I}^{(h)}\widehat{\varphi}^j\right) \boxed{-\frac{\chi^{AB}}{2}\tau\left(\varphi^{j-1}_h - \varphi^j_h, \varphi^j_h - \mathcal{I}^{(h)}\widehat{\varphi}^j\right)} \\
&\qquad + \boxed{\alpha\tau(1-\theta)\left((-\Delta_h)^{-1}\left(\varphi^{j-1}_h - \varphi^j_h\right), \varphi^j_h - \mathcal{I}^{(h)}\widehat{\varphi}^j\right)} = \tau\left(\psi^j_h, \varphi^j_h - \mathcal{I}^{(h)}\widehat{\varphi}^j\right),
\end{aligned} \tag{B.450}$$

after using the hint in Corollary 3.6 of Blowey and Elliott (1992) which says that

$$\left(\varphi^{j-1}_h, \varphi^j_h - \mathcal{I}^{(h)}\widehat{\varphi}^j\right) = \left(\varphi^j_h, \varphi^j_h - \mathcal{I}^{(h)}\widehat{\varphi}^j\right) + \left(\varphi^{j-1}_h - \varphi^j_h, \varphi^j_h - \mathcal{I}^{(h)}\widehat{\varphi}^j\right), \tag{B.451a}$$

and similarly noting that

$$\left(\left(-\Delta_h\right)^{-1}\left(\varphi_h^j-m\right)_{\{\theta\}},\varphi_h^j-\mathcal{I}^{(h)}\widehat{\varphi}^j\right)=\left(\left(-\Delta_h\right)^{-1}\left(\varphi_h^j-m\right),\varphi_h^j-\mathcal{I}^{(h)}\widehat{\varphi}^j\right)$$
$$+(1-\theta)\left(\left(-\Delta_h\right)^{-1}\left(\varphi_h^{j-1}-\varphi_h^j\right),\varphi_h^j-\mathcal{I}^{(h)}\widehat{\varphi}^j\right). \quad \text{(B.451b)}$$

The two *red* terms on the left of (B.450) are additional to those in (B.414). They are due to the location of the linear term (at the lower time level), and the θ-method we attached to the non-local part of the problem.

ii) To deal with the first additional term on the left of (B.450), we set

$$u_h=\frac{\chi^{AB}}{2}\tau^2\left(\varphi_h^j-\mathcal{I}^{(h)}\widehat{\varphi}^j\right)=\frac{\chi^{AB}}{2}\tau^2\left(\varphi_h^j-P^{(h)}\widehat{\varphi}^j+P^{(h)}\widehat{\varphi}^j-\mathcal{I}^{(h)}\widehat{\varphi}^j\right)\in V^h$$

in (B.390b), and discover that (cf. (B.416))

$$\begin{aligned}\frac{\chi^{AB}}{2}\tau\left(\varphi_h^{j-1}-\varphi_h^j,\varphi_h^j-\mathcal{I}^{(h)}\widehat{\varphi}^j\right)&=\frac{\chi^{AB}}{2}\tau^2\left(\nabla\psi_h^j,\nabla\left(\varphi_h^j-\mathcal{I}^{(h)}\widehat{\varphi}^j\right)\right)\\&=\frac{\chi^{AB}}{2}\tau^2\left(\nabla\psi_h^j,\nabla\left(\varphi_h^j-P^{(h)}\widehat{\varphi}^j+P^{(h)}\widehat{\varphi}^j-\mathcal{I}^{(h)}\widehat{\varphi}^j\right)\right)\\&=\frac{\chi^{AB}}{2}\tau^2\left(-\Delta_h\psi_h^j,\varphi_h^j-\widehat{\varphi}^j\right)+\frac{\chi^{AB}}{2}\tau^2\left(-\Delta_h\psi_h^j,\widehat{\varphi}^j-\mathcal{I}^{(h)}\widehat{\varphi}^j\right).\end{aligned} \quad \text{(B.452)}$$

We re-write (B.390b) as

$$\left(-\Delta_h\psi_h^j,u_h\right)=-\left(\delta^{(\tau)}\varphi_h^j,u_h\right), \quad \text{(B.453a)}$$

for every $u_h\in V^h$. Setting $u_h=-\Delta_h\psi_h^j\in V^h$ leads to

$$\left\|-\Delta_h\psi_h^j\right\|^2\leq\left\|\delta^{(\tau)}\varphi_h^j\right\|\left\|-\Delta_h\psi_h^j\right\| \qquad \Rightarrow \qquad \left\|-\Delta_h\psi_h^j\right\|\leq\left\|\delta^{(\tau)}\varphi_h^j\right\|, \quad \text{(B.453b)}$$

by the Cauchy–Schwarz inequality.

iii) To deal with the second (non-local) additional term on the left of (B.450), we re-write (B.390b) as (cf. (B.342), (B.416))

$$\left(\left(-\Delta_h\right)^{-1}\delta^{(\tau)}\varphi_h^j,v_h\right)+\left(\psi_h^j,v_h\right)=0 \quad \text{(B.454)}$$

for every $v_h\in V^h$. Setting

$$v_h=\alpha\tau^2(1-\theta)\left(\varphi_h^j-\mathcal{I}^{(h)}\widehat{\varphi}^j\right)=\alpha\tau^2(1-\theta)\left(\varphi_h^j-P^{(h)}\widehat{\varphi}^j+P^{(h)}\widehat{\varphi}^j-\mathcal{I}^{(h)}\widehat{\varphi}^j\right)$$

in the above yields

$$\alpha\tau(1-\theta)\left(\left(-\Delta_h\right)^{-1}\left(\varphi_h^j-\varphi_h^{j-1}\right),\varphi_h^j-\mathcal{I}^{(h)}\widehat{\varphi}^j\right)$$
$$=-\alpha\tau^2(1-\theta)\left(\psi_h^j,\varphi_h^j-\widehat{\varphi}^j\right)-\alpha\tau^2(1-\theta)\left(\psi_h^j,\widehat{\varphi}^j-\mathcal{I}^{(h)}\widehat{\varphi}^j\right). \quad \text{(B.455)}$$

iv) The additional terms in (B.450) above express on the right side of a modified version of (B.424), using (B.452) and (B.455), as

$$\begin{aligned}\sum_{j=1}^{k} A_j \leq\ & \text{(IV)} - \text{(V)} + \text{(VI)} + \text{(VII)} + (8) + (9) + (10) + (11) \\ & + \underbrace{\frac{\chi^{AB}}{2} \sum_{j=1}^{k} \tau^2 \left(-\Delta_h \psi_h^j, \varphi_h^j - \widehat{\varphi}^j \right)}_{(12)} + \underbrace{\frac{\chi^{AB}}{2} \sum_{j=1}^{k} \tau^2 \left(-\Delta_h \psi_h^j, \widehat{\varphi}^j - \mathcal{I}^{(h)} \widehat{\varphi}^j \right)}_{(13)} \\ & \underbrace{-\alpha \sum_{j=1}^{k} \tau^2 (1-\theta) \left(\psi_h^j, \varphi_h^j - \widehat{\varphi}^j \right)}_{(14)} \underbrace{-\alpha \sum_{j=1}^{k} \tau^2 (1-\theta) \left(\psi_h^j, \widehat{\varphi}^j - \mathcal{I}^{(h)} \widehat{\varphi}^j \right)}_{(15)}. \end{aligned} \tag{B.456}$$

The other terms are unchanged. We bound the four new terms (12)–(15).

(12): this term has a similar structure to term (10) (cf. (B.436)). We find that

$$\begin{aligned} |(12)| &= \frac{\chi^{AB}}{2} \left| \sum_{j=1}^{k} \tau^2 \left(-\Delta_h \psi_h^j, \varphi_h^j - \widehat{\varphi}^j \right) \right| \\ &\leq \frac{\chi^{AB}}{2} \sum_{j=1}^{k} \tau \left\| -\Delta_h \psi_h^j \right\| \int_{t_{j-1}}^{t_j} \left\| e_{\varphi,h}(t) \right\| \, \mathrm{d}t \\ &\leq \frac{\chi^{AB}}{2} \sum_{j=1}^{k} \tau \left\| \delta^{(\tau)} \varphi_h^j \right\| \left\{ \tau^{1/2} \left(\int_{t_{j-1}}^{t_j} c_P^2 \left| e_{\varphi,h}(t) \right|_1^2 \, \mathrm{d}t \right)^{1/2} \right\} \\ &\leq C\tau^{1/2} \left(\sum_{j=1}^{k} \left\| \varphi_h^j - \varphi_h^{j-1} \right\|^2 \right)^{1/2} \left(\int_{t_0}^{t_k} \left| e_{\varphi,h}(t) \right|_1^2 \, \mathrm{d}t \right)^{1/2} \\ &\leq C\tau^{1/2} \left(\int_{t_0}^{t_k} \left| e_{\varphi,h}(t) \right|_1^2 \, \mathrm{d}t \right)^{1/2} \\ &\leq \frac{C\tau}{\varepsilon_\varphi^2 \nu} + \frac{\varepsilon_\varphi^2 \nu}{4} \int_0^{t_k} \left| e_{\varphi,h}(t) \right|_1^2 \mathrm{d}t, \end{aligned} \tag{B.457}$$

for any $\nu > 0$, after using (B.453b) and (B.406), and then Young's inequality.

(13): this term is structurally similar to term (8). Consequently,

$$\begin{aligned} |(13)| &= \left| \frac{\chi^{AB}}{2} \sum_{j=1}^{k} \tau^2 \left(-\Delta_h \psi_h^j, \widehat{\varphi}^j - \mathcal{I}^{(h)} \widehat{\varphi}^j \right) \right| \\ &\leq \frac{\chi^{AB}}{2} \sum_{j=1}^{k} \tau \left\| \delta^{(\tau)} \varphi_h^j \right\| \int_{t_{j-1}}^{t_j} \left\| \mathcal{I}^{(h)} \varphi(t) - \varphi(t) \right\| \mathrm{d}t \\ &\leq Ch^2 \left(\sum_{j=1}^{k} \left\| \varphi_h^j - \varphi_h^{j-1} \right\|^2 \right)^{1/2} \left(\int_0^{t_k} \left| \varphi(t) \right|_2^2 \, \mathrm{d}t \right)^{1/2} \\ &= Ch^2, \end{aligned} \tag{B.458}$$

after recalling (B.453b), (B.406) and that $\varphi \in L^2\left(0, T; H^2(\Omega)\right)$.

(14): this term has a similar structure to term (12). For $\frac{1}{2} \leq \theta < 1$,

$$\begin{aligned}
|(14)| &= \alpha\left(1-\theta\right)\left|\sum_{j=1}^{k}\tau^{2}\left(\psi_{h}^{j},\varphi_{h}^{j}-\widehat{\varphi}^{j}\right)\right| \\
&\leq C\sum_{j=1}^{k}\tau\left\|\psi_{h}^{j}\right\|\left\{\tau^{1/2}\left(\int_{t_{j-1}}^{t_{j}}\left|e_{\varphi,h}\left(t\right)\right|_{1}^{2}\,\mathrm{d}t\right)^{1/2}\right\} \\
&\leq C\tau\left(\sum_{j=1}^{k}\tau\left\|\psi_{h}^{j}\right\|^{2}\right)^{1/2}\left(\int_{0}^{t_{k}}\left|e_{\varphi,h}\left(t\right)\right|_{1}^{2}\,\mathrm{d}t\right)^{1/2} \\
&\leq \frac{CT^{1/2}\tau^{2}}{\varepsilon_{\varphi}^{2}\nu}+\frac{\varepsilon_{\varphi}^{2}\nu}{4}\int_{0}^{t_{k}}\left|e_{\varphi,h}\left(t\right)\right|_{1}^{2}\mathrm{d}t,
\end{aligned} \tag{B.459}$$

for any $\nu > 0$, after using (B.401).

(15): this final term has a similar structure to term (13). As such,

$$\begin{aligned}
|(15)| &= \alpha\left(1-\theta\right)\left|\sum_{j=1}^{k}\tau^{2}\left(\psi_{h}^{j},\widehat{\varphi}^{j}-\mathcal{I}^{(h)}\widehat{\varphi}^{j}\right)\right| \\
&\leq \alpha\left(1-\theta\right)\sum_{j=1}^{k}\tau\left\|\psi_{h}^{j}\right\|\int_{t_{j-1}}^{t_{j}}\left\|\mathcal{I}^{(h)}\varphi\left(t\right)-\varphi\left(t\right)\right\|\mathrm{d}t \\
&\leq Ch^{2}\tau^{1/2}\left(\sum_{j=1}^{k}\tau\left\|\psi_{h}^{j}\right\|^{2}\right)^{1/2}\left(\int_{0}^{t_{k}}\left|\varphi\left(t\right)\right|_{2}^{2}\,\mathrm{d}t\right)^{1/2} \\
&\leq CTh^{2}\left\|\varphi\right\|_{L^{2}\left(0,T;H^{2}(\Omega)\right)} = Ch^{2},
\end{aligned} \tag{B.460}$$

since $\tau \leq T$.

Remark. Terms (14) and (15) vanish if $\theta = 1$ (i.e. the non-local term is fully implicit).

As in the fully implicit case, the new terms above can all be absorbed into $\sigma\left(h,\tau\right)$ in (B.438b). The rest of the proof is thus (structurally) identical, apart from a few choices for constants.

Remark. The convex splitting formulation does not result in unconditional convergence viz. we can only prove convergence if $\tau \lesssim \varepsilon_{\varphi}^{2}$ as in (B.443).

□

Notes

[1]Blowey and Elliott (1991) omit the details of the proof of their Proposition 3.1, which corresponds to this result.

[2]See the sections 'a. Coercivity' and 'b. Lower semicontinuity' in Section 8.2.1 of Evans (1998).

[3]This is because $(\mathcal{E}[\varphi_k])_{k\in\mathbb{N}}$ is a convergent sequence of real numbers. Consequently, it contains, at most, a finite number of unbounded terms which we can remove.

[4]See Theorem 1 in Appendix B of Evans (1998).

[5]See the definition in Section 8.2.1 of Evans (1998).

[6]Ordinarily, when performing a variation, we would make $|\theta|$ small, but θ itself could be negative.

[7]$\mathbb{R}^N$ is clearly not compact, but the boundedness of T means that bounded sets $\{\boldsymbol{c}_i\} \subset \mathbb{R}^N$ map to bounded (closed) and compact sets in $\mathbb{R}^N$, which have convergence sub-sequences.

[8]The weak convergence that follows means that (cf. Defn 4.11 of Robinson (2001)) $\left\langle \eta, \varphi_\mu^{(N)} \right\rangle_1 \to \langle \eta, \varphi_\mu \rangle_1$ (in $\mathbb{R}$) as $N \to \infty$ for every $\eta \in \left(H^1(\Omega)\right)'$, i.e.

$$\left(\eta, \varphi_\mu^{(N)}\right) + \left(\nabla\eta, \nabla\varphi_\mu^{(N)}\right) \to (\eta, \varphi_\mu) + (\nabla\eta, \nabla\varphi_\mu) \qquad \text{(in } \mathbb{R}\text{) as} \qquad N \to \infty, \tag{B.461a}$$

for every $\eta \in \left(H^1(\Omega)\right)'$. Consequently, by symmetry, there are sub-sequences for which

$$\left(\varphi_\mu^{(N)}, \eta\right) \to (\varphi_\mu, \eta) \qquad \text{and} \qquad \left(\nabla\varphi_\mu^{(N)}, \nabla\eta\right) \to (\nabla\varphi_\mu, \nabla\eta) \qquad \text{(in } \mathbb{R}\text{) as} \qquad N \to \infty, \tag{B.461b}$$

for every $\eta \in H^1(\Omega)$ (and $\nabla\eta \in \left(L^2(\Omega)\right)^d$).

[9]Note the extraneous term '$|u_\epsilon|_0$' in the corresponding line in Blowey and Elliott (1991) – line 13, from the top of p. 254 of that article.

[10]The following result matches (2.49) of Blowey and Elliott (1991).

[11]See (2.50) of Blowey and Elliott (1991).

[12]See (3.5) of Blowey and Elliott (1991).

[13]A useful fact in this regard is that

$$\frac{1}{p} + \frac{1}{q} = 1 \qquad \Rightarrow \qquad (p-1)\,q = p.$$

We include the next derivation in detail because of the error in the corresponding part of Blowey and Elliott (1991).

[14]Only $W^{2,2}(\Omega) = H^2(\Omega)$ is a Hilbert space. We exclude $p = \infty$ because $L^\infty(\Omega)$ is not reflexive.

[15]See (3.8) of Blowey and Elliott (1991).

[16]See 3.4(b), (d) of Blowey and Elliott (1991).

[17]See (3.9) of Blowey and Elliott (1991).

[18]See the remarks above Proposition 3.1 in Blowey and Elliott (1991).

[19]What follows is our equivalent to problem $(\hat{\mathbf{S}}_\mu)$ in (3.10) of Blowey and Elliott (1991).

[20]See (3.11) of Blowey and Elliott (1991).

[21]This basic idea is from Section 2.3.1 of Parsons (2012).

[22]See (2.6) of Blowey and Elliott (1991).

[23]See (2.26) of Blowey and Elliott (1991).

[24]See (2.27) of Blowey and Elliott (1991).

[25]If $\|\varphi\|_{L^\infty\left(0,T;H^1(\Omega)\right)} \leq C$ independent of T then $\|\varphi\|_{L^2\left(0,T;H^1(\Omega)\right)} \leq C(T)$ i.e. the $L^2(0,T)$ bound is *not* uniform in T. This is because

$$\|\varphi\|^2_{L^2(0,T;V)} = \int_0^T \|\varphi\|_V^2 \;\mathrm{d}t \leq \int_0^T \operatorname*{ess\,sup}_{0\leq t\leq T} \|\varphi\|_V^2 \;\mathrm{d}t = T\,\|\varphi\|^2_{L^\infty(0,T;V)},$$

i.e. $\|\varphi\|_{L^2(0,T;V)} \leq \sqrt{T}\,\|\varphi\|_{L^\infty(0,T;V)}$. Unless there is another way to get this $L^2(0,T)$ bound (not shown in Blowey and Elliott (1991)), there is an error in this paper.

[26]This is identical to (2.56) in Blowey and Elliott (1991).

[27]See (2.57) of Blowey and Elliott (1991).

[28]As δ gets small, this last quantity will become very large. For $\delta > 0$ (strictly), it remains finite i.e. we do *not* consider a limiting process in which $\delta \downarrow 0$.

[29]This result says that if $u \in H^1\left(0,T;H^1\left(\Omega\right)\right)$, then $u \in C\left(\left[0,T\right];H^1\left(\Omega\right)\right)$, too. We replace the time interval $(0,T)$ in the theorem with our (δ,T).

[30]See (2.33) of Blowey and Elliott (1991); notice their typo 'u_k' on the left.

[31]We prove what follows:

$$\left(u-\overline{u},v-\overline{v}\right)=\left(u,v-\overline{v}\right)-\overline{u}\underbrace{\left(1,v-\overline{v}\right)}_{=0}=\left(u-\overline{u},v\right)-\overline{v}\underbrace{\left(u-\overline{u},1\right)}_{=0}=\left(u,v\right)-\overline{u}\left(1,v\right).$$

[32]See (2.35) of Blowey and Elliott (1991).

[33]See (2.36) of Blowey and Elliott (1991).

[34]See (2.37) of Blowey and Elliott (1991); notice their typo.

[35]This means that

$$\left\langle \varphi,\varphi_{\mu}^{(N)}\right\rangle _{L^{2}\left(0,T;H^{1}\left(\Omega\right)\right)}\rightarrow\left\langle \varphi,\varphi_{\mu}\right\rangle _{L^{2}\left(0,T;H^{1}\left(\Omega\right)\right)}$$

for every

$$\varphi\in\left(L^{2}\left(0,T;H^{1}\left(\Omega\right)\right)\right)'=L^{2}\left(0,T;\left(H^{1}\left(\Omega\right)\right)'\right),$$

where we have identified $L^2\left(0,T\right)$ with its dual $\left(L^2\left(0,T\right)\right)'$. In particular,

$$\int_{0}^{T}\left\langle \varphi,\varphi_{\mu}^{(N)}\right\rangle _{1}\,\mathrm{d}t\rightarrow\int_{0}^{T}\left\langle \varphi,\varphi_{\mu}\right\rangle _{1}\,\mathrm{d}t\qquad\qquad\text{(in }\mathbb{R}\text{) as}\qquad\qquad N\rightarrow\infty$$

for every $\varphi\in L^{2}\left(0,T;\left(H^{1}\left(\Omega\right)\right)'\right)$. This statement holds for any pairing between members of $\left(H^1\left(\Omega\right)\right)'$ and $H^1\left(\Omega\right)$, including those for which we choose the $L^2\left(\Omega\right)$ inner product.

[36]If we apply the Riesz Representation Theorem to the pairing $\left\langle \cdot,\cdot\right\rangle _{1}$, then

$$\int_{0}^{T}\left(\eta,\varphi_{\mu}^{(N)}\right)+\left(\nabla\eta,\nabla\varphi_{\mu}^{(N)}\right)\,\mathrm{d}t\rightarrow\int_{0}^{T}\left(\eta,\varphi_{\mu}\right)+\left(\nabla\eta,\nabla\varphi_{\mu}\right)\,\mathrm{d}t \tag{B.462}$$

(in $\mathbb{R}$) as $N\rightarrow\infty$, for every $\eta\in L^{2}\left(0,T;H^{1}\left(\Omega\right)\right)$. Now, the (sub-)sequence $\left(\nabla\varphi_{\mu}^{(N)}\right)$ is bounded in $L^{2}\left(0,T;L^{2}\left(\Omega\right)\right)$, another Hilbert space, and so it also has a sub-sequence which converges weakly, viz.

$$\nabla\varphi_{\mu}^{(N)}\rightharpoonup\nabla\varphi_{\mu}\qquad\qquad\text{in}\qquad\qquad L^{2}\left(0,T;L^{2}\left(\Omega\right)\right), \tag{B.463}$$

which leads to (B.113c). Combining (B.462) and (B.113c) leads to (B.113b).

[37]In detail (cf. Defn 4.16 of Robinson (2001)),

$$\left\langle \partial_{t}\varphi_{\mu}^{(N)},\psi\right\rangle _{L^{2}\left(0,T;H^{1}\left(\Omega\right)\right)}\rightarrow\left\langle \dot{\varphi},\psi\right\rangle _{L^{2}\left(0,T;H^{1}\left(\Omega\right)\right)}$$

for every $\psi\in L^{2}\left(0,T;H^{1}\left(\Omega\right)\right)$, where, by the reflexivity of Hilbert spaces,

$$\left(L^{2}\left(0,T;\left(H^{1}\left(\Omega\right)\right)'\right)\right)'=L^{2}\left(0,T;H^{1}\left(\Omega\right)\right).$$

[38]We show that $\dot{\varphi}=\partial_{t}\varphi_{\mu}$, so that in fact, $\partial_{t}\varphi_{\mu}^{(N)}\overset{\star}{\rightharpoonup}\partial_{t}\varphi_{\mu}$. Set $\psi=\phi\left(t\right)w\left(x\right)$ with $\phi\in C_{c}^{1}\left(0,T\right)$

(viz. $\phi(0) = \phi(T) = 0$) and $w \in H^1(\Omega)$. Integrating by parts in time yields

$$\begin{aligned}\int_0^T \left(\partial_t \varphi_\mu^{(N)}, \phi w\right) \mathrm{d}t &= \int_\Omega w(x) \left(\int_0^T \partial_t \varphi_\mu^{(N)} \phi(t) \ \mathrm{d}t\right) \mathrm{d}\Omega \\ &= \int_\Omega w(x) \left(\varphi_\mu^{(N)} \phi\Big|_{t=0}^{t=T} - \int_0^T \varphi_\mu^{(N)} \phi'(t) \ \mathrm{d}t\right) \mathrm{d}\Omega \\ &= -\int_0^T \left(\phi' w, \varphi_\mu^{(N)}\right) \mathrm{d}t \\ &\to -\int_0^T \left(\phi' w, \varphi_\mu\right) \mathrm{d}t = -\int_0^T \left(\varphi_\mu, \phi' w\right) \mathrm{d}t\end{aligned}$$

by (B.113b). But according to (B.114) and uniqueness of limits, we must have

$$\int_0^T \left(\phi' w, \varphi_\mu\right) \mathrm{d}t = -\int_0^T \left(\phi w, \dot{\varphi}\right) \mathrm{d}t$$

for every $\phi \in C_c^1(0,T)$ and $w \in H^1(\Omega)$. Hence, using the definition of weak derivatives of Banach space valued functions (cf. Section 5.9.2 of Evans (1998)) $\partial_t \varphi_\mu = \dot{\varphi}$.

The treatment of this part of Section 7.4.3 of Robinson (2001) is erroneous. See (27) in Theorem 3 of Section 7.1 of Evans (1998) and Problem 4 of that chapter.

[39]The existence of this convergent sub-sequence follows from the Alaoglu Theorem (Theorem 4.18 of Robinson (2001), 6.64 of Renardy and Rogers (2004) or Theorem 10 of Yosida (1980)) if we recall that $L^\infty(0,T)$ can be identified with the dual of $L^1(0,T)$, a separable Banach space. By contrast, we *cannot* identify $L^1(0,T)$ with the dual of $L^\infty(0,T)$; see Sections 4.2.3 and 4.2.4 of Robinson (2001). In fact, $L^\infty(0,T)$ is neither separable nor reflexive, whereas $L^1(0,T)$ is separable as in Proposition 1.15 of Robinson (2001), but not reflexive. See Sections 1.4.3 and 4.4 of Robinson (2001).

[40]Note the typo in the corresponding part of Theorem 2.1 of Blowey and Elliott (1991): passing to the limit in their (2.21b) leads to (2.17a), not (2.7a).

[41]See (2.39) of Blowey and Elliott (1991).

[42]Note the error in the corresponding result in Blowey and Elliott (1991), in the identity immediately after their (2.40).

[43]See (2.40) of Blowey and Elliott (1991).

[44]This is because we must have $\varphi_\mu(t) \in H^1(\Omega)$ for the energy to be finite.

[45]See (2.47) of Blowey and Elliott (1991).

[46]Note the typo at the corresponding point in Blowey and Elliott (1991): they pass to the limit in their (2.17b), and should recover (2.7a), not (2.7b) as printed.

[47]This corresponds to (2.48) of Blowey and Elliott (1991).

[48]See (2.50) of Blowey and Elliott (1991).

[49]See (2.51) in Blowey and Elliott (1991). In what follows, we use the notation

$$\|u\|_{L^2\left(0,T;H^1(\Omega)\right)} := \left(\|u\|^2_{L^2(\Omega_T)} + |u|^2_{L^2\left(0,T;H^1(\Omega)\right)}\right)^{1/2}.$$

[50]In what follows, we subtract off the mass average of the potential ω to ensure well-posedness.

[51]Intuitively, we may substitute (4.37a) into the term on the right-hand side of (4.37b) to arrive at (4.38).

[52]The results in (B.166) match the corresponding unnumbered results in Blowey and Elliott (1991).

[53]See also (2.54) of Blowey and Elliott (1991).

[54]This result uses the same 'stop-start' argument as in the latter stages of Theorem 2.2 of Blowey and Elliott (1991).

[55]See (2.61) of Blowey and Elliott (1991).

[56]Notice the missing factor of $\frac{1}{2}$ in the last term in (2.61) of Blowey and Elliott (1991).

[57]See (2.62) of Blowey and Elliott (1991).

[58]See (2.68) of Blowey and Elliott (1991).

[59]See Defn 5.2 in Sutherland (2009) or Defn 1.1-1 of Kreyszig (1978): a metric space is a non-empty set X, together a metric d satisfying the following axioms:

(M1) $d(x,y) \geq 0$ for all $x, y \in X$ and $d(x,y) = 0 \Leftrightarrow x = y$;

(M2) (Symmetry): $d(x,y) = d(y,x)$ for all $x, y \in X$; and

(M3) (Triangle inequality): $d(x,z) \leq d(x,y) + d(y,z)$ for all $x, y, z \in X$.

[60]This means that its closure, $\overline{\bigcup_{\tau \geq t} S(\tau)\varphi_0}$, is compact.

[61]Notice the two test-space function typos in (2.73) and (2.74) ($\eta \in K_m, K$ should be χ) of Blowey and Elliott (1991).

[62]See also (2.27) of Blowey and Elliott (1991).

[63]We can also bound $\|\psi(t)\|_1$. To do so, we need a bound on $|(\psi, 1)|$. We set $\nu_2 = 1$ in (B.215c) and, using (4.7) and (4.22c), find that (cf. (B.105))

$$|(\psi,1)| \leq \frac{\chi^{AB}}{2} |(\varphi_\mu,1)| + (|\zeta_\mu(\varphi_\mu)|, 1) \leq \frac{\chi^{AB}}{2} |(\varphi_\mu,1)| + (\zeta_\mu(\varphi_\mu), \varphi_\mu).$$

Setting $\nu_2 = \varphi_\mu$ in (B.215c) and rearranging then yields (cf. (B.106))

$$(\zeta_\mu(\varphi_\mu), \varphi_\mu) \leq \frac{\chi^{AB}}{2} \|\varphi_\mu\|^2 + (\psi, \varphi_\mu) - (F, \varphi_\mu)$$

after recalling (B.107) and that $\varepsilon_\varphi^2 |\varphi_\mu|_1^2 \geq 0$. Combining the last two results, and noting that $(\varphi_\mu, 1) = m|\Omega|$ for a.e. t, we determine that (cf. (B.108))

$$|(\psi,1)| \leq \frac{\chi^{AB}}{2} |m| |\Omega| + \frac{\chi^{AB}}{2} \|\varphi_\mu\|^2 - (F, \varphi_\mu) + (\psi, \varphi_\mu). \tag{B.464}$$

Setting $u = \psi$ and $v = \varphi_\mu$ in (B.109) leads to (cf. (B.110))

$$\begin{aligned}(\psi, \varphi_\mu) &= (\psi, \varphi_\mu - m) + \overline{\psi}(\varphi_\mu, 1) = \left(\nabla\psi, \nabla(-\Delta_n)^{-1}(\varphi_\mu - m)\right) + m(\psi, 1) \\ &\leq |\psi|_1 \left|(-\Delta_n)^{-1}(\varphi_\mu - m)\right|_1 + m(\psi,1) \leq |\psi|_1 \|\varphi_\mu - m\|_{-1} + |m| |(\psi,1)|,\end{aligned} \tag{B.465}$$

where we used (2.1), (2.9), (2.11), mass conservation, and the Cauchy–Schwarz inequality. Combining (B.464) and (B.465) with $|m| < 1$ leads to (cf. (B.111))

$$|(\psi,1)| \leq \frac{\frac{\chi^{AB}}{2} |m| |\Omega| + \frac{\chi^{AB}}{2} \|\varphi_\mu\|^2 + \frac{1}{2}\|F\|^2 + \frac{1}{2}\|\varphi_\mu\|^2}{1 - |m|} + \frac{c_P^2 |\varphi_\mu|_1}{1 - |m|} |\psi|_1$$

after using Young's inequality, (A.28) to obtain $\|\varphi_\mu - m\|_{-1} \leq c_P^2 |\varphi_\mu|_1$, and rearranging. Since (4.62) holds, we have discovered that (cf. (B.112b))

$$|(\psi(t), 1)| \leq C + C|\psi(t)|_1 \tag{B.466}$$

for a.e. $t \in (0,T)$, where both constants C are independent of μ. A comparison of (B.466) and Poincaré's inequality (A.2) reveals that

$$\|\psi(t)\| \leq c_P \left\{ |(\psi(t), 1)| + |\psi(t)|_1 \right\} \tag{B.467}$$

for a.e. $t \in (0,T)$, and since (B.238) is true, we conclude that

$$\psi \in L^\infty\left(0, T; H^1(\Omega)\right). \tag{B.468}$$

[64]We originally noted what follows in Parsons (2012); see also the equation following (2.40) in Blowey and Elliott (1991).

[65]See (2.45) of Parsons (2012).

[66]See also (2.47) of Parsons (2012).

[67]See (2.39b) of Blowey and Elliott (1991).

[68]This result matches Lemma 10.52 of Renardy and Rogers (2004).

[69]Note that if $\varphi \in H^1_*(\Omega)$, then $\overline{\varphi + m} = m$. Then Poincaré's inequality gives

$$\|\varphi + m\| \leq c_P \left|\varphi + m - \overline{\varphi + m}\right|_1 = c_P \left|\varphi\right|_1 .$$

[70]Zeidler (1990) shows that strong monotonicity generally implies coercivity.

[71]In the above, we can apply Lemma A.1.10, if we note that (5.8) implies that φ^j satisfies (cf. (A.40))

$$\left(\nabla\varphi^j, \nabla\nu\right) = (g, \nu)$$

for every $\nu \in H^1_*(\Omega)$ with

$$g = \frac{1}{\varepsilon_\varphi^2}\left(\frac{\chi^{AB}}{2}\varphi^{j-1} - (-\Delta_n)^{-1}\delta^{(\tau)}\varphi^j - \zeta_\mu\left(\varphi^j\right) - \alpha\,(-\Delta_n)^{-1}\left(\varphi^j - \overline{\varphi^j}\right)_{\{\theta\}} + (-\Delta_n)^{-1}\widetilde{f}^j\right).$$

The fact that the test space has zero mass has no impact on the application of Lemma A.1.10.

[72]The details are

$$\int_\Omega \delta^{(\tau)}\varphi^j \,\mathrm{d}\Omega - \underbrace{\int_\Omega \Delta\omega^j \,\mathrm{d}\Omega}_{=0} + \alpha \underbrace{\int_\Omega \left(\varphi^j - \overline{\varphi^j}\right)_{\{\theta\}} \mathrm{d}\Omega}_{=0} = \underbrace{\int_\Omega \widetilde{f}^j \,\mathrm{d}\Omega}_{=0}.$$

[73]As in (B.175),

$$\left(\zeta_\mu\left(\varphi^j\right), -\Delta\varphi^j\right) + \alpha\left((-\Delta_n)^{-1}\left(\varphi^j - m\right), -\Delta\varphi^j\right) \geq 0.$$

[74]See also (2.39) of Blowey and Elliott (1991).

[75]Each $\varphi^k \in H^1_*(\Omega) \subset L^2_*(\Omega)$ and we showed that $\|\cdot\|_{-1}$ is a norm on $L^2_*(\Omega)$ in Appendix A.1.2.

[76]See (3.2) of Blowey and Elliott (1992).

[77]See (2.15) of Blowey and Elliott (1992).

[78]See (3.1 b) of Blowey and Elliott (1992).

[79]See (3.7)–(3.8) of Bosch et al. (2014a); notice that the last term on the right of their (3.8) should be $\langle y_2, \psi\rangle$, not $\langle y_1, \varphi\rangle$.

[80]Our (B.368) corresponds to the unnumbered equation after (3.8) in Bosch et al. (2014a), which appears to be erroneous.

[81]See (3.9) of Bosch et al. (2014a).

[82]See (3.10)-(3.11) of Bosch et al. (2014a).

[83]See (3.5) of Bosch et al. (2014a).

[84]Note that φ_h^j does not have a zero Neumann BC (it can't), but that the $-\Delta_h$ operates in V^h as if it did.

[85]This form of the problem most closely resembles (1.2a) of Blowey and Elliott (1992).

[86]See (3.29) of Blowey and Elliott (1992) as the basis for what follows. We avoid some of the complexity in that reference as we do not use the $(\cdot,\cdot)^h$ inner product.

[87]We mimic the build-up to (3.26)–(3.27) of Blowey and Elliott (1992).

[88] For the third part of what follows, we use

$$\begin{aligned}
&\int_{t_{j-1}}^{t_j} \left(\delta^{(\tau)}\varphi_h^j, (-\Delta_n)^{-1}(\varphi - m)\right)\mathrm{d}t \\
&\quad= \left(\delta^{(\tau)}\varphi_h^j, (-\Delta_n)^{-1}\int_{t_{j-1}}^{t_j}(\varphi - m)\,\mathrm{d}t\right) \\
&\quad= \left(\varphi_h^j - \varphi_h^{j-1}, (-\Delta_n)^{-1}\frac{1}{\tau}\int_{t_{j-1}}^{t_j}(\varphi - m)\,\mathrm{d}t\right) \\
&\quad= \left(\varphi_h^j - \varphi_h^{j-1}, (-\Delta_n)^{-1}\left(\widehat{\varphi}^j - \varphi_{j-1}\right)\right) + \left(\varphi_h^j - \varphi_h^{j-1}, (-\Delta_n)^{-1}(\varphi_{j-1} - m)\right),
\end{aligned}$$

and

$$\begin{aligned}
&-\left(\varphi_j-\varphi_{j-1},(-\Delta_n)^{-1}\left(\varphi_h^j-m\right)\right)-\left(\varphi_h^j-\varphi_h^{j-1},(-\Delta_n)^{-1}\left(\varphi_{j-1}-m\right)\right)\\
&\quad=-\left((-\Delta_n)^{-1}\left(\varphi_j-m\right),\varphi_h^j\right)+\left((-\Delta_n)^{-1}\left(\varphi_{j-1}-m\right),\varphi_h^j\right)\\
&\qquad-\left(\varphi_h^j-\varphi_h^{j-1},(-\Delta_n)^{-1}\left(\varphi_{j-1}-m\right)\right)\\
&\quad=-\left(\varphi_j,(-\Delta_n)^{-1}\left(\varphi_h^j-m\right)\right)+\left(\varphi_h^{j-1},(-\Delta_n)^{-1}\left(\varphi_{j-1}-m\right)\right).
\end{aligned}$$

[89]In what follows, it is useful to note that

$$\begin{aligned}
\left\|\varphi_j-\varphi_h^j\right\|_{-1}^2&=\left(\varphi_j-\varphi_h^j,(-\Delta_n)^{-1}\left(\varphi_j-m+m-\varphi_h^j\right)\right)\\
&=\left(\varphi_j,(-\Delta_n)^{-1}\left(\varphi_j-m\right)\right)-2\left(\varphi_j,(-\Delta_n)^{-1}\left(\varphi_h^j-m\right)\right)\\
&\quad+\left(\varphi_h^j,(-\Delta_n)^{-1}\left(\varphi_h^j-m\right)\right)\\
&=\left\|\varphi_j-m\right\|_{-1}^2-2\left(\varphi_j,(-\Delta_n)^{-1}\left(\varphi_h^j-m\right)\right)+\left\|\varphi_h^j-m\right\|_{-1}^2,
\end{aligned}$$

since

$$\left(\varphi_h^j,(-\Delta_n)^{-1}\left(\varphi_j-m\right)\right)=\left((-\Delta_n)^{-1}\left(\varphi_h^j-m\right),\varphi_j\right).$$

[90]See (3.26) of Blowey and Elliott (1992).

[91]See (3.30) and (3.31) of Blowey and Elliott (1992). We do not have terms corresponding to their (VIII)–(X), as we ignore the effects of numerical quadrature.

[92]See (3.32) of Blowey and Elliott (1992), but note that our IC is different from theirs.

[93]In what follows, we frequently use the Cauchy–Schwarz inequality for sums

$$\left(\sum_i a_i b_i\right)^2\le\left(\sum_i {a_i}^2\right)\left(\sum_i {b_i}^2\right)$$

in the form

$$\sum_i a_i^{1/2}b_i^{1/2}\le\left(\sum_i a_i\right)^{1/2}\left(\sum_i b_i\right)^{1/2}.$$

[94]Our reasoning in (B.434) closely matches that in (3.38) of Blowey and Elliott (1992).

[95]See (3.42) of Blowey and Elliott (1992).

[96]See (3.44) of Blowey and Elliott (1992). Notice that those authors have retained δ in their (3.44), even though they have already specified that $\delta=1-\nu$.

[97]See (3.45) of Blowey and Elliott (1992).

[98]See (3.46) of Blowey and Elliott (1992).

[99]See (3.47) of Blowey and Elliott (1992).

Appendix C

The 2-phase problem in 1D

C.1 Alternative proof of Lemma 6.1.1

Proof.

i) We recall Leibnitz's rule, which says that

$$\frac{\mathrm{d}}{\mathrm{d}y}\int_{h(y)}^{g(y)} f(x,y)\,\mathrm{d}x = f(g(y),y)\,g'(y) - f(h(y),y)\,h'(y) + \int_{h(y)}^{g(y)} \partial_y f(x,y)\,\mathrm{d}x. \tag{C.1}$$

ii) Using the above, initially with y in (C.1) set to x_L,

$$\begin{aligned}
\partial_{x_L}\mathscr{L} = {} & \frac{\varepsilon_\varphi^2}{2}\left(-\left(\widetilde{\varphi}'(x_L)\right)^2\right) + \varepsilon_\varphi^2\int_{x_L}^{x_R}\left(\partial_{x_L}\widetilde{\varphi}'\right)\widetilde{\varphi}'\,\mathrm{d}x \\
& -\frac{\chi^{AB}}{4}\underbrace{\left(1-\widetilde{\varphi}^2(x_L)\right)}_{=0} - \frac{\chi^{AB}}{2}\int_{x_L}^{x_R}\left(\partial_{x_L}\widetilde{\varphi}\right)\widetilde{\varphi}\,\mathrm{d}x + \alpha\int_{-L/2}^{L/2}\left(\partial_{x_L}\Phi'\right)\Phi'\,\mathrm{d}x \\
& -\lambda\Bigg(\underbrace{\int_{-L/2}^{x_L}\partial_{x_L}\varphi\,\mathrm{d}x}_{=0} + \int_{x_L}^{x_R}\partial_{x_L}\widetilde{\varphi}\,\mathrm{d}x + \underbrace{\int_{x_R}^{L/2}\partial_{x_L}\varphi\,\mathrm{d}x}_{=0}\Bigg) \\
& -\partial_{x_L}\lambda\left(\int_{-L/2}^{L/2}\varphi\,\mathrm{d}x - mL\right)
\end{aligned}$$

(since $\widetilde{\varphi}(x_L) = -1$ and noting that λ is constant in x, but may depend on x_L)

$$\begin{aligned}
= {} & -\frac{\varepsilon_\varphi^2}{2}\left(\widetilde{\varphi}'(x_L)\right)^2 + \varepsilon_\varphi^2\left(\partial_{x_L}\widetilde{\varphi}\right)\widetilde{\varphi}'\big|_{x_L}^{x_R} + \alpha\left(\partial_{x_L}\Phi'\right)\Phi\big|_{-L/2}^{L/2} \\
& +\int_{x_L}^{x_R}\left(\varepsilon_\varphi^2\left(-\widetilde{\varphi}''\right) - \frac{\chi^{AB}}{2}\widetilde{\varphi} - \lambda\right)\left(\partial_{x_L}\widetilde{\varphi}\right)\mathrm{d}x \\
& -\partial_{x_L}\lambda\left(\int_{-L/2}^{L/2}\varphi\,\mathrm{d}x - mL\right) + \alpha\Bigg(\int_{-L/2}^{x_L}\partial_{x_L}\left(\varphi-\overline{\varphi}\right)\Phi\,\mathrm{d}x \\
& +\int_{x_L}^{x_R}\partial_{x_L}\left(\widetilde{\varphi}-\overline{\varphi}\right)\Phi\,\mathrm{d}x + \int_{x_R}^{L/2}\partial_{x_L}\left(\varphi-\overline{\varphi}\right)\Phi\,\mathrm{d}x\Bigg)
\end{aligned}$$

(integrating by parts twice, swapping $\partial_{x_L} \leftrightarrow \partial_x$ and noting that $-\Phi'' = \varphi - \overline{\varphi}$)

$$\begin{aligned}
= {} & -\frac{\varepsilon_\varphi^2}{2}\left(\widetilde{\varphi}'(x_L)\right)^2 + \varepsilon_\varphi^2\left(\partial_{x_L}\widetilde{\varphi}\right)\widetilde{\varphi}'\big|_{x_L}^{x_R} - \alpha\partial_{x_L}\overline{\varphi}\underbrace{\int_{-L/2}^{L/2}\Phi\,\mathrm{d}x}_{=0} \\
& +\int_{x_L}^{x_R}\left(\varepsilon_\varphi^2\left(-\widetilde{\varphi}''\right) - \frac{\chi^{AB}}{2}\widetilde{\varphi} - \lambda + \alpha\Phi\right)\left(\partial_{x_L}\widetilde{\varphi}\right)\mathrm{d}x - \partial_{x_L}\lambda\left(\int_{-L/2}^{L/2}\varphi\,\mathrm{d}x - mL\right)
\end{aligned}$$

(C.2)

using (6.1b), noting that $\varphi := \widetilde{\varphi}$ on (x_L, x_R), and recalling that $\varphi \equiv -1$ on $\left[-\frac{L}{2}, x_L\right)$ and $\varphi \equiv 1$ on $\left(x_R, \frac{L}{2}\right]$ means that $\partial_{x_L}\varphi \equiv 0$ on $\left[-\frac{L}{2}, x_L\right) \cup \left(x_R, \frac{L}{2}\right]$. In addition, according to (6.8), $\partial_{x_L}\Phi' = 0$ at $x = -\frac{L}{2}, \frac{L}{2}$; we also note that $\overline{\varphi}$ is constant on Ω (i.e. in x), but clearly depends on x_L. Now, viewing $\widetilde{\varphi}$ as a function of x_L, x_R and $x = x(x_L, x_R)$, it is clear that

$$\frac{\mathrm{d}}{\mathrm{d}x_L}\widetilde{\varphi}\left(x\left(x_L,x_R\right),x_L,x_R\right) = \partial_x\widetilde{\varphi}\left(x\left(x_L,x_R\right),x_L,x_R\right)\frac{\mathrm{d}x}{\mathrm{d}x_L} + \partial_{x_L}\widetilde{\varphi}\left(x\left(x_L,x_R\right),x_L,x_R\right)$$

and similarly,

$$\frac{\mathrm{d}}{\mathrm{d}x_R}\widetilde{\varphi}\left(x\left(x_L,x_R\right),x_L,x_R\right) = \partial_x\widetilde{\varphi}\left(x\left(x_L,x_R\right),x_L,x_R\right)\frac{\mathrm{d}x}{\mathrm{d}x_R} + \partial_{x_R}\widetilde{\varphi}\left(x\left(x_L,x_R\right),x_L,x_R\right)$$

by the Chain Rule. Consequently, setting $x(x_L, x_R) = x_L$ (or $x(x_L, x_R) = x_R$ as appropriate), and differentiating the conditions $\widetilde{\varphi}(x_L) = -1$ and $\widetilde{\varphi}(x_R) = 1$ from (6.4a), we see that

$$\partial_x\widetilde{\varphi}(x_L,x_L,x_R) + \partial_{x_L}\widetilde{\varphi}(x_L,x_L,x_R) = 0 \qquad \Rightarrow \qquad \partial_{x_L}\widetilde{\varphi}(x_L) = -\widetilde{\varphi}'(x_L), \tag{C.3a}$$

and likewise,

$$\partial_x\widetilde{\varphi}(x_R,x_L,x_R) + \partial_{x_R}\widetilde{\varphi}(x_R,x_L,x_R) = 0 \qquad \Rightarrow \qquad \partial_{x_R}\widetilde{\varphi}(x_R) = -\widetilde{\varphi}'(x_R). \tag{C.3b}$$

Similarly, at $x = x_L$,

$$\frac{\mathrm{d}}{\mathrm{d}x_R}\widetilde{\varphi}(x_L,x_L,x_R) = \partial_x\widetilde{\varphi}(x_L,x_L,x_R)\underbrace{\frac{\mathrm{d}x_L}{\mathrm{d}x_R}}_{=0} + \partial_{x_R}\widetilde{\varphi}(x_L,x_L,x_R) = \partial_{x_R}\widetilde{\varphi}(x_L) = 0; \tag{C.3c}$$

moreover, taking total derivatives in x_L at $x = x_R$ leads to

$$\partial_{x_L}\widetilde{\varphi}(x_R) = 0. \tag{C.3d}$$

Hence, the boundary terms in (C.2) above simplify, and we obtain

$$\begin{aligned}\partial_{x_L}\mathscr{L} = \frac{\varepsilon_\varphi^2}{2}\left(\widetilde{\varphi}'(x_L)\right)^2 - (\partial_{x_L}\lambda)\left(\int_{-L/2}^{L/2}\varphi\,\mathrm{d}x - mL\right)\\ + \int_{x_L}^{x_R}\left(\varepsilon_\varphi^2\left(-\widetilde{\varphi}''\right) - \frac{\chi^{AB}}{2}\widetilde{\varphi} - \lambda + \alpha\Phi\right)(\partial_{x_L}\widetilde{\varphi})\,\mathrm{d}x.\end{aligned} \tag{C.4a}$$

By an analogous argument, we find that (notice the sign change in the boundary term),

$$\begin{aligned}\partial_{x_R}\mathscr{L} = -\frac{\varepsilon_\varphi^2}{2}\left(\widetilde{\varphi}'(x_R)\right)^2 - (\partial_{x_R}\lambda)\left(\int_{-L/2}^{L/2}\varphi\,\mathrm{d}x - mL\right)\\ + \int_{x_L}^{x_R}\left(\varepsilon_\varphi^2\left(-\widetilde{\varphi}''\right) - \frac{\chi^{AB}}{2}\widetilde{\varphi} - \lambda + \alpha\Phi\right)(\partial_{x_R}\widetilde{\varphi})\,\mathrm{d}x.\end{aligned} \tag{C.4b}$$

iii) We now vary $\widetilde{\varphi}$ (viz. the interface layer) by $\theta\eta$ for $\theta \in \mathbb{R}$ and $\eta \in C_c^\infty(x_L, x_R)$, a smooth function with compact support in the interface layer.[1] Using (6.5), but replacing the non-local energy term with that appearing in (6.3), we conclude that[2]

$$\begin{aligned}\mathscr{L}[\varphi+\theta\eta;\boldsymbol{x},\lambda] - \mathscr{L}[\varphi;\boldsymbol{x},\lambda] = \int_{x_L}^{x_R}\Big\{\frac{\varepsilon_\varphi^2}{2}\left(2\theta\widetilde{\varphi}'\eta' + \theta^2\left(\eta'\right)^2\right) - \frac{\chi^{AB}}{4}\left(2\theta\widetilde{\varphi}\eta + \theta^2\eta^2\right)\\ - \lambda\theta\eta + \frac{\alpha}{2}\eta\left(2\theta\Phi + \theta^2\left(-\Delta_n\right)^{-1}(\eta - \overline{\eta})\right)\Big\}\,\mathrm{d}x.\end{aligned} \tag{C.5}$$

Hence, the Gâteaux variation of $\mathscr{L}$ at φ (cf. Defn 1.5 of Sagan (1969)) is

$$\delta\mathscr{L}\left[\eta\right] := \lim_{\theta\to 0}\left\{\frac{\mathscr{L}\left[\varphi+\theta\eta;\boldsymbol{x},\lambda\right]-\mathscr{L}\left[\varphi;\boldsymbol{x},\lambda\right]}{\theta}\right\} = \int_{x_L}^{x_R}\varepsilon_\varphi^2\widetilde{\varphi}'\eta' - \frac{\chi^{AB}}{2}\widetilde{\varphi}\eta - \lambda\eta + \alpha\Phi\eta\ \mathrm{d}x.$$

Integrating by parts in the first term of the right-hand side above leads to

$$\int_{x_L}^{x_R}\widetilde{\varphi}'\eta'\ \mathrm{d}x = \widetilde{\varphi}'\eta\big|_{x_R}^{x_L} - \int_{x_L}^{x_R}\widetilde{\varphi}''\eta\ \mathrm{d}x = \int_{x_L}^{x_R}\left(-\widetilde{\varphi}''\right)\eta\ \mathrm{d}x$$

since $\eta\in C_c^\infty\left(x_L,x_R\right)$ which means that $\eta\left(x_L\right)=\eta\left(x_R\right)=0$. We determine that

$$\delta\mathscr{L}\left[\eta\right] = \int_{x_L}^{x_R}\left(\varepsilon_\varphi^2\left(-\widetilde{\varphi}''\right) - \frac{\chi^{AB}}{2}\widetilde{\varphi} - \lambda + \alpha\Phi\right)\eta\ \mathrm{d}x \tag{C.6}$$

and conclude that $\frac{\delta\mathscr{L}}{\delta\widetilde{\varphi}}=0$ if $\delta\mathscr{L}\left[\eta\right]=0$ for every $\eta\in C_c^\infty\left(x_L,x_R\right)$. It follows that (6.10) is necessary for a stationary stationary $B\to A$ interface layer. Alternatively, we could work directly from the Euler–Lagrange equation. Write the Lagrangian (6.5) as

$$\mathscr{L}\left[\varphi;\boldsymbol{x},\lambda\right] = \int_{-L/2}^{L/2}L\left(x,\varphi,\varphi'\right)\mathrm{d}x \tag{C.7a}$$

where

$$L\left(x,\varphi,\varphi'\right) = \frac{\varepsilon_\varphi^2}{2}\left(\varphi'\right)^2 + \frac{\chi^{AB}}{4}\left(1-\varphi^2\right) + \frac{\alpha}{2}\left(\varphi-\overline{\varphi}\right)\left(\left(-\Delta_n\right)^{-1}\left(\varphi-\overline{\varphi}\right)\right) - \lambda\left(\varphi-m\right). \tag{C.7b}$$

The bulk and interfacial components are zero where $\varphi=\pm1$ (i.e. outside of the interface layer) as a result of our solution *ansatz*. From the Euler–Lagrange equation (cf. (2.3.8) of Section 2.3 of Sagan (1969)),

$$\frac{\delta\mathscr{L}}{\delta\widetilde{\varphi}} = -\frac{\mathrm{d}}{\mathrm{d}x}\left(\partial_{\widetilde{\varphi}'}L\right) + \partial_{\widetilde{\varphi}}L = \varepsilon_\varphi^2\left(-\widetilde{\varphi}''\right) - \frac{\chi^{AB}}{2}\widetilde{\varphi} - \lambda + \alpha\Phi$$

which leads to (6.10).

iv) Setting $\partial_\lambda\mathscr{L}=0$ retrieves the mass constraint $\overline{\varphi}=m$ (6.1c) which we write as (6.11), and removes the two $\left(\int_{-L/2}^{L/2}\varphi\ \mathrm{d}x - mL\right)$ terms from (C.4).

v) Specifying that $\partial_{x_L}\mathscr{L}=\partial_{x_R}\mathscr{L}=0$, for an energy minimising $\boldsymbol{x}$ leads to (6.9).

□

C.2 Interfacial structure in Region I

First, we have the following useful result, which we state without proof.

Lemma C.2.1. (Monotone morphologies) *Any monotone, single-layer morphology solving the ODE* (6.17)*, is bounded as in* (7.1a)*, viz.* $\left\|\widetilde{\varphi}\right\|_{0,\infty}\leq 1$.

We assert that all of the morphologies in Region I are monotone, and thus bounded.

Conjecture C.2.2. (Properties of c_A) *For* $\widehat{q}_h>\widehat{q}_\ell$, $c_A\left(\widehat{\ell},\widehat{\alpha}\right)$ *in* (6.29b) *on p. 129, has*

$$\widehat{\ell} < \frac{\pi}{\sqrt{\widehat{q}_h}} \qquad\Rightarrow\qquad c_A\left(\widehat{\ell},\widehat{\alpha}\right) < 0; \tag{C.8a}$$

viz. c_A *is negative inside Region I, and*

$$c_A\left(\widehat{\ell},\widehat{\alpha}\right)\uparrow 0 \qquad \textit{as} \qquad \widehat{\ell}\downarrow 0 \qquad \textit{for any} \qquad \widehat{\alpha}\in\left(0,\frac{1}{4}\right). \tag{C.8b}$$

Evidence.

i) For (C.8a), see Fig. C.1. c_A is clearly smooth and note that

$$c_A\left(\widehat{\ell}=0\right)=0, \qquad c_A\left(\widehat{\alpha}=0\right)=0, \qquad c_A\left(\widehat{\alpha}=\frac{1}{4}\right)=0, \tag{C.9}$$

by substitution.

ii) (C.8b) is clear from the above.

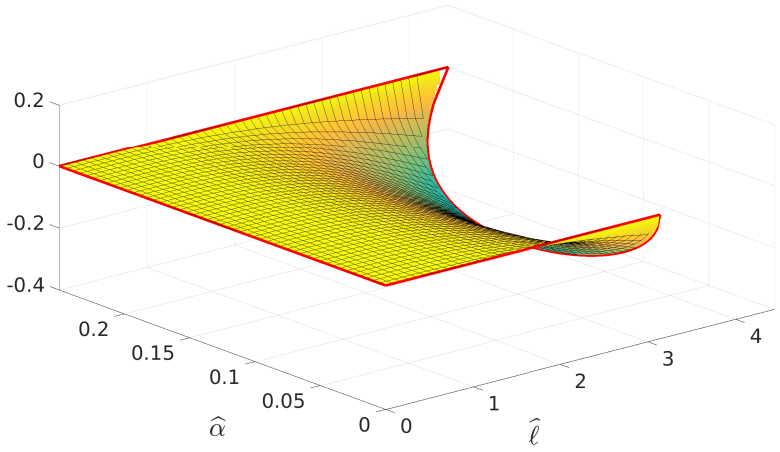

Figure C.1: The function $c_A\left(\widehat{\ell},\widehat{\alpha}\right)$ over Region I. The edges of Region I have been embedded in the surface in **red**.

□

As a consequence of Conjecture C.2.2 and recalling the relationship between c_1, c_3 and c_A in (6.59c), we see that

$$c_1\left(\widehat{\ell}\right)\to-\infty \qquad \text{and} \qquad c_3\left(\widehat{\ell}\right)\to+\infty \qquad \text{as} \qquad \widehat{\ell}\downarrow 0, \tag{C.10}$$

which means that the high (c_3)/low (c_1) frequency coefficients are related as

$$\frac{\text{high frequency coefficient}}{\text{low frequency coefficient}}=\frac{c_3}{c_1}=-\frac{\sqrt{\widehat{q}_\ell}\cos\left(\sqrt{\widehat{q}_\ell}\,\frac{\widehat{\ell}}{2}\right)}{\sqrt{\widehat{q}_h}\cos\left(\sqrt{\widehat{q}_h}\,\frac{\widehat{\ell}}{2}\right)}\to-\sqrt{\frac{\widehat{q}_\ell}{\widehat{q}_h}} \qquad \text{as} \qquad \widehat{\ell}\downarrow 0.$$

We depict these phenomena in Fig. C.2(b).

Conjecture C.2.3. (Region I interface layers are monotone) *All of the interface layers in Region I ($0<\widehat{\ell}\leq\pi/\sqrt{\widehat{q}_h}$) are monotone. Consequently, they all satisfy $\|\widetilde{\varphi}\|_\infty\leq 1$. The second derivative of these interface layers admits a single zero (only) at $\widehat{x}=0$.*

Evidence. We show that morphologies in Region I have zero derivative only at $\widehat{x}=\pm\frac{\widehat{\ell}}{2}$.

i) The spatial derivative of the interface layer (6.59b) is

$$\frac{\mathrm{d}\widetilde{\varphi}}{\mathrm{d}\widehat{x}} = \sqrt{\widehat{q}_h\widehat{q}_\ell}\frac{\cos\left(\sqrt{\widehat{q}_h}\frac{\widehat{\ell}}{2}\right)\cos\left(\sqrt{\widehat{q}_\ell}\widehat{x}\right) - \cos\left(\sqrt{\widehat{q}_\ell}\frac{\widehat{\ell}}{2}\right)\cos\left(\sqrt{\widehat{q}_h}\widehat{x}\right)}{c_A\left(\widehat{\ell},\widehat{\alpha}\right)}. \tag{C.11}$$

This is zero for $\widehat{x} = \pm\frac{\ell}{2}$, as we would expect, given our BCs (6.17c).

ii) We know from Conjecture C.2.2 that $c_A\left(\widehat{\ell},\widehat{\alpha}\right)$ is negative inside Region I. It remains to show that the numerator of (C.11) is also of a single sign for $\widehat{x} \in \left(\frac{-\widehat{\ell}}{2},\frac{\widehat{\ell}}{2}\right)$, or since the interface layer is odd about $\widehat{x}=0$, for $\widehat{x}\in\left[0,\frac{\widehat{\ell}}{2}\right)$. We explored this with CHEBFUN; results are depicted in Fig. 6.7(a) (see the blue shaded areas). See also Appendix C.4.

Likewise,

$$\frac{\mathrm{d}^2\widetilde{\varphi}}{\mathrm{d}\widehat{x}^2} = \sqrt{\widehat{q}_h\widehat{q}_\ell}\frac{-\sqrt{\widehat{q}_\ell}\cos\left(\sqrt{\widehat{q}_h}\frac{\widehat{\ell}}{2}\right)\sin\left(\sqrt{\widehat{q}_\ell}\widehat{x}\right) + \sqrt{\widehat{q}_h}\cos\left(\sqrt{\widehat{q}_\ell}\frac{\widehat{\ell}}{2}\right)\sin\left(\sqrt{\widehat{q}_h}\widehat{x}\right)}{c_A\left(\widehat{\ell},\widehat{\alpha}\right)}, \tag{C.12}$$

and for $0<\widehat{\ell}<\pi/\sqrt{\widehat{q}_h}$, we assert that this second derivative has only one zero, viz.

$$-\sqrt{\widehat{q}_\ell}\cos\left(\sqrt{\widehat{q}_h}\frac{\widehat{\ell}}{2}\right)\sin\left(\sqrt{\widehat{q}_\ell}\widehat{x}\right) + \sqrt{\widehat{q}_h}\cos\left(\sqrt{\widehat{q}_\ell}\frac{\widehat{\ell}}{2}\right)\sin\left(\sqrt{\widehat{q}_h}\widehat{x}\right) = 0 \tag{C.13}$$

only has the solution $\widehat{x}=0$ (it is clear that $\widehat{x}=0$ is *a* solution). We explored this with CHEBFUN; results are depicted in Fig. 6.7(a) (see the yellow shaded areas). See also Appendix C.4.

□

Remark. There is no restriction *per se* as $\ell \downarrow 0$ and so we can accommodate (almost) arbitrarily steep candidate interface layers. We do however demand that $\widehat{\ell}\neq 0$ as this would imply a morphology with a step discontinuity. We illustrate a typical small-$\widehat{\ell}$ response (for $\widehat{\alpha}=0.02$) inside Region I in Fig. C.2(a).

C.2.1 The effect of sending $\widehat{L}\downarrow 0$

We now examine what happens in un-scaled parameter space as $\widehat{\ell}=\widehat{L}\leq\pi/\sqrt{\widehat{q}_h}$ and $\widehat{L}\downarrow 0$.

We observed previously that in Region I, the single-layer energy minimising interface layer is M1I (cf. Fig. 6.7(a)) and fills the domain entirely i.e. $\widehat{\ell}_{\mathrm{opt}}=\widehat{L}$. Hence, for (un-scaled) $L=1$ and (scaled) $\widehat{\alpha}\in\left(0,\frac{1}{4}\right)$, the *un-scaled* single-layer energy minimiser on the unit domain fills $\left(-\frac{1}{2},\frac{1}{2}\right)$, and we can investigate the effect of sending $\widehat{L}\downarrow 0$ in this setting. For the specified interface layer, (6.59) implies that the scaled interface layer is

$$\widehat{\varphi}_{\widehat{L}}\left(\widehat{x};\widehat{\alpha}\right) = \frac{\sqrt{\widehat{q}_h}\cos\left(\sqrt{\widehat{q}_h}\frac{\widehat{L}}{2}\right)\sin\left(\sqrt{\widehat{q}_\ell}\widehat{x}\right) - \sqrt{\widehat{q}_\ell}\cos\left(\sqrt{\widehat{q}_\ell}\frac{\widehat{L}}{2}\right)\sin\left(\sqrt{\widehat{q}_h}\widehat{x}\right)}{\sqrt{\widehat{q}_h}\cos\left(\sqrt{\widehat{q}_h}\frac{\widehat{L}}{2}\right)\sin\left(\sqrt{\widehat{q}_\ell}\frac{\widehat{L}}{2}\right) - \sqrt{\widehat{q}_\ell}\cos\left(\sqrt{\widehat{q}_\ell}\frac{\widehat{L}}{2}\right)\sin\left(\sqrt{\widehat{q}_h}\frac{\widehat{L}}{2}\right)}, \tag{C.14a}$$

for $\widehat{x}\in\left(-\frac{\widehat{L}}{2},\frac{\widehat{L}}{2}\right)$ where we have included $\widehat{\alpha}$ as a parameter. Scaling back to the unit domain with $L=1$ via $\widehat{x}=\widehat{L}x$ leads us to the un-scaled

$$\varphi_{\widehat{L}}\left(x;\widehat{\alpha}\right) = \frac{\sqrt{\widehat{q}_h}\cos\left(\sqrt{\widehat{q}_h}\frac{\widehat{L}}{2}\right)\sin\left(\sqrt{\widehat{q}_\ell}\widehat{L}x\right) - \sqrt{\widehat{q}_\ell}\cos\left(\sqrt{\widehat{q}_\ell}\frac{\widehat{L}}{2}\right)\sin\left(\sqrt{\widehat{q}_h}\widehat{L}x\right)}{\sqrt{\widehat{q}_h}\cos\left(\sqrt{\widehat{q}_h}\frac{\widehat{L}}{2}\right)\sin\left(\sqrt{\widehat{q}_\ell}\frac{\widehat{L}}{2}\right) - \sqrt{\widehat{q}_\ell}\cos\left(\sqrt{\widehat{q}_\ell}\frac{\widehat{L}}{2}\right)\sin\left(\sqrt{\widehat{q}_h}\frac{\widehat{L}}{2}\right)}, \tag{C.14b}$$

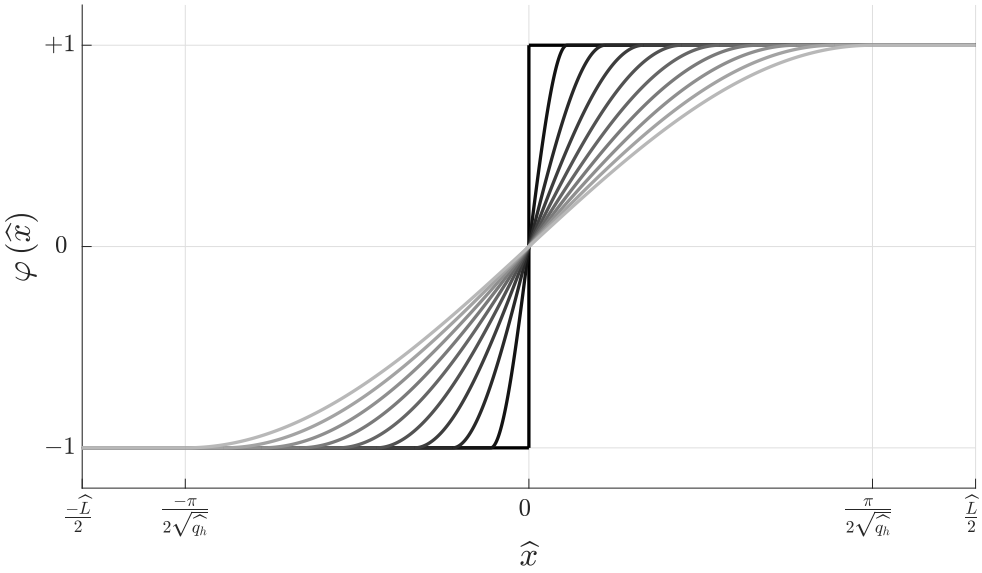

(a) Morphology response for small $\widehat{\ell}$ at $\widehat{\alpha} = 0.02$: we depict ten thin M1I interface layers for $\widehat{\ell} \in \left\{0, \ldots, \pi/\sqrt{\widehat{q}_h}\right\}$. As $\widehat{\ell} \downarrow 0$, the monotone interface layer becomes steeper, but they are all monotone (and thus bounded). Interfaces of larger $\widehat{\ell}$ are coloured in lighter shades of grey.

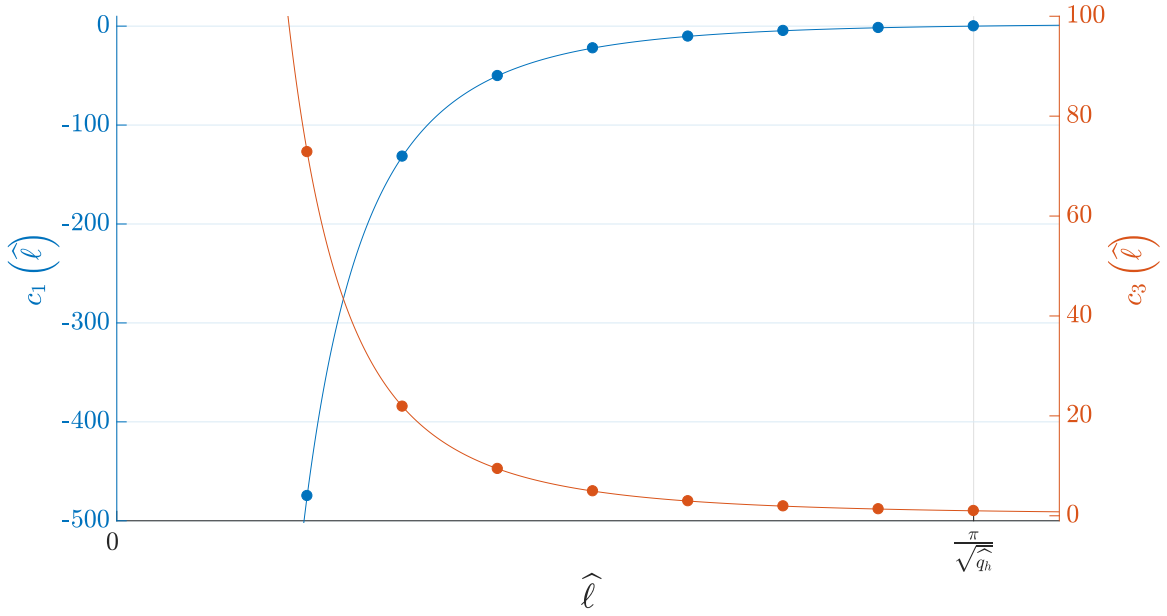

(b) c_1, c_3 response for small $\widehat{\ell}$: we mark off with large dots the values c_1 and c_3 corresponding to the values of $\widehat{\ell}$ for which we plotted interface layers in part (a) above. $c_1 \to -\infty$ and $c_3 \to +\infty$ as $\widehat{\ell} \downarrow 0$, as we noted in (C.10) (and so we are unable to include markers for the very small values of $\widehat{\ell}$ featured as interface layers in part (a) above).

Figure C.2: Small $\widehat{\ell}$ morphological response.

for $x \in \left(-\frac{1}{2}, \frac{1}{2}\right)$. We therefore seek to understand the function

$$\varphi_{\widehat{\alpha}}(x) := \lim_{\widehat{L}\downarrow 0} \left\{\varphi_{\widehat{L}}(x;\widehat{\alpha})\right\}, \tag{C.14c}$$

assuming tentatively that this limit exists. Taking $\widehat{L} \downarrow 0$ in (C.14b) by hand is hard, and so we perform a numerical investigation for a set of $\widehat{\alpha}$ values. For $\widehat{L} = \frac{\pi}{\sqrt{\widehat{q}_h}}$ i.e. $\sqrt{\widehat{q}_h}\frac{\widehat{L}}{2} = \frac{\pi}{2}$ and $\cos\left(\sqrt{\widehat{q}_h}\frac{\widehat{L}}{2}\right) = 0, \sin\left(\sqrt{\widehat{q}_h}\frac{\widehat{L}}{2}\right) = 1$, (C.14b) reduces to

$$\varphi_{\widehat{L}}(x;\cdot) = \sin(\pi x), \tag{C.15}$$

independent of $\widehat{\alpha}$. We plot (C.14b) for various $\widehat{\alpha}$-values and a set of small $\widehat{L}$-values in Fig. C.3. It is not clear what function $\varphi_{\widehat{L}}(x;\cdot)$ is but these very preliminary results suggest this function exists and has $\left|\varphi'_{\widehat{L}}\right|_\infty$ independent of $\widehat{L}$ for any $\widehat{\alpha} \in \left(0, \frac{1}{4}\right)$.

C.3 Interfacial structure outside of Region I

We explore some of the typical structures in cool parameter space. Our approach will be to examine c_1 and c_3 on and near the various contours of interest that we drew in Fig. 6.4. To start we consider the zero contours of $\cos\left(\sqrt{\widehat{q}_h}\frac{\widehat{\ell}}{2}\right)$ and $\cos\left(\sqrt{\widehat{q}_\ell}\frac{\widehat{\ell}}{2}\right)$, and recall that

$$\sin\left(\sqrt{\widehat{q}_h}\frac{\widehat{\ell}}{2}\right) = 0 \quad \Rightarrow \quad \cos\left(\sqrt{\widehat{q}_h}\frac{\widehat{\ell}}{2}\right) = \pm 1; \qquad \sin\left(\sqrt{\widehat{q}_\ell}\frac{\widehat{\ell}}{2}\right) = 0 \quad \Rightarrow \quad \cos\left(\sqrt{\widehat{q}_\ell}\frac{\widehat{\ell}}{2}\right) = \pm 1,$$

and vice versa. We now analyse the various lines in Fig. 6.4.

- First, we consider the solid **blue** lines that are *not* at the solid round intersection points with the **black** lines. On these,

  $$\cos\left(\sqrt{\widehat{q}_\ell}\frac{\widehat{\ell}}{2}\right) = 0 \qquad \text{but} \qquad \cos\left(\sqrt{\widehat{q}_h}\frac{\widehat{\ell}}{2}\right) \neq 0.$$

  Then $\sin\left(\sqrt{\widehat{q}_\ell}\frac{\widehat{\ell}}{2}\right) = \pm 1$ so

  $$c_A\left(\widehat{\ell}\right) = \pm\sqrt{\widehat{q}_h}\cos\left(\sqrt{\widehat{q}_h}\frac{\widehat{\ell}}{2}\right) \qquad \text{and} \qquad c_B\left(\widehat{\ell}\right) = \pm\sqrt{\widehat{q}_\ell}\cos\left(\sqrt{\widehat{q}_h}\frac{\widehat{\ell}}{2}\right)$$

  and so since $\cos\left(\sqrt{\widehat{q}_h}\frac{\widehat{\ell}}{2}\right) \neq 0$, we have $c_A\left(\widehat{\ell}\right), c_B\left(\widehat{\ell}\right) \neq 0$ which means that

  $$c_1 = \pm\frac{\cos\left(\sqrt{\widehat{q}_h}\frac{\widehat{\ell}}{2}\right)}{\cos\left(\sqrt{\widehat{q}_h}\frac{\widehat{\ell}}{2}\right)} = \pm 1 \qquad \text{and} \qquad c_3 = \mp\frac{\sqrt{\widehat{q}_\ell}\cos\left(\sqrt{\widehat{q}_\ell}\frac{\widehat{\ell}}{2}\right)}{\sqrt{\widehat{q}_h}\cos\left(\sqrt{\widehat{q}_h}\frac{\widehat{\ell}}{2}\right)} = 0. \tag{C.16}$$

  Such interface layers have form (cf. (6.59b), (6.66))

  $$\widetilde{\varphi}\left(x;\widehat{\ell}\right) = (-1)^s \sin\left(\sqrt{\widehat{q}_\ell}x\right) \qquad \text{for} \qquad x \in \frac{(2s+1)\pi}{2\sqrt{\widehat{q}_\ell}}(-1,1); \qquad s \in \{0,1,2,\ldots\}, \tag{C.17a}$$

  and for such morphologies, $\|\widetilde{\varphi}\|_\infty = 1$. The $(-1)^s$ pre-multiplication term in (C.17a) ensures that all of the morphologies respect our $B \to A$ *ansatz* as s increases. The structure of such interface layers is easily seen if we scale $x \to \widehat{x}$ so that each one occupies $\widehat{x} \in [-1,1]$. Setting

  $$x = \frac{(2s+1)\pi}{2\sqrt{\widehat{q}_\ell}}\widehat{x}$$

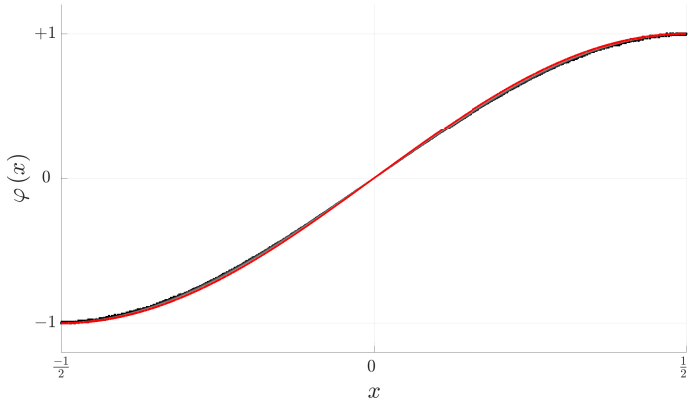

(a) $\widehat{\alpha} = 0.2390$

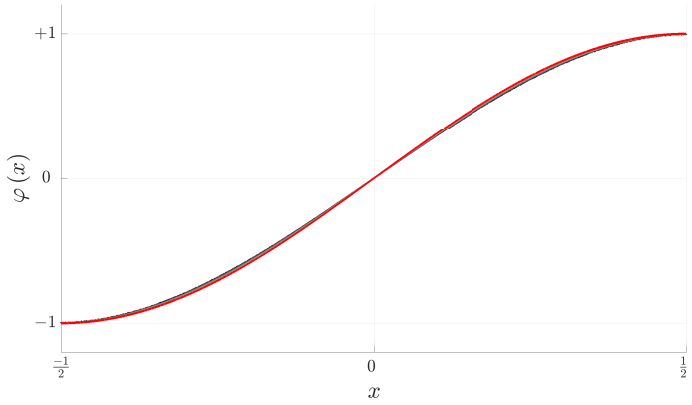

(b) $\widehat{\alpha} = 0.0996$

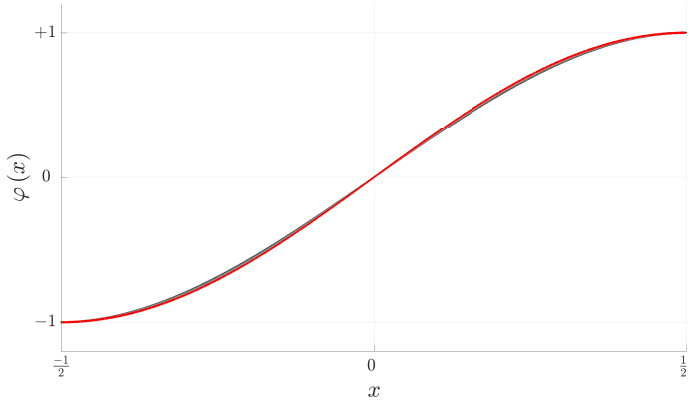

(c) $\widehat{\alpha} = 0.0100$

Figure C.3: Un-scaled single-layer energy minimisers inside Region I, with $\widehat{\ell} = \widehat{L}$ for various $\widehat{\alpha}$ and small $\widehat{L}$-values. In each case, $\sin(\pi x)$ corresponding to $\widehat{L} = \frac{\pi}{\sqrt{\widehat{q_h}}}$ as in (C.15) is plotted in red for reference. The black line in each plot corresponds to $\widehat{L} = 10^{-6}$.

means we can replace (C.17a) with

$$\widetilde{\varphi}\left(\widehat{x};\widehat{\ell}\right)=(-1)^{s}\sin\left(\frac{(2s+1)\,\pi}{2}\widehat{x}\right)\qquad\text{for}\qquad\widehat{x}\in(-1,1)\,;\qquad s\in\{0,1,2,\ldots\}\,,\tag{C.17b}$$

and each interface layer is comprised of $2s+1$ (internal) P2P transitions on $(-1,1)$. We recall that s describes the particular zero of $\cos\left(\sqrt{\widehat{q}_\ell}\frac{\widehat{\ell}}{2}\right)$, so for instance $s=0$ describes the first solid dark blue line in Fig. 6.4 (the upper bound of the cold region), $s=1$ the second one, and so on. Clearly, as $\widehat{\ell}$ (i.e. s) increases, the interface layers become more and more 'wiggly'.

- Now consider the solid **black** lines *not* at the solid round intersection points with the **blue** lines. On these,

$$\cos\left(\sqrt{\widehat{q}_h}\frac{\widehat{\ell}}{2}\right)=0\qquad\qquad\text{but}\qquad\qquad\cos\left(\sqrt{\widehat{q}_\ell}\frac{\widehat{\ell}}{2}\right)\neq 0,$$

which means that, $\sin\left(\sqrt{\widehat{q}_h}\frac{\widehat{\ell}}{2}\right)=\pm1$ so

$$c_A\left(\widehat{\ell}\right)=\pm\sqrt{\widehat{q}_\ell}\cos\left(\sqrt{\widehat{q}_\ell}\frac{\widehat{\ell}}{2}\right)\qquad\text{and}\qquad c_B\left(\widehat{\ell}\right)=\pm\sqrt{\widehat{q}_h}\cos\left(\sqrt{\widehat{q}_\ell}\frac{\widehat{\ell}}{2}\right)$$

and so since $\cos\left(\sqrt{\widehat{q}_h}\frac{\widehat{\ell}}{2}\right)\neq 0$, we have $c_A\left(\widehat{\ell}\right),c_B\left(\widehat{\ell}\right)\neq 0$ which means that

$$c_1=\pm\frac{\sqrt{\widehat{q}_h}\cos\left(\sqrt{\widehat{q}_h}\frac{\widehat{\ell}}{2}\right)}{\sqrt{\widehat{q}_\ell}\cos\left(\sqrt{\widehat{q}_\ell}\frac{\widehat{\ell}}{2}\right)}=0\qquad\text{and}\qquad c_3=\mp\frac{\sqrt{\widehat{q}_\ell}\cos\left(\sqrt{\widehat{q}_\ell}\frac{\widehat{\ell}}{2}\right)}{\sqrt{\widehat{q}_\ell}\cos\left(\sqrt{\widehat{q}_\ell}\frac{\widehat{\ell}}{2}\right)}=\mp1.\tag{C.18}$$

Such interface layers have form (cf. (6.59b), (6.66), (C.17a))

$$\widetilde{\varphi}\left(x;\widehat{\ell}\right)=(-1)^{s}\sin\left(\sqrt{\widehat{q}_h}x\right)\qquad\text{for}\qquad x\in\frac{(2s+1)\,\pi}{2\sqrt{\widehat{q}_h}}(-1,1)\,;\qquad s\in\{0,1,2,\ldots\}\,,\tag{C.19}$$

and for such morphologies, $\|\widetilde{\varphi}\|_\infty=1$. This time, the $(-1)^s$ pre-multiplication term ensures that all of the morphologies respect our $B\to A$ *ansatz* as s increases. Re-scaling as we did above, we find that each interface layer is comprised of $2s+1$ (internal) P2P transitions on $(-1,1)$ where s describes the particular zero of $\cos\left(\sqrt{\widehat{q}_h}\frac{\widehat{\ell}}{2}\right)$.

Intersections of the solid **black** and **blue** lines are points at which

$$\cos\left(\sqrt{\widehat{q}_h}\frac{\widehat{\ell}}{2}\right)=0\qquad\qquad\textit{and}\qquad\qquad\cos\left(\sqrt{\widehat{q}_\ell}\frac{\widehat{\ell}}{2}\right)=0.$$

Under such conditions, we must also have $c_A\left(\widehat{\ell}\right)=0$ and $c_B\left(\widehat{\ell}\right)=0$ i.e. the **red** and dashed **green** lines also intersect at these points (this is also clearly visible in Fig. 6.4). If we let the integer r count the zeros of $\cos\left(\sqrt{\widehat{q}_h}\frac{\widehat{\ell}}{2}\right)$ for a given $\widehat{q}_h$ i.e. $\widehat{\alpha}$, and s serve the same purpose for the zeros of $\cos\left(\sqrt{\widehat{q}_\ell}\frac{\widehat{\ell}}{2}\right)$, then for the solid black dots in Fig. 6.4, we can use (6.66). It follows that

$$\sqrt{\frac{\widehat{q}_h}{\widehat{q}_\ell}}=\frac{2r+1}{2s+1}=:k_{\text{odd}}\qquad\Rightarrow\qquad\frac{\widehat{q}_h}{\widehat{q}_\ell}=\left(\frac{2r+1}{2s+1}\right)^2=:k_{\text{odd}}^2\qquad\text{for}\qquad r,s\in\mathbb{N}_0,$$

or, in words, $\sqrt{\frac{\widehat{q_h}}{\widehat{q_\ell}}}$ is the ratio of two odd, positive integers, which ratio we will call k_{odd}. Rearranging, we see that

$$\widehat{\alpha} = \frac{1}{4}\left(1 - \left(\frac{k_{\text{odd}}^2 - 1}{k_{\text{odd}}^2 + 1}\right)^2\right) = \left(\frac{k_{\text{odd}}}{k_{\text{odd}}^2 + 1}\right)^2, \tag{C.20a}$$

and so

$$\widehat{q_h} = \frac{1}{2}\left(1 + \left(\frac{k_{\text{odd}}^2 - 1}{k_{\text{odd}}^2 + 1}\right)\right) = \frac{k_{\text{odd}}^2}{k_{\text{odd}}^2 + 1} \qquad \text{and} \qquad \widehat{q_\ell} = \frac{1}{2}\left(1 - \left(\frac{k_{\text{odd}}^2 - 1}{k_{\text{odd}}^2 + 1}\right)\right) = \frac{1}{k_{\text{odd}}^2 + 1}. \tag{C.20b}$$

The easiest way to find all of these points is to consider each of the zero contours of the low frequency term $\cos\left(\sqrt{\widehat{q_\ell}}\frac{\widehat{\ell}}{2}\right)$ (the low frequency zero contours) and their intersections with the zero contours of $\cos\left(\sqrt{\widehat{q_h}}\frac{\widehat{\ell}}{2}\right)$ (the high frequency zero contours). We have:

$s = 0$: the first low frequency zero contour intersects with all of the high frequency zero contours for which $r = 0, 1, 2, \ldots$. Along this line, $\cos\left(\sqrt{\widehat{q_\ell}}\frac{\widehat{\ell}}{2}\right) = 0$ and in fact $\widehat{\ell} = \frac{\pi}{\sqrt{\widehat{q_\ell}}}$, so if we substitute the second part of (C.20b) we arrive at

$$\widehat{\ell} = \pi\sqrt{k_{\text{odd}}^2 + 1} \qquad \Rightarrow \qquad k_{\text{odd}} = \sqrt{\frac{\widehat{\ell}^2}{\pi^2} - 1} \tag{C.21}$$

where, in the second part of the calculation, we replace k_{odd} with the continuous $k > 0$. Consequently, we may define the set

$$k_{\text{odd}}^{(s=0)} \in \{2r + 1\}_{r=0,1,2,\ldots} = \{1, 3, 5, 7, 9, \ldots\}.$$

Using these values and (6.66), (C.20a) we can find corresponding intersection points $(\ell, \widehat{\alpha})$; we post the first few of these (corresponding to the intersections we plotted in Fig. 6.4) in Table C.1.

$s = 1$: the second low frequency zero contour intersects with the second and higher high frequency zero contours for which $r = 1, 2, \ldots$. This time, we have

$$k_{\text{odd}}^{(s=1)} \in \left\{\frac{2r+1}{3}\right\}_{r=1,2,\ldots} = \left\{1, \frac{5}{3}, \frac{7}{3}, 3, \ldots\right\}.$$

The same process we followed for $s = 0$ leads to the data in the third column of Table C.1.

$s = 2$: the third low frequency zero contour intersects with the third and higher high frequency zero contours for which $r = 2, 3, \ldots$. This time, we have

$$k_{\text{odd}}^{(s=2)} \in \left\{\frac{2r+1}{5}\right\}_{r=2,3,\ldots} = \left\{1, \frac{7}{5}, \frac{9}{5}, \ldots\right\}.$$

We calculate the entries in the fourth column of Table C.1.

$\ldots$: and so on.

Summary results are noted in Table C.1.

Intersections of the dashed **black** and **blue** lines are points at which

$$\sin\left(\sqrt{\widehat{q_h}}\frac{\widehat{\ell}}{2}\right) = 0 \qquad \textit{and} \qquad \sin\left(\sqrt{\widehat{q_\ell}}\frac{\widehat{\ell}}{2}\right) = 0.$$

The approach to finding the coordinates of these points is similar to what we did above; the primary difference this time, is that both the high and low frequency terms have zeros at $\widehat{\ell} = 0$ (which we are not interested in).

The main difference is that (6.67) means that $k_{\rm odd}$ in (C.20a) is replaced with the ratio of (not necessarily odd) integers $k_{\rm int} := \frac{r}{s}$, where

$$\widehat{\alpha} = \left(\frac{k_{\rm int}}{k_{\rm int}^2 + 1} \right)^2 . \tag{C.22}$$

We present the results in Table C.2.

Intersections of the **red** and *dashed* **green** lines correspond to points at which

$$c_A\left(\widehat{\ell}\right) = 0 \qquad \text{and} \qquad c_B\left(\widehat{\ell}\right) = 0. \tag{C.23}$$

An examination of Fig. 6.4 reveals that these functions intersect along $\widehat{\alpha} = \frac{1}{4}$ (for any $\widehat{\ell} \geq 0$) and along $\widehat{\ell} = 0$ (for any $0 \leq \widehat{\alpha} \leq \frac{1}{4}$). In addition, the points of intersection inside the cool parameter region are either those at which $\cos\left(\sqrt{\widehat{q}_h}\frac{\widehat{\ell}}{2}\right) = 0$ and $\cos\left(\sqrt{\widehat{q}_\ell}\frac{\widehat{\ell}}{2}\right) = 0$, or have the property that $\sin\left(\sqrt{\widehat{q}_h}\frac{\widehat{\ell}}{2}\right) = 0$ and $\sin\left(\sqrt{\widehat{q}_\ell}\frac{\widehat{\ell}}{2}\right) = 0$. We have discussed these above.

	s = 0		**s = 1**		**s = 2**	
r	$k_{\rm odd}$	$(\ell, \widehat{\alpha})$	$k_{\rm odd}$	$(\ell, \widehat{\alpha})$	$k_{\rm odd}$	$(\ell, \widehat{\alpha})$
0	1	$\left(\sqrt{2}\pi, \frac{1}{4}\right)$	–		–	
1	3	$\left(\sqrt{10}\pi, \frac{9}{100}\right)$	1	$\left(3\sqrt{2}\pi, \frac{1}{4}\right)$	–	
2	5	$\left(\sqrt{26}\pi, \frac{25}{676}\right)$	$\frac{5}{3}$	$\left(\sqrt{34}\pi, \frac{225}{1156}\right)$	1	$\left(5\sqrt{2}\pi, \frac{1}{4}\right)$
3	7	$\left(5\sqrt{2}\pi, \frac{49}{2500}\right)$	$\frac{7}{3}$	$\left(\sqrt{58}\pi, \frac{441}{3364}\right)$	$\frac{7}{5}$	$\left(\sqrt{74}\pi, \frac{1225}{5476}\right)$
4	9	$\left(\sqrt{82}\pi, \frac{81}{6724}\right)$	3	$\left(3\sqrt{10}\pi, \frac{9}{100}\right)$	$\frac{9}{5}$	$\left(\sqrt{106}\pi, \frac{2025}{11236}\right)$

Table C.1: Sample intersections of $\cos\left(\sqrt{\widehat{q}_h}\frac{\widehat{\ell}}{2}\right)$ and $\cos\left(\sqrt{\widehat{q}_\ell}\frac{\widehat{\ell}}{2}\right)$ for various odd ratios $k_{\rm odd} = \sqrt{\frac{\widehat{q}_h}{\widehat{q}_\ell}}$, as depicted in Fig. 6.4 with filled black dots.

	$\mathbf{s=1}$		$\mathbf{s=2}$		$\mathbf{s=3}$	
$\mathbf{r}$	$\frac{r}{s}$	$(\ell,\widehat{\alpha})$	$\frac{r}{s}$	$(\ell,\widehat{\alpha})$	$\frac{r}{s}$	$(\ell,\widehat{\alpha})$
1	1	$\left(2\sqrt{2}\pi,\frac{1}{4}\right)$	–		–	
2	2	$\left(2\sqrt{5}\pi,\frac{4}{25}\right)$	1	$\left(4\sqrt{2}\pi,\frac{1}{4}\right)$	–	
3	3	$\left(2\sqrt{10}\pi,\frac{9}{100}\right)$	$\frac{3}{2}$	$\left(2\sqrt{13}\pi,\frac{36}{169}\right)$	1	$\left(6\sqrt{2}\pi,\frac{1}{4}\right)$
4	4	$\left(2\sqrt{17}\pi,\frac{16}{289}\right)$	2	$\left(2\sqrt{5}\pi,\frac{4}{25}\right)$	$\frac{4}{3}$	$\left(10\pi,\frac{144}{625}\right)$
5	5	$\left(2\sqrt{26}\pi,\frac{25}{676}\right)$	$\frac{5}{2}$	$\left(2\sqrt{29}\pi,\frac{100}{841}\right)$	$\frac{5}{3}$	$\left(2\sqrt{34}\pi,\frac{225}{1156}\right)$

Table C.2: Sample intersections of $\sin\left(\sqrt{\widehat{q}_h}\frac{\widehat{\ell}}{2}\right)$ and $\sin\left(\sqrt{\widehat{q}_\ell}\frac{\widehat{\ell}}{2}\right)$ for various integer ratios $k_{\text{int}}=\frac{r}{s}=\sqrt{\frac{\widehat{q}_h}{\widehat{q}_\ell}}$ as depicted in Fig. 6.4 with filled black squares.

C.4 Interface layer feasibility in $\left(\widehat{\ell},\widehat{\alpha}\right)$ parameter space

Feasible sub-regions of parameter space are discussed.

Boundedness

We wish to find the (edges of the) set

$$\left(\widehat{\ell},\widehat{\alpha}\right)_{\text{bdd}}:=\left\{\left(\widehat{\ell},\widehat{\alpha}\right)\in\left(\widehat{L},\widehat{\alpha}\right)_{\text{cool}}\,\middle|\,\|\widetilde{\varphi}\|_\infty\leq 1\right\},\tag{C.24}$$

viz. the interface layers satisfy (7.1a). It is clear that the extrema of $\widetilde{\varphi}$ occur at the zeros of its derivative. Consequently, we can consider instead the equivalent

$$p\left(\widehat{\ell}\right):=\max_{\widehat{x}\in\left\{\left(\frac{-\widehat{\ell}}{2},\frac{\widehat{\ell}}{2}\right)\cap\widetilde{\varphi}'(\widehat{x})=0\right\}}\left|\widetilde{\varphi}\left(\widehat{x}\right)\right|-1,\tag{C.25}$$

which means we need to solve the equation $\widetilde{\varphi}'\left(\widehat{x}\right)=0$ for $\widehat{x}\in\left(\frac{-\widehat{\ell}}{2},\frac{\widehat{\ell}}{2}\right)$, viz.

$$\frac{1}{c_A\left(\widehat{\ell}\right)}\left(\cos\left(\sqrt{\widehat{q}_h}\frac{\widehat{\ell}}{2}\right)\cos\left(\sqrt{\widehat{q}_\ell}\widehat{x}\right)-\cos\left(\sqrt{\widehat{q}_\ell}\frac{\widehat{\ell}}{2}\right)\cos\left(\sqrt{\widehat{q}_h}\widehat{x}\right)\right)=0,\tag{C.26}$$

and consider the values of $\widetilde{\varphi}$ on this (discrete) set as we continuously vary $\widehat{\ell}$, the total interface layer width.

Remark. We probed this numerically using Chebfun, and the results suggest that bounded parameter solution sets (viz. where $\|\widetilde{\varphi}\|_\infty\leq 1$) are bounded by the lines indicated in Fig. 6.7(a) (the grey shaded areas). But these are precisely the lines on which $\det(A)$ blows up, and so even though the limits seem quite well-behaved, it is very hard to pin down the corresponding morphologies. Finding these edges to any sort of accuracy, even with a tool as accurate as Chebfun, is extremely challenging.

The structure of interface layers in cool parameter space

Having identified those parts of the cool parameter space which yield bounded interface layers ($\|\widetilde{\varphi}\|_\infty \leq 1$), we can go one step further to understand their internal structure. To do this, we count the number of turning points inside the interface layer and define

$$\#\text{ of internal walls} = \#\text{ of turning pts } +1.$$

We illustrate the process with some specific results in Fig. 6.6, and summarise the results of our sweep of parameter space in Fig. 6.7(b). The number of turning points is always even; the number of internal walls is odd.

Monotonicity

We wish to find the (edges of the) set of monotone interface layers,

$$\left(\widehat{\ell},\widehat{\alpha}\right)_{\text{mono.}} := \left\{ \left(\widehat{\ell},\widehat{\alpha}\right) \in \left(\widehat{\ell},\widehat{\alpha}\right)_{\text{bdd}} \;\middle|\; \frac{\mathrm{d}\widetilde{\varphi}_{BA}}{\mathrm{d}\widehat{x}} \geq 0 \text{ or } \frac{\mathrm{d}\widetilde{\varphi}_{AB}}{\mathrm{d}\widehat{x}} \leq 0 \,\forall\, |\widehat{x}| < \frac{\widehat{\ell}}{2} \right\}, \tag{C.27}$$

viz. the interface layers satisfy (7.1b). In the context of BA P2P transitions, we require

$$\frac{\mathrm{d}\widetilde{\varphi}_{BA}}{\mathrm{d}\widehat{x}} \geq 0. \tag{C.28a}$$

Using (C.11) with (6.29b), we state this requirement as

$$\frac{\cos\left(\sqrt{\widehat{q}_h}\frac{\widehat{\ell}}{2}\right)\cos\left(\sqrt{\widehat{q}_\ell}\widehat{x}\right) - \cos\left(\sqrt{\widehat{q}_\ell}\frac{\widehat{\ell}}{2}\right)\cos\left(\sqrt{\widehat{q}_h}\widehat{x}\right)}{\sqrt{\widehat{q}_h}\cos\left(\sqrt{\widehat{q}_h}\frac{\widehat{\ell}}{2}\right)\sin\left(\sqrt{\widehat{q}_\ell}\frac{\widehat{\ell}}{2}\right) - \sqrt{\widehat{q}_\ell}\cos\left(\sqrt{\widehat{q}_\ell}\frac{\widehat{\ell}}{2}\right)\sin\left(\sqrt{\widehat{q}_h}\frac{\widehat{\ell}}{2}\right)} \geq 0 \qquad \text{for} \qquad |\widehat{x}| \leq \frac{\widehat{\ell}}{2}. \tag{C.28b}$$

Remark. As above, we probed this with CHEBUN, and found this to be a very hard problem. Results, such as they are, are depicted in Fig. 6.7(a) (the blue shaded areas).

The single inflexion point constraint

Our third feasibility requirement in (7.1c) was the single inflexion point constraint. To satisfy it, we seek

$$\left(\widehat{\ell},\widehat{\alpha}\right)_{\text{uw}} := \left\{ \left(\widehat{\ell},\widehat{\alpha}\right) \in \left(\widehat{\ell},\widehat{\alpha}\right)_{\text{mono.}} \;\middle|\; \frac{\mathrm{d}^2\widetilde{\varphi}}{\mathrm{d}\widehat{x}^2} = 0 \text{ has one solution } \widehat{x} < \left|\frac{\widehat{\ell}}{2}\right| \right\}. \tag{C.29}$$

Using (C.12) with (6.29b), we find that $\frac{\mathrm{d}^2\widetilde{\varphi}}{\mathrm{d}\widehat{x}^2} = 0$ is equivalent to

$$\sqrt{\widehat{q}_h}\cos\left(\sqrt{\widehat{q}_\ell}\frac{\widehat{\ell}}{2}\right)\sin\left(\sqrt{\widehat{q}_h}\widehat{x}\right) = \sqrt{\widehat{q}_\ell}\cos\left(\sqrt{\widehat{q}_h}\frac{\widehat{\ell}}{2}\right)\sin\left(\sqrt{\widehat{q}_\ell}\widehat{x}\right) \tag{C.30a}$$

or

$$\mathscr{U}\left(\widehat{x}\right) := \frac{\sin\left(\sqrt{\widehat{q}_h}\widehat{x}\right)}{\sin\left(\sqrt{\widehat{q}_\ell}\widehat{x}\right)} = \sqrt{\frac{\widehat{q}_\ell}{\widehat{q}_h}}\frac{\cos\left(\sqrt{\widehat{q}_h}\frac{\widehat{\ell}}{2}\right)}{\cos\left(\sqrt{\widehat{q}_\ell}\frac{\widehat{\ell}}{2}\right)} =: \mathscr{Q}\left(\widehat{\ell}\right) \tag{C.30b}$$

as long as $c_A\left(\widehat{\ell},\widehat{\alpha}\right) \neq 0$. In (C.30b) we observe a fixed function of $\widehat{\ell}$ (for a given $\widehat{\alpha}$) on the right, and an even function of $\widehat{x}$ on the left. An examination of (C.30a) reveals that $\widehat{x} = 0$ is a solution for any $\widehat{\ell}$, and so we are

looking for bounds (on $\widehat{\ell}$) for which we can ensure that the problem has no further solutions. We explore the problem graphically in Fig. C.4. In this series of graphs, we plot $\mathscr{U}\left(\widehat{x};\widehat{\alpha}\right)$ for given parameter $\widehat{\alpha}$ in **blue** and the corresponding $\mathscr{Q}\left(\widehat{\ell};\widehat{\alpha}\right)$ with $\widehat{x}=\frac{\widehat{\ell}}{2}\Rightarrow\widehat{\ell}=2\widehat{x}$ in **red**. We then vary $\widehat{x}$ looking for intersections of the black lines with $\mathscr{U}\left(\widehat{x};\widehat{\alpha}\right)$ for $\widehat{x}\leq\frac{\widehat{\ell}}{2}$. Summary observations are as follows:

i) For $\widehat{\alpha}>0.09$ (cf. Fig. C.4(a)), there is an M1I region from $\widehat{\ell}=0$ to $\widehat{\ell}=\widehat{\ell}_{\max}$ satisfying

$$\lim_{\widehat{x}\downarrow 0}\left\{\frac{\sin\left(\sqrt{\widehat{q}_h}\widehat{x}\right)}{\sin\left(\sqrt{\widehat{q}_\ell}\widehat{x}\right)}\right\}=\sqrt{\frac{\widehat{q}_h}{\widehat{q}_\ell}}=\sqrt{\frac{\widehat{q}_\ell}{\widehat{q}_h}}\frac{\cos\left(\sqrt{\widehat{q}_h}\frac{\widehat{\ell}}{2}\right)}{\cos\left(\sqrt{\widehat{q}_\ell}\frac{\widehat{\ell}}{2}\right)}$$

$$\Leftrightarrow\qquad \widehat{q}_\ell\cos\left(\sqrt{\widehat{q}_h}\frac{\widehat{\ell}_{\max}}{2}\right)-\widehat{q}_h\cos\left(\sqrt{\widehat{q}_\ell}\frac{\widehat{\ell}_{\max}}{2}\right)=0 \tag{C.31}$$

where we used L'Hôpital's rule on the left. We denote by $\widehat{\ell}_{\max}$ the value of $\widehat{\ell}$ satisfying (C.31) for $\alpha>0.09$. This is the only M1I region for $\widehat{\alpha}>0.09$.

ii) For $\widehat{\alpha}=0.09$ (cf. Fig. C.4(b)), there is an M1I region from $\widehat{\ell}=0$ to the first intersection of $\mathscr{Q}\left(2\widehat{x}\right)$ and $\mathscr{U}\left(\widehat{x}\right)$, for which

$$\frac{\sin\left(\sqrt{\widehat{q}_h}\frac{\widehat{\ell}}{2}\right)}{\sin\left(\sqrt{\widehat{q}_\ell}\frac{\widehat{\ell}}{2}\right)}=\sqrt{\frac{\widehat{q}_\ell}{\widehat{q}_h}}\frac{\cos\left(\sqrt{\widehat{q}_h}\frac{\widehat{\ell}}{2}\right)}{\cos\left(\sqrt{\widehat{q}_\ell}\frac{\widehat{\ell}}{2}\right)}\qquad\Leftrightarrow\qquad c_B\left(\frac{\widehat{\ell}}{2}\right)=0 \tag{C.32}$$

with c_B as in (6.29c). We denote by $\widehat{\ell}_{\max}$ the value of $\widehat{\ell}$ satisfying (C.32) for $\alpha\leq 0.09$; it is the smallest non-zero, positive zero of c_B. Clearly, this is the only M1I region for $\widehat{\alpha}=0.09$.

According to Fig. 6.7(a), $\sqrt{\widehat{q}_h}=3\sqrt{\widehat{q}_\ell}$ and $\sqrt{\widehat{q}_\ell}=\frac{1}{\sqrt{10}}$ for $\widehat{\alpha}=0.09$ and so we can solve (C.32) exactly to find that $\widehat{\ell}_{\max}=\sqrt{10}\pi$ as in the $(r=1,k_{\text{odd}})$-entry of Table C.1.

iii) For $\alpha<0.09$ (cf. Fig. C.4(c)), there is an M1I region from $\widehat{\ell}=0$ to the first intersection of $\mathscr{Q}\left(2\widehat{x}\right)$ and $\mathscr{U}\left(\widehat{x}\right)$ as in (C.32) above. A second M1I region is observed from $\widehat{\ell}=\widehat{\ell}_2$ satisfying (C.31), up to $\widehat{\ell}=\widehat{\ell}_3$ satisfying

$$\underbrace{\left.\frac{\sin\left(\sqrt{\widehat{q}_h}\widehat{x}\right)}{\sin\left(\sqrt{\widehat{q}_\ell}\widehat{x}\right)}\right|_{(\mathscr{U}'(\widehat{x})=0)}}_{:=U_1}=\sqrt{\frac{\widehat{q}_\ell}{\widehat{q}_h}}\frac{\cos\left(\sqrt{\widehat{q}_h}\frac{\widehat{\ell}}{2}\right)}{\cos\left(\sqrt{\widehat{q}_\ell}\frac{\widehat{\ell}}{2}\right)}$$

$$\Leftrightarrow\qquad \sqrt{\widehat{q}_\ell}\cos\left(\sqrt{\widehat{q}_h}\frac{\widehat{\ell}_3}{2}\right)-U_1\sqrt{\widehat{q}_h}\cos\left(\sqrt{\widehat{q}_\ell}\frac{\widehat{\ell}_3}{2}\right)=0. \tag{C.33}$$

We use $\left(\widehat{\ell}_2,\widehat{\ell}_3\right)$ to denote this second M1I sub-domain. More generally, we seek the first two values of $\widehat{x}$ corresponding to turning points of $\mathscr{U}\left(\widehat{x};\widehat{\alpha}\right)$ (the smaller of which is always zero). For each of these, we then seek the smallest corresponding values of $\widehat{\ell}$ from $\mathscr{Q}\left(\widehat{\ell};\widehat{\alpha}\right)$. It is clear that for any larger values of $\widehat{\ell}$, we always have at least two intersections of a black line and a blue one i.e. there are no further M1I regions.

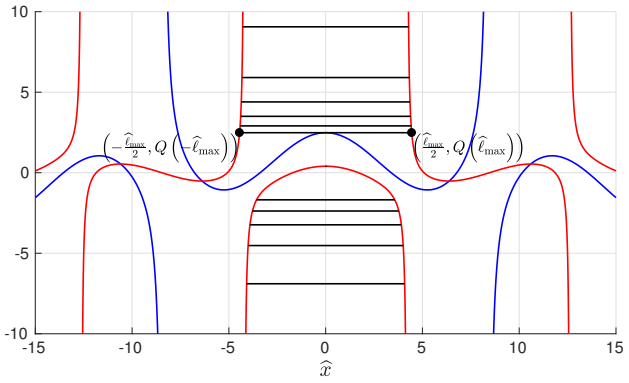

(a) $\alpha = 0.12 > 0.09$: the solid black lines correspond to M1I values of $\widehat{\ell} \in \left(0, \widehat{\ell}_{\max}\right)$.

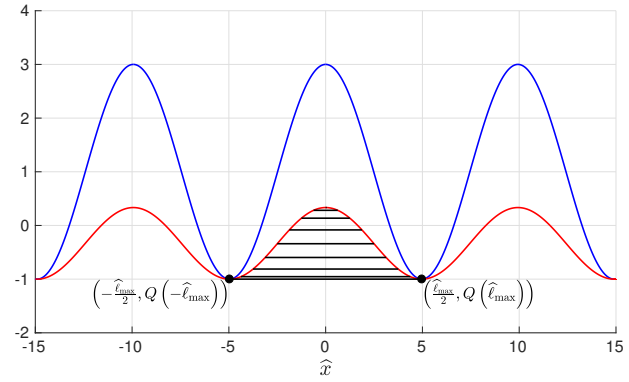

(b) $\widehat{\alpha} = 0.09$: the solid black lines correspond to M1I values of $\widehat{\ell} \in \left(0, \widehat{\ell}_{\max}\right)$ where $\widehat{\ell}_{\max} = \sqrt{10}\pi$.

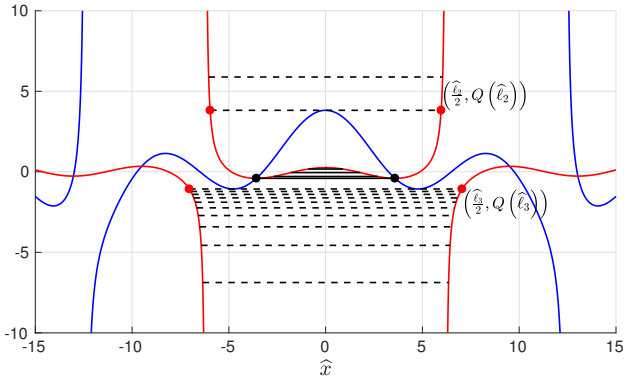

(c) $\widehat{\alpha} = 0.06 < 0.09$: the solid black lines correspond to M1I values of $\widehat{\ell} \in \left(0, \widehat{\ell}_{\max}\right)$ with the two black dots marking off the sub-domain $\frac{1}{2}\left(-\widehat{\ell}_{\max}, \widehat{\ell}_{\max}\right)$. The dashed lines correspond to M1I values of $\widehat{\ell} \in \left(\widehat{\ell}_2, \widehat{\ell}_3\right)$; the red dots have $\widehat{x}$ coordinates of $\frac{\widehat{\ell}_2}{2}$ and $\frac{\widehat{\ell}_3}{2}$. Numerical calculations give $\ell_{\max} = 7.162$, $\widehat{\ell}_2 = 11.935$ and $\widehat{\ell}_3 = 14.092$.

Figure C.4: M1I regions for three values of $\widehat{\alpha}$ (cf. Fig. 6.7(a))

C.5 The function $\widetilde{g}$ in the ID-ELE

We assume that $\widehat{\alpha}$ has been specified and that functions of $\left(\widehat{\ell},\widehat{\alpha}\right)$ have reduced to functions of $\widehat{\ell}$ only (i.e. we suppress the $\widehat{\alpha}$ dependency). Fig. C.5 depicts the $\widetilde{g}$-profile for $\widehat{\alpha}=0.1$.

- $\widetilde{g}$ blows up (with non-removable poles) at those zeros of $c_A\left(\widehat{\ell}\right)$ which are not also zeros of g_{num} (6.63b). We will call the pieces of $\widetilde{g}$ between such points, *branches*, number them 1, 2, ..., and abbreviate them as b_i (for the i-th branch of $\widetilde{g}$). Between each pair of poles, $\widetilde{g}$ is a strictly non-decreasing function with a multi-step character resembling a series of tan profiles that have been glued together. For any given $\widehat{L}$, $\widetilde{g}\left(\widehat{\ell}\right)=\widehat{L}$ has precisely one solution on each and every branch of $\widetilde{g}$.

- $\widetilde{\ell}$ is defined as the smallest solution of $\widetilde{g}\left(\widehat{\ell}\right)=\widehat{\ell}=\widehat{L}$ as in (6.63a), viz.

$$\frac{g_{\text{num}}\left(\widehat{\ell}\right)}{c_A\left(\widehat{\ell}\right)}=0 \qquad \text{i.e.} \qquad \cos\left(\sqrt{\widehat{q_h}}\frac{\widehat{\ell}}{2}\right)=0. \tag{C.34}$$

  In this case, we define the corresponding monolayer width $\widehat{L}$ as

$$\widetilde{L}:=\widetilde{g}\left(\widetilde{\ell}\right)=\widetilde{\ell}, \tag{C.35}$$

  as illustrated in Fig. C.5(b). We will use $\widetilde{\ell}$ and $\widetilde{L}$ somewhat interchangeably in what follows depending on context. They both measure the width of the thinnest possible P2P monolayer that solves the ID-ELE. Evidently, there is a value of $\widehat{L}$ below which the ID-ELE has no solutions; for the ID-ELE (written as (6.63a)) to admit a solution, we require

$$\widehat{L}\geq\widetilde{L}=\widetilde{L}\left(\widehat{\alpha}\right)=\frac{\pi}{\sqrt{\widehat{q_h}\left(\widehat{\alpha}\right)}}. \tag{C.36}$$

  This condition matches the definition of Region I. When $\widehat{L}=\widetilde{L}$, (6.63a) becomes

$$\widehat{\ell}+2\left(\frac{\widehat{q_h}-\widehat{q_\ell}}{\sqrt{\widehat{q_\ell}\widehat{q_h}}c_A\left(\widehat{\ell},\widehat{\alpha}\right)}\right)\cos\left(\sqrt{\widehat{q_h}}\frac{\widehat{\ell}}{2}\right)\cos\left(\sqrt{\widehat{q_\ell}}\frac{\widehat{\ell}}{2}\right)=\frac{\pi}{\sqrt{\widehat{q_h}}},$$

  with (minimum positive) solution

$$\widehat{\ell}=\frac{\pi}{\sqrt{\widehat{q_h}}}=\widehat{L}. \tag{C.37}$$

We conclude that:

Lemma C.5.1. (The ID-ELE has no solutions in Region I) *The ID-ELE* (6.63a) *has no solutions in Region I. Along the right edge of Region I/left edge of the cold region,* (6.63a) *admits the solution* $\widehat{\ell}=\widehat{L}$.

Corollary C.5.2. (All Region I candidates are at the edges) *Candidate, single-layer energy minimisers in Region I can only come from Source (2). In particular, for any* $\left(\widehat{L},\widehat{\alpha}\right)$ *in Region I, we need only consider* $\widehat{\ell}=0$ *(which we discard by continuity) and* $\widehat{\ell}=\widehat{L}$. *Consequently, the minimum energy single layer P2P morphology in Region I has* $\widehat{\ell}=\widehat{L}$.

Proof.

i) We saw in Conjecture C.2.3 that all of the configurations in Region I are monotone (and bounded).

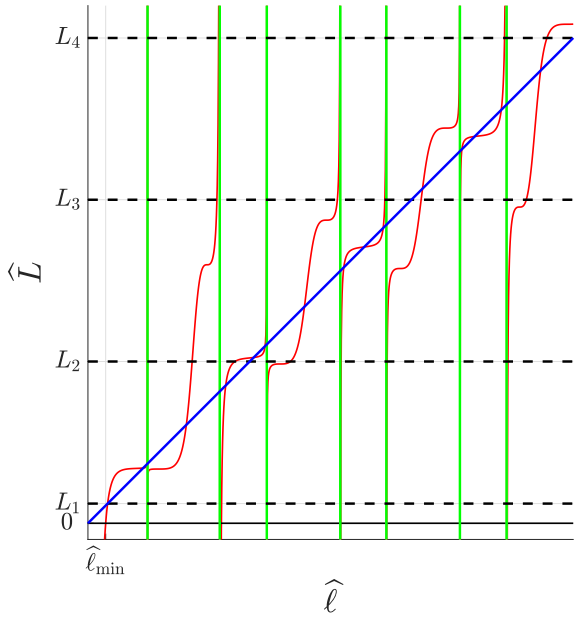

(a) $\widetilde{g}\left(\widehat{\ell}, \widehat{\alpha} = 0.1\right) = \widehat{L}$ for various $\widehat{L}$, showing the step-like, but strictly non-decreasing nature of $\widetilde{g}$ between its many non-removable poles.

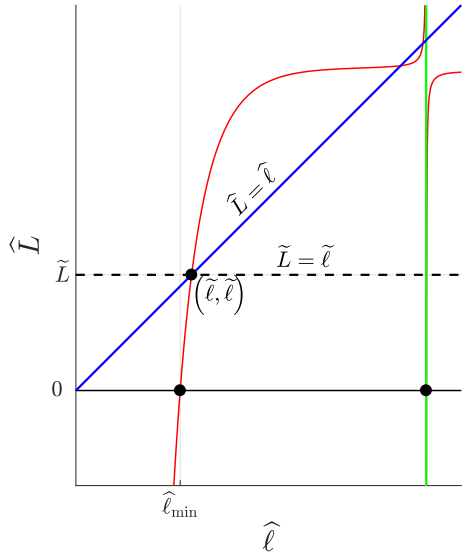

(b) A zoomed-in version of the figure in (a) to more clearly show the relationship between $\widehat{\ell}_{\min}$ and $\widetilde{\ell} = \widetilde{L}$

Figure C.5: The function $\widetilde{g}$ from (6.63a) is shown in red. The line $\widehat{L} = \widehat{\ell}$ is drawn in dark blue. The green lines correspond to values at which $\widetilde{g}$ in (6.63a) blows up. $\widehat{\ell}_{\min}$ is the smallest zero of $\widetilde{g}\left(\widehat{\ell}, \widehat{\alpha}\right)$ and $\widetilde{\ell}$ is the smallest solution of $\widetilde{g}\left(\widehat{\ell}, \widehat{\alpha}\right) = \widehat{\ell}$ with value $\widetilde{\ell} = \frac{\pi}{\sqrt{\widehat{q}_h}}$. Notice that $0 < \widehat{\ell}_{\min} < \widetilde{\ell} = \widetilde{L}$.

ii) We noted in Lemma C.5.1 that the ID-ELE has no solutions inside Region I; in addition from Fig. 6.7(a), it is clear that the function $c_A\left(\widehat{\ell},\widehat{\alpha}\right)$ has no zeros in this area. Consequently, we are left with candidates from Source (3) only.

This follows by consideration of Conjecture C.2.3, Lemma C.5.1 and Fig. 6.7(a) which shows that $c_A\left(\widehat{\ell},\widehat{\alpha}\right)$ has no zeros in Region I. □

Remark. The situation is quite different in the multi-layer problem where we can move other monolayers around to make space for interface layers with $\widehat{\ell} > \widehat{L}$. See layer $\boxed{2}$ in Fig. 7.6(b) on p. 158 for an illustration of such a morphology.

The simplicity of the result in Lemma C.5.2 means that we can create the minimum P2P energy function over this part of parameter space explicitly and exactly.

- More generally, we may find contours in parameter space for which the ID-ELE admits the solution $\widehat{\ell} = \widehat{L}$. Making the appropriate substitution into (6.63), we are led to

$$\widehat{L} + \frac{g_{\text{num}}\left(\widehat{\ell},\widehat{\alpha}\right)}{c_A\left(\widehat{\ell},\widehat{\alpha}\right)} = \widehat{L} \qquad \Rightarrow \qquad \cos\left(\sqrt{\widehat{q}_h}\frac{\widehat{\ell}}{2}\right) = 0 \qquad \text{or} \qquad \cos\left(\sqrt{\widehat{q}_\ell}\frac{\widehat{\ell}}{2}\right) = 0, \tag{C.38}$$

as long as $c_A\left(\widehat{\ell},\widehat{\alpha}\right) \neq 0$.

Remark. Just because the ID-ELE admits these simple solutions along this set of contours does not make them bounded. According to Fig. 6.7(a), the corresponding solutions $\widetilde{\varphi}$ to the ID-ELE have $\|\widetilde{\varphi}\|_\infty > 1$ in much of parameter space.

- We define $\widehat{\ell}_{\min}$ as the smallest solution of $\widetilde{g}\left(\widehat{\ell}\right) = 0$, viz.

$$\widehat{\ell} + 2\left(\frac{\widehat{q}_h - \widehat{q}_\ell}{\sqrt{\widehat{q}_\ell\widehat{q}_h}c_A\left(\widehat{\ell}\right)}\right)\cos\left(\sqrt{\widehat{q}_h}\frac{\widehat{\ell}}{2}\right)\cos\left(\sqrt{\widehat{q}_\ell}\frac{\widehat{\ell}}{2}\right) = 0; \tag{C.39}$$

it is the (smallest) stationary interface layer width for a monolayer of width $\widehat{L} = 0$. We illustrate this in Fig. C.5(b).

Remark. This scenario makes no sense in the single-layer context, but in the multi-layer situation, we can shift monolayers around to (effectively) create a zero width monolayer.

If we reconsider Fig. 6.4 in light of the above, we discover that the zero contour of c_A, giving the blow-ups of $\widetilde{g}$, is shown by the (dashed) green line, and the zero contour of $\frac{g_{\text{num}}}{c_A}$, giving the solutions of $\widetilde{g}\left(\widehat{\ell}\right) = \widehat{\ell}$ (for which $\widehat{\ell} = \widehat{L} = \widetilde{L}$), correspond to the solid **black** and **blue** lines (on which $\cos\left(\sqrt{\widehat{q}_h}\frac{\widehat{\ell}}{2}\right) = 0$ or $\cos\left(\sqrt{\widehat{q}_\ell}\frac{\widehat{\ell}}{2}\right) = 0$).

Notes

[1]Recall that we are seeking a stationary condition on $\widetilde{\varphi}$ which has Dirichlet BCs; consequently, the set of admissible functions comprises those functions satisfying (6.4a). Likewise, the set of admissible variations must satisfy zero Dirichlet BCs on the interface layer.

[2]We used the following facts in the derivation:

- The mass average, $\bar{\cdot}$, and inverse Laplacian, $(-\Delta_n)^{-1}(\cdot)$, operations are linear;
- For any zero mass, square integrable u, v,

$$\int_\Omega u\left((-\Delta_n)^{-1} v\right) \mathrm{d}\Omega = \int_\Omega v\left((-\Delta_n)^{-1} u\right) \mathrm{d}\Omega.$$

  To show this, let $(-\Delta_n)^{-1} u = f \Rightarrow -\Delta_n f = u$ and $(-\Delta_n)^{-1} v = g \Rightarrow -\Delta_n g = v$. Then

$$\begin{aligned}\int_\Omega u\left((-\Delta_n)^{-1} v\right) \mathrm{d}\Omega &= \int_\Omega (-\Delta_n f)\, g \ \mathrm{d}\Omega \\ &= \underbrace{-\int_{\partial\Omega} g \partial_n f \ \mathrm{d}s}_{=0} + \int_\Omega \nabla f \cdot \nabla g \ \mathrm{d}\Omega \\ &= \int_\Omega (-\Delta_n g)\, f \ \mathrm{d}\Omega + \underbrace{\int_{\partial\Omega} f \partial_n g \ \mathrm{d}s}_{=0} = \int_\Omega v\left((-\Delta_n)^{-1} u\right) \mathrm{d}\Omega.\end{aligned}$$

- The integral

$$\int_{-L/2}^{L/2} \overline{\eta}\Phi \ \mathrm{d}x = \overline{\eta} \int_{-L/2}^{L/2} \Phi \ \mathrm{d}x = 0,$$

  by virtue of the third part of (6.1b).
- We notice that

$$\int_{-L/2}^{L/2} \eta f \ \mathrm{d}x = \int_{x_L}^{x_R} \eta f \ \mathrm{d}x$$

  for any f, by virtue of the compact support of η on the interface layer.

Appendix D

Models of 3-phase materials

This appendix complements Chapter 9, and has four sections:

- In Section D.1, we construct a set of gradient flow dynamics for the 3-phase problem in terms of the underlying phases ϕ_A, ϕ_B, ϕ_V, and then apply the incompressibility condition (9.2) to these dynamics via a Lagrange parameter function. We then extract dynamics for (φ, ψ) as in (9.3), and reconcile the mobilities of the two formulations.
- In Section D.2, we apply the incompressibility condition (9.2) directly to the 3-phase energy, and then study 3-phase mass conservation in the (φ, ψ) dynamics.
- In Section D.3, we consider mass control for 3-phase materials. This allows us to write down some simple, exact solutions of our dynamical model.
- Finally, in Section D.4 we confirm that the 3-phase discrete time-stepping scheme we posed in Defn 9.2.2 inherits the mass conservation and control properties of the continuous model it approximates.

To facilitate some of the transformations in the next section, we first define (cf. (9.4))

$$\phi_A = \phi_A(\xi, \eta) = \xi \quad \text{and} \quad \phi_B = \phi_B(\xi, \eta) = \eta \quad \text{so that} \quad \phi_V = \phi_V(\xi, \eta) = 1 - \xi - \eta, \tag{D.1a}$$

whence,

$$\xi = \frac{1}{2}(\psi + \varphi), \qquad \eta = \frac{1}{2}(\psi - \varphi) \qquad \text{and so} \qquad \overline{\xi} = \frac{1}{2}\left(\overline{\psi} + \overline{\varphi}\right), \qquad \overline{\eta} = \frac{1}{2}\left(\overline{\psi} - \overline{\varphi}\right). \tag{D.1b}$$

D.1 Dynamics: a Lagrange parameter for incompressibility

We propose the following dynamics:

$$\begin{cases} \partial_t \phi_i = \nabla \cdot \left(M^{(i)} \nabla \mu_i \right) \\ \mu_i = \dfrac{\delta \mathcal{E}}{\delta \phi_i} + \lambda = -\nabla \cdot \left(\partial_{\nabla \phi_i} \mathcal{I} \right) + \partial_{\phi_i} \left(\mathcal{B} + \mathcal{N} \right) + \lambda \end{cases} \qquad \text{for } i = A, B, V, \tag{D.2}$$

where each mobility matrix is diagonal, viz.

$$M^{(i)} = M_i I_d \tag{D.3}$$

and each M_i is a constant scalar. We proceed as we did in Section 3.1.2, and assume that we may take partial derivatives of the homogeneous density $\mathcal{B}$, for instance by using the regularised $\mathcal{B}_\mu$ of (9.32). The six-part system of PDEs governing the dynamics is (cf. (3.22) and equations (6)–(8) of Zhang et al. (2005))

$$\partial_t \phi_A - M_A \Delta \left(\frac{\delta \mathcal{E}}{\delta \phi_A} + \lambda \right) = 0 \qquad \text{or} \qquad \begin{cases} \partial_t \phi_A - M_A \Delta \mu_A = 0 \\ \text{where} \quad \mu_A = \dfrac{\delta \mathcal{E}}{\delta \phi_A} + \lambda; \end{cases} \tag{D.4a}$$

$$\partial_t \phi_B - M_B \Delta \left(\frac{\delta \mathcal{E}}{\delta \phi_B} + \lambda \right) = 0 \qquad \text{or} \qquad \begin{cases} \partial_t \phi_B - M_B \Delta \mu_B = 0 \\ \text{where} \quad \mu_B = \dfrac{\delta \mathcal{E}}{\delta \phi_B} + \lambda; \end{cases} \tag{D.4b}$$

and,

$$\partial_t \phi_V - M_V \Delta \left(\frac{\delta \mathcal{E}}{\delta \phi_3} + \lambda \right) = 0 \qquad \text{or} \qquad \begin{cases} \partial_t \phi_V - M_V \Delta \mu_V = 0 \\ \text{where} \quad \mu_V = \dfrac{\delta \mathcal{E}}{\delta \phi_V} + \lambda, \end{cases} \tag{D.4c}$$

subject to incompressibility as in (9.2), the zero Neumann BCs

$$\partial_n \phi_A|_{\partial\Omega} = \partial_n \phi_B|_{\partial\Omega} = \partial_n \phi_V|_{\partial\Omega} = 0,$$

and

$$\partial_n \left(\frac{\delta \mathcal{E}}{\delta \phi_A} + \lambda \right)\Big|_{\partial\Omega} = \partial_n \left(\frac{\delta \mathcal{E}}{\delta \phi_B} + \lambda \right)\Big|_{\partial\Omega} = \partial_n \left(\frac{\delta \mathcal{E}}{\delta \phi_V} + \lambda \right)\Big|_{\partial\Omega} = 0, \tag{D.4d}$$

and the ICs

$$\begin{aligned} & \phi_A(x,0) = \phi_{A_0}(x), && \text{where} && \overline{\phi_{A_0}} = a, \\ & \phi_B(x,0) = \phi_{B_0}(x), && \text{where} && \overline{\phi_{B_0}} = b, \\ \text{and} \quad & \phi_V(x,0) = \phi_{V_0}(x), && \text{where} && \overline{\phi_{V_0}} = v = 1 - (a+b). \end{aligned} \tag{D.4e}$$

We proceed as follows:

1. Find the Lagrange function $\lambda = \lambda(x,t)$ and use it to re-write (D.4);
2. Derive the dynamics in φ and ψ (from (9.3a) and (9.3c)).

The Lagrange parameter function λ: redundant dynamics

From (A.93a) and (A.93b), we deduce that

$$\lambda = -\frac{1}{M_A + M_B + M_V} \left(M_A \frac{\delta \mathcal{E}}{\delta \phi_A} + M_B \frac{\delta \mathcal{E}}{\delta \phi_B} + M_V \frac{\delta \mathcal{E}}{\delta \phi_V} \right), \tag{D.5a}$$

and

$$\mu_i = \frac{1}{M_A + M_B + M_V} \left(\left(\sum_{\substack{j \in \{A,B,V\} \\ j \neq i}} M_j \right) \frac{\delta \mathcal{E}}{\delta \phi_i} - \sum_{\substack{j \in \{A,B,V\} \\ j \neq i}} M_j \frac{\delta \mathcal{E}}{\delta \phi_j} \right) \qquad \text{for} \qquad i = A, B, V. \tag{D.5b}$$

If we substitute these into (D.4a)–(D.4c) and add the results, we get

$$\sum_{i \in \{A,B,V\}} \mu_i = \frac{1}{M_A + M_B + M_V} \sum_{i \in \{A,B,V\}} \left(\left(\sum_{\substack{j \in \{A,B,V\} \\ j \neq i}} M_j \right) \frac{\delta \mathcal{E}}{\delta \phi_i} - \sum_{\substack{j \in \{A,B,V\} \\ j \neq i}} M_j \frac{\delta \mathcal{E}}{\delta \phi_j} \right) = 0 \tag{D.5c}$$

as expected i.e. with λ as in (D.5a), we have a redundant system of PDEs. In particular, if we drop (D.4c) and substitute (D.5b) into (D.4a) and (D.4b), we have

$$\partial_t \phi_A - \frac{M_A}{M_A + M_B + M_V} \Delta \left((M_B + M_V) \left(\frac{\delta \mathcal{E}}{\delta \phi_A} - \frac{\delta \mathcal{E}}{\delta \phi_V} \right) - M_B \left(\frac{\delta \mathcal{E}}{\delta \phi_B} - \frac{\delta \mathcal{E}}{\delta \phi_V} \right) \right) = 0; \tag{D.6a}$$

and

$$\partial_t \phi_B - \frac{M_B}{M_A + M_B + M_V} \Delta \left((M_A + M_V) \left(\frac{\delta \mathcal{E}}{\delta \phi_B} - \frac{\delta \mathcal{E}}{\delta \phi_V} \right) - M_A \left(\frac{\delta \mathcal{E}}{\delta \phi_A} - \frac{\delta \mathcal{E}}{\delta \phi_V} \right) \right) = 0, \tag{D.6b}$$

where we have added/subtracted convenient terms.

We now switch to (φ, ψ). Using (D.1), we find that

$$\frac{\delta \mathcal{E}}{\delta \xi} = \frac{\delta \mathcal{E}}{\delta \phi_A} \partial_\xi \phi_A + \frac{\delta \mathcal{E}}{\delta \phi_B} \partial_\xi \phi_B + \frac{\delta \mathcal{E}}{\delta \phi_V} \partial_\xi \phi_V = \frac{\delta \mathcal{E}}{\delta \phi_A} - \frac{\delta \mathcal{E}}{\delta \phi_V} \tag{D.7a}$$

$$\text{and} \quad \frac{\delta \mathcal{E}}{\delta \eta} = \frac{\delta \mathcal{E}}{\delta \phi_A} \partial_\eta \phi_A + \frac{\delta \mathcal{E}}{\delta \phi_B} \partial_\eta \phi_B + \frac{\delta \mathcal{E}}{\delta \phi_V} \partial_\eta \phi_V = \frac{\delta \mathcal{E}}{\delta \phi_B} - \frac{\delta \mathcal{E}}{\delta \phi_V}. \tag{D.7b}$$

If we use this result to re-write (D.6) in terms of (ξ, η), we are led to the pair

$$\partial_t \xi - \frac{M_A}{M_A + M_B + M_V} \Delta \left((M_B + M_V) \frac{\delta \mathcal{E}}{\delta \xi} - M_B \frac{\delta \mathcal{E}}{\delta \eta} \right) = 0 \tag{D.8a}$$

$$\text{and} \qquad \partial_t \eta - \frac{M_B}{M_A + M_B + M_V} \Delta \left((M_A + M_V) \frac{\delta \mathcal{E}}{\delta \eta} - M_A \frac{\delta \mathcal{E}}{\delta \xi} \right) = 0. \tag{D.8b}$$

For $M_A = M_B = M_V = k$, this simplifies to

$$\partial_t \xi - \frac{k}{3} \Delta \left(2 \frac{\delta \mathcal{E}}{\delta \xi} - \frac{\delta \mathcal{E}}{\delta \eta} \right) = 0 \qquad \text{and} \qquad \partial_t \eta - \frac{k}{3} \Delta \left(2 \frac{\delta \mathcal{E}}{\delta \eta} - \frac{\delta \mathcal{E}}{\delta \xi} \right) = 0; \tag{D.9}$$

In this latter case, we can always re-scale t so that $k = 1$. More generally, we could re-scale time so that one of $M_A, M_B, M_V = 1$; we explicitly choose *not* to do so, however.

Having transformed to a system which satisfies the incompressibility constraint, we now transform to a set of order parameters (φ, ψ) that are useful/convenient. We consider an invertible, linear transformation

$$\begin{pmatrix} \psi \\ \varphi \end{pmatrix} = \begin{pmatrix} c_1 & d_1 \\ c_2 & d_2 \end{pmatrix} \begin{pmatrix} \xi \\ \eta \end{pmatrix} \qquad \text{with} \qquad c_1 d_2 - d_1 c_2 \neq 0, \tag{D.10}$$

for real constants c_i, d_i. We regard the underlying component mobilities $M_A, M_B, M_V > 0$ as prescribed (by the physics, by measurement or otherwise), and we choose the c_i, d_i for convenience. We consider dynamics in which the macro mobility $M^{(\psi)} = M_\psi I$, and the micro mobility $M^{(\varphi)} = M_\varphi I$, are constant multiples of the identity matrix, viz.

$$\partial_t \psi - \nabla \cdot \left(M^{(\psi)} \nabla \frac{\delta \mathcal{E}}{\delta \psi} \right) = \partial_t \psi - \Delta \left(M_\psi \frac{\delta \mathcal{E}}{\delta \psi} \right) = 0, \tag{D.11a}$$

$$\text{and} \quad \partial_t \varphi - \nabla \cdot \left(M^{(\varphi)} \nabla \frac{\delta \mathcal{E}}{\delta \varphi} \right) = \partial_t \varphi - \Delta \left(M_\varphi \frac{\delta \mathcal{E}}{\delta \varphi} \right) = 0. \tag{D.11b}$$

We summarise the process in Fig. D.1, and pose the following questions:

- For a given set of mobilities M_i, can we choose the parameters c_i, d_i at will?
- For given M_i, can we choose the c_i, d_i such that $M_\varphi = M_\psi = 1$?
- What can be said about the special transformation in which

$$c_1 = d_1 = c_2 = 1, \qquad d_2 = -1 \qquad \text{viz.} \qquad \psi(\xi, \eta) = \xi + \eta \qquad \text{and} \qquad \varphi(\xi, \eta) = \xi - \eta? \tag{D.12}$$

  Are there restrictions on the mobilities M_i if (D.12) holds *and* $M_\varphi = M_\psi = 1$?

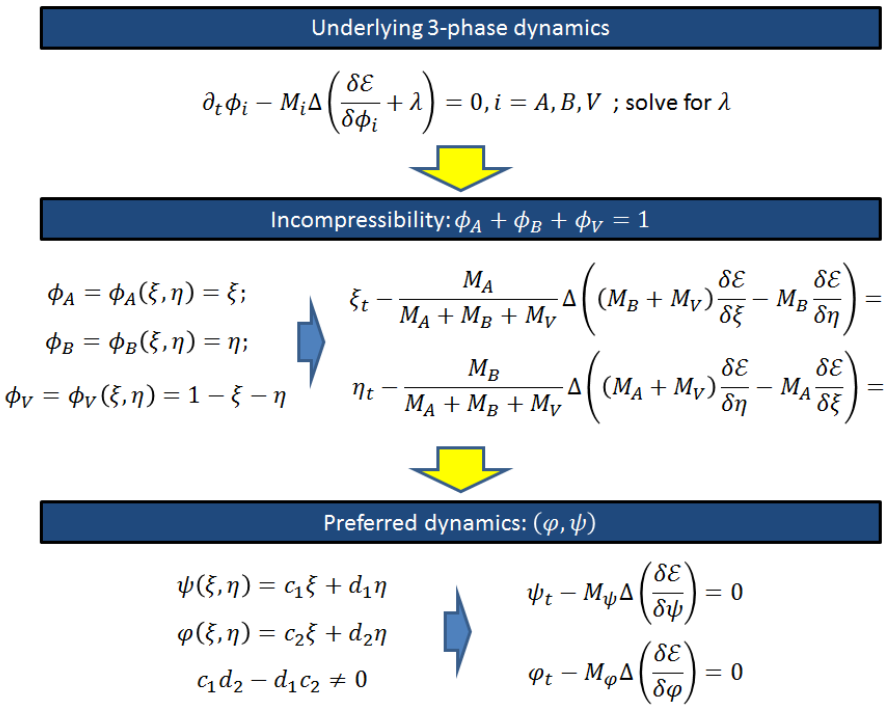

Figure D.1: Converting from the dynamics in $\boldsymbol{\phi}$ to dynamics in (φ, ψ). We are interested in transformations with $c_1 = d_1 = c_2 = 1$ and $d_2 = -1$.

To answer these questions, we add and subtract appropriate multiples of (D.8a) and (D.8b), using (D.10) to arrive at

$$\partial_t \psi - \Delta\left(\frac{M_A\left((c_1 - d_1)M_B + c_1 M_V\right)}{M_A + M_B + M_V}\frac{\delta \mathcal{E}}{\delta \xi} + \frac{M_B\left((d_1 - c_1)M_A + d_1 M_V\right)}{M_A + M_B + M_V}\frac{\delta \mathcal{E}}{\delta \eta}\right) = 0 \tag{D.13a}$$

and

$$\partial_t \varphi - \Delta\left(\frac{M_A\left((c_2 - d_2)M_B + c_2 M_V\right)}{M_A + M_B + M_V}\frac{\delta \mathcal{E}}{\delta \xi} + \frac{M_B\left((d_2 - c_2)M_A + d_2 M_V\right)}{M_A + M_B + M_V}\frac{\delta \mathcal{E}}{\delta \eta}\right) = 0. \tag{D.13b}$$

Using (D.10), we see that

$$\frac{\delta \mathcal{E}}{\delta \xi} = \frac{\delta \mathcal{E}}{\delta \psi}\partial_\xi \psi + \frac{\delta \mathcal{E}}{\delta \varphi}\partial_\xi \varphi = c_1 \frac{\delta \mathcal{E}}{\delta \psi} + c_2 \frac{\delta \mathcal{E}}{\delta \varphi} \quad \text{and} \quad \frac{\delta \mathcal{E}}{\delta \eta} = \frac{\delta \mathcal{E}}{\delta \psi}\partial_\eta \psi + \frac{\delta \mathcal{E}}{\delta \varphi}\partial_\eta \varphi = d_1 \frac{\delta \mathcal{E}}{\delta \psi} + d_2 \frac{\delta \mathcal{E}}{\delta \varphi} \tag{D.14}$$

or

$$\begin{pmatrix} \frac{\delta \mathcal{E}}{\delta \xi} \\ \frac{\delta \mathcal{E}}{\delta \eta} \end{pmatrix} = \begin{pmatrix} c_1 & c_2 \\ d_1 & d_2 \end{pmatrix} \begin{pmatrix} \frac{\delta \mathcal{E}}{\delta \psi} \\ \frac{\delta \mathcal{E}}{\delta \varphi} \end{pmatrix} \quad \Rightarrow \quad \begin{pmatrix} \frac{\delta \mathcal{E}}{\delta \psi} \\ \frac{\delta \mathcal{E}}{\delta \varphi} \end{pmatrix} = \frac{1}{c_1 d_2 - d_1 c_2} \begin{pmatrix} d_2 & -c_2 \\ -d_1 & c_1 \end{pmatrix} \begin{pmatrix} \frac{\delta \mathcal{E}}{\delta \xi} \\ \frac{\delta \mathcal{E}}{\delta \eta} \end{pmatrix}. \tag{D.15}$$

Hence, to write down dynamics as in (D.11), we need to choose c_i, d_i in terms of M_A, M_B and M_V such that, from (D.13) and (D.15),

$$\frac{M_\psi}{c_1 d_2 - d_1 c_2}\left(d_2 \frac{\delta \mathcal{E}}{\delta \xi} - c_2 \frac{\delta \mathcal{E}}{\delta \eta}\right) = \frac{M_A\left((c_1 - d_1)M_B + c_1 M_V\right)}{M_A + M_B + M_V}\frac{\delta \mathcal{E}}{\delta \xi} + \frac{M_B\left((d_1 - c_1)M_A + d_1 M_V\right)}{M_A + M_B + M_V}\frac{\delta \mathcal{E}}{\delta \eta}$$

and

$$\frac{M_\varphi}{c_1 d_2 - d_1 c_2}\left(-d_1 \frac{\delta \mathcal{E}}{\delta \xi} + c_1 \frac{\delta \mathcal{E}}{\delta \eta}\right) = \frac{M_A\left((c_2 - d_2)M_B + c_2 M_V\right)}{M_A + M_B + M_V}\frac{\delta \mathcal{E}}{\delta \xi} + \frac{M_B\left((d_2 - c_2)M_A + d_2 M_V\right)}{M_A + M_B + M_V}\frac{\delta \mathcal{E}}{\delta \eta}.$$

Notice that the two right-hand sides above are structurally identical, with c_1 replaced by c_2, and d_1 by d_2 in the second. Upon equating components, we find that

$$\frac{d_2 M_\psi}{c_1 d_2 - d_1 c_2} = \frac{M_A\left(\left(c_1 - d_1\right) M_B + c_1 M_V\right)}{M_A + M_B + M_V}; \tag{D.16a}$$

$$\frac{-c_2 M_\psi}{c_1 d_2 - d_1 c_2} = \frac{M_B\left(\left(d_1 - c_1\right) M_A + d_1 M_V\right)}{M_A + M_B + M_V}; \tag{D.16b}$$

$$\frac{-d_1 M_\varphi}{c_1 d_2 - d_1 c_2} = \frac{M_A\left(\left(c_2 - d_2\right) M_B + c_2 M_V\right)}{M_A + M_B + M_V}; \tag{D.16c}$$

and

$$\frac{c_1 M_\varphi}{c_1 d_2 - d_1 c_2} = \frac{M_B\left(\left(d_2 - c_2\right) M_A + d_2 M_V\right)}{M_A + M_B + M_V}. \tag{D.16d}$$

Evidently, we cannot choose c_i, d_i at will. We recall the following restrictions:

- Strictly positive mobilities: $M_A, M_B, M_V > 0 \Rightarrow M_A + M_B + M_V > 0$; and
- Invertibility (cf. (D.10)): $c_1 d_2 - d_1 c_2 \neq 0$.

Dividing (D.16a) and (D.16b), we have

$$\frac{d_2}{c_2} = \frac{M_A\left(\left(c_1 - d_1\right) M_B + c_1 M_V\right)}{M_B\left(\left(c_1 - d_1\right) M_A - d_1 M_V\right)} = \frac{f\left(c_1, d_1\right)}{g\left(c_1, d_1\right)}. \tag{D.17a}$$

Likewise, from (D.16c) and (D.16d), we obtain

$$\frac{d_1}{c_1} = \frac{M_A\left(\left(c_2 - d_2\right) M_B + c_2 M_V\right)}{M_B\left(\left(c_2 - d_2\right) M_A - d_2 M_V\right)} = \frac{f\left(c_2, d_2\right)}{g\left(c_2, d_2\right)}. \tag{D.17b}$$

It is clear that these two equations form a redundant pair.

Remark. We could also relabel $c_1 \leftrightarrow c_2$ and $d_1 \leftrightarrow d_2$ to switch between (D.17a) and (D.17b).

We may choose the pair (c_1, d_1) (or (c_2, d_2)), at which point the ratio of c_2 to d_2 (or c_1 to d_1) becomes fixed. There are two distinct cases to consider:

1. $c_1 = d_1 = C$, and $c_2 \neq d_2$; and
2. $c_1 \neq d_1$ and $c_2 \neq d_2$.

Remark. By symmetry, $c_1 = d_1, c_2 \neq d_2$ and $c_1 \neq d_1, c_2 = d_2$ refer to the same scenario.

For simplicity, we consider only the first case. From (D.17b), we determine that

$$c_2 M_A = -d_2 M_B \quad \Rightarrow \quad \frac{d_2}{c_2} = -\frac{M_A}{M_B}. \tag{D.18}$$

Hence, if $M_A, M_B > 0$, c_2 and d_2 must have opposite signs. (D.16) rearranges to

$$M_\psi = \frac{C^2 M_V\left(M_A + M_B\right)}{M_A + M_B + M_V} \qquad \text{and} \qquad M_\varphi = M_A\left(\frac{M_A}{M_B} + 1\right) c_2^2. \tag{D.19a}$$

Dividing the first of these into the second gives

$$\frac{M_\varphi}{M_\psi} = \frac{c_2^2 M_A\left(M_A + M_B + M_V\right)}{C^2 M_B M_V}. \tag{D.19b}$$

We consider three special sub-cases:

i) The same underlying mobilities, $M_A = M_B = M_V =: \widetilde{M}$: from (D.18) and (D.19b),

$$d_2 = -c_2 =: D \qquad \Rightarrow \qquad M_\psi = \frac{2}{3} C^2 \widetilde{M}, \qquad M_\varphi = 2 D^2 \widetilde{M}, \qquad \frac{M_\varphi}{M_\psi} = \frac{3 D^2}{C^2}. \tag{D.20}$$

Notice that $d_2 = -c_2$ only requires $M_A = M_B$ (with $M_V > 0$ free).

ii) Equal (unit) mobilities on ψ and φ, i.e. $M_\psi = M_\varphi\,(=1)$: to achieve this, we require

$$\frac{C^2}{c_2^2} = \frac{M_A\,(M_A + M_B + M_V)}{M_B M_V}. \tag{D.21}$$

For $M_\psi = M_\varphi$ and $M_A = M_B = M_V = \widetilde{M}$ (so $c_2 = -D$ as above), it is clear that

$$\frac{C^2}{D^2} = 3 \qquad \Rightarrow \qquad C = \pm\sqrt{3}D \qquad \Leftrightarrow \qquad D = \frac{\pm C}{\sqrt{3}} \tag{D.22}$$

(since we regard C as independent). To achieve $M_\psi = M_\varphi = 1$ requires

$$C = \sqrt{\frac{3}{2\widetilde{M}}}, \qquad \text{and} \qquad D = \frac{1}{\pm\sqrt{2\widetilde{M}}}.$$

Choosing

$$\psi\,(\xi,\eta) = \sqrt{\frac{3}{2\widetilde{M}}}\,(\xi+\eta) \qquad \text{and} \qquad \varphi\,(\xi,\eta) = \frac{1}{\sqrt{2\widetilde{M}}}\,(\xi-\eta)\,, \tag{D.23}$$

leads to $M_\psi = M_\varphi = 1$, as required. For underlying unit mobilities, $M_A = M_B = M_V = 1$, we would need to use the transformation

$$\psi\,(\xi,\eta) = \sqrt{\frac{3}{2}}\,(\xi+\eta) \qquad \text{and} \qquad \varphi\,(\xi,\eta) = \frac{1}{\sqrt{2}}\,(\xi-\eta)\,, \tag{D.24}$$

in order to arrive at $M_\psi = M_\varphi = 1$.

iii) The transformation (D.12), in which $c_2/d_2 = D = -1$: (D.18) implies that

$$M_A = M_B =: \widehat{M}. \tag{D.25}$$

Likewise, using (D.19), it is clear that

$$M_\psi = \frac{M_V\,(M_A+M_B)}{M_A+M_B+M_V} = \frac{2M_V\widehat{M}}{2\widehat{M}+M_V} \qquad \text{and} \qquad M_\varphi = \frac{M_A\,(M_A+M_B)}{M_B} = 2\widehat{M}, \tag{D.26a}$$

and so

$$\frac{M_\varphi}{M_\psi} = \frac{M_A\,(M_A+M_B+M_V)}{M_B M_V} = \frac{2\widehat{M}+M_V}{M_V} = 1 + \frac{2\widehat{M}}{M_V} > 1. \tag{D.26b}$$

Then

$$M_r := \frac{M_\psi}{M_\varphi} = \frac{\overline{M}+2}{\overline{M}} = \qquad \text{where} \qquad \overline{M} := \frac{M_V}{\widehat{M}} \tag{D.26c}$$

relates the ratio of the macro to micro mobilities, to the ratio of the void mobility to the A, B mobilities (assumed equal). We summarise their relationship in Fig. D.2.

According to (D.26b), it is impossible to have $M_\psi = M_\varphi > 0$. But, if $M_A = M_B = M_V = M\,(=1)$, then (cf. the red point in Fig. D.2, (9.31))

$$M_\psi = \frac{2M}{3}\left(=\frac{2}{3}\right) \qquad \text{and} \qquad M_\varphi = 2M\,(=2)\,. \tag{D.27}$$

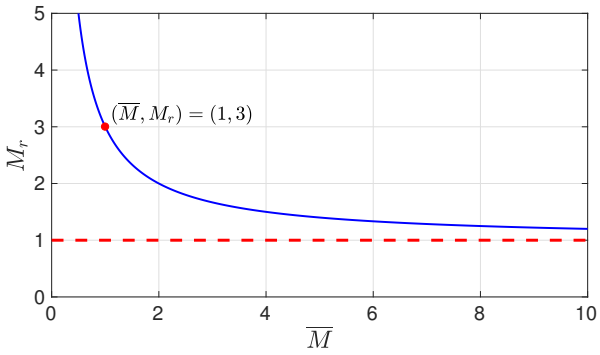

Figure D.2: Ratio of macro to micro mobilities, M_r, as a function of $\overline{M}$ in (D.26c). The **red** dot indicates the M_r implied by $\overline{M} = 1$ (cf. (D.27)). Notice that $M_r \to 1$ as $\overline{M} \to \infty$: it is impossible to have $M_\psi \leq M_\varphi$ i.e. $M_r \leq 1$ for (φ, ψ) as in (D.12).

Remark. Going forward, we choose (φ, ψ) as in (D.12) (cf. (9.3)), and insist that the underlying mobilities M_i satisfy (D.25); viz. $M_A = M_B = \widehat{M}$. The dynamics of our system have the form (cf. (D.11), (D.26))

$$\partial_t \psi - \Delta \left(M_\psi \frac{\delta \mathcal{E}}{\delta \psi} \right) = 0, \qquad \text{where} \qquad M_\psi = \frac{2 M_V \widehat{M}}{2\widehat{M} + M_V}, \tag{D.28a}$$

$$\text{and} \qquad \partial_t \varphi - \Delta \left(M_\varphi \frac{\delta \mathcal{E}}{\delta \varphi} \right) = 0, \qquad \text{where} \qquad M_\varphi = 2\widehat{M}, \tag{D.28b}$$

which we summarise in (9.35).

We now repeat the calculation above with specific reference to our energy functional, initially switching to (ξ, η) parameters as we did in (D.6), (D.8) and then to (φ, ψ) (cf. (9.3a)–(9.3c)).

Examining (9.14), and recalling (A.87), (A.88) and (A.89), we find that

$$\frac{\delta \mathcal{E}}{\delta \phi_j} = - \sum_{i \in \{A,B,V\}} \varepsilon_{ji}^2 \left(-\Delta\right) \phi_i + \partial_{\phi_j} \mathcal{B} + \sum_{i \in \{A,B,V\}} \gamma_{ji} \left(-\Delta_n\right)^{-1} \left(\phi_i - \overline{\phi_i}\right), \tag{D.29}$$

and so, if we use this in (D.5b), we have

$$\mu_i = \frac{1}{M_A + M_B + M_V} \left(\left(\sum_{\substack{j \in \{A,B,V\} \\ j \neq i}} M_j \right) \left(\text{Row}_i \left(\boldsymbol{\mathcal{I}} \left(-\Delta\right) \boldsymbol{\phi} \right) + \partial_{\phi_i} \mathcal{B} + \left(-\Delta_n\right)^{-1} \left(\text{Row}_i \left(\boldsymbol{\Gamma \Phi} \right) \right) \right) \right.$$

$$\left. - \sum_{\substack{j \in \{A,B,V\} \\ j \neq i}} M_j \left(\text{Row}_j \left(\boldsymbol{\mathcal{I}} \left(-\Delta\right) \boldsymbol{\phi} \right) + \partial_{\phi_j} \mathcal{B} + \left(-\Delta_n\right)^{-1} \left(\text{Row}_j \left(\boldsymbol{\Gamma \Phi} \right) \right) \right) \right), \tag{D.30}$$

for $i = A, B, V$. At this stage, it is convenient to recall (9.14b) and (9.18b), and note that

$$\boldsymbol{\mathcal{I}} \left(-\Delta\right) \boldsymbol{\phi} = \begin{pmatrix} \varepsilon_A^2 \left(-\Delta\right) \phi_A + \varepsilon_{AB}^2 \left(-\Delta\right) \phi_B + \varepsilon_{AV}^2 \left(-\Delta\right) \phi_V \\ \varepsilon_{BA}^2 \left(-\Delta\right) \phi_A + \varepsilon_B^2 \left(-\Delta\right) \phi_B + \varepsilon_{BV}^2 \left(-\Delta\right) \phi_V \\ \varepsilon_{AV}^2 \left(-\Delta\right) \phi_A + \varepsilon_{BV}^2 \left(-\Delta\right) \phi_B + \varepsilon_V^2 \left(-\Delta\right) \phi_V \end{pmatrix},$$

and

$$\boldsymbol{\Gamma \Phi} = \begin{pmatrix} \gamma_A \left(\phi_A - \overline{\phi_A}\right) + \gamma_{AB} \left(\phi_B - \overline{\phi_B}\right) + \gamma_{AV} \left(\phi_V - \overline{\phi_V}\right) \\ \gamma_{AB} \left(\phi_A - \overline{\phi_A}\right) + \gamma_B \left(\phi_B - \overline{\phi_B}\right) + \gamma_{BV} \left(\phi_V - \overline{\phi_V}\right) \\ \gamma_{AV} \left(\phi_A - \overline{\phi_A}\right) + \gamma_{BV} \left(\phi_B - \overline{\phi_B}\right) + \gamma_V \left(\phi_V - \overline{\phi_V}\right) \end{pmatrix}.$$

If we now substitute into (D.4), we arrive at

$$\begin{aligned}\partial_t\phi_A - \frac{M_A}{M_A+M_B+M_V}\Delta\Bigg(&\left((M_B+M_V)\,\varepsilon_A^2 - M_B\varepsilon_{AB}^2 - M_V\varepsilon_{AV}^2\right)(-\Delta)\,\phi_A\\ &+\left((M_B+M_V)\,\varepsilon_{AB}^2 - M_B\varepsilon_B^2 - M_V\varepsilon_{BV}^2\right)(-\Delta)\,\phi_B\\ &+\left((M_B+M_V)\,\varepsilon_{AV}^2 - M_B\varepsilon_{BV}^2 - M_V\varepsilon_V^2\right)(-\Delta)\,\phi_V\\ &+(M_B+M_V)\,\partial_{\phi_A}\mathcal{B} - M_B\partial_{\phi_B}\mathcal{B} - M_V\partial_{\phi_V}\mathcal{B}\\ &+(-\Delta_n)^{-1}\Bigg(\left((M_B+M_V)\,\gamma_A - M_B\gamma_{AB} - M_V\gamma_{AV}\right)\left(\phi_A-\overline{\phi_A}\right)\\ &+\left((M_B+M_V)\,\gamma_{AB} - M_B\gamma_B - M_V\gamma_{BV}\right)\left(\phi_B-\overline{\phi_B}\right)\\ &+\left((M_B+M_V)\,\gamma_{AV} - M_B\gamma_{BV} - M_V\gamma_V\right)\left(\phi_V-\overline{\phi_V}\right)\Bigg)\Bigg) = 0; \quad \text{(D.31a)}\end{aligned}$$

$$\begin{aligned}\partial_t\phi_B - \frac{M_B}{M_A+M_B+M_V}\Delta\Bigg(&\left((M_A+M_V)\,\varepsilon_{AB}^2 - M_A\varepsilon_A^2 - M_V\varepsilon_{AV}^2\right)(-\Delta)\,\phi_A\\ &+\left((M_A+M_V)\,\varepsilon_B^2 - M_A\varepsilon_{AB}^2 - M_V\varepsilon_{BV}^2\right)(-\Delta)\,\phi_B\\ &+\left((M_A+M_V)\,\varepsilon_{BV}^2 - M_A\varepsilon_{AV}^2 - M_V\varepsilon_V^2\right)(-\Delta)\,\phi_V\\ &+(M_A+M_V)\,\partial_{\phi_B}\mathcal{B} - M_A\partial_{\phi_A}\mathcal{B} - M_V\partial_{\phi_V}\mathcal{B}\\ &+(-\Delta_n)^{-1}\Bigg(\left((M_A+M_V)\,\gamma_{AB} - M_A\gamma_A - M_V\gamma_{AV}\right)\left(\phi_A-\overline{\phi_A}\right)\\ &+\left((M_A+M_V)\,\gamma_B - M_A\gamma_{AB} - M_V\gamma_{BV}\right)\left(\phi_B-\overline{\phi_B}\right)\\ &+\left((M_A+M_V)\,\gamma_{BV} - M_A\gamma_{AV} - M_V\gamma_V\right)\left(\phi_V-\overline{\phi_V}\right)\Bigg)\Bigg) = 0; \quad \text{(D.31b)}\end{aligned}$$

and

$$\begin{aligned}\partial_t\phi_V - \frac{M_V}{M_A+M_B+M_V}\Delta\Bigg(&\left((M_A+M_B)\,\varepsilon_{AV}^2 - M_A\varepsilon_A^2 - M_B\varepsilon_{AB}^2\right)(-\Delta)\,\phi_A\\ &+\left((M_A+M_B)\,\varepsilon_{BV}^2 - M_A\varepsilon_{AB}^2 - M_B\varepsilon_B^2\right)(-\Delta)\,\phi_B\\ &+\left((M_A+M_B)\,\varepsilon_V^2 - M_A\varepsilon_{AV}^2 - M_B\varepsilon_{BV}^2\right)(-\Delta)\,\phi_V\\ &+(M_A+M_B)\,\partial_{\phi_V}\mathcal{B} - M_A\partial_{\phi_A}\mathcal{B} - M_B\partial_{\phi_B}\mathcal{B}\\ &+(-\Delta_n)^{-1}\Bigg(\left((M_A+M_B)\,\gamma_{AV} - M_A\gamma_A - M_B\gamma_{AB}\right)\left(\phi_A-\overline{\phi_A}\right)\\ &+\left((M_A+M_B)\,\gamma_{BV} - M_A\gamma_{AB} - M_B\gamma_B\right)\left(\phi_B-\overline{\phi_B}\right)\\ &+\left((M_A+M_B)\,\gamma_V - M_A\gamma_{AV} - M_B\gamma_{BV}\right)\left(\phi_V-\overline{\phi_V}\right)\Bigg)\Bigg) = 0. \quad \text{(D.31c)}\end{aligned}$$

At this stage, we impose the incompressibility condition and switch to (ξ,η) order parameters. Using (D.1) to discard the equation for ϕ_V (i.e. (D.31c)) (we could just as easily have dropped either of the other two), we note that (cf. (D.7))

$$\partial_\xi\mathcal{B} = \partial_{\phi_A}\mathcal{B} - \partial_{\phi_V}\mathcal{B} \qquad \text{and} \qquad \partial_\eta\mathcal{B} = \partial_{\phi_B}\mathcal{B} - \partial_{\phi_V}\mathcal{B}. \quad \text{(D.32)}$$

Substituting, we thus arrive at a two-part system of PDEs (D.33) in (ξ,η), viz.

$$\partial_t\xi - \frac{M_A}{M_A+M_B+M_V}\Delta\mu_\xi = 0, \quad \text{(D.33a)}$$

where

$$\begin{aligned}\mu_\xi = &\left((M_B+M_V)\,\varepsilon_A^2 - M_B\varepsilon_{AB}^2 - (M_B+2M_V)\,\varepsilon_{AV}^2 + M_B\varepsilon_{BV}^2 + M_V\varepsilon_V^2\right)(-\Delta)\,\xi\\ &+\left((M_B+M_V)\,\varepsilon_{AB}^2 - M_B\varepsilon_B^2 - (M_B+M_V)\,\varepsilon_{AV}^2 + (M_B-M_V)\,\varepsilon_{BV}^2 + M_V\varepsilon_V^2\right)(-\Delta)\,\eta\\ &+(M_B+M_V)\,\partial_\xi\mathcal{B} - M_B\partial_\eta\mathcal{B}\\ &+(-\Delta_n)^{-1}\Big(\left((M_B+M_V)\,\gamma_A - M_B\gamma_{AB} - (M_B+2M_V)\,\gamma_{AV} + M_B\gamma_{BV} + M_V\gamma_V\right)\left(\xi-\overline{\xi}\right)\\ &+\left((M_B+M_V)\,\gamma_{AB} - M_B\gamma_B - (M_B+M_V)\,\gamma_{AV} + (M_B-M_V)\,\gamma_{BV} + M_V\gamma_V\right)(\eta-\overline{\eta})\Big) = 0;\end{aligned}\tag{D.33b}$$

and, likewise

$$\partial_t\eta - \frac{M_B}{M_A+M_B+M_V}\Delta\mu_\eta = 0,\tag{D.33c}$$

where

$$\begin{aligned}\mu_\eta = &\left((M_A+M_V)\,\varepsilon_{AB}^2 - M_A\varepsilon_A^2 + (M_A-M_V)\,\varepsilon_{AV}^2 - (M_A+M_V)\,\varepsilon_{BV}^2 + M_V\varepsilon_V^2\right)(-\Delta)\,\xi\\ &+\left((M_A+M_V)\,\varepsilon_B^2 - M_A\varepsilon_{AB}^2 - (M_A+2M_V)\,\varepsilon_{BV}^2 + M_A\varepsilon_{AV}^2 + M_V\varepsilon_V^2\right)(-\Delta)\,\eta\\ &+(M_A+M_V)\,\partial_\eta\mathcal{B} - M_A\partial_\xi\mathcal{B}\\ &+(-\Delta_n)^{-1}\Big(\left((M_A+M_V)\,\gamma_{AB} - M_A\gamma_A + (M_A-M_V)\,\gamma_{AV} - (M_A+M_V)\,\gamma_{BV} + M_V\gamma_V\right)\left(\xi-\overline{\xi}\right)\\ &+\left((M_A+M_V)\,\gamma_B - M_A\gamma_{AB} - (M_A+2M_V)\,\gamma_{BV} + M_A\gamma_{AV} + M_V\gamma_V\right)(\eta-\overline{\eta})\Big) = 0.\end{aligned}\tag{D.33d}$$

We now use (D.33) to calculate dynamics in φ and ψ. Assuming that $M_A = M_B = \widehat{M}$ (as in (D.25)) we define M_ψ as in (D.26a), viz.

$$M_\psi = \frac{2M_V\widehat{M}}{2\widehat{M}+M_V} \qquad \text{and} \qquad \mu_\psi = \frac{\mu_\xi+\mu_\eta}{2M_V},$$

and add the equations above, to obtain $\partial_t\psi - M_\psi\Delta\mu_\psi = 0$ (cf. (D.28a)), where

$$\begin{aligned}\frac{\mu_\xi+\mu_\eta}{2M_V} = &\frac{1}{4}\left(\varepsilon_A^2+\varepsilon_B^2+2\varepsilon_{AB}^2-4\varepsilon_{AV}^2-4\varepsilon_{BV}^2+4\varepsilon_V^2\right)(-\Delta)\,\psi\\ &\frac{1}{4}\left(\varepsilon_A^2-\varepsilon_B^2+2\varepsilon_{BV}^2-2\varepsilon_{AV}^2\right)(-\Delta)\,\varphi + \partial_\psi\mathcal{B}(\varphi,\psi)\\ &+\frac{1}{4}(-\Delta_n)^{-1}\left((\gamma_A+\gamma_B+2\gamma_{AB}-4\gamma_{AV}-4\gamma_{BV}+4\gamma_V)\left(\psi-\overline{\psi}\right)\right.\\ &\left.+(\gamma_A-\gamma_B+2\gamma_{BV}-2\gamma_{AV})\,(\varphi-\overline{\varphi})\right) = 0,\end{aligned}$$

if we use (D.1b) and use (D.15) to write

$$\partial_\psi\mathcal{B}(\varphi,\psi) = \frac{1}{2}\left(\partial_\xi\mathcal{B}+\partial_\eta\mathcal{B}\right) \quad \text{and} \quad \partial_\varphi\mathcal{B}(\varphi,\psi) = \frac{1}{2}\left(\partial_\xi\mathcal{B}-\partial_\eta\mathcal{B}\right).\tag{D.34}$$

Similarly, if we define M_φ as in (D.26a), viz.

$$M_\varphi = 2\widehat{M} \qquad \text{and} \qquad \mu_\varphi = \frac{\mu_\xi-\mu_\eta}{2\left(2\widehat{M}+M_V\right)},$$

and *subtract* the equations above, we obtain $\partial_t\varphi - M_\varphi\Delta\mu_\varphi = 0$ (cf. (D.28b)), where

$$\begin{aligned}\frac{\mu_\xi-\mu_\eta}{2\left(2\widehat{M}+M_V\right)} = &\frac{1}{4}\left(\varepsilon_A^2-\varepsilon_B^2+2\varepsilon_{BV}^2-2\varepsilon_{AV}^2\right)(-\Delta)\,\psi + \frac{1}{4}\left(\varepsilon_A^2-2\varepsilon_{AB}^2+\varepsilon_B^2\right)(-\Delta)\,\varphi + \partial_\varphi\mathcal{B}(\varphi,\psi)\\ &+\frac{1}{4}(-\Delta_n)^{-1}\left((\gamma_A-\gamma_B+2\gamma_{BV}-2\gamma_{AV})\left(\psi-\overline{\psi}\right)+(\gamma_A-2\gamma_{AB}+\gamma_B)\,(\varphi-\overline{\varphi})\right) = 0.\end{aligned}$$

Finally, using (9.24), we re-write this latter system in the more familiar form (9.36).

We define the interfacial parameters as in (9.21), and the non-local parameters as in (9.24) and close the dynamics by imposing the zero Neumann BCs (9.36e) (cf. (3.35d)), along with the ICs (9.36f) (cf. (3.35c), (D.4e)).

D.2 A 3-phase model in two order parameters

Starting from (9.12) and (9.14), we now use (9.4) and (9.8) to express the energy in terms of (φ, ψ), and then use this form of the energy to derive the related dynamic equations.

D.2.1 Energy

The **interfacial energy** density is

$$\mathcal{I}(\nabla \boldsymbol{\phi}) = \frac{1}{2}\Big(\varepsilon_A^2 |\nabla\phi_A|^2 + 2\varepsilon_{AB}^2 |\nabla\phi_A \cdot \nabla\phi_B| + 2\varepsilon_{AV}^2 |\nabla\phi_A \cdot \nabla\phi_V| \\ + \varepsilon_B^2 |\nabla\phi_B|^2 + 2\varepsilon_{BV}^2 |\nabla\phi_B \cdot \nabla\phi_V| + \varepsilon_V^2 |\nabla\phi_V|^2 \Big)$$

and so if we cast this into (φ, ψ) order parameters, we have

$$\mathcal{I}(\nabla\psi, \nabla\varphi) = \frac{\varepsilon_\varphi^2}{2} |\nabla\varphi|^2 + \varepsilon_{\varphi\psi}^2 |\nabla\psi \cdot \nabla\varphi| + \frac{\varepsilon_\psi^2}{2} |\nabla\psi|^2 ,$$

where we have used (9.21). **The non-local energy** expands as

$$\int_\Omega \mathcal{N}(\boldsymbol{\phi})\, \mathrm{d}\Omega = \frac{\gamma_A}{2} \left\|\phi_A - \overline{\phi_A}\right\|_{-1}^2 + \gamma_{AB} \left(\phi_A - \overline{\phi_A}, \phi_B - \overline{\phi_B}\right)_{-1} + \gamma_{AV} \left(\phi_A - \overline{\phi_A}, \phi_V - \overline{\phi_V}\right)_{-1} \\ + \frac{\gamma_B}{2} \left\|\phi_B - \overline{\phi_B}\right\|_{-1}^2 + \gamma_{BV} \left(\phi_B - \overline{\phi_B}, \phi_V - \overline{\phi_V}\right)_{-1} + \frac{\gamma_V}{2} \left\|\phi_V - \overline{\phi_V}\right\|_{-1}^2 .$$

Casting this into (φ, ψ) order parameters yields

$$\int_\Omega \mathcal{N}(\varphi, \psi)\ \mathrm{d}\Omega = \frac{\alpha}{2} \|\varphi - \overline{\varphi}\|_{-1}^2 + \beta \left(\varphi - \overline{\varphi}, \psi - \overline{\psi}\right)_{-1} + \frac{\gamma}{2} \left\|\psi - \overline{\psi}\right\|_{-1}^2 ,$$

if we use (9.24). The homogeneous free energy density $\mathcal{B}$ is discussed in detail in the main text. Combining these terms yields (9.19).

FEniCS

We discuss the task of evaluating the non-local energy in FEniCS. We consider

$$\int_\Omega \left((-\Delta)^{-1}(\varphi - \overline{\varphi})\right)\left(\psi - \overline{\psi}\right) \mathrm{d}\Omega,$$

and focus on solving the Neumann Poisson PDE

$$(-\Delta)^{-1}(\varphi - \overline{\varphi}) = u \qquad \Leftrightarrow \qquad -\Delta u = \varphi - \overline{\varphi} =: f.$$

We wish to solve $-\Delta_n u = f$ subject to the global uniqueness constraint $\overline{u} = 0$. We recast the problem as one in which we wish to find u such that

$$\mathcal{E}(u) := \int_\Omega \left(\frac{1}{2}|\nabla u|^2 - fu\right) \mathrm{d}\Omega \to \min \qquad \text{with} \qquad \int_\Omega u\ \mathrm{d}\Omega = 0,$$

and we assume that f satisfies the Neumann Poisson solvability constraint $\overline{f} = 0$ (this is obviously true for our function $f = \varphi - \overline{\varphi}$). We define the Lagrangian

$$\mathcal{L}(u, \lambda) := \int_\Omega \left(\frac{1}{2} |\nabla u|^2 - fu \right) \, \mathrm{d}\Omega + \lambda \int_\Omega u \, \mathrm{d}\Omega,$$

with Lagrange parameter $\lambda \in \mathbb{R}$. First order optimality conditions are

$$\begin{aligned} \frac{\delta \mathcal{L}}{\delta u} = 0 \qquad &\Rightarrow \qquad -\Delta_n u + \lambda = f \\ \partial_\lambda \mathcal{L} = 0 \qquad &\Rightarrow \qquad \int_\Omega u \, \mathrm{d}\Omega = 0. \end{aligned}$$

Introduce the test elements $\omega \in H^1(\Omega)$ and $\nu \in \mathbb{R}$ and the weak form of the problem is to find $(u, \lambda) \in H^1(\Omega) \times \mathbb{R}$ such that

$$(\nabla u, \nabla \omega) + (\lambda, \omega) = (f, \omega) \qquad \text{and} \qquad (\nu, u) = 0,$$

for every $(\omega, \nu) \in H^1(\Omega) \times \mathbb{R}$.

Remark. The FEniCS project website has useful documentation based on this problem, but the URLs change frequently. The reader may find it useful to search http://fenicsproject.org for more information on the above.

D.2.2 Dynamics

For gradient stable dynamics, we use (D.28) with zero Neumann BCs for φ and ψ. We find that

$$\frac{\delta \mathcal{E}}{\delta \varphi} = \varepsilon_\varphi^2 (-\Delta) \varphi + \varepsilon_{\varphi\psi}^2 (-\Delta) \psi + \partial_\varphi \mathcal{B}(\varphi, \psi) + (-\Delta_n)^{-1} \left(\alpha (\varphi - \overline{\varphi}) + \beta \left(\psi - \overline{\psi} \right) \right), \tag{D.35}$$

$$\frac{\delta \mathcal{E}}{\delta \psi} = \varepsilon_{\varphi\psi}^2 (-\Delta) \varphi + \varepsilon_\psi^2 (-\Delta) \psi + \partial_\psi \mathcal{B}(\varphi, \psi) + (-\Delta_n)^{-1} \left(\beta (\varphi - \overline{\varphi}) + \gamma \left(\psi - \overline{\psi} \right) \right). \tag{D.36}$$

Using all of this material, we arrive at the coupled system (9.36).

D.2.3 Mass conservation: from non-local to local dynamics

Equations (9.36a) and (9.36c) reference the non-local averages $\overline{\varphi}$ and $\overline{\psi}$. These originate from the inverse Laplacian present in the non-local contribution to the energy functional (9.19). Computing with such non-local terms is hard, and so we wish to replace them with fixed control parameters. We integrate (9.36a) over Ω and divide by $|\Omega|$ to obtain

$$\partial_t \overline{\varphi} - M_\varphi \underbrace{\overline{\Delta_n \omega_\varphi}}_{=0} + M_\varphi \Big(\alpha \underbrace{\overline{(\varphi - \overline{\varphi})}}_{=0} + \beta \underbrace{\overline{\left(\psi - \overline{\psi} \right)}}_{=0} \Big) = 0 \qquad \Rightarrow \qquad \overline{\varphi}(t) = \overline{\varphi_0}; \tag{D.37a}$$

i.e. $\overline{\varphi}(t)$ is constant in time. Likewise, from (9.36c), we conclude that

$$\partial_t \overline{\psi} = 0 \qquad \Rightarrow \qquad \overline{\psi}(t) = \overline{\psi_0}, \tag{D.37b}$$

and so $\overline{\psi}(t)$ is also constant. We have shown that, given initial masses $\overline{\varphi_0}$ and $\overline{\psi_0}$, the dynamics in (9.36) are mass conserving; m in (9.11) is also conserved. Consequently, we switch $\overline{\varphi_0}$ for $m\mathcal{M}$ and $\overline{\psi_0}$ for $\mathcal{M}$, understood to be the *initial* mass averages, and replace (9.36a) and (9.36c) with

$$\partial_t \varphi + M_\varphi \left[(-\Delta) \omega_\varphi + (\alpha (\varphi - m\mathcal{M}) + \beta (\psi - \mathcal{M})) \right] = 0, \tag{D.38a}$$

$$\text{and} \quad \partial_t \psi + M_\psi \left[(-\Delta) \omega_\psi + (\beta (\varphi - m\mathcal{M}) + \gamma (\psi - \mathcal{M})) \right] = 0, \tag{D.38b}$$

with ω_φ and ω_ψ as in (9.36b)–(9.36d). We will occasionally find it useful to eliminate ω_φ and ω_ψ, and work with the equivalent fourth order pair

$$\partial_t\varphi - M_\varphi\Delta\left(\varepsilon_\varphi^2\left(-\Delta\right)\varphi + \varepsilon_{\varphi\psi}^2\left(-\Delta\right)\psi + \mathcal{B}_\varphi\left(\varphi,\psi\right)\right) + M_\varphi\left(\alpha\left(\varphi - m\mathcal{M}\right) + \beta\left(\psi - \mathcal{M}\right)\right) = 0 \tag{D.39a}$$

and

$$\partial_t\psi - M_\psi\Delta\left(\varepsilon_{\varphi\psi}^2\left(-\Delta\right)\varphi + \varepsilon_\psi^2\left(-\Delta\right)\psi + \mathcal{B}_\psi\left(\varphi,\psi\right)\right) + M_\psi\left(\beta\left(\varphi - m\mathcal{M}\right) + \gamma\left(\psi - \mathcal{M}\right)\right) = 0. \tag{D.39b}$$

We will use (local) dynamics of this form for all further work.

D.3 Mass control

In Section D.2.2 we replaced the non-local averages $\overline{\varphi}$ and $\overline{\psi}$ with the control masses $m\mathcal{M}$ and $\mathcal{M}$ to write down (D.38), (D.39). If $\left(\overline{\varphi_0},\overline{\psi_0}\right) = \left(m\mathcal{M},\mathcal{M}\right) = \boldsymbol{m}$, this change is ostensibly cosmetic. On the other hand, suppose that

$$\left(\overline{\varphi_0},\overline{\psi_0}\right)^\top = \boldsymbol{m} + \left(\delta\varphi_0,\delta\psi_0\right)^\top \qquad \text{where} \qquad \boldsymbol{m} := \mathcal{M}\left(m,1\right)^\top, \tag{D.40}$$

for non-zero $\left(\delta\varphi_0,\delta\psi_0\right)^\top$, which we denote the *initial mass drift*. We would like to understand the conditions under which $\overline{\varphi}\to m\mathcal{M}$, $\overline{\psi}\to M$ (cf. (3.50) in the 2-phase case) and $\frac{\overline{\varphi}}{\overline{\psi}}\to m$ (cf. (9.11)). We will find that our dynamics in (D.38), (D.39) are not (generally) mass conserving, but rather mass *controlling*, in a sense we will make precise.

We refine our understanding and notation as follows:

- We interpret m and $\mathcal{M}$ as target/control parameters. The former encodes information about the DBC molecule; the latter the total proportion of polymer material in Ω. In modelling DBCs, we expect $\overline{\psi_0} = M$ and $\overline{\varphi_0} = m\mathcal{M}$, but in this section, we drop this assumption and investigate the PDEs (D.38), (D.39).

- We define a new time-dependent quantity (cf. (9.11))

$$\widetilde{m}\left(t\right) := \frac{\overline{\varphi}\left(t\right)}{\overline{\psi}\left(t\right)}, \tag{D.41}$$

  to measure the *actual* recorded (molecular) ratio of $\overline{\varphi}\left(t\right)$ to $\overline{\psi}\left(t\right)$.

Integrating (D.38) over Ω and diving by $\left|\Omega\right|$ (noting the zero Neumann BCs on ω_φ and ω_ψ), we are quickly led to the system

$$\partial_t\overline{\varphi} + M_\varphi\left(\alpha\left(\overline{\varphi} - m\mathcal{M}\right) + \beta\left(\overline{\psi} - \mathcal{M}\right)\right) = 0 \tag{D.42a}$$

$$\text{and} \qquad \partial_t\overline{\psi} + M_\psi\left(\beta\left(\overline{\varphi} - m\mathcal{M}\right) + \gamma\left(\overline{\psi} - \mathcal{M}\right)\right) = 0. \tag{D.42b}$$

We now define (cf. (5.14))

$$\overline{\boldsymbol{\varphi}} = \begin{pmatrix} \overline{\varphi} \\ \overline{\psi} \end{pmatrix} \qquad \text{and} \qquad \overline{\mathring{\boldsymbol{\varphi}}} = \begin{pmatrix} \overline{\mathring{\varphi}} \\ \overline{\mathring{\psi}} \end{pmatrix} = \begin{pmatrix} \overline{\varphi} - m\mathcal{M} \\ \overline{\psi} - \mathcal{M} \end{pmatrix} = \overline{\boldsymbol{\varphi}} - \boldsymbol{m}, \tag{D.43}$$

where $\overline{\mathring{\boldsymbol{\varphi}}}\left(t\right)$ is the mass drift as a function of time, $\overline{\mathring{\boldsymbol{\varphi}}}\left(0\right) = \left(\delta\varphi_0,\delta\psi_0\right)^\top$. Using (D.42),

$$\overline{\boldsymbol{\varphi}}\left(t\right) = \boldsymbol{m} + \overline{\mathring{\boldsymbol{\varphi}}}\left(t\right) \qquad \text{with} \qquad \partial_t\overline{\mathring{\boldsymbol{\varphi}}} = A\overline{\mathring{\boldsymbol{\varphi}}} \qquad \text{where} \qquad A = -\begin{pmatrix} M_\varphi\alpha & M_\varphi\beta \\ M_\psi\beta & M_\psi\gamma \end{pmatrix}. \tag{D.44}$$

For $\beta \neq 0$, the eigenvalues and vectors of A are given by

$$\lambda_1 = -\frac{1}{2}\left(M_\varphi\alpha + M_\psi\gamma + \chi\right) \qquad \text{with} \qquad \boldsymbol{v}_1 = \begin{pmatrix} \dfrac{M_\varphi\alpha - M_\psi\gamma + \chi}{M_\psi} \\ 2\beta \end{pmatrix}, \tag{D.45a}$$

and

$$\lambda_2 = -\frac{1}{2}\left(M_\varphi\alpha + M_\psi\gamma - \chi\right) \qquad \text{with} \qquad \boldsymbol{v}_2 = \begin{pmatrix} \dfrac{M_\varphi\alpha - M_\psi\gamma - \chi}{M_\psi} \\ 2\beta \end{pmatrix}, \tag{D.45b}$$

where we have defined

$$\chi := \sqrt{\left(M_\varphi\alpha - M_\psi\gamma\right)^2 + 4M_\varphi M_\psi\beta^2} = \sqrt{\left(M_\varphi\alpha + M_\psi\gamma\right)^2 - 4M_\varphi M_\psi\left(\alpha\gamma - \beta^2\right)}. \tag{D.45c}$$

Remark. We work with the matrix above as it is simpler than A; note that if $\overline{A}\boldsymbol{x} = \mu\boldsymbol{x}$, then $-\frac{3}{2}A\boldsymbol{x} = \mu\boldsymbol{x}$ and so $A\boldsymbol{x} = -\frac{2}{3}\mu\boldsymbol{x}$ i.e. μ an eigenvalue of $\overline{A} \Rightarrow -\frac{2}{3}\mu$ an eigenvalue of A.

It is clear that these eigenvalues:

- are real for any real α, β, γ and $M_\varphi, M_\psi > 0$;
- repeat only when $\chi = 0$, viz.

$$\beta = 0 \qquad \text{and} \qquad \frac{M_\varphi}{M_\psi} = \frac{\gamma}{\alpha};$$

- are both negative (assuming $M_\varphi\alpha + M_\psi\gamma > 0$) when

$$M_\varphi\alpha + M_\psi\gamma > \chi \qquad \Leftrightarrow \qquad \left(M_\varphi\alpha + M_\psi\gamma\right)^2 > \left(M_\varphi\alpha + M_\psi\gamma\right)^2 - 4M_\varphi M_\psi\left(\alpha\gamma - \beta^2\right)$$

  which is true if and only if $\alpha\gamma > \beta^2$; and
- have opposite signs when $\alpha\gamma < \beta^2$.

In our original variables, the time ODE for the mass averages has the general solution

$$\overline{\boldsymbol{\varphi}}\left(t\right) = \boldsymbol{m} + C_1\begin{pmatrix} \dfrac{M_\varphi\alpha - M_\psi\gamma + \chi}{M_\psi} \\ 2\beta \end{pmatrix}\mathrm{e}^{\lambda_1 t} + C_2\begin{pmatrix} \dfrac{M_\varphi\alpha - M_\psi\gamma - \chi}{M_\psi} \\ 2\beta \end{pmatrix}\mathrm{e}^{\lambda_2 t}$$

subject to the IC (D.40), viz.

$$\left(\delta\varphi, \delta\psi\right)^\top = C_1\boldsymbol{v}_1 + C_2\boldsymbol{v}_2$$

which, according to MATLAB, implies that

$$\begin{pmatrix} C_1 \\ C_2 \end{pmatrix} = \frac{1}{4\beta\chi}\begin{pmatrix} \delta\psi_0\left(\chi - \left(M_\varphi\alpha - M_\psi\gamma\right)\right) + 2M_\psi\beta\delta\varphi_0 \\ \delta\psi_0\left(\chi + M_\varphi\alpha - M_\psi\gamma\right) - 2M_\psi\beta\delta\varphi_0 \end{pmatrix}.$$

For $\beta \neq 0$, if $\lambda_1, \lambda_2 < 0$ (i.e. $\alpha\gamma > \beta^2$), it is clear that we have mass control in the sense that

$$\overline{\varphi}\left(t\right) \to m\mathcal{M}, \qquad \overline{\psi}\left(t\right) \to \mathcal{M} \qquad \text{and} \qquad \widetilde{m}\left(t\right) \to m \qquad \text{as} \qquad t \to \infty,$$

irrespective of the magnitude of the initial mass drift. There are additional, special cases of the above which are relevant to DBC modelling, which we now explore.

i) For $\beta = 0$ (and $M_\varphi \alpha \neq M_\psi \gamma$), we have the simpler eigenvalue/vector pairs

$$\lambda_1 = -M_\psi \gamma \qquad \text{with} \qquad \boldsymbol{v}_1 = \begin{pmatrix} 0 \\ 1 \end{pmatrix} \qquad \text{and} \qquad \lambda_2 = -M_\varphi \alpha \qquad \text{with} \qquad \boldsymbol{v}_2 = \begin{pmatrix} 1 \\ 0 \end{pmatrix}. \tag{D.46}$$

The solution of (D.44) becomes

$$\overline{\boldsymbol{\varphi}}\,(t) = \boldsymbol{m} + \begin{pmatrix} 0 \\ \delta\psi_0 \end{pmatrix} \mathrm{e}^{-M_\psi \gamma t} + \begin{pmatrix} \delta\varphi_0 \\ 0 \end{pmatrix} \mathrm{e}^{-\alpha M_\varphi t}. \tag{D.47}$$

Once again, as long as $\alpha, \gamma > 0$,

$$\overline{\varphi}\,(t) \to m\mathcal{M}, \qquad \overline{\psi}\,(t) \to \mathcal{M} \qquad \text{and} \qquad \widetilde{m}\,(t) \to m \qquad \text{as} \qquad t \to \infty,$$

irrespective of the magnitude of the initial mass drift.

ii) For $\beta^2 = \alpha\gamma$, $\chi = M_\varphi \alpha + M_\psi \gamma$ (cf. (D.45c)), the coefficient matrix A is singular, having a zero eigenvalue. Substituting $\beta = \sqrt{\alpha\gamma} \geq 0$, leads to the eigenvalue/vector pairs

$$\lambda_1 = -\left(M_\varphi \alpha + M_\psi \gamma\right); \qquad \boldsymbol{v}_1 = \begin{pmatrix} \dfrac{M_\varphi}{M_\psi}\sqrt{\alpha} \\ \sqrt{\gamma} \end{pmatrix} \qquad \text{and} \qquad \lambda_2 = 0; \qquad \boldsymbol{v}_2 = \begin{pmatrix} -\sqrt{\gamma} \\ \sqrt{\alpha} \end{pmatrix}, \tag{D.48a}$$

for which (D.44) admits the general solution, assuming $M_\varphi \alpha + M_\psi \gamma \neq 0$,

$$\overline{\boldsymbol{\varphi}}\,(t) = \boldsymbol{m} + C_1 \begin{pmatrix} \dfrac{M_\varphi}{M_\psi}\sqrt{\alpha} \\ \sqrt{\gamma} \end{pmatrix} \mathrm{e}^{-\left(M_\varphi \alpha + M_\psi \gamma\right)t} + C_2 \begin{pmatrix} -\sqrt{\gamma} \\ \sqrt{\alpha} \end{pmatrix}, \tag{D.48b}$$

with

$$\begin{pmatrix} C_1 \\ C_2 \end{pmatrix} = \frac{1}{M_\varphi \alpha + M_\psi \gamma} \begin{pmatrix} M_\psi \left(\sqrt{\gamma}\delta\psi_0 + \sqrt{\alpha}\delta\varphi_0\right) \\ M_\varphi \sqrt{\alpha}\delta\psi_0 - M_\psi \sqrt{\gamma}\delta\varphi_0 \end{pmatrix}. \tag{D.48c}$$

We now relate these results to the α, β, γ of the DBC model in (9.24). For these,

$$\beta = -m\alpha, \qquad \gamma = (-m)^2 \alpha \qquad \text{and} \qquad \alpha\gamma = (-m)^2 \alpha^2 = \beta^2,$$

which means that we are in scenario (ii) above viz. $\det A = 0$, and

$$M_\varphi \alpha + M_\psi \gamma = \left(M_\varphi + M_\psi m^2\right) \alpha > 0.$$

Consequently, we can express the general DBC mass evolution solution (D.48) as

$$\overline{\boldsymbol{\varphi}}\,(t) = \boldsymbol{m} + C_1 \begin{pmatrix} \dfrac{M_\varphi}{M_\psi} \\ -m \end{pmatrix} \mathrm{e}^{-\alpha\left(M_\varphi + M_\psi m^2\right)t} + C_2 \begin{pmatrix} m \\ 1 \end{pmatrix}, \tag{D.49a}$$

where we recall that $\sqrt{\gamma} = -m\sqrt{\alpha}$, and

$$\begin{pmatrix} C_1 \\ C_2 \end{pmatrix} = \frac{1}{M_\varphi + M_\psi m^2} \begin{pmatrix} M_\psi \left(-m\delta\psi_0 + \delta\varphi_0\right) \\ M_\varphi \delta\psi_0 + M_\psi m \delta\varphi_0 \end{pmatrix}. \tag{D.49b}$$

We interpret these results as follows:

- If $\overline{\varphi_0} = m\mathcal{M}$ and $\overline{\psi_0} = \mathcal{M}$ then $\delta\varphi_0 = \delta\psi_0 = 0$, so $C_1 = C_2 = 0$ in (D.49b), and the system *conserves* the initial masses as in (D.37),

$$\overline{\varphi}(t) = m\mathcal{M}, \qquad \overline{\psi}(t) = \mathcal{M} \qquad \text{and} \qquad \widetilde{m}(t) = m \qquad \text{for every} \qquad t \in [0, T]. \tag{D.50}$$

- In the symmetric case $m = 0$, (D.49) becomes (cf. (D.47))

$$\overline{\boldsymbol{\varphi}}(t) = \begin{pmatrix} 0 \\ \overline{\psi_0} \end{pmatrix} + \begin{pmatrix} \delta\varphi_0 \\ 0 \end{pmatrix} \mathrm{e}^{-\alpha M_\varphi t}, \tag{D.51}$$

after recalling (D.40), which means that

$$\overline{\psi}(t) = \overline{\psi_0} \,\forall\, t \qquad \text{and} \qquad \overline{\varphi}(t) = \delta\varphi_0 \mathrm{e}^{-\alpha M_\varphi t} \to 0 \qquad \Rightarrow \qquad \widetilde{m}(t) \to 0 \qquad \text{as} \qquad t \to \infty, \tag{D.52}$$

for any $M_\varphi > 0$, *irrespective of the magnitude of the initial mass drift*. Hence, ψ is *conserved* (but $\mathcal{M}$ has no impact whatsoever), whereas φ is *controlled*. This result is not surprising in light of (9.36) and (D.39): if $\beta = \gamma = 0$, then we eliminate all of the non-local terms other than $\alpha(\varphi - m\mathcal{M}) = \alpha\varphi$ (for $m = 0$) i.e. $\mathcal{M}$ is not present.

- In the asymmetric case, the second term on the right-hand side of (D.49a) tends to zero as $t \to \infty$, for $M_\psi > 0$, and so

$$\overline{\boldsymbol{\varphi}}(t) \to \boldsymbol{m} + \begin{pmatrix} \varphi_\epsilon \\ \psi_\epsilon \end{pmatrix} \qquad \text{as} \qquad t \to \infty, \tag{D.53a}$$

where we define the long-time mass drift as

$$\begin{pmatrix} \varphi_\epsilon \\ \psi_\epsilon \end{pmatrix} := C_2 \begin{pmatrix} m \\ 1 \end{pmatrix} \qquad \text{with} \qquad C_2 = \frac{M_\varphi \delta\psi_0 + M_\psi m \delta\varphi_0}{M_\varphi + M_\psi m^2}. \tag{D.53b}$$

Hence $\left(\overline{\varphi}, \overline{\psi}\right)^\top \not\to \boldsymbol{m}$ as $t \to \infty$, even though $m\mathcal{M}$ and $\mathcal{M}$ are both present. Yet,

$$\widetilde{m}(t) = \frac{\overline{\varphi}(t)}{\overline{\psi}(t)} \to \frac{m\mathcal{M} + \varphi_\epsilon}{\mathcal{M} + \psi_\epsilon} = \frac{m\mathcal{M} + mC_2}{\mathcal{M} + C_2} = m \qquad \text{as} \qquad t \to \infty,$$

which means we recover the correct molecular ratio m as $t \to \infty$, *irrespective of the magnitude of the initial mass drift*. Even if $\delta\psi_0 = 0$, but $\delta\varphi_0 \neq 0$ (i.e. $\overline{\psi_0} = \mathcal{M}$ but $\widetilde{m}(0) \neq m$) the system will gain/lose *polymer* material as $\widetilde{m} \to m$, as in Fig. D.3.

D.3.1 Exact solutions: constant ICs

Finding exact, closed-form solutions to (D.39) is impossible in most situations. However, for constant ICs, progress is possible. Suppose that

$$\varphi_0 \equiv c_1 \qquad \text{and} \qquad \psi_0 \equiv c_2. \tag{D.54}$$

For such φ and ψ, $(-\Delta)\varphi = (-\Delta)\psi = 0$, and since $\partial_\varphi \mathcal{B}(\varphi, \psi)$ and $\partial_\psi \mathcal{B}(\varphi, \psi)$ are constant functions of space, $\Delta\mathcal{B}_\varphi(\varphi, \psi) = \Delta\mathcal{B}_\psi(\varphi, \psi) = 0$, too. Hence, for these ICs, (D.39) reduces to

$$\partial_t\varphi + M_\varphi(\alpha(\varphi - m\mathcal{M}) + \beta(\psi - \mathcal{M})) = 0 \tag{D.55a}$$

$$\text{and} \qquad \partial_t\psi + M_\psi(\beta(\varphi - m\mathcal{M}) + \gamma(\psi - \mathcal{M})) = 0, \tag{D.55b}$$

which is the same as (D.42), if we replace φ and ψ with their mass averages. In particular, neither $\partial_t\varphi$ nor $\partial_t\psi$ is necessarily zero (unless $c_1 = m\mathcal{M}$ and $c_2 = \mathcal{M}$), but both of these time derivatives are independent of x, and we end up with a system of linear ODEs (in time). Hence, $\overline{\varphi}$ and $\overline{\psi}$ of (D.42) evolve in the same way as φ and ψ in (D.55).

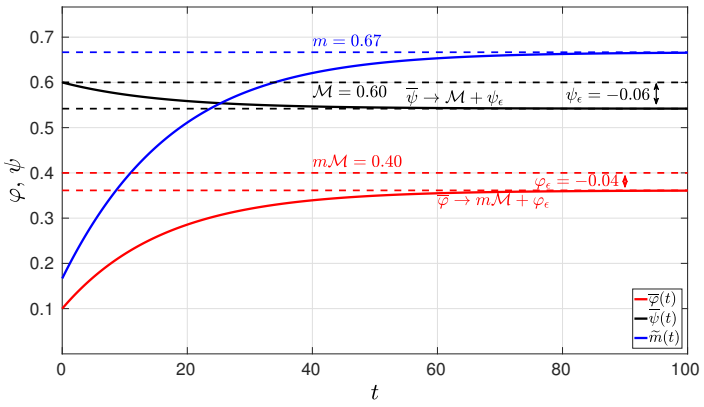

(a) $(\delta\varphi_0, \delta\psi_0) = (-0.3, 0)$ i.e. $\left(\overline{\varphi_0}, \overline{\psi_0}\right) = (0.1, 0.6)$: $\mathcal{M} = \overline{\psi_0}$

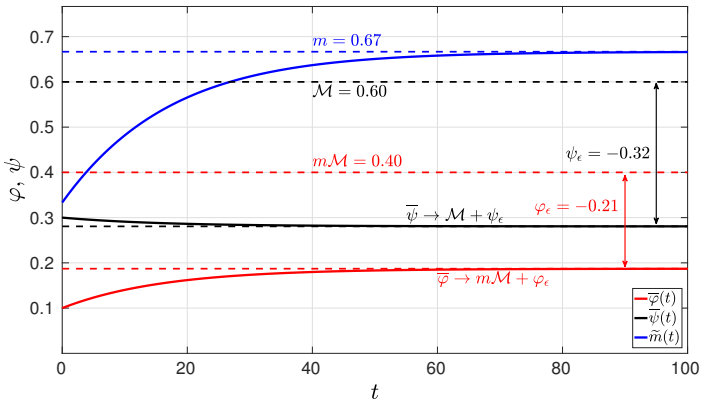

(b) $(\delta\varphi_0, \delta\psi_0) = (-0.3, -0.3)$ i.e. $\left(\overline{\varphi_0}, \overline{\psi_0}\right) = (0.1, 0.3)$: $\mathcal{M} \neq \overline{\psi_0}$

Figure D.3: Mass evolution for an asymmetric DBC with $\mathcal{M}(m, 1) = (0.4, 0.6)$ (i.e. $m = \frac{2}{3}$) and the indicated initial mass drifts, (D.40). $M_\varphi = 2$, $M_\psi = \frac{2}{3}$ (cf. (D.27))) and $6\varepsilon\gamma_c = 0.005$ in (9.24a), so that $\alpha = 0.027$, $\beta = -0.018$ and $\gamma = 0.012$; $T = 100$. The molecular ratio $\widetilde{m}(t)$ from (D.41) is drawn in **blue**. In both cases, $\left(\overline{\varphi}, \overline{\psi}\right) \to (m\mathcal{M} + \varphi_\epsilon, \mathcal{M} + \psi_\epsilon)$ as $t \to \infty$, and $\widetilde{m} \to m$, the correct molecular ratio, despite the large initial mass drift. In (a), the system loses polymer material during this process.

D.4 Numerical simulations of gradient flow dynamics

D.4.1 Discrete time mass control

We now study mass conservation and control in the time discretisation of Defn 9.2.2. If we set $\nu_1 = \nu_3 \equiv 0$ in (9.44), and divide by $|\Omega|$, we arrive at the *linear* equations (cf. (5.22))

$$\frac{\overline{\mathring{\varphi}^j} - \overline{\mathring{\varphi}^{j-1}}}{\tau} + M_\varphi\left(\alpha\overline{\mathring{\varphi}^j} + \beta\overline{\mathring{\psi}^j}\right) = 0 \qquad \text{and} \qquad \frac{\overline{\mathring{\psi}^j} - \overline{\mathring{\psi}^{j-1}}}{\tau} + M_\psi\left(\beta\overline{\mathring{\varphi}^j} + \gamma\overline{\mathring{\psi}^j}\right) = 0, \tag{D.56a}$$

for the mass averages (cf. (D.43))

$$\overline{\mathring{\boldsymbol{\varphi}}^j} = \begin{pmatrix} \overline{\mathring{\varphi}^j} \\ \overline{\mathring{\psi}^j} \end{pmatrix} := \begin{pmatrix} \overline{\varphi^j} - m\mathcal{M} \\ \overline{\psi^j} - \mathcal{M} \end{pmatrix}. \tag{D.56b}$$

Remark. We switch from the averages $\overline{\varphi^j}$ and $\overline{\psi^j}$ to $\overline{\mathring{\varphi}^j}$ and $\overline{\mathring{\psi}^j}$ above using the discrete version of the fact that constant functions have zero derivative.

We express (D.56a) in matrix form as

$$K\overline{\mathring{\boldsymbol{\varphi}}^j} = \overline{\mathring{\boldsymbol{\varphi}}^{j-1}} \qquad \text{where} \qquad K = \begin{pmatrix} 1 + M_\varphi \tau\alpha & M_\varphi \tau\beta \\ M_\psi \tau\beta & 1 + M_\psi \tau\gamma \end{pmatrix} = I_2 - \tau A, \tag{D.57}$$

with A as in (D.44). We have clearly arrived at the time-discrete version of the problem we analysed in Section D.3; we focus here on the DBC model version of the problem. Now

$$\det K = 1 + M_\varphi \tau\alpha + M_\psi \tau\gamma + M_\varphi M_\psi \tau^2 \left(\alpha\gamma - \beta^2\right),$$

and so for our DBC model with $\alpha\gamma = \beta^2$ (cf. (9.24)), we find that

$$\det K = 1 + \tau\left(M_\varphi \alpha + M_\psi \gamma\right) > 0.$$

Hence, we assume K is invertible, and write

$$\overline{\mathring{\boldsymbol{\varphi}}^j} = K^{-1}\overline{\mathring{\boldsymbol{\varphi}}^{j-1}} = K^{-1}\left(K^{-1}\overline{\mathring{\boldsymbol{\varphi}}^{j-2}}\right) = \ldots = \left(K^{-1}\right)^j \overline{\mathring{\boldsymbol{\varphi}}^0} \tag{D.58a}$$

or (cf. (D.44))

$$\overline{\boldsymbol{\varphi}^j} = \boldsymbol{m} + \left(K^{-1}\right)^j \overline{\mathring{\boldsymbol{\varphi}}^0}, \tag{D.58b}$$

and thus explicitly predict $\overline{\mathring{\boldsymbol{\varphi}}^j}$ for each j. Clearly, if $\overline{\mathring{\boldsymbol{\varphi}}^0} = \mathbf{0}$, then $\overline{\boldsymbol{\varphi}^j} = \boldsymbol{m}$ for every j and our scheme *conserves* the initial mass. For K as in (D.57), the eigenvalues of K^{-1} are related to those of A as

$$Ax = \lambda x \qquad \Leftrightarrow \qquad K^{-1}x = \widehat{\lambda}x \qquad \text{where} \qquad \widehat{\lambda} := (1 - \tau\lambda)^{-1}, \tag{D.59}$$

as long as $\tau \neq \frac{1}{\lambda}$ i.e. K^{-1} and A share eigenvectors. Using (D.48) we find that

$$\widehat{\lambda}_1 = \frac{1}{1 + \tau\left(M_\varphi \alpha + M_\psi \gamma\right)}; \qquad \boldsymbol{v}_1 = \begin{pmatrix} \frac{M_\varphi}{M_\psi}\sqrt{\alpha} \\ \sqrt{\gamma} \end{pmatrix} \qquad \text{and} \qquad \widehat{\lambda}_2 = 1; \qquad \boldsymbol{v}_2 = \begin{pmatrix} -\sqrt{\gamma} \\ \sqrt{\alpha} \end{pmatrix}, \tag{D.60}$$

and we assume that $\tau\left(M_\varphi \alpha + M_\psi \gamma\right) > 0$ i.e. $\widehat{\lambda}_1 \neq \widehat{\lambda}_2$, and so $\{\boldsymbol{v}_1, \boldsymbol{v}_2\}$ spans $\mathbb{R}^2$. Consequently, if $\overline{\mathring{\boldsymbol{\varphi}}^0} \neq \mathbf{0}$, there exist constants C_1, C_2 (at least one non-zero) such that

$$\overline{\mathring{\boldsymbol{\varphi}}^0} = C_1\boldsymbol{v}_1 + C_2\boldsymbol{v}_2 \qquad \text{i.e.} \qquad \begin{pmatrix} \delta\varphi_0 \\ \delta\psi_0 \end{pmatrix} = \begin{pmatrix} \frac{M_\varphi}{M_\psi}\sqrt{\alpha} & -\sqrt{\gamma} \\ \sqrt{\gamma} & \sqrt{\alpha} \end{pmatrix} \begin{pmatrix} C_1 \\ C_2 \end{pmatrix}$$

viz. as in (D.48c),

$$\begin{pmatrix} C_1 \\ C_2 \end{pmatrix} = \frac{1}{M_\varphi \alpha + M_\psi \gamma} \begin{pmatrix} M_\psi\left(\sqrt{\gamma}\delta\psi_0 + \sqrt{\alpha}\delta\varphi_0\right) \\ M_\varphi\sqrt{\alpha}\delta\psi_0 - M_\psi\sqrt{\gamma}\delta\varphi_0 \end{pmatrix}. \tag{D.61}$$

Setting $\sqrt{\gamma} = -m\sqrt{\alpha}$ for our DBC model we arrive at

$$\overline{\mathring{\boldsymbol{\varphi}}^0} = C_1 \begin{pmatrix} \frac{M_\varphi}{M_\psi} \\ -m \end{pmatrix} + C_2 \begin{pmatrix} m \\ 1 \end{pmatrix}; \qquad \begin{pmatrix} C_1 \\ C_2 \end{pmatrix} = \frac{1}{M_\varphi + M_\psi m^2} \begin{pmatrix} M_\psi \left(-m\delta\psi_0 + \delta\varphi_0\right) \\ M_\varphi \delta\psi_0 + M_\psi m \delta\varphi_0 \end{pmatrix}, \tag{D.62}$$

as in (D.49). Consequently in (D.58),

$$\left(K^{-1}\right)^j \overline{\mathring{\boldsymbol{\varphi}}^0} = C_1 \widehat{\lambda}_1^j \boldsymbol{v}_1 + C_2 \widehat{\lambda}_2^j \boldsymbol{v}_2 = \frac{C_1}{\left(1 + \tau\alpha\left(M_\varphi + M_\psi m^2\right)\right)^j} \begin{pmatrix} \frac{M_\varphi}{M_\psi} \\ -m \end{pmatrix} + C_2 \begin{pmatrix} m \\ 1 \end{pmatrix}, \tag{D.63}$$

which specifies the mass drift at each time-step. For $j = 0$,

$$\left(K^{-1}\right)^0 \overline{\mathring{\boldsymbol{\varphi}}^0} = \frac{1}{M_\varphi + M_\psi m^2} \begin{pmatrix} \left(M_\varphi + M_\psi m^2\right) \delta\varphi_0 \\ \left(M_\varphi + M_\psi m^2\right) \delta\psi_0 \end{pmatrix} = \begin{pmatrix} \delta\varphi_0 \\ \delta\psi_0 \end{pmatrix},$$

as expected. For $j > 0$, as in the symmetric, continuous time case (D.51),

$$\left(K^{-1}\right)^j \overline{\mathring{\boldsymbol{\varphi}}^0} = \frac{1}{\left(1 + \tau\alpha M_\varphi\right)^j} \begin{pmatrix} \delta\varphi_0 \\ 0 \end{pmatrix} + \begin{pmatrix} 0 \\ \delta\psi_0 \end{pmatrix} \to \begin{pmatrix} 0 \\ \delta\psi_0 \end{pmatrix} \qquad \text{as } j \to \infty. \tag{D.64}$$

Hence, as in (D.52)

$$\overline{\psi^j} = \overline{\psi_0}, \quad j = 1, 2, \ldots \quad \text{and} \quad \overline{\varphi^j} = \frac{\delta\varphi_0}{\left(1 + \tau\alpha M_\varphi\right)^j} \to 0 \quad \Rightarrow \quad \widetilde{m}^j \to 0 \quad \text{as} \quad j \to \infty, \tag{D.65}$$

for any $\tau, \alpha, M_\varphi > 0$, where we have defined the discrete analogue to (D.41),

$$\widetilde{m}^j := \frac{\overline{\varphi^j}}{\overline{\psi^j}}. \tag{D.66}$$

Likewise, in the asymmetric case $m \neq 0$, if $\tau\alpha\left(M_\varphi + M_\psi m^2\right) > 0$, then

$$\overline{\boldsymbol{\varphi}^j} = \boldsymbol{m} + \left(K^{-1}\right)^j \overline{\mathring{\boldsymbol{\varphi}}^0} \to \boldsymbol{m} + \frac{M_\varphi \delta\psi_0 + M_\psi m \delta\varphi_0}{M_\varphi + M_\psi m^2} \begin{pmatrix} m \\ 1 \end{pmatrix}, \tag{D.67}$$

which is essentially the same as the continuous (D.53). Hence, the time discretisation in Defn (9.2.2) captures continuous time mass conservation and control. We illustrate this for various τ in Fig. D.4.

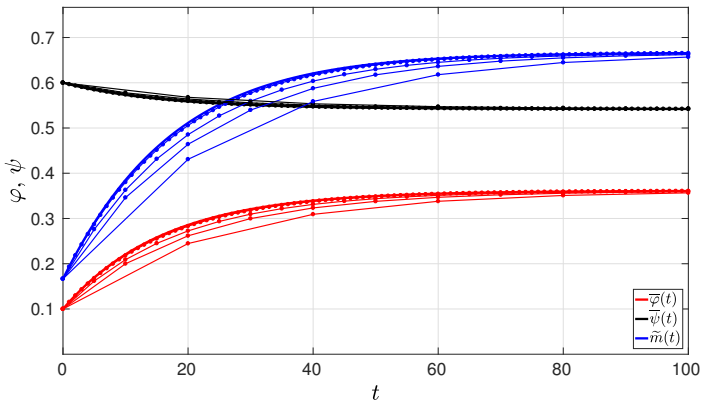

(a) $(\delta\varphi_0, \delta\psi_0) = (-0.3, 0)$ i.e. $\left(\overline{\varphi_0}, \overline{\psi_0}\right) = (0.1, 0.6)$: $\mathcal{M} = \overline{\psi_0}$

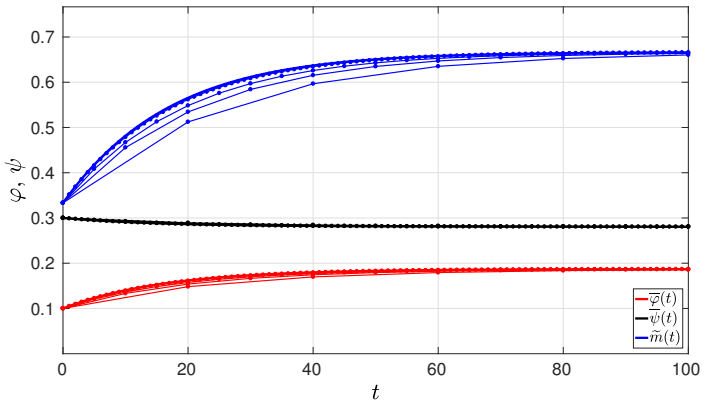

(b) $(\delta\varphi_0, \delta\psi_0) = (-0.3, -0.3)$ i.e. $\left(\overline{\varphi_0}, \overline{\psi_0}\right) = (0.1, 0.3)$: $\mathcal{M} \neq \overline{\psi_0}$

Figure D.4: Predicted discrete time mass evolution for the asymmetric DBC scenarios in Fig. D.3 with $T = 100$ and $\tau \in \{1, 5, 10, 20\}$. It is clear that the smaller τ is, the closer the discrete mass evolution is to that in continuous time.